Title

Selected Works of L. Jackson Laslett Volume II

Author

Lawrence Berkeley National Laboratory

Publication Date

1987-09-01

PUB-616
Volume II
September 1987

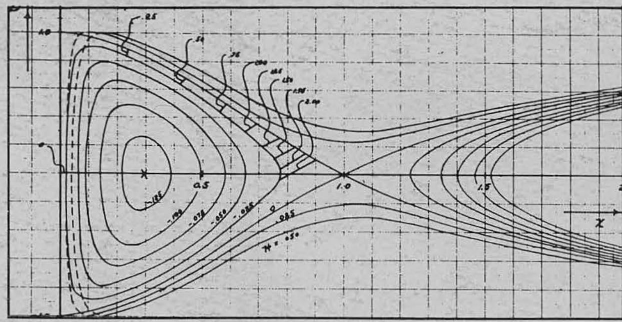

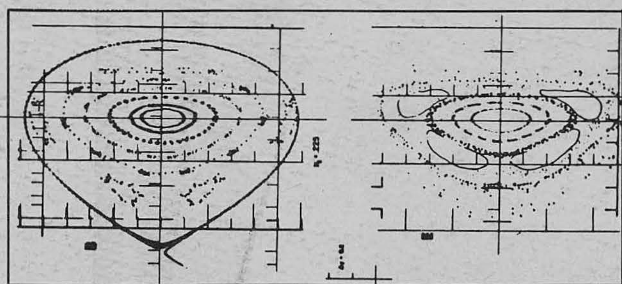

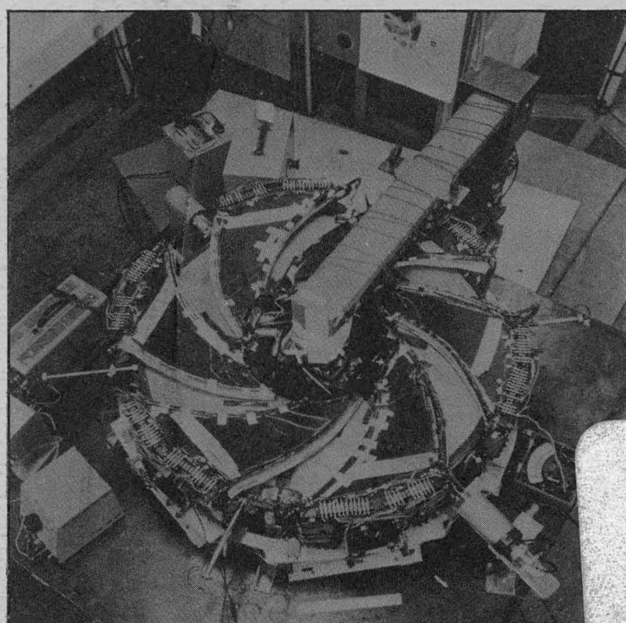

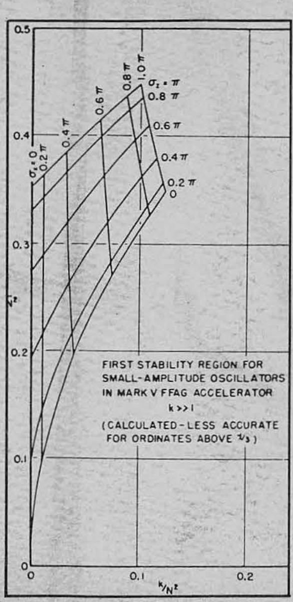

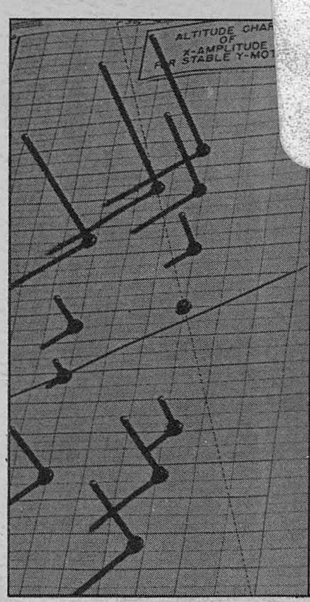

Selected Works of L. Jackson Laslett

Lawrence Berkeley Laboratory
University of California
Berkeley, California 94720

Prepared for the U.S. Department of Energy
under Contract DE-AC03-76SF00098

PUB-616
Volume II
September 1987

Selected Works of L. Jackson Laslett

Lawrence Berkeley Laboratory
University of California
Berkeley, California 94720

Prepared for the U.S. Department of Energy under Contract DE-AC03-76SF00098

Table of Contents

Volume I

MURA Notes and Other Documents

Section 4: Coherent Collective Instabilities

Section 5. Impedances

1

Single Particle Dynamics in Fixed Field Alternating Gradient Accelerators

MU–RA "NOTES" [Treble Clef]

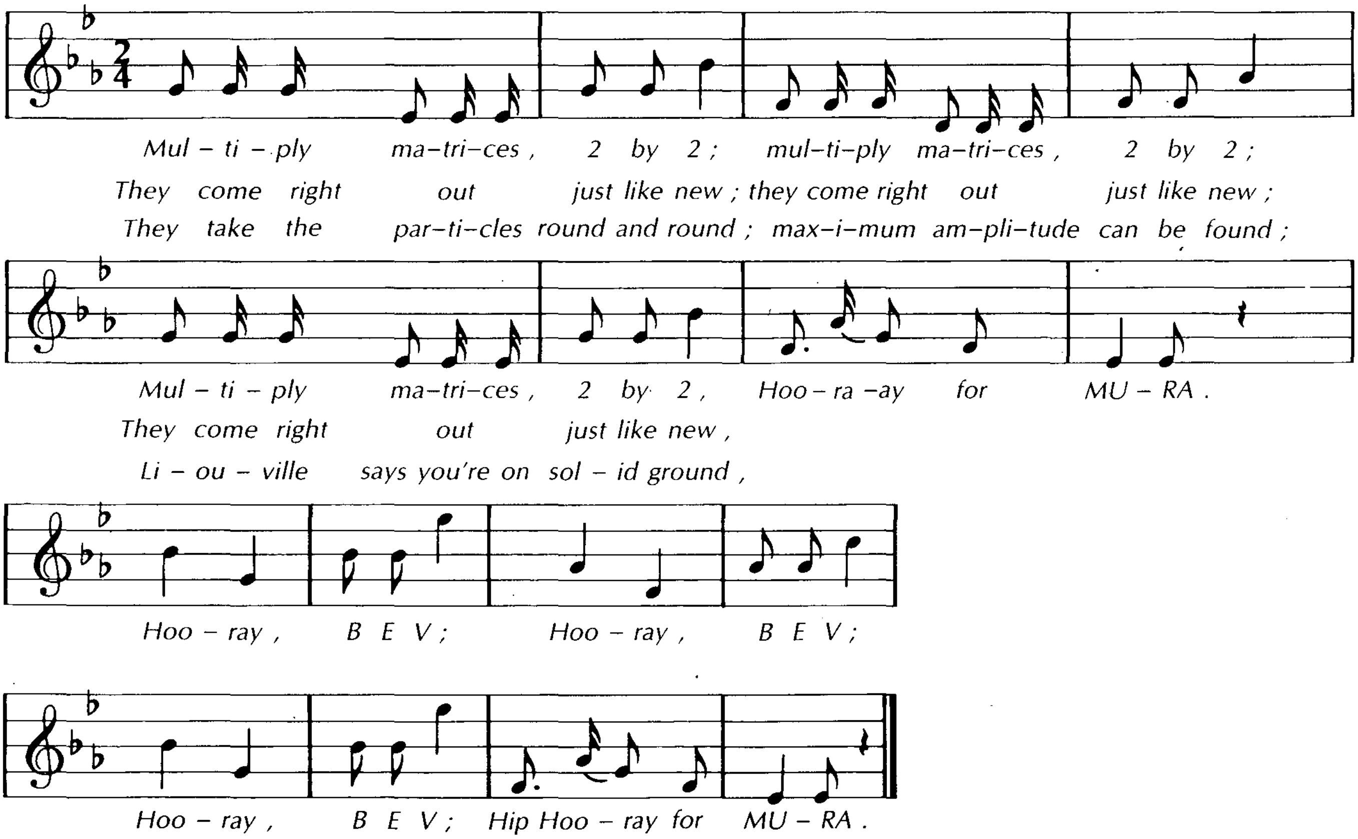

Reprinted from SCIENCE, October 26, 1956, Vol. 124, No. 3226, pages 781–787.

Fixed-Field Alternating-Gradient Accelerators

L. Jackson Laslett

Developments in the art of designing high-energy particle accelerators may be of interest not only to nuclear physicists but also to those working in chemical and engineering fields, to biologists, and to workers engaged in medical research. For the physicist, the possibility of studying particle reactions at increasingly *high energies* may be the most exciting aspect of such developments, although a substantial increase of *intensity,* at energies presently available, would make possible definitive experiments that are now difficult to perform. For production of radiation effects on matter *en gros,* as in the production of cross-linkages in polymers or in various investigations of radiation damage, intensity may be the more important characteristic of an accelerator. In the present article (*1*), I attempt to outline a potential new development in the accelerator art which appears to offer not only the prospect of certain engineering advantages but also the promise of a substantial increase of intensity or of the energy available for the study of particle reactions. Analysis of the particle orbits to be expected in the proposed structures affords a number of important and challenging mathematical problems concerning which, it may be hoped, an improved analytic understanding will be built up to supplement results obtained by digital computation.

The developments discussed here are the result of study by a group of midwestern physicists (*2*) who were stimulated by the broad class of new accelerators apparently made possible by the use of the alternating-gradient principle, which was first announced from the Brookhaven National Laboratory (*3*). Specifically, in contrast to the present Brookhaven efforts, the midwestern group has concentrated on a class of cyclic accelerators employing magnetic fields that are *constant* in time.

In any cyclic accelerator, such as the cyclotron, betatron, or synchrotron, a charged particle makes a great number of revolutions within the structure, gaining a relatively small amount of energy on each turn, and the provision of suitable focusing forces is essential. It may be of interest to note in this connection that, in a number of typical accelerators now in use, the distance covered by the particle during the acceleration process ranges from one-third of the distance across the United States to some 6 or 8 times around the earth. Since particles with energies that are at least slightly different will be simultaneously present, a related property of an annular accelerator of importance in its effect on the cost of the structure is the ability to accommodate particles with various energies within an annular region of limited radial extent.

If, as is customary, the particles are guided by a magnetic field as they follow their orbits around the accelerator, it is particularly convenient to achieve the requisite focusing by adjustment of the spatial variation of this field. In the case in which the fields show no variation with azimuth, a suitable index to characterize this spatial variation is

$$n \equiv \frac{r}{B}\frac{dB}{dr}$$

where r represents the distance from the central axis of the machine, and B represents the strength of the (axial) field in the median plane. In the absence of an azimuthal variation, stability in both the radial and axial directions is obtained only if the condition

$$-1 < n < 0$$

is satisfied. The energy or momentum content of such a machine is expressed by the quantity

$$\alpha \equiv \frac{r}{p}\frac{dp}{dr} = n + 1$$

where p denotes the particle momentum, and α is so small than an annular accelerator must then be operated in a pulsed manner to provide an increasing field adequate to hold particles of increasing energy within the machine.

In a conventional continuous-wave cyclotron, with the index n constrained to lie between 0 and -0.2 in order to avoid a coupling resonance between the radial and axial oscillations, the requirement that the frequency of revolution be independent of energy imposes a limitation on the attainable energy when the relativistic increase of mass becomes significant.

Description

A markedly greater energy content can be achieved in an annular accelerator if a rapid radial increase of the guide field is permitted by introduction of alternating-gradient focusing to maintain orbit stability. The field may then be capable of accommodating simultaneously particles of a wide range of energy, and the field strength could be independent of time. Such a modification, although it introduces complications associated with the significantly nonlinear character of the differential equations governing the particle motion, evidently promises a number of significant advantages.

1) Direct-current magnet construction and excitation may be employed.

2) The magnetic field need only be adjusted for operation at a single level of excitation, thus avoiding the difficulties associated with remanence, saturation, and eddy currents in a pulsed accelerator.

3) There is greater freedom in the choice of injection energy, and the time schedule for the acceleration process is flexible.

4) High intensity appears possible, owing to the permissible flexibility in planning the means of particle acceleration. Azimuthal variation of the field in a cyclotron, with the associated alternating-gradient focusing effects, can also be advantageous, because it allows higher energies to be reached than otherwise would be permitted by the relativistic increase of mass with energy.

In subsequent paragraphs I discuss a number of specific types of structures in which fixed-field alternating-gradient focusing is present (*4–6*). The structures are of two general types, one employing radial sectors and the other a spiral sector pattern. The first-mentioned type is in some ways simpler and easier to construct, while the second appears to permit a smaller accelerator for a given energy. In all the structures, particles with a wide range of energies can be simultaneously accommodated by virtue of a magnetic field whose average value around the machine varies with radius as r^k, and focusing forces leading to stable motion are obtained by a suitable spatial variation of the field.

The author is at present on leave of absence from Iowa State College to work at the University of Illinois as a member of the Technical Group of the Midwestern Universities Research Association. Some of the material on which this article is based was discussed at the International Conference on Accelerators in Geneva, Switzerland, during the week of 11 June and at a meeting of the Canadian Association of Physicists on 14 June 1956.

Reversed-Field Design

In the reversed-field type of fixed-field alternating-gradient (FFAG) accelerator, the direction of the field is reversed from one sector to the next. The sector boundaries are usually supposed to be formed by geometric planes that extend radially from the axis of the accelerator. The strength of the field in the reversed-field sectors, or the length of the reversed-field sectors, must, of course, be less than for the sectors of positive field in order that the particle orbits will ultimately be bent around through 360 degrees and permit a closed equilibrium orbit to be drawn (Fig. 1).

The magnitude of the field in the reversed-field accelerator varies at every azimuth as r^k, where r is the radius from the central axis of the machine. If k is positive, there is axial defocusing in the positive-field sectors and axial focusing in the reversed-field sectors. The alternating-gradient action is found to yield reasonable stability for small-amplitude oscillations in both the radial and axial directions, provided that the combined circumference of the forward and reversed-field magnets is some 5 times that required by an azimuthally constant magnetic field of the same maximum field strength. The ratio of the combined circumference to that required for a constant magnetic field is termed the *circumference factor, C.*

Within the individual sectors, the fields would normally be such that the complete equilibrium orbit would be formed from a series of circular arcs with their centers displaced from the axis of the machine. Denoting the radius of curvature of the orbit by ρ, the local focusing index is $n = k \cdot \rho/r$ and, if the same magnitude of field strength prevails in the positive and negative sectors, $\rho = r/C$. In linear approximation the radial and axial oscillations in such structures can then be expressed reasonably accurately, when the number of sectors is large, by the equations

$$\frac{d^2x}{d(s/r)^2} \pm kCx = 0$$

$$\frac{d^2z}{d(s/r)^2} \mp kCz = 0$$

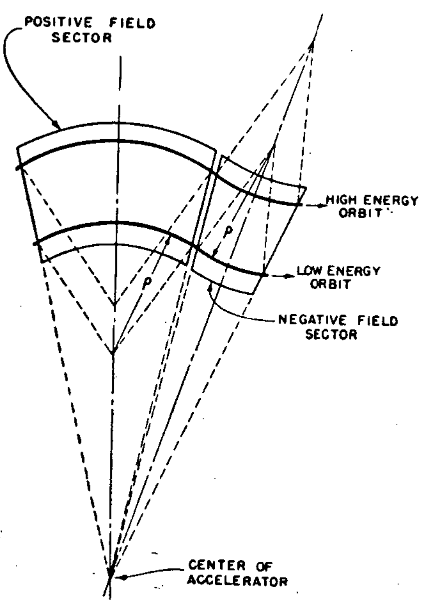

Fig. 1. Orbits in a reversed-field FFAG accelerator.

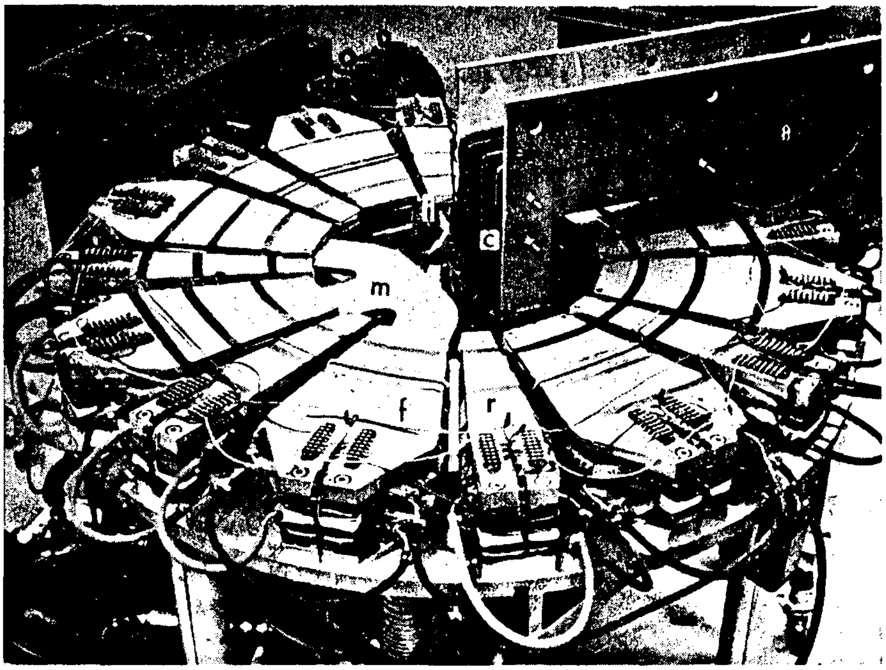

Fig. 2. An operating electron model of a reversed-field FFAG accelerator. Eight sectors of positive field and eight narrower sectors of negative field are employed. The betatron core is seen linking the region occupied by the particle orbits. (f) Magnet sector with forward or positive field; (r) magnet sector with reversed or negative field; (c) betatron core; (i) injector; (m) pump manifold.

where s denotes arc length along a reference circle of radius r, the upper and lower signs refer, respectively, to the sectors of positive and negative field, and centrifugal effects have been neglected since we assume that $kC \gg 1$. These equations may be solved by the aid of the matrix methods that are customarily employed in analysis of alternating-gradient focusing. If the phase change per sector for the radial oscillations and the corresponding phase change for the axial oscillations are permitted to assume widely different values, lying near the upper and lower limits of the stable range, a design with C as low as 5 may be feasible. A more accurate calculation must, of course, take account of the edge effects that arise at the sector boundaries and would involve an expansion about an equilibrium orbit which, accordingly, must be determined first. For a complete account of the motion, the effect of nonlinear terms would also have to be included.

Attention is directed to the important scaling property of the orbits in this accelerator. Possible orbits of particles of different energies, or momenta, are scaled replicas of each other. In consequence, the frequencies of the oscillations will be independent of energy, and harmful resonances may be avoided at all energies by a consistent design. The momentum content is represented by $p \propto r^{k+1}$, so that the momentum compaction factor α is given by

$$\alpha = k + 1$$

and can be either positive or negative in a reversed-field accelerator.

A small working model of a reversed-field FFAG accelerator has been put into operation (7). This model, shown in Fig. 2, employs eight sectors of positive field and eight shorter sectors of negative field. Electrons are accelerated, at present by betatron action, from 25 kev to 400 kev. Tuning controls have been provided for the model, so that various oscillation frequencies can be produced. These frequencies can be measured accurately by a radio-frequency knock-out technique (8) and the effect of certain resonances on the beam noted. The model affords an opportunity to study operation with a high duty factor, as is possible in FFAG accelerators employing betatron acceleration. Radio-frequency acceleration methods will also be investigated.

Possible parameters for a large-scale reversed-field FFAG accelerator for the production of 10 Bev protons have been examined. Although such a machine would be expected to have many desirable characteristics, the large magnet mass and power requirements direct interest to other FFAG designs of smaller circumference factor. By virtue of its essential simplicity, however, the reversed-field type may remain of interest for accelerators of low or intermediate energy, especially if a high duty factor can be efficiently realized with betatron acceleration.

Spiral-Sector Design

To avoid the considerable circumference required for a reversed-field FFAG accelerator, an alternative arrangement has been suggested by D. W. Kerst and others of the Midwestern Universities Research Association (MURA) group in which the alternating-gradient action is provided by a smaller but more rapid spatial variation of the field, the field being alternatively high and low along spiral curves which all particles must cross. Illustrative of the type of field present in the median plane of such a structure, one may take

$$B_{z_0} = \langle B \rangle (r/r_0)^k \left\{ 1 + f \sin \left[\frac{\ln(r/r_0)}{w} - N\Phi \right] \right\}$$

From this expression it is seen that N is the number of spiraling ridges passed over by a particle in going around the machine once. The coefficient f is the fractional flutter in the magnetic field owing to the ridges. Finally, if the radial width of the annulus is small in comparison with the outer radius, r_0, $\lambda \cong 2\pi r_0 w$ is substantially the radial separation of the ridges. The exponent k is taken to be positive.

In the spiral-sector design, as in the radial-sector case, the fields and the orbits satisfy the scaling condition. In passing from one energy to another, there is, however, a *rotation* of the geometrically similar orbits, which presents complications if one wishes to introduce straight-sections (field-free regions) whose boundaries extend radially from the central axis of the machine.

The equilibrium orbit in the spiral-sector machine departs from a circle by an amount that affects significantly the character of the small-amplitude oscillations. For analytic work (*9*) it is appropriate to expand the equations of motion about the scalloped equilibrium orbit. In terms of cylindrical coordinates (r, z, θ) we introduce the notation

$$x \equiv \frac{r - r_1}{r_1}$$

$$y \equiv \frac{z}{r_1}$$

$$N\theta \equiv N\Phi - \frac{1}{w} \ln(r_1/r_0)$$

and choose r_1 so that the dimensionless variable x will be small. The forced motion that produces the noncircular equilibrium orbit is found to be quite well represented by

$$x_f = -\frac{f}{N^2 - (k+1)} \sin N\theta$$

and the linearized equations describing small-amplitude oscillations are represented by Hill equations of substantially the following form:

$$u'' + (a_u + b_u \cos N\theta + c_u \cos 2N\theta) u = 0$$

$$y'' + (a_y + b_y \cos N\theta + c_y \cos 2N\theta) y = 0$$

where

$$u \equiv x - x_f$$

$$a_u \cong k + 1 - \tfrac{1}{2} \frac{(f/w)^2}{N^2 - (k+1)}$$

$$b_u \cong \frac{f}{w}$$

$$c_u \cong \tfrac{1}{2} \left(\frac{f}{wN}\right)^2$$

$$a_y \cong -k + \tfrac{1}{2} \frac{(f/w)^2}{N^2 - (k+1)}$$

$$b_y \cong -\frac{f}{w}$$

$$c_y \cong -\tfrac{1}{2} \left(\frac{f}{wN}\right)^2$$

Nonlinear terms in the equations of motion can also be obtained.

The frequencies and other characteristics of the oscillations characterized by the foregoing linear equations can be obtained by the use of tables prepared with the aid of the electronic digital computer of the Graduate College of the University of Illinois (ILLIAC). Useful orientation is provided, however, by writing the frequencies that are given by a simple approximate solution (*10*), ignoring the relatively small effect of the terms involving $\cos 2N\theta$ and taking $N^2 \gg k + 1$:

$$\nu_x = [k+1]^{1/2}$$

$$\nu_y = \left[\left(\frac{f}{wN}\right)^2 - k \right]^{1/2}$$

It is thus seen that the frequency of the free radial oscillations is substantially determined by the exponent k characterizing the radial increase of average field strength, so that $k + 1$ must be positive, and that axial stability may be obtained if the term $(f/wN)^2$ is sufficiently large to dominate $-k$. The stability region for the small-amplitude oscillations represented by the Hill equations cited has been mapped by aid of the ILLIAC tables and is depicted in Fig. 3.

The nonlinearities associated with large-amplitude motion in the spiral-sector accelerator make the use of automatic digital computation particularly helpful in trajectory studies. Results pertaining to motion with 1 degree of freedom are appropriately and conveniently represented by phase plots that depict the position and associated momentum of a particle as it progresses through successive "sectors" (periods of the structure) from one homologous point to another (Fig. 4). For small-amplitude motion, the particle is represented by a point that moves around an elliptical curve in phase space, while, with larger amplitudes, curves departing from the elliptical shape may be followed. At still larger amplitudes, unstable fixed points—representing an unstable equilibrium orbit—make their appearance. Associated with the unstable fixed points, one finds a separatrix, constituting an effective stability limit to the motion, which in the majority of cases the ILLIAC results depict as a sharp boundary and outside of which it is frequently possible to draw the initial portion of unstable phase curves.

Because of the nonlinear character of the oscillations, it is not surprising (*11*, *12*) that the permissible amplitude of oscillation is much curtailed if σ, the phase change per sector, lies near $2\pi/3$ or $2\pi/4$. It has, in fact, also been found (*13*) that the amplitude limit is reduced,

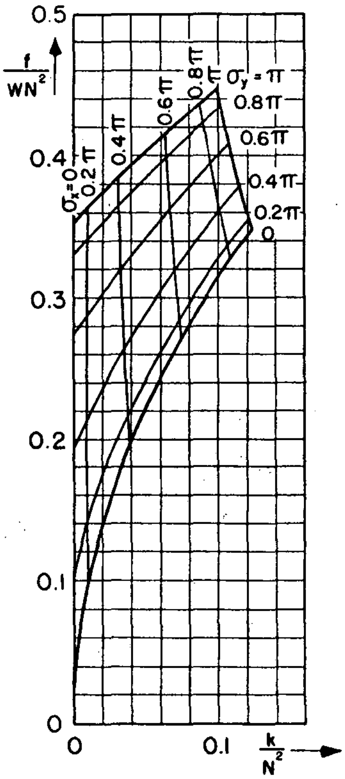

Fig. 3. First stability region ($0 < \sigma \equiv 2\pi\nu/N < \pi$) for small-amplitude oscillations in spiral-sector FFAG accelerators. The curves are calculated for the case $k \gg 1$ and are believed to be the most accurate for ordinates less than ⅓. When the condition $k \gg 1$ is not satisfied, the diagram can best be used by entering at the point $(k/N^2, f/wN^2)$ and proceeding up a curve of constant σ_y until an abscissa of $(k+1)/N^2$ is reached.

although not to zero, for $\sigma = 2\pi/5$. For cases in which σ_x is near $2\pi/3$, the limit of radial stability is characterized by the appearance of three unstable fixed points. In this case, an examination of the nonlinear differential equation for the trajectory permits a rough estimate to be made of the limiting amplitude (*14*):

$$A_x \cong 2(w^2N^2/f)|(\sigma_x/\pi)^2 - (2/3)^2|$$

It may be noted that, since the oscillation frequencies are essentially determined by k and f/wN, this formula suggests that a desirable increase of stable amplitude might be expected if f and w were each increased by the same factor.

Introduction of axial motion into a study of spiral-sector accelerators produces complications for all but the smallest amplitude oscillations, since there is coupling between this motion and that occurring in the radial direction. Surveys can be made, however, to determine the initial conditions that appear to exhibit short-time stability. In typical cases the permissible amplitude for axial motion appears to be materially smaller, possibly by a factor of 5, that is allowable for the radial motion. When oscillations in 2 degrees of freedom are treated, the characteristics of the axial motion and inferences concerning stability limits are materially affected by proximity to certain coupling resonances, notably those for which $\sigma_x = 2\sigma_y$, $\sigma_x + 2\sigma_y = 2\pi$, or $2\sigma_x + 2\sigma_y = 2\pi$. Near such resonances the amplitude of axial motion exhibits an exponential increase, over a considerable amplitude range, the rate of growth being the greater, the more the radial amplitude exceeds a certain threshold value, and the closer one is to the resonance in question. Some quantitative success in accounting for the growth of axial amplitude can be obtained by treating the differential equation for the axial motion as linear and inserting a prescribed expression for the radial oscillations into certain coupling terms that are linear in the axial coordinate.

In an actual accelerator, the N individual sectors will not be exactly identical, owing to the presence of unavoidable small differences in construction, excitation, or alignment. The basic period of the structure will thus be strictly N sectors, representing the machine as a whole, and additional resonances based on values of $N\sigma$ may be of importance. Computational study of the effect of realistic misalignments can be very informative prior to the fixing of specifications of a proposed machine. By way of example, studies of a proposed five-sector model ($\nu_x = 1.41$, $\nu_y = 0.87$) indicated that an axial displacement of one sector by 1/300 of the radius effected a reduction of the stable radial and axial amplitudes by factors of about 2 and 3, respectively.

Separated-Sector Modification

In the spiral-sector accelerator discussed in the foregoing paragraphs, an unnecessary and probably undesirable limitation was introduced by requiring that the field in the median plane have a precisely sinusoidal variation. The aperture that is magnetostatically possible is severely limited (*15*), especially if f differs markedly from the value ¼. In addition, the angle $\tan^{-1} Nw$ of the ridges (measured with respect to a reference circle) may be inconveniently small in a large machine, and a convenient construction may be difficult to realize. Attention is accordingly directed to structures involving separated poles (Fig. 5), a design that affords improved accessibility to the vacuum chamber and beam, easy realization of a more generous magnet gap, a considerably higher value for the root-mean-square field flutter, and a corresponding increase of the spiral angle. In this design it would be important to retain the scaling feature of the field and to take note of the high-order Fourier components that some pole configurations may introduce into the field. Retention of the scaling requirement makes it possible to solve the magnetostatic problem, which is defined by a specified pole contour, by relaxation methods on a *two-dimensional* grid which represents variables conveniently taken as

$$\xi \equiv \frac{1}{2\pi}\left[\frac{\ln(1+x)}{w} - N\theta\right]$$

$$\eta \equiv \frac{\sqrt{1+(wN)^2}}{2\pi w}\,\frac{y}{1+x}$$

The result of such computations may then be stored, again on a two-dimensional grid, for use in trajectory computations (*16*).

Plans are being completed for the construction, at the University of Illinois, of electron models that will provide experience pertaining to spiral-sector and separated-sector FFAG accelerators. These models will be similar in size to the reversed-field model mentioned in a previous section and likewise will employ betatron acceleration in the initial tests. Provisional designs of a large-scale machine have been attempted. It has been estimated that a separated-sector FFAG magnet for the production of 15-Bev protons would weigh about 12,000 tons and consume some 5 megawatts of electric power. This estimated magnet weight

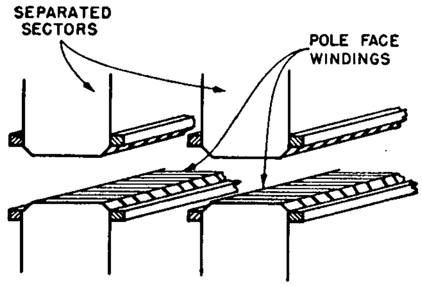

Fig. 5. Pole configuration illustrative of the separated-sector modification of a spiral-sector magnet. The currents carried by the pole-face windings are instrumental in achieving the r^k dependence of the magnetic field.

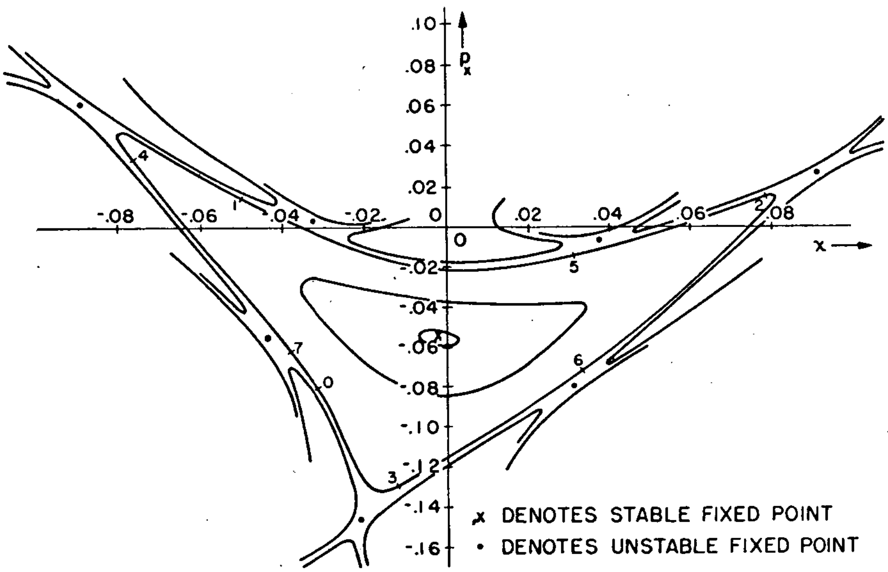

Fig. 4. Phase plot representing radial motion, at $N\theta = 0$ *mod.* 2π, in a spiral-sector FFAG accelerator. The machine parameters are those of a proposed model, for which $k = 0.8$, $1/w = 23.0$, $f = ¼$, and $N = 5$. In this case σ_x is close to 0.571π for small-amplitude motion. **The value of σ_x does not change greatly with increasing amplitude, and it is noteworthy that ultimately *seven* unstable fixed points make their appearance in this particular example.**

is intermediate between estimates that one would make for reversed-field and spiral-sector magnets, for which the estimated weights would be roughly 3 times greater or one-third as great, respectively. Although such a separated-sector structure may be some 6 times as massive as a pulsed accelerator of the same design energy, it may be felt that this feature is compensated to a considerable degree by the many simplifications which a direct-current design affords and that, as will be emphasized in a subsequent section, the increased freedom in detailed acceleration methods may permit a very significant increase of intensity.

Cyclotrons

It is attractive to consider the possible applicability of a spiral field variation to continuous-wave cyclotrons, as a generalization of the early suggestions of Thomas (*5*), in the interests of increasing the attainable energy. If, to permit continuous-wave operation, the frequency of revolution is to be independent of particle energy, the field index k that characterizes (differentially) the radial increase of the average field must satisfy the relationship

$$k + 1 = (E/E_0)^2$$

where E and E_0 are, respectively, the total energy and the rest energy of the particle. In a cyclotron, therefore, k must increase with energy, the oscillations will not satisfy the scaling requirement, and the possibility of encountering dangerous resonances during the acceleration process must be carefully considered. If we regard the relationship $\nu_x = [k+1]^{1/2}$ as sufficiently accurate for the present purpose, then $\nu_x \cong E/E_0$, the first half-integral and integral machine resonances for the radial motion ($\nu_x = 3/2$ and $\nu_x = 2$) would be encountered at kinetic energies of $\frac{1}{2}E_0$ and E_0, respectively (*17*), and the $\sigma_x = 2\pi/3$ inherent resonance at $[N/3 - 1]E_0$. The design of FFAG cyclotrons is currently being pursued by a number of groups, and design modifications that hold the promise of ameliorating the foregoing difficulties are being explored.

Acceleration Methods

In small-size annular accelerators that employ the FFAG principle, the use of betatron acceleration is highly attractive from the standpoint of intensity. If charged particles are injected into the gap of the fixed-field magnet during a substantial portion of the time the central flux is rising, they may be accelerated and arrive at the target with full energy so long as the flux continues to rise (Fig. 6). If the total change of flux within the core is twice that required to accelerate the beam from the low to the high magnetic-field region, the duty cycle would approach 25 percent.

For larger machines, radio-frequency acceleration methods would appear to be more practicable. The lack of dependence on a fixed magnet excitation cycle may permit in the FFAG accelerators a more rapid recycling of the radio-frequency program and a desirable flexibility in the design of this program. In analyzing the synchrotron motion, it is noteworthy that, in distinction to pulsed machines, the orbit radius and revolution frequency are a function only of the particle energy rather than of energy and time. To study in detail the effects of radio-frequency handling systems, it is helpful to employ a Hamiltonian theory for the synchrotron oscillations, in order that general theorems such as that of Liouville may be brought to bear on the problem. With $\omega(E)$ denoting 2π times the revolution frequency of the particle and E the energy, suitable canonical coordinates are the electric phase-angle ϕ with which the particle crosses the acceleration gap and the quantity w, related to energy, defined as

$$w \equiv \int^{E} \frac{dE}{\omega(E)}$$

For a single cavity of peak voltage V, frequency $\nu/2\pi$, and operating at the hth harmonic of the nominal particle frequency, the equations characterizing the synchrotron motion can then be derived from the Hamiltonian expression

$$\mathcal{H} = V\cos\phi + 2\pi[\nu w - hE(w)]$$

in which V and ν are specified functions of time.

To avoid the large frequency swing—perhaps as great as a factor of 11—which would be required to carry a proton from its initial to its final energy in a single modulation cycle, it is attractive to think of raising the particle energy in a series of steps, each involving a comparatively small amount of frequency modulation. Such an arrangement provides a sort of "bucket-lift" process whereby groups of particles are simultaneously and progressively accelerated by means of a single radio-frequency source whose frequency is successively a smaller multiple of the increasing revolution frequency of the particle. If one commences with an oscillator frequency that is $s \cdot p^M$ times the rotation frequency of the injected particle and modulates by a factor p/q, the particle frequency is raised by this factor and the particle may be further accelerated in the $s \cdot q \cdot p^{M-1}$ harmonic during the next frequency-modulation cycle. The modulation cycle may thus be employed by the particle some $M+1$ times, as it progresses to higher energies, before synchronism is lost. The modulation factor p/q could be 3/2, for example, and a factor 2/1 might be particularly suitable.

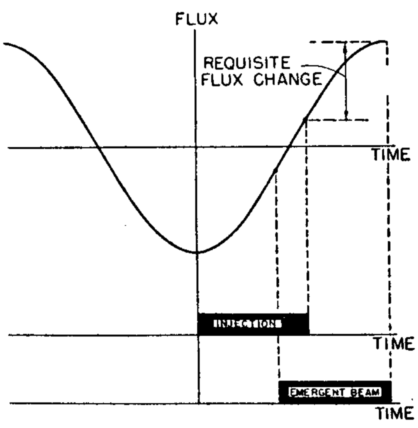

Fig. 6. Operation cycle of a FFAG betatron with a high duty factor.

If one thinks of using a bucket-lift process to stack particles at some intermediate energy prior to a final acceleration of the accumulated group by a second radio-frequency system, conservation of area in (ϕ, w) phase space tells us that the particles in successive buckets cannot be superposed exactly. Physically speaking, one group is slightly disturbed and displaced by the oscillator when it brings up a later group. This displacement has been studied computationally and is not sufficient to preclude the practicality of stacking a number of groups in a region of synchrotron phase space sufficiently limited that a second radio-frequency system could then accommodate them all.

For efficient stacking, it is of interest to ascertain the number of buckets that may be brought up empty at the end of the process. If $q = 1$ and $p = 2$, and if particles are injected only once per frequency-modulation cycle, the number of such empty buckets may readily be shown to be s, but these extra buckets can presumably be used with a consequent increase of intensity by more frequent injection.

There are several variants of this bucket-lift arrangement, which may present advantages chiefly of convenience. With an *unscheduled* bucket lift, particles not caught in a bucket at the onset of a particular frequency-modulation cycle will usually be displaced downward in energy by a passing bucket, but will be caught on occasional frequency-modulation cycles and in the end may be carried up in energy. The use of a completely stochastic acceleration method has been discussed in a Soviet paper (*18*) and shown to lead to acceleration of some particles by a sort of random-walk process.

It seems clear that the flexibility that fixed-field accelerators permit in regard to design of particle-handling methods offers many promising possibilities. These possibilities are being further studied within the MURA group, chiefly by A. M. Sessler and K. R. Symon, both analytically and with the aid of digital computation. As a related endeavor, the characteristics of mechanically modulated radio-frequency cavities are being studied by Zaffarano and his associates at Iowa State College. The accumulation of intense beams within an accelerator or in adjacent storage rings (*19*), by a suitable stacking process may open the door to study of a new field of high-energy physics.

Intersecting-Beam Accelerators

With the possibility in sight of attaining beam intensities higher than have been possible heretofore, the opportunity arises (*20*) of studying high-energy particle interactions by directing one beam against another (Fig. 7). The outstanding advantage of such a system would be the large increase of effective center-of-mass energy which could be reached in this way. If two beams, each of energy E_1, are directed against each other, the total energy is, of course, $E_{CM} = 2E_1$. In contrast, a single beam of energy E_1' (measured in units of the rest energy) directed against a stationary target makes available a center-of-mass energy that is approximately $E_{CM} = (2E_1')^{1/2}$ for $E_1' \gg 1$. Thus two 15-Bev proton beams, oppositely directed, are equivalent to a single beam of 500 Bev directed against a stationary target, and two 21.6-Bev accelerators would be equivalent to one machine of 1 Tev (10^{12} ev).

In estimating the practicality of intersecting-beam accelerators, one must, of course, judge whether it is feasible to produce beam intensities that will result in a sufficiency large reaction rate. The interactions of interest must, moreover, be studied in the presence of background radiation produced by the individual beams and will bear a more favorable ratio to the background the greater the density of intersecting particles. In this regard, however, it may be noted that the background radiations will be confined to directions differing little from the beam direction, while the reactions of interest will be essentially isotropic in the laboratory system. The background and beam survival will be directly dependent on the degree of vacuum that can be maintained in the system; hence, recent developments for the realization of high pumping speeds (*21*) and the measurement of high vacuums (*22*) will be of importance. The additional focusing or defocusing effects that arise from space-charge forces, possibly modified by the effect of any electrons that may be captured by the beam, and the difficul-

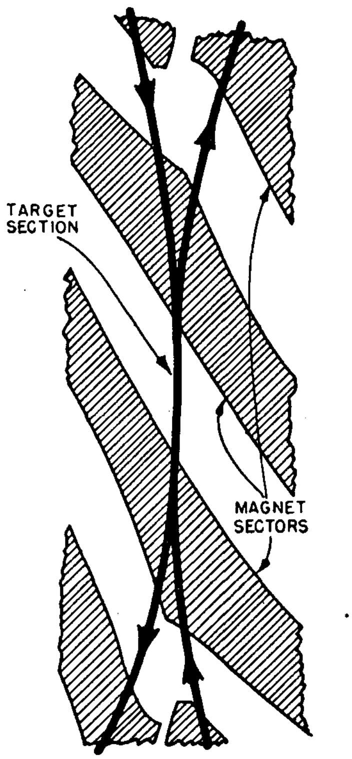

Fig. 7. Schematic method of effecting the intersection of high-energy beams. In the case illustrated, the individual accelerators are considered to be of the separated-sector type.

ties of handling safely a concentrated beam that may possess an energy of 1 megajoule will also require careful attention.

The intensities that one may be able to build up will certainly depend on the efficiency of stacking and on the ingenuity employed in the injection process. Although these techniques may be developed and improved as experience is gained with completed FFAG accelerators, an upper limit to the particle density in a stacked beam is imposed by Liouville's theorem. In regard to this limitation, we may estimate the number of injected pulses that theoretically could be assembled, after acceleration, in a region of reasonably small cross-sectional area. With respect to the energy spread associated with the motion in synchrotron phase space, we may consider the fate of particles injected with an energy spread ΔE_1, assuming for simplicity that synchrotron and betatron phase space are separately conserved. If the most efficient particle-handling system is used, the number of pulses that can be contained within a region ΔE_2 in energy at the completion of the acceleration process is

$$n_p = (\Delta E_2/\Delta E_1)/(\omega_2/\omega_1)$$

for $\Delta\phi$ constant, since the area in phase space is $\Delta\phi_2\Delta E_2/\omega_2 = n_p\Delta\phi_1\Delta E_1/\omega_1$. The quantity ΔE_2 in turn may be expressed conveniently in terms of the associated radial spread of the beam

$$\Delta E_2 = (k+1)(p_2^2c^2/E_2)(\Delta r_2/r_2)$$
$$\cong (k+1)E_2(\Delta r_2/r_2)$$

ultrarelativistically. Thus, if $k+1 = 100$, $E_2 = 15 \times 10^9$ ev, $\Delta r_2 = 0.5$ cm, $r_2 = 10^4$ cm, $\omega_2/\omega_1 = 11$, and $\Delta E_1 = 4 \times 10^3$ ev, we find that $\Delta E_2 = 7.5 \times 10^7$ ev and $n_p = 1700$ particle pulses.

Similarly, in regard to the phase space for betatron oscillations, if the injector is imagined to scan the aperture, the number of horizontal and vertical scans that theoretically could be accommodated can be written

$$n_x = \frac{p_2}{p_1}\frac{(\Delta r_2)^2}{r_2\beta_x\Psi_x\Delta r_1}$$

$$n_y = \frac{p_2}{p_1}\frac{(\Delta z_2)^2}{r_2\beta_y\Psi_y\Delta z_1}$$

where Ψ_x, Ψ_y denote the angular spread of the injected beam, β_x, β_y relate the angular and linear displacements experienced during the course of a betatron oscillation ($\Delta r = r\beta_x\Psi_x$), and the momentum ratio p_2/p_1 accounts for the adiabatic damping of the oscillations. Accordingly, approximating $\beta_{x,y}$ by $2/\nu_{x,y}$,

$$n_x n_y = \left(\frac{p_2}{p_1}\right)^2 \frac{\nu_x\nu_y(\Delta r_2)^2(\Delta z_2)^2}{4r_2^2\Psi_x\Psi_y\Delta r_1\Delta r_2}$$

If we now substitute $p_2/p_1 = 100$, $\nu_x = 10$, $\nu_y = 5$, $r_2 = 10^4$ cm, $\Delta r_2 = \Delta z_2 = 0.5$ cm, and $\Psi_x\Delta r_1 = \Psi_y\Delta z_1 = 0.5 \times 10^{-3}$ radian cm, we find that $n_x n_y = 1250$.

This large value for the theoretically admissible number of scans implies a very complex scanning procedure and suggests that an injector with a much larger beam spread and correspondingly higher current would be desirable (*23*).

On the basis of the considerations of the preceding paragraphs, one would estimate that a 1-milliampere injector would permit the accumulation of

$$N_P = \frac{10^{-3}}{1.6 \times 10^{-19}} \times \frac{2\pi \times 10^4}{3 \times 10^{10}/11} \times 1700 \times 1250$$
$$\cong 3 \times 10^{17}$$

particles within a tube of about 1 square centimeter cross-sectional area. If we estimate that we actually may have 1/600 as large a beam as this, or 5×10^{14} particles circulating in each machine, some 10^7 interactions per second (proportional to N_P^2) may be expected to be produced in an interaction region that is 1 meter in length (*20*). With a vacuum of the order of 10^{-6} mm-Hg of nitrogen gas, the background produced in this target volume may be expected to be larger by about one order of magnitude, but, as is pointed out previously, the background radiations will be confined primarily to the median plane. Interaction with the residual gas also has the effect of limiting the beam life, possibly to a time not much longer than 1000 seconds in the present example, so that groups of particles must be injected to replenish the beam at a rate not less than the reasonable value of one group per second.

It is the hope of the MURA group that further theoretical and experimental work will lead to the design and construction of models that will permit testing means for efficient particle acceleration, the investigation of high-current beams, and the eventual realization of a research machine that will take full advantage of the benefits to be derived from the FFAG principle.

References and Notes

1. It is impossible here to give explicit credit to the many physicists who have contributed to the development of these ideas, but it is fitting to indicate our special appreciation of the courtesy which the University of Illinois has extended to the MURA group in making the ILLIAC available for numerous computational studies and our indebtedness to J. N. Snyder for directing this phase of the program. I wish also to express my appreciation to D. W. Kerst, K. R. Symon, and A. M. Sessler for assistance in the preparation of this article and to K. Lark-Horovitz for his courtesy in reading the manuscript in draft form.
2. The technical group has been under the direction of D. W. Kerst. As the interest in the work grew, a number of midwestern institutions formalized this cooperative effort by forming the Midwestern University Research Association (MURA). The work of the technical group has been assisted by the National Science Foundation, the Office of Naval Research, and the U.S. Atomic Energy Commission.

3. E. D. Courant, M. S. Livingston, H. S. Snyder, *Phys. Rev.* 88, 1190 (1952).

4. The interest of the midwestern group in fixed-field alternating-gradient (FFAG) accelerators arose from the original suggestions of K. R. Symon, made during meetings of the technical group in the summer of 1954. The idea of accelerators employing annular direct-current magnets was also proposed earlier, in at least one form, by T. Ohkawa at a meeting of the Physical Society of Japan and appears to have received brief consideration by others working in the accelerator field. A special form of cyclotron employing an azimuthal variation of field is the design proposed by Thomas (*5*).

5. L. H. Thomas, *Phys. Rev.* 54, 580, 588 (1938).

6. Discussion of FFAG accelerators has been given in papers presented before the American Physical Society and in a paper by K. R. Symon *et al.*, "Fixed-field alternating-gradient particle accelerators" (*Phys. Rev.*, in press), in which a general theory of orbits, applicable to a variety of types of cyclic accelerators, is derived in linear approximation.
7. The reversed-field model was constructed at the University of Michigan under the direction of K. M. Terwilliger and L. W. Jones. The magnet design was carried to completion by R. Haxby of Purdue University, and injectors were supplied from Kerst's laboratory at the University of Illinois. A substantial portion of the theoretical work was contributed by F. T. Cole of the State University of Iowa.

8. C. L. Hammer, R. W. Pidd, K. M. Terwilliger, *Rev. Sci. Instr.* 26, 555 (1955).
9. Details of some of the analytic work pertaining to spiral-sector accelerators are given in a series of MURA reports: L. J. Laslett, *Character of Particle Motion in the Mark V FFAG Accelerator*, LJL(MURA)-5, *et seq.* (1955); D. L. Judd, *Analytical Approximation in Mark V Scalloped Orbits and to Radial Betatron Oscillations about Them*, MURA DLJ-1 (1955); D. L. Judd, *Non-Linear Terms in Mark V Radial Betatron Equation*, MURA DLJ-2 (1955); F. T. Cole, *Mark V Expanded Equations of Motion*, MURA/FTC-3 (1956).
10. A useful method for obtaining approximate characteristics of solutions to linear or nonlinear differential equations with periodic coefficients is the "smooth approximation" developed by K. R. Symon and summarized in two MURA reports: K. R. Symon, *A Smooth Approximation to the Alternating Gradient Orbit Equations*, KRS(MURA)-1 (1954); K. R. Symon, *An Alternative Derivation of the Formulas for the Smooth Approximation*, KRS(MURA)-4 (1954).
11. J. Moser, *Nachr. Akad. Wiss. Göttingen Math.-physik Kl. IIa* 1955, No. 6, 87 (1955); *Commun. Pure and Appl. Math.* 8, 409 (1955).
12. P. A. Sturrock, *Static and Dynamic Electron Optics* (Cambridge Univ. Press, Cambridge, 1955), chap. 7. In place of the quantity that I have denoted σ, Moser (*11*) employs $2\pi\omega$ or $2\pi\alpha$, and Sturrock employs θ. My quantity σ may be related to the number of betatron oscillations, ν, executed by the particle as it passes through N sectors to make a complete circuit of the accelerator, by the relationship $N\sigma = 2\pi\nu$.
13. R. Christian, unpublished.
14. This relationship was derived originally by A. M. Sessler and me, and it has recently been treated more carefully by G. Parzen, unpublished.
15. In the absence of back-wound currents on the pole surface and with f assuming its optimum value, 0.24, the available magnet gap is limited to $G = 0.28(2\pi w)r = 0.28\lambda$, where λ is the radial wavelength of the magnet structure.
16. This computational method is outlined and certain useful general features of the fields are treated, respectively, in the following MURA reports: L. J. Laslett, *Proposed Method for Determining Mark V Trajectories by Aid of Grid Storage*, MURA-LJL-8 Rev. (1956); J. L. Powell, *Mark V FFAG Equations of Motion for Illiac Computation*, MURA-JLP-6 (1955).
17. Compare D. S. Falk and T. A. Welton, *Bull. Am. Phys. Soc. II*, 1, 60, (1956).
18. E. L. Burshtein, V. I. Veksler, A. A. Kolomensky, *A Stochastic Method of Particle Acceleration*, translated by V. N. Rimsky-Korsakoff from *Certain Problems of the Theory of Cyclic Accelerators* (U.S.S.R. Akad. Sci., Moscow, 1955), pp. 3–6.
19. D. Lichtenberg, R. Newton, M. Ross, *Intersecting Beam Accelerator with Storage Ring*, MURA Rept. MURA-DBL/RGN/MHR-1 (1956); G. K. O'Neill, *The Storage-Ring Synchrotron—a device for High-Energy Physics Research* (Princeton Univ. Rept., 1956); G. K. O'Neill, *Phys. Rev.* 102, 1418 (1956).
20. D. W. Kerst *et al.*, *Phys. Rev.* 102, 590 (1956).
21. R. H. Davis and A. S. Divatia, *Rev. Sci. Instr.* 25, 1193 (1954).
22. D. Alpert, *Science* 122, 729 (1955).
23. Interesting information concerning working designs of high-current linear accelerators has been given by E. O. Lawrence, *Science* 122, 1127 (1955).

PARTICLE ORBITS IN FIXED FIELD ALTERNATING GRADIENT ACCELERATORS

L. J. LASLETT

Iowa State College, Iowa (Ia) and

K. R. SYMON

University of Wisconsin, Madison (Wisc.) and Midwestern Universities Research Association, U.S.A. *

(presented by K. R. Symon)

I. Linearized orbit equations

1. Geometry of the equilibrium orbits

In order to develop a theory of orbit stability applicable to FFAG accelerators generally, it is convenient to characterize a particular accelerator by specifying its equilibrium orbits. We will therefore assume that a set of closed equilibrium orbits lying in the median plane is given. If instead, the magnetic field pattern is specified, the equilibrium orbits must be found by integrating the equations of motion.

The geometrical properties of each orbit, and the relations between orbits, will be periodic in the azimuthal angle θ with period $2\pi/N$. Each orbit is to be specified by its equivalent radius R defined by

$$S = 2\pi R, \tag{1.1}$$

where S is the length of the orbit. In general, R will be slightly larger than the mean radius $\langle r \rangle_{av}$. We define an azimuthal coordinate Θ by the equation

$$s = \Theta R, \tag{1.2}$$

where s is the distance measured along the orbit from some reference point (say at azimuthal angle Θ_0). We shall require that the orbit be perpendicular to the radius from the center of the machine at the reference point, and that the reference points lie along a continuous curve. The parameter Θ will be equal to the azimuthal angle $\theta - \theta_0$ plus a small periodic function with period $2\pi/N$.

Each orbit will now be specified by a periodic parameter $\mu(\Theta, R)$ defined by

$$\mu(\Theta, R) = R/\rho(\Theta, R) \tag{1.3}$$

where ρ is the radius of curvature. Specification of $\mu(\Theta, R)$, together with the requirement that the center of the orbit lie at the origin in the median plane, completely determines the orbit R, provided the reference point $\Theta = 0$ is specified. For our purposes, it will be sufficient to specify the angle $\zeta(R)$ between the radius from the origin and the reference curve $\Theta = 0$ where it crosses the orbit R (figure 1). Choice of the parameter $\mu(\Theta, R)$ is restricted by the requirement that it be periodic in Θ with, period $2\pi/N$ and mean value

$$\langle \mu \rangle_{av} = \frac{1}{2\pi}\int_0^{2\pi} \mu \, d\Theta = \frac{1}{2\pi}\int_0^{S} \frac{ds}{\rho} = 1. \tag{1.4}$$

The function $\mu(\Theta, R)$ is also restricted by the requirement that at the point $\Theta = 0$ the orbit R must be perpendicular to the radius from the origin. This requirement leads to a rather complicated analytical restriction on the function μ. It is sufficient if $\Theta = 0$ is a point of symmetry of the orbit, i.e.,

$$\mu(-\Theta, R) = \mu(\Theta, R) \tag{1.5}$$

We will need also parameters $\eta(\Theta, R)$ and $\varepsilon(\Theta, R)$ relating the perpendicular distance dx between two nearby orbits, and the increment $d\Theta$ in Θ along an orthogonal trajectory to the orbits, to the increment dR in the parameter R (see figure 1):

$$dx = \eta \, dR \tag{1.6}$$

$$d\Theta = \varepsilon \, dR/R \tag{1.7}$$

* Assisted by the National Science Foundation and the Office of Naval Research.

Published in CERN Symposium on High Energy Accelerators and Pion Physics, 1956, v. 1, pp. 279-289. Reproduced with permission by CERN.

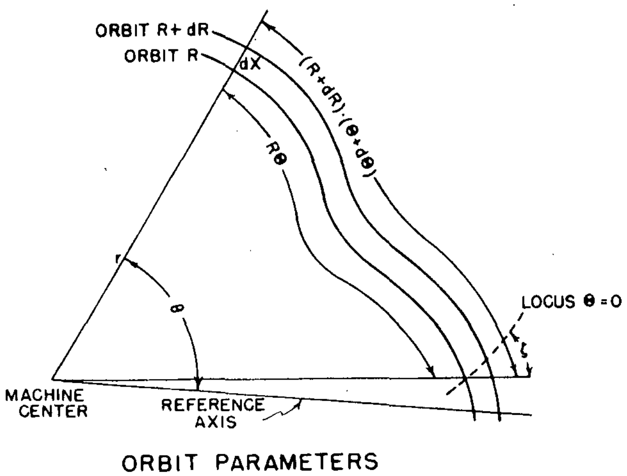

Fig. 1.

It can be shown that η, ε satisfy the differential equations

$$\partial\varepsilon/\partial\Theta = \mu\eta - 1, \tag{1.8}$$

$$\partial\eta/\partial\Theta = -\mu\varepsilon - \int R\ \partial\mu/\partial R \cdot d\Theta, \tag{1.9}$$

where the three constants of integration are to be chosen so that ε and η are periodic functions of Θ (i.e. so that the right hand members of equations (1.8) and (1.9) have zero mean values), and so that

$$[\varepsilon/\eta]_{\theta=0} = \tan\zeta. \tag{1.10}$$

If all equilibrium orbits are geometrically similar, the parameter μ depends only on Θ and not on R. In the interest of simplicity, we will usually restrict our attention to machines of this type. If in addition, ζ is independent of R, then by equations (1.8)-(1.10), the parameters η and ε will be independent of R. In this case, we will say that the quilibrium orbits *scale*; the equilibrium orbits scale if any set of neighboring orbits can be obtained by photographic enlargement or reduction from a set of orbits in the neighborhood of any other orbit.

Let us set

$$\mu = 1 + f g(N\Theta), \tag{1.11}$$

where f is the flutter factor, and the flutter function $g(N\Theta)$ has period 2π in $N\Theta$, zero mean, and is normalized so that its mean square value is $^1/_2$. For example,

$$g(N\Theta) = \cos N\Theta. \tag{1.12}$$

Then an approximate solution of equations (1.8)-(1.9) which is adequate to exhibit the principal features of FFAG orbits is

$$\eta \doteq 1 - f \tan\zeta/N \cdot g_1(N\Theta), \tag{1.13}$$

$$\varepsilon \doteq \tan\zeta, \tag{1.14}$$

where for any function $g(\xi)$, periodic in ξ with zero mean, we define

$$g_1(\xi) = \int g(\xi)\, d\xi, \tag{1.15}$$

where the constant of integration is to be chosen so that $g_1(\xi)$ has zero mean.

2. *Betatron oscillations*

If a particle of momentum p moves in an equilibrium orbit R, then we have by equation (1.3)

$$p c = e H\rho = (e H R)/\mu, \tag{2.1}$$

where H is the magnitude of the magnetic field, so that

$$H(R, \Theta) = pc/eR\ \mu(\Theta, R). \tag{2.2}$$

The magnetic field is thus given in terms of the coordinates R, Θ.

If we differentiate equation (2.1) with respect to x, where x is measured perpendicular to the orbit, we have

$$H\ \partial\rho/\partial x + \rho\ (\partial H/\partial x) = c/e \cdot \partial\rho/\partial x. \tag{2.3}$$

The field index is therefore

$$n = -\rho/H \cdot \partial H/\partial x$$
$$= \partial\rho/\partial x - \rho \cdot \partial \ln p/\partial x. \tag{2.4}$$

Making use of equations (1.3), (1.6) and (1.7), we find

$$n = -1/\eta\mu^2\,[k\mu + \varepsilon\ \partial\mu/\partial\Theta + R\ \partial\mu/\partial R], \tag{2.5}$$

where k is a parameter which measures the momentum compaction:

$$k = R(d \ln p)/dR - 1. \tag{2.6}$$

In terms of the mean magnetic field $\overline{H} = pc/eR$, we can write k also as a mean field index:

$$k = R/\overline{H} \cdot d\overline{H}/dR, \tag{2.7}$$

The linearized equations for betatron oscillations about an equilibrium orbit are

$$d^2x/ds^2 - (1 - n)/\rho^2 \cdot x = 0, \tag{2.8}$$
$$d^2z/ds^2 - (n/\rho^2)\, z = 0, \tag{2.9}$$

where x and z are the deviations from the equilibrium orbit in the radial and vertical directions. These become by equations (1.2) and (1.3),

$$d^2x/d\Theta^2 + \mu^2\,(1 - n)\, x = 0, \tag{2.10}$$

$$d^2z/d\Theta^2 - \mu^2\, n\, z = 0. \tag{2.11}$$

The character of the betatron oscillations is therefore determined by the functions $\mu^2(\Theta, R)$ and

$$\mu^2 n = -1/\eta - (k\mu + \varepsilon\, \partial\mu/\partial\Theta + R\partial\mu/\partial R). \quad (2.12)$$

By making use of equations (1.8) and (1.9) we can rewrite equation (2.12) in the form

$$\mu^2(1-n) = (k+1)\mu/\eta - 1/\eta\, \partial^2\eta/\partial\Theta^2. \quad (2.13)$$

If the equilibrium orbits scale, then μ, η and ε are functions only of Θ. Thus μ^2 n will be a function of Θ only, and the betatron oscillations will also scale, provided k is constant. Accelerators with this property will be referred to as accelerators which scale. For accelerators which scale, we have

$$p = p_0 (R/R_0)^{k+1} \quad (2.14)$$

and

$$H = H_0 (R/R_0)^k \mu(\Theta). \quad (2.15)$$

3. Approximate solution for betatron oscillations

In this section we develop some approximate formulas which give a useful general picture of the properties of FFAG accelerators. If the betatron wavelengths are long on comparison with the sector length (say at least four sectors), then the smooth approximation equations are applicable[1, 2]. The "smooth" betatron oscillation equations become in this case

$$d^2X/d\Theta^2 - \nu_x^2 X = 0, \quad (3.1)$$

$$d^2Z/d\Theta^2 - \nu_z^2 Z = 0, \quad (3.2)$$

where,

$$\nu_x^2 = <\mu^2(1-n)>_{av} + <\{\mu^2(1-n)\}_1^2>_{av}, \quad (3.3)$$

$$\nu_z^2 = <\mu^2 n>_{av} + <\{\mu^2 n\}_1^2>_{av}. \quad (3.4)$$

The curly brackets {} indicate that only the oscillatory part of the enclosed function is to be taken; i.e., the mean value is to be subtracted.

The solutions of equations (3.1), (3.2) are

$$X = A \cos \nu_x\Theta + B\sin \nu_x\Theta, \quad (3.5)$$

$$Z = C \cos \nu_z\Theta + D\sin \nu_z\Theta. \quad (3.6)$$

Superposed upon these smooth solutions is a ripple which has the periodicity of the sectors. It is clear that ν_x, ν_z are the numbers of radial and vertical betatron wavelengths around the circumference of the accelerator. The approximate formulas (3.3), (3.4) give ν_x, ν_z within about 10% provided that ν_x, ν_z are *both* less than N/4.

In order to avoid resonance buildup of betatron oscillations, it is necessary to avoid integral and half-integral values for ν_z, ν_z and also to avoid integral values for $\nu_x + \nu_z$. This implies that ν_x, ν_z, must be the same for all orbits, or nearly so, and this is the principal limiting condition on FFAG designs. In accelerators which scale ν_x, ν_z are necessarily the same for all orbits; this is the advantage in designs which scale.

The relation between betatron wavelengths and machine parameters depends upon which term in eq. (2.13) predominates in giving alternating gradient focusing. In a radial sector FFAG accelerator with $\zeta = 0$, and with a large number of sectors (say $N > 10$) η is very nearly unity, and the second term in eq. (2.13) is small except near the edges of the magnets where it gives rise to edge focusing effects. The edge focusing comes from the term $-\eta^{-1} \cdot \varepsilon\, \partial\mu/\partial\Theta$ in eq. (2.12). This term has a non-zero mean value, part of which is included in the μ term in eq.(2-13); thus eq. (3.7) and (3.8) below include most of the mean focusing effect due to edges in radial sector machines. We will call the first term in eq. (2.13) the "μ term" and the second, the "η term". In a spiral sector FFAG accelerator, the alternating gradient focusing comes predominantly from the η term.

It may be noted that the η term includes the term $(R/\eta)(\partial\mu/\partial R)$ which appears when the orbits do not scale. It is not hard to see that in a conventional AG synchrotron this is the dominant alternating gradient term.

Let us first consider a radial sector FFAG accelerator with a large number of sectors, and let us neglect the η term. If $f/N \ll 1$, then $\eta \doteq 1$ according to eq. (1.13), let us write μ in the form given by eq. (1.11). Then eq. (3.3), (3.4) yield, if we substitute from eq. (2.13), with $\eta = 1$,

$$\nu_x^2 = k + 1 + \frac{(k+1)^2 f^2}{N^2} <g_1^2>_{av}, \quad (3.7)$$

$$\nu_z^2 = -k + \frac{f^2}{2} + \frac{(k-1)^2 f^2}{N^2} <g_1^2>_{av}, \quad (3.8)$$

where we have neglected a small term involving $g^2 - \overline{g^2}$ in eq. (3.8). The betatron oscillation advances in phase by an angle

$$\sigma = 2\pi\nu/N \quad (3.9)$$

per sector. For stability, σ must be less than π, and for the smooth approximation to be valid, σ must be less than about $\pi/2$. If we solve eq. (3.7), (3.8) for k, f in terms of σ_x, σ_z, we obtain

$$k + 1 = \frac{N^2}{8\pi^2}(\sigma_x^2 - \sigma_z^2 - b), \quad (3.10)$$

$$f = \frac{4\pi}{[2 <g_1^2>_{av}]^{1/2}} \frac{[\sigma_x^2 + \sigma_z^2 - b]^{1/2}}{|\sigma_x^2 - \sigma_z^2 - b|}, \quad (3.11)$$

where

$$b = 4\pi^2/N^2 [1 - f^2 - 4kf^2/N^2 <g_1^2>_{av}]. \quad (3.12)$$

The quantity b is negligible for sufficiently large N.

By appropriate choice of σ_x, σ_z, k can be made either positive or negative, i.e., in a radial sector FFAG synchrotron, with N large, the high energy orbits may be either on the outside or the inside of the donut. The b-term, which is important when N is small, is positive and therefore favors machines with positive k, i.e., with a given N, /k/ can be larger and f smaller if $k>0$. For maximum momentum compaction, i.e., minimum radial aperture, k, and hence N, should be as large as practicable. If we define a circumference factor C as the ratio between mean and minimum radii of curvature of the equilibrium orbit, then

$$C = |\mu|_{max} = |1 + fg(N\Theta)|_{max}. \quad (3.13)$$

It is desirable to minimize C, since for a given maximum magnetic field, this yields the smallest accelerator design. It is clear from eq. (3.11), that for a given form of g, the minimum circumference factor is obtained by making σ_z as small, and σ_x as large as possible (or vice versa, if k is to be negative).

Let us assume a rectangular field flutter, with unit mean square:

$$g(\xi) = \begin{cases} \left[\dfrac{1-q}{2q}\right]^{\frac{1}{2}}, -q\pi < \xi < q\pi, & \text{(I)} \\ -\left[\dfrac{q}{2(1-q)}\right]^{\frac{1}{2}}, q\pi < \xi < 2\pi - q\pi, & \text{(II)} \end{cases} \quad (3.14)$$

$$g(\xi + 2\pi) = g(\xi). \quad (3.15)$$

When $\xi = N\ \Theta$ lies in regions labeled I, we say that Θ is in a positive half sector; regions labeled II we call negative half sectors. We need to calculate

$$<g_1^2>_{av} = \pi^2/\sigma \cdot q(1-q). \quad (3.16)$$

If now

$$K = f[<g_1^2>_{av}]^{1/2} \quad (3.17)$$

is fixed by eq. (3.11), then by eq. (3.13), the circumference factor is

$$C = 1 + \frac{\sqrt{3}K}{\pi q}, \text{ or } \frac{\sqrt{3}K}{\pi(1-q)} - 1, \quad (3.18)$$

whichever is greater. The minimum value of C occurs when q is chosen so that the two values of the right member of eq. (3.18) are equal. We then have

$$\mu = 1 + fg(N\Theta) = \begin{cases} C, -q\pi < N\Theta < q\pi, & \text{(I)} \\ -C, q\pi < N\Theta < 2\pi - q\pi, & \text{(II)} \end{cases} \quad (3.19)$$

The radius of curvature, and consequently also the magnetic field, is constant in magnitude along the equilibrium orbit and opposite in sign in the two half sectors. The ratio of half sector lengths is

$$\Gamma = \frac{q}{1-q} = \frac{C+1}{C-1}, \quad (3.20)$$

and the circumference factor is

$$C = \frac{\Gamma + 1}{\Gamma - 1} = \left[1 - \frac{f^2}{2}\right]^{\frac{1}{2}} \quad (3.21)$$

If we take $\sigma_z = \pi/6$, $\sigma_x = \pi/2$, $b = 0$, and use the approximate formulas (3.10), (3.11), we obtain $K = 3\sqrt{5}$, $\Gamma = 1.31$, $C = 7.5$, $f = 10.5$, $k = N^2/36$. It will be shown in the next section by a more accurate calculation that the minimum value of C where N is large is about 5.

In a spiral sector FFAG accelerator, ζ is near 90° and the η - term in eq. (2.13) is large. It is then possible to use a much smaller flutter factor, so that the oscillatory part of the μ - term is small. We will again assume that μ is given by eq. (2.11) and will use the approximation (1.13) for η. If we expand $1/\eta$ in a power series in the second term of formula (1.13), we may calculate

$$<\mu/\eta>_{av} = 1 - (f^2\tan^2\zeta)/N^2 <g_1^2>_{av} - \ldots \quad (3.22)$$

We will neglect the second and higher order terms, and will neglect also the oscillatory part of μ/η. The η - term can be rewritten in the following way:

$$1/\eta\ \partial^2\eta/\partial\Theta^2 = \partial/\partial\Theta\,(1/\eta\ \partial\eta/\partial\Theta) + (1/\eta\ \partial\eta/\partial\Theta)^2. \quad (3.23)$$

The first term on the right is large and oscillatory with zero mean, and the second is smaller but has a positive mean value. We neglect the oscillatory part of the second term, and substitute in eq. (3.3) and (3.4), using (2.13) to obtain

$$\nu_x^2 = k + 1, \quad (3.24)$$

$$\nu_x^2 = -k + f^2/2 + 2 <(1/\eta\ \partial\eta/\partial\Theta)^2>_{av}. \quad (3.25)$$

Note that the η - term does not contribute in this approximation to the radial focusing. If we take η as given by formula (1.13), we have

$$\left\langle\left(\frac{1}{\eta}\frac{\partial\eta}{\partial\Theta}\right)^2\right\rangle_{av} = f^2\tan^2\zeta\left\langle\frac{g^2}{(1 - fN^{-1}\tan\zeta\ g_1)^2}\right\rangle_{av}$$

$$= f^2\tan^2\zeta\left[\frac{1}{2} + \frac{2f^2\tan^2\zeta}{N^2}\left\langle g^2 g_1^2\right\rangle_{av} + \ldots\right] \quad (3.26)$$

We will neglect the second and higher order terms in square brackets and substitute in eq. (3.24), (3.25), to obtain

$$f^2 \tan^2\zeta = (\nu_x^2 + \nu_z^2 - 1), \quad (3.27)$$

where we have also neglected f^2. Note that, to this order of approximation, formulas, (3.24) and (3.27) are independent of the form of the flutter function $g(N\Theta)$; only the circumference factor [eq. (3.13)] depends on $g(N\Theta)$. We can rewrite these formulas in terms of the phase shifts σ per sector:

$$k + 1 = (N^2 \sigma_x^2)/4\pi^2, \quad (3.28)$$

$$f^2 \tan^2\zeta = N^2/4\pi^2 \cdot (\sigma_x^2 - \sigma_z^2) - 1. \quad (3.29)$$

The reference curve $\Theta = 0$, satisfies, in polar coordinates r, θ, the equation

$$1/r \, dr/d\theta = \cot\zeta. \quad (3.30)$$

The radial separation between ridges (points of maximum magnetic field), in units of r is therefore

$$\lambda = \Delta r/r = 2\pi/N \tan\zeta. \quad (3.31)$$

Thus for a given choice of σ_x, σ_z, and N the ratio f/λ is fixed. The maximum allowable gap between the poles of the magnet is proportional to λ; if the field flutter is to be obtained by shaping the poles, without extra forward windings, it can be shown that for f/λ fixed the maximum gap is about $^1/_4\,\lambda\, r$ and is obtained for $f \doteq {}^1/_4$. Under these conditions, the field flutter will necessarily be very nearly sinusoidal,

$$g(\xi) = \cos\xi, \quad (3.33)$$

and hence the circumference factor will be

$$C = 1 + f = 1.25.$$

If we take, as above, $\sigma_z = \pi/6$, $\sigma_x = \pi/2$, with $f = {}^1/_4$, we obtain $k + 1 = N^2/16$, $\lambda = 5.95\ N^{-2}\,[1\text{-}14.4N^{-2}]^{-1/2}$, $\tan\zeta = 1.05\ N\,[1\text{-}14.4N^{-2}]^{-1/2}$.

4. *Linear stability for radial sectors*

In order to get more accurate relations between the parameters, we return to the betatron oscillation equations (2.10), (2.11). Making use of eq. (2.12), (1.13) and (1.14), with $\zeta = 0$, we rewrite eq. (2.10), (2.11) for the case of a rectangular field flutter of the form (3.19):

$$d^2x/d\Theta^2 \pm kCx = 0, \quad (4.1)$$

$$d^2z/d\Theta^2 \mp kCz = 0, \quad (4.2)$$

where the upper signs apply in positive half sectors, and the lower in negative half-sectors. The term $\varepsilon\, \partial\mu/\partial\Theta$ in eq. (2.12) gives rise to terms in eq. (2.10), (2.11) which represent the focusing which occurs at the sector edges, which we will here neglect. These approximations are valid only when $N \gg f$, and we have accordingly also neglected 1 in comparison with n. When N is small, edge effects and higher order terms in η must be taken into account. The oscillatory terms in η will give rise to effects resulting from the fact that neighboring equilibrium orbits are not everywhere equidistant. For small N, edge effects turn out to increase the vertical focusing and decrease the radial focusing, so that considerably smaller values of the flutter factor f may be used if $k > 0$, without losing vertical stability.

Let $N\Theta_0 = -q\pi$, $N\Theta_1 = q\pi$, $N\Theta_2 = (2\text{-}q)\pi$. Then the solutions of eq. (4.1) within the positive and negative halfsectors separately yield the following matrix relations between x and $x' = dx/d\Theta$ at the points Θ_0, Θ_1, Θ_2:

$$\begin{pmatrix} x_1 \\ x_1' \end{pmatrix} = M_+ \begin{pmatrix} x_0 \\ x_0' \end{pmatrix}, \quad \begin{pmatrix} x_2 \\ x_2' \end{pmatrix} = M_- \begin{pmatrix} x_1 \\ x_1' \end{pmatrix}, \quad (4.3)$$

where

$$M_+ = \begin{pmatrix} \cos\psi_+ & (KC)^{-1/2}\sin\psi_+ \\ -(KC)^{1/2}\sin\psi_+ & \cos\psi_+ \end{pmatrix}, \quad M_- = \begin{pmatrix} \cosh\psi_- & (KC)^{-1/2}\sinh\psi_- \\ (KC)^{1/2}\sinh\psi_- & \cosh\psi_- \end{pmatrix}, \quad (4.4)$$

$$\psi_+ = \frac{2\pi q}{N}(KC)^{1/2}, \quad \psi_- = \frac{2\pi(1\text{-}q)}{N}(KC)^{1/2} \quad (4.5)$$

We thus obtain

$$\begin{pmatrix} x_2 \\ x'_2 \end{pmatrix} = M \begin{pmatrix} x_0 \\ x'_0 \end{pmatrix}, \quad (4.6)$$

with

$$M = M_- M_+ = \begin{pmatrix} \cos\psi_+\cosh\psi_- - \sin\psi_+\sinh\psi_-, & (KC)^{-1/2}(\cos\psi_+\sinh\psi_- - \sin\psi_+\cosh\psi_-) \\ (KC)^{1/2}(\cos\psi_+\sinh\psi_- + \sin\psi_+\cosh\psi_-), & \cos\psi_+\cosh\psi_- + \sin\psi_+\sinh\psi_- \end{pmatrix} \quad (4.7)$$

We can now calculate

$$\cos \sigma_x = \tfrac{1}{2} \text{Trace}(M) = \cos \psi_+ \cosh \psi_- \tag{4.8}$$

and in the same way,

$$\cos \sigma_z = \cos \psi_- - \cosh \psi_+. \tag{4.9}$$

In terms of the local field index

$$n = k/C, \tag{4.10}$$

within the magnets (we take n as positive here), and the ratio Γ of sector lengths [eq. (3.20)], we may rewrite ψ_+ and ψ_- :

$$\psi_+ = \frac{2\pi}{N} \frac{\Gamma}{\Gamma - 1} n^{1/2}, \quad \psi_- = \frac{2\pi}{N} \frac{1}{\Gamma - 1} n^{1/2}. \tag{4.11}$$

Formulas (4.5), (4.8), (4.9) and (4.11) have been written for $k > 0$. However they may also be used for $k < 0$, in which case it is convenient to regard C as negative.

The smallest circumference factor is obtained by choosing σ_x as large as possible and σ_z as small as possible (or vice versa). If we choose $\sigma_x = 3\pi/4$, $\sigma_z = \pi/6$, we calculate from eq. (4.8), (4.9), $\psi_+ = 1.32$, $\psi_- = 1.93$. From eq. (4.11), (3.21) we have

$$\Gamma = \psi_+/\psi_- = 1.46, \; C = 5.35 \tag{4.12}$$

The theoretical minimum value of C is 4.45 for $\sigma_x = \pi$, $\sigma_z = 0$. In order to keep the amplitude of betatron oscillations within reasonable bounds, the above choices of σ_x, σ_z run about as close to the stability limits as it is safe to go. (For the choice $\sigma_x = \pi/2$, $\sigma_z = \pi/6$, these more exact formulas give $\Gamma = 1.29$, $C = 7.9$, which may be compared with the approximate values 1.31, 7.5 obtained in the preceding section.)

5. *Linear stability for spiral sectors*

For spiral sector accelerators, the circumference factor is close to unity, and minimizing C is no longer a major consideration. The ridge separation λ is, however, rather small, and if the gap between magnet poles is to be kept as large as possible, it appears that the field flutter in the median plane must be at least approximately sinusoidal. We will therefore assume a field in the median plane of the form.

$$B_{z0} = B_0 (r/r_0)^k [1 - f \sin (1/w \cdot \ln (r/r_0) - N\theta)], \tag{5.1}$$

where r, θ are polar coordinates in the median plane. The argument of the sine function is made logarithmic rather than linear in r in order to make the magnetic field (and hence the particle orbits) scale. The constant w is related to the spiral angle and the ridge separation (eq. 3.31) by

$$1/w = N \tan \zeta = 2\pi/\lambda. \tag{5.2}$$

The linearized equations for the betatron oscillations in the field (5.1) can be obtained from the general analysis of the first two sections, but it is perhaps more illuminating to derive them directly.

If one undertakes to write the linear terms in the differential equations characterizing the departure of the particle from a reference circle of radius $r_1 = p/eB_0(r_0/r_1)^k$ one obtains substantially the following, where $x = (r - r_1)/r_1$ and $y = z/r_1$.

$$x'' + [1 + k + f/w \cdot \cos N\theta]\, x \doteq f \sin N\theta \tag{5.3}$$

$$y'' - [k + f/w \cdot \cos N\theta]\, y \doteq 0. \tag{5.4}$$

These equations suggest alternate gradient focusing of the type characterized by the Mathieu differential equation, but the presence of the forcing term on the right hand side of the equation for the x-motion indicates that a forced oscillation will be expected and will be given approximately by

$$x = -\frac{f}{N^2 - (k + 1)} \sin N\theta. \tag{5.5}$$

Because of the presence of this forced motion one realizes that not only will the nonlinear terms in the differential equations be large but that a noticeable influence upon the betatron oscillation wavelength can result.

It is appropriate, therefore, to perform an expansion about a more suitable reference curve by writing

$$v = x - \frac{f}{N^2 - (k + 1)} \sin N\theta \tag{5.6}$$

In this way one obtains equations of which the most significant terms appear below :

$$v'' + \left[k + 1 - \tfrac{1}{2}\frac{f^2/w^2}{N^2 - (k + 1)} + \frac{f}{w}\cos N\theta + \tfrac{1}{2}\frac{f^2/w^2}{N^2 - (k + 1)}\cos 2N\theta\right] v = 0 \tag{5.7}$$

$$y'' - \left[k - \tfrac{1}{2}\frac{f^2/w^2}{N^2 - (k + 1)} + \frac{f}{w}\cos N\theta + \tfrac{1}{2}\frac{f^2/w^2}{N^2 - (k + 1)}\cos 2N\theta\right] y = 0 \tag{5.8}$$

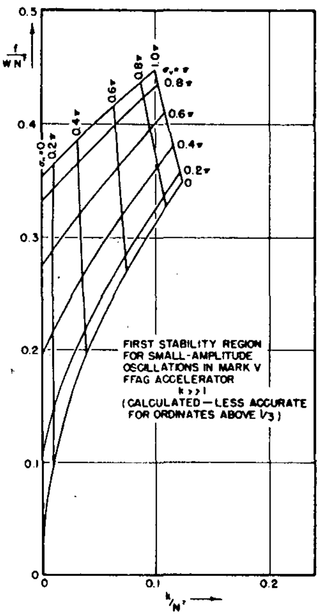

Fig. 2.

Each of these equations is of the form

$$d^2z/dr^2 + [A + B\cos 2\tau + C\cos 4\tau]\, z = 0.$$

Tables of the characteristic exponent (σ/π) of the extended Mathieu equation (5.9) have been computed on the ILLIAC, using a variational method[3]). Values of A are tabulated for a range of values of σ, B, C covering the significant portion of the first stability region. Results for the Mathieu equation (C = 0) are included. So far as we are aware there are at present no published tables of characteristic exponents for the Mathieu equation within the stability region.

In fig. 2 we plot a stability diagram for a spiral sector FFAG accelerator with $k \gg 1$ computed from the above formulas and the tabulated solutions. If $k \gg 1$, the coefficients A, B, C, depend only on k/N^2 and $f/w\,N^2$. We accordingly plot curves of constant σ_x and σ_z vs k/N^2 and f/WN^2. If we take $\sigma_z = \pi/6$, $\sigma_x = \pi/2$, with $f = 1/4$, we obtain $k = .057N^2$, $f/WN^2 = .25$, $\lambda = 6.3N^{-2}$, which may be compared with the approximate values $k = .062\,N^2$, $f/WN^2 = .265$, $\lambda = 5.95\,N^{-2}$ obtained in Section 3.

II. Non-linear effects in FFAG orbits

6. *General description of non-linear effects*

The preceding analysis of betatron oscillations has been based on an expansion of the equations of motion in powers of the displacement from the equilibrium orbit, keeping only the linear terms. The small amplitude betatron oscillations in x and z are then found to satisfy linear differential equations with coefficients periodic in the independent variable Θ.

In a perfectly constructed accelerator, the only periodicity would be that associated with the N identical sectors around the machine, and the period of the coefficients would be $2\pi/N$. In an actual accelerator, there will be imperfections, so that the coefficients will be strictly periodic with the period 2π in Θ, and approximately periodic with period $2\pi/N$. Associated with the period $2\pi/N$ is the requirement that σ_x and σ_z must not be integral or half integral multiples of 2π; in practice it appears that σ should be less than π since otherwise the tolerances on magnet construction and alignment become very severe. Associated with the period 2π is the requirement that ν_x and ν_z must not be integral or half-integral if imperfection resonances are to be avoided, and, in addition, if imperfections can couple the x - and z - motions, $\nu_x + \nu_z$ must not be an integer.

The study of the effects of non-linear terms in the equations of motion has not advanced nearly as far as the study of the linearized equations. Approximate analytic methods of treating non-linear equations with periodic coefficients have been developed by J. Moser[4]) and P. A. Sturrock[5]). Their results can be summarized as follows. If the coefficients in the equations have period 2π in Θ, and if ν_x, ν_z are the numbers of betatron oscillations in one period 2π, then imperfection resonances can occur when

$$n_x\,\nu_x + n_z\,\nu_z = \text{any integer, for} \qquad (6.1)$$

$$n_x,\ n_z = 0,\ 1,\ 2, \ldots\ldots$$

Let

$$n_x + n_z = q. \qquad (6.2)$$

Then if q = 1 or q = 2, the motion is unstable even in linear approximation (this is the rule stated in the preceding paragraph). If q = 3, then in general, the effects of quadratic terms in the differential equations are such as to make the motion unstable even at very small amplitudes. If q = 4, then the effects of cubic terms may be to render the motion unstable, depending on the form of the cubic (and linear) terms. If $q > 4$, then, in general, the motion is stable for sufficiently small amplitudes of betatron oscillation. In any case, if $q \geqslant 4$, and if the equations of motion are non-linear, then there will be in general a limiting amplitude of betatron oscillations beyond which the oscillations are unstable in the sense that they leave the donut. Numerical studies carried out on the ILLIAC at the University of Illinois seem to confirm these conclusions.

If we apply the above criteria to the sector periodicity $2\pi/N$, then we must replace ν_x, ν_z in eq. (6.1) by $\sigma_x/2\pi$, $\sigma_z/2\pi$, the number of betatron oscillations per sector. We then conclude that values of σ_x or σ_z near $2\pi/3$ are to be avoided as well as values such that $\sigma_x + 2\sigma_z$ or $\sigma_z + 2\,\sigma_x$ is nearly 2π. We call these resonances with the periodicity of the structure itself "sector resonances". We have indeed found in numerical studies that the limiting amplitude for betatron oscillations in spiral sector machines become very small when σ approaches $2\pi/3$.

It should be pointed out that non-linear terms in the equations for the radial sector accelerator are not very large, being not greater in order of magnitude than non-linear terms which arise in some conventional alternating gradient accelerators which have been contemplated. However, the non-linear terms which arise when the sectors spiral are much larger and play a very important role in determining the character of the betatron oscillations. Numerical studies indicate that although the motion in spiral sector synchrotrons exhibits marked non-linear effects, the amplitude limits are large enough to accommodate reasonable betatron oscillations provided σ is not close to $2\pi/3$. (Say $\sigma_x < .6\pi$).

7. *Characteristics of particle motion in spiral sector structures*

The digital computer studies have been carried out with the aid of the Electronic Digital Computer of the Graduate College of the University of Illinois (ILLIAC). A large fraction of the computations pertained to structures for which the parameters fell in the range suitable for the spiral-sector model, which is under development at the University of Illinois, but the majority of the orbit characteristics revealed in this way appear to be common to large-scale spiral-sector machines, including cyclotrons of the type currently being studied by groups in other laboratories.

The computational studies for spiral-sector machines have so far involved integration of differential equations describing the particle-trajectories, although attention is being directed towards the formulation of transformations (suitable for rapid computation of particle-motion through successive sectors) akin to those employed earlier as part of an analogous study of non-linear alternate-gradient structures similar in form to the Courant-Livingston-Snyder design.

The differential equations have involved (i) a set of exact equations covering motion in the median plane and (ii) a set of approximate, but Hamiltonian, equations describing both radial and exial motion in a magnetic field of the form necessarily associated with that prescribed in the median plane. The present programs have confined attention to fields with a sinusoidal dependence upon azimuth angle, but active programming has been begun on others free of this restriction. The utility of structures possessing poles which do not lead to pure sinusoidal fields is under study. The analytic work for a two-part computational program has been completed, involving (i) solution of the magnetostatic problem in the space between such poles, employing only two position variables

$$\xi \equiv \frac{1}{2\pi}\left[\frac{ln\,(1+x)}{w} - N\theta\right] \text{ and } \eta \equiv \frac{\sqrt{1+(wN)^2}}{2\pi w}\,\frac{y}{1+x}$$

when use is made of the scaling property of the structure, and (ii) solving the differential equations for trajectories in this field, which will, in effect, be stored in the computer memory.

The results of computations pertaining to motion with one degree of freedom are appropriately and conveniently represented by means of phase plots, depicting on invariant curves the position and associated momentum of a particle as it progresses through successive " sectors " (periods of the structure) from one homologous point to another. Such studies provide information concerning the location of "fixed-points", corresponding to an equilibrium orbit; the phase-change of the betatron oscillation per sector (σ); the displacement associated with trajectory directions different from that of the equilibrium orbit; and the extent of the region within which stable motion is possible. The characteristics of small-amplitude motion found in this way agree well, for sinusoidal fields, with the predictions of the analytic theory. At large amplitudes, unstable fixed-points—representing unstable equilibrium orbits—make their appearance. These fixed-points are usually 3 or 4 in number, corresponding to an unstable periodic solution 3 or 4 sectors in wavelength, although other cases have also been observed.

Associated with the unstable fixed-points one finds a separatrix, constituting an effective stability limit, which in the majority of cases the ILLIAC results depict as a sharp boundary and outside of which it is frequently possible to draw the initial portions of what appear to be invariant curves for unstable motion. Fig. 3 shows a number of invariant curves, on a phase plot of this nature, for parameters not far from those which would be suitable for a model. In this case the phase change per sector is close to $\sigma_x = .571\pi$ for small-amplitude motion; σ_x does not change greatly with increasing amplitude and it is noteworthy that ultimately 7 unstable fixed-points ($\sigma_x = 4\pi/7 \doteq .5714\pi$ make their appearance. In this example a rather large permissible amplitude of stable motion is found ($|\Delta r|$ approximately 0.08 or 0.09 times the radius, at $N\theta = 0$, mod 2π). The existence of this relatively large region of stability is connected with the fact that

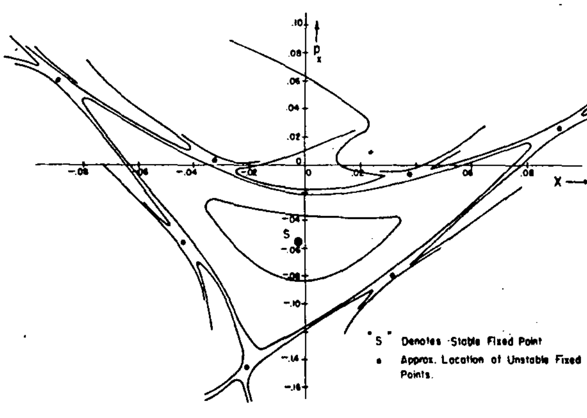

Fig. 3.

σ_{x0} differs materially from the value $2\pi/3$, for which a prominent non-linear sector-resonance makes its presence felt.

When axial motion is also permitted, there is in general coupling between this motion and that occurring in the radial direction. For small-amplitude oscillations about the equilibrium orbit, however, the motion is virtually decoupled. Limits of axial stability can be readily examined for special cases such as that in which the radial motion is introduced with initial conditions characteristic of the stable equilibrium orbit. For the structure with the parameters to which fig. 3 pertains, one finds in this way an axial amplitude limit of slightly over 0.014r—this limit applies to locations such that $N\theta = 0 \pmod{2\pi}$, near the center of an axially defocusing region, and has associated with it amplitude limits which become almost twice as large at intermediate points.

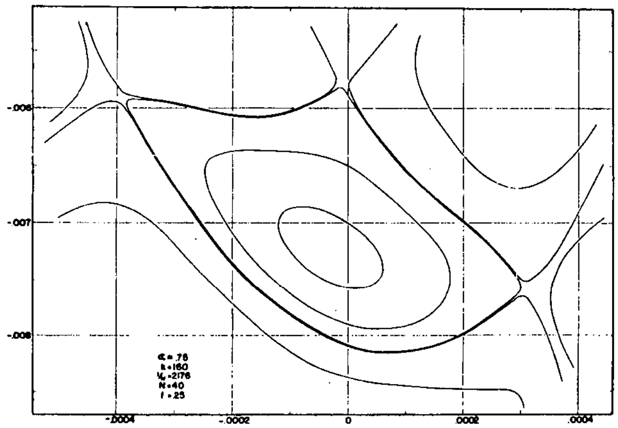

Fig. 4.

Similarly constructed phase plots for other values of machine parameters are shown in fig. 4 and the following figures. We are indebted to N. Vogt-Nilsen for supplying these plots from his studies of orbit stability.

Coupled axial and radial motion is more difficult to study systematically. By examining the behavior of the axial motion for various amplitudes of radial oscillation, however, some progress has already been made in the examination of the importance of various resonances involving the two frequencies which characterize the small-amplitude motion.

When the machine as-a-whole is considered, as it must because the presence of unavoidable misalignments makes the basic period strictly not one sector but one complete revolution, numerous additional resonances become possible. The effect of some of these has been examined with the ILLIAC, and further active investigation of this question is planned.

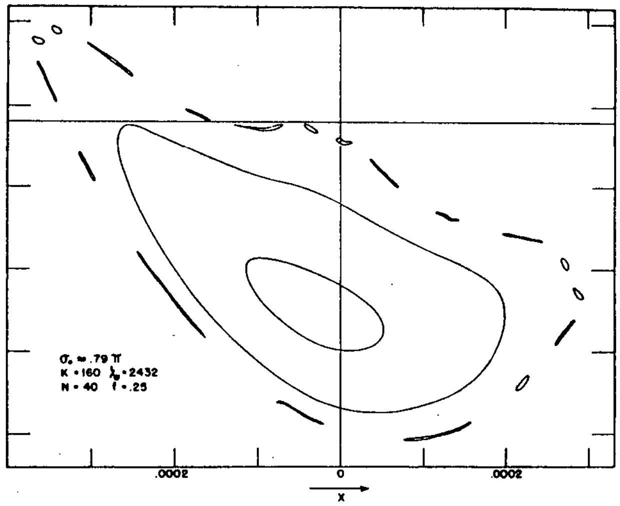

Fig. 5.

8. Application of Walkinshaw's equation to the $2\sigma_y = \sigma_x$ resonance

A method of analysis which appears to account for the behavior of the axial motion, in the presence of appreciable radial oscillation, has been developed by Walkinshaw[6]. The differential equation characterizing the axial motion is trated as *linear*, but contains a coefficient which involves the radial motion. As is well-known, the forced radial motion enhances the A-G focusing which appears in the axial equation—now, however, the additional effect of the free radial betatron oscillations is also included in the axial equation. The super-position of the comparatively-long-wavelength radial oscillations on the forced motion in effect modulates the smooth-approximation coefficient in the axial equation, to yield a Mathieu equation with a coefficient *having the period of the radial motion.* Under "resonant" conditions, which will be seen to include the case of interest here, this equation may have unstable solutions and, in such cases, the characteristic exponent of the solution appears to compare reasonably in magnitude with the lapserate characterizing the exponential growth of the ILLIAC solutions of the "Feckless Five" equations.

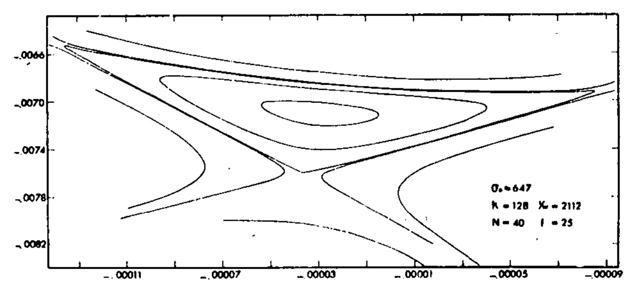

Fig. 6.

Walkinshaw's analysis pertains to differential equations which, in the MURA notation (f. ex., LJL(MURA) - 5), are taken to be of the form

$$x'' + (k + 1)\,x = -f \sin(x/w - N\theta), \tag{8.1}$$

$$y'' + [-k - (f/w)\cos(x/w - N\theta)\,y = 0 \tag{8.2}$$

(cf. LJL MURA Notes 6-22 Oct. 1955, Sect. 6, for $y/w \ll 1$). A solution for the radial motion, representing a free oscillation of amplitude A superposed on the forced motion, is taken of the form

$$x = A\cos(\nu_x\theta + \varepsilon) - (f/\Omega^2)\sin\!\int\Omega d\theta, \tag{8.3}$$

where

$$\Omega \simeq N + A(\nu_x/w)\sin(\nu_x\theta + \varepsilon) \text{ and } \nu_x \doteq (k+1)^{1/2} \tag{8.4}$$

This solution is substituted into the axial equation to yield, after some approximation (and a shift of the origin of θ which we introduce for convenience),

$$y'' + \left[-k + \frac{f^2}{w^2N^2}\left(1 + \frac{2A\,\nu_x}{wN}\cos\nu_x\theta\right)\right]y = 0. \tag{8.5}$$

It is noted that, when $A = 0$, this equation reduces to that given by the smooth approximation—we accordingly write

$$y'' + \left[\nu_y^2 + \frac{2Af^2\,\nu_x}{w^3N^3}\cos\nu_x\theta\right]y = 0, \tag{8.6}$$

to obtain an equation of the Mathieu type with a coefficient of period $2\pi/\nu_x$ in θ. By the transformation $\nu_x\theta = 2t$, we have the standard form

$$d^2y/dt^2 + \left[(2\,\nu_y/\nu_x)^2 + \frac{8\,f^2}{w^3N^3}\frac{A}{\nu_x}\cos 2t\right]y = 0 \tag{8.7}$$

with a coefficient of period π in the independent variable t.

A solution of the Mathieu equation

$$d^2y/dt^2 + [a + b\cos 2t]\,y = 0, \tag{8.8}$$

for b small but not zero, will exhibit instability when the coefficient a is equal or close to the square of an integer. In the present application stop-bands may thus be expected at operating points such that $2\,\nu_y/\nu_x = m$, the broad band of instability at $2\,\nu_y/\nu_x = 1$ (or $z\,\sigma_y/\sigma_x = 1$) being of chief interest in connection with the work presented here. It appears, moreover, possible to employ the Mathieu equation to account semi-quantitatively for (i) the range of b, and hence of the amplitude of free radial oscillation, which may be permitted when the oscillation frequencies depart by a specified amount from the resonant condition, and (ii) the lapse rate found to characterize the growth of the axial motion when the radial oscillations exceed this limit.

The numerical application of the Mathieu equation to specific problems of stability or instability may be accomplished by reference to ILLIAC solutions for the stability boundaries or for the characteristic exponent characterizing the solution.

(i) A useful estimate of the expected restrictions on the radial motion may be obtained, however, by appeal to the fact that near $a = 1$, $b = 0$ the stability boundaries can be represented rather well by the condition

$$|b| \doteq 2\,|a - 1|. \tag{8.9}$$

We find in this way the following estimate for the limiting amplitude:

$$A_1 = \frac{w^3N^3}{4f^2}\,\nu_x\,|(2\,\nu_y/\nu_x)^2 - 1|$$

$$\cong \frac{w^3N^3}{2f^2}\,|\,2\nu_y - \nu_x\,|\;\left(\text{for } \frac{2\nu_y}{\nu_x} - 1 \ll 1\right). \tag{8.10}$$

It may be noted that this result, although expressed in terms of ν_x and ν_y, concerns an inherent *sector resonance* which arises when $2\,\sigma_y/\sigma_x = 1$. This resonance is particularly interesting in that it does not appear to fall under the general criteria outlined in Section 6.

(ii) An estimate of the lapse rate characterizing unstable solutions near $a = 1$, $b = 0$ may, moreover, be made by taking

$$\mu \doteq \frac{\pi}{4}\sqrt{b^2 - 4(a-1)^2} \text{ nepers for } \Delta t = \pi \qquad \text{when } (|b| > 2|a-1|)$$

$$= \frac{\pi}{4}\frac{\nu_x}{N}\sqrt{b^2 - 4(a-1)^2} \text{ nepers per sector}$$

$$= \frac{\pi/4}{N}\sqrt{\left(\frac{8F^2A}{w^3N^3}\right)^2 - 4\left[(2\,\nu_y)^2 - \nu_x^2\right]^2/\nu_x^2} \text{ nepers per sector}$$

$$= \frac{0.68}{N}\sqrt{\left(\frac{4f^2A}{w^3N^3}\right)^2 - \left[(2\,\nu_y)^2 - \nu_x^2\right]^2/\nu_x^2} \text{ decades per sector} \tag{8.11}$$

A convenient alternative form for this last result is

$$\mu \doteq \frac{2\pi F^2}{w^3N^4}\sqrt{A^2 - A_1^2} \text{ nepers/sector}$$

$$\frac{2.73\,F^2}{w^3N^4}\sqrt{A^2 - A_1^2} \text{ decades/sector.} \tag{8.12}$$

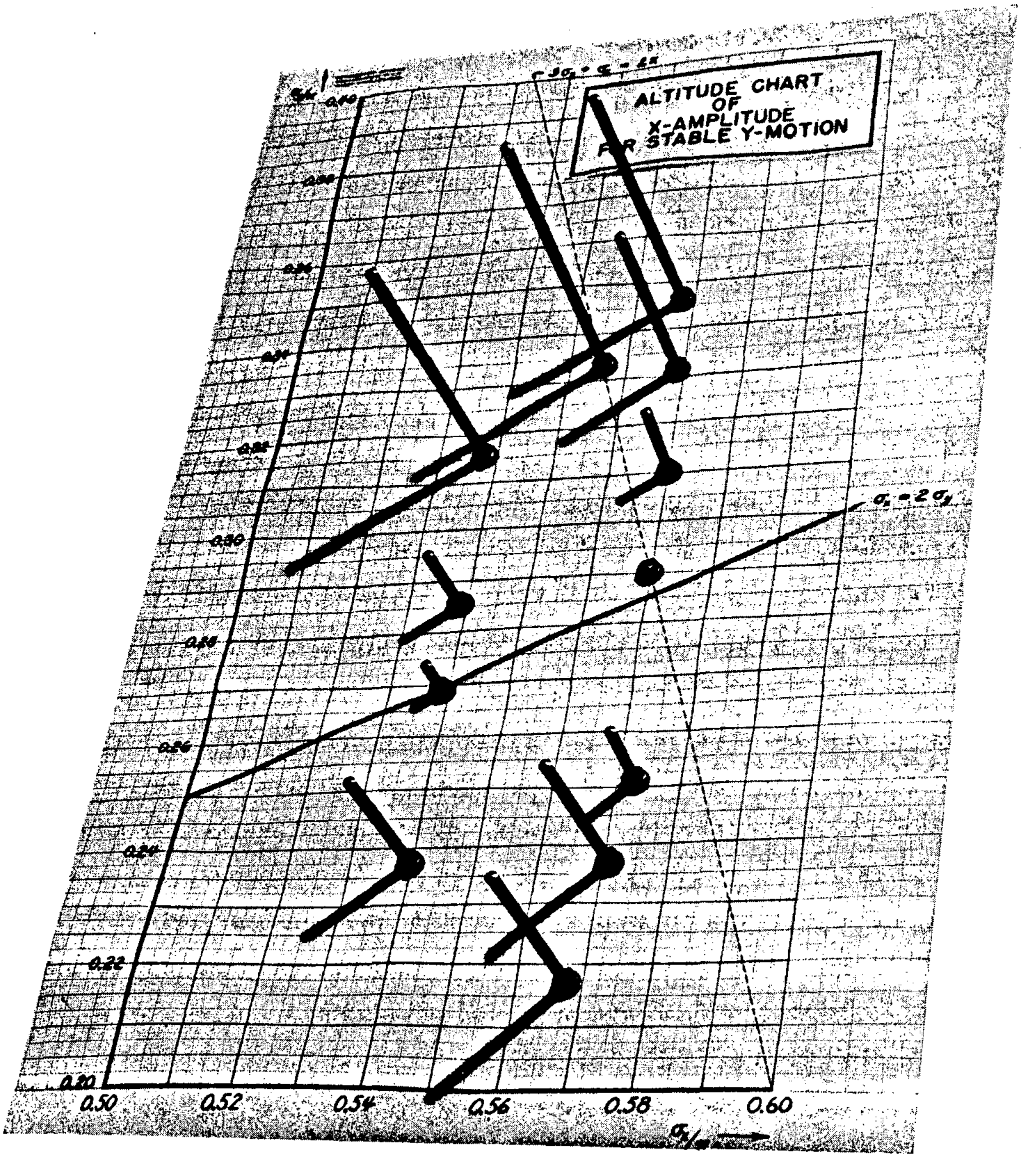
ALTITUDE CHART
OF
X-AMPLITUDE
FOR STABLE Y-MOTION
0.50
0.52
0.54
0.56
0.58
0.60
0.20
0.22
0.24
0.26
0.28
0.30
0.32
0.34
0.36
0.38
0.40

Fig. 7.

Results obtained with the ILLIAC, for 5-sector machines with model-like parameters such that $0.5\pi < \sigma_{x_0} < 0.6\pi$ and $0.2\pi < \sigma_{y_0} < 0.4\pi$, appear fairly close to these estimates. In all the ILLIAC runs the radial amplitudes were measured, however, near the center of a focusing region, at $N\theta = 0$ (Mod. 2π), where the amplitudes of the non-sinusoidal A-G oscillations can exceed those corresponding to the smooth approximation representation of the motion. By way of example we present here the results for an accelerator for which

$$k = 0.6436 \qquad 1/w = 20.82 \qquad f = {}^1/_4 \qquad N = 5:$$

In this case the oscillation frequencies are such that

$$\left.\begin{array}{l}\sigma_{x_0} = 0.5388\pi \\ \sigma_{y_0} = 0.2855\pi\end{array}\right\} \text{ or } \left\{\begin{array}{l}\nu_{x_0} = 1.347 \\ \nu_{y_0} = 0.714\end{array}\right.$$

and the limiting amplitude for x appeared to be some 0.0075 units to the left of the stable fixed point ($N\theta = 0$, mod. 2π). For these machine parameters the equation for A_1 yields

$$A_1 = \frac{500}{(20.82)^3}\, 1.347\,[(1.06)^2 - 1]$$

$= 0.0092$, the observed limiting amplitude at $N\theta = 0$ (mod 2π) thus being within 20% of this estimate. With respect to the lapse rate, we continue this example by consideration of the case $A = 0.0225$. Then $\sqrt{A^2 - A_1^2} = 0.02035$, and one expects

$$\mu = \frac{0.171\,(20.82)^3}{625}\,(0.02035)$$

$$= 0.050 \text{ decades/sector,}$$

in close agreement with the value 0.055 decades/sector found from the ILLIAC work. (For this case the coefficients in the Mathieu equation are $a = 1.12$, $b = 0.604$, for which an independent extrapolation of coarse tables extending to $a \leqslant 1$ suggests $\mu = 0.107$ nepers/sector $=$ 0.046 decades/sector.) In fig. 7, we plot the amplitude of radial motion for which the vertical motion becomes unstable (represented by the lengths of the rods) at various points in the σ_x, σ_z - plane.

Growth of the axial motion, similar in appearance to that reported here, has also been observed in the neighborhood of the $2\,\sigma_x + 2\,\sigma_y = 2\pi$ and $\sigma_x + 2\sigma_y = 2\pi$ resonances. It appears that these sum resonances may be connected with the presence of terms in the y-equation which involve $u^2 y \cos N\theta$ and $uy \sin N\theta$, where u represents the radial oscillation about the scalloped equilibrium orbit.

LIST OF REFERENCES

1. Symon, K. R. An alternative derivation of the formulas for the smooth approximation (MURA-KRS-4). Midwestern Universities Research Assoc., 1954. (unpublished.)
2. Sigurgeirsson, T. Focussing in a synchrotron with periodic field perturbation treatment. CERN-T/TS 3, 1953. (unpublished.)
3. Laslett, L. J., Snyder, J. N. and Hutchinson, D. Tables for the determination of stability boundaries and characteristic exponents for a Hill's equation characterizing the Mark V FFAG synchrotron. (MURA Notes). Midwestern Universities Research Assoc., 1955. (unpublished.)
4. Moser, J. Stabilitätsverhalten kanonischer Differentialgleichungssysteme. Nachr. Akad. Wiss. Göttingen, IIa, Nr. 6, p. 87-120, 1955.
5. Sturrock, P. A. Static and dynamic electron optics. Cambridge, University Press, 1955.
6. Walkinshaw, W. A Spiral Ridged Bevatron. A.E.R.E., Harwell, 1955. (unpublished.)

FIXED FIELD ALTERNATING GRADIENT PARTICLE ACCELERATORS

D. W. KERST, K. R. SYMON, L. J. LASLETT, L. W. JONES, and K. M. TERWILLIGER

Midwestern Universities Research Association *, U.S.A.

(presented by L. W. Jones)

I. General description

Alternating gradient (AG) focusing [1] provides a high degree of stability for both the radial and vertical modes of betatron oscillations in circular particle accelerators. This stability makes possible the construction of many kinds of circular accelerators with magnetic guide fields which are constant in time, called fixed field alternating gradient (hereafter FFAG) accelerators. These machines contain stable equilibrium orbits for all particles from the injection energy to the output energy. These orbits may all be in an annular ring, as in a synchrotron or betraton; the magnetic field must then change rapidly with radius to provide orbits for the different energy particles. If the guide field gradient were made independent of azimuth, one of the modes of betatron oscillation would be clearly unstable. Application of alternating gradient focusing, however, can keep both modes of betatron oscillation stable even with the rapid radial change of magnetic field. It is interesting to note that circular particle accelerators can be classified into four groups according to the type of guide field they use : fixed field constant gradient (conventional cyclotrons, synchro-cyclotrons and microtrons), pulsed field constant gradient (weak focusing synchrotrons and betatrons), pulsed field alternating gradient (AG synchrotrons), and fixed field alternating gradient (FFAG synchrotrons, betatrons, and cyclotrons).

Two types of FFAG design appear the most practical. The radial sector type** achieves AG focusing by having the fields in the successive focusing and defocusing magnets vary in the same way with radius but with alternating signs (or in certain cases alternating magnitudes). Since the orbit in the reverse field magnet bends away from the center, the machine is considerably larger than a conventional AG machine [1] of the same energy having an equal peak magnetic field. This serious disadvantage is largely overcome in the spiral sector type (suggested by D. W. Kerst), in which the magnetic field consists of a radially increasing azimuthally independent field on which is superimposed a radially increasing azimuthally periodic field. The peaks and troughs of the periodic field spiral outward at a small angle to the orbit. The radial separation between peaks is small compared to the radial aperture. The particle, crossing the field ripples at a small angle, experiences alternating gradient focusing. Since the fields need not be anywhere reversed, the size of this machine can be comparable to that of an equivalent conventional AG machine.

FFAG synchrotrons have a number of important advantages over conventional synchrotrons. A major one is beam intensity. Since the magnetic field is time independent in an FFAG synchrotron, the beam pulse rate is determined only by the repetition rate of the radio frequency modulation cycle. In a conventional synchrotron, the beam pulse rate is limited by the time to complete the pulsed magnetic field cycle. It is reasonable to assume that RF cycle repetition rates can be made considerably higher than field recycling rates. In addition, one may consider accelerating several groups of particles simultaneously, so that the interval between times when groups of particles are accepted from the injector may be made much less than the time required to accelerate one group to full energy.

The radio-frequency acceleration may follow a more arbitrary frequency-versus-time program with FFAG synchrotrons since there is no magnetic field tracking requirement as in pulsed-field synchrotrons. This allows the use of a mechanical modulation system with high-Q cavities. With the high-Q realized in unloaded cavities, the required voltage gain per turn could be given the particles by one cavity driven at reasonable pover. Modulation could be accomplished by a moving diaphragm or similar device to tune the cavity capacity. With such a system, model tests indicate a frequency change of a factor of greater than 3:1 is practical. Using 5 Mev injection, a frequency change of 10 : 1 is required to reach relativistic velocities. One might then use one cavity operating as a self-excited oscillator to accelerate particles from injection to about 50 Mev. The voltage on that cavity would then be turned off as voltage on a second cavity is turned on, and acceleration continued with the

* Assisted by the National Science Foundation and the Office of Naval Research.

** Suggested by K. R. Symon. This structure was also suggested independently earlier (1953) by T. Ohkawa, University of Tokyo, Tokyo, Japan. (private communication.)

second cavity. The change-over could be triggered by frequency comparison between cavities. The relative phases of the cavities could be controlled by a loose coupling between them. (With the University of Michigan electron synchrotron two cavity RF system, it was observed that is was possible to make the transition from one cavity to another without an observable beam loss.) A third cavity might be added and a second transition made if desired, since it is observed that most of the energy is given the particles after they have reached almost constant velocity, c, and this third cavity could be designed to provide very high voltage over a small frequency range. Fine frequency adjustments would be made with reactance tube loading of the cavities. With this RF system it appears reasonable to accelerate protons to 20 Bev with a repetition rate of two or three per second. While the above system is suggested on the basis of experimental tests already in progress, it is realized that other RF systems might prove more practical. In alternating gradient synchrotrons, phase stability vanishes at a transition energy. It is possible in the radial sector FFAG designs to have k large and negative. In this case there is no transition energy, and high energy orbits lie on the inner radius of the machine. Negative k designs appear o be not practical with spiral sectors.

Another reason for high beam intensity is the large injection aperture possible in the FFAG designs. Whereas injection from a 50 Mev proton linear accelerator is planned for 25 Bev pulsed-field accelerators, a 5 Mev Van de Graaff electrostatic generator might be used to inject into FFAG synchrotrons for the following reasons. Eddy current effects on the magnetic fields are absent in FFAG synchrotrons and the effects of remanent magnetic fields can be reduced by properly distributed currents (or by a demagnetizing procedure at the end of an operating day), so that injection into weaker magnetic fields appears practical. By enlarging the injection aperture space charge and gas scattering effects may be reduced, allowing the lower injection energy. Conventional synchrotrons must inject into a region where the magnetic field will later be pulsed to its maximum value, so that an increase in injection aperture would require an increase in peak magnet power and stored energy. The use of electrostatic generator injection with FFAG synchrotrons would have the advantages of higher pulse currents, greater simplicity, lower cost, and better beam energy and size resolution than are at present realized with proton linear accelerators. Although one-turn injection using a pulsed inflector with a pulsed current of milliamperes is the most obvious injection system, many-turn injection might be used to give greater beam currents if methods of circumventing the space charge limit are found.

Other advantages of the FFAG synchrotron are engineering and maintenance simplifications. The direct current magnet power supply is simpler and cheaper than a pulsed supply to construct and to maintain. The magnets do not have to be laminated, and field trimming is all time independent. Disadvantages of the FFAG synchrotron are the large increase in circumference for the radial sector type (at least a factor of three) and the increase in complexity of the magnetic fields, particularly for the spiral sector machine.

Fixed field betatrons have potentially a much higher intensity than conventional betatrons.* Beam can be injected for a considerable fraction of a cycle, if extra accelerating flux is available, rather than the few tenths of a microsecond presently possible. The only beam current limitation appears to be space charge at injection, and this may be decreased by such techniques as high voltage injection. An FFAG betatron has no problems of tracking a pulsed guide field with the accelerating flux, and has also other engineering simplifications mentioned in the synchrotron case.

Application of the FFAG principle to a cyclotron allows the radial dependence of the magnetic field to be such as to keep the particle revolution rate constant, independent of energy even in the relativistic region. Present high energy cyclotrons must be frequency modulated to compensate for the relativistic increase of mass. A constant frequency cyclotron should increase the beam output about two orders of magnitude. A radial sector cyclotron, in which the field alternates between high and low values, was first suggested by Thomas [2]. The spiral sector design seems even more advantageous for application to the cyclotron.

II. Types of FFAG design

1. Radial sector type

Circular particle accelerators with radial sectors can be built with the high energy orbits at the outer edge of the machine and the injection orbits at the inside edge, or vice versa. This discussion assumes the highest energy orbits are at the outside edge. (We will refer specifically to FFAG synchrotrons, but most of our comments will apply also to betatrons and cyclotrons.) In the radial sector design the magnet structure consists of N identical sectors, each composed of a focusing magnet and a defocusing magnet. The magnet which is focusing for radial oscillations is of course defocusing for vertical oscillations and vice versa. The azimuthal boundaries of the magnets are on radii from the machine center (hence the name). The magnetic field direction in one magnet of a sector is opposite to that of the other, while the radial dependence of the field is the same in both. The field in the median plane at any azimuth is

$$H = H_0 \left(\frac{r}{r_0}\right)^k \qquad (1.1)$$

where r is the distance from the machine center to the equilibrium orbit and k is a constant for the machine. This field shape requires that orbits for different energy particles are similar, i.e. photographic images of each other. Ideally,

* This has been pointed out independently by Miyamoto, Tokyo University, Tokyo, Japan, at a symposium on nuclear physics of the Physical Society of Japan in October, 1953. (private communication.)

the field along a closed equilibrium orbit is constant through each magnet, and the path is composed of arcs of circles. This situation is perturbed by the impossibility of a sharp field boundary. If we assume the ideal situation, a particularly simple case occurs when the fields for a given energy orbit have the same magnitude in the positive and negative field magnets.

It is evident that particles deviating from the equilibrium orbit experience AG focusing. The numbers of radial and vertical betatron oscillations around the machine, ν_x and ν_z, are determined by k and the magnet lengths. Both ν_x and ν_z are constant for all energies.

It is desirable to make the negative field magnets as short as possible, to keep the radius of the machine small; the minimum length of the negative field magnet is of course determined by the necessity for preserving stability of the vertical betatron oscillations. Some vertical focusing and radial defocusing occur because the orbits are scalloped and do not cross the magnet edges at right angles. In machines in which the number of sectors is large and the effects of orbit scalloping small, the negative field magnet can be made no shorter than about $^2/_3$ of the positive field magnet if we wish to preserve vertical stability. This means that, neglecting straight sections, the circumference of the machine is five times that necessary if there were no negative field magnets. The ratio (in this case, five) between the actual orbit circumference of a circle whose radius is the minimum radius of curvature at any point along the orbit, we call the circumference factor. The fixed magnetic field in an FFAG machine can be made considerably larger than the pulsed field of a conventional accelerator, so a machine of the radial sector type might actually be about three times the size of a pulsed field AG accelerator of the same energy. It is also desirable to make the radial extent of the magnets as small as possible, which requires a high field gradient. The allowable gradient is determined by the effect of magnet misalignments. Reasonable values indicate a minimum radial aperture of about 2% of the radius of the machine.

2. *Spiral sector type*

The spiral sector design of FFAG accelerator has the high energy orbits at the outside edge of the machine. It is not practical to have the high energy orbits on the inside and inject at the outside edge, because stability of the radial oscillations becomes virtually impossible to achieve.

The guide field on the median plane, if there are no straight sections, is given by

$$H = H_0 \, (r/r_0)^k \, \{1 + f \cos [N\,\theta - N \tan \zeta \; \ln \, (r/r_0)]\} \tag{2.1}$$

where r is again the distance from the center of the machine; k, the mean field index; θ, the azimuthal angle, also measured from the center of the machine; f, the flutter factor (the fraction of field variation); N, the number of sectors (periods of the field variation) around the machine; and ζ is the spiral angle between the field maximum and the radius. The equilibrium orbits are all similar figures, whose linear dimensions are proportional to the radius, but their positions rotate with radius due to the spiraling periodic field. A particle going around the machine experiences a gradient first of one sign then the opposite as it crosses the periodic field peaks and troughs at a small angle, so there is AG focusing of the betatron oscillations. The negative gradient is less than the positive gradient, due to the radial increase of field. This is somewhat compensated by the scalloping of the orbits, which causes the particle to experience a longer path in the negative gradient and a shorter path in the positive gradient than if it moved on a circle. The strength of betatron focusing depends on the rate of radial increase of the field, the spiral angle, and the number of sectors. The minimum size of radial aperture is limited primarily by the difficulty of achieving strong AG focusing with a periodic field while requiring a given vertical aperture. A flutter factor of about $^1/_4$ gives the largest vertical gap for a fixed strength of focusing when iron magnet poles are used without distributed backwindings and forward windings. This small flutter factor means the machine has a circumference factor (in this case, $1 + f$), close to unity, so the radius of an FFAG spiral sector synchrotron is about the same as that of an equivalent energy conventional synchrotron. By using a field variation in the median plane which is more rectangular than sinusoidal, some increase in vertical aperture and also in the maximum stable amplitude of vertical oscillations is achieved at some sacrifice of circumference factor. The minimum radial aperture for reasonable parameters is about 3% of the radius.

3. *Other FFAG types*

Both the radial sector and spiral sector designs discussed above have equilibrium orbits of constant shape scaled in proportion to the orbit radius. There are many modifications of these designs. Some differ only in that the fields are not the square wave type used in the radial sector design described or the sinusoidal shape used in the spiral sector design. There are other variations of these designs which preserve betatron oscillation stability, hold ν_x and ν_z constant, but do not retain the property of similarity of equilibrium orbits. The magnet edges of focusing and defocusing sectors can be made non-radial, and the fields in the positive and negative field magnets made different functions of radius (the negative field magnet can even be designed to have zero field). The magnet edges, radial or non-radial, can be tipped in the same direction, approaching the spiral sector design. Machines made with these modifications do not seem to show any strong advantages with perhaps the following exception. It is conceivable, using backwindings, to transform from a spiral sector at the outside edge of the machine, with a small circumference factor where it is needed, to a radial sector at the inside edge, with a large vertical aperture for injection. Such a design would have the advantages of both types with, however, a considerable increase in magnet complexity.

Another modification is the spiral sector constant frequency cyclotron. In this machine, the frequency of revolution of the particles can be made independent of energy even at relativistic energies, but the orbits in this case do not scale, and the number of betatron oscillations, ν_x and ν_z cannot be kept constant.

LIST OF REFERENCES

1. Courant, E. D., Livingston, M. S. and Snyder, H. S. The strong-focusing synchrotron — a new high energy accelerator. Phys. Rev., *88*, p. 1190-6, 1952.
2. Thomas, L. H. The paths of ions in the cyclotron. Phys. Rev., *54*, p. 580-98, 1938.

RESONANT STABILITY LIMITS FOR SYNCHROTRON OSCILLATIONS *

K. R. Symon and J. D. Steben

Midwestern Universities Research Association, Stoughton, Wisconsin (USA)

L. J. Laslett

Lawrence Radiation Laboratory, University of California, Berkeley, California (USA)

(Presented by K. R. Symon)

I. INTRODUCTION

The synchrotron frequency is given in the usual approximation (1) (valid for $\nu_s \ll 1$) by

$$\nu_s = \frac{f_{synchrotron}}{f_{revolution}} = \left[\frac{h\,KV\cos\Phi_s}{2\pi E_s}\right]^{1/2} \qquad [1.1]$$

where ν_s is the number of synchrotron oscillations per revolution, V is the peak voltage gain per turn, Φ_s is the stable phase, h the harmonic number, and

$$K = \frac{E}{f}\frac{df}{dE} \qquad [1.2]$$

Ordinarily, $\nu_s \ll 1$, but if h is very large, as it conceivably could be in the 100-1000 GeV accelerators, ν_s can be of the order 1 or even larger. We may then expect to encounter resonant behavior when

$$\nu_s = \frac{m}{n_s} \qquad [1.3]$$

just as is the case with betatron oscillations, and for $n_s \leq 4$ similar instabilities and nonlinear stability limits may occur. Since ν_s changes during acceleration, and eventually decreases to small values, a value such as $\nu_s > 1/4$ will necessitate crossing a quarter-integral resonance during acceleration, and higher values of ν_s will necessitate crossing more serious resonances. We may also expect coupling resonances with the radial betatron oscillations whenever

$$n_s\nu_s \pm n_r\nu_r = m \qquad [1.4]$$

* Work supported by the U. S. Atomic Energy Commission

In the present report we will consider only synchrotron resonances of type [1.3], and we will study only the stability limits introduced by these resonances when the acceleration parameters are held constant.

A resonance of type [1.3] may be regarded as driven by neighboring harmonics in the acceleration signal. That is, if the synchronous revolution frequency is

$$f_s = f_o/h \qquad [1.5]$$

where f_o is the frequency at the accelerating r. f. gap, then a particle at frequency

$$f_{s-} = f_o/(h-1) \qquad [1.6]$$

would also be synchronous. In the case of a single accelerating gap, when all traveling wave components into which we can resolve the accelerating voltage have equal amplitudes, it is of interest to compare the energy extension of a bucket with the distance between adjacent harmonics, which is

$$\Delta E_h = \frac{E}{f}\frac{f_{s-}-f_s}{|K|} = \frac{E}{h\,|K|} \qquad [1.7]$$

when $h \gg 1$. The maximum excursion from the synchronous energy is (1) given roughly by

$$\Delta E_m = (1-\Gamma)\left[\frac{2\,V\,E}{\pi\,h\,|K|}\right]^{1/2},\ \Gamma = \sin\Phi_s \qquad [1.8]$$

As a result, the usual bucket formulas certainly break down (buckets would overlap) when

$$(1-\Gamma)\left[\frac{2\,V\,E}{\pi\,h\,|K|}\right]^{1/2} > \frac{E}{2\,h\,|K|} \qquad [1.9]$$

or, in view of Eq. [1.1], for $\nu_s \gtrsim 1/4$, for reasonable values of Γ.

In the next section, we formulate the acceleration problem in terms of canonical variables suitable for applying Moser's (2) techniques to study the behavior at resonant values of ν_s. We then apply these in succeeding sections.

II. SYNCHROTRON ACCELERATION EQUATIONS

The time derivative of the phase of the r.f. voltage when a particle crosses an accelerating gap is

$$\dot{\Phi} = 2\pi(f_o - hf) = 2\pi h(f_s - f) \qquad [2.1]$$

where f is the particle revolution frequency, f_o the frequency of the gap voltage, h tre harmonic number, and f_s the synchronous particle frequency. For the case of a single accelerating gap of negligible width at $\theta = 0$, where θ is the azimuthal coordinate of the accelerator, the rate at which the energy E of a particle increases is given by (1)

$$\dot{E} = 2\pi f\,\delta(\theta)\,V \sin 2\pi f_o t =$$

$$= \sum_{n=-\infty}^{\infty} - f V \sin(n\theta - 2\pi f_o t) \qquad [2.2]$$

where V is the peak gap voltage (which we take as independent of time). Letting

$$\Phi = 2\pi f_o t - h\theta \qquad [2.3]$$

leads to a rate of energy gain given by

$$\dot{E} = f V \sin\Phi + \sum_{\substack{m=-\infty \\ m\neq 0}}^{\infty} f V \sin\left[(1+\frac{h}{m})\Phi - 2\pi m f_s t\right] \qquad [2.4]$$

The first term, which corresponds to $n = h$, represents the component of the r.f. which revolves with the synchronous particle. The other terms are commonly dropped, but they are important here as they may drive resonances when ν_s is not small. We will, however, assume that quantities such as f_o vary so slowly that they may be taken as constant (during a few synchrotron oscillation periods). Expanding f(E, t) about the synchronous energy E_s (which corresponds to the frequency f_s) gives

$$f = f_s + f_E(E - E_s), \qquad f_E = \left.\frac{\partial f}{\partial E}\right|_{E=E_s} \qquad [2.5]$$

to first order. Note that the synchronous phase Φ_s is given by

$$\dot{E}_s = f_s V \sin\Phi_s \qquad [2.6]$$

(where $\cos\Phi_s$ has the same sign as $\partial f/\partial E$).

Dimensionless phase, energy, and time variables may be introduced by (')

$$\varphi = \Phi - \Phi_s \qquad [2.7]$$

$$y = -\frac{h f_E}{f_s}(E - E_s) \qquad [2.8]$$

$$\tau = 2\pi f_s t \qquad [2.9]$$

so that Eqs. [2.], [2.4] become

$$\frac{d\varphi}{d\tau} = y, \qquad [2.10]$$

$$\frac{dy}{d\tau} = \nu_s^2\left(-\sin\varphi + 2\tan\Phi_s \sin^2\frac{\varphi}{2}\right)\left[1 + 2\sum_{m=1}^{\infty}\cos m\tau\right] \qquad [2.11]$$

where ν_s is given by Eq. [1.1] and where we have assumed h to be large (neglected m/h relative to 1). Equations [2.10], [2.11] may be derived from the Hamiltonian

$$H = \frac{1}{2}y^2 + \nu_s^2\left[2\sin^2\frac{\varphi}{2} - \tan\Phi_s(\varphi - \sin\varphi)\right]$$

$$\left[1 + 2\sum_{m=1}^{\infty}\cos m\tau\right] \qquad [2.12]$$

For N properly phased and evenly spaced gaps with identical peak voltages V/N, one would again arrive at Eq. [2.11] except that only those values of m which are divisible by N appear. A few evenly spaced gaps can thus eliminate the terms which drive low order resonances. However, any error in position, voltage, or phase will give rise to small terms in $\cos m\tau$ for which m is not divisible by N. If, for example, a single gap has errors $\delta\theta$, δV, $\delta\varphi$ in position, voltage, and phase, the errors will contribute to the sum the terms

$$2\sum_{m=1}^{\infty} E\cos(m\tau + \zeta),$$

$$E = \left\{\left[\frac{\delta V}{V}\right]^2 + \left[\delta\varphi + (m+h)\,\delta\theta\right]^2\right\}^{1/2}$$

$$\zeta = \tan^{-1}\frac{\delta\varphi + (m+h)\,\delta\theta}{\delta V/V} \qquad [2.13]$$

Note that our y is not the same as that used in Ref. 1.

In the usual treatment in which the time-dependent terms in Eq. [2.11] are neglected, it is clear if we linearize Eq. [2.11] that ν_s is the angular frequency of small phase oscillations. Since the time τ is measured here in radians of revolution of the synchronous particle, ν_s will be the frequency in phase oscillations per revolution. We will see later that the time-dependent terms have a negligible effect if $\nu_s \ll 1$. In that case the usual treatment yields, for the nonlinear problem, a region of stable phase oscillations, a "bucket", whose area in phase space, in the present units, is

$$A_\Gamma = 16\,\nu_s\,\alpha_1(\Gamma)/(1-\Gamma^2)^{1/4} = 16\,\nu_s\,\alpha(\Gamma),$$

$$\alpha(\Gamma) = \frac{\alpha_1(\Gamma)}{(1-\Gamma^2)^{1/4}}, \qquad [2.14]$$

where the Γ dependence, $\alpha_1(\Gamma)$, is a numerical factor shown graphically in (1). We consider first the linearized Eqs. [2.10], [2.11], with time-dependent terms neglected. Let us make a canonical transformation $(y, \varphi) \to (\rho, \gamma)$ to canonical polar coordinates, defined by

$$y = (2\,\nu_s\,\rho)^{1/2}\cos\gamma, \qquad [2.15]$$

$$\varphi = \left(\frac{2\rho}{\nu_s}\right)^{1/2}\sin\gamma. \qquad [2.16]$$

The quadratic part of the Hamiltonian [2.12] is then

$$H_2 = \frac{1}{2}y^2 + \frac{1}{2}\nu_s^2\,\varphi^2 = \nu_s\,\rho \qquad [2.17]$$

The phase trajectories are circles of constant ρ.

If the time-dependent terms are included, then the linearized equations [2.10], [2.11] lead to a Hill equation. The solution is of Floquet type with a linear oscillation frequency ν_0 replacing from ν_s. We shall determine ν_0 later. Instabilities appear when ν_0 approaches an integral or half-integral value. When the linearized motion is stable, it is again possible to find a canonical transformation (now periodic in τ) which transforms the quadratic part of the Hamiltonian to form [2.17], with ν_0 replacing ν_s. Thus in suitable variables, the linear motion is again reduced to a circle of constant ρ in phase space. Using further canonical transformations of types introduced by Birkhoff (3), one could formally eliminate the γ and τ dependence from successively higher order terms of H, so that to any desired order one may formally transform the phase curves into circles of constant ρ, obtaining

$$H = F(\rho), \qquad [2.18]$$

$$\frac{d\rho}{d\tau} = -\frac{\partial H}{\partial \gamma} = 0, \quad \frac{d\gamma}{d\tau} = \frac{\partial H}{\partial \rho} = \nu_c(\rho) \qquad [2.19]$$

where now ρ, γ are new canonical variables related by a sequence of transformations to the original ρ, γ variables introduced in the linear problem. The transformations are such that the new variables differ from the original ones only by nonlinear terms, so that the difference between them is only important at large amplitudes. The frequency of phase oscillations, $\nu_c(\rho)$, is a function of the amplitude ρ, or equivalently of the area A of the phase trajectory, since

$$\rho = \frac{A}{2\pi} \qquad [2.20]$$

Although it would be possible to find the function $F(\rho)$ and hence $\nu_c(\rho)$ by thus transforming Eq. [2.12], we may obtain an approximate result in a simpler way by noticing that $\nu_c \xrightarrow[\rho\to 0]{} \nu_0$, and $\nu_c(\rho) \xrightarrow[\rho\to\rho_c]{} 0$ with vertical slope. Letting $\rho \to \rho_c$ label the separatrix, one obtains

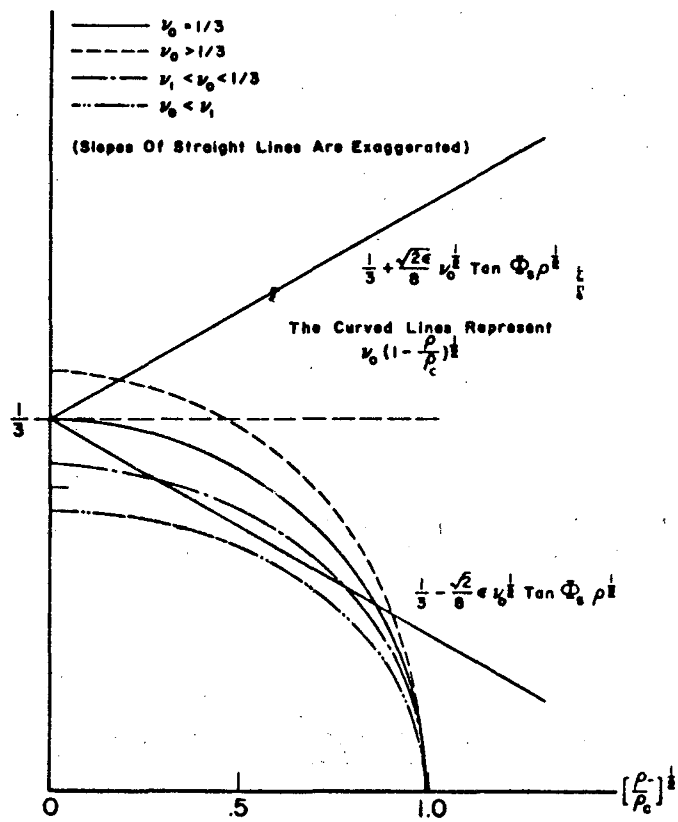

Fig. 1 - Graphical solution of Eq. (3.6) near 1/3 integral resonance.

$$\rho_c = \frac{A_r}{2\pi} \approx \frac{8\,\nu_s\,\alpha(\Gamma)}{\pi}, \qquad [2.21]$$

where A_r is the bucket area, given in the usual approximation by Eq. [2. 14]. A function with the desired behavior at the limiting values of ρ is

$$\nu_r(\rho) = \nu_o\left(1-\frac{\rho}{\rho_c}\right)^x, 0 < x < 1 \qquad [2.22]$$

which corresponds to the Hamiltonian

$$H = \frac{1}{x+1}\nu_o\rho_c\left[1-\left(1-\frac{\rho}{\rho_c}\right)^{x+1}\right] \qquad [2.23]$$

The function [2. 22] has the correct limiting values at $\rho = 0$, $\rho = \rho_c$ for any exponent x in the range indicated, and hence may be expected to yield topologically correct prediction about phase trajectories. By expanding Eq. (2. 12), one may show that the value of $d\nu_r/d\rho$ is also correctly matched near $\rho = 0$ (when τ^--dependent terms are neglected) if we take

$$x = \alpha(\Gamma)/\pi \qquad [2.24]$$

Near the separatrix, it can be shown that $\nu_r \to 0$ more slowly than formula [2. 22] no matter how small x is taken. However formula [2. 22] gives a reasonably good fit to the actual function $\nu_r(\rho)$ if the value [2. 24] is taken for x.

When ν_s/N is not small we may treat the linearized equations exactly, with discrete transformations. It may be shown, for the case of N identical accelerating gaps, that the transformation matrix[1] giving the energy and phase of a particle at the $(n+1)^{th}$ accelerating gap crossing, in terms of that at the n^{th} gap crossing is

$$\begin{vmatrix} \varphi \\ E - E_s \end{vmatrix}_{n+1} = \begin{vmatrix} 1 & \dfrac{2\pi h K}{N E} \\ \dfrac{V}{N}\cos\Phi_s & 1 - \dfrac{2\pi h K V}{N^2 E}\cos\Phi_s \end{vmatrix} \begin{vmatrix} \varphi \\ E - E_s \end{vmatrix}_n \qquad [2.25]$$

From this, we conclude in the usual way (4), using Eq. [1. 1], that there is a relationship

$$\cos\frac{2\pi\nu_o}{N} = 1 - \frac{\left(2\pi\dfrac{\nu_s}{N}\right)^2}{2} \qquad [2.26]$$

between the actual synchrotron oscillation frequency ν_o and the approximate frequency ν_s, valid

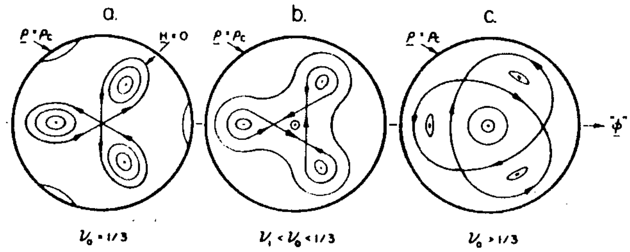

Fig. 2 - Phase trajectories in neighborhood of $\nu_o = 1/3$ resonance. Arrows show direction of motion. a) For $\nu_o = 1/3$; b) For $\nu_1 < \nu_o < 1/3$; c) Phase trajectories for $\nu_o > 1/3$.

for $\nu_s \ll 1$. Equation [2.26] is exhibited graphically as the curve in Fig. 5. This equation predicts a cuthoff frequency; for ν_s greater than N/π which corresponds to $\nu_o = N/2$), synchrotron motion is unstable.

It can further be shown that the amount of beam one may accelerate (in a fixed orbit synchrotron) becomes strongly limited before the $\nu_o = N/2$ resonance is reached, approaching zero at the resonance. If we let E_L denote the maximum energy excursion $(E - E_s)$ that is acceptable within the radial aperture of the synchrotron, (where E_L is small compared to the bucket height) then the usable phase space is confined to an ellipse for which the maximum excursion from the synchronous phase is

$$\varphi_{max} = \sqrt{\frac{2\pi h K}{E V\cos\Phi_s}}\,E_L \qquad [2.27]$$

Thea area of this ellipse (in units of energy and phase) is

$$A = \pi\sqrt{\frac{2\pi h K}{V\cos\Phi_s E}}\sqrt{1-\frac{\pi h K V\cos\Phi_s}{2N^2E}}\,E_L^2 = \qquad [2.28]$$

$$= \frac{2\pi^2\nu_s}{V\cos\Phi_s}\sqrt{1-\left(\frac{\pi\nu_s}{N}\right)^2}\,E_L^2$$

This formula, however, is modified by other resonances and nonlinear effects.

III. N^{th}-INTEGRAL RESONANCES

The equations of motion, [2. 10] and [2.11], include terms of all orders in φ, if $\tan\Phi_s \neq 0$, so one expects resonance effects whenever Eq. [1. 3] is satisfied. The m/n. resonances whith odd integers n become very strongly driven an $\Gamma \longrightarrow 1$ ($\tan\Phi_s \longrightarrow \infty$) and disappear for $\Gamma = 0$. For brevity we shall mainly examine one of the

[1] The authors are indebted to L. Smith for this approach to the problem.

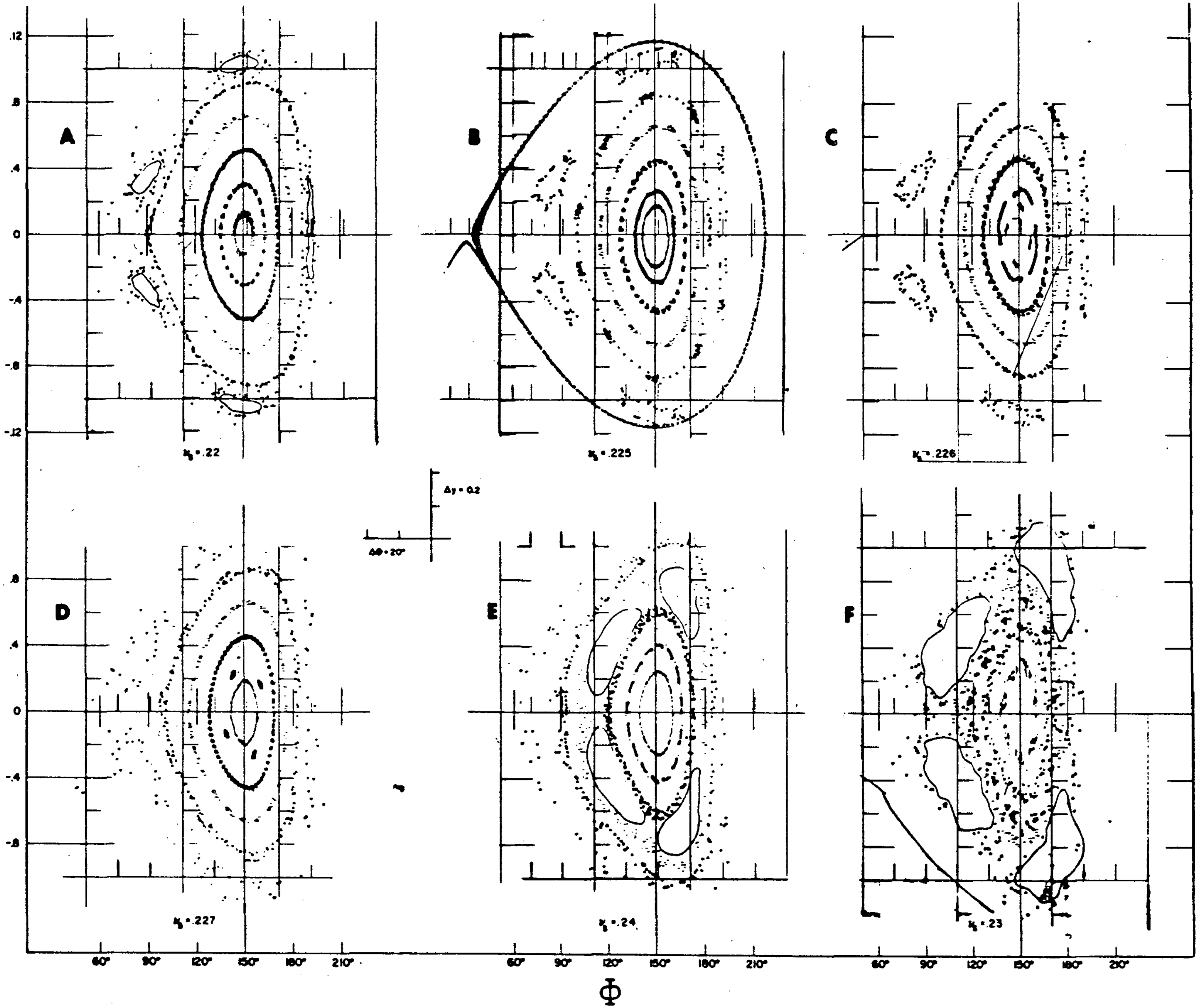

Fig. 3 - Particle trajectories in single gap accelerator in neighborhood of 1/4 and 1/5 resonances. $\Gamma = 0.5$ in all cases ($\Phi_s = 150°$). Values of ν_o represented: (a) 0.242 ($\nu_s = 0.22$); (b) 0.248 (also shown is separatrix obtained for $\nu_o = 0.01$, i.e., normal bucket shape); (c) 0.250; (d) 0.252; (e) 0.27; (f) 0.285. In this and the following figures, horizontal divisions represents ($\Delta\Phi =$) 60° each, and vertical divisions are shown at intervals of ($\Delta y =$) 0.2 ν_s each.

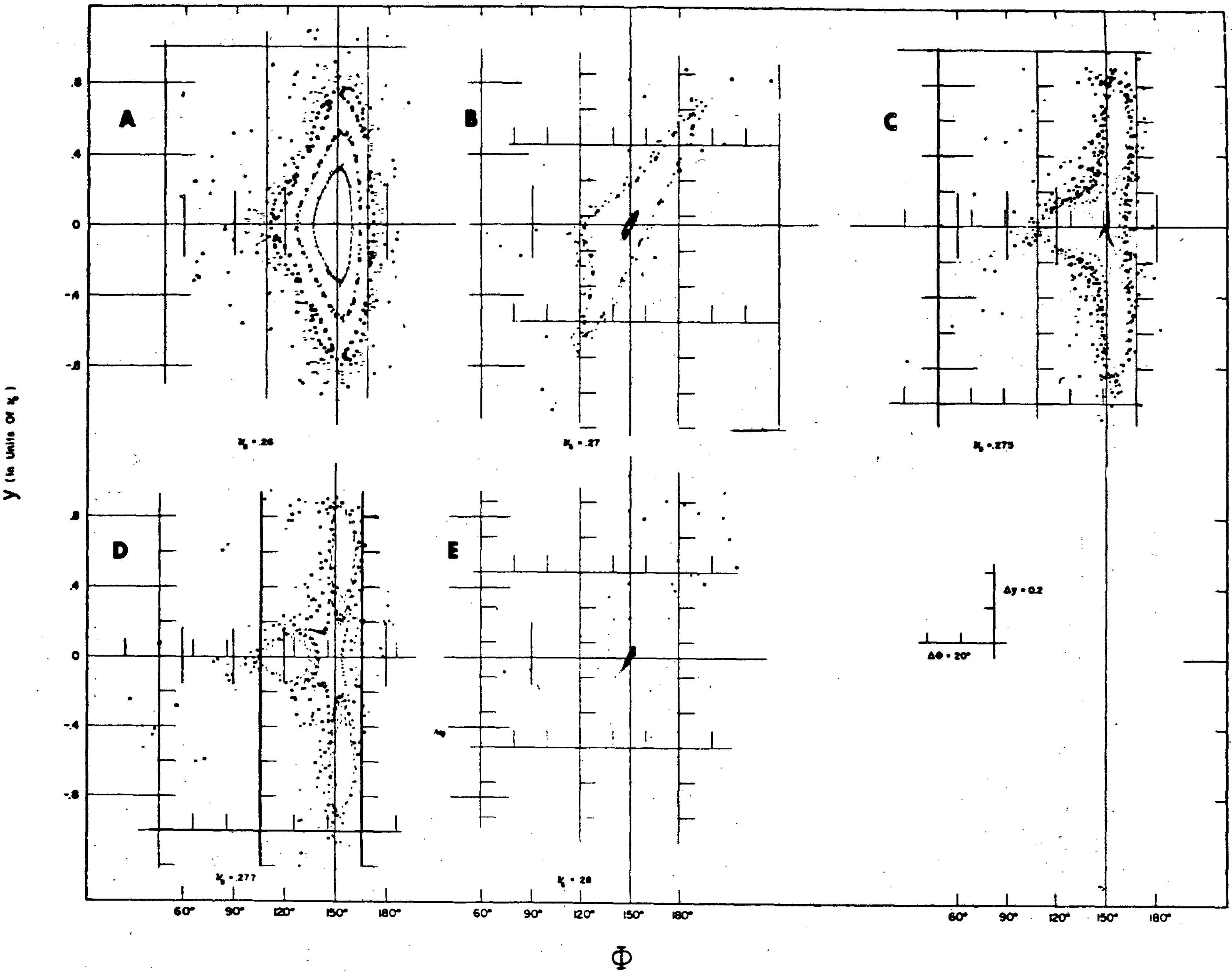

Fig. 4 - Particle trajectories near 1/3 integral resonance. (The tilt of these graps is unimportant and just corresponds to having the r.f. gap non symmetrically located with respect to the particle observation point.) Again, $\Gamma = 0.5$. Values of ν_o represented: (a) 0.305 ($\nu_s = 0.26$); (b) 0.323; (c) 0.333; (d) 0.337; (e) 0. 342.

most important resonances, $\nu = 1/3$, and just indicate important results of the other ones.[3]

Assume that all terms in the equation of motion for synchrotron oscillations have been transformed away, so the Hamiltonian is a function only of ρ, except for the $\nu_0 = 1/3$ driving term from Eq. [2.11]. This driving term

$$\left(\frac{dy}{d\tau}\right)_{\nu=1/3} = \varepsilon\nu_s^2 \tan\Phi_s\,\varphi^2\cos\tau = -\frac{\partial H_{\nu=1/3}}{\partial\varphi} \qquad [3.1]$$

may be integrated, and added to Eq. [2.23] to obtain the Hamiltonian H applicable to the resonance, namely

$$H = \frac{\nu_0\rho_c}{1+x}\left[1-\left(1-\frac{\rho}{\rho_c}\right)^{1+x}\right] + \qquad [3.2]$$
$$+\frac{\sqrt{2}}{12}\tan\Phi_s\,E\nu_0^{1/2}\rho^{3/2}\sin(3\gamma-\tau)$$

plus ignorable terms which do not drive the resonance. To eliminate the time dependence, we make a canonical transformation to a coordinate system rotating in the phase space. The generating function is

$$S = \underline{\rho}\left(\gamma - \frac{1}{3}\tau\right) \qquad [3.3]$$

so that the new variables become

$$\underline{\gamma} = \gamma - \frac{\tau}{3}, \quad \underline{\rho} = \frac{dS}{d\gamma} = \rho \quad \underline{H} = H - \frac{\underline{\rho}}{3} \qquad [3.4]$$

Curves of constant H have singular points where

$$\frac{\partial H}{\partial\underline{\gamma}} = \frac{\sqrt{2}}{4}\tan\Phi_s\,E\nu_0^{1/2}\rho^{3/2}\cos 3\underline{\gamma} = 0, \quad \frac{\partial\underline{H}}{\partial\underline{\rho}} = 0 \qquad [3.5]$$

so that

$$\underline{\gamma} = \left(n+\frac{1}{2}\right)\frac{\pi}{3}, \quad n = 0, 1 \ldots 5;$$

$$\nu_0\left(1-\frac{\rho}{\rho_c}\right)^{x} = \frac{1}{3} + \left(-1\right)^{n+1}\frac{\sqrt{2}}{8}E\tan\Phi_s\,\nu_0^{1/4}\,\underline{\rho}^{1/2} \qquad [3.6]$$

This latter equation is solved graphically in Fig. 1.

We consider first the case $\nu_0 = 1/3$, for which one solution of Eq. [3.6] is $\underline{\rho} = 0$. In this case the curve $\underline{H} = 0$ has six branches radiating from the origin at angles $\underline{\gamma} = n\pi/3$. The criterion as to whether Eq. [3.6] has another solution is (if we put $x = 1/\alpha$ for algebraic convenience).

$$|E|\nu_0\left[\frac{\Gamma^2\alpha(\Gamma)}{1-\Gamma^2}\right]^{1/2} < \frac{2\sqrt{\pi}}{3} \qquad [3.7]$$

in view of Fig. 1 and Eqs. [2.21]. Since it may be shown that $\alpha\tan^2\Phi_s \leq \Gamma/2$, the previous inequality is certainly satisfied, so there are always some stable loops for $\nu_0 = 1/3$. These are shown in Fig. 2a. The present treatment is not valid for $\underline{\rho} > \rho_c$. (Cf. Eq. [2.26] which defines ρ).

For $\nu_0 \neq 1/3$ there is stability near the origin, i.e., arbitrarily small closed orbits exist. It is evident from Fig. 1 that if ν_0 is small enough, Eq. [3.6] has no roots and the bucket is topologically normal. However, for ν_0 equal to some value ν_1, there is a double root, and for $\nu_1 < \nu_0 < 1/3$ there are two roots, leading to the trajectories shown in Fig. 2b. We may show, after some manipulation, that (again with $x = 1/\alpha$)

$$\nu_1 = \frac{1}{3}\left[1+\frac{\varepsilon^2\alpha\Gamma^2}{4\pi(1-\Gamma^2)}\right]^{-1/2} \qquad [3.8]$$

(thus ν_1 is very close to $1/3$) and that the inner separatrix encloses less than a fraction $0.04\Gamma^2$ of the normal bucket area. For $\nu_0 > 1/3$, there is one root in each branch of the equation (see Fig. 1). The phase trajectories are then as shown in Fig. 2c, with the inner separatrix occurring at a value of $\underline{\rho}$ given by $\nu_s(\rho) = 1/3$ or we now take x from Eq. [2.24]

$$\rho = \rho_c\left[1-\left(\frac{1}{3\nu_0}\right)^{\frac{\pi}{\alpha(\Gamma)}}\right] \qquad [3.9]$$

For the case of an inherent resonance (i.e., $\varepsilon = 1$) computations showed no stable orbits outside the beads (see Sec. IV) for $\nu_0 > 1/3$. Furthermore, the loops may be unstable (unless they occur at small values of $\underline{\rho}$), so that Eq. [3.9] is a crude estimate of the shrinkage of bucket size due to the third integral resonance. For $E \ll 1$, however, a small structure of 3 pearls (in a normal sized bucket) is all that is observed.

The linearized equation for the analogous function $\underline{H}$ for the half-integral resonance,

$$\underline{H} = \left(\nu_0 - \frac{1}{2} - \frac{1}{2}E\nu_0\cos 2\underline{\gamma}\right)\underline{\rho} \qquad [3.10]$$

yields stopbands, areas where curves of constant $\underline{H}$ are not closed around the origin, since the coefficient of $\underline{\rho}$ can be zero if

[3] A more detailed discussion will be given in a forthcoming paper by the present authors.

$$\frac{1}{2+|E|} < \nu_o < \frac{1}{2-|E|} \qquad [3.11]$$

If there is only one accelerating gap, $E = 1$ and the stopband extends from $\nu_s = 1/3$ * to $\nu_s = 1$. This lower limit is close to the $\nu_s = 1/\pi$ cut-off predicted by Eq. [2.26].

For the quarter-integral resonance, we can show, by similar manipulations, that no major instability occurs at or below $\nu_o = 1/4$ but that four pearls are obtained when $\nu_o > 1/4$. We solve the analogue of Eq. [3.6] in this case, but use the more accurate value of x given by Eq. [2.24] since at $\nu_o = 1/4$ both the resonant and central parts have the same ϱ dependence as $\varrho \longrightarrow 0$, making the coefficients important. The central forces dominate, as the inequality

$$\frac{1}{4} - \nu_o \left(1 - \frac{\varrho}{\rho_c}\right)^{\frac{\alpha(\Gamma)}{\pi}} > \frac{|E|\,\varrho}{24} \qquad [3.12]$$

holds at the resonance, yielding stability, or trajectories which are topologically normal (near $\rho = 0$).

IV. COMPUTATIONS: COMPARISON WITH THEORY

Some of the preceding theoretical arguments have been checked by computer calculations and the results of these will be described.

As a simplyfying device in most of these calculations, a constant energy loss dy/dt has been inserted and adjusted so that an energy boost Γ V is required to make a synchronous particle stay synchronous. Configurations of one and more than one accelerating gaps have been examined.

The Hamiltonian is time-varying, and the presence of errors in voltages or phases of r.f. gaps makes the over-all period of H equal to the orbital frequency of the synchronous particle. Particle positions have been plotted for time increments equal to this period, i.e., essentially, the position (phase) and energy have been plotted once per revolution (of the synchronous particle). Each different symbol corresponds to the « foot prints » of a given particle with different initial conditions generally selected to represent a different value of ρ.

Relevant effects of the theory which have been examined include the comparison of ν_o with ν_s, sizes of stopbands, detailed shape of the phase-space diagrams, effect of error signals on stable phase area, and behavior in the neighborhood of particular resonances. The general shape of the trajectories and structure resemble closely the shape of the predicted energy contours (Cf. Fig. 2c with Fig. 4d or 7d, for instance).

A dramatic result is the enhancement of ν_o with respect to ν_s, which leads to the stopband discussed in Sections II and III. Figure 5 shows a graph of ν_o versus ν_s obtained from the computer calculations and a comparison with values of ν_o calculated from relations [2.26]. The agreement is excellent, for cases of either 1 or 5 accelerating gaps. For the 1/4 and 1/5 integral resonances, prominent beads are observed for values ν_o above the resonance in a single gap configuration (Fig. 3). Some trace of these persists in the five-gap case (for a 10% error signal, see Fig. 7b).

One can see by comparing Fig. 3 with Fig. 4 that while the quarter-integral case does not affect stability near the center of the bucket, the 1/3 integral resonance destroys even this, as was shown in Section III.

For the case of many accelerating gaps, predicted effects are verified in Figs. 6-8, namely, stability is restored and the resonances are minimized. The following examples, unless otherwise noted, are for the case of five evenly spaced accelerating gaps. For simplicity, the gap voltages have been chosen equal for four of the gaps, and 1%, 10%, or 25% different for the fifth gap. This provides a simple example of a type of inhomogeneity which is likely to occur in an actual accelerator. Such an error signal will weakly drive the resonances experienced in a single gap machine. Then, instead of resem-

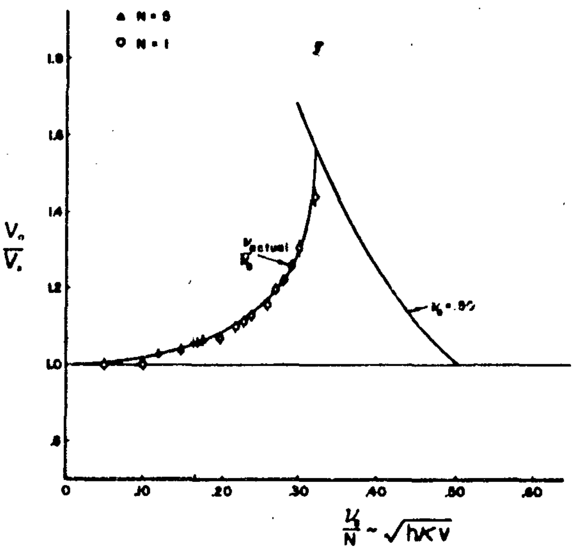

Fig. 5 - Graph of ν_o versus ν_s and comparison of computational values with theoretical approximate values derived from Eq. (2.26). N represents the number of r.f. stations.

* In this case, the most important time-dependent term ($\cos 2\gamma$) is being treated explicitly, so that one should use ν_s instead of ν_o in Eq. [3.1].

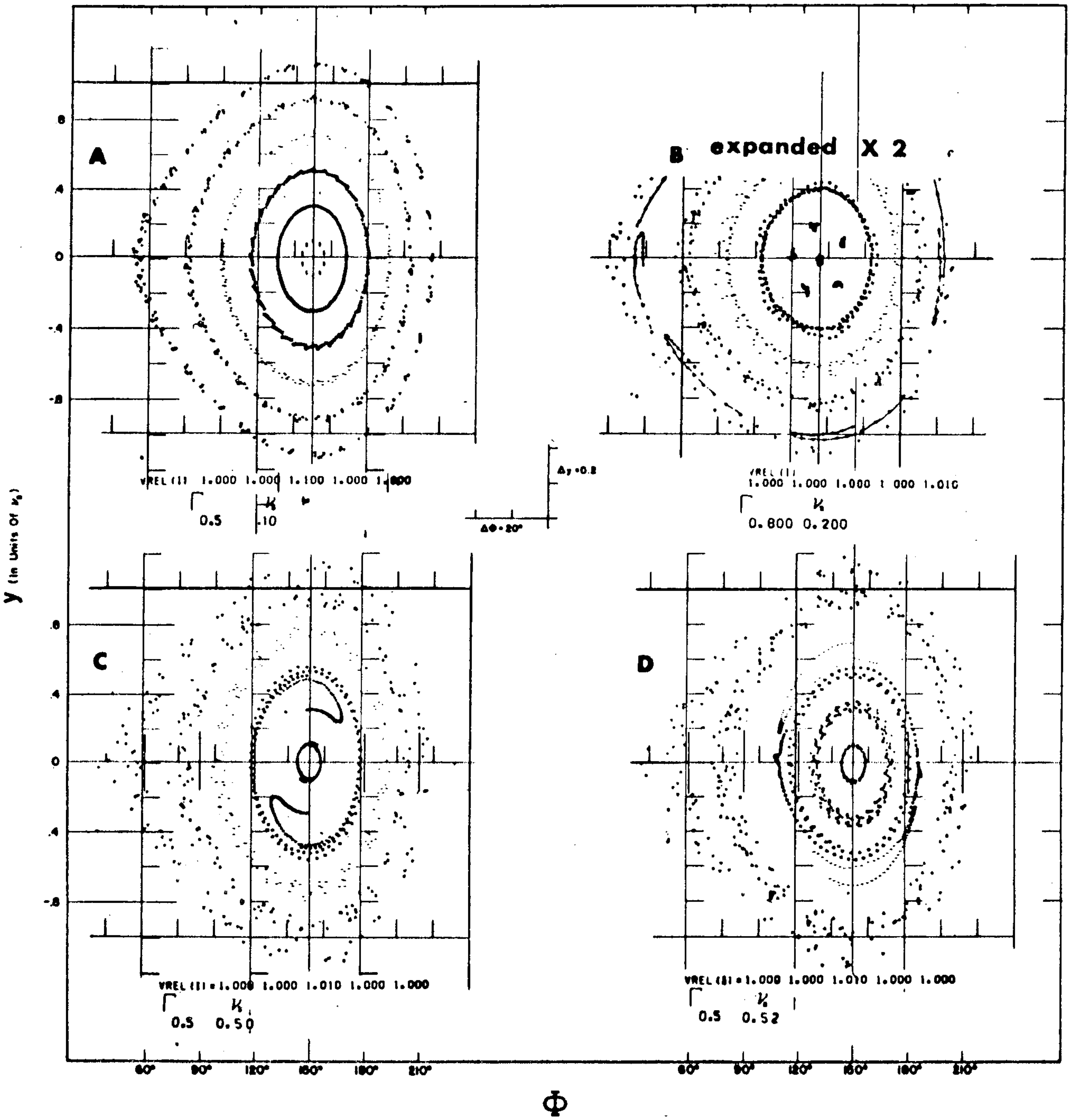

Fig. 6 - Particle paths for five accelerating gaps. In this and succeeding figures, VREL(I) denotes the relative voltages on the five gaps, located respectively at angles $(2n - 1)\ \pi/5$ relative to the measurement point.

a) $\nu_o = 0.10$ (smal ν), $\Gamma = 0.5$

b) $\nu_o = 0.201$ $\Gamma = 0.8$ ($\Phi_s = 126.8°$)

c) $\nu_o = 0.507$, 1% voltage error, $\Gamma = 0.5$

d) $\nu_o = 0.527$, 1% voltage error, $\Gamma = 0.5$

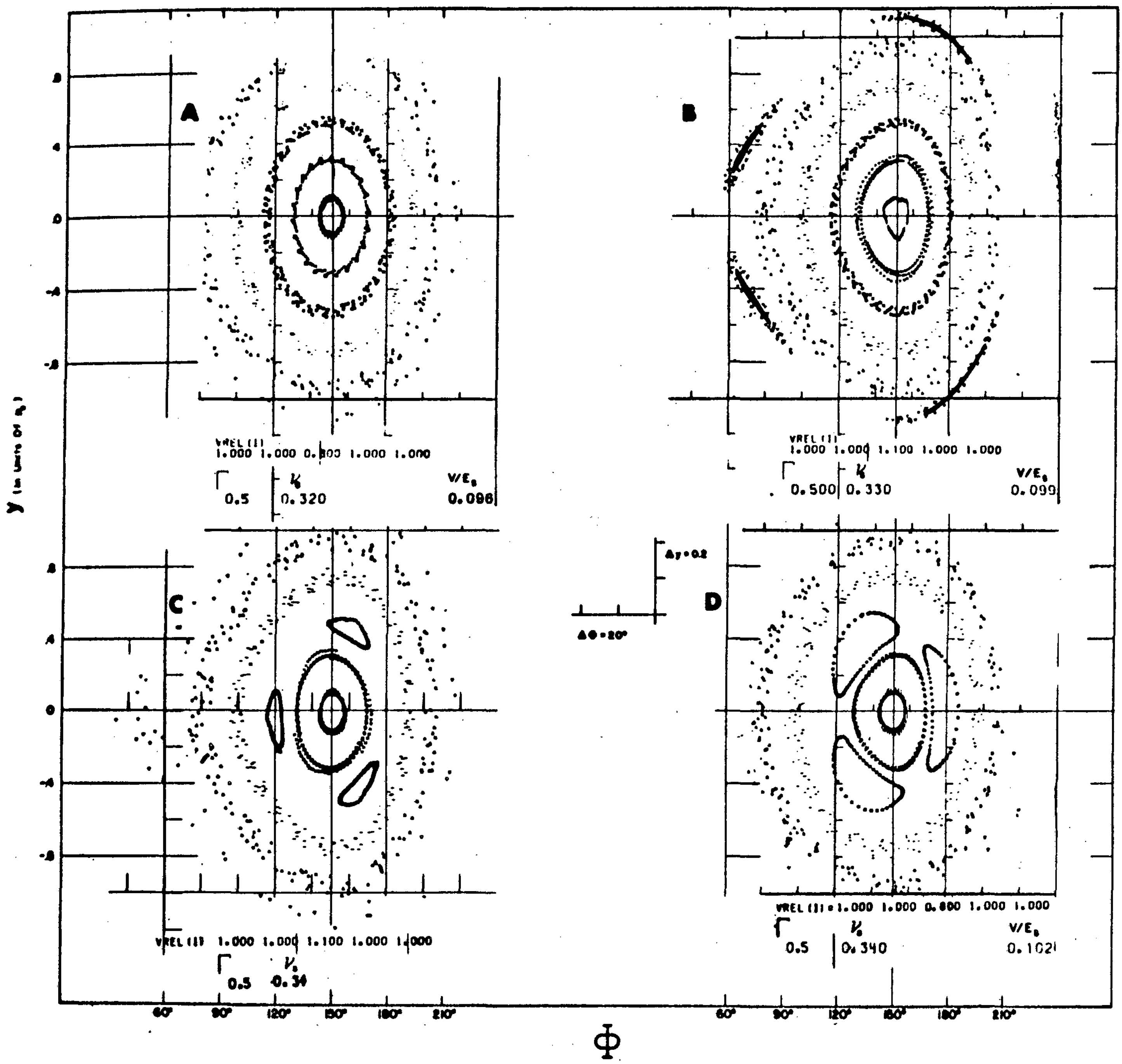

Fig. 7 - Particle trajectories for five accelerating gaps, mainly near 1/3 integral resonance. The following cases are shown, where $\nu_s \approx \nu_x$.

a) $\nu_s = 0.32$ -20% voltage error

b) $\nu_s = 0.33$ 10% voltage error

c) $\nu_s = 0.34$ 10% voltage error

d) $\nu_s = 0.34$ -20% voltage error

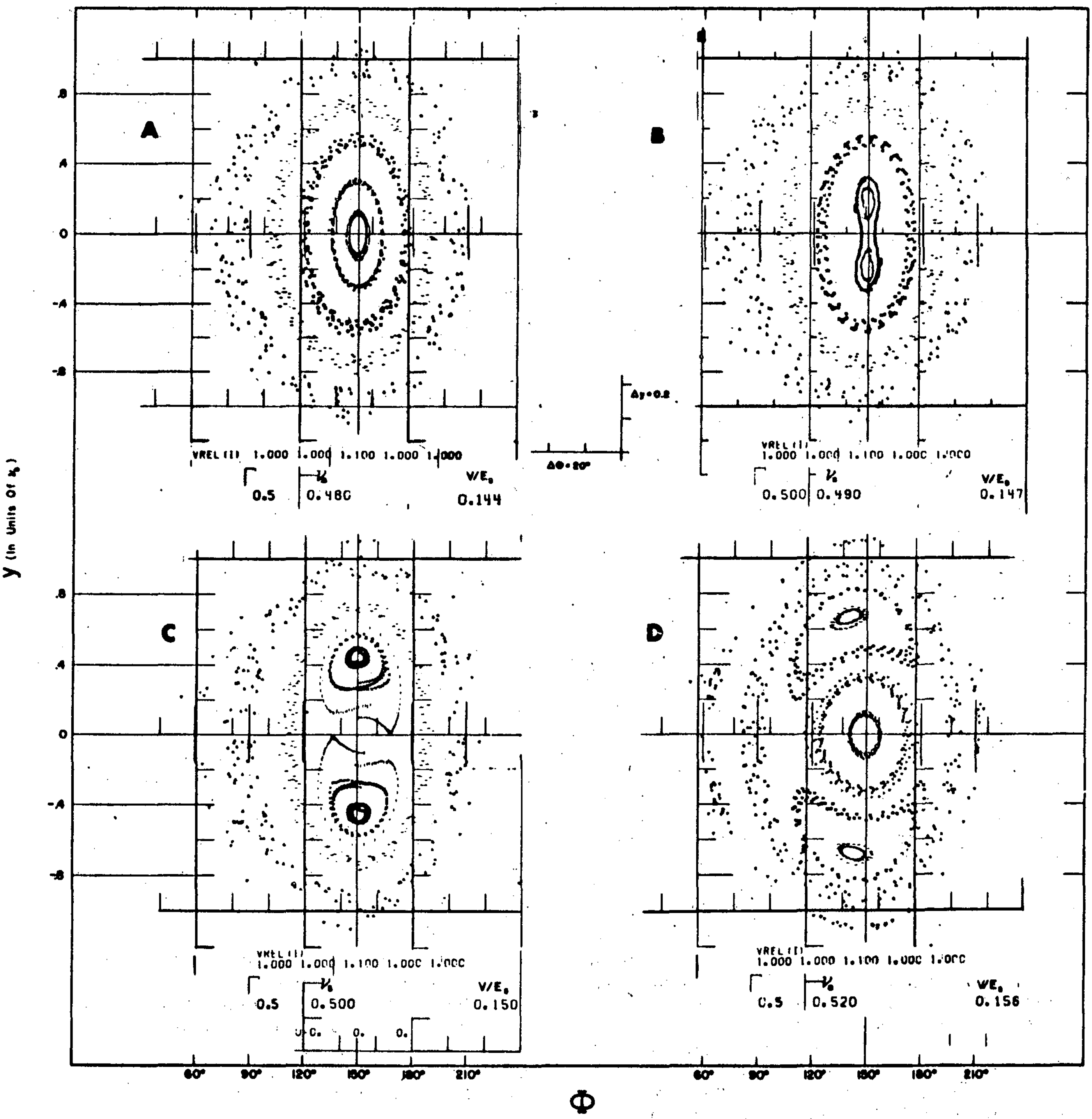

Fig. 8 - Particle trajectories for five accelerating gaps for ν_0 near half integral resonance; resonance driven by 10% voltage error. $\Gamma = 0.5$ and $\varepsilon = 0.02$ (as opposed to 0.002 in Fig. 6, parts c and d). Cases shown are: (a) $\nu_s = 0.487$ ($\nu_0 = 0.48$); (b) $\nu_s = 0.497$; (c) $\nu_0 = 0.507$; (d) $\nu_s = 0.528$.

bling the wild patterns of Fig. 4 in which the phase plot had degenerated into islands, the $^1/_3$ integral resonance no longer causes a complete breakdown of the bucket, and graphs of Fig. 7 merely show a string of (3) beads enclosing a stable area. These three stable beads observed here are quite similar, for instance, to the five stable beads which are observed in Fig. 3a with one accelerating gap. Computer runs with a suppressed voltage on one of four gaps ($E \approx 0.0$ to -0.25, $N. = 4$) have shown that the $^1/_3$ integral resonance could cause a reduced region of stability, even as an error signal. For $|E| \leqslant 0.1$, stable motion only occurred for values of ρ smaller than that at which $\nu_s(\rho) = {}^1/_3$. The $\nu_o = {}^1/_4$ resonance, however, had little effect when driven by an error signal of this magnitude.

We have also investigated the reduced stopband predicted in Eq. [3.11] when the $^1/_2$ integral resonance is driven by an error signal (in this case $\varepsilon = 0.02$). This is shown in Fig. 8, where first-order stability (stability at $\rho = 0$) is observed for $\nu_s = 0.487$ (but with vertically elongated ellipses) and 0.527 but not for $\nu_o = 0.497$ or 0.507. For the calculations shown in Figs. 8a-d, $\delta V = 10\%$ and $E = 0.02$, and as expected, the stopband (for which small oscillations about the origin are unstable) extends from $\nu_o = 0.49$ to 0.51.

One phenomenon which seems common to the $\nu_s = {}^1/_2$, $^1/_3$, and $^1/_4$ resonances is that the effect of an instability near the outside of a nominal bucket appears much more dramatic than the effects when the instability is near the center. Thus the major bucket perturbations are seen when ν_o is greater than $^1/_4$, $^1/_3$, or $^1/_2$ at the center of the "bucket". An investigation of $\nu_s(\rho)$ versus ρ gave reasonably good agreement with predictions of Eqs. [2.22] and [2.24]. In particular, for $\Gamma = 0.5$, the prediction is $x = 0.11$, and the computations verified this slow rate of decline of frequency with oscillation amplitude.

A search for the (outermost) separatrix as a function of voltage errors on the accelerating gaps (calculated for the case of four accelerating gaps) has shown that large errors may reduce the stable area considerably.

A value of $K = -0.03$ has been used in most of the computer calculations. These calculations have been carried out on an IBM 704 computer, employing eight decimal digits of accuracy, and the scatter in the experimental points is believed to be due to this. Preliminary results with "double precision" computation (16 digit accuracy) showed smooth curves for the trajectories, but otherwise little change in the structure.

V. CONCLUSIONS

We conclude from the above results that in accelerators with a single accelerating gap, or with unsymmetrically placed gaps, the resonance $\nu_o = {}^1/_2$ must be avoided. The resonance $\nu_o = {}^1/_3$ should probably also be avoided, although in certain cases it may be possible to accelerate through this resonance. In applying these considerations, it is important to remember that the true synchrotron frequency ν_o can be considerably greater than the value ν_s given by the usual formula [1.1] when $\nu_s \gtrsim 0.2$.

With symmetrically placed accelerating gaps, these resonances may be made relatively harmless, provided the voltage and phase errors are not too large. The resonant beads produced by r.f. errors are small and disappear at values of ν_o at or slightly below the resonance in each case. Since ν_o generally decreases during acceleration, the beads will move in toward the synchronous point as the resonance is approached, then shrink and disappear. Beads near the bucket boundary can result in instabilities which reduce the stable bucket area. If however the r.f. phase trajectories at injection are stable in the region occupied by the injected particles, and if there are no resonant beads outside this region, then no difficulty due to imperfection resonances may be expected during acceleration. This conclusion may not hold, however, if the injected particles cover only a small ellipse at the center of the bucket. In that case, as a resonance is crossed, the bounding ellipse is distorted, and its energy dimension may be considerably increased, as discussed at the end of Section II. Furthermore, the resonant beads, as they move into the bucket center, will bring with them empty phase space which becomes mixed with the phase space occupied by particles; the phase area containing the accelerated particles will therefore be increased after the resonance is crossed, by the area of the resonant beads.

REFERENCES

(1) K. R. Symon and A. M. Sessler: Proc. Symp. on High Energy Accelerators Geneve, 1956, Vol. 1, p. 44.
(2) J. Moser: Nachr. Aakd. Wiss. Göttingen, Math-Physik Kl. *IIa, 6,* 87 (1955).
(3) Geo. Birkhoff: Dynamical Systems, Amer. Math. Soc. Colloquium Publications (Amer. Math. Soc., New. York, 1927), Vol. IX, Chapter 3.
(4) E. D. Courant and H. S. Snyder, Ann. Phys. 3, 1 (1958).

DISCUSSION

PENTZ: You have explained the effect described in terms of the picture of two buckets, corresponding to two harmonic members of the radio-frequency acceleration differing by unity (h, h$\pm$1), which may overlap. Is it correct, then, that the effect will occur when the bucket height is large enough for such overlap to occur?

SYMON: Yes.

PENTZ: Could one then study the effect experimentally by using two accelerating gaps separately programmed so as to locate two buckets at energy separations comparable to the buckets heights?

SYMON: Yes, this would be approximatively equivalent situation to that which would exit in the case of acceleration at high harmonic number.

KOLOMENSKY: In your paper you have considered one-dimensional (longitudinal) motion. I think that the two-dimensional character of motion (i.e. coupling with the radial betatron oscillation) would be taken into account particularly in the case of large number of accelerating stations?

SYMON: Yes, I agree.

Reprinted from THE PHYSICAL REVIEW, Vol. 103, No. 6, 1837–1859, September 15, 1956
Printed in U. S. A.

Fixed-Field Alternating-Gradient Particle Accelerators*

K. R. SYMON,† D. W. KERST,‡ L. W. JONES,§ L. J. LASLETT,‖ AND K. M. TERWILLIGER§
Midwestern Universities Research Association
(Received June 6, 1956)

It is possible, by using alternating-gradient focusing, to design circular accelerators with magnetic guide fields which are constant in time, and which can accommodate stable orbits at all energies from injection to output energy. Such accelerators are in some respects simpler to construct and operate, and moreover, they show promise of greater output currents than conventional synchrotrons and synchrocyclotrons. Two important types of magnetic field patterns are described, the radial-sector and spiral-sector patterns, the former being easier to understand and simpler to construct, the latter resulting in a much smaller accelerator for a given energy. A theory of orbits in fixed-field alternating-gradient accelerators has been worked out in linear approximation, which yields approximate general relationships between machine parameters, as well as more accurate formulas which can be used for design purposes. There are promising applications of these principles to the design of fixed-field synchrotrons, betatrons, and high-energy cyclotrons.

INTRODUCTION

ALTERNATING–GRADIENT (AG) focusing[1] provides a high degree of stability for both radial and vertical modes of betatron oscillations in circular particle accelerators. This stability makes possible the construction of many kinds of circular accelerators with magnetic guide fields which are constant in time, called fixed-field alternating-gradient (hereafter FFAG) accelerators. These machines contain stable equilibrium orbits for all particles from the injection energy to the output energy. These orbits may all be in an annular ring, as in a synchrotron or betatron; the magnetic field must then change rapidly with radius to provide orbits for the different energy particles. If the guide field gradient is made independent of azimuth, one of the modes of betatron oscillation is clearly unstable. Application of alternating-gradient focusing, however, can keep both modes of betatron oscillation stable even with the rapid radial change of magnetic field. Circular particle accelerators can be classified into four groups according to the type of guide field they use: fixed-field constant-gradient (conventional cyclotrons, synchrocyclotrons, and microtrons), pulsed-field constant-gradient (weak-focusing synchrotrons and betatrons), pulsed-field alternating-gradient (AG synchrotrons), and fixed-field alternating-gradient (FFAG synchrotrons, betatrons, and cyclotrons).

Two types of FFAG design appear the most practical. The radial-sector type[2] achieves AG focusing by having the fields in the successive focusing and defocusing magnets vary in the same way with radius but with alternating signs (or in certain cases alternating magnitudes). Since the orbit in the reverse field magnet bends away from the center, the machine is considerably larger than a conventional AG machine[1] of the same energy having an equal-peak magnetic field. This serious disadvantage is largely overcome in the spiral-sector type[3] in which the magnetic field consists of a radially increasing azimuthally independent field on which is superimposed a radially increasing azimuthally periodic field. The ridges (maxima) and troughs (minima) of the periodic field spiral outward at a small angle to the orbit. The radial separation between ridges is small compared to the radial aperture. The particle, crossing the field ridges at a small angle, experiences alternating-gradient focusing. Since the fields need not be reversed anywhere, the circumference of this machine can be comparable to that of an equivalent conventional AG machine.

FFAG synchrotrons have a number of important advantages over conventional synchrotrons. A major one is beam intensity. Since the magnetic field is time-independent in an FFAG synchrotron, the beam pulse rate is determined only by the repetition rate of the radio-frequency modulation cycle. In a conventional synchrotron, the beam pulse rate is limited by the time to complete the pulsed magnetic field cycle. It is reasonable to assume that frequency-modulation repetition rates can be made considerably higher than field recycling rates. Another reason for high beam intensity is the large injection aperture possible in the FFAG designs (larger for the radial sector than for the spiral sector). Other advantages of the FFAG synchrotron are engineering and maintenance simplifications. The direct-current magnet power supply is simpler and cheaper to construct and to maintain than a pulsed supply. The magnets do not have to be laminated, there are no eddy current problems, and remanent field and saturation difficulties are less serious than in pulsed-field

* Supported by National Science Foundation.
† University of Wisconsin, Madison, Wisconsin.
‡ University of Illinois, Champaign, Illinois.
§ University of Michigan and Michigan Memorial Phoenix Project, Ann Arbor, Michigan.
‖ Iowa State College Institute for Atomic Research, Ames, Iowa.
[1] Courant, Livingston, and Snyder, Phys. Rev. 88, 1190 (1952).
[2] K. R. Symon, Phys. Rev. 98, 1152(A) (1955). This structure was also suggested independently earlier by T. Ohkawa, University of Tokyo, Tokyo, Japan at a Symposium on Nuclear Physics of the Physical Society of Japan in October, 1953 (private communication), and independently by H. Snyder at Brookhaven National Laboratory.
[3] Suggested by D. W. Kerst [Kerst, Terwilliger, Jones, and Symon, Phys. Rev. 98, 1153(A) (1955)].

accelerators. All field trimming is time independent. The necessity for accurate tracking of the rf accelerating voltage with a pulsed magnetic field is eliminated, with a resulting greater freedom and ease in design of the rf system. Injection should be possible at a lower energy than is contemplated for a conventional synchrotron, because of the fewer low-field problems and the easier frequency-modulation program and the possibility of large apertures at the injection radius; the complexity of the injection system will then be decreased. Disadvantages of the FFAG synchrotron are the large increase in circumference for the radial-sector type (at least a factor of three) and the increase in complexity of the magnetic fields, particularly for the spiral-sector machine.

Fixed-field betatrons have potentially a much higher intensity than conventional betatrons.[4] The beam can be injected for a considerable fraction of a cycle, if extra accelerating flux is available, rather than the few tenths of a microsecond presently possible. The only beam current limitation appears to be space charge at injection, and this may be decreased by such techniques as high-voltage injection. An FFAG betatron has no problems of tracking a pulsed guide field with the accelerating flux, and also has other engineering simplifications mentioned in the synchrotron case.

Application of the FFAG principle to a cyclotron allows the radial dependence of the magnetic field to be such as to keep the particle revolution rate constant, independent of energy even in the relativistic region. Present high-energy cyclotrons must be frequency-modulated to compensate for the relativistic increase of mass. A constant-frequency cyclotron should increase the beam output by two orders of magnitude. A radial-sector cyclotron, in which the field alternates between high and low values, was first suggested by Thomas.[5] The spiral-sector design seems even more advantageous for application to the cyclotron.

In Part I of this paper we discuss the radial- and spiral-sector types of FFAG accelerator in detail. In Part II the theory of particle trajectories in FFAG machines is developed. Part III contains a description of a 10-Bev radial-sector synchrotron, a 20-Bev spiral-sector synchrotron, and FFAG betatrons and cyclotrons.

I. TYPES OF FFAG DESIGN

1. Radial-Sector Type

Circular particle accelerators with radial sectors can be built with the high-energy orbits at the outer edge of the machine and the injection orbits at the inside edge, or vice versa. This discussion assumes that the highest energy orbits are at the outside edge. (We will refer specifically to FFAG synchrotrons, but most of our comments will apply also to betatrons and cyclotrons.) In radial-sector design the magnet structure consists of N-identical sectors, each composed of a focusing magnet and a defocusing magnet. The magnet which is focusing for radial oscillations is of course defocusing for vertical oscillations and vice versa. The azimuthal boundaries of the magnets are on radii from the machine center (hence the name). The magnetic field direction in one magnet of a sector is opposite to that of the other, while the radial dependence of the field is the same in both. The field in the median plane at any azimuth is

$$H\sim(r/r_0)^k, \tag{1.1}$$

where r is the distance from the machine center to the equilibrium orbit and k is a constant for the machine. Figure 1 shows this type of field pattern. This field shape requires that orbits for different energy particles be similar, i.e., photographic images of each other. Ideally, the field along a closed equilibrium orbit is constant through each magnet, and the path is composed of arcs of circles. This ideal orbit cannot be attained because of the impossibility of a sharp field boundary. However, if we assume the ideal situation, a particularly simple case occurs if the fields for a given energy orbit have the same magnitude in the positive- and negative-field magnets. Equilibrium orbits for this case are shown in Fig. 2.

It is evident that particles deviating from the equilibrium orbit experience AG focusing. The numbers of radial and vertical betatron oscillations around the machine, ν_x and ν_z, are determined by k and the magnet lengths. Both ν_x and ν_z are constant for all energies.

It is desirable to make the negative-field magnets as short as possible, to keep the radius of the machine small; the minimum length of the negative-field magnet is of course determined by the necessity for preserving stability of the vertical betatron oscillations. Some vertical focusing and radial defocusing occur because the orbits are scalloped and do not cross the magnet edges at right angles. In machines in which the number of sectors is large and the effects of orbit scalloping small, the negative-field magnet can be made no shorter than about $\frac{2}{3}$ of the positive-field magnet if we wish to preserve vertical stability. This means that, neglecting

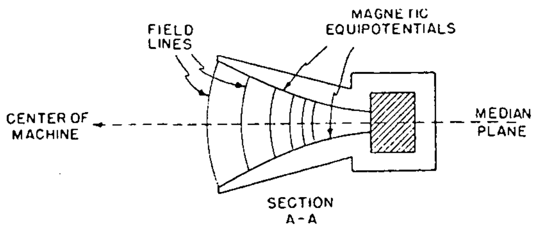

FIG. 1. Vertical section through positive or negative radial-sector magnets.

[4] Terwilliger, Jones, Kerst, and Symon, Phys. Rev. 98, 1153(A) (1955). This had been pointed out independently by G. Miyamoto, Tokyo University, Tokyo, Japan, at a meeting of the Physical Society of Japan in April, 1952 (private communication).

[5] L. H. Thomas, Phys. Rev. 54, 580, 588 (1938).

straight sections, the circumference of the machine is five times that which would be necessary if there were no negative-field magnets. The ratio (in this case, five) between the actual orbit circumference and the circumference of a circle whose radius is the minimum radius of curvature, we call the circumference factor. The fixed magnetic field in an FFAG machine can be made considerably larger than the pulsed field of a conventional accelerator, so a machine of the radial-sector type might actually be about three times the size of a pulsed-field AG accelerator of the same energy. It is also desirable to make the radial extent of the magnets as small as possible, which requires a high field gradient. The allowable gradient is determined by the effect of magnet misalignments. Reasonable values indicate a minimum radial aperture of about 2% of the radius of the machine.

2. Spiral-Sector Type

The spiral-sector design of FFAG accelerator has the high-energy orbits at the outside edge of the machine. It is not practical to have the high-energy orbits on the inside and to inject at the outside edge, because stability of the radial oscillations becomes virtually impossible to achieve.

The guide field on the median plane, if there are no straight sections, is given by

$$H=H_0(r/r_0)^k\{1+f\cos[N\theta-N\tan\zeta\ln(r/r_0)]\}, \quad (2.1)$$

where r is again the distance from the center of the machine; k, the mean field index; θ, the azimuthal angle, also measured from the center of the machine; f, the flutter factor (the fraction of field variation); N, the number of sectors (periods of the field variation) around the machine; and ζ is the spiral angle between the locus of the field maximum and the radius.

Figure 3 shows how the ridges and troughs of the periodic field spiral toward the outside of the machine and indicates the equilibrium orbits for this design. The equilibrium orbits are all similar figures, whose linear dimensions are proportional to the radius, but their

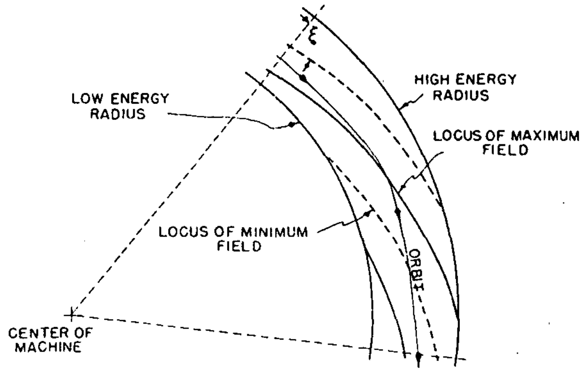

FIG. 3. Spiral-sector configuration.

positions rotate with radius due to the spiraling periodic field. Figure 4 is a plot of the radial dependence of the median-plane magnetic field. A particle going around the machine experiences a gradient first of one sign then of the opposite sign as it crosses the periodic field ridges and troughs at a small angle, so there is AG focusing of the betatron oscillations. The negative gradient is less than the positive gradient, due to the radial increase of field. This is somewhat compensated by the scalloping of the orbits, which causes the particle to experience a longer path in the negative gradient and a shorter path in the positive gradient than if it moved on a circle. The strength of betatron focusing depends on the rate of radial increase of the field, the flutter factor, and the spiral angle.

The minimum size of radial aperture is limited primarily by the difficulty of achieving strong AG focusing with a periodic field while requiring a given vertical aperture. If we restrict ourselves to a sinusoidal variation of field, a flutter factor of $f=\frac{1}{4}$ gives the largest vertical gap for a fixed strength of focusing when iron magnet poles are used without distributed back windings and forward windings. This small flutter factor means that the machine has a circumference factor (in this case, $1+f$), close to unity, so the radius of an FFAG spiral-sector synchrotron is about the same as that of an equivalent-energy conventional synchrotron. The minimum radial aperture for reasonable parameters is about 3% of the radius.

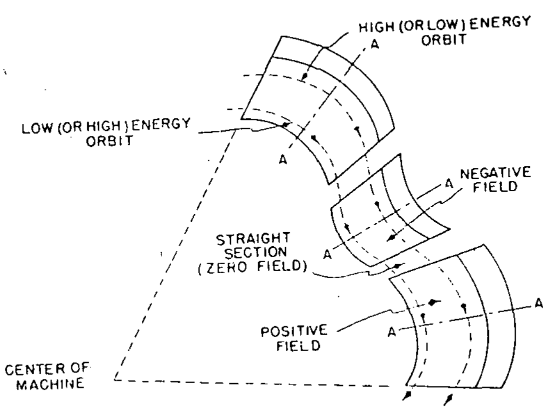

FIG. 2. Plan view of radial-sector magnets.

3. Other FFAG Types

Both the radial-sector and spiral-sector designs discussed above have equilibrium orbits of constant shape scaled in proportion to the orbit radius. There are many modifications of these designs. Some differ only in that the fields are not the square-wave type used in the radial-sector design described or the sinusoidal shape used in the spiral-sector design. Changes of this kind will not affect the constancy of shape of the equilibrium orbits and will modify other machine characteristics only slightly. There are other variations of these designs which preserve betatron oscillation

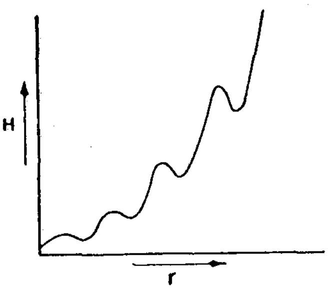

FIG. 4. Radial dependence of the axial magnetic field in the median plane.

stability, hold ν_x and ν_z constant, but do not retain the property of similarity of equilibrium orbits. The magnet edges of focusing and defocusing sectors can be made nonradial, and the fields in the positive- and negative-field magnets made different functions of radius; (the negative-field magnet can even be designed to have zero field). The magnet edges, radial or nonradial, can be tipped in the same direction, approaching the spiral-sector design. It is conceivable, using back windings, to transform from a spiral sector at the outside edge of the machine, with a small circumference factor where it is needed, to radial sector at the inside edge, with a large vertical aperture for injection. Such a design would have the advantages of both types with, however, a considerable increase in magnet complexity.

Another modification is the spiral-sector constant-frequency cyclotron. In this machine, the frequency of revolution of the particles can be made independent of energy even at relativistic energies, but the orbits in this case do not scale, and the number of betatron oscillations, ν_x and ν_z, cannot easily be kept constant.

II. ORBIT THEORY

4. Geometry of the Equilibrium Orbits

In order to develop a theory of orbit stability applicable to FFAG accelerators generally, it is convenient to characterize a particular accelerator by specifying its equilibrium orbits. We will therefore assume that a set of closed equilibrium orbits lying in the median plane is given. If instead, the magnetic field pattern is specified, the equilibrium orbits must be found by integrating the equations of motion.

The geometrical properties of each orbit, and the relations between orbits, will be periodic in the azimuthal angle θ with period $2\pi/N$. Each orbit is to be specified by its equivalent radius R defined by

$$S=2\pi R, \tag{4.1}$$

where S is the length of the orbit. In general, R will be slightly larger than the mean radius $\langle r\rangle_{\text{Av}}$. We define an azimuthal coordinate Θ by the equation

$$s=\Theta R, \tag{4.2}$$

where s is the distance measured along the orbit from some reference point (say at azimuthal angle θ_0). We shall require that the orbit be perpendicular to the radius from the center of the machine at the reference point, and that the reference points lie along a continuous curve. The parameter Θ will be equal to the azimuthal angle $\theta-\theta_0$ plus a small periodic function with period $2\pi/N$.

Each orbit will now be specified by a periodic parameter $\mu(\Theta,R)$ defined by

$$\mu(\Theta,R)=R/\rho(\Theta,R), \tag{4.3}$$

where ρ is the radius of curvature. Specification of $\mu(\Theta,R)$, together with the requirement that the center of the orbit lie at the origin in the median plane, completely determines the orbit R, provided the reference point $\Theta=0$ is specified. For our purposes, it will be sufficient to specify the angle $\zeta(R)$ between the radius from the origin and the reference curve $\Theta=0$ where it crosses the orbit R (Fig. 5). Choice of the parameter $\mu(\Theta,R)$ is restricted by the requirement that it be periodic in Θ with period $2\pi/N$ and mean value

$$\langle\mu\rangle_{\text{Av}}=\frac{1}{2\pi}\int_0^{2\pi}\mu d\Theta=\frac{1}{2\pi}\int_0^S\frac{ds}{\rho}=1. \tag{4.4}$$

The function $\mu(\Theta,R)$ is also restricted by the requirement that at the point $\Theta=0$ the orbit R must be perpendicular to the radius from the origin. This requirement leads to a rather complicated analytical restriction on the function μ. It is sufficient if $\Theta=0$ is a point of symmetry of the orbit, i.e.,

$$\mu(-\Theta,R)=\mu(\Theta,R). \tag{4.5}$$

If there are no points of symmetry, it is necessary to construct the orbit in order to locate properly the reference point $\Theta=0$. Fortunately, an error in properly locating the reference point will produce only a very small error (of order $1/N^2$) in the equations for the betatron oscillations, provided the angle ζ is correctly specified.

We will need also parameters $\eta(\Theta,R)$ and $\epsilon(\Theta,R)$ relating the perpendicular distance dx between two nearby orbits, and the increment $d\Theta$ in Θ along an orthogonal trajectory to the orbits, to the increment

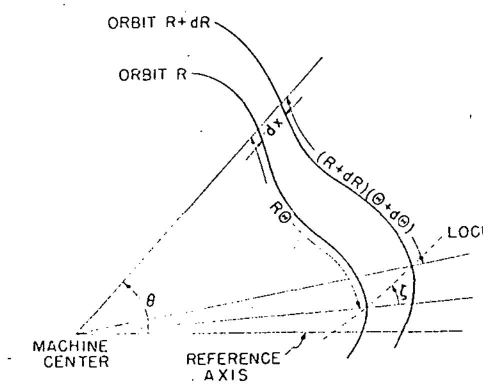

FIG. 5. Equilibrium orbit notation.

dR in the parameter R (see Fig. 5)

$$dx=\eta dR, \tag{4.6}$$

$$d\Theta=\epsilon dR/R. \tag{4.7}$$

It can be shown[6] that η, ϵ satisfy the differential equations

$$\frac{\partial\epsilon}{\partial\Theta}=\mu\eta-1, \tag{4.8}$$

$$\frac{\partial\eta}{\partial\Theta}=-\mu\epsilon-\int R\frac{\partial\mu}{\partial R}d\Theta, \tag{4.9}$$

where the three constants of integration are to be chosen so that ϵ and η are periodic functions of Θ [i.e., so that the right-hand members of Eqs. (4.8) and (4.9) have zero mean values], and so that

$$[\epsilon/\eta]_{\Theta=0}=\tan\zeta. \tag{4.10}$$

If all equilibrium orbits are geometrically similar, the parameter μ depends only on Θ and not on R. In the interest of simplicity, we will usually restrict our attention to machines of this type. If in addition, ζ is independent of R, then by Eqs. (4.8)–(4.10), the parameters η and ϵ will be independent of R. In this case, we will say that the equilibrium orbits *scale*; the equilibrium orbits scale if any set of neighboring orbits can be obtained by photographic enlargement or reduction from a set of orbits in the neighborhood of any other orbit.

The solution of Eqs. (4.8) and (4.9) may be obtained by successive approximations. Let us set

$$\mu=1+fg(N\Theta), \tag{4.11}$$

where $g(N\Theta)$ has period 2π in $N\Theta$, has mean value zero, and is normalized so that its mean square is $\frac{1}{2}$; f is the flutter factor. Since the right members of Eqs. (4.8) and (4.9) have period $2\pi/N$ (and zero mean), they contribute to η and ϵ oscillatory terms of order $1/N$. The integral in Eq. (4.9) is constant, if we assume that μ is independent of R; it will in any case contribute only very small oscillatory terms unless μ changes appreciably within a very small fractional increase in radius. The quantity $\tan\zeta$ is zero in radial-sector FFAG machines, but is of order N in spiral-sector FFAG machines. We therefore write as a zero-order approximation to η and ϵ the constant values

$$\eta\doteq1,\quad \epsilon\doteq\tan\zeta, \tag{4.12}$$

which satisfy the conditions imposed on ϵ and η.

If $F(\xi)$ is any periodic function of ξ with period 2π, it is convenient to introduce the notations

$$\langle F\rangle_{\mathrm{Av}}=\frac{1}{2\pi}\int_0^{2\pi}F(\xi)d\xi, \tag{4.13}$$

$$\{F\}=F(\xi)-\langle F\rangle_{\mathrm{Av}}, \tag{4.14}$$

$$F'=dF/d\xi, \tag{4.15}$$

$$F_1=\int\{F\}d\xi, \tag{4.16}$$

$$F_{n+1}=\int F_n d\xi, \tag{4.17}$$

where the integration constants in the last two equations are to be chosen so that F_n has mean value zero. All the functions defined by Eqs. (4.14)–(4.17) have period 2π and mean value zero.

We now substitute Eqs. (4.11) and (4.12) in (4.8) and (4.9) and integrate again to get a first approximation

$$\eta\doteq1-\frac{f\tan\zeta}{N}g_1(N\Theta), \tag{4.18}$$

$$\epsilon\doteq\tan\zeta-\frac{fg_1(0)}{N}\sec^2\zeta+\frac{f}{N}g_1(N\Theta), \tag{4.19}$$

where the integration constants have been chosen as required. [Note that

$$\langle g_1g\rangle_{\mathrm{Av}}=\frac{1}{2\pi}\int_0^{2\pi}g_1dg_1=0, \tag{4.20}$$

and that if $g(\xi)$ is even, then $g_1(\xi)$ is odd, and $g_1(0)=0$. In any case, $g_1(0)$ is ordinarily small.]

A second approximation may be obtained by substituting η, ϵ from Eqs. (4.18) and (4.19) in the right members of Eqs. (4.8) and (4.9) and integrating again. Each successive iteration yields terms of order $1/N^2$ and f^2/N^2 times the preceding terms.

5. Betatron Oscillations

If a particle of momentum p moves in an equilibrium orbit R, then we have by Eq. (4.3)

$$pc=eH\rho=eHR/\mu, \tag{5.1}$$

where H is the magnitude of the magnetic field, so that

$$H(\Theta,R)=(pc/eR)\mu(\Theta,R). \tag{5.2}$$

The magnetic field is thus given in terms of the coordinates R and Θ.

If we differentiate Eq. (5.1) with respect to x, where x is measured perpendicular to the orbit, we have

$$H\frac{\partial\rho}{\partial x}+\rho\frac{\partial H}{\partial x}=\frac{c}{e}\frac{\partial p}{\partial x}. \tag{5.3}$$

[6] K. R. Symon, Midwestern Universities Research Association report, MURA-KRS-8 (unpublished). A more elegant derivation has been given by B. Hamermesh and E. A. Crosbie [Argonne Accelerator Group, Progress Report No. 7, July 13, 1955 (unpublished)].

The field index is therefore

$$n=-\left(\frac{\rho}{H}\right)\frac{\partial H}{\partial x}$$

$$=\frac{\partial \rho}{\partial x}-\rho\frac{\partial \ln p}{\partial x}. \tag{5.4}$$

Making use of Eqs. (4.3), (4.6), and (4.7), we find

$$n=-\frac{1}{\eta\mu^2}\left[k\mu+\epsilon\frac{\partial\mu}{\partial\Theta}+R\frac{\partial\mu}{\partial R}\right], \tag{5.5}$$

where k is a parameter which measures the momentum compaction:

$$k=R\frac{d\ln p}{dR}-1. \tag{5.6}$$

In terms of the mean magnetic field $\bar{H}=pc/eR$, we can write k also as a mean field index:

$$k=\left(\frac{R}{\bar{H}}\right)\frac{d\bar{H}}{dR}. \tag{5.7}$$

The linearized equations for betatron oscillations about an equilibrium orbit are[7]

$$\frac{d^2x}{ds^2}+\frac{1-n}{\rho^2}x=0, \tag{5.8}$$

$$\frac{d^2z}{ds^2}+\frac{n}{\rho^2}z=0, \tag{5.9}$$

where x and z are the deviations from the equilibrium orbit in the radial and vertical directions. These become, by Eqs. (4.2) and (4.3),

$$\frac{d^2x}{d\Theta^2}+\mu^2(1-n)x=0, \tag{5.10}$$

$$\frac{d^2z}{d\Theta^2}+\mu^2nz=0. \tag{5.11}$$

The character of the betatron oscillations is therefore determined by the functions $\mu^2(\Theta,R)$ and

$$\mu^2n=-\frac{1}{\eta}\left(k\mu+\epsilon\frac{\partial\mu}{\partial\Theta}+R\frac{\partial\mu}{\partial R}\right). \tag{5.12}$$

By making use of Eqs. (4.8) and (4.9) we can rewrite Eq. (5.12) in the form

$$\mu^2(1-n)=\frac{(k+1)\mu}{\eta}-\frac{1}{\eta}\frac{\partial^2\eta}{\partial\Theta^2}. \tag{5.13}$$

[7] N. M. Blachman and E. D. Courant, Rev. Sci. Instr. 20, 596 (1949), Eq. (15).

If the equilibrium orbits scale, then μ, η, and ϵ are functions only of Θ. Thus μ^2n will be a function of Θ only, and the betatron oscillations will also scale provided k is constant. Accelerators with this property will be referred to as accelerators which scale. For accelerators which scale, we have

$$p=p_0(R/R_0)^{k+1}, \tag{5.14}$$

and

$$H=H_0(R/R_0)^k\mu(\Theta). \tag{5.15}$$

6. Approximate Solution for Betatron Oscillations

In this section we develop some approximate formulas which give a useful general picture of the properties of FFAG accelerators. If the betatron wavelengths are long in comparison with the sector length (say at least four sectors), then the smooth approximation equations developed in the appendix are applicable. The "smooth" betatron oscillation equations become in this case

$$d^2X/d\Theta^2+\nu_x^2X=0, \tag{6.1}$$

$$d^2Z/d\Theta^2+\nu_z^2Z=0, \tag{6.2}$$

where, by Eqs. (5.10), (5.11), and (A.13) of the appendix,

$$\nu_x^2=\langle\mu^2(1-n)\rangle_{\mathrm{Av}}+\langle\{\mu^2(1-n)\}_1{}^2\rangle_{\mathrm{Av}}, \tag{6.3}$$

$$\nu_z=\langle\mu^2n\rangle_{\mathrm{Av}}+\langle\{\mu^2n\}_1{}^2\rangle_{\mathrm{Av}}. \tag{6.4}$$

The solutions of Eqs. (6.1) and (6.2) are

$$X=A\cos\nu_x\Theta+B\sin\nu_x\Theta, \tag{6.5}$$

$$Z=C\cos\nu_z\Theta+D\sin\nu_z\Theta. \tag{6.6}$$

To these smooth solutions must be added a ripple which can be computed from Eq. (A.7). It is clear that ν_x and ν_z are the numbers of radial and vertical betatron wavelengths around the circumference of the accelerator. The approximate formulas (6.3) and (6.4) give ν_x and ν_z within about 10% provided that ν_x and ν_z are *both* less than $N/4$.

In order to avoid resonance buildup of betatron oscillations, it is necessary to avoid integral and half-integral values for ν_x and ν_z, and also to avoid integral values for $\nu_x+\nu_z$.[8] This implies that ν_x and ν_z must be the same for all orbits, or nearly so, and this is the principal limiting condition on FFAG designs. In accelerators which scale, ν_x and ν_z are necessarily the same for all orbits; this is the advantage in designs which scale.

The relation between betatron wavelengths and machine parameters depends upon which term in Eq. (5.13) predominates in giving alternating-gradient focusing. In a radial-sector FFAG accelerator with $\zeta=0$ and with a large number of sectors (say $N>10$),

[8] P. A. Sturrock, *Static and Dynamic Electron Optics* (Cambridge University Press, Cambridge, 1955), Chap. 7.

η is very nearly unity, and the second term in Eq. (5.13) is small except near the edges of the magnets where it gives rise to edge focusing effects. The edge focusing comes from the term $-(\epsilon/\eta)(\partial\mu/\partial\Theta)$ in Eq. (5.12). This term has a nonzero mean value, part of which is included in the μ term in Eq. (5.13); thus Eqs. (6.7) and (6.8) below include most of the mean focusing effect due to edges in radial sector machines. We will call the first term in Eq. (5.13) the "μ term" and the second, the "η term." In a spiral-sector FFAG accelerator, the alternating-gradient focusing comes predominantly from the η term. It may be noted that the η term includes the term $(R/\eta)(\partial\mu/\partial R)$ which appears when the orbits do not scale. It is not hard to see that in a conventional AG synchrotron[1] this is the dominant alternating-gradient term.

Let us first consider a radial-sector FFAG accelerator with a large number of sectors, and let us neglect the η term. If $f/N \ll 1$, then $\eta=1$ according to the discussion in Sec. 4. Let us write μ in the form given by Eq. (4.11). Then Eqs. (6.3) and (6.4) yield, if we substitute from Eq. (5.13), with $\eta=1$,

$$\nu_x^2=k+1+\frac{(k+1)^2f^2}{N^2}\langle g_1^2\rangle_{\mathrm{Av}}, \qquad (6.7)$$

$$\nu_z^2=-k+\frac{f^2}{2}+\frac{(k-1)^2f^2}{N^2}\langle g_1^2\rangle_{\mathrm{Av}}, \qquad (6.8)$$

where we have neglected a small term involving $\{g^2\}$ in Eq. (6.8). The betatron oscillation advances in phase by an angle

$$\sigma=2\pi\nu/N, \qquad (6.9)$$

per sector. For stability,[1] σ should be less than π, and for the smooth approximation to be valid, σ must be less than about $\pi/2$. If we solve Eqs. (6.7) and (6.8) for k and f in terms of σ_x and σ_z, we obtain

$$k+1=\frac{N^2}{8\pi^2}(\sigma_x^2-\sigma_z^2+b), \qquad (6.10)$$

$$f=\frac{4\pi}{[2\langle g_1^2\rangle_{\mathrm{Av}}]^{\frac{1}{2}}}\frac{[\sigma_x^2+\sigma_z^2-b]^{\frac{1}{2}}}{|\sigma_x^2-\sigma_z^2+b|}, \qquad (6.11)$$

where

$$b=\frac{4\pi^2}{N^2}\left[1+\frac{f^2}{2}-\frac{4kf^2}{N^2}\langle g_1^2\rangle_{\mathrm{Av}}\right]. \qquad (6.12)$$

The quantity b is negligible for sufficiently large N.

By appropriate choice of σ_x and σ_z, k can be made either positive or negative; i.e., in a radial-sector FFAG synchrotron, with N large, the high-energy orbits may be either on the outside or the inside of the donut. The b-term, which is important when N is small, is positive and therefore favors machines with positive k, i.e., with a given N, $|k|$ can be larger and f smaller if $k>0$. For maximum momentum compaction, i.e., minimum radial

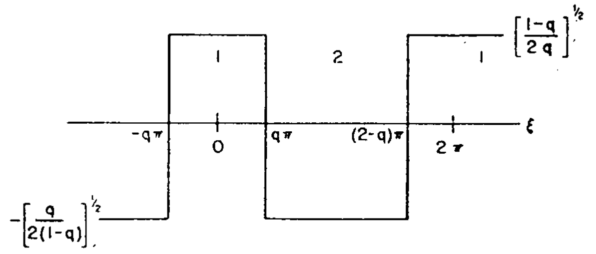

FIG. 6. Rectangular field flutter.

aperture, k, and hence N, should be as large as practicable. If we define a circumference factor C as the ratio between mean and minimum radii of curvature of the equilibrium orbit, then

$$C=|\mu|_{\max}=|1+fg(N\Theta)|_{\max}. \qquad (6.13)$$

It is desirable to minimize C, since for a given maximum magnetic field, this yields the smallest accelerator design. It is clear from Eq. (6.11), that for a given form of g, the minimum circumference factor is obtained by making σ_z as small, and σ_x as large as possible (or vice versa, if k is to be negative).

Let us assume a rectangular field flutter, with mean square value $\frac{1}{2}$:

$$g(\xi)=\left[\frac{1-q}{2q}\right]^{\frac{1}{2}}, \quad -q\pi<\xi<q\pi, \quad \text{(I)}$$

$$=-\left[\frac{q}{2(1-q)}\right]^{\frac{1}{2}}, \qquad (6.14)$$

$$q\pi<\xi<2\pi-q\pi, \quad \text{(II)}$$

$$g(\xi+2\pi)=g(\xi). \qquad (6.15)$$

This function is plotted in Fig. 6. When $\xi=N\Theta$ lies in regions labeled I, we say that Θ is in a positive half-sector; regions labeled II we call negative half-sectors. We need to calculate

$$\langle g_1^2\rangle_{\mathrm{Av}}=\tfrac{1}{6}\pi^2q(1-q). \qquad (6.16)$$

If now

$$K=f[\langle g_1^2\rangle_{\mathrm{Av}}]^{\frac{1}{2}}, \qquad (6.17)$$

is fixed by Eq. (6.11), then by Eq. (6.13), the circumference factor is

$$C=1+\frac{\sqrt{3}K}{\pi q}, \quad \text{or} \quad \frac{\sqrt{3}K}{\pi(1-q)}-1, \qquad (6.18)$$

whichever is greater. The minimum value of C occurs when q is chosen so that the two values of the right member of Eq. (6.18) are equal. We then have

$$\mu=1+fg(N\Theta)=C, \quad -q\pi<N\Theta<q\pi, \quad \text{(I)}$$
$$=-C, \quad q\pi<N\Theta<2\pi-q\pi. \quad \text{(II)} \qquad (6.19)$$

The radius of curvature, and consequently also the magnetic field, is constant in magnitude along the equilibrium orbit and opposite in sign in the two half-sectors. The ratio of half-sector lengths is

$$\Gamma = q/(1-q) = (C+1)/(C-1), \tag{6.20}$$

and the circumference factor is

$$C = (\Gamma+1)/(\Gamma-1) = [1+\tfrac{1}{2}f^2]^{\frac{1}{2}}. \tag{6.21}$$

If we take $\sigma_z = \pi/6$, $\sigma_x = \pi/2$, $b=0$, and use the approximate formulas (6.10) and (6.11), we obtain $K=\sqrt{5}$, $\Gamma = 1.31$, $C=7.5$, $f=10.5$, and $k=N^2/36$. It will be shown in the next section by a more accurate calculation that the minimum value of C where N is large is about 5.

In a spiral-sector FFAG accelerator, ζ is nearly 90° and the η term in Eq. (5.13) is large. It is then possible to use a much smaller flutter factor, so that the oscillatory part of the μ term is small. We will again assume that μ is given by Eq. (4.11) and will use the approximation (4.18) for η. If we expand $1/\eta$ in a power series in the second term of formula (4.18), we may calculate

$$\left\langle\frac{\mu}{\eta}\right\rangle_{\mathrm{Av}} = 1+\frac{f^2\tan^2\zeta}{N^2}\langle g_1{}^2\rangle_{\mathrm{Av}}+\cdots. \tag{6.22}$$

We will neglect the second and higher order terms, and will neglect also the oscillatory part of μ/η. The η term can be rewritten in the following way:

$$\frac{1}{\eta}\frac{\partial^2\eta}{\partial\Theta^2} = \frac{\partial}{\partial\Theta}\left(\frac{1}{\eta}\frac{\partial\eta}{\partial\Theta}\right)+\left(\frac{1}{\eta}\frac{\partial\eta}{\partial\Theta}\right)^2. \tag{6.23}$$

The first term on the right is large and oscillatory with zero mean value, and the second is smaller but has a positive mean value. We neglect the oscillatory part of the second term, and substitute in Eqs. (6.3) and (6.4), using (5.13) to obtain

$$\nu_x{}^2 = k+1, \tag{6.24}$$

$$\nu_z{}^2 = -k+\tfrac{1}{2}f^2+2\left\langle\left(\frac{1}{\eta}\frac{\partial\eta}{\partial\Theta}\right)^2\right\rangle_{\mathrm{Av}}. \tag{6.25}$$

Note that the η term does not contribute in this approximation to the radial focusing. If we take η as given by formula (4.18), we have

$$\left\langle\left(\frac{1}{\eta}\frac{\partial\eta}{\partial\Theta}\right)^2\right\rangle_{\mathrm{Av}}$$

$$= f^2\tan^2\zeta\left\langle\frac{g^2}{(1-fN^{-1}\tan\zeta g_1)^2}\right\rangle_{\mathrm{Av}}$$

$$= f^2\tan^2\zeta\left[1+\frac{2f^2\tan^2\zeta}{N^2}\langle g^2g_1{}^2\rangle_{\mathrm{Av}}+\cdots\right]. \tag{6.26}$$

We will neglect the second and higher order terms in square brackets and substitute in Eqs. (6.24) and (6.25), to obtain

$$f^2\tan^2\zeta = (\nu_x{}^2+\nu_z{}^2-1), \tag{6.27}$$

where we have also neglected f^2. Note that, to this order of approximation, formulas (6.24) and (6.27) are independent of the form of the flutter function $g(N\Theta)$; only the circumference factor Eq. (6.13) depends on $g(N\Theta)$. We can rewrite these formulas in terms of the phase shifts σ per sector:

$$k+1 = \frac{N^2\sigma_x{}^2}{4\pi^2}, \tag{6.28}$$

$$f^2\tan^2\zeta = \frac{N^2}{4\pi^2}(\sigma_x{}^2+\sigma_z{}^2)-1. \tag{6.29}$$

The reference curve $\Theta=0$, satisfies, in polar coordinates r and θ, the equation

$$\frac{1}{r}\frac{dr}{d\theta} = \cot\zeta. \tag{6.30}$$

The radial separation between ridges (points of maximum magnetic field), in units of r is therefore

$$\lambda = \Delta r/r = 2\pi/(N\tan\zeta). \tag{6.31}$$

Thus for a given choice of σ_x, σ_z, and N the ratio f/λ is fixed. The maximum allowable gap between the poles of the magnet is proportional to λ; if the field flutter is to be obtained by shaping the poles, without extra forward windings, it can be shown (Sec. 13) that for f/λ fixed the maximum gap is about $\frac{1}{4}\lambda r$ and is obtained for $f\doteq\frac{1}{4}$. Under these conditions, the field flutter may be very nearly sinusoidal,

$$g(\xi) = \cos\xi, \tag{6.32}$$

and then the circumference factor will be $C=1+f=1.25$.

If we take, as above, $\sigma_z=\pi/6$, $\sigma_x=\pi/2$, with $f=\frac{1}{4}$, we obtain $k+1=N^2/16$, $\lambda=5.95N^{-2}[1-14.4N^{-2}]^{-\frac{1}{2}}$, and $\tan\zeta = 1.05N[1-14.4N^{-2}]^{-\frac{1}{2}}$.

7. Linear Stability for Radial Sectors

In order to get more accurate relations between the parameters, we return to the betatron oscillation equations (5.10) and (5.11). Making use of Eqs. (5.12), (4.18), and (4.19), with $\zeta=0$, we rewrite Eqs. (5.10) and (5.11) for the case of a rectangular field flutter of the form (6.19):

$$\frac{d^2x}{d\Theta^2}\pm kCx=0, \tag{7.1}$$

$$\frac{d^2z}{d\Theta^2}\mp kCz=0, \tag{7.2}$$

where the upper signs apply in positive half-sectors, and the lower, in negative half-sectors. The term $\epsilon\partial\mu/\partial\Theta$ in Eq. (5.12) gives rise to terms in Eqs. (5.10) and (5.11) which represent the focusing that occurs at the sector edges, which we will neglect for the present. These approximations are valid only when $N\gg f$, and we have accordingly also neglected 1 in comparison with n. When N is small, edge effects and higher order terms in η must be taken into account. The oscillatory terms in η will give rise to effects resulting from the fact that neighboring equilibrium orbits are not everywhere equidistant. For small N, edge effects turn out to increase the vertical focusing and to decrease the radial focusing, so that considerably smaller values of the flutter factor f may be used if $k>0$, without losing vertical stability.

Let $N\Theta_0=-q\pi$, $N\Theta_1=q\pi$, $N\Theta_2=(2-q)\pi$. Then the solutions of Eq. (7.1) within the positive and negative half sectors separately yield the following matrix relations between x and $x'=dx/d\Theta$ at the points Θ_0, Θ_1, and Θ_2:

$$\begin{pmatrix} x_1 \\ x_1' \end{pmatrix}=M_+\begin{pmatrix} x_0 \\ x_0' \end{pmatrix},\quad \begin{pmatrix} x_2 \\ x_2' \end{pmatrix}=M_-\begin{pmatrix} x_1 \\ x_1' \end{pmatrix},\qquad (7.3)$$

where

$$M_+=\begin{pmatrix} \cos\psi_+ & (kC)^{-\frac{1}{2}}\sin\psi_+ \\ -(kC)^{\frac{1}{2}}\sin\psi_+ & \cos\psi_+ \end{pmatrix},$$
$$M_-=\begin{pmatrix} \cosh\psi_- & (kC)^{-\frac{1}{2}}\sinh\psi_- \\ (kC)^{\frac{1}{2}}\sinh\psi_- & \cosh\psi_- \end{pmatrix},\qquad (7.4)$$

$$\psi_+=\frac{2\pi q}{N}(kC)^{\frac{1}{2}},\quad \psi_-=\frac{2\pi(1-q)}{N}(kC)^{\frac{1}{2}}.\qquad (7.5)$$

We thus obtain

$$\begin{pmatrix} x_2 \\ x_2' \end{pmatrix}=M\begin{pmatrix} x_0 \\ x_0' \end{pmatrix},\qquad (7.6)$$

with

$$M=M_-M_+=\begin{pmatrix} \cos\psi_+\cosh\psi_- -\sin\psi_+\sinh\psi_-, & (kC)^{-\frac{1}{2}}(\cos\psi_+\sinh\psi_- -\sin\psi_+\cosh\psi_-) \\ (kC)^{\frac{1}{2}}(\cos\psi_+\sinh\psi_- +\sin\psi_+\cosh\psi_-), & \cos\psi_+\cosh\psi_- +\sin\psi_+\sinh\psi_- \end{pmatrix}.\qquad (7.7)$$

We can now calculate[8]

$$\cos\sigma_x=\tfrac{1}{2}\,\mathrm{trace}(M)=\cos\psi_+\cosh\psi_-,\qquad (7.8)$$

and in the same way,

$$\cos\sigma_z=\cos\psi_-\cosh\psi_+.\qquad (7.9)$$

In terms of the local field index

$$n=k/C,\qquad (7.10)$$

within the magnets (we take n as positive here), and the ratio Γ of sector lengths [Eq. (6.20)], we may rewrite ψ_+ and ψ_-:

$$\psi_+=\left(\frac{2\pi}{N}\right)\left(\frac{\Gamma}{\Gamma-1}\right)n^{\frac{1}{2}},\quad \psi_-=\left(\frac{2\pi}{N}\right)\left(\frac{1}{\Gamma-1}\right)n^{\frac{1}{2}}.\qquad (7.11)$$

Formulas (7.5), (7.8), (7.9), and (7.11) have been written for $k>0$. However, they may also be used for $k<0$, in which case it is convenient to regard C as negative.

The smallest circumference factor is obtained by choosing σ_x as large as possible and σ_z as small as possible (or vice versa). If we choose $\sigma_x=3\pi/4$, $\sigma_z=\pi/6$. we calculate from Eqs. (7.8) and (7.9) that $\psi_+=1.32$, $\psi_-=1.93$. From Eqs. (7.11) and (6.21), we have

$$\Gamma=\psi_+/\psi_-=1.46,\quad C=5.35.\qquad (7.12)$$

The theoretical minimum value of C is 4.45 for $\sigma_x=\pi$, $\sigma_z=0$. In order to keep the amplitude of betatron oscillations within reasonable bounds, the former choices of σ_x and σ_z run about as close to the stability limits as it is safe to go. (For the choice $\sigma_x=\pi/2$, $\sigma_z=\pi/6$, these more exact formulas give $\Gamma=1.29$, $C=7.9$, which may be compared with the approximate values 1.31, 7.5 obtained in the preceding section.)

A more general calculation, including straight sections between magnets, and taking edge effects into account, can be carried out in a similar way. We assume that along an equilibrium orbit the magnetic fields have equal and opposite constant values within the positive and negative half-sectors, and that the positive and negative half-sectors are separated by straight sections where the field is zero; (see Fig. 7). Let the fractions of orbit length within the positive and negative magnets be q_1 and q_2, respectively, and let the fraction of orbit

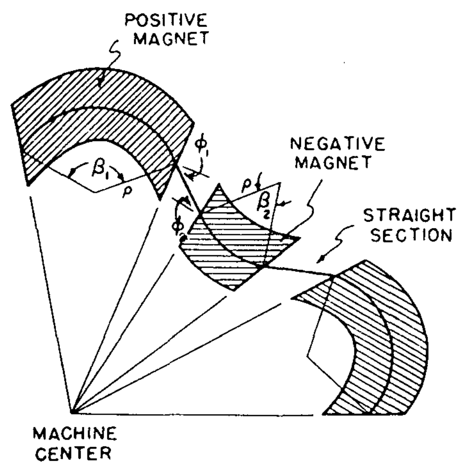

FIG. 7. Equilibrium orbit notation for radial sectors with straight sections.

length in each straight section be q_0, so that

$$2q_0+q_1+q_2=1. \tag{7.13}$$

The angles β_1 and β_2 shown in Fig. 7 are

$$\beta_1=2\pi Cq_1/N, \quad \beta_2=2\pi Cq_2/N. \tag{7.14}$$

The number of sectors is

$$N=2\pi/(\beta_1-\beta_2), \tag{7.15}$$

so that the circumference factor is

$$C=1/(q_1-q_2). \tag{7.16}$$

The angles ϕ_1 and ϕ_2 shown in Fig. 7 are the edge angles between the orbit and the normal to the magnet edges. It is convenient to define

$$\delta=2\pi Cq_0/N, \tag{7.17}$$

$$\psi_1=\beta_1(n_1+1)^{\frac{1}{2}}, \quad \psi_2=\beta_2(n_2-1)^{\frac{1}{2}}, \tag{7.18}$$

$$\psi_3=\beta_1 n_1^{\frac{1}{2}}, \quad \psi_4=\beta_2 n_2^{\frac{1}{2}}. \tag{7.19}$$

The indices n_1 and n_2 are the local field indices at the centers of the positive and negative magnets:

$$n=k/(\eta C), \tag{7.20}$$

where

$$\eta_1=1-2q_2\left(1-\frac{\sin(\pi Cq_2/N)}{Cq_2\sin(\pi/N)}\right)-2q_0\left(1-\frac{\cos(\pi Cq_2/N)}{(N/\pi)\sin(\pi/N)}\right), \tag{7.21}$$

and

$$\eta_2=1-2q_1\left(1-\frac{\sin(\pi Cq_1/N)}{Cq_1\sin(\pi/N)}\right)-2q_0\left(1-\frac{\cos(\pi Cq_1/N)}{(N/\pi)\sin(\pi/N)}\right). \tag{7.22}$$

We do not neglect 1 relative to n here. We do, however, neglect variation of η within the magnets. The result is

$$\begin{aligned}\cos\sigma_x=&\left[1+2\delta(\tan\phi_1+\tan\phi_2)+2\delta^2\tan\phi_1\tan\phi_2\right]\cos\psi_1\cosh\psi_2\\&+\left[(n_1+1)^{-\frac{1}{2}}(\tan\phi_1+\tan\phi_2+\delta\tan^2\phi_1+2\delta\tan\phi_1\tan\phi_2+\delta^2\tan^2\phi_1\tan\phi_2)-(n_1+1)^{\frac{1}{2}}(\delta+\delta^2\tan\phi_2)\right]\sin\psi_1\cosh\psi_2\\&+\left[(n_2-1)^{-\frac{1}{2}}(\tan\phi_1+\tan\phi_2+\delta\tan^2\phi_2+2\delta\tan\phi_1\tan\phi_2+\delta^2\tan^2\phi_2\tan\phi_1)+(n_2-1)^{\frac{1}{2}}(\delta+\delta^2\tan\phi_1)\right]\cos\psi_1\sinh\psi_2\\&+\tfrac{1}{2}\left[-(n_1+1)^{\frac{1}{2}}(n_2-1)^{\frac{1}{2}}\delta^2-(n_1+1)^{\frac{1}{2}}(n_2-1)^{-\frac{1}{2}}(1+\delta\tan\phi_2)^2+(n_1+1)^{-\frac{1}{2}}(n_2-1)^{\frac{1}{2}}(1+\delta\tan\phi_1)^2\right.\\&\left.+(n_1+1)^{-\frac{1}{2}}(n_2-1)^{-\frac{1}{2}}(\tan\phi_1+\tan\phi_2+\delta\tan\phi_1\tan\phi_2)^2\right]\sin\psi_1\sinh\psi_2,\end{aligned} \tag{7.23}$$

$$\begin{aligned}\cos\sigma_z=&\left[1-2\delta(\tan\phi_1+\tan\phi_2)+2\delta^2\tan\phi_1\tan\phi_2\right]\cos\psi_4\cosh\psi_3\\&+\left[n_2^{-\frac{1}{2}}(-\tan\phi_1-\tan\phi_2+\delta\tan^2\phi_2+2\delta\tan\phi_1\tan\phi_2-\delta^2\tan^2\phi_2\tan\phi_1)-n_2^{\frac{1}{2}}(\delta-\delta^2\tan\phi_1)\right]\sin\psi_4\cosh\psi_3\\&+\left[n_1^{-\frac{1}{2}}(-\tan\phi_1-\tan\phi_2+\delta\tan^2\phi_1+2\delta\tan\phi_1\tan\phi_2-\delta^2\tan^2\phi_1\tan\phi_2)+n_1^{\frac{1}{2}}(\delta-\delta^2\tan\phi_2)\right]\cos\psi_4\sinh\psi_3\\&+\tfrac{1}{2}\left[-n_2^{\frac{1}{2}}n_1^{\frac{1}{2}}\delta^2-n_2^{\frac{1}{2}}n_1^{-\frac{1}{2}}(1-\delta\tan\phi_1)^2+n_2^{-\frac{1}{2}}n_1^{\frac{1}{2}}(1-\delta\tan\phi_2)^2\right.\\&\left.+n_2^{-\frac{1}{2}}n_1^{-\frac{1}{2}}(-\tan\phi_1-\tan\phi_2+\delta\tan\phi_1\tan\phi_2)^2\right]\sin\psi_4\sinh\psi_3.\end{aligned} \tag{7.24}$$

8. Linear Stability for Spiral Sectors

For spiral-sector accelerators, the circumference factor is close to unity, and minimizing C is no longer a major consideration. The ridge separation λ is, however, rather small, and if the gap between magnet poles is to be kept as large as possible, it appears that the field flutter in the median plane must be at least approximately sinusoidal. We will therefore assume a field in the median plane of the form (2.1).

$$H=H_0(r/r_0)^k\{1+f\sin[N\theta-(1/w)\ln(r/r_0)]\}, \tag{8.1}$$

where we have set

$$1/w=N\tan\zeta=2\pi/\lambda. \tag{8.2}$$

The form of Eq. (8.1) is chosen so as to guarantee that the accelerator scales.

The linearized equations for the betatron oscillations in the field (8.1) can be obtained from the general analysis of the first two sections, but it is perhaps more illuminating to derive them directly. If one undertakes to write the linear terms in the differential equations characterizing the departure of the particle from a reference circle of radius

$$r_1=cp/[eH,(r_0/r_1)^k], \tag{8.3}$$

one obtains substantially the following:

$$r''+[1+k+(f/w)\cos N\theta](r-r_1)\doteq fr_1\sin N\theta, \tag{8.4}$$

$$z''-[k+(f/w)\cos N\theta]z\doteq 0. \tag{8.5}$$

These equations suggest alternating-gradient focusing of the type characterized by the Mathieu differential equation, but the presence of the forcing term on the right hand side of the equation for the radial motion indicates that a forced oscillation will be expected and will be given approximately by

$$r-r_1=-\frac{f}{N^2-(k+1)}r_1\sin N\theta. \tag{8.6}$$

Because of the presence of this forced motion, one realizes that not only will the nonlinear terms in the differential equations be large, but that a noticeable influence upon the betatron oscillation wavelength can result.

It is appropriate, therefore, to perform an expansion about a more suitable reference curve by writing

$$x=r-r_1+\frac{f}{N^2-(k+1)}r_1\sin N\theta. \qquad (8.7)$$

In this way one obtains linearized equations, of which the most significant terms appear below:

$$x''+\left[k+1-\tfrac{1}{2}\frac{f^2/w^2}{N^2-(k+1)}+\frac{f}{w}\cos N\theta\right.$$
$$\left.+\tfrac{1}{2}\frac{f^2/w^2}{N^2-(k+1)}\cos 2N\theta\right]x=0, \qquad (8.8)$$

$$z''-\left[k-\tfrac{1}{2}\frac{f^2/w^2}{N^2-(k+1)}+\frac{f}{w}\cos N\theta\right.$$
$$\left.+\tfrac{1}{2}\frac{f^2/w^2}{N^2-(k+1)}\cos 2N\theta\right]z=0. \qquad (8.9)$$

These equations have the form of an extended Mathieu equation

$$d^2u/d\tau^2+(A+B\cos 2\tau+C\cos 4\tau)u=0. \qquad (8.10)$$

The neglected terms in the coefficients A and C in Eq. (8.10) as given by Eqs. (8.8) and (8.9) are of order k^2w^2 times the main terms, so that for $f=\frac{1}{4}$, the error in these coefficients is less than 2% over most of the region of stability (Fig. 8). The neglected terms in the coefficients B are of order $\frac{1}{8}(f/N^2w)^2$ and $\frac{1}{2}(f/N^2w)^2$ in Eqs. (8.8) and (8.9), respectively, so that the errors will be less than 2% and 8%, respectively, over most of the region of stability. The coefficient of the third harmonic term (which has been omitted) is of order $\frac{1}{8}(f/N^2w)^2$ and $\frac{1}{2}(f/N^2w)^2$, respectively, times the coefficient B; since the third harmonic contributes to σ an amount proportional to $\frac{1}{9}$ the square of the coefficient, its contribution is completely negligible.

Tables of the characteristic exponent (σ/π) of the extended Mathieu equation (8.10) have been computed on the ILLIAC, using a variational method.[9] Values of A are tabulated for a range of values of σ, B, and C, covering the significant portion of the first stability region. Results for the Mathieu equation $C=0$ are included. So far as we are aware, there are at present no published tables of characteristic exponents for the Mathieu equation within the stability region.

In Fig. 8 we plot a stability diagram for a spiral-sector FFAG accelerator with $k\gg 1$ computed from the above formulas and tabulated solutions of Eq. (8.20). If $k\gg 1$, the coefficients A, B, and C depend only on k/N^2 and f/N^2w. We accordingly plot curves of constant σ_x and σ_z vs k/N^2 and f/N^2w. If we take $\sigma_z=\pi/6$ and $\sigma_x=\pi/2$, with $f=\frac{1}{4}$, we obtain $k=0.057N^2$, $f/N^2w=0.25$, and $\lambda=6.3N^{-2}$, which may be compared with the approximate values $k=0.062N^2$, $f/N^2w=0.265$, and $\lambda=5.95N^{-2}$ obtained at the end of Sec. 6.

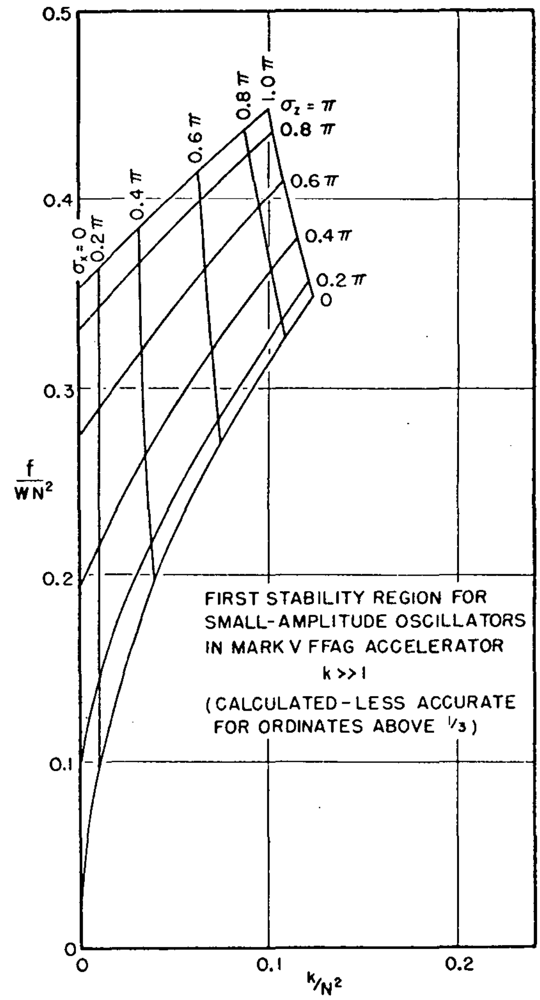

FIG. 8. Dependence of σ_x and σ_z within the stable region on spiral-sector parameters for $N\gg 1$.

9. Nonlinear Effects

The preceding analysis of betatron oscillations has been based on an expansion of the equations of motion in powers of the displacement from the equilibrium orbit, keeping only the linear terms. The small-amplitude betatron oscillations in x and z are then found to satisfy linear differential equations with coefficients periodic in the independent variable Θ.

In a perfectly constructed accelerator, the only periodicity would be that associated with the N-identical sectors around the machine, and the period of the coefficients would be $2\pi/N$. In an actual accelerator, there will be imperfections, so that the coefficients will be

[9] Laslett, Snyder, and Hutchinson, "Tables for the determination of stability boundaries and characteristics exponents for a Hill's equation characterizing the Mark V FFAG synchrotron." Midwestern Universities Research Association Notes, April 20, 1955 (unpublished).

strictly periodic with the period 2π in Θ, and approximately periodic with period $2\pi/N$. Associated with the period $2\pi/N$ is the requirement that σ_x and σ_z must not be integral or half-integral multiples of 2π; in practice it appears that σ should be less than π, since otherwise the tolerances on magnet construction and alignment become very severe. Associated with the period 2π is the requirement that ν_x and ν_z must not be integral or half-integral if imperfection resonances are to be avoided, and, in addition, if imperfections can couple the x and z motions, $\nu_x+\nu_z$ must not be an integer.

The study of the effects of nonlinear terms in the equations of motion has not advanced nearly as far as the study of the linearized equations. Approximate analytic methods of treating nonlinear equations with periodic coefficients have been developed by Moser,[10] Sturrock,[8] and Hagedorn.[11] Their results can be summarized as follows: If the coefficients in the equations have period 2π in Θ, and ν_x, ν_z are the numbers of betatron oscillations in one period 2π, then resonances can occur when

$$n_x\nu_x+n_z\nu_z=\text{any integer, for}$$
$$n_x,n_z=0,1,2\cdots. \tag{9.1}$$

Let

$$n_x+n_z=q. \tag{9.2}$$

Then if $q=1$ or $q=2$, the motion is unstable even in linear approximation. (This is the rule stated in the preceding paragraph.) If $q=3$, then in general, the effects of quadratic terms in the differential equations are such as to make the motion unstable even at very small amplitudes. If $q=4$, then the effects of cubic terms may be to render the motion unstable, depending on the form of the cubic (and linear) terms. If $q>4$, then, in general, the motion is stable for sufficiently small amplitudes of betatron oscillation. In any case, if $q\geqslant 4$, and if the equations of motion are nonlinear, then there will be in general a limiting amplitude of betatron oscillations beyond which the oscillations are unstable at least in the sense that they leave the donut.

Numerical studies carried out on the ILLIAC at the University of Illinois seem to confirm these conclusions. It was also reported by the Brookhaven group[12] that experiments with the electron-analog alternating-gradient accelerator have confirmed these conclusions.

If we apply the above criteria to the sector periodicity $2\pi/N$, then we must replace ν_x and ν_z in Eq. (9.1) by $\sigma_x/2\pi$ and $\sigma_z/2\pi$, the number of betatron oscillations per sector. We then conclude for example that values of σ_x or σ_z near $2\pi/3$ are to be avoided, as well as values such that $\sigma_x+2\sigma_z$ or $\sigma_z+2\sigma_x$ is nearly 2π. We call these resonances with the periodicity of the structure itself "sector resonances." We have indeed found in numerical studies that the limiting amplitudes for betatron oscillations in spiral sector machines become very small when σ approaches $2\pi/3$.

If we apply the above criteria to the once-around period 2π, then we find that the values of ν_x and ν_z excluded by the above rules are as shown in Fig. 9. We plot ν_x horizontally and ν_z vertically. The lines labeled $q=1$, 2, 3, and 4 represent the values excluded by the above rules. The lines $q=1$ are integral resonances. The lines $q=2$ are half-integral resonances (vertical and horizontal) and sum resonances (diagonal). The lines $q=3$, 4 are third and fourth integral resonances. It is not yet altogether clear how serious the third and fourth integral resonances are, since they arise only from nonlinear imperfections in the machine. Experiments with the electron analog at Brookhaven[12] seem to indicate that these resonances must be excited by deliberately inserted nonlinear imperfections in order to be detected. This is not true of course of the $\sigma=2\pi/3$ resonances discussed in the preceding paragraph, which are resonances with the inherent periodicity of the structure. It would at present seem wise to avoid all the excluded lines on Fig. 9 if this can be done.

It should be pointed out that nonlinear terms in the equations for the radial sector accelerator are not very large, being not greater in order of magnitude than nonlinear terms which arise in some conventional alternating-gradient accelerators which have been contemplated. However, the nonlinear terms which arise when the sectors spiral are much larger and play a very important role in determining the character of

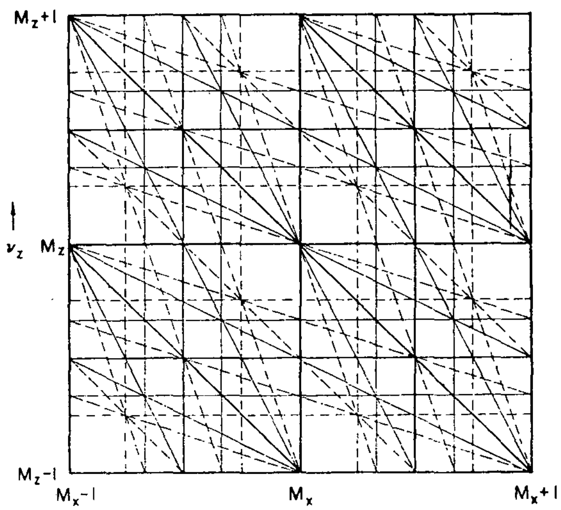

FIG. 9. Linear and nonlinear resonances in an AG accelerator. M_x and M_z are integers.

[10] J. Moser, Nachr. Akad. Wiss. Göttingen, Math.-physik. Kl. IIa, No. 6, 87 (1955). We are indebted to Dr. Moser for a very helpful discussion of his results.

[11] R. Hagedorn, CERN Report, CERN-PS/RH 9, November, 1955 (unpublished).

[12] Courant, Kassner, Raka, Smith, and Spiro, Phys. Rev. 100, 1269(A) (1955).

the betatron oscillations. Numerical studies indicate that although the motion in spiral-sector synchrotrons exhibits marked nonlinear effects, the amplitude limits are large enough to accommodate reasonable betatron oscillations provided σ is not close to $2\pi/3$ (say $\sigma_x < 0.6\pi$).

10. Momentum Content and Phase Stability

The momentum $p(R)$ is determined by integrating Eq. (5.6):

$$p = p_0 \exp\left[\int_{R_0}^{R} \frac{k+1}{R} dR\right]. \tag{10.1}$$

If k is independent of R, this reduces to the simple relation (5.14). Thus momentum and energy are determined as functions of the orbit size R. Since R is essentially a mean radius of the orbit, the radial aperture required for any given initial and final momentum can be determined from Eq. (10.1). It is clear that for a given momentum content, the radial aperture decreases with increasing k. If $k \gg 1$, then the radial aperture is much less than R, and we have approximately, for constant k,

$$\frac{R_1 - R_0}{R_0} \doteq \left(\frac{1}{k+1}\right) \ln\left(\frac{p_1 - p_0}{p_0}\right). \tag{10.2}$$

The angular velocity of a particle in an orbit R is

$$\omega = \frac{d\Theta}{dt} = \frac{\beta c}{R} = \frac{pc^2}{ER}, \tag{10.3}$$

where E is the total energy, including rest energy. By squaring Eq. (10.3) and differentiating, we obtain

$$\frac{E}{\omega}\frac{d\omega}{dE} = \frac{1}{(E^2/E_0^2) - 1} - \frac{1}{(R/E)(dE/dR)}. \tag{10.4}$$

We now differentiate the equation

$$E^2 = p^2c^2 + E_0^2, \tag{10.5}$$

and use Eq. (5.6) to obtain

$$\frac{E}{\omega}\frac{d\omega}{dE} = \frac{(k-1)E_0^2 - E^2}{(E^2 - E_0^2)(k+1)}. \tag{10.6}$$

We may integrate this equation if k is constant to obtain

$$\frac{\omega}{\omega_1} = \frac{E_1}{E}\left(\frac{E^2 - E_0^2}{E_1^2 - E_0^2}\right)^{k/[2(k-1)]}, \tag{10.7}$$

where ω_1 is the angular frequency of revolution at any particular energy E_1. A graph of ω/ω_t is shown in Fig. 10, where ω_t is the angular frequency at the transition energy, and we have taken $k = 99$. If we define the transition energy

$$E_t = (k+1)^{\frac{1}{2}} E_0, \tag{10.8}$$

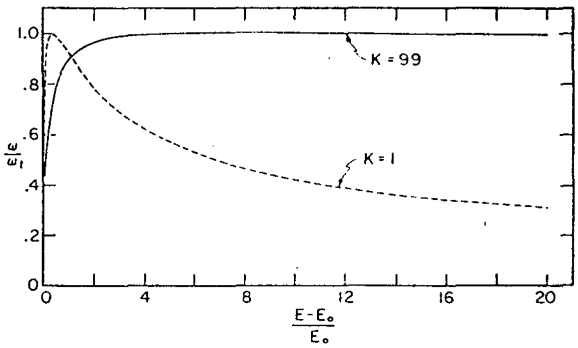

FIG. 10. Frequency of revolution as a function of energy.

then for $E < E_t$, $d\omega/dE$ is positive, while for $E > E_t$, $d\omega/dE$ is negative. If particles are accelerated by radio-frequency voltages applied to one or more accelerating gaps, then the theory of phase stability in FFAG accelerators is similar to that for conventional cyclotrons and synchrotrons.[13] When $d\omega/dE$ is positive, particles may execute stable synchrotron oscillations about a phase on the rising side of the voltage wave at the accelerating gap. When $d\omega/dE$ is negative, the stable phase is on the falling side of the voltage wave. At $E = E_t$, there is no phase stability. In order to accelerate particles beyond the transition energy, it is necessary to shift the relative phase at which the particle arrives at the accelerating gap from the rising to the falling side of the voltage wave.

In a cyclotron, the frequency of revolution, $\omega/2$, must be the same for all energies, and Eq. (10.6) then furnishes a relation between k and E:

$$k + 1 = E^2/E_0^2. \tag{10.9}$$

In a cyclotron, k must increase with energy, and the betatron oscillations therefore do not scale even when the equilibrium orbits scale.

III. APPLICATIONS

11. FFAG Proton Synchrotrons

As an illustration of the application of the FFAG principles to high-energy accelerator design, possible parameters are given below for a radial-sector and a spiral-sector synchrotron. Many of the considerations governing choices of parameters are common to these synchrotrons, and to pulsed-field alternating-gradient synchrotrons,[1] e.g., resonances, alignment tolerances, and gas scattering. It is anticipated that injection and acceleration might be accomplished somewhat differently than in pulsed-field synchrotrons of comparable energy.

Whereas injection from a 50-Mev proton linear accelerator is planned for 25-Bev pulsed-field accelerators, a 5-Mev Van de Graaf electrostatic generator might be

[13] D. Bohm and L. Foldy, Phys. Rev. **70**, 249 (1946); D. M. Dennison and T. H. Berlin, Phys. Rev. **69**, 542 (1946); R. Q. Twiss and N. H. Frank, Rev. Sci. Instr. **20**, 1 (1949).

used to inject into FFAG synchrotrons for the reasons mentioned in the introduction. Electrostatic-generator injection with FFAG synchrotrons would have the advantages of higher pulse currents, greater simplicity, lower cost, and better beam energy and size resolution than are at present realized with proton linear accelerators. Although one-turn injection using a pulsed inflector with a pulsed current of milliamperes is the most obvious injection system, many-turn injection may be used to give greater beam currents by scanning the aperture with the injected beam up to the space charge limit.

While the possibility of low-energy injection was evident when FFAG accelerators were conceived, it was also realized that it is usually uneconomical to use iron at a low flux density and that large momentum content in an FFAG accelerator requires much pole face area working at a very low flux density. This suggested the use of FFAG accelerators in succession with high flux density in the iron and with regenerative beam extractors used backward to inject particles from one accelerator into the next at high energy. Such regenerative peeler systems for extraction have been used for some time on betatrons and recently on cyclotrons; time reversal of the orbits would allow the system to be used for injection provided the injected beam can be caused to move away from the magnetic perturbation at the same time the excited oscillation in the beam is damped. This would require very careful adjustment. The feasibility of this sytem is being given extensive theoretical study by Teng,[14] and by others at the Argonne National Laboratory. Teng emphasizes that the use of high-energy injection largely avoids the frequency modulation problem and the problems of controlling the shape of low magnetic fields needed for low-energy injection. However, the radio-frequency modulation problem has many interesting possibilities of solution not available to pulsed-field accelerators.

The arbitrary frequency-*versus*-time program of FFAG synchrotrons allows the use of a mechanical modulation system with high-Q cavities. With the high Q realized in unloaded cavities, the required voltage gain per turn could be given the particles by one cavity driven at reasonable power. Modulation could be accomplished by moving a diaphragm to tune the cavity capacity. With such a system, model tests indicate a frequency change of a factor of 3:1 is practical. Using 5-Mev injection, a frequency change of 10:1 is required to reach relativistic velocities. One might then use one cavity operating as a self-excited oscillator to accelerate particles from injection to about 50 Mev. The voltage on that cavity would then be turned off as voltage on a second cavity is turned on, and acceleration continued with the second cavity. The change-over could be triggered by frequency comparison between cavities. The relative phases of the cavities could be controlled by a loose coupling between them. (With the University of Michigan electron synchrotron two-cavity rf system, it was observed that it was possible to make the transition from one cavity to another without an observable beam loss.) A third cavity might be added and a second transition made if desired, since it is observed that most of the energy is given the particles after they have reached almost constant velocity, c (see Fig. 10), and this third cavity could be designed to provide very high voltage over a small frequency range. Fine frequency adjustments would be made with reactance-tube loading of the cavities. With this rf system, it appears reasonable to accelerate protons to 20 Bev with a repetition rate of several per second.

While the above system is suggested on the basis of experimental tests already in progress, it is realized that other rf systems might prove more practical. Some of these are:

1. Many ferrite-loaded, low-voltage, low-Q cavities operated as tuned, driven amplifiers. Tuning would be accomplished by biasing the ferrites with currents. This is the system planned for the CERN and Brookhaven pulsed AG synchrotrons.
2. The use of drift tubes or operation of one or more entire magnet units as a drift tube on a high harmonic of the particle rotational frequency. In this case tuning over a wide frequency range appears difficult.
3. Several rf schemes have been proposed in which many groups of particles of different energies are present in the donut simultaneously. If any of these schemes proves practicable, large increases in duty factor and hence in beam output will become possible.

In alternating-gradient synchrotrons, phase stability vanishes at a transition energy, E_t, given by Eq. (10.8). It is possible in the radial-sector FFAG designs to have k large and negative. In this case there is no transition energy, and high-energy orbits lie on the inner radius of the machine. Negative-k designs appear to be not practical with spiral sectors. Figure 11 illustrates

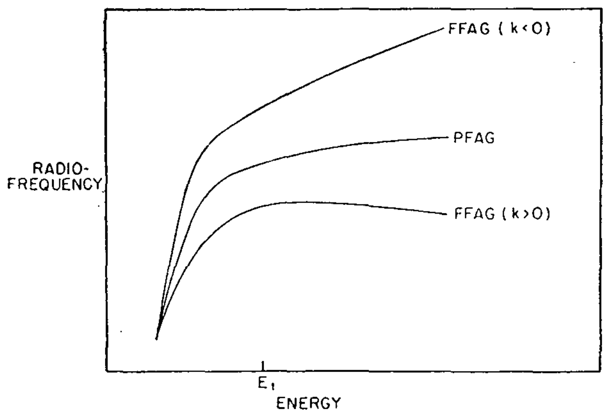

FIG. 11. Radio-frequency program for pulsed-field AG and FFAG synchrotrons.

[14] L. C. Teng, Phys. Rev. 100, 1247 (1955).

qualitatively the radio-frequency *versus* energy program in a pulsed-field AG accelerator, and in comparable FFAG accelerators with positive and negative k.

12. A 10-Bev FFAG Proton Synchrotron with Radial Sectors

The following design for a high-energy proton synchrotron is intended to illustrate the features of the radial-sector FFAG synchrotron. This design type is at present the most completely understood of the FFAG accelerators thus far suggested, although spiral sectors certainly offer the possibility of more economical design. From the expressions (7.23 and (7.24), values of σ_x and σ_z may be found for a given choice of N, n, β_1, β_2, and δ. In Table I, typical values of the parameters are given for a 64-sector radial-sector accelerator. For this example we choose 10 Bev as the maximum proton energy and 20 000 gauss as the magnetic field for the equilibrium orbit of that energy. The limit on the strength of the focusing, radially and vertically, is set by the tolerances which must be placed on parameters of the machine such as n to avoid resonances. Since, if σ_x is kept constant, ν_x is roughly proportional to the square root of n, weaker focusing relaxes these tolerances. In cases where the simple expressions (7.8), (7.9) hold, the tolerance on n for $\Delta\nu=\frac{1}{2}$ is, by differentiating,

$$\frac{dn}{n}=\frac{2\pi\sin\sigma}{N(\psi_1\sin\psi_1\cosh\psi_2-\psi_2\cos\psi_1\sinh\psi_2)}. \tag{12.1}$$

For the above design figures, the tolerance on n is about one percent. A closer tolerance might be held on n in the fixed-field case than in the pulsed-field case since all field adjustments are time-independent.

Misalignment of magnets in alternating-gradient accelerators has been shown to give rise to large deviations of equilibrium orbits.[15] In radial-sector accelerators, the equilibrium orbit deviation for a given rms sector misalignment may be shown[15] to be worse, by approximately the ratio of circumference factors, than in a conventional AG accelerator of the same number of magnet units and comparable ν_x and ν_z. Here the simplifying assumptions are made that misalignments occur for magnet units as a whole, and that they are random and independent. For the accelerator in this example, an rms misalignment of the 128 magnets of 0.02 cm would be expected to result in a maximum deviation of the equilibrium orbit of ± 2.0 cm.

TABLE I. Illustrative values of the parameters for a radial sector accelerator.

$N=64$	$\beta_1=15.00°$	$\sigma_x=122.1°$
$n_1\doteq n_2=36$	$\beta_2=9.37°$	$\sigma_z=22.0°$
$C=5.35$	$\delta=0.05°$	$\nu_x=21.7$
$k=192.5$	$\phi_1\doteq\phi_2=5.74°$	$\nu_z=3.91$

TABLE II. Physical dimensions of a radial sector accelerator. Subscript 0 refers to maximum energy, subscript i refers to injection.

$E_0=10$ Bev	$E_i=5$ Mev	proton kinetic energy
$r_0=97.3$ m	$r_i=95.0$ m	synchrotron radius
$B_0=20\,000$ gauss	$B_i=200$ gauss	magnet guide field
$\rho_0=18.2$ m	$\rho_i=17.8$ m	radius of curvature
$Z_0=3.0$ cm	$Z_i=15.0$ cm	vertical semiaperture
$r_0-r_i=2.3$ m	radial aperture	
$E_t=12$ Bev	transition energy	
$Z_i=2.5$ cm	vertical semiheight of injected beam	
$\delta_i=\pm 0.001$ radian	angular spread of injected beam	
$p=5\times10^{-6}$ mm Hg	pressure in the vacuum chamber	

The effects of space charge and gas scattering have been treated by Blachman and Courant[16] and others.[17] In this example, an injected beam from a typical Van de Graaf electrostatic accelerator would fill ± 10 cm of aperture after gas scattering. Adiabatic damping of betatron oscillations as the momentum increases by a factor of 100 during acceleration would then reduce these oscillations to ± 1.0 cm. At a reasonable rate of acceleration (75 kilovolts per turn), 3×10^{11} protons per pulse could be accepted.

The values of physical quantities consistent with the parameters of Table I and the above considerations are given in Table II.

Figure 12 illustrates in cross section a possible method of constructing the magnets. Much of the large change in field would be accomplished by back-winding coils on the pole sufaces. Table III illustrates the magnet parameters for the accelerator described above in Tables I and II.

With the rf system described above, the repetition rate is limited only by the rf voltage which can be applied and by the rate of mechanical frequency modulation attainable. Using this rf system with the accelerator of this illustration, one to three pulses per second of 3×10^{11} ten-Bev protons appear attainable.

13. 20-Bev FFAG Proton Synchrotron with Spiral Sectors

As an example of an accelerator made with a ring magnet producing loci of maximum field which cross the path of the particle at a small angle, we take a field of the form (8.1). The motion for this case is treated in Part II. Equations (6.24), (6.27), and (6.31) show that in the smooth approximation

$$\nu_x^2=1+k, \tag{13.1}$$

$$\nu_z^2=-k+(f/wN)^2+\tfrac{1}{2}f^2, \tag{13.2}$$

[15] E. D. Courant and H. S. Snyder, Internal Brookhaven National Laboratory Report, June 1, 1953 (unpublished); G. Lüders, CERN reports CERN-PS/GL 4, GL6, GL7, GL8, and GL9 (unpublished); E. Crosbie, Argonne Accelerator Group, Progress Report No. 5, February 24, 1955 (unpublished).

[16] N. M. Blachman and E. D. Courant, Phys. Rev. **74**, 140 (1948); **75**, 315 (1949).

[17] J. Seiden, Compt. rend. **237**, 1075 (1953); D. W. Kerst, Phys. Rev. **60**, 47 (1941); J. P. Blewett, Phys. Rev. **69**, 87 (1946).

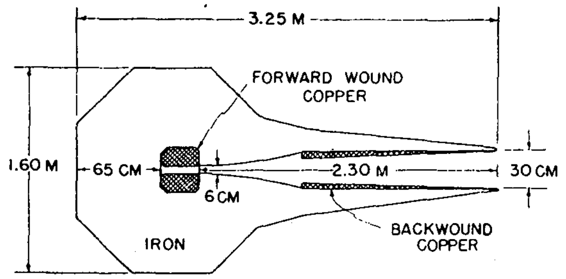

FIG. 12. Cross section of radial-sector magnet and coils.

where $w=\lambda/2\pi$ and λ is the radial separation between adjacent ridges in units of the radius.

Parameters for a 20-Bev ring magnet will be derived using this smooth-approximation result and the condition $\sigma=2\pi\nu/N<\pi$, the stability limit for a Hill equation. Later the alteration of these parameters resulting from exact solution of the linearized differential equation by the use of the Illiac digital computer will be shown.

We can choose from many types of injectors—linear accelerators of 50 Mev, cyclotrons, or, for much lower energy, Van de Graaf electrostatic accelerators. For the purpose of this example, suppose we choose an extreme case in which the ring magnet is able to hold orbits of 5-Mev injected protons at its inside rim and orbits of 20-Bev protons at its outside rim. We can choose $k=82.5$, $r_0=5000$ cm, where r_0 is the mean radius of the high-energy orbit using 14 000 gauss for the average field strength at the orbit. This gives $r_i=4688$ cm as the mean radius of the 5-Mev orbit. A radial extent of the magnet gap of approximately $d=r_0-r_i=312$ cm is needed. The ratio of the average field at the high-energy orbit to the average field at the low-energy orbit is $\bar{H}_0/\bar{H}_i=203$.

Since $k=82.5$, $\nu_x=9.15$ radial betatron oscillations around the machine according to the smooth approximation. To remain within the stability limit for the linearized differential equation with varying coefficients we must have $2\nu<N$. Choose $N=31$ sectors or ridges crossed in one passage around the machine. This gives $\sigma_x=0.6\pi$. We can then choose $\sigma_z=0.268\pi$, so that $\nu_z=4.15$. This choice of ν_x and ν_z avoids the forbidden lines on Fig. 9. The working point chosen is then in one of the two largest squares available in (ν_x,ν_z) space. The ridge characteristics can now be found by the second smooth approximation Eq. (13.2) which gives $f/w=218$ with the above values of N and k.

Thus if we take $f=\frac{1}{4}$, then $\lambda=0.00506$ in units of the radius, so that the radial separation of the ridges at the outside edge is 25.3 cm. This result is only approximate.

TABLE III. Magnet parameters characterizing a radial sector accelerator.

Total weight of iron	9650 tons
Total weight of copper	670 tons
Required current	112 000 ampere turns
Required magnet excitation power	5.5 megawatts

The accurate solution to the linearized equations can be summarized in the form shown in Fig. 8 which exhibits the "necktie" for the case of a magnetic field of our prescribed form in the median plane. According to this diagram, take $\sigma_x=0.615\pi$ and $\sigma_z=0.25\pi$; then $f/wN^2=0.303$ and $k/N^2=0.075$. If we choose $N=33$ sectors, we have: $\nu_x=10.15$, $\nu_z=4.15$. Both values are now in the middle of a different large square allowed by the integral, half-integral, and third integral rules. (To be in the center of the largest allowed squares, the working point ν_x, ν_z should be 0.15 units above integers for both dimensions or 0.15 units below integers for both dimensions.) If we again take $f=\frac{1}{4}$, then $w=1/1320$, so $\lambda r_0=23.8$ cm radial ridge separation.

At this point, consideration must be given to the possible magnitude of f which can be achieved. The shapes of magnetic potential surfaces which will produce a flutter $f=\frac{1}{4}$ with $k=150$ are shown in Fig. 13. The curves are loci of constant magnetic potential for several different values of the potential. These curves were determined by digital computation. They show deep crevices developing in the surfaces or poles when the ridge is about 0.13λ away from the median plane. Apparently when the gap between ridges exceeds $\frac{1}{4}$ of the radial separation of the ridges, the crevices in the surfaces occur. These crevices mean that a pole of opposite polarity is needed in the crevices to produce the required flutter when the gap is large. If we do not want pole faces with these reverse poles embedded in them, then the gap between ridges must not exceed one fourth of the radial separation of the ridges. The same result has been obtained analytically.

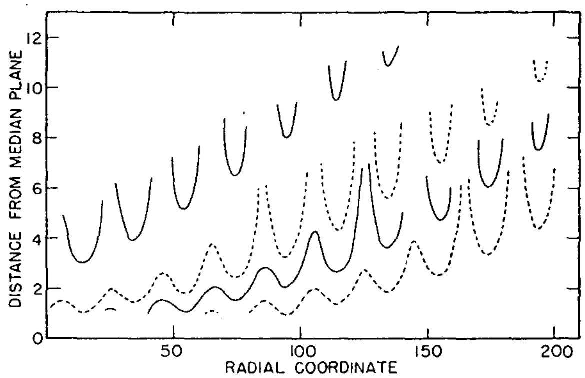

FIG. 13. Spiral-sector equipotentials for $k=150$ and $f=0.25$. Ordinates and abscissas are in the same units.

Figure 14 shows the calculated shape of the equipotential surfaces for $f=\frac{1}{4}$. The dependence of gap is shown in Fig. 15 where G is the maximum gap at ridge tops without forward windings. If we require that the ν's be constant, f/w must be constant. Thus we plot Gf/w vs f in Fig. 1. We see that the flutter f which gives the maximum possible gap at the ridges, under conditions of constant alternating-gradient focusing, that is, constant f/w, is $f=\frac{1}{4}$, and the maximum gap is $G=0.275$ in units of the ridge separation. The curves show that flutter factors from 0.14 to 0.36, without crevices in the poles, require that the gap be only 10% less than the maximum possible gap. These analytical results are similar to those from digital computation as already mentioned.

For the example we are considering, we had $\lambda r_0 = 2\pi w r_0 = 23.8$ cm radial separation between ridges at r_0. This means that if we choose $G=0.275\lambda r_0$, then $G=6.15$ cm at the injection radius and 6.6 cm at the high-energy radius.

To make the magnetic field 203 times larger at the high-energy radius than at the injection radius, this gap would have to be reduced by a factor of 203 unless currents are distributed on the pole face. By placing such windings between iron ridges, the gap can be kept full size at all radii. Thus, by proper winding, $G(r)$ could always be about 0.275 times the ridge separation,

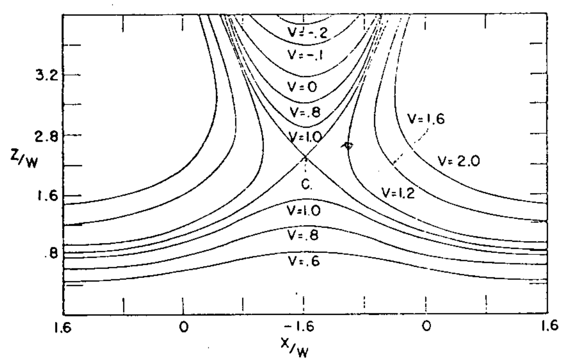

FIG. 14. Magnetic potentials, $V=Z/W+f\sin(X/W)\sin[H(Z/W)]$, for $k=0$ and $f=0.25$. Poles corresponding to $V=1.1$ have the widest gap without crevices in the pole surface.

which is practically constant. However, it is not most desirable to have the gap essentially constant at all radii because the amplitude of betatron oscillations decreases as $p^{-\frac{1}{2}}$ while the particle is being accelerated. Thus if the momentum increases by a factor of $\sim$203, then the space required for betatron oscillations decreases by a factor of $(200)^{\frac{1}{2}}$ or $\sim$14. Consequently it would be best to have the gap at the injection radius about 10 times larger than the gap at high energy and it would be desirable to fill this large aperture with beam at the injection time. Actually the gap at successive energies should be big enough to accommodate not only the decreasing betatron oscillations but also the misalignment distortion of the equilibrium orbit. If we maintain a gap as large as possible without the addition of opposite poles between ridges, that is if we keep $G=0.275\lambda r$, then the aperture available actually increases slightly during acceleration due to the slight increase in r. To reverse this gap variation without decreasing the gap below about 6.2 cm would require

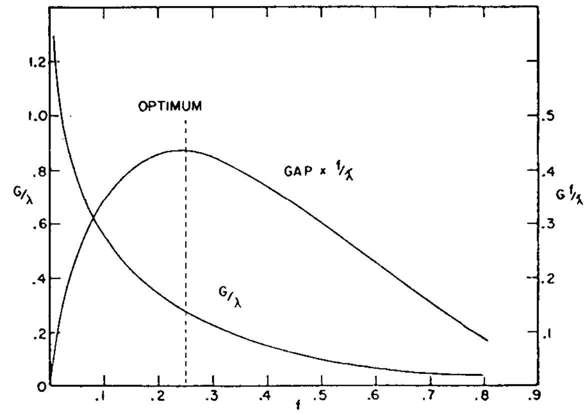

FIG. 15. Maximum gap, G, times (f/λ), for fixed tune as a function of f. The criterion of no crevice in the pole face is used. The field variation in the orbital plane is sinusoidal.

introduction of reverse poles between ridges where it is most easily done, that is at the low-field rim. In practice this can be accomplished by running currents in two directions between a few of the low-field ridges. Then the iron surfaces may be separated farther to give an increased vertical aperture. It seems reasonable that the gap at the injection radius could be doubled this way.

A configuration of the ridges and coils which produces the correct field shape is shown in Fig. 16 which shows iron contours as magnetic equipotentials. The location of current-carrying copper between the ridges is shown. This current terminates some magnetic potential surfaces, allowing the iron to be brought down to the same gap magnitude at successive ridges. Since the magnetic field decreases by the same factor between all adjacent ridges, the amount of back-wound current in the slot decreases by the same factor between slots. Thus the slot at the high-field ridge carries the largest number of back-wound ampere turns. The figure shows how the gap at the injection radius might be doubled by using forward and backward currents in the slot. Such a magnet requires about 1.8 megawatts of power.

With this method of providing the field shaping, it would be necessary to carry current over the ridges of iron as they spiral outwardly. A way to do this is to have the gap between ridge tops close a little as they spiral outward to produce the field increasing as r^k, and then to have the wires carrying current come back to the

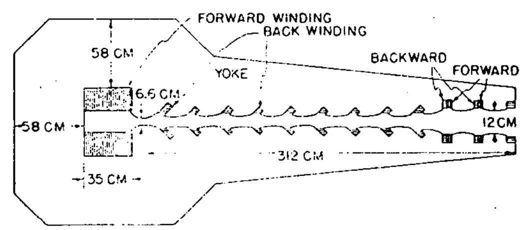

FIG. 16. Spiral-sector magnetic structure. The insertion of back-wound current carrying conductors allows the gap between the poles to be about the same for all ridges.

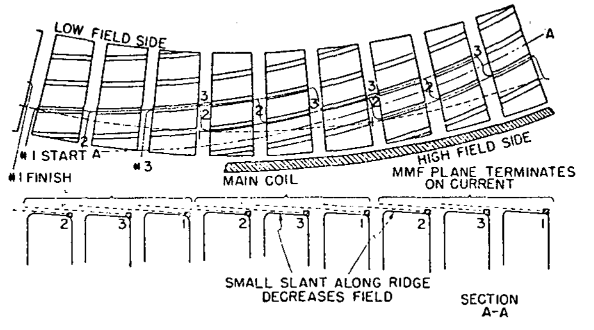

FIG. 17. Method of bringing conductors back across ridges at straight sections.

beginning radius at the start of the next sector around the magnet. Straight sections between sectors provide the opportunity to bring the conductors back to the same radius. Since the field changes by about 35% from ridge to ridge, the gap would have to change by about 35% between the crests of ridges from one end of a sector to the other. A less drastic change in gap along ridges results if the sectors, which are about 32 feet long, are subdivided say 3 times to form approximately 10-foot lengths with straight sections between. Then the gap needs to vary only about 12% along a ridge top and the wires between ridges can come back to the same radius every 11 feet around the circumference. This is shown in Fig. 17.

This brings up the problem of straight sections where the magnet is separated and where the field is approximately zero. If such cuts in the magnet are made along approximately radial lines, the machine and the orbits do not scale. Consequently σ varies periodically as the radius of the orbit grows. This problem is one of the most important being studied by the MURA technical group and there are indications that the distribution of the straight sections, such as subdivision of sectors into several parts as just mentioned, minimizes the variation of σ to a tolerable value with a useful length of straight section.

There is another example of a method to attain the desired field shape which simplifies some of the problems and which has been studied in the form of magnetic models by the MURA technical group. Such a structure is shown in Fig. 18. The average radial dependence of field (r^k) is produced by back-windings on iron poles similar to those used in a radial-sector magnet. The magnetic equipotential surfaces so formed are distorted or kinked by some other means such as the presence of iron rods having the same shape as the desired magnetic equipotentials on the side toward the orbits. These rods assume their magnetic potential from their positions in the gap. Since the rods spiral from one radius to another, they must be segmented with a few nonmagnetic spacers such as brass washers to prevent magnetic flux from traveling along the rod. Such ridges and the proper fields were achieved in the models made by F. L. Peterson and T. B. Elfe of the MURA technical group.

An interesting observation which they made shows that there is the possibility of relaxing the requirements for a small gap in a spiral sector magnet. They were able to increase f greatly above the design figure of $\frac{1}{4}$ without closing the gap and without using reverse poles or deep crevices between ridges. It was done merely by deviating slightly from a simple sinusoidal field variation. A value of $f \sim 0.38$ was reached without a great harmonic distortion of the field in the median plane. Further studies of this possibility will be needed to show how much the alternating-gradient term in ν_z is increased by the attainable field shapes. Any increase would allow opening the gap more.

An important question must be answered before it is known how large a gap is useful. As pointed out in Sec. 9, the motion of a particle in a magnetic field which causes nonlinear restoring forces generally has a limit to the amplitude for stable motion or an amplitude limit beyond which the particle starts to oscillate about a second closed equilibrium orbit in or outside the accelerator. If oscillation about this second orbit takes the particle out of the aperture, the particle is lost. In the radial direction this limit can be as large as 0.1 to 0.3 of a ridge separation and in the axial direction it is smaller. The example given does not have an especially large limit because σ_x is near $2\pi/3$. The increase of such stability limits by suppression of some of the nonlinear forces would make it worthwhile to open the gap farther than 0.275 of the ridge separation because more vertical space useful for betatron oscillations would become available. For some vertical stability limits observed with the digital computer, there would be no value in opening the gap wider because the stability limit is within the gap available. The sources of the nonlinear effects are being studied with the purpose of designing a spiral-sector system to make larger gaps useful. In general, if the angle ζ is made smaller so the oscillations do not cause a large variation in sector length, the stability limit increases.

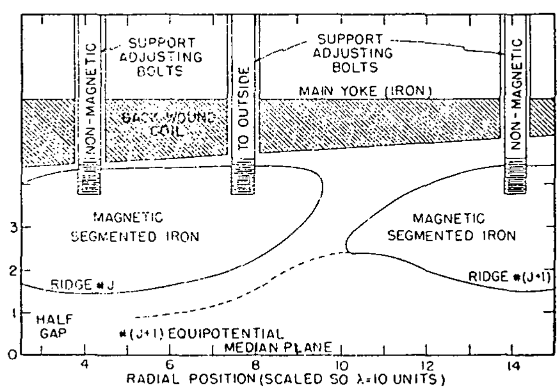

FIG. 18. Floating equipotentials which produce sinusoidal field variation.

The most promising method of decreasing ζ and hence decreasing the nonlinearities so that the stability limit is increased is to use magnets which produce a large flutter, f. Two very promising cases of this type follow:

One case has rectangular ridges of iron with the gap between ridges $\frac{1}{4}$ as big as the gap at the valleys. (See Fig. 19.) Taking account of the fringing flux, we can produce an $f=\sqrt{2}\langle\Delta H\rangle_{\mathrm{rms}}/\bar{H}=0.71$ in the favorable case of $A=2$ and $D=9$, where A and D are in units of half-gaps. If we want $f/w=330$, as in the previous example, then $w=0.00215$. This case gives a good size for the injection aperture:

$$G=[4\pi w/(A+D)]\times 4688 \text{ cm}=11.1 \text{ cm}.$$

The circumference factor is less than $(A+D)/(A+\frac{1}{4}D)=2.3$ which could be tolerated at the injection radius. If we do not require that the equilibrium orbits scale, then the ridge proportions can change and the circumference factor can be improved at the high-energy radius. For example, a gradual transition could be made to $A=9$, $D=8$, and $G=7$ cm, with the same f/w including fringing effects. The circumference factor, including fringing effects, is then 1.38.

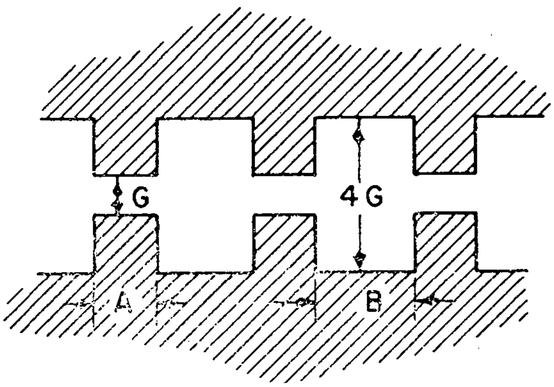

FIG. 19. Rectangular spiral ridges. The distributed back-winding is circumferential.

A structure which has many desirable features is a separated spiral-sector magnet. By winding each spiral ridge separately with a forward coil and with distributed back-windings on the pole face (in the manner shown in Fig. 12 for radial sector magnets), the ridges can be spaced widely enough to bring the field down to approximately zero between ridges; this increases f greatly. If the field shape is that shown in Fig. 20, which gives a circumference factor of 2, the flutter f is 1.28 and the gap can be about 30 cm. The angle between the sector edge and the orbit is large enough to allow a large-amplitude betatron oscillation before the stability limit is reached—possibly as much as 90-cm amplitude. Sector dimensions are shown in Fig. 21.

The gap at the high-field radius can be made much less than 30 cm in order to conserve power, but it is highly desirable to keep this large gap at the low-energy radius for injection purposes.

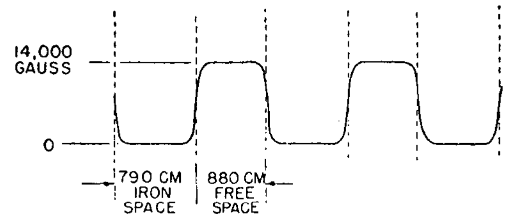

FIG. 20. Circumferential distribution of axial field for separated spiral sectors, at 10 000-cm radius with 30-cm gap.

While this structure requires a large circumference (not all occupied by iron), it has many conveniences compared to magnets already described. The fabrication has simplifying features. The vacuum tube is more easily constructed. Access to the beam for targets is better. The sectors can be separated more where longer straight sections are desired and scaling is still possible. The nonlinear stability limit should be comfortably large, permitting a large useful injection aperture.

14. FFAG Betatrons

The large momentum spread which can be held by FFAG magnets allows a great increase in the acceptance time of injected particles if betatron acceleration is used.[4] The injected particles may be accepted into stable orbits in the dc magnet gap at the low-energy radius all the time that the central magnetic flux is rising; as the particles gain energy, they spiral toward the high-field radius. After each particle orbit has linked a certain change of flux, $\Delta\phi$, corresponding to an increase in momentum to its final value, it reaches the target (or ejector) radius. Charged particles continue to arrive at the target as long as the flux continues to rise beyond $\Delta\phi$. If $\Delta\phi$ is less than the maximum core flux, ϕ_0, useful injection and ejection may occur as much as 25% of the time by cycling the core flux between $+\phi_0$ and $-\phi_0$. When sinusoidal core excitation is used, the duty factor D (the fraction of time for useful

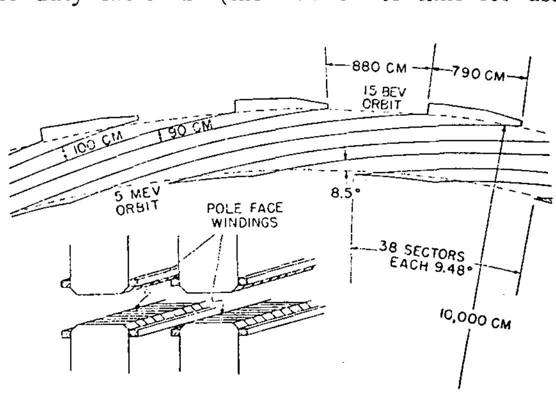

FIG. 21. Separated spiral-sector geometry. Each ridge has its own windings.

injection) is given as follows (see Fig. 22):

$$D=\frac{1}{2\pi}\cos^{-1}\left[\frac{\Delta\phi}{\phi_0}-1\right]. \tag{14.1}$$

In order to miss an injector structure, a certain minimum rate of acceleration (rate of rise of flux) at injection is required; this will reduce the duty factor in practice.

Since the particle equilibrium orbit is not circular and since its radius changes with acceleration, the relationship between $\Delta\phi$ and the momentum increase differs from that for conventional betatrons.

The voltage gain per revolution is, in Gaussian units,

$$V=(1/c)(d\phi/dt), \tag{14.2}$$

where ϕ is the flux in the betatron core. The rate of increase in energy is therefore

$$\frac{dE}{dt}=\left(\frac{e\omega}{2\pi c}\right)\frac{d\phi}{dt}, \tag{14.3}$$

where $\omega/2\pi$ is the frequency of revolution [Eq. (10.3)]. We have, therefore,

$$Rdp=\frac{dE}{\omega}=\left(\frac{e}{2\pi c}\right)d\phi, \tag{14.4}$$

and the required accelerating flux change is determined by

$$\phi_2-\phi_1=\frac{2\pi c\bar{R}}{e}(p_2-p_1), \tag{14.5}$$

where

$$\bar{R}=\frac{1}{p_2-p_1}\int_{p_1}^{p_2}Rdp. \tag{14.6}$$

If k is constant, we have, by Eq. (5.14),

$$\bar{R}=R_2\left(\frac{k+1}{k+2}\right)\frac{1-(p_1/p_2)^{(k+2)/(k+1)}}{1-(p_1/p_2)}$$

$$\doteq\left(\frac{k+1}{k+2}\right)R_2,\quad \text{if}\quad p_1\ll p_2. \tag{14.7}$$

With FFAG guide fields in the 20- to 300-Mev energy range, the duty factor could be increased by more than a factor of 10^4 over that in existing betatrons and synchrotrons. The beam current increase would probably be less because of space-charge effects at injection.

In pulsed-field betatrons, large amounts of energy are stored in the pulsed-guide field magnet gap, and equipment capable of handling the large circulating currents and voltages must be used. In FFAG betatrons, only the accelerating core is pulsed, and it would be a closed iron circuit which would require much less energy storage, and therefore a much smaller condenser bank and less ac power equipment.

Either the radial-sector or the spiral-sector type of FFAG magnet could be used for electron betatron acceleration up to a few hundred Mev, and the design would be subject to the same considerations as discussed above for synchrotrons. Since the core flux change for a given particle momentum increase is proportional to the particle period of revolution, the smaller circumference of the spiral sector type is doubly important for betatrons. In focusing magnets designed for the betatron energy range, an N of 10 to 30 appears more suitable than the higher N values suggested for multi-Bev synchrotrons.

The output beam of electrons from an FFAG betatron would be nearly monoenergetic and spread over a long time corresponding to the duty factor. Present betatrons and synchrotrons achieve a lengthened output beam pulse at the expense of energy homogeneity, since the electrons are in a sinusoidally varying field at essentially constant radius. This and the prospect of beam currents approaching time-average values of milliamperes makes this an attractive accelerator for electrons from a few Mev to several hundred Mev.

15. FFAG Cyclotrons

To make semirelativistic particles revolve in a cyclotron at constant frequency and in orbits that are approximately circles, it is necessary to have the average magnetic field increase with radius. In order to avoid the resultant axial defocusing, alternating-gradient focusing may be employed. There are a number of possible magnetic field configurations for such a fixed-field alternating-gradient cyclotron. The first such cyclotron was proposed by Thomas.[5] The Thomas cyclotron is essentially a radial-sector FFAG machine having three or more sectors with a roughly sinusoidal field flutter. Thomas showed that such a machine has stable orbits for energies up to a limit depending upon the number of sectors. A considerable amount of experimental and theoretical work on the Thomas

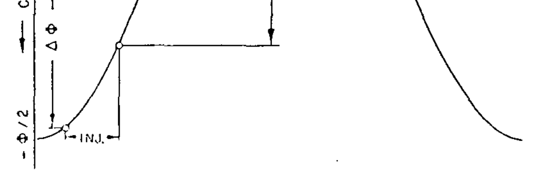

FIG. 22. Time dependence of betatron flux showing duty factor.

cyclotron has been carried out at the University of California, culminating in the successful construction and operation of two electron models which accelerate electrons up to half the speed of light.[18] We will here discuss briefly the general features of FFAG cyclotrons with particular reference to spiral-sector configurations.

In Sec. 10, we have obtained a relation (10.9) between the total energy E and the mean field index k for a cyclotron, in which the frequency of revolution is independent of energy. We have also the approximate expressions developed in Sec. 7 relating k to the betatron oscillation frequencies. For spiral sectors, the simple approximate relation (6.24) holds:

$$\nu_x = (1+k)^{\frac{1}{2}}. \tag{15.1}$$

According to Eq. (10.9), ν_x is given directly in terms of the energy by the relation

$$\nu_x \doteq E/E_0. \tag{15.2}$$

It is clear that the orbits in such a cyclotron start at the center at $E=E_0$ with $\nu_x=1$ (as in a conventional cyclotron), and that as E increases, successive integral and half-integral radial resonances are encountered at energies which are approximately integral and half-integral multiples of E_0. If we regard the first integral resonance as the limiting energy, then the maximum kinetic energy is about one rest energy (actually somewhat less, according to more accurate calculations[19]). If sufficiently high dee voltage is applied, and if magnetic field errors are sufficiently small, it may be possible to drive the particle energy through resonances fast enough to avoid buildup of oscillations. In any case, for stability, ν_x must be less than $\frac{1}{2}N$, so that E can never be greater than about $\frac{1}{2}NE_0$. The predicted existence (Sec. 9) of a strong third integral resonance at $\sigma_x = 2\pi/3$, $(\nu_x = N/3)$, may set an even lower limit on E for a given number of sectors N.

In a *radial*-sector configuration in which the number of sectors is small ($N<8$), the alternating-gradient focusing also comes primarily from the η term in Eq. (5.13), and consequently the relations (15.1) and (15.2) are still roughly correct and the preceding considerations are still qualitatively correct. In particular, this is true of a Thomas cyclotron.

In a cyclotron in which the η term in Eq. (5.13) predominates, we see from Eqs. (6.24) and (6.25) that the focusing depends on k and on the quantity

$$F = 2\left\langle \left(\frac{1}{\eta}\frac{\partial \eta}{\partial \Theta}\right)^2 \right\rangle_{\text{Av}} + \tfrac{1}{2}f^2. \tag{15.3}$$

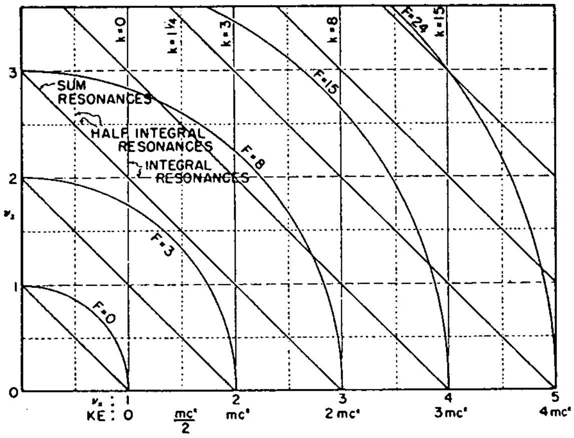

FIG. 23. Working point diagram for a spiral-sector cyclotron. F is the AG focusing parameter.

The focusing parameter F is determined, according to Eqs. (6.24) and (6.25), by the relation

$$F = \nu_x^2 + \nu_z^2 - 1. \tag{15.4}$$

In Sec. 6, we have noted that with spiral sectors, the optimum flutter factor f is about $\frac{1}{4}$, for maximum vertical aperture without extra forward pole-face windings. With this value of f, the focusing parameter F may be written, with the help of Eq. (6.26),

$$F \doteq \tfrac{1}{16}(\tan^2\zeta + \tfrac{1}{2}). \tag{15.5}$$

In Fig. 23, we plot circles of constant F *vs* ν_x and ν_z. Vertical lines of constant k (hence constant E) are marked in the figure. We show also lines representing integral and half integral resonances (ν_x, ν_z = integer or half-integer) and sum resonances ($\nu_x+\nu_z$ = integer). As the energy increases from E_0 to E, the working point (ν_x,ν_z) will trace out a curve connecting the line $k=0$ with the line $K=(E/E_0)^{\frac{1}{2}}-1$. The form of this working point curve will depend on the way F varies with radius. In a practical magnet, F will almost necessarily be zero at the center so that the curve will start near ($\nu_x=1$, $\nu_z=0$). Difficulties may be expected in accelerating particles beyond a point where the working point crosses any of the resonance lines, particularly integral resonances, or resonances involving the vertical motion (since the vertical aperture is not large). It is clear from Fig. 23 that the working point necessarily crosses a half-integral radial resonance near $E=E_0+\frac{1}{2}E_0$, and a sum resonance and an integral radial resonance before reaching $E=2E_0$.

In order to get a picture of an FFAG cyclotron, we note that the frequency of revolution of an ion in a cyclotron is

$$\omega/2\pi = \beta c/2\pi R = c/2\pi\lambda\!\!\!^{-}, \tag{15.6}$$

where $2\pi\lambda\!\!\!^{-}$ is the wavelength of the radio-frequency voltage required to drive the dees (we assume first-harmonic operation). We have therefore the following

[18] D. L. Judd, Phys. Rev. **100**, 1804(A) (1955); Pyle, Kelly, Richardson, and Thornton, Phys. Rev. **100**, 1804(A) (1955); Heusinkveld, Jakobson, Ruby, Smith, and Wright, Phys. Rev. **100**, 1804(A) (1955). We are indebted to Dr. Judd for a discussion of the work done at Berkeley, which is described in University of California Radiation Laboratory Reports No. 2344 and No. 2435 (unpublished).

[19] D. S. Falk and T. A. Welton, Bull. Am. Phys. Soc. Ser. II, 1, 60 (1956).

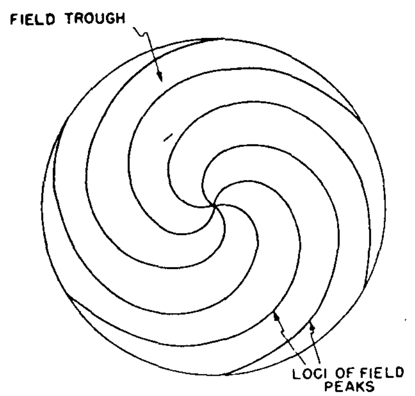

FIG. 24. Plan view of ridges in a 6-sector spiral-sector cyclotron.

relation between energy and radius:

$$E/E_0=\lambda/(\lambda^2-R^2)^{\frac{1}{2}}. \tag{15.7}$$

The momentum $p(R)$ is

$$p=mcR/(\lambda^2-R^2)^{\frac{1}{2}}, \tag{15.8}$$

the mean magnetic field is

$$\bar{H}=\frac{pc}{eR}=\frac{mc^2/e}{(\lambda^2-R^2)^{\frac{1}{2}}}, \tag{15.9}$$

and the mean field index [Eq. (10.9)] is

$$k=R^2/(\lambda^2-R^2). \tag{15.10}$$

The relations (15.6)–(15.10) are exact. In order to determine the shape of the spiral ridges, we must solve the equations for betatron oscillations. We can get a rough idea of the ridge pattern from the approximate relations (15.1), (15.4), and (15.5). If we combine these formulas with (15.10), we obtain

$$\tan^2\zeta=\frac{16R^2}{\lambda^2-R^2}+\nu_z^2-\tfrac{1}{2}. \tag{15.11}$$

Let us now assume for example that the working point

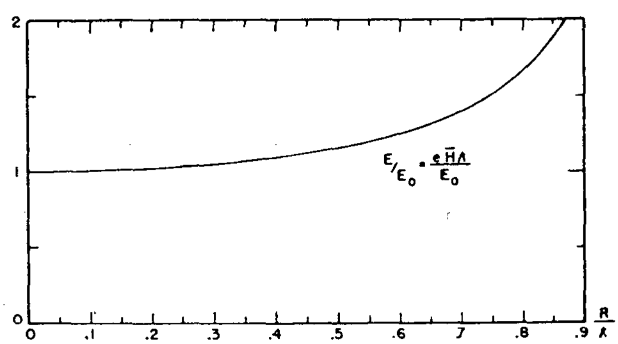

FIG. 25. Total energy and magnetic field as a function of radius in a constant-frequency cyclotron. (E_0 is the rest mass and $2\pi\lambda$ is the oscillator wavelength.)

in Fig. 23 moves along the horizontal $\nu_z=1/\sqrt{2}$, so that

$$\tan\zeta \doteq \frac{4R}{(\lambda^2-R^2)^{\frac{1}{2}}}. \tag{15.12}$$

If we neglect the scalloping of the equilibrium orbit, we may replace R by the radius r, and substitute in Eq. (6.30) to obtain the equation for a spiral ridge in polar coordinates:

$$\theta_0=4\sin^{-1}(r/\lambda). \tag{15.13}$$

If we assume a sinusoidal field flutter, the function μ is

$$\mu=1+\tfrac{1}{4}\cos[N(\theta-\theta_0)], \tag{15.14}$$

and the magnetic field is given by

$$H=\bar{H}\mu=\frac{mc^2/e}{(\lambda^2-R^2)^{\frac{1}{2}}}\times\{1+\tfrac{1}{4}\cos[N\theta-4N\sin^{-1}(r/\lambda)]\}. \tag{15.15}$$

The number of sectors N is, to this approximation, still arbitrary. If the output energy is to be $E=2E_0$, (about 1-Bev kinetic energy for protons), then $\nu_x\doteq 2$ at the output radius, and N must be at least 4, for linear stability of the betatron oscillations. In order to avoid the third integral nonlinear resonance at $\sigma_x=2\pi/3$, we should probably take $N=6$. In Fig. 24, we plot the ridges and troughs given by Eq. (15.13) for a cyclotron with six spiral sectors and an output energy $E=2E_0$. In Fig. 25, we plot E and $\bar{H}$ *vs* R for such a cyclotron.

ACKNOWLEDGMENTS

We wish to acknowledge many helpful discussions with H. R. Crane, F. T. Cole, Nils Vogt-Nilsen, J. N. Snyder, and other members of the Midwestern Universities Research Association technical group.

APPENDIX A. THE SMOOTH APPROXIMATION

Let the alternating-gradient equation of motion in one dimension be written in the form

$$d^2x/d\theta^2=f(x,\theta), \tag{A.1}$$

where the force $f(x,\theta)$ is periodic in θ with period $2\pi/N$. We will assume that $N\gg\nu$, that is, that the betatron wavelength is long compared with the sector length. It is then reasonable to seek an approximate solution of the form

$$x=X+\xi(X,\theta), \tag{A.2}$$

where the "smooth" oscillation $X(\theta)$ satisfies an equation of the form

$$d^2X/d\theta^2=F(X), \tag{A.3}$$

independent of the sector periodicity, and the "ripple" $\xi(X,\theta)$ is periodic in θ with period $2\pi/N$ and with zero mean, for fixed X. We will assume that the ripple ξ

and the derivatives $dX/d\theta$, $d^2X/d\theta^2$ are small in a sense to be made more precise presently.

We substitute Eq. (A.2) in (A.1) to obtain

$$X''+\xi_{\theta\theta}+2\xi_{X\theta}X'+\xi_{XX}X'^2+\xi_X X''=f(X+\xi,\theta), \quad (A.4)$$

where primes deonote derivatives with respect to θ. We now average over θ, keeping X, X', X'' fixed, remembering that $\langle\xi\rangle_{Av}=0$, to obtain an equation corresponding to (A.3):

$$d^2X/d\theta^2=\langle f(X+\xi,\theta\rangle_{Av}. \quad (A.5)$$

We subtract Eq. (A.5) from (A.4):

$$\xi_{\theta\theta}=\{f(X+\xi,\theta)\}-2\xi_{X\theta}X'-\xi_{XX}X'^2-\xi_X X''. \quad (A.6)$$

We use the notation introduced in the definition (4.14). It is easy to see that the last two terms are of order $(\sigma/2\pi)^2$ relative to the first term, and are therefore negligible if $N\gg\nu$. The second term is only of order σ/π relative to the first, but its effect on the smooth equation (A.5) can be shown to cancel out to first order. We therefore neglect the last three terms in Eq. (A.6) and replace $\{f(X+\xi,\theta)\}$ by $\{f(X,\theta)\}$, i.e., we assume that $\{\xi f_X\}\ll\{f\}$. We can then integrate Eq. (A.6) to obtain, as a first approximation to the ripple,

$$\xi=f_2(X,\theta), \quad (A.7)$$

in the notation introduced in definitions (4.16) and (4.17). If we substitute the ripple (A.7) in Eq. (A.5), we obtain, to first order in ξ, the smooth approximation

$$d^2X/d\theta^2=\langle f\rangle_{Av}+\langle f_2 f_X\rangle_{Av}. \quad (A.8)$$

(Essentially the same result has been obtained by Sigurgiersson.[20]) To the solution of Eq. (A.8) is to be added the ripple (A.7) to obtain an approximate solution to Eq. (A.1). The second term on the right in Eq. (A.8) can be integrated by parts and rewritten in the form

$$d^2X/d\theta^2=\langle f\rangle_{Av}-\langle f_1 f_{X1}\rangle_{Av}. \quad (A.9)$$

If the force in Eq. (A.1) is linear in x,

$$f(x,\theta)=g(\theta)x, \quad (A.10)$$

[20] T. Sigurgiersson, CERN report, CERN-T/TS-1, December, 952; CERN-T/TS-3, May, 1953 (unpublished).

then Eq. (A.9) can be written as a linear equation

$$d^2X/d\theta^2=[\langle g\rangle_{Av}-\langle g_1^2\rangle_{Av}]X, \quad (A.11)$$

and the approximate solution (A.2) then can be written in the Floquet form

$$x=e^{\pm i\nu\theta}[1+g_2(\theta)], \quad (A.12)$$

where

$$\nu^2=\langle g_1^2\rangle_{Av}-\langle g\rangle_{Av}. \quad (A.13)$$

The above results can be immediately generalized to the two-dimensional case

$$\begin{aligned} d^2x/d\theta^2&=f(x,z,\theta),\\ d^2z/d\theta^2&=g(x,z,\theta). \end{aligned} \quad (A.14)$$

We assume a solution of the form

$$\begin{aligned} x&=X+\xi,\\ z&=Z+\zeta. \end{aligned} \quad (A.15)$$

We have the approximate equations

$$\begin{aligned} \xi&=f_2(X,Z,\theta),\\ \zeta&=g_2(X,Z,\theta), \end{aligned} \quad (A.16)$$

where X, Z satisfy

$$\begin{aligned} d^2X/d\theta^2&=\langle f\rangle_{Av}+\langle f_2 f_X\rangle_{Av}+\langle g_2 f_Z\rangle_{Av},\\ d^2Z/d\theta^2&=\langle g\rangle_{Av}+\langle f_2 g_X\rangle_{Av}+\langle g_2 g_Z\rangle_{Av}, \end{aligned} \quad (A.17)$$

where averages are over θ with X, Z fixed.

In practice, we have found that Eq. (A.13) gives values of ν or $\sigma(=2\pi\nu/N)$ which are accurate to within about 10% of $[\langle g_1^2\rangle_{Av}]^{\frac{1}{2}}$, provided that $[\langle g_1^2\rangle_{Av}]^{\frac{1}{2}}\lesssim N/4$. A few nonlinear cases have been studied, and solutions of Eqs. (A.8) and (A.17) have yielded results in fair agreement with more accurate calculations except near stability boundaries. Stability boundaries where the betatron wavelength becomes infinite are fairly accurately predicted by Eqs. (A.8) and (A.17) but the (more interesting) stability boundaries due to sector resonances when the betatron wavelength becomes a small integral number of sectors are not predicted at all by the smooth equations.

Reprinted from THE REVIEW OF SCIENTIFIC INSTRUMENTS, Vol. 28, No. 11, 970–971, November, 1957
Printed in U. S. A.

Operation of a Spiral Sector Fixed Field Alternating Gradient Accelerator*

D. W. KERST,† H. J. HAUSMAN,‡ R. O. HAXBY,§ L. J. LASLETT,|| F. E. MILLS, T. OHKAWA,¶ F. L. PETERSON, A. M. SESSLER,‡ J. N. SNYDER,† AND W. A. WALLENMEYER

Midwestern Universities Research Association, Madison, Wisconsin

(Received September 26, 1957)

FIXED field alternating gradient particle focusing[1] by a ring of sectors provides the possibility of accelerating large currents of particles in direct current magnets by the application of the alternating gradient principle. There are two characteristically different types of FFAG magnets—radial sector and spiral sector. A successful radial sector model was constructed by the group of MURA Universities in 1956.[2] The radial sector type requires some magnets to have a reversed magnetic field to reverse the gradient with a consequently large circumference. This letter describes a successfully operating spiral sector accelerator (see Fig. 1) in which the magnetic field is unidirectional and the alternation of the gradient is achieved by the edge focusing of the spiral sectors.[1] This spiral type can have a smaller circumference because the field is unidirectional.

Nonlinear focusing forces are prominent in FFAG accelerators, because the average magnetic field varies as r^k where r is the radius and k is a constant and because the orbit crosses magnet edges at an angle other than $\pi/2$. The latter fact causes very strong quadratic forces in the spiral sector type. For this reason the new model was thoroughly tested before construction by digital computers, the ILLIAC at Illinois and the IBM 704 at MURA. Magnetic fields resulting from iron and current configurations were determined by the computers by solving the magnetic potential problem. This problem is reducible to a two-dimensional problem because the structures were chosen to scale proportionally with the radius. The fields were stored on a mesh and the orbits of particles passing through these fields were computed. Radial and axial betatron oscillation frequencies and phase space stability limits due to nonlinear forces were determined. A working point was chosen sufficiently far from the difference resonance, $2\nu_z=\nu_r$, to avoid axial oscillation growth (ν_z=number of axial betatron oscillations per revolution, ν_r=radial oscillations per revolution). The chosen point was $\nu_z=1.13$ and $\nu_r=1.40$. Structural tolerances were obtained by calculating the effects of displaced sectors and sectors with erroneous k in the digital computer runs. Errors of one millimeter in sector positions had minor effects on the computed stability limits. The magnet with 6 sectors and an injection radius at 30.5 cm and a final radius of 55 cm was constructed well within these tolerances. k was trimmed by adding small coils to supply the magnetomotive force lost by the finite iron permeability and not taken into account in the computer tests. The radial component of magnetic field in the orbital plane was detected by an iron strip second harmonic generating magnetometer. This component was brought below the value equivalent to a one millimeter axial displacement of a sector (about 0.1 gauss) by adjusting coil positions and by slight corrections on reluctance differences between top and bottom poles.

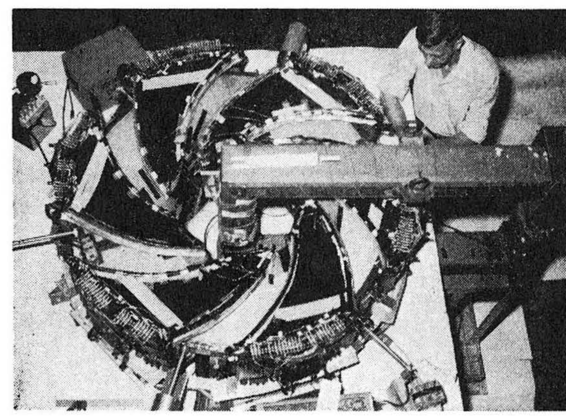

FIG. 1.

An injector of the type used in betatrons directs its focus into a inflector which turns the beam into the equilibrium orbit. Electrons injected at 30 kev are accelerated to ~120 kev by action of a betatron induction core. The values of ν_z and ν_r measured by a radio-frequency knock-out probe are 1.05 and 1.41, respectively. Coils for tuning radial frequency by changing k and for tuning axial frequency by changing the flutter of the field are available for examining other working points. Without these tuning coils energized the backwinding on the magnet pole face produces measured values of 0.7 for k and 1.02 for the flutter, defined as $f=\sqrt{2}\langle\Delta B\rangle_{\mathrm{rms}}/\bar{B}$, averages being taken around a circle. This measured flutter is less than the design flutter and causes the lower value of ν_z. The angle between the normal to the magnet edge and the radius of the machine is 43°. The gap at the low-energy radius was chosen to be 8 cm and the structure, including the gap, scales up with the radius. This conservative choice of parameters provides structural simplicity without eliminating the nonlinearity difficulties which must be faced in a spiral sector accelerator. Preliminary estimates indicate that injection for four microseconds gives 10^9 electrons accelerated to the target.

* This work was supported by the U. S. Atomic Energy Commission, The National Science Foundation, and The Office of Naval Research.

† University of Illinois, Urbana, Illinois.

‡ The Ohio State University, Columbus, Ohio.

§ Purdue University, Lafayette, Indiana.

|| Iowa State College, Institute for Atomic Research, Ames, Iowa.

¶ University of Tokyo, Tokyo, Japan.

[1] Symon, Kerst, Jones, Laslett, and Terwilliger, Phys. Rev. **103**, 1837 (1956).

[2] Cole, Haxby, Jones, Pruett, and Terwilliger, Rev. Sci. Instr. **28**, 403 (1957).

Reprinted from Proceedings of the Intern. Conf.
on High-Energy Accelerators and Instrumentation--
CERN 1959

EXPERIENCE WITH A SPIRAL SECTOR FFAG ELECTRON ACCELERATOR

R. O. Haxby (*), **L. J. Laslett** (**), **F. E. Mills, F. L. Peterson, E. M. Rowe and W. A. Wallenmeyer**

Midwestern Universities Research Association, Madison, Wis. (***)

(presented by K. R. Symon)

I. INTRODUCTION

In fixed-field alternating gradient (FFAG) accelerators [1-4], particles with a large range of momenta can be accommodated simultaneously within an annular magnet of limited radial extent, thus providing a desirable flexibility in the methods of accelerating the particles and affording the promise of high beam intensities. The spiral sector type is an attractive form of FFAG accelerator, since a smaller circumference factor may be employed than is feasible with the radial sector design and a significant economy thus can be obtained in the construction. A six-sector spiral ridge FFAG accelerator has been constructed and successfully operated to accelerate electrons from 35 to 180 keV kinetic energy [5, 6]. Acceleration was by betatron action, supplemented by radio-frequency acceleration when desired. The design was based on magnetostatic and orbit computations (****), and the subsequent performance was found to be in good accord with these computations. The model permitted not only the acquisition of design experience and the demonstration of predicted stability regions, but also afforded the opportunity of studying coupling and multi-particle effects not investigated in detail theoretically.

The number of sectors (N) was selected as 6, in the interests of a conservative design, and the remaining basic parameters characterizing the model then were selected on the basis of digital computations pertaining to the magnetostatic problem and to the orbit dynamics in the resultant magnetic field. The inner radius of the accelerator was determined by the need to accommodate the betatron core and for convenience of access to ancillary components, while the strength of the magnetic field at that radius was dictated by the selection of 35 keV as a convenient injection energy. The maximum energy attainable by the model ($\simeq$ 180 keV) was sufficiently greater than the transition energy (155 keV) so that experience was obtained in the use of radio-frequency programs suitable for traversing this possibly critical region.

II. DESIGN

A separated-sector magnet design was adopted in the interests of simplicity and to achieve conveniently a field with a large azimuthal variation such as would be expected to affect favorably the non-linear stability limits [4]. Guard rings, effectively at zero magnetostatic potential, further enhanced the field variation and, secondarily, provided some additional shielding from external magnetic fields present in the laboratory. The character of the magnetic field which would result from specific magnet structures of this type (Fig. 1) was determined computationally by a relaxation

(*) On leave of absence from Purdue University, Lafayette, Indiana.

(**) Iowa State University, Ames, Iowa.

(***) Supported by the United States Atomic Energy Commission.

(****) The computations were primarily made by aid of the electronic digital computer of the Graduate College of the University of Illinois (ILLIAC), corroborated and supplemented by later computations made with the IBM-704 computer in the MURA Laboratory at Madison. The invaluable contributions to this work by J. N. Snyder and A. M. Sessler are gratefully acknowledged, as is also the cooperation of J. P. Nash, R. E. Meagher, and others at the University of Illinois, who facilitated initiation of this work.

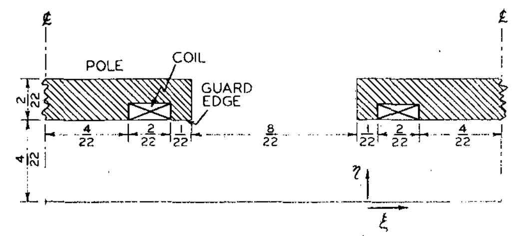

Fig. 1 Cross section of magnet pole. $\xi = \frac{1}{2\pi}\left[\frac{1}{w}\ln\frac{r}{r_o} - N\theta\right]$ and $\eta = \frac{[(1/w)^2 + N^2]^{1/2}}{2\pi}\frac{z}{r}$. Where r, θ, z are cylindrical co-ordinates, and w is the spatial period radially divided by $2\pi r$. The pole profile in the ξ, η -plane represents a section taken at constant radius, but with *unequal scale factors* in the azimuthal and axial directions. The outline represents more truly a cross section *perpendicular* to the spiral save that the general increase of all linear dimensions with radius is not depicted. Azimuthal distances at constant radius are given by $2\pi r/N$ times the increment of ξ and axial distances by $2\pi r[(1/w)^2 + N^2]^{1/2}$ times the increment of η. For the present model $1/w = 6.25$ and these distances become $1.0472\, r\Delta\xi$ and $0.7252\, r\Delta\eta$, respectively.

procedure, wherein it was possible to employ a two-dimensional mesh [7] by taking advantage of the scaling feature of the field. The resultant magnetostatic potential, suitably scaled, was then stored in the computer memory for use in orbit computations.

Three operating points considered in the design of the model are indicated on Fig. 2, where the abscissa and ordinate (σ_x, σ_y) of each point respectively denote the phase change per sector of the radial and axial betatron oscillations. Studies of orbit dynamics for point A of Fig. 2 indicated strong coupling of radial to axial motion, a behaviour attributed to the proximity to the $\sigma_x = 2\sigma_y$ resonance. The coupling was found to be less pronounced for point B, but the radial stability limit was found to be rather small ($\simeq r/25$) and the value of σ_y was also undesirably low. The operation point chosen

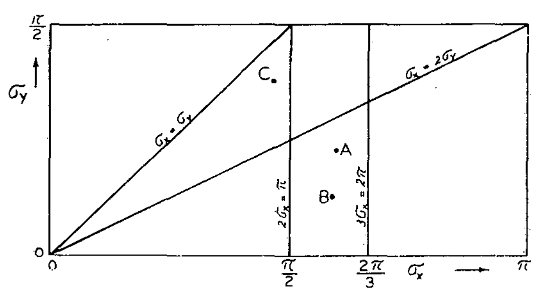

Fig. 2 Location of operating points for which detailed computations were made. For these three points the phase changes per sector of the betatron oscillations, σ, were as follows: A ($0.597\,\pi$, $0.225\,\pi$), B ($0.595\,\pi$, $0.129\,\pi$), C ($0.466\,\pi$, $0.375\,\pi$).

for the model was, accordingly, that denoted by point C on Fig. 2 ($\sigma_x = 0.466\pi$, $\sigma_y = 0.375\pi$), situated a considerable distance *above* the $\sigma_x = 2\sigma_y$ resonance. Here the stability region was found to be at least as large as for point A and the axial oscillation frequency was more acceptable; coupling effects, moreover, were no longer apparent and the sensitivity to misalignments (such as sector displacements) appeared to be much less pronounced. In practice, the model was provided with tuning coils to permit an experimental investigation of performance for operation under other conditions, in order that the effect of various resonance lines in the neighbourhood of point C could be determined.

TABLE I

Parameters of the spiral sector model

Parameter	*Symbol*	*Value*
Number of sectors	N	6
Mean field index	k	
$k = (r/\langle B\rangle_{av})(\partial\langle B\rangle_{av}/\partial r)$		
design value		0.7
adjustable within the range		0.2 to 1.16
Spatial period, radially/$2\pi r$	w	0.16
Spiral angle with radius	ζ	46°
$\cot\zeta = Nw$		
Field flutter	f_{eff}	
$f_{eff} = [2\langle(B - \langle B\rangle_{av})^2\rangle_{av}/\langle B\rangle^2_{av}]^{1/2}$		
design value		1.087
adjustable within the range		0.57 to 1.60
Betatron oscillations per revolution		
$\nu = N\sigma/2\pi$		
radial, design value	ν_x	1.398
axial, design value	ν_y	1.125
Vacuum chamber dimensions, interior :		
inner radius	r_1	27 cm
outer radius	r_2	55 cm
height	h	3.8 cm
Injection radius	r_i	31 cm
Detector radius, useful, maximum	r_f	52 cm
Injection energy, nominal	E_i	35 keV
Final Energy	E_f	
at $k = 0.7$		124 keV
at $k = 1.16$		180 keV
Transition energy	E_t	155 keV
Revolution frequency, maximum	f_t	62.45 Mc/s
Radial stability limit/r, computed	A_x	$\pm$ 0.11

(near the center of a radially-focusing region and when the radial momentum has the value corresponding to the stable fixed point. The radial motion at the limit of stability actually covers a range $\Delta r/r = \pm$ 0.18 at this azimuth.)

The basic parameters of the model are given in Table I and a general view of the assembled accelerator is shown in Fig. 3. The brass vacuum chamber was constructed as two hollow semi-circular annuli, insulated from each other, so that the accelerating

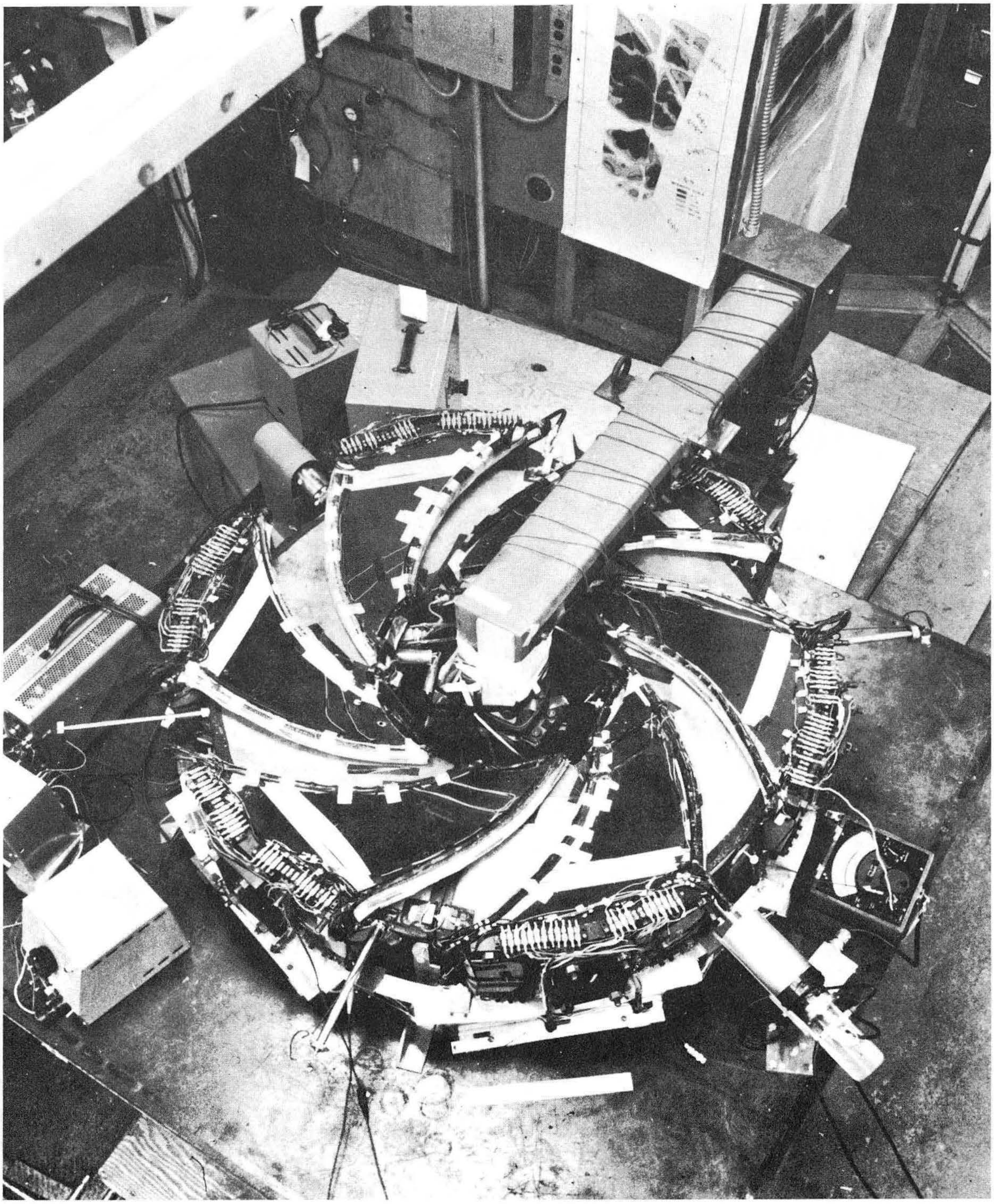

Fig. 3 View of the assembled spiral sector accelerator.

76a

voltages could be applied. A movable scintillation detector and a current probe were provided for detection and analysis of the accelerated beam. An additional probe carried an offset molybdenum wire which, by rotation about the probe axis, served to measure the vertical location of the equilibrium orbit, to indicate the amplitude of the axial oscillations, and to limit these amplitudes when desired. Various electrodes were also provided to permit the application of auxiliary perturbing fields required for some of the performance tests.

III. PERFORMANCE

A. Intensity survey

Following assembly of the model, and after careful measurement and correction of the magnetic field, a betatron-accelerated beam was immediately obtained. Tests were then made to determine the betatron oscillation frequencies and the variation of beam intensity over the accessible portion of the ν_x, ν_y stability region. The oscillation frequencies were determined in this work by the method[8,9] of resonant radio-frequency enhancement of the betatron oscillations. The value of ν_y was found to vary significantly with amplitude (axial or radial amplitude) and an estimated 1 to 2 per cent inaccuracy arose from this effect in the intensity survey. The betatron oscillation frequencies observed in the model, without current in the tuning coils, were close to the values resulting from the digital computations (*see above*) and a small current in the flutter-tuning coils sufficient to raise f_{eff} from 1.03 to its design value of 1.087 raised ν_y from 1.026 to the predicted value of 1.12. The resonance diagram which resulted from the intensity survey, with low emission from the injector, is shown in Fig. 4. A sizable region of maximum intensity is seen to occur centered about the design point and the importance of several resonances which cross the accessible region is also apparent.

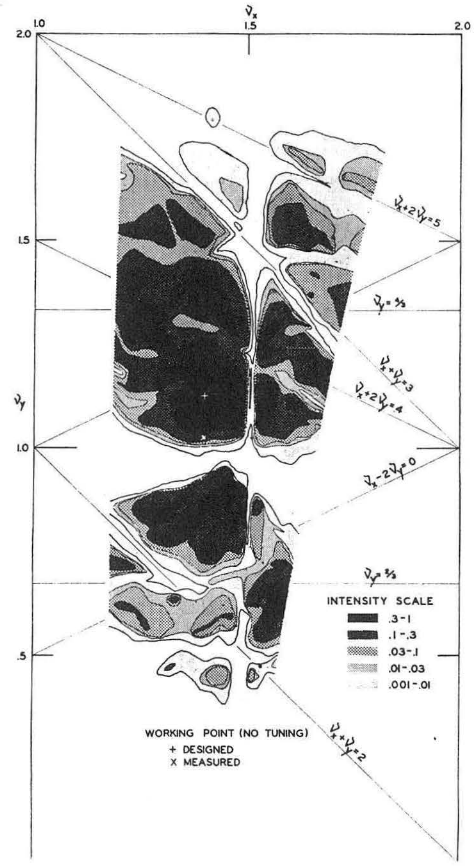

Fig. 4 Beam intensity as determined by the resonance survey of the spiral sector model, using low emission from the injector. + denotes the design values for the oscillation frequencies and is seen to be surrounded by a sizable region of high intensity. The strong influence of several resonances is also evident, the occasional slight departure of the resonance lines from the positions of minimum intensity being believed chiefly ascribable to the imprecise scaling of the field when substantial tuning currents are applied.

B. Stability limits

In measuring the radial stability limits in a fixed-field accelerator, one may examine the range of energies throughout which particles can be captured at the injection radius. On the supposition that the minimum-energy particles are injected into an equilibrium orbit which just misses the injector and that the maximum-energy particles oscillate about an equilibrium orbit which is situated a distance away from the injector equal to the stability limit, a measurement of this energy difference—or, equivalently, of the variation in the time taken for acceleration—permits the stability limit to be calculated.

The calculation to convert the variation of the required acceleration time to the radial range of stable motion at the injection radius requires use of the known rate of acceleration (betatron voltage) and correction for the adiabatic damping which occurs in the course of acceleration ($\propto B^{-1/2}$). With either method it must be recognized that the spatial stability limits will vary with azimuth, due to the alternating-gradient nature of the magnetic focusing.

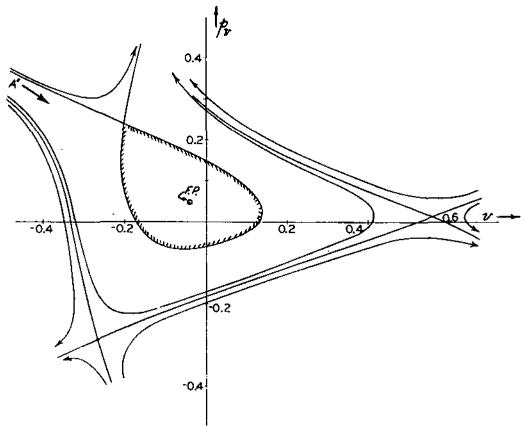

Fig. 3 Phase plot of solutions to Eq. (6), with the same values for the coefficients as were used in Fig. 2 but pertaining to solutions at $s = \pi/2 \pmod{3\pi}$.

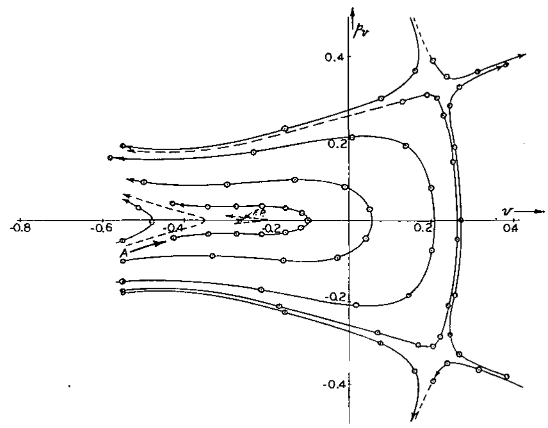

Fig. 5 Phase plot, for $s = 0 \pmod{3\pi}$, of solutions to Eq. (6) with $\nu_r/N = 0.3$ and $B = 1.15$ when λ has the critical value $\lambda_c = 0.01136$. The point designated F.P. represents the confluent fixed point.

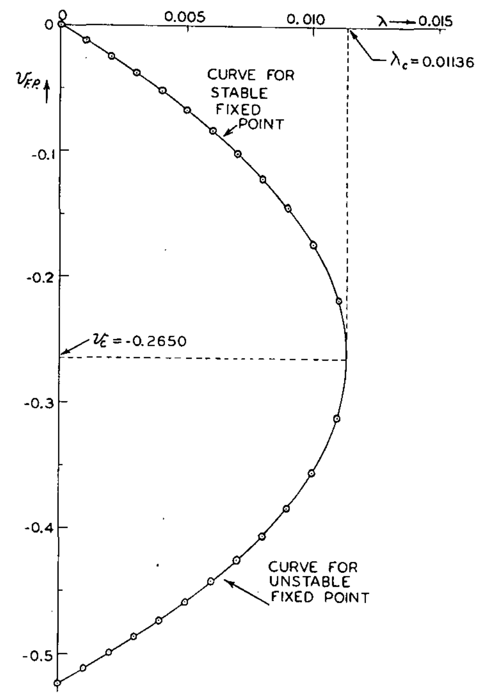

Fig. 4 Coordinates of the stable and unstable fixed points situated on the coordinate axis, for solutions of Eq. (6) with $\nu_r/N = 0.3$, $B = 1.15$, $s = 0 \pmod{3\pi}$ *vs* λ. These two fixed points are seen to approach one another as the strength of the perturbation is increased, becoming coincident when λ assumes the critical value $\lambda_c = 0.01136$.

The detailed characteristics of phase plots which are obtained for any particular value of λ depend, of course, on the particular value of $s \pmod{3\pi}$—or of $\theta \pmod{6\pi/N}$—to which they apply, but the topological features are independent of s (compare Figs. 2 and 3, which apply respectively to $s = 0$ and to $s = \pi/2 \pmod{3\pi}$. Firstly, it is found that, as desired, the application of the perturbation ($\lambda > 0$) does open up the phase curves which originally intersected at one of the unstable fixed points and, secondly, that this fixed point and the stable fixed point approach one another as the strength of the perturbation is increased (Fig. 4), to result in the complete disappearance of the stable region at a critical strength of the perturbation, $\lambda_c = 0.01136$ (Fig. 5).

It may be noted in passing that, for small λ, the locations of these two fixed points which lie on the $p_v = 0$ axis when $s = 0 \pmod{3\pi}$ may be estimated by [15]

$$v_1(\lambda) \simeq -\frac{\lambda}{4/9-(2\nu_r/N)^2} \tag{11a}$$

$$v_2(\lambda) \simeq \nu_{2,0}+\frac{\lambda}{4/9-(2\nu_r/N)^2}, \tag{11b}$$

where $v_{2,0}$ denotes the coordinate value of the unstable fixed point when $\lambda = 0$. A parabolic fit, tangent to the lines (11a, b) at $\lambda = 0$, may be written

$$\lambda = \frac{v\cdot[v-v_{2,0}]}{v_{2,0}}\cdot[4/9-(2\nu_r/N)^2], \tag{12}$$

for which the maximum value of λ,

$$\lambda_c = [1/9-(\nu_r/N)^2]\,[-v_{2,0}], \tag{13a}$$

is attained at

$$v_c = \tfrac{1}{2}v_{2,0}. \tag{13b}$$

With $\nu_r/N = 0.3$ and $-v_{2,0} = 0.5238$, Eqs. (13*a*, *b*) suggest

$$\lambda_c = 0.01106 \tag{14a}$$

$$v_c = -0.2619\,, \tag{14b}$$

which may be compared with the computational results

$$\lambda_c = 0.01136 \tag{14a'}$$

$$v_c = -0.2650\,. \tag{14b'}$$

Finally, we note that suitably injected particles —e.g. with their initial phase points lying in the region A of Fig. 2— will move so that their phase points pass completely around the stable region which is formed as the perturbation is being removed. We may expect, therefore, that particles captured in this way will fill the stable region with a phase density equal to the maximum theoretically attainable.

V. INJECTION WITH A SECULARLY-DECREASING PERTURBATION

We imagine the injector situated physically at radii less than those of the stable region into which it is desired to inject—say with $v \leq -0.55$ at $s = 0$ (Fig. 1)—to avoid any interference by the injector with the captured beam. With an assumed particular value for the rate of decrease of the perturbation, one then seeks to find, by digital computations, the regions of phase space within which particles may start, at various initial values of λ, to become captured within the final stable region. The possible difficulties which conceivably could be discovered in such a search would be :

(i) an appreciable fraction of the region of interest might be found not to pass through regions to the left of $v = -0.55$;

(ii) the location of the region with respect to momentum, p_v, might vary strongly with the initial value of λ;

(iii) the region in phase space might be found to be seriously filamented; and

(iv) the coupling between radial and axial motion may be found to play a more dominant role than is usually the case with stable motion, with a consequent complexity of the four-dimentional phase space and of its projections onto the radial and axial sub-spaces.

A. Characteristics when only radial oscillations are present.

For an initial computational investigation it is convenient to confine one's attention to motion in the median plane (axial oscillations absent). One may then commence by finding the range of momenta, p_v, which, at $v = -0.55$ and for various representative initial values of λ, lead to capture into the stability region. From such values other suitable initial conditions could be found by integration backwards in s, to obtain a transformed set of points situated at smaller radii, although with a three-sector accelerator (or with injectors located at every third sector around a larger accelerator) such a reverse transformation should only be carried through a three-sector interval in order to avoid the inclusion of points which would encounter physical interference by the injector structure. The region between these two lines in the radial phase plane—i.e. between the line at $v = -0.55$ and its transform through $\Delta s = 3\pi$—can then be explored to find the boundaries of the regions suitable for injection.

Such a computational survey of the radial phase plane has been made for the case $d\lambda/ds = -0.002/3\pi = -2.122 \times 10^{-4}$, which corresponds to a linear decrease of the perturbation at a rate such that the strength of the perturbation would decrease from its critical value, λ_c, to zero in the time taken by the particle to traverse 17 sectors of the unperturbed machine. The results of this survey are summarized below.

For the initial value $v = -0.55$, the range of "momenta", p_v, within which particles are captured for various initial values of λ, are as shown in Fig. 6. It is noted that the useful values of λ extend consider-

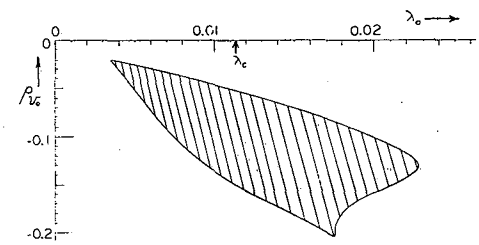

Fig. 6 Range of initial momenta, p_{v0}, vs. the initial value, λ_0, of λ, for capture of particles into the stable area of Fig. 1 when the initial coordinate is $v_0 = -0.55$. The results were obtained computationally for solutions of Eq. (6) with the perturbation decreased to zero at the rate $\frac{d\lambda}{ds} = -\frac{0.002}{3\pi}$.

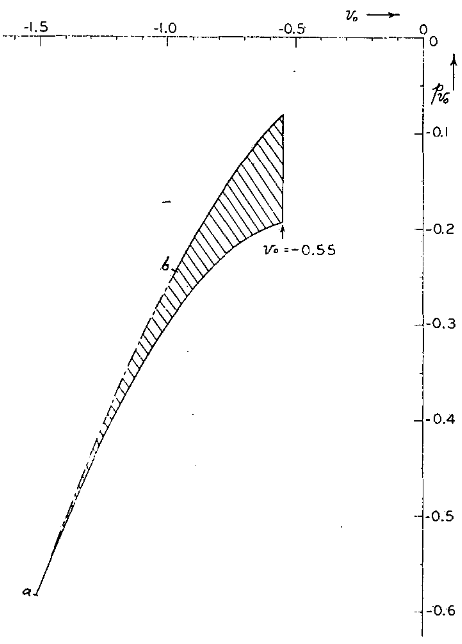

Fig. 7 Range of initial conditions for capture of particles into the stable area of Fig. 1 when the initial strength of the perturbation is $\lambda_0 = 0.0165$ and $\frac{d\lambda}{ds} = -\frac{0.002}{3\pi}$. The boundary *ab* transforms, after three sectors ($\Delta s = 3\pi$), to $v = -0.55$.

ably beyond the critical value, λ_c, since λ will decrease during the time the phase points of the particles progress through the region wherein the stable area is being established. As mentioned above, each such range of values was then projected backward in s to give a second locus of values, applicable three sectors earlier (and for a value of λ greater by 0.002). The intermediate region of the phase plane, between $v = -0.55$ and its transform, was then surveyed to obtain results of which those portrayed in Fig. 7 are typical. For the particular case studied, filamentation of the " phase fluid " was almost entirely absent throughout the entire phase area which was mapped out in this way, although in a few cases the computations appeared to show definite evidence of an incipient filamentation developing along the lower edge of the region (Fig. 8).

The areas of radial phase space which thus should be covered by the injector were obtained from curves of the type shown in Fig. 7. These areas, $A(\lambda)$, have been plotted, vs. the initial value of λ, in Fig. 9 and lead to the integrated result

$$\int A(\lambda)d\lambda = 0.00046. \tag{15}$$

If the injector is capable of delivering n particles per unit area of radial phase space per unit time, the total number of particles which thus could be successfully injected by this means would be

$$\begin{aligned} \mathcal{N} &= \int nA(\lambda)dt \\ &= \frac{n}{|d\lambda/dt|}\int A(\lambda)d\lambda \\ &= \frac{n}{\omega N}\frac{2}{|d\lambda/ds|}\int A(\lambda)d\lambda \\ &= \frac{n}{\omega N}\frac{6\pi}{0.002}0.00046 \\ &= 4.3\,\frac{n}{\omega N}, \end{aligned} \tag{16}$$

where $\omega \equiv d\theta/dt$ denotes the angular velocity of the particles in the accelerator. This result may be compared with the maximum theoretically obtainable

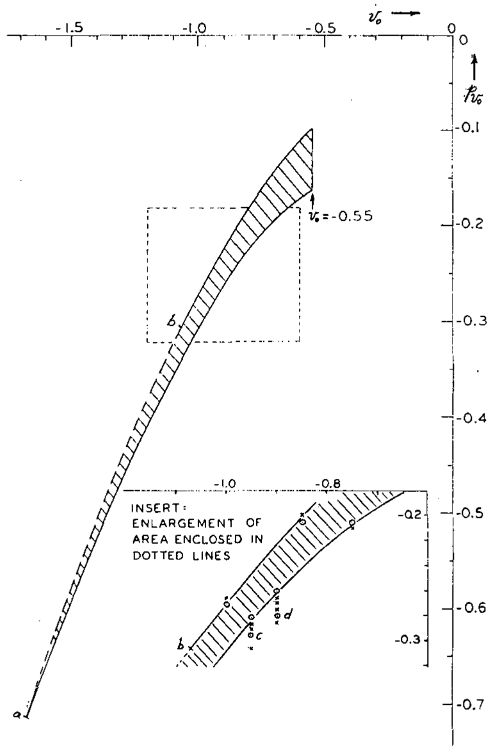

Fig. 8 Detailed portion of diagram, similar to Fig. 7, for capture of particles with $\lambda_0 = 0.0195$. Particles with initial values represented by circles are captured and those depicted by the crossses are not. The boundary *ab* transforms after three sectors to $v = -0.55$. The points denoted by *c* and *d* represent initial values which were found to lead to stable motion and thus provide evidence of incipient filamentation.

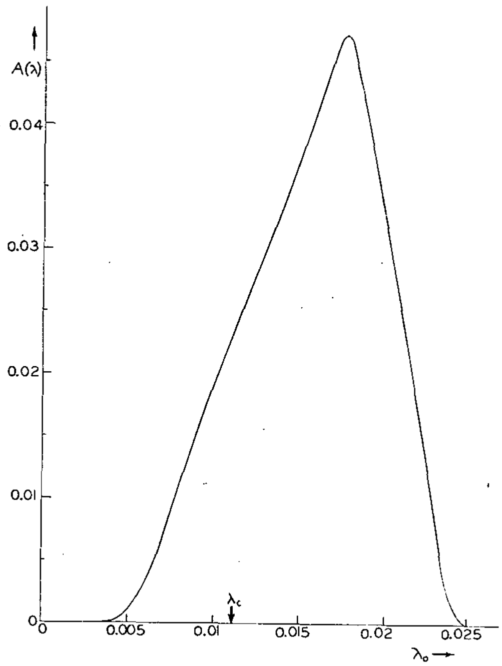

Fig. 9 Area of phase space from which particles may be successfully injected into the stable area of Fig. 1, as a function of λ_0, for $\frac{d\lambda}{ds} = -\frac{0.002}{3\pi}$. The ordinates were obtained from diagrams of the type illustrated in Fig. 7, in which one boundary represented the locus of points which transform after three sectors to $v = -0.55$. From the date shown here, the result $\int A(\lambda)\, d\lambda = 0.00046$ was obtained.

by direct injection, during a three-sector interval, into the stable area without violation of Liouville's theorem, namely

$$\mathcal{N} = \frac{n}{\omega}\left(\frac{6\pi}{N}\right) \cdot [\text{Area of stable phase plot}]$$

$$= \frac{n}{\omega}\left(\frac{6\pi}{N}\right)(0.223)$$

$$= 4.2\frac{n}{\omega N}. \tag{17}$$

It is evident, from comparison of the results (16) and (17), that excellent efficiency of injection into radial phase space has been obtained from the region mapped in this example, although with injection through more than three sectors, or with more complicated differential equations, a more pronounced filamentation of phase space might well develop to present practical difficulties. The transfer of radial phase space from outside the stable region to the interior appears to be quite orderly in the case which we examined and so encourages a continuation of the investigation of this injection (or extraction) method. The exact azimuth at which the injector might best be situated might be adjusted, in practice, to achieve a convenient match to the properties of the injector; it probably would be convenient to select a location where the usable values of p_v vary the least during the interval that the secularly-changing perturbation is being employed and for which the phase diagrams might be similar to that shown in Fig. 10.

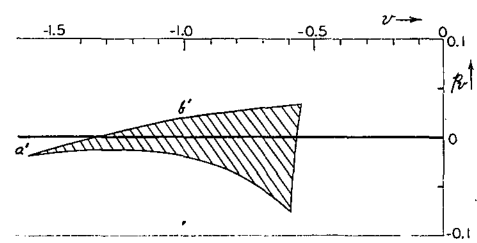

Fig. 10 Transformation of the shaded area depicted in Fig. 7 from $s = 0$ to $s = 3\pi/32$, so that this region becomes more centrally located with respect to $p_v = 0$ (compare Figs. 2 and 3, for which the corresponding values of s differ by $\pi/2$). The segment $a'b'$ of the boundary represents the transformation of the portion denoted as ab on Fig. 7. In either case the shaded region has an area estimated as 0.042 vp_v-*units*.

B. The effect of axial motion.

As in other accelerator investigations, the inclusion of the additional, axial degree-of-freedom in the present study introduces considerable complication and requires a rather extended amount of computation if a comprehensive picture is to be obtained. The importance of including the axial motion in such studies is clear, however, as has been emphasized by Terwilliger in connection with a computational investigation[16, 17] of a method which proved to afford a promising means of beam *extraction* from a spiral sector accelerator. Basically, this latter work was concerned with the use of a pulsed localized field bump which served to perturb the entire beam into a region of strong d.c. magnetic field, whence it would be bent down the spiral and out of the accelerator. Terwilliger's investigation[16] of combined radial and axial motion indicated considerable phase distortion (and, effectively, loss of phase density) in the unperturbed accelerator if one employed amplitudes comparable with stability limits. Specifically, with a beam for which the oscillation amplitudes were originally about one-half as great as the stability limits, so that the coupling was not pronounced, and for which the amplitudes each were further damped by a factor of about 7 during the acceleration process, use of the pulsed field was then found to permit orderly *extraction* with high efficiency. The results which we are able to cite at the present time in regard to the inclusion of axial motion in the problem reported here are certainly not sufficiently complete to afford a comprehensive picture—as we shall see, however, the preliminary results which have already been obtained do indicate that, as expected, the axial motion exerts a marked effect on the performance and may detract materially from the utility of the method if efficient *injection into the entire stability region* of the accelerator is required.

A search for the y-stability limit for solutions to Eqs. (*7a, b*) in the absence of the perturbation indicated that this limit lay between 0.72 and 0.85 if the amplitude of the radial motion was initially zero (i.e. corresponding to the origin of the radial phase plot shown in Fig. 1). For larger amplitudes the permissible initial axial amplitudes were somewhat reduced, as shown in Table III.

TABLE III

Computational estimates of limiting axial amplitudes, with various initial radial amplitudes, for solutions to Eqs. (7a, b) with $\lambda = 0$

$p_{v_0} = p_{y_0} = 0$

v_0	y_0	
	Stable	Unstable
0	0.72	0.85
– 0.1	0.61	0.72
– 0.25	0.52	0.61

To illustrate the influence of axial motion on the proposed injection method, we have made preliminary computations for the case in which the initial strength of the perturbations is $\lambda_0 = 0.0165$ (and $d\lambda/ds = —0.002/3\pi$) and for which Fig. 7 applies in the absence of axial motion. The y-stability limits for Eqs. (*7a, b*) were then sought for $v_0 = —0.55$ and for $v_0 = —0.85$, in each case assigning to the initial radial momentum, p_{v_0}, a value near the center of the previously permissible range of values. The results of this search, summarized in Table IV, indicate that the axial stability limits for these representative cases were materially smaller than those shown in Table III.

TABLE IV

Computational estimates of limiting axial amplitudes, with representative initial conditions for the radial motion, for solutions to Eqs. (*7a, b*) with $\lambda_0 = 0.0165$ and $d\lambda/ds = —0.002/3\pi$

$p_{y_0} = 0$

v_0	p_{v_0}	y_0	
		Stable	Unstable
– 0.55	– 0.13625	0.31	0.37
– 0.85	– 0.22	0.19	0.21

Guided by the results shown in Table IV, the range of permissible values of p_{v_0}, leading to stable motion, was then examinaed at $v_0 = —0.55$ and at $v_0 = —0.85$ for several initial axial amplitudes. The results of this survey are summarized in Table V.

TABLE V

Computational estimates of range of permissible radial momenta, with representative initial radial and axial coordinates, for solutions to Eqs. (*7a, b*) with $\lambda_0 = 0.0165$ and $d\lambda/ds = -0.002/3\pi$

$p_{y_0} = 0$

y_0	v_0	p_{v_0}			
		Unstable	Stable	Stable	Unstable
0	– 0.55	– 0.0775	– 0.0800	– 0.1925	– 0.1950
0.19		– 0.09	– 0.10	– 0.19	– 0.20
0.22		– 0.09	– 0.10	– 0.19	– 0.20
0.26		– 0.10	– 0.11	– 0.19	– 0.20
0.31		– 0.12	– 0.13	– 0.19	– 0.20
0.37		– 0.14	– 0.15	– 0.20	– 0.21
0.44		– 0.18	– 0.19	– 0.21	– 0.22
0.52		– 0.22	– 0.23	– 0.24	– 0.25
0	– 0.85	– 0.190	– 0.195	– 0.245	– 0.250
0.19		– 0.21	– 0.22	– 0.25	– 0.26
0.22		– 0.22	– 0.23	– 0.26	– 0.27
0.26		– 0.23	– 0.24	– 0.27	– 0.28
0.31		– 0.25	– 0.26	– 0.28	– 0.29

It is clear that axial amplitudes much smaller than those which appear in Table III result in a material reduction of the useful range of p_{v_0}. The larger values of y_0 listed in Table V are seen, moreover, to be associated with values of p_{v_0} differing from those suitable for $y_0 = 0$, and injection with values of y_0 as large as those listed near the end of each section of Table V may be of rather limited utility.

VI. CONCLUSION

The particular injection method discussed in this paper was found to permit efficient transfer of *radial* phase space between regions exterior and interior to the accelerator, although complications might be expected ro arise if the physical limitation imposed at the time the beam returns to the injector azimuth were deferred for longer than the three sectoıs considered here. The results of the method appear to show a close resemblance to those which previously [6] have indicated the potential utility of a similar perturbation for the efficient *extraction* of a beam from a three-sector fixed-field accelerator.

The preliminary studies of the influence of substantial axial oscillation amplitudes on the particle behavior indicated that this influence was pronounced and so might detract materially from the practicality of the method unless additional considerations, such as the limitation of axial amplitudes by the vacuum chamber or the damping of oscillation amplitudes prior to use of the method for *ejection*, served to limit the axial amplitudes to values considerably less than are dynamically stable in the absence of the perturbation.

It is hoped that the method and results reported here will prove suggestive of other possible methods of utilizing a secularly-changing perturbation in conjunction with the non-linear dynamical properties of the orbits, including methods in which the perturbation may have a greater period than that employed here and so would interact with a machine resonance rather than with an inherent sector resonance.

It is a pleasure to acknowledge the assistance of Mr. Seymour J. Wolfson, a MURA summer visitor from Wayne State University, in some of the algebraic and numerical calculations connected with the analytic phases of this investigation, and to thank Mr. Igor Sviatoslavsky for assistance with some of the graphical work.

LIST OF REFERENCES

1. Symon, K. R., Kerst, D. W., Jones, L. W., Laslett, L. J. and Terwilliger, K. M. Fixed-field alternating-gradient particle accelerators. Phys. Rev., *103*, p. 1837-59, 1956.
2. Laslett, L. J. Fixed-field alternating-gradienst accelerators. Science, *124*, p. 781-7, 1956.
3. Kerst, D. W., Symon, K. R., Laslett, L. J., Jones, L. W. and Terwilliger, K. M. Fixed field alternating gradient particle accelerators. CERN Symp. 1956. *1*, p. 32-5.
4. Kerst, D. W., Cole, F. T., Crane, H. R., Jones, L. W., Laslett, L. J., Ohkawa, T., Sessler, A. M., Symon, K. R., Terwilliger, K. M. and Vogt-Nilsen, N. Attainment of very high energy by means of intersecting beams of particles. Phys. Rev., *102*, p. 590-1, 1956.
5. Kerst, D. W. Properties of an intersecting-beam accelerating system. CERN Symp. 1956. *1*, p. 36-9.
6. Blosser, H. G. et al. A proposal for a nuclear research facility in the medium energy range utilizing a 64″ variable energy multiparticle cyclotron. Michigan State University. Department of Physics and Astronomy report. East Lansing, Michigan. 1958. Section III-A.1-C, p. 67-76. (unpublished).
7. Laslett, L. J. and Symon, K. R. Particle orbits in fixed field alternating gradient accelerators. CERN Symp. 1956. *1*, p. 279-89.
8. Moser, J. Nonexistence of integrals for canonical systems of differential equations. Commun. pure appl. Math., *8*, p. 409-36, 1955.
9. Cole, F. T. Mark V FFAG expanded equations of motion. MURA (*) 95. 19 January, 1956.
10. Courant, E. D. and Snyder, H. S. Theory of the alternating-gradient synchrotron. Ann. Phys. New-York, *3*, p. 1-48, 1958. Equations (4.4) and (4.5) on p. 18.
11. Hagedorn, R., Hine, M. G. N. and Schoch, A. Non-linear orbit problems in synchrotrons. CERN Symp. 1956. *1*, p. 237-53.
12. Hagedorn, R. Note on an instability on a difference resonance line. CERN Symp. 1956. *1*, p. 293-4.
13. Moser, J. Stabilitätsverhalten Kanonischer Differentialgleichungssysteme. Nachr. Akad. Wiss. Göttingen. Math. Phys. Kl. 1955. p. 87-120.
14. Laslett, L. J. Concerning the $\nu/N \to 1/3$ resonance. I. Application of a variational procedure and of the Moser method to the equation $d^2v/dt^2+(2\nu/N)^2v+(1/2)(\sin 2t)v^2=0$. MURA (*) 452. April 13, 1959.
15. Laslett, L. J. and Wolfson, S. J. Concerning the $\nu N \to 1/3$ resonance. V: Analysis of the equation $d^2v/ds^2+(2\nu/N)^2v-(b/2)(\cos 2s)v^2-\lambda\cos(2s/3)=0$. MURA (*) 497. 1959.
16. Terwilliger, K. M. Beam extraction from an FFAG synchrotron. MURA (*) 427. 1958.
17. Jones, L. W. and Terwilliger, K. M. Beam extraction from FFAG accelerators. See p. 48.

(*) see note on reports p. 696.

Reprinted from THE REVIEW OF SCIENTIFIC INSTRUMENTS, Vol. 32, No. 2, 144–149, February, 1961
Printed in U. S. A.

Resonant Beam Extraction from an A. G. Synchrotron*

C. L. HAMMER AND L. JACKSON LASLETT†
Institute for Atomic Research and Department of Physics, Iowa State University, Ames, Iowa, and Midwestern Universities Research Association, Madison, Wisconsin

(Received July 22, 1960)

The resonant extraction method previously proposed for the normally constant gradient synchrotron has been extended to alternate gradient accelerators. It is found that perturbation field gradients which contain circular functions of arguments $2\nu_x$, $2\nu_x+1$, $2\nu_x+2$ are particularly effective in causing the radial betatron oscillations to grow exponentially at a particular azimuthal position. The analytical procedure for predicting which perturbations give optimum results, and digital computer calculations verifying these predictions, are presented.

I. INTRODUCTION

THE use of the half-integral resonance,[1] $\nu_x=\frac{1}{2}$, to effect rapid beam knockout, or extraction, from a normally constant gradient synchrotron (or betatron) has been previously published[2,3] and successfully applied to the Iowa State University synchrotron and to the Allis-Chalmers betatrons. More recently a convenient analytic description has been reported.[4] The use of the analytical approach to guide a broader investigation of resonant extraction seems timely in view of the great enhancement of utility and versatility which a successful method would provide for alternate gradient accelerators now nearing completion, or, which have been completed.[5,6] In the following sections an investigation of a resonant method for alternate gradient synchrotrons is made.

It may be recalled that the method used with the constant gradient synchrotron[2–4] employed an azimuthally dependent perturbation of the field gradient (n bump) to drive the operating point into the $\nu_x=\frac{1}{2}$ unstable zone (stopband), which opened up with a width proportional to the perturbation strength and within which the solution for the exponentially increasing betatron oscillations attained its maximum value at *one particular azimuth* in the accelerator *regardless* of the initial conditions of the particular particle under investigation. This implies that, in principle, the beam can be extracted on *successive* revolutions with no spread in the angle tangent to the equilibrium orbit, thus making the radial phase space of the *extracted* beam zero. In the application to the alternate gradient case, all these features are retained except that the use of a half-integral, as distinct from an integral, resonance does not seem essential and the selection of the particular resonance to be employed may be based on secondary considerations peculiar to the particular accelerator to which the method might be applied. However, with the integral resonance, half the particles are driven toward the outer radius at a particular azimuth while the other half are driven toward the inner radius, so that at most 50% of the particles can be extracted at one port. In contrast, with the half-integral resonance, the particles go alternately to large and small radii on successive revolutions, so that in principle all the particles can be extracted at one port. As in the case with the constant gradient accelerators, the use of the n bump seems desirable, since the perturbing windings then have very little coupling from the main magnetic field of the accelerator. Basically, then, one visualizes driving the accelerator to a nearby half-integral or integral resonance and this stopband is then opened by a suitable perturbation (see Fig. 1). The unstable oscillations grow exponentially, predominantly at one particular azimuth in the accelerator.

Attention is directed to achieving *radial* instability, it being presumed that axial stability can be maintained. Throughout the paper the equations of motion are taken as linear, and typically may be regarded as of the Hill form. In the numerical examples the unperturbed accelerator is considered to consist of N identical A-G sectors (full sectors) with $N=48$ and $\nu_x=7.5$ or, alternatively, with $N=12$ and $\nu_x=2.5$. This illustrative material will not include the complications of straight sections, superperiods, or auxiliary lenses, it being felt that nothing significant is lost in the exposition by omitting such elaborations.

II. THEORY

A. Basic Equations

The equation characterizing the radial betatron oscillations may be taken to be of the form

$$\partial^2 x+[p+mF(\theta)+\lambda f(\theta)]x=0, \qquad \partial=d/d\theta, \tag{1}$$

where the alternate gradient flutter is given by

$$F(\theta)=+1 \quad \text{for} \quad -\pi/2N<(\theta, \bmod 2\pi/N)<\pi/2N,$$
$$F(\theta)=-1 \quad \text{for} \quad \pi/2N<(\theta, \bmod 2\pi/N)<3\pi/2N,$$

* Contribution No. 916. Work was performed in the Ames Laboratory of the U. S. Atomic Energy Commission.
† Now in London with the Office of Naval Research.
[1] ν_x is the number of radial betatron oscillations per circumference.
[2] C. L. Hammer and A. J. Bureau, Rev. Sci. Instr. 26, 594 (1955).
[3] C. L. Hammer and A. J. Bureau, Rev. Sci. Instr. 26, 598 (1955).
[4] C. L. Hammer and L. J. Laslett, "Electron beam control in a conventional synchrotron," 2nd Intern. Conf. Peaceful Uses Atomic Energy Geneva 30, 151 (1958).
[5] For example the Cornell 1-Bev electron synchrotron or the synchrotron planned by the Cambridge Design Study Group, M. Stanley Livingston, Director.
[6] V. V. Vladimirski *et al.*, *Proceedings of the* CERN *Symposium on High Energy Accelerators and Pion Physics* (UN, Geneva, 1956), Vol. 1, p. 133.

and where the perturbation of strength λ has the form

$$f(\theta)=\sum_\sigma \xi_\sigma \cos(\sigma\theta+\delta_\sigma). \tag{2}$$

The magnitude of the unperturbed field gradient is therefore given by m, and the constant p represents the usually small "centrifugal focusing" term. It is seen that $\theta=0$ corresponds to the center of a radially focusing semisector. The solutions to Eq. (1) have the Floquet form[7]

$$x=Ae^{\mu\theta}\Phi_1+Be^{-\mu\theta}\Phi_2, \tag{3}$$

where μ is real for operation inside an unstable zone and where Φ_1 and Φ_2 are periodic functions determined by the structure $mF(\theta)$ and the perturbation $\lambda f(\theta)$. It is clear from Eq. (3) that for suitable values of μ, the ascending exponential soon dominates the solution, so that the betatron oscillations have the periodicity given by Φ_1 regardless of the initial conditions. Therefore, the problem reduces to that of determining $f(\theta)$ so that Φ_1 has the periodicity and spatial dependence desired for beam extraction from a particular accelerator and so that μ has a value which permits the ascending exponential to dominate.

It is convenient to solve Eq. (1) by use of perturbation theory,[8] with the complete set of functions, $\chi_{\nu,\tau}$,[9] as the basis vectors where

$$\partial^2\chi_{\nu,\tau}{}^k+[p+m_\nu F(\theta)]\chi_{\nu,\tau}{}^k=-a_{\nu,\tau}{}^k\chi_{\nu,\tau}{}^k. \tag{4}$$

The functions $\chi_{\nu,\tau}{}^k$ are the eigenfunctions of Eq. (4) which are associated with the eigenvalues $a_{\nu,\tau}{}^k$. Choosing the value of m_ν so that[10] $a_{\nu,\nu}{}^k=0$, ensures that $\chi_{\nu,\nu}{}^k$ is also the eigenfunction of Eq. (1) in the absence of the perturbation with the eigenvalue $m=m_\nu$. As a consequence of Eq. (4),

$$\langle k,\tau|l,\sigma\rangle\equiv\int \chi_{\nu,\tau}{}^k\chi_{\nu,\sigma}{}^l d\theta=\delta_{k,l}\delta_{\tau,\sigma}, \tag{5}$$

reference 11. Excellent approximations[12] for $\chi_{\nu,\tau}{}^k$ and $a_{\nu,\tau}{}^k$ are given by

$$\chi_{\nu,\tau}{}^k=-D_\tau\{\cos[\tau\theta+k\pi/2]+B_\tau\cos[(N-\tau)\theta-k\pi/2] +C_\tau\cos[(N+\tau)\theta+k\pi/2]\}, \tag{6}$$

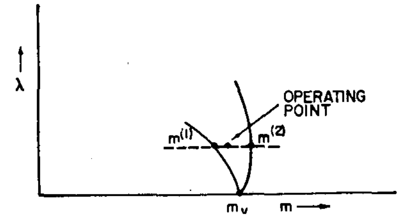

FIG. 1. Stability diagram.

where D_τ is a normalization constant and

$$B_\tau=2m_\nu\pi^{-1}[(N-\tau)^2-p-a_{\nu,\tau}{}^{(1)}]^{-1},$$
$$C_\tau=2m_\nu\pi^{-1}[(N+\tau)^2-p-a_{\nu,\tau}{}^{(1)}]^{-1}, \tag{7}$$

$$\tau^2=a_{\nu,\tau}{}^{(1)}+p+(2m_\nu\pi^{-1})^2\{[(N-\tau)^2-p-a_{\nu,\tau}{}^{(1)}]^{-1} +[(N+\tau)^2-p-a_{\nu,\tau}{}^{(1)}]^{-1}\}, \tag{8}$$

for $(\tau/N)<\frac{1}{2}$. The quantity m_ν may be obtained from Eq. (8) by setting $\tau=\nu$ and $a_{\nu,\nu}{}^k=0$. More approximate equations for m_ν and $a_{\nu,\tau}{}^k$ are given by

$$a_{\nu,\tau}{}^k=[\tau^2-\nu^2][1+4(\nu/N)^2]^{-1}, \tag{9}$$

$$2(2m_\nu\pi^{-1})^2=\nu^2(N^2-\nu^2)^2(N^2+\nu^2)^{-1}. \tag{10}$$

The centrifugal term p has been neglected. The quantities m, μ, and Φ_1 can be expanded in powers of the perturbation strength λ according to

$$m=\alpha m^{(1)}+(1-\alpha)m^{(2)},$$
$$m^k=m_\nu+\lambda m_1{}^k+\lambda^2 m_2{}^k+\cdots\quad [k=(1),(2)],$$
$$\mu=\lambda\mu_1+\lambda^2\mu_2+\cdots,$$
$$\Phi_1=\sum_k b_k\chi_{\nu,\nu}{}^k+\lambda\sum_k[c_k\chi_{\nu,\nu}{}^k+\sum_{\sigma\neq\nu}(a_{\nu,\sigma}{}^k)^{-1}d_{\nu,\sigma}{}^k\chi_{\nu,\sigma}{}^k] +\lambda^2\sum_k[e_k\chi_{\nu,\nu}{}^k+\sum_{\sigma\neq\nu}(a_{\nu,\sigma}{}^k)^{-1}f_{\nu,\sigma}{}^k\chi_{\nu,\sigma}{}^k]+\cdots,$$

where $m^{(1)}$ and $m^{(2)}$, $m^{(2)}>m^{(1)}$, correspond to the values of m at the edges of the stopband (see Fig. 1). Substituting for these quantities in Eq. (1) and applying the orthogonality condition given by Eq. (5) and the normalization condition,

$$\int\Phi_1{}^2d\theta=1 \tag{11}$$

one obtains,[13]

$$m_1{}^k=-\langle k,\nu|f|k,\nu\rangle\langle k,\nu|F|k,\nu\rangle^{-1}, \tag{12}$$

reference 14,

$$m_2{}^k=-\sum_l\sum_{\sigma\neq\nu}\langle k,\nu|m_1{}^kF+f|l,\sigma\rangle^2(a_{\nu,\sigma}{}^l)^{-1} \times\langle k,\nu|F|k,\nu\rangle^{-1}, \tag{13}$$

$$\mu_1=(m_1{}^{(2)}-m_1{}^{(1)})(2\langle 2,\nu|\partial|1,\nu\rangle)^{-1} \times\langle 1,\nu|F|1,\nu\rangle[\alpha(1-\alpha)]^{\frac{1}{2}}, \tag{14}$$

[7] E. T. Whittaker and G. N. Watson, *Modern Analysis* (Cambridge University Press, Cambridge, 1927), Sec. 19.4.

[8] See, for example, Leonard I. Schiff, *Quantum Mechanics* (McGraw-Hill Book Company, Inc., New York, 1955), ed. 2, Chap. VII.

[9] The latin superscript refers to the parity of the eigenfunction and takes the value (1) for odd and (2) for even. The subscript ν refers to the fact that $a_{\nu,\nu}{}^k$ is chosen to give a particular value m_ν and the subscript τ refers to the fundamental frequency of oscillation in the eigenfunction $\chi_{\nu,\tau}{}^k$.

[10] It is assumed that m_ν is such that $a_{\nu,\nu}{}^{(1)}=a_{\nu,\nu}{}^{(2)}$. This assumption is valid as long as $(\nu_x/N)<\frac{1}{2}$, which is the case for all accelerators. In general, as long as $\tau/N\neq\frac{1}{2}$, $a_{\nu,\tau}{}^{(1)}=a_{\nu,\tau}{}^{(2)}$.

[11] The notation indicated by Eq. (5) will be used throughout. Note that the subscript ν has been suppressed (see reference 9). Further, $\langle k,\tau|g(\theta)|l,\sigma\rangle\equiv\int\chi_{\nu,\tau}{}^k g(\theta)\chi_{\nu,\sigma}{}^l d\theta$. The integration interval is assumed over a full period of $\chi_{\nu,\tau}{}^l$ in which these functions form a complete orthonormal set. The interval 0 to 4π is sufficient for all cases to be discussed.

[12] L. Jackson Laslett, "Approximation of eigenvalues, and eigenfunctions, by variational methods," MURA Notes (February 1, 1955). See also L. Jackson Laslett and C. L. Hammer, MURA Report 445 (February 2, 1959).

[13] It is assumed here that $\langle 1,\nu|f(\theta)|2,\nu\rangle=0$ so that nondegenerate perturbation theory applies. Also, the algebra is simplified if one recognizes that $\langle 1,\nu|\partial|2,\sigma\rangle=-\langle 2,\sigma|\partial|1,\nu\rangle$ and $\langle 1,\nu|F(\theta)|1,\nu\rangle=\langle 2,\nu|F(\theta)|2,\nu\rangle$, $\nu\neq(nN/2)$, n being any integer.

[14] This equation identifies $m^{(2)}$ with the even eigenfunctions which may not be consistant with the assumption $m^{(2)}>m^{(1)}$. If an inconsistancy results, however, it can be removed by redefining $k=(1)$ as even and $k=(2)$ as odd.

$$\mu_2=\{[16\alpha(1-\alpha)]^{-\frac{1}{2}}\langle 2,\nu|\partial|1,\nu\rangle^{-1}\}\{(2\alpha-1)\mu_1^2 + (2\alpha-1)[\alpha m_2^{(1)}+(1-\alpha)m_2^{(2)}]\langle 1,\nu|F|1,\nu\rangle - 2\mu_1\sum_l\sum_k\sum_{\sigma\neq\nu}(-1)^l b_l(a_{\nu,\sigma}^k)^{-1}d_{\nu,\sigma}^k\langle l,\nu|\partial|k,\sigma\rangle - \sum_l\sum_k\sum_{\sigma\neq\nu}(-1)^l b_l(a_{\nu,\sigma}^k)^{-1}d_{\nu,\sigma}^k \times\langle l,\nu|[\alpha m_1^{(1)}+(1-\alpha)m_1^{(2)}]F+f|k,\sigma\rangle\}, \quad (15)$$

$$b_1=(\alpha)^{\frac{1}{2}}, \quad (16)$$

$$b_2=(1-\alpha)^{\frac{1}{2}}, \quad (17)$$

$$c_1=-(1-\alpha)^{\frac{1}{2}}W, \quad (18)$$

$$c_2=(\alpha)^{\frac{1}{2}}W, \quad (19)$$

$$W=\{[4\alpha(1-\alpha)]^{-\frac{1}{2}}[(m_1^{(2)}-m_1^{(1)})\langle 1,\nu|F|1,\nu\rangle]^{-1}\} \times\{\mu_1^2+[\alpha m_2^{(1)}+(1-\alpha)m_2^{(2)}]\langle 1,\nu|F|1,\nu\rangle + 2\mu_1\sum_l\sum_k\sum_{\sigma\neq\nu}b_l(a_{\nu,\sigma}^k)^{-1}d_{\nu,\sigma}^k\langle l,\nu|\partial|k,\sigma\rangle + \sum_l\sum_k\sum_{\sigma\neq\nu}b_l(a_{\nu,\sigma}^k)^{-1}d_{\nu,\sigma}^k \times\langle l,\nu|[\alpha m_1^{(1)}+(1-\alpha)m_1^{(2)}]F+f|k,\sigma\rangle, \quad (20)$$

$$d_{\nu,\sigma}^k=2\mu_1\sum_l b_l\langle k,\sigma|\partial|l,\nu\rangle + \sum_l b_l\{[\alpha m_1^{(1)}+(1-\alpha)m_1^{(2)}]\langle k,\sigma|F|l,\nu\rangle + \langle k,\sigma|f|l,\nu\rangle\}, \quad (\sigma\neq\nu). \quad (21)$$

The formulas for m_2^k, μ_2, W, and $d_{\nu,\sigma}^k$ simplify greatly if the additional restrictions

$$\langle k,\nu|F|l,\sigma\rangle=\langle k,\nu|\partial|l,\sigma\rangle=0 \quad (\nu\neq\sigma), \quad (22)$$

are imposed. This does not limit the problem at hand since the values of σ for which Eq. (22) is not true give rise to values of $a_{\nu,\sigma}^k$ sufficiently large that the omitted terms are negligible. Thus,

$$m_2^k=-\sum_l\sum_{\sigma\neq\nu}\langle k,\nu|f|l,\sigma\rangle^2(a_{\nu,\sigma}^l)^{-1}\langle k,\nu|F|k,\nu\rangle^{-1}, \quad (23)$$

$$\mu_2\{(m_2^{(2)}-m_2^{(1)})(2\langle 2,\nu|\partial|1,\nu\rangle)^{-1} \times\langle 1,\nu|F|1,\nu\rangle[\alpha(1-\alpha)]^{\frac{1}{2}}+(2\alpha-1)(\mu_1^2/4) \times[\alpha(1-\alpha)]^{-\frac{1}{2}}\langle 2,\nu|\partial|1,\nu\rangle^{-1}\}, \quad (24)$$

$$W=\sum_k\sum_{\sigma\neq\nu}(a_{\nu,\sigma}^k)^{-1}\langle 1,\nu|f|k,\sigma\rangle\langle k,\sigma|f|2,\nu\rangle \times\langle 1,\nu|F|1,\nu\rangle^{-1}(m_1^{(2)}-m_1^{(1)})^{-1}+(m_1^{(2)}-m_1^{(1)}) \times[\alpha(1-\alpha)]^{\frac{1}{2}}\langle 1,\nu|F|1,\nu\rangle 8^{-1}\langle 2,\nu|\partial|1,\nu\rangle^{-2}, \quad (25)$$

and

$$d_{\nu,\tau}^k=\sum_l b_l\langle k,\tau|f|l,\nu\rangle, \quad (\tau\neq\nu) \quad (26)$$

In summary, letting $\lambda=1$, one obtains

$$\mu=(m^{(2)}-m^{(1)})(2\langle 2,\nu|\partial|1,\nu\rangle)^{-1}\langle 1,\nu|F|1,\nu\rangle[\alpha(1-\alpha)]^{\frac{1}{2}} + (2\alpha-1)(m^{(2)}-m^{(1)})^2 16^{-1}\langle 2,\nu|\partial|1,\nu\rangle^{-3} \times[\alpha(1-\alpha)]^{\frac{1}{2}}\langle 1,\nu|F|1,\nu\rangle^2, \quad (27)$$

through second order and

$$\Phi_1=(\alpha)^{\frac{1}{2}}[\chi_{\nu,\nu}^{(1)}+W\chi_{\nu,\nu}^{(2)}+\sum_k\sum_{\sigma\neq\nu}(a_{\nu,\sigma}^k)^{-1} \times\langle 1,\nu|f|k,\sigma\rangle\chi_{\nu,\sigma}^k]+(1-\alpha)^{\frac{1}{2}}[\chi_{\nu,\nu}^{(2)}-W\chi_{\nu,\nu}^{(1)} + \sum_k\sum_{\sigma\neq\nu}(a_{\nu,\sigma}^k)^{-1}\langle 2,\nu|f|k,\sigma\rangle\chi_{\nu,\sigma}^k], \quad (28)$$

through first order. Except for the second term in Eq. (25), the square-bracketed terms of Eq. (28) are the eigenfunctions associated with the $m^{(1)}$ and the $m^{(2)}$ boundaries, respectively.

One sees from Eq. (28) and Eqs. (6) and (7) that the dominant term in Φ_1 is a circular function of frequency ν. Thus if ν is integral, those particles whose displacements x initially are such that A in Eq. (3) is positive will reach their maximum displacement always towards the outer radius of the accelerator (positive x) while those particles with A less than zero will always reach their maxima toward the inner radius. In contrast, if ν is a half-odd integer, the particles reach their maxima alternately toward the inner and outer radius.

B. Form of the Perturbation

The perturbation $f(\theta)$ is intended both to open the stopband as economically as possible and to introduce harmonics into the betatron oscillations such that the orbits reach a maximum displacement at a particular azimuth in the accelerator. As one sees from Eqs. (12), (23), (27), and (28), to accomplish these purposes, one need only consider the matrix elements $\langle k,\nu|f|l,\tau\rangle$. To obtain the frequencies that must be contained in $f(\theta)$ it is sufficient to approximate $\chi_{\nu,\tau}^k$ by the circular functions of frequency τ, which are the first terms of Eqs. (6) and (7). In fact, this approximation is, in general, good to order (ν/N), so that it is also adequate for most calculational purposes. Thus, the matrix element becomes the simple integral over the product of three circular functions, giving

$$\langle k,\nu|f|l,\tau\rangle =2^{-1}\xi_{\nu+\tau}\cos[\delta_{\nu+\tau}-(k+l)(\pi/2)]+2^{-1}\xi_{|\nu-\tau|} \times\cos[\delta_{|\nu-\tau|}-(k-l)(\pi/2)(\nu-\tau)|\nu-\tau|^{-1}], \quad \nu\neq\tau, \quad (29)$$

and

$$\langle k,\nu|f|k,\nu\rangle=2^{-1}\xi_{2\nu}\cos(\delta_{2\nu}-k\pi)+2^{-1}\xi_0\cos\delta_0. \quad (30)$$

From Eq. (12) it is seen that the opening of the stopband will occur to first order if $\langle 1,\nu|f|1,\nu\rangle\neq\langle 2,\nu|f|2,\nu\rangle$. Inspection of Eq. (30) shows that only the $\xi_{2\nu}\cos(2\nu\theta+\delta_{2\nu})$ term in the perturbation will accomplish this purpose. While it is possible to find an $f(\theta)$ to open the stopband in second order using the condition

$$\sum_l\langle 1,\nu|f|l,\sigma\rangle^2\neq\sum_l\langle 2,\nu|f|l,\sigma\rangle^2,$$

given by Eq. (23) (recall $a_{k,\sigma}^{(1)}=a_{k,\sigma}^{(2)}$), it would seem from the standpoint of minimizing the magnitude of the perturbation required that this case need not be considered. However, for a particular accelerator, if it is not convenient to use a perturbation which contains a 2ν harmonic, it may be necessary to examine the second-order effects further.[15]

To choose the perturbation so that the maximum displacement occurs at a particular azimuth it is necessary to separate the analysis into two parts, obtaining first the harmonics required in the perturbation and second the choice of the phase shifts δ_σ. If the maximum is to

[15] The opening of a stopband to second order in the perturbation is considered in some detail by the authors in MURA Report 445 (February 2, 1959).

be enhanced at some θ_0 it would be desirable for the perturbation to add to the unperturbed solution a function (see Fig. 2)

$$\begin{aligned} g(\theta) &= g_0 \cos\nu(\theta-\theta_0), \quad (2n\nu-1)(\pi/2\nu) \leq (\theta-\theta_0), \bmod 2\pi, \leq (2n\nu+1)(\pi/2\nu), \\ &= 0, \quad (2n\nu+1)(\pi/2\nu) \leq (\theta-\theta_0), \bmod 2\pi, \leq [(2n+2)\nu-1](\pi/2\nu), \end{aligned} \tag{31}$$

where n is an even integer and ν is the fundamental frequency of the unperturbed solution. The Fourier analysis of $g(\theta)$ gives coefficients

$$g_\tau = 2g_0\nu\pi^{-1}(\nu^2-\tau^2)^{-1}\cos(\pi\tau/2\nu); \quad \tau=1, 2, 3, \cdots. \tag{32}$$

The dominant terms in the series can be ascertained from the ratio

$$\begin{aligned} (g_\tau/g_\nu) &= 4\pi^{-1}\nu^2(\nu^2-\tau^2)^{-1}\cos(\pi\tau/2\nu), \\ &\geq 0; \quad \tau \leq 3\nu. \end{aligned} \tag{33}$$

Since Φ_1 already contains the dominant term of the Fourier expansion as its fundamental, it is apparent from Eq. (33) that the additional terms to be added should contain harmonics close to ν. Furthermore, since (g_τ/g_ν) becomes more slowly varying for large ν, more terms will be needed for large ν than for small ν. On this basis, and from Eqs. (28) and (29), one concludes that the perturbation should include either harmonics 1, 2, or 3, etc., or harmonics $(2\nu\pm1)$, $(2\nu\pm2)$, etc. However, one observes that the coefficients g_τ have the same sign for $\tau \leq 3\nu$, whereas the coefficients of $\chi_{\nu,\tau}{}^k$ in Φ_1 alternate in sign [see Eqs. (9) and (29)] depending upon whether τ is greater or less than ν. Therefore, having frequencies 1, 2 etc., or $(2\nu-1)$, $(2\nu-2)$, etc., in the perturbation is desirable since they introduce harmonics $\nu\pm1$, $\nu\pm2$, etc., or $(\nu-1, 3\nu-1)$, $(\nu-2, 3\nu-2)$, etc., into the solution. In the latter case, however, this distinction is academic since the fact that $a_{\nu,3\nu-\rho}{}^k \gg a_{\nu,\nu-\rho}{}^k$ makes the $(3\nu-\rho)$ terms negligible.

The azimuthal position of the maximum displacement can be obtained approximately by examining the maximum of Φ_1 alone, ignoring the exponential factor $\exp\mu\theta$, and using the approximate formulas given by Eq. (6). Thus, letting

$$\begin{aligned} K\sin\varphi_0 &= (\alpha)^{\frac{1}{2}} - W(1-\alpha)^{\frac{1}{2}}, \\ K\cos\varphi_0 &= (1-\alpha)^{\frac{1}{2}} + W(\alpha)^{\frac{1}{2}}, \\ \tan\varphi_0 &= [\alpha/(1-\alpha)]^{\frac{1}{2}} + (2\alpha-1\alpha)W, \end{aligned} \tag{34}$$

one obtains

$$\begin{aligned} \Phi_1 \sim & \cos\nu(\theta-\varphi_0/\nu) \\ &+ B_\nu \cos[(N-\nu)(\theta-\varphi_0/\nu)+(N\varphi_0/\nu)] \\ &+ C_\nu \cos[(N+\nu)(\theta-\varphi_0/\nu)+(N\varphi_0/\nu)] \\ &+ (2a_{\nu,\nu+\rho}{}^{(1)})^{-1}\xi_{2\nu+\rho}\{\cos[(\nu+\rho)(\theta-\varphi_0/\nu)+\gamma_\rho] \\ &+ B_{\nu+\rho}\cos[(N-\nu-\rho)(\theta-\varphi_0/\nu)-\gamma_\rho+(N\varphi_0/\nu)] \\ &+ C_{\nu+\rho}\cos[(N+\nu+\rho)(\theta-\varphi_0/\nu) \\ &\qquad +\gamma_\rho+(N\varphi_0/\nu)]\}, \end{aligned} \tag{35}$$

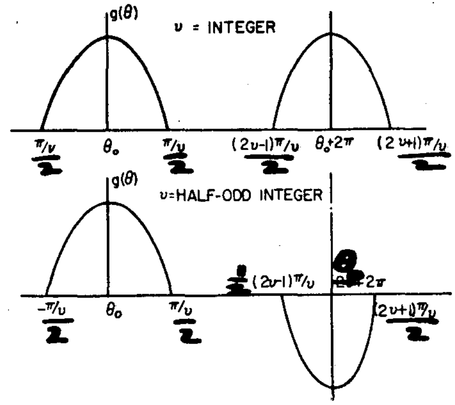

FIG. 2. Form of the function $g(\theta)$.

where $\gamma_\rho = \delta_{2\nu+\rho} + (\rho\varphi_0/\nu) + 2\varphi_0$, $\rho = \pm1, \pm2$, etc., for a typical perturbation term $\xi_{2\nu+\rho}\cos[(2\nu+\rho)\theta+\delta_{2\nu+\rho}]$. For convenience the higher-order terms

$$-W(1-\alpha)^{\frac{1}{2}}\textstyle\sum_k \sum_{\sigma\neq\nu}(a_{\nu,\sigma}{}^k)^{-1}\langle 1,\nu|f|k,\sigma\rangle\chi_{\nu,\sigma}{}^k$$

and

$$W(\alpha)^{\frac{1}{2}}\textstyle\sum_k \sum_{\sigma\neq\nu}(a_{\nu,\sigma}{}^k)^{-1}\langle 2,\nu|f|k,\sigma\rangle\chi_{\nu,\sigma}{}^k$$

were added to Eq. (28) to derive the above result.[16] The maximum will occur at the azimuth $\theta_0 = (\varphi_0/\nu)$ with the dominant terms reinforcing the fundamental if one chooses

$$\xi_{2\nu+\rho} = \rho|\rho|^{-1}|\xi_{2\nu+\rho}|, \tag{36}$$

$$(N\varphi_0/\nu) = 2\pi l; \quad l=1, 2, 3, \cdots, \tag{37}$$

$$\begin{aligned} \delta_{2\nu+\rho} &= -(2\varphi_0+\rho\varphi_0/\nu) \\ &= -2\pi N^{-1}l(2\nu+\rho). \end{aligned} \tag{38}$$

The condition expressed by Eq. (37) places the maximum in the center of a radially focusing sector. Since maximum growth for the betatron oscillations occurs for $\alpha=0.5$ [see Eq. (27)] one obtains the auxiliary condition $\varphi_0 = (n+\frac{1}{4})\pi$, $n=1, 2, 3, \cdots$, from Eq. (34). Imposing this condition gives

$$l = (8\nu)^{-1}(4n+1)N. \tag{39}$$

Because this equation cannot be satisfied for arbitrary N and ν, it would be desirable to include it in the design specifications of the accelerator. However, since $[\alpha(1-\alpha)]^{\frac{1}{2}}$ varies so slowly in the neighborhood of $\alpha=0.5$, growth is achieved for quite modest values of α. Thus Eq. (39) can be relaxed sufficiently to include any N and ν. From Eqs. (12) and (30) one sees that the assumption $m^{(2)} > m^{(1)}$ is justified if one chooses

$$\xi_{2\nu} < 0, \quad \delta_{2\nu} = 0. \tag{40}$$

C. Summary

In the previous sections it has been determined that a field gradient perturbation of the type

$$-|\xi_{2\nu}|\cos 2\nu\theta + \textstyle\sum_\rho \rho|\rho|^{-1}|\xi_{2\nu+\rho}|\cos[(2\nu+\rho)\theta+\delta_{2\nu+\rho}], \quad \rho=\pm1, \pm2, \text{etc.}, \tag{41}$$

[16] The normalization factor D_τ does not appear in Eq. (35) since the use of the simpler functions in the matrix elements requires the same constant for each of the eigenfunctions. The more sophisticated treatment, however, gives the same results.

TABLE I. Coefficients of $\cos\sigma(\theta-\varphi_0/\nu)$ in the function Φ_1 for the perturbation given in Eq. (41).

σ	Coefficient
ν	1
$N-\nu$	B_ν
$N+\nu$	C_ν
$+\rho$	$\xi_{2\nu+\rho}(2a_{\nu,\nu+\rho}^{(1)})^{-1}$
$N-\nu+\rho$	$\xi_{2\nu+\rho}(2a_{\nu,\nu+\rho}^{(1)})^{-1}B_{\nu+\rho}$
$N+\nu+\rho$	$\xi_{2\nu+\rho}(2a_{\nu,\nu+\rho}^{(1)})^{-1}C_{\nu+\rho}$
$3\nu+\rho$	$\xi_{2\nu+\rho}(2a_{\nu,3\nu+\rho}^{(1)})^{-1}$
$N-3\nu+\rho$	$\xi_{2\nu+\rho}(2a_{\nu,3\nu+\rho}^{(1)})^{-1}B_{3\nu+\rho}$
$N+3\nu+\rho$	$\xi_{2\nu+\rho}(2a_{\nu,3\nu+\rho}^{(1)})^{-1}C_{3\nu+\rho}$

will open the stopband associated with the radial frequency ν to first order and that the maximum displacement of the betatron oscillations will occur in the center of only one of the radial focusing sectors if the phase shifts $\delta_{2\nu+\rho}$ are chosen in accordance with Eqs. (37) and (38) and if $|\xi_{2\nu+\rho}|$ is chosen approximately in accordance with the Fourier coefficients given in Eq. (33). The exact number of terms required in the perturbation depends upon the magnitude of ν. In the following section two examples are given; one involving $\nu=7.5$, $N=48$ in which four perturbation terms are required, and the other involving $\nu=2.5$, $N=12$, in which only two are necessary.

Simplified, approximate formulas for the matrix elements, in addition to those given in Eqs. (29) and (30),

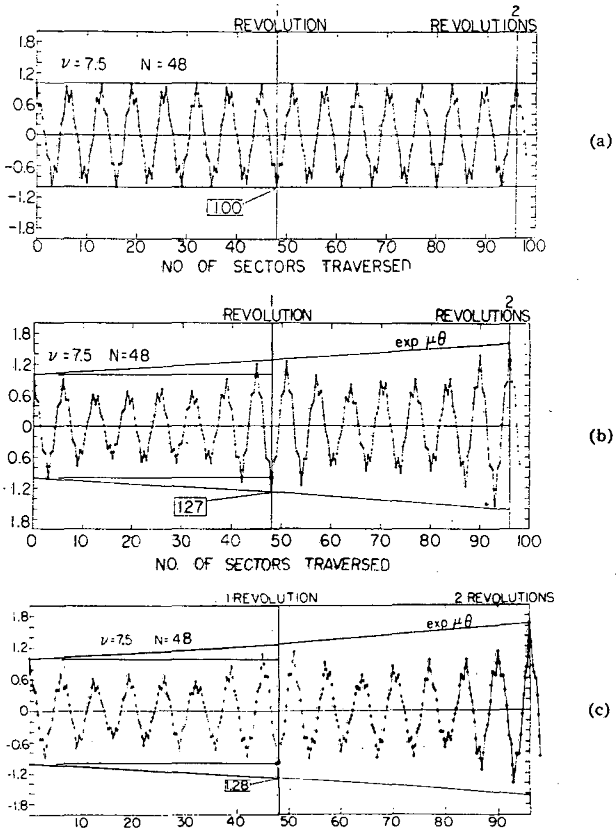

FIG. 3. Digital results for $N=48$, $\nu=7.5$. (a) No perturbation; (b) $f(\theta)=-\cos 15\theta+5.2\cos 16\theta+10.17\cos[17\theta+(\pi/2)]$; (c) $f(\theta)=-\cos 15\theta+5.2\cos 16\theta+10.17\cos[17\theta+(\pi/2)]+21.65\cos 20\theta$.

which are necessary to estimate the growth rate μ and the function Φ_1 are

$$\langle 1,\nu|F|1,\nu\rangle=(2\nu^2/m_\nu),\qquad \langle 2,\nu|\partial|1,\nu\rangle=\nu. \tag{42}$$

Using these values one obtains for the perturbation suggested in Eq. (41),

$$\mu=(2\nu)^{-1}\xi_{2\nu}[\alpha(1-\alpha)]^{\frac{1}{2}}[1+(8\nu^2)^{-1}(2\alpha-1)\xi_{2\nu}], \tag{43}$$

and the coefficients for the harmonics in Φ_1 shown in Table I.

III. DIGITAL COMPUTATIONS

To verify that the perturbation suggested in Eq. (41) gives the desired results, digital computations for the solutions of Eq. (1) were made using the Iowa State University "Cyclone" and the MURA IBM 704 computers. To simplify both the digital and analytic calculations, the small "centrifugal focusing" term p is ignored and the function $F(\theta)$ replaced by the first term in its Fourier analysis, $(4/\pi)\cos N\theta$. This latter approximation has been shown[15] to make essentially no change in the functions Φ_1 or $\chi_{\nu,\sigma}{}^k$ and all the equations given in the previous section remain valid.

The particular example chosen is for an accelerator consisting of 48 full sectors operating near the $\nu=7.5$ resonance and being perturbed by an $f(\theta)$ as given by Eq. (41) for the two values $\rho=1, 2$. Thus the equations of interest are

$$\partial^2x+[(4/\pi)m\cos 48\theta-\cos 15\theta+5.20\cos 16\theta+10.17\cos(17\theta+\pi/2)]x=0, \tag{44}$$

where the phase shifts have been chosen in accordance with Eqs. (37), (38), and (39) with $n=11$, $l=36$, and

$$\partial^2\chi_{7.5,\tau}{}^k+(4/\pi)m_{7.5}\cos 48\theta\chi_{7.5,\tau}{}^k=-a_{7.5,\tau}{}^k\chi_{7.5,\tau}{}^k. \tag{45}$$

TABLE II. Eigenfunctions and eigenvalues for the equation $\partial^2\chi_{\nu,\sigma}{}^k+(4/\pi)m_\nu\cos N\theta\chi_{\nu,\sigma}{}^k=-a_{\nu,\sigma}{}^k\chi_{\nu,\sigma}{}^k$.

Eigenvalues $a_{\nu,\tau}{}^k$ τ	Digital	Predicted by Eq. (10) and Eq. (8)	or Eq. (9)
7.5	0	0	0
8.5	14.34	14.34	14.58
9.5	30.37	30.37	30.97
22.5	310.49	322	409
23.5	317.82	330	452
$m_{7.5}$	384.74	385.48	

Coefficients of circular functions in $\chi_{7.5,\tau}{}^k$

τ	D_τ Digital	D_τ Predicted	B_τ Digital	B_τ Predicted	C_τ Digital	C_τ Predicted
7.5	1.394	1.394	0.1500	0.1496	0.07972	0.07967
8.5	1.392	1.393	0.1593	0.1588	0.07727	0.07723
9.5	1.390	1.391	0.1697	0.1691	0.07496	0.07490
22.5	1.1314	1.1318	0.7467	0.7477	0.05321	0.05280
23.5	1.0464	1.0461	0.9061	0.9082	0.05190	0.05131

TABLE III. Coefficients of $\cos\sigma(\theta-\varphi_0/\nu)$ in the function Φ_1.

σ	Digital	Predicted
7.5	1	1
40.5	0.148	0.150
55.5	0.0787	0.0797
8.5	(0.181)(1.34)	0.181
39.5	(0.0282)(1.34)	0.0289
56.5	(0.0138)(1.34)	0.0140
9.5	0.155	0.167
38.5	0.0256	0.0278
57.5	0.0115	0.0123

A comparison between the digital and the analytic calculations is shown in Tables II, III, and IV. In the analytic calculations, the simplified expressions using Eqs. (29), (30), and (42) are used throughout. In general it is seen that the agreement is quite good. The disagreement shown in Table III by the multiplication factor 1.34 arises primarily from a relatively large contribution to the function $\chi_{7.5,8.5}{}^k$ in Φ_1 from the second-order terms which were ignored. These same terms which enter in the third order in the value of μ, account for the disagreement shown in Table IV. The value of α cannot be predicted as well as the other quantities since the additional assumption is made that the factor $\exp\mu\theta$ does not affect the position of the maximum. The difference in α shown in Table IV corresponds to a shift in the maximum of only 1.67°. Thus, the analytical approach, as represented by the simplified formulas, serves as an excellent guide to the digital calculations which must be done to extract a beam from a particular accelerator.

Graphs of the digital solution to Eq. (44) are shown in Fig. 3(b). For comparison purposes, the solution in the absence of the perturbation is given in Fig. 3(a). The maxima at the sectors 0 and 96 and the minimum at sector 48 have been enhanced as predicted by the theory. The more complete interference shown in Fig. 3(c) is accomplished through the additional perturbation term $21.65\cos 20\theta$, which is chosen specifically to reduce the maxima near sector 48 [see Fig. 3(b)]. The substantial increase in the amplitude of the betatron oscillations shown in Fig. 3 for each revolution plus the constructive interference at the appropriate azimuth attests to the usefulness of the resonance method of extraction. In addition all the perturbation terms used in the example are less than 6% of the normal A.G. flutter.

Fewer perturbations are necessary if the resonance used

TABLE IV. Eigenvalues m^k, growth rate μ, and the position α within the stopband.

	Digital	Predicted
$m^{(1)}$	378.21	378.39
$m^{(2)}$	381.77	381.78
μ	0.039	0.036
α	0.71	0.75

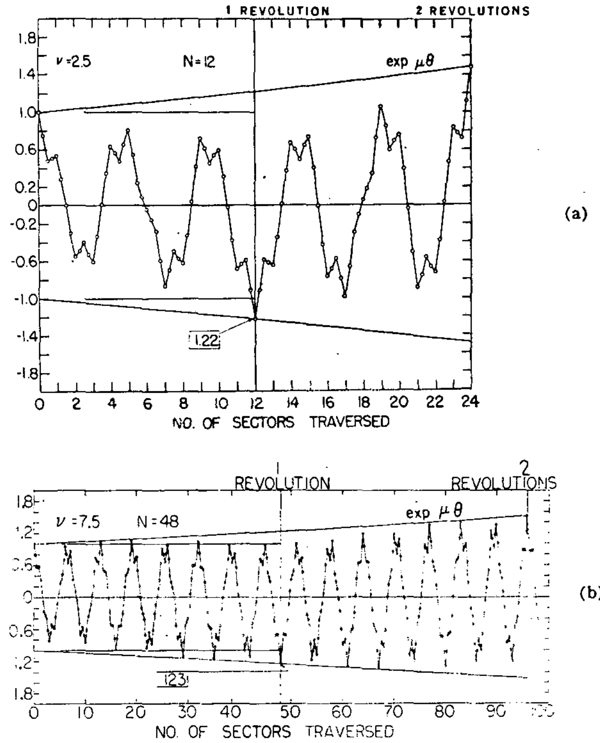

FIG. 4. Digital results comparing the effectiveness of a $\cos(\theta/2)$ term in the solution. (a) $N=12$, $\nu=2.5$, $f(\theta)=-.25\cos 5\theta+2.5\cos 2\theta$; (b) $N=48$. $\nu=7.5$, $f(\theta)=-\cos 15\theta+9.24\cos 8\theta$.

is a small integer or half-integer. To demonstrate this one considers an accelerator with 12 full sectors operating near the $\nu=2.5$ resonance. In this case the differential equation is

$$\partial^2 x+[(4/\pi)(31.42)\cos 12\theta-0.25\cos 5\theta+2.5\cos 2\theta]x=0.$$

The $\cos 2\theta$ term in the perturbation introduces a $\cos(\theta/2)$ term in the solution. The results are shown in Fig. 4(a). For comparison purposes, the solution for the 48 sector accelerator with $\nu=7.5$ for the perturbation $(-\cos 15\theta+9.24\cos 8\theta)$ is shown in Fig. 4(b). In this case it is the $\cos 8\theta$ term that introduces the $\cos(\theta/2)$ dependence of the solution. One sees immediately that whereas the solution for the $\nu=2.5$ resonance is quite satisfactory, the solution for the $\nu=7.5$ resonance shows very little preference for one sector over the others.

ACKNOWLEDGMENTS

The authors wish to thank the members of the MURA and Cyclone computer groups for their cooperation and especially to acknowledge the efforts of Mr. Bill Lewish and Mr. George Westlund for making many of the digital computations possible. The authors are also indebted to Dr. George A. Kolstad for stimulating remarks concerning the potential utility of an effective resonant extraction method for alternate gradient accelerators.

Reprinted from THE REVIEW OF SCIENTIFIC INSTRUMENTS, Vol. 31, No. 10, 1076–1106, October, 1960
Printed in U. S. A.

Electron Model of a Spiral Sector Accelerator*

D. W. KERST,† E. A. DAY,† H. J. HAUSMAN,‡ R. O. HAXBY,§ L. J. LASLETT,|| F. E. MILLS, T. OHKAWA,¶ F. L. PETERSON, E. M. ROWE, A. M. SESSLER,‡ J. N. SNYDER,** AND W. A. WALLENMEYER

Midwestern Universities Research Association, Madison, Wisconsin

(Received June 23, 1960; and in final form, July 29, 1960)

A six-sector spiral ridge FFAG accelerator has been constructed and successfully operated to accelerate electrons from 35 to 180 kev kinetic energy. Acceleration was by betatron action, supplemented by radio-frequency acceleration when desired. The design was based on magnetostatic and orbit computations performed with the Illiac digital computer, and the subsequent performance was found to be in good accord with these computations. Tuning coils permitted variation of the basic parameters about the design values suggested by the computations, so that an experimental investigation could be made concerning the importance of nearby resonances. The theoretical basis of the computational work and the specific results obtained are first described, followed by a *résumé* of the constructional features and magnetostatic measurements. Tests with the operating model are then reported, comprising a resonance survey, injection studies, perturbation studies, and the use of radio-frequency acceleration. The frequencies of radial and axial betatron oscillation at the nominal operating point were, respectively, $\nu_x=1.40$ and $\nu_y=1.12$, and the resonance survey indicated this operating point to be centrally located within a region of relatively large intensity which was bounded by the resonances $\nu_y=1.0$, $\nu_x=1.5$, and (less markedly) $2\nu_y-\nu_x=1$. Injection from a deflector structure with a thin septum permitted efficient injection to be achieved either by concomitant rapid acceleration of the injected electrons or, alternatively, by use of a time dependent radial electric field applied as a perturbation. Experiments with a protracted injection pulse permitted the observation of phenomena attributable to space charge effects. A suitable frequency-modulation schedule permitted successful acceleration of a substantial fraction of stacked electrons through the transition energy. Appendices describe a modulator, with negative feedback stabilization, to permit protracted injection, a magnetometer, used in the magnetic field measurements, and the essentials of Parzen's theory of perturbations, which was found to account satisfactorily for the results of the perturbation experiments.

I. INTRODUCTION

IN fixed field alternating gradient (FFAG) accelerators[1,2] particles with a large range of momenta can be simultaneously accommodated within an annular magnet of limited radial extent, thus permitting a desirable flexibility in the methods of accelerating the particles and affording the promise of high beam intensities. The nature and general theory of FFAG accelerators have been described previously[1,2] and the operation of a radial sector electron model reported.[3] The spiral sector type is an attractive alternative form of a FFAG accelerator, since smaller circumference factors may be utilized than appear feasible with the radial sector type and a significant economy may thus be achieved in the magnet design. Nonlinear features of the orbit dynamics, on the other hand, would be expected to be materially more prominent than for a comparable radial sector accelerator. The present article describes the design, construction, and operation of a model FFAG electron accelerator employing

* This work was supported by the U. S. Atomic Energy Commission, the National Science Foundation, and the Office of Naval Research.

† Present address: General Atomic Division of General Dynamics Corporation, San Diego, California.
‡ The Ohio State University, Columbus, Ohio.
§ On leave from Purdue University, Lafayette, Indiana.
|| Iowa State University, Ames Iowa.
¶ On leave from the University of Tokyo, Tokyo, Japan.
** University of Illinois, Urbana, Illinois.

[1] K. R. Symon, D. W. Kerst, L. W. Jones, L. J. Laslett, and K. M. Terwilliger, Phys. Rev. 103, 1837 (1956).
[2] L. Jackson Laslett, Science 124, 781 (1956).
[3] F. T. Cole, R. O. Haxby, L. W. Jones, C. H. Pruett, and K. M. Terwilliger, Rev. Sci. Instr. 28, 403 (1957).

spiral sectors,[4] which was constructed to provide an empirical test of theoretical predictions, to contribute further evidence of orbit stability over intervals longer than could be examined computationally or under conditions in which multiparticle effects are important, and to permit the acquisition of experience with various acceleration methods possible in accelerators of this type.

As in other FFAG designs the magnet was such as to provide a field whose average value varies with radius as r^k, and use of logarithmically spiraled poles permitted possible orbits of particles with different energies, or momenta, to be geometrically similar. A separated sector design,[2] employing separate spiral magnets, was used in the interests of simplifying construction. More significantly, a field with a large azimuthal variation was thereby obtained, in an aperture not excessively limited, and larger stability limits could be expected. The flutter, or azimuthal variation of the field, was further enhanced by the use of guard edges or "ears," of zero magnetostatic potential at the edges of the spiral sectors.[5] Initially the model was operated with betatron acceleration, although in later work fairly extensive tests of radio-frequency acceleration methods were undertaken.

The design of the spiral sector model was based, as discussed in Sec. II, on computations performed with the electronic digital computer of the Graduate College of the University of Illinois (Illiac), corroborated and supplemented later by some computations with an IBM-704 computer in the MURA Laboratory at Madison, Wisconsin. Constructional work was begun in the Physics Research Laboratory of the University of Illinois and completed in Madison, where magnetic field tests were made, the model put into operation, and a beam immediately obtained.

With the number of sectors (N) selected as six, in the interests of a conservative design which would permit avoiding an excessive number of resonances, the remaining

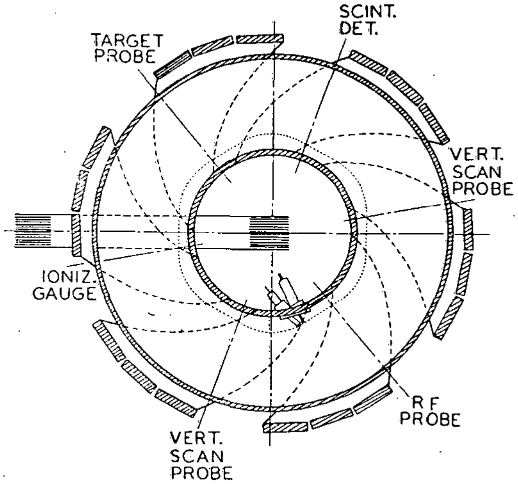

FIG. 1. Over-all view of the spiral sector model.

basic parameters characterizing the model were selected by digital computations pertaining to the magnetostatic problem and to the orbit dynamics in the resultant magnetic field. The computational work included study of the effect of misalignments and the values finally recommended for the basic parameters were taken as central design values about which adjustments could later be made to determine empirically the effect of possible harmful resonances.

The inner radius of the accelerator was determined by the need to accommodate the betatron core and for convenience of access to various ancillary components, while the associated injection energy ($\cong$35 kev) was dictated by the specifications of the injector, which was originally planned to be of the type used in the University of Illinois 80-Mev betatron.[6] From the field strength thus found to be appropriate at the inner radius, and from the value of the field index k suggested by the digital computations, the maximum radius obtainable with readily available forgings of Armco iron thus determined the maximum energy which could be attained in the model ($\cong$180 kev). With the dimensions selected in this way the model permitted study of beam behavior in the neighborhood of the transition energy (155 kev), which was reached by particles moving in orbits situated an adequate distance within the outer wall of the vacuum chamber.

Figure 1 presents a general view of the accelerator. In the following sections we review the theoretical and computational design studies, summarize the constructional features and test program, and report the results of experiments made with the operating model to determine the effects of resonances and the characteristics of various acceleration methods.

[4] Preliminary accounts of this model have been given in the following references: (a) D. W. Kerst *et al.*, Rev. Sci. Instr. **28**, 970 (1957); (b) L. J. Laslett, A. M. Sessler, and J. N. Snyder, Bull. Am. Phys. Soc. **II** 2, 337 (1957); (c) H. J. Hausman *et al.*, Bull. Am. Phys. Soc. **II** 2, 337 (1957); (d) R. O. Haxby *et al.*, Bull. Am. Phys. Soc. **II** 2, 337 (1957); (e) D. W. Kerst and F. E. Mills, Bull. Am. Phys. Soc. **II** 2, 337 (1957); (f) R. Stump, B. Waldman, and W. A. Wallenmeyer, Bull. Am. Phys. Soc. **II** 2, 337 (1957); (g) F. L. Peterson and W. A. Wallenmeyer, Bull. Am. Phys. Soc. **II** 3, 168 (1958); (h) F. E. Mills and D. S. Roiseland, Bull. Am. Phys. Soc. **II** 3, 168 (1958); (i) F. L. Peterson, Bull. Am. Phys. Soc. **II** 3, 331 (1958); and (j) R. O. Haxby *et al.*, "Experience with a spiral sector FFAG electron accelerator," *Proceedings of the CERN Conference on High Energy Accelerators and Instrumentation* (European Organization for Nuclear Research, Geneva, 1959), p. 75.

[5] In addition to effecting a more rapid decrease of the magnetic field at the edges of each sector, the ears provide additional shielding from the magnetic field of the earth, which is not entirely negligible in comparison to the rather low field strengths employed in the electron model. The influence of the earth's field was further reduced by use of large compensation coils surrounding the accelerator, similar to Helmholtz pairs, and with a hexagonal shape employed for the pair intended to neutralize the vertical component.

[6] D. W. Kerst *et al.*, Rev. Sci. Instr. **21**, 462 (1950), especially Fig. 12.

II. THEORY

The general theory of fixed field accelerators, as well as that specific to the spiral sector design, has been discussed extensively elsewhere.[1,2] Many of the approximate analytic techniques which have been developed[7] were of great value in the preliminary theoretical design studies. This work, however, is not essentially unique, whereas the methods used to design this model are distinct from those used to design any other particle accelerator in that, to the best of our knowledge, this is the first time that a digital computer was used to determine completely the essential parameters of an accelerator by computation of the performance which would result from various choices of magnet design.

There were two digital computer programs which were essential to the design of the model. The first program started with any chosen magnet contour (provided only that the pole "scales"[1,2]) and calculated the magnetostatic potential at all points in the region between the poles. The second program constituted a *dynamics* program, as differentiated from the aforementioned *potential* program, and served to calculate the trajectory of a monoenergetic particle in the fields resulting from the solution to the potential problem. In effect, by use of these programs, it was possible by digital computation to construct a large number of poles and study in detail the resulting magnetic fields or, more generally, to construct a large number of accelerators and study the consequent particle dynamics. It cannot be overemphasized that this is an essentially exact procedure, save for possible long range dynamical instabilities which would not be exhibited in digital computer runs corresponding to particle trajectories carried through a few hundred revolutions or for possible many particle effects such as the limitations due to space charge. Thus, provided the accelerator was assembled according to the specifications and tolerances obtained from the computer, there could be no real doubt that the accelerator would operate successfully.

The remainder of this section is devoted to a description of the digital computer programs mentioned and to the various calculations which were performed in order to determine a suitable set of design parameters.

A. The Potential Problem

Fixed field accelerators must be designed so that the betatron oscillation frequencies are substantially independent of radius. This may be accomplished most directly by having the orbits and the fields themselves simply scaled replicas, possibly rotated, of the orbits and fields at any other radius. In the case that such scaling is maintained, it is clear that the fields throughout the entire gap can be characterized by the fields on a *two-dimensional* surface (for example on a cylinder). Limiting our attention then to scaling fields, we can reduce a three-dimensional potential problem to a *two-dimensional* problem—namely, to a problem which is quite tractable with present high speed digital computers.

The median plane field $[H_r(r,\phi,0)=H\phi(r,\phi,0)=0]$ in a spiral sector, scaling accelerator can be written

$$H_z(r,\phi,0)=-H_0\left(\frac{r}{r_0}\right)^k F\left(\frac{1}{w}\ln\frac{r}{r_0}-N\phi\right), \tag{1}$$

where r is the radial coordinate, ϕ is the azimuthal angle, and F is a periodic function (period 2π) of average value unity. The constant H_0 denotes the average magnetic field at the reference radius r_0. The parameter k represents the field index, the number of sectors is N, and the spiral ridge makes an angle $\zeta=\cot^{-1}(Nw)$ with a radius vector.

From Eq. (1) the magnetic scalar potential V may be written as

$$V=\left(\frac{r}{r_0}\right)^{k+1} G\left(\frac{1}{w}\ln\frac{r}{r_0}-N\phi,\frac{z}{r}\right), \tag{2}$$

where G is a periodic function (of period 2π) with respect to its first argument, r is the radial coordinate in a cylindrical coordinate system, and z is the vertical coordinate. If we define a new function by the equation

$$\Omega(\xi,\eta)=V/H_0r_0(r/r_0)^{k+1}, \tag{3}$$

where

$$\xi=\frac{1}{2\pi}\left[\frac{1}{w}\ln\frac{r}{r_0}-N\phi\right] \tag{4a}$$

$$\eta=\frac{[(1/w)^2+N^2]^{\frac{1}{2}}}{2\pi}\frac{z}{r}, \tag{4b}$$

$\Omega(\xi,\eta)$ is periodic with the period unity with respect to ξ and it becomes evident that the fields can be expressed in terms of the *two* variables ξ and η.

In terms of the function $\Omega(\xi,\eta)$, Laplace's equation in three dimensions reduces to the following partial differential equation with *two* independent variables:

$$\frac{\partial^2\Omega}{\partial\xi^2}+\left[1+\frac{4\pi^2\eta^2}{(1/w)^2+N^2}\right]\frac{\partial^2\Omega}{\partial\eta^2}-\frac{4\pi(1/w)}{(1/w)^2+N^2}\eta\frac{\partial^2\Omega}{\partial\xi\partial\eta}$$
$$+\frac{4\pi(k+1)/w}{(1/w)^2+N^2}\frac{\partial\Omega}{\partial\xi}-\frac{4\pi^2(2k+1)}{(1/w)^2+N^2}\eta\frac{\partial\Omega}{\partial\eta}$$
$$+\frac{4\pi^2(k+1)^2}{(1/w)^2+N^2}\Omega=0, \tag{5}$$

[7] The linear orbit equations may be approximated by aid of the "smooth approximation" (see reference 1, p. 1842) or by use of tabulated solutions to a Hill's equation (see reference 1, footnote 9). Results for the nonlinear orbit equations may be approximated by techniques developed independently by a number of workers [see, for example, L. J. Laslett and A. M. Sessler, Midwestern Universities Research Association Rept. MURA-263 (1957, unpublished)].

in which Ω is an odd function of η, vanishing at $\eta=0$, and is periodic in ξ with the period unity. The potential problem was accordingly solved with the Illiac digital computer through application of a relaxation method to Eq. (5), the input data being the parameters k, $1/w$, N, and the values of Ω on a boundary curve.[8] For a typical problem, the computation time required to obtain Ω with sufficient accuracy for studies of particle dynamics was of the order of 1 or 2 hr.

B. The Dynamics Program

The solution of the potential problem, Ω (or strictly Ω/η), was stored in the fast memory of the Illiac computer as $\frac{1}{2}$-words so that a mesh of up to 2000 points was available. The fields which enter into the differential orbit equations were computed from these stored values by differentiation-interpolation[8] as needed during the course of the integration of the dynamical equations. The field components are given by

$$H_z=-\frac{H_0}{r_0}\frac{[(1/w)^2+N^2]^{\frac{1}{2}}}{2\pi}\left(\frac{r}{r_0}\right)^k\left[\frac{\Omega}{\eta}+\eta\frac{\partial}{\partial\eta}\left(\frac{\Omega}{\eta}\right)\right] \tag{6a}$$

$$H_r=-\frac{H_0}{r_0}\left(\frac{r}{r_0}\right)^k\left[k\left(\frac{\Omega}{\eta}\right)+\frac{1}{2\pi w}\frac{\partial}{\partial\xi}\left(\frac{\Omega}{\eta}\right)-\eta\frac{\partial}{\partial\eta}\left(\frac{\Omega}{\eta}\right)\right] \tag{6b}$$

$$H_\phi=\frac{H_0}{r_0}\frac{N}{2\pi}\left(\frac{r}{r_0}\right)^k\eta\frac{\partial}{\partial\xi}\left(\frac{\Omega}{\eta}\right), \tag{6c}$$

and the dynamical equations, employing these field components, are

$$dx/d\phi=(1+x)p_x(1-p_x^2-p_y^2)^{-\frac{1}{2}} \tag{7a}$$

$$dy/d\phi=(1+x)p_y(1-p_x^2-p_y^2)^{-\frac{1}{2}} \tag{7b}$$

$$dp_x/d\phi=(1-p_x^2-p_y^2)^{-\frac{1}{2}}+\frac{1}{H_0}(1+x)\times[H_z-p_y(1-p_x^2-p_y^2)^{-\frac{1}{2}}H_\phi] \tag{7c}$$

$$dp_y/d\phi=\frac{1}{H_0}(1+x)[p_x(1-p_x^2-p_y^2)^{-\frac{1}{2}}H_\phi-H_r] \tag{7d}$$

in terms of the dependent variables $y\equiv z/r_0$ and $x\equiv(r-r_0)/r_0$.[9]

In order to study the effects of misalignments and field imperfections for the purpose of obtaining tolerances for construction of the model, the dynamics program was arranged so that certain simple algebraic transformations could be inserted periodically. Such transformations, which are called "bumps," were of the following types:

(*1*) *Axially-displaced sector bump.* At the entrance to some chosen sector the following transformation was introduced to relate the initial values (x_i, etc.) of the orbit variables to the values (x_f, etc.) which result from application of the transformation

$$\begin{aligned} x_f&=x_i & y_f&=y_i-\Delta y\\ p_{xf}&=p_{xi} & p_{yf}&=p_{yi}. \end{aligned} \tag{8}$$

The program then proceeded with the integration until the end of the sector, at which point the transformation

$$\begin{aligned} x_f&=x_i & y_f&=y_i+\Delta y\\ p_{xf}&=p_{xi} & p_{yf}&=p_{yi} \end{aligned} \tag{9}$$

used introduced. This same bump was then used repetitively on each revolution.

(*2*) *Radially-displaced sector bump.* The transformation used to simulate a radially displaced sector was identical to that used for a vertical displacement, except that the displacement was made in the x coordinate rather than in y.

(*3*) *Rotated sector bump.* At the entrance to a chosen sector the transformation

$$\begin{aligned} x_f&=x_i-(\pi/N)(\Delta\theta) & y_f&=y_i\\ p_{xf}&=p_{xi}+\Delta\theta & p_{yf}&=p_{yi} \end{aligned} \tag{10}$$

was made. The transformation was then followed, at the end of the sector, by

$$\begin{aligned} x_f&=x_i-(\pi/N)(\Delta\theta) & y_f&=y_i\\ p_{xf}&=p_{xi}-\Delta\theta & p_{yf}&=p_{yi}. \end{aligned} \tag{11}$$

As with the other bumps, this series of transformations was repeated on each revolution of the particle.

C. Computational Results

Figure 2 depicts the operating region of interest, in terms of the quantities $\sigma_x/\pi=2\nu_x/N$ and $\sigma_y/\pi=2\nu_y/N$, where ν_x and ν_y denote the number of radial or axial betatron oscillations per revolution. The important intrinsic resonances have been indicated on Fig. 2, as well as imperfection resonances through third order. On the basis of linear theory, and guided by the theory of imperfections for the linear problem,[1,3,7] three possible operating points

[8] A more complete description of this computational method is given by L. J. Laslett, Midwestern Universities Research Association Rept. MURA-99 (1956, unpublished). The nature of a more elaborate program, subsequently prepared for an IBM-704 computer, is summarized by L. J. Laslett, Midwestern Universities Research Association Rept. MURA-221 (1957, unpublished). The technical difficulties of constructing an efficient relaxation program which would fit the capacities of the Illiac were by no means trivial, but are not discussed here.

[9] Actually the program worked with the variables S and T, rather than x and y, where $S\equiv\ln(1+x)$ and $T\equiv y/(1+x)$. This procedure avoided the use of a logarithm routine in the computational program and thus provided memory capacity for a more detailed representation of the field. For details concerning this feature, the interpolation and differentiation algorisms (which are constructed to provide field components which were continuous from one cell of the mesh to another), and for other details of the computational method see L. J. Laslett, Midwestern Universities Research Association Rept. MURA-99 (1956, unpublished). A description of a similar program subsequently written for an IBM-704 computer is given by L. J. Laslett, Midwestern Universities Research Association Rept. MURA-222 (1957, unpublished).

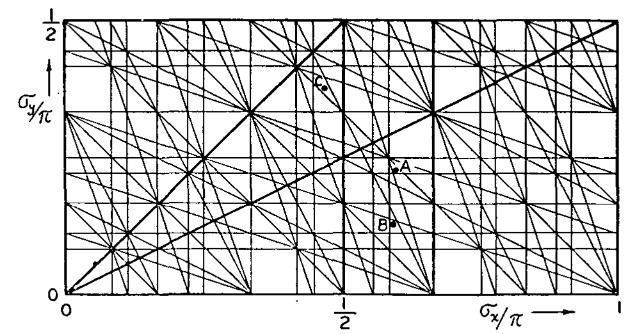

FIG. 2. Resonance diagram for $N=6$. Three possible operating points, for which detailed computations were made, are indicated by the letters A, B, and C.

were selected for detailed study. For each of these operating points, indicated on Fig. 2 by the letters A, B, and C, a realistic pole profile and gap were selected and suitable values of the parameters k and $1/w$ determined computationally to give the desired frequencies for small amplitude betatron oscillations. In Table I we list the parameters which correspond to the three operating points and in Fig. 3 we show a cross section, in the ξ, η plane, of the pole shape used for point C. It may be noted that a pole profile, depicted in this way in the ξ, η plane, represents a section taken at constant r, but with *unequal scale factors* in the azimuthal and axial directions. The outline represents more truly a cross section *perpendicular* to the spiral, save that the general increase of all linear dimensions with radius is not depicted.

The results of a computational study of orbit dynamics for the three operating points are summarized in Table II, wherein we include some refined estimates of radial stability limits determined with the MURA IBM-704 in Madison. To ensure that the computations would not ignore the possibility of strong coupling between radial and axial motion at certain operating points, the Illiac searches for radial stability limits were made with a small initial axial displacement ($y_0=10^{-5}$) in cases which otherwise would have been entirely free of axial motion, and likewise, the subsequent IBM-704 studies of radial motion

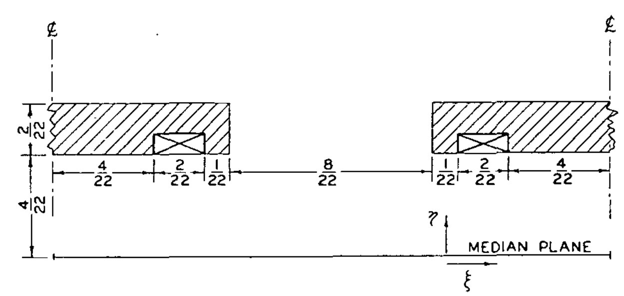

FIG. 3. Cross section of magnet pole, in the ξ, η plane, for operating point C. The pole contour is periodic in the variable ξ, with period 1. Azimuthal distances at constant radius are given by $2\pi r/N$ times the increment of ξ and axial distances by $2\pi r[(1/w)^2+N^2]^{-\frac{1}{2}}$ times the increment of η. For the present structure $1/w=6.25$ and these distances become $1.0472\ r\ \Delta\xi$ and $0.7252\ r\ \Delta\eta$, respectively.

included searches made with an initial axial displacement which was about 12% of the corresponding axial stability limit. Despite the relatively short duration of the individual computer runs for the estimation of stability limits, the introduction of this modest amount of initial axial motion led to substantially reduced, but it is believed more realistic, radial limits for operation at points A and B. For point C, however, the radial stability limits were found to be substantially independent of the presence of such axial motion. Although the data of Table II may be subject to some sampling errors, a significant trend seems unmistakable which served as a helpful guide in selection of a suitable operating point for the model.

The radial stability limits for point A appeared undesirably low when even small amounts of axial motion were present. This result, attributed to proximity to the $\nu_x=2\nu_y$ resonance, motivated the investigation of point B, situated somewhat further from this coupling resonance. As is seen from Table II, the stability limits, although significantly greater than for point A, were still rather small and, in view of the low value of ν_y associated with point B, the usable volume of phase space was again regarded as undesirably small.

Attention was therefore finally directed to point C, lying a considerable distance *above* the $\nu_x=2\nu_y$ resonance. Here the stability region was found to be materially greater than for points A and B, and the axial oscillation frequency was also comparatively large. Most important, moreover, coupling effects were no longer apparent and the sensitivity to misalignments did not appear to be pronounced.

On the basis of the Illiac computations included in Table II, which incidentally were obtained with a total of approximately 200 hr of computer time,[10] it accordingly was decided to proceed with the construction of the model at operating point C. It was, of course, planned to be able to tune the model, but the central design parameters were taken as those associated with point C. It is encouraging to note that the subsequent performance of the model,

TABLE I. Parameters for the three operating points studied computationally.

Parameter	Point A	Point B	Point C
k	1.62	1.65	0.70
$1/w$	6.65	6.00	6.25
N	6	6	6
f_{eff}[a]	1.083	1.085	1.087
σ_x	0.597 π	0.595 π	0.466 π
σ_y	0.225 π	0.129 π	0.375 π
ν_x	1.791	1.785	1.398
ν_y	0.675	0.387	1.125

[a] f_{eff} denotes the *effective flutter*, defined as $f_{eff}=[2(\langle H^2\rangle-\langle H\rangle^2)/\langle H\rangle^2]^{\frac{1}{2}}=[2\langle(H-\langle H\rangle)^2\rangle/\langle H\rangle^2]^{\frac{1}{2}}$.

[10] This estimate does not include code checking, various simplified problems which were studied to test the programs, or checks of internal consistency used to confirm that the results were substantially independent of mesh size. Some tests of the effect of mesh size are described in reference 11.

TABLE II. Summary of the dynamics studies for the three operating points A, B, and C.[a]

Perturbation	Length of individual run	Point A Radial ampl.[b]	Point A Axial ampl.	Point B Radial ampl.[b]	Point B Axial ampl.	Point C Radial ampl.[b]	Point C Axial ampl.
Unperturbed							
	30 sectors	0.088[c]		0.117[c]		0.106[c]	
		0.028[d]		0.052[d]		0.106[d]	
	80 sectors		0.029		0.033		0.036
	Max ampl., stable[e]		0.073		0.072		0.075
Threshold							
	90 sectors, growth	0.032		0.049		0.092	
	no growth	0.027		0.031		0.074	
Axially displaced sector							
$\Delta y=0.00351$ ($\Delta z\cong 1$ mm)	90 sectors	0.019[d]	0.029	0.036[d]	0.033	0.099[c,d]	0.040
$\Delta y=0.00702$ ($\Delta z\cong 2$ mm)		0.019[d]	0.028	0.030[d]	0.035	0.077[c,d]	0.033
Radially displaced sector							
$\Delta x=0.00351$ ($\Delta r\cong 1$ mm)	90 sectors	0.026[d]	0.025	0.037[d]	0.032	0.100[c,d]	0.036
$\Delta x=0.00702$ ($\Delta r\cong 2$ mm)		0.023[d]	0.020	0.034[d]	0.029	0.097[c,d]	0.036
Rotated sector							
$\Delta\theta=0.0015$	90 sectors, unstable	0.032[d]	0.032	0.060[d]	0.034	0.126[c,d]	0.039
	stable	0.023[d]	0.029	0.042[d]	0.030	0.100[c,d]	0.034
$\Delta\theta=0.0060$	unstable	0.036[d]	0.027	0.065[d]	0.030	0.104[c,d]	0.044
	stable	0.023[d]	0.025	0.046[d]	0.028	0.078[c,d]	0.039

[a] The numbers in the body of the table give the magnitudes of the limiting amplitudes, for the free betatron oscillations, in units of the radius. Save where otherwise indicated, the amplitudes refer to the center of a radially focusing region. The threshold for y growth denotes the amplitude of radial oscillation above which coupling results in a marked (exponential) increase in the amplitude of initially small axial oscillations. Approximate magnitudes of the various sector displacements are given in millimeters for a nominal radius of 30 cm.
[b] Amplitude to left of stable fixed point when p_x has the value corresponding to the fixed point.
[c] With no axial amplitude present.
[d] With a small amount of axial amplitude introduced initially.
[e] Amplitude at center of axially focusing region.

reported in Sec. V, indicated that point C fell within a region of maximum beam intensity.

Following initiation of construction of the model, further digital computation was performed on the MURA IBM-704 at Madison. This work proved to be completely consistent with all the results as described, but, because the pressure to obtain a satisfactory design point was no longer present, the opportunity presented itself to obtain a more complete description of the accelerator represented by point C.[11] Some of these supplementary results are described as follows:

(*1*) *Median-plane field.* A Fourier analysis was obtained for the magnetic field in the median plane, with the results given in Table III.

(*2*) *Large amplitude radial oscillations.* A phase plot for large amplitude radial oscillations is illustrated in Fig. 4 for the model free of imperfections.

(*3*) *Small amplitude radial oscillations.* The small amplitude betatron oscillations occur about an equilibrium orbit for which the major terms in its Fourier representation were found to be

$$x_f\cong -0.0211-0.0290\sin N\theta-0.0071\cos N\theta -0.0011\cos 2N\theta -0.0001\sin 3N\theta-0.0002\cos 3N\theta. \quad (12)$$

The elements of the matrix $\begin{pmatrix}A & B\\ C & D\end{pmatrix}$ which serves to carry the vector $(x-x_f,\ p_x-p_{xf})$, characterizing a small amplitude betatron oscillation, through one sector also were computed. These elements, as a function of the starting point within the sector, are plotted in Fig. 5. The parameter β, defined as $B/\sin\sigma$, has been introduced by Courant and Snyder[12] for convenience in treating the response of an

TABLE III. The prominent Fourier components of the normalized magnetic field for operating point C.

m	f_m (the coeff. of $\sin 2\pi m\xi$)	g_m (the coeff. of $\cos 2\pi m\xi$)
0		1 (normalized)
1	1.0688	−0.1312
2	−0.0258	−0.0875
3	0.0742	−0.0357
4	−0.0087	−0.0122
f_{eff}	1.084	

[11] A more complete description of this work is given by L. J. Laslett, Midwestern Universities Research Association Rept. MURA-213 (1957, unpublished).

[12] E. D. Courant and H. S. Snyder, Ann. Phys. 3, 1 (1958).

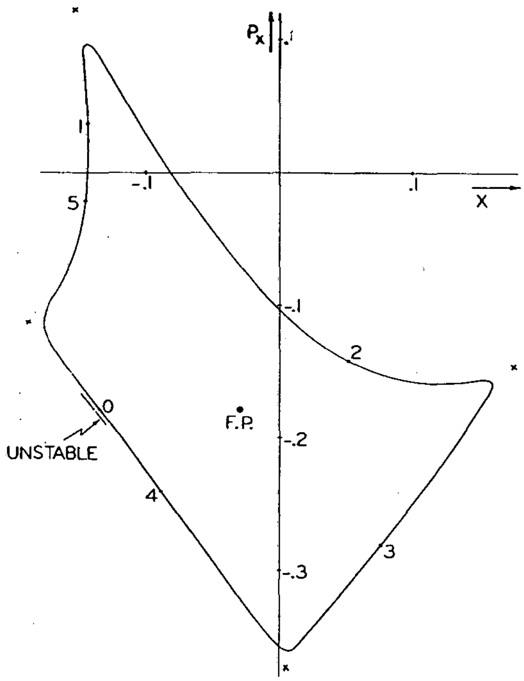

FIG. 4. Phase plot of limiting amplitude stable radial motion, obtained from computer results pertaining to $N\theta=0$ (*mod.* 2π). The stable fixed point is designated by F. P. and the four unstable fixed points by x.

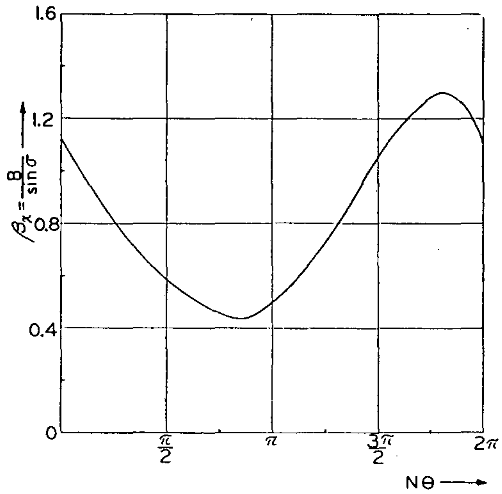

FIG. 6. The parameter β_x for propagation of small amplitude radial oscillations through one sector of the model.

orbit to scattering and other disturbances. For the present structure β_x varies between about 0.43 and 1.29, as can be seen from Fig. 6, and the value at the reference point used in the earlier work ($N\theta=0$, *mod.* 2π) is about 1.12.

(*4*) *Small amplitude axial oscillations.* Corresponding results for axial motion in the model are plotted in Figs. 7 and 8. The values of β_y at $N\theta=0$ and $N\theta=\pi$ (*mod.* 2π) are, respectively, 0.62 and 1.40.

Motivated by the unexpected comparative behavior of three Illiac runs, 22 runs, each of 400 sectors duration, were made with the IBM-704. None of these runs gave evidence of instability and many gave reasonably definite p_y vs y phase plots, of which some were characterized by a rotation number close to $2\pi/5$. The initial conditions for the axial motion were varied over a considerable range within the stability limits quoted in Table II, while the

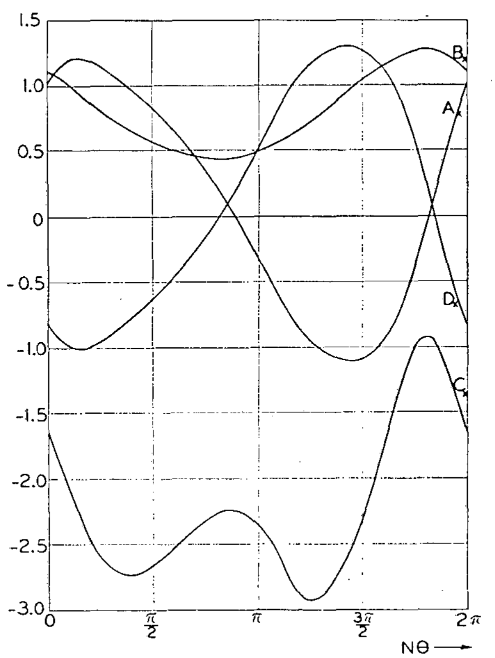

FIG. 5. Matrix elements characterizing propagation of small amplitude radial oscillations through one sector of the model, as a function of the starting point within the sector.

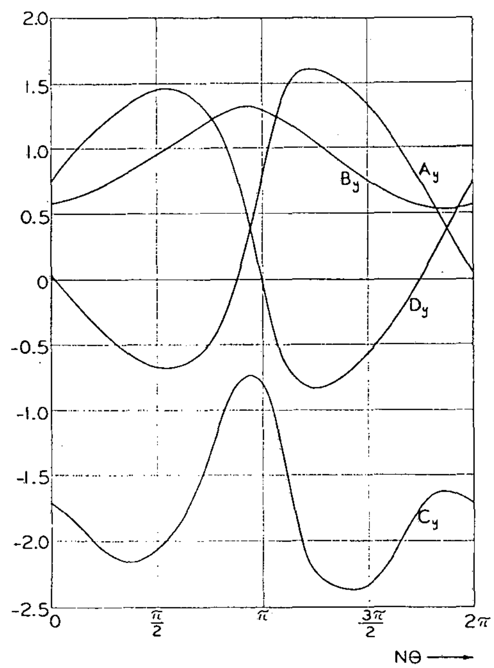

FIG. 7. Matrix elements characterizing propagation of small amplitude axial oscillations through one sector of the model, as a function of the starting point within the sector.

initial values for the radial motion were the coordinates of the fixed point which characterizes the equilibrium orbit.[11]

A careful study[13] was made of the effect of k assuming in one sector the value 0.8, while in the remaining sectors it retained its design value 0.7. It was found that there were no notable effects attributable to the decrease of periodicity of the structure, but only a partial decrease of the radial phase space available for stable oscillations which was similar to the larger decrease found when k was increased in *all* sectors.

III. CONSTRUCTION

A. Magnets

As mentioned previously, it was the intention that the accelerator design should scale and accordingly that all annular rings of the magnet should be *similar*, with the

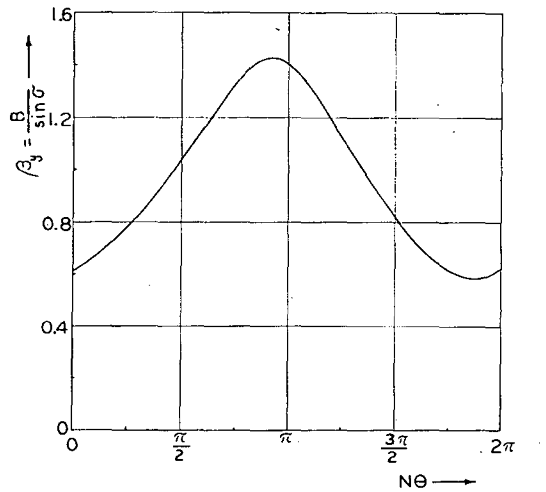

FIG. 8. The parameter β_y for propagation of small amplitude axial oscillations through one sector of the model.

dimensions increasing in direct proportion to the radius. In addition the edges, and other equivalent points of each magnet sector, should progress radially outward along a logarithmic spiral which makes an angle $\zeta=\cot^{-1}(Nw)=46°$ with a radius vector. With such a design, computations made for one radius in the accelerator should be immediately applicable to other radii.

It was appropriate, therefore, to cut the magnet poles from a surface having the correct conical angle to satisfy the scaling requirements of the machine. The sectors were made from forgings of Armco iron, $1\frac{1}{4}$ in. thick, from which annular rings of 25 cm inner radius and 61 cm outer radius were flame-cut. These annular rings were then placed upon a template, pressed into the desired conical shape, and subsequently annealed.

The individual magnet pole pieces were cut from the

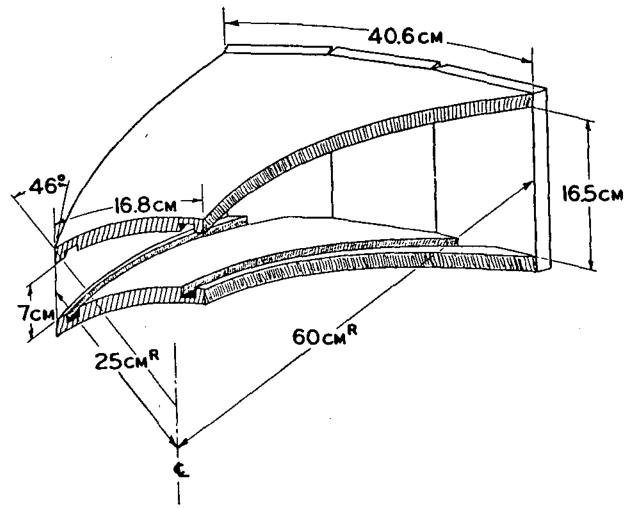

FIG. 9. Schematic drawing of one magnet sector.

conical rings, mounted on a turntable, and machined to the final conical surface. Grooves were machined in the pole surfaces, near the sector edges, to carry the magnetizing windings and tuning coils. The rim of iron remaining beyond the coils could thus be regarded as remaining at zero magnetostatic potential, thereby increasing the effective flutter of the resultant magnetic field by effecting a more abrupt falloff and serving to provide additional shielding against external magnetic fields. The back leg and pole faces of each magnet sector were finally assembled on a jig and pinned by dowels in the final position. Figure 9 illustrates an assembled sector, prior to winding.

Since the magnet gap increases in direct proportion to the radius and the magnetic field as $r^{0.7}$, the magnetostatic potential of the pole face must vary as $r^{1.7}$. It was therefore necessary to use distributed pole-face windings. These were so designed that a single layer of wire gave the requisite field dependence if infinite permeability were assumed for the iron. Current densities in the wires were kept below 2000 amp/in.^{2}, thus obviating the need for water cooling. The coil configuration is shown in Fig. 10.

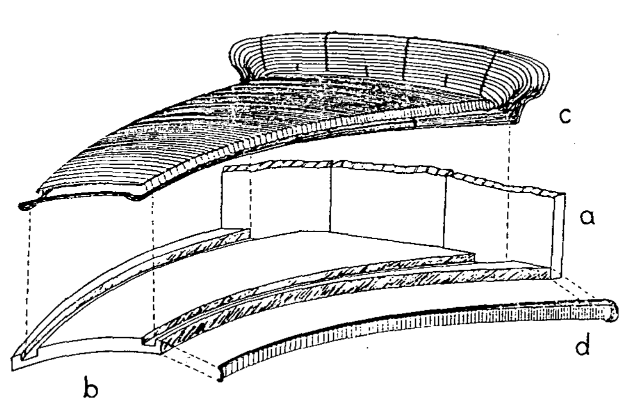

FIG. 10. Exploded view, showing one of the main magnet coils above a magnet pole. The yoke, magnet pole, pole-face windings, and flutter-tuning coils are, respectively, denoted by a, b, c, and d.

[13] L. J. Laslett, Midwestern Universities Research Association Rept. MURA-257 (1957, unpublished).

The main pole-face windings were formed of No.16 Formex-insulated wire and employed 110 turns on each pole, of which 86 were distributed across the pole face, on circular arcs concentric with the accelerator. The wires crossing the pole were secured with polystyrene cement into grooves machined in a Lucite form $\frac{1}{8}$ in. thick. The return copper bundles were then rigidly formed to fit into the edge slots and were carefully mounted on the magnet faces, using fish paper and varnished cambric for insulation.

To provide a desirable flexibility in the operation of the model, both k-tuning coils and flutter-tuning coils were provided for adjusting the operating point of the accelerator. From an expansion of the desired magnetic field through terms of first order in Δk,

$$H(k+\Delta k)\cong H_0(r/r_0)^k+H_0(r/r_0)^k\ln(r/r_0)\Delta k, \quad (13)$$

one is led to a distribution of a single layer of supplemental pole-face windings adequate to produce a suitable change in k with no more than a small nonscaling error. These distributed windings were fabricated in the same way as the main field coils. They were wound with 97 turns of No. 22 Formex-insulated wire, following a schedule similar to that for the main coils, and the return copper bundles were also buried in the edge slots. The flutter-tuning coils were wound on thin Lucite strips which then were secured to the guard edges of each pole so that the edges could be adjusted to magnetostatic potentials different from zero. During the installation of all the coils, the resistances were continually monitored and great care taken to avoid short circuits or grounds.

The main coils were all connected in series, so that they carried the same current ($\cong$3.4 amp). The k-tuning coils had their own series circuit with an adjustable current supply and the flutter-tuning coils were similarly in series with a separate control. Power for these currents was provided by a stabilized Nobatron power supply. A current of ± 1 amp in the k-tuning coils produced a change in k of $\pm 40\%$, and ± 1 amp in the flutter-tuning coils effected a $\pm 30\%$ change of the effective flutter. It should be noted, however, that if *both* types of tuning coils are simultaneously employed, a significant departure from the desired scaling property of the magnetic field will result.

B. Vacuum Chamber and Detectors

(1) The Vacuum Chamber

The vacuum chamber was designed to permit utilization of as much of the magnet gap as possible, this consideration being of particular importance at the injection radius where the largest oscillation amplitudes occur, and to afford a flexibility which would permit modifications of the experimental arrangements to be made readily. It was necessary to provide at least one insulated gap across which accelerating voltages could be placed when required, and several access ports for the insertion of probes and detectors were considered desirable. For adequate beam lifetime, ultimate pressures in the neighborhood of 10^{-6} mm Hg were considered appropriate and an operating pressure of 2×10^{-6} mm Hg was typical for most of the tests described in the following sections.

The chamber, Fig. 11, was constructed as two hollow semicircular annuli, sealed together by means of a $\frac{1}{8}$-in. flat rubber gasket compressed by insulated bolts. The rubber gasket was located behind a metal shoulder, which served to shield the insulating gasket from the beam and assisted in assembly of the chamber. The inner and outer chamber walls were formed by brass rings, $\frac{5}{8}$ in. thick, to which the top and bottom plates of $\frac{1}{2}$-in. brass were brazed to form a chamber with an interior height of $1\frac{1}{2}$ in. The top and bottom exterior surfaces were chamfered, on the inner portion, to fit closely between the magnet poles.

The chamber was pumped continuously through two of eight 4-in. holes in the bottom plate, selection of the particular holes to be used being determined by the desired azimuthal location of the chamber with respect to the magnet sectors. Two Consolidated Electrodynamics type MCF-300 oil diffusion pumps, trapped by baffles which were Freon-cooled to $-40°C$, evacuated the chamber through 4-in. gate valves. The forevacuum was provided by a Welch type 1397 rotary pump which, by a suitable system of ball-valves and use of ballast tanks, also served as a roughing pump. Pressures in the high vacuum system

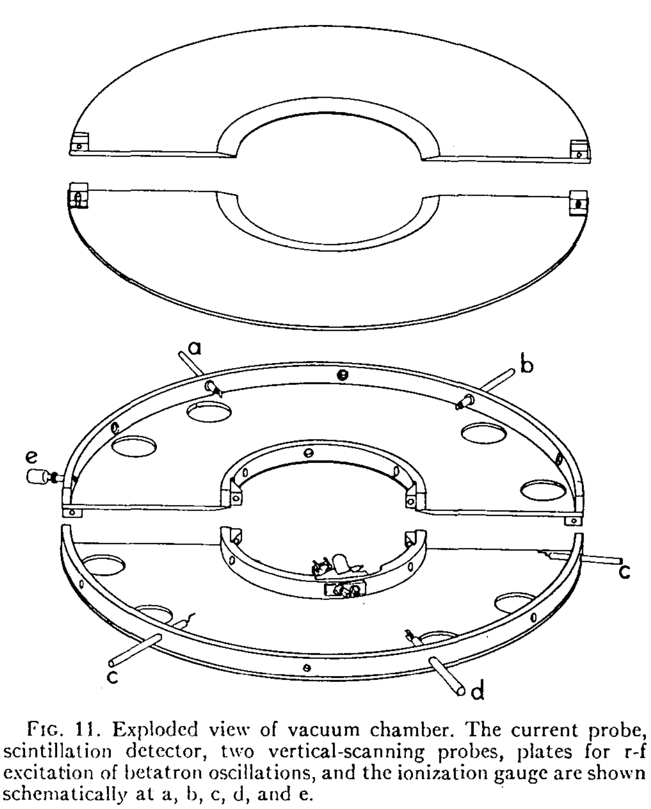

FIG. 11. Exploded view of vacuum chamber. The current probe, scintillation detector, two vertical-scanning probes, plates for r-f excitation of betatron oscillations, and the ionization gauge are shown schematically at a, b, c, d, and e.

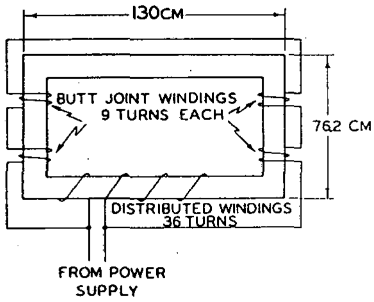

FIG. 12. Betatron core and excitation windings.

were measured with Consolidated Electrodynamics VG-1*A* ionization gauges and forepressures by thermocouple gauges. Gauges of the latter type also served to actuate protective vacuum interlocks.

(2) *Detectors*

For direct detection and analysis of the accelerated electron beam a scintillation detector was constructed for insertion into the vacuum chamber. The scintillator proper consisted of a 1-in. diam cylinder of Sintilon plastic, attached to the end of a brass tube which passed through an O-ring sliding seal at the vacuum chamber wall. The scintillator was covered on its front surface by an evaporated aluminum layer which was lighttight and yet sufficiently thin to permit electrons to strike the plastic. Electrical pulses were then obtained from an RCA type 6342 photomultiplier situated at the end of the brass tube and were either viewed directly on an oscilloscope or integrated to give a signal indicative of the total beam striking the scintillator.

In moving the scintillator radially within the vacuum chamber, it necessarily crosses the spirals of the magnet structure and in consequence presents a variable aspect to the scalloped particle orbits. To avoid variations in the geometrical acceptance it was therefore necessary to make the front of the scintillator chisel-shaped.

A second detector consisted of a current probe, constructed to provide an absolute measurement of beam intensity. This probe was in the form of a Mo flag $\frac{5}{8}$ in. high, $\frac{3}{8}$ in. wide, and 0.010 in. thick. Tests indicated that secondary emission caused no detectable error in measurements made with this probe. An additional type of probe carried an offset 0.040-in. Mo wire which, through rotation of the probe, served to measure the vertical location of the equilibrium orbit, to indicate the amplitudes of vertical oscillations, and to limit these amplitudes when desirable.

For accurate measurement of the betatron oscillation frequencies and of the revolution frequency in tests of the operating model, it was planned to use destructive radio-frequency excitation of the betatron motion.[3,14] For this purpose a pair of plates was introduced near the upper and lower surfaces of the vacuum chamber. These electrodes consisted of 0.010-in. Mo, $\frac{1}{2}$ in. wide, 2 in. long, separated vertically by 1 in. They were electrically insulated, both from each other and from the chamber wall, and, by exciting them either in opposition or together, suitable vertical or radial electric fields could be placed in resonance with the corresponding betatron oscillations. An additional electrode of $\frac{1}{16}$-in. Cu, 6 in. long and $\frac{27}{32}$ in. high, was also provided to permit application of a radial electric field near the injection radius.

[14] C. L. Hammer, R. W. Pidd, and K. M. Terwilliger, Rev. Sci. Instr. 26, 555 (1955).

C. Accelerating System

Betatron acceleration alone was used when the model was first put into operation, and later supplemented the radio-frequency fields employed in the series of experiments described in Sec. VIII. The dimensions and windings of the betatron core, which was constructed of 0.014-in. transformer laminations, are illustrated in Fig. 12. The four butt joints were surrounded, as shown, by separate windings connected in parallel with the main distributed windings and the resultant flux-forcing served to reduce the leakage flux. Measurements made at the center of the betatron-core window, before insertion of the vacuum chamber, indicated a leakage flux-density of approximately 1 gauss and a residual field of about 1/7 gauss from the core—the $\frac{1}{2}$-in. brass plates of the vacuum chamber would be expected, of course, to effect a further reduction of stray time-varying fields.

At the time the core was designed the final basic parameters of the model had not been selected and it was believed desirable to provide an induction field of as much as 50 v/turn with continuous operation from a 500-cps alternator. In practice, however, it proved convenient to operate the core from a pulsed power supply, for which the circuits and resultant waveforms are illustrated by Fig. 13. By use of this circuit electrons could be accelerated in two stages, first being carried to an intermediate radius and then, after a short interval, further accelerated to the final

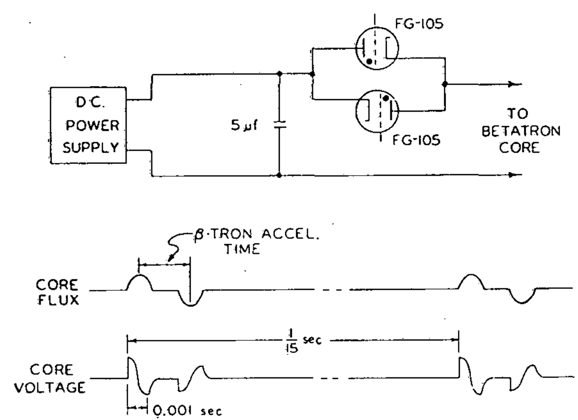

FIG. 13. Circuit and waveforms for pulsed excitation of betatron core.

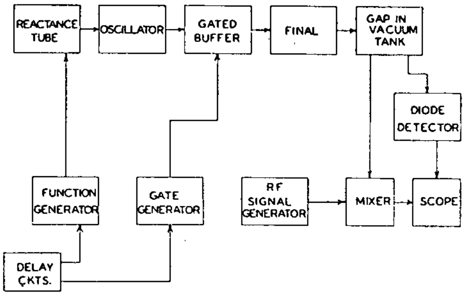

FIG. 14. Block diagram of rf system.

energy. During this interval experiments on radio-frequency acceleration could be performed.

The radio-frequency system is illustrated by the block diagram of Fig. 14. Since the required frequency change was small for the radio-frequency experiments with the model, a 6CL6 reactance tube was used to modulate the 6C4 oscillator. A 6CL6 gated buffer drove the 829-B final stage, which was then coupled to one of the insulated gaps of the vacuum chamber. Since at 60 Mc the gap presents a reactance of very low Q, it was feasible to connect it to a tuning coil to provide a broadband resonant circuit. The frequency-modulation function generator used to control the reactance tube was sufficiently versatile to control, independently, the initial radio-frequency program as well as the program in the neighborhood of the transition[1] energy.

D. Injector

Although it was possible to employ as an injector a simple gun of the type customarily used for injection into betatrons,[6] it was considered preferable in the model tests to use an injection system with a very narrow septum so that one could inject into a region as small as several millimeters. To avoid voltage limitations within the injector assembly it proved convenient to employ an auxiliary deflector which permitted a septum as thin as 0.005 in. to direct the beam emerging from the injector.

The injector assembly is shown in Fig. 15. The electron optics of the gun itself were determined by a rubber dam method, leading to a design in which the focus was several millimeters in front of the gun save for space-charge effects which would displace this focus toward the deflector system. The deflector was constructed to bend the electrons through 15°, so that they would emerge through a slit 0.080 in. wide and effectively 0.365 in. high. The electric fields of the deflector were shielded by a box, of which the 0.005-in. septum formed the grounded wall, in order to preclude disturbance of the electron orbits within the accelerator. This deflector system provided a small amount of radial focusing and substantially no vertical focusing. When changing injectors, the mounting and alignment provisions permitted a pretested assembly to be inserted and a beam obtained within 20 min.

Tests of the injector in a separate vacuum system indicated an emittance of 0.2 mm·rad horizontally (± 1 mm, ± 0.05 rad) and 2 mm·rad vertically (± 5 mm, ± 0.1 rad). The emergent intensity, amounting to about $\frac{1}{5}$ the total emission from the tungsten filament, was typically 25 to 50 ma at operating conditions which would ensure a filament life of at least 600 hr. The radial admittance[11] of the accelerator at the point where the injector was located, as determined by the digital computations for the design point C, was expected to be 18 mm·rad (Fig. 4) and the axial admittance (as limited by the vacuum chamber) about 2.6 mm·rad, so that multiturn injection radially warranted consideration. The injector was normally located at the center of a vertically focusing sector, where the envelope of vertical oscillation is greatest.

Two distinct pulse circuits were constructed for the injector, to permit operation with short or protracted pulses, as desired. In the short pulse circuit an artificial delay line was discharged, by a 5C22 hydrogen thyratron, through the primary winding of a 7.5:1 iron-cored oil-insulated pulse transformer. The secondary of the transformer was connected to the injector and used a bifilar winding to provide power for the filament transformer. Resonant charging of the delay line was provided through a choke and high vacuum rectifier circuit. An inverse diode served to clip overshoot and to prevent continuous conduction by the thyratron. The output impedance of this pulse supply was sufficiently low that variation of the load through its entire range caused no measurable voltage change. Pulses up to 40 kv in height and 4 μsec duration were available from this circuit, with a flat top which was

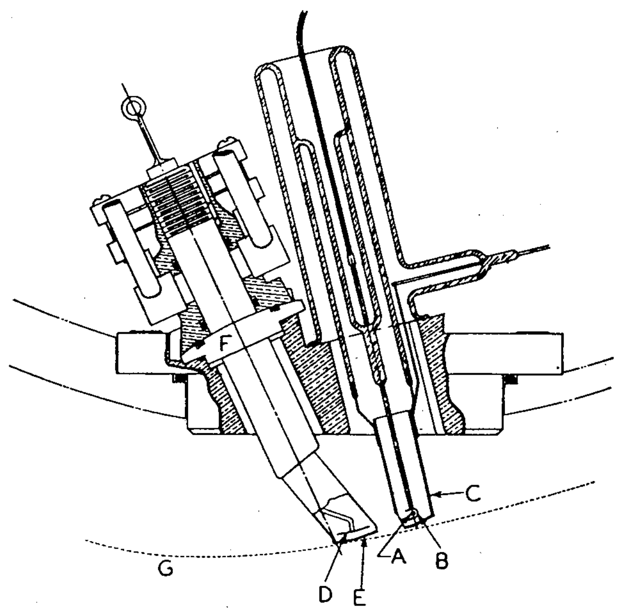

FIG. 15. Injector assembly, with deflector. The cathode, shield, injector housing, deflector electrode, grounded septum, spherical bearing surface, and a typical equilibrium orbit arc, respectively, shown at A, B, C, D, E, F, and G.

achieved by careful adjustment of matching resistors provided at the primary of the pulse transformer and by adjustment of the lengths of the individual delay-line sections.

The detailed construction of the modulator designed to produce long pulses is described in Appendix I. It could provide pulses up to 45 kv in height and 1 msec duration, with a rise time of 8 μsec. By negative feedback the output was stabilized to 0.1%.

IV. MEASUREMENT AND CORRECTION OF THE MAGNETIC FIELD

To ensure that the model would operate in the manner suggested by the computational work, and to make it effective for quantitative performance studies, it was necessary to measure the magnetic field carefully throughout the entire aperture of the machine. The numerical value and constancy of the field index k, the nature of the azimuthal variation of the magnetic field, and the character of the median plane were examined. Adjustments were then made so that magnetic fields could be obtained which were substantially the same as those used in the orbit computations. The measurements were made difficult by the low value of the magnetic field, the maximum value being 60 gauss, and by the complication of the spiral geometry. In following an initial investigation, it was found that the original magnet surfaces differed 2 or 3 mm from a conical shape and would have required corrective pole-face windings over the entire pole surface. Accordingly, the poles were carefully remachined before making the final set of measurements and adjustments.

For most of the magnetic measurements small flip coils about 1 cm in length and diameter were used. To measure k three coils were used in an arrangement similar to that previously described.[3] The coils were mounted on an arm which was rotatable about the center of the accelerator and could be changed in radius. The radial and azimuthal positions were determined by suitable scales (to an accuracy of a few tenths of a millimeter in radius and a few tenths of a degree in azimuth). The end two coils were equally spaced from the center coil and were located along an axis, intersecting the axis of the center coil, which made an angle of 46° with the radius so as to be tangent to the central spiral locus of the magnet-sector (Fig. 16). The three coils could be flipped simultaneously, through 180°, about this axis.

The arrangement just described was only satisfactory for measuring k along the central spiral of each magnet (shown as a broken line in Fig. 16), since a large error results in regions where the field varies rapidly at right angles to the rotation axis and the error is greatly enhanced if the magnetic axes of the coils do not intersect this line accurately. Despite this limitation, however, the results obtained with the aforementioned method were

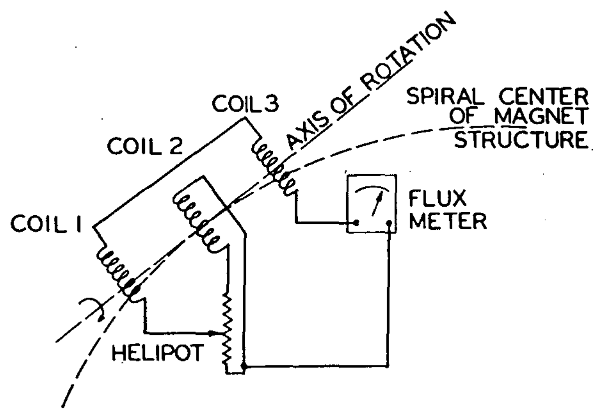

FIG. 16. Diagram of the null-reading flip coil arrangement used to determine the field-gradient index of the magnets.

found to be adequate when taken in conjunction with measurements of the average value of k by means to be described later.

Preliminary measurements indicated a value of k which was low and varied with radius. With the remachined poles the addition of a suitable number of back-leg turns in series with the main magnet windings made it possible to hold k constant within 5% at low and intermediate radii—i.e., out to about 48 cm. In order to keep k constant at large radii, it was found necessary to distribute the main forward windings and the extra back-leg turns very carefully across the inside surface of the back legs. It will be noted from Fig. 9 that, for these larger radii, the region in which a good field is desired is as close to the back legs as to the pole-face windings.

Measurements of the magnetic field dependence on azimuth were first made using a single flip coil (the center coil of the three-coil arrangement), connected directly to a General Electric fluxmeter. Some of the later measurements were taken with a peaker-strip magnetometer (Appendix II), which was constructed and kindly made available to us by Dr. Joseph Ballam of Michigan State University. These measurements were analyzed in the form of a Fourier series, using the IBM-704 computer. The program calculated both the Fourier components of the field and also the "effective flutter," $f_{eff}=[2(\langle H^2\rangle-\langle H\rangle^2)/\langle H\rangle^2]^{\frac{1}{2}}$. From the average values of the field at different radii, the average value of k could be computed. From the components of the Fourier analysis it was possible to determine which magnets had too large or too small a field. It was found that the effective flutter was slightly lower than desired, even when the vertical component of the earth's magnetic field was removed by means of a large hexagonal Helmholtz coil pair placed around the accelerator, but final adjustments of course could be made by use of the flutter-tuning coils described in Sec. IIIA. In addition to the hexagonal coil pair just mentioned, a second set of coils was installed to remove the horizontal component of the earth's field.

In order to measure the horizontal component of field in the geometric median plane of the model, a piece of plate glass was carefully leveled and adjusted so that its top surface was parallel to and below the geometric median plane of the magnets. A peaker-strip magnetometer (Appendix II), sensitive to small fields, was connected to a zero-center meter and set on this glass plate so that its axis was at the height of the median plane. By moving the magnetometer about on this surface it was found that there were fairly large and random horizontal fields of magnitudes up to more than 1 gauss. Since the radial component of the horizontal field was felt to be the more harmful, attempts were made to reduce this as much as possible. To this end the magnets were raised or lowered, and tipped, and it was also necessary to wind turns properly positioned about the poles of the magnets, forward on one pole and backward on the other. In some cases it also was necessary to provide "plaster" coils on the inside of the back legs of the magnets. With these various adjustments it was possible to reduce the horizontal field to a maximum of about 10 milligauss at all radii less than about 52 cm. Beyond this radius, the many back-leg windings seemed to make the attempt excessively difficult.

When the flutter coils were added to the edges of the magnets, it was found necessary to adjust their feeder-windings carefully along the slots to reduce their effect on the horizontal field. Careful adjustments were made until the horizontal field was no more than 20 milligauss when the coils were excited sufficiently to change the effective flutter by $\pm 40\%$.

V. RESONANCE SURVEY AND STABILITY LIMITS

A. Method Employed in Resonance Survey

A detailed measurement of the variation in beam intensity over a large part of the ν_x, ν_y stability region of the model was made [4f,15,16] in order to study the effects of various resonances on the operation of the accelerator. The field index was varied within the range 0.20 to 1.16 by the k-tuning coils (Sec. IIIA) and the flutter from 0.57 to 1.60 by the flutter-tuning coils. The measurements were chiefly made at a radius of 37 cm, which was as close to the injection radius as it was possible to operate and still clearly differentiate the accelerated beam from newly injected electrons. The beam intensity was obtained from the integrated signal of the plastic scintillation detector (Sec. IIIB2). During the intensity survey the injector filament current was kept low and constant; likewise the betatron core voltage, the gas pressure, and the injection timing were held fixed.

To correlate the measurements of beam intensity versus

TABLE IV. Determination of ν_x and ν_y from resonant radio frequencies at the central operating point (tuning coils de-energized).

Measured frequency (Mc)	Character of resonance	f_0 (Mc)	f_{rf}/f_0, Av	Assignment (f_{rf}/f_0)	Result
50.53	y, strong	49.25	1.025	ν_y	$\nu_y=1.025$
47.96	y, strong		0.974	$2-\nu_y$	1.026
27.48	y, medium	49.24	0.558	$3-(\nu_x+\nu_y)$	$\nu_x+\nu_y=2.442$
21.76	y, strong		0.442	$(\nu_x+\nu_y)-2$	2.442
29.74	y, medium	49.40	0.604	$1-(\nu_x-\nu_y)$	$\nu_x-\nu_y=0.396$
19.66	y, strong		0.399	$\nu_x-\nu_y$	0.399
49.27		49.27	1.000	1	
70.23	x, very strong	49.43	1.426	ν_x	$\nu_x=1.426$
28.63	x, very strong	49.43	0.581	$2-\nu_x$	1.419
20.80	x, very strong		0.422	ν_x-1	1.422
41.13	x, strong	49.26	0.835	$2\nu_x-2$	$2\nu_x=2.835$
57.38	x, medium		1.163	$4-2\nu_x$	2.837
46.40	x, medium		0.941	$3-2\nu_y$	$2\nu_y=2.059$
Average		49.3			$\nu_x=1.420$ $\nu_y=1.026$

tuning currents with the betatron-oscillation frequencies, the method[3,14] of radio-frequency resonant enhancement of the betatron oscillations was employed. Enhancement of the axial oscillations was detected by loss of beam due to interception by the vertical-scanning probe (Sec. IIIB2) or by the walls of the vacuum chamber, while enhancement of the radial oscillations was identified by a shift in the time of arrival of the beam at the detector. The frequencies at which such resonances are observed are related to the betatron-oscillation frequencies by a relation of the form[3]

$$f_{rf}=|p\nu_x\pm q\nu_y\pm m|f_0, \tag{14}$$

where f_0 is the revolution frequency of the particles and p, q, and m are integers. The radio-frequency oscillator used for these measurements covered a range from 12 to 74 Mc, while the frequency of revolution at the 37 cm radius varied from 42 to 58 Mc as the tuning was changed within the range of interest. A typical set of frequency measurements, assignments, and results is given in Table IV. In order to make the correct assignments and thus determine the oscillation frequencies, approximate values for these frequencies of course should be known by other means.

B. Results

The intensity survey as a function of the tuning currents was taken in a series of runs where one of the tuning currents was kept constant (generally that for the k-tuning coils) and the other was varied over most of its range in order to determine most of the maxima and minima of intensity. A typical plot obtained by this procedure is shown in Fig. 17. This plot shows the relative beam intensity measured by the scintillation detector as a function of the current in the flutter-tuning coils for the case where there was no current in the k-tuning coils. The experimentally measured flutter at three points is also indicated on the abscissa. Values of the axial and radial betatron oscillation frequencies are indicated above the curve, as are also the locations of certain significant resonances. By measuring the betatron-oscillation frequencies as a func-

[15] R. Stump and B. Waldman, Midwestern Universities Research Association Rept. MURA-361 (1957, unpublished).
[16] W. A. Wallenmeyer, Midwestern Universities Research Association Rept. MURA-407 (1958, unpublished).

tion of the tuning currents, interpolation graphs were prepared which permitted the results of the intensity survey to be replotted in terms of these frequencies. The resonance diagram which resulted is shown in Fig. 18, in which the increasing width of the resonances at points further from the center of the diagram is chiefly attributed to the increasing nonscaling of the field as the tuning currents are increased (Sec. IIIA). An indication of the degree to which the untuned fields satisfy the scaling condition is provided by Fig. 19, in which the measured frequencies are shown as a function of radius.

C. Discussion

Interpretation of the results just reported is subject to some uncertainty due to incomplete control of the betatron-oscillation amplitudes. In the intensity survey the injector and deflector potentials were adjusted for each point so as to obtain maximum intensity and the amplitudes of the radial oscillations necessarily increased or decreased with the injection energy. The amplitudes of the axial oscillations, moreover, were limited during the intensity measurements only by the upper and lower walls of the vacuum chamber. In the measurements of the betatron-oscillation frequencies by the radio-frequency resonance method, however, no quantitative attempt was made to return to the injection conditions previously used except that adjustments were again made to attain maximum intensity. Also the axial amplitudes were here deliberately limited, by the vertical-scanning probe, in the interests of observing a sharp radio-frequency resonance with the axial oscillations. The observed frequencies of the betatron oscillations as a function of oscillation amplitude are shown in Fig. 20 for the central operating point of the model. It is seen that although the variation of ν_x with amplitude is small, the variation of ν_y is considerable and presents some uncertainty in the values determined for ν_y in the intensity survey (Fig. 18). It should also be mentioned that the radio-frequency resonance method is difficult when operation is near one of the intensity minima of Fig. 18 and that reliance must be placed, in such cases, on interpolation from results obtained in regions of good beam intensity. This fact, the amplitude dependence of the oscillation frequencies, and the nonscaling character of the magnetic field when substantial tuning currents are applied may account for the observation that the positions of the resonance lines drawn on Fig. 18 do not coincide exactly with the observed positions of minimum intensity.

It may be noted that the betatron-oscillation frequencies observed in the model (Table IV), without current in the tuning coils, were close to the values resulting from the digital computations[4b,11] (Table I) and that a small current in the flutter-tuning coils sufficient to raise f_{eff} to its design value of 1.087 raised ν_y from 1.026 to the predicted value of 1.12 (cf. Fig. 17). A sizable region of maximum intensity was found to occur centered about the design point in Fig. 18. The resonance diagram indicates the importance of several resonances in the region accessible by the tuning controls. Although the computer studies summarized in Table I suggested that the coupling resonance $\nu_x = 2\nu_y$ could affect the intensity markedly in the neighborhood of operating point A, the specific influence of this resonance on beam intensity, when no misalignments were deliberately introduced, was less clearly marked in the results of the intensity survey illustrated by Fig. 18. An additional investigation, reported in Sec. VE, was therefore directed toward the examination of effects associated with operation near the accessible portion of this resonance line.

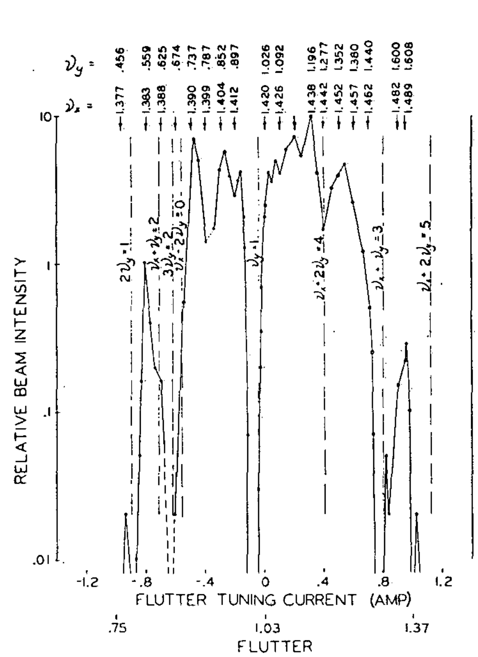

FIG. 17. Beam intensity as a function of the flutter-tuning current, with no current in the k-tuning coils. The values of ν_x and ν_y, as measured by radio-frequency excitation of the betatron oscillations, are indicated above the curve. Points where certain resonances were crossed are also indicated.

D. Stability Limits

Experimental measurements were made of the axial and radial stability limits at the design point of the model. At a given working point there is a range of energies at which electrons will be accepted into stable orbits in the accelerator. If one assumes that the minimum energy particles are injected onto an equilibrium orbit which just misses the injector and that the maximum energy particles oscillate about an equilibrium orbit which is situated a distance from the injector corresponding to the radial stability limit, it is possible to obtain a measurement of the radial stability limit.

In one method it is convenient to apply a long pulse (Appendix I) to the injector, modified to give a waveform

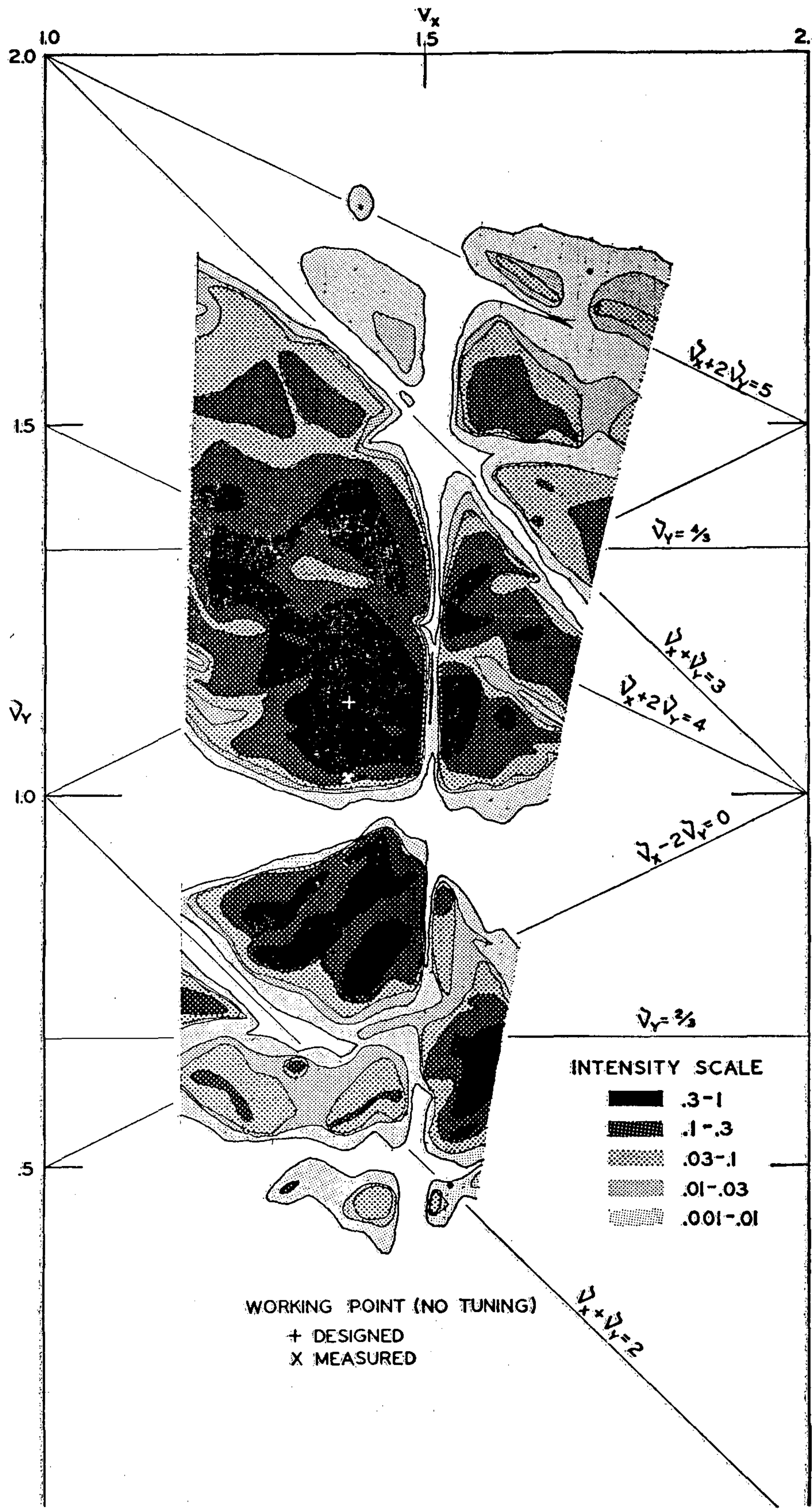

FIG. 18. Beam intensity as determined in the resonance survey of the spiral sector model.

having a linearly falling portion and with the maximum injector voltage set above the high voltage limit for injection of a beam into the accelerator. By suddenly dropping the deflector potential to zero at a time which is adjustable with respect to the waveform applied to the injector, the time interval over which injection occurs may be measured. From the rate of decrease of the injector voltage the acceptable energy range for injection may then be computed and hence the corresponding radial displacements of the injected particles from their respective equilibrium orbits. In a second method a long rectangular pulse which drops rapidly to zero (Appendix I) is applied to the injector, so that injection occurs over a quite short interval of time, and the time interval over which the accelerated beam is received at the target is measured. In this case electrons injected with a higher energy, and undergoing larger betatron oscillations, will arrive at the target earlier than electrons injected onto an equilibrium orbit which just misses the injector. From the known properties of the accelerator, in particular the value of the betatron accelerating voltage, the radial stability limit may again be evaluated. The adiabatic damping of the radial betatron oscillations must be taken into account, of course, in this calculation.

Axial stability limits are conveniently obtained by use of the vertical-scanning probe (Sec. IIIB2). For all these measurements, where the injector, detector, and vertical-scanning probe were at different azimuthal and radial locations, some adjustments had to be made to the measured values so as to have the radial and axial limits refer to the same value of ξ. These adjustments could be made with the aid of the curves of β vs $N\theta$ (Sec. IIC; Figs. 6 and 8) for small amplitude oscillations, taking the betatron oscillation amplitude as proportional to $\beta^{\frac{1}{2}}$,[12] or by use of similar computer information pertaining to larger amplitude oscillations.

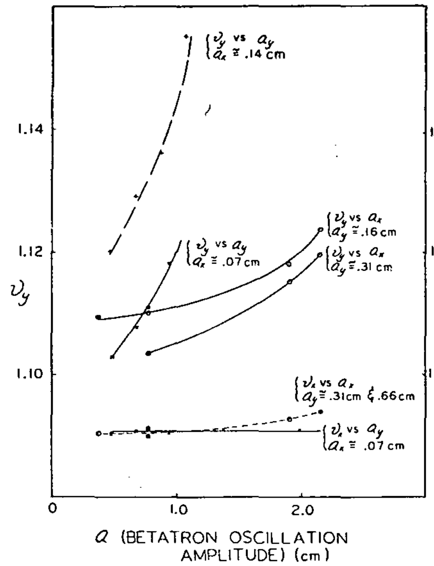

FIG. 20. Measured variation of betatron oscillation frequencies with amplitude, without tuning currents.

A measurement of the radial stability limit by the second of the methods described led to a value at the azimuth of the injector given by $\pm(0.058\pm0.006)r$, or ±1.75 cm, for the design point. This result corresponds to a limit of approximately $\pm0.08r$ at the azimuth to which Table II applies (cf. Fig. 6) and is in reasonable agreement with the value of approximately $\pm0.09r$ found computationally. The measured value for the axial stability limit similarly was $\pm(0.045\pm0.006)r$. This result is somewhat smaller than the maximum amplitude which would be permitted by the internal dimension of the vacuum chamber, as would necessarily be the case if the magnetic median plane were not quite centrally located within the vacuum chamber, while the computational result given in Table II suggests a dynamical limit at the injector somewhat greater than the available aperture.

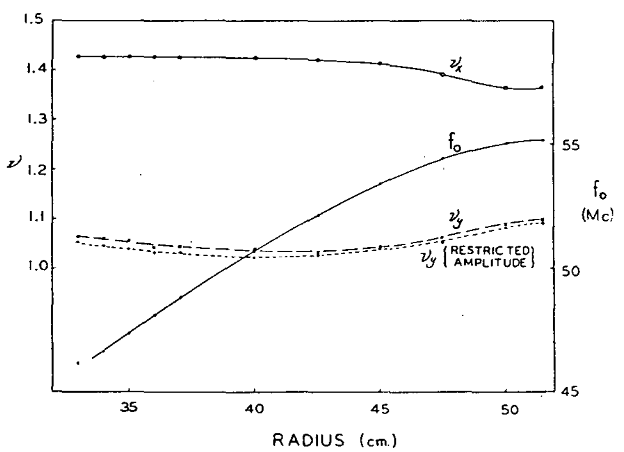

FIG. 19. Measured values of the revolution frequency and the betatron oscillation frequencies as a function of radius, without tuning currents. If the scaling condition were satisfied *exactly*, the oscillation frequencies ν_x and ν_y would be independent of radius.

E. The Resonance $\nu_x=2\nu_y$

The design point for the model was deliberately chosen (Sec. II) to be far from the difference resonance $\nu_x=2\nu_y$. As noted in Fig. 18, however, it was possible with the tuning controls to reach operating points in the vicinity of this resonance line, although the accessible portion was of somewhat limited extent and fell in a region where other important resonances were also present. It is apparent from Fig. 18 that the beam intensities in the neighborhood of the $\nu_x=2\nu_y$ resonance are generally low, although no pronounced decrease of beam intensity is unambiguously attributable to this particular resonance. For this reason, and because of the general interest in the $\nu_x=2\nu_y$ resonance, additional information was sought experimentally for operation near this resonance, with $\nu_x\cong1.46$, and the inter-

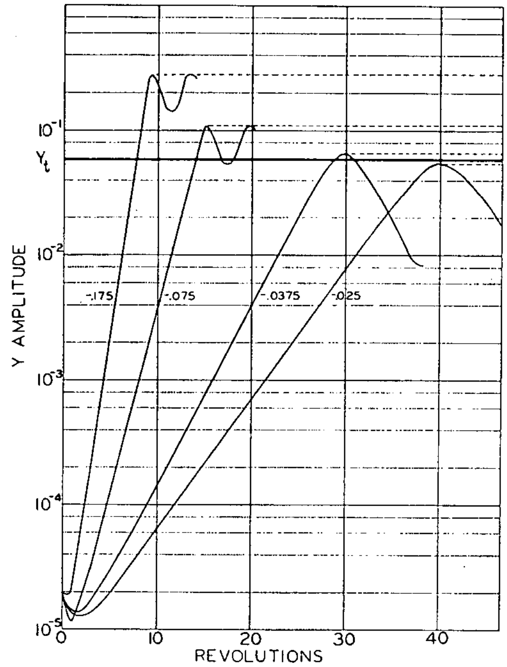

FIG. 21. Semilogarithmic plot illustrating growth of the amplitude of axial oscillations for operation near the $\nu_x = 2\nu_y$ resonance, as obtained by digital computation with $\nu_x = 1.25$ and $\nu_y = 0.62$. The number appended to each individual curve denotes the initial radial displacement for that run. Y_t denotes the semi-aperture of the vacuum chamber at the injection radius.

pretation was guided by the results of digital computations made specifically for the point $\nu_x = 1.25$, $\nu_y = 0.62$.

From the computations it appeared that the radial motion, if present alone, would have very generous stability limits but, as is typical of performance on a coupling resonance,[17,18] a very small amount of radial oscillation would be accompanied by a marked growth of the axial oscillations. This growth of axial oscillation-amplitude is shown in the semilogarithmic plot of Fig. 21, wherein it is evident that a radial amplitude in excess of about $0.022r$, or about 0.7 cm measured at the injector, will carry the axial motion to amplitudes in excess of $0.06\,r$ (1.9 cm) and result in interception of the beam by the chamber wall. If the wall were not present, however, this physical limitation would not occur and stable motion with axial amplitudes up to about $0.1\,r$ might then be considered possible.

Experimental measurement of the radial stability limit at the operating point assumed in the computations, using the methods described in Sec. VD, led to an effective limit of 0.51 cm and, as was the case for the design point, axial amplitudes in excess of 1.3 cm were found. In a more detailed set of measurements, made with $\nu_x \cong 1.46$, results were obtained to suggest that the effective radial limit was indeed decreased if the axial amplitudes were restricted, the effect becoming more pronounced when operating close to the resonance line (Fig. 22). In summary, it is felt that the empirical measurements, when recognition is given to possible small departures of the magnetic median plane from the mid-plane of the vacuum chamber, are consistent with the computational results and that the growth of axial amplitude associated with operation near the $\nu_x = 2\nu_y$ coupling resonance can effect a pronounced loss of intensity.

VI. INJECTION METHODS

A. General Considerations

It is impossible to trap particles in a static field, since particles injected externally ultimately will re-emerge and those injected from a source in the field eventually will return to strike the source. The imposition of secularly changing fields, the presence of gas-scattering, or the use of time-varying fields arising from the particles themselves therefore is essential for injection. It frequently may be convenient, however, to analyze such injection methods by a study of the equilibrium orbit and the oscillations about it for a static field, followed by corrections for the secular changes which are necessarily present. With this procedure one can determine, for example, the time required before a particle injected with particular initial conditions from a source in the static field will return to strike the injector. Attention can then be directed to effecting a modification of the equilibrium orbit, or a damping of the betatron oscillations, sufficient to move the orbits away from the deflector structure.

For efficient injection it is also necessary, of course, that the injected particles be sufficiently limited in their initial positions and directions that they can be contained within the stable region of phase space for particles in the accelerator. If the emittance of the injector is substantially smaller than the corresponding admittance of the accelerator, however, it may then be profitable to inject many turns successively. When many particles are present, their

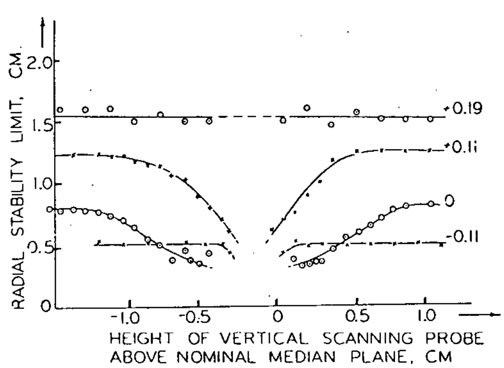

FIG. 22. Observed apparent radial stability limits as a function of the limitations imposed on the axial motion, for operation near the $\nu_x = 2\nu_y$ resonance with $\nu_x \cong 1.46$. The number appended to each individual curve denotes the value of $2\nu_y - \nu_x$ for that curve.

[17] L. J. Laslett and K. R. Symon, *Proceedings of the CERN Symposium on High Energy Accelerators and Pion Physics* (European Organization for Nuclear Research, Geneva, 1956), vol. 1, p. 279.

[18] L. Jackson Laslett and A. M. Sessler, Midwestern Universities Research Association Rept. MURA-263 (1957, unpublished).

mutual interactions may cause a shift of the betatron-oscillation frequencies by such an amount that the effect of one or more resonances (possibly due to imperfections) is materially enhanced and thereby particles are lost from the beam. The limit to beam density which results from such space-charge effects will impose a less serious limit on the total current which it is possible to contain within the accelerator if the area utilized by the beam can be increased. An increase of the intensity of the injected beam at the expense of increased energy spread may be a chimerical gain, however, if beams ultimately are to be stacked by a repetitive acceleration system. Similarly, arranging a *rapid* energy change, in an effort to move the equilibrium orbit away from the injector and to suppress space-charge effects by increasing the beam area, may augment the amplitude of the betatron oscillations appreciably and somewhat reduce the effectiveness of this injection method.

B. Methods Employed with Short-Pulse Injection

In the spiral sector model one method of injection undertook to accelerate the electrons rapidly, but under conditions such that the amplitudes of the radial betatron oscillations remained smaller than the radial width of the beam due to energy spread. Under these circumstances, it is to be expected that the total number of particles successfully injected will be proportional to the radial width of the beam and that this, in turn, will be proportional to the energy gain per turn. With an acceleration voltage of 150 v/turn, successful injection for a 4-μsec interval was accomplished and led to individual beam pulses containing in excess of 10^{10} electrons. The electron density in this case was estimated as 3×10^6 cm^{-3}, which may be compared with the calculated limit[19] of 10^7 cm^{-3} at which space-charge effects would induce beam loss from the $\nu_y=1$ resonance.

A second method which was successfully applied to the model did not require acceleration of the electrons but employed an azimuthally localized time-dependent radial electric field. This electric field, by producing a forced oscillation, resulted in a perturbation of the equilibrium orbit (Fig. 23). The injection conditions were chosen so that, with the perturbation present, the betatron oscillations of the accelerated electrons were of small amplitude. By presuming that the strength of the perturbation is decreased to zero adiabatically, the orbits of these electrons will follow the changing equilibrium orbit with little change of oscillation amplitude, thus, in effect, being pulled away from the injector structure. Electrons injected somewhat later also can be accepted, with somewhat larger

[19] L. Jackson Laslett, Midwestern Universities Research Association Rept. MURA-14 (1954, unpublished). Our present estimate is one-half the value which would follow from the formulas of this reference, since in place of a toroidal beam we here consider a beam which is significantly more extended radially than in the axial direction.

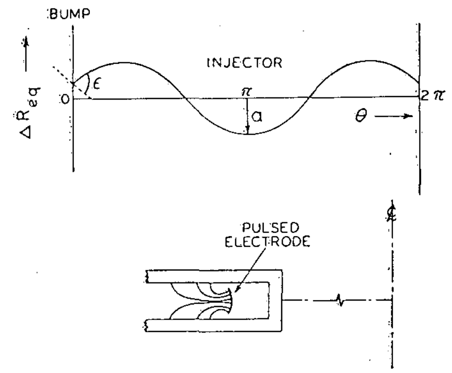

FIG. 23. Perturbation of the equilibrium orbit by an azimuthally localized radial electric field, illustrated for $\nu_x=1.40$ with the unperturbed equilibrium orbit drawn as a straight line and ignoring the scalloping which arises from the alternating gradient structure. *Insert*: Cross-sectional shape of electrode, intended to produce a region of substantially constant field.

amplitudes of oscillation, and they too would be removed from the region of the injector as the perturbation was turned off. Despite the objective that the perturbation be removed adiabatically, it is necessary, of course, that the radial motion of the equilibrium orbit in the neighborhood of the injector be sufficiently rapid to preclude interception of the beam by some portion of the injector structure. If the vertical admittance of the accelerator were considerably larger than the vertical emittance of the injector, the injection structure could be displaced from the median plane, the perturbation could be turned off more slowly, and an improved utilization of phase space in this way might be possible. In the spiral sector model, however, the vertical emittance was not such as to permit such use of the vertical motion to assist in injection.

The perturbation was applied by a radial electric field, from an electrode inserted into the vacuum chamber. The electrode was shaped, as shown on Fig. 23, to produce a field of fairly constant strength throughout a region of several centimeters radial extent, and modulation provided by discharge of a capacitor with a thyratron. When injection with large amplitude betatron oscillations was attempted, the electric field apparently effected a coupling between radial and axial motion which resulted in beam loss; the system otherwise appeared to work well, however, permitting multiturn injection to be achieved and leading to beam densities of approximately one-sixth the space-charge limit.

C. Long-Pulse Injection

One of the desirable possibilities[1,2] for use of fixed-field accelerators is that in which a large betatron core might be employed in conjunction with a fixed-field magnet structure in such a way that particles may be injected and accelerated to the target or extractor with a duty cycle approaching 30 or 40%. Use of the long-pulse modulator (Appendix I) permitted the injection of high intensity

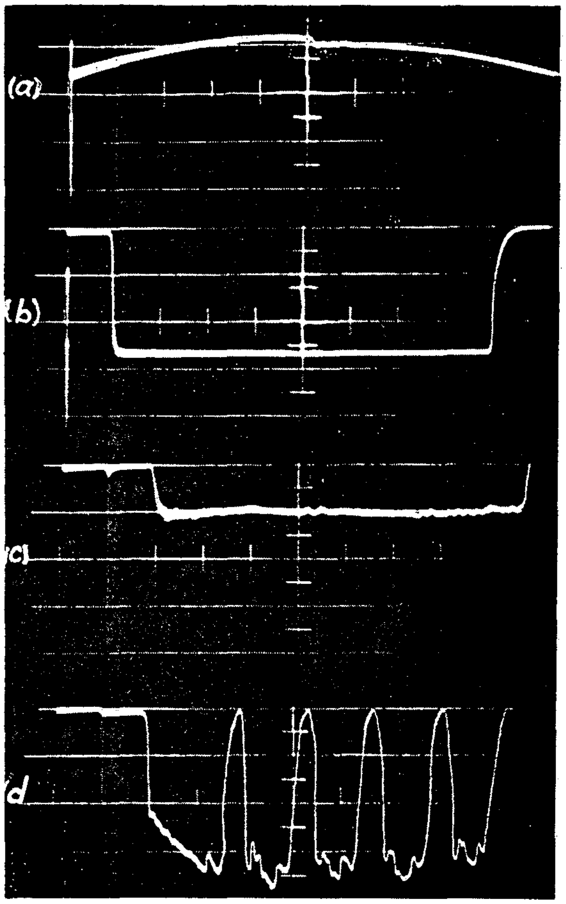

FIG. 24. Oscillograms to illustrate phenomena observed with long-pulse injection: (a) betatron voltage; (b) injector voltage; (c) beam current to target when the injector is operated at low emission; and (d) beam current at high emission, showing effects attributable to space-charge and positive-ion neutralization.

beams into the spiral sector model for times as long as the 500-cps flux-wave in the betatron core could accelerate them and enabled a study to be made of ionization phenomena which would be unnoticeable with a short-pulse injection system.

The accelerating voltage was provided by the positive half of the 500-cps sinusoidal excitation of the betatron core and usually amounted to about 20 v/turn. Electrons could be accelerated thereby from the injection energy (30 kev) to the target, situated at a 45 cm radius (80 kev), in approximately 80 μsec. The equilibrium orbits of individual electrons thus moved outward at a rate of roughly 2×10^5 cm/sec during the course of acceleration. Injection could be maintained for periods as long as several milliseconds, but usually occupied only 400 μsec at the peak of the accelerating-voltage wave, during which time the accelerating voltage was comparatively constant. Injection conditions otherwise were as described in Sec. IIID.

Space-charge forces limit the density of electrons at injection to about 10^7 cm^{-3} (Sec. VIB).[20] The injector can supply more electrons than are required to reach this density and in consequence we would expect that the frequencies of betatron oscillations would decrease significantly as a result of space charge, possibly to be limited by the nearest lower resonance. In the course of time during the injection pulse, ions formed by interaction of the beam with the residual gas in the vacuum chamber should collect in the beam and begin to neutralize the space-charge forces due to the electrons themselves. The initial value of the potential well which acts to trap these ions is of the order of several electron volts and this process may be aided to some extent by the configuration of the applied magnetic field. The ions would not, in general, gain enough energy to escape the potential well of the beam and one accordingly visualizes a sheet of charge, originally some 2 cm thick, whose density is limited initially by the space-charge forces at injection and within which ions are being formed and trapped to neutralize these forces. It may be supposed, finally, that the accumulated ion density will serve to *increase* the frequencies of the electron betatron oscillations, possibly until the stability limitations imposed by the nearest resonance of *higher* frequency begin to affect the beam.

When the injector is operated at low emission currents with a good vacuum in the chamber, one observes a current at the target such as that shown in Fig. 24(c). This current is quite uniform with respect to time and only becomes more intense when the betatron voltage is increased. The current is proportional to the emission from the injector and no effects of space charge or of ionization are observed. As the emission from the injector is increased, however, several more complicated phenomena are seen to occur. In this case the output current presents a time dependence shown in Fig. 24(d), of which the essential features are sketched in Fig. 25. The time dependence is extremely reproducible from pulse to pulse, as is illustrated by the several hundred pulses contributing to the oscillogram of Fig. 24(d).

The initial current I_0 (Fig. 25) is found to be directly proportional to emission when this latter current is small and to reach a constant value at high emission currents. At high currents, I_0 is directly proportional to the betatron

[20] The change of the oscillation frequency $\nu_y \equiv N\sigma_y/2\pi$ may be estimated readily for the simplified case of a beam of uniform density in a constant gradient field (cf. reference 19, in which a *toroidal* beam is considered). With the particle density denoted by n_e for the electrons of velocity βc, and by n_i for the singly charged stationary positive ions, one obtains

$$\delta(\nu_y^2) = -4\pi r_0 R_0^2 \beta^{-2}(1-\beta^2)^{\frac{1}{2}}[n_e(1-\beta^2)-n_i],$$

in which r_0 denotes the classical electron radius and R_0 represents the radius of the accelerator. It is seen that the space-charge effect of the electron density is to *decrease* the oscillation frequency, by an amount which depends on $1-\beta^2$ because of the partial cancellation of electrostatic defocusing by magnetic focusing effects, but that the accumulation of positive ions can reduce this decrease and ultimately lead to a net *increase* of the oscillation frequency.

voltage—i.e., upon the rate of progression of the equilibrium orbits away from the injector—and is independent of gas pressure, save for single-scattering losses estimable by other means. The electron density corresponding to I_0, when calculated from dr/dt and the other known parameters of the accelerator, is approximately 2×10^6 cm^{-3}, so that this limiting value of the output current evidently may be related to the space-charge limit mentioned in Sec. VIB.

Following attainment of the current value I_0, but depending on the particular operating point chosen, the output current may or may not undergo a further rise to reach a plateau value, I_{max} (Fig. 25). At a time T_1 the output current drops to zero and is restored only after an interval T_d. At the time T_2 the current again drops to zero and from then on the phenomenon reproduces itself in the manner indicated. It is found that T_1 is inversely proportional to the product of vacuum-chamber pressure and emission current, while the interval T_d is generally slightly less than the time required to accelerate electrons from the injector to the target and appears to be relatively independent of emission current. Evidently at time T_1 the sheet of charge extending from the injector to the target becomes unstable and is lost. Specifically it was found that when the operating point lay just below an axial resonance a probe situated above or below the beam would receive a large amount of charge at the time T_1, whereas when operating just below a radial resonance a probe inserted near the inner or outer radii would receive a burst of charge at T_1. The instability usually appeared to begin at the injection radius and proceed outward to the target radius, taking approximately 5 μsec to do so.

Since the slope dI/dt (Fig. 25) and I_{max} are each proportional to emission current and T_1 varies inversely with pressure and emission, the phenomena appear attributable to ionization of the gas in the vacuum chamber. The initial space-charge limited current I_0 can increase as ions are formed and collected in the beam until the current I_{max} is reached, which may represent the maximum current available from the injector. As additional ions are collected, the oscillation frequencies increase to approach a resonant value, whereupon, at T_1, the beam is lost. Following this, after a sufficient number of ions have migrated to the chamber walls, injected electrons may once again build up a new sheet of charge, commencing at the injection radius, and the phenomena then repeat themselves as long as the emission and accelerating voltage are both present. Radio-frequency measurements of the betatron oscillation frequencies,[3,14] made at various times during the acceleration process, confirmed that with high emission currents the initial oscillation frequencies are lowered, as expected, and that at later times the frequencies increased to values which were above those obtained with low emission and

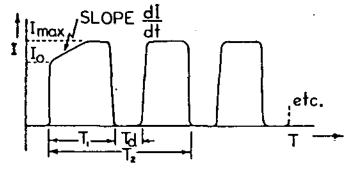

FIG. 25. Sketch depicting the essential features of the beam current observed at high emission, as obtained from the oscillogram of Fig. 24(d).

which approached a half-integral resonance (e.g., $\nu_z=1.5$). Once the operating point enters a stop-band and some electrons become quickly lost, the ions remaining behind may be expected to drive the operating point further into the stop-band and the beam must necessarily be lost very rapidly.

Although the foregoing explanation in terms of beam neutralization by ionization of residual gas appears to account for the phenomena described, additional phenomena involving the collective motion of particles undoubtedly occur. Thus, for example, a strong rf electromagnetic field was found to arise from the beam, with frequencies which usually were half-integral multiples of the electron revolution frequency at the injector radius. The strength, frequency spectrum, and duration of this electromagnetic field depended quite markedly on the operating point of the accelerator. Since the intensity usually was particularly strong just prior to the time at which the beam was lost, the radiation may, at least in part, have been due to coherent motion of the charges as the operating point entered a stop-band. In one instance, moreover, it appeared that the current which arrived at the target was bunched at the revolution frequency of the electrons.

VII. PERTURBATION STUDIES

A. General Description

It was of interest to obtain experimental information concerning the effects of misalignments on the operation of the model to permit a comparison with computational and analytic results and to provide information concerning constructional tolerances for an accelerator of the spiral type. Four types of perturbations were specifically studied in turn: (1) The magnetic field in one of the six sectors was reduced 7% by reducing the currents in the main field coils which produced the excitation for that sector; (2) the field index, k, in a sector was raised from 0.7 to 0.8 by adjustment of the current in the k-tuning coils for that sector; (3) a sector was raised by 1 mm with respect to the remaining five sectors; and (4) a sector was rotated approximately 2° about a pin on its inner radius. For each such perturbation, measurements were made of, (1) the resultant radial and axial displacements of the equilibrium orbit, (2) changes in the frequencies of radial and axial betatron oscillations, and (3) changes in the radial and axial stability limits.

B. Results of Perturbations at the Design Point

The radial displacement of the equilibrium orbit which resulted from lowering the field by 7% in one of the sectors is shown by the points in Fig. 26(a). The solid line of Fig. 26(a) represents the displacement predicted by digital computation with the IBM-704, using the measured values of the magnetic field at a given radius together with the design values for k and w, while the dotted line represents the result predicted by Parzen[21] from an analytic treatment of this problem where the indicated shape is obtained from the addition of a $\cos\theta$ first harmonic term and a negative $\cos 2\theta$ second harmonic term. As expected, no significant vertical movement of the equilibrium orbit arose from this type of perturbation. As a result of this perturbation, the frequencies and amplitudes of the betatron oscillations were changed by the amounts listed in Table V.

A perturbation in which the field index k is raised from 0.7 to 0.8 in a sector has the effect of leaving the field unchanged at a radius of 25 cm but strengthens the field by increasing amounts at larger radii within the perturbed sector (cf. Sec. IIIA). The effect of such a perturbation on the equilibrium orbit appears[21] to be essentially due to the associated increase of the field strength at the radius of interest. The shift of the radial position of the equilibrium orbit as obtained experimentally at a radius of 37 cm is indicated by the points plotted in Fig. 26(b) together with computational and analytic results obtained by considering only the increased field strength within the perturbed sector. Again, as expected, no vertical movement of the equilibrium orbit was found to occur. The change in the field strength at 37 cm as a result of the change in k is about half that which was produced by the preceding field perturbation and in the opposite sense. Changes in the frequencies of the betatron oscillations and the stability limits which were observed to occur from the perturbation of k and the resulting field perturbation are summarized in Table V. Also included are the results of computations[13] made with the IBM-704 prior to operation of the model. As noted previously (Sec. IIC), the main effect of this perturbation appears to be a partial decrease of the phase space available for stable oscillations similar to the larger decrease found when k was increased in all sectors.

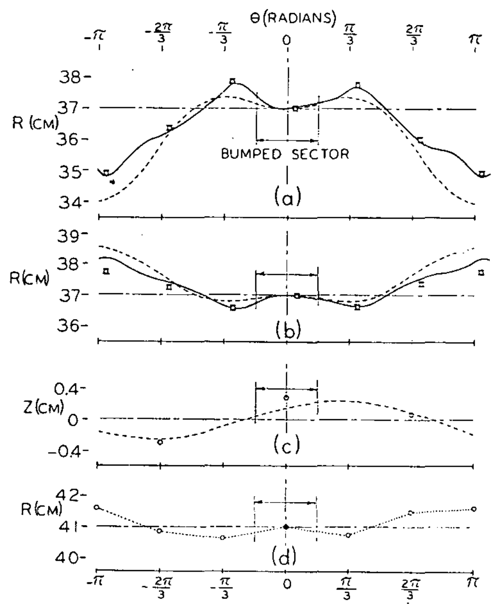

FIG. 26. Effect of perturbations on the equilibrium orbit: (a) radial displacement of the equilibrium orbit as a result of a 7% field reduction in one magnet sector; (b) radial displacement of the equilibrium orbit as a result of raising the field index k from 0.7 to 0.8 in one sector, the effect being regarded as chiefly attributable to the 3.5% increase of field at the detection radius of the perturbed sector; (c) axial displacement of the equilibrium orbit as a result of raising one magnet sector 1 mm; and (d) radial displacement of the equilibrium orbit as a result of rotating one sector approximately 1° about its front pin, the effect being regarded as chiefly the result of the accompanying 2 to 2.5% increase of field at any given radius within the perturbed sector. The solid lines represent computational results, the dashed lines are based on the perturbation theory summarized in Appendix III, and the circles connected by a dotted line in (d) are the observed displacements. Circles barred on top and bottom represent experimental results (a) and (b).

[21] The results of an analytic treatment by G. Parzen of the effect of perturbations in a spiral ridge accelerator are given in Appendix III. The authors are very grateful to Dr. Parzen for his courtesy in permitting this material to be included in the present paper.

The vertical movement of a sector by 1 mm resulted in an equilibrium orbit displaced from the median plane by amounts shown in Fig. 26(c), and produced no detectable change in the radial position. The effects on the betatron oscillation frequencies and on the limiting stable amplitudes are summarized in Table V, together with computer results obtained by means of the Illiac prior to construction of the model.

Clockwise rotation of a sector, through 2° about a vertical axis at its inner radius, will necessarily increase somewhat the field strength at a given radius—in the present

TABLE V. Effect of perturbations on the oscillation frequencies and stability limits at the design point.

Perturbation	Item	Theory[a]	Computer	Experiment
Unperturbed	ν_x	1.32	1.40	1.41
	ν_y	1.15	1.12	1.12
	A_x		$0.097\,{}^{+0.005}_{-0.000}$	0.058 ± 0.006
	A_y		$0.058\,{}^{+0.005}_{-0.000}$	0.045 ± 0.006
Field decreased 7% in one sector	$\Delta\nu_x$		0 ± 0.001	$+0.006\pm0.003$
	$\Delta\nu_y$		-0.002 ± 0.0005	-0.006 ± 0.005
	$\Delta A_x/A_x$		-0.18 ± 0.05	-0.25 ± 0.08
	$\Delta A_y/A_y$		-0.31 ± 0.05	-0.22 ± 0.08
Field index k changed from 0.7 to 0.8 in one sector	$\Delta\nu_x$		$+0.01\pm0.001$	$+0.011\pm0.003$[b]
	$\Delta\nu_y$		-0.01 ± 0.001	-0.015 ± 0.005[b]
	$\Delta A_x/A_x$			-0.20 ± 0.08[b]
	$\Delta A_y/A_y$			-0.23 ± 0.08[b]
Axially displaced sector (raised 1 mm)	$\Delta\nu_x$			$+0.001\pm0.004$
	$\Delta\nu_y$			$+0.002\pm0.006$
	$\Delta A_x/A_x$			-0.20 ± 0.10
	$\Delta A_y/A_y$			-0.08 ± 0.10
Rotated sector (approx. 2°)	$\Delta\nu_x$			$+0.004\pm0.006$
	$\Delta\nu_y$			$+0.003\pm0.007$
	$\Delta A_x/A_x$			0.0 ± 0.15
	$\Delta A_y/A_y$			0.0 ± 0.15

[a] Theoretical results from Appendix III.
[b] The experimental values for the perturbation in k also include the effect of the field being increased by about 3½% at the detection radius in the perturbed sector.

case by about $2\frac{1}{2}\%$. The change in the equilibrium orbit which results from this perturbation is shown in Fig. 26(d) and is believed to arise primarily from the increase of field strength associated with rotation of the sector. The changes produced in the betatron oscillation frequencies and the stability limits appear to be small.

C. Results Near the $\nu_x = 2\nu_y$ Resonance

To supplement the results just reported it was considered of interest to obtain information concerning the effect of perturbations applied to the model when operating in the neighborhood of the difference resonance $\nu_x = 2\nu_y$. Unfortunately, as noted in Sec. V, the accessible portion of this resonance line was of somewhat limited extent and fell in a region where other important resonances were also present. The computer results obtained for the operating points A and B considered in Sec. IIC indicated that the radial stability limits were very greatly reduced in the neighborhood of the $\nu_x = 2\nu_y$ resonance when even small amounts of axial motion were introduced, and misalignments of course were found to effect a further reduction of these stability limits. In practice, the pronounced exchange of amplitude between radial and axial oscillations which occurs when operating near a coupling resonance presents a complication in making it difficult to distinguish experimentally motions in these two degrees of freedom.

Two types of perturbations were studied at a point near the $\nu_x = 2\nu_y$ resonance: (1) The magnetic field was lowered by 5% in a sector, and (2) a sector was raised 1 mm. The same measurements were made as at the design point. The radial displacement of the equilibrium orbit which resulted from lowering the magnetic field by 5% was about the same as at the design point with the exception that the negative $\cos 2\theta$ part had less of an effect here, as expected.[21] The changes in the betatron oscillation frequencies and the stability limits were less than the indeterminancies of the measurements. The vertical displacement of a sector caused a small vertical displacement of the equilibrium orbit and no detectable radial displacement. The observed changes in the betatron frequencies and stability limits were again very small. Computer studies made specifically for $\nu_x = 1.25$, $\nu_y = 0.62$ appeared to confirm the result that little further reduction of the radial stability limit would occur at this operating point with an axial sector displacement of 1 mm.

VIII. STUDIES OF RADIO-FREQUENCY ACCELERATION

A. General Discussion

The objective of the radio-frequency acceleration experiments reported here for the spiral ridge model was to determine empirically the frequency-modulation programs which could most successfully be applied to accelerate par-

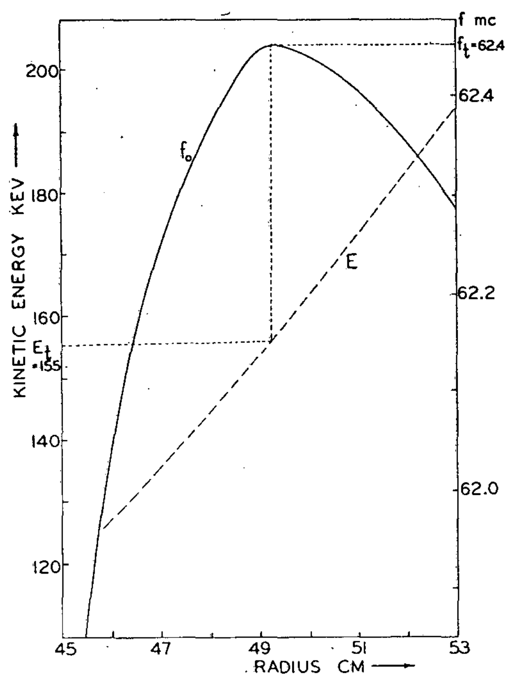

FIG. 27. Electron energy, E, and revolution frequency f vs radius. E_t and f_t denote, respectively, the transition energy and the associated revolution frequency.

ticles through the transition energy. The magnet excitation and the injector voltage were adjusted so that the transition radius was 49 cm. This allowed electrons to be accelerated through the transition to at least a 52 cm radius before edge effects in the magnets reduced the beam. Figure 27 shows the energy and revolution frequency as a function of radius under these operating conditions. The energy was calculated on the basis of field measurements and the known value k, while the frequency was measured by radio-frequency excitation of betatron oscillations (Secs. IIIB and V)[3,14] and by the more accurate method which we now describe. The first of two successive betatron acceleration pulses (Sec. IIIC) was adjusted so that practically all the electrons were taken out to the target. The remaining electrons could be assumed to have extremely small betatron oscillations and could be observed striking the target at the start of the second betatron pulse. In the interval between these betatron pulses radio-frequency power was applied to the vacuum chamber at a constant frequency close to the revolution frequency and tuned to bring these electrons with small oscillation amplitudes onto the target, possibly by exciting synchrotron oscillations. In this way the frequency could be determined quite accurately as a function of radius.

The transition energy for fixed-field alternating-gradient accelerators is given by[1]

$$E_t = E_0(k+1)^{\frac{1}{2}} \qquad (15)$$

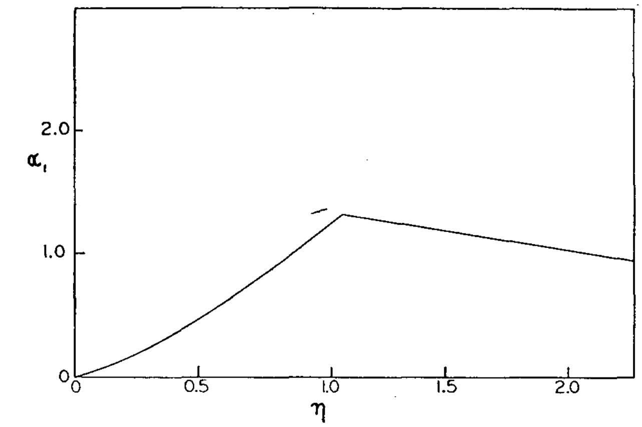

FIG. 28. The parameter α_1, to which the bucket area is proportional, versus the parameter η of the Symon-Sessler theory (reference 22).

and the transition radius, in centimeters, by

$$r_t=\left[\frac{E_0^2\, k\, r_0^{2k}\, 10^8}{9H_0^2}\right]^{1/(2k+2)}, \tag{16}$$

where E_0= electron rest energy in Mev, E_t= transition energy (including rest energy) in Mev, k= mean field index, and H_0 is the average field in gauss at r_0 cm.

In discussing radio-frequency acceleration methods, reference is made to the electrical phase angle ϕ at which a particle crosses the acceleration gap; the peak value V of the voltage applied to the gap; the phase angle ϕ_s for an equilibrium particle; and the gap voltage V_s appearing across the gap at the time of transit of the equilibrium particle. It is convenient to introduce the quantity Γ, defined by

$$\Gamma\equiv\sin\phi_s=V_s/V, \tag{17}$$

and to note that

$$V_s=df/dt/f\, df/dE, \tag{18}$$

where f denotes the revolution frequency of a particle in the given magnetic field (Fig. 27).

The Symon-Sessler theory[22] of radio-frequency acceleration in fixed-field alternating-gradient accelerators further employs the variable W, shown to be canonically-conjugate to ϕ, defined by

$$W=\int_{E_0}^{E} dE/f(E). \tag{19}$$

The stable area in W, ϕ phase space, within which stable synchrotron oscillations may occur, is termed a "bucket." For a given machine and a constant radio-frequency voltage, the bucket area is proportional to a quantity α_1, which is given by the Symon-Sessler theory[22] in terms of a parameter η. The latter quantity is proportional to $1-f/f_t$ and α_1 approaches zero as the revolution frequency f approaches the transition frequency f_t, in the manner illustrated by Fig. 28.

Typical buckets above and below the transition energy are shown in Fig. 29. As a bucket approaches the transition energy, the stable area approaches zero and, in passing to operation above the transition energy, particles may be expected to be deposited in a band lying just above the transition energy in the W, ϕ plane. If, however, the frequency is modulated nonadiabatically to a value slightly greater than the transition frequency and then decreased, it is possible to pick up some particles from this region and accelerate them further. This procedure requires a carefully scheduled program of frequency modulation so that, in effect, the correct phase slip required to continue acceleration above the transition energy is introduced.

B. Experimental

In the experimental work ϕ_s was normally between 11° and 55° when operating below the transition energy, with Γ correspondingly between 0.2 and 0.8; in going through the transition energy, Γ has little meaning as defined by Eq. (17); and, finally, in the operation above the transition energy, ϕ_s typically approached the value 150°. The frequency-modulation program in the neighborhood of the transition energy was then adjusted empirically to obtain effectively the optimum phase slip and thereby achieve the most efficient transfer of electrons to states of stable synchrotron motion above the transition energy.

The effectiveness of the various frequency-modulation programs was determined by a method which paralleled that used in similar studies[23] with the radial sector model.[3]

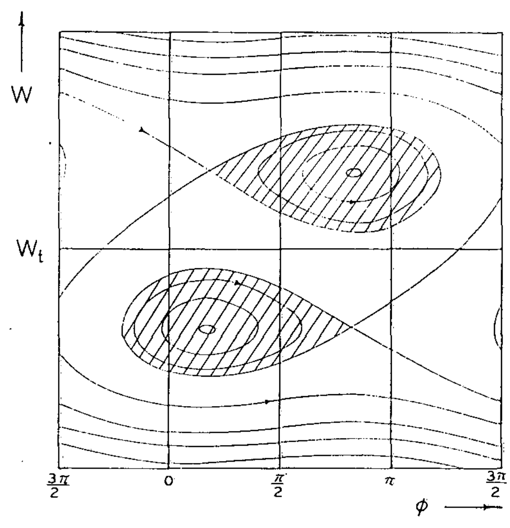

FIG. 29, Regions of W, ϕ phase space, showing typical phase-stable areas, or "buckets," (a) above and (b) below the transition energy. The shaded areas represent the buckets and the curves indicate possible particle trajectories in W, ϕ space.

[22] K. R. Symon and A. M. Sessler, *Proceedings of the CERN Symposium on High Energy Accelerators and Pion Physics* (European Organization for Nuclear Research, Geneva, 1956), vol. 1, p. 44.

[23] K. M. Terwilliger, L. W. Jones, and C. H. Pruett, Rev. Sci. Instr. 28, 987 (1957).

Figure 30 illustrates this method schematically. With curve A no radio-frequency acceleration is provided, so that electrons are accelerated by an initial betatron pulse to an energy of about 118 kev and to a radius of 45.5 cm, to remain at that radius for about 1230 μsec before being further accelerated by a second betatron pulse which carries them to the scintillation detector at a radius of 52 cm. In the case depicted by curve B the radio-frequency voltage is used to carry the electrons, which have been stacked at the intermediate radius of 45.5 cm, up to the transition energy and the voltage is then turned off. In this case the electrons are once again brought to the detector by the further acceleration provided by the second betatron pulse, but arrive 150 μsec earlier than with curve A. Finally, with curve C, the radio-frequency voltage is applied in accordance with a frequency-modulation schedule intended to provide acceleration through the transition energy and electrons successfully accelerated in this way will appear at the detector at a time *preceding* onset of the second betatron pulse.

Typical results of the method just described are illustrated by the oscilloscope traces drawn in Fig. 31. The upper trace of each pair shows the beam received at the detector and the lower trace represents the rf voltage. In actuality the first betatron pulse had dropped to zero by the time the sweep started, but the second betatron pulse appeared on the trace and the radio-frequency voltage, when present, was also displayed. In the first pair of traces

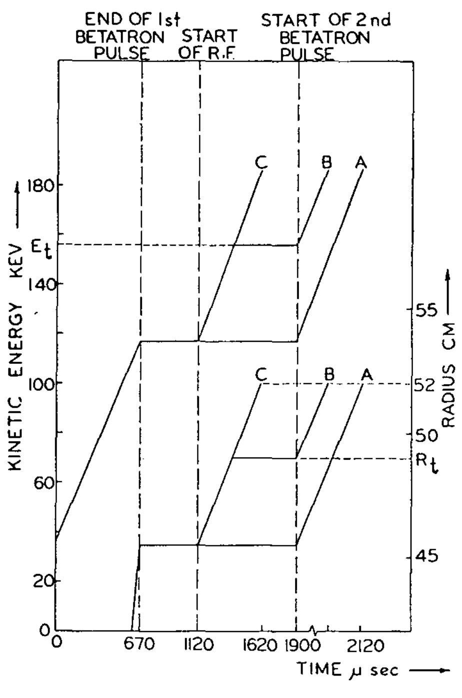

FIG. 30. Particle energy and orbit radius versus time for three acceleration programs.

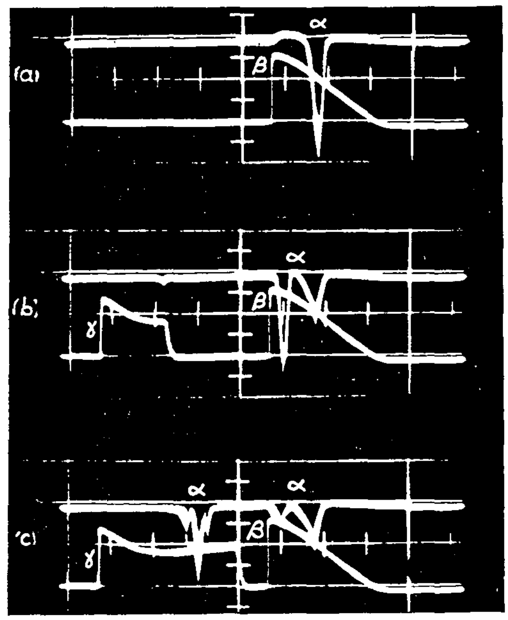

FIG. 31. Oscillograms of (α) the beam received at the detector, (β) the betatron voltage, and (γ) the envelope of the rf voltage in experiments designed to investigate acceleration through the transition energy. The first pair of traces (a) correspond to curve A of Fig. 30, for which no rf acceleration is employed. Traces (b) correspond to curve B, with rf acceleration up to the transition energy. In (c), corresponding to curve C, some of the stacked beam is seen to have been successfully accelerated through the transition energy. In this figure one horizontal division corresponds to 200 μsec and, on the lower member of each pair, one vertical division represents 5 v.

in Fig. 31 no radio-frequency voltage was used and the single beam pulse shown represents the electrons accelerated entirely by betatron action. In the second pair the radio-frequency voltage served to carry about 60% of the stacked electrons to the neighborhood of the transition energy (155 kev) and these electrons gave rise to the earlier of the two pulses shown. Finally, the third set of traces illustrates the case in which some electrons were successfully accelerated *through* the transition energy to arrive at the detector prior to the onset of the second betatron pulse, while others were dropped at the transition energy and the remainder were not captured by the radio-frequency system at all. In the quantitative interpretation of results such as those illustrated by Fig. 31 it must be recognized that the true efficiency (50%) is somewhat less than that indicated directly by the data (70%), since the pressure in the vacuum chamber was of the order of 3×10^{-6} mm Hg at the time the experiments were performed and the consequent half-life of the beam due to gas scattering was approximately 400 μsec.

The adjustment of the frequency-modulation schedule to obtain efficient traversal of the transition energy is, of course, critical. This is illustrated by Fig. 32, in which three frequency schedules are shown, of which the second

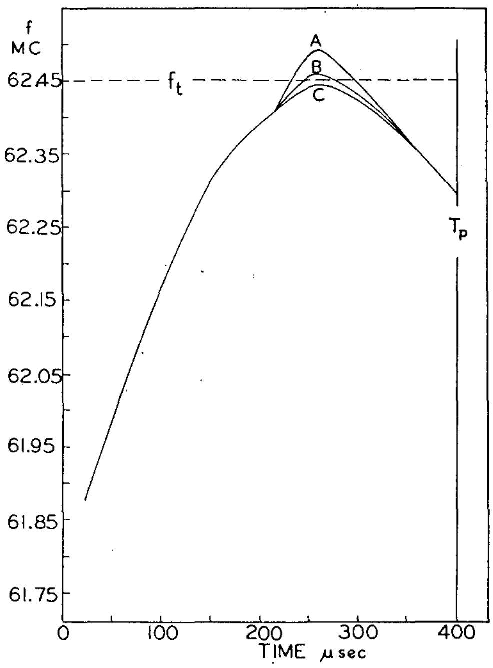

FIG. 32. Frequency of rf oscillator versus time for three acceleration programs leading to different efficiencies for traversal of the transition energy. The efficiencies for curves A, B, and C were measured as 10, 50, and 10%, respectively.

(denoted B) gave an efficiency approximately five times as great as with either of the other two.

IX. ACKNOWLEDGMENTS

We would like to express our indebtedness to the several universities which, by granting leaves of absence, made it possible for many of the authors to contribute to the success of the model. We particularly appreciate the cooperation of the Graduate College of the University of Illinois in the arrangements permitting extensive use of the Illiac computer, the willingness of the Physics Research Laboratory to assume the burdens of initial construction, and the assistance of the mechanical engineering shop at the University of Illinois in making available a large press for initial shaping of the magnet poles.

Invaluable assistance in programming the digital computations was provided by Dr. R. F. King, Mrs. G. Belford, and D. Hutchinson. Use of the computers was greatly facilitated by the cooperation of Dr. J. P. Nash and Dr. R. E. Meagher of the Digital Computer Laboratory, by Jess Anderson who prepared the individual problems for the computer, and by Melvin Storm who supervised some of the later work with the IBM-704 installation in Madison.

The initial construction was implemented by the administrative assistance of J. J. Cochrane and by the work of T. B. Elfe. The final assembly and portions of the test program received substantial contributions from Dr. Carl E. Nielsen, of the Ohio State University, and Dr. R. Stump, of the University of Kansas. Assistance was provided by G. F. Dell, of the Ohio State University; C. Bernhardt, G. E. Bush, and E. C. Weinberg, of Purdue University; C. W. Owen, D. S. Roiseland, D. Schroeder, and M. G. Silbert, of the University of Wisconsin; and by J. D. Hogan, E. S. Kennedy, J. Mulady, and C. A. Radmer, of the MURA Laboratory.

The cooperation of Dr. Joseph Ballam of Michigan State University in providing a field magnetometer was very helpful in facilitating the magnetic measurements and the contributions of Dr. E. S. Akeley, Dr. F. T. Cole, Dr. G. Parzen, and Dr. K. R. Symon to the basic theory are also gratefully acknowledged.

APPENDIX I. DESIGN OF THE LONG-PULSE MODULATOR

For the studies of stability limits and space-charge effects described in Secs. V and VI, it was necessary to inject electrons into the accelerator for relatively long periods of time. The long injection time and the required constancy of injection energy demanded by the specifications for the modulator (Table VI) precluded the use of conventional delay line and pulse transformer techniques for driving the injector. Fortunately, a power tetrode capable of withstanding 50-kv plate potentials became available at the time these experiments were being considered, so that the use of a plate-loaded amplifier for driving the injector appeared to be an attractive possibility. The problem then became one of constructing from available components an amplifier with adequate frequency response and output capability. This appendix describes briefly the design and performance of such an amplifier.

The values of pulse amplitude, current, and duration listed in Table VI represent, of course, maximum values and are much greater than necessary for the present purpose. It was felt, however, that the amplifier should be designed to make full use of the output stage. The characteristics of the output tube (Eimac type X556) are given in Table VII.

A simplified circuit diagram of the amplifier output stage is shown in Fig. 33, wherein C_s denotes the parasitic capacitance of the output circuit, including the injector, and R_L represents the resistive load presented by the injector. Because the output of the amplifier is to be a moderately fast pulse at high potential, the choice of the coupling capacitor is severely limited with respect to its capacitance. The largest commercially available capacitance

TABLE VI. Specifications for the long-pulse modulator.

Pulse amplitude	Pulse current	Pulse length	Rise time	Flatness
−45 kv	250 ma	10^{-3} sec	10^{-5} sec	0.25%

in the 50-kv range with reasonable physical size and electrical properties seems, in fact, to be about 0.1 μf. With the output tube specified, the design of the amplifier then must start with the coupling capacitor since it alone will determine the flatness of the output pulse under the assumption that all other time constants ahead of the output stage may be made long compared to 10^{-3} sec.

The injector operates in the emission-limited region and consequently the expression

$$\Delta V = (I_L/C_c)\Delta t \tag{20}$$

is exact. In taking C_c to be 0.1 μf, I_L to be 250 ma, and Δt to be 10^{-3} sec, ΔV is found to be 2.5×10^3 v and a 20-kv output pulse of 1 msec duration thus would be expected to drop by 12.5% as a result of the capacitative coupling. An amplitude of 20 kv was chosen for this calculation because it corresponds to the minimum pulse amplitude that will be required of the amplifier and therefore gives the maximum percentage drop for a given output current. Moreover, even if it were possible to increase the size of C_c without limit to obtain the required flatness of the output pulse, there will be variations in the output level due to shifts in the 50-kv power supply, which is not regulated. These latter variations might be as large as $\pm5\%$ and would appear in the output because the dynamic plate impedance of the X556 tetrode is fairly low. It was considered essential, therefore, to incorporate a feedback loop to stabilize the gain of the amplifier and to decrease the drop of the output pulse to the required 0.25%.

Before calculating the value of the loop gain βA_0 necessary for the required degree of stability, the rest of the amplifier must be considered. The output stage requires a driving signal of at least 500 v peak from a low-impedance source in order that it can conduct heavily during the rise of the pulse. The heavy conduction is necessary to discharge the parasitic capacitance C_s, which was estimated to be as high as 150 $\mu\mu$f. In order for this discharge to occur in approximately 5 μsec for a 45-kv pulse, a current at least as large as that given by

$$I_p = C_s(\Delta V/\Delta t) = 1.2 \text{ amp} \tag{21}$$

must pass through the tube. This requires that the output tube be driven into the region of grid conduction. A

TABLE VII. Characteristics of Eimac type X556[a] power tetrode.

Dc plate voltage	50 kv max
Pulse cathode current	6 amp max
Average control grid dissipation	5 w max
Average screen grid dissipation	25 w max
Average plate dissipation	250 w max
Transconductance (estimated)[b]	6000 μmho
Grid bias for 10-μa anode current[c]	−450 v

[a] Now Eimac type Y 158.
[b] Screen potential = 1 kv, anode current = 1 amp.
[c] Anode potential = 50 kv, screen potential = 1 kv.

FIG. 33. Schematic circuit of the output stage for the long-pulse amplifier.

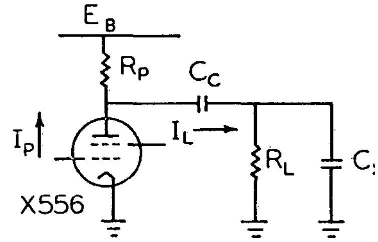

cathode follower using a high powered tube such as a 3E29 dual beam power tube would be expected to prove satisfactory as a driver. It furthermore seems reasonable to expect that a two-stage amplifier ahead of the cathode follower then could supply the necessary 500- to 600-v signal.

If the arbitrary assumption is made that the gains of the first two amplifier stages and of the output stage may change in the course of time by $\pm10\%$ due to aging of components, power supply variations, etc., then the loop gain will vary by $\pm33\%$. The cathode follower is not inincluded in this estimate since it is a degenerative device. The necessary value of loop gain βA_0 would then follow from the relation[24]

$$\frac{1}{\beta A_0}\cdot\frac{1}{2}\left(\frac{1}{0.67}-\frac{1}{1.33}\right)\leqslant 0.0025, \tag{22a}$$

whence

$$\beta A_0 \cong 150. \tag{22b}$$

It can be seen that this value of βA_0 is considerably greater than that necessary to reduce the 12.5% drop of the output pulse to the required 0.25%. It now remains only to pick a reasonable closed-loop gain in order to calculate the required over-all gain of the amplifier. Taking the closed-loop gain to be 10^3, the necessary over-all gain is then $A_0 = 10^3 \times 1.5\times10^2 = 1.5\times10^5$. This value may seem excessive for three stages until it is recalled that the transconductance of the output stage is 6000 μmho. For a plate-load resistance of 50 kΩ this gives a gain of 300 for this stage alone and the preceding two stages should be able to provide a gain of 500 quite easily.

The seemingly arbitrary choice in the previous paragraph for the plate-load resistor in the output stage was actually motivated by consideration of the power dissipation in the output tube. It was expected that the duty cycle for the amplifier might be as high as 0.03. If 5 kv is assumed as the plate voltage during the pulse and 250 w as the maximum permissible plate dissipation, the pulse plate current should be less than 1.7 amp. Since there is a significant contribution to plate dissipation during the rise of current at the beginning of the pulse when heavy

[24] Duncan MacRae, Jr., in *Vacuum Tube Amplifiers*, edited by G. E. Valley, Jr., and H. Wallmann (McGraw-Hill Book Company, Inc., New York, 1948), Massachusetts Institute of Technology Radiation Laboratory Series, vol. 18, Chap. 9, p. 366, Eq. (45).

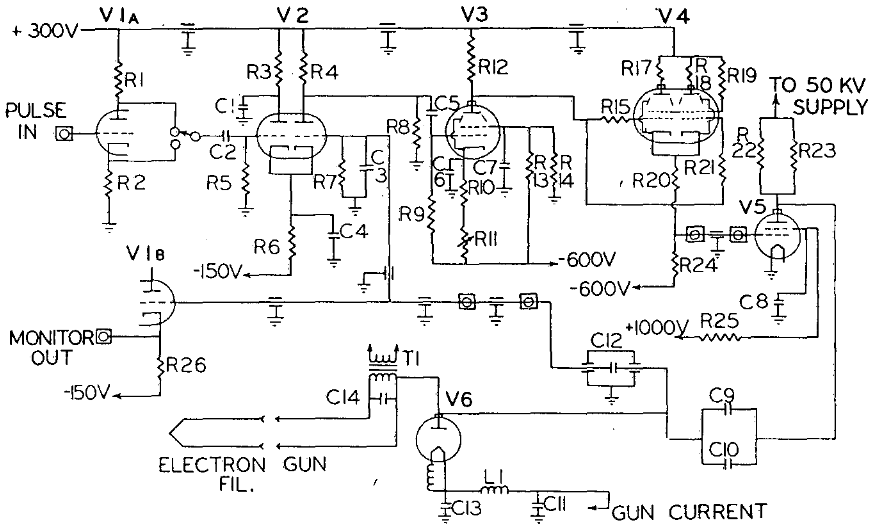

FIG. 34. Amplifier circuit for the long-pulse modulator.

conduction at high plate potential takes place, it seemed advisable to reduce the plate current to 1.25 amp and a value of 50 kΩ accordingly was selected for the plate resistor.

Figure 34 shows the circuit of the complete amplifier. The design of all stages is conventional and will not be discussed in any great detail. Feedback from the output is obtained from a capacitive voltage divider with a ratio of 1000:1. The first stage is a standard noninverting amplifier with a gain of approximately 30. The second grid is used as a feedback terminal. The second stage is biased unsymmetrically to obtain a large positive pulse of short rise time. The cathode follower is of low impedance since it must supply the grid current of the final stage as well as drive a rather high parasitic capacitance. Small resistors were included in the plate, grid, and cathode circuits of of the cathode follower to serve as parasitic suppressors. The direct coupling used in the last two stages serves two purposes: First, it reduces the number of low frequency phase-shifting networks in the loop and, second, it provides a convenient method of adjusting the bias on the final amplifier stage. The small capacitors in the cathode circuits of the first and second stages and the RC series circuit to ground from the plate of the first stage are networks required for stabilization of the feedback amplifiers.

The measured performance of the amplifier was rather close to the original specifications (Table VI). The closed-loop gain was 995 and the rise time was 8 μsec. A 4-μsec rise time could be obtained, in fact, at the expense of a single 5% overshoot. The flatness of the output pulse was measured with a differential amplifier and oscilloscope. For a 1-msec 30-kv pulse applied to a 120-kΩ load the voltage drop was less than 0.1%.

In summary, the modulator design reported here appeared to represent a straightforward method of generating long pulses of moderate rise time with a good constancy of amplitude at high voltage. There seem to be no complications arising from the high voltages that cannot be circumvented by the usual techniques. Faster rise and decay times undoubtedly may be obtained at the expense of pulse length as tubes with higher maximum plate current became available. Again, however, feedback could be used to reduce the value of coupling capacitance necessary for good reproduction of the flat top of the pulse and this would appear to be of some advantage since the cost of increasing loop gain is much less than that of increasing the size of the coupling capacitor. Since the modulator is a linear amplifier, the output pulse is an accurate reproduction of the input pulse subject to the limitations of frequency response. In some of the stability-limit measurements described in the text (Secs. VD, E) the input pulse, which ordinarily was a square pulse of variable amplitude derived from a multivibrator circuit, was shaped so as to exhibit a region with a substantially linear and moderately slow decrease of potential.

APPENDIX II. THE MAGNETOMETERS

The two magnetometers used in measuring the magnetic field and locating the median plane were basically of the same type. The operation of these instruments is based on the fact that if one excites a transformer wound on a ferromagnetic core with a sinusoidally varying current, the magnetic field within the core and hence the secondary voltage may be represented by a series which involves only the fundamental and odd-order harmonics, provided the hysteresis loop of the core is symmetrical about the origin. If this symmetry is destroyed by the presence of a dc magnetic field which displaces the hysteresis loop along the H axis, even harmonics will appear in the output. The amplitude of the even harmonic content of the output is, to a first approximation, proportional to the superimposed dc field. In principle, then, the magnitude of the superimposed field may be obtained from the amplitude of the second harmonic component. There are, however, other considerations that enter in the practical application of this method. For example, the shape and symmetry of the hysteresis loop are very dependent on the mechanical and magnetic history of the core. Also, since the magnetometers used with the spiral sector model were required to give good spatial resolution in an inhomogeneous field, the active volume of the core had to be extremely small. This latter requirement led to considerable difficulty with heat dissipation in the primary winding, because it was necessary that the core be driven into saturation in both directions to avoid its taking a permanent "set."

As is understandable, the aforementioned problems could not all be overcome conveniently in any one instrument. Accordingly, two magnetometers were constructed—one for fairly large fields (1 to 300 gauss) and one for very small fields ($\approx 10^{-2}$ gauss). The magnetometer for "large" fields incorporated a feedback circuit that energized a quadrupole coil mounted coaxially with the core to ensure that the core was never operated in a field of more than a few tenths of a gauss and thus reduce the driving power in the primary winding. This instrument was essentially a copy of the device described by Voelker and Leavitt[25,26] and was used in mapping the vertical component of the magnetic field in the region of the geometric median plane. This magnetometer was entirely adequate for the use described, but suffered from two significant drawbacks which made it unsuitable for finding the magnetic median plane. The first such defect arose because the bias coil produced a small but not negligible external magnetic field at distances from the coil of as much as 3 cm (or half a gap width at the injection radius) and it was initially feared that in the magnet measurements (Sec. IV) the low field ends of the magnets would be highly sensitive to external fields. Secondly, since the bias current was supplied by series vacuum tubes, the magnetometer could be used only in fields of one polarity, for otherwise the core might become saturated and thus take on a "set" which would give an appreciable error when measuring small fields. The situation just described could readily occur when making measurements in the fringing-field region with large currents in the flutter-tuning coils.

The "sensitive" magnetometer for measurement of weak fields is shown schematically in Fig. 35. The oscillator-amplifier circuit operated at 3500 cps and incorporated current feedback to stabilize the driving field. The reject filter was included to keep the fundamental component of the signal from overloading the tuned amplifier and thus generating a spurious second-harmonic component. The

[25] F. Voelker and M. A. Leavitt, University of California Radiation Laboratory Rept. UCRL-3084 (Berkeley, California, 1955, unpublished).
[26] F. Voelker, Electronics 31 (No. 11), 152 (March 14, 1958).

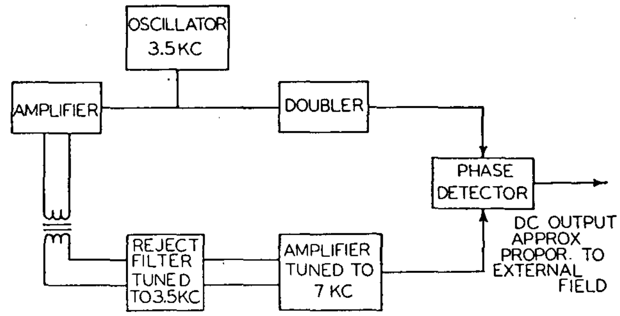

FIG. 35. Schematic diagram illustrating the principle of the magnetometers.

pickup transformer consisted of two 20-turn windings of No. 40 B&S gauge Formvar-insulated wire wound directly on a 1×10-mm strip of Mo permalloy, 0.5 mil thick. This magnetometer was insensitive to transverse magnetic fields as great as 200 gauss, while showing good sensitivity for longitudinal fields of 10^{-2} gauss. Because of the small driving field, considerable care had to be exercised to keep the pickup transformer out of longitudinal fields in excess of 10 gauss. In practice, the magnetometer was not used to determine the magnitude of the horizontal field in the region of the median plane, but rather to implement adjustments directed toward reduction of the radial component of magnetic field in this plane.

APPENDIX III. PERTURBATION THEORY

In this appendix theoretical results for the linear orbit properties and for effects of field perturbations will be presented. No derivations of the results will be given here.

We will first give some results for the linear orbit properties of a scaling FFAG accelerator. Somewhat more general and accurate results, and their derivations are available in MURA reports.[27]

We will write the magnetic field in the median plane as

$$H_z=-\{H_0(r)+2H_1(r)\cos[N\theta-\beta_1(r)] +2H_2(r)\cos[2N\theta-\beta_2(r)]+\cdots\}, \quad (23a)$$

where

$$H_n(r)=-B_0(r/r_0)^k h_n, \quad (23b)$$

$$\beta_n(r)=(n/w)\ln(r/r_0)+\alpha_n. \quad (23c)$$

The average radius of the equilibrium orbit R and the momentum p are related by

$$p=eRH_{ef}/c, \quad (24a)$$

where H_{ef} the effective magnetic field is given by

$$H_{ef}=B_0(R/r_0)^k/b, \quad (24b)$$

$$b=\frac{2}{h_0+[h_0^2+8h_1^2(k+3/2)/N^2]^{\frac{1}{2}}}. \quad (24c)$$

[27] G. Parzen, Midwestern Universities Research Association Repts. MURA-454, 451, 397 (1959, 1958, unpublished).

TABLE VIII. A comparison of the theoretical and computer results for the tune and beat factors of the spiral sector model.

	Computer	Theory
ν_x	1.40	1.32
ν_y	1.12	1.15
B_x	1.73	1.66
B_y	1.51	1.41

The equilibrium orbit is given by $r(\theta)=R[1+x(\theta)]$, where

$$x(\theta)=(2bh_1/N^2)\cos[N\theta-(1/w)\ln(R/r_0)-\alpha_1]. \quad (25)$$

The radial tune ν_x is given by

$$\nu_x^2=bh_0(k+2)-1+4b^2h_1^2(k^2+3k+2)/N^2. \quad (26)$$

The vertical tune ν_y is given by

$$\nu_y^2=2b^2(h_1^2+h_2^2+\cdots)-bh_0k+2b^2h_1^2(2/w^2+1/4)/N^2. \quad (27)$$

The beat factor B_x which gives the ratio of the largest amplitude of betatron oscillation to the smallest amplitude as one goes around the machine is related to β_x by

$$B_x=[\beta_{x,\max}/\beta_{x,\min}]^{\frac{1}{2}}. \quad (28)$$

B_x is given by

$$B_x=1+4bh_1[(k+3/2)^2+i/w^2]^{\frac{1}{2}}/(N^2-4\nu_x^2). \quad (29)$$

The beat factor for the vertical betatron oscillations B_y is given by

$$B_y=1+4bh_1[(k+1/2)^2+1/w^2]^{\frac{1}{2}}/(N^2-4\nu_y^2). \quad (30)$$

A comparison of the results given by the theory with results found by numerical integration of the equations is given in Table VIII for the tune and beat factors of the spiral sector model.

We will now give some theoretical results for the effects of field perturbations. No derivations of the results will be given here.

We assume that the magnetic field in the median plane for the unperturbed machine is written as

$$H_z=-\sum_{n=0,\pm N,\pm 2N\cdots} G_n(r)\exp(in\theta). \quad (31)$$

The harmonics $G_n(r)$ may also be written as

$$G_n(r)=H_n(r)\exp[-i\beta_n(r)], \quad (32)$$

where H_n and β_n are real. The effect of the perturbation on the median plane field is to change the field components by the amount ΔH_z, ΔH_r, ΔH_θ. We will first treat the case where only $\Delta H_z\neq 0$. This is a particularly important case as all deliberate perturbations like straight sections fall into this case.

We assume that the field perturbation ΔH_z is written as

$$\Delta H_z=-\sum_{n=-\infty}^{\infty}\Delta G_n(r)\exp(in\theta), \quad (33)$$

$$\Delta G_n(r)=\Delta H_n(r)\exp[-i\alpha_n(r)]. \quad (34)$$

This field perturbation will affect the equilibrium orbit and the tune ν_x, ν_y. For the sake of simplicity, the results will not be presented in the most general or accurate form that has been obtained, but the results will be given for the particular case of the spiral sector model and for perturbations that were introduced into this model. The following results should be accurate within about 20%.

The following assumptions will also be made. It will be assumed that the field gradient is large, which for the spiral sector machine means that $1/w\gg 1$. It will be assumed that the perturbing field does not shift the tune appreciably, that the unperturbed tune is not too close to the stop bands introduced by the perturbation, and that neither ν_x nor ν_y are close to $\frac{1}{2}N$.

We find the change in the equilibrium orbit. The effect of the perturbation on the equilibrium orbit can be broken down into two parts. There is the effect due to the harmonics of ΔH_z for $n=0$, $\pm N$, $\pm 2N\cdots$, and there is the effect due to the harmonics for which $n\neq 0$, $\pm N$, $\pm 2N\cdots$. These two effects are calculated separately and the effect of the harmonics for $n=0$, $\pm N$, $\pm 2N$ is treated first.

Let us consider an orbit of the unperturbed field which corresponds to the momentum p and the average radius R. p and R are related by

$$p=eRH_{\mathrm{ef}}/c, \quad (35a)$$

where H_{ef}, the effective field, is given by

$$H_{\mathrm{ef}}=\frac{1}{2}\left\{H_0+\left[H_0^2+8H_N\left(RH_N'+\frac{3}{2}H_N\right)\Big/N^2\right]^{\frac{1}{2}}\right\}, \quad (35b)$$

where H_0, H_N are evaluated at $r=R$ and the prime indicates differentiation with respect to r.

The equilibrium orbit corresponding to the particle momentum p is shifted by the amount $R\Delta x$, where R is the average radius of the equilibrium orbit of the unperturbed field.

We write $\Delta x(\theta)$ in Fourier series form as

$$\Delta x=\sum_n\Delta x_n\exp(in\theta). \quad (36)$$

The Δx_n for $n=0$, $\pm N$, $\pm 2N\cdots$ are given by

$$\Delta x_n=(\Delta x_n)_1+(\Delta x_n)_2, \quad (37a)$$

where

$$(\Delta x_0)_1=-\frac{1}{\nu_x^2}\left[\frac{eR}{pc}\Delta H_0+2\left(\frac{eR}{pc}\right)^2\sum_{n>0}^{N}\frac{1}{n^2}\times(RH_n'\Delta H_n+R\Delta H_n'H_n+3H_n\Delta H_n)\right], \quad (37b)$$

$$(\Delta x_n)_1 = (eR/pc)(1/n^2)[\Delta G_n + (RG_n' + 2G_n)(\Delta x_0)_1], \quad (37c)$$

for $n = \pm N, \pm 2N \cdots$.

$$(\Delta x_n)_2 = \frac{1}{n^2 - \nu_x^2} \sum_m{}' \frac{\Delta G_{n+m}}{(m+n)^2 - \nu_x^2} (R\Delta G_{-m}' + 2\Delta G_{-m})$$
$$+ \frac{1}{n^2 - \nu_x^2} \frac{1}{2} \sum_s^N [(R^2 G_s'' + 2RG_s' + 2G_s) \times \sum_m{}' \Delta x_m \Delta x_{-s-m}]. \quad (37d)$$

In Eqs. (37),

$$\sum_s^N$$

signifies a sum over $s = 0, \pm N, \pm 2N \cdots$ and

$$\sum_m{}'$$

signifies a sum over m but omitting $m = 0, \pm N, \pm 2N \cdots$. The Δx_m for $m \neq 0, \pm N, \pm 2N$ are given in the following.

We may note that the $(\Delta x_n)_1$ are due to the harmonics ΔG_n for which $n = 0, \pm N \cdots$ and the $(\Delta x_n)_2$ are due to the harmonics for which $n \neq 0, \pm N \cdots$. The G_n and ΔG_n are to be evaluated at $r = R$.

For $n \neq 0, \pm N \cdots$ we find

$$\Delta x_n = a_n - \sum_{s \neq 0}^N \frac{g_s}{s(-s+2n)} a_{n-s}, \quad (38a)$$

where

$$a_n = \frac{1}{n^2 - \nu_x^2} \left[\frac{eR}{pc} \Delta G_n + \frac{eR}{pc} \sum_{s \neq 0}^N x_s (R\Delta G_{n-s}' + 2\Delta G_{n-s}) - \sum_{s \neq 0}^N \frac{eR}{pc} \Delta G_{n+s} \frac{g_{-s}}{s(s+2n)} \right], \quad (38b)$$

$$g_s = -\frac{eR}{pc} \left(RG_s' + \frac{3}{2} G_s \right), \quad (38c)$$

$$x_s = \frac{1}{s^2} \frac{eR}{pc} G_s. \quad (38d)$$

Equation (38a) is not valid for $n = \frac{1}{2}N$, and we find for the case $n = \frac{1}{2}N$,

$$\Delta x_n = \frac{eR}{pc} \Delta G_n \exp[i(\gamma_N + \alpha_n)] \left[\frac{\cos(\gamma_N + \alpha_n)}{n^2 - \nu_x^2 - |g_N|} - i \frac{\sin(\gamma_N + \alpha_n)}{n^2 - \nu_x^2 + |g_N|} \right], \quad (38e)$$

where γ_N is the phase of the complex number g_N.

The second term in Eq. (38a) is usually of the order of 10% of the first term and may be neglected unless the first term is absent.

A somewhat simplified but useful expression for the oscillatory part of the equilibrium orbit is given by

$$\Delta x(\theta) = A \sum_n \frac{eR}{pc} \frac{1}{n^2 - \nu_x^2} \Delta G_n \exp(in\theta), \quad (39a)$$

$$A = 1 + |g_N|^2/(N^2 - 4\nu_x^2). \quad (39b)$$

We will now treat the general case where we have not only a ΔH_z but also a ΔH_r and ΔH_θ perturbations. Usually such perturbations are accidental and the exact form of the perturbation is not known. Also, the r and z motions are now coupled. Instead of having an r tune and a z tune, one now has two normal modes whose tunes we may still label as ν_x and ν_y since one mode is predominantly r motion and the other is predominantly z motion.

The equilibrium orbit corresponding to the particle momentum is shifted by the amount $R\Delta x$ and $R\Delta y$. The radial shift is given by Eqs. (37) to (39). The vertical shift is given by

$$\Delta y = -B \frac{eR}{pc} \sum_n \frac{1}{n^2 - \nu_y^2} \Delta G_{r,n} \exp(in\theta), \quad (40a)$$

$$B = 1 + \frac{1}{1 - (2\nu_y/N)^2} \frac{|f_N|^2}{N^2}, \quad (40b)$$

$$f_N = \frac{eR}{pc} |RG_N' + \tfrac{1}{2} G_N|, \quad (40c)$$

and we represent the perturbation ΔH_r as

$$\Delta H_r = -\sum_n \Delta G_{r,n}(r) \exp(in\theta). \quad (40d)$$

The foregoing result for Δy holds if the perturbation does not change the tune very much in the same manner as was assumed in the case of a pure ΔH_z perturbation.

We will now apply the foregoing theoretical results to the various field perturbations that were introduced into the spiral sector model.

Sector Bump

A bump that was applied to the radial sector model was to decrease the field in one sector by 7%. To apply the results given above we must first calculate the ΔG_n due to the perturbation. The ΔG_n are given by

$$\Delta G_n = \frac{1}{2\pi} \int_0^{2\pi} d\theta \exp(-in\theta) \Delta H_z(r,\theta). \quad (41)$$

For the spiral sector model we may write the unperturbed field as

$$H_z = -B_0 (r/r_1)^k h(\theta, r), \quad (42a)$$

$$h(\theta, r) = \sum_n h_n \exp\{[inN[\theta - (1/wN) \ln(r/r_1)]\}, \quad (42b$$

and the perturbation may be written as

$$\Delta H_z = -B_0(r/r_1)^k \Delta h(\theta,r), \tag{43}$$

where Δh is different from zero in only one sector and reduces the field by 7% in that sector. An approximate result for ΔG_n, valid for $n \ll N$, is

$$\Delta G_n = B_0\left(\frac{r}{r_1}\right)^k \exp\left[-\frac{in}{wN}\ln\frac{r}{r_1}\right]\frac{(\Delta h)_{\rm av}}{N}, \tag{44}$$

$(\Delta h)_{\rm av}$ being the average value of Δh over the sector where it is not zero.

One may also note that for this unperturbed machine

$$(eR/p_c) \simeq 1/G_0. \tag{45}$$

Using these results for ΔG_n one now computes the shift in the orbit and tune.

The change in the equilibrium orbit shown in Fig. 26 may be easily understood. Since the tune $\nu_x = 1.40$, the orbit shift is primarily due to the first and second harmonics of the perturbing field. The theoretical curve in Fig. 26 only takes into account the first and second harmonics, and including the higher harmonics would have improved the agreement with experiment. Equation (39) was used to calculate the equilibrium orbit.

Δk Bump

In this bump, k was changed in one sector from $k=0.7$ to $k=0.8$. The value of the magnetic field was unchanged at $r=25$ cm and the measurements were made at $r=37$ cm.

We can write the unperturbed field as

$$H_z = -B_0(r/r_1)^k h(\theta,r), \tag{46}$$

where $r_1 = 25$ cm, and the perturbed field as

$$\bar{H}_z = -B_0(r/r_1)^{k'} h(\theta,r), \tag{47}$$

where $k' = k + \Delta k$ and $\Delta k = 0.1$ in one sector, $\Delta k = 0$ in the other five sectors.

The field perturbation $\Delta H_z = \bar{H}_z - H_z$ is then given by

$$\Delta H_z = -B_0(r/r_1)^k \Delta k \ln(r/r_1) h(\theta,r), \tag{48}$$

where we have expanded in powers of Δk keeping just the lowest term.

This perturbation ΔH_z has the same form as the perturbation for the 7% sector bump where $\Delta h(\theta,r)$ is given by

$$\Delta h(\theta,r) = \Delta k \ln(r/r_1) h(\theta,r). \tag{49}$$

This Δk bump then shifts the equilibrium orbit in the same way as a sector bump where the field is changed by the fraction $\Delta k \ln(R/r_1)$ where R is the radial distance to the point of measurement.

Vertical Displacement Bump

In this bump a magnet was raised 1 mm. Raising a magnet introduces a radial component ΔH_r, in the magnetic field in the median plane. ΔH_r is given by

$$\Delta H_r = -\left.\frac{\partial H_z}{\partial r}\right|_{z=0} \Delta z, \tag{50}$$

in the sector where the magnet is raised, and Δz is the distance the magnet is raised.

If we write the unperturbed field as

$$H_z = -B_0(r/r_1)_k h(\theta,r), \tag{51a}$$

$$h/\theta,r) = 1 + f\cos[N\theta - (1/w)\ln(r/r_1)], \tag{51b}$$

then

$$\Delta H_r = \frac{\Delta z}{r} B_0\left(\frac{r}{r_1}\right)^k\left\{\frac{f}{w}\sin\left(N\theta - \frac{1}{w}\ln\frac{r}{r_1}\right) + k\left[1 + f\cos\left(N\theta - \frac{1}{w}\ln\frac{r}{r_1}\right)\right]\right\}. \tag{52}$$

We find $\Delta G_{r,n}$ from

$$\Delta G_{r,n} = -\frac{1}{2\pi}\int_0^{2\pi} \exp(-in\theta)\Delta H_r. \tag{53}$$

An approximate result for $\Delta G_{r,n}$ is

$$\Delta G_{r,n} = -\frac{\Delta z}{r} B_0\left(\frac{r}{r_1}\right)^k\left(\frac{k}{N}h_{\rm av} - i\frac{n\pi}{2N^2}\left|\frac{\partial h}{\partial r}\right|_{\rm av}\right) \exp\left(\frac{-in}{wN}\ln\frac{r}{r_1}\right), \tag{54a}$$

$$h_{\rm av} \simeq \tfrac{2}{3}(1+f), \tag{54b}$$

$$\left|\frac{\partial h}{\partial r}\right|_{\rm av} \simeq \tfrac{2}{3} f/w. \tag{54c}$$

Reprinted from THE REVIEW OF SCIENTIFIC INSTRUMENTS, Vol. 31, No. 11, 1225-1228, November, 1960
Printed in U. S. A.

Theory of a High Dispersion Double Focusing Beta-Ray Spectrometer*

H. DANIEL† AND L. JACKSON LASLETT
Institute for Atomic Research and Department of Physics, Iowa State University, Ames, Iowa

(Received April 25, 1960; and in final form, August 3, 1960)

A "flat" high dispersion double focusing beta-ray spectrometer is proposed and results of computations are presented. The high dispersion is achieved by making the electrons orbit around the field axis more than once. The source and detector are displaced radially, in opposite directions, from the stationary circular orbit. A suitable baffle is mounted between the source and detector to shield the detector against unwanted electrons. The electron-optical properties are almost the same as for the $\pi\sqrt{2}$ spectrometer except that the dispersion is increased. Numerical results are presented for two instruments with focusing angles of 565.88° and 909.02°, with respective dispersions of 21.5 and 50.6, to be compared with a dispersion of 4 for the $\pi\sqrt{2}$ spectrometer.

I. INTRODUCTION

IN a beta-ray spectrometer with moderate dispersion, high resolution requires a very narrow source which, furthermore, must be quite well adjusted. If one uses a high dispersion, however, both disadvantages are greatly reduced.

The need for a high dispersion has already been pointed out and suitable magnetic fields have been described.[1,2] In reference 1 a double focusing spectrometer was proposed,

* Contribution No. 885. This work was performed in the Ames Laboratory of the U. S. Atomic Energy Commission.

† Present address: Max Planck Institute for Nuclear Physics, Heidelberg, Germany. The major portion of the present work was performed while the author was on leave from the Max Planck Institute.

[1] G. E. Lee-Whiting, Can. J. Phys. 35, 570 (1957).

[2] H. Daniel, Rev. Sci. Instr. 31, 249 (1960).

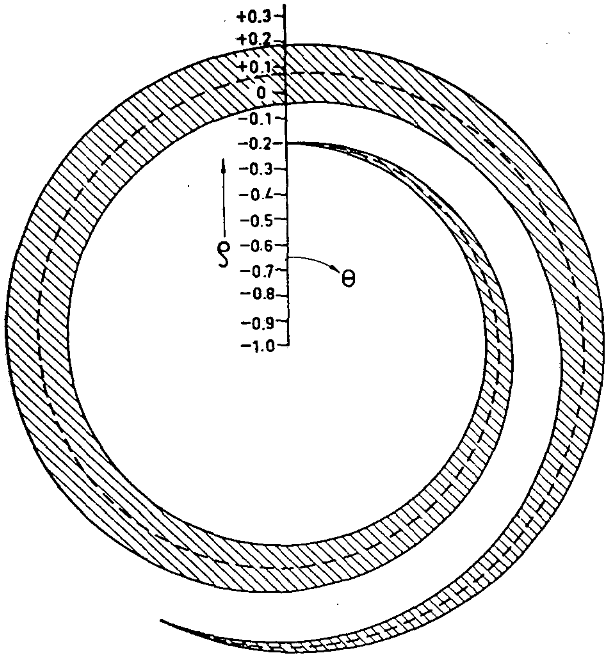

FIG. 1. Electron bundle in the case $l=3$. Three orbits all in the symmetry plane are shown: $\zeta_r=+0.04$ and $\zeta_r=-0.04$ (solid lines) and $\zeta_r=0$ (dashed line). The shaded area represents the cross section of the electron bundle for $|\zeta_r|\leqslant 0.04$. The electrons start at $\rho=-0.2$.

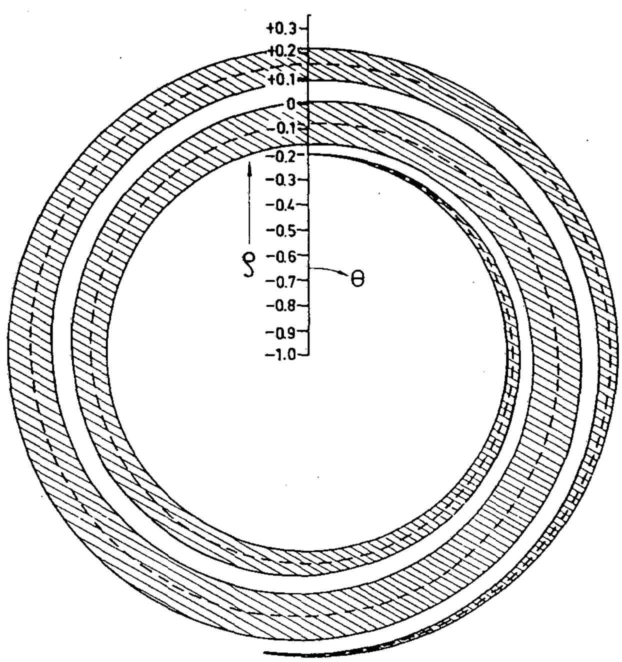

FIG. 2. Electron bundle in the case $l=5$. Three orbits all in the symmetry plane are shown: $\zeta_r=+0.02$ and $\zeta_r=-0.02$ (solid lines) and $\zeta_r=0$ (dashed line). The shaded area represents the cross section of the electron bundle for $|\zeta_r|\leqslant 0.02$. The electrons start at $\rho=-0.2$.

while in reference 2 a spectrometer with a curved exit slit was proposed. In both cases the angle θ_1 between source and detector must be larger than 2π in order to obtain the desired high dispersion. If θ_1 is larger than 2π, some electrons of undesired momenta will reach the detector if there are no special arrangements to stop these electrons. Lee-Whiting[1] estimates this background. If, however, the source is displaced from the stationary circular orbit, it is possible to shield the detector completely against these unwanted electrons.[2] In this case the detector is shifted by about the same amount in the opposite direction. Figures 1 and 2 show two examples of such an arrangement.

It is the purpose of the present paper to give more detailed information about a high dispersion double focusing spectrometer with a displaced source. In Sec. II some results of a second-order perturbation calculation are summarized. Because of the magnitude of the requisite source shift, however, which is not small, these results are not sufficiently accurate to draw definite conclusions. Section III gives the results of electronic computer calculations.

II. SECOND-ORDER TREATMENT

The notation of reference 2 will be used in the following analysis. Assume for the moment that there is no source shift, so $\rho_0=0$. Then the formulas of reference 2 lead to the following expressions for the image coordinates ρ_1, ξ_1 as functions of the source coordinates ρ_0, ξ_0, the emission angles ζ_r, ζ_z, and the field coefficients α, β:

$$\rho_1=-\rho_0-\frac{3+7\alpha+4\beta}{3(1+\alpha)^2}\zeta_r^2-\frac{1+5\alpha+4\beta}{(1+\alpha)(1+5\alpha)}\zeta_z^2$$
$$-\frac{2}{3}\frac{\alpha+\beta}{1+\alpha}\rho_0^2+\frac{\alpha(1+5\alpha)+2\beta(1+3\alpha)}{(1+\alpha)(1+5\alpha)}\xi_0^2, \quad (1)$$

$$\xi_1=-\xi_0-\frac{2(1+4\beta+5\alpha)}{(1+\alpha)(1+5\alpha)}\zeta_r\zeta_z-\frac{4\beta}{1+5\alpha}\rho_0\xi_0. \quad (2)$$

Equation (2) holds for the only practically important case

$$l=(-\alpha)^{\frac{1}{2}}/(1+\alpha)^{\frac{1}{2}}=\text{odd integer}, \quad (3)$$

in which l denotes the number of axial oscillations per radial oscillation. As in the $\pi\sqrt{2}$ case[3] there are two main types of design, in which the aperture aberration is independent of ζ_r^2 or, alternatively, of ζ_z^2. In the former case one has

$$\beta=-(3+7\alpha)/4, \quad (4)$$

and in the latter,

$$\beta=-(1+5\alpha)/4. \quad (5)$$

TABLE I. Numerical results of the second-order theory.

l	ρ_0	α	β	γ	δ	θ_1	ρ_1	D	a_2/D	b_1
1	0	−0.500	0.375	...	...	255.56°	0	4.0	−0.333	−0.500
3	0	−0.900	0.875	...	...	569.21°	0	20.0	−0.333	−0.500
5	0	−0.962	0.952	...	...	917.82°	0	52.0	−0.333	−0.500

[3] K. Siegbahn, *Beta- and Gamma-Ray Spectroscopy*, edited by K Siegbahn (Interscience Publishers, Inc., New York, 1955), Chap. II.

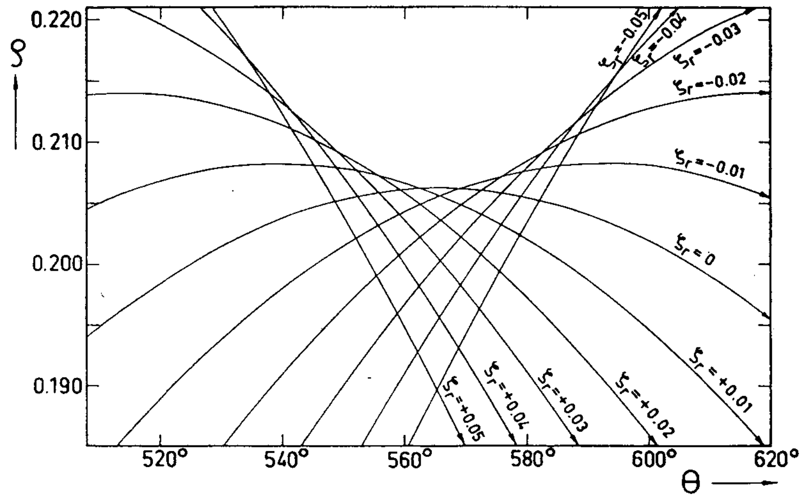

FIG. 3. Electron orbits near the exit slit in the case $l=3$. All orbits shown are in the symmetry plane.

The remaining aperture aberrations are then

$$\Delta\rho_1 = \frac{2}{1+5\alpha}\zeta_z^2 \tag{6}$$

and

$$\Delta\rho_1 = a_2 D\zeta_r^2 = -\frac{1}{3}\frac{2}{1+\alpha}\zeta_r^2, \tag{7}$$

respectively. Similarly, the aberration connected with the source height is

$$\Delta\rho_1 = b_2\xi_0^2 = -\tfrac{1}{2}\xi_0^2. \tag{8}$$

Finally, the dispersion D is given by

$$D = 2/(1+\alpha). \tag{9}$$

High dispersion requires that α be close to -1. The coefficient of ζ_r^2 in Eq. (7) is therefore much larger than the coefficient of ζ_z^2 in Eq. (6). For a given maximum bundle diameter, however, the aberrations given by Eqs. (6) and (7) are nearly equal. This has been discussed in greater detail by Lee-Whiting.[1] For a spectrometer employing a source shift, the high transmission requirement favors strongly the type characterized by Eq. (5). Therefore, only this type will be treated in the remainder of this paper. Note that ρ_0 does not appear in Eqs. (6) through (9). Finally it should be noted that, according to Eq. (3) of reference 2, there is no first- or second-order shift in θ_1 in the case $\rho_0 \neq 0$. Numerical results of the second-order theory are given in Table I.

III. COMPUTER CALCULATIONS

Because of the large source shift necessary to combine high dispersion and medium transmission in an arrangement like that of Figs. 1 or 2, it was decided to perform computer calculations which, automatically, included higher-order terms not taken into account in the analysis of Sec. II. The second-order theory of Sec. II served as a guide in this work.

The general procedure for the numerical calculations was to determine the electron orbits as a function of the angle

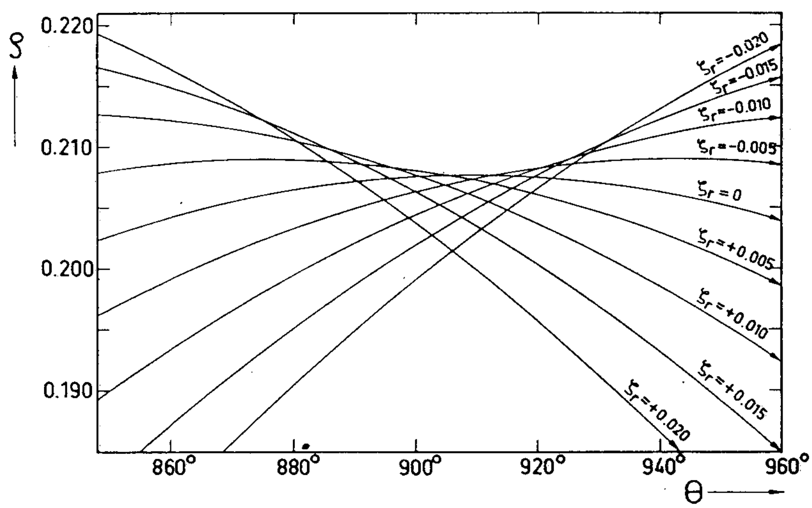

FIG. 4. Electron orbits near the exit slit in the case $l=5$. All orbits shown are in the symmetry plane.

TABLE II. Field coefficients and results of the computer calculations.

l	ρ_0	α	β	γ	δ	θ_1	ρ_0	D	a_2/D	b_2
3	−0.2	−0.898	0.875	−0.895	0.880	565.88°	0.2063	21.5	−0.350	−0.612
5	−0.2	−0.961	0.952	−0.961	0.953	909.02°	0.2077	50.6	−0.308	−0.580

θ. This was done with an electronic computer and the results of these computations were then evaluated by hand. The orbits were determined with the MURA IBM-704 computer by use of the Ill-Tempered Five Program.[4] The step length was chosen to be 4°. Linear interpolation was used between two steps when evaluating the data. In order to obtain a point on the exit slit two orbits were used, both with $\zeta_z=0$: $\zeta_r=+\zeta_r^{(1)}$ and $\zeta_r=-\zeta_r^{(1)}$, where $\zeta_r^{(1)}$ denotes a selected value for the magnitude of the angle ζ_r. Other orbits were chosen to determine the aberrations connected with axial aperture, source height, electron momentum, and combinations of these quantities with each other and with the radial aperture. Before starting computations pertaining to the present problem, the procedure was checked for the $\pi\sqrt{2}$ spectrometer, which exhibits almost perfect focusing in ζ_z and for which there is an elaborate theory available[5] for comparison.

Computations were performed for $l=3$ and $l=5$, Eq. (3), with the source shift held constant at $\rho_0=-0.2$. Table II contains the values selected for the field coefficients, α, β, γ, and δ. These values were previously determined by exploratory computations so as to give, approximately, first-order double focusing and small axial-aperture aberration. The higher-order field coefficients were taken to be zero. Figures 3 and 4 show some orbits near the exit slit in the cases $l=3$ and $l=5$, respectively. The intersections of two orbits with $\zeta_r=+\zeta_r^{(1)}$ and $\zeta_r=-\zeta_r^{(1)}$ describe a curve for different $\zeta_r^{(1)}$ values which is almost a straight line but is not perpendicular to the circle $\rho=$const, for $\zeta_r^{(1)}$ not too large. The angle between this focal line and the circle $\rho=$const is found to be 76° in the case for which $l=3$ and 5.5° in the case $l=5$. Obviously it is most advantageous to make the exit slit follow this focal line and this has been assumed, in the following, when calculating the resolution.

[4] Elizabeth Z. Chapman, Midwestern Universities Research Association Rept. MURA-457, *Ill-Tempered Five Program 220* (1959, unpublished). The authors are indebted to Mrs. Chapman for her work in constructing this versatile program, which was well adapted for performing the computations reported here.

[5] G. E. Lee-Whiting and E. A. Taylor, Can. J. Phys. 35, 1 (1957).

The computational results have been analyzed in terms of a_2, b_2, and D of Eqs. (7) through (9) and are summarized in Table II. There is almost perfect double focusing and, as expected for a spectrometer with β given by Eq. (5), only a negligible ζ_z^2 dependence of ρ_1. At large values of ζ_z, of course, higher-order terms contribute, but for $l=3$ and $\zeta_z=0.305$ one still has $\Delta\rho_1/D=-5.4\times10^{-5}$, and for $l=5$ and $\zeta_z=0.253$ one has $\Delta\rho_1/D=-1.05\times10^{-4}$.

When comparing the proposed high dispersion spectrometer with the $\pi\sqrt{2}$ type, it is seen that they have almost the same electron-optical properties except for the dispersion. This means that, for a given transmission, resolution, and apparatus size, one may use a source which is wider and higher by about a factor of $D/4$ than the source in the $\pi\sqrt{2}$ spectrometer. To the same extent the source positioning is less critical. Table III gives rough estimates of the expected efficiency at the listed values of solid angle and source dimensions. The quantity ω is the fractional solid angle selected by the entrance slit and η is the total width of the resolution curve at half-maximum. The radius r_0 of the stationary circular orbit has been taken to be 20 cm, which implies an instrument of only moderate size.

TABLE III. Typical data for a spectrometer with a 20 cm mean radius r_0.

	ω	Total source height	Total source width	η
3	0.4%	5 cm	2 mm	~0.12%
5	0.15%	4 cm	1 mm	~0.025%

IV. ACKNOWLEDGMENTS

It is a pleasure to thank M. Storm and the staff of the MURA Computer Section for kindly performing the computations. The authors are indebted to B. McDaniel and C. Engler for their help in evaluating the data.

Reprinted from THE REVIEW OF SCIENTIFIC INSTRUMENTS, Vol. 32, No. 11, 1235–1252, November, 1961
Printed in U. S. A.

Coupling Resonances in Spiral Sector Accelerators*

L. J. LASLETT† AND A. M. SESSLER‡
Midwestern Universities Research Association, Madison, Wisconsin
(Received May 18, 1961; and in final form, August 9, 1961)

Theoretical and computational results are presented to illustrate the behavior of single particle motion in spiral sector FFAG accelerators of small flutter factor when operated in the neighborhood of vertical-radial coupling resonances. The theoretical analysis proceeds from the approximation in which the radial motion is determined without consideration of the vertical motion, and this solution is then inserted into the linearized equation for the vertical motion. The resulting generalized Hill equation is analyzed by a variational technique which yields both the bands of instability of the vertical motion and the exponential rate of growth within these zones. This mathematical analysis is confirmed by a computational study of the Hill equation used in the theoretical analysis. Extensive computational results are presented of the actual particle motion near coupling resonances for a choice of parameters characteristic of both full-scale accelerators and models. Attention is concentrated on defining the regions of instability and determining the rate of vertical growth, both of which are seen to be in semiquantitative agreement with the theoretical analysis.

I. INTRODUCTION

THIS paper is concerned with certain phenomena pertaining to particle motion with two degrees of freedom in a spiral sector accelerator. Briefly, the behavior to which we direct our attention is an exponential growth of the amplitude of axial oscillations, from very small initial amplitudes, when the structure is such that the oscillation frequencies lie in the neighborhood of certain "coupling resonances." This "y growth" appears to be the more rapid the greater the amplitude of the radial motion, above a certain threshold, and more pronounced when the operating point is near the resonance in question. For certain of the resonances, the exponential growth may be found ultimately to terminate, at relatively large y amplitudes, if the amplitude of the radial oscillation is not too great. Despite the possible termination, or "turnover," of the exponential growth in certain cases,[1] it is suggested that it deserves serious recognition by the accelerator designer due to the possibility that this growth may lead to ultimate instability through the mechanism of other inherent or imperfection resonances.

The studies of this paper have been confined to FFAG accelerators with spiral sectors,[2,3] which is an attractive form of a FFAG accelerator, since smaller circumference factors may be utilized than appear feasible with the alternative radial sector design. Considerable effort has been expended by the MURA Group in successfully constructing and operating a spiral sector electron model,[4] while spiral sector cyclotrons are now in operation or under construction in a large number of laboratories. Thus, the results of this study may be of direct interest to a number of groups, but more importantly, the authors would like to emphasize that both the computational and theoretical approaches should have wide applicability to the study of many particle-handling devices.

The contents of this paper have appeared during the last five years in a number of unpublished MURA Reports[5–9]; but only here, for the first time, will be found a comprehensive description of the phenomena.

A. Theoretical Analysis

In the theoretical work, attention is directed to appropriate coupling terms in the differential equation for the vertical amplitude y which are *linear* in the dependent variable y but involve the radial coordinate u, measured with respect to the stable equilibrium orbit.[2] Suitable solutions of an approximate differential equation for u, obtained on the supposition that $y=0$, are introduced into the coupling terms of the y equation to obtain a linear differential equation for y with coefficients involving both the period of the structure *and* that of the radial oscillations. This introduction in a non-Hamiltonian way of what is taken in effect to be a *prescribed* u motion was

* This work was supported by the National Science Foundation, the Office of Naval Research, and the U. S. Atomic Energy Commission.

† Department of Physics and Institute for Atomic Research, Iowa State University, Ames, Iowa. Present address: Division of Research, U. S. Atomic Energy Commission, Washington 25, D. C.

‡ The Ohio State University, Columbus, Ohio. Present address: Lawrence Radiation Laboratory, University of California, Berkeley 4, California.

[1] Theoretical analysis of a single nonlinear resonance has suggested that, ultimately, turn over may be expected for the case of a *difference* resonance [cf. references 12 and 13, and R. Hagedorn, *Proceedings of the CERN Symposium on High Energy Accelerators and Pion Physics, Geneva, 1956* (CERN, Geneva, 1956), Vol. 1, p. 293].

[2] K. R. Symon, D. W. Kerst, L. W. Jones, L. J. Laslett, and K. M. Terwilliger, Phys. Rev. **103**, 1837 (1956).

[3] L. Jackson Laslett, Science **124**, 781 (1956).

[4] D. W. Kerst, E. A. Day, H. J. Hausman, R. O. Haxby, L. J. Laslett, F. E. Mills, T. Ohkawa, F. L. Peterson, E. M. Rowe, A. M. Sessler, J. N. Snyder, and W. A. Wallenmeyer, Rev. Sci. Instr. **31**, 1076 (1960).

[5] L. Jackson Laslett and A. M. Sessler, Midwestern Universities Research Association Report MURA-263 (1957, unpublished).

[6] L. Jackson Laslett, Midwestern Universities Research Association Report MURA-320 (1957, unpublished).

[7] Roger E. Mills, Midwestern Universities Research Association Report MURA-319 (1957, unpublished).

[8] A. M. Sessler, Midwestern Universities Research Association Report MURA-596 (1961, unpublished).

[9] C. A. Lassettre, Midwestern Universities Research Association Report MURA-595 (1961, unpublished).

originally suggested by W. Walkinshaw[10] and appears to be entirely defensible when the y amplitudes are as small as those obtaining in the greater part of the present work. Since coupling terms are actually also present in the differential equation for u, it must be acknowledged that the development of a large amplitude y oscillation will "react back" on the u motion, but this is generally a small effect unless the y motion has grown to exceedingly large amplitudes, and is ignored in the remainder of this paper so that the results strictly are only applicable to y growth in its initial stages where the amplitude is small.

Subsequently, considerable attention has been given to these problems by Parzen[11] employing perturbation methods similar to those applied in solid-state physics, and by Symon and co-workers,[12] using the mathematical methods developed by Moser.[13] These techniques are capable of reproducing the results of this paper as well as predicting aspects of the phenomenon of "turnover," but the mathematical methods are more involved than those employed in this paper.

The differential equations used in the theoretical analysis are taken from the analysis of Cole[14] which is appropriate to a FFAG accelerator with a pure sinusoidal variation of the median plane field. Only the coefficients which are dominant for small values of the flutter f are retained. The radial displacement (in units of a convenient reference radius) is written

$$x=x_f+u, \tag{1.1}$$

where x_f represents the forced motion resulting in the (periodic) equilibrium orbit. The free radial oscillation satisfies the following approximate differential equation:

$$u''+[a_x+b_x\cos N\theta]u=-\frac{f}{2w^2}\sin N\theta\, u^2+\frac{f}{6w^3}\cos N\theta\, u^3, \tag{1.2}$$

where

$$a_x=k+1-\frac{f^2}{2w^2[N^2-(k+1)]}\simeq k+1-\frac{f^2}{2w^2N^2}, \tag{1.3}$$

$$b_x=f/w, \tag{1.4}$$

and the notation is that of reference 2. The y equation governing the axial motion is taken to be

$$y''+[a_y+b_y\cos N\theta]y=\frac{f}{w^2}\sin N\theta\, uy-\frac{f}{2w^3}\cos N\theta\, u^2y-\frac{f}{6w^4}\sin N\theta\, u^3y, \tag{1.5}$$

where

$$a_y=-k+\frac{f^2}{2w^2[N^2-(k+1)]}\simeq -k+\frac{f^2}{2w^2N^2} \tag{1.6}$$

and

$$b_y=-f/w. \tag{1.7}$$

These equations restrict the theoretical analysis to a special class of FFAG accelerators, namely those which employ a sinusoidally varying median plane field with a small flutter factor (typically $f\approx 0.25$). The methods used are more general, of course, but all specific results will only be applicable to this case.

By changing variables, we may simplify the above equations; namely, let

$$\tau=\tfrac{1}{2}N\theta,\quad \rho=u/w,\quad \psi=y/w,\quad \lambda=f/wN^2, \tag{1.8}$$

in which case Eqs. (1.2) and (1.5) become

$$d^2\rho/d\tau^2+4[(a_x/N^2)+\lambda\cos 2\tau]\rho=-2\lambda\sin 2\tau\,\rho^2+\tfrac{2}{3}\lambda\cos 2\tau\,\rho^3 \tag{1.9}$$

and

$$d^2\psi/d\tau^2+4[(a_y/N^2)-\lambda\cos 2\tau]\psi=4\lambda\sin 2\tau\,\rho\psi-2\lambda\cos 2\tau\,\rho^2\psi-\tfrac{2}{3}\lambda\sin 2\tau\,\rho^3\psi. \tag{1.10}$$

Since the small amplitude "tune" σ_{x0} and σ_{y0} [betatron frequency phase change per sector[2] ($\sigma=2\pi\nu/N$, where ν is the number of betatron wavelengths about the circumference)] may be used to eliminate a_x/N^2 and a_y/N^2, it can be seen that all results are simply a function of the linear tune σ_{x0}, σ_{y0} and the parameter λ which may be thought of as a measure of the nonlinearities whose presence creates the coupling resonance. In particular, the y motion can be characterized by σ_{x0}, σ_{y0}, λ, and the amplitude of the x motion, A, expressed in units of $1/w$.

The theoretical analysis is carried out in Sec. III, where five distinct resonances are treated. Before that, we must develop approximate solutions to the nonlinear radial equation and a method of determining the regions of instability of the linear Hill equation which determines the y motion. These mathematical preliminaries are carried out in Sec. II. Although the methods are standard, this particular mathematical procedure may be of interest in that it should be useful in the analysis of the behavior of a variety of particle-handling devices.

B. Computational Studies

The results of the theoretical analysis are summarized in Sec. III F, and the subsequent sections of the paper are devoted to computational studies designed to test these predictions. This work falls into two classes, first a com-

[10] W. Walkinshaw, "A spiral ridged bevatron," A.E.R.E. Report, Harwell (1956, unpublished).

[11] G. Parzen, Midwestern Universities Research Association Report MURA-217 (1957, unpublished); G. Parzen, Midwestern Universities Research Association Report MURA-250 (1957, unpublished).

[12] H. Meier and K. R. Symon, *Proceedings of the CERN Symposium on High-Energy Accelerators, Geneva, 1959* (CERN, Geneva, 1959), p. 253.

[13] J. Moser, Nachr. Akad. Wiss. Göttingen, Math.-physik. Kl. IIa, No. 6, 87 (1955); J. Moser, Commun. Pure and Appl. Math. **8**, 409 (1955).

[14] F. T. Cole, Midwestern Universities Research Association Report MURA-95 (1955, unpublished). The change in sign of b_1 corrects an inadvertent error in this report.

putational study of the simplified equations[15] used in the theoretical analysis [essentially Eqs. (1.9) and (1.10)], and secondly a computational study of the exact equations of motion of a particle in a spiral sector accelerator.[16–21]

The computational study of the equations used in the theoretical analysis is given in Sec. IV, while Sec. V is devoted to the computational study of the equations governing a particle in an actual accelerator. These equations—involving as they do many more effects than are included in the simplified equations—lead to a poorer agreement with the theoretical analysis. The agreement is nevertheless sufficiently good to allow the use of the theoretical formulas as a guide in the design and analysis of accelerator behavior.

Analysis of the results was aided by computing, once per sector, the quantity K_y, which is the square root of a quadratic form which remains invariant for linear uncoupled motion. This quantity was taken to be

$$K_y \equiv (\xi y^2 + \eta y p_y + \zeta p_y^2), \tag{1.11}$$

where, in terms of the matrix

$$\begin{pmatrix} A & B \\ C & D \end{pmatrix}$$

which carries a particle through successive sectors from one homologous point to the next,

$$\xi = \frac{-C}{\sin^2\sigma}B, \quad \eta = \frac{A-D}{\sin^2\sigma}B, \quad \zeta = \frac{B^2}{\sin^2\sigma}. \tag{1.12}$$

The coefficients ξ, η, ζ, as well as the oscillation frequencies, were determined by preliminary short small-amplitude runs. Physically, for linear uncoupled motion, K_y represents the maximum value which y can attain at those homologous points for which the invariant K_y applies and so represents the *amplitude* of the motion at such points.

II. MATHEMATICAL PRELIMINARIES

In this section, certain mathematical properties of Eqs. (1.2) and (1.5) will be established. The results of this analysis are summarized in Sec. II E, and the reader who is willing to assume these results may skip to that section and then continue with the theoretical analysis of Sec. III.

Many of these results may be obtained by an alternative "smooth approximation" method which is described in reference 5, but not included in this paper.

A. Estimation of Stability Boundaries for a Mathieu Equation

To orient our analysis of Sec. II C, we outline here a variational method for determining the first few stability boundaries of the Mathieu equation

$$y'' + [a + b\cos N\theta]y = 0. \tag{2.1}$$

At stability boundaries, the differential equation admits a periodic solution such that, formally,

$$\delta \int_0^{4\pi/N} \tfrac{1}{2}[y'^2 - (a + b\cos N\theta)y^2]d\theta = 0. \tag{2.2}$$

(1) At the first stability boundary, corresponding[22] to ce_0 and for which $a=0$ when $b=0$, a suitable trial function is

$$y = A_0 + A_1 \cos N\theta. \tag{2.3}$$

Insertion of this trial function into the integral and setting the partial derivatives of the result (taken with respect to A_0, A_1) equal to zero leads to simultaneous linear homogeneous algebraic equations, which for a nontrivial solution require

$$2a(N^2 - a) + b^2 = 0. \tag{2.4}$$

For b small, one then obtains

$$\begin{aligned} a &\approx -b^2/(2N^2), \\ A_1/A_0 &\approx b/N^2, \end{aligned} \tag{2.5}$$

which are, of course, the initial terms of well-known series expansions.[22]

(2) At the second stability boundary, near $a=N^2/4$ and corresponding to ce_1, we take

$$y = B_1 \cos N\theta/2 + B_2 \cos 3N\theta/2 \tag{2.6}$$

as the trial function. One then obtains in a similar manner

$$\begin{aligned} a &\approx N^2/4 - b/2, \\ B_2/B_1 &\approx b/(4N^2). \end{aligned} \tag{2.7}$$

(3) At the third stability boundary, again near $a=N^2/4$ but corresponding to se_1, we take

$$y = C_1 \sin N\theta/2 + C_2 \sin 3N\theta/2. \tag{2.8}$$

In this case, one obtains

$$\begin{aligned} a &\approx N^2/4 + b/2, \\ C_2/C_1 &\approx b/(4N^2). \end{aligned} \tag{2.9}$$

(4) At the fourth stability boundary, near $a=N^2$ and corresponding to se_2, a suitable trial function may be

[15] J. N. Snyder, Midwestern Universities Research Association Report MURA-237 (1957, unpublished).
[16] L. Jackson Laslett, Midwestern Universities Research Association Report MURA-75 (1955, unpublished).
[17] L. D. Fosdick, Midwestern Universities Research Association Report MURA-226 (1957, unpublished).
[18] L. D. Fosdick, Midwestern Universities Research Association Report MURA-241 (1957, unpublished).
[19] L. Jackson Laslett and J. N. Snyder, Midwestern Universities Research Association Report MURA-222 (1957, unpublished).
[20] J. N. Snyder, Midwestern Universities Research Association Report MURA-231 (1957, unpublished).
[21] E. Z. Chapman, Midwestern Universities Research Association Report MURA-457 (1959, unpublished).

[22] Notation of E. T. Whittaker and G. N. Watson, *Modern Analysis* (Cambridge University Press, New York, 1927), Sec. 19.3. These authors use $16q$ in place of our coefficient b and take $N=2$.

taken of the form

$$y=D_1 \sin N\theta+D_2 \sin 2N\theta. \quad (2.10)$$

One obtains in this case

$$a\approx N^2-b^2/(12N^2),$$
$$D_2/D_1\approx b/(6N^2). \quad (2.11)$$

(5) At the other stability boundary near $a=N^2$, one may employ the trial function

$$y=E_0+E_1 \cos N\theta+E_2 \cos 2N\theta \quad (2.12)$$

to obtain

$$a\approx N^2+5b^2/(12N^2),$$
$$E_0/E_1\approx -b/(2a)\approx -b/(2N^2), \quad (2.13)$$
$$E_2/E_1\approx b/[2(4N^2-a)]\approx b/(6N^2).$$

It is of interest to note, from the results of this and the preceding subsection, that the stability boundaries are not symmetrically located about $a=N^2$.

Series expansions for all these various stability boundaries are, as has been noted, given in published texts.[22,23]

(6) A case involving a special *Hill equation* may also be considered here because of certain similarities to (4) and (5) above. The equation

$$y''+[\alpha+\beta \cos\omega\theta+\gamma \cos 2\omega\theta]y=0, \quad (2.14)$$

with β and γ considered small, will exhibit a narrow zone of instability for α near ω^2. When $\beta=0$, the equation is of the form considered in subsections (2) and (3) (with 2ω corresponding to N) and the width of the unstable region will be proportional to γ; when $\gamma=0$, the resonance in question is that considered in subsections (4) and (5) (with $\omega=N$) and the width will be proportional to β^2.

The corresponding result for the general case (β and γ both different from zero) may be obtained for circumstances in which β^2 and γ are of the same order of magnitude. The variational statement

$$\delta\int \tfrac{1}{2}\{y'^2-[\alpha+\beta \cos\omega\theta+\gamma \cos 2\omega\theta]y^2\}d\theta=0 \quad (2.15)$$

is used, with the trial functions

$$y=D_1 \sin\omega\theta+D_2 \sin 2\omega\theta,$$
$$y=E_0+E_1 \cos\omega\theta+E_2 \cos 2\omega\theta. \quad (2.16)$$

One then finds that instability will occur when $\alpha-\omega^2$ lies between

$$-\beta^2/(12\omega^2)+\gamma/2 \quad \text{and} \quad 5\beta^2/(12\omega^2)-\gamma/2. \quad (2.17)$$

B. Approximate Solution of a Mathieu Equation

We are again concerned with the Mathieu equation

$$y''+[a+b \cos N\theta]y=0, \quad (2.18)$$

seeking an approximate representation of the Floquet solutions and an estimate of the characteristic oscillation frequency. A simplification results if one imagines that the characteristic period of the solution and the period of the coefficient $\cos N\theta$ are commensurate in some (possibly large) interval and that the Floquet solution is accordingly periodic in this interval.

By the foregoing ruse we then again write

$$\delta\int \tfrac{1}{2}[y'^2-(a+b \cos N\theta)^2]yd\theta=0, \quad (2.19)$$

with the integral now covering a sufficient number of periods of the cosine coefficient that the periodicity of the solution in this interval may be exploited. Seeking a solution whose variation with θ is roughly that of $\cos\nu\theta$ or $\sin\nu\theta$, effective trial functions are

$$y=A_1 \cos\nu\theta+B_1 \cos(N-\nu)\theta+C_1 \cos(N+\nu)\theta \quad (2.20)$$

or

$$y=A_2 \sin\nu\theta+B_2 \sin(N-\nu)\theta+C_2 \sin(N+\nu)\theta. \quad (2.21)$$

We proceed to a solution of the problem by use of these trial functions under the supposition that ν is small in comparison to N, results containing this limitation being suitable for the present purposes.[24]

The first of the trial functions, when adjusted to make the integral stationary, leads to the simultaneous equations

$$\begin{aligned}
&(\nu^2-a)A_1 && -(b/2)B_1 && -(b/2)C_1 &&=0\\
&-(b/2)A_1 && +[(N-\nu)^2-a]B_1 && &&=0 \quad (2.22)\\
&-(b/2)A_1 && && +[(N+\nu)^2-a]C_1 &&=0.
\end{aligned}$$

Approximate solution of these equations gives

$$B_1\approx (b/2N^2)[1+(2\nu/N)]A_1,$$
$$C_1\approx (b/2N^2)[1-(2\nu/N)]A_1, \quad (2.23)$$

and

$$\nu^2\approx a+b^2/(2N^2), \quad (2.24)$$

this last relation being in agreement with the "smooth approximation" result.[2]

The second trial function, involving sine terms, leads similarly to

$$\begin{aligned}
&(\nu^2-a)A_2 && +(b/2)B_2 && -(b/2)C_2 &&=0,\\
&(b/2)A_2 && +[(N-\nu)^2-a]B_2 && &&=0, \quad (2.25)\\
&-(b/2)A_2 && && +[(N+\nu)^2-a]C_2 &&=0,
\end{aligned}$$

with approximate solutions identical in form to those for the cosine series, save for a change in sign for B_2. Thus, although the procedure employed is formally similar to that which can be used to find stability boundaries (cf. Sec.

[23] N. W. McLachlan, *Theory and Application of Mathieu Functions* (Clarendon Press, Oxford, England, 1947), Secs. 4.90–4.91.

[24] This problem has been extensively studied, and the reader is referred to the following references for more accurate solutions. L. Jackson Laslett and A. M. Sessler, Midwestern Universities Research Association Report MURA-252 (1957, unpublished); R. E. Mills, Midwestern Universities Research Association Report MURA-340 (1957, unpublished); G. Parzen, Midwestern Universities Research Association Report MURA-397 (1958,unpublished).

II A), the relations connecting ν, a, and b are *identical* for the two cases considered here and we may write the general approximate solution as an arbitrary linear combination of the two solutions

$$A_1[\cos\nu\theta+(b/N^2)\cos N\theta\cos\nu\theta+2b\nu/N^3\sin N\theta\sin\nu\theta] \quad (2.26)$$

and

$$A_2[\sin\nu\theta+(b/N^2)\cos N\theta\sin\nu\theta-2b\nu/N^3\sin N\theta\cos\nu\theta]; \quad (2.27)$$

viz:

$$y=A_y[\sin(\nu\theta+\epsilon)+(b/N^2)\sin(\nu\theta+\epsilon)\cos N\theta - (2b\nu/N^3)\cos(\nu\theta+\epsilon)\sin N\theta], \quad (2.28)$$

with

$$\nu^2\approx a+b^2/2N^2. \quad (2.29)$$

A detailed comparison of the approximate solution with a small-amplitude numerical solution of the exact (axial) equation of motion may be found in reference 5, where it is seen that for $\nu/N\approx 0.1$ the approximate solution is accurate to a few percent.

C. Stability Limits for a Hill Equation

We are concerned here with the differential equation

$$y''+[a+b\cos N\theta+(c/2)\cos(N-\nu_x)\theta \pm(c/2)\cos(N+\nu_x)\theta+d\cos\nu_x\theta]y=0, \quad (2.30)$$

where we presume that $p\equiv N/\nu_x$ may be regarded as a rational number and the coefficients c and d are regarded as small. For the work to follow, the differential equation is replaced by the variational statement

$$\delta\int\tfrac{1}{2}\{y'^2-[a+b\cos p\nu_x\theta+(c/2)\cos(p-1)\nu_x\theta \pm(c/2)\cos(p+1)\nu_x\theta+d\cos\nu_x\theta]y^2\}d\theta=0. \quad (2.31)$$

We then proceed to determine, in turn, stability boundaries near

$$\nu_x=2\nu_{y0},\quad \nu_x+2\nu_{y0}=N,\quad\text{and}\quad 2\nu_x+2\nu_{y0}=N.$$

(1a) The location of the first stability limit of interest here is determined by aid of the trial function

$$y=B_1\cos\nu_x\theta/2+B_2\cos3\nu_x\theta/2 +R_1\cos(2p-3)\nu_x\theta/2+P_1\cos(2p-1)\nu_x\theta/2 +P_2\cos(2p+1)\nu_x\theta/2+R_2\cos(2p+3)\nu_x\theta/2, \quad (2.32)$$

although, as will be seen, inclusion of the terms with coefficients B_2, R_1, and R_2 is unnecessary for the accuracy desired here. Insertion of this trial solution into the integral and formation of the appropriate derivatives leads to a complicated set of simultaneous equations. (See reference 5 for details.) Neglecting terms of second and higher order in c and d, and terms of order $d/(2p^2\nu_x^2)$ and $d/2N^2$ compared to unity, these equations may be solved to yield

$$P_1\approx\frac{b+c/2}{2p^2\nu_x^2}[1+1/p]B_1 \quad (2.33)$$

and

$$P_2\approx\frac{b\pm c/2}{2p^2\nu_x^2}[1-1/p]B_1 \quad (2.34)$$

as the dominant coefficients supplementing B_1 in Eq. (2.32). Furthermore, one obtains, if the ***upper sign*** is used,

$$\frac{\nu_x^2}{4}-\left(a+\frac{b^2}{2N^2}\right)\approx\frac{bc}{2N^2}+\frac{d}{2}. \quad (2.35)$$

If the *lower sign* is used, one obtains instead

$$\frac{\nu_x^2}{4}-\left(a+\frac{b^2}{2N^2}\right)\approx\frac{\nu_x bc}{2N^2}+\frac{d}{2}. \quad (2.36)$$

Since, by the results of Sec. II B, $\nu_{y0}^2\equiv a+b^2/(2N^2)$ represents the square of the frequency of the y oscillations for the case $c=d=0$, we may conveniently write

$$(\nu_x/2)^2-\nu_{y0}^2\approx bc/(2N^2)+d/2, \quad (2.37)$$

for the upper sign, and

$$(\nu_x/2)^2-\nu_{y0}^2\approx \nu_x bc/(2N^3)+d/2, \quad (2.38)$$

for the lower sign.

(1b) A second stability limit to the differential equation is similarly obtained in the same neighborhood by use of the trial function

$$y=C_1\sin\nu_x\theta/2+\cdots+Q_1\sin(2p-1)\nu_x\theta/2 +Q_2\sin(2p+1)\nu_x\theta/2+\cdots. \quad (2.39)$$

In this case, one finds

$$Q_1\approx-\frac{b-c/2}{2p^2\nu_x^2}[1+1/p]C_1,\qquad Q_2\approx\frac{b\mp c/2}{2p^2\nu_x^2}[1-1/p]C_1, \quad (2.40)$$

with the relation

$$\nu_{y0}^2-(\nu_x/2)^2\approx bc/(2N^2)+d/2, \quad (2.41)$$

for the upper sign, and

$$\nu_{y0}^2-(\nu_x/2)^2\approx \nu_x bc/(2N^3)+d/2 \quad (2.42)$$

for the lower sign.

The associated stability limits derived in subsections (1a) and (1b) for Eq. (2.30) may thus be summarized as follows:

$$|\nu_x^2-(2\nu_{y0})^2|\approx 2|bc/N^2+d|, \quad (2.43)$$

when the upper sign is taken, and

$$|\nu_x^2-(2\nu_{y0})^2|\approx 2|\nu_x bc/N^3+d| \quad (2.44)$$

when the lower sign applies.

(2a) An additional zone of instability occurs near $\nu_x+2\nu_{y0}=N$. We write for convenience $N=q\nu_0$ and $\nu_x=(q-1)\nu_0$, where $\nu_0\equiv N-\nu_x$. The equations

$$y''+[a+b\cos q\nu_0\theta+(c/2)\cos\nu_0\theta \pm(c/2)\cos(2q-1)\nu_0\theta+d\cos(q-1)\nu_0\theta]y=0 \quad (2.45)$$

or

$$\delta\int \tfrac{1}{2}\{y'^2-[a+b\cos q\nu_0\theta+(c/2)\cos\nu_0\theta \pm(c/2)\cos(2q-1)\nu_0\theta+d\cos(q-1)\nu_0\theta]y^2\}d\theta=0 \quad (2.46)$$

are then solved approximately by the trial function

$$y=E_1\cos\nu_0\theta/2+T_1\cos(2q-1)\nu_0\theta/2 +T_2\cos(2q+1)\nu_0\theta/2. \quad (2.47)$$

The following conditions are found to apply [for either sign of the coefficient of $\cos(2q-1)\nu_0\theta$]:

$$T_1\approx[(b+d)/(2q^2\nu_0^2)]E_1,\qquad T_2\approx[b/(2q^2\nu_0^2)]E_1, \quad (2.48)$$

and, again noting $\nu_{y0}^2=a+b^2/(2N^2)$,

$$(\nu_0/2)^2-\nu_{y0}^2\approx c/4+bd/(2N^2). \quad (2.49)$$

(2b) A similar result, with a reversal in sign of the entire right-hand side of the equation, can be obtained for the companion stability boundary if sine functions are used in place of cosine functions in the trial solution. We accordingly write

$$|\nu_0^2-(2\nu_{y0})^2|\approx|c+2bd/N^2|, \quad (2.50)$$

or

$$|(N-\nu_x)^2-(2\nu_{y0})^2|\approx|c+2bd/N^2|. \quad (2.51)$$

D. Estimate of the Characteristic Exponent in the Unstable Region of a Hill Equation

An approximate expression may be derived for the characteristic exponent μ, which characterizes the lapse-rate of an exponentially-growing solution in the unstable region of a Hill equation. For this purpose, we follow a procedure analogous to that described by McLachlan.[23]

We denote the even and odd characteristic solutions at the associated stability boundaries by $c(\theta)$ and $s(\theta)$, respectively. The solutions near the vertex of the zone of instability may then be written approximately as

$$y=e^{\pm\mu\theta}[Cc(\theta)\pm Ss(\theta)] \quad (2.52)$$

in place of representing the Floquet factor within the bracket by expansion in a complete orthogonal set of functions. Substitution of this solution into the differential equation

$$y''+f(a,\theta)y=0 \quad (2.53)$$

yields

$$Cc''(\theta)\pm Ss''(\theta)\pm2\mu[Cc'(\theta)\pm Ss'(\theta)] +[\mu^2+f(a,\theta)][Cc(\theta)\pm Ss(\theta)]=0. \quad (2.54)$$

The eigensolutions satisfy

$$c''+f(a_1,\theta)c=0,\quad s''+f(a_2,\theta)s=0, \quad (2.55)$$

and a_1 and a_2 are eigenvalues corresponding to the stability boundaries of the problem. Thus,

$$\pm2\mu[Cc'(\theta)\pm Ss'(\theta)]+C[\mu^2+a-a_1]c(\theta) \pm S[\mu^2+a-a_2]s(\theta)=0. \quad (2.56)$$

The coefficients of the even and odd functions in this approximate identity may be related by multiplying through by $c(\theta)$ and by $s(\theta)$ in turn and integrating, making use of the orthogonality of the (periodic) eigenfunctions which correspond to the two distinct eigenvalues a_1 and a_2. In this way, one obtains

$$C[\mu^2+a-a_1]\langle c^2\rangle+2\mu S\langle cs'\rangle=0,\qquad 2\mu C\langle sc'\rangle+S[\mu^2+a-a_2]\langle s^2\rangle=0, \quad (2.57)$$

where $\langle\,\rangle$ denotes that the average value is taken. An approximate solution of the resulting determinantal equation yields

$$\mu^2\approx-\frac{(a-a_1)(a_2-a)\langle c^2\rangle\langle s^2\rangle}{4\langle sc'\rangle\langle cs'\rangle}. \quad (2.58)$$

If the parameter "a" lies midway between the two eigenvalues a_1 and a_2, the lapse rate will thereby be maximized,

$$\mu_{\max}{}^2\approx-\frac{\langle c^2\rangle\langle s^3\rangle}{\langle sc'\rangle\langle cs'\rangle}\left[\frac{a_2-a_1}{4}\right]^2 \quad (2.59)$$

for $a=(a_1+a_2)/2$.

The foregoing expressions for μ^2 may readily be applied to estimate the lapse rates associated with the resonances which form the subject of this report, employing the estimates for their respective stability boundaries derived in Sec. II C. For the eigenfunctions $c(\theta)$ and $s(\theta)$, it is convenient merely to take the cosine and sine functions which constitute the dominant terms of the trial functions employed in estimating the stability boundaries.

E. Summary of Mathematical Results

We have established, in Sec. II, the following results, which are organized according to the section in which they have been established.

A. Estimation of Stability Boundaries for a Mathieu Equation

(1) For the Mathieu equation

$$y''+[a+b\cos N\theta]y=0, \quad (2.1)$$

regions of instability are

$a < -b^2/(2N^2)$, from Eq. (2.5);

$N^2/4 - b/2 < a < N^2/4 + b/2$, from Eqs. (2.7) and (2.9); (2.60)

$N^2 - b^2/(12N^2) < a < N^2 + 5b^2/(12N^2)$, from Eqs. (2.11) and (2.13).

(2) For the Hill equation

$$y'' + [\alpha + \beta \cos\omega\theta + \gamma \cos 2\omega\theta]y = 0, \tag{2.14}$$

a region of instability exists for α between

$$\omega^2 - \beta^2/(12\omega^2) + \gamma/2 \quad \text{and} \quad \omega^2 + 5\beta^2/(12\omega^2) - \gamma/2. \tag{2.17}$$

B. Approximate Solution of a Mathieu Equation

For the Mathieu equation

$$y'' + [a + b \cos N\theta]y = 0, \tag{2.18}$$

we take the solution to be, when ν/N is small,

$$y = A_y[\sin(\nu\theta + \epsilon) + (b/N^2)\sin(\nu\theta + \epsilon)\cos N\theta - (2b\nu/N^3)\cos(\nu\theta + \epsilon)\sin N\theta], \tag{2.28}$$

with

$$\nu^2 \approx a + b^2/(2N^2). \tag{2.24}$$

C. Stability Limits for a Hill Equation

Stability limits for the equation

$$y'' + [a + b\cos N\theta + (c/2)\cos(N - \nu_x)\theta \pm (c/2)\cos(N + \nu_x)\theta + d\cos\nu_x\theta]y = 0 \tag{2.30}$$

are found associated with zones of instability as follows:

(1) $$|\nu_x^2 - (2\nu_{y0})^2| \approx 2|(bc/N^2) + d|, \tag{2.43}$$

when the upper sign is taken;

$$|\nu_x^2 - (2\nu_{y0})^2| \approx 2|(\nu_x bc/N^3) + d|, \tag{2.44}$$

when the lower sign is taken.

(2) $$|(N - \nu_x)^2 - (2\nu_{y0})^2| \approx |c + (2bd/N^2)| \tag{2.51}$$

for either sign of the term which involves $\cos(N + \nu_x)\theta$.
(3) If ν_x is replaced by $2\nu_x$ in this last result, the equation

$$y'' + [a + b\cos N\theta + (c/2)\cos(N - 2\nu_x)\theta \pm (c/2)\cos(N + 2\nu_x)\theta + d\cos 2\nu_x\theta]y = 0 \tag{2.61}$$

has a zone of instability defined by

$$|(N - 2\nu_x)^2 - (2\nu_{y0})^2| \approx |c + (2bd/N^2)|. \tag{2.62}$$

D. Estimate of the Characteristic Exponent in the Unstable Region of a Hill Equation

Summary: The lapse rate, μ nepers/rad, characterizing unstable solutions of the differential equation

$$y'' + f(a,\theta)y = 0 \tag{2.53}$$

is given in terms of the eigenvalues a_1, a_2 and eigenfunctions $c(\theta)$, $s(\theta)$ associated with the boundaries of the unstable region

$$\mu^2 \approx -\frac{(a - a_1)(a_2 - a)\langle c^2\rangle\langle s^2\rangle}{4\langle sc'\rangle\langle cs'\rangle}, \tag{2.58}$$

$$\mu_{\max}^2 \approx -\frac{\langle c^2\rangle\langle s^2\rangle}{\langle sc'\rangle\langle cs'\rangle}\left[\frac{a_2 - a_1}{4}\right]^2. \tag{2.59}$$

III. THEORETICAL ANALYSIS

In this section we shall use the results of the previous section to analyze the behavior in the region of various coupling resonances. The various cases are treated in turn, and the results summarized in Sec. III F.

A. The $\sigma_x = 2\sigma_y$ Resonance

For the analysis of axial motion as affected by the relatively strong coupling resonance which prevails when σ_x lies in the neighborhood of $2\sigma_{y0}$, it is sufficient to characterize the radial motion by a linear equation in u and to represent the coupling by inclusion of the term of the form uy in the axial equation. The equations considered then are

$$u'' + [a_x + (f/w)\cos N\theta]u = 0, \tag{3.1a}$$

$$y'' + [a_y - (f/w)\cos N\theta - (f/w^2)(\sin N\theta)u]y = 0. \tag{3.1b}$$

The solution to the u equation is then given by the results of Sec. II B as

$$u = A\left[\sin\nu_x\theta + \frac{f}{wN^2}\sin\nu_x\theta\cos N\theta - 2\frac{f\nu_x}{wN^3}\cos\nu_x\theta\sin N\theta\right], \tag{3.2}$$

where we have dropped the phase shift for convenience. Substitution of this expression for u into the y equation and neglect of terms in $2N\theta$ then leads to

$$y'' + \left[a_y - (f/w)\cos N\theta - \frac{Af}{w^2}\sin\nu_x\theta\sin N\theta + \frac{Af^2\nu_x}{w^3N^3}\cos\nu_x\theta\right]y = 0. \tag{3.3}$$

This equation is of the form of that considered in the first part of Sec. II C1 with the lower sign, viz.,

$$y'' + [a + b\cos N\theta + c\sin\nu_x\sin N\theta + d\cos\nu_x\theta]y = 0, \tag{3.4}$$

for which the stability boundaries are given by

$$|\nu_x^2 - (2\nu_{y0})^2| = 2|(\nu_x bc/N^3) + d|. \tag{3.5}$$

With the identification

$$b = -f/w, \quad c = -Af/w^2, \quad d = Af^2\nu_x/w^3N^3, \tag{3.6}$$

the stability boundaries accordingly are given by

$$|\nu_x^2-(2\nu_{y0})^2|=4(f^2\nu_x/w^3N^3)|A| \qquad (3.7)$$

and the "threshold" amplitude for radial motion, above which y growth may occur, correspondingly by

$$|A|_{\text{thr}}=\frac{w^3N^3}{4f^2\nu_x}|\nu_x^2-(2\nu_{y_0})^2|$$

$$=\frac{1}{16}w\left(\frac{wN^2}{f}\right)^2\frac{N}{\nu_x}\left|\left(\frac{\sigma_x}{\pi}\right)^2-\left(2\frac{\sigma_{y0}}{\pi}\right)^2\right|. \qquad (3.8)$$

An estimate for the lapse-rate characterizing exponential growth in the unstable region is likewise obtainable directly from Eq. (2.58), Sec. II D

$$\mu^2=\frac{(a-a_1)(a_2-a)\langle c^2\rangle\langle s^2\rangle}{4\langle sc'\rangle\langle cs'\rangle}. \qquad (3.9)$$

Since the differences of "a" are identical to differences ν_{y0}^2 and, for the present purpose, the functions c and s may be taken as proportional to the cosine and sine of $\nu_x\theta/2$,

$$\mu=\{[\nu_{y0}^2-(\nu_{y0})_1^2][(\nu_{y0})_2^2-\nu_{y0}^2]/\nu_x^2\}^{\frac{1}{2}}$$

$$=\left\{\left[\frac{f^2\nu_x}{w^3N^3}A+\left(\nu_{y0}^2-\frac{\nu_x^2}{4}\right)\right]\right.$$

$$\left.\times\left[\frac{f^2\nu_x}{w^3N^3}A-\left(\nu_{y0}^2-\frac{\nu_x^2}{4}\right)\right]\Big/\nu_x^2\right\}^{\frac{1}{2}} \qquad (3.10)$$

$$=\frac{f^2}{w^3N^3}(A^2-A_{\text{thr}}^2)^{\frac{1}{2}}\text{ nepers/rad}$$

$$=2.73\left(\frac{f}{wN^2}\right)^2\frac{(A^2-A_{\text{thr}}^2)^{\frac{1}{2}}}{w}\text{ decades/sector.}$$

In particular the maximum lapse-rate, for a given amplitude A, is given by

$$\mu_{\max}=2.73\left(\frac{f}{wN^2}\right)^2\frac{A}{w}\text{ decades/sector.} \qquad (3.11)$$

B. The $\sigma_x+2\sigma_y=2\pi$ Resonance

An analytic treatment of small-amplitude axial motion in the case that $\sigma_x+2\sigma_y$ lies in the neighborhood of 2π may be based on the same differential equation as employed for discussion of the $\sigma_x=2\sigma_y$ resonance, namely

$$y''+\left[a_y-(f/w)\cos N\theta-\frac{Af}{w^2}\sin\nu_x\theta\sin N\theta\right.$$

$$\left.+\frac{Af^2\nu_x}{w^3N^3}\cos\nu_x\theta\right]y=0. \qquad (3.12)$$

In the present application it will be seen that the term involving $\cos\nu_x\theta$ in this last equation is of relatively small effect and hence that it would have been sufficient to make the substitution $u=A\sin\nu_x\theta$ in the original y equation.

We now refer to the results of Sec. II C, and in particular to Eq. (2.30) with stability limits as given by Eq. (2.51). We identify $b=-f/w$, $c=-Af/w^2$ [taking the lower sign in Eq. (2.30)], and $d=Af^2\nu_x/w^3N^3$. Note that the term in $2bd/N^2$ is negligible compared to c in Eq. (2.51), so that we find

$$|(N-\nu_x)^2-(2\nu_{y0})^2|\approx|c| \qquad (3.13)$$
$$=(f/w^2)|A|,$$

with the threshold amplitude then being explicitly

$$|A|_{\text{thr}}=(w^2/f)|(N-\nu_x)^2-(2\nu_{y0})^2|$$

$$=\frac{w}{4}\left(\frac{wN^2}{f}\right)\left|\left(2-\frac{\sigma_x}{\pi}\right)^2-\left(2\frac{\sigma_y}{\pi}\right)^2\right|. \qquad (3.14)$$

An estimate of the lapse-rate for y growth in the unstable region is again given by Eq. (2.58) with c and s now represented by circular functions of argument $(N-\nu_x)/2$. Accordingly

$$\mu=\left\{\left(\frac{f}{4w^2}A+\left[\nu_{y0}^2-\left(\frac{N-\nu_x}{2}\right)^2\right]\right)\right.$$

$$\left.\times\left(\frac{f}{4w^2}A-\left[\nu_{y0}^2-\left(\frac{N-\nu_x}{2}\right)^2\right]\right)\Big/(N-\nu_x)^2\right\}$$

$$=0.682\frac{f}{wN^2}\frac{1}{1-\nu_x/N}\frac{(A^2-A_{\text{thr}}^2)^{\frac{1}{2}}}{w}\text{ decades/sector.} \qquad (3.15)$$

The maximum μ, for a given amplitude A, is

$$\mu_{\max}=0.682\frac{f}{wN^2}\frac{1}{1-\nu_x/N}\frac{A}{w}\text{ decades/sector.} \qquad (3.16)$$

It is noted that for a *sum* resonance, such as the one considered here, ν_x and ν_y cannot both be arbitrarily small in comparison to N.

C. The $\sigma_x=\sigma_y$ Resonance

A narrow zone of instability would be expected to arise from a $\sigma_{x0}=\sigma_{y0}$ resonance, in analogy to the second zone of instability for Mathieu's equation. Since, however, the resonance is second order in its dependence on the u amplitude A,[25] a consistent analysis of the problem requires consideration of (i) possible contributions from the u^2y term in the y equation and (ii) supplementary terms, proportional to A^2, which will enter in uy when a solution to the *nonlinear* u equation is attempted. These features complicate the analytic work considerably, so we here undertake an approximate treatment, taking f/wN^2 and ν_x^2/N^2

[25] To emphasize the second-order nature of this resonance, it preferably should be designated $2\sigma_x=2\sigma_{y0}$.

to be small and employing for convenience at one point the "smooth-approximation" method.[2] [Curiously, retention of the u^2y term appears to affect noticeably the intermediate steps of the analysis but not, in the present approximation, the final result.] An analysis which does not employ the "smooth approximation" has been made and shown to lead to the same results as the treatment given here.

The equations with which we commence are, from Eqs. (1.2) and (1.5),

$$u''+[a_x+f/w\cos N\theta]u=-\tfrac{1}{2}(f/w^2)\sin N\theta\, u^2, \tag{3.17}$$

$$y''+[a_y-f/w\cos N\theta]y=(f/w^2)\sin N\theta\, uy - (f/2w^3)\cos N\theta\, u^2y. \tag{3.18}$$

The solution of the u equation is now taken to be of the form previously taken from Sec. II B for use in analyzing the $\sigma_{x0}=2\sigma_{y0}$ resonance (Sec. III A), but supplemented by additional terms, proportional to A^2, obtained therefrom by a perturbation procedure,

$$\begin{aligned} u=&\left[A\sin\nu_x\theta+\frac{f}{wN^2}\sin\nu_x\theta\cos N\theta - 2\frac{f\nu_x}{wN^3}\cos\nu_x\theta\sin N\theta\right]\\ &+\frac{fA^2}{4w^2N^2}\left[\sin N\theta-\cos 2\nu_x\theta\sin N\theta+4\frac{\nu_x}{N}\sin 2\nu_x\theta\cos N\theta\right]. \end{aligned} \tag{3.19}$$

For the purpose at hand we also take, then,

$$u^2\approx A^2\left[\sin^2\nu_x\theta+2\frac{f}{wN^2}\sin^2\nu_x\theta\cos N\theta - 4\frac{f\nu_x}{wN^3}\sin\nu_x\theta\cos\nu_x\theta\sin N\theta\right]. \tag{3.20}$$

In forming the coupling terms, we drop terms involving the sine or cosine of $2N\theta$ to obtain

$$\frac{f}{w^2}\sin N\theta\, u\approx\frac{f}{w^2}\left[A\sin\nu_x\theta\sin N\theta-\frac{f\nu_xA}{wN^3}\cos\nu_x\theta+\frac{fA^2}{8w^2N^2}-\frac{fA^2}{8w^2N^2}\cos 2\nu_x\theta\right] \tag{3.21}$$

and

$$\begin{aligned} -\frac{f}{2w^3}\cos N\theta\, u^2&\approx-\frac{1}{2}\frac{fA^2}{w^3}\left[\sin^2\nu_x\theta\cos N\theta+\frac{f}{wN^2}\sin^2\nu_x\theta\right]\\ &=-\frac{1}{2}\frac{fA^2}{w^3}\left[\sin^2\nu_x\theta\cos N\theta+\frac{f}{2wN^2}-\frac{f}{2wN^2}\cos 2\nu_x\theta\right]. \end{aligned} \tag{3.22}$$

The differential equation for y now becomes expressible in the form

$$y''+\left[\nu_{y0}^2-\frac{f^2}{2w^2N^2}+\frac{f^2A^2}{8w^4N^2}+\frac{f^2\nu_xA}{w^3N^3}\cos\nu_x\theta - \frac{f^2A^2}{8w^4N^2}\cos 2\nu_x\theta-\frac{f}{w}\cos\left(N\theta-\frac{A}{w}\sin\nu_x\theta\right)\right]y=0, \tag{3.23}$$

with the "smooth-approximation equivalent"[2]

$$y''+\left\{\nu_{y0}^2-\frac{f^2}{2w^2N^2}+\frac{f^2A^2}{8w^4N^2}+\frac{f^2\nu_xA}{w^3N^3}\cos\nu_x\theta - \frac{f^2A^2}{8w^4N^2}\cos 2\nu_x\theta+\frac{f^2}{2w^2N^2}\left(1-\frac{A\nu_x}{wN}\cos\nu_x\theta\right)^{-2}\right\}y=0 \tag{3.24}$$

or, recalling that ν_x^2 is negligible compared to N^2,

$$y''+\left\{\nu_{y0}^2+\frac{f^2A^2}{8w^4N^2}+2\frac{f^2\nu_xA}{w^3N^3}\cos\nu_x\theta - \frac{f^2A^2}{8w^4N^2}\cos 2\nu_x\theta\right\}y=0. \tag{3.25}$$

The stability boundaries near $\nu_x=\nu_{y0}$ for this last equation may now be obtained by appeal to the results of Sec. II A 6 in which the Eq. (2.14) was considered.

We set

$$\begin{aligned} &\omega=\nu_x &&\beta=2f^2\nu_xA/w^3N^3\\ &\alpha=\nu_{y0}^2+(f^2A^2/8w^4N^2) &&\gamma=-f^2A^2/8w^4N^2 \end{aligned} \tag{3.26}$$

and obtain from Eq. (2.17)

$$\begin{aligned} &\omega^2-\beta^2/(12\omega^2)+\gamma/2\leqslant\alpha\leqslant\omega^2+5\beta^2/(12\omega^2)-\gamma/2\\ &-\frac{3}{16}\frac{f^2A^2}{w^4N^2}\leqslant\nu_{y0}^2-\nu_x^2\leqslant-\frac{1}{16}\frac{f^2A^2}{w^4N^2}-\frac{3}{4}\left(\frac{f}{wN^2}\right)^2\left(\frac{A}{w}\right)^2\\ &\leqslant\left(\frac{\sigma_{y0}}{\pi}\right)^2-\left(\frac{\sigma_x}{\pi}\right)^2\leqslant-\frac{1}{4}\left(\frac{f}{wN^2}\right)^2\left(\frac{A}{w}\right)^2, \end{aligned} \tag{3.27}$$

the terms which arise from β^2 being neglected since they involve an additional factor $[f/(wN^2)]^2$.

This approximate result for estimating the stability boundaries associated with the $\sigma_x\approx\sigma_{y0}$ resonance suggests a relatively narrow zone of instability whose width is proportional to the *square* of the radial amplitude and which will be found exclusively for values of σ_{y0} *below* σ_x. Moreover, there thus appear to be two "threshold" amplitudes (for specified ν_x, ν_{y0}), an upper limit

$$|A_2|=4w\frac{wN^2}{f}\frac{(\nu_x^2-\nu_{y0}^2)^{\frac{1}{2}}}{N} =2w\frac{wN^2}{f}\left[\left(\frac{\sigma_x}{\pi}\right)^2-\left(\frac{\sigma_{y0}}{\pi}\right)^2\right]^{\frac{1}{2}} \tag{3.28}$$

and the more pertinent lower limit

$$|A_1| = (4/\sqrt{3})w\frac{wN^2}{f}\frac{(\nu_x^2-\nu_{y0}^2)^{\frac{1}{2}}}{N}$$

$$= (2/\sqrt{3})w\frac{wN^2}{f}\left[\left(\frac{\sigma_x}{\pi}\right)^2-\left(\frac{\sigma_{y0}}{\pi}\right)^2\right]^{\frac{1}{2}}. \quad (3.29)$$

The lapse-rate which characterizes exponential growth in the unstable region may be estimated from the result of Sec. II D, noting that the functions c and s are now primarily represented by cosine and sine functions of $\nu_x\theta$, and is conveniently expressed in terms of the threshold amplitude A_1,

$$\mu=\left\{\left[\frac{3}{16}\frac{f^2A^2}{w^4N^2}-(\nu_x^2-\nu_{y0}^2)\right]\right.$$

$$\left.\times\left[(\nu_x^2-\nu_{y0}^2)-\frac{1}{16}\frac{f^2A^2}{w^4N^2}\right]\Big/(4\nu_x^2)\right\}^{\frac{1}{2}}$$

$$=0.1477\left(\frac{f}{wN^2}\right)^2\frac{N}{\nu_x}\frac{[(A^2-A_1^2)(3A_1^2-A^2)]^{\frac{1}{2}}}{w^2}$$

$$\text{decades/sector.} \quad (3.30)$$

The maximum lapse-rate, for a given amplitude A, is then estimated to be

$$\mu_{\max}=0.085\left(\frac{f}{wN^2}\right)^2\frac{N}{\nu_x}\left(\frac{A}{w}\right)^2 \text{ decades/sector.} \quad (3.31)$$

D. The $2\sigma_x+2\sigma_y=2\pi$ Resonance

In an analysis of the resonance to be expected when $2\sigma_x+2\sigma_{y0}$ is close to 2π, the obvious term to invoke in the y equation is the u^2y term. It is necessary, however, also to consider the double-frequency ($2\nu_x$) terms which can enter the term in uy by virtue of supplementary terms in u obtainable by a perturbation solution of the nonlinear u equation. It will appear that the direct contribution from the u^2y term nonetheless definitely dominates.

The solution of the u equation is taken to be that employed previously in Sec. III C, namely Eq. (3.19). In forming $-\frac{1}{2}(f/w^3)(\cos N\theta)u^2$, the term of major importance in exciting the resonance of present interest is $\frac{1}{4}(fA^2/w^3)\cos 2\nu_x\theta\cos N\theta$, although the following terms might all be kept in mind:

$$-\frac{f}{2w^3}\cos N\theta\, u^2=-\frac{fA^2}{4w^3}\cos N\theta+\frac{fA^2}{4w^3}\cos 2\nu_x\theta\cos N\theta$$

$$-\frac{f^2A^2}{4w^4N^2}+\frac{f^2A^2}{4w^4N^2}\cos 2\nu_x\theta+\cdots. \quad (3.32)$$

Likewise, the following terms might be noted to arise from $(f/w^2)(\sin N\theta)u$:

$$\frac{f}{w^2}\sin N\theta\, u=\frac{f^2A^2}{8w^4N^2}-\frac{f^2A^2}{8w^4N^2}\cos 2\nu_x\theta. \quad (3.33)$$

With the foregoing expressions for the u-dependent terms, the differential equation for axial motion becomes

$$y''+[a+b\cos N\theta+c\cos 2\nu_x\theta\cos N\theta+d\cos 2\nu_x\theta]y=0, \quad (3.34)$$

where

$$a=a_y+\text{terms of order } \frac{f^2}{w^2N^2}\left(\frac{A}{w}\right)^2,$$

$$b=-\frac{f}{w}\left[1+\text{terms of order}\left(\frac{A}{w}\right)^2\right],$$

$$c=-\frac{f}{4w}\left(\frac{A}{w}\right)^2,$$

and

$$d \text{ is of order} \frac{f^2}{w^2N^2}\left(\frac{A}{w}\right)^2.$$

This equation is of the form considered in Sec. II C [see Eqs. (2.61) and (2.62)], for which the stability boundaries are represented by

$$|(N-2\nu_x)^2-(2\nu_{y0})^2|=\left|c+\frac{2bd}{N^2}\right|. \quad (3.35)$$

In this last relation, ν_{y0}^2 refers to the square of the y frequency when the coefficients c and d vanish; it differs, however, only by terms of order $(f^2/w^2N^2)(A/w)^2$ from the square of the y frequency for $A=0$. The factor $2bd/N^2$, moreover, is less than c by a factor of order $[f/(wN^2)]^2$. Regarding $f/(wN^2)$ as small in comparison to unity, we are thus led to the result which would have been obtained if only the term $\frac{1}{4}(fA^2/w^3)\cos 2\nu_x\theta\cos N\theta$ in the u^2 term had been retained,

$$|(N-2\nu_x)^2-(2\nu_{y0})^2|\approx\frac{f}{4w}\left(\frac{A}{w}\right)^2, \quad (3.36)$$

this result involving A *squared*, as was also the case for the $2\sigma_x=2\sigma_{y0}$ resonance treated in Sec. III C.

The threshold amplitude is correspondingly

$$|A|_{\text{thr}}=2w\left[\frac{w}{f}|(N-2\nu_x)^2-(2\nu_{y0})^2|\right]^{\frac{1}{2}}$$

$$=2w\left[\frac{wN^2}{f}\left|\left(1-\frac{\sigma_x}{\pi}\right)^2-\left(\frac{\sigma_{y0}}{\pi}\right)^2\right|\right]^{\frac{1}{2}}. \quad (3.37)$$

An estimate of the lapse-rate for the axial amplitude in the unstable region is given by Eq. (2.58) with c and s represented by circular functions of argument $(N-2\nu_x)/2$. Accordingly,

$$\mu=\left\{\left(\frac{fA^2}{16w^3}+\left[\nu_{y0}^2-\left(\frac{N}{2}-\nu_x\right)^2\right]\right)\right.$$

$$\left.\times\left(\frac{fA^2}{16w^2}-\left[\nu_{y0}^2-\left(\frac{N}{2}-\nu_x\right)^2\right]\right)\Big/(N-2\nu_x)^2\right\}^{\frac{1}{2}}$$

$$=0.17\frac{f}{wN^2}\frac{1}{1-2\nu_x/N}\frac{(A^4-A_{\text{thr}}^4)^{\frac{1}{2}}}{w^2}\text{ decades/sector.}\quad(3.38)$$

The maximum μ, for a given amplitude A, is then

$$\mu_{\max}=0.17\frac{f}{wN^2}\frac{1}{1-2\nu_x/N}\left(\frac{A}{w}\right)^2\text{ decades/sector,}\quad(3.39)$$

with a quadratic dependence on A.

E. The $3\sigma_x+2\sigma_y=2\pi$ Resonance

Examination of this fifth-order resonance is complicated by the need for an appropriate solution of the nonlinear radial equation. The resonance will be driven by terms in the y equation of frequencies $3\nu_x$, $3\nu_x\pm N$, $3\nu_x\pm 2N$, $\cdots$, and we keep only the dominant first three terms.

Solving the u equation [Eq. (1.2)] by perturbation theory and, dropping terms of order $(\nu_x/N)^2$ and $[f/(wN^2)]^2$ compared to unity, we obtain

$$u=A\left[\sin\nu_x\theta+\frac{f}{wN^2}\sin\nu_x\theta\cos N\theta-2\left(\frac{f}{wN^2}\right)\frac{\nu_x}{N}\cos\nu_x\theta\sin N\theta\right]$$

$$+\frac{fA^2}{4w^2N^2}\left[\sin N\theta-\sin N\theta\cos 2\nu_x\theta+\frac{4\nu_x}{N}\cos N\theta\sin 2\nu_x\theta\right]$$

$$+\frac{fA^3}{48w^3N^2}\left[\sin 3\nu_x\theta\cos N\theta-\frac{6\nu_x}{N}\cos 3\nu_x\theta\sin N\theta\right],\quad(3.40)$$

where certain secular terms have been dropped, and correspondingly, ν_x is the frequency associated with amplitude A rather than zero amplitude. (See reference 8 for a detailed derivation.) If this solution is inserted into the y equation [Eq. (1.5)] and terms of frequency $3\nu_x$ and $3\nu_x\pm N$ are retained, we obtain

$$y''+\left[a_y-\frac{f}{w}\cos N\theta+\frac{f^2A^3}{w^5N^3}\left(\frac{7\nu_x}{16}\right)\cos 3\nu_x\theta\right.$$

$$\left.-\frac{fA^3\sin 3\nu_x\sin N\theta}{24w^4}\right]y=0,\quad(3.41)$$

which, upon comparison with Eqs. (2.30) and (2.51), yields

$$|(N-3\nu_x)^2-(2\nu_{y0})^2|=\frac{fA^3}{24w^4}.\quad(3.42)$$

The threshold is consequently given by

$$A_{\text{thr}}=2w\left(\frac{3wN^2}{f}\right)^{\frac{1}{3}}\left|\left(1-\frac{3\sigma_x}{2\pi}\right)^2-\left(\frac{\sigma_{y0}}{\pi}\right)^2\right|^{\frac{1}{3}},\quad(3.43)$$

while use of Sec. II D yields for the lapse-rate

$$\mu=0.0284\left(\frac{f}{wN^2}\right)\frac{1}{1-3\nu_x/N}\left[\left(\frac{A}{w}\right)^6-\left(\frac{A_{\text{thr}}}{w}\right)^6\right]^{\frac{1}{2}}$$

$$\text{decades/sector,}\quad(3.44)$$

and a maximum lapse-rate for a given amplitude A of

$$\mu_{\max}=0.0284\left(\frac{f}{wN^2}\right)\frac{1}{1-3\nu_x/N}\left(\frac{A}{w}\right)^3$$

$$\text{decades/sector.}\quad(3.45)$$

A similar analysis could be made for the $3\sigma_x-2\sigma_y=2\pi$ *difference* resonance, but operating points in the neighborhood of this resonance line are considered to be of lesser interest for the design of FFAG accelerators and no computational results have been sought for such points.

F. Summary of the Theoretical Results

We have established in Sec. III the following results, which are organized according to the section in which they have been established.

A. The $\sigma_x=2\sigma_y$ Resonance

$$|A|_{\text{thr}}=\frac{1}{16}w\left(\frac{wN^2}{f}\right)^2\frac{N}{\nu_x}\left|\left(\frac{\sigma_x}{\pi}\right)^2-\left(2\frac{\sigma_{y0}}{\pi}\right)^2\right|,\quad(3.8)$$

$$\mu=2.73\left(\frac{f}{wN^2}\right)^2\frac{(A^2-A_{\text{thr}}^2)^{\frac{1}{2}}}{w}\text{ decades/sector,}\quad(3.10)$$

$$\mu_{\max}=2.73\left(\frac{f}{wN^2}\right)^2\frac{A}{w}\text{ decades/sector.}\quad(3.11)$$

B. The $\sigma_x+2\sigma_y=2\pi$ Resonance

$$|A|_{\text{thr}}=\frac{w}{4}\left(\frac{wN^2}{f}\right)\left|\left(2-\frac{\sigma_x}{\pi}\right)^2-\left(2\frac{\sigma_y}{\pi}\right)^2\right|,\quad(3.14)$$

$$\mu=0.682\frac{f}{wN^2}\frac{1}{1-\nu_x/N}\frac{(A^2-A_{\text{thr}}^2)^{\frac{1}{2}}}{w}$$

$$\text{decades/sector,}\quad(3.15)$$

$$\mu_{\max}=0.682\frac{f}{wN^2}\frac{1}{1-\nu_x/N}\frac{A}{w}\text{ decades/sector.}\quad(3.16)$$

C. The $\sigma_x=\sigma_y$ Resonance

$$|A_2|=2w\left(\frac{wN^2}{f}\right)\left[\left(\frac{\sigma_x}{\pi}\right)^2-\left(\frac{\sigma_{y0}}{\pi}\right)^2\right]^{\frac{1}{2}},\quad(3.28)$$

$$|A_1|=\frac{2}{\sqrt{3}}w\left(\frac{wN^2}{f}\right)\left[\left(\frac{\sigma_x}{\pi}\right)^2-\left(\frac{\sigma_{y0}}{\pi}\right)^2\right]^{\frac{1}{2}}, \quad (3.29)$$

$$\mu=0.1477\left(\frac{f}{wN^2}\right)^2\frac{N}{\nu_x}\frac{[(A^2-A_1^2)(3A_1^2-A^2)]^{\frac{1}{2}}}{w^2}$$

decades/sector, (3.30)

$$\mu_{\max}=0.085\left(\frac{f}{wN^2}\right)^2\frac{N}{\nu_x}\left(\frac{A}{w}\right)^2 \text{decades/sector.} \quad (3.31)$$

D. The $2\sigma_x+2\sigma_y=2\pi$ Resonance

$$|A|_{\text{thr}}=2w\left(\frac{wN^2}{f}\right)^{\frac{1}{2}}\left|\left(1-\frac{\sigma_x}{\pi}\right)^2-\left(\frac{\sigma_{y0}}{\pi}\right)^2\right|^{\frac{1}{4}}, \quad (3.37)$$

$$\mu=0.17\frac{f}{wN^2}\frac{1}{1-2\nu_x/N}\frac{(A^4-A_{\text{thr}}^4)^{\frac{1}{2}}}{w^2}$$

decades/sector, (3.38)

$$\mu_{\max}=0.17\frac{f}{wN^2}\frac{1}{1-2\nu_x/N}\left(\frac{A}{w}\right)^2 \text{decades/sector.} \quad (3.39)$$

E. The $3\sigma_x+2\sigma_y=2\pi$ Resonance

$$A_{\text{thr}}=2w\left(\frac{3wN^2}{f}\right)^{\frac{1}{4}}\left|\left(1-\frac{3\sigma_x}{2\pi}\right)^2-\left(\frac{\sigma_{y0}}{\pi}\right)^2\right|^{\frac{1}{4}}, \quad (3.43)$$

$$\mu=0.0284\left(\frac{f}{wN^2}\right)\frac{1}{1-3\nu_x/N}\left[\left(\frac{A}{w}\right)^6-\left(\frac{A_{\text{thr}}}{w}\right)^6\right]^{\frac{1}{2}}$$

decades/sector, (3.44)

$$\mu_{\max}=0.0284\left(\frac{f}{wN^2}\right)\frac{1}{1-3\nu_x/N}\left(\frac{A}{w}\right)^3$$

decades/sector. (3.45)

IV. COMPUTATIONAL STUDIES OF THE SIMPLIFIED EQUATIONS

In this section we shall describe certain computational studies which were made of the simplified equations used in the theoretical analysis. A more detailed description of this work can be found in reference 7, and the authors are indebted to Mr. Roger Mills for permission to use his results in this section. It will be seen that the agreement between the theoretical results and the computations is reasonably good; and the reader who is willing to accept these results may turn to the computational studies of the equations governing particle motion in an actual accelerator, as are described in Sec. V.

The various resonances studied in Sec. III will be treated in turn, with the exception of the high-order resonance $3\sigma_x+2\sigma_y=2\pi$ which was not subject to the study of this section.

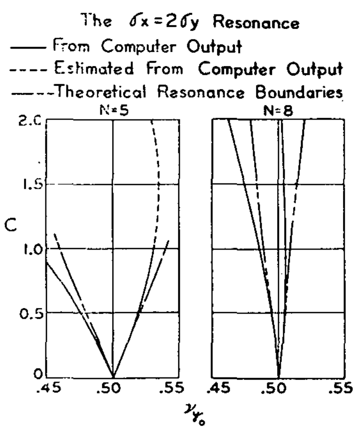

FIG. 1. Resonance boundaries in the region of $\sigma_x=2\sigma_y$, both theoretically predicted and according to computations employing the simplified equations used in the theoretical analysis.

A. The $\sigma_x=2\sigma_y$ Resonance

1. Equations

The theoretical treatment of this resonance (Sec. III A) employs the linear equation for the vertical motion

$$y''+[a+b\cos N\theta+c\sin\nu_x\theta\sin N\theta+d\cos\nu_x\theta]y=0 \quad (4.1)$$

with the resonance boundaries given (Sec. II C) by

$$\nu_{y0}^2=\left(\frac{\nu_x}{2}\right)^2-\frac{\nu_x bc}{2N^3}-\frac{d}{2},$$
$$\nu_{y0}^2=\left(\frac{\nu_x}{2}\right)^2+\frac{\nu_x bc}{2N^3}+\frac{d}{2}, \quad (4.2)$$

and a maximum lapse-rate obtained as in Sec. III A to be

$$\mu_{\max}=\frac{\pi}{N}\left|\frac{bc}{N^3}+\frac{d}{\nu_x}\right| \text{nepers/sector.} \quad (4.3)$$

The mathematical study was undertaken by identifying the parameters of Eq. (4.1) as

$$a=a_y,\ b=-f/w,\ c=-A_xf/w^2,\ d=A_x\nu_xf_2^2/(w^3N^3), \quad (4.4)$$

and then choosing $\nu_x=1$, $w=1/20$, $f=1/4$, and $N=5$ or 8, as would be characteristic of a model-size accelerator. The value of a was chosen so as to vary ν_{y0} through the resonance, while the amplitude A_x in effect was adjusted by the independent variable c.

2. Results

Figure 1 shows the portions of the stability diagrams for this resonance, and the theoretical boundaries. It can be seen that the resonance as described by the computer tends to "bend" toward lower values of ν_{y0} as c increases. However, when $c\lesssim 1$, the agreement is fairly good.

Because of the "bending," it would be expected that lapse-rate comparisons between theory and the output at the same ν_{y0} would be rather poor. Perhaps though, it is possible to compare the maximum theoretical and observed lapse-rates at a given value of c, and thus at least

TABLE I. Comparison between computational results employing simplified equations and theoretical predictions for the maximum lapse-rate, in the neighborhood of the $\sigma_x=2\sigma_y$ resonance, as a function of the coupling parameter c.

	c	μ_{max} (nepers/sector) Theoret	Obs
$N=5$	0	0	0
	0.5	0.0251	0.0283
	1.0	0.0503	0.0540
$N=8$	0	0	0
	1.00	0.0077	0.0079
	1.43	0.0110	0.0125
	1.83	0.0140	0.0153

get an upper limit on the lapse-rate. This comparison is shown in Table I, where it can be seen that the agreement is fairly good even when the "bending" has become pronounced.

B. The $\sigma_x+2\sigma_y=2\pi$ Resonance and the $2\sigma_x+2\sigma_y=2\pi$ Resonance

1. Equations

The theoretical treatment of these resonances employs the linear equation [Eq. (4.1)] with resonance boundaries for the first resonance given (Sec. II C 3) by

$$\begin{aligned}(2\nu_{y0})^2&=(N-\nu_x)^2-(c+2bd/N^2),\\(2\nu_{y0})^2&=(N-\nu_x)^2+(c+2bd/N^2).\end{aligned}\tag{4.5}$$

The maximum lapse-rate may be found as in Sec. III B, and is

$$\mu_{max}=\frac{\pi|c+2bd/N^2|}{2N(N-\nu_x)}\text{ nepers/sector.}\tag{4.6}$$

The second resonance yields the same results except for the substitution of $2\nu_x$ for ν_x and hence does not require a separate mathematical check.

The numerical study proceeded as in the previous section, with the variable c taken as the independent variable and the coefficients evaluated in terms of the same accelerator parameters.

2. Results

Figure 2 gives a comparison of the predicted and observed resonances, which is seen to be quite good. The maximum lapse-rates are compared in Table II.

C. The $\sigma_x=\sigma_y$ Resonance

1. Equations

The mathematical methods employed in the study of this resonance (Sec. III C) may be checked by starting with the equation

$$\begin{aligned}y''+[a_y-d+b\cos N\theta+c\cos\nu_x\theta+d\cos 2\nu_x\theta\\+e\sin\nu_x\theta\sin N\theta+g\sin^2\nu_x\theta\cos N\theta]y=0,\end{aligned}\tag{4.7}$$

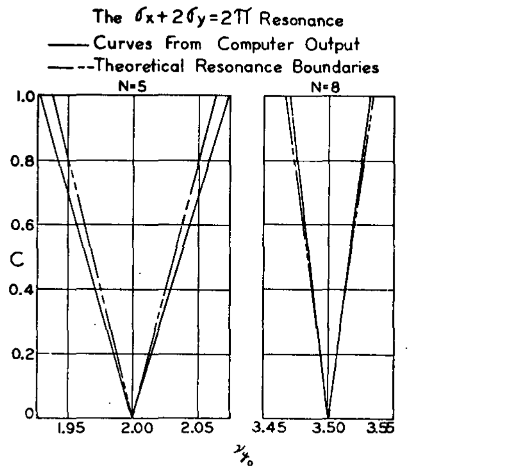

FIG. 2. Resonance boundaries in the region of $\sigma_x+2\sigma_y=2\pi$, both theoretically predicted and according to computations employing the simplified equations used in the theoretical analysis.

with the following conditions on the coefficients:

$$\begin{aligned}b&=-e^2/(2g),\\(c/\nu_x)^2&\ll|d|,\\ [e^3/(2gN^3)]^2&\ll|d|.\end{aligned}\tag{4.8}$$

It can be seen that, by making the identifications

$$\begin{aligned}b=-f/w,\quad c=f^2\nu_xA/(w^3N^3),\quad d=-f^2A^2/(8w^4N^2),\\e=-fA/w^2,\quad g=fA^2/(2w^3),\end{aligned}\tag{4.9}$$

and employing the fact that $A/w\ll1$, Eq. (4.7) is identical with Eq. (3.23); the latter formed the basis for the analysis of the $\sigma_x=\sigma_y$ resonance. That the inequalities of Eq. (4.8) are satisfied by the substitution of Eq. (4.9) may be easily seen to only require $[f/(wN^2)]^2<1$.

Analysis now proceeds by "smooth approximation", as was employed following Eq. (3.23), Sec. III C, to yield

$$y''+\left[\left(a_y-d+\frac{e^4}{8g^2N^2}\right)+\left(c-\frac{e^3\nu_x}{2gN^3}\right)\cos\nu_x\theta+d\cos 2\nu_x\theta\right]y=0.\tag{4.10}$$

TABLE II. Comparison between computational results employing simplified equations and theoretical predictions for the maximum lapse-rate, in the neighborhood of the $\sigma_x+2\sigma_y=2\pi$ resonance, as a function of the coupling parameter c.

	c	μ_{max} (nepers/sector) Theoret	Obs
$N=5$	0	0	0
	0.5	0.0393	0.0566
	1	0.0785	0.0976
$N=8$	0	0	0
	0.5	0.0140	0.0148
	1	0.0281	0.0292

TABLE III. Comparison between computational results employing simplified equations and theoretical preductions for the maximum lapse-rate, in the neighborhood of the $\sigma_x=\sigma_y$ resonance, as a function of the coupling parameter c.

	c	$\mu_{\max}$ (nepers/sector) Theoret	Obs
$N=5$	0	0	0
	0.3	0.000141	0.000138
	0.5	0.000392	0.000512
	1	0.00157	0.00165
	2	0.00628	0.0130
$N=8$	0	0	0
	0.5	0.000096	0.00006
	1	0.00038	0.00040
	2	0.00153	0.00169

Employing the relation $\nu_{y0}^2 \approx a_y + b^2/2N^2 = a_y + e^4/8g^2N^2$, and the results of Sec. II A 6 [Eq. (2.17)], we obtain [after use of Eq. (4.8)] for instability the condition

$$\nu_{y0}^2 \text{ lies between } \begin{cases} \nu_x^2+\frac{3}{2}d \\ \text{and} \\ \nu_x^2+\frac{1}{2}d. \end{cases} \tag{4.11}$$

This may be seen to agree with Eq. (3.27) after use of Eq. (4.9).

The maximum lapse rate is given by

$$\mu_{\max} = \frac{\pi|d|}{2\nu_x N} \text{ nepers/sector.} \tag{4.12}$$

2. Results

The numerical studies employed Eq. (4.7) with the identifications of Eq. (4.9) and the choice of parameters used in Sec. IV A. It can be seen that the inequalities are in fact satisfied, and the results are exhibited in Table III and Fig. 3.

V. COMPUTATIONAL STUDIES OF THE ACTUAL ACCELERATOR EQUATIONS

In this section we will describe some of the computational studies made of motion in spiral sector FFAG accelerators operated in the region of coupling resonances. A more detailed description of this work may be found in references 5, 6, and 9, and the authors are indebted to Mr. C. A. Lassettre for permission to use his results in this section. The various resonances studied will be treated in order, with most of the results exhibited in graphical and tabular form.

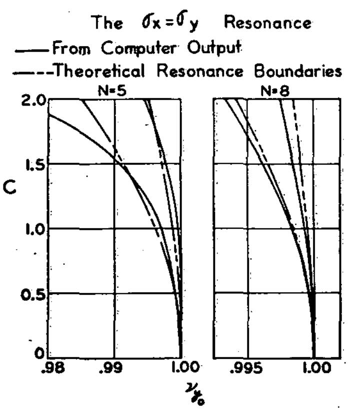

FIG. 3. Resonance boundaries in the region of $\sigma_x=\sigma_y$, both theoretically predicted and according to computations employing the simplified equations used in the theoretical analysis.

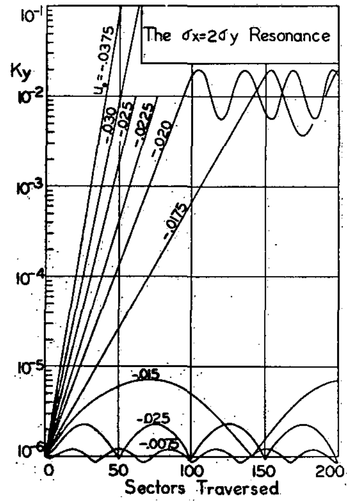

FIG. 4. Schematic graph illustrating y growth near $\sigma_x=2\sigma_y$. The parameters for this operating point are $k=0.668$, $1/w=19.6$, $f=\frac{1}{4}$, and $N=5$, resulting in $\sigma_x/\pi=0.5400$ and $\sigma_y/\pi=0.2365$. High frequency, small- amplitude components of K_y have been smoothed out.

In all of these studies, "runs" were made in which the computer was used to integrate the coupled equations of motion subject to the initial conditions $u_0'=y_0'=0$, while u_0 was varied, and y_0 taken to be very small. The small amplitude tunes were usually determined by auxiliary runs which were also used to determine the coefficients in the "y invariant" K_y (recall the discussion in Sec. I). The resulting K_y was plotted as a function of the number of sectors traversed, and a typical set of such runs is indicated in Fig. 4. In this figure we have smoothed K_y so as to remove small amplitude and wavelength fluctuations of the order of a few sectors. From these graphs, the amplitude of radial motion for which y growth is initiated may be determined,[26] as well as the lapse-rate of the motion in the

TABLE IV. Computational parameters used in the studies of the $\sigma_x=2\sigma_y$ resonance, and the resulting tunes. For this study $N=40$ and $f=\frac{1}{4}$, with a sinusoidal median plane field.

Point	$1/w$	k	σ_x/π	σ_y/π
1	896.0	26.52	0.2693	0.1106
2	901.3	26.32	0.2675	0.1170
3	906.6	26.12	0.2667	0.1232
4	910.2	25.99	0.2662	0.1271
5	913.7	25.85	0 2664	0 1309
6	917 3	25.72	0.2654	0.1347
7	920.8	25.59	0.2650	0.1382
8	924.4	25.45	0.2644	0.1420
9	927.9	25.32	0.2643	0.1454

[26] This may usually be done most accurately by determining the lapse-rate for various u amplitudes, and then plotting the lapse-rate against the radial amplitude and extrapolating to zero rate of growth.

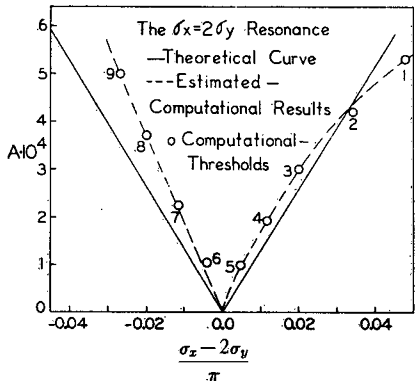

FIG. 5. A comparison between theoretical and computational studies in the neighborhood of $\sigma_x=2\sigma_y$. The graph shows the amplitude of radial motion at which y growth starts, as a function of "tune."

region of growth. Finally, plots are made of radial amplitude for initiation of y growth as a function of "tune."

It will be realized that the computational study of a resonance, especially as a function of machine parameters, is an extremely lengthy (and consequently expensive) process. Studies were limited to two ranges of parameters: models (typically with $k=0.7$, $1/w=20$, $f=\frac{1}{4}$, $N=5$), and full-scale accelerators (typically with $k=26$, $1/w=900$, $f=\frac{1}{4}$, $N=40$). The comparison between theory and experiment is a sensitive function of flutter—being good only for small f (the modifications of the basic equations are severe for f not small compared to unity), but is only slightly improved as N is increased. This is presumably because the nonscaling terms (which are ignored in the analysis, and decrease in importance as N increases) are not the major source of error.

A. The $\sigma_x=2\sigma_y$ Resonance

The threshold amplitudes found in a computational study of the $\sigma_x=2\sigma_y$ resonance in large accelerators, are

TABLE V. A comparison between theoretical and computational results for the lapse-rate in the neighborhood of the $\sigma_x=2\sigma_y$ resonance. The points refer to Table IV.

	$\frac{\sigma_x-2\sigma_y}{\pi}$	$u_0\times10^4$	μ_{obs} (decades/sector)	μ_{theoret} (decades/sector)
	0.0335	−10	0.0552	0.0438
Point 2		− 8	0.0634	0.0268
		− 6	0.0167	0.0132
	0.0120	−10	0.0544	0.0493
		− 8	0.0427	0.0390
Point 4		− 6	0.0304	0.0286
		− 4	0.0195	0.0176
	−0.0040	−10	0.0499	0.0511
		− 8	0.0386	0.0408
Point 6		− 6	0.0287	0.0304
		− 4	0.0188	0.0198
	−0.0196	−10	0.0464	0.0490
		− 8	0.0358	0.0375
Point 8		− 6	0.0231	0.0250
		− 4	0.0095	0.0085

TABLE VI. Computational parameters used in the studies of the $\sigma_x+2\sigma_y=2\pi$ resonance, and the resulting "tunes." For this study $N=40$ and $f=\frac{1}{4}$, with a sinusoidal median plane field.

Point	$1/w$	k	σ_x/π	σ_y/π
1	2395	30	0.3066	0.8681
2	2390	30	0.3064	0.8627
3	2385	30	0.3041	0.8575
4	2380	30	0.3043	0.8523
5	2375	30	0.3014	0.8474
6	2370	30	0.3017	0.8426
7	2365	30	0.3018	0.8379
8	2360	30	0.3021	0.8333
9	2355	30	0.3025	0.8288
10	2350	30	0.3031	0.8245

depicted in Fig. 5, where the semiquantitative agreement between the theoretical predictions and the computational results may be seen. The results for model size accelerators are similar.[5]

The parameters used in the computation are listed in Table IV. The comparison between computed and theoretical lapse-rates for full-size accelerators is presented in Table V.

B. The $\sigma_x+2\sigma_y=2\pi$ Resonance

Figure 6 summarizes the computational studies in large size accelerators. The parameters are listed in Table VI.

Comparison between computational and theoretical results for the lapse-rate are presented in Table VII. Similar results have been obtained for model size accelerators,[5] but are not included here.

C. The $\sigma_x=\sigma_y$ Resonance

The parameters of the computational studies are listed in Table VIII, while the computational results are depicted on Fig. 7. In Table IX we have compared the computational results with theory, for a few characteristic points.

With regard to the lapse-rate, we consider point 4 with $u=-0.000306$. The lapse-rate calculated from the theo-

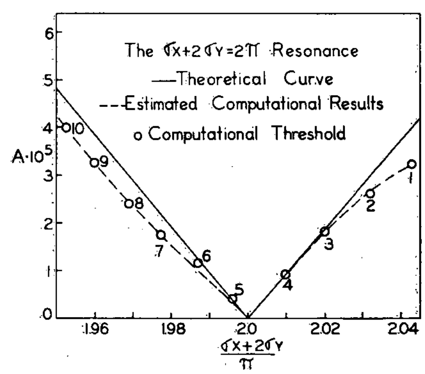

FIG. 6. A comparison between theoretical and computational studies in the neighborhood of $\sigma_x+2\sigma_y=2\pi$. The graph shows the amplitude of radial motion at which y growth starts, as a function of "tune."

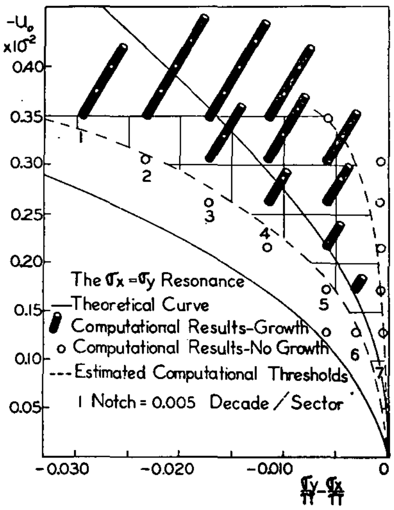

FIG. 7. Altitude chart of lapse-rate in the neighborhood of $\sigma_x=\sigma_y$ for $\sigma\approx 0.37\pi$. In this study, $f=\frac{1}{4}$, $N=50$, the median plane field is sinusoidal, $1/w=2500$, and k is given in Table VIII. In this graph the horizontal axis was shifted slightly to make the $\mu_0=0$ vertex of the unstable zone coincide with an abscissa of zero. This was necessary in view of small systematic errors in the computational determination of the "tune." One notch is 0.005 decades/sector.

retical estimate using the observed value of A_1, is 0.0157_6 decades/sector and the observed lapse-rate for this case is 0.0125 decades/sector.

We were surprised that an early computational search for the $2\sigma_x=2\sigma_y$ resonance with parameters characteristic of models ($N=5$) failed to reveal its presence. It may be that the search was misdirected because, as we now find, the zone of instability is associated with values of σ_y *considerably less* than σ_x; when the machine size becomes small, however, our basic equations are a less accurate description of the motion and the characteristics of a narrow resonance may depart significantly from the description in this report.

D. The $2\sigma_x+2\sigma_y=2\pi$ Resonance

In Table X are listed the parameters used in the computational study of this resonance, while Fig. 8 displays the results.

In Table XI we compare lapse-rates for two characteristic points.

It can be seen that for the higher order resonances the agreement between theory and computational results is decidedly poorer than for the lower order resonances. Presumably, this is due to the interaction between the lower order resonances and the one under study—an effect ignored in the theoretical analysis.

E. The $3\sigma_x+2\sigma_y=2\pi$ Resonance

Computational studies[6] of this resonance, for an accelerator with $f\approx 1$, indicated that the width of resonance varied with amplitude as expected theoretically, but with a numerical coefficient differing by a factor of ten from the

TABLE VII. A comparison between theoretical and computational results for the lapse-rate in the neighborhood of the $\sigma_x+2\sigma_y=2\pi$ resonance. The points refer to Table VI.

$(\sigma_x+2\sigma_y)/\pi$	$u_0\times 10^5$	μ_{obs} (decades/sector)	$\mu_{theoret}$ (decades/sector)
	−10.0	0.0959	0.0694
	− 9.0	0.0853	0.0619
	− 8.0	0.0760	0.0544
	− 7.0	0.0638	0.0467
2.0318	− 6.0	0.0532	0.0389
	− 5.0	0.0437	0.0307
Point 2	− 4.0	0.0300	0.0218
	− 3.0	0.0149	0.0107
	−10.0	0.0929	0.0709
	− 9.0	0.0822	0.0638
	− 8.0	0.0739	0.0566
	− 7.0	0.0635	0.0494
2.0089	− 6.0	0.0550	0.0422
	− 5.0	0.0453	0.0350
Point 4	− 4.0	0.0347	0.0278
	− 3.0	0.0243	0.0204
	− 2.0	0.0147	0.0127
	−10.0	0.0912	0.0706
	− 9.0	0.0818	0.0635
	− 8.0	0.0727	0.0565
	− 7.0	0.0625	0.0494
	− 6.0	0.0538	0.0423
1.9962	− 5.0	0.0444	0.0352
	− 4.0	0.0336	0.0280
Point 5	− 3.0	0.0248	0.0209
	− 2.0	0.0163	0.0136
	− 1.0	0.0070	0.0060
	−10.0	0.0862	0.0691
	− 9.0	0.0766	0.0620
	− 8.0	0.0682	0.0548
	− 7.0	0.0580	0.0476
1.9776	− 6.0	0.0502	0.0403
	− 5.0	0.0408	0.0329
Point 7	− 4.0	0.0292	0.0253
	− 3.0	0.0201	0.0172
	− 2.0	0.0086	0.0071

theoretical expectation. On the assumption that for a smaller flutter the agreement would be improved, extensive computations were undertaken for an accelerator with $f=\frac{1}{4}$. The increased agreement with theory more than justified this expectation, although the agreement when $f=\frac{1}{4}$ is still not as good as for the lower order resonances.

Parameters are listed in Table XII, and the results presented in Fig. 9.

In Table XIII are presented the results for the lapse-rate, as well as a comparison with the theoretical predictions.

TABLE VIII. For the study of the $\sigma_x=\sigma_y$ resonance $N=40$, $f=\frac{1}{4}$, $1/w=2500$, and k was chosen as indicated in the table. The resulting "tunes" are also tabulated.

Point	k	σ_{x0}/π	σ_{y0}/π
1	81.7	0.3854	0.3564
2	80.4	0.3826	0.357_7
3	79.1	0.379_8	0.362_9
4	77.8	0.376_9	0.366_1
5	76.5	0.3741	0.369_4
6	75.85	0.372_7	0.371_0
7	75.2	0.371_3	0.372_6

TABLE IX. For three of the points of Table VIII, a comparison is given between the theoretical and computed threshold amplitudes for y growth.

Point	$\frac{\sigma y_0}{\pi}$ $\frac{\sigma x_0}{\pi}$	$\lvert u_1\rvert_{\rm thr}$	$\lvert A_1\rvert_{\rm theoret}$
3	-0.0169	0.00028	0.00021
4	-0.0108	0.00023	0.00017
5	-0.0047	0.00018	0.00011

VI. DISCUSSION

In addition to the resonances reported here, for which positive evidence of y growth was obtained, operating points near $2\sigma_{x0}\approx 3\sigma_{y0}$ and others near $3\sigma_{x0}+\sigma_{y0}\approx 2\pi$ were also studied. These latter resonances (for which the coefficient of σ_{y0} is *odd*) showed no evidence of y growth, in agreement with theoretical expectations.

TABLE X. Computational parameters used in the studies of the $2\sigma_x+2\sigma_y=2\pi$ resonance, and the resulting "tunes." For this study $N=40$, and $f=\frac{1}{4}$, with a sinusoidal median plane field.

Point	$1/w$	k	σ_x/π	σ_y/π
1	2241	27.03	0.2982	0.7552
2	2233	26.72	0.2945	0.7516
3	2225	26.40	0.2915	0.7471
4	2217	26.09	0.2877	0.7431
5	2207	25.70	0.2890	0.7382
6	2196	25.31	0.2858	0.7328
7	2188	25.00	0.2809	0.7290
8	2180	24.69	0.2780	0.7252
9	2172	24.38	0.2752	0.7215
10	2157	23.81	0.2685	0.7146
11	2142	23.23	0.2611	0.7079

For the resonances treated in the present report, the computational results and the theoretical estimates are in fair agreement—generally within a factor of two. This agreement may be considered satisfactory at this stage in view of (i) the data inaccuracies associated with determining the small-amplitude oscillation frequencies and extrapolated thresholds, (ii) the approximations inherent in the analytic work. We would like to infer, therefore, that the equations presented in this report afford a semiquantitative account of the resonances considered,

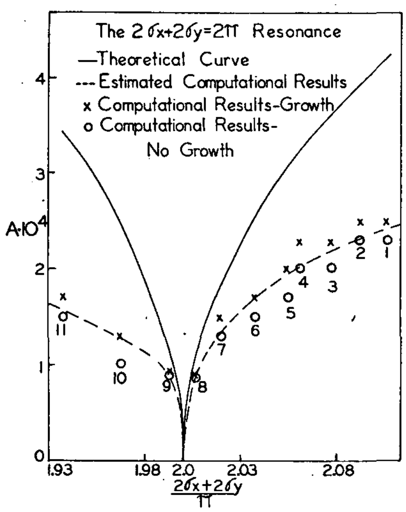

FIG. 8. A comparison between theoretical and computational studies in the neighborhood of $2\sigma_x+2\sigma_y=2\pi$. The graph shows the amplitude of radial motion at which y growth starts, as a function of "tune".

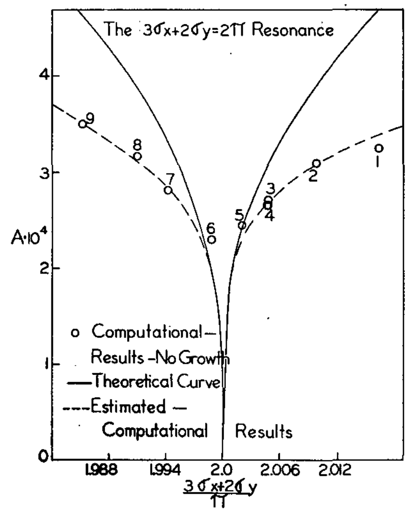

FIG. 9. A comparison between theoretical and computational studies in the neighborhood of $3\sigma_x+2\sigma_y=2\pi$. The graph shows the amplitude of radial motion at which y growth starts, as a function of "tune".

TABLE XI. A comparison between theoretical and computational results for the lapse-rate in the neighborhood of the $2\sigma_x+2\sigma_y=2\pi$ resonance. The points refer to Table X.

Point	$u_0\times 10^4$	$\mu_{\rm obs}$ (decades/sector)	$\mu_{\rm theoret}$ (decades/sector)
8	-2.0	0.0537	0.0149
	-1.8	0.0415	0.0120
	-1.6	0.0302	0.0093
	-1.4	0.0206	0.0068
	-1.2	0.0134	0.0046
	-1.0	0.0074	0.0023
9	-2.0	0.0555	0.0147
	-1.8	0.0439	0.0118
	-1.6	0.0334	0.0091
	-1.4	0.0241	0.0067
	-1.2	0.0170	0.0045

TABLE XII. Computational parameters used in the studies of the $3\sigma_x+2\sigma_y=2\pi$ resonance, and the resulting "tunes." For this study $N=40$ and $f=\frac{1}{4}$, with a sinusoidal median plane field.

Point	$1/w$	k	σ_x/π	σ_y/π
1	1695	69.2	0.4463	0.3387
2	1692	69.0	0.4447	0.3378
3	1688	68.7	0.4436	0.3369
4	1686	68.5	0.4438	0.3366
5	1684	68.3	0.4431	0.3363
6	1682	68.2	0.4425	0.3356
7	1678	67.9	0.4416	0.3347
8	1671	67.3	0.4414	0.3334
9	1664	66.7	0.4404	0.3320

TABLE XIII. A comparison between theoretical and computational results for the lapse-rate in the neighborhood of the $3\sigma_x+2\sigma_y=2\pi$ resonance. The points refer to Table XII.

Point	$u_0\times 10^4$	μ_{obs} (decades/sector)	$\mu_{theoret}$ (decades/sector)
1	−5.0	0.0659	0.0333
	−4.5	0.0474	0.0234
	−4.0	0.0294	0.0150
	−3.5	0.0136	0.0072
3	−4.0	0.0312	0.0164
	−3.8	0.0261	0.0138
	−3.6	0.0197	0.0114
	−3.4	0.0158	0.0091
	−3.2	0.0120	0.0070
6	−3.5	0.0195	0.0108
	−3.3	0.0159	0.0089
	−3.1	0.0128	0.0072
8	−4.5	0.0462	0.0219
	−4.0	0.0302	0.0142
	−3.5	0.0151	0.0073

when the median plane field has a sinusoidal variation characterized by a modest flutter factor ($f\approx\frac{1}{4}$, or smaller).

As was pointed out in the Introduction, the viewpoint taken in the analysis has been that a *prescribed u* oscillation is assumed for the radial motion and is introduced into a linear differential equation for y which is taken to characterize the axial oscillations. If large axial amplitudes are built up, the radial motion will certainly be affected, however, and the amplitude of radial oscillations has then been seen to decrease noticeably in certain cases.

It is of interest to extend this investigation, possibly with a more refined theoretical approach, to cases in which the flutter factor f is large (so that additional terms, which here could be considered negligible, become important) and to cases in which a significant harmonic content is present in the magnetic field (as for separated-sector structures). Theoretical efforts in this direction by Parzen[11] have had considerable success.

Interpretation of the "leveling off" which the y growth may exhibit (cf. Fig. 4) is beyond the scope of this work, but considerable progress in this direction has been made by Symon and co-workers[12] using the methods of Moser.[13] The danger that y growth arising from a difference resonance (which might be innocuous in itself, as is predicted by the theory) would aggravate the effects of other resonances is a subject needing further study. A brief report of such a study of the $\sigma_x=2\sigma_y$ resonance, correlated with observational experience acquired with a FFAG model has been reported elsewhere.[4]

Computations directed to a study of "turnover",[12] suggest questions concerning the ultimate stability of particles whose axial motion is subject to growth and exhibits turnover. The repeated rise and fall of y amplitude in such cases appears to conceal an ultimate instability which is observable only if undesirably protracted runs are made.

The phenomena discussed here of course have their analogues in "machine resonances," which may be engendered when misalignments are present. It would be desirable ultimately also to obtain a semiquantitative understanding of the corresponding effects produced by such imperfections, both in regard to their ability to excite machine resonances and with respect to their effect on the true stability or instability of orbits strongly affected by some inherent sector resonance. It may be noted that one can expect to encounter certain imperfection resonances whose analogous sector resonances are absent by virtue of median-plane symmetry, since in the presence of misalignments symmetry about the "median-plane" need no longer obtain.

ACKNOWLEDGMENTS

The authors are happy to have had the opportunity of discussing these phenomena at a very early stage of the investigation, with Dr. W. Walkinshaw. They wish to thank Dr. J. N. Snyder for his invaluable assistance with the computational phases of the work. They are indebted to Mr. Roger E. Mills and Mr. Carroll A. Lassettre for their extensive computational studies which have been incorporated into this paper. The authors wish to thank numerous members of the MURA Technical Group who have contributed to this work either through computational assistance, helpful conversations, or stimulating comments. Finally they wish to thank the Graduate College of the University of Illinois for liberal time allotments on the Illiac.

CHAPTER 5.3

STRONG FOCUSING IN CIRCULAR PARTICLE ACCELERATORS

L. Jackson Laslett

LAWRENCE RADIATION LABORATORY AND DEPARTMENT OF PHYSICS
UNIVERSITY OF CALIFORNIA, BERKELEY, CALIFORNIA

5.3.1. Introduction

High-energy particles are used for research in nuclear and elementary-particle physics, for tracer production, and for industrial and biomedical

Reprinted by permission of the Academic Press, from Focusing of Charged Particles, Albert Septier, Ed., Academic Press, Inc., Florida (1967), pp. 355-420.

applications of high-energy radiation. The desired high energies are imparted to such particles by means of particle accelerators, of which the chief types are (1) the linear accelerator, (2) the betatron, (3) the microtron, (4) the cyclotron, (5) the synchrocyclotron, and (6) the synchrotron. A connected discussion of several types of high-energy accelerators has been given by Livingood (1961) and Bruck (1966), and principles and techniques applicable to the design of synchrotrons and linear accelerators have been presented in detail by Livingston and Blewett (1962). Green and Courant (1959) have extensively reviewed specific proton synchrotrons, and Judd (1958) has given a broad discussion of several significant new concepts in accelerator design.

The principles of alternating-gradient focusing, frequently termed "strong focusing," can be applied advantageously to the design of accelerators of each of the aforementioned types, and only through the use of these principles has it proven practicable to design synchrotrons for the production of particles with energies of tens of GeV.[1] In this chapter we treat chiefly the application of strong focusing to high-energy synchrotrons, but many of the principles find a parallel application to other types of particle accelerators.

A. NATURE AND LIMITATIONS OF CONVENTIONAL SYNCHROTRONS

The synchrotron, in its most elementary form, employs a magnetic field throughout an annularly shaped region in order to guide and to focus the particles as they gain energy within the vacuum chamber of this accelerator. Energy is added to the particles by radio-frequency (rf) fields, applied to one or more drift-tube structures or developed within resonant cavities. The strength of the magnetic field is caused to rise during the acceleration, either by application of a pulsed wave form or by resonant excitation of the magnet circuit, so as to maintain a constant equilibrium-orbit radius for particles of increasing energy and momentum. The frequency of the rf fields increases concurrently in direct proportion to the angular velocity of the accelerated particles. Stability of energy oscillations about the energy

[1] 1 GeV = 10^9 eV. The highest energy weak-focusing proton synchrotrons in existence are the 10-GeV "synchrophasotron" at the Joint Institute for Nuclear Research, Dubna, U.S.S.R., and the 12.5-GeV "Zero-Gradient Synchrotron" at the Argonne National Laboratory, Lemont, Illinois. The latter accelerator actually is designed so that a uniform field is produced within the eight sectors that constitute the guide magnet ("zero gradient"), and supplemental focusing is introduced by "edge focusing" that results from the provision of slanting edges at the ends of each of these octant blocks.

that is appropriate to the frequency of the accelerating system at any instant results from the principle of phase stability discovered independently by Veksler (1944a, b, 1945) and McMillan (1945). An accurately programmed relationship between the rf frequency and the instantaneous strength of the magnetic guide field can be obviated by the use of a "phase lock" system that enables the accelerated groups of particles to control the rf system (Green and Courant, 1959, pp. 289-293).

A synchrotron is of the "constant-gradient" type if the focusing character of the field is the same at all azimuthal positions around the accelerator. The radial variation of the magnetic field normal to the median plane, at points in the neighborhood of a circular equilibrium orbit of radius R, is conveniently characterized in such a case by the "field index"

$$n = -\frac{R}{B}\frac{dB}{dR} \tag{1}$$

and the frequencies of small-amplitude radial and axial oscillations about the equilibrium orbit then are given in units of the orbital frequency by (Kerst and Serber, 1941)

$$Q_r \equiv f_r/f_0 = (1-n)^{1/2} \tag{2a}$$

$$Q_v \equiv f_v/f_0 = (n)^{1/2} \tag{2b}$$

respectively. It is seen that the requirement of stability with respect to motion in *both* transverse dimensions requires that $0 < n < 1$ and, hence, that Q_r and Q_v be less than unity. An angular spread, $\pm\,\delta\theta$, of a beam injected onto the equilibrium orbit, or an angular deflection resulting from a field error or similar misalignment, thus can lead to sinusoidal oscillations of an amplitude as great as

$$A = (R/Q)\,\delta\theta \tag{3}$$

More explicitly, an aperture of linear half width A could accommodate a beam whose emittance in position-angle phase space for one transverse degree of freedom is limited to an elliptical region of area

$$Y = \pi\,\delta r\,\delta\theta = \pi Q A^2/R \tag{4}$$

It is informative to consider the implications of Eq. (4) with respect to single-turn injection of a group of particles into a constant-gradient synchrotron. Thus, for example, if one planned to inject a beam that occupied, in the phase space of one transverse dimension, an area of $(2 \times 10^{-5})\pi$ radian·meter into an accelerator of 100-m radius and for which Q is approx-

imately $0.6^{1/2}$, the semiaperture allowance required to accommodate the free oscillations of this group of particles would be[2]

$$\begin{aligned} A &= (Y/\pi)^{1/2}R^{1/2}Q^{-1/2} \\ &= (2\times 10^{-5})^{1/2}(100)^{1/2}(0.6)^{-1/4} \\ &= 0.05 \text{ meter} \end{aligned}$$

In contrast, in a similar accelerator that employs the principles of alternating-gradient focusing (to be described in Section 5.3.3), a Q value some eight times greater can be practically realized. Despite the presence of a *flutter factor* in the free-oscillation amplitudes that arises from the kinematical orbit characteristics in an alternating-gradient structure and that typically may be approximately 1.5, the necessary aperture to be provided to accommodate these oscillations of the injected beam will be reduced to 40–50% of the value previously found.

A second important characteristic of an accelerator, which also affects directly the aperture required, the magnet dimensions, and hence the cost of construction and operation, is its ability to accommodate simultaneously particles of appreciably different momenta. Momentum variations not only occur because of the "synchrotron" oscillations in energy and phase that arise from the action of the rf fields, but also because such variations are present in the initially injected particles. The radial shift due to a prescribed fractional momentum deviation, $\delta p/p_0$ in a constant-gradient synchrotron is given directly by

$$\delta r = \frac{R}{1-n}\frac{\delta p}{p_0} \tag{5a}$$

$$= \frac{R}{Q_r^2}\frac{\delta p}{p_0} \tag{5b}$$

and, since $1-n$ or Q_r^2 cannot be large in such an accelerator, the aperture needed to accommodate a given energy spread may be undesirably great. Thus, for $\delta p/p = 2\times 10^{-3}$, $R = 100$ m, and $Q_r^2 = 0.4$, we obtain the quite large radial excursion

$$\delta r = 0.5 \text{ meter}$$

For an alternating-gradient synchrotron Eq. (5b) represents a good approximation to the mean deviation of the closed orbit, although again a

[2] Such an emittance might contain a substantial portion of the beam from a well designed and well aligned 50-MeV proton linear accelerator (AGS Staff, 1961).

flutter factor of 1.3 or greater will be present. Use of alternating-gradient focusing accordingly would afford a means for reducing the radial excursions due to momentum errors to about 2% of the value found for this example of a constant-gradient accelerator, and this property of the alternating-gradient technique may be regarded as its outstanding advantage in this application.

5.3.2. Use of Alternating-Gradient Focusing

The initial impetus to the present extensive use of alternating-gradient principles in the design of particle accelerators now operating or being planned arose from results of a study reported by Courant *et al.* (1952), of the Brookhaven National Laboratory, although application of similar principles had previously been proposed independently in a patent issued to Christofilos (1950). A constructive proposal to employ azimuthally varying fields in the design of cw (unmodulated) cyclotrons was made, however, as early as 1938 by Thomas (1938) and the analysis of Thomas was extended shortly thereafter by Schiff (1938), but the application of this work was not reported until the latter part of the 1950's (Pyle *et al.*, 1955; Kelly *et al.*, 1956; Heyn and Khoe, 1958). The "racetrack synchrotron" (Crane, 1946a, b), in which field-free "straight sections" were introduced, of course in principle involved a departure from the use of focusing that was strictly constant all along the particle orbit. Although this modification resulted in the occurrence of some additional potentially dangerous resonant relationships between the values of Q_r and Q_v (Blackman and Courant, 1949), the initial racetrack synchrotron remained a weak-focusing accelerator in that Q_r and Q_v were both less than unity. Concepts closely akin to those later employed in alternating-gradient theory also appeared in the work of Le Couteur (1951) in analyzing orbit dynamics in the regenerative deflector proposed by Tuck and Teng (1951) for the resonant extraction of particle beams from a circular accelerator such as the synchrotron.

5.3.3. Principles of Alternating-Gradient Focusing

As was shown by Courant *et al.* (1952), the limitations of a constant-gradient type of focusing can be removed if the field index is caused to vary with azimuthal position in a suitable manner so as to alternate between large positive and negative values. The ability of a periodic sequence of focusing

and defocusing magnetic lenses to produce a net focusing action may be visualized by considering the optical analogue of a series of lenses (Fig. 1). It is evident that a given trajectory will on the whole be a greater distance from the optic axis in the regions occupied by positive lenses, and hence may experience a net focusing under the action of the lens sequence.

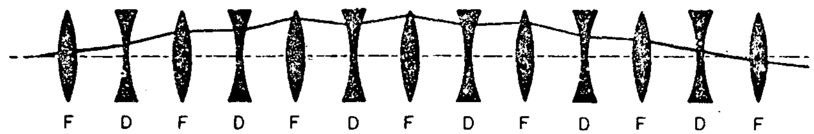

FIG. 1. Optical analogue of alternating-gradient focusing, showing a ray traversing a periodic sequence of focusing (F) and defocusing (D) lenses.

It remains to be discussed, however, what values of Q_r and Q_v in practice can be attained in this way, and what improvements in orbit characteristics can thereby be achieved. In the simplest application to a circular accelerator, the strong alternating lens action is provided by the spatial variation of the magnetic field that also serves to guide the particles on a circular orbit. A sequence of alternating-gradient lenses can be usefully introduced, however, to provide focusing action in a linear accelerator (or for beam transport generally), without introducing any bending in the trajectory of a particle moving along the axis of the system, and such separate magnetic lenses also have played an important role for the adjustment of orbit characteristics in cyclic accelerators and in the design of so-called "separated-function" accelerators or storage rings. Examples of such separated-function devices have been described by Amman *et al.* (1964) and by Ferger *et al.* (1964). Analogously, one can obtain alternating-gradient focusing action by means of suitably shaped *electric* fields, as was done in the "electron analogue" (Brookhaven Staff, 1955), constructed at the Brookhaven National Laboratory in preparation for work on a large proton synchrotron, and as has been proposed (Paul and Steinwedel, 1953; Taubert, 1957) for mass-spectrometry applications.

A. Equations of Motion

In analyzing orbit characteristics in a circular accelerator it is convenient to develop the equations for the trajectories by expansion about a closed equilibrium orbit, of circumference C_0 and local curvature $1/\varrho_0$, for a reference particle of momentum p_0. Distance along this curve will be denoted by s, and $R_0 = C_0/2\pi$ represents the effective radius of this equilibrium orbit.

For simplicity in the discussion we shall assume that the equilibrium orbit is planar, and employ $n(s) = -(\varrho_0/B_0)(dB/dr)$ to characterize the focusing that is provided by the spatial variation of the magnetic field [cf. Eq. (1)]. For particle momenta and field strengths that are constant or only slowly varying with time, the linear differential equations for the radial and vertical (axial) transverse displacements (x and y, respectively) for a particle of momentum $p = p_0 + \delta p$ then are[3]

$$\frac{d}{ds}\left(p_0 \frac{dx}{ds}\right) + \frac{1 - n(s)}{\varrho_0^2(s)} p_0 x = \frac{\delta p}{\varrho_0(s)} \tag{6a}$$

$$\frac{d}{ds}\left(p_0 \frac{dy}{ds}\right) + \frac{n(s)}{\varrho_0^2(s)} p_0 y = 0 \tag{6b}$$

As Adams (1953) has pointed out, however, it should be noted that the focusing coefficient which a strictly linear field presents to particles with a momentum different from p_0 will not be identical to that for an equilibrium particle (an effect that for relatively small variations of momentum may be represented by $n_{\text{eff}} \propto 1/p$ for $|n| \gg 1$)—this effect, not represented by the linearized equations (6a) and (6b), in practice may be compensated by the inclusion of sextupole lenses in the sequence of magnetic elements that constitute the accelerator.[4]

It follows from Eqs. (6a) and (6b) that the free transverse oscillations

[3] In static magnetic fields (in which the energy and mechanical momentum of an individual particle remain constant), the spatial differential equations for the trajectories may be obtained conveniently from the principle of least action,

$$\delta \int (\mathbf{p} + e\mathbf{A}) \cdot d\mathbf{s} = 0\,,$$

where $\mathbf{A}$ denotes the vector potential from which the magnetic field is derived. The possibility of linear coupling between the two transverse degrees of freedom normally would arise in practice only through the agency of misalignments or similar imperfections; such effects are not included in the equations presented in this subsection, but are extensively treated, for example, in Sect. 4c of an excellent monograph by Courant and Snyder (1958) on the theory of alternating-gradient synchrotrons.

[4] It will be noted that, in the case of a circular accelerator with no azimuthal variation of n, solution of Eqs. (6a) and (6b) will lead to simple-harmonic transverse oscillations of frequencies $\sqrt{1-n}\,f_0$ and $\sqrt{n}\,f_0$ in agreement with the expressions cited previously for Q_r and Q_v in such a case [Eqs. (2a, b)], and the equilibrium-orbit radius will change by $\delta x = [\varrho_0/(1-n)](\delta p/p_0)$ for off-momentum particles [as stated in Eq. (5a)]. Equations (6a) and (6b) also indicate that the transverse free-oscillation amplitudes of a particle whose momentum is caused to change in a magnetic field of gradually increasing strength will vary as $(\varrho_0/p_0)^{1/2}$; that is, the amplitudes will experience an adiabatic damping inversely proportional to the square root of the magnetic field strength.

1-146

of particles in an alternating-gradient synchrotron will be characterized by an equation of the form

$$\frac{d}{ds}\left(p_0 \frac{dx}{ds}\right) + p_0 K_x(s) x = 0 \tag{7}$$

or equivalently by

$$\frac{dp_x}{ds} = -p_0 K_x(s) x \tag{8a}$$

and

$$p_x = p_0 \frac{dx}{ds}\,, \tag{8b}$$

and by analogous equations for motion in the axial degree of freedom. The first-order equations (8a) and (8b) are derivable from a Hamiltonian function

$$H(x, p_x; s) = \frac{1}{2p_0} p_x^2 + \frac{1}{2} p_0 K_x(s) x^2 \tag{9}$$

with p_x and x constituting canonically conjugate variables that will be subject to Liouville's theorem (Judd, 1958, p. 193 ff.; Courant and Snyder, 1958, p. 45 ff.).[5]

Aside from possible slow secular variations, the focusing coefficient K_x (and the corresponding coefficient K_y) will be strictly a periodic function of s with a basic period equal to the circumference C_0. In practice a strong-focusing synchrotron will be designed so that *ideally*—in the absence of constructional errors, misalignments, and similar perturbations—the period of K_x and K_y will be a substantial submultiple N of C_0. Also in its simplest form [for example, as presented by Courant *et al.* (1952)], n vs s will be described by a rectangular graph, of period C_0/N, in which the positive and negative values may be of equal magnitude and cover equal intervals of s. Small regions devoid of focusing may occur periodically as field-free intervals between the magnet blocks, and additional lenses likewise may be introduced for correction or control at intervals of the magnet structure.[6] The functions $K_x(s)$ and $K_y(s)$ then will have a similar piecewise constant form, and, for $|n| \gg 1$, $K_x(s) \simeq -K_y(s)$.

[5] The result of Liouville's theorem applied to the x, p_x phase space for the uncoupled radial motion is related to the constancy of p_0 times the Wronskian of solutions to Eq. (7).

[6] The edge focusing that is produced by magnet blocks whose end faces are oblique to the equilibrium orbit would, in effect, be represented by such lenses.

B. General Characteristics of the Solution

Although the analysis of orbit characteristics is particularly direct, and most closely applicable to actual accelerators, for the case in which $K_x(s)$ and $K_y(s)$ are piecewise constant, some general results may be obtained without restriction to this particular functional form. We consider for this purpose the equation

$$\frac{d^2x}{ds^2} + K_x(s)x = 0 \tag{10}$$

that describes the free oscillations when we ignore the possible slow variation of p_0 in Eq. (7). Equation (10) has the form of Hill's equation, for which by Floquet's theorem (Whittaker and Watson, 1927, pp. 412–413),[7] a complete solution is

$$x = c_1 \exp(\mu s)\, \Phi(s) + c_2 \exp(-\mu s)\, \Psi(s) \tag{11}$$

where $\Phi(s)$ and $\Psi(s)$ are periodic in s with the period $L = C_0/N$ of $K_x(s)$. There thus exists a fundamental set of solutions, $v_1(s)$ and $v_2(s)$, such that

$$v_1(s + L) = \lambda_1 v_1(s) \tag{12a}$$

and

$$v_2(s + L) = \lambda_2 v_2(s) \tag{12b}$$

where $\lambda_1 = \exp(\mu L)$ and $\lambda_2 = \exp(-\mu L)$. The characteristic factors, λ_1 and λ_2, constitute a reciprocal pair—in addition, with $K_x(s)$ real, they either will be both real or will be a complex conjugate pair of absolute value unity.

The propagation of a particle trajectory through the accelerator structure can be conveniently expressed in terms of the fundamental set of solutions,

[7] In the special case that μ is zero or has an imaginary value such that $\exp(\mu C_0/N) = \pm 1$, one solution to Eq. (10) will be truly periodic and a second solution may be represented by a periodic function plus s times this first solution. We use the symbol μ here to denote the characteristic exponent, as indicated in Eq. (11), and we shall employ σ to represent $-i\mu L = -i\mu C_0/N$; in much of the published work on alternating-gradient accelerators, however, both μ and σ are used to denote this latter quantity. In the interest of brevity, we omit in these paragraphs the use of subscripts $_x$ or $_y$ that strictly should be appended to μ, σ, and similar quantities [such as the matrix $\mathbf{M}$ and the functions α, β, γ introduced subsequently in Eqs. (24a–c)] in order to distinguish between the properties of the free oscillations in the two transverse degrees of freedom.

$v_1(s)$, $v_2(s)$. In matrix notation[8] with primes denoting d/ds,

$$\begin{bmatrix} x \\ x' \end{bmatrix}_s = \begin{pmatrix} \dfrac{v_2'(s_0)v_1(s) - v_1'(s_0)v_2(s)}{W} & \dfrac{v_1(s_0)v_2(s) - v_2(s_0)v_1(s)}{W} \\ \dfrac{v_2'(s_0)v_1'(s) - v_1'(s_0)v_2'(s)}{W} & \dfrac{v_1(s_0)v_2'(s) - v_2(s_0)v_1'(s)}{W} \end{pmatrix} \cdot \begin{bmatrix} x \\ x' \end{bmatrix}_{s_0} \tag{13}$$

in which W denotes the (constant) Wronskian

$$W = v_1 v_2' - v_2 v_1' \tag{14}$$

and the determinant of the matrix will be seen to be unity. For an advance through *one period* of the structure

$$\begin{pmatrix} x \\ x' \end{pmatrix}_{s_0 + C_0/N} = \begin{pmatrix} \dfrac{\lambda_1 v_1 v_2' - \lambda_2 v_2 v_1'}{W} & (\lambda_2 - \lambda_1)\dfrac{v_1 v_2}{W} \\ (\lambda_1 - \lambda_2)\dfrac{v_1' v_2'}{W} & \dfrac{\lambda_2 v_1 v_2' - \lambda_1 v_2 v_1'}{W} \end{pmatrix} \begin{pmatrix} x \\ x' \end{pmatrix}_{s_0} \tag{15}$$

with v_1, v_2, and their derivatives evaluated at s_0. It is noted that the trace of the matrix appearing in Eq. (15) is the invariant $\lambda_1 + \lambda_2$ and its absolute value will be less than 2 if and only if the characteristic factors are complex. In addition, denoting the matrix in Eq. (15) by $\mathbf{M}$, it follows that[9]

$$\frac{dM_{1,1}}{ds_0} = M_{1,2}(s_0)K_x(s_0) + M_{2,1}(s_0) \tag{16a}$$

$$\frac{dM_{1,2}}{ds_0} = M_{2,2}(s_0) - M_{1,1}(s_0) \tag{16b}$$

$$\frac{dM_{2,1}}{ds_0} = [M_{2,2}(s_0) - M_{1,1}(s_0)]K_x(s_0) \tag{16c}$$

$$\frac{dM_{2,2}}{ds_0} = -[M_{1,2}(s_0)K_x(s_0) + M_{2,1}(s_0)] \tag{16d}$$

[8] Since, for a given solution, the values of x and x' at successive values of s are related by a sequence of linear algebraic transformations, it will be seen that matrix algebra will be applicable.

[9] Equations (16a–d) may be established directly, using Eq. (10) and the periodicity of $K_x(s)$, by developing the first-order relation

$$\begin{pmatrix} 1 & \delta s \\ -K_x(s_0)\delta s & 1 \end{pmatrix} \begin{pmatrix} M_{1,1}(s_0) & M_{1,2}(s_0) \\ M_{2,1}(s_0) & M_{2,2}(s_0) \end{pmatrix}$$
$$= \begin{pmatrix} M_{1,1}(s_0) + \delta M_{1,1} & M_{1,2}(s_0) + \delta M_{1,2} \\ M_{2,1}(s_0) + \delta M_{2,1} & M_{2,2}(s_0) + \delta M_{2,2} \end{pmatrix} \begin{pmatrix} 1 & \delta s \\ -K_x(s_0)\delta s & 1 \end{pmatrix}$$

It in turn follows from Eqs. (10) and (16 a–d) that the quadratic form

$$I^2 = M_{1,2}x'^2 + (M_{1,1} - M_{2,2})xx' - M_{2,1}x^2 \tag{17}$$

remains invariant throughout the motion of any given particle.

1. *Phase-Amplitude Variables*

The relations expressed by Eqs. (13) and (15) can be expressed conveniently in terms of solutions to Eq. (10) expressed in a "phase-amplitude" form that was introduced by Courant and Snyder (1958) and that has been widely employed in the analysis of alternating-gradient accelerators. Since we shall be concerned with the representation of *stable* solutions to Eq. (10), we shall employ the quantity

$$\begin{aligned}\sigma &= -i\mu C_0/N \\ &= -i\mu L\end{aligned} \tag{18}$$

in preference to μ. By defining

$$w = \left(\frac{2}{i}\,\frac{v_1v_2}{W}\right)^{1/2} \tag{19a}$$

and

$$\psi = \frac{i}{2}\ln\frac{v_2}{v_1} \tag{19b}$$

one finds that the expressions

$$w\exp(\pm i\psi) = \begin{cases}\left(\dfrac{2}{iW}\right)^{1/2} v_1 & \text{(20a)}\\[2ex] \left(\dfrac{2}{iW}\right)^{1/2} v_2 & \text{(20b)}\end{cases}$$

provide a form in which the fundamental set of solutions may be expressed.

The amplitude function, $w(s)$, is a periodic function of s with the period L of $K_x(s)$, and the phase function, $\psi(s)$, will increase by σ in this interval. It follows that $w^2\psi'$ is a constant with the normalization of w so chosen that

$$w^2\psi' = 1\,, \tag{21a}$$

and w satisfies the differential equation

$$w'' + K_x(s)w - \frac{1}{w^3} = 0 \tag{21b}$$

By noting from Eq. (21 a) that ψ' must be periodic, it is also seen that one may write

$$\psi = \sigma\frac{s}{L} + \chi(s) \tag{22}$$

where $\chi(s)$ is periodic (period L).

The matrix $\mathbf{M}$ of Eq. (15) now may be written as

$$\mathbf{M} = \begin{bmatrix}\cos\sigma + \alpha\sin\sigma & \beta\sin\sigma \\ -\gamma\sin\sigma & \cos\sigma - \alpha\sin\sigma\end{bmatrix}, \tag{23}$$

in which α, β, and γ are periodic functions of s_0 given by

$$\alpha = -w\,w' \tag{24a}$$

$$\beta = w^2 = \frac{1}{\psi'} \tag{24b}$$

$$\gamma = \frac{1+\alpha^2}{\beta} = \frac{1}{w^2} + w'^2 \tag{24c}$$

and the invariant quantity $\cos\sigma$ is one half the trace of $\mathbf{M}$. The relations (16 a–d) imply that

$$\alpha' = K_x \cdot \beta - \gamma \tag{25a}$$

$$\beta' = -2\alpha \tag{25b}$$

and

$$\gamma' = 2K_x \cdot \alpha \tag{25c}$$

Similarly, the invariant quadratic form of Eq. (17) becomes

$$I^2 = [\beta x'^2 + 2\alpha xx' + \gamma x^2]\sin\sigma \tag{26}$$

The form of $\mathbf{M}$ given in Eq. (23) is convenient in that

$$\mathbf{M}^m = \begin{bmatrix}\cos m\sigma + \alpha\sin m\sigma & \beta\sin m\sigma \\ -\gamma\sin m\sigma & \cos m\sigma - \alpha\sin m\sigma\end{bmatrix} \tag{27}$$

and affords a useful representation of the matrix that serves to propagate particle trajectories from s_0 through m periods of the accelerator structure. The general matrix that appears in Eq. (13) may also be expressed in terms of w and w', determined at the points s and s_0, and the difference $\psi(s) - \psi(s_0)$ between the phase function at these two points.

It is evident from Eqs. (17) or (26) that x and x' for any given particle trajectory will describe an ellipse if plotted for homologous points of the accelerator, since the coefficients α, β, and γ assume identical values at points separated by an integral number of periods. The area of this ellipse in x, x' space ($1/p_0$ times the area of the corresponding ellipse in x, p_x phase space), or of such an ellipse at any point along the trajectory, is $\pi I^2/\sin\sigma$. At any given s the maximum value of x for a point on this ellipse is $(\beta/\sin\sigma)^{1/2}I$, with β evaluated at s, and x would not exceed $(\beta_{\max}/\sin\sigma)^{1/2} I$ at *any* point along the orbit. The aperture allowance that must be provided to accommodate the free oscillations of a particle beam of specified emittance thus will be directly related to the maximum value of $\beta(s)$ for the transverse degree of freedom under consideration. [Note, from Eq. (25b), that $\beta(s)$ has its maximum and minimum values at points for which $\alpha(s) = 0$.]

2. *Angle-Action Variables*

The s-dependence of the focusing coefficient, $K_x(s)$, in Eq. (10) may be formally eliminated by a canonical transformation to "angle-action variables" (φ, J) through use of the generating function (Goldstein, 1950)

$$F(x, J; s) = \left[\sin^{-1}\frac{x}{(2\beta J)^{1/2}} - \chi\right] J + \frac{x}{2\beta}(2\beta J - x^2)^{1/2} - \frac{\alpha}{2\beta}x^2 . \quad (28)$$

1-149

The new variables are, in terms of x and x',[10]

$$J = \tfrac{1}{2}[\beta x'^2 + 2\alpha x x' + \gamma x^2] \quad (29a)$$

$$\varphi = \tan^{-1}\left(\frac{x}{\alpha x + \beta x'}\right) - \chi , \quad (29b)$$

with the new Hamiltonian function

$$\bar{H}(\varphi, J; s) = \frac{\sigma}{L} J . \quad (29c)$$

Then

$$\varphi' = \frac{\partial \bar{H}}{\partial J} = \frac{\sigma}{L}, \quad \text{so} \quad \varphi = \frac{\sigma}{L}s + \text{const} \quad (30a)$$

and

$$J' = -\frac{\partial \bar{H}}{\partial \varphi} = 0, \quad \text{so} \quad J \text{ is constant.} \quad (30b)$$

The angle variable φ, thus is a *linear* function of s, increasing by σ when s increases by $L = C_0/N$ and by $N\sigma = 2\pi Q_x$ for a complete circuit of the accelerator.

[10] It is seen that J is $1/(2\sin\sigma)$ times the invariant I^2 of Eq. (26).

An alternative transformation for eliminating the s-dependence in the differential equation for *one* of the transverse degrees of freedom employs a "scaling" of both the dependent and independent variables (cf. Courant and Snyder, 1958, p. 18),

$$\eta = \frac{1}{\sqrt{\beta}} x \quad (31a)$$

$$\psi = \int^s \frac{ds}{\beta} \quad (31b)$$

so that Eq. (10) becomes

$$\frac{1}{\beta^{3/2}}\left[\frac{d^2\eta}{d\psi^2} + \eta\right] = 0 \quad (32)$$

The solutions η thus will be simple-harmonic in the variable ψ, with the argument of the circular functions increasing by σ in a single period and by $N\sigma = 2\pi Q_x$ in an entire revolution. Transformations related to those just presented can be of value in extending the analysis of alternating-gradient systems to situations in which nonlinear restoring forces are present.

C. Solutions for Piecewise-Constant Focusing Factor

In the application of alternating-gradient principles to the design of high-energy synchrotrons, the most practical and most common form for the function $n(s)$ is such that this quantity alternates, in equal intervals of s, between large positive and negative values of equal magnitude, provided we ignore the presence of shorter field-free sections $n(s) = 0$ between the individual magnet blocks. The coefficients $K_x(s)$ and $K_y(s)$ then each have the form of a rectangular wave, and will alternate between values of equal magnitude if we neglect the difference between $1 - n(s)$ and $-n(s)$. The stability regions for solutions to such an equation were derived in an early paper by van der Pol and Strutt (1928) and in the previously cited work of Courant *et al.* (1952).

Since the particle trajectories are describable by simple circular or hyperbolic functions within the individual regions of constant $n(s)$, individual matrices are readily formed to represent the traversal of any portion of such a region, and the matrix **M** that characterizes traversal of a full period may be obtained by matrix multiplication. One thus finds, with s measured from the center of an interval wherein there is positive focusing for the degree of freedom under consideration, elements of **M** such that

$$\cos\sigma = \cosh\pi\frac{|n|^{1/2}}{N}\cos\pi\frac{|n|^{1/2}}{N} \tag{33a}$$

$$\alpha = \frac{\sinh\pi\dfrac{|n|^{1/2}}{N}\sin 2\dfrac{|n|^{1/2}s}{\varrho_0}}{\sin\sigma} \qquad -\frac{C_0}{4N} \le s\left(\mathrm{mod}\,\frac{C_0}{N}\right) \le \frac{C_0}{4N}$$

$$= \frac{\sin\pi\dfrac{|n|^{1/2}}{N}\sinh 2|n|^{1/2}\left(\dfrac{\pi}{N}-\dfrac{s}{\varrho_0}\right)}{\sin\sigma} \qquad \frac{C_0}{4N} \le s\left(\mathrm{mod}\,\frac{C_0}{N}\right) \le \frac{3C_0}{4N} \tag{33b}$$

$$\beta = \frac{\varrho_0}{|n|^{1/2}}\,\frac{\cosh\pi\dfrac{|n|^{1/2}}{N}\sin\pi\dfrac{|n|^{1/2}}{N} + \sinh\pi\dfrac{|n|^{1/2}}{N}\cos 2\dfrac{|n|^{1/2}s}{\varrho_0}}{\sin\sigma}$$

$$= \frac{\varrho_0}{|n|^{1/2}}\,\frac{\cos\pi\dfrac{|n|^{1/2}}{N}\sinh\pi\dfrac{|n|^{1/2}}{N} + \sin\pi\dfrac{|n|^{1/2}}{N}\cosh 2|n|^{1/2}\left(\dfrac{\pi}{N}-\dfrac{s}{\varrho_0}\right)}{\sin\sigma} \tag{33c}$$

The condition for the stability of particle orbits in the assumed periodic structure is given from Eq. (33a) by the condition $|\cos\sigma| < 1$,[11] and Eq. (33a) permits computation of the oscillation frequencies ($Q_x = N\sigma/2\pi$) or of the lapse rate ($\mu = iN\sigma/C_0$) for orbits in a specific accelerator structure. A graph of σ vs $|n|^{1/2}/N$, as given by Eq. (33a), is shown in Fig. 2 for the first (and by far the most useful) zone of stability. This zone corresponds to $0 < \sigma < \pi$ and occurs for $|n| < 0.3562\,N^2$. The value $\sigma = \pi/2$ occurs for $|n|/N^2 = 1/4$.[12] For small values of σ, an expansion of Eq. (33a) leads to the approximate relation

$$\frac{\sigma}{\pi} \doteq \frac{\pi}{\sqrt{3}}\frac{|n|}{N^2}\left[1 + \frac{4\pi^4}{315}\left(\frac{n}{N^2}\right)^2 + \cdots\right] \tag{34}$$

[11] A more detailed analysis, covering the case of unequal values of $|n|$ in the focusing and defocusing regions and including the presence of straight sections, has been outlined by Livingood (1961, Sect. 12.3).

[12] It is of interest to note that if $K_z(s)$ had been replaced by $(4n/\pi)\cos Ns/\varrho_0$, which represents the first term in a Fourier development of our assumed piecewise-constant function, the first stability region for the resultant Mathieu equation would occur for

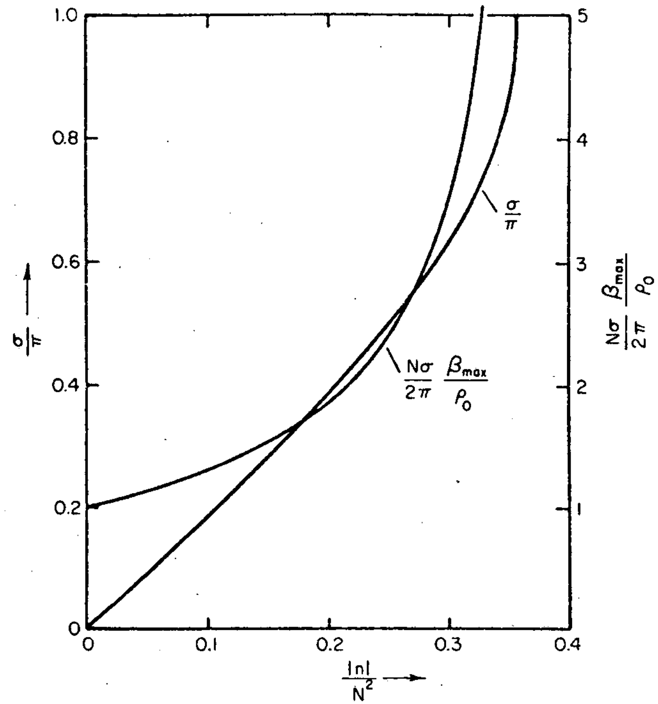

FIG. 2. Plot of the phase advance per period, in units of π, and of the maximum value of β, in units of $2\pi\varrho_0/N\sigma$, vs $|n|/N^2$ for the first stability zone of an alternating-gradient synchrotron ($|n| \gg 1$).

The average value of $(\beta/\varrho_0)^{-1}$ will be equal to $N\sigma/2\pi$, the number of oscillations per circumference [see Eq. (31b)], but β will vary significantly as s advances through one period. The maximum value of β, expressed in units of $(2\pi/N\sigma)\varrho_0$, is depicted on Fig. 2. It is evident that β_{max} will become nearly 50% greater than $(2\pi/N\sigma)\varrho_0$ for $\sigma = \pi/4$, and very much greater values of $(N\sigma/2\pi)(\beta_{max}/\varrho_0)$ occur in regions of the diagram that are closer to the upper boundary of the first stability region. The variation of β with s, as given by Eq. (33c), and the corresponding variations of α and ψ, are illustrated in Fig. 3 for a case in which $\sigma = 49°$ ($\pi|n|^{1/2}/N = 1.2$).

$|n| < 0.3566\,N^2$, $\sigma = \pi/2$ would result for $|n|$ near $0.251\,N^2$, and σ/π would be approximately $1.8006\,|n|/N^2$ for small values of σ. These values have been obtained from numerical tables relating to the Mathieu function (Belford *et al.*, 1957; National Bureau of Standards, 1951). The use of a Mathieu equation to represent, to a good degree of approximation, the transverse oscillations of particles in an alternating-gradient synchrotron has been noted by Meixner and Schäfke (1954, pp. 338–343).

We mentioned earlier (Section 5.3.1, A) the advantage of a synchrotron design that permits an aperture of modest dimensions to accommodate the momentum variations of the particles that are to be accelerated. Not only will such momentum variations be present initially as a result of an energy

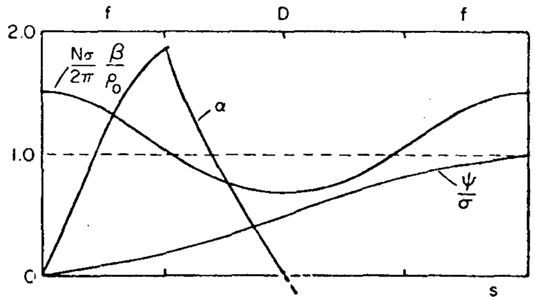

FIG. 3. Plot of the functions $\alpha(s)$, $\beta(s)$, and $\psi(s)$ within one period of an alternating-gradient synchrotron for which $\pi |n|^{1/2}/N = 1.2$ ($\sigma = 49°$), commencing at the center of a focusing region. The symbols f, D, and f at the top of the diagram denote the portions of the plot that correspond to half of a focusing interval, a defocusing interval, and half of the following focusing interval.

spread in the injected beam, but the "phase oscillations" of individual particles under the action of the radio-frequency acceleration system also will necessarily be accompanied by corresponding oscillations of the particle momentum. In order to examine the character and magnitude of the influence that momentum variations will have on the closed orbit, we refer to the inhomogeneous equation for the radial motion [cf. Eq. (6a), with $K_x(s)$ written for $(1-n)/\varrho_0^2$ and p_0 treated as substantially constant]

$$\frac{d^2x}{ds^2} + K_x(s)x = \frac{1}{\varrho_0}\frac{\delta p}{p_0} \tag{35}$$

The periodic solution to Eq. (35) of course can be expressed generally through use of the solutions to the corresponding homogeneous equation,[13] but the piecewise-constant character of $K_x(s)$ for an alternating-gradient accelerator makes it straightforward to find the periodic solution to Eq.

[13] The expression

$$X(s) = \frac{\delta p}{p_0}\frac{1}{2\sin\sigma/2}\int_{s-C_0/N}^{s}\frac{\beta^{1/2}(s)\,\beta^{1/2}(\tau)}{\varrho_0}\cos\left[\psi(s)-\psi(\tau)-\frac{\sigma}{2}\right]d\tau$$

may be verified to be a periodic solution of Eq. (35).

(35) by joining simple solutions for the focusing and defocusing regions. For $|n| \gg 1$, one obtains (cf. Livingood, 1961, pp. 208–213)

$$\frac{X}{\varrho_0} = \frac{1}{|n|}\left[2\,\frac{\sinh\dfrac{\pi|n|^{1/2}}{2N}\cos|n|^{1/2}\dfrac{s}{\varrho_0}}{\cosh\dfrac{\pi|n|^{1/2}}{2N}\sin\dfrac{\pi|n|^{1/2}}{2N}-\sinh\dfrac{\pi|n|^{1/2}}{2N}\cos\dfrac{\pi|n|^{1/2}}{2N}}+1\right]\frac{\delta p}{p_0}$$

$$-\frac{C_0}{4N} \le s\left(\mathrm{mod}\,\frac{C_0}{N}\right) \le \frac{C_0}{4N}$$

$$= \frac{1}{|n|}\left[2\,\frac{\sin\dfrac{\pi|n|^{1/2}}{2N}\cosh|n|^{1/2}\left(\dfrac{\pi}{N}-\dfrac{s}{\varrho_0}\right)}{\cosh\dfrac{\pi|n|^{1/2}}{2N}\sin\dfrac{\pi|n|^{1/2}}{2N}-\sinh\dfrac{\pi|n|^{1/2}}{2N}\cos\dfrac{\pi|n|^{1/2}}{2N}}-1\right]\frac{\delta p}{p_0}$$

$$\frac{C_0}{4N} \le s\left(\mathrm{mod}\,\frac{C_0}{N}\right) \le \frac{3C_0}{4N}, \tag{35a}$$

where s is measured from the center of a focusing region. The maximum value of X is given by

$$\left.\frac{X/\varrho_0}{\delta p/p_0}\right|_{\max} = \frac{1}{|n|}\left[2\,\frac{\sinh\dfrac{\pi|n|^{1/2}}{2N}}{\cosh\dfrac{\pi|n|^{1/2}}{2N}\sin\dfrac{\pi|n|^{1/2}}{2N}-\sinh\dfrac{\pi|n|^{1/2}}{2N}\cos\dfrac{\pi|n|^{1/2}}{2N}}+1\right] \tag{35b}$$

and the average value by (see *Note I*, Section 5.3.6)

$$\frac{1}{\xi} = \frac{\langle X\rangle_{\mathrm{av}}/\varrho_0}{\delta p/p_0} = \frac{4}{\pi}\frac{N}{|n|^{3/2}}\,\frac{1}{\coth\dfrac{\pi|n|^{1/2}}{2N}-\cot\dfrac{\pi|n|^{1/2}}{2N}} \tag{35c}$$

The reciprocals of the quantities given by Eqs. (35b) and (35c) are plotted, in units of Q_x^2, in Fig. 4 for values of σ lying in the first stability zone ($0 < \sigma < \pi$). It is seen that $\langle X\rangle_{\mathrm{av}}/\varrho_0$ does not exceed $(1/Q_x^2)(\delta p/p_0)$ by more than about 20% for values of σ less than $\pi/2$, but that $X_{\max}$ will become about 30% greater than $\langle X\rangle_{\mathrm{av}}$ when σ is close to $\pi/2$. The fact that X/ϱ_0 is roughly of the magnitude of $(1/Q_x^2)(\delta p/p_0)$ directly indicates, however, the ability of an alternating-gradient structure, by virtue of its higher Q_x,

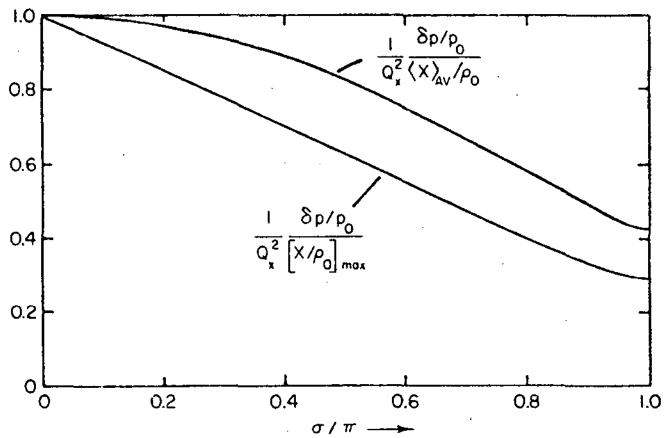

FIG. 4. Graphs illustrating the relation between closed-orbit amplitude and momentum error, as a function of σ/π, for an alternating-gradient synchrotron.

to contain particles with a markedly greater momentum spread than could be accommodated by a constant-gradient structure of the same radial aperture.

1-152

In the realistic design of an alternating-gradient accelerator, certain features may be introduced that will cause the linear differential equations of motion to assume a more complicated detailed form than has been treated in the examples presented above, but much of the general analysis will still apply. The introduction of special straight sections at a small number of locations around the accelerator will reduce the basic periodicity of the magnet structure, and the presence of misalignments or other errors results in a structure with a fundamental period that is strictly equal to the circumference of the machine. If we disregard these latter effects (to which we give further attention in a subsequent subsection, E), then the presence of gaps between magnet blocks, the introduction of correcting lenses or correction windings, and the possible edge focusing from end faces on the magnet blocks that are oblique to the equilibrium orbit all constitute features to which the methods just described are readily adaptable.

D. EFFECT OF COUPLING

In addition to the effects mentioned, there may also be linear periodic terms that couple the two transverse degrees of freedom, x and y. The differential equations will still be Hamiltonian in this case, however, with the linear equations derivable from a quadratic form. If forcing terms are absent, so that the differential equations are homogeneous, the coupled equa-

tions [analogous to Eq. (10)] for motion in a Maxwell field are of the form

$$\frac{d^2x}{ds^2} - K_x(s)x - \left[G(s) + \frac{1}{2}\frac{dH}{ds}\right]y - H(s)\frac{dy}{ds} = 0 \qquad (36a)$$

$$\frac{d^2y}{ds^2} + K_y(s)y - \left[G(s) - \frac{1}{2}\frac{dH}{ds}\right]x + H(s)\frac{dx}{ds} = 0 \qquad (36b)$$

where $H(s)$ is e/p_0 times whatever longitudinal magnetic field may be present along the orbit and the factors containing $G(s)$ represent e/p_0 times the coefficients of a "skew quadrupole field" (oriented at an angle of 45° to the quadrupole component of the normal focusing field of the magnets). Canonically conjugate momenta, which include the appropriate transverse components of a vector potential, could be taken to be

$$p_x = p_0\left[\frac{dx}{ds} - \frac{1}{2}H(s)y\right] \qquad (36c)$$

$$p_y = p_0\left[\frac{dy}{ds} + \frac{1}{2}H(s)x\right] \qquad (36d)$$

As in the case of uncoupled motion, any solution to Eqs. (36a, b) is expressible as a linear homogeneous algebraic function of the initial conditions—a relation that may be represented by a matrix that transforms a four-component vector (for example, with components x, p_x, y, and p_y) from s_0 to s. The matrix for a transformation from s_0 to $s_0 + C_0/N$, in particular, would be composed of two-by-two matrices [similar to the one shown in Eq. (23)] situated on the principal diagonal in the uncoupled case, and the stability of the coupled motion would be determined by the nature of the characteristic values ($\lambda_1, \cdots \lambda_4$) of the four-by-four matrix when the coupling effects are included. A quadratic invariant form, analogous to the quantity I^2 defined by Eq. (17), is

$$\begin{aligned} I_c^2 = {} & M_{1,2}p_x^2/p_0^2 + (M_{1,1} - M_{2,2})xp_x/p_0 - M_{2,1}x^2 \\ & + (M_{1,4} + M_{3,2})p_xp_y/p_0^2 + (M_{3,1} - M_{2,4})xp_y/p_0 \\ & + (M_{1,3} - M_{4,2})yp_x/p - (M_{4,1} + M_{2,3})xy \\ & + M_{3,4}p_y^2/p_0^2 + (M_{3,3} - M_{4,4})yp_y/p_0 - M_{4,3}y^2 \end{aligned} \qquad (37)$$

For any two solutions, designated by subscripts i and j,

$$U_{i,j} \equiv x_ip_{x_j} - y_ip_{y_j} - x_jp_{x_i} - y_jp_{y_i} = \text{constant (independent of } s), \qquad (38)$$

as may be shown directly from the differential equations. If the solutions are taken, in particular, to be *characteristic* solutions (associated respectively with characteristic factors λ_i and λ_j), then for any i there will be a j such that $U_{i,j} \neq 0$ [since a particular solution, representable as a linear combination of the characteristic solutions, certainly could be chosen with initial conditions such that this quantity does not vanish]. The invariance of $U_{i,j}$, if applied for values of s one period apart, then requires that $\lambda_i\lambda_j = 1$ for such a pair of characteristic solutions. Thus not only are the four characteristic factors such that their product is unity, but they may be grouped into reciprocal pairs. In addition, of course, complex values will occur in complex conjugate pairs.

For uncoupled motion that is stable in both degrees of freedom, the four characteristic values will occur in complex conjugate pairs and all will lie on the unit circle in the complex plane (Fig. 5 a). If the introduction of a small (infinitesimal) amount of coupling were to have the effect of shifting these values, subject to the conditions just mentioned, off the unit circle (Fig. 5c)—so that the coupled motion would be unstable—it therefore would be necessary that the characteristic values for the uncoupled x and y equations be (infinitesimally) close (Fig. 5b). Thus a coupling instability will occur in such cases only if

$$\cos \sigma_x \doteq \cos \sigma_y\,; \tag{39a}$$

that is, only if

$$\frac{\sigma_x \mp \sigma_y}{2\pi} \text{ is close to an integer} \tag{39b}$$

In the absence of coupling, the invariant I_c is a simple linear combination of two invariant quadratic expressions of the form indicated by Eqs. (26):

$$\begin{aligned} I_c^2 = {} & [\beta_x p_x^2/p_0^2 + 2\alpha_x x p_x/p_0 + \gamma_x x^2] \sin \sigma_x \\ & + [\beta_y p_y^2/p_0^2 + 2\alpha_y y p_y/p_0 + \gamma_y y^2] \sin \sigma_y \end{aligned} \tag{40}$$

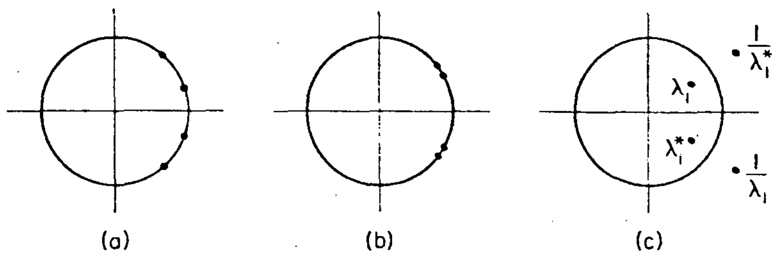

FIG. 5. Location, with respect to the unit circle in the complex plane, of the characteristic factors for coupled motion: (a) For stable motion when the coupling is absent; (b) for stable motion near a coupling resonance; (c) for unstable coupled motion.

and, for stable motion in each of the individual degrees of freedom, each of the square brackets will be positive definite. Under such circumstances I_c^2 will then constitute a quadratic form of definite sign if $\sin \sigma_x$ and $\sin \sigma_y$ are each positive or are each negative, whereas it will be a *difference* of two positive definite forms if these factors have opposite signs. Although the detailed structure of I_c^2 will be slightly modified when a small amount of coupling is present, it will be expected to remain a quadratic form of definite sign near a *difference* resonance (where $\sin \sigma_x \cong \sin \sigma_y$) and the particle motion would then remain stable.[14] Near a sum resonance (where $\sin \sigma_x \cong -\sin \sigma_y$), on the other hand, it would be possible for the solutions to grow without limit. The magnitudes of the individual quadratic forms may be taken as indicative of the amplitudes of x and y motion (proportional to areas in x, p_x and y, p_y space) if the coupling is weak, and operation near a difference resonance can lead to a pronounced interchange of amplitude between the x and y oscillations.

E. SELECTION OF PARAMETERS AND MAGNET CONFIGURATION

The selection of suitable parameters for an alternating-gradient synchrotron involves consideration of many factors. Great importance normally is attached to achieving a design in which the aperture required to accommodate the beam will be small, since slight increases in the vertical dimension of the magnet gap can greatly increase the cost of a large machine. The necessary aperture dimensions will be determined not only by the parameters of the magnet structure itself, and by the stability of its foundations, but also by the characteristics of ancillary equipment that forms a part of the entire accelerator facility. Thus, in particular, the energy and emittance of the injector can have an important effect on the choice of other parameters, and the specifications of the injector therefore should be included as variables in a careful cost optimization.

Since the magnet ring in practice is built from a large number of individual blocks, gaps (typically of the order of 1 m in length) may conveniently be provided between these blocks to accommodate correcting lenses and other items of ancillary equipment. If focusing and, defocusing magnets are combined in a single block, with gaps situated at points of mirror symmetry between focusing and defocusing regions, the basic configuration is denoted FOFDOD. [Such a configuration was selected for the CERN proton synchrotron in Geneva, in which 1.6-m gaps are normally

[14] A complete derivation of this result has been presented by Courant and Snyder (1958, p. 27 ff.), and references are cited to earlier perturbation treatments of the problem.

employed, and the provision of 10 special 3-m gaps at 10-block intervals results in a structure comprising 10 superperiods.] An alternative arrangement, denoted FODO, situates the gaps between magnets of opposite type. The latter arrangement in principle has the advantage of producing a greater phase advance for a given field gradient, since the lens actions of adjacent F and D regions in the FOFDOD configuration partially annul one another because of their proximity. The FOFDOD arrangement has the advantage, however, of permitting quadrupole lenses to be situated at mid-F and mid-D points, thereby providing a means for independent control of Q_x and Q_y, and this same arrangement has also been found to make more feasible the realization of long straight sections of the type proposed by Collins (Section 5.3.3, F). It is definitely desirable to provide some straight sections of a length considerably greater than that normally introduced between the magnet blocks, in order to accommodate radiofrequency acceleration stations and to facilitate injection and extraction of the beam.

The detailed determination of a suitable field index requires, of course, that the design and spacing of the magnet blocks be explicitly considered. Because of fringing, the "gradient length" of an individual magnet in typical cases may be about 4 cm greater than the physical length of the block itself, and the "bending length" may exceed the physical length by as much as 12 cm; a corresponding adjustment of n (for example, an increase of 1 or 2 per cent) accordingly will be required in the magnet design because of these effects. The integrated field also may be found to have a nonlinear variation with radius, and such a characteristic will contribute to the variation of Q with momentum at any stage of the acceleration cycle. To correct and control such variations it is prudent to supplement the quadrupole corrections (that can be provided by pole-face windings and individual quadrupole lenses) with sextupole and octupole fields. Skew quadrupoles (quadrupole lenses whose axes are rotated by 45° from the orientation of the units used for adjusting Q_x and Q_y) are desirable to eliminate coupling between radial and axial oscillations that may result from stray fields, and auxiliary steering magnets may also provide useful corrections and assist in injection or extraction of the beam.

1. *Influence of Misalignments*

In recent years the possibility of attaining beam currents of substantial size (for example, 0.1—1 A) within a high-energy accelerator has come to have some bearing on the choice of aperture dimensions (or of injection energy), since the space-charge forces that act on such a beam arise in part

from image charges and currents whose effect is reduced if the aperture dimensions are increased (Laslett, 1963). A major, if not dominant, factor in determining the parameters that affect the aperture, however, normally proves to be the accuracy with which the magnet blocks can be positioned and their alignment maintained. Quantitative analysis of the effects that positional errors will have on the particle orbits is somewhat specific to the survey and support system that is planned, since possible correlations between the errors of individual magnet blocks will be of importance. For considering the general application of present technology to the construction of accelerators for higher energy, however, one may regard σ or $|n|/N^2$ as fixed and suppose that closed-orbit deviations approximately proportional to $\sqrt{N}$ times the root-mean-square alignment error could be expected. Important contributions to the closed-orbit error could also arise from perturbations of the magnetic field due to remanence, eddy currents, and stray fields from magnetized supports or equipment in the neighborhood of the accelerator. These latter effects can be kept from dominating, however, if the injection energy is sufficiently high that the accelerator is not required to operate with flux densities below a few hundred gauss at the orbit. If the quality of the injected beam, as specified by the emittance of the injector, is also assumed to be given, the corresponding linear aperture dimensions would be proportional to $(R/Q)^{1/2}$, or to $(R/N)^{1/2}$ for a constant value of σ. Achievement of an optimum balance between this factor and the aperture to be provided for closed-orbit displacements thus would appear to require values of N, and hence of Q, to be so selected for accelerators of similar configuration that they would be proportional to the square root of the orbit radius, that is to the square root of the final energy of the synchrotron.

As a rough approximation, we might suppose that a semiaperture allowance of $7\sqrt{N}\,\varepsilon$ typically would be required to accommodate, with a factor of safety, a variety of alignment errors having a root-mean-square value ε (see *Note II*, Section 5.3.6). With ε not exceeding 10^{-4} m, this allowance then becomes $\pm 0.7 \times 10^{-3}\sqrt{N}$ m. Also, with single-turn injection of a high-energy beam occupying an area of $10^{-6}\,\pi$ radian · meter in phase space, with $Q \cong N/8$ (corresponding to $\sigma = \pi/4$), and with a flutter factor $\beta_{\max}\langle 1/\beta\rangle_{\text{av}} \cong 1.5$, the additional aperture required to accommodate the beam oscillations would be

$$\pm\,[(\beta_{\max}\langle 1/\beta\rangle_{\text{av}})\,(Y/\pi)\,(2\pi/\sigma)\,(R/N)]^{1/2}$$
$$= \pm\,[1.5 \times 10^{-6} \times \overset{8\times}{R/N}]^{1/2} = \pm\,0.0035\,(R/N)^{1/2}$$

Under these circumstances, then, one would expect that an optimum value of N would lie in the neighborhood of $N = 5\sqrt{R}$, for R in meters. Correspondingly, for $\sigma \cong \pi/4$, $|n| = 0.1346\,N^2 \cong 3.4\,R$ and $(1/B_0)\,(dB/dx) \cong 3.4\ \mathrm{m}^{-1}$.

It is interesting to note that proton synchrotrons now operating at energies near 30 GeV and accelerators that are being planned for the attainment of energies in the 200–1000 GeV range all employ values of $(1/B_0)\,(dB/dx)$ close to 3 or 4 m^{-1}. Such values of the relative field gradient permit the realization of an efficient magnet design. The 30-GeV accelerators were intended, however, to accept beams injected from a 50-MeV linear accelerator of markedly greater emittance (AGS Staff, 1961) than that assumed in the present discussion, and a correspondingly greater allowance also was provided in these pioneering machines to accommodate mechanical misalignments. Accordingly, the apertures proposed for new multihundred GeV accelerators in fact are not increased by the fourth root of the radius ratio (as would follow from the analysis indicated here) but actually have dimensions slightly *smaller* than in the present machines. In principle it thus appears desirable, as Sands (1961) and his colleagues have emphasized, to inject into the larger synchrotrons at energies in the multi-GeV range and to consider the use of one or more "booster synchrotrons" in cascade for this purpose.

2. *Computational Aids*

Detailed orbit characteristics of specific accelerator designs frequently are obtained most conveniently by means of digital computation, either by direct integration of the differential equations or (more efficiently, when the linear character of the equations permits) through the appropriate multiplication of matrices that characterize simple portions of the focusing system. The simplest computations of this type would employ 2×2 matrices that act on the vector $(x, p_0 dx/ds)$ or on $(y, p_0 dy/ds)$, and this technique could be directly extended to the use of 4×4 matrices to describe motion with linear coupling.

In the study of uncoupled motion in one degree of freedom it at times has proven convenient, however, to employ 3×3 matrices in order to investigate the orbit characteristics for particles with different values of the momentum, and such matrices alternatively can be applied to determine the closed-orbit response to a sequence of magnet misalignments. For the first of these applications, such 3×3 matrices would be designed to act on a vector whose third component is δp or, more commonly, $\delta p/p_0$. From ref-

erence to the inhomogeneous Eq. (6a), it may be seen that a matrix of the type indicated in Eq. (13) then becomes extended to the 3×3 form

$$\begin{bmatrix} \cos\dfrac{|n|^{1/2}}{\varrho_0}\Delta s & \dfrac{\varrho_0}{|n|^{1/2}}\sin\dfrac{|n|^{1/2}}{\varrho_0}\Delta s & \dfrac{\varrho_0}{|n|}\left(1-\cos\dfrac{|n|^{1/2}}{\varrho_0}\Delta s\right) \\ -\dfrac{|n|^{1/2}}{\varrho_0}\sin\dfrac{|n|^{1/2}}{\varrho_0}\Delta s & \cos\dfrac{|n|^{1/2}}{\varrho_0}\Delta s & \dfrac{1}{|n|^{1/2}}\sin\dfrac{|n|^{1/2}}{\varrho_0}\Delta s \\ 0 & 0 & 1 \end{bmatrix} \tag{41a}$$

for a focusing segment of an alternating-gradient structure with $|n| \gg 1$, and to

$$\begin{bmatrix} \cosh\dfrac{|n|^{1/2}}{\varrho_0}\Delta s & \dfrac{\varrho_0}{|n|^{1/2}}\sinh\dfrac{|n|^{1/2}}{\varrho_0}\Delta s & \dfrac{\varrho_0}{|n|}\left(\cosh\dfrac{|n|^{1/2}}{\varrho_0}\Delta s - 1\right) \\ \dfrac{|n|^{1/2}}{\varrho_0}\sinh\dfrac{|n|^{1/2}}{\varrho_0}\Delta s & \cosh\dfrac{|n|^{1/2}}{\varrho_0}\Delta s & \dfrac{1}{|n|^{1/2}}\sinh\dfrac{|n|^{1/2}}{\varrho_0}\Delta s \\ 0 & 0 & 1 \end{bmatrix} \tag{41b}$$

for a defocusing segment. By constructing from such matrices the 3×3 matrix (**M**) for a period of the structure, the values of X and X' for the periodic solution (relative to the orbit of the "equilibrium particle" with momentum p_0) are obtained as

$$X = \frac{M_{1,3} + M_{1,3}^{-1}}{2(1-\cos\sigma)}\frac{\delta p}{p_0} \tag{42a}$$

and

$$X' = \frac{M_{2,3} + M_{2,3}^{-1}}{2(1-\cos\sigma)}\frac{\delta p}{p_0} \tag{42b}$$

for the end points of this interval, where

$$M_{1,3}^{-1} = M_{1,2}M_{2,3} - M_{1,3}M_{2,2} \tag{42c}$$

$$M_{2,3}^{-1} = M_{1,3}M_{2,1} - M_{1,1}M_{2,3} \tag{42d}$$

and

$$\cos\sigma = \tfrac{1}{2}(M_{1,1} + M_{2,2}) \tag{42e}$$

Alternatively, the misalignment of any particular magnet block (or of other components of the structure) may be represented in a similar way through the use of a matrix whose 1,3 element represents the amount by which the end of this magnet is displaced with respect to the adjacent end of the following magnet, the 2,3 element is the slope of the magnet block with respect to the slope of the following component, and the 3,3 element equals unity. Such a matrix, operating on a vector $(x, x', 1)$, introduces the proper discontinuities to describe the trajectory relative to the centerline of the perturbed structure, evaluated at points immediately following the discontinuity. The closed-orbit deviations again will be given in terms of the matrix constructed for a complete period (that now will constitute a complete revolution) by expressions that correspond to Eqs. (42a, b).

A modification to the 3×3 matrix employed to represent the radial motion of a particle with a momentum $p_0 + \delta p$ has been recently suggested by Courant (1964), with the object of generating directly the additional length (Δl) of the paths that such particles describe. In this proposed method the matrix would operate on a four-element vector that has components x, $p_0(dx/ds)$, Δl, and δp—or, more simply, the components x, dx/ds, Δl, and $\delta p/p_0$. In the latter case, the first-order relation

$$\Delta l = \int_0^{\Delta s} \frac{x}{\varrho_0}\, ds \tag{43a}$$

$$= \begin{cases} \displaystyle\int_0^{\Delta s} \left[\frac{1}{|n|}\frac{\delta p}{p_0}\left(1 - \cos\frac{|n|^{1/2}}{\varrho_0} s\right) + \frac{x_0}{\varrho_0}\cos\frac{|n|^{1/2}}{\varrho_0} s \right. \\ \displaystyle\qquad \left. + \frac{1}{|n|^{1/2}} x_0' \sin\frac{|n|^{1/2}}{\varrho_0} s\right] ds, \\ \displaystyle\int_0^{\Delta s} \left[\frac{1}{|n|}\frac{\delta p}{p_0}\left(\cosh\frac{|n|^{1/2}}{\varrho_0} s - 1\right) + \frac{x_0}{\varrho_0}\cosh\frac{|n|^{1/2}}{\varrho_0} s \right. \\ \displaystyle\qquad \left. + \frac{1}{|n|^{1/2}} x_0' \sinh\frac{|n|^{1/2}}{\varrho_0} s\right] ds \end{cases} \tag{43b}$$

$$= \begin{cases} \displaystyle\frac{x_0}{|n|^{1/2}}\sin\frac{|n|^{1/2}}{\varrho_0}\Delta s + \frac{\varrho_0}{|n|} x_0'\left(1 - \cos\frac{|n|^{1/2}}{\varrho_0}\Delta s\right) \\ \displaystyle\qquad + \frac{1}{|n|}\frac{\delta p}{p_0}\left(\Delta s - \frac{\varrho_0}{|n|^{1/2}}\sin\frac{|n|^{1/2}}{\varrho_0}\Delta s\right), \\ \displaystyle\frac{x_0}{|n|^{1/2}}\sinh\frac{|n|^{1/2}}{\varrho_0}\Delta s + \frac{\varrho_0}{|n|} x_0'\left(\cosh\frac{|n|^{1/2}}{\varrho_0}\Delta s - 1\right) \\ \displaystyle\qquad + \frac{1}{|n|}\frac{\delta p}{p_0}\left(\frac{\varrho_0}{|n|^{1/2}}\sinh\frac{|n|^{1/2}}{\varrho_0}\Delta s - \Delta s\right) \end{cases} \tag{43c}$$

for focusing and defocusing regions, gives directly the elements of an additional row (with the diagonal element equal to unity and the new column elements zero) that may be inserted into the 3×3 matrix to form a 4×4 matrix capable of transforming Δl. By multiplication of such matrices to obtain a matrix (M) characteristic of a period of the structure, one then may derive the closed-orbit characteristics from the equations represented by

$$(\mathbf{M}) \begin{pmatrix} x \\ x' \\ 0 \\ \delta p/p_0 \end{pmatrix} = \begin{pmatrix} x \\ x' \\ \Delta l \\ \delta p/p_0 \end{pmatrix} \tag{44}$$

and, in particular, evaluate the momentum compaction factor directly by

$$\frac{1}{\xi} = \frac{N \Delta l / C_0}{\delta p/p_0} \tag{45}$$

3. *Machine Resonances*

The detailed selection of parameters for an alternating-gradient synchrotron will be determined not only with the object of achieving a desirable value of σ and suitable properties of such functions as $\beta(s)$ that characterize the unperturbed structure, but also so as to avoid harmful effects from so-called "machine resonances." We have already seen that in a strictly periodic structure we must avoid values of σ_x and σ_y that are multiples of π, as well as sum resonances for which $\sigma_x + \sigma_y$ is a multiple of 2π. In an accelerator with misalignments, the true period of the structure becomes a complete circumference, and analogous restrictions therefore apply to $N\sigma_x$ and to $N\sigma_y$. Linear resonances thus occur in general for integral and half-integral values of Q_x and Q_y, and for values such that $Q_x + Q_y$ is an integer. Misalignments and field errors that act to produce an inhomogeneous term in the orbit equations, but do not materially influence K_x or K_y, lead specifically to large excursions of the closed orbit in the neighborhood of an integral resonance and thus, in effect, contribute to the widths of the integral stop bands. These stop bands, in practice, are normally found to be more prominent than those that develop at half-integral values of Q. Because of these machine resonances, values selected for Q_x and for Q_y normally are close to an integer plus or minus one quarter, and quadrupole lenses are commonly provided to permit adjustment and control of these quantities throughout the operating cycle of the accelerator.[15]

[15] The position of the beam within the accelerator aperture can be determined by means of electrostatic or magnetic pick-up devices called "difference electrodes." The provision of several such pick-up units, for each transverse degree of freedom, per oscillation wave-

F. Introduction of Long, Straight Sections

The introduction of straight sections or other special features at equally spaced but infrequent intervals will increase the fundamental period of a perfectly constructed magnet ring from C_0/N to C_0/N', where N' denotes the total number of "super periods" of which the structure is comprised. Accordingly, unless the modifications to the basic structure are introduced in a well-matched way, one may expect prominent resonances to develop when Q_x/N' or Q_y/N' is an integer or half integer [and, if coupling is present, when $(Q_x + Q_y)/N'$ is an integer]. Such resonances therefore should be avoided in the selection of parameters.

A relatively simple method of introducing a long, straight section in a matched way (when $\delta p = 0$) has been suggested by Collins (1961) and affords a means of obtaining an unobstructed region whose length is approximately a free-oscillation wavelength divided by 2π. Similar concepts have been discussed by Holt and Newns (1961), of the Liverpool-Manchester-Glasgow Electron Accelerator Project ("NINA," at Daresbury, Cheshire). The arrangement of Collins employs a field-free region of length L_1, a focusing quadrupole lens of focal length F, a (longer) field-free region of length L_2, a defocusing quadrupole of focal length $-F$, and a final field-free region of length L_1 (Fig. 6). This sequence of elements is inserted into the regular magnet lattice between defocusing and focusing magnet units so that, by suitable adjustment of the parameters, the orbit characteristics may be matched simultaneously for both transverse degrees of freedom.

1-157

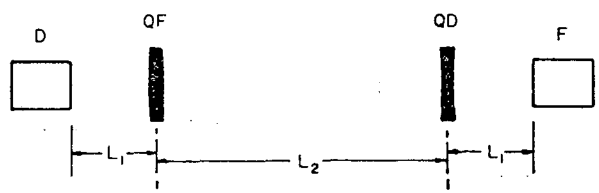

FIG. 6. Sequence of elements in a Collins straight section. QF and QD denote, respectively, focusing and defocusing quadrupole lenses. The elements D and F represent defocusing and focusing magnet elements in the preceding and following normal portions of the accelerator.

length is desirable in order to permit a thorough diagnosis to be made of an imperfectly aligned beam and to guide the corrective measures that may be taken. The frequencies of the free oscillations similarly may be measured through the use of radial or vertical radio-frequency "knock-out" fields by a technique that first was described in connection with operation of the race-track synchrotron at the University of Michigan (Hammer *et al.*, 1955).

If we neglect the geometrical length of the quadrupole lenses, the transfer matrix for such a Collins straight section is

$$(\mathbf{M}_T)_{\text{Collins}} = \begin{pmatrix} 1 - L_2/F - L_1L_2/F^2 & 2L_1 + L_2 - L_1{}^2L_2/F^2 \\ -L_2/F^2 & 1 + L_2/F - L_1L_2/F^2 \end{pmatrix} \tag{46}$$

By choosing

$$F = \frac{|\alpha|}{\gamma} \tag{47a}$$

and

$$L_2 = \frac{2L_1\alpha^2}{1 + L_1{}^2\gamma^2} \tag{47b}$$

the matrix (46) may be expressed in the form

$$(\mathbf{M}_T)_{\text{Collins}} = \begin{pmatrix} \cos\theta - |\alpha|\sin\theta & \beta\sin\theta \\ -\gamma\sin\theta & \cos\theta + |\alpha|\sin\theta \end{pmatrix} \tag{48a}$$

where

$$\theta = \cos^{-1}\frac{1 - L_1{}^2\gamma^2}{1 + L_1{}^2\gamma^2} = \sin^{-1}\frac{2L_1\gamma}{1 + L_1{}^2\gamma^2} \tag{48b}$$

The straight section is seen then to be matched to the impedance ellipse of the magnet structure and introduces a phase advance of θ in the free oscillations. The maximum value of L_2 is obtained by choosing

$$L_1 = 1/\gamma \tag{49a}$$

so that

$$L_2 = \alpha^2L_1 = \alpha^2/\gamma = \frac{\beta}{1 + 1/\alpha^2} \tag{49b}$$

and

$$\theta = \pi/2 \tag{49c}$$

Since β will be approximately $2\pi\varrho_0/N\sigma$ at the boundary between focusing and defocusing regions and $|\alpha|$ typically is close to 2 at such points, L_2 will be about equal to $1/2\pi$ times an oscillation wavelength and the shorter field-free regions (L_1) each will be approximately one quarter of L_2.

It should be noted, however, that *within* the Collins section, in the neighborhood of the focusing quadrupole, β will attain a value that is close to twice the value that it has at the endpoints of this structure. It thus will become materially greater than $\beta_{\max}$ within the normal magnet structure, and a sufficiently large aperture must be provided within the straight section to accommodate this increase. This type of straight section also leads to radial excursions of the closed orbit for particles whose momentum differs from p_0 that are 1.7–2 times as great as would occur in a simple alternating-gradient magnet.

The use of such straight sections (or of others of greater complexity that can be designed to suppress the mismatch for off-momentum particles and to provide longer field-free regions than can be realized with the Collins design) is attractive in affording room for radio-frequency acceleration structures, for work with internal targets, and for injection or extraction of the particle beam. Rapid beam extraction has been accomplished, with high efficiency, by means of rapidly pulsed kicker magnets that deflect a desired portion of the beam into bending magnets situated further "downstream" (Bertolotto *et al.*, 1964). For slow extraction, particularly desirable for counter experiments with an external beam, the beam may be caused to experience a radial resonance. As various portions of the beam become subjected to this resonant condition, or as the oscillations of particles with small initial amplitudes become large, the trajectories "lock in" to a mode that is characterized by a definite phase angle with respect to the perturbation, and the radial displacement increases sufficiently during successive revolutions that the beam can enter the channel of a septum magnet (Hammer and Bureau, 1955; Hammer and Laslett, 1958, 1961; Hereward, 1964).

5.3.4. Basic Parameters of Existing High-Energy Alternating-Gradient Accelerators

Basic design parameters of several alternating-gradient synchrotrons designed for the production of protons or electrons with energies in the multi-GeV range are listed in Table I. Intensities are not cited for these accelerators, since this important parameter of an accelerator is sensitive to many details of the design and frequently increases markedly as operating experience is acquired. Linear accelerators are most frequently employed, in place of electrostatic generators, as injectors for the higher-energy alternating-gradient synchrotrons, but the 1.2-GeV alternating-gradient electron synchrotron at the University of Lund, Sweden (where $R \simeq 5.3$ m, $\varrho_0 = 3.65$ m, $N = 8$, and $|n| \simeq 11$) successfully employs a microtron with a hot-cathode source for the injection of a well-defined 6-MeV beam into this accelerator (Wernholm, 1964). Figure 7 shows a portion of the magnet ring and supporting concrete beam, together with a section of a magnet block, for the 6-GeV alternating-gradient electron synchrotron in Hamburg, Germany, for which the dedication ceremonies took place in November, 1964.

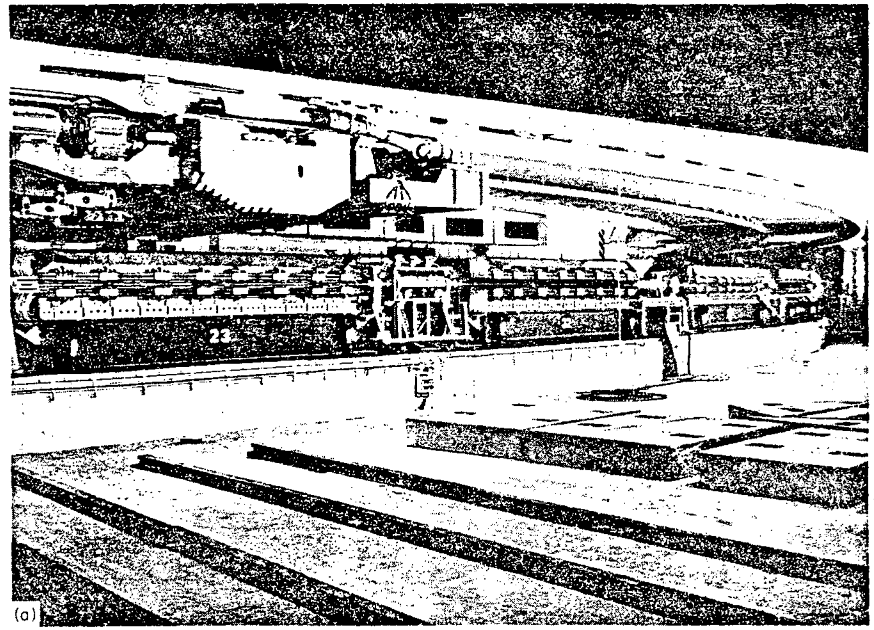

FIG. 7. (a) A portion of the magnet ring and supporting beam of the 6-GeV Deutsches Elektronen-Synchrotron (DESY) that was completed in Hamburg, Germany, in 1964. (b) Cross section of a magnet block for the DESY accelerator. [Courtesy of Professor Willibald K. Jentschke, Director, Deutsches-Elektronen-Synchrotron and II Institut für Experimentalphysik, Hamburg.]

As is apparent from the data given in Table I, the high-energy alternating-gradient accelerators are of such a size as to warrant very careful attention to optimization of design and to critical engineering details. Provisions for efficient use of the facility must be carefully planned, and the accelerator should be adaptable to future unforeseen experimental needs.

The magnet power required for the individual accelerators listed in Table I is in the range of 1–100 Mw. This excitation power can be supplied in pulsed form, by use of ignitrons or solid-state devices, from motor-generator sets with fly-wheel energy storage. Continuous excitation to produce a current whose wave form is that of a biased sinusoid has proven feasible, by use of a resonant condenser and ring-choke arrangement, for magnets with a power consumption of 1–2 Mw. [Initial plans for the application

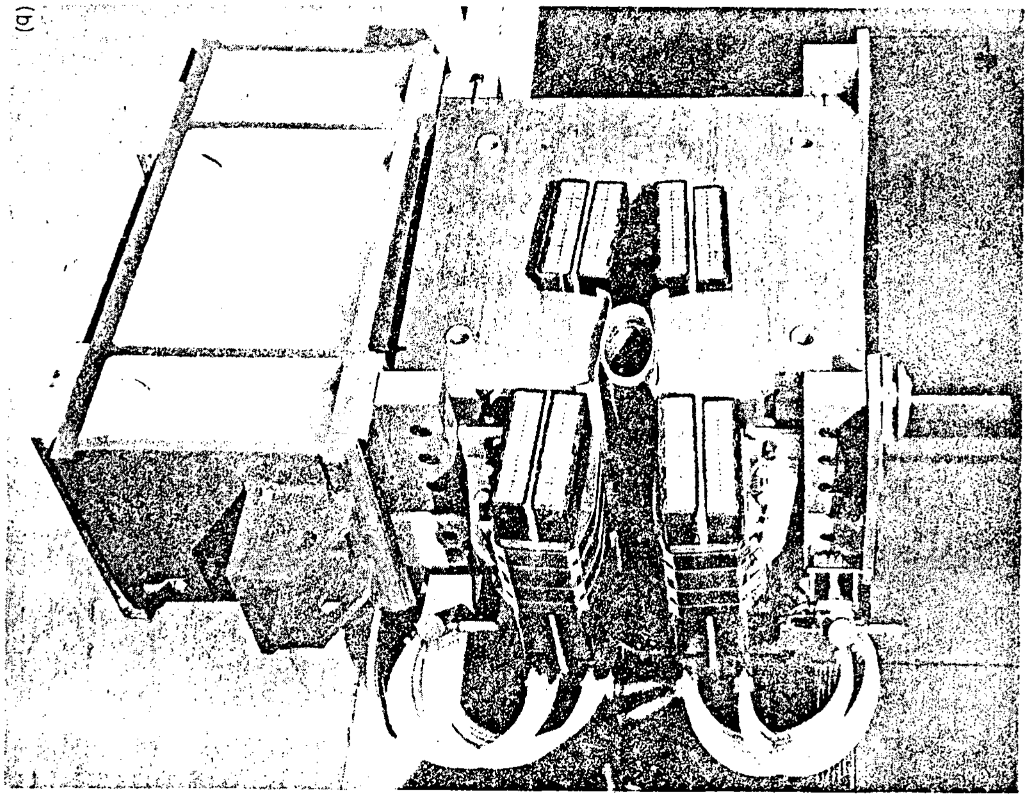

FIG. 7. (b).

of such a system to a 3-GeV weak-focusing proton synchrotron, designed to operate at a repetition frequency of 19 pulses per second, are described by White, *et al.* (1956)]. With the use of pulsed power, care must be taken to avoid both ripple and delay-line transient effects that could lead to unequal excitation of the individual magnet units in the accelerator ring. This latter effect can be reduced by the introduction of a saturable reactor in series with the magnet (to reduce the initial value of $\dot{B}/B$) and by the provision of damping resistors at several points in the circuit, but multiple

TABLE I

MAJOR DESIGN PARAMETERS OF ALTERNATING-GRADIENT SYNCHROTRONS FOR ENERGIES OF SEVERAL GeV OR ABOVE

Proton synchrotrons	CERN, Geneva, Switzerland	Brookhaven, New York	I.T.E.P., Moscow, USSR	Serpukov, USSR	
Maximum energy (kinetic)	28	33	7.3	60–70	GeV
Injection energy	50	50[a]	3.8	100	MeV
Radius, $C_0/2\pi$	100.00	128.44	39.98	236.13	m
Radius of curvature	70.08	85.37	31	194.12	m
N	50	60	56[b]	48[d]	—
$k = (1/B_0)(dB/dx)$	4.1	4.2	14.8[c]	2.3	m^{-1}
Q	6.25	8.75	12.75	9.7	—
Magnet weight, with coils (approx.)	3,500	4,000	2,700	20,700	tonnes
Vacuum chamber					
width	14	15	11	17[e]	cm
height	7	7	8	11.5	cm
Electron synchrotrons	**CEA, Cambridge, Massachusetts, USA**	**DESY, Hamburg, Germany**	**Physical Inst., Yerevan, Armenia, USSR**	**NINA, Daresbury, England**	
Maximum energy (kinetic)	6	6	6	4.0–5.5	GeV
Injection energy	28[f]	40	50	40	MeV
Radius, $C_0/2\pi$	36.0	50.42	34.49	35.0937	m
Radius of curvature	26.4	31.70	25.25	20.7697	m
N	24	24	24	20	—
$k = (1/B_0)(dB/dx)$	3.4	2.2	4.55	2.22, 2.28	m^{-1}
Q	6.4	6.25	5.38	5.25	—
Magnet weight, with coils (approx.)	310	650	425	380	tonnes
Vacuum chamber					
width	13.4	F: 14.4; D: 9.2	12.0	F: 13[e] D: 9[e]	cm
height	3.9	F: 4.5; D: 8.0	4.2	~7	cm

[a] Plan to replace by 500-MeV injector.
[c] Employs a neutral pole. [d] 12 superperiods.
[e] Useful width. [f] Hope to obtain 40–50 MeV injector.
[b] 14 superperiods, containing seven C-magnets and one quadrupole in a FODO sequence designed to eliminate the transition energy by raising it to 18.3 GeV (kinetic).

feed points would be desirable in the design of larger accelerators of this type.

The main magnet units of alternating-gradient accelerators require particularly careful design and close manufacturing control if good performance is to be realized with the relatively small apertures that result from cost optimization. The contour of the magnetic poles is basically hyperbolic in the central region, with modifications at each side of the gap, in order to achieve in the median plane the desired linear variation of magnetic field with radius. The use of *H* magnets (yokes on each side of the aperture) or the introduction of neutral poles can be attractive as a means for obtaining a magnet design that is inherently more efficient, but a C-type magnet is usually preferred in order to facilitate access to the central-field region.

To reduce distortions arising from eddy currents and from remanence, the magnet blocks are frequently constructed from laminations of thin ($\sim$1 mm) silicon steel, cut with precision dies. These laminations can advantageously be shuffled before stacking to insure that steel sheets from the various heats, rollings, and annealing processes in their manufacture are distributed among the magnet units. The effect of residual variations between the individual magnet blocks can be reduced, moreover, by arranging these units in a sequence that introduces these variations with a high periodicity.

Deterioration of the field shape as a result of saturation can be forestalled by a favorable design of the core and yoke of the magnet, by the introduction of suitably located holes in the top and bottom yokes near the corners of the coils (as developed by M. H. Foss for the *H* magnets of the 12.5-GeV zero-gradient accelerator and reported by the Argonne National Laboratory Staff, 1964), and by use of crenelated poles (Bruck, *et al.*, 1956; Princeton University Staff, 1959). The use of superconducting materials to achieve field strengths markedly in excess of those attainable with iron or steel, with corresponding reductions of dimensions and magnet power, would appear to present especially grave difficulties in a pulsed accelerator, and a substantial reduction of size would result in appreciable inconvenience in the use of the magnet as an accelerator component. [The possibility of using superconducting surfaces to shape a magnetic field (del Castillo, 1963, 1965) may be mentioned, however, for its possible application to the fixed-field alternating-gradient type of accelerator (Section 5.3.5).] Distortions of the field due to eddy currents, including currents induced in the excitation coils and in a metal vacuum chamber (for example, in a chamber with 2-mm walls, formed from material with a specific resistivity of 100 $\mu\Omega$-cm) must be reduced to an acceptable level at the time of injection. Such low-field

distortions, the effect of remanence, space-charge phenomena, and the desirability of introducing a high quality (low admittance) beam all favor high-energy injection into the synchrotron ring. Further details concerning the design and construction of alternating-gradient proton synchrotrons are included in the comprehensive review of Green and Courant (1959).

5.3.5. Fixed-Field Alternating-Gradient Accelerators

An interesting, and useful, application of alternating-gradient focusing methods occurs in the fixed-field alternating-gradient (FFAG) type of accelerator, wherein the magnetic fields that guide and focus the accelerated particles are constant with respect to time but have an azimuthal variation that gives rise to alternating-gradient focusing (Symon *et al.*, 1956; Laslett, 1956).[16] An important form of FFAG accelerator is similar to the more conventional type of synchrotron, in that a magnetic field is provided only within an *annular* region. The similar use of azimuthally varying fields in the design of cyclotrons intended to produce continuous beams affords, however, a means of meeting the otherwise conflicting requirements of axial stability and isochronism for relativistic particles. Related applications may also be found in the development of separated-sector microtrons and in betatron design.

In the annular form of an FFAG accelerator, the strength of the magnetic field increases rapidly ($\propto r^k$) with radius. The azimuthal variations of this field overcompensate the axial defocusing that otherwise would result, and produce a strong-focusing action in this transverse degree of freedom. Particles with a wide range of momentum can be accommodated simultaneously in such a field, so that there is an opportunity for great flexibility in the acceleration techniques and other particle-handling procedures in an accelerator of this type. The design thus offers the technical convenience of requiring a magnetic field that is constant with respect to time, it may permit the designer to realize more rapid cycling rates for the acceleration (with a corresponding increase of the average beam intensity), and it presents the opportunity to build up ("stack") intense beams that can be stored within the accelerator. Various types of FFAG design have been proposed, and their theoretical and technological problems extensively analyzed, by members of the Midwestern Universities Research Association.

[16] Similar design concepts, in at least one form, had been presented earlier by T. Ohkawa at a meeting of the Physical Society of Japan (1953) and also were considered by L. J. Haworth and H. Snyder of the Brookhaven National Laboratory.

A. Radial-Sector Design, with Reversed Fields

A simple form of FFAG accelerator is the reversed-field type, in which the direction of the magnetic field is caused to reverse from one magnet sector to the next. The sector boundaries are formed by geometrical planes that extend radially from the axis of the accelerator, and the length of the reversed-field sectors (or the strength of the reversed field) then normally would be chosen to be less than for the sectors of positive field in order that a closed orbit may be formed without requiring an excessively great circumference. Because of the strong radial increase of field strength and the alternating sense of the curvature of the equilibrium orbit, there will be a marked alternation in the sign and magnitude of the local focusing index $|n| = k\varrho_0/R$. This alternation of the focusing action within the individual magnet sectors, with some contribution from the edge focusing that results from the equilibrium orbit crossing the sector boundaries obliquely, can result in a net strong-focusing effect on the beam. Model accelerators of this type have been built (Cole *et al.*, 1957), and have operated in the manner expected from prior analysis, but the design is such that the circumference may be some 5 times that required for a constant-field device and the magnet consequently must be undesirably massive.

B. Spirally Ridged Design

To avoid the large circumference required for a reversed-field FFAG accelerator, it is advantageous to provide a field variation such that the field is alternately high and low along spiral curves that the particles will cross. Specifically, the field is taken as proportional to R^k times a periodic function of $(1/w)\ln(R/R_1)-N\theta$, where θ denotes the azimuthal angle. With the period of this function taken as 2π, N denotes the number of periods (or full sectors) per circumference and the periodic function is constant along curves that make an angle $\tan^{-1}(1/Nw)$ with the radius. A field variation of this form retains the important scaling property that is also satisfied in the reversed-field design; that is, possible orbits of particles of different momenta are scaled replicas of each other, with such geometrically similar orbits shifted azimuthally with respect to one another in the spirally ridged design.[17] Because of this property, the essential characteristics of the transverse oscillations of particles with different energies will be identi-

[17] It will be observed that the relative azimuthal displacement of geometrically similar orbits for particles of different momenta in a scaling field presents complications if it is desired to introduce field-free straight sections whose boundaries extend radially from

cal, and harmful resonances may be avoided at all energies by a suitable choice of parameters.

The characteristics of the transverse oscillations of particles in a spirally ridged accelerator lend themselves to analytic examination most readily if the periodic variation is expressible by a simple sine function and if the amplitude of this variation is not large. We then consider the particle motion in a median-plane field of the form

$$B_y = -B_1(R/R_1)^k\left\{1 + f\sin\left[\frac{\ln(R/R_0)}{w} - N\theta\right]\right\} \tag{50}$$

with f small in comparison to unity (for example $f \leq 1/4$); quantitative examination of orbits in fields that fail to meet these simplifying conditions may be obtained conveniently by digital computations, but will generally exhibit qualitative characteristics similar to those that can be derived from use of Eq. (50).

1. *Analysis of Equations of Motion*

The closed equilibrium orbit in the spiral-sector field of Eq. (50) departs from a circle by an amount that affects significantly the character of the oscillations about this orbit. For a particle of magnetic rigidity p_0/e, the equilibrium orbit may be approximately expressed by

$$R_{\mathrm{eq}} = R_0\left[1 - \frac{f}{N^2-(k+1)}\sin N\theta\right] \tag{51a}$$

where

$$R_0 = R_1\cdot\left(\frac{p_0}{eB_1R_1}\right)^{1/(k+1)} \tag{51b}$$

It is immediately apparent that, in conformity with Eq. (51b), the momentum-compaction factor in the assumed scaling field is

$$\xi = k+1\,; \tag{51c}$$

for investigation of the transverse oscillations it is appropriate to expand the equations of motion about the solution given by Eq. (51a).

If we initially retain only terms that are linear in the departure from the

the central axis of the accelerator—see, for example, Cole and Morton (1959, pp. 31–37). The spiral angle facilitates, however, the extraction of a beam that is circulating in the direction of the spiral.

equilibrium orbit and neglect terms of order $(f/wN)^2$, the equations of motion are of the form

$$\frac{d^2u}{d\theta^2} + (a_x + b_x \cos N\theta)u = 0 \tag{52a}$$

$$\frac{d^2v}{d\theta^2} + (a_y + b_y \cos N\theta)v = 0 \tag{52b}$$

where

$$u = \frac{R - R_{eq}}{R_0} \tag{53a}$$

$$v = \frac{y}{R_0} \tag{53b}$$

and

$$a_x \cong k + 1 - \frac{1}{2}\,\frac{(f/w)^2}{N^2 - (k+1)} \tag{54a}$$

$$a_y \cong -k + \frac{1}{2}\,\frac{(f/w)^2}{N^2 - (k+1)} \tag{54b}$$

$$b_x \cong \frac{f}{w} \tag{54c}$$

$$b_y \cong -\frac{f}{w} \tag{54d}$$

The frequencies of small-amplitude transverse oscillations may be obtained for the Mathieu equations (52a, b) by numerical integration (Belford *et al.*, 1957) or estimated by approximate formulas (Symon *et al.*, 1956, Appendix A; Laslett and Sessler, 1961, Eq. (2.24)) that are valid when f/wN^2 is small. The approximate formulas lead to

$$Q_x^2 \cong a_x + \frac{b_x^2}{2N^2}$$
$$\cong k + 1 \tag{55a}$$

$$Q_y^2 \cong \left(\frac{f}{wN}\right)^2 - k \tag{55b}$$

for k/N^2 and f/wN^2 small in comparison to unity. The boundaries of the first stability zone for solutions to Eqs. (52a, b) may be similarly approximated by the stability condition (Laslett and Sessler, 1961, Sect. IIa)

$$-\frac{b^2}{2N^2} < a < \frac{N^2}{4} - \frac{|b|}{2} \tag{56}$$

or, more accurately, by well-known series expansions (Whittaker and Watson, 1927, Section 19.3, Ex. 2; McLachlan, 1947, Sections 4.90–4.91) for the first characteristic values of the Mathieu equation.

Equations (55a, b) are of good accuracy throughout the present range of interest for the parameters if $2Q/N \leq 1/3$, and for values of $2Q/N$ as great as 2/3 if $|b| \leq N^2/4$. More accurate values for the boundaries and oscillation frequencies for the first region of stable solutions to Eqs. (52a, b) are listed in Table II (from Belford *et al.*, 1957; National Bureau of Standards, 1951) and are illustrated by Fig. 8. A stability diagram for the two degrees of freedom represented by Eqs. (52a) and (52b) is shown in Fig. 9.

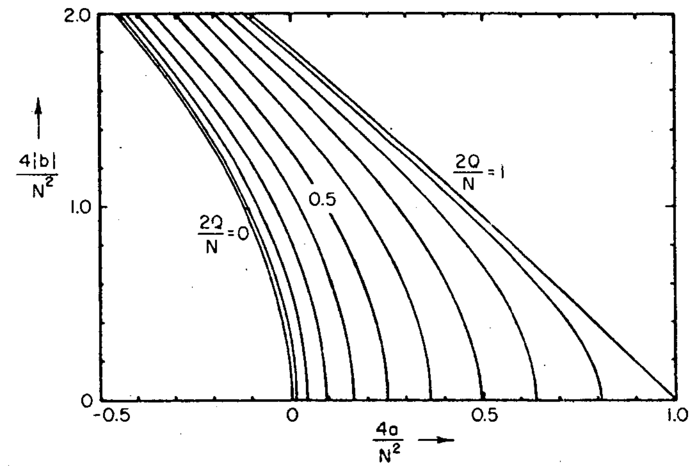

Fig. 8. Diagram showing the relation between the coefficients of Eqs. (52a) or (52b) for various values of the oscillation frequency. Curves are given for increments of 0.1 in the quantity $2Q/N = \sigma/\pi$.

2. *Physical Origin of Axial Focusing*

It is informative to examine the physical origin of the several terms that contribute to the result expressed by Eq. (55b). The results of such an analysis (Laslett, 1961) suggest an interpretation that is summarized below for terms that arise in the coefficient of v in Eq. (52 b). This coefficient may be written

$$K = \frac{eR_0^2}{p_0}\,\frac{[-(\mathbf{V}/V) \times \mathbf{B}] \cdot \hat{e}_y}{y},$$

with $p_0 = e\,|\,B_0 R_0\,|$ and with the guide field (B_y) negative for positively charged particles. Also we may assume $k \ll N^2$.

TABLE II

STABILITY BOUNDARIES AND VALUES OF $2Q/N$ FOR SOLUTIONS TO EQS. (52a) OR (52b)

$\frac{4b}{N^2}$:	0	± 0.2	± 0.4	± 0.6	± 0.8	± 1.0	± 1.2	± 1.4	± 1.6	± 1.8	± 2.0
$\frac{4a}{N^2}$ for $Q = 0$:	0	−0.004995	−0.019913	−0.044566	−0.078649	−0.121766	−0.173445	−0.233169	−0.300393	−0.374564	−0.455139
$\frac{4a}{N^2}$	*Values of 2Q/N*										
−0.4	—	—	—	—	—	—	—	—	—	—	0.295293
−0.3	—	—	—	—	—	—	—	—	0.022886	0.331822	0.513820
−0.2	—	—	—	—	—	—	—	0.204739	0.372817	0.523586	0.700020
−0.15	—	—	—	—	—	—	0.166996	0.326529	0.461670	0.606491	0.809354
−0.12	—	—	—	—	—	0.044613	0.252886	0.382727	0.509724	0.655910	0.907994
−0.09	—	—	—	—	—	0.189606	0.317003	0.432744	0.555508	0.706820	—
−0.06	—	—	—	—	0.142084	0.264945	0.370904	0.478689	0.599985	0.761485	—
−0.03	—	—	—	0.123432	0.229781	0.323667	0.418648	0.521836	0.644024	0.824726	—
0	0	0.070850	0.142551	0.216059	0.292566	0.373744	0.462249	0.563066	0.688564	0.915909	—
0.03	0.173205	0.187553	0.225760	0.279688	0.344378	0.418350	0.502904	0.603071	0.734854	—	—
0.06	0.244949	0.255622	0.285758	0.331479	0.389651	0.459144	0.541413	0.642470	0.784973	—	—
0.09	0.300000	0.309063	0.335254	0.376367	0.430487	0.497137	0.578370	0.681903	0.843572	—	—
0.12	0.346410	0.354556	0.378399	0.416607	0.468086	0.533008	0.614259	0.722151	0.931173	—	—
0.15	0.387298	0.394858	0.417174	0.453456	0.503214	0.567255	0.649518	0.764339	—	—	—
0.2	0.447214	0.454188	0.474973	0.509361	0.557654	0.621757	0.708125	0.845489	—	—	—
0.3	0.547723	0.554252	0.573974	0.607483	0.656567	0.726441	0.837583	—	—	—	—
0.4	0.632456	0.639073	0.659316	0.694701	0.749493	0.838962	—	—	—	—	—
0.5	0.707107	0.714238	0.736433	0.776983	0.847508	—	—	—	—	—	—
$\frac{4a}{N^2}$ for $Q = \frac{N}{2}$:	1.000000	0.898766	0.795124	0.689166	0.580981	0.470654	0.358271	0.243912	0.127656	0.009578	−0.110249

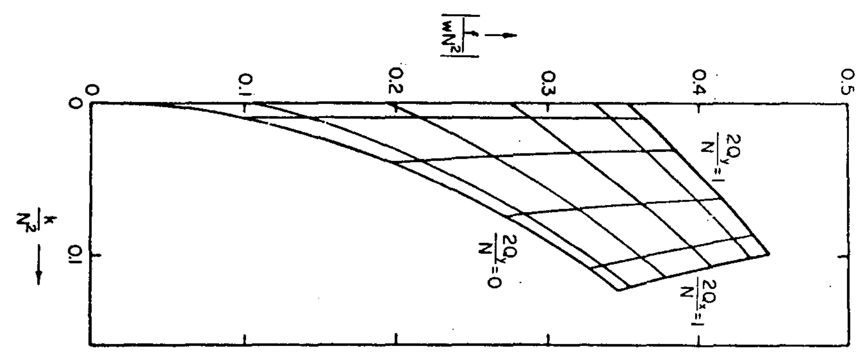

FIG. 9. Diagram of the first stability region for oscillations that are characterized in the two degrees of freedom by Eqs. (52a) and (52b).

(1) For a particle on a circular orbit K will then include terms due to

$$V_\theta B_r = -\left[V_\theta \frac{\partial(-B_y)}{\partial r}\right] y$$

that are

(α) $-k$ from the R^k-dependence of the average strength of the field, and

(β) $-(f/w)\cos N\theta$ due to the radial variation of the spiral term in B_y;

(2) Because the radial motion departs from a circle to the extent given by Eq. (51a), there are additional terms in K:

(α) $(f^2/w^2N^2)\sin^2 N\theta = (1/2)(f^2/w^2N^2)(1-\cos 2N\theta)$ from an additional term $[-R_0(f/N^2)\sin N\theta][-V_\theta\partial^2(-B_y)/\partial r^2]y$ in the development of $V_\theta B_r$, and

(β) $f^2 \cos^2 N\theta = (f^2/2)(1 + \cos 2N\theta)$ due to $-V_r B_\theta \doteq (V_r/R_\theta)[\partial(-B_y)/\partial\theta]\,y$.

The several terms listed above contribute to the value of Q_y^2 as follows:

(1, α) $-k$, the normal value of Q_y^2 in a constant-gradient accelerator;

(1, β) $(1/2)(f^2/w^2N^2)$, by an approximation of the alternating-gradient focusing that arises from radial fields attributable to the spiral ridges;

(2, α) $(1/2)(f^2/w^2N^2)$, from the constant component of force that arises from the additional radial fields experienced by particles that cross the spiral ridges on a noncircular equilibrium orbit; and

(2, β) $f^2/2$, from the constant component of force that arises from azimuthal components of magnetic field, in a configuration such that B_y varies with θ, that act on the radial component of velocity for particles whose equilibrium orbit is noncircular.

Disregarding the term $f^2/2$, that quantitatively is of little importance in a spirally ridged accelerator, the terms listed are seen to combine to give the result expressed by Eq. (55b). It is noteworthy, however, that only one of the terms (namely, 1, β) truly arises from an alternating-gradient focusing action. The last two of the terms listed (2, α, β) have their physical origin in the noncircularity of the equilibrium orbit, and their effect thus corresponds to that noted by Thomas (1938) in his paper that suggested the application of radial ridges to a cyclotron field.

1-164

C. Application to the Cyclotron, Microtron, and Betatron

1. *Cyclotron with Azimuthally Varying Field*

It is evident that the use of azimuthally varying fields, with or without spiral ridges, affords a means of maintaining isochronism and stability for particles accelerated in a cyclotron.[18] An azimuthal variation of the field will lead to a significant scalloping of the particle orbits, but, to the extent that the revolution time of a particle is not greatly affected by the noncircularity of the orbits, one may readily derive the radial variation of magnetic field that is required to insure isochronism. In this case, $\beta \equiv V/c$ must be proportional to radius and the average field strength will be proportional

[18] The conflicting character of the requirements for isochronism and stability in a conventional cyclotron was noted by Bethe and Rose (1937) and by Rose (1938). *Cf.* also the experimental work reported by Wilson (1938).

to $\gamma \equiv (1 - \beta^2)^{-1/2}$. A simple differentiation then shows that the value of k at any radius is[19]

$$k \equiv \frac{R}{B}\frac{dB}{dR} = \gamma^2 - 1 \tag{57}$$

The radial oscillations are characterized by a value of Q_x^2 that is close to $k + 1$, so it then follows that

$$Q_x \cong \gamma \tag{58}$$

in an isochronous cyclotron. The scaling condition that was introduced for annular fixed-field accelerators in which isochronism was not required cannot be maintained if Eq. (57) is to be satisfied, but Eq. (58) indicates the possibility of achieving a design in which Q_x remains bounded by the integral values 1 and 2 as the kinetic energy of the particles increases from zero to a value in the neighborhood of M_0c^2. A precise analysis of particle dynamics in fields that are suitable for isochronous cyclotrons is too detailed for presentation here; an early analysis was given by Dunn *et al.* (1956), a comprehensive review of cyclotron technology has been presented by Cohen (1959), and an excellent résumé of both the theory and design principles for sector-focused cyclotrons has been given by Richardson (1965).

With $k > 0$, some form of azimuthal variation of field strength is required to provide axial focusing. As has been noted earlier, one obtains

$$Q_y = [(f^2/2) - k]^{1/2} \tag{59}$$

with "Thomas focusing," and more modest values of f will suffice if spiral focusing is introduced.[20] The Thomas design (Thomas, 1938; Schiff, 1938; Judd, 1955) received an initial experimental test in two electron models (Pyle *et al.*, 1955; Kelly *et al.*, 1956), and both radially and spirally ridged cyclotrons have since come into successful operation for the acceleration of

[19] Alternatively, one may note that the momentum compaction is given directly by $\xi = k + 1$ and the condition of isochronism ($\delta T = 0$) requires $\xi = \gamma^2$ (refer to *Note I*), so that Eq. (57) then follows immediately.

[20] An ingenious radial-ridge design was adopted for a three-sector cyclotron built at the Karlsruhe Nuclear Research Center (Leopoldshafen, Germany) to provide a continuous beam of 50-MeV deuterons. The large value of f required in this case was realized by locating *three* radio-frequency electrodes in the regions where the magnet gap is large and driving them together at the third harmonic of the orbital frequency (Steimel and Lerbs, 1959; Steimel, 1963).

semirelativistic beams of positively charged ions.[21] An electron model of an eight-sector "Mc^2 cyclotron" (Livingston and Martin, 1964) has successfully demonstrated the ability to obtain a beam whose kinetic energy is close to the rest energy of the particles and then to extract this beam efficiently through the excitation of the "8/4 essential resonance" that occurs for $Q_x = 2$. Theoretical and experimental work also has been directed (Haddock *et al.*, 1964) to the design of a negative-ion cyclotron from which proton beams of variable energy up to 625 MeV could be efficiently extracted magnetically following charge stripping of the negative ions in their passage through thin carbon foils.

The selection of parameters for sector-focused cyclotrons and detailed determination of their engineering design have come to constitute an important field of specialization in accelerator technology (Howard, 1959; Siegbahn and Howard, 1962; Howard and Vogt-Nilsen, 1963). Twenty six isochronous cyclotrons have been listed by Howard and Vogt-Nilsen (1963) as in operation or under construction in the spring of 1963. With suitable designs, energy variation may be achieved over a wide range, a change to a new type of particle can be accomplished rapidly, and beams of good emittance may be extracted efficiently. In determining the desired variation of magnetic field strength with radius it may be desirable to forego precise isochronism and to give special attention to the central region where the size of the gap prevents reliance on flutter focusing. Thus, in the three-sector "88-inch" cyclotron at the Lawrence Radiation Laboratory in Berkeley (California), for which the pole diameter is 224 cm and the minimum internal magnet gap is 19 cm, the flutter focusing becomes effective only for radii greater than about 19 cm and electric focusing is effective only within a 7.6 cm radius (Watson, 1962). The use of trimming coils in various configurations is helpful to control and to correct the spatial variation of the magnetic field. "Ion pullers" and "beam clippers" can assist in obtaining from the internal ion source a beam whose initial conditions are suitably defined for subsequent extraction from the cyclotron (Willax and Garren, 1962). An alternative method of injection introduces the beam through a

[21] An extensive series of papers on the theory and design of cyclotrons with azimuthally varying fields will be found in the *Proceedings of the International Conference on High Energy Accelerators, Dubna, USSR, 1963* (Atomizdat, Moscow, USSR, 1964) and in earlier publications cited therein. For collections of papers specifically concerned with detailed problems in the design, construction, and use of cyclotrons with azimuthally varying fields, see the proceedings of the 1959, 1962, and 1963 international conferences on sector-focused cyclotrons (edited respectively by Howard, Siegbahn and Howard, and Howard and Vogt-Nilsen).

hole on the axis of the magnet pole, as has been done on the 3-sector radial-ridge cyclotron at the University of Birmingham (Cox *et al.*, 1962).

The acceleration of negative ions requires good vacuum conditions and the use of somewhat lower field strengths than otherwise would normally be selected, in order to avoid premature dissociation of a substantial fraction of the ions [see résumé by Judd (1962)]. The acceleration of polarized protons and deuterons—injected as atomic beams and ionized at the center of the accelerator—has proven feasible in constant-field cyclotrons, provided that refrigerated surfaces maintain the vapor pressure of water at a sufficiently low value to avoid excessive background from nonpolarized protons (cf. Dick *et al.*, 1963; Thirion, 1963; and references cited therein). There is a corresponding interest in the possibility of accelerating such polarized particles in cyclotrons (or other circular accelerators) with azimuthally varying fields (Cox *et al.*, 1962; Luccio *et al.*, 1962), and this interest has motivated an examination of the possibly significant enhancement of depolarization through the agency of unavoidable energy-dependent resonances (that can occur between the precession frequency and the frequency of some oscillatory component of the field felt by the particle). Several analyses have been made of this potential depolarizing mechanism (cf. Khoe and Teng, 1963, and earlier work cited therein) and suggest that a reasonable rate of acceleration in a sector-focused cyclotron will preserve the greater part of the initial polarization.

Table III lists a few of the published characteristics of the "88-inch"

TABLE III

APPROXIMATE SPECIFICATIONS OF THE LRL AND OAK RIDGE ISOCHRONOUS CYCLOTRONS

Characteristic	LRL, Berkeley	Oak Ridge, Tennessee	
Maximum particle energies	59 p 65 d 130 α	~75 p ~40 d ~80 α	MeV
Pole diameter	224	193	cm
Minimum gap	19	19	cm
Average field at r_{max}	17	17	kG
Sectors	3	3	—
Maximum spiral angle	55	30	deg
Magnet weight	260	190	tonne
Magnet power	1000	2000	kw
R-f electrodes	One, 180° dee	One, 180° dee	
kV/turn (max.)	140	200	kV

and 76-inch (ORIC) isochronous cyclotrons that have been operating respectively since 1961 and 1962 at the Lawrence Radiation Laboratory in Berkeley (Kelly, 1962; Grunder and Selph, 1963) and at the Oak Ridge National Laboratory (Tennessee). Each of these cyclotrons permits the final particle energy to be varied and can accelerate various ionic species. The LRL radio-frequency system covers the range from 16.5 MHz to one-third this value, thus permitting a transfer to third-harmonic operation without leaving a gap in the energy range of the accelerator. Similarly the ORIC system is continuously tunable from 22.1 to 7.3 MHz. The first of these cyclotrons was designed primarily as a deuteron accelerator. The usable radius of the ORIC is about 80% as great as that available in the 88-inch cyclotron, and the limiting energies for deuterons and alpha particles for this reason are correspondingly smaller. The limiting oscillator frequency of 16.5 MHz similarly restricts proton energies (at an extraction radius of 100 cm) to 59 MeV in the LRL machine.

2. *Microtron*

The microtron (Veksler, 1945) or "electron ~~synchro~~cyclotron" normally employs a spatially constant dc magnetic field,[22] and achieves vertical focusing only through the provision of a region of slightly increased magnetic field in the immediate region of the radio-frequency cavity (Redhead *et al.*, 1950; Aitken *et al.*, 1961) or by virtue of the focusing action of the rf fields within this cavity (Bell, 1953; Reich, 1960). A modification that promises to afford a flexibility in the design that could be advantageous in several respects is that in which separated sectors, or sectors of unequal field strength, are employed to guide the particles on the orbits to be described between successive transits of the rf cavity. In such a separated-sector design there then may be the opportunity to introduce a desirable amount of edge focusing at the sector boundaries, and the incorporation of spiral boundaries may deserve consideration. Although the dynamics of particles in a microtron are strictly not describable by differential equations with simple periodic coefficients, some of the analytical methods employed for the analysis of alternating-gradient accelerators will be applicable. The utility of microtrons employing separated sectors (Moroz, 1956, 1957, 1958) has been discussed in a general article by Roberts (1958), and an electron accelerator of this type has been successfully operated (Brannen *et al.*, 1960; Brannen and Froelich, 1961; Froelich, 1962) at the University of Western Ontario (London, Ontario, Canada).

[22] For a general discussion of the microtron (and of other particle accelerators), see for example, Kollath (1955), or Kolomensky and Lebedev (1966).

3. *FFAG Betatron*

An annular FFAG field, with a value of k sufficiently great that particles with a large range of momentum may be simultaneously held by this field, affords a means of providing a beam with a very high duty factor by use of betatron acceleration. The accelerating electric fields would be generated in such a case by the change of flux in a large separate magnetic core. If the excitation of the core is such that the total flux change is approximately twice that required to accelerate particles to the full energy that the guide field can accommodate, particles injected during the first quarter cycle of increasing flux will be accelerated to full energy and produce an intense beam with a duty factor approaching 25% (Fig. 10). Betatron acceleration has

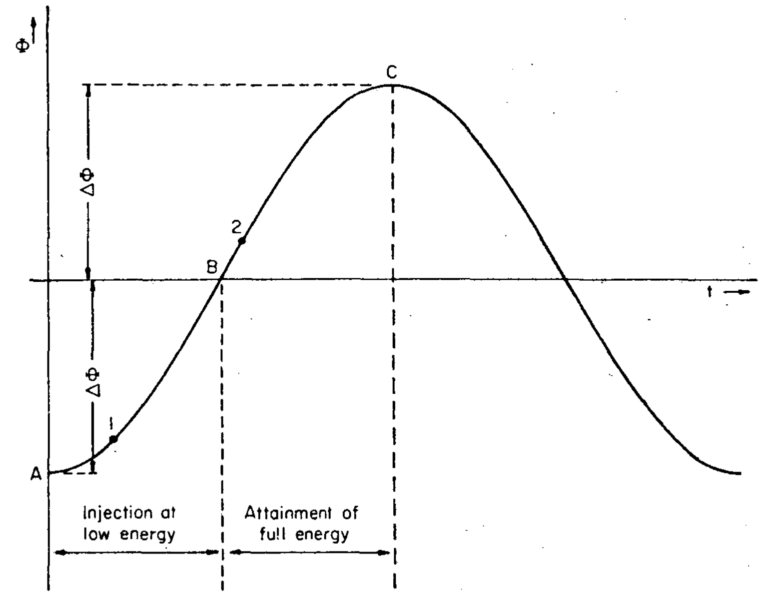

FIG. 10. Time dependence of magnetic flux for betatron acceleration of particles in a FFAG field, indicating the possibility of achieving a high duty factor. $\Delta\Phi$ denotes the change of flux that is required to accelerate a given particle from its initial to its final energy. Particles injected during the interval AB (for example, at 1) will attain full energy during the time interval BC (for example, at 2) as a result of acceleration produced by the action of $\Delta\Phi$.

been tested in electron models as one means of accelerating particles in FFAG machines (Cole *et al.*, 1957) and design studies have indicated the possibility of realizing high performance electron accelerators based on these methods.

D. Nonlinear Resonances

Nonlinear terms in the equations that govern the motion of particles in a circular accelerator may influence the orbits significantly in some situations, particularly through the mechanism of nonlinear resonances that can impair the stability of the motion. Such nonlinear effects deserve particular attention in analysis of FFAG accelerators, since the character of the fields in this type of accelerator is inherently such that appreciable nonlinear terms necessarily will be present.

In the spirally ridged FFAG design considered earlier, consideration of nonlinear phenomena requires that Eqs. (52 a,b) be supplemented by the inclusion of additional terms (Cole, 1956):

$$\frac{d^2u}{d\theta^2} + (a_x + b_x \cos N\theta)u + \frac{f}{2w^2}(\sin N\theta)(u^2 - v^2) - \frac{f}{6w^3}(\cos N\theta)(u^3 - 3uv^2) = 0 \tag{60a}$$

$$\frac{d^2v}{d\theta^2} + (a_y + b_y \cos N\theta)v - \frac{f}{w^2}(\sin N\theta)\, uv + \frac{f}{2w^3}(\cos N\theta)\, u^2v = 0 \tag{60b}$$

1-167

It will be noted that Eqs. (60a, b) are derivable from a Hamiltonian and that only terms linear in v have been included. A simple scaling of these equations will show that, if u and v are expressed in units of w, the properties of the solutions are expressible in terms of the phase advance per sector (σ_x and σ_y) of solutions to the uncoupled linearized equations and a parameter $\lambda \equiv f/wN^2$ that measures the strength of the nonlinearities (Laslett and Sessler, 1961).

Inspection of Eq. (60a), with v set equal to zero, suggests that the quadratic term can lead to a resonant action when Q_x is near $N/3$ (σ_x near $2\pi/3$). Solutions to the linearized equation will contain terms of frequency Q_x, $N \mp Q_x$, ... ; $u^2 \sin N\theta$ will have a strong component of frequency $N - 2Q_x$; and this term can represent a resonant driving function if $Q_x \cong N/3$. By virtue of such action by low-order nonlinear resonances, phase diagrams that depict the radial oscillations (when constructed for successive homologous points in the structure) become markedly distorted from simple elliptical curves, and a separatrix then can occur to represent a limiting amplitude beyond which the oscillations effectively are unstable. At the amplitude corresponding to the boundary of stable motion, there will be a periodic solution (for example, with a fundamental frequency represented by $N\theta/3$ for the $Q_x = N/3$ resonance) that is represented on the phase diagram by unstable fixed points (Fig. 11).

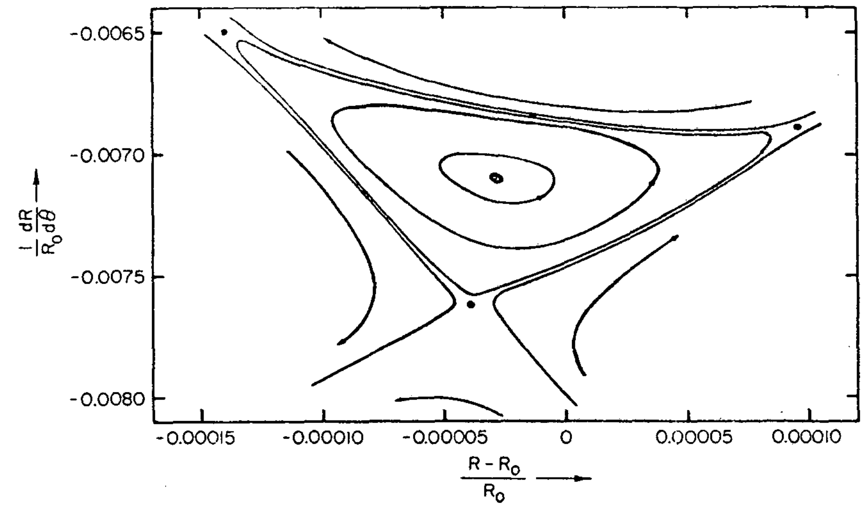

Fig. 11. Phase curves depicting the radial motion in a spirally ridged FFAG accelerator. The curves were constructed from points computed for the parameters $N = 40$, $k = 128$, $f = 0.25$, $1/w = 2112$, and the corresponding small-amplitude oscillation frequency is such that $\sigma_x = 0.647\pi$. For larger amplitudes the frequency departs from this value, and at the limiting amplitude for stable motion σ_x attains the value $2\pi/3$ that is characteristic of the unstable equilibrium orbit associated with this nonlinear resonance. The stable equilibrium orbit is represented by the point at the center of the diagram, and the unstable orbit by the three "unstable fixed points" depicted by solid dots on the figure.

1. *Limiting Amplitude When Q_x is Close to $N/3$*

The limiting amplitude for a simple nonlinear resonance may be conveniently estimated through use of an approximate solution of a suitable form for which the coefficients are adjusted to achieve a harmonic balance of the terms in the differential equation. Thus a useful estimate of the radial stability limit that results from the quadratic term in Eq. (60a) may be obtained very simply by replacing the coefficient of u by Q_x^2 and employing a trial solution of the form $u = A \sin N\theta/3$. One thus obtains (Laslett and Sessler, 1956) the approximate result

$$A \doteq \frac{8w^2}{f}\left[Q_x^2 - \left(\frac{N}{3}\right)^2\right] \tag{61a}$$

$$\frac{|A|}{w} \doteq 2\left(\frac{f}{wN^2}\right)^{-1}\left|\left(\frac{\sigma_x}{\pi}\right)^2 - \left(\frac{2}{3}\right)^2\right| \tag{61b}$$

indicating the pronounced limitation of stable amplitude that is imposed by the quadratic term of Eq. (60a) when Q_x is close to $N/3$.

Systematic approaches to the analysis of nonlinear equations with periodic coefficients have been given by Moser (1955a, b, 1956) and by Sturrock (1955, 1958a, b). Since it has been seen possible by a suitable transformation [Eqs. (31a, b)] to remove the alternating-gradient character of the coefficient of u, it will suffice for present purposes to illustrate a procedure similar to that of Moser by its application (for the $Q_x \cong N/3$ resonance) to the equation

$$\frac{d^2\eta}{d\psi^2} + \left(\frac{2Q}{N}\right)^2 \eta + \frac{1}{2}(\sin 2\psi)\eta^2 = 0 \tag{62}$$

that is derivable from the Hamiltonian

$$H = \frac{1}{2}P^2 + \frac{1}{2}\left(\frac{2Q}{N}\right)^2 \eta^2 + \frac{1}{6}(\sin 2\psi)\eta^3 \tag{63}$$

It will be the purpose to transform the variables (η, P) in such a way that the ψ dependence is removed from the cubic term in H; the resultant Hamiltonian, through terms of this order (and including ψ-independent terms of the next higher order), may then be taken as an approximate constant of the motion from which invariant phase curves can be constructed and fixed points determined. This technique in principle can be extended (Moser, 1955a) to displace the ψ-dependence to terms of increasingly high order in the dependent variable.

We shall employ a series of canonical transformations (Goldstein, 1950), defined by generating functions G_0, G_1, and G_2, to transform the conjugate variables and their associated Hamiltonian functions successively from (η, P) to (γ_0, J_0), (γ_1, J_1), and (γ_2, J_2):

1. $$G_0(\eta, \gamma_0) = (Q/N)\,\eta^2 \cot\gamma_0 \tag{64a}$$

$$P = \partial G_0/\partial\eta = (2Q/N)\eta\cot\gamma_0 \tag{64b}$$

$$J_0 = -\,\partial G_0/\partial\gamma = (Q/N)\eta^2\csc^2\gamma_0 \tag{64c}$$

$$\begin{aligned} H_0 &= (2Q/N)J_0 + \frac{1}{48}(N/Q)^{3/2}J_0^{3/2} \\ &\quad \times [3\cos(\gamma_0 - 2\psi) - 3\cos(\gamma_0 + 2\psi) \\ &\quad + \cos(3\gamma_0 + 2\psi) - \cos(3\gamma_0 - 2\psi)]. \end{aligned} \tag{64d}$$

2. $$G_1(\gamma_0, J_1) = J_1\gamma_0 - \frac{1}{96}(N/Q)^{3/2}J_1^{3/2}\left[3\frac{\sin(\gamma_0 - 2\psi)}{1 - Q/N} + 3\frac{\sin(\gamma_0 + 2\psi)}{1 + Q/N} - \frac{\sin(3\gamma_0 + 2\psi)}{1 + 3Q/N}\right] \tag{65a}$$

$$J_0 = \partial G_1/\partial\gamma_0 = J_1 + \frac{1}{32}(N/Q)^{3/2}J_1^{3/2}\left[\frac{\cos(\gamma_0 - 2\psi)}{1 - Q/N} + \frac{\cos(\gamma_0 + 2\psi)}{1 + Q/N} - \frac{\cos(3\gamma_0 + 2\psi)}{1 + 3Q/N}\right] \tag{65b}$$

$$\gamma_1 = \partial G_1/\partial J_1 = \gamma_0 + \frac{1}{64}(N/Q)^{3/2}J_1^{1/2}\left[3\frac{\sin(\gamma_0 - 2\psi)}{1 - Q/N} + 3\frac{\sin(\gamma_0 + 2\psi)}{1 + Q/N} - \frac{\sin(3\gamma_0 + 2\psi)}{1 + 3Q/N}\right] \tag{65c}$$

$$\begin{aligned} H_1 &= (2Q/N)J_1 - \frac{1}{48}(N/Q)^{3/2}J_1^{3/2}\cos(3\gamma_1 - 2\psi) \\ &\quad + \frac{1}{2048}(N/Q)^3 J_1^2\left[\frac{6Q/N}{1 - Q^2/N^2} - \frac{1}{1 + 3Q/N}\right] \end{aligned} \tag{65d}$$

in which only terms independent of ψ and of γ_1 have been retained in the coefficient of J_1^2.

3. $$G_2(\gamma_1, J_2) = J_2 \cdot \left(\gamma_1 - \frac{2}{3}\psi\right) \tag{66a}$$

$$J_1 = \partial G_2/\partial\gamma_1 = J_2 \tag{66b}$$

$$\gamma_2 = \partial G_2/\partial J_2 = \gamma_1 - \frac{2}{3}\psi \tag{66c}$$

$$\begin{aligned} H_2 &= -\left(\frac{2}{3} - \frac{2Q}{N}\right)J_2 - \frac{1}{48}(N/Q)^{3/2}J_2^{3/2}\cos 3\gamma_2 \\ &\quad + \frac{1}{2048}(N/Q)^3 J_2^2\left[\frac{6Q/N}{1 - Q^2/N^2} - \frac{1}{1 + 3Q/N}\right] \end{aligned} \tag{66d}$$

again with ψ-dependent terms omitted from the coefficient of J_2^2.

The detailed algebraic steps required in the transformations (64a) *et seq.* have not been shown, but the effect of these transformations is apparent. The first transformation results in a Hamiltonian that would be a constant of the motion if no nonlinear terms had been present in Eq. (62)—that is, if only quadratic terms had been present in the Hamiltonian shown in Eq. (63). The second transformation was so chosen as to remove from the Hamiltonian all ψ-dependent terms in the coefficient of $J_1^{3/2}$ save that associated with the resonance $Q/N \sim 1/3$. The third transformation removes this remaining ψ-dependence from the cubic $(J_2^{3/2})$ term.

Without pursuing the analysis further, the Hamiltonian shown in Eq. (66d) may be taken as an approximate constant of the motion and the inverse transformations employed to obtain equations for the "invariant phase curves" of a P, η-diagram. Other characteristics of the motion, such as the variation of the oscillation frequency with amplitude, may similarly be determined (Laslett, 1959).

Of particular interest in defining the limits of stability are the three unstable fixed points, for which the Hamiltonian is stationary. From Eq. (66d), this condition is satisfied when

$$\gamma_2 = -\pi/3,\ \pi/3,\ \text{or}\ \pi \tag{67a}$$

$$J_2^{1/2} = 64\,\varkappa \left(\frac{1}{3} - \frac{Q}{N}\right)\left(\frac{Q}{N}\right)^{3/2} \tag{67b}$$

where

$$\varkappa \equiv \frac{(1+4g)^{1/2}-1}{2g} \doteq 1 - g + 2g^2 - 5g^3 + 14\,g^4 - \cdots \tag{67c}$$

and

$$g = 2\left(\frac{1}{3} - \frac{Q}{N}\right)\left[\frac{6Q/N}{1-(Q/N)^2} - \frac{1}{1+3Q/N}\right] \tag{67d}$$

The inverse transformation to the original variables (P, η), although tedious, is straightforward. For a phase diagram pertaining to $\psi = 0$ (*mod* π) one obtains

$$\eta = \pm 32\sqrt{3}\left(\frac{1}{3} - \frac{Q}{N}\right)\left(\frac{Q}{N}\right)\varkappa \times \left\{1 - \left[\frac{2}{1-(Q/N)^2} - \frac{1}{1+3Q/N}\right]\left(\frac{1}{3} - \frac{Q}{N}\right)\varkappa\right\} \tag{68a}$$

$$P = 64\left(\frac{1}{3} - \frac{Q}{N}\right)\left(\frac{Q}{N}\right)^2\varkappa \times \left\{1 + \left[\frac{10}{1-(Q/N)^2} + \frac{1}{1+3Q/N}\right]\left(\frac{1}{3} - \frac{Q}{N}\right)\varkappa\right\} \tag{68b}$$

and

$$\eta = 0 \tag{69a}$$

$$P = -128\left(\frac{1}{3} - \frac{Q}{N}\right)\left(\frac{Q}{N}\right)^2\varkappa \times \left\{1 - \left[\frac{2}{1-(Q/N)^2} - \frac{1}{1+3Q/N}\right]\left(\frac{1}{3} - \frac{Q}{N}\right)\varkappa\right\} \tag{69b}$$

for the coordinates of the three unstable fixed points. From Eq. (68a)

it is seen that, for operation close to the resonance, the displacement of the unstable equilibrium orbit at $\psi = 0$ (mod π) attains the magnitude

$$\text{Displ}\Big|_{\psi=0} = \frac{32}{\sqrt{3}}\left|\frac{Q}{N} - \frac{1}{3}\right| \tag{70a}$$

since $Q/N \simeq 1/3$ and $\varkappa \simeq 1$ [Eq. (67c)]; for $\psi = \mp\pi/4$ (mod π), however, a similar analysis leads to the amplitude

$$\text{Ampl}\Big|_{\psi=-\pi/4} = \frac{64}{3}\left|\frac{Q}{N} - \frac{1}{3}\right| \tag{70b}$$

in agreement with the approximate result suggested for this case by Eq. (61a) of the text.

2. *Analysis of Coupling Resonances*

Analytic methods analogous to that just presented for the $Q_x = N/3$ resonance can be applied to other essential resonances in one degree of freedom, to the effect of forcing terms that can result in effects attributable to a machine resonance (perturbation of period C_0), and to coupling resonances.[23] The effects of coupling, due to a sum or difference resonance, have been examined computationally and analyzed by a technique similar to that of Moser (1955a) by Meier and Symon (1959). In this latter work the coupling term in the Hamiltonian was taken to be proportional to $uv^2 \cdot \Delta(N\theta)$ where $\Delta(N\theta)$ is a periodic delta function of period $2\pi/N$, since the computational work could then employ a sequence of simple linear and nonlinear algebraic transformations that made it feasible to perform individual computational runs extending through as many as 10^6 sectors.

Of particular interest is the character of orbits that are influenced by sum or difference resonances. Because of such coupling resonances, an initially small amplitude of axial oscillation may experience a pronounced growth, provided the amplitude of the radial oscillations is above a certain threshold value. This threshold will be low, and the rate of growth correspondingly large, if the oscillation frequencies are close to values that satisfy a resonance relation [$g_xQ_x + g_yQ_y = g$ or gN (for machine resonances or essential resonances, respectively), where g_x, g_y, and g are integers (of small absolute value) and with g_y *even* if there exists a symmetry plane that excludes odd powers of y from the Hamiltonian.] Although the axial growth

[23] The effect of a perturbation whose wavelength is equal to three periods of the magnet structure has been reported by Laslett and Symon (1959).

attributable to a single *difference* resonance in principle may be bounded, it could lead to orbit excursions that are undesirable in practice and may in fact result in loss of particles through an enhanced action of other resonances (Meier and Symon, 1959).

Estimates of the threshold for axial growth, and of the initial growth rate to be expected if this threshold is exceeded, may be obtained conveniently by regarding the axial motion as governed by a linear differential equation in which the coefficients have been modified by the substitution of a prescribed radial oscillation in the coupling terms. This introduction of a specified radial motion in a non-Hamiltonian manner was suggested by Walkinshaw (1956); the technique has been applied (Laslett and Sessler, 1961) with considerable success to the analysis of several coupling resonances that are expected to be significant in a spirally ridged FFAG accelerator, and appears to be entirely justifiable for the rather small axial amplitudes that this type of accelerator normally can accept.

To apply this technique to the prominent $Q_x \doteq 2Q_y$ resonance in particular, one retains in Eq. (60b) the coupling term that is proportional to uv, and substitutes for u an approximate solution to the linear equation for the radial motion [Eq. (52a)]:

$$u \doteq A\left[\sin Q_x\theta + \frac{f}{wN^2}\sin Q_x\theta\cos N\theta - 2\frac{fQ_x}{wN^3}\cos Q_x\theta\sin N\theta\right] \quad (71)$$

The resulting differential equation for v then becomes

$$\frac{d^2v}{d\theta^2} + [a_y + b_y\cos N\theta + c_y\sin Q_x\theta\sin N\theta + d_y\cos Q_x\theta]v = 0 \quad (72)$$

where a_y and b_y are given by Eqs. (54b) and (54d), respectively,

$$c_y = -Af/w^2, \quad (73a)$$

and

$$d_y = Af^2Q_x/w^3N^3 \quad (73b)$$

Equation (72) may be regarded as a Hill equation if we suppose (artificially) that N/Q_x is rational, and it will have unstable solutions in regions whose boundaries can be found conveniently by a variational method (Laslett and Sessler, 1961)[24]:

[24] Insertion of a trial function

$$v \doteq B_1\cos Q_x\theta/2 + P_1\cos(N - Q_x/2)\theta + P_2\cos(N + Q_x/2)\theta$$

into

$$\delta\int \tfrac{1}{2}\{(dv/d\theta)^2 - [a_y + b_y\cos N\theta + c_y\sin Q_x\theta\sin N\theta + d_y\cos Q_x\theta]v^2\}\,dv = 0$$

leads to

$$P_{1,2}/B_1 \simeq \tfrac{1}{2}(b_y \pm c_y/2)(1 \pm Q_x/N)/N^2$$

and to a stability boundary that has been cited in the text. The second boundary to the zone of instability is similarly given by use of sine functions in the trial expression for v.

1-170

$$|Q_x^2 - (2Q_y)^2| \doteq 2\,|b_yc_yQ_x/N^3 + d_y| \quad (74a)$$

$$= 4\frac{f^2}{w^3}\frac{Q_x}{N^3}|A| \quad (74b)$$

The threshold amplitude for radial motion, above which growth of the axial amplitude will occur, thus becomes

$$|A|_{\text{thr}} = \frac{w^3N^3}{4f^2Q_x}|Q_x^2 - (2Q_y)^2| \quad (75a)$$

or

$$\frac{|A|_{\text{thr}}}{w} = \frac{1}{16}\left(\frac{f}{wN^2}\right)^{-2}\left(\frac{Q_x}{N}\right)^{-1}\left|\left(\frac{\sigma_x}{\pi}\right)^2 - \left(\frac{2\sigma_y}{\pi}\right)^2\right| \quad (75b)$$

Similarly, the growth rate when this threshold is exceeded may be estimated (Laslett and Sessler, 1961) as

$$\mu_y = 2\pi\left(\frac{f}{wN^2}\right)^2\frac{(A^2 - A_{\text{thr}}^2)^{1/2}}{w}\ \text{nepers/sector}, \quad (76a)$$

with a maximum value

$$(\mu_y)_{\max} = 2\pi\left(\frac{f}{wN^2}\right)^2\frac{|A|}{w}\ \text{nepers/sector} \quad (76b)$$

E. Application of FFAG Principles to Annular Accelerators

Electron models of annular FFAG accelerators have been constructed (Cole *et al.*, 1957; Kerst *et al.*, 1960; MURA Staff, 1959, 1961b; Curtis *et al.*, 1964), and have been operated both with betatron and synchrotron acceleration. Larger accelerators of this type are of interest because of their flexible duty factor, and because of the resultant potentiality of providing intense beams and the ability of building up very strong circulating currents within the accelerator. High intensities, if not precluded by unanticipated instabilities arising from collective effects, would be advantageous in experimental investigation of fundamental processes of low cross section that are significant in the study of elementary-particle physics, for the production of high quality secondary beams, and to permit the use of colliding beams to achieve center-of-mass energies greatly in excess of those that result when a beam strikes a stationary target.[25]

The Midwestern Universities Research Association staff has completed designs for spirally ridged FFAG proton accelerators with maximum energies of 10 GeV (*cf.* MURA Staff, 1961a) and 12.5 GeV, and recently prepared a similar analysis for a 500-MeV machine of this type that could serve as a high-intensity injector in a cascade-synchrotron facility (Snowdon, 1964). Table IV presents the major design parameters of these proposed facilities.

TABLE IV

MAJOR DESIGN PARAMETERS FOR HIGH-INTENSITY FFAG PROTON ACCELERATORS (AFTER M.U.R.A.)

Maximum energy (kinetic)	0.500	10.0	12.5 GeV
Injection energy	20	200	200 MeV
Radius ($C_0/2\pi$)	6.858 [a]	72.0 [b]	88.6 [c] m
N	16 [d]	48 [d]	48 [d]
$k = (\varrho/B)(dB/d\varrho)$	8.2	85	85
$1/w$	75	536	548
Q_x	3.211	9.78	9.78
Q_y	2.256	6.29	6.29
Aperture			
radial [e]	1.346	2.75	3.42 m
axial [f]	5.08	19	15.2 cm at inject.
	2.54 [g]	10 [h]	7.6 [i] cm
Magnet weight (total)	410	15000	22000 ton (metric)
Magnet-excitation power	3.4	31.5	47.2 Mw

[a] For 0.5-GeV equilibrium orbit.
[b] For 10.0-GeV equilibrium orbit.
[c] For 12.5-GeV equilibrium orbit.
[d] Number of superperiods is $\frac{1}{2}N$
[e] Region of good field
[f] Within chamber
[g] At $R = 6.934$ m
[h] At $R = 72.1$ m
[i] At $R = 88.75$ m

[25] At highly relativistic energies, the reaction energy that is available in the center-of-mass system when a particle of rest energy M_0c^2 and total energy E_1 strikes a similar stationary particle is $E_{cm} \simeq [2E_1(M_0c^2)]^{1/2}$, whereas two colliding beams of particles with energy E make available an energy of $2E$. This latter energy thus is equivalent to that obtained by a beam of energy $E_1 = 2E^2/M_0c^2$ directed against a stationary target. A "two-way" design (MURA Staff, 1959, 1961b; Curtis *et al.*, 1964) for a FFAG accelerator represents one means by which colliding beams of sufficient intensity might be achieved, but recent interest in the construction of a facility for colliding proton beams has been

The magnet design employs radial blocks, to which are bolted spirally oriented poles that are provided with individual excitation coils. A non-energized "zero pole" is located between each pair of spiral poles in order to increase the effective flutter (~ 1) that can be produced in the magnetic field. Induced radioactivity and radiation damage can present problems in the maintenance of high-energy accelerators of this type, or of any other that is designed to achieve high intensity. Efficient beam-handling techniques, especially for extraction of the high-energy beam, and the selection of suitable construction materials therefore should be regarded as highly important features of the design.

5.3.6. Notes

Note I

The quantity ξ is commonly termed the "momentum compaction factor" in the literature and is frequently denoted by α or $1/\alpha$. Since the time for a particle to complete one revolution around the accelerator is given in terms of its speed and its average orbit radius by

$$T = 2\pi(\varrho_0 + \langle X\rangle_{\text{av}})/V,$$
$$\delta T/T = \langle X\rangle_{\text{av}}/\varrho_0 - \delta V/V_0 = [1/\xi - (E/m_0c^2)^{-2}](\delta p/p_0).$$

The quantity $1/\xi - (E/m_0c^2)^{-2}$, accordingly, will enter as a factor in determining the frequency of phase oscillations. If $\xi > 1$, as is the case for alternating-gradient synchrotrons of the type considered here, there will be a "transition energy," $E_T = \sqrt{\xi}\, m_0c^2$, above which the equilibrium phase angles possible for stable phase oscillations are no longer less than $\pi/2$ but become greater than $\pi/2$. An expansion of Eq. (35c) leads to

$$\xi \doteq (\pi^2/12)\,(n/N)^2[1 + (\pi^4/2520)\,(n/N^2)^2 + \cdots]$$

so that, through use of Eq. (34), we obtain

$$\xi \doteq Q_x^2[1 + (\pi^4/40)\,(n/N^2)^2]^{-1} = Q_x^2[1 + 3\sigma_x^2/40]^{-1}$$

for small σ_x. It is noted that replacement of Eq. (35) by the nonalternating-gradient equation $d^2x/ds^2 + (Q_x^2/\varrho_0^2)x = (1/\varrho_0)\,(\delta p/p_0)$, for which the

directed toward the use of separated-function alternating-gradient "storage rings," into which particles could be injected from an accelerator such as the CERN 28-GeV proton synchrotron (Hereward *et al.*, 1961; Johnsen *et al.*, 1964; Schnell, 1964; Fischer, 1964; Ferger *et al.*, 1964).

same transverse-oscillation frequency would apply, would lead directly to $\xi = Q_x^2$. ξ will tend toward zero as the $\sigma_x = 0$ stability boundary is approached, but it appears infeasible to attain *negative* momentum compaction within the first zone of stability for the free radial oscillations ($0 < \sigma_x < \pi$) in a conventional alternating-gradient accelerator. By use of reversed fields in a fraction of the magnets, however, a noncircular equilibrium orbit will result for particles with the nominal momentum p_0, and it has been found possible to achieve in this way a very large momentum compaction factor (and so obtain a very high transition energy, that may be placed above the maximum energy of the accelerator). Reversed fields were proposed for this purpose by Vladimirskij and Tarasov, and the method has been used with the 7-GeV "synchrophasotron" at the Institute for Theoretical and Experimental Physics in Moscow—for parameters and discussion of the design of this accelerator see Vladimirskij (1959).

Note II

1-172

As an example of one source of closed-orbit deviation for which provision would be made in selecting the radial aperture of the accelerator, we consider a surveying system based on M monuments that nominally are equally spaced within the magnet enclosure. The assumed surveying procedure will involve (1) measurement of the inter-monument separations (S) and (2) measurement of the perpendiculars (h_i) dropped from monuments M_i to the straight lines connecting monuments M_{i-1} and M_{i+1}. When M is large, the *radial* position of the monuments is determined primarily through these latter measurements. A least-squares analysis of the appropriate difference equations leads to a radial error in the position of the jth monument, expressed relative to the mean radius, that is given in terms of errors δh_i in the individual quantities h_i by (Laslett and Smith, 1966)

$$\delta r_j = \frac{1}{6M} \sum_{i=1}^{M} [M^2 - 1 - 6M\,|\,j-i\,| + 6\,|\,j-i\,|^2]\delta h_i$$

The magnet structure will be assumed to be such that there is an integral number, $m = N/M$, of periods between adjacent monuments and each monument will be assumed to be at a point of symmetry where $\alpha = 0$ and $\beta = \beta_{\max}$. If each magnet block is then positioned with respect to the two nearest monuments, the deviations of the closed orbit (from the center line of the magnet blocks) at the monument locations are

$$x_k = 2\frac{\beta}{S}\,\frac{\sin^2 \pi Q/M}{\sin \pi Q} \sum_{j=1}^{M}\left[1 - \frac{\tan \pi Q}{\tan \pi Q/M}\,\delta_{k,j}\right] \cos\left(1 - 2\frac{|k-j|}{M}\right)\pi Q\,\delta r_j$$

where $\delta_{k,j}$ is unity for $j = k$ and zero otherwise; similar deviations arise at the centers of the other focusing regions, that are situated between two monuments.

If the independent surveying measurements have a common standard deviation, ε_h, the standard deviation of any particular x_k that results from these uncorrelated errors δh_i is

$$(x_k)_{\text{rms}} = \left\{ \sum_{i=1}^{M} \left[\sum_{j=1}^{M} \left(\frac{\partial x_k}{\partial(\delta r_j)}\right) \left(\frac{\partial(\delta r_j)}{\partial(\delta h_i)}\right)\right]^2\right\}^{1/2} \varepsilon_h$$

The value of this sum may be readily approximated when Q is close (but not equal) to an integer H (so that $|\,Q - H\,| \ll M$), since the effect of this single harmonic then will dominate in the orbit response. The Fourier amplitudes of the monument displacement that results from a single surveying error and of the closed-orbit response to the movement of a single monument are, for this harmonic,

$$A_1 = \frac{1}{M}\csc^2\frac{\pi H}{M} \qquad (\text{for } H \ll M)$$

and

$$A_2 = \frac{4}{M}\,\frac{\beta}{S}\left|\frac{\sin\dfrac{2\pi Q}{M}}{\cos\dfrac{2\pi Q}{M} - \cos\dfrac{2\pi H}{M}}\right| \sin^2\frac{\pi H}{M}$$

$$\cong \frac{2}{\pi}\,\frac{\beta}{S}\,\frac{\sin^2 \pi H/M}{|\,Q - H\,|}$$

respectively. Then

$$\begin{aligned}(x)_{\text{rms}} &\cong (M/2)^{3/2}(A_1 A_2)\varepsilon_h \\ &= \frac{1}{\pi}(M/2)^{1/2}\frac{\beta}{S}\,\frac{1}{|\,Q - H\,|}\,\varepsilon_h \\ &= \frac{1}{\pi^2}(M/2)^{3/2}\frac{\beta}{R}\,\frac{1}{|\,Q - H\,|}\,\varepsilon_h\end{aligned}$$

The more tedious evaluation of the exact sum has been carried through by Smith (1964), with the result

$$(x)_{\text{rms}} = \frac{1}{\pi}(M/2)^{3/2}\frac{\beta}{R}\,\frac{1}{|\sin \pi Q\,|}\,\varepsilon_h$$

Although the closed-orbit deviation at any particular observation point may be expected to have a probability distribution that is Gaussian, and will be strongly correlated with the deviations at other observation points, the probability distribution for $|x|_{\max}$ in each member of an ensemble of accelerators should be considered in selecting the amount of aperture that is to be provided to accommodate the orbit distortions that result from errors such as have been considered here. To insure that the aperture will accommodate these deviations *all around* the accelerator with a high degree of probability ($\geq 98\%$), a semiaperture allowance of $2\sqrt{2}\,(x)_{\text{rms}}$ has been proposed (Courant and Snyder, 1958) and independent Monte-Carlo computations suggest the advisability of increasing this estimate by an additional 20% (Keil, 1965; Laslett, 1965). One thus obtains a desirable semiaperture allowance of

$$\pm \frac{1.2}{\pi} M^{3/2} \frac{\beta}{R} \frac{1}{|\sin \pi Q|} \varepsilon_h$$

$$= \pm \frac{1.2}{\pi} M^{3/2} \frac{\beta\langle 1/\beta\rangle_{\text{av}}}{Q\,|\sin \pi Q|} \varepsilon_h$$

$$= \pm \frac{2.4}{\sigma} \frac{\beta\langle 1/\beta\rangle_{\text{av}}}{m^{3/2}} \frac{\sqrt{N}}{|\sin \pi Q|} \varepsilon_h .$$

If $m = 2$, $\sigma = \pi/4$, $\beta\langle 1/\beta\rangle_{\text{av}} = 1.57$, and $\sin \pi Q = 1/\sqrt{2}$, this last result suggests a contribution of $2.4\sqrt{N}\,\varepsilon_h$ to the required semiaperture. Since this analysis illustrates the effect of only *one* source of closed-orbit deviation, and other constructional errors may lead to somewhat greater effects, the value $7\sqrt{N}\,\varepsilon_h$ adopted in the text may be considered reasonably representative of the semiaperture allowance that should be made to accommodate all such errors.

REFERENCES

Adams, J. B. (1953). *In* "Lectures on the Theory and Design of an Alternating-Gradient Proton Synchrotron" (M. H. Blewett, ed.), Art. III—4.10, p. 102. CERN, Geneva, Switzerland.

AGS Staff (1961). *Proc. Intern. Conf. High Energy Accelerators, Brookhaven Natl. Lab., Upton, N. Y., 1961.* Fig. 3, p. 42. U.S. Govt. Print. Office, Washington, D.C.

Aitken, D. K., Heymann, F. F., Jennings, R. E., and Kalmus, P. I. P. (1961). *Proc. Phys. Soc.* (*London*) **77**, 769–785.

Amman, F., Andreani, R., Bassetti, M., Bernardini, M., Cattoni, A., Cerchia, R., Chimenti, V., Corazza, G., Ferlenghi, E., Mango, L., Massarotti, A., Pellegrini, C., Placidi, M., Puglisi, M., Renzler, G., and Tazzioli, F. (1964). *Proc. Intern. Conf. High Energy Accelerators, Dubna, USSR, 1963*, pp. 249-273. Atomizdat, Moscow, USSR.

1-173

Argonne National Laboratory Staff, Particle Accelerator Division (1964). *Proc. Intern. Conf. High Energy Accelerators, Dubna, USSR, 1963*, pp. 187–195. Atomizdat, Moscow, USSR.

Belford, G., Laslett, L. J., and Snyder, J. N. (1957). *Math. Tables Other Aids Computation* **11**, 79–81 and 110.

Bell, J. S. (1953). *Proc. Phys. Soc.* (*London*) **B60**, 802–804.

Bertolotto, R., van Breugel, H., Caris, L., Consigny, E., Hijkhuisen, H., Goni, J., Hirsbrunner, J. J., Kuiper, B., Milner, S., Pichler, S., and Plass, G. (1964). *Proc. Intern. Conf. High Energy Accelerators, Dubna, USSR, 1963*, pp. 669–689. Atomizdat, Moscow, USSR.

Bethe, H. A., and Rose, M. E. (1937). *Phys. Rev.* **52**, 1254–1255.

Blackman, N. M., and Courant, E. D. (1949). *Rev. Sci. Instr.* **20**, 596–601.

Brannen, E., and Froelich, H. (1961). *J. Appl. Phys.* **32**, 1179-1180.

Brannen, E., Froelich, H., and Stewart, T. W. W. (1960). *J. Appl. Phys.* **31**, 1829.

Brookhaven Staff (1955). *Phys. Rev.* **100**, 1268–1269.

Bruck, H. (1966), "Accélérateurs Circulaires de Particles." Presses Universitaires de France, Paris.

Bruck, H., Bronca, G., Hamelin, J., Neyret, G., and Parain, J. (1956). *Proc. CERN Symp. High Energy Accelerators Pion Phys., Geneva, 1956*, Vol. 1, pp. 330–338. CERN, Geneva, Switzerland.

Christofilos, N. C. (1950). U.S. Patent, 2,736,799 (issued Feb. 28, 1956).

Cohen, B. L. (1959). *In* "Handbuch der Physik" (S. Flügge and E. Creutz, eds.), Vol. 44, pp. 105-169. Springer, Berlin.

Cole, F. T. (1956). Mark V FFAG expanded equations of motion. Unpublished Rept. MURA-95, in which the dominant term of b_1 should be reversed in sign. Midwestern Universities Research Association, Stoughton, Wisconsin.

Cole, F. T., and Morton, P. L. (1959). *Proc. Intern. Conf. High Energy Accelerators Instrumentation, CERN, Geneva, 1959*, pp. 31–37. CERN, Geneva, Switzerland.

Cole, F. T., Haxby, R. O., Jones, L. W., Pruett, C. H., and Terwilliger, K. M. (1957). *Rev. Sci. Instr.* **28**, 403–420.

— Collins, T. L. (1961). Long straight sections for AG synchrotrons. Unpublished Rept. CEA-86. Cambridge Electron Accelerator, Cambridge, Massachusetts.

Courant, E. D. (1964). Unpublished material.

Courant, E. D., and Snyder, H. S. (1958). *Ann. Phys.* (*N.Y.*) **3**, 1–48.

Courant, E. D., Livingston, M. S., and Snyder, H. S. (1952). *Phys. Rev.* **88**, 1190-1196.

Cox, A. J., Kidd, D. E., Powell, W. B., Reece, B. L., and Waterton, P. J. (1962). *Nucl. Instr. Methods* **18–19**, 25–32 (esp. Sec. 3).

Crane, H. R. (1946a). *Phys. Rev.* **69**, 542.

Crane, H. R. (1946b). *Phys. Rev.* **70**, 800–801.

Curtis, C. D., Galonsky, A., Hilden, R. H., Mills, F. E., Otte, R. A., Parzen, G., Pruett, C. H., Rowe, E. M., Shea, M. F., Swenson, D. A., Wallenmeyer, W. A., and Young, D. E. (1964). *Proc. Intern. Conf. High Energy Accelerators, Dubna, USSR, 1963*, pp. 620–651. Atomizdat, Moscow, USSR.

del Castillo, G. (1963). *In* "Proceedings of the 1963 Summer Study on Storage Rings, Accelerators and Experimentation at Super-High Energies" (J. W. Bittner, ed.), BNL No. 7534, pp. 449–477. Brookhaven Natl. Lab., Upton, New York.

del Castillo, G. (1965). *Bull. Am. Phys. Soc.* [II] **10**, No. 4, 456–457.

Dick, L., Lévy, Ph., and Vermeulen, J. (1963). *Proc. Intern. Conf. Sector-Focused Cyclotrons Meson Factories, CERN, Geneva, 1963*, pp. 127–129. CERN, Geneva, Switzerland.

Dunn, P. D., Mullett, L. B., Pickavance, T. G., Walkinshaw, W., and Wilkins, J. J. (1956). *Proc. CERN Symp. High Energy Accelerators Pion Phys., Geneva, 1956*, Vol. 1, pp. 9–31. CERN, Geneva, Switzerland.

Ferger, F. A., Fischer, E., Jones, E., Kirstein, P. T., Koziol, H., and Pentz, M. J. (1964). *Proc. Intern. Conf. High Energy Accelerators, Dubna, USSR, 1963*, pp. 338–346. Atomizdat, Moscow, USSR.

Fischer, E. (1964). *Proc. Intern. Conf. High Energy Accelerators, Dubna, USSR, 1963*. pp. 347–352. Atomizdat, Moscow, USSR.

Froelich, H. R. (1962). Theory and design of a race-track microtron with application to the generation of millimeter waves. Thesis. University of Western Ontario, London, Ontario, Canada.

Goldstein, H. (1950). "Classical Mechanics," Sects. 8-1 and 9-5. Addison-Wesley, Reading, Massachusetts.

Green, G. K., and Courant, E. D. (1959). *In* "Handbuch der Physik" (S. Flügge and E. Creutz, eds.), Vol. 44, pp. 218–340. Springer, Berlin.

Grunder, H. A., and Selph, F. B. (1963). *Proc. Intern. Conf. Sector-Focused Cyclotrons Meson Factories, CERN, Geneva, 1963*, pp. 8–16a. CERN, Geneva, Switzerland.

Haddock, R. P., MacKenzie, K. R., Richardson, J. R., and Wright, B. T. (1964). *Proc. Intern. Conf. High Energy Accelerators, Dubna, USSR, 1963*, pp. 568–576. Atomizdat, Moscow, USSR.

1-174

Hammer, C. L., and Bureau, A. J. (1955). *Rev. Sci. Instr.* 26, 594-598 and 598-600.

Hammer, C. L., and Laslett, L. J. (1958). *Proc. 2nd Intern. Conf. Peaceful Uses At. Energy, Geneva, 1958*. Vol. 30, pp. 151–157. Columbia Univ., Press. (I.D.S.), New York.

Hammer, C. L., and Laslett, L. J. (1961). *Rev. Sci. Instr.* 32, 144–149.

Hammer, C. L., Pidd, R. W., and Terwilliger, K. M. (1955). *Rev. Sci. Instr.* 26, 555–556.

Hereward, H. G. (1964). *Proc. Intern. Conf. High Energy Accelerators, Dubna, USSR, 1963*, pp. 690–692. Atomizdat, Moscow, USSR.

Hereward, H. G., Johnsen, K., Schoch, A., and Zilverschoon, C. J. (1961). *Proc. Intern. Conf. High Energy Accelerators, Brookhaven Natl. Lab., Upton, N. Y. 1961*, pp. 265–271. U.S. Govt. Print. Office, Washington, D.C.

Heyn, F. A., and Khoe, K. T. (1958). *Rev. Sci. Instr.* 29, 662.

Holt, J. R., and Newns, H. C. (1961). *Proc. Intern. Conf. High Energy Accelerators, Brookhaven Natl. Lab., Upton, N. Y., 1961*, pp. 217–220. U.S. Govt. Print. Office, Washington, D.C.

Howard, F. T., ed. (1959). "Sector-Focused Cyclotrons—Proceedings of an Informal Conference at Sea Island, Georgia," Publ. No. 656, Natl. Acad. Sci.-Natl. Res. Council, Washington, D.C.

Howard, F. T. (1963). *Proc. Intern. Conf. Sector-Focused Cyclotrons Meson Factories, CERN, Geneva, 1963*; Appendix, pp. 414–415. CERN, Geneva, Switzerland.

Howard, F. T., and Vogt-Nilsen, N. (eds.) (1963). *Proc. Intern. Conf. Sector-Focused Cyclotrons Meson Factories.* CERN Rept. No. 63–19. CERN, Geneva, Switzerland.

Johnsen, K., Middelkoop, W. C., de Raad, B., Resegotti, L., Schoch, A., Symon, K. R., and Zilverschoon, C. J. (1964). *Proc. Intern. Conf. High Energy Accelerators, Dubna, USSR, 1963*, pp. 312–325. Atomizdat, Moscow, USSR.

Judd, D. L. (1955). *Phys. Rev.* 100, 1804.

Judd, D. L. (1958). *Ann. Rev. Nucl. Sci.* 8, 181–216.

Judd, D. L. (1962). *Nucl. Instr. Methods* 18–19, 70–73.

Keil, E. (1965). Unpublished Internal Rept. AR/Int. SG/65-3. CERN, Geneva, Switzerland.

Kelly, E. L. (1962). *Nucl. Instr. Methods* 18–19, 33–40.

Kelly, E. L., Pyle, R. V., Thornton, R. L., Richardson, J. R., and Wright, B. T. (1956). *Rev. Sci. Instr.* 27, 493–503.

Kerst, D. W., and Serber, R. (1941). *Phys. Rev.* 60, 53–58.

Kerst, D. W., Day, E. A., Hausman, H. J., Haxby, R. O., Laslett, L. J., Mills, F. E., Ohkawa, T., Peterson, F. L., Rowe, E. M., Sessler, A. M., Snyder, J. N., and Wallenmeyer, W. A. (1960). *Rev. Sci. Instr.* 31, 1076–1106.

Khoe, T. K., and Teng, L. C. (1963). *Proc. Intern. Conf. Sector-Focused Cyclotrons Meson Factories, CERN, Geneva, 1953*, pp. 118–126. CERN, Geneva, Switzerland.

Kollath, R. (1955). "Teilchenbeschleuniger," Sect. IIC. Vieweg & Sohn, Braunschweig.

Kolomensky, A. A., and Lebedev, A. N. (1966). "Theory of Cyclic Accelerators." North-Holland Publishing Co., Amsterdam (English translation by M. Barbier).

Laslett, L. J. (1956). *Science* 124, 781–787.

Laslett, L. J. (1959). Unpublished Repts. MURA-452, 459, 461, 463, 497 (with S. J. Wolfson), and 515. Midwestern Universities Research Association, Stoughton, Wisconsin.

Laslett, L. J. (1961). Analysis of FFAG accelerators and the evolution of circular accelerators, Unpublished Rept. CEA 1912. Institut National des Sciences et Techniques Nucléaires, Centre d'Études Nucléaires de Saclay, Gif-sur-Yvette (S.-et-O.), France.

Laslett, L. J. (1963). *In* "Proceedings of the 1963 Summer Study on Storage Rings, Accelerators and Experimentation at Super-High Energies" (J. W. Bittner, ed.), BNL 7534, pp. 324-367. Brookhaven Natl. Lab., Upton, New York.

Laslett, L. J. (1965). Computational results concerning the maximum displacement of a closed orbit for one and two transverse degrees of freedom. Unpublished Rept. UCID-10158. Lawrence Radiation Laboratory, Berkeley, California.

Laslett, L. J., and Sessler, A. M. (1956). The x-stability limit in spiral sector accelerators. Unpublished Rept. MURA-120. Midwestern Universities Research Association, Stoughton, Wisconsin.

Laslett, L. J., and Sessler, A. M. (1961). *Rev. Sci. Instr.* 32, 1235–1252.

Laslett, L. J., and Smith, L. (1966). Analysis of surveying procedures that only employ distance measurements and the effect of surveying errors on the closed orbit. Unpublished Rept. UCID-10161. Lawrence Radiation Laboratory, Berkeley, California.

Laslett, L. J. and Symon, K. R. (1959). *Proc. Intern. Conf. High Energy Accelerators Instrumentation, CERN, Geneva, 1959*, pp. 38–47. CERN, Geneva, Switzerland.

LeCouteur, K. J. (1951). *Proc. Phys. Soc.* (*London*) B64, 1073–1084.

Livingood, J. J. (1961). "Principles of Cyclic Particle Accelerators." Van Nostrand, Princeton, New Jersey.

Livingston, M. S., and Blewett, J. P. (1962). "Particle Accelerators." McGraw-Hill, New York.

Livingston, R. S., and Martin, J. A. (1964). *Proc. Intern. Conf. High Energy Accelerators, Dubna, USSR, 1963*, pp. 561–567. Atomizdat, Moscow, USSR.

Luccio, A., Pavanati, G., Resmini, F., Succi, C., and Tagliaferri, G. (1962). *Nucl. Instr. Methods* 18–19, 74–80.

McLachlan, N. W. (1947). "Theory and Application of Mathieu Functions," Sec. 4.90–4.91. Oxford Univ. Press (Clarendon), London and New York.
McMillan, E. M. (1945). *Phys. Rev.* 68, 143–144.
Meier, H., and Symon, K. R. (1959). *Proc. Intern. Conf. High Energy Accelerators Instrumentation, CERN, Geneva, 1959*, pp. 253–262. CERN, Geneva, Switzerland.
Meixner, J., and Schäfke, F. W. (1954). "Mathieusche Funktionen und Sphäroidfunctionen," Sect. 4.23, pp. 338–343. Springer, Berlin. Wherein N denotes *twice* the number of magnet periods in the accelerator structure.
Moroz, E. M. (1956). *Dokl. Akad. Nauk SSSR* **108**, 436–439.
Moroz, E. M. (1957). *Dokl. Akad. Nauk SSSR* **115**, 78–79.
Moroz, E. M. (1958). *At. Energ. USSR* 4, 228.
Moser, J. (1955a). *Nachr. Akad. Wiss. Goettingen, Math.-Physik. Kl. II-a*, No. 6, 87–120.
Moser, J. (1955b). *Commun. Pure Appl. Math.* 8, 409–436.
Moser, J. (1956). *Proc. CERN Symp. High Energy Accelerators Pion Phys., Geneva, 1956*, Vol. 1, pp. 290–292. CERN, Geneva, Switzerland.
MURA Staff (1959). *Proc. Intern. Conf. High Energy Accelerators Instrumentation, CERN, Geneva, 1959*, pp. 71–74. CERN, Geneva, Switzerland.
MURA Staff (1961a). *Proc. Intern. Conf. High Energy Accelerators, Brookhaven Natl. Lab., Upton, N. Y., 1961*, pp. 57–63. U.S. Govt. Print. Office, Washington, D.C.
MURA Staff (1961b). *Proc. Intern. Conf. High Energy Accelerators, Brookhaven Natl. Lab., Upton, N. Y., 1961*, pp. 344–350. U.S. Govt. Print. Office, Washington D.C.
MURA Staff (1964). *Rev. Sci. Instr.* **35**, 1393–1482.
National Bureau of Standards, U.S. (1951). (Computation Laboratory, National Applied Mathematics Laboratories) "Tables Relating to Mathieu Functions." Columbia Univ. Press, New York.
Paul, W., and Steinwedel, H. (1953). *Z. Naturforsch.* **8a**, 448–450.
Princeton University Staff (1959). *Proc. Intern. Conf. High Energy Accelerators Instrumentation, CERN, Geneva, 1959*, pp. 362–365. CERN, Geneva, Switzerland.
Pyle, R. V., Kelly, E. L., Richardson, J. R., and Thornton, R. L. (1955). *Phys. Rev.* 100, 1804.
Redhead, P. A., LeCaine, H., and Henderson, W. J. (1950). *Can. J. Res.* **A28**, 73–91.
Reich, H. (1960). *Z. Angew. Phys.* 12, 481–493.
Richardson, J. R. (1965). *In* "Progress in Nuclear Techniques and Instrumentation" (F. J. M. Farley, ed.), Vol. I, "Sector Focusing Cyclotrons." North-Holland Publishing Co., Amsterdam.
Roberts, A. (1958). *Ann. Phys. (N. Y.)* 4, 115–165.
Rose, M. E. (1938). *Phys. Rev.* 53, 392–408.
Sands, M. (1961). *Proc. Intern. Conf. High Energy Accelerators, Brookhaven Natl. Lab., Upton, N. Y., 1961*, pp. 145–153. U.S. Govt. Print. Office, Washington, D.C.
Schiff, L. I. (1938). *Phys. Rev.* **54**, 1114–1115.
Schnell, W. (1964). *Proc. Intern. Conf. High Energy Accelerators, Dubna, USSR, 1963*, pp. 326–331. Atomizdat, Moscow, USSR.
Siegbahn, K., and Howard, F. T. (eds.) (1962). "Sector-Focused Cyclotrons—Proc. Intern. Conf. Sector-Focused Cyclotrons, University of California at Los Angeles." North-Holland Publishing Co., Amsterdam. (*Nucl. Instr. Methods* **18–19**).
Smith, L. (1964). Unpublished material.
Snowdon, S. C. (1964). Study of a 500 MeV high intensity injector. Unpublished Rept. MURA-700. Midwestern Universities Research Association, Stoughton, Wisconsin.

1-175

Steimel, K. (1963). *Proc. Intern. Conf. Sector-Focused Cyclotrons Meson Factories, CERN, Geneva, 1963*, pp. 24–29. CERN, Geneva, Switzerland.
Steimel, K., and Lerbs, A. (1959). *Atomwirtschaft* 4, Nos. 7–8, 345–348.
Sturrock, P. A. (1955). "Static and Dynamic Electron Optics." Cambridge Univ. Press, London and New York.
Sturrock, P. A. (1958a). *Ann. Phys. (N. Y.)* 3, 113–189.
Sturrock, P. A. (1958b). *Ann. Phys. (N. Y.)* 4, 306–324.
Symon, K. R., Kerst, D. W., Jones, L. W., Laslett, L. J., and Terwilliger, K. M. (1956). *Phys. Rev.* 103, 1837–1859.
Taubert, R. (1957). *Z. Naturforsch.* 12a, 169–170.
Thirion, J. (1963). *Proc. Intern. Conf. Sector-Focused Cyclotrons Meson Factories, CERN, Geneva, 1963*, pp. 107–117. CERN. Geneva, Switzerland.
Thomas, L. H. (1938). *Phys. Rev.* 54, 580–588 and 588–598.
Tuck, J. L., and Teng, L. C. (1951). *Phys. Rev.* **81**, 305.
van der Pol, B., and Strutt, M. J. O. (1928). *Phil. Mag.* [7], 5, 18–38.
Veksler, V. I. (1944a). *Compt. Rend. Acad. Sci. USSR* 43, 444.
Veksler, V. I. (1944b). *Compt. Rend. Acad. Sci. USSR* 44, 393.
Veksler, V. I. (1945). *J. Phys. (USSR)* 9, 153–158.
Vladimirskij, V. V. (1959). *Proc. Intern. Conf. High Energy Accelerators Instrumentation, CERN, Geneva, 1959*, pp. 371–372. CERN, Geneva, Switzerland.
Walkinshaw, W. (1956). A spiral ridged bevatron. Unpublished Rept. At. Energy Res. Establ., Harwell, England.
Watson, P. G. (1962). *Nucl. Instr. Methods* **18–19**, 362–369.
Wernholm, O. (1964). *Arkiv Fysik* 26, 527–573.
White, M. G., Shoemaker, F. C., and O'Neill, G. K. (1956). *Proc. CERN Symp. High Energy Accelerators Pion Phys., Geneva, 1956*, Vol. I, pp. 525–529. CERN, Geneva, Switzerland.
Whittaker, E. T., and Watson, G. N. (1927). "A Course of Modern Analysis," Cambridge Univ. Press, London and New York.
Willax, H. A., and Garren, A. A. (1962). *Nucl. Instr. Methods* **18–19**, 347–361.
Wilson, R. R. (1938). *Phys. Rev.* 53, 408–420.

LJL(MAC)-2
January, 1954

DISCUSSION OF SPACE-CHARGE EFFECTS IN THE ALTERNATE-GRADIENT SYNCHROTRON

by

L. Jackson Laslett

Institute for Atomic Research and Department of Physics

Iowa State College

and

Mid-West Accelerator Conference

1. Introduction:

As a sequel to the January 9 meeting of the Mid-West Technical Group, Dr. Kerst suggested that it would be desirable to record equations which have been used in discussion of space-charge effects and to exhibit some of the grave consequences suggested by use of these equations. The present report is in compliance with this suggestion, but is written with the following reservations in mind.

(i) Concentration of attention on space-charge effects, which will be most prominent at low energy, should not cause one to overlook other phenomena,[1,2] not readily analyzed, which may play important rôles at injection.

(ii) Analysis of space-charge effects on the basis of an assumed form for the charge distribution may be seriously in error if the particles of the group considered can execute oscillations which result in a distribution differing from that assumed.[3]

It is suggested, however, that application of the present formulas to a group of particles moving non-coherently will provide an approximate indication of dangerous values for design parameters.

2. Statement of Formulas:

A. Effective Change of "n", Rudimentary Derivation--

For a beam of constant charge density ρ throughout a cross-sectional area of constant radius Δ, the total charge q is

$$q = (\pi\Delta^2)(2\pi R_o)$$
$$= 2\pi^2 \Delta^2 R_o \rho , \qquad (1)$$

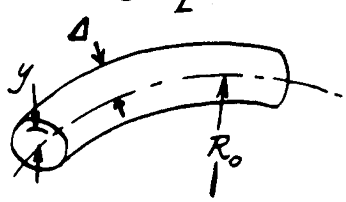

where R_o represents the orbit radius.

The net defocusing electric and magnetic force experienced, as a result of the space-charge, by a particle within the beam at a distance y from the axis, is

$$F_{s.c.} = \frac{e}{2}\left(\frac{1}{\epsilon_o} - \mu_o v^2\right) y\rho$$

$$= \frac{e}{2\epsilon_o}(1-\beta^2)\, y\rho$$

$$= \frac{qe(1-\beta^2)y}{4\pi^2\epsilon_o\Delta^2 R_o}, \quad \text{in "rationalized" (MKS) units.} \tag{2}$$

The focusing and defocusing forces produced by the magnetic field of the accelerator are

$$F_z = n\,\frac{evB_o y}{R_o} = n\,\frac{E_T\beta^2 y}{R_o^{\,2}}, \quad \text{or} \tag{3a}$$

$$F_r = (1-n)\,\frac{E_T\beta^2 y}{R_o^{\,2}}, \tag{3b}$$

with E_T representing the <u>total</u> energy of the particle.

The force indicated in equation (2) is thus equivalent to a reduction of n in the equation of axial motion, and an increase in n in the radial equation, by

$$|\delta n| = \frac{qeR_o}{4\pi^2\epsilon_o\Delta^2}\,\frac{1-\beta^2}{\beta^2 E_T}; \tag{4}$$

$$q = \frac{4\pi^2\epsilon_o}{e}\,\frac{\Delta^2}{R_o}\,\beta^2\,\frac{E_T^{\,3}}{E_o^{\,2}}\cdot|\delta n|$$

$$= \frac{(E_o/e)_{volts}}{60_{ohms}}\left(\frac{2\pi R_o}{c}\right)_{sec}\left(\frac{\Delta}{R_o}\right)^2\beta^2\left(\frac{E_T}{E_o}\right)^3|\delta n|.^{(a)} \tag{5}$$

(a)
$$\epsilon_o = \left[\frac{1}{(4\pi\times 10^{-7})_{H/M}\; c_{M/sec}^{\;2}}\right]_{farad/M} = \frac{1}{(120\pi)_{ohms}\; c_{M/sec}}.$$

If this analysis is accepted, it can be seen that the result of the space-charge is equivalent to effecting a translation of the operating point at right angles to the diagonal of the "necktie" diagram.

For comparison with similar results stated elsewhere, it is also of interest to write the associated "current"

$$i \equiv q\ (\beta c/\text{circumference})$$

$$= \frac{(E_o/e)_{\text{volts}}}{60_{\text{ohms}}} \left(\frac{\Delta}{R_o}\right)^2 \beta^3 \left(\frac{E_T}{E_o}\right)^3 \cdot |\delta n| \quad \text{amperes.} \tag{6}$$

B. Comparison with Previous Results --

Equation (5) is consistent with a non-relativistic result given by Kerst[4] for a conventional betatron, if we identify $|\delta n|$ with the limiting tolerance $(1-n)$ for radial stability. Again in application to a conventional synchrotron, Judd[5] considers unequal radial and axial focusing and derives the aperture requirements for a beam of elliptical cross-section. His results also agree with our equation (5) in the case $n = 1-n = 1/2 = |\delta n|$. Similarly, J. P. Blewett[6] has also considered an elliptical beam in a conventional betatron with $n = 3/4$ and $R_o = 0.833$ Meter. Finally, Barden[7] originated the equation (5) in the form cited here and has suggested considering its application to an alternate-gradient accelerator in terms of the permissible variation of n.

C. Estimate of a Tolerable $|\delta n|$ --

In application of equation (5) to an alternate-gradient accelerator, Barden[7] originally suggested that one require

$$|\delta n| < 0.006\ N_s^2, \tag{7}$$

where N_s represents the number of magnet sectors. This suggested limitation was possibly motivated by the observation that the overall width of the necktie diagram, projected onto the n_1 or n_2 axis, corresponds approximately to $|\delta n| = 0.03\ N_s^2$. Thus a variation of about the amount suggested by Barden would carry the operation point from the diagonal almost half-way towards the edge of the stable region.

In view, however, of the present concern about integral and half-integral resonances (as well as sum resonances), it appears more prudent to allow variations of n only within one of the small diamonds situated along the diagonal of the necktie diagram. Since the characteristic solutions for the particle trajectories involve a factor exp(+ik) for traversal of a sector pair, the separation of integral resonances corresponds to

$$|\delta k| = \frac{2\pi}{N_s/2}, \quad \text{or} \tag{8a}$$

$$|\delta(\cos k)| = \frac{2\pi \sin k}{N_s/2}; \tag{8b}$$

similarly, movement from the center of a small diamond, bounded by integral and half-integral resonances, half way[(b)] towards the edge corresponds to

$$|\delta k| = \frac{\pi/4}{N_s/2}, \quad \text{or} \tag{9a}$$

$$|\delta(\cos k)| = \frac{(\pi/4)\sin k}{N_s/2}. \tag{9b}$$

With the index n alternating between n_1 and $n_2 \equiv -m$ in sectors of equal length,[8]

$$\cos k = \cos\frac{2\pi n_1^{1/2}}{N_s}\cosh\frac{2\pi m^{1/2}}{N_s} - \frac{n_1 - m}{2n_1^{1/2}m^{1/2}}\sin\frac{2\pi n_1^{1/2}}{N_s} \times \sinh\frac{2\pi m^{1/2}}{N_s}. \tag{10}$$

For variations such that $\delta n_1 = -\delta m$, and in the neighborhood of the diagonal,

$$\delta(\cos k) = \left\{\frac{\pi}{n^{1/2}N_s}\left[\cos\frac{2\pi n^{1/2}}{N_s}\sinh\frac{2\pi n^{1/2}}{N_s} + \sin\frac{2\pi m^{1/2}}{N_s}\cosh\frac{2\pi n^{1/2}}{N_s}\right] + \frac{1}{n}\sin\frac{2\pi n^{1/2}}{N_s}\sinh\frac{2\pi m^{1/2}}{N_s}\right\}[-\delta n]. \tag{11}$$

A conservative limit to the acceptable $|\delta n|$ thus appears to be

$$|\delta n| \leq \frac{(n^{1/2}/2)\sin k}{\cos\frac{2\pi n^{1/2}}{N_s}\sinh\frac{2\pi n^{1/2}}{N_s} + \sin\frac{2\pi n^{1/2}}{N_s}\cosh\frac{2\pi n^{1/2}}{N_s} + \frac{N_s}{\pi n^{1/2}} \times \sin\frac{2\pi n^{1/2}}{N_s}\sinh\frac{2\pi n^{1/2}}{N_s}} \tag{12}$$

continuation of denominator

(b) To afford some latitude for other possible variations of the accelerator characteristics, as would arise for example from remanence. It may also be noted that, as J. B. Adams[14] has pointed out, particles with momentum different from the equilibrium momentum are presented with a different n value ($|\delta n| \simeq n_0 \cdot \Delta p/p_0$).

Accordingly, near the center of the necktie where $n^{1/2}/N_s \cong 0.25$, $\sin k \cong 1$ and

$$|\delta n| \leq \frac{n^{1/2}/2}{\cosh \pi/2 + (4/\pi) \sinh \pi/2} = 0.0919\ n^{1/2} = 0.0230\ N_s; \qquad (13a)$$

similarly at an operation point for which $n^{1/2}/N_s \cong 0.1778$, $\sin k \cong 0.671$ and

$$|\delta n| \leq \frac{(n^{1/2}/2)\ 0.671}{4.314} = 0.078\ n^{1/2} = 0.0138\ N_s. \qquad (13b)$$

The above criteria suggest, as a typical tolerance in an accelerator with n in the range of 400 to 500,

$$|\delta n| \simeq 1.8.$$

Livingston[9] appears to have considered a similar approach to the problem of estimating space-charge limitations.

3. Numerical Results:

In application of equation (5) to estimate the beam which can be held in an alternate-gradient synchrotron at the time of injection, two alternative view-points may be considered. If one considers that the injected beam spirals inward,[10,11] due to the rising magnetic field, equation (5) may be considered as giving the maximum charge per turn and Δ might be taken as one-half of the pitch required for the spiral to clear the inflector comfortably;[(c)] in this case the acceptable injection current is the limiting charge per turn divided by the period of revolution and the total charge is the charge per turn times the number of turns accepted. If, on the other hand, the details of the injection process are ignored, equation (5) might be regarded as giving the total possible charge, with Δ representing the useful semi-aperture of the accelerator, and the acceptable injection current would be this charge divided by the estimated duration of the useful injection interval. In either case, the expected useful beam from the accelerator will be no more than about one-half of that successfully injected, due to (for example) incomplete capture into the synchrotron phase.

In estimating the manner in which the acceptable injection currents will depend on injection energy, one must take account (in the non-relativistic case) of the energy dependence of the period of revolution. The bunching action of a R.F. linear accelerator has been suggested[12] as aggravating the space-charge effects, but it appears[12,13] that a slight inherent energy inhomogeneity suffices to smooth out the charge distribution within a distance less than one circumference.

[(c)] Supposedly this pitch would be at least twice the beam radius plus the radial thickness of the deflecting electrode.

A numerical example of space-charge limitations has been given by J. B. Adams[14] in connection with a proposed CERN accelerator design. Adams states his conclusions in terms of maximum current, which is presumably $i = q(\beta c/\text{circumference})$. With $n = 392$, we expect $|\delta n| \cong 3$ to carry the operating point to near the edge of a diamond.[(d)] If, following Adams, we take $\Delta = 0.4$ cm (the radius of the injected beam), $R_o = 8600$ cm, Kinetic Energy = 50 Mev, and $\beta = 0.314$, we find from equation (6) that

$$i = 1.2 \times 10^{-3} \cdot |\delta n| \quad \text{amperes}$$

constitutes a limiting current (for one-turn injection) similar to the 3 ma cited by Adams.

We give below a table of permissible values, calculated from equation (5), for a circular accelerator of 8650 cm radius[(e)] and with the permissible $|\delta n|$ limited to 1.8. Kinetic energies for proton injection of 4 Mev and 50 Mev are considered. In addition, we first consider an injected beam of 0.3 cm radius, spiraling inward so that injection continues for six turns; secondly we consider a total beam of 4.0 cm radius, without regard to the details of the injection process. It is noted that the estimated acceptable injection currents for 50 Mev injection are about 45 times those for 4 Mev (proportional non-relativistically to the three-halves power of the kinetic energy).

4. Conclusions:

From the foregoing examples it is clear that space-charge may seriously limit the beam currents in certain of the accelerator designs presently under consideration. It is important, therefore, to be as certain as possible concerning the following points:

(i) Is the conventional analysis presented here valid?[3]

(ii) Are the integral and half-integral resonances so important that space-charge should not be permitted to displace the operating point across such resonances?[9]

(iii) If the present analysis is considered adequate, is it best to associate Δ with the radial width of the proposed injected beam,[9,14] with the pitch of the spiral[10,11] described by the injected beam, or with the semi-aperture of the accelerator?

The advantage of injection at high energy is apparent, if the injector supply can deliver the currents desired. It would be unfortunate to have an injector system incapable of delivering the desired currents, but it would also be frustrating to have designed an accelerator which could not accept the injection

(d) Or see diagram VI of Adams' paper.[14]

(e) Such a radius would permit, for example, attainment of 25 Gev in a field of 10,000 gauss (1 weber/M^2).

EXAMPLES OF ESTIMATED SPACE-CHARGE LIMITATIONS

$R_o = 8650$ cm, $|\delta n| = 1.8$

			$\Delta = 0.3$ cm				$\Delta = 4.0$ cm			
Kinetic Energy of Protons	β	Revolution Period μsec	Charge / Revolution (coulombs)	i (ma)	Charge / 6 Rev. (coulombs)	Particles, assuming 50% capture	Total Charge (Coulombs)	i (ma), if inject for 1 Rev	6 Rev	Particles, assuming 50% capture
50 Mev	0.314	5.76	7.1×10^{-9}	1.2	42×10^{-9}	13×10^{10}	1.26×10^{-6}	220	36	3.9×10^{12}
4 Mev	0.092	19.7	5.3×10^{-10}	0.027	3.2×10^{-9}	1.0×10^{10}	9.4×10^{-8}	4.8	0.80	0.3×10^{12}

The computed acceptable charge is rather considerably greater for electrons (which one could easily inject at high energy from a linear accelerator of the Stanford type) than for protons of the same energy. For injection energies which are relativistic for electrons and non-relativistic for protons, the ratio $q_{electrons}/q_{protons}$ appears to be approximately

$$\frac{(\text{Total Electron Energy})^3}{2\ (\text{Proton Kinetic Energy})\ (\text{Electron Rest Energy})^2},$$

or about 5000 for 50 Mev injection.

currents which it was planned to attain. Attention should be given, moreover, to the avoidance of R.F. voltages which would bunch the beam to an extent that space-charge would cause the beam to expand beyond the bounds of the effective aperture. The space-charge effects appear to be considerably less serious in comparable electron accelerators.

5. References:

1. D. W. Kerst, Phys. Rev. 74, 503 (1948).
2. D. L. Judd, "A Study of the Injection Process in Betatrons and Synchrotrons", California Institute of Technology Thesis (Pasadena, 1950).
3. The possible importance of the mutual interaction between the particle trajectories and the space-charge distribution was suggested by M. Hamermesh following a discussion of this topic at the January 9 MAC meeting.
4. D. W. Kerst, Phys. Rev. 60, 47 (1941). In our equation (5), $\beta^2 E_0$ may be identified in the non-relativistic limit with $2E_{Kinetic}$ and $E_T/E_0 \rightarrow 1$; we obtain in this way agreement with Kerst's expression

$$(I/f)_{coulombs} = \pi\Delta^2 \text{ (Injection Voltage)}(1-n)/(15r_0 \cdot c).$$

In discussion of this phenomenon, Kerst also comments on the nature of the relativistic effect.

5. D. L. Judd, op. cit.[2] At the bottom of p. 91 Judd gives for the total charge the expression $q = 2\pi^2 \epsilon_0 B_0 R^2 v \left(\frac{1-n}{n}\right)^{1/2}$ $(1-v^2/c^2)^{-1}$.(relative radial semi-aperture)^2. When $n = 1/2$ this result assumes the form $q = 2\pi^2 \epsilon_0 B_0 \frac{v}{1-\beta^2} \Delta^2$; with the substitution $\frac{B_0 v}{1-\beta^2} = \frac{\beta^2 E_0}{eR}\left(\frac{E_T}{E_0}\right)^3$, one has

$q = \frac{2\pi^2 \epsilon_0}{e} \beta^2 \frac{E_T^3}{E_0^2} \frac{\Delta^2}{R}$, in agreement with our expression leading to equation (5) if $|\delta n|$ is set equal to one-half.

Judd's expression may be compared similarly with the result of Blewett[6] [equation (18), p. 90] by writing the circulating current as

$$i = \pi \epsilon_0 B_0 R \frac{v^2}{1-v^2/c^2} \left(\frac{1-n}{n}\right)^{1/2} \left(\frac{w/2}{R}\right)^2 = \frac{\pi}{4} \epsilon_0 \left(\frac{e}{m_0}\right)^2 B_0^{\,3} R \left(\frac{1-n}{n}\right)^{1/2}$$
$$\times w^2 = 1.0 \times 10^{11} B_0^{\,3} w^2,$$

after numerical substitution of Blewett's values [$n = 3/4$, $R = 0.833$ M, and $\frac{e}{m_0} = 1.76 \times 10^{-11}$ cou/Kg].

6. J. P. Blewett, Phys. Rev. 69, 87 (1946). Blewett's equation (18) appears to be consistent with our equation (6) if we take $|\delta n| = 1/2$ and replace Δ^2 by an effective value $w^2/(4\sqrt{3})$.

7. S. E. Barden, private communication to Dr. E. D. Courant (1953).
8. Courant, Livingston, and Snyder, Phys. Rev. 88, 1190 (1952). Our equation (10) results from the substitution of $n_2 = -m$ in their equation (4).
9. M. Stanley Livingston, "Design Study for a 15 Mev Accelerator", MIT Technical Report No. 60 (Cambridge, Massachusetts; June 30, 1953), §8.9. In the belief that the factor $(1-\beta^2)$ in Livingston's equations (98)-(99) has been lumped into his equation (101) for ω_p^2, his results for the defocusing effect of space-charge appear similar to the implications of our equation (5). He points out (p. 154) that for his design injection of 3 ma at 4 Mev, "the space-charge density is great enough to shift the beam through 3 or 4 π-resonances, allowing for the space-charge defocusing in the straight sections. ...We conclude that there is an upper limit to the space-charge density that can be held in stable orbits in the A.G.S. In the present design it is probable that the maximum useful current is appreciably less than 3 ma." In Livingston's estimates, a beam radius of 0.5 cm at injection was considered.
10. Livingston, Blewett, Green, and Haworth, Rev. Sci. Inst. 21, 7 (1950).
11. Kerst, Adams, Koch, and Robinson, Rev. Sci. Inst. 21, 462 (1950).
12. D. W. Kerst, private communication concerning discussion at the 26-28 October 1953 CERN conference (November 25, 1953).
13. J. H. Williams, comments at the meeting of the MAC Technical Group (January 9, 1954).
14. J. B. Adams, "The design of an alternate gradient synchrotron based on the linear theory", CERN, Geneva (October 24, 1953). Adams suggests (cf. his Fig. IX) a working diamond which "allows the n values of the different magnet sectors to have a random variation in n between the limits ± 1 per cent of n." Scaling his figure indicates a permissible consistent variation of n within the limits n±2. Adams points out explicitly that "for an injected current of 3 ma and an injection energy of 50 Mev the working point moves to the edge of the diamond. Dropping the injection energy to 25 Mev puts the working point outside the diamond. If a 4 Mev Van de Graaff generator were used the working point would be right outside the stability diagram."
15. Servo control of certain features of the beam trajectories was mentioned by L. Jones in a preliminary discussion at the meeting of the MAC Technical Group (January 9, 1954).

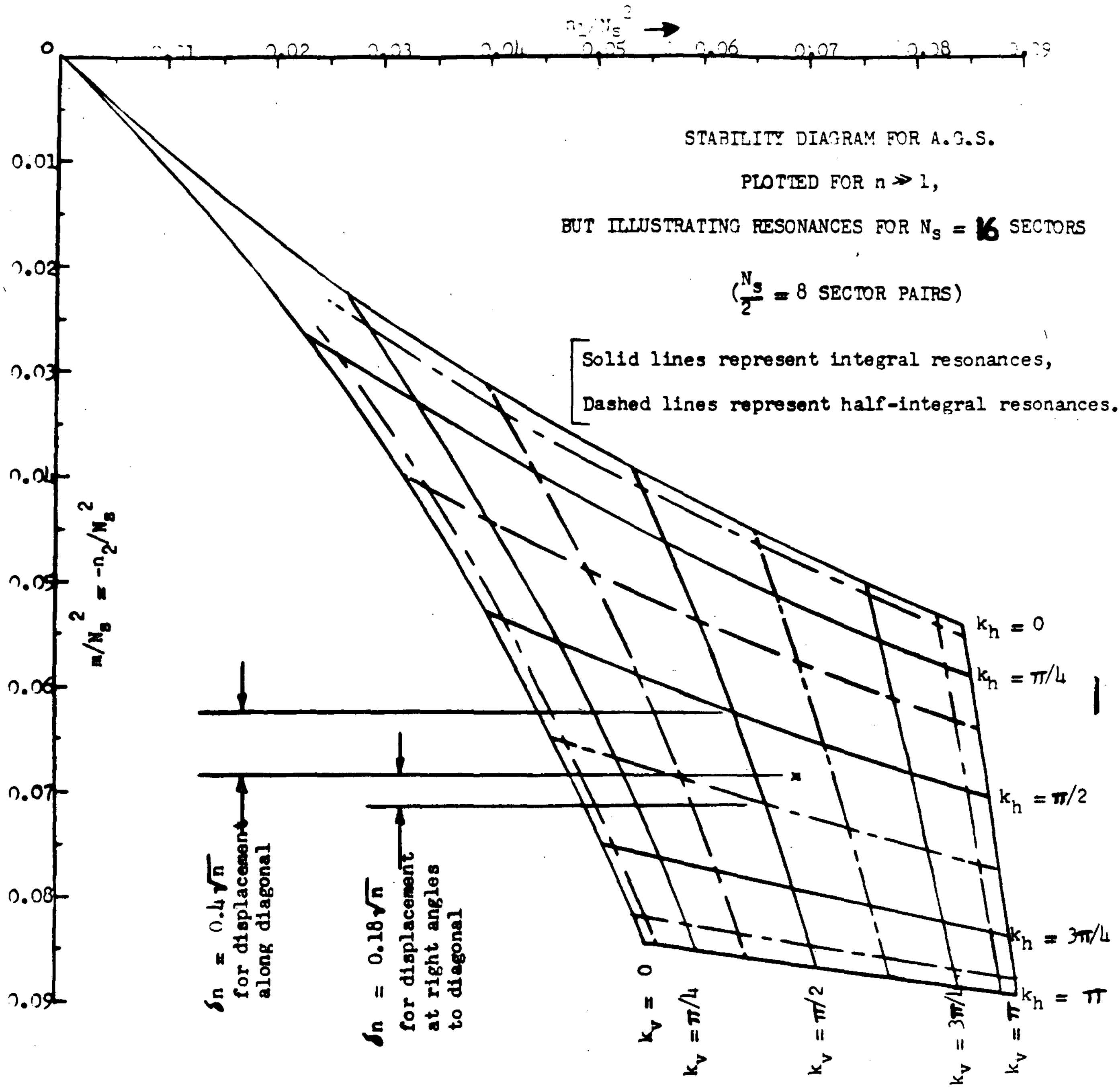
STABILITY DIAGRAM FOR A.G.S.
PLOTTED FOR n ≫ 1,
BUT ILLUSTRATING RESONANCES FOR N_s = 16 SECTORS
($\frac{N_s}{2}$ = 8 SECTOR PAIRS)
Solid lines represent integral resonances,
Dashed lines represent half-integral resonances.
n_1/N_s^2
0
0.01
0.02
0.03
0.04
0.05
0.06
0.07
0.08
0.09
$m/N_s^2 = -n_2/N_s^2$
$k_h = 0$
$k_h = \pi/4$
$k_h = \pi/2$
$k_h = 3\pi/4$
$k_h = \pi$
$k_v = 0$
$k_v = \pi/4$
$k_v = \pi/2$
$k_v = 3\pi/4$
$k_v = \pi$
$\delta n = 0.4\sqrt{n}$ for displacement along diagonal
$\delta n = 0.18\sqrt{n}$ for displacement at right angles to diagonal

L. Jackson Laslett
1 February 1955

APPROXIMATION OF EIGENVALUES, AND EIGENFUNCTIONS, BY VARIATIONAL METHODS

1. Motivation

In consideration of various accelerator designs employing the alternate-gradient principle, one is often faced with the problem of determining the values of the design parameters at the limits of stability. If one knows the general character of the solution to the differential equation at such points one may substitute a suitable simple trial function (or simple trial functions), containing adjustable parameters, into the associated variation problem and readily determine the eigenvalues with considerable accuracy.[1] It is the purpose of the present note (i) to illustrate the use of variational methods in a simple boundary-value problem where the dependent variable is fixed at the boundaries, (ii) to apply a similar technique to the Mathieu equation, for which the eigen-solutions are periodic, and finally (iii) to point out the applicability of the method to a problem arising in connection with the analysis of a Mk. V FFAG accelerator.

2. Example Concerning a Boundary-Value Problem in which the Dependent Variable is Fixed at the Boundaries

We consider the differential equation

$$y'' + \lambda y = 0 , \qquad \text{with} \qquad y(\pm 1) = 0 .$$

The simplest solution to this problem is known to be of the form.

$$y_1 = \cos\frac{\pi}{2}x \quad \text{and is obtained when} \quad \lambda = \frac{\pi^2}{4} .$$

The above problem is equivalent to the isoperimetric variation problem in which we seek a function, such that $y(\pm 1) = 0$, for which

$$\delta \int_{-1}^{1} y'^2 dx = 0 , \quad \text{subject to} \quad \int_{-1}^{1} y^2 dx = \text{const. (say 1)};$$

that is, introducing the Lagrange multiplier $-\lambda$, Euler's equation for

$$\delta \int_{-1}^{1} (y'^2 - \lambda y^2)\, dx = 0$$

is our original differential equation $y'' + \lambda y = 0$.

A trial solution (even in x), satisfying the boundary conditions, may be taken of the form

$$y = (1 - x^2)(a_1 + a_2 x^2) ,$$

for which $\int_{-1}^{1} (y'^2 - \lambda y^2) dx = (\frac{8}{3} - \frac{16}{15}\lambda) a_1^2 + (\frac{16}{15} - \frac{32}{105}\lambda) a_1 a_2 + (\frac{88}{105} - \frac{16}{315}\lambda) a_2^2.$

The latter expression will be stationary when

$$(\frac{16}{3} - \frac{32}{15}\lambda) a_1 + (\frac{16}{15} - \frac{32}{105}\lambda) a_2 = 0$$

$$(\frac{16}{15} - \frac{32}{105}\lambda) a_1 + (\frac{176}{105} - \frac{32}{315}\lambda) a_2 = 0 .$$

We accordingly find that λ must be given by

$$\lambda^2 - 28\lambda + 63 = 0,$$

of which the lesser root is $\lambda = 14 - (133)^{1/2} = 2.4674_{37}$ and $\frac{a_2}{a_1} = -0.22075$.

This value of λ may be compared with $\frac{\pi^2}{4} = 2.467\,401\,100\,022\,\cdots$; the inclusion of additional parameters in the trial function would permit further improvement of the estimated value. [The use of three constants (a_1, a_2, a_3) has been reported (Buck) to give $\lambda = 2.467\,401\,10_8$.]

It may be noted that with the trial solution normalized so that our auxiliary integral (in this case $\int_{-1}^{1} y^2\,dx$) is unity, the value obtained for $\int_{-1}^{1} y'^2 dx$ may be shown to be our value of λ and will be greater than the exact eigenvalue.

The equivalent variation problems for other differential equations with other types of boundary conditions are presented in Courant-Hilbert[2], Ch. IV, Sect. 5, esp. p.182. One may further note that, in particular, with J of the form

$$J = \int_{x_1}^{x_2} F(x, y, y')\,dx,$$

$$\delta J = \frac{\partial F}{\partial y'}\,\delta y\Big|_{x_1}^{x_2} - \int_{x_1}^{x_2}\Big[\frac{d}{dx}\Big(\frac{\partial F}{\partial y'}\Big) - \frac{\partial F}{\partial y}\Big]\,\delta y\,dx\,;$$

accordingly if $\frac{\partial F}{\partial y'}$ is independent of x or periodic (period $x_2 - x_1$) in x, boundary conditions requiring y to be periodic (period $x_2 - x_1$) result in the variation problem again reducing to the problem governed by Euler's equation

$$\frac{d}{dx}\Big(\frac{\partial F}{\partial y'}\Big) - \frac{\partial F}{\partial y} = 0\,.$$

3. Character of the Eigensolutions of the Mathieu Equation

At the stability boundaries for the Mathieu equation,

$$\frac{d^2y}{dx^2} + (a + 16q\cos 2x)\,y = 0\,,$$

the characteristic bounded solutions are periodic, with period π or 2π. When $q = 0$, the periodic solutions are, of course,

$$\begin{array}{ccccc} 1 & \cos x & \cos 2x & \cos 3x & \cdots \\ & \sin x & \sin 2x & \sin 3x & \cdots\,; \end{array}$$

the Mathieu functions which reduce to these forms when $q \to 0$ are designated (notation of Whittaker and Watson[3])

$$\begin{array}{ccccc} ce_0(x,q) & ce_1(x,q) & ce_2(x,q) & ce_3(x,q) & \cdots \\ & se_1(x,q) & se_2(x,q) & se_3(x,q) & \cdots\,, \end{array}$$

the functions in the first line being even functions of x and those in the second line odd functions.

The stability boundaries are given in series form for the first few cases[3] and are also listed in tables[4]; coefficients for the Fourier expansion of the eigenfunctions are likewise available[3,4]. The stability boundaries are graphed in Fig. 1 and the character of the solutions illustrated in the accompanying Table I. The solutions of the table are arranged in the same order as the quantities appear on the graph. The quatities be_0, bo_1, be_1, ... are tabulated as functions of $s = 2|16q|$ in ref.[4], as are the coefficients in Fourier expansions of the even functions Se_0, Se_1, ... and of the odd functions So_1, So_2, ...; for $q < 0$, these functions give the desired solutions if we set $s = 2(-16q)$, while, for $q > 0$, we set $s = 2(16q)$ and replace the argument by $x \mp \pi/2$.

4. Approximation, by Variational Methods, of Eigenvalues and Eigenfunctions for Mathieu Equation

The first eigenvalues of Mathieu's equation (given by be_0, bo_1, be_1, bo_2) may be approximated by a procedure paralleling that employed in the example of Section 2. We consider, in this connection, the variation problem for the form of the eigenfunctions

$$\delta\int_0^{2\pi}(y'^2 - ay^2 - 16\,q\,y^2\cos 2x)\,dx = 0$$

into which we introduce periodic trial solutions.

(i) For the first stability boundary we employ trial solutions, even in x and of period π, of the form

$$A_0 + A_1\cos 2x + A_2\cos 4x + \cdots.$$

If only two terms are retained, the integral becomes

$$2\pi\left[-a A_0^2 - 16\,q A_0 A_1 + (2 - \tfrac{a}{2})A_1^2\right].$$

This expression is stationary if

$$\begin{aligned} -2a\,A_0 - 16\,q\,A_1 &= 0 \\ -16q\,A_0 + (4 - a)\,A_1 &= 0\,; \end{aligned}$$

and gives us a relation from which one obtains a good first estimate of the first stability boundary:

$$(16\,q)^2 = 2a\,(a - 4).$$

We thus obtain, for the first stability boundary,

$$a \doteq -2\left[(1 + 32\,q^2)^{1/2} - 1\right], \quad A_1/A_0 \doteq \frac{(1 + 32\,q^2)^{1/2} - 1}{4q} \quad \text{and,}$$

by way of example, if $16\,q = \pm 4$,

$$a \doteq -1.464\ , \quad A_1/A_0 \doteq \pm 0.732 \quad \text{(the sign being that of } q\text{)}.$$

[The second root for "a" is $2\left[(1 + 32q^2)^{1/2} + 1\right]$ or, in this example, 5.464 with $A_1/A_0 \doteq \mp 2.732$.]

Fig. 1

Stability Boundaries and Eigen solutions for Mathieu Equation

$$\frac{d^2y}{dx^2} + (a + 16q\cos 2x)\,y = 0 .$$

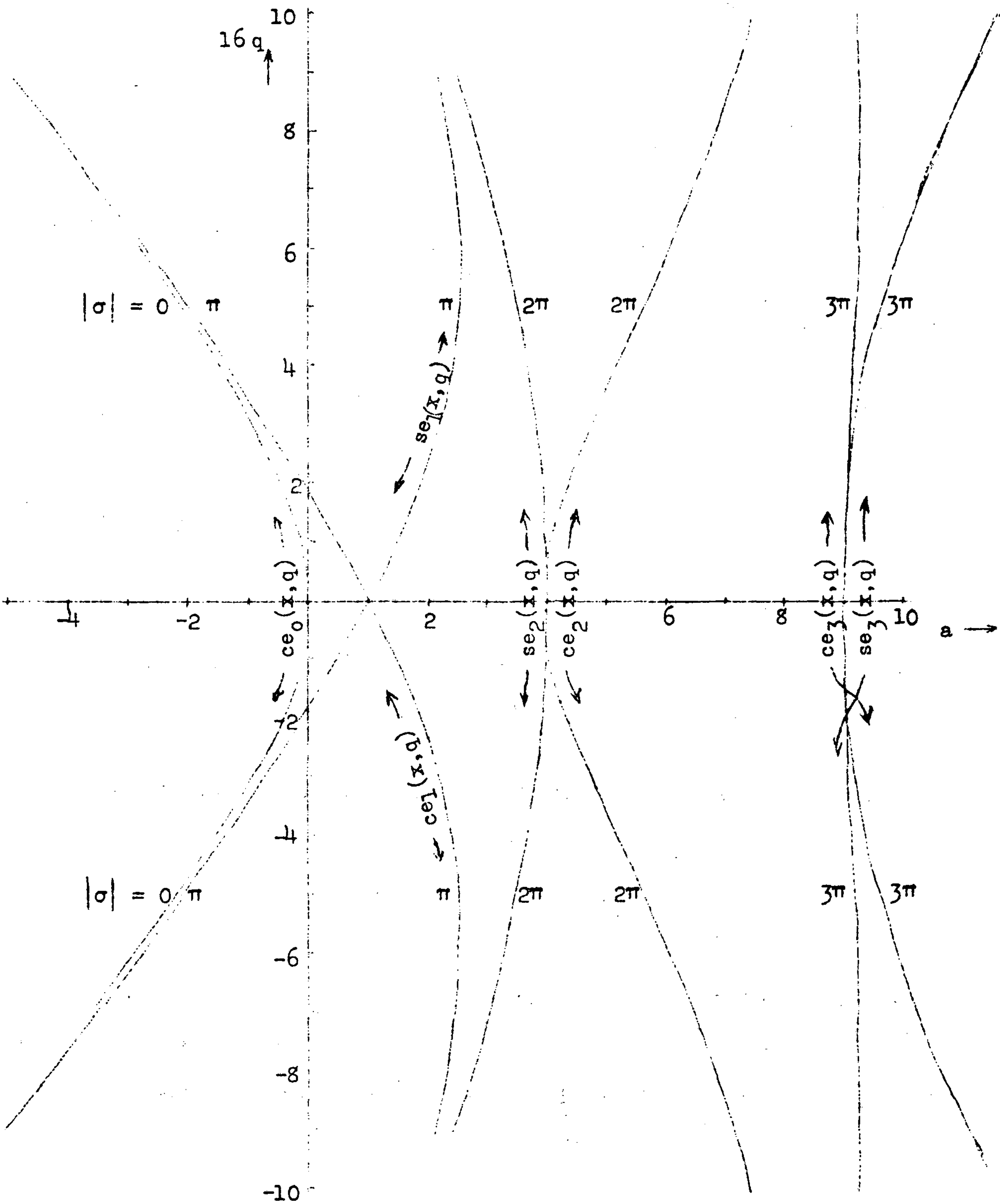

TABLE I

CHARACTER OF EIGENSOLUTIONS TO MATHIEU EQUATION

σ	0	π	π	2π	2π	3π	3π
a	$be_o(32q) - 16q$	$bo_1(32q) - 16q$	$be_1(32q) - 16q$	$bo_2(32q) - 16q$	$be_2(32q) - 16q$	$bo_3(32q) - 16q$	$be_3(32q) - 16q$
16 q	ce_o	ce_1	se_1	se_2	ce_2	ce_3	se_3
4.0	1.0 + 0.7570 cos 2x + 0.0870 cos 4x	cos x + 0.1953 cos 3x + 0.0148 cos 5x	sin x + 0.3104 sin 3x + 0.0275 sin 5x	sin 2x + 0.1639 sin 4x + 0.0102 sin 6x	− 0.3866 + cos 2x + 0.1870 cos 4x	− 0.1972 cos x + cos 3x + 0.1269 cos 5x	− 0.3140 sin x + sin 3x + 0.1288 sin 5x
1.367	1.0 + 0.3260 cos 2x + 0.0138 cos 4x	cos x + 0.0785 cos 3x + 0.0022 cos 5x	sin x + 0.0930 sin 3x + 0.0027 sin 5x				
0	1	cos x	sin x	sin 2x	cos 2x	cos 3x	sin 3x
16 q	ce_o (From Se_o)	se_1 (From So_1)	ce_1 (From Se_1)	se_2 (From Se_2)	ce_2 (From Se_2)	se_3 (From So_3)	ce_3 (From Se_3)
0	1	sin x	cos x	sin 2x	cos 2x	sin 3x	cos 3x
-1.367	1.0 − 0.3260 cos 2x + 0.0138 cos 4x	sin x − 0.0785 sin 3x + 0.0022 sin 5x	cos x − 0.0930 cos 3x + 0.0027 cos 5x				
-4.0	1.0 − 0.7570 cos 2x + 0.0870 cos 4x	sin x − 0.1953 sin 3x + 0.0148 sin 5x	cos x − 0.3104 cos 3x + 0.0275 cos 5x	sin 2x − 0.1639 sin 4x + 0.0102 sin 6x	0.3866 + cos 2x − 0.1870 cos 4x	0.1972 sin x + sin 3x − 0.1269 sin 5x	0.3140 cos x + cos x − 0.1288 cos 5x
a	$be_o(\|32q\|)$ $- \|16q\|$	$bo_1(\|32q\|)$ $- \|16q\|$	$be_1(\|32q\|)$ $- \|16q\|$	$bo_2(\|32q\|)$ $- \|16q\|$	$be_2(\|32q\|)$ $- \|16q\|$	$bo_3(\|32q\|)$ $- \|16q\|$	$be_3(\|32q\|)$ $- \|16q\|$
Period of Eigenfcn.	π	2π	2π	π	π	2π	2π

If we refine our approximation by including three parameters in the trial function, the integral becomes

$$2\pi\left[-aA_0^2 - 16\,q\,A_0A_1 + (2-\tfrac{a}{2})A_1^2 - 8\,q\,A_1A_2 + (8-\tfrac{a}{2})A_2^2\right].$$

We thus obtain the simultaneous equations

$$\begin{aligned} -2a\,A_0 \quad - 16q\,A_1 \qquad\qquad &= 0\\ -16\,q\,A_0 + (4-a)\,A_1 - 8\,q\,A_2 &= 0\\ -8\,q\,A_1 + (16-a)A_2 &= 0\,; \end{aligned}$$

we thus obtain for the first stability boundary (for $16\,q = \pm 4$)

$$a = -1.5136_5, \qquad A_1/A_0 = \pm 0.7568_2, \qquad A_2/A_0 = +0.0864$$

and a second solution

$$a \doteq +5.176, \qquad A_1/A_0 \doteq \mp 2.588, \qquad A_2/A_1 \doteq \pm 0.1848\,.$$

We thus are obtaining what appears to be a good approximation to the first eigenvalue and its associated solution as well as a reasonable estimate[5] of the value and solution corresponding to ce_2. The correct values are[4]

First solution: $a = -1.51396$, $A_1/A_0 = \pm 0.7570$, $A_2/A_0 = +0.0870$;
Second solution: $a = 5.17266$, $A_1/A_0 = \mp 2.5863$, $A_2/A_1 = \pm 0.1870$.

The first stability limit may, of course, be alternatively estimated by use of the smooth approximation;[7] in this way we find $a = -32\,q^2$, which represents a good approximation to the correct value when q is small (as is seen by expansion of our first result or by reference to the series given on p.411 of ref.3) and gives the numerical value -2 for $16\,q = \pm 4$.

(ii) One may proceed similarly to locate the second stability boundary and to examine the character of the associated eigensolutions. In this case (when $q > 0$) we employ trial solutions (with period 2π) of the form

$$B_1\cos x + B_2\cos 3x + B_3\cos 5x + \cdots.$$

Retaining three terms, the integral becomes

$$2\pi\left[(\tfrac{1}{2}-4q-\tfrac{a}{2})B_1^2 - 8qB_1B_2 + (\tfrac{9}{2}-\tfrac{a}{2})B_2^2 - 8qB_2B_3 + (\tfrac{25}{2}-\tfrac{a}{2})B_3^2\right]$$

and leads to the equations

$$\begin{aligned} (1-8q-a)B_1 - 8q\,B_2 \qquad\qquad &= 0\\ -8q\,B_1 + (9-a)B_2 - 8q\,B_3 &= 0\\ -8q\,B_2 + (25-a)B_3 &= 0\,. \end{aligned}$$

The location of the first stability boundary of the present type is then estimated to be, when $16\,q = 4$,

$$a = -1.39066, \quad \text{with } B_2/B_1 = 0.1953_3 \text{ and } B_3/B_1 = 0.0148_{03}\,.$$

The correct values are[4]

$$a = -1.39068, \quad \text{and } B_2/B_1 = 0.1953_4, \quad B_3/B_1 = 0.014848\,.$$

(iii) Proceeding to the next stability limit, one assumes trial solutions (again of period 2π) of the form

$$C_1 \sin x + C_2 \sin 3x + C_3 \sin 5x + \cdots .$$

Since we are concerned only with this problem as an illustration, we keep merely two terms here to obtain

$$2\pi\left[\left(\frac{1}{2} + 4q - \frac{a}{2}\right)C_1^{\,2} - 8qC_1 C_2 + \left(\frac{9}{2} - \frac{a}{2}\right)C_2^{\,2}\right]$$

for the integral.

We then obtain the equations

$$\begin{aligned} (1 + 8q - a)C_1 - 8q\, C_2 &= 0 \\ -8q\, C_1 + (9 - a)C_2 &= 0 , \end{aligned}$$

with the solution of interest, for $16q = 4$,

$$a = 6 - (13)^{1/2} = 2.3944, \quad C_2/C_1 = 0.3028 .$$

The correct values are[4]

$$a = 2.3792 , \qquad C_2/C_1 = 0.3104 .$$

(iv) The fourth type of stability limit is investigated by aid of the trial function (period π)

$$D_1 \sin 2x + D_2 \sin 4x + D_3 \sin 6x + \cdots .$$

Again we retain only two terms to obtain

$$2\pi\left[\left(2 - \frac{a}{2}\right)D_1^{\,2} - 8qD_1 D_2 + \left(8 - \frac{a}{2}\right)D_2^{\,2}\right]$$

for the integral.

We then obtain the equations

$$\begin{aligned} (4 - a)D_1 - 8q\, D_2 &= 0 \\ -8q\, D_1 + (16 - a)D_2 &= 0 , \end{aligned}$$

with the solution of interest, for $16q = 4$,

$$a = 10 - (40)^{1/2} = 3.6754, \quad D_2/D_1 = 0.1623 .$$

The correct values are[4]

$$a = 3.6722, \qquad D_2/D_1 = 0.1639 .$$

5. Application of Variation Methods to a Problem arising in a Mk.V FFAG

In the analysis[8] of the oscillations about a scalloped orbit, as for a Mk.V FFAG accelerator, one obtains differential equations of the form

$$\frac{d^2y}{dt^2} + \left\{a + \left[b\cos 2t + c\cos(4t+\delta)\right]\right\} y = 0,$$

or

$$\frac{d^2y}{dt^2} + \left\{a + \left[b\cos 2t + c\cos\delta\,\cos 4t - c\sin\delta\,\sin 4t\right]\right\} y = 0.$$

In a typical case,

$b = \pm 1.3672$, $c = \pm 0.2462$, and $\delta = 0.0331$ radian.

It is desired to determine values of the parameter "a" at those stability limits which lie near zero.

(i) Since δ is small it may be experted that a good estimate of the stability boundaries may, in fact, be obtainable by setting $\delta = 0$ and using trial solutions

$A_0 + A_2\cos 2t + A_4\cos 4t$ for one boundary

and $A_1\cos t + A_3\cos 3t$ (in the case the upper sign for "b" is taken) at the other boundary.

In these respective cases, proceding by methods similar to those used before, one finds the determanental equations

$$\begin{vmatrix} -2a & -b & -c \\ -b & 4-a-\frac{c}{2} & -\frac{b}{2} \\ -c & -\frac{b}{2} & 16-a \end{vmatrix} = 0 \quad \text{and} \quad \begin{vmatrix} 1-a-\frac{b}{2} & -\frac{b}{2}-\frac{c}{2} \\ -\frac{b}{2}-\frac{c}{2} & 9-a \end{vmatrix} = 0 .$$

The first determanental equation leads to the first boundary location (when b and c have the values indicated)

$a = -0.234_{29}$ for $c > 0$,

$a = -0.215_{45}$ for $c < 0$.

The values obtained in general from this first determanental equation approach, when b and c are small, the value given by the smooth approximation[7]:

$$a \cong -\left(\frac{b^2}{8} + \frac{c^2}{32}\right)$$

but, in third order (order of b^2c), appear to permit a slightly more negative value of "a" when the maximum positive excursions of the $\cos 2t$ and $\cos 4t$ terms add in phase. For the values of b and c assumed here the smooth approximation gives $a \cong -0.2355$.

The second determanental equation leads to the second stability boundary estimated to be given by

$a \doteq 0.2421$ for $c > 0$,

$a \doteq 0.2804$ for $c < 0$.

(ii) If we do not neglect δ in the given problem, it then appears appropriate to take trial functions of a more general form, although the determanental equation will be found to factor into two equations, corresponding to eigensolutions of periods π and 2π.

We accordingly take as a trial function

$$\begin{aligned} y = A_0 &+ A_1\cos t + A_2\cos 2t + A_3\cos 3t + A_4\cos 4t \\ &+ B_1\sin t + B_2\sin 2t + B_3\sin 3t + B_4\sin 4t\,, \end{aligned}$$

for which the integral which is to take on a stationary value is

$$\begin{aligned} 2\pi\Big[&- aA_0^2 - bA_0A_2 - c\cos\delta\,A_0A_4 + c\sin\delta\,A_0B_4 \\ &+ \left(\tfrac{1}{2} - \tfrac{a}{2} - \tfrac{b}{4}\right)A_1^2 + \left(-\tfrac{b}{2} - \tfrac{c}{2}\cos\delta\right)A_1A_3 + \tfrac{c}{2}\sin\delta\,A_1B_3 \\ &+ \left(2 - \tfrac{a}{2} - \tfrac{c}{4}\cos\delta\right)A_2^2 - \tfrac{b}{2}A_2A_4 + \tfrac{c}{2}\sin\delta\,A_2B_2 \\ &+ \left(\tfrac{9}{2} - \tfrac{a}{2}\right)A_3^2 + \tfrac{c}{2}\sin\delta\,A_3B_1 + \left(8 - \tfrac{a}{2}\right)A_4^2 \\ &+ \left(\tfrac{1}{2} - \tfrac{a}{2} + \tfrac{b}{4}\right)B_1^2 + \left(-\tfrac{b}{2} + \tfrac{c}{2}\cos\delta\right)B_1B_3 \\ &+ \left(2 - \tfrac{a}{2} + \tfrac{c}{4}\cos\delta\right)B_2^2 - \tfrac{b}{2}B_2B_4 \\ &+ \left(\tfrac{9}{2} - \tfrac{a}{2}\right)B_3^2 + \left(8 - \tfrac{a}{2}\right)B_4^2 \Big]. \end{aligned}$$

The resulting determanental equation may be factored to read

$$\begin{vmatrix} -2a & -b & -c\cos\delta & 0 & c\sin\delta \\ -b & 4-a-\frac{c}{2}\cos\delta & -b/2 & \frac{c}{2}\sin\delta & 0 \\ -c\cos\delta & -b/2 & 16-a & 0 & 0 \\ 0 & \frac{c}{2}\sin\delta & 0 & 4-a+\frac{c}{2}\cos\delta & -b/2 \\ c\sin\delta & 0 & 0 & -b/2 & 16-a \end{vmatrix} \times$$

$$\begin{vmatrix} 1-a-\frac{b}{2} & -\frac{b}{2}-\frac{c}{2}\cos\delta & 0 & \frac{c}{2}\sin\delta \\ -\frac{b}{2}-\frac{c}{2}\cos\delta & 9-a & \frac{c}{2}\sin\delta & 0 \\ 0 & \frac{c}{2}\cos\delta & 1-a+\frac{b}{2} & -\frac{b}{2}+\frac{c}{2}\cos\delta \\ \frac{c}{2}\sin\delta & 0 & -\frac{b}{2}+\frac{c}{2}\cos\delta & 9-a \end{vmatrix} = 0.$$

and is seen to reduce to the previous result if δ is set equal to zero. Vanishing of the first determanent would permit one to obtain ratios of non-vanishing coefficients A_0, A_2, A_4, B_2, B_4, corresponding to a solution of period π, and the vanishing of the second permit an independent similar determination of A_1, A_3, B_1, B_3, corresponding to a solution of period 2π.

With regard to the 5×5 determanent, it has been noted that it will factor when $\delta = 0$ to give the earlier result. If $\delta \neq 0$, the determanent may be expanded as a sum of 3×3 minors and their associated 2×2 cofactors to give a correction of order $c^2\delta^2$ to the original 3×3 determanent. In addition, it is to be noted that the original 3×3 determanent is itself modified by a term of order $c\delta^2$; a rough numerical check seems to indicate that this latter effect is somewhat the greater and would result (as might be expected) in bringing together the estimates of the first stability boundary for the two cases $b \gtrless 0$. With the present value of δ, however, the change of "a" is believed to be small -- perhaps of the order of ± 0.003 -- and a direct revaluation has not been undertaken.

With regard to the 4×4 determanent associated with the next stability limit a similar situation is seen to apply. Expansion in a series of products of 2×2 determanents and adjustment of the original determanent to take account of $\cos\delta \neq 1$ is seen once again to introduce corrections of the order of δ^2.

6. Approximate Association of Parameters in Mathieu Equation with the Value of σ

It appears possible, with a bit more algebraic complexity, to employ variational methods to relate the parameters of the Mathieu equation to values of σ away from the stability boundaries. To this end we note that, as pointed out by Courant and Snyder [EDC-15], stable solutions to equations of the form considered here may be written in the form

$$x(t) = w(t)\, e^{\pm i\,\phi(t)},$$

where $\phi(t) = \frac{\sigma}{T} t + \psi(t)$,

$w(t)$ and $\psi(t)$ are real functions, each periodic with the period T of the coefficients in our differential equation, and

σ is a real constant.

In connection with the differential equation

$$\frac{d^2y}{dt^2} + (a + b\cos 2t)\,y = 0,$$

we accordingly express solutions in the form

$$y = w(t)\, e^{\pm i\left[\frac{\sigma}{\pi} + \psi(t)\right]},$$

with w and ψ each periodic with period π. We then consider the variational problem

$$\delta \int_0^{\pi} \left[\tfrac{1}{2} w'^2 - \tfrac{1}{2} b (\cos 2t) w^2 + \tfrac{1}{2}\left(\tfrac{\sigma}{\pi} + \psi'\right)^2 w^2 \right] dt = 0,$$

with $\int_0^{\pi} \frac{1}{2} w^2\, dt = 1.$

With the introduction of the Lagrange multiplier $-a$, we then obtain

$$\delta\int_0^\pi \frac{1}{2}\left[w'^2 - aw^2 - b(\cos 2t)w^2 + \left(\frac{\sigma}{\pi} + \psi'\right)^2 w^2\right] dt = 0 ,$$

with the restriction that the average value of ψ' shall vanish. From this variational statement we then obtain the differential equations

$$w'' + \left[a + b\cos 2t\right] w - \left(\frac{\sigma}{\pi} + \psi'\right)^2 w = 0$$

$$\left(\frac{\sigma}{\pi} + \psi'\right) w^2 = \text{const.},$$

which are the differential equations governing the periodic functions w and ψ from which the solutions to our original differential equation may be constructed.

If, to proceed in a simple way, we take the trial functions

$$w = A_0 + A_1 \cos 2t$$

$$\psi' = B\cos 2t ,$$

the integral becomes

$$\frac{\pi}{2}\left[2A_1^2 - aA_0^2 - a\frac{A_1^2}{2} - bA_0A_1 + \left(\frac{\sigma}{\pi}\right)^2\left(A_0^2 + \frac{A_1^2}{2}\right) + \frac{A_0^2B^2}{2} + 2\frac{\sigma}{\pi}A_0A_1B + \frac{3}{8}A_1^2B^2\right].$$

We accordingly obtain the simultaneous equations

$$\left[-2a + 2\left(\frac{\sigma}{\pi}\right)^2 + B^2\right]A_0 + \left[-b + 2\frac{\sigma}{\pi}B\right]A_1 = 0$$

$$\left[-b + 2\frac{\sigma}{\pi}B\right]A_0 + \left[4 + \left(\frac{\sigma}{\pi}\right)^2 - a + \frac{3}{4}B^2\right]A_1 = 0$$

$$\left[A_0^2 + \frac{3}{4}A_1^2\right]B + 2\frac{\sigma}{\pi}A_0A_1 = 0 .$$

It is desired to determine values of the parameters such that the solution of these simultaneous equations does not require the coefficients A_0, A_1, and B to vanish.

By way of example, we take $q = 0.09$ or $b = 16q = 1.44$ and $\cos\sigma = 0.6$ or $\sigma = 0.9273 = 0.29517\,\pi$.

The simultaneous equations then become

$$\left[0.17425 - 2a + B^2\right]A_0 + \left[-1.44 + 0.59033B\right]A_1 = 0$$

$$\left[-1.44 + 0.59033B\right]A_0 + \left[4.087125 - a + \frac{3}{4}B^2\right]A_1 = 0$$

$$\left[A_0^2 + \frac{3}{4}A_1^2\right]B + 0.59033A_0A_1 = 0 .$$

The algebraic complexity of these equations suggests that a solution be obtained by trial. We find in this way

$$a = -0.17564 \qquad (A_1/A_0 = 0.3624, \quad B = -0.1948) .$$

This result may be compared with that obtained by constructing a graph for $\cos\sigma$ by numerical integration and adjustment to the known stability boundaries -- viz. $a = -0.180$.

7. References

1. W. Ritz, J. für reine u. angew. Math. CXXXV, 1-61 (1909). Cited in Courant-Hilbert[2], I, 157.

2. R. Courant u. D. Hilbert, Meth. der Math. Physik I (Springer, Berlin, 1924).

3. E. T. Whittaker and E. N. Watson, Modern Analysis (Cambridge University Press, 1927), Sect. 19.3.

4. f. ex. NBS Computation Laboratory "Tables Relating to Mathieu Functions" (Columbia University Press, N.Y., 1951).

5. For further discussion of these general methods see N. Kryloff, Mem. des Sciences Math. 49. See also comments and further references in Bateman's[6] introduction.

6. H. Bateman, Partial Differential Equations (Cambridge University Press, 1932; Dover, N.Y., 1944).

7. K. R. Symon, KRS(MURA)-1, -4 (1954).

8. Work in progress, summarized in letters to Dr. Kerst dated 21, 23, 25 January 1955, and based on the original model proposed by Kerst [cf. MURA-DWK/KMT/LWJ/KRS-3 and MURA-DWK-7].

MU-RA "NOTES" [Treble Clef]
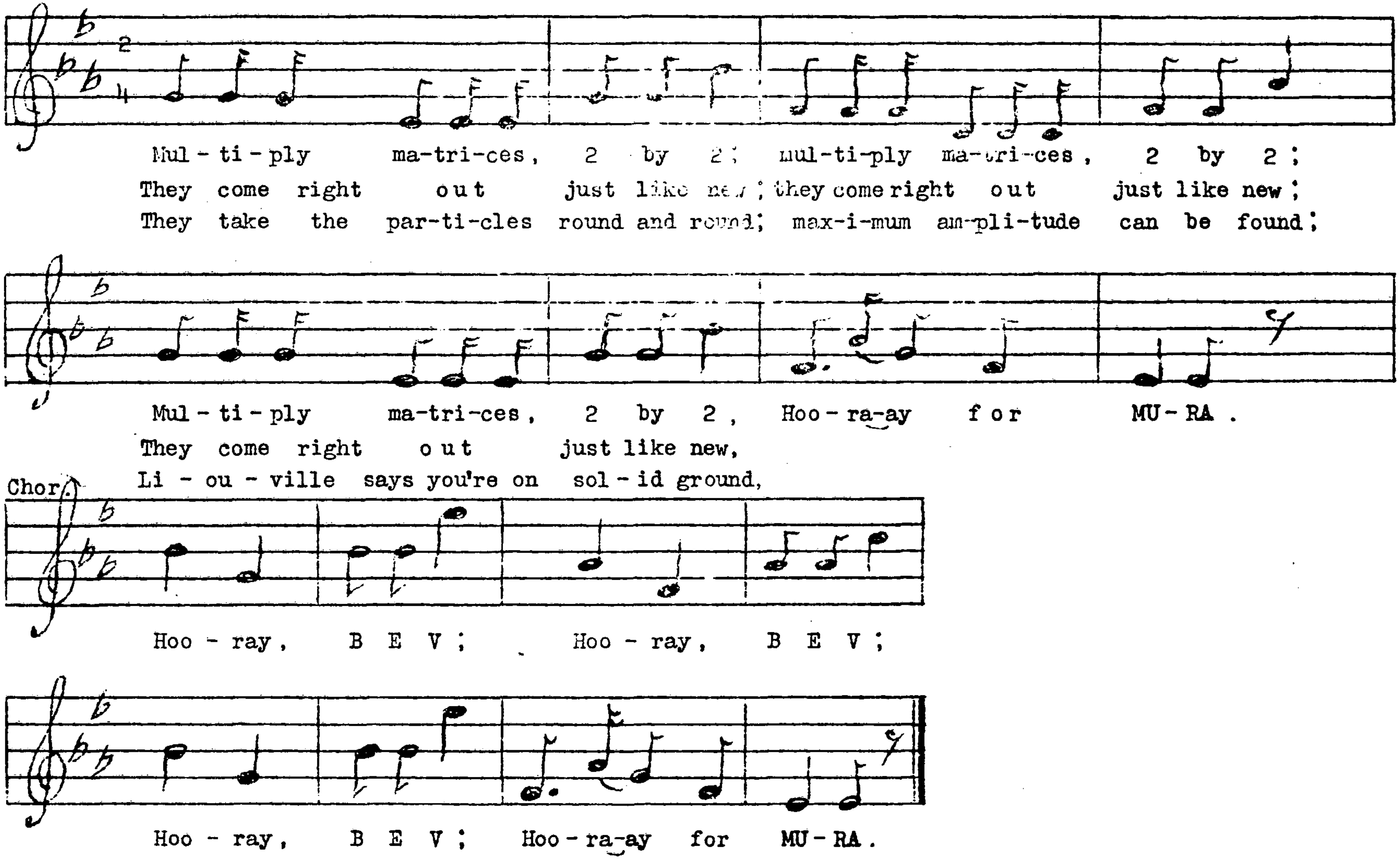
APPLICATION OF WALKINSHAW'S EQUATION TO THE $2\sigma_y = \sigma_x$ RESONANCE

L. Jackson Laslett*

Midwestern Universities Research Association†

A method of analysis which appears to account for the behavior of the axial motion, in the presence of appreciable radial oscillation, has been developed by Walkinshaw, [W. Walkinshaw, "A Spiral Ridged Bevatron," A.E.R.E., Harwell (1956)]. The differential equation characterizing the axial motion is treated as linear, but contains a coefficient which involves the radial motion. As is well-know, the forced radial motion enhances the A-G focusing which appears in the axial equation – now, however, the additional effect of the free radial betatron oscillations is also included in the axial equation. The super-position of the comparatively-long-wavelength radial oscillations on the forced motion in effect modulates the smooth-approximation coefficient in the axial equation, to yield a Mathieu equation with a coefficient having the period of the radial motion. Under "resonant" conditions, which will be seen to include the case of interest here, this equation may have unstable solutions and, in such cases, the characteristic exponent of the solution appears to compare reasonably in magnitude with the lapse-rate characterizing the exponential growth of the ILLIAC solutions of the "Feckless Five" equations.

---

*At the University of Illinois, on leave from Iowa State College.

†Assisted by the National Science Foundation, the Office of Naval Research, and the Atomic Energy Commission.

Walkinshaw's analysis pertains to differential equations which, in the MURA notation [f.ex., LJL(MURA)-5], are taken to be of the form

$$x'' + (k+1)x = -f\sin(x/w - N\theta)$$
$$y'' + [-k - (f/w)\cos(x/w - N\theta)]y = 0$$

[cf. LJL MURA Notes 6-22 Oct. 1956, Sec. 6, for y/w << 1]. A solution for the radial motion, representing a free oscillation of amplitude A superposed on the forced motion, is taken of the form

$$x = A\cos(\nu_x\theta + \epsilon) - (f/\Omega^2)\sin\int\Omega\, d\theta,$$

where $\Omega \simeq N + A(\nu_x/w)\sin(\nu_x\theta + \epsilon)$ and $\nu_x \doteq (k+1)^{1/2}$

This solution is substituted into the axial equation to yield, after some approximation (and a shift of the origin of θ which we introduce for convenience),

$$y'' + \left[-k + \frac{f^2}{w^2N^2}\left(1 + \frac{2A\nu_x}{wN}\cos\nu_x\theta\right)\right]y = 0$$

It is noted that, when A = 0, this equation reduces to that given by the smooth approximation – we accordingly write

$$y'' + \left[\nu_y^2 + \frac{2Af^2\nu_x}{w^3N^3}\cos\nu_x\theta\right]y = 0$$

to obtain an equation of the Mathieu type with a coefficient of period $2\pi/\nu_x$ in θ. By the transformation $\nu_x\theta = 2t$, we have the standard form

$$\frac{d^2y}{dt^2} + \left[\left(\frac{2\nu_y}{\nu_x}\right)^2 + \frac{8f^2}{w^3N^3}\frac{A}{\nu_x}\cos 2t\right]y = 0$$

with a coefficient of period π in the independent variable t.

A solution of the Mathieu equation

$$\frac{d^2y}{dt^2} + \left[a + b \cos 2t \right] y = 0 \quad ,$$

for b small but not zero, will exhibit instability when the coefficient a is equal or close to the square of an integer. In the present application stop-bands may thus be expected at operating points such that $2\nu_y/\nu_x = m$, the broad band of instability at $2\nu_y/\nu_x = 1$ (or $2\sigma_y/\sigma_x = 1$) being of chief interest in connection with the work presented here. It appears, moreover, possible to employ the Mathieu equation to account semi-quantitatively for (i) the range of b, and hence of the amplitude of free radial oscillation, which may be permitted when the oscillation frequencies depart by a specified amount from the resonant condition, and (ii) the lapse-rate found to characterize the growth of the axial motion when the radial oscillations exceed this limit.

The numerical application of the Mathieu equation to specific problems of stability or instability may be accomplished by reference to ILLIAC solutions for the stability boundaries or for the characteristic exponent characterizing the solution.

(i) A useful estimate of he expected restrictions on the radial motion may be obtained, however, by appeal to the fact that near $a = 1$, $b = 0$ the stability boundaries can be represented rather well by the condition

$$|b| \doteq 2\,|a-1|$$

We find in this way the following estimate for the limiting amplitude:

$$A_1 = \frac{\omega^3 N^3}{4 f^2}\,\nu_x \left|\left(\frac{2\nu_y}{\nu_x}\right)^2 - 1\right|$$

$$\simeq \frac{\omega^3 N^3}{4 f^2}\,\left|2\nu_y - \nu_x\right| \quad \text{for } \frac{2\nu_y}{\nu_x} - 1 \ll 1$$

It may be noted that this result, although expressed in terms of ν_x and ν_y, concerns an inherent sector resonance which arises when $2\sigma_y/\sigma_x = 1$.

(ii) An estimate of the lapse-rate characterizing unstable solutions near a = 1, b = 0 may, moreover, be made by taking

$$\mu \doteq \frac{\pi}{4}\sqrt{b^2 - 4(a-1)^2} \quad \text{nepers for } \Delta t = \pi \quad (\text{when } |b| > 2|a-1|)$$

$$= \frac{\pi}{4}\frac{\nu_x}{N}\sqrt{b^2 - 4(a-1)^2} \quad \text{nepers per sector}$$

$$= \frac{\pi}{4N}\sqrt{\left(\frac{8 f^2 A}{\omega^3 N^3}\right)^2 - 4\left[(2\nu_y)^2 - \nu_x^2\right]/\nu_x^2} \quad \text{nepers per sector}$$

$$= \frac{1.57}{N}\sqrt{\left(\frac{4 f^2 A}{\omega^3 N^3}\right)^2 - \left[(2\nu_y)^2 - \nu_x^2\right]^2/\nu_x^2} \quad \text{nepers per sector}$$

$$= \frac{0.68}{N}\sqrt{\left(\frac{4 f^2 A}{\omega^3 N^3}\right)^2 - \left[(2\nu_y)^2 - \nu_x^2\right]/\nu_x^2} \quad \text{decades per sector.}$$

A convenient alternative form for this last result is

$$\mu = \frac{2\pi f^2}{\omega^3 N^4}\sqrt{A^2 - A_1^2} \qquad \text{nepers/sector}$$

$$= \frac{2.73 f^2}{\omega^3 N^4}\sqrt{A^2 - A_1^2} \qquad \text{decades/sector.}$$

Results obtained with the ILLIAC, for 5-sector machines with model-like parameters such that $0.5\pi < \sigma_{xo} < 0.6\pi$ and $0.2\pi < \sigma_{yo} < 0.4\pi$, appear fairly close to these estimates. In all the ILLIAC runs the radial amplitudes were measured, however, near the center of a focusing region, at $N\theta = 0$ (Mod. 2π), where the amplitudes of he non-sinusoidal A-G oscillations can exceed those corresponding to the smooth approximation representation of the motion. By way of example we present here the results for an accelerator for which

$$k = 0.6436 \qquad \frac{1}{\omega} = 20.82 \qquad f = \frac{1}{4} \qquad N = 5 \; :$$

In this case the oscillation frequencies are such that

$$\sigma_{xo} = 0.5388\,\pi \qquad \text{or} \qquad \nu_{xo} = 1.347$$

$$\sigma_{yo} = 0.2855\,\pi \qquad \qquad \nu_{yo} = 0.714$$

and the limiting amplitude for x appeared to be some 0.0075 units to the left of the stable fixed point ($N\theta = 0$, mod. 2π). For these machine parameters the equation for A_1 yields

$$A_1 = \frac{500}{(20.82)^3}\ 1.347\ \left[(1.06)^2 - 1\right]$$

$$= \frac{500 \times 1.347 \times 0.1236}{9025}$$

= .0092, the observed limiting amplitude at $N\theta = 0$ (Mod. 2π) thus being within 20% of this estimate.

With respect to the lapse-rate, we continue this example by consideration of the case A = 0.0225. Then $\sqrt{A^2 - A_1^2} = 0.02035$, and one expects

$$\mu = \frac{0.171\ (20.82)^3 (0.02035)}{625}$$

$$\simeq 0.050 \text{ decades/sector}$$

in close agreement with the value 0.055 decades/sector found from the ILLIAC work.

[For this case the coefficients in the Mathieu equation are a = 1.12, b = 0.604, for which an independent extrapolation of coarse tables extending to a > 1 suggests μ = 0.107 nepers/sector = 0.046 decades/sector.]

LECTURE AT MADISON, WISCONSIN - 20 JUNE 1956

CALCULATIONS CONCERNING PARTICLE MOTION IN SPIRALLY-RIDGED AND SEPARATED-SECTOR FFAG ACCELERATORS

L. Jackson Laslett

MURA

(On leave from Iowa State College)

I. INTRODUCTION

The subject with which I shall be concerned today is the particle motion in a Fixed-Field accelerator of the spirally-ridged type,[1] including computational preparations for examination of the separated-sector variety, but with no reference to acceleration processes.

To define the problem, the starting point in analysis of the spirally-ridged structure is the assumed median-plane field, which we prescribe. In contrast, the separated-sector machine, or even certain slightly-modified spiral sector machines, make the specification of the pole contour more natural. If the pole contour is specified, one has the preliminary problem of determining the fields (or the magnetostatic potential) which they produce, while with the median-plane field prescribed at the start one must find the fields at other points and the location of equipotential surfaces along which the poles may be located.

It may be noted that, perhaps through lack of ingenuity, we have *not* attempted to start with a system of orbits and then endeavored to find a Maxwell field which would give rise to the prescribed orbits. We have, however, always imposed a scaling requirement in a sufficiently strict sense that not only are the number of radial and axial betatron oscillations around the machine independent of particle energy, but the orbits for different energy particles are themselves geometrically similar.

The basic idea in these structures is that the average field around the machine shall vary with radius as r^k, with k sufficiently great as to give an adequately large momentum content, and that stability will be provided by the A-G action which arises from having the field alternatively higher and lower than average along spiral curves which all particles must cross. The most general type of median-plane field which is considered is, then,

$$B_{z_0} = -\langle B\rangle\left(\frac{r}{r_0}\right)^k\left\{1+\sum_{m=1} f_m \sin m\left[\frac{\ln(r/r_0)}{w}-N\phi\right] + g_m \cos m\left[\frac{\ln r/r_0}{w}-N\phi\right]\right\}.$$

Powell[2] has shown how such a field may be developed for points out of the median-plane, to give the various field components, the vector-potential components, or the magnetostatic scalar potential. For these various quantities Powell's development is quite similar in form and is expressed in terms of the dimensionless parameters

$$x = \frac{r-r_1}{r_1} \qquad y = \frac{z}{r_1} \qquad N\theta = N\phi - \ln\left(\frac{r_1}{r_0}\right),$$

where r_1 is chosen so that, for the particle momentum under consideration, x will be small. Then the scalar potential, for example, is written

$$\psi = (1+x)^{k+1}\sum_{i=0}\left\{\tau_i + \sum_{m=1}\nu_{i,m}\sin m\left[\frac{\ln(1+x)}{w}-N\theta\right] + \mu_{i,m}\cos m\left[\frac{\ln(1+x)}{w}-N\theta\right]\right\}\frac{(y/1+x)^{2i+1}}{(2i+1)!}$$

where recursion relations are given by Powell for the coefficients. It is noted that the definition of x is based on use of a cylindrical coordinate system; it may be pointed out that Dr. Akeley has suggested that reference to a system of spherical coordinates may have certain advantages and has written a report on this topic. This series of Powell's has formed the basis of a computer program--the "Potentate"--whereby the height (y) of a specified equipotential (ψ) may be found digitally as a function of θ and x. By a quite similar program--the so-called "MKV Stormesh Leader"--values proportional to

$$\frac{\psi/(1+x)^{k+1}}{y/(1+x)}$$

may be obtained.

II. PROGRAMS FOR COMPUTING TRAJECTORIES[3]

For the computation of trajectories in the spiral ridge accelerator no direct use has been made so far of Powell's expansion, although it has assisted in providing the base for some new programs which may come into use soon. What has already been done computationally has been with two programs which I shall now discuss--

First, the "Ridge Runner", based on exact equations for motion in the median plane, and, second, what was supposed to have been an interim program for combined radial and axial motion, the so-called "Feckless Five". In these two programs the prescribed median plane field is taken to be of the form[4]

$$(1+x)^{k}\left[1 + f\sin\left(\frac{\ln(1+x)}{w} - N\theta\right)\right],$$

no harmonic components being admissible.

1. Ridge Runner[4a]

The differential equations for the Ridge Runner program are written quite readily, since the fields, and hence the forces, may be explicitly formulated immediately. The equations are written as first order equations, in terms of the canonically conjugate variables

$$x \quad \text{and} \quad p_x \equiv \frac{x'}{\sqrt{(1+x)^2 + x'^2}},$$

and are integrated by the Runge-Kutta procedure. Computation takes 0.37 sec/RK, or, with 32 RK/sector, about 12 sec/sector plus punching time.

2. Feckless Five[4b]

For inclusion of axial motion in the computations attention must first be given to the development of the field out of the median-plane.

One wishes, in fact, to obtain the vector potential, in order that the equations of motion (which involve the velocity-dependent $\vec{v} \times \vec{B}$ forces) may be strictly Hamiltonian in character. The systematic development of the vector potential has been treated in reports by Dr. Akeley[5] about a year and a half ago--the process is strictly an infinite one, involving the repeated application of the ∇ operator to vector quantities, and becomes rather elaborate if carried out properly in cylindrical coordinates. In setting up the "Feckless Five" equations this type of development was kept in mind--the view was taken, however, that curvature effects of the sort which distinguish a cylindrical coordinate system from a Cartesian one could be regarded as small corrections which need not be included exactly and that the dominant y-dependence would be given by hyperbolic functions of an argument close to y/w. In this way an approximate vector potential with components A_y and A_z was contrived, from which a set of exactly-Hamiltonian equations was derived with the dependent variables x, y,

$$p_x = \frac{x'}{1+x} \quad , \quad p_y = \frac{y'}{1+x} + \frac{e}{p_1} A_z \ .$$

One supposes that the variables x and y themselves will be small, but that $\frac{x}{w}$ and $\frac{y}{w}$ may be comparable with unity.

This program requires 0.71 sec/RK-step, or, with 32 RK/sector, about 23 sec/sector plus punching time.

The program is to be regarded as an approximate one, whose accuracy is expected to be good for large-scale machines but not as great for models where curvature effects play a more pronounced role.

The Feckless Five program is seen to be substantially half as fast as the Ridge Runner and it would be nice if we had some equivalent transformation which could be used to carry the particle rapidly through sector after sector in studies which require continued computations through a large number of sectors.

3. Overwrites:

Available for use with these programs are various embellishments or "overwrites". Thus the Ridge Runner may be adapted to permit the introduction of an algebraic transformation to simulate passage of a particle through a straight section. The Feckless Five may be supplemented by an overwrite which gives once or twice a sector the square root of the quadratic forms which remain invariant in the linear approximation:

$$K_x = \sqrt{\xi_x (x-x_f)^2 + \eta_x (x-x_f)(p-p_{x_f}) + \zeta_x (p_x-p_{x_f})^2}$$

and K_y similarly.

In addition, as we shall illustrate later, it is possible to introduce various kinds of "bumps" into the Feckless Five program, to simulate certain misalignments.

4. Small Five:[2]

It has been hoped that the Feckless Five will be replaced by the proposed "Small Five" program, in which a more systematic development of the magnetic field would be employed, based on Powell's series, and with which it would be possible to study cases in which a limited number of harmonic components would be present in the field. Programming of the Small Five was begun and then interrupted in the interest of other work considered to be more pressing--it is hoped, however, that work on the Small Five will be recommenced and this program completed.

5. Stormesh:[6]

Since the first of the calendar year it has become increasingly apparent that one is unnecessarily and undesirably restricting oneself by confining attention to fields which in the median-plane are strictly sinusoidal or which are even restricted to a very limited number of harmonics. This recognition was reinforced by the result of some simple field-surveys,[7] made by solving Laplace's two-dimensional equation on a "50 x 50" Cartesian not (49 units x 14 units), and by the increased interest which the separated-sector type of structure appears to warrant. It seemed important therefore to bring into operation a double program, which (i) would commence with the contour of the pole boundary, on which the magnetostatic potential would be considered as given, and solve Laplace's equation for the space between this boundary and the median-plane, and then (ii) would permit investigation of particle trajectories in this potential field. It was felt that mesh-storage would be the most practicable approach and that storage should be confined to the fast-memory of the ILLIAC, when solving the dynamical problems, in the interests of achieving reasonable speed. It was further recognized that considerable simplification would result in the potential problem and a considerable reduction of the subsequent storage requirements if advantage were taken from the start of the scaling property of the field. The desire to economize to the utmost in storage suggested that the computational programs be planned in terms of the scalar potential, despite the impossibility of strictly Hamiltonian equations of motion when using fields derived from a somewhat-in-exact scaler potential.

The scaling character of the field can be seen by reference to Powell's expansion, cited previously. It has evident from this development that $\psi/(1+x)^{k+1}$ has the same value at all points for which both $y/(1+x)$ and $\phi = \frac{\ln(1+x)}{w} - N\theta$ have the same values. Also, with $y/(1+x)$ constant, $\psi/(1+x)^{k+1}$ is periodic in ϕ with period 2π. The potential, with its scaling factor $(1+x)^{k+1}$ is thus conveniently expressed in terms of two independent variables which we take to be

$$\xi \equiv \frac{1}{2\pi}\left[\frac{\ln(1+x)}{\omega} - N\theta\right]$$

$$\eta \equiv \frac{\sqrt{1+(\omega N)^2}}{2\pi\,\omega}\,\frac{y}{1+x}$$

$$\psi = \frac{1}{A}(1+x)^{k+1}\,\Omega\,(\xi,\eta),$$

with Ω periodic in ξ with period unity.

This last equation may be alternatively interpreted (i) as referring $\psi/(1+x)^{k+1}$ to the value at a suitable point in the $\theta = 0$ plane or (ii) relating it to the value at a suitable point in the cylinder x = 0. By virtue of this relationship, Laplace's equation for this scaling field may be reduced to a second order differential equation for Ω with only two independent variables (ξ and η). The magnetic fields, moreover, may be obtained from Ω and hence storage on a two-dimensional net will suffice. For most efficient storage it was felt appropriate to store a quantity proportional to Ω/η , since this quantity will be more nearly constant than Ω itself and a greater number of significant figures would be retained. The field-strengths which enter into the (First-order) differential equations of motion are then to be obtained by First-order differentiation of Ω/η , interpolation and interpolation-differentiation being necessary because these quantities are stored on a net. To insure continuity in the differential equations it was then felt desirable to use an interpolation formula which would exhibit a continuous derivative upon crossing from the region covered by one cell to that covered by an adjacent cell. Such an interpolation Formula, being the only reasonable one of its type extending through u^3 and based on four values of the function, is used <u>throughout</u> in preference to Bessel's more conventional but only slightly-different form.

This formula is:

$$\Lambda(t_0+uh) = u\Lambda_1 + (1-u)\Lambda_0 + \frac{1}{4}u(1-u)(-\Lambda_2+\Lambda_1+\Lambda_0-\Lambda_{-1})$$
$$+ \frac{1}{2}u\left(\frac{1}{2}-u\right)(1-u)(\Lambda_2-3\Lambda_1+3\Lambda_0-\Lambda_{-1}),$$

in contrast to Bessel's form:

$$\Lambda(t_0+uh) = u\Lambda_1 + (1-u)\Lambda_0 + \frac{1}{4}u(1-u)(-\Lambda_2+\Lambda_1+\Lambda_0-\Lambda_{-1})$$
$$+ \frac{1}{6}u\left(\frac{1}{2}-u\right)(1-u)(\Lambda_2-3\Lambda_1+3\Lambda_0-\Lambda_{-1}).$$

The quantity $\Omega/y / \langle \Omega / y \rangle_0$ is stored for each of as many as some 2000 mesh points as 13 binary bits. The differential equations are written in terms of coordinates

$$S = \ln (1+x) \quad \text{and} \quad T = \frac{y}{1+x}$$

to avoid the complications of a logarithm routine in the program, although print-out is performed in terms of the more-familiar variables x, y, px, and py.

The part of this program which seeks a solution to the p.d. equ. for Ω is termed the "SCAPOCYL" and the dynamics portion, the "Stormesh". Trouble-shooting of the first portion and testing of the second is currently in progress. The speed of the Stormesh program has been found to be intermediate between that of the Ridge Runner and that of the Feckless Five.

III. COMPUTATIONAL RESULTS

By use of the Ridge Runner and Feckless Five programs, surveys have been made of the particle motion in spirally-ridged structures. Although the larger portion of this work was with parameters characteristic of models, the general features of the results no doubt apply also to large-scale machines.

1. Radial Motion[8]

The results of computation pertaining to motion with one degree of freedom are appropriately and conveniently represented by means of phase plots, depicting on invariant curves the position and associated momentum of a particle as it progresses through successive "sectors" (periods of the structure) from one homologous point to another. Such studies provide information concerning the location of "fixed-points", corresponding to an equilibrium orbit; the phase-change of the betatron oscillation per sector ( ); the displacement associated with trajectory directions different from that of the equilibrium orbit; and the extent of the region within which stable motion is possible. The characteristics of small-amplitude motion found in this way agree well, for the sinusoidal fields, with the analytic work to be discussed later. At large amplitudes, unstable fixed points--representing an unstable equilibrium orbit--make their appearance. Associated with the unstable fixed-points one finds a separatrix, constituting an effective stability limit, which in the majority of cases the ILLIAC results depict as a sharp boundary and outside of which it is frequently possible to draw the initial portions of what appears to be invariant curves for the unstable motion.

With regard to stability the requirement for a strictly linear system is that the condition

$$0 < \sigma < \pi$$

be satisfied for operation in the first stability zone. Due to the non-linear character of the oscillations in a spirally-ridge FFAG, however, it is not surprising that for such structures the permissible amplitude of oscillation is much curtailed if σ lies near $2\pi/3$ or $2\pi/4$. In fact Dr. Christian at Los Alamos has made computations which show the amplitude limit to be reduced, although not to zero, for $\sigma = 2\pi/5$. If the small-amplitude σ is in the neighborhood of $2\pi/3$, σ will at first change only slowly but then quite near the stability boundary will rapidly approach $2\pi / 3$, and three unstable fixed-points will appear. These correspond to an unstable equilibrium orbit which repeats after progress through three sectors. Similarly, near $2\pi/4$, four unstable fixed-points may be expected to develop. When the machine parameters are such that σ is essentially midway between the values $2\pi/3$ and $2\pi/4$, a comparatively large stable region is found and the apparent limit of stability is defined by a separatrix which may be associated with a larger number of unstable Fixed-points, 7 such points being found in one example. In special cases rather elaborate island-structure is seen to develop within the main stability region. In some cases the phase curves near the stability boundary do not appear well defined and the location of the stability boundary can not be fixed with high precision.

A case with one of the largest radial-amplitude limits for machines with model-like parameters has a σ_x near $4\pi/7$. In this case $k = 0.8$ $\frac{1}{w} = 23.0$ $f = \frac{1}{4}$ $N = 5$, and the "ears" of the phase-plot (at $N\theta = 0$, mod. 2π) extend to $x = \pm 0.09$; similarly for a case currently of considerable interest in connection with freezing the parameters of the Illinois spiral-sector model $k = 0.74$, $1/w = 23.7$, $f = 1/4$, $N = 5$, ($\sigma_{x_0} = 0.563\pi$), and the ears extend beyond $x =$ 0.06. It has been noted that, for reasons which will be suggested later, if F is increased and 1/w concurrently decreased to maintain a similar σ_{y_0} , the amplitude limit may be made substantially greater--for comparison with this last example, the case $k = 0.74$ $\frac{1}{w} = 5.925$ $f = 1$ $N = 5$ (with $\sigma_{x_0} = 0.5896\pi$) led to a material change in the shape of the phase-plot but to a radial amplitude limit some 2.5 times that found in the earlier case. A similar result for the limit of stable axial motion would not be unexpected.

2. Axial Motion:[9]

Introduction of axial motion into a study of spiral-sector accelerators produces complications for all but the smallest-amplitude oscillations, since in general there is coupling between this motion and that occurring in the radial direction. For small-amplitude axial motion one can find the σ_{y_0} and the various matrix elements which characterize linear oscillations. For large-amplitude axial motion one can undertake an experimental survey to determine how large an initial y-amplitude can be tolerated if the motion is to "hold on" (i.e., not exceed the limits of the computer, which are normally given by $y < 3.1w$) for some arbitrary number of sectors (e.g., 80 sectors). By way of example, one finds in this manner for the first of the model-like structures cited earlier ($k = 0.8$ $\frac{1}{w} = 23$ $f = \frac{1}{4}$ $N = 5$) an axial amplitude limit close to y = 0.014; this limit applies to locations such that $N\theta = 0 \pmod{2\pi}$, near the center of an axially defocusing region, and has associated with it amplitude limits which become almost twice as large at intermediate points. As with the radial motion, the limiting amplitude is curtailed if the operating point approaches such "resonant" values as $2\pi/3$. Analysis of such resonances has been given by Moser,[10] Hagedorn,[11] Sturrock,[12] and others.

3. Motion in Two Degrees of Freedom:

With motion in two degrees of freedom one can make searches with a wide variety of initial conditions to determine emperical stability limits. Beyond this, however, it is difficult to proceed systematically. As a result of a suggestion by Sturrock,[13a,b] it was hoped that investigation of motion in two degrees of freedom could be systemitized by use of the quadratic forms K_x^2 and K_y^2, mentioned earlier, which remain invarient on the basis of linear theory. We were led to expect that plots of K_y vs K_x would depict the point which represents a single trajectory moving on a portion of a conic curve and that regions of stability or instability could be distinguished. From a limited number of results obtained to-date, it appears that the expectation is an over-simplification--the values of K_x and K_y scatter sufficiently that a true curve is not defined, the nature of a curve near which the points lie appears sometimes to be elliptical and sometimes hyperbolic, and the regions of stability or instability are not readily apparent. It may be that further work along these lines is merited, however. A possible refinement of this technique would involve the plotting of running averages of K_x and of K_y, averaged over possibly 20 values in the interests of smoothness; in addition, one could consider use of more elaborate algebraic forms,[13a] in place of K_x and K_y themselves, between which simple relationships may be expected to apply.

4. Coupling Resonances:

Evidence of apparent instability appears for operating points in the neighborhood of certain "coupling resonances", notably:

$$\sigma_x = 2\sigma_y$$
$$\sigma_x + 2\sigma_y = 2\pi$$
$$2\sigma_x + 2\sigma_y = 2\pi$$

In such cases one finds a exponential growth of y-amplitude, conveniently represented by semi-logarithmic plot of K_y vs. the number of sectors traversed, which may begin with very small initial y-amplitudes (or even in the "noise" of the computer) and extends over many orders of magnitude. The y-growth appears to be the more rapid the greater the amplitude of the radial motion, above a certain threshold, and the more pronounced the closer one is to the resonance in question. This phenomenon has so far been studied in greatest detail for the $\sigma_x = 2\sigma_y$ resonance. If the initial radial amplitude is not too great, the exponential growth may be seen eventually to terminate rather suddenly (For example, near y = 0.01 or y = 0.02 in some typical cases involving model-like parameters) and to change to an exponential decrease for a time. This decrease may then be followed by an interval characterized by an exponential growth. When one is very close to the $\sigma_x = 2\sigma_y$ resonance, so that the y-growth occurs for even a rather small amplitude of the radial oscillation, it is possible to see from the computed values of K_x and K_y that as the axial amplitude increases there is some decrease of the amplitude of the radial oscillation. Because of the cessation of growth at axial amplitudes not far from those at which violent instability might be expected to occur, it is questionable whether machine operation would be satisfactory under such conditions--in such cases the majority of the particles would be expected to find themselves near the outer limits of the beam from time-to-time and misalignments may be expected to reap a heavy toll in such cases. These matters are being further explored computationally at the present time and theoretical progress has been made with respect to those aspects of the phenomena which concern the initial exponential growth.

5. Studies of Misalignments:

Some computational investigations of the effects of various "bumps" have been made before making a final commitment concerning the parameters of the Illinois spiral sector model. The results obtained will be reported in a factual way, little theory being available for organization of the results, and the work will be seen to represent no more than a coarse survey of the effects which certain misalignments can cause in a specific case. The slowness of such computational work is a real handicap, which arises in part from the misalignments being a property of the machine-as-a-whole and the consequent necessity of going through a number of sectors to traverse one period of the perturbed structure. It may, moreover, be noted that, as Symon and Christian have emphasized, certain types of bumps may excite certain potentially dangerous resonances only indirectly; hence, unless a suitable, and perhaps unrealistic, perturbation is selected, a resultant instability may develop so slowly as to pass unnoticed in a run of reasonable duration. It would be of considerable convenience in such work to have at hand the most general transformation required to represent the effects of harmful misalignments and a knowledge of the manner in which the parameters of such transformation are related to the magnitudes of the constructional misalignments which the transformation represents.

The work reported here pertained primarily to an operating point chosen to be clear of the $\sigma_x = 2\sigma_y$ resonance, to lie between $\sigma_x = 2\pi/4$ (For which $\nu_x = 5/4$) and the half-integer resonance $\nu_x = 3/2$ and to fall below $\nu_y = 1$. The nearby inherent resonance $3\sigma_x + \sigma_y = 2\pi$ had not been found harmful in a machine free of imperfections. The nearest other imperfection resonances, aside from difference resonances, were those for which $3\nu_y + \nu_x = 4$ and $3\nu_x = 4$. The parameters of the machine selected for most of the studies (denoted "d") were:

$$k = 0.74 \qquad \frac{1}{\omega} = 23.7 \qquad f = \frac{1}{4} \qquad N = 5$$

for which $\nu_x = 1.408$ and $\nu_y = 0.873$.

In studying certain bumps, neighboring operating points were also included. The computations were performed by aid of various overwrites, applicable to the Feckless Five master program.

Results

(i) Bumps Absent:

In the absence of bumps, radial motion was stable in machine "d" for an x-displacement $\left\{ \begin{matrix} -.033 \\ +.040 \end{matrix} \right.$ from the stable fixed point, and the ears of the phase plot extended beyond $\pm$ .06. Similarly an initial y-displacement of $\pm$ .011 appeared to be stable. These displacements refer to points for which $N\theta = 0$, Mod. 2π.

(ii) Momentum Bumps:

As a first attempt at the introduction of bumps, the combination was introduced once a revolution. The permissible amplitude of the radial phase plot appeared to be reduced by a factor of about 2.

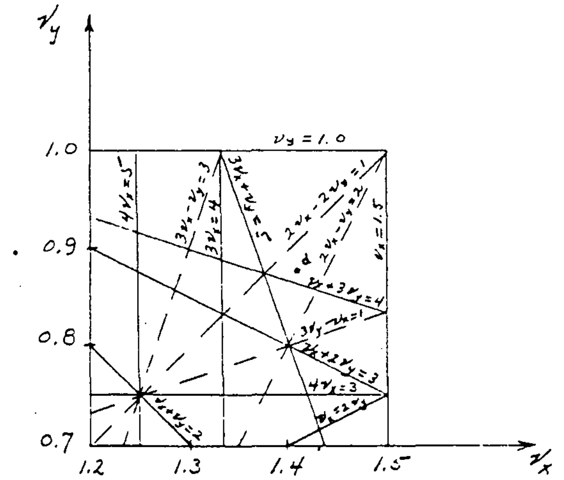

RESONANCES IN NEIGHBORHOOD OF "d".

RESONANCES IN NEIGHBORHOOD OF "d".

(iii) Coordinate-Dependent Momentum Bumps:

In this series of runs a few different combinations of momentum bumps (Δp_x , Δp_y) were abruptly introduced into the computations once every 5 sectors--i.e., once per revolution. In one case the combination

$$\Delta p_x = -.005 - .2x - 2x^2 - 10x^3$$

$$\Delta p_y = + .0005 - .2y \quad ,$$

For which the Jacobian of the transformation is unity, was employed. In this case the stable region of the radial phase plot was very materially reduced, each dimension of the plot being reduced by a factor estimated as close to 3. With the signs of the x-dependent terms reversed, the decrease of each dimension was similarly by a factor close to two.

(iv) Radically-Displaced Sector:

In this series a displacement, Δx , was introduced for an interval $2\pi/N$ to simulate a radially-displaced sector. Various phases for introduction of the bump were investigated, as well as various magnitudes of Δx . In this case a reduction of the stable region, of the radial phase plot, by a factor of 2 seemed to result from a displacement, Δx , lying between 0.0021 and 0.0063. Thus, with the smaller bump, motion with an initial x lying .0250 to the left of the fixed point was stable regardless of the phase of the bump while motion with an initial x lying .0375 to the left was stable in none of the cases studied; with the larger bump, an initial x lying .0250 to the left of the fixed point led to instability in most cases.

(v) Axially-Displaced Sector:

With an axially-displaced sector there resulted a very noticeable increase in the frequency of axial betatron oscillations, an increase which varied predominantly as the square of the sector displacement Δy . Because of the proximity of the integer resonance $\nu_y = 1$, it was felt appropriate to suppose that in actual practice suitable tuning controls would be employed to restore the operating point to its desired location despite the presence of unavoidable misalignments. For this reason the work to be reported here is concerned with a structure (denoted "e") for which

$$k = 0.7464 \qquad \frac{1}{w} = 23.252 \qquad f = \frac{1}{4} \qquad N = 5 \;;$$

in the absence of any sector-displacement

$$\nu_x = 1.405 \qquad \nu_y = 0.834$$

but with a displacement $|\Delta y| = .00350$ for one sector

$$\nu_y = 0.8747 \; .$$

The axially displaced sector, $\Delta y = -.00350$, was found to effect a reduction of the stable x-amplitude by a factor of 2 and the y-amplitude by a factor of 3.

(vi) Tilted Sector:

In this series a tilted sector was simulated by introducing, once per revolution, two bumps, $(\Delta y_1, \Delta p_{y_1})$ and $(\Delta y_2, \Delta p_{y_2})$, at points one sector apart. Specifically, $\Delta y_1 = \Delta y_2$, $\Delta p_{y_1} = -\frac{5}{\pi}\Delta y_1$, $\Delta p_{y_2} = +\frac{5}{\pi}\Delta y_1$. A reduction of the stable amplitudes of radial and axial motion by a factor of nearly 2 was found to occur when $\Delta y_1 = -.00350$.

(vii) Parameter-Shift:

In this series the parameter $1/w$ was changed for an interval corresponding to one sector and a concurrent change was made in f in an effort to allow for the increased spatial modulation of the field which would be expected to result if the ridges of a spiral sector accelerator were separated. Work has been confined to the case in which one sector of accelerator "d" was modified as follows:

Unperturbed Sectors: $1/w = 23.7$, $f = 0.25$;

Perturbed Sectors: $1/w_s = 23.07423$, $f_s = 0.2533996$.

In this case little reduction of the stable region appeared to result, although a radial phase plot of a nearly-limiting amplitude run appeared to be a bit more ragged than for the unperturbed case.

In summary, it is seen that displacements which correspond to about 1 mm, when $r_1 = 300$ mm, under a number of circumstances can cause a serious reduction of the stability region.

IV. ANALYTIC WORK PERTAINING TO UNPERTURBED STRUCTURES

1. The Equilibrium Orbit:

One of the distinctive features of the spirally-ridged accelerator is that the equilibrium orbit is not circular.[4] If one expands the equations which govern the motion in the median plane about a reference circle, a forcing term makes its appearance and leads to a scalloped equilibrium orbit. The departure from a circle is, in fact, close to a sinusoid, given by[4]

$$x_f \doteq \frac{f}{N^2 - (k+1)} \sin N\theta$$

and has been determined with greater accuracy by Judd[14] and by Cole.[15]

2. The Small-Amplitude Betatron Oscillations:

The character of small-amplitude betatron oscillations must be obtained by expansion of the equations of motion about the equilibrium orbit and leads to frequencies materially different[4,16] from those which would be obtained by ignoring the effect of the forcing term. Qualitatively this is to be expected, since the field gradient is in a sense to favor radial focusing over a smaller interval of 0 if one examines the gradient in the neighborhood of the scalloped orbit instead of along a circular path.

We will not undertake here to discuss development of the equations for betatron oscillations on the basis of Symon's unified theory of FFAG machines,[17] but shall outline a more specific approach developed with increasing degrees of completeness by myself,[4] by Judd,[14,18] and by Cole.[15] From the prescribed median plane field, vector potential components are developed and employed in a space-like Lagrangian from which, by the principle of least action, the differential equations for the trajectories may be derived directly:[19]

$$\begin{aligned}\mathcal{L}(x,y;x',y';\theta) &= p\, ds/dO + e\,\bar{A} \cdot \bar{ds}/d\theta \\ &= p r_1 \sqrt{(1+x)^2 + x'^2 + y'^2} \\ &\qquad + e r_1 \left[(1+x)A_\theta + x'A_r + y'A_z\right] .\end{aligned}$$

A change of variable is then made ($u \equiv x - x_f$) to modify the Lagrangian so as to eliminate the forced motion, and the differential equations which result from the modified Lagrangian are then taken as the equations governing the betatron oscillations. In this way the coefficients of the linearized equations, applying to small-amplitude motion, are obtained and the major non-linear terms also may be noted.

The linear equations are of the Hill form and, if relatively small terms are ignored, are substantially of the form

$$u'' + (a_x + b_x \cos N\theta + c_x \cos 2N\theta)u = 0 ,$$

and similarly for the y-equation. For orientation, it is helpful to note the frequencies which the smooth approximation[20] gives for the solutions to these equations. Ignoring the relatively small contribution from the term involving $c \cos 2N\theta$, one obtains

$$\nu_x^2 \cong a_x + \frac{1}{2}\frac{b_x^2}{N^2}$$

$$\doteq \left[(k+1) - \frac{1}{2}\frac{(f/w)^2}{N^2-(k+1)}\right] + \frac{1}{2}\frac{(f/w)^2}{N^2}$$

$$\doteq k+1$$

$$\nu_y^2 \cong \left[-k + \frac{1}{2}\frac{(f/w)^2}{N^2-(k+1)}\right] + \frac{1}{2}\frac{(f/w)^2}{N^2}$$

$$\doteq -k + \left(\frac{f}{wN}\right)^2 .$$

It is thus seen that the frequency of the free radial oscillations is substantially determined by the exponent k characterizing the radial increase of average field strength, so that $k = 1$ must be positive, and that axial stability may simultaneously be obtained if the enhanced A-G term, $(f/wN)^2$, is sufficiently large to dominate $-k$.

More exact information concerning the solutions of the Hill equation, with the term $c \cos 2N\theta$ retained, may be obtained by use of tables pertaining to this equation and which were calculated by aid of the ILLIAC digital computer. The first set of tables was prepared by a variational method which is believed to be quite accurate at the stability limits, $\sigma = 0$ or π, and also for the smaller values of σ in general. The most satisfactory form in which to use these results is by recourse to the graphs which accompany the tables. A second set of finer-mesh tables has been subsequently prepared for the Hill equation by direct integration of the differential equation. These tables, which have been duplicated and are about to be distributed, give $\cos\sigma$, σ/π, and selected values of a quantity $\left(\frac{\sin\sigma}{\phi'}\right)$ proportional to the square of the amplitude function and from which the Floquet solutions in the phase-amplitude form can be obtained. In each of these tables an independent variable is used such that the argument of the cosine functions is 2t, and multiples thereof.

By use of the foregoing theory, and by aid of the available tables or graphs, the first stability region may be plotted in terms of machine parameters. The basic variables, when $k \gg 1$, are k/N^2 and $f/(wN^2)$. The result of direct integration of the equations of motion, by use of the Ridge Runner or Feckless Five programs, yield results which for small-amplitude motion are consistent with the predictions of the analytic theory.

3. The Limiting Stable Amplitudes:

(i) The stability-limit for radial oscillations:

In a large fraction of cases the limit of stability for the radial motion is characterized by the appearance of three fixed points. For such cases a convenient approximate formula may be developed by recourse to a differential equation in which the important non-linear term is taken from Cole's report:[15]

$$u'' + (a + b \cos N\theta)u = \frac{f}{2w^2}(\sin N\theta)\, u^2 .$$

One may attempt the solution of this equation by substitution of the trial solution $u = A \sin(N\theta/3)$ and application of harmonic balance. One may alternatively replace the differential equation by an equivalent variational statement and then employ the same type of trial solution as before. Finally one may employ a variational procedure of the type outlined by Sturrock.[13] These various methods appear to agree in giving for the limiting amplitude the expression

$$|A| \cong 8(w^2/f)\left|\nu_x^{\,2} - \frac{N^2}{9}\right| = 2(w^2N^2/f)\left|(\sigma_x/\pi)^2 - (2/3)^2\right|$$

$$\doteq (8/3)(w^2N^2/f)\left|\frac{\sigma_x}{\pi} - \frac{2}{3}\right| .$$

It is noted that the character of the trial function taken in this work was extremely simple; the formula appears, however, to give estimates in good accord with the Ridge Runner stability limits in both model-like and full-scale machines for which the nearest resonance is that for which $\sigma_x = 2\pi/3$. It may be noted that, since the betatron frequencies are essentially determined by k/N^2 and $f/(wN^2)$, a desirable increase of stable amplitude might be expected if f and w were each increased by the same factor. Dr. Sessler has extended this formula in an attempt to take account of fields containing higher-order Fourier components.

(ii) The Stability Limit for Axial Oscillations:

In considering the stability limit for axial motion, it has been pointed out that larger amplitudes of axial oscillation cause the particle to sample fields of a necessarily greater flutter-factor. The flutter-factor of a simple sinusoidal variation increases approximately by the factor $\cosh(y/w)$ for points out of the median plane. The suggestion has then been advanced that the effect of this increased flutter in the field is to "tune" the oscillation frequency towards the next higher resonance and that instability will result when this resonant value is reached. On the basis of this simple, and perhaps not entirely true, idea, one may proceed to write

$$\nu_y^2 = \frac{f^2}{N^2 w^2} - k$$

$$\Delta\nu_y = \frac{f\,\Delta f}{\nu_y\, N^2 w^2} .$$

With $f = f_o \operatorname{Cosh}\frac{\langle y\rangle_{eff}}{w}$,

$$\Delta f \doteq \frac{f\langle y^2\rangle}{2\, w^2} ,$$

and $\Delta\nu_y = \dfrac{f^2\,\langle y^2\rangle}{2\,\nu_y N^2\, w^4}$.

If we write $\langle y^2\rangle = A^2/2$ and consider σ_y to be below but fairly close to the value $2\pi/3$,

$$A^2 \doteq \frac{4\nu_y\, N^2\, w^4}{f^2}\left[\frac{N}{3} - \nu_y\right]$$

$$\doteq \frac{2\nu_y\, N^3\, w^4}{f^2}\left[\frac{2}{3} - \frac{\sigma_y}{\pi}\right] .$$

Since ν_y is presumed close to N/3 (i.e., σ_y close to $2\pi/3$), this result may be expressed in the simpler form

$$A \simeq \sqrt{\frac{2}{3}}\,\frac{N^2 w^2}{f}\sqrt{\frac{2}{3} - \frac{\sigma_y}{\pi}}$$

$$\simeq 0.8\,\frac{N^2 w^2}{f}\sqrt{\frac{2}{3} - \frac{\sigma_y}{\pi}} .$$

Comparison of this equation with Feckless Five results suggests that the formula may over-estimate the permissible amplitude but that within a factor of about 4 it gives a correct estimate in a variety of cases. Again, the desirability of increasing f and w together by the same factor is suggested. Sessler has undertaken to extend this formula, by the same type of reasoning, to cases in which higher-order Fourier components are present in the field.

4. y-Growth:

We shall discuss here analytical work relevant to the exponential growth of axial amplitude observed in the neighborhood of certain resonances, with particular emphasis on the $\;_x = 2\;_y$ resonance.

(i) Walkinshaw's approach:

In a recent memorandum, Walkinshaw[21] has pointed out that the differential equation for axial motion, although properly treated as linear in y for small amplitudes, contains a coefficient which involves the radial motion. Just as the forced radial motion is known, as we have seen, to affect the axial focusing, so the presence of an appreciable amplitude of radial oscillation may be expected to affect the axial motion under suitable circumstances. The view is taken that the superposition of the comparatively-long-wavelength radial oscillations on the forced motion in effect modulates the smooth-approximation coefficient in the axial equation, to yield a Mathieu equation with a coefficient having the period of the radial motion. Under "resonant" conditions, which appear to include the case $\sigma_x = 2\sigma_y$, the equation may have unstable solutions.

Walkinshaw commences with the basic differential equations (in our notation):

$$x'' + (k + 1)x = -f \sin\left(\frac{x}{w} - N\theta\right) ,$$

$$y'' + \left[-k - \frac{f}{w}\cos\left(\frac{x}{w} - N\theta\right)\right] y = 0 .$$

A solution for the radial motion, representing a free oscillation of amplitude A superimposed on the forced motion, is taken of the form:

$$x = x_\beta + x_f ,$$

with $x_\beta = A \sin(\nu_x\theta + \alpha)$,

$$x_f = -(f/N^2)\left(1 - \frac{x_\beta'}{w} N\right)^{-2} \sin\left(N\theta - \frac{x_\beta}{W}\right) ,$$

and $\nu_x = \sqrt{k + 1} \ll N.$

This solution is then introduced into the axial equation and, after some approximation, gives

$$y'' + \left[-k + \frac{1}{2}\frac{f^2}{w^2N^2}\left(1 - \frac{x_\beta'}{wN}\right)^{-2} - \frac{f}{w}\cos\left(N\theta - \frac{x_\beta}{w}\right)\right] y = 0 .$$

At this point the attempt is made to eliminate the cosine term by application of the "smooth approximation", in effect replacing the N which usually appears by $N - x_\beta'/w$:

$$y'' + \left[-k + \frac{f^2}{w^2N^2}\left(1 - \frac{x_\beta'}{wN}\right)^{-2}\right] y = 0 ,$$

or $$y'' + \left[-k + \frac{f^2}{w^2N^2} + \frac{2f^2\, x_\beta'}{w^3N^3}\right] y = 0 .$$

It is noted that the terms within the square bracket and which do not contain x_β' are just those which normally give $\nu_{y_o}^2$ by the smooth approximation. Hence, with this substitution and replacement of x_β' by $A\nu_x\cos(\nu_x\theta + \alpha)$, one obtains

$$y'' + \left[\nu_{y_o}^2 + \frac{2A\, f^2 \nu_x}{w^3N^3}\cos(\nu_x\theta + \alpha)\right] y = 0 .$$

This Mathieu equation may be put into standard form by the change of independent variable

$$\nu_x\,\theta + \alpha = 2\tau ,$$

to obtain

$$\frac{d^2y}{d\tau^2} + \left[(2\,\nu_{y_o}/\nu_x)^2 + \frac{8A\, f^2}{w^3N^3\nu_x}\cos 2\tau\right] y = 0 ,$$

with a coefficient whose period is π in the independent variable τ. Such a Mathieu equation will exhibit instability when the constant term in the coefficient is equal or close to the square of an integer -- in particular, there is a fairly broad band of instability near

$$(2\nu_{y_o}/\nu_x)^2 = 1 ,$$

corresponding to $\nu_x = 2\nu_{y_o}$. This instability will be expected to extend over a wider range of values of ν_{y_o} the greater is A, the amplitude of the radial betatron oscillation; similarly, for a fixed value of $2\nu_{y_o}/\nu_x$ and within the unstable zone, the lapse rate characterizing the growth of the axial amplitude will be the greater the larger the radial oscillations. The predictions of this theory, both with respect to the threshold at which instability sets in and with respect to the lapse rate in the unstable region, appear to be in good accord with the results of the ILLIAC computations.

(ii) An Alternative Approach:

Despite the success of Walkinshaw's ingenious and successful account of the $\sigma_x = 2\sigma_y$ resonance, it was felt that the method involved some uncertainties, especially in the first application of the "smooth approximation", which were difficult to rationalize. It was thought desirable to develop an alternative, and perhaps more general, method which would be applicable to other resonances and which would be based in a straight forward way on the differential equations developed by Cole.[15]

If we regard the amplitude of the betatron oscillations themselves, taken with respect to the closed equilibrium orbit, as small, they may be supposed adequately represented by the linear differential equation

$$u'' + \left[a_x + b_x \cos N\theta\right] u = 0 \quad ,$$

with

$$a_x = k + 1 - \frac{f^2}{2w^2\left[N^2 - (k+1)\right]} \simeq k + 1 - \frac{f^2}{2w^2N^2} \quad \text{and}$$

$$b_x = f/w \quad .$$

A suitable solution to this equation may be sought conveniently by a variational method in a variety of ways. A method which we shall employ again imagines that the frequency of the oscillation and the basic frequency of the structure are commensurate in a sufficiently large interval and, hence, that the solution may be regarded as "periodic" in such an interval. Such a periodic solution might normally be thought to correspond to a stability boundary, but in the present instance we find that there are two periodic solutions and the zone of instability which one might imagine to be present is of zero width.

We write, then, the variational statement

$$\delta \int \frac{1}{2}\left[u'^2 - (a_x + b_x \cos N\theta)\, u^2\right] d\theta = 0$$

as equivalent to the differential equation.

A trial solution of the form

$$u = A \cos \nu\theta + B \cos(\nu + N)\theta + C \cos(\nu - N)\theta$$

may be introduced into the integral, the integration performed, and the resultant algebraic expression adjusted to be stationary by proper selection of the frequency ν and proper proportioning of the coefficients A, B, C. One finds in this way

$$\nu^2 \cong a_x - \frac{b_x^2}{2N^2}$$

$$B \cong \frac{b_x}{2N^2}(1 - 2\nu/N)\,A$$

$$C \cong \frac{b_x}{2N^2}(1 + 2\nu/N)\,A.$$

Thus the value found for ν in this approximation is concordant with the result of the smooth approximation and we have the approximate solution for u:

$$u = A\left[\cos\nu\theta + \frac{b_x}{2N^2}(1 - 2\nu/N)\cos(\nu + N)\theta + \frac{b_x}{2N^2}(1+\frac{2\nu}{N})\cos(\nu - N)\theta\right]$$

$$= A\left[\cos\nu\theta + \frac{b_x}{N^2}\cos\nu\theta\cos N\theta + \frac{2b_x\nu}{N^3}\sin\nu\theta\sin N\theta\right].$$

Likewise, if a trial function employing sine functions had been employed, a similar result would have been obtained:

$$u = A\left[\sin\nu\theta + \frac{b_x}{N^2}\sin\nu\theta\cos N\theta - \frac{2b_x\nu}{N^3}\cos\nu\theta\sin N\theta\right].$$

We accordingly take the general solution to be:

$$u = A\left[\sin(\nu_x\theta + \epsilon) + \frac{b_x}{N^2}\sin(\nu_x\theta + \epsilon)\cos N\theta - \frac{2b_x\nu_x}{N^3}\cos(\nu_x\theta + \epsilon)\sin N\theta\right]$$

$$= A\left[\sin(\nu_x\theta + \epsilon) + \frac{f}{wN^2}\sin(\nu_x\theta + \epsilon)\cos N\theta - \frac{2f\nu_x}{wN^3}\cos(\nu_x\theta + \epsilon)\sin N\theta\right].$$

The complete radial motion is $x = -\frac{f}{N^2}\sin N\theta + u$ and is found to agree with Walkinshaw's form when the latter is expanded.

For study of the y-motion near the $\sigma_x = 2\sigma_y$ resonance we again refer to Cole's report[15] to write the linear equation in y:

$$y'' + \left[a_y + b_y\cos N\theta - b_5 u\right]y = 0,$$

where

$$a_y = -k + \frac{f^2}{2w^2\left[N^2 - (k+1)\right]} \cong -k + \frac{f^2}{2w^2N^2} ,$$

$$b_y = - f/w ,$$

and

$$b_5 \cong (f/w^2) \sin N\theta .$$

to sufficient accuracy for the present purpose.

We then substitute our solution u into this equation, ignoring terms in $2N\theta$ and dropping the phase-shift ϵ as a matter of convenience, to obtain

$$y'' + \left[a_y + b_y \cos N\theta - \frac{Af}{w^2} \sin N\theta \sin \nu_x\theta + \frac{Af^2\nu_x}{w^3 N^3} \cos \nu_x\theta\right] y = 0 .$$

This equation is of the form

$$y'' + \left[a_y + b_y \cos N\theta + \tfrac{1}{2}c_y \cos(N - \nu_x)\theta - \tfrac{1}{2}c_y \cos(N + \nu_x)\theta + d_y \cos \nu_x\theta\right] y = 0 ,$$

with a_y and b_y as before,

with $c_y = - Af/w^2$, and

with $d_y = + Af^2\nu_x/(w^3N^3)$.

The equation may be case in the form of a variational statement and stability boundaries sought by the use of trial functions

$$y_1 = B \cos \frac{\nu_x}{2} + P_1 \cos \frac{2N-\nu_x}{2} \theta + P_2 \cos \frac{2N+\nu_x}{2} \theta ,$$

$$y_2 = C \sin \frac{\nu_x}{2} + Q_1 \sin \frac{2N-\nu_x}{2} \theta + Q_2 \sin \frac{2N+\nu_x}{2} \theta .$$

One finds in this way that the stability boundaries in the neighborhood of $\nu_x = 2\nu_{y_o}$ (where $\nu_{y_o}^2 \cong a_y + b_y^2/(2N^2)$ corresponds to solutions of the y-equation when $A = 0$) are given by

$$\left| \nu_x^2 - (2\nu_{y_o})^2 \right| = 2\left| \frac{\nu_x b_y c_y}{N^3} + d_y \right|$$

$$= 4\frac{\nu_x f^2}{w^3 N^3} \left| A \right| .$$

This result is in agreement with the location of the stability boundaries of the "equivalent" Mathieu equation originally suggested by Walkinshaw.

Continuation of the analysis of our equation, along lines indicated for the Mathieu equation by McLachlan,[22] moreover leads to lapse rates in the unstable zone which agree with the values implied by Walkinshaw's equation and which appear to be in reasonable accord with the ILLIAC results.

(iii) Other Resonances:

We have applied our methods to the examination of other resonances where y-growth may occur. It appears possible in this way to account for the behavior at the resonance $\sigma_x + 2\sigma_y = 2\pi$ and at $2\sigma_x + 2\sigma_y = 2\pi$. In this latter case one should consider not only the term $\frac{1}{2}c_{10}\, u^2 y$ in the y-equation but also the double frequency ($2\nu_x$) terms which can enter the term $b_5 uy$ by use of supplementary terms in u obtained by a perturbation solution of the non-linear u-equation. It appears, however, that the direct contribution from $\frac{1}{2}c_{10}\, u^2 y$ definitely dominates.

In the neighborhood of the possible $\sigma_x = \sigma_y$ resonance, the ILLIAC results have revealed no y-growth. Our analysis, differing in detail from Walkinshaw's, indicates that instability leading to y-growth would occur over a quite restricted range of radial amplitudes and that the lapse rate within this narrow zone of instability would be so small as to be far beneath notice.

V. REFERENCES

1. D. W. Kerst, et al., Bull. Amer. Phys. Sec. 30, #1, Paper D 5, (January 27, 1955).

2. J. L. Powell, MURA Report MURA-JLP-6 (August 16, 1955).

3. Details concerning the use of these programs are given in a MURA Report by J. N. Snyder, "The MURA Program For Illiac".

4. L. J. Laslett, MURA Report LJL(MURA)-5 (July 30, 1955).

a) Appendix I

b) Appendix II

5. E. S. Akeley, MURA Report ESA(MURA-1), (January 26, 1955).

6. L. J. Laslett, MURA Report MURA-LJL-8, Revised (February 21, 1956).

7. L. J. Laslett, MURA Report MURA-LJL-9 (in press).

8. F. T. Cole, L. J. Laslett, and J. N. Snyder, Bull. Amer. Phys. Soc., Sec. II, #1, Paper U 8, (January 30, 1956).

9. F. T. Cole, L. J. Laslett, and J. N. Snyder, Bull. Amer. Phys. Soc., Sec. II, #4, Paper G 5 (April 26, 1956).

10. J. Meser, Nachr. Akad, Wiss. Gottingen, Math-Physik Kd. II-a, #6, 87 (1955); Communications on Pure and Applied Mathematics, vd. VIII, 409-436 (1955).

11. R. Hagedorn, CERN Report, CERN-PS/RH 9 (November 1955).

12. P. A. Sturrock, States and Dynamic Electron Optics, Cambridge University Press (1955), Chapter 7.

13. P. A. Sturrock, (a) A.E.R.E. Harwell, Report X/R 1771;
(b) Urbana Lectures (November 30, 1955).

14. D. L. Judd, MURA Report MURA DLJ-1 Internal (August 10, 1955).

15. F. T. Cole, MURA Report MURA/FTC-3 (January 19, 1956).

16. L. J. Laslett, Bull. Amer. Phys. Soc. 30, #3, Paper T8 (April 30, 1955).

17. K. R. Symon, et al., "Fixed Field Alternating Gradient Particle Accelerations" (Submitted for publication).

18. D. L. Judd, MURA Reporting MURA DLJ-2 Internal (August 12, 1955).

19. L. J. Laslett, LJL(MAC)-4 (March-April, 1954), eq. (2).

20. K. R. Symon, MURA Reports KRS(MURA)-1, -4 (July 1 and August 10, 1954).

21. W. Walkinshaw, "A Spiral Ridged Bevatron", A.E.R.E., Harwell (1956).

22. N. W. McLachlan, "Theory and Application of Mathieu Functions", Clarendon Press, Oxford (1947), Sect. 4.90 - 4.91.

Internal Report
MURA-LJL-Int.-11

AXIAL-AMPLITUDE LIMITATIONS EFFECTED BY $\sigma_x + 2\sigma_y = 2\pi$

L. Jackson Laslett*
Midwestern Universities Research Association†
Madison 5, Wisconsin
11 September 1956

ABSTRACT

Evidence, based on Feckless Five computations, is presented appearing to support Parzen's suggestion that the $\sigma_x + 2\sigma_y = 2\pi$ resonance, rather than $\sigma_y = 2\pi/3$, is responsible for the limit of stable y-amplitude in spirally-ridged accelerations free of imperfections. The computations covered a small number of structures with $k = 0.2$, $f = 1/4$, and $N = 5$, for which σ_x was in the neighborhood of $\pi/2$.

1. Introduction:

The question has been raised by Parzen (Madison summer session) whether the stable limit of y-amplitude observed[1] in Feckless Five[2] runs with σ_x near 0.6π is attributable to the $\sigma_x + 2\sigma_y = 2\pi$ resonance rather than to $\sigma_y = 2\pi/3$. Because of the importance of this question in connection with the design of spirally-ridged (or separated-sector) FFAG accelerators,[3] a quick computational examination was made to distinquish between the two possibilities. The computations were performed by aid of the Feckless Five ILLIAC Program. The results of this study are summarized below and, although unfortunately carried out with σ_x undesirably close to $\pi/2$, appear to substantiate Parzen's proposition.

- - - - - - - - - - -

*On leave from Iowa State College.

†Assisted by the National Science Foundation, the Office of Naval Research, and the Atomic Energy Commission

2. Results:

The parameters and characteristics of the structures studied are summarized in Table I. The results of 80-sector searches for the axial stability limit are also included in the table. In all cases the x-motion was started substantially on the fixed point. Figures 1 and 2 depict the y-stability limit, expressed in terms of the initial value y(0) with $y^1(0) = 0$, as a function of $1/w$ and of σ_{y_0}/π.

3. Conclusion:

The results of this brief survey appear to substantiate Parzen's suggestion that the $\sigma_x + 2\sigma_y = 2\pi$ resonance, rather than $\sigma_y = 2\pi/3$, is responsible for the limitation of stable axial motion in this region of the working diagram for a structure free of misalignments. It is expected that this matter will receive further study. It may be of interest to mention in closing that it has been conjectured that generally, in structures free os misalignments, resonances of the form

$$p\,\sigma_x + q\,\sigma_y = r(2\pi) \qquad (p,q,r = \text{integers})$$

are significant only if q is <u>even</u>.

4. References:

1. F. T. Cole, L. J. Laslett, and J. N. Snyder, Bull. Amer. Phys. Soc., Ser. II, #4, Paper G5 (April 26, 1956).

2. L. J. Laslett, MURA Report LJL(MURA)-5 (July 30, 1955), Appendix II.

3a. D. W. Kerst, et al., Bull. Amer. Phys. Soc. 30, #1, Paper D5 (January 27, 1955).

b. K. R. Symon, et al., "Fixed Field Alternating Gradient Particle Accelerators" (to be published in The Physical Review).

c. Pop. Mech. 106, #1, P. 94 (July 1956).

TABLE I

EXAMINATION OF 80-SECTOR AXIAL STABILITY LIMIT
IN THE NEIGHBORHOOD OF $\sigma_y = 2\pi/3$ AND $\sigma_x + 2\sigma_y = 2\pi$

$k = 0.2$ $\quad f = 1/4$ $\quad N = 5$									
	Small-Ampl. Freqs.			Last Unstable Run	First Stable Run				
$1/\omega$	σ_{x_0}/π	σ_{y_0}/π	$\sigma_{x_0}/\pi + 2\sigma_{y_0}/\pi$	Initial y_0	Initial y_0	Max. $\lvert y \rvert$ $N\theta = 0 \bmod 2\pi$	Max. $\lvert y \rvert$ $N\theta = \pi \bmod 2\pi$	x_f	p_{x_f}
29.69	0.4782	0.626	1.730	0.00530	0.00460	0.0055648	0.0126041	-.002400	-.054863
30.49	0.4809	0.650	1.781	0.00460	0.00400	0.0052565	0.0126207	-.002409	-.054863
31.00	0.4811	0.666	1.812	0.00348	0.00300	0.0035865	0.0089536	-.002415	-.054905
31.5243	0.4830	0.682	1.847	0.00264	0.00230	0.0028005	0.0073961	-.002421	-.054921
32.2167	0.4851	0.702	1.889	0.00174	0.00150	0.0018110	0.0052916	$-.002428_5$	-.054940
32.9091	0.4871	0.729	1.945	0.00087	0.00075	0.0009169	0.0029405	-.002432	-.054958
33.5555	0.4891	0.753	1.995	($\cong 0.00037_5$)		----	----	-.002443	-.054973
34.7676	0.4930	0.805	2.103	0.00150	0.00132	0.0016944	0.0077997	-.002560	$-.054998_5$

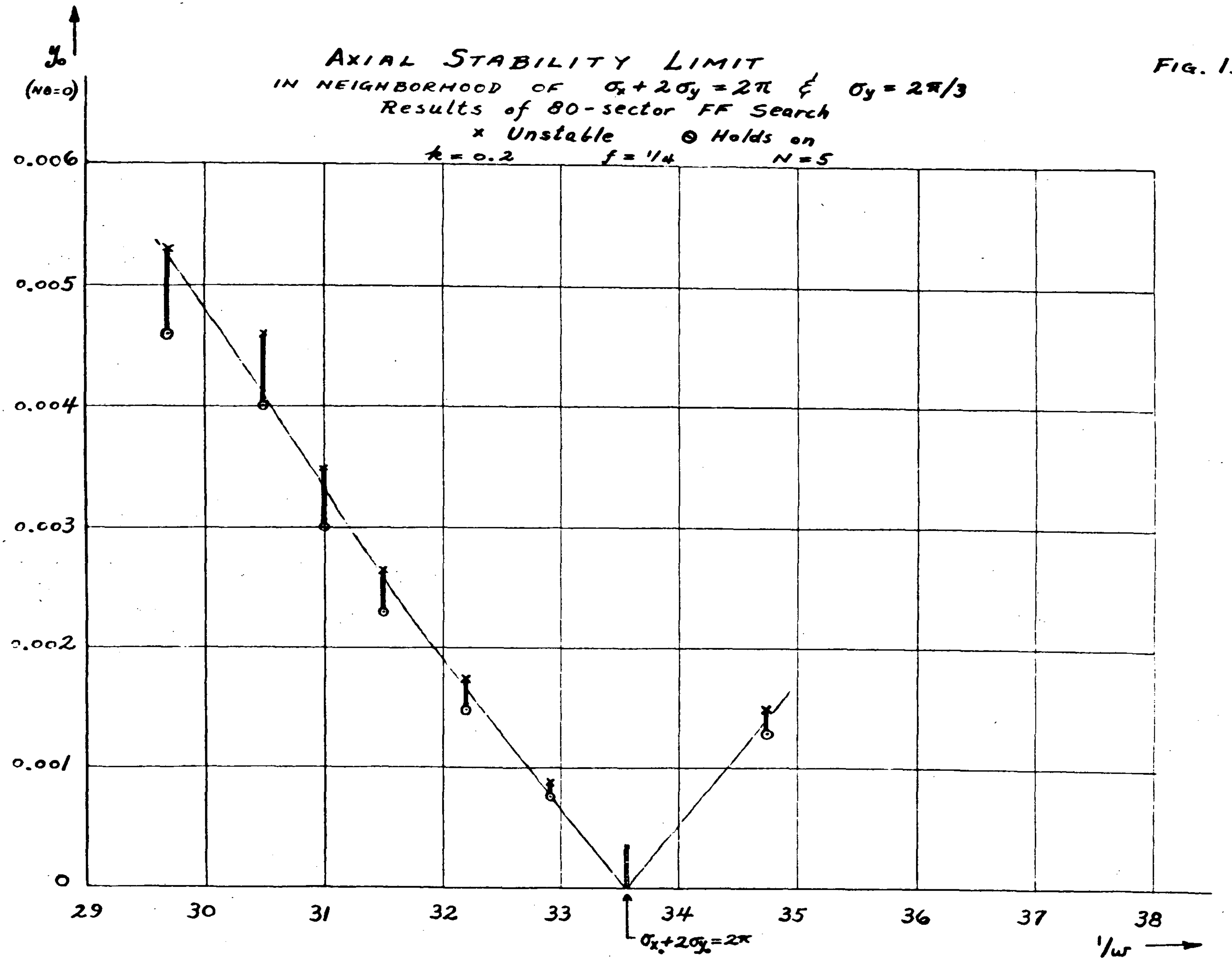
FIG. 1.
AXIAL STABILITY LIMIT
IN NEIGHBORHOOD OF $\sigma_x + 2\sigma_y = 2\pi$ & $\sigma_y = 2\pi/3$
Results of 80-sector FF Search
× Unstable ⊙ Holds on
$k = 0.2$ $f = 1/4$ $N = 5$
y_0 (NB=0)
0.006
0.005
0.004
0.003
0.002
0.001
0
29
30
31
32
33
34
35
36
37
38
$\sigma_{x_0} + 2\sigma_{y_0} = 2\pi$
$1/\omega$

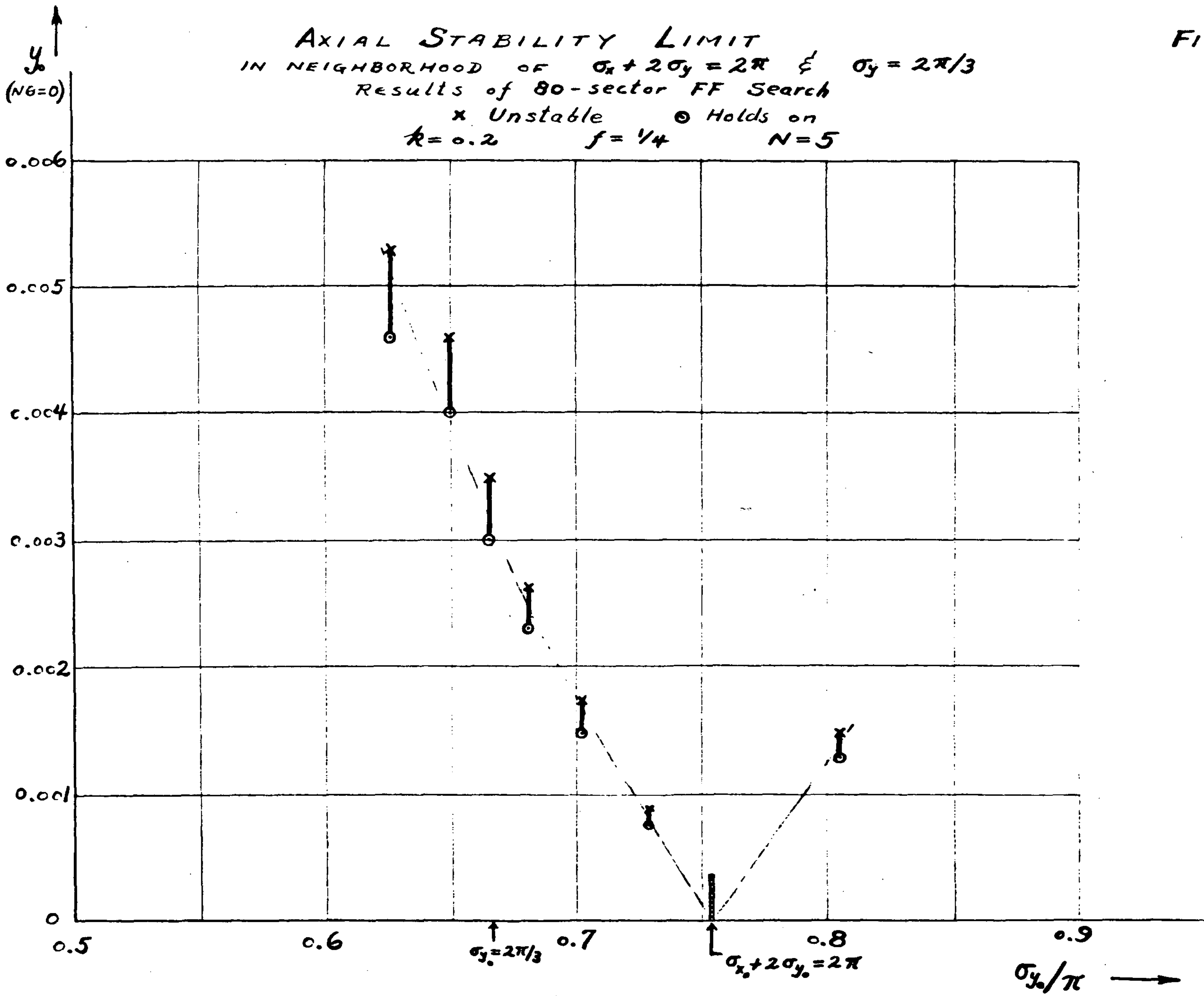
AXIAL STABILITY LIMIT
IN NEIGHBORHOOD OF $\sigma_x + 2\sigma_y = 2\pi$ & $\sigma_y = 2\pi/3$
Results of 80-sector FF Search
× Unstable ⊙ Holds on
$k = 0.2$ $f = 1/4$ $N = 5$
y_0 (NG=0)
0.006
0.005
0.004
0.003
0.002
0.001
0
0.5
0.6
$\sigma_{y_0} = 2\pi/3$
0.7
$\sigma_{x_0} + 2\sigma_{y_0} = 2\pi$
0.8
0.9
σ_{y_0}/π

FIG. 2.

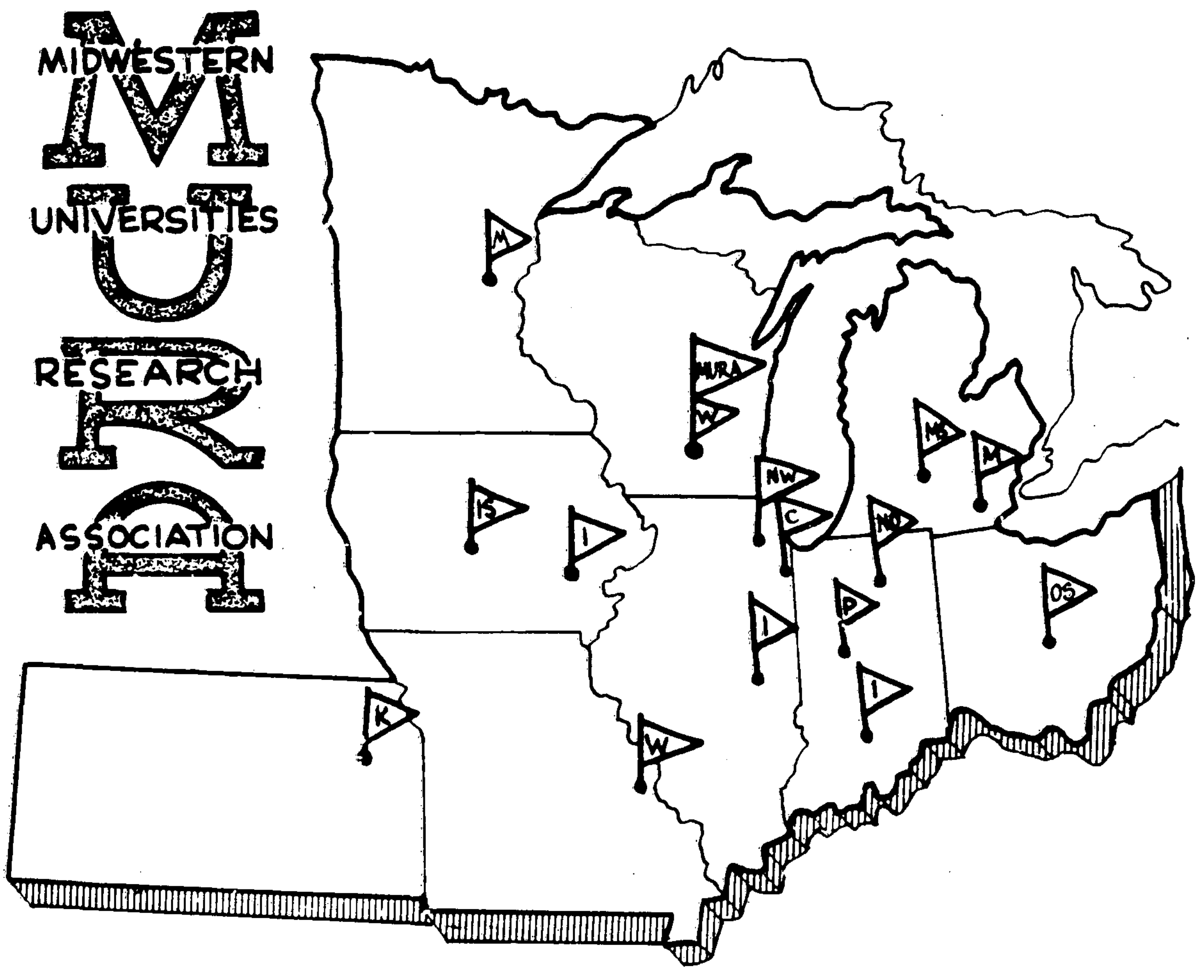

Damping of Oscillations - Requisite Energy Tolerance
At Injection - Coherent Radiation

REPORT **NUMBER** 23

MURA NOTES May-June, 1954

L. Jackson Laslett
Iowa State College

The following notes deal (i) with the possible supplementary damping of oscillations in a synchrotron, (ii) with the energy tolerance required at injection, and (iii) with certain aspects of coherent radiation. These provisional notes do not represent a complete analysis of these subjects, but were begun in preparation for the May 22-23 meeting of the technical group and to a small extent reflect the discussion at that meeting.

I. DAMPING OF OSCILLATIONS

1. Introduction:

At recent meetings of the technical group attention has been given to the possibility of damping synchrotron oscillations, through the use of a radio-frequency E.M.F. per turn which varies across the radial aperture of the accelerator.[1] This possibility has also received attention by the Princeton group[2] and in an early Berkeley report[3] recently called to the writer's attention. Since it appears from the analysis that one may expect an undamping of betatron oscillations if the synchrotron oscillations are damped in this way, the arguments are outlined hereunder (i) as a review, (ii) as a challenge to devise (if possible) an acceptable damping mechanism, (iii) as an indication of the tolerances required in cavity construction, and (iv) with the thought that in some accelerators some additional damping of one of the oscillations may be desirable, even at the expense of a certain undamping of the other.

2. The Phase-Equation:

The equation governing the phase oscillations may be obtained in a manner suggested by the work of Twiss and Frank,[4] recently reviewed by Livingood,[5] by writing the equations for a general particle and for the synchronous particle as follows:[6]

We consider the E.M.F. per turn to vary in a substantially linear manner across the useful aperture of the accelerator

$$\text{E.M.F.} = V_0 \left(1 - \sigma n \frac{\Delta r}{r_s}\right) \sin\phi,$$

where $\Delta r = r - r_s$.

Introducing the vector potential of the guide field $[rA = (\text{flux})_z / 2\pi]$,

$$\frac{d}{dt}(pr + erA) = \frac{eV_0}{2\pi}\left(1 - \sigma n \frac{\Delta r}{r_s}\right)\sin\phi$$

$$\frac{d}{dt}(p_s r_s + e r_s A_s) = \frac{eV_0}{2\pi} \sin\phi_s .$$

By subtraction:

$$\frac{d}{dt}\left(p_s r_s \frac{\Delta p}{p_s}\right) = \frac{eV_o}{2\pi}(\sin\phi - \sin\phi_s) - \sigma n\left(\frac{eV_o}{2\pi}\right)\frac{\Delta r}{r_s}\sin\phi$$

$$\frac{d}{dt}\left(\frac{E_s}{-\gamma}\dot\phi\right) = -\omega_o^2 h\frac{eV_o}{2\pi}(\sin\phi - \sin\phi_s) + \omega_o^2 h\frac{eV_o}{2\pi}\sigma n\frac{\Delta r}{r_s}\sin\phi,$$

where ω_o represents $\dfrac{2\pi}{\text{period of revolution}}$ for a hypothetical particle moving on the radius r_s with the speed of light.

In the traversal of several cavities (or of a single cavity several times), we write in the usual notation,

$$\frac{\Delta r}{r_s} \cong \frac{[\Delta r]_{AV}}{r_s} = a\frac{\Delta p}{p_s} = \frac{a}{\gamma\omega_s h}\dot\phi = \frac{a}{\beta\gamma h\omega_o}\dot\phi$$

and obtain:

$$\frac{d}{dt}\left(\frac{E_s}{-\gamma}\dot\phi\right) = -\omega_o^2 h\frac{eV_o}{2\pi}(\sin\phi - \sin\phi_s) + \frac{a\sigma n}{\beta\gamma}\omega_o\frac{eV_o}{2\pi}\dot\phi\sin\phi,$$

which is of the form:

$$\frac{d}{dt}(M\dot\phi) = -A(\sin\phi - \sin\phi_s) + a\dot\phi\sin\phi,$$

with $M = \dfrac{E_s}{-\gamma}$, $A = \dfrac{\omega_o^2 heV_o}{2\pi}$, $a = \dfrac{a\sigma n}{\beta\gamma}\omega_o\dfrac{eV_o}{2\pi}$.

This result appears concordant with the non-relativistic eq. (15) of ref. 3 for a conventional synchrotron in which P_s increases linearly with time, where

$h = 1$ $\quad \sigma n = -6$ $\qquad \omega_o = \dfrac{c}{r_s\left(1 + \frac{\Sigma L}{2\pi r_s}\right)}$

$a = \dfrac{1}{1-n}$

$\gamma = \dfrac{1}{1-n}\,\dfrac{1}{1+\frac{\Sigma L}{2\pi r_s}} - 1$ $\qquad \phi \cong \phi_s$

$E_s/\epsilon_s \cong 0$ and

$$\frac{1}{E_s}\frac{\omega_o}{\beta}\frac{eV_o}{2\pi}\sin\phi_s = \frac{1}{E_s}\frac{\omega}{\beta^2}\frac{eV_o}{2\pi}\sin\phi_s = \frac{(dE/dt)_s}{\beta^2 E_s} = \frac{(dp/dt)_s}{p_s}.$$

The conclusions of ref. 3 concerning the damping of the resultant motion will thus be found to be consistent with ours for this case, as will also the results stated for the extreme relativistic situation.

3. <u>Solution of the Phase Equation</u>:

To facilitate solution of the phase equation we replace $\sin\phi$ by $\sin\phi_s$ in the damping term and, rather then proceed directly with the differential equation, note that the motion may be derived from a Lagrangian

$$L = (M/2)\left[\exp\left(-\sin\phi_s \int \frac{a}{M}\,dt'\right)\right]\dot{\phi}^2 + A\left[\exp\left(-\sin\phi_s \int \frac{a}{M}\,dt'\right)\right]\left[U(\phi) - U(\phi_s)\right],$$

where $U(\phi) = \cos\phi + \phi \sin\phi_s$.

The motion accordingly may be characterized by the Hamiltonian

$$H = \frac{1}{2M}\left[\exp\left(\sin\phi_s \int \frac{a}{M}\,dt'\right)\right]p^2 - A\left[\exp\left(-\sin\phi_s \int \frac{a}{M}\,dt'\right)\right]\left[U(\phi) - U(\phi_s)\right]$$

$$\cong \frac{1}{2M}\left[\exp\left(\sin\phi_s \int \frac{a}{M}\,dt'\right)\right]p^2 + \frac{A}{2}\left[\exp\left(-\sin\phi_s \int \frac{a}{M}\,dt'\right)\right]\cos\phi_s\,(\phi - \phi_s)^2,$$

with the canonically conjugate momentum $p = M\left[\exp\left(-\sin\phi_s \int \frac{a}{M}\,dt'\right)\right]\dot{\phi}$.

In adiabatic changes of the roughly periodic motion, the invariance of the action integral insures that $p_{max} \cdot (\phi - \phi_s)_{max}$ remains constant: thus $\Omega M\left[\exp\left(-\sin\phi_s \int \frac{a}{M}\,dt'\right)\right](\phi - \phi_s)^2_{max}$

$$= (AM\cos\phi_s)^{1/2}\left[\exp\left(-\sin\phi_s \int \frac{a}{M}\,dt'\right)\right](\phi - \phi_s)^2_{max}$$

remains constant, or

$$(\phi - \phi_s)_{max} \propto (AM\cos\phi_s)^{-1/4} \exp\left[(1/2)(\sin\phi_s)\int \frac{a}{M}\,dt'\right].$$

The factor $(AM\cos\phi_s)^{-1/4}$ represents the customary damping of synchrotron phase oscillations and leads to the familiar $E^{-1/4}$ damping at energies such that γ is substantially constant. It is of interest, therefore, to estimate the exponential factor which is introduced by the variation of E.M.F. with radius.

$$\frac{a}{M}\sin\phi_s = -\frac{a\sigma n}{\beta E_s}\,\omega_0\,\frac{eV_0}{2\pi}\sin\phi_s = -a\sigma n\,\frac{(dp/dt)_s}{p_s},$$

$$(1/2)(\sin\phi_s)\int \frac{a}{M}\,dt' = -(a\sigma n/2)\ln\frac{p_f}{p_i},$$

and

$$\exp\left[(1/2)(\sin\phi_s)\int \frac{a}{M}\,dt'\right] = (p_f/p_i)^{-a\sigma n/2}$$

$$= (p_f/p_i)^{-\frac{4.81}{2}\sigma}$$

$$= (p_f/p_i)^{-2.4\sigma}$$

in agreement with the results of ref. 3 when $a = \frac{1}{1-n}$, $\sigma n = -\epsilon$, and $p \propto t$ for an alternate-gradient synchrotron operated near the center of the stability diagram.

In a typical example an increase of momentum from that corresponding to an injection energy of 50 Mev (pc = 0.31 Gev) to an energy in the neighborhood of a transition energy such that pc = 9.70 Gev then leads to the additional damping factor

$$(9.70/0.31)^{-2.4\sigma} = (31.2)^{-2.4\sigma},$$

or approximately 0.18 for $\sigma = 1/4.8$. It is noted that the sense of the damping is unaffected by flipping the phase at the transition energy.

It appears from the foregoing that, from the standpoint of the synchrotron oscillations, this damping mechanism would be desirable in reducing the difficulties associated with traversal of the transition energy, since the increase of amplitude resulting from an inexactly-timed change of phase would start from a lower level of amplitude. It is necessary, however, to consider the effect of this mechanism on the radial betatron oscillations.

4. <u>Associated build-up of Betatron Oscillations</u>:

It appears that consideration should be given to two ways in which the mechanism suggested may influence the magnitude of the radial betatron oscillations. The first of these[7] involves the $e[\bar{v} \times \bar{B}]$ forces arising from the magnetic flux-leakage within the cavity, and presumably a similar radial impulse would be expected in case a resonator with an oblique gap were employed. The second effect[3] is that resulting from the abrupt change in the equilibrium orbit at each traversal of the acceleration cavity. We proceed to consider these effects in turn.

5. <u>Evaluation of Impulse from Leakage Flux-Density</u>:

Writing the E.M.F. per cavity as $V_1 [1 - \sigma n \frac{\Delta r}{r_s}] \cdot \sin(h\omega_s t)$,

we have
$$V_1 \left[1 - \sigma n \frac{\Delta r}{r_s}\right] \cdot \sin(h\omega_s t) = -\iint \dot{B}\, dS$$
$$= -\int_0^r \int r \dot{B}(r,\theta)\, dr\, d\theta$$
$$\frac{V_1 \sigma n}{r_s} \sin(h\omega_s t) = \int r \dot{B}(r,\theta)\, d\theta$$
$$\frac{V_1}{h\omega_s} \frac{\sigma n}{r_s} \cos\phi = -\int r\, B(r,\theta)\, d\theta$$
$$= -\int B(r,\theta)\, ds,$$
integrated through the cavity.

It is realized that the R.F. electric and magnetic fields must constitute a self-consistent solution to Maxwell's equations and that difficulties could in fact arise if one attempted to achieve an E.M.F. which over an extended region were strictly independent of the path. The statements made herein appear to be satisfactory, however, for an E.M.F. of the form assumed, and considerations based on curl $\bar{H} = \dot{\bar{D}}$ suggest that neglecting the μH so implied by a spatially constant E.M.F. affects the amplitude $\Delta r \cong \lambda \Delta r'$ by an amount negligible (5 to 30 percent in a typical case) in comparison with the term $-a(\frac{\Delta p}{p_s}) \cos\psi$ considered later.

We thus obtain for the impulse
$$\Delta p_r = \int F\, dt = e\int B \frac{ds}{dt}\, dt$$
$$= e\int B\, ds = -\frac{eV_1}{h\omega_s} \frac{\sigma n}{r_s} \cos\phi$$

$$\Delta\left(\frac{dr}{dt}\right) = -\frac{(eV_1)\sigma n}{mh\omega_s r_s}\cos\phi$$
$$= -\frac{eV_1}{p}\,\frac{\sigma n}{h}\cos\phi$$
$$\Delta\left(\frac{d(r/r_s)}{d\theta}\right) = \frac{1}{v_s}\,\Delta\left(\frac{dr}{dt}\right) = -\frac{eV_1}{pv_s}\,\frac{\sigma n}{h}\cos\phi \doteq -\frac{eV_1}{\beta^2 E_s}\,\frac{\sigma n}{h}\cos\phi_s$$
$$= -\left(\frac{\Delta E_1}{\beta^2 E}\right)_s \frac{\sigma n}{h}\,\mathrm{ctn}\,\phi_s = -\left(\frac{dp_1}{p}\right)_s \mathrm{ctn}\,\phi_s$$

If this impulse were the only mechanism affecting the betatron oscillations, it would be reasonable to consider the use of cavities in pairs, spaced by a half-wavelength of the radial betatron oscillations. The maximum extra relative displacement which would then be expected to arise in this way <u>between</u> the members of a <u>cavity-pair</u> would not exceed

$$2\left(\frac{\lambda}{r_s}\right)\left|\Delta\left(\frac{d(r/r_s)}{d\theta}\right)\right| = 2\,\frac{\lambda}{r_s}\,\left(\frac{dp_1}{p}\right)_s \frac{\sigma n}{h}\,\mathrm{ctn}\,\phi_s\,.$$

(The factor 2 is that estimated by Courant, Livingston, and Snyder[8] to allow for the non-sinusoidal character of the oscillations in an A.G.S.)

With h_c cavities in all, each excited to a similar R.F. level, $\left(\frac{dp_1}{p}\right)_s$ or $\left(\frac{\Delta E_1}{\beta^2 E}\right)_s$ equals

$$\frac{2\pi r_s\left[1+\frac{\Sigma L}{2\pi r_s}\right]}{h_c\beta^2 E_s}\left(\frac{dp}{dt}\right)_s \quad \text{or substantially} \quad \frac{2\pi r_s\left[1+\frac{\Sigma L}{2\pi r_s}\right]}{h_c\beta^2 c\,(\text{acc. time})}\;\frac{E_f}{E_s};$$

in addition we may take $\lambda/r_s = 2/\sqrt{n}$ radians and obtain

$$n\left[\frac{\Delta r}{r_s}\Big|_{max}\right] \le \frac{4\,(n)^{3/2}}{hh_c}\;\sigma\;\frac{2\pi r_s\left[1+\frac{\Sigma L}{2\pi r_s}\right]\mathrm{ctn}\,\phi_s}{c\cdot\text{acceleration time}}\cdot\frac{E_f}{\beta^2 E_s} \quad \text{from a single cavity.}$$

Typically, with $n = 400$, $h_c = h = 16$, acceleration from an injection energy of 50 Mev (kinetic) to a final energy of 25 Gev, and a rise-time of one second,

$$n\left[\frac{\Delta r}{r_s}\Big|_{max}\right] \le \frac{4\times 8000}{16\times 16}\;\frac{2\pi\times 86.50\times 1.3\times\sqrt{3}}{3\times 10^8\times 1}\;\frac{26\times 10^9}{97\times 10^6}\,\sigma$$
$$= 0.14\,\sigma \text{ at injection,}$$

which is considerably less than unity (for the harmonic number assumed) with any reasonable choice of σ.

The impulse from the leakage field of such cavities also will imply an accumulative displacement in the case of particles for which the betatron wavelength is not exactly twice the separation of a cavity-pair. For estimating this effect we presume that through careful control of the magnet performance n is not permitted to wander more than from the center of a small stability diamond half-way to the edge. We accordingly consider $|\delta K| = \frac{\pi/4}{N_s/2} = \frac{\pi}{8\sqrt{n}}$, or $|\delta n| = 0.2\sqrt{n}$, (where k enters as $\exp(\pm i\kappa)$ in the characteristic solutions for traversal of a sector-pair).[9] Since the increase of relative amplitude from traversal of a sector-pair spaced by $\frac{\lambda \pm \Delta\lambda}{2}$ will not exceed $\frac{|\Delta\lambda|}{r_s} \Delta \left(\frac{d(r/r_s)}{d\theta}\right)$ and typically $|\Delta\lambda| = \frac{\lambda}{\kappa}|\delta\kappa| = \frac{32 r_s}{N_s}|\delta\kappa| = \frac{16\pi r_s}{N_s{}^2} = \frac{\pi r_s}{n}$,

$$n\left[\frac{\Delta r}{r_s}\Big|_{max}\right] \leq \pi\Delta\left(\frac{d(r/r_s)}{d\theta}\right) = \pi\left(\frac{\Delta E_1}{\beta^2 E}\right)_s \frac{\sigma n}{h} \operatorname{ctn}\phi_s$$

$$= \frac{\pi n}{h r_c}\,\sigma\,\frac{2\pi r_s\left[1 + \frac{\Sigma L}{2\pi r_s}\right]\operatorname{ctn}\phi_s}{c \cdot \text{acceleration time}}\;\frac{E_\rho}{\beta^2 E_s}$$

$$= \frac{\pi \times 400}{16 \times 16}\;\frac{2\pi \times 86.50 \times 1.3 \times \sqrt{3}}{3 \times 10^8 \times 1}\;\frac{26 \times 10^9}{97 \times 10^6}\,\sigma$$

$$= 0.0054\,\sigma.$$

The increase of amplitude per revolution would, at the worst, be $\frac{h_c}{2}$ times the above result and after several revolutions might be about 2.62 times larger still, if we stay away from resonances by no less than the amount suggested.

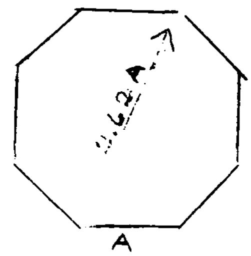

We accordingly write

$$n\left[\frac{\Delta r}{r_s}\Big|_{max}\right]_{overall} \leq \frac{4.1\,n}{h}\,\sigma\,\frac{2\pi r_s\left[1 + \frac{\Sigma L}{2\pi r_s}\right]\operatorname{ctn}\phi_s}{c \cdot \text{acceleration time}}\;\frac{E_\rho}{\beta^2 E_s}$$

$= 0.11\,\sigma$, for the example considered
($h = 16$, 50 Mev injection, etc.),

With σ somewhat less than unity, this result does not appear to be excessive in a magnet whose radial semi-aperture is comparable with $\pm r_s/n$

6. The Growth of Oscillations from step-wise Shifts of Equilibrium Orbits.

It has been pointed out in the Berkeley report[3] to which reference has been made earlier that in traversal of a R.F. cavity the instantaneous equilibrium orbit is suddenly displaced by an amount

$$\left(\frac{\Delta r}{r_s}\right)_{equil.} = a\frac{\Delta p_\perp}{p} = a\left(\frac{\Delta p_\perp}{p}\right)_s\left(1 - \sigma n\frac{\Delta r}{r_s}\right).$$

With this displacement there is associated an increase of the square of the relative amplitude x_m of the betatron oscillations which, for sinusoids, would amount to

$$\Delta(x_m^2) \geq -2 a x_m \cos\psi \, (1 - \sigma n x_m \cos\psi) \left(\frac{\Delta p_1}{p}\right)_s ,$$

where ψ is the phase of the oscillation at the time of traversal. If we take over this expression as roughly indicative of the behaviour in an A.G.S., we note that

$$\langle \Delta x_m^2 \rangle_{av} = a \sigma n \left(\frac{\Delta p_1}{p}\right)_s x_m^2$$

and hence there results a growth of amplitude on this account:

$$x_m \propto p^{a\sigma n/2} \simeq p^{2.4\sigma}$$

The growth-factor so found for the betatron oscillations is thus as rapid as the attenuation factor found in section 3 for the synchrotron oscillations.

The effect just described appears definitely to detract from the utility of a system in which the E.M.F. decreases as one moves radially outward across the aperture. In some circumstances, however, the radial betatron oscillations may be of somewhat secondary importance to the synchrotron oscillations -- in such a situation consideration might be given to the use of cavities for which σ is such that the effect in question is just sufficient to cancel the customary $1/\sqrt{p}$ adiabatic damping of the betatron oscillations:

$$\sigma < 1/4.8 \simeq 0.2$$

As has been remarked at the May 22-23 meeting of the mid-west technical group, however, a more adequate treatment of these effects would consider the betatron and synchrotron motions together in a general unified analysis.

It may be noted that Kerst has pointed out[10] that a betatron inherently involves an induced E.M.F. which increases with radius. Although "gaps" may in a sense be present, due to the shielding effect of the conducting sections of the vacuum chamber wall, phase stability is not involved and the effect on the betatron oscillations may be beneficial.

7. Possible Statistical Growth of Induced Betatron-Oscillation Amplitude:

In section 6 it was indicated that, when $\sigma = 0$, the betatron oscillation amplitude changes upon traversal of a cavity by

$$\Delta(x_m^2) \cong -2 a x_m \left(\frac{\Delta p_1}{p}\right)_s \cos\psi$$

$$\text{or} \quad \Delta x_m \cong -a \left(\frac{\Delta p_1}{p}\right)_s \cos\psi .$$

Although as previously stated, the values of cos ψ may be presumed to average to zero, there could conceivably be random variations of n such that the values of ψ are distributed in a substantially random way statistically. In such a case we have a situation similar to the projection of a two-dimensional "ramdom walk" problem and may write for ν cavity traversals

$$\frac{d\langle(\Delta x_m)^2\rangle}{d\nu} = \frac{1}{2}\left[a\left(\frac{\Delta p_1}{p}\right)_s\right]^2 = \frac{a^2}{2}\left[\left(\frac{\Delta E_1}{\beta^2 E}\right)_s\right]^2 = \frac{a^2(\Delta E_1)^2}{2}\,\frac{E^2}{(E^2-E_0{}^2)^2}$$

$$\frac{d\langle(\Delta x_m)^2\rangle}{dE} = \frac{a^2\Delta E_1}{2}\,\frac{E^2}{(E^2-E_0{}^2)^2}.$$

Integrating,

$$\langle(\Delta x_m)^2\rangle = \frac{a^2\Delta E_1}{4E_0}\left[\mathrm{ctnh}^{-1}\frac{E_i}{E_0} - \mathrm{ctnh}^{-1}\frac{E_f}{E_0} + \frac{E_i/E_0}{(E_i/E_0)^2-1} - \frac{E_f/E_0}{(E_f/E_0)^2-1}\right]$$

$$\cong \frac{a^2}{8}\,\frac{\Delta E_1}{E_i-E_0} \qquad (\text{for } E_i-E_0 \ll E_0,\ E_f \gg E_0)$$

$$= \frac{a^2}{8h_c}\,\frac{2\pi r_s\left[1+\frac{\Sigma L}{2\pi r_s}\right]}{c\cdot(\text{acc. time})}\,\frac{E_f}{E_i-E_0}$$

$$= \left(\frac{4.81}{n}\right)^2 \frac{1}{8h_c}\,\frac{2\pi\times 56.50\times 1.3}{3\times 10^8\times 1}\,\frac{26\times 10^9}{50\times 10^6}$$

$$= \left(\frac{4.81}{n}\right)^2 \frac{1}{h_c}\,1.53\times 10^{-4}$$

$$\langle(\Delta x_m)^2\rangle^{1/2} = \frac{4.81}{n h_c{}^{1/2}}\,1.24\times 10^{-2}$$

$$= \frac{0.06}{n h_c{}^{1/2}}$$

$$n\langle(\Delta x_m)^2\rangle^{1/2} = \frac{0.06}{h_c{}^{1/2}} \cong 0.015,$$

In the case of the electron synchrotron described in an earlier report,[11] we similarly write

$$\langle(\Delta x_m)^2\rangle \cong \frac{a^2\Delta E_1}{2E_i} \qquad (E_f \gg E_i \gg E_0)$$

$$= \left(\frac{4.81}{n}\right)^2 \frac{1}{2h_c}\,\frac{0.892\times 10^6}{50\times 10^6}$$

$$= \left(\frac{4.81}{n}\right)^2 \frac{1}{h_c}\,0.892\times 10^{-2}$$

$$\langle(\Delta x_m)^2\rangle^{1/2} = \frac{4.81\times 0.094}{n\,h_c{}^{1/2}}$$

$$= \frac{0.455}{n\,h_c{}^{1/2}}$$

$$n\langle(\Delta x_m)^2\rangle^{1/2} = \frac{0.455}{h_c{}^{1/2}} = 0.08 \qquad (\text{since } h_c = 32).$$

8. Operation with a Single Cavity:

The effects considered in the preceding sections do not appear to preclude operation of a high-energy proton synchrotron with a single cavity, since even with random phases we find from the results of page 8 that $n\langle(\Delta x_m)^2\rangle^{1/2} \cong 0.06$ when $h_c = 1$; due to the non-sinusoidal character of the oscillations, we might consider that this result could be as great as a little over twice the value found there -- say 0.14.

In a single traversal of such a cavity

$$
\begin{aligned}
|n \cdot \Delta x_m| &= 4.81 \left.\frac{\Delta E/v}{p}\right|_s \cos\psi \\
&\leq 4.81 \left.\frac{\Delta E}{\beta^2 E}\right|_s \\
&= 4.81 \frac{58.6 \times 10^3}{97.5 \times 10^6} \\
&= 0.0029 .
\end{aligned}
$$

Again, due to the non-sinusoidal character of the oscillations we may better write

$$n|\Delta x_m| \leq 0.007 .$$

II. REQUISITE ENERGY TOLERANCE AT INJECTION

1. Motivation:

The question has been raised concerning the requisite energy tolerances at injection and whether there exists a disparity between the Linac requirements as specified at Brookhaven and those currently conceived in the mid-west group and elsewhere.

2. Acceptance into Stable Synchrotron Oscillations:

One approach to this problem has been given by K. Johnsen[12] in the CERN proton-synchrotron lectures. In this approach the requirement considered has been that the initial momentum spread shall be no greater than that acceptable into synchrotron phase oscillations. For the case of no frequency error Johnsen cites [cf. his eq. (3)] the result

$$
\begin{aligned}
\frac{\Delta p}{p} &= \pm \frac{2}{\beta} \sqrt{\frac{e}{mc^2} \frac{r_m r_0 \dot{B}_0 [-\operatorname{ctn}\phi_0 - (\phi_0 - \pi/2)]}{h}} \\
&= \pm \frac{2}{\beta} \sqrt{\frac{eV_0/2\pi}{mc^2} \frac{[-\cos\phi_0 - (\phi_0 - \pi/2)\sin\phi_0]}{h}} ,
\end{aligned}
$$

which is consistent with eq. (16) of a report[6] by the present writer if $|\gamma|$ in this latter equation is regarded as substantially unity.[13]

For the similar accelerators considered in the CERN and MAC reports we list the following parameters and find

	CERN (October 1953)	LJL(MAC)-3	
Inj. Energy, Kinetic	50	50	Mev
" " Total	0.99	0.99	Gev
β	0.314	0.314	
$\lvert\gamma\rvert$	$\cong 1$	0.88	
$eV_o/2\pi$	23.1 x 103 based on $\dot{B}$ = 12 KG/sec	18.7×10^3	$\frac{ev}{radian}$
h	38	(38)	
$\Delta p/p$	$\pm 1.80 \times 10^{-2}/h^{1/2} = \pm 0.29 \times 10^{-2}$	$\pm 1.73 \times 10^{-2}/h^{1/2} = \pm 0.28 \times 10^{-2}$	
$\frac{\Delta E}{E_{Kin}} = \frac{\beta^2}{1-\sqrt{1-\beta^2}}\left(\frac{\Delta p}{p}\right)$	$\pm 0.56 \times 10^{-2}$	$\pm 0.55 \times 10^{-2}$	

These results may be compared with what would then be a satisfactory expected performance of the linac, as reported by L. H. Johnston:[14]

$$E_{Kin} = 50 \pm 0.2 \text{ Mev}, \quad \text{or} \quad \Delta E/E_{Kin.} = \pm 0.4 \times 10^{-2}.$$

The momentum spread tabulated above appears to constitute the basis of the CERN design specifications [p.6 of the CERN report 12]. For the Brookhaven design a higher harmonic number may be under consideration -- the foregoing example with the harmonic number changed to 88 would lead to

$$\frac{\Delta p}{p} = \pm 0.19 \times 10^{-2}$$

$$\frac{\Delta E}{E_{Kin.}} = \pm 0.37 \times 10^{-2},$$

Note added in proof: The Brookhaven Accelerator Development Division minutes (#57) of their March 16, 1954 meeting suggest the requirement $\pm 1/2\%$ in energy, $\pm 10^{-3}$ radian, and a width of 1/2 inch.

3. Avoidance of Resonances:

The change in effective n due to momentum error should for safety be no greater than that which will displace the operation point from the center of a small diamond, bounded by 2π- and π-resonances, half-way to the edge. The momentum spread which is tolerable on this acount has been estimated earlier[6] as $\pm 0.20/\sqrt{n}$ for operation near the center of the "necktie diagram" ($\sigma = \pi/2$), or $\pm 0.31/\sqrt{n}$ for a point situated on the diagonal but closer to the origin ($\sigma = 0.3\pi$). For a field index (n) in the neighborhood of 400, these considerations necessitate a tolerance of about ± 1 per cent in momentum or ± 2 percent in energy and are evidently less demanding than the requirements discussed previously cf. Fig. 9A, p. 111 of the CERN report[12] and the accompanying discussion by Adams (Sect. III-4, esp. p. 102).

4. Clearance of Inflector Electrode:

An additional and more severe limitation of the tolerable energy spread may arise if the beam is obliged to clear the electrode of an electrostatic inflector structure as it spirals inward during the injection interval. It should be noted that such an arrangement presents, possibly, serious difficulties in machines of the types presently under consideration, due to the very small pitch of the spiral in the presence of a linearly-rising magnetic field -- about 0.6 mm per turn. If it is intended to inject at the start of the injection interval particles whose trajectories have initially the scolloped appearance of the repetitive orbits illustrated by Courant, Livingston, and Snyder [ref. 8, Fig. 4], it may be noted that for some particles an excess momentum will require the superposition of a betatron oscillation (of an initially negative sign) of amplitude $(6.39/n)\ (\Delta p/p)$. In the course of a revolution, this betatron motion may come to represent a positive displacement at the inflector location. The radial error from this effect can then amount to

$$\frac{\Delta r}{r} = 2 \times \frac{6.39}{n} \frac{\Delta p}{p}$$

and would restrict the permissible excess momentum to

$$\frac{\Delta p}{p} = \frac{n}{2 \times 6.39} \frac{\Delta r}{r}.$$

With, for example, $\Delta r = 0.6$ mm $= 0.6 \times 10^{-3}$ M, $n = 400$, and $r = 86.50$ M as before, we thus find the comparatively severe limitation

$$\frac{\Delta p}{p} = \frac{400}{2 \times 6.39} \frac{0.6 \times 10^{-3}}{86.50} = 0.22 \times 10^{-3},$$

$$\text{or} \quad \frac{\Delta E}{E_{K}} = 0.43 \times 10^{-3} = 0.043 \text{ percent}.$$

The discussion of this section presumably leads only to a rough estimate of the desired energy tolerance when an inflector is used -- to obtain a more definitive idea of the requirements it would seem appropriate to study in some detail the individual trajectories of representative particles injected with various amounts of momentum- and angular-error at various times within the injection interval.

III. COHERENT RADIATION

1. Introduction:

Since there has been within the mid-west group some expression of interest in the construction of a circular electron accelerator, the attention of the Technical Group was directed to a recent report[15] by Nodvick and Saxon "On the Suppression of Coherent Radiation by Electrons in a Synchrotron". Since some general discussion of coherent radiation resulted at the May 22-23 meeting, the following comments are appended for whatever interest and reference value they may have. The mathematical notes are somewhat crude but may have the merit of affording a simple feel for the phenomenon.

2. Rough Formulation of Form-Factor for Coherent Radiation:

If the power radiated non-coherently is $P_0(\omega)\,d\omega$ per electron, the coherent radiation power from a small bunch of N electrons characterized by a symmetrical distribution density ρ is

$$P = N^2 \int_0^\infty \left[F(\omega)\right]^2 P_0(\omega)\,d\omega,$$

where $$F(\omega) = \frac{\int \rho(x)\cos\frac{\omega x}{c}\,dx}{\int \rho(x)\,dx}.$$

3. List of Form-Factors:

We consider the following form-factors:

(i) For a uniform bunch of length L,

$$F = \frac{\sin\frac{L\omega}{2c}}{\frac{L\omega}{2c}}.$$

(ii) For a Guassian bunch, of width L between 1/e points:

$$F = \exp\left[-\left(\frac{L\omega}{4c}\right)^2\right].$$

(iii) For a group of particles moving with S.H.M. and with amplitudes uniformly distributed from 0 to L/2: In this case

$$\rho(x) \propto \int_x^{L/2} ds/(s^2-x^2)^{1/2} = \cosh^{-1}\frac{L}{2x}$$ and

$$F = \frac{4}{\pi L}\int_0^{L/2} \cosh^{-1}\frac{L}{2x}\cos\frac{\omega x}{c}\,dx$$

$$= \frac{2}{\pi}\int_0^1 \cosh^{-1}\frac{1}{y}\cos\frac{L\omega y}{2c}\,dy.$$

4. Introduction of the Incoherent Spectral Distribution, $P_0(\omega)$:

If, for the low-frequency radiation important in the coherent effects, we write

$$P_0(\omega) = K\omega^{1/3},$$

the coherent radiation in the cases considered becomes

(i) For a uniform bunch,

$$P_{(1)} = \frac{2\pi}{\sqrt{3}\,\Gamma(5/3)} K N^2 \left(\frac{c}{L}\right)^{4/3}$$

$$= 4.02\, K N^2 \left(\frac{c}{L}\right)^{4/3}.$$

(ii) For a Gaussian bunch,

$$\mathcal{P}_{(2)} = 3\Gamma\left(\tfrac{5}{3}\right) K N^2 \left(\tfrac{c}{L}\right)^{4/3}$$
$$= 2.71\, K N^2 \left(\tfrac{c}{L}\right)^{4/3}$$

(iii) For S.H.M. oscillations with uniformly-distributed amplitudes the integration is more complex, but it appears safe to take

$$\mathcal{P}_{(3)} \cong 6\, K N^2 \left(\tfrac{c}{L}\right)^{4/3}.$$

The factor of 6 represents a (pessimistic) estimate of the integral

$$\left(\tfrac{2}{\pi}\right)^2 (2)^{4/3} \int_0^\infty z^{1/3}\, dz \left[\int_0^1 \cosh^{-1}\left(\tfrac{1}{y}\right) . \cos zy \, dy\right]^2 .$$

5. Resultant Formulas for the Coherent Radiation:

From eq. (II.20) of a paper by Schwinger[16] we find ($E >> E_0$)

$$\mathcal{P}_0(\omega)\, d\omega = \frac{(3)^{7/6}}{2\pi} \Gamma\left(\tfrac{5}{3}\right) \frac{e^2}{R} \left(\tfrac{R}{c}\right)^{1/3} \omega^{1/3} d\omega, \quad \text{or}$$

$$K = \frac{(3)^{7/6}}{2\pi} \Gamma\left(\tfrac{5}{3}\right) \frac{e^2}{R} \left(\tfrac{R}{c}\right)^{1/3}, \quad \text{e.s.u. being used.}$$

We then find

(i) for a uniform bunch

$$\mathcal{P}_{(1)} = 2\pi\, (3)^{2/3} \frac{N^2 e^2}{R} \left(\tfrac{R}{L}\right)^{4/3} . \frac{c}{2\pi R} .$$

The E.M.F. loss per turn is, accordingly,

$$V_{(1)} = 2\pi\, (3)^{2/3} \frac{Ne}{R} \left(\tfrac{R}{L}\right)^{4/3} \quad \text{statvolts/turn}$$
$$= 600\pi\, (3)^{2/3} \frac{Ne}{R} \left(\tfrac{R}{L}\right)^{4/3} \quad \text{volts/turn}$$
$$= 3.92 \times 10^3 \frac{Ne}{R} \left(\tfrac{R}{L}\right)^{4/3} \quad \text{volts/turn,}$$

with e still in e.s.u. and R in cm.

This result may also be expressed as a "radiation resistance":

$$R_{rad.} = \frac{V}{(Ne)f} = \frac{(2\pi)^2 (3)^{2/3}}{c} \left(\tfrac{R}{L}\right)^{4/3} \text{statohms}$$
$$= 120\pi^2 \left(\tfrac{\sqrt{3}R}{L}\right)^{4/3} \text{ohms,}$$

in agreement with a result stated by Schwinger.[17]

(ii) For a Gaussian bunch

$$T(2) = 4\,(3)^{1/6}\,[\Gamma(\tfrac{2}{3})]^2\,\frac{N^2e^2}{R}\,(\tfrac{R}{L})^{4/3}\,\frac{c}{2\pi R}$$

in agreement with eq. (20) of a paper by Schiff.[18]

$$V(2) = 4\,(3)^{1/6}\,[\Gamma(\tfrac{2}{3})]^2\,\frac{Ne}{R}\,(\tfrac{R}{L})^{4/3} \quad \text{statvolts/turn}$$

$$= 2.64 \times 10^3\,\frac{Ne}{R}\,(\tfrac{R}{L})^{4/3}$$ volts/turn, again with e in e.s.u. and R in cm.

(iii) For the S.H.M. case with distributed amplitudes we estimate

$$V(3) \cong 6 \times 10^3\,\frac{Ne}{R}\,(\tfrac{R}{L})^{4/3}$$ volts/turn, with e and R in the same units as before.

6. Numerical Examples:

By way of an example, first consider a single bunch of electrons for which

$$N = 10^{11}$$
$$R = 5140 \text{ cm, and}$$
$$L/R = 0.8\,;$$

then $V(3) \cong 6 \times 10^3 \times \dfrac{10^{11} \times 4.8 \times 10^{-10}}{5.14 \times 10^3} \times \dfrac{1}{0.744} = 75\ \dfrac{\text{volts}}{\text{turn}}$.

If, on the other hand,

$N = 3 \times 10^{11}$ per bunch,

$R = 700$ cm, and

$L/R = 0.037$, as might be expected with operation in a high harmonic,

then $V(3) \cong 6 \times 10^3 \times \dfrac{3 \times 10^{11} \times 4.8 \times 10^{-10}}{700} \times \dfrac{1}{0.0123} = 10^5$ v/turn.

For comparison, the incoherent loss, for electron-energies of 10 Gev and 2 Gev correspond in these respective cases to:

$$V_{incoh.} = 400\pi\,\frac{4.8 \times 10^{-10}}{5140}\,\left(\frac{10000}{0.51}\right)^4 = 17 \times 10^6 \text{ v/turn;}$$

$$V_{incoh.} = 400\pi\,\frac{4.8 \times 10^{-10}}{700}\,\left(\frac{2000}{0.51}\right)^4 = 2 \times 10^5 \text{ v/turn.}$$

7. Effect of Shielding:

The coherent radiation, which is of relatively long wavelength, may be reduced considerably by suitable shielding. By use of a suitably modified Green's function, Schwinger[19] has considered the case of a uniform bunch between infinite parallel conducting shields, of separation a, and obtained a shielding factor $(1/2)(1/3)^{1/6}\ (a/R)(R/L)^{2/3}$, for $L > a$. Saxon has reviewed the derivation of this factor, which he considers may assume the value 0.071 in a typical case ($R/a = 50$, $L/R = 0.04$), to include an estimate of the shielding effect for parallel conducting sheets of finite width.

IV. REFERENCES

1. Eg. MAC meeting, State University of Iowa, Iowa City, Iowa (April 16, 1954); see also (a) informal note "Possible Damping of Phase Oscillations" (L.J.L., April 1, 1954), based on informal discussion with Drs. Haxby and Palfrey at Bloomington, Indiana (12 February 1954) and (b) letter to D.W. Kerst (April 9, 1954). Damping of phase oscillations was considered attractive in the interest of facilitating the phase change at the transition energy.

2. cf. W. Aron and R.F.Mozley, Minutes of Princeton meeting (July 15, 1953, p.2): "It is known that in the conventional synchrotron the use of a sloped acceleration gap gives increased phase stability at the expense of increased radial oscillation. The first question considered here was whether the same held in both phase stability regions for the strong-focusing synchrotron, and for both "positive" gaps (where the voltage gain increases with particle radius) and "negative" gaps (where the voltage decreases with particle radius). It remains true in all circumstances that the synchrotron amplitude is reduced only if the betatron amplitude is increased, and vice versa. However, since "positive" and "negative" gaps have always oppositely directed effects the use of alternating gaps as previously suggested for the transition region was not ruled out in principle.

The possibility of using such sloped gaps to damp out the betatron oscillation aroused some interest. If the energy from the betatron oscillation were coupled into a slow increase in mean radius then the problem of adjusting the radius might prove easier of solution than any other damping approach (though this was just speculation)."

3. A.A. Garren, R. L. Gluckstern, L. R. Henrich, and Lloyd Smith, "Theoretical Considerations in the Design of a Proton Synchrotron", Sect. IIID--[UCRL-547 (December 9, 1949)]. In this section the authors consider both a cavity device in which the energy gain can be a function of radius because of leakage effects and a dee-type electrode in which a radial variation may be introduced, because of the time-of-flight, by shaping the dee faces. These mechanisms are shown to give similar damping effects.

4. R. Q. Twiss and N. H. Frank, Rev. Sci. Inst. 20, 1 (1949).

5. J. J. Livingood, hectographed Argonne National Laboratory notes (November, 1953).

6. LJL(MAC)-3 (February, 1954) -- esp. ref. 7.

7. This phenomenon was suggested to the writer by his interpretation of a letter from Dr. D. W. Kerst (April 5, 1954).

8. Courant, Livingston, and Snyder, Phys. Rev. 88, 1190-1196 (December 1, 1952).

9. LJL(MAC)-2 (January, 1954) -- esp. p. 4.

10. Private telephone conversation (May 20, 1954).

11. Lawrence W. Jones and L. Jackson Laslett, LWJ-LJL/MAC-5 (September, 1953).

12. K. Johnsen, CERN proton-synchrotron lectures [M. Hildred Blewett, Ed Sect. III-3 (October, 1953).

13. The factor 1.17 in eq. (16) of the MAC report[6] represents the numerical value of $2\left[-\cos \phi_o - (\phi_o - \pi/2) \sin \phi_o\right]^{1/2}$, for $\phi_o = 5\pi/6$.

$\gamma \equiv -(d\omega/\omega_s) / (dp/p_s)$ and is only slightly less than unity under the conditions prevailing at injection and for which Johnsen's equation was written.

14. L. H. Johnston, Bull. of the American Physical Society, 1954 meeting in Washington D.C., paper C1.

15. John S. Nodvick and David S. Saxon, "on the Suppression of Coherent Radiation by Electrons in a Synchrotron", Technical Report No. 21, Department of Physics, University of California at Los Angeles Los Angeles, Calif., (May, 1954).

16. J. Schwinger, Phys. Rev. 75,1912-1925 (June 15, 1949).

17. J. Schwinger, Harvard Lectures, Autumn 1945.

18. L. I. Schiff, Rev. Sci. Inst. 17, 6-14 (January, 1946) -- esp. appendix, pp. 12-14.

19. J. Schwinger, "On Radiation by Electrons in a Betatron" (1945), unpublished manuscript kindly communicated by Professor Schwinger and cited as ref. 2 of our ref. 15.

CHARACTER OF PARTICLE MOTION

IN THE

MARK V FFAG ACCELERATOR

L. Jackson Laslett*

Department of Physics, Iowa State College†

and Midwestern Universities Research Association‡

(30 July 1955)

CONTENTS

LJL.MURA.5

I. INTRODUCTION

The Mark V or "spiral ridge" FFAG accelerator is a version, originally proposed by Kerst,[1,2] of the fixed-field class of A-G machines. In this design the general r^k increase of field with radius is modified, to produce alternate gradient focusing with no marked increase of circumference, by introducing a spatial ripple into the guide field so that the particles encounter regions in which the local "n" and restoring forces alternate. This is achieved by constructing a field which, in comparison with the average field at a given radius, is alternately higher and lower along oblique curves which all particles must cross. In practice such a field would be attained by the use of spiral ridges on the pole surfaces, supplemented, when required, by similarly disposed current-carrying conductors.

It is the purpose of this report to derive analytically information concerning the particle motion in the Mark V accelerator and, in Appendices, to record some techniques useful for further study of the motion by aid of the ILLIAC digital computer.

II. THE MAGNETIC FIELD

A. Form Assumed in the Median Plane:

Without the use of poles excessively close to the median plane, the type of variation of magnetic field which is most readily realizable is sinusoidal. To obtain a field which would subject the particles to alternate focusing forces, it was originally conceived that the field prescribed in the median plane be of the form

$$B_{zo} = -B_o (r/r_o)^k \left\{1 + f \sin\left[\frac{r - r_o}{\lambda\!\!\!^-}\right) - N\phi\right]\right\} .$$

In order that the field scale, however, in such a way that the essential features of its effect on all particles be the same,[3] it appears desirable to make the quantitatively minor modification of adopting the form

$$B_{zo} = -B_o (r/r_o)^k \left\{1 + f \sin\left[\frac{\ln(r/r_o)}{w} - N\phi\right]\right\} ,$$

with w constant. This revised form for the median plane field will be the basis for the remainder of this report. The momentum compaction is then clearly given by $(\Delta r/r)/(\Delta p/p) = \frac{1}{k+1}$.

From these expressions it is seen that N is the number of spiralling ridges passed over by a particle in going around the machine once in the θ direction. f is the fractional flutter, in the magnetic field, due to the ridges. Finally, if the radial width of the annulus is small in comparison to the outer radius, r_o, $\lambda = 2\pi\lambda\!\!\!^- = 2\pi r_o w$ is substantially the radial separation of the ridges. The angle by which the ridges spiral out from a reference circle is of the order N_W and in practice will be quite small. The exponent k is taken to be positive.

It will be convenient in what follows to work with dimensionless quantities defined as follows:

$$\left(\frac{r_1}{r_0}\right)^{k+1} \equiv \frac{p_1}{eB_0 r_0}$$

$$x \equiv \frac{r - r_1}{r_1}$$

LJL.MURA.5

$$y \equiv \frac{z}{r_1} \quad ;$$

the median plane field may then be written

$$B_{zo} = -\frac{p_1}{er_1}(1+x)^k \left\{1 + f \sin\left[\frac{1}{w}\ln(1+x) - N\theta\right]\right\},$$

where $N\phi = N\theta + \ln(r_1/r_o)$.

B. Development of Vector Potential:

To obtain the differential equations governing the particle motion it is desirable to characterize the magnetic field by a vector potential, which should be at least approximately compatible with the prescribed median plane field and with Maxwell's equations, in order that the resulting equations be rigorously Hamiltonian and the solutions thus satisfy Lieuville's theorem. In attempting to write suitable expansions for components of the field and vector potential, one may be guided by the consideration that x and y will themselves be quite small but that x/w and y/w may, in cases of practical interest, be comparable with unity. In the work described in the body of this report terms involving powers of these latter quantities will be retained so far as practicable, but no more than quite limited accuracy may be expected for values of x or y nearly as large as w. kx and ky, however, will be typically rather small (0.1). Also Nx and Ny are normally less than kx and ky.

We undertake an expansion of the median plane field, through cubic terms in x, to obtain

$$B_{zo} = -\frac{p_1}{er_1}(1+x)^k\left[1 + f\sin\left(\frac{x - \frac{1}{2}x^2 + \frac{1}{3}x^3}{w} - N\theta\right)\right]$$

$$= -\frac{p_1}{er_1}\left[A_0 + A_1x + A_2x^2 + A_3x^3\right],$$

where

$$A_0 = 1 - f\sin N\theta$$

$$A_1 = k + f\left(\frac{1}{w}\cos N\theta - k\sin N\theta\right)$$

$$A_2 = \frac{k(k-1)}{2} + f\left[\frac{k-\frac{1}{2}}{w}\cos N\theta + \left(\frac{1}{2w^2} - \frac{k(k-1)}{2}\right)\sin N\theta\right]$$

$$A_3 = \frac{k(k-1)(k-2)}{6} + f\left\{\frac{-\frac{1}{w^2} + 3k(k-2) + 2}{6w}\cos N\theta + \left[\frac{k-1}{2w^2} - \frac{k(k-1)(k-2)}{6}\right]\sin N\theta\right\}$$

Likewise, for use in what follows,

$$(1+x)B_{zo} = -\frac{p_1}{er_1}\left[B_o + B_1x + B_1x + B_2x^2 + B_3x^3\right],$$

where

$$B_o = 1 - f\sin N\theta$$

$$B_1 = k+1 + f\left(\frac{1}{w}\cos N\theta - (k+1)\sin N\theta\right)$$

$$B_2 = \frac{k(k+1)}{2} + f\left[\frac{k+\frac{1}{2}}{w}\cos N\theta + \left(\frac{1}{2w^2} - \frac{k(k+1)}{2}\right)\sin N\theta\right]$$

$$B_3 = \frac{(k+1)(k)(k-1)}{6} + f\left\{\frac{-\frac{1}{\omega^2}+3k^2-1}{6\omega}\cos N\theta + \left[\frac{k}{2\omega^2} - \frac{(k+1)(k)(k-1)}{6}\right]\sin N\theta\right\}$$

We now seek a vector potential such that A_r and A_z vanish at $z = 0$ (in general, the components A_θ and A_r will be even functions of z or y with A_r involving only y^2 and higher even powers of y, while A_z will be an odd function). Then in the median plane A_θ must satisfy[4]

$$\frac{1}{r_1}\frac{\partial}{\partial x}\left[(1+x)\, A_{\theta o}\right] = (1+z)B_{zo} \quad ,$$

leading to the possible solution

$$\frac{e}{p_1}(1+x)\, A_{\theta o} = C_1 x + C_2 x^2 + C_3 x^3 + C_4 x^4 \quad , \quad \text{or}$$

$$\frac{e}{p_1} A_{\theta o} = D_1 x + D_2 x^2 + D_3 x^3 + D_4 x^4 \quad ,$$

where

$$C_1 = -B_o = -1 + f\sin N\theta$$

$$C_2 = -\frac{B_1}{2} = -\frac{k+1}{2} + f\left(-\frac{1}{2\omega}\cos N\theta + \frac{k+1}{2}\sin N\theta\right)$$

$$C_3 = -\frac{B_2}{3} = -\frac{k(k+1)}{6} + f\left[-\frac{2k+1}{6\omega}\cos N\theta + \left(-\frac{1}{6\omega^2} + \frac{k(k+1)}{6}\right)\sin N\theta\right]$$

$$C_4 = -\frac{B_3}{4} = -\frac{k(k+1)(k-1)}{24} + f\left\{\frac{\frac{1}{\omega^2}-3k^2+1}{24\omega}\cos N\theta + \frac{1}{24}\left[-\frac{3k}{\omega^2} + k(k+1)(k-1)\right]\sin N\theta\right\}$$

$$D_1 = C_1 = -1 + f\sin N\theta$$

$$D_2 = C_2 - C_1 = -\frac{k-1}{2} + f\left(-\frac{1}{2\omega}\cos N\theta + \frac{k-1}{2}\sin N\theta\right)$$

$$D_3 = C_3 - C_2 + C_1 = -\frac{k^2-2k+3}{6} + f\left[-\frac{k-1}{3\omega}\cos N\theta + \left(-\frac{1}{6\omega^2} + \frac{k^2-2k+3}{6}\right)\sin N\theta\right]$$

$$\begin{aligned} D_4 &= C_4 - C_3 + C_2 - C_1 \\ &= -\frac{k^3-4k^2+7k-12}{24} \\ &\quad + f\left\{\frac{\frac{1}{\omega^2} - 3k^2+8k-7}{24\omega}\cos N\theta + \frac{1}{24}\left[\frac{-(3k+4)}{\omega^2} + k^3-4k^2+7k-12\right]\sin N\theta\right\} \end{aligned}$$

To develop the vector potential for points not in the median plane we employ a gauge in which div $\bar{A} = 0$ and note that, in the notation of E. S. Akeley,[4]

$$\begin{aligned} \bar{A}_t &\doteq \left\{1 - \frac{z^2\Delta_t}{2} + \frac{z^4\Delta_t\Delta_t}{24}\right\}\left[A_{\theta_0}\hat{e}_\theta\right] \\ &= A_{\theta_0}\hat{e}_\theta - \frac{z^2}{2}\left\{\left[(\nabla_t^2 A_{\theta_0}) - \frac{A_{\theta_0}}{r^2}\right]\hat{e}_\theta - \frac{2}{r^2}\frac{\partial A_{\theta_0}}{\partial\theta}\hat{e}_r\right\} \\ &\quad + \frac{z^4}{24}\left\{\left[\nabla_t^2\left(\nabla_t^2 A_{\theta_0} - \frac{A_{\theta_0}}{r^2}\right) - \frac{4}{r^4}\frac{\partial^2 A_{\theta_0}}{\partial\theta^2} - \frac{\nabla_t^2 A_{\theta_0} - \frac{A_{\theta_0}}{r^2}}{r^2}\right]\hat{e}_\theta\right. \\ &\quad \left. + \left[-\frac{2}{r^2}\frac{\partial}{\partial\theta}\left(\nabla_t^2 A_{\theta_0} - \frac{A_{\theta_0}}{r^2}\right) - 2\nabla_t^2\left(\frac{1}{r^2}\frac{\partial A_{\theta_0}}{\partial\theta}\right) + \frac{2}{r^4}\frac{\partial A_{\theta_0}}{\partial\theta}\right]\hat{e}_r\right\}. \end{aligned}$$

Likewise

$$A_z = -\left\{z - \frac{z^3}{6}\Delta_t\right\}\nabla_t\cdot\bar{A}_{\theta 0} .$$

In this way we find

$$\frac{e}{p_1} A_\theta = D_1 x + D_2 x^2 + D_3 x^3 + D_4 x^4$$

$$- \frac{y^2}{2} \Big[(D_1 + 2D_2) + (-2D_1 + 2D_2 + 6D_3 + D_1'')x$$

$$+ (3D_1 - 3D_2 + 3D_3 + 12D_4 - 2D_1'' + D_2'')x^2 \Big]$$

$$+ \frac{y^4}{24} \Big[3D_1 - 6D_2 + 12D_3 + 24D_4 - 2D_1'' + 4D_2'' \Big],$$

$$\frac{e}{p_1} A_r = \Big[D_1' x + (-2D_1' + D_2')x^2 \Big] y^2 + \frac{D_1' - 2D_2'}{6} y^4 \quad , \quad \text{and}$$

$$\frac{e}{p_1} A_z = -y \Big[D_1' x + (-D_1' + D_2')x^2 + (D_1' - D_2' + D_3')x^3 \Big]$$

$$+ \frac{y^3}{6} \Big[(-D_1' + 2D_2') + (3D_1' - 4D_2' + 6D_3' + D_1''')x \Big],$$

primes denoting differentiation with respect to θ. These components of the vector potential represent expansions through fourth order in x or y and, as a check, can be verified to satisfy

$$r_1 \nabla \cdot \bar{A} \equiv \frac{\partial A_z}{\partial y} + \frac{\partial A_r}{\partial x} + \frac{A_r}{1+x} + \frac{\partial A_\theta / \partial \theta}{1+x} = 0$$

through third order.

III. THE EQUATIONS OF MOTION

A. "Lagrangian" for Use in Principle of Least Action:

The differential equations governing the particle trajectories in the aforementioned magnetic field may be conveniently obtained from the principle of least action by use of the "space Lagrangian"

$$
\begin{aligned}
\mathcal{L}(x,y;x',y';\theta) &= pr_1\sqrt{(1+x)^2 + x'^2 + y'^2} + er_1\left[(1+x)A_\theta + x'A_r + y'A_z\right] \\
&\approx 1 + x + \frac{1}{2}\,\frac{x'^2+y'^2}{1+x} - \frac{1}{8}\left(x'^2+y'^2\right)^2 \\
&\qquad + \frac{e}{p}\left[(1+x)A_\theta + x'A_r + y'A_z\right] \\
&\cong 1 + \frac{1}{2}\,\frac{x'^2+y'^2}{1+x} - \frac{1}{8}\left(x'^2+y'^2\right)^2 + x \\
&\qquad + \frac{p_1}{p}\Big\{ D_1'x'xy^2 + \Big\{\left[-D_1'x + (D_1'-D_2')x^2\right]y \\
&\qquad\qquad + \left[-D_1'+2D_2'\right]\frac{y^3}{6}\Big\}\, y' + C_1x + C_2x^2 + C_3x^3 + C_4x^4 \\
&\qquad - \frac{y^2}{2}\Big[(D_1+2D_2) + (-D_1+4D_2+6D_3+D_1'')x \\
&\qquad\qquad + (D_1 - D_2 + 9D_3 + 12D_4 - D_1'' + D_2'')x^2 \\
&\qquad + \frac{y^4}{24}\left[3D_1 - 6D_2 + 12D_3 + 24D_4 - 2D_1'' + 4D_2''\right]\Big\},
\end{aligned}
$$

in which we have treated x′ and y′ as of the same order as x and y despite the fact that these derivatives may be expected to be some N times greater than the dependent variables themselves.

The Euler-Lagrange equations, if applied to the Lagrangian of the preceding paragraph, lead to differential equations for the motion which might be susceptible to solution by digital computations,[5] but which are not in a form most suitable for analytic study. The equation for the radial motion, in particular, is marked by the presence of a forcing

LJL.MURA.5

term f $\sin N\theta$ derived from the term $(1+C_1)x$ in the Lagrangian. It can, in fact, be shown that the magnitude of the (periodic) response to this forcing term is sufficient ($\cong - f/N^2$) that non-linear terms in the differential equations affect significantly the character of small amplitude betatron oscillations.[6,7] It is desirable, therefore, to undertake a change of dependent variable such that the forcing term is suppressed and the resulting equations, if then linearized, may be used to provide an analytic basis for determining the character of small-amplitude free oscillations.

The Lagrangian as written is in a form somewhat inconvenient for the analytical work to follow because of the presence of terms arising from centrifugal effects. Since the first derivative terms which result in the differential equations are in practice small for excursions of the order of the forced motion (at least in the case of "full-scale" high-energy accelerators), it is expedient to simplify the Lagrangian in such a way that the troublesome terms are removed but with the remaining terms of the differential equation modified only slightly. We accordingly continue by use of the following Lagrangian, which yields differential equations free from terms involving first derivatives of the dependent variables and, in the remaining terms of the equations, modifies only slightly the original terms involving y^2, xy, xy^2, x^2y, xy^3, and x^4:

$$\mathcal{L} \cong \frac{x'^2 + y'^2}{2} + x + \frac{x^2}{2}$$

$$+ \frac{P_1}{P}\left[E_1 x + E_2 x^2 + E_3 x^3 + E_4 x^4 + F_0 y^2 + F_1 x y^2 + F_2 x^2 y^2 + G y^4\right]$$

with $E_1 = C_1 \qquad F_0 = -\frac{D_1}{2} - D_2$

$$E_2 = C_2 + \frac{C_1}{2} \qquad F_1 \doteq \frac{D_1}{4} - \frac{5}{2}D_2 - 3D_3 - \frac{D_1''}{4}$$

$$E_3 = C_3 + \frac{2}{3}C_2 \qquad F_2 \doteq \frac{3}{8}D_1 - D_2 - \frac{27}{4}D_3 - 6D_4 - \frac{D_1''}{8} - \frac{D_2''}{4}$$

$$E_4 = C_4 + \frac{3}{4}C_3 \qquad G = \frac{D_1}{24} - \frac{D_2}{4} + \frac{D_3}{2} + D_4 - \frac{D_1''}{24} + \frac{D_2''}{12} .$$

B. The Forced Motion:

With the aim of separating out the major effect of the forced oscillations we now introduce the new dependent variable u by the substitution

$$x = K_1 \sin N\theta + K_2 \cos N\theta + u$$

a numerical integration for a particular example having suggested that the forced motion is in fact close to sinusoidal. The resulting Lagrangian (after subtracting a term which is a function only of θ) is:

$$\begin{aligned}
\mathcal{L} \doteq\ & \frac{u'^2 + y'^2}{2} + N(K_1 \cos N\theta - K_2 \sin N\theta)u' + [1 + K_1 \sin N\theta + K_2 \cos N\theta]u + \frac{u^2}{2} \\
& + \frac{p_1}{p}\Big\{\Big[E_1 + 2E_2(K_1 \sin N\theta - K_2 \cos N\theta) + 3E_3(K_1 \sin N\theta + K_2 \cos N\theta)^2 \\
& + 4E_4(K_1 \sin N\theta + K_2 \cos N\theta)^3\Big]u \\
& + [E_2 + 3E_3(K_1 \sin N\theta + K_2 \cos N\theta) + 6E_4(K_1 \sin N\theta + K_2 \cos N\theta)^2]u^2 \\
& + [E_3 + 4E_4(K_1 \sin N\theta + K_2 \cos N\theta)]u^3 + E_4 u^4 \\
& + [F_0 + F_1(K_1 \sin N\theta + K_2 \cos N\theta) + F_2(K_1 \sin N\theta + K_2 \cos N\theta)^2]y^2 \\
& + [F_1 + 2F_2(K_1 \sin N\theta + K_2 \cos N\theta)uy^2 \\
& + F_2 u^2 y^2 + G y^4\Big\} ,
\end{aligned}$$

LJL.MURA.5

of which we shall be chiefly interested in terms of second or lower order in the variables u, y.

This Lagrangian leads to a residual forcing term in the equation for the u-motion given by

$$
\begin{aligned}
&1+(N^2+1)(K_1 \sin N\theta + K_2 \cos N\theta) + \frac{p_1}{p}\Big[E_1 + 2E_2(K_1 \sin N\theta + K_2 \cos N\theta) \\
&\quad + 3E_3(K_1 \sin N\theta + K_2 \cos N\theta)^2 + 4E_4(K_1 \sin N\theta + K_2 \cos N\theta)^3\Big] \\
&\cong 1 + (N^2+1)(K_1 \sin N\theta + K_2 \cos N\theta) \\
&\quad + \frac{p_1}{p}\Big\{-1 + f \sin N\theta + \Big[-(k+2) + f\Big(-\frac{1}{\omega}\cos N\theta + (k+2)\sin N\theta\Big)\Big] \\
&\qquad\qquad [K_1 \sin N\theta + K_2 \cos N\theta] \\
&\quad + \Big[-\frac{k^2}{2} + f\Big(-\frac{k}{\omega}\cos N\theta + \Big(-\frac{1}{2\omega^2} + \frac{k^2}{2}\Big)\sin N\theta\Big)\Big](K_1 \sin N\theta + K_2 \cos N\theta)^2 \\
&\quad + \Big[-\frac{k^3}{6} + f\Big(\Big(-\frac{k^2}{2\omega} + \frac{1}{6\omega^3}\Big)\cos N\theta + \Big(-\frac{k}{2\omega^2} + \frac{k^3}{6}\Big)\sin N\theta\Big)\Big] \\
&\qquad\qquad (K_1 \sin N\theta + K_2 \cos N\theta)^3
\end{aligned}
$$

and is to be suppressed by suitable choice of the constants p_1/p, K_1, and K_2. It appears from this development that a measure of the adequacy of the analysis is afforded by the degree to which the values found for K_1/w and K_2/w are small in comparison to unity.

The forcing term contains the following Fourier-components, which may be made to vanish:

Constant Term: $1 + \frac{p_1}{p}\Big[-1 + \frac{1}{2}f\beta K_2 - \frac{1}{2}f\alpha K_1 + \frac{a}{2}(K_1^2 + K_2^2)$
$\quad + \frac{3}{8}f\,BK_2(K_1^2+K_2^2) + \frac{3}{8}f\,CK_1(K_1^2+K_2^2)\Big]$,

Coeff. of sin $N\theta$: $(N^2+1)K_1 + \frac{p_1}{p}\Big[f + \alpha K_1 + \frac{fc}{4}(3K_1^2 + K_2^2) + \frac{fb}{2}K_1K_2 + \frac{3}{4}AK_1(K_1^2+K_2^2)\Big]$,

LJL.MURA.5

Coeff. of cos $N\theta$: $(N^2+1)K_2 + \frac{p_1}{p}\left[\alpha K_2 + \frac{fb}{4}(K_1^2+3K_2^2) + \frac{fc}{2}K_1K_2 + \frac{3}{4}AK_1(K_1^2+K_2^2)\right]$,

where

$$\alpha = -(k+2) \qquad \beta = -\frac{1}{w}$$

$$a = -\frac{k^2}{2} \qquad b = -\frac{k}{w} \qquad c = -\frac{1}{2w^2} + \frac{k^2}{2}$$

$$A = -\frac{k^3}{6} \qquad B = -\frac{k^2}{2w} + \frac{1}{6w^3} \qquad C = -\frac{k}{2w^2} + \frac{k^3}{6} \quad .$$

We have attempted to find solutions which make these coefficients vanish when the machine parameters lie within what may be considered the normal range of values. In this way we find:

$$K_1 \doteq -\frac{f}{N^2-(k+1)+\frac{3}{8}\left(\frac{f}{\omega N}\right)^2} \doteq \frac{f}{N^2-(k+1)} \;,$$

$$K_2 \doteq \frac{f^3 k}{4\omega N^6}$$ or very nearly zero, and

$$p_1/p \doteq 1 - \frac{k+2}{2}\left(\frac{f}{N}\right)^2 .$$

The forced motion is thus represented approximately by:

$$x_{\text{forced}} \doteq -\frac{1}{2}\,\frac{k+2}{k+1}\left(\frac{f}{N}\right)^2 - \frac{f}{N^2-(k+1)}\left[\sin N\theta - \frac{k}{4w}\left(\frac{f}{N^2}\right)^2\cos N\theta\right]$$

$$\cong -\frac{1}{2}\left(\frac{f}{N}\right)^2 - \frac{f}{N^2-(k+1)}\sin N\theta$$

$$x'_{\text{forced}} \doteq -\frac{Nf}{N^2-(k+1)}\left[\cos N\theta + \frac{k}{4\omega}\left(\frac{f}{N^2}\right)^2\sin N\theta\right]$$

$$\cong -\frac{Nf}{N^2-(k+1)}\cos N\theta \;;$$

accordingly, at $\theta = 0$, the "fixed points" are given by

$$x_{\text{fixed}} \cong -\frac{1}{2}\left(\frac{f}{N}\right)^2$$

$$x'_{\text{fixed}} \cong -\frac{Nf}{N^2-(k+1)}$$

and the amplitude of the forced motion is given approximately by the magnitude of the coefficient $-\frac{f}{N^2-(k+1)}$.

The validity of these results is expected, as noted previously, to be measured by the degree to which K_1/w or $\frac{f/w}{N^2-(k+1)}$ is small in comparison to unity.

C. Character of Small-Amplitude Betatron Oscillations:

For small-amplitude oscillations about the equilibrium orbit, the governing differential equations will be of the form

$$u'' + F_u u = 0$$

$$y'' + F_y y = 0 \quad .$$

On the basis of the Lagrangian of the previous sub-section, the spring factors which determine the frequencies of the oscillations are respectively (neglecting $\frac{p_1 - p}{p}$, K_2, and powers of K_1 above the first):

$$\begin{aligned} F_u &= -1 - 2\,E_2 - 6\,K_1\,E_3 \sin N\theta \\ &\cong k+1+\frac{f}{\omega}\cos N\theta - \frac{(f/\omega)^2}{N^2-(k+1)}\sin^2 N\theta \\ &= k+1-\frac{1}{2}\frac{(f/\omega)^2}{N^2-(k+1)} + \frac{f}{\omega}\cos N\theta + \frac{1}{2}\frac{(f/\omega)^2}{N^2-(k+1)}\cos 2N\theta \end{aligned}$$

$$F_y = -2\, F_o - 2\, K_1\, F_1 \sin N\theta$$
$$\cong -k - \frac{f}{\omega} \cos N\theta + \frac{(f/\omega)^2}{N^2-(k+1)} \sin^2 N\theta$$
$$= -k + \frac{1}{2}\frac{(f/\omega)^2}{N^2-(k+1)} - \frac{f}{\omega}\cos N\theta - \frac{1}{2}\frac{(f/\omega)^2}{N^2-(k+1)}\cos 2N\theta \; .$$

The linearized equations representing small-amplitude betatron oscillations are seen to be of the Hill type. Some aids for the solution of these equations -- especially for the determination of stability boundaries and the characteristic exponents (σ_u and σ_y) of the motion -- are noted in Appendix III. As Kerst has pointed out,[8] useful orientation is readily provided, however, by application of the "smooth approximation" technique introduced by Symon.[9] If the normally-small contributions from the cos $2N\theta$ terms are ignored and if k+1 is neglected in comparison to N^2, the smooth approximation leads to differential equations of the form

$$u'' + \nu_u^2\, u = 0$$

$$y'' + \nu_y^2\, y = 0 \; ,$$

where
$$\nu_u^2 \doteq k+1 - \frac{1}{2}\left(\frac{f}{\omega N}\right)^2 + \frac{1}{2}\left(\frac{f}{\omega N}\right)^2$$
$$= k+1 \qquad \text{and}$$
$$\nu_y^2 \doteq -k + \frac{1}{2}\left(\frac{f}{\omega N}\right)^2 + \frac{1}{2}\left(\frac{f}{\omega N}\right)^2$$
$$= \left(\frac{f}{\omega N}\right)^2 - k \; .$$

It is thus seen that the frequency of the free radial oscillations is substantially determined by the exponent characterizing the radial

LJL.MURA.5

increase of average field strength, while axial stability may be obtained concurrently if $(\frac{f}{w\ N})^2$ is sufficiently large to dominate -k.

It will be noted that these features of the betatron motion differ markedly from the performance which would be expected on the basis of an expansion about a circular reference orbit while ignoring the presence of the forced oscillations. This situation can be understood physically[6,7] by reference to a diagram on which are drawn contours of constant magnetic field strength in the median plane, with the expected equilibrium orbit superposed (Fig. 1). One notes that the field gradient is in a sense to favor radial focusing over a smaller interval of θ if one examines the gradient in the neighborhood of the scalloped curve than if one merely examined it along a line of constant radius.

IV. ILLIAC STUDIES OF THE PARTICLE MOTION

Although the results of the foregoing analytical work are believed to describe reasonably well the general character of particle motion in typical Mark V machines, it is clearly desirable to study the motion in representative structure of this type by means of digital computation. Such a program not only would provide a useful check on the analytical results and provide information concerning structures for which the approximations which we have introduced are invalid, but can take account of the inherently non-linear character of the dynamical equations and provide accurate information concerning stability regions. Work directed toward these ends is listed below:

(i) Exact differential equations governing the motion in the median plane have been prepared for use with the ILLIAC ("Ridge Runner" program).

(ii) Relatively simple, approximate differential equations for the three-dimensional motion have been prepared, attempting to take account of the fact that x/w and y/w may be large (comparable with unity), but supposing that variables x and y themselves will be small ("Feckless Five" program).

(iii) More accurate, but somewhat more elaborate, differential equations for the three-dimensional motion have also been set up by Vogt-Nilsen, based on recent vector-potential developments[4] of E. S. Akeley ("Feckful Five" program).[10] These computer programs are being directed toward a comprehensive study of the particle dynamics in Mark V machines, chiefly through the efforts of the Illinois group.

In Appendices I and II to follow we outline the development of the equations listed as (i) and (ii) above. In Appendix III we describe some techniques which have been applied for obtaining information concerning solutions to the Hill equation developed in Section IV of this report. In Appendix IV we make some numerical comparisons, in certain examples, between results obtained from the analytic theory and from the ILLIAC computer. As Appendix V we present a stability diagram computed from the analytic theory.

V. NOTES AND REFERENCES

*Temporarily at Accelerator Development Department, Brookhaven National Laboratory, Upton, L.I., N.Y.

†Institute for Atomic Research and Ames Laboratory of the U.S. Atomic Energy Commission.

‡Assisted by the National Science Foundation.

[1]D. W. Kerst, et al., MURA-DWK/KMT/LWJ/KRS-3 (November 12, 1954); D. W. Kerst, MURA-DWK-7 (November 17, 1954); Revision MURA-DWK-7 (March 2, 1955); D. W. Kerst, et al., Bull. Amer. Phys. Soc. 30, No. 1, Paper D5 (January 27, 1955).

[2]Subsequent relevant reports include D. W. Kerst, MURA/DWK-10 (May 10, 1955); MURA-DWK-11 (June 27, 1955).

[3]The failure of the originally proposed field to scale the essential features exactly would, on the basis of linear theory applicable to small amplitude betatron oscillations, result in the traversal of a couple of resonances (integral or half-integral) by the operating point of some typical machines.

[4]While this work was in progress a report by E. S. Akeley [ESA(MURA-1), dated January 26, 1955] appeared which systematizes this procedure. Subsequent reports, ESA(MURA-2) and ESA(MURA-3) have extended this technique.

[5]A more accurate formulation for use with digital computation is presented, however, in Appendix II.

[6]This point has been brought out previously in informal communication: letters to D. W. Kerst, dated 21, 23, and 25 January 1955; 1955 Sesquimonthly MURA technical meetings at Northwestern University, Indiana University, and the University of Minnesota.

[7]L. J. Laslett, Bull. Amer. Phys. Soc. 30, No. 3, Paper T8 (April 30, 1955).

[8]D. W. Kerst, private telephone conversation, 25 January 1955.

[9]K. R. Symon, KRS(MURA)-1, -4 (July 1 and August 10, 1954).

[10]Cf.Nils Vogt-Nilsen, MURA/NVN/2 (June, 1955), where a more general complex field is treated.

[11]L. J. Laslett, LJL(MAC)-4 (March-April, 1954), eq. (4), p. 2.

[12]I am indebted to Dr. J.N. Snyder for advice on this point.

[13]Cf. L. J. Laslett, MURA Notes (1 February 1955).

[14]E. Courant and H. Snyder, B.N.L. Report EDC-15 (September 2, 1954).

[15]L.J. Laslett, supplement to MURA Notes cited[15] (31 May 1955).

[17]Letter to J. N. Snyder (11 July 1955).

APPENDIX I

EXACT DIFFERENTIAL EQUATIONS FOR MOTION IN THE MEDIAN PLANE

For the accurate exploration of the character of particle motion in the median plane of the Mark V accelerator, and for aid in checking results obtained by other methods, exact differential equations governing this motion were prepared in a form suitable for ILLIAC computation. It is clear that this is possible, since the field -- and hence the nature of the forces -- is prescribed in the median plane. The resultant program has been termed the "Ridge Runner."

For z identically zero, the equation of motion is [11]

$$\frac{d}{d\phi}\left(\frac{r'}{\sqrt{r^2+r'^2}}\right) = \frac{r}{\sqrt{r^2+r'^2}} + \frac{e}{P}\, r B_z$$

With $r = r_1\,(1+x)$,

$$\frac{d}{d\phi}\left(\frac{x'}{\sqrt{(1+x)^2+x'^2}}\right) = \frac{1+x}{\sqrt{(1+x)^2+x'^2}} + \frac{e r_1}{P}\,(1+x) B_z$$

We let $p_x = \dfrac{x'}{\sqrt{(1+x)^2+x'^2}}$, or $x' = (1+x)\dfrac{p_x}{\sqrt{1-p_x^2}}$,

and put $eB_o(r_1/r_o)^k\, r_1 = p_1$, $\qquad N\theta = N\phi + \ln(r_o/r_1)$

to obtain the simultaneous first order differential equations

$$p_x' = \sqrt{1-p_x^2} - \frac{p_1}{p}(1+x)^{k+1}\left\{1 + f\sin\left[\frac{1}{w}\ln(1+x) - N\theta\right]\right\}$$

$$x' = (1+x)\frac{p_x}{\sqrt{1-p_x^2}} .$$

[These equations are clearly in Hamiltonian form, since $\partial x'/\partial x = -\partial p_x'/\partial p_x$, the "Hamiltonian" being

$$H \propto -(1+x)\sqrt{1-p_x^2} - \frac{er_1}{p}\int^x (1+x) B_z \, dx$$

$$= -(1+x)\sqrt{1-p_x^2} + \frac{p_1}{p}\int^x (1+x)^{k+1}\left\{1 + f \sin\left[\frac{1}{w} \ln(1+x) - N\phi\right]\right\} dx$$

in which the second term represents the contribution $-\frac{e}{p}\frac{r}{r_1} A_0$ from the vector potential.] For automatic digital computation, r_1 may be taken so that $p_1 = p$ (for convenience).

LJL.MURA.5

APPENDIX II

APPROXIMATE DIFFERENTIAL EQUATIONS OF MOTION

In the attempt to permit relatively simple exploration of three-dimensional Mark V motion with the ILLIAC, relatively simple differential equations of motion have been formulated. The intention was to retain the dominant influence of the quantity x/w, which is not necessarily small in comparison to unity, but to make approximations consistent with the supposition that z and kx will be small in most cases of interest. The resulting program is termed the "Feckless Five".

We employ the notation

$$x = \frac{r - r_1}{r_1} \qquad y = \frac{z}{r_1} \qquad (r_1/r_o)^k = \frac{p_1}{e\,B_o\,r_1}$$

$$\delta = \tan^{-1}\left[(k+1)w\right] \qquad \sec\delta = \left[1 + (k+1)^2 w^2\right]^{1/2}$$

$$\alpha - i\beta = \left[1 - (k^2 + k + 1 - N^2)w^2 - i2(k+1)w\right]^{1/2}$$

$$\doteq \left[1 - (k^2 - N^2)w^2 - 2i\,k\,w\right]^{1/2}$$

$$N\theta = N\phi + \ln(r_o/r_1) \quad .$$

The field in the median plane is taken to be

$$B_{zo} = -\frac{p_1}{er_1}(1+x)^k\left\{1 + f\sin\left[\frac{1}{w}\ln(1+x) - N\theta\right]\right\}$$

$$\cong -\frac{p_1}{er_1}\left\{(1+x)^k + f\frac{e^{(k+1)x}}{1+x}\left(1 - \frac{k+1}{2}x^2\right)\left[\sin\left(\frac{x}{w} - N\theta\right) - \frac{x^2}{2w}\cos\left(\frac{x}{w} - N\theta\right)\right]\right\}$$

$$\cong -\frac{p_1}{er_1}\left\{(1+x)^k + f\frac{e^{(k+1)x}}{1+x}\sin\left(\frac{x}{w} - N\theta\right) - \frac{f\sec\delta}{1+x}\frac{x^2}{2w}\cos(N\theta+\delta)\right\} ,$$

in which we regard the last term as a small correction.

If the vector potential in the median plane is taken to have a θ-component only, we employ the relation

$$(1+x)\ B_{zo} = \frac{\partial}{\partial x}\left[\frac{1+x}{r_1} A_{\theta o}\right]$$

to obtain

$$-\frac{e}{p_1}(1+x)A_{\theta_o} \doteq \frac{(1+x)^{k+2}}{k+2} - \frac{f\omega e^{(k+1)x}}{\sec\delta}\cos\left(\frac{x}{\omega} - N\theta + \delta\right)$$
$$- f\sec\delta\frac{x^3}{6\omega}\cos(N\theta+\delta)$$

or
$$-\frac{e}{p_1} A_{\theta_o} \doteq \frac{(1+x)^{k+1}}{k+2} - \frac{f\omega e^{kx}}{\sec\delta}\cos\left(\frac{x}{\omega} - N\theta+\delta\right)$$
$$- f\sec\delta\ \frac{x^3}{6\omega}\cos(N\theta+\delta)\ .$$

For developing the vector potential at points not necessarily in the median plane, we note

$$\mathrm{div}_t\ A_{\theta o} \doteq Nf\omega\ \frac{e^{(k+1)x}}{\sec\delta}\ \sin\left(\frac{x}{\omega} - N\theta + \delta\right)$$
$$+\ \text{Term of order}\ \frac{Nf x^3}{3\omega}$$

and apply the methods[4] used previously in Section IIB to obtain

$$-\frac{e}{p_1}(1+x)A_\theta \doteq \frac{(1+x)^{k+2}}{k+2} - k\frac{y^2}{2}(1+x)^k + \frac{k^2(k-2)}{24}y^4(1+x)^{k-2}$$
$$-\frac{f\omega}{\sec\delta}e^{(k+1)x}\left[\frac{\cos\left(\frac{x}{\omega} - N\theta+\delta\right)\ \cosh\frac{\alpha y}{\omega}\cos\beta y}{\sin\left(\frac{x}{\omega} - N\theta+\delta\right)\ \sinh\frac{\alpha y}{\omega}\sin\beta y}\right],$$

$$-\frac{e}{p_1}A_z \doteq \frac{Nf\omega}{\sec\delta}\ y\ e^{(k-1)x}\ \sin\left(\frac{x}{\omega} - N\theta + \delta\right).$$

$-\frac{e}{p_1} A_r \doteq 0$ (being of order wy^2).

The equations of motion are now obtained by use of these vector potential components in the Lagrangian[11]

$$\mathcal{L} = \left[(1+x)^2 + x'^2 + y'^2\right]^{1/2} + \frac{e}{p}\left[(1+x)A_\theta + x'A_r + y'A_z\right]$$

$$\doteq 1 + x + \frac{x'^2 + y'^2}{2(1+x)} + \frac{e}{p}\left[(1+x)A_\theta + y'A_z\right] \quad \text{(since we take } A_r \doteq 0\text{)}$$

or the Hamiltonian

$$\mathcal{H} = -(1+x)\left[1 - p_x 2 - (p_y - \frac{e}{p}A_z)^2\right]^{1/2} - \frac{e}{p}(1+x)A_\theta$$

$$\doteq -(1+x)\left[1 - \frac{p_x 2 + (p_y - \frac{e}{p}A_z)^2}{2}\right] - \frac{e}{p}(1+x)A_\theta \quad .$$

One thus obtains, if p_1 is set equal to p:

$$x' = (1+x)\, p_x$$

$$y' = (1+x)\, A$$

$$\begin{aligned} p_x' = & -(k+1)x - \frac{k(k+1)}{2}x^2 - \frac{(k+1)k(k-1)}{6}x^3 + \frac{k^2}{2}y^2 + \frac{k^2(k-1)}{2}xy^2 \\ & - \frac{f}{\sec\delta} e^{(k+1)x}\Big\{\left[\sin(\tfrac{x}{w} - N\theta + \delta) - (k+1)w\cos(\tfrac{x}{w} - N\theta + \delta)\right]\cosh\tfrac{\alpha y}{w}\cos\beta y \\ & \quad - \left[\cos(\tfrac{x}{w} - N\theta + \delta) + (k+1)w\sin(\tfrac{x}{w} - N\theta + \delta)\right]\sinh\tfrac{\alpha y}{w}\sin\beta y\Big\} \\ & + \frac{f\sec\delta}{2w}(x^2 - y^2)\cos(N\theta + \delta) - \frac{p_x^2}{2} - \frac{A^2}{2} \\ & - \frac{Nf}{\sec\delta}(1+x)\,y\,e^{(k-1)x} A\left[\cos(\tfrac{x}{w} - N\theta + \delta) + (k-1)w\sin(\tfrac{x}{w} - N\theta + \delta)\right]. \end{aligned}$$

$$
\begin{aligned}
p_y' = {} & ky + k^2 xy + \frac{k^2(k-1)}{2} x^2 y - \frac{k^2(k-2)}{6} y^3 \\
& + \frac{f}{\sec\delta} e^{(k+1)x} \Big\{ \Big[\alpha \sin\left(\tfrac{x}{w} - N\theta + \delta\right) - \beta w \cos\left(\tfrac{x}{w} - N\theta + \delta\right) \Big] \cosh \tfrac{\alpha}{w} y \sin \beta y \\
& \qquad + \Big[\alpha \cos\left(\tfrac{x}{w} - N\theta + \delta\right) + \beta w \sin\left(\tfrac{x}{w} - N\theta + \delta\right) \Big] \sinh \tfrac{\alpha}{w} y \cos \beta y \Big\} \\
& - \frac{f \sec\delta}{w} xy \cos(N\theta + \delta) - \frac{Nfw}{\sec\delta} (1+x) e^{(k-1)x} A \sin\left(\tfrac{x}{w} - N\theta + \delta\right),
\end{aligned}
$$

where

$$
A = p_y + \frac{Nf\,w}{\sec\delta}\, y\, e^{(k-1)x} \sin\left(\frac{x}{w} - N\theta + \delta\right) .
$$

It is believed that solutions of these equations for certain cases, involving motion in the median plane only, have been in good agreement with solutions of the exact equations of the "Ridge Runner" program. More accurate, and more elaborate, differential equations for the three dimensional motion have been in preparation by N. Vogt-Nilsen,[10] guided by E. S. Akeley's treatment[4] of the vector potential.

APPENDIX III

VARIATIONAL METHOD FOR DETERMINING STABILITY BOUNDARIES AND CHARACTERISTIC EXPONENTS FOR THE HILL EQUATION

By the change of variable $N\theta = 2\tau$, the Hill equation encountered in the body of this report may be put into the standard form:

$$\frac{d^2Y}{d\tau^2} + (A + B\cos 2\tau + C\cos 4\tau)Y = 0 .$$

Information relating the coefficients of this equation at the stability boundaries may be obtained conveniently by variational methods, since the equation then has a periodic solution. By considering the "isoperimetric" problem

$$\delta \int_0^\pi \left[\frac{1}{2} Y'^2 - (B\cos 2\tau + C\cos 4\tau)Y^2\right] d\tau = 0$$

$$\int_0^\pi \frac{1}{2} Y^2 \, d\tau = 1 ,$$

with A playing the role of the Lagrange multiplier, we arrive at the result

$$A = \left[\frac{\int_0^\pi \frac{1}{2}\left[Y'^2 - (B\cos 2\tau + C\cos 4\tau)Y^2\right] d\tau}{\int_0^\pi \frac{1}{2} Y^2 d\tau}\right]_{min.}$$

By use of trial solutions

$$Y = 1 + 2P\cos 2\tau + 2Q\cos 4\tau + \ldots$$

or $Y = \cos\tau + U\cos 3\tau + V\cos 5\tau + \ldots$

the expression to be minimized may be put into an algebraic form appropriate to the $\sigma = 0$ or $\sigma = \pi$ boundaries, respectively. This form is suited to rapid solution by a high-speed digital computer[12] -- by the minor modification of leaving the normalization of the trial functions unspecified, the same general technique may be used to provide simultaneous homogeneous linear equations suitable for solution with a desk computer.[13]

With a bit more algebraic complexity similar methods may be applied to estimate the relation between the parameters of the differential equation and values of σ away from the stability boundaries. For this purpose one notes that on the basis of the Floquet theory, as Courant and Snyder have pointed out,[14] solutions may be written in the "phase-amplitude" form

$$Y(\tau) = w(\tau)\, e^{+i\left[L\tau + \psi(\tau)\right]} ,$$

where, in the stable case, $w(\tau)$ and $\psi(\tau)$ are real periodic functions with the period (π) of the equation and L is a real constant equal to σ/π. One then considers the variational statement

$$\delta \int_0^\pi \frac{1}{2}\left[w'^2 - (B\cos 2\tau + C\cos 4\tau)w + (L+\psi')^2 w^2\right. d\tau = 0$$

$$\int_0^\pi \frac{1}{2} w^2\, d\tau = 1 ,$$

LJL.MURA.5

to obtain

$$A = \left[\frac{\int_0^{\pi} \frac{1}{2} \left[w'^2 - (B \cos 2\tau + C \cos 4\tau) w^2 + (L + \psi')^2 w^2 \right] d\tau}{\int_0^{\pi} \frac{1}{2} w^2 \, d\tau} \right]_{min}$$

By use of trial functions

$$w = 1 + 2P \cos 2\tau + 2Q \cos 4\tau + \ldots,$$

$$\psi' = 2R \cos 2\tau + 2S \cos 4\tau + \ldots,$$

the expression to be minimized again assumes an algebraic form which, by aid of high-speed computation, can give estimates of the value of A associated with specified values of B, C, and $L = \sigma/\pi$.

The foregoing methods have been used in ILLIAC computations to provide tables[15] giving the estimated values of A for values of the remaining parameters in the range

L: 0 (0.1) 1.0

B: 0 (0.2) 5.0

C: -2.5 (0.5) 2.5 ,

together with the values found for the coefficients of the trial functions. For convenient use, and because the estimates of A are somewhat inaccurate for values of L close to but less than unity, supplementary graphs[16] have been prepared from these data giving (i) A vs. $\cos\sigma$ for various values of B and C and (ii) A vs. B for various values of C and σ.

LJL.MURA.5

As has been remarked, the foregoing methods appear to suffer somewhat in regard to accuracy for values of L near but less than unity, although very close agreement with known values for the stability limits is found in those cases for which comparison can be made. It is believed that close to the $= \pi$ limit the form assumed for the trial function which represents ψ' is not favorable. It may, therefore, be appropriate to mention a modification[17] of the variational procedure which might be useful if more accurate results should be desired for other applications. In this modification the single trial function w is employed, use being made of the identity $w^2(L+\psi') = K^2$, a constant.

Specifically,

$$\pi L \equiv \sigma = \int_0^{\pi} (L+\psi')\, d\tau = K^2 \int_0^{\pi} \frac{1}{w^2}\, d\tau = K^2 \pi \left\langle \frac{1}{w^2} \right\rangle,$$

or $$K^2 = \frac{L}{\left\langle \frac{1}{w^2} \right\rangle} .$$

Since, as has been noted,

$$A = \left[\frac{\left\langle w'^2 - (B\cos 2\tau + C\cos 4\tau) w^2 + (L+\psi')^2 w^2 \right\rangle}{\langle w^2 \rangle} \right]_{min.},$$

we obtain the equivalent result

$$A = \left[\frac{\langle w'^2 \rangle - \langle (B\cos 2\tau + C\cos 4\tau) w^2 \rangle + \frac{L^2}{\left\langle \frac{1}{w^2} \right\rangle}}{\langle w^2 \rangle} \right]_{min.}$$

For convenience one may make the change of variable

$$v \equiv w^2$$

LJL.MURA.5

to obtain

$$A = \left[\frac{\frac{1}{4}\left\langle \frac{v'^2}{v} \right\rangle - \left\langle (B\cos 2\tau + C\cos 4\tau)v \right\rangle + \frac{L^2}{\left\langle \frac{1}{v} \right\rangle}}{\langle v \rangle} \right]_{min.}$$

These expressions are conveniently homogeneous of degree zero in their respective trial functions. The trial functions should be non-zero, continuous, have a continuous derivative, be periodic with the period π, and (in the case considered here) be even about 0 and $\pi/2$. By virtue of the property last mentioned, the averaging need then be taken only over the interval 0 to $\pi/2$. A limited number of hand-computed exampled with simple trial functions indicate that this modified procedure will give good results, even for values of L near unity, although in practice some of the integrations associated with the averaging process may have to be performed numerically.

If the trial function v is taken to be of the form

$$v = 1 + 2P_1 \cos 2\tau + 2P_2 \cos 4\tau \ldots,$$

we thus obtain

$$A \leq \left[\frac{1}{4}\left\langle \frac{(4P_1 \sin 2\tau + 8P_2 \sin 4\tau + \cdots)}{1 + 2P_1\cos 2\tau + 2P_2 \cos 4\tau + \cdots} \right\rangle + \frac{L^2}{\left\langle \frac{1}{1+2P_1\cos 2\tau + 2P_2 \cos 4\tau + \cdots} \right\rangle} - BP_1 - CP_2 \right]_{min}$$

In tabulating the results of a minimization procedure based on this method, it would be desirable to include the value of $\langle 1/v \rangle$, since an estimate of $1/(L+\psi')^{1/2}$, which equals $\left[\frac{v}{L}\left\langle\frac{1}{v}\right\rangle\right]^{1/2}$, is useful in judging the amplitude resulting from scattering and for determining the displacement of the equilibrium orbit due to misalignments.

LJL.MURA.5

APPENDIX IV

NUMERICAL COMPARISON WITH ILLIAC RESULTS

In the table which follows we give comparisons between the results obtained for radial motion with the ILLIAC, using the exact equations of motion, and the corresponding values predicted by the equations of this report.

The theoretical equations used for estimation of the fixed points are

$$x_{fixed} = -\frac{1}{2}(f/N)^2$$

$$x'_{fixed} = -\frac{Nf}{N^2 - (k+1)} \cong F x_{fixed} .$$

For comparison with known results in one case, we take the predicted amplitude (about the fixed point) for the forced oscillation as

$$= \frac{f}{N^2 - (k+1)} .$$

The phase shift, σ_u, experienced by the small-amplitude radial betatron oscillations in traversing one period is given by the smooth approximation as

$$\sigma_u = \frac{2\pi\sqrt{k+1}}{N} .$$

For a more reliable estimate, we determine the coefficients A, B, and C in the standard Hill equation

$$\frac{d^2u}{d\tau^2} + (A + B \cos 2\tau + C \cos 4\tau)u = 0 \quad ,$$

using the relations

$$A = \left(\frac{2}{N}\right)^2 \left[k + 1 - \frac{1}{2} \frac{(f/\omega)^2}{N^2 - (k+1)} \right]$$

$$B = \left(\frac{2}{N}\right)^2 \frac{f}{\omega}$$

$$C = \left(\frac{2}{N}\right)^2 \frac{1}{2} \frac{(f/\omega)^2}{N^2 - (k+1)} \quad ,$$

and then interpolate σ_u from the graphs mentioned in Appendix III.

As one measure of the extent to which one might expect in advance accurate results from the theory, we list the quantity $\frac{f/w}{N^2 - (k+1)}$, which should be small in comparison to unity.

It should also be mentioned that the examples given do not necessarily represent practicable combinations of machine parameters, the first example being in fact axially unstable and others having possibly undesirably large values for σ_u.

COMPARISON WITH ILLIAC RESULTS

Machine Parameters						Fixed Points		Forced Amplitude				
k	k' = k+1	f	1/w	N	$\frac{f/w}{N^2-(k+1)}$	Theor. x / x'	Observed	Theoretical	Observed	A / B / C		
75	76	0.25	167	27	0.064	-0.000043	-0.00004			0.4097	0.65π	
						-0.01034	-0.0104			0.2291	0.65π	0.65π
										0.0073		
75	76	0.25	1047	27	0.401	-0.000043	-0.00004			0.1291	0.65π	
						-0.01034	-0.0108			1.4372	0.82π	0.79π
							Approx.			0.2879		
299	300	0.25	4000	52	0.416	-0.0000116	-0.0000144	0.000104	0.0000987	0.137		
						-0.00541	-0.00564			1.48		
										0.307		
150	151	0.25	2094	37	0.430	-0.000023	-0.00004			0.1125	0.66π	
						-0.0076	-0.0079			1.53	0.91π	0.86π
							Approx.			0.3287		

APPENDIX V

DIAGRAM OF STABILITY REGION

The first stability region has been plotted (Fig. 2) as a function of machine parameters on the basis of the theory presented in this report and assisted by the graphs[16] describing the character of solutions to the Hill equation. The basic variables are k/N^2 and $f/(wN^2)$, for $k \gg 1$, and the computed results are expected to apply for small-amplitude betatron oscillations most accurately when the ordinates are small in comparison to unity (say $\frac{f}{wN^2} < \frac{1}{3}$). A more accurate plot of this character could be prepared, if required, by use of ILLIAC solutions of more accurate equations of motion.

LJL(MURA)-5, Sequel
1 August 1955

PARTICLE MOTION

IN THE

MARK V FFAG

[The following material is intended to represent an abbreviated presentation containing the essential elements of the material in Sections II B & III A,B, C of LJL(MURA)-5 .]

Expansion of the Magnetic Field:

We proceed on the supposition that there is interest in examining the particle motion under conditions such that

$$k < \frac{1}{w}, \quad N^2 < \frac{k}{w}, \quad \text{and} \quad \frac{x}{w} < 1,$$

this last inequality being consistent with the results to be obtained if $\frac{f}{wN^2} < 1$ and if attention is confined to small-amplitude betatron oscillations about the (non-circular) equilibrium orbit.

The prescribed median- plane field may be expanded

$$B_{zo} \doteq -\frac{p_1}{er_1}\left[1+kx+\frac{k(k-1)}{2}x^2\right]\left[1+f\sin\left(\frac{x-1/2\ x^2}{w}-N\theta\right)\right]$$

$$= -\frac{p_1}{er_1}\left[1+kx+\frac{k(k-1)}{2}x^2\right]\left[1+f\,\frac{x-1/2\ x^2}{w}\cos N\theta \right.$$

$$\left. -f\left(1-\frac{x^2}{2w^2}\right)\sin N\theta\right]$$

$$= -\frac{p_1}{er_1}\left\{\left[1-f\sin N\theta\right] + \left[k+f\left(\frac{1}{w}\cos N\theta-k\sin N\theta\right)\right]x\right.$$

$$+\frac{k(k-1)}{2} + f\left(\frac{k-1/2}{w}\cos N\theta + \left[\frac{1}{2w^2} - \frac{k(k-1)}{2}\right]\sin N\theta\right)\Bigg] x^2\Bigg\}$$

$$\cong \frac{-p_1}{er_1}\left\{\left[1 - f\sin N\theta\right] + \left[k + f\left(\frac{1}{w}\cos N\theta - k\sin N\theta\right)\right]x + \frac{f}{2}\left[\frac{2k}{w}\cos N\theta + \frac{1}{w^2}\sin N\theta\right] x^2\right\}.$$

The magnetic field components off the median plane may be written by aid of series expansions consistent with the vanishing of the curl and divergence (cylindrical coordinates) [Cf. LJL(MAC)-4, with

$$\alpha = 0 \qquad a = 0$$

$$\beta = -f\sin N\theta \qquad b \cong -\frac{f}{3}\left[\frac{2k}{w}\cos N\theta + \frac{1}{w^2}\sin N\theta\right]$$

$$\Phi = 0 \qquad c = 0$$

$$n = -k + f\left[-\frac{1}{w}\cos N\theta + k\sin N\theta\right)\Bigg]:$$

$$B_z = \frac{-p_1}{er_1}\left\{\left[1 - f\sin N\theta\right] + \left[k + f\left(\frac{1}{w}\cos N\theta - k\sin N\theta\right)\right]x + \frac{f}{2}\left[\frac{2k}{w}\cos N\theta + \frac{1}{w^2}\sin N\theta\right](x^2 - y^2)\right\}$$

$$B_r = -\frac{p_1}{er_1}\left\{\left[k + f\left(\frac{1}{w}\cos N\theta - k\sin N\theta\right)\right]y + f\left(\frac{2k}{w}\cos N\theta + \frac{1}{w^2}\sin N\theta\right)xy\right\}$$

$$B_\theta = \frac{p_1}{er_1}\left\{Nfy\cos N\theta + \ldots\right\}$$

and will be ignored since it can only interact with the velocity components x' or y' and does not contain $\frac{1}{w}$ in its coefficient.

For subsequent use we then take, to this order,

$$\frac{er_1}{p_1}(1+x)^2 B_z = \left[-1 + f\sin N\theta\right] + \left[-(k+2) + f\left(-\frac{1}{w}\cos N\theta\right.\right.$$
$$\left.\left. + (k+2)\sin N\theta\right)\right] x + \frac{f}{2}\left[\frac{2k}{w}\cos N\theta + \frac{1}{w^2}\sin N\theta\right](y^2 - x^2)$$

$$\frac{er_1}{p_1}(1+x) B_r = \left[-k + f\left(-\frac{1}{w}\cos N\theta + k\sin N\theta\right)\right] y - \left[\frac{2k}{w}\cos N\theta\right.$$
$$\left. + \frac{1}{w^2}\sin N\theta\right] xy$$

$$B_\theta = 0.$$

The Equations of Motion:

The equations of motion are given rigorously by [LJL(MAC)-4, Sect. 2]:

$$\frac{d}{d\theta}\left\{\frac{x'}{\sqrt{(1+x)^2 + x'^2 + y'^2}}\right\} = \frac{1+x}{\sqrt{(1+x)^2 + x'^2 + y'^2}}$$
$$+ \frac{er_1}{p}\left[(1+x)\ B_z - y'\ B_\theta\right]$$

$$\frac{d}{d\theta}\left\{\frac{y'}{\sqrt{(1+x)^2 + x'^2 + y'^2}}\right\} = -\frac{er_1}{p}\left[(1+x)\ B_r - x'\ B_\theta\right].$$

These equations of motion will be reasonably-well duplicated (if x'^2 and $y'^2 << 1$ and if B_θ is ignored) by the differential equations resulting from the Lagrangian

$$\mathcal{L} = \frac{x'^2 + y'^2}{2} + x + 1/2\ x^2 + \psi(x,y,\theta),$$

if $\quad \dfrac{\partial \psi}{\partial x} = \dfrac{er_1}{p}(1+x)^2 B_z \quad$ and $\quad \dfrac{\partial \psi}{\partial y} = -\dfrac{er_1}{p}(1+x)B_r .$

We thus find it possible to work with a simple Lagrangian or Hamiltonian system, selecting

$$\psi = \frac{p_1}{p}\Big\{\Big[-1+f\sin N\theta\Big] x + 1/2\Big[-(k+2) + f\Big(-\frac{1}{w}\cos N\theta + (k+2)\sin N\theta\Big)\Big] x^2 + 1/2\Big[k + f\Big(\frac{1}{w}\cos N\theta - k\sin N\theta\Big)\Big] y^2 + \frac{f}{6}\Big[\frac{2k}{w}\cos N\theta + \frac{1}{w^2}\sin N\theta\Big](3xy^2 - x^3)\Big\} .$$

For convenience we shall select r_1 so that $p_1 = p$.

The Forced Motion:

Because of the presence of a forced oscillation in the x-motion, we undertake to study the free oscillations by suppressing the forcing term through a suitable change of dependent variable. We select for this purpose the transformation

$$x = K_0 + K_1 \sin N\theta + K_2 \cos N\theta + u,$$

a numerical integration in a particular case having suggested that the forced motion is close to sinusoidal; we shall, in fact, find that of the three coefficients introduced in this transformation, the coefficient K_1 plays the dominant role.

The Lagrangian then becomes effectively (dropping terms which depend only on θ):

$$
\begin{aligned}
\mathcal{L} = {} & \frac{u'^2 + y'^2}{2} + (NK_1\cos N\theta - NK_2\sin N\theta)\,u' + \Big\{ \left[f\sin N\theta\right] \\
& + \left[-(k+1) + f\left(-\tfrac{1}{w}\cos N\theta + (k+2)\sin N\theta\right)\right] (K_0 + K_1\sin N\theta \\
& + K_2\cos N\theta\,)\Big\}\,u \; -1/2\, f\left[\frac{2k}{w}\cos N\theta + \frac{1}{w^2}\sin N\theta\right](K_0 \\
& + K_1\sin N\theta + K_2\cos N\theta)^2 + 1/2\Big\{\Big[-(k+1) + f\left(-\tfrac{1}{w}\cos N\theta\right. \\
& \left.+ (k+2)\sin N\theta\right)\Big] - f\left[\frac{2k}{w}\cos N\theta + \frac{1}{w^2}\sin N\theta\right] \cdot \left[K_0 + K_1\sin N\theta + K_2\cos N\theta\right]\Big\}\,u^2 \\
& + 1/2\Big\{\left[k + f\left(\tfrac{1}{w}\cos N\theta - k\sin N\theta\right)\right] + f\left[\frac{2k}{w}\cos N\theta + \frac{1}{w^2}\sin N\theta\right] \cdot \left[K_0 + K_1\sin N\theta + K_2\cos N\theta\right]\Big\}\,y^2
\end{aligned}
$$

$+$ terms of order uy^2 and u^3.

The forcing term extracted from this Lagrangian has the main Fourier components

<u>Constant term</u>: $\quad -(k+1)K_0 + f\,\dfrac{k+2}{2}K_1 - \dfrac{f}{2w}K_2$;

<u>Coeff. of sin Nθ</u>: $\quad f + \left[N^2 - (k+1)\right]K_1 - \dfrac{3}{8}\,\dfrac{f}{w^2}K_1^2 + f(k+2)K_2$; and

<u>Coeff. of cos Nθ</u>: $\quad -\dfrac{f}{w}K_0 - f\dfrac{k}{4w}K_1^2 + \left[N^2 - (k+2)\right]K_2$;

in which we have neglected additional terms of second or higher order in the quantities K_0, K_1, K_2 and which prove to be comparatively small.

For values of the machine parameters lying in the range of interest, these Fourier components can be caused to vanish by selecting the constants to have values given approximately as follows:

$$K_1 \doteq -\frac{f}{N^2 - (k+1) + \frac{3}{8}\left(\frac{f}{wN}\right)^2}$$

$$\cong -\frac{f}{N^2 - (k+1)} \quad ;$$

$$K_0 \doteq \frac{k+2}{k+1} \; \frac{f}{2} \; K_1$$

$$\cong -1/2\left(\frac{f}{N}\right)^2 \quad \text{and is fairly small;}$$

K_2 is very small, being of the order

$$\cong \frac{f}{4} \; \frac{k}{w} \; \frac{K_1^2}{N^2} \cong \frac{k f^3}{4wN^6} .$$

The forced motion is thus represented approximately by:

$$x_{\text{forced}} \doteq -1/2\left(\frac{f}{N}\right)^2 - \frac{f}{N^2 - (k+1)} \sin N\theta ,$$

$$x'_{\text{forced}} \doteq -\frac{Nf}{N^2 - (k+1)} \cos N\theta ,$$

and the "fixed points", evaluated at $\theta = 0$, are given by

$$x_{\text{fixed}} \doteq -1/2\left(\frac{f}{N}\right)^2, \quad x'_{\text{fixed}} \doteq -\frac{Nf}{N^2 - (k+1)} .$$

Likewise, the amplitude of the forced motion is given approximately by the magnitude of the coefficient $-\frac{f}{N^2 - (k+1)}$.

In closing this section it may be re-emphasized that the foregoing analysis will not be expected to apply unless $|K_1|/w$, or $\frac{f/w}{N^2 - (k+1)}$, is small in comparison to unity.

Character of Small-Amplitude Betatron Oscillations:

For small-amplitude oscillations about the equilibrium orbit, the governing differential equations will be of the form:

$$u'' + F_u u = 0$$

$$y'' + F_y y = 0$$

On the basis of the Lagrangian indicated previously, the spring factors which determine the frequencies of the free oscillations are respectively:

$$F_u = k + 1 + f\left(\frac{1}{w}\cos N\theta - (k+2)\sin N\theta\right) + f\left(\frac{2k}{w}\cos N\theta + \frac{1}{w^2}\sin N\theta\right)(K_0 + K_1 \sin N\theta + K_2 \cos N\theta)$$

$$\cong k + 1 + \frac{f}{w}\cos N\theta + \frac{fK_1}{w^2}\sin^2 N\theta$$

$$= \left[(k+1) + \frac{fK_1}{2w^2}\right] + \frac{f}{w}\cos N\theta - \frac{fK_1}{2w^2}\cos 2N\theta$$

$$\triangleq \left[(k+1) - 1/2\,\frac{(f/w)^2}{N^2 - (k+1)}\right] + \frac{f}{w}\cos N\theta + 1/2\,\frac{(f/w)^2}{N^2 - (k+1)}\cos 2N\theta,$$

$$F_y = -k + f\left(-\frac{1}{w}\cos N\theta + k\sin N\theta\right) - f\left(\frac{2k}{w}\cos N\theta + \frac{1}{w^2}\sin N\theta\right)(K_0 + K_1 \sin N\theta + K_2 \cos N\theta)$$

$$\cong -k - \frac{f}{w}\cos N\theta - \frac{fK_1}{w^2}\sin^2 N\theta$$

$$= \left[-k - \frac{fK_1}{2w^2}\right] - \frac{f}{w}\cos N\theta + \frac{fK_1}{2w^2}\cos 2N\theta$$

$$\doteq \left[-k + 1/2 \frac{(f/w)^2}{N^2 - (k+1)}\right] - \frac{f}{w} \cos N\theta$$

$$- 1/2 \frac{(f/w)^2}{N^2 - (k+1)} \cos 2N\theta ,$$

in which we have rejected small out-of-phase terms.

These linearized equations representing small-amplitude betatron oscillations are seen to be of the Hill type. Some approximate tables have been constructed to aid in the solution of these differential equations. As Kerst has pointed out, however, useful orientation is readily provided by application of the "smooth approximation" technique introduced by Symon. If the nomally - small contributions from the cos 2Nθ terms are ignored and if $k+1$ is neglected (for convenience) in comparison to N^2, the smooth approximation leads to differential equations of the form

$$u'' + v_u^2 \; u = 0$$

$$y'' + v_y^2 y = 0,$$

where

$$v_u^2 \doteq k + 1 - 1/2 \left(\frac{f}{wN}\right)^2 + 1/2 \left(\frac{f}{wN}\right)^2$$

$$= k + 1$$

$$v_y^2 \doteq -k + 1/2 \left(\frac{f}{wN}\right)^2 + 1/2 \left(\frac{f}{wN}\right)^2$$

$$= \left(\frac{f}{wN}\right)^2 - k.$$

It is thus seen that the frequency of the free radial oscillations is substantially determined by the exponent characterizing the radial increase of average field-strength, while axial stability may be obtained concurrently if $(\frac{f}{wN})^2$ is sufficiently large to dominate - k. The nature of the restoring forces, and hence the magnitudes of the oscillation frequencies, when recognition is taken of the scalloped equilibrium orbit, differ markedly from what would be expected from an expansion about a circular reference orbit with the effect of the forcing terms ignored.

L. Jackson Laslett
Iowas State College

ADDENDUM - August 12, 1955

The following calculated coordinates may be of use although a more accurate story would be given by a remaping based on ILLIAC solutions of more accurate equations of motion. For large values of the orginate (values of f/wN^2 near the top of the diagram ∽ say $> 1/3$), my theory may overestimate σ_H a bit.

Values of k/N^2

σ_H	0	0.2 π	0.4 π	0.6 π	0.8 π	1.0 π
f/wN^2=0	0	0.01	0.04	0.09	0.16	0.25
0.1	0	0.007(?)	0.038	0.087_5	0.155	0.205
0.2	0	0.009	0.038	0.082	0.135	0.169
0.3	-0.0006(?)	0.0098	0.034	0.072	0.114_5	0.138
0.4	-0.0009(?)	0.0086	0.030	0.064	0.094	0.110
0.5	-0.006(?)	0.009	0.028	0.054	0.079	0.093

σ_V	0	0.2 π	0.4 π	0.6 π	0.8 π	1.0 π
f/wN^2=0	0	-0.01	-0.04	-0.09	-0.16	-0.25
0.1	0.010	0	-0.028	-0.078	-0.142	-0.196
0.2	0.040	0.030	+0.003	0.043	-0.095	-0.128
0.3	0.091	0.082	0.056	+0.018	-0.025	-0.049
0.4	0.167	0.159	0.134	0.100	+0.065	+0.046
0.5	0.280	0.269	0.244	0.210	0.179	0.164

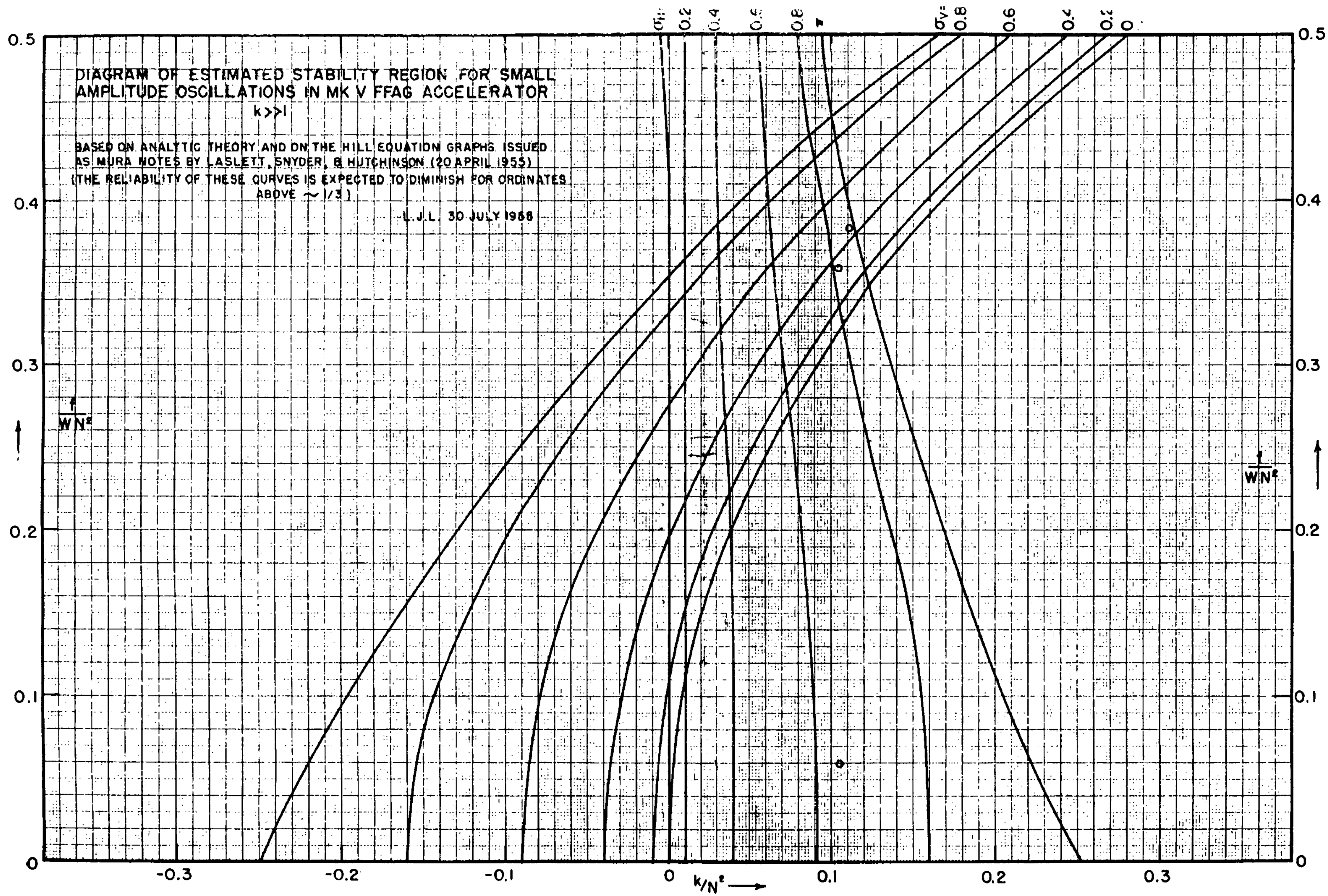
DIAGRAM OF ESTIMATED STABILITY REGION FOR SMALL AMPLITUDE OSCILLATIONS IN MK V FFAG ACCELERATOR
k>>1
BASED ON ANALYTIC THEORY AND ON THE HILL EQUATION GRAPHS ISSUED AS MURA NOTES BY LASLETT, SNYDER, & HUTCHINSON (20 APRIL 1955)
(THE RELIABILITY OF THESE CURVES IS EXPECTED TO DIMINISH FOR ORDINATES ABOVE ~ 1/3)
L.J.L. 30 JULY 1955
f/WN²
k/N²
σv= 0.8
0.6
0.4
0.2
0
0.2
0.4
0.6
0.8
π
-0.3
-0.2
-0.1
0
0.1
0.2
0.3
0.5
0.4
0.3
0.2
0.1

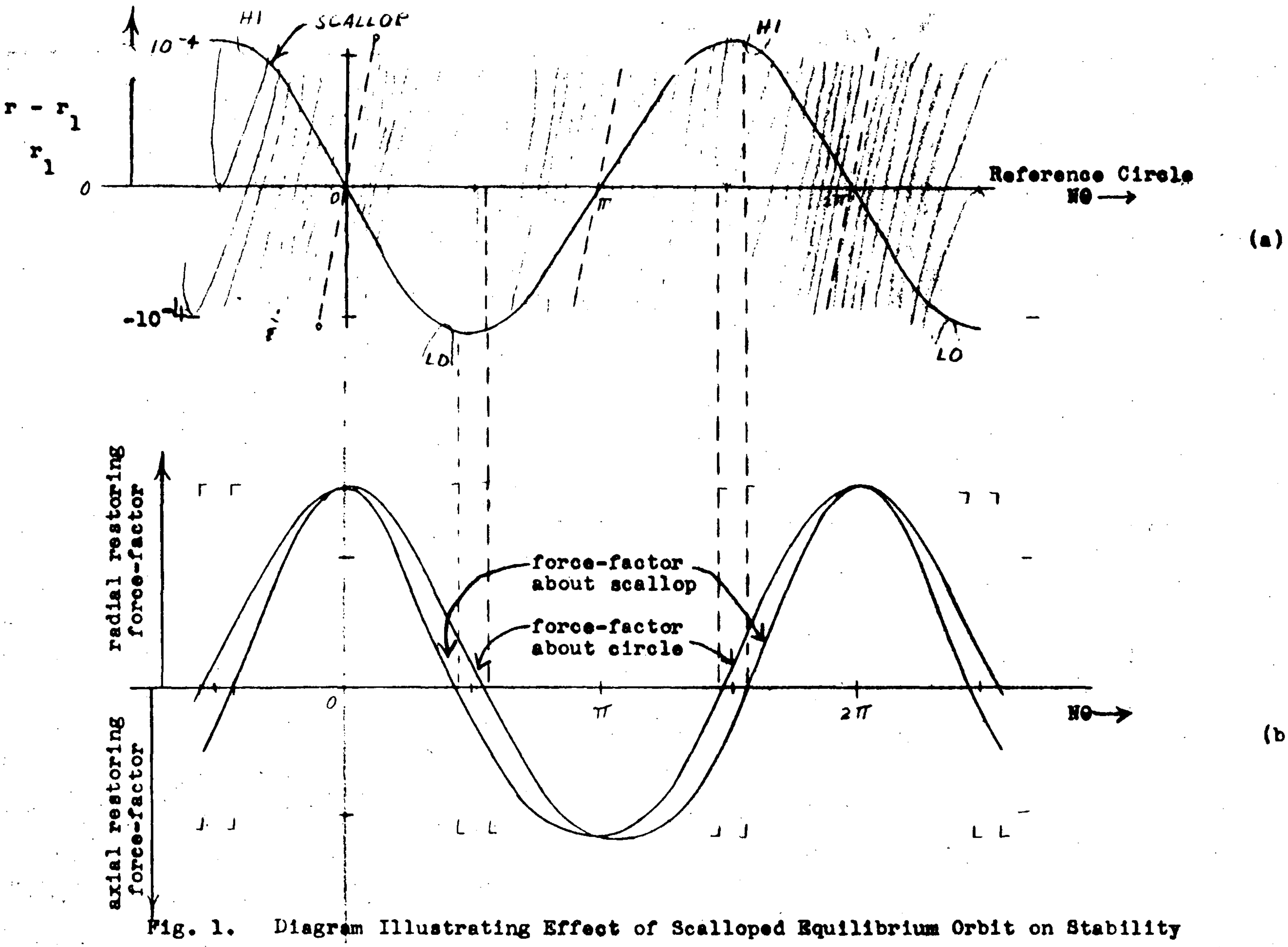

Fig. 1. Diagram Illustrating Effect of Scalloped Equilibrium Orbit on Stability

(a). Contour lines of Magnetic Field

(b). Force-factors for Motion about Circular and Scalloped Reference Curve

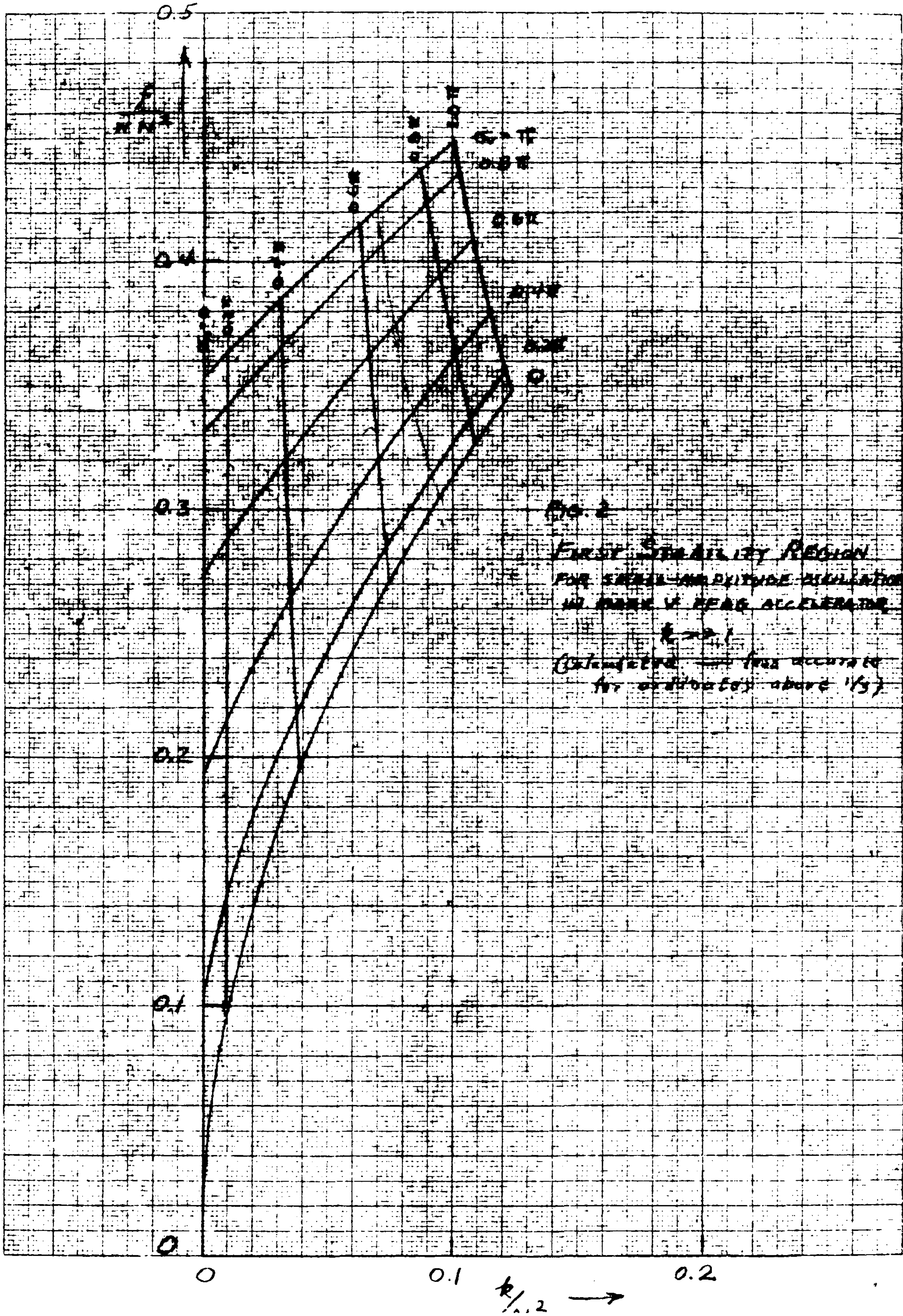

Fig. 2

First Stability Region

for small-amplitude oscillations in Mark V FFAG accelerator

$k \to 1$

(Calculated — less accurate for ordinates above 1/3)

MURA-206
Internal

MIDWESTERN UNIVERSITIES RESEARCH ASSOCIATION*

REMARKS ON THE INVARIANT QUADRATIC FORMS PERTAINING TO MOTION CHARACTERIZED BY A LINEAR DIFFERENTIAL EQUATION WITH PERIODIC COEFFICIENT

L. Jackson Laslett+

November 21, 1956

ABSTRACT: The nature and interpretation of the invariant quadratic forms are reviewed and means for determining the coefficients are outlined. Computation of such quadratic forms can be helpful in following the secular growth of "amplitude" in certain cases involving coupling resonances.

* Supported by Contract AEC #AT(11-1)-384

+ On leave from Iowa State College.

1. The solutions of the linear equation (forced motion absent)

$$x'' + F(\theta)\, x = 0,$$

with $F(\theta)$ periodic with period T, may be conveniently expressed

$$\begin{pmatrix} x \\ x' \end{pmatrix}_{\theta+T} = \begin{pmatrix} A & B \\ C & D \end{pmatrix} \begin{pmatrix} x \\ x' \end{pmatrix}_{\theta}.$$

Here A, B, C, D are periodic functions of θ (period T) such that

$$\begin{vmatrix} A & B \\ C & D \end{vmatrix} = 1 \qquad \text{(constancy of the Wronskin)}$$

$$\frac{dA}{d\theta} = BF + C \qquad \frac{dB}{d\theta} = D - A$$

$$\frac{dC}{d\theta} = (D - A)F \qquad \frac{dD}{d\theta} = -(BF + C) \qquad \text{(Appendix A)}$$

$$1/2 \text{ Trace} \equiv 1/2\,(A + D) = \cos\sigma\text{, an invariant.}$$

Solutions at homologous points may be related by

$$\begin{pmatrix} x \\ x' \end{pmatrix}_{\theta+nT} = \begin{pmatrix} A & B \\ C & D \end{pmatrix}^n \begin{pmatrix} x \\ x' \end{pmatrix}_{\theta} = \begin{pmatrix} \cos n\sigma - \frac{1}{2}\frac{B_0'}{\sin\sigma}\sin n\sigma & \frac{B_0}{\sin\sigma}\sin n\sigma \\ \frac{1}{B_0\sin\sigma}\left[\sin^2\sigma + \frac{1}{4}B_0'\right]\sin n\sigma & \cos n\sigma + \frac{1}{2}\frac{B_0'}{\sin\sigma}\sin n\sigma \end{pmatrix} \begin{pmatrix} x \\ x' \end{pmatrix}_{\theta};$$

the solution at an <u>any</u> θ may moreover be expressed in terms of the initial values x_0 and x_0'

$$y(\theta) = \sqrt{\frac{B(\theta)}{B_0}}\left\{\left[\cos\phi - \frac{1}{2}\frac{B_0'}{\sin\sigma}\sin\phi\right]x_0 + \left[\frac{B_0}{\sin\sigma}\sin\phi\right]x_0'\right\},$$

where $\varphi = (\sin\sigma)\displaystyle\int_0^\theta \frac{d\theta}{B}$

2. The quantity

$$I^2 = -Cx^2 + (A - D)\, x x' + B x'^2$$

constitutes an invariant of the motion. (Appendix B)

In particular it is of interest to construct from this the two quantities

$$R^2 = \frac{-C}{\sin\sigma}x^2 + \frac{A-D}{\sin\sigma}x x' + \frac{B}{\sin\sigma}x'^2,$$ an invariant throughout the motion,

and

$$K^2 = \frac{-CB}{\sin^2\sigma} x^2 + \frac{(A-D)B}{\sin^2\sigma} x x' + \frac{B^2}{\sin^2\sigma} x'^2 ,$$

an invariant at homologous points.

The first of these gives the invariant R^2 which is $1/\pi$ times the area of the ellipse described by the phase-point (x, x') plotted at homologous points; the second gives the quantity K representing the maximum displacement for the particular set of homologous points chosen.

3. Writing

$$R^2 = a x^2 + b x x' + c x'^2$$

and

$$K^2 = \xi x^2 + \eta x x' + \zeta x'^2 ,$$

the coefficients may be expressed in terms of the parameters of the ellipse described by the phase-point $(x, x' = y)$ (Appendix C):

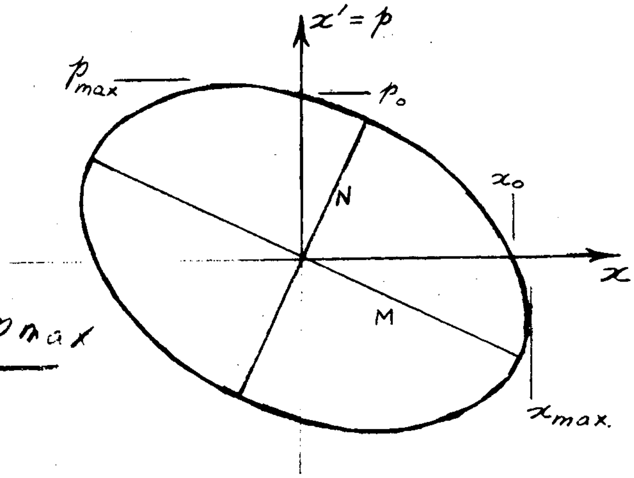

$$a = \frac{p_{max}}{x_o}$$

$$b = \pm 2 \sqrt{\frac{x_{max}\, p_{max}}{x_o\, p_o} - 1}$$

$$c = \frac{x_{max}}{p_o}$$

$$ac - 1 = \left(\frac{b}{2}\right)^2$$

$$\xi = \left(\frac{x_{max}}{x_o}\right)^2 = \left(\frac{p_{max}}{p_o}\right)^2 = \frac{x_{max}\, p_{max}}{x_o\, p_o}$$

$$\eta = \pm 2 \frac{x_{max}}{p_o} \sqrt{\frac{x_{max}\, p_{max}}{x_o\, p_o} - 1}$$

$$\zeta = \left(\frac{x_{max}}{p_o}\right)^2$$

$$\xi\zeta - 1 = \frac{\eta^2}{4\xi}$$

with the sign of the square root selected to be positive if the major axis lies in the II^{nd} & IV^{th} quadrants, and conversely.

4. Alternatively, of course, the coefficients a, b, c; ξ, η, ζ may be computed from the matrix elements A, B, C, D by aid of two one-sector runs between successive homologous points of the type of interest.

Thus, most simply, if a run is commenced with $y' = 0$,

$$A = y_1/y_0$$

$$C = y_1'/y_0 \, ;$$

and a run commenced with $y = 0$,

$$B = y_1/y_0'$$

$$D = y_1'/y_0' \, .$$

(If $F(\theta)$ possesses symmetry about the reference point, $A = D = \cos\sigma$ & $-C = \frac{\sin^2\sigma}{B}$; The matrix elements and $\cos\sigma$ may then be obtained, if desired, through the use of formulas pertaining to two runs each of length T/2.)

5. The square root of a quadratic form, such as R, may be evaluated by a convenient construction:

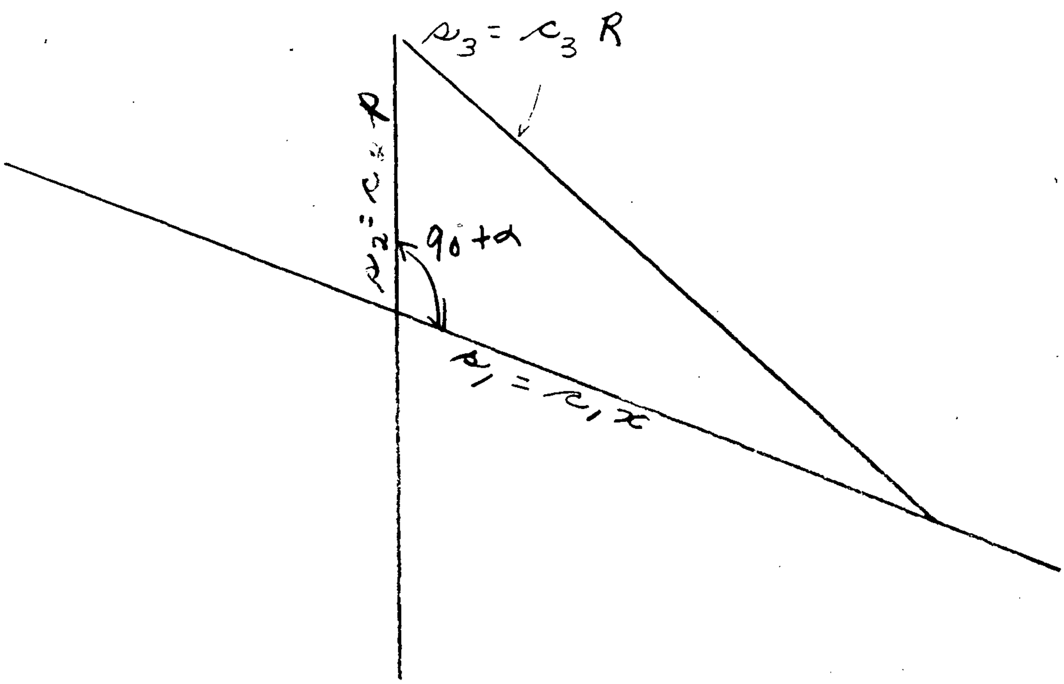

$$c_3^2 R^2 = c_1^2 x^2 + 2 c_1 c_2 (\sin\alpha) x p + c_2^2 p^2$$

Choose $\left(\frac{c_1}{c_3}\right)^2 = a$, i.e., $c_1 = c_3\sqrt{a}$;

$$\left(\frac{c_2}{c_3}\right)^2 = c , \qquad c_2 = c_3\sqrt{c} ;$$

$$2\,\frac{c_1 c_2}{c_3^2}\sin\alpha = b, \qquad \sin\alpha = \frac{1}{2}\,\frac{b}{\sqrt{ac}} .$$

APPENDIX A -- Proof of the differential relations for A, B, C, D:

To first order we expand

$$((M[\theta|\theta+\delta\theta]))((M)) = ((M+\delta M))((M[\theta|\theta+\delta\theta]))$$

$$\begin{pmatrix} 1 & \delta\theta \\ -F\delta\theta & 1 \end{pmatrix}\begin{pmatrix} A & B \\ C & D \end{pmatrix} = \begin{pmatrix} A+\delta A & B+\delta B \\ C+\delta C & D+\delta D \end{pmatrix}\begin{pmatrix} 1 & \delta\theta \\ -F\delta\theta & 1 \end{pmatrix}$$

$$\begin{pmatrix} A+C\delta\theta & B+D\delta\theta \\ C-AF\delta\theta & D-BF\delta\theta \end{pmatrix} = \begin{pmatrix} A+\delta A-BF\delta\theta & B+\delta B+A\delta\theta \\ C+\delta C-DF\delta\theta & D+\delta D+C\delta\theta \end{pmatrix}$$

$$\delta A = (BF+C)\,\delta\theta \qquad \delta B = (D-A)\,\delta\theta$$

$$\delta C = (D-A)F\,\delta\theta \qquad \delta D = -(BF+C)\,\delta\theta\,.$$

APPENDIX B — Proof of the invariance of I:

Differentiation of the expression given for I^2 leads to:

$$\frac{dI^2}{d\theta} = -2Cxx' + (A-D)(x'^2 + xx'') + 2Bx'x'' - C'x^2 + (A'-D')xx' + B'x'^2$$

The terms $(A - D)\, x'^2$ and $B' x'^2$ cancel by virtue of the relation $B' = D - A$. Employing the relation $x'' = -Fx$,

$$\frac{dI^2}{d\theta} = (-2C + A' - D' - 2BF)xx' - [C' + F(A-D)]x^2,$$

which vanishes by virtue of the relation

$$A' = -D' = BF + C$$

$$C' = (D-A)F.$$

APPENDIX C -- The interpretation of R^2 and K^2:

in the ellipse

$$\left(\frac{x\cos\beta - p\sin\beta}{M}\right)^2 + \left(\frac{x\sin\beta + p\cos\beta}{N}\right)^2 = 1,$$

$$x_0 = \left[\left(\frac{\cos\beta}{M}\right)^2 + \left(\frac{\sin\beta}{N}\right)^2\right]^{-1/2}$$

$$p_0 = \left[\left(\frac{\sin\beta}{M}\right)^2 + \left(\frac{\cos\beta}{N}\right)^2\right]^{-1/2}$$

$$x_{max} = MN/p_0$$

$$p_{max} = MN/x_0 .$$

1. We form

$$R^2 = \frac{p_{max}}{x_0} x^2 \pm 2\left[\frac{x_{max}\,p_{max}}{x_0 p_0} - 1\right]^{1/2} xp + \frac{x_{max}}{p_0} p^2$$

$$= MN\left\{\left[\left(\frac{\cos\beta}{M}\right)^2 + \left(\frac{\sin\beta}{N}\right)^2\right]x^2 \pm 2\left[\sin^2\beta\cos^2\beta\left(\frac{1}{M^4}+\frac{1}{N^4}\right) - \frac{1-\sin^4\beta-\cos^4\beta}{M^2N^2}\right]^{1/2} xp + \left[\left(\frac{\sin\beta}{M}\right)^2 + \left(\frac{\cos\beta}{N}\right)^2\right]p^2\right\}$$

$$= MN\left\{\left[\left(\frac{\cos\beta}{M}\right)^2 + \left(\frac{\sin\beta}{N}\right)^2\right]x^2 + 2\sin\beta\cos\beta\left(\frac{1}{N^2}-\frac{1}{M^2}\right)xp + \left[\left(\frac{\sin\beta}{M}\right)^2 + \left(\frac{\cos\beta}{N}\right)^2\right]p^2\right\}$$

$$= MN = \frac{\text{area}}{\pi} .$$

2. The quantity K^2 is $\frac{x_{max}}{p_0} R^2$ and hence is invariant for any particular set of homologous points.

x_{max} occurs when $p = -\frac{\eta}{2\xi} x$ and

$$K^2 = \left(\xi - \frac{\eta^2}{4\xi}\right) x_{max}^2 = x_{max}^2 .$$

3. The maximum amplitude at <u>any</u> point along a given orbit may be expressed in terms of K at some reference point, or in terms of R or I:

$$x_{max,max} = K_{max} = \sqrt{\frac{\beta_{max}}{\beta_{ref}}}\, K_{ref}$$

$$= \sqrt{\frac{\beta_{max}}{\sin\sigma}}\, R$$

$$= \frac{\sqrt{\beta_{max}}}{\sin\sigma}\, I .$$

MURA-246
Internal

MIDWESTERN UNIVERSITIES RESEARCH ASSOCIATION*

CONCERNING THE y-GROWTH PHENOMENON EXHIBITED BY ALGEBRAIC TRANSFORMATIONS

L. Jackson Laslett**

March 11, 1957

ABSTRACT:

Hamiltonian algebraic transformations which can lead to extensive exponential y-growth are discussed in regard to the threshold for y-growth. Computational examples are given.

Contents

---

* Supported by Contract AEC No. AT(11-1)-384.

** On leave from Iowa State College, Ames, Iowa.

1. Motivation:

As is well known, non-linear coupling between the radial and axial motion in particle accelerators can lead to extensive exponential growth of the axial oscillations. The y-growth appears to be more rapid the further the x-amplitude is above a critical threshold value and the threshold becomes zero as a resonant relation between the radial and axial frequencies is approached. The amplitudes resulting from y-growth may differ sufficiently from those prevailing originally that instability is soon seen to develop, but in other cases the y-growth is found to "turn-over" and stability, for at least a limited interval of time, appears indicated.

Certain aspects of these phenomena have been studied both analytically and computationally. The computations may be based either on differential equations which represent closely those which govern particle motion in an actual accelerator or they may employ idealized differential equations which, it is supposed, contain the essential significant features of the exact equations. In either case, however, the computational time required for the integration of any particular problem is sufficiently great as normally to preclude carrying a single computation beyond a few hundred "sectors" -- i.e., through perhaps 100 oscillations.

It appears noteworthy that the y-growth and turn-over found by integration of differential equations for an AG (alternating-gradient) accelerator may be replicated fairly closely by a suitable non-AG problem and that, in the latter case, the particle does not appear to enter during the computation all regions of phase-space which are energetically available to it. Since some of the particles which the computations thus indicate as "stable", in the equivalent non-AG structure under consideration, have sufficient energy to become unstable by traversal of a pass in the potential-energy surface, there is some interest in the ultimate fate of such particles.

Because of the interest in more extended computations, attention is directed to the use of algebraic transformations, which may be performed with a speed perhaps two orders of magnitude greater than typical for solution of differential equations. Although a close equivalence between the differential equations and some specific transformation may be difficult to establish definitively, it appears possible to find transformations which describe well the general features of the solutions found computationally for the differential equations of interest.

We consider in this report a particular type of algebraic transformations which may be representative of motion influenced by the $\sigma_x = 2\sigma_y$ resonance. The scaling features and threshold for y-growth are discussed. Examples of computations through 1200 sectors, performed by the ALGYTEE program are also given.

2. Statement of the Algebraic Transformation Under Consideration:

We consider here a transformation in which the coupling is provided by the addition of y^2 terms to the equations for x, p_x and by the addition of xy terms to the equations for y, p_y:

$$\left.\begin{aligned}
x_n &= a_x x_{n-1} + b_x p_{x_{n-1}} + (\lambda/2)(b_x/b_y)\, y_{n-1}^2 \\
p_{x_n} &= c_x x_{n-1} + d_x p_{x_{n-1}} + (\lambda/2)(d_x/b_y)\, y_{n-1}^2 \\
y_n &= a_y y_{n-1} + b_y p_{y_{n-1}} + \lambda\, x_{n-1}\, y_{n-1} \\
p_{y_n} &= c_y y_{n-1} + d_y p_{y_{n-1}} + \lambda (d_y/b_y)\, x_{n-1}\, y_{n-1}
\end{aligned}\right\}, \qquad (1)$$

with $\begin{vmatrix} a_x & b_x \\ c_x & d_x \end{vmatrix} = 1, \quad \begin{vmatrix} a_y & b_y \\ c_y & d_y \end{vmatrix} = 1$, and the coupling terms selected to have coefficients which depend on a single parameter λ to insure that the transformation be Hamiltonian* (as adjudged from the bracket expressions).

If, for simplicity, we wish the diagonal members of the linear part of the x, p_x transformation to be equal and likewise for the y, p_y transformation (corresponding to the situation in which the amplitude functions for the associated Floquet solutions are stationary at the point of reference), we may put

$$\left.\begin{aligned} \begin{pmatrix} X \\ P_X \end{pmatrix}_j &= \begin{pmatrix} \alpha_x & 0 \\ \dfrac{a_x - d_x}{2\alpha_x b_x} & \dfrac{1}{\alpha_x} \end{pmatrix} \begin{pmatrix} x \\ p_x \end{pmatrix}_j \\ \text{and} \quad \begin{pmatrix} Y \\ P_Y \end{pmatrix}_j &= \begin{pmatrix} \alpha_y & 0 \\ \dfrac{a_y - d_y}{2\alpha_y b_y} & \dfrac{1}{\alpha_y} \end{pmatrix} \begin{pmatrix} y \\ p_y \end{pmatrix}_j . \end{aligned}\right\} \quad (2)$$

In terms of the upper-case variables the transformation then reads

$$\left.\begin{aligned} X_n &= \frac{a_x + d_x}{2} X_{n-1} + \alpha_x^2 b_x P_{X_{n-1}} + \frac{\lambda}{2} \frac{\alpha_x}{\alpha_y^2} \frac{b_x}{b_y} Y_{n-1}^2 \\ P_{X_n} &= \frac{\left[\frac{1}{2}(a_x + d_x)\right]^2 - 1}{\alpha_x^2 b_x} X_{n-1} + \frac{a_x + d_x}{2} P_{X_{n-1}} + \frac{\lambda}{2\alpha_x \alpha_y^2} \frac{a_x + d_x}{2 b_y} Y_{n-1}^2 \\ Y_n &= \frac{a_y + d_y}{2} Y_{n-1} + \alpha_y^2 b_y P_{Y_{n-1}} + \frac{\lambda}{\alpha_x} X_{n-1} Y_{n-1} \\ P_{Y_n} &= \frac{\left[\frac{1}{2}(a_y + d_y)\right]^2 - 1}{\alpha_y^2 b_y} Y_{n-1} + \frac{a_y + d_y}{2} P_{Y_{n-1}} + \frac{\lambda}{\alpha_x \alpha_y^2} \frac{a_y + d_y}{2 b_y} X_{n-1} Y_{n-1} . \end{aligned}\right\} \quad (3)$$

---

* The equations actually iterated on the computer in ALGYTEE runs 10-18 were strictly not Hamiltonian, but would become so by a trivial (non-canonical) transformation such that the y and p_y values employed by the computer be each multiplied by the scale factor $\sqrt{-c_y b_y}$ to obtain the corresponding canonical quantities.

This transformation is seen to be of the same form as (1) ($\lambda' \equiv \lambda/\alpha_x$ now playing the role of λ), with symmetry in the diagonal elements of the linear portion. By suitably choosing α_x and α_y, the off-diagonal elements may also be made equal save for sign -- specifically, identifying $(1/2)(a_x + d_x) = \cos \nu$ and $(1/2)(a_y + d_y) = \cos \kappa$, we choose $\alpha_x^2 = \frac{\sin \nu}{b_x}$ and $\alpha_y^2 = \frac{\sin \kappa}{b_y}$. As a result we finally obtain

$$\left.\begin{aligned}
X_n &= (\cos \nu) X_{n-1} + (\sin \nu) P_{X_{n-1}} + \frac{\lambda'}{2} \frac{\sin \nu}{\sin \kappa} Y_{n-1}^2 \\
P_{X_n} &= -(\sin \nu) X_{n-1} + (\cos \nu) P_{X_{n-1}} + \frac{\lambda'}{2} \frac{\cos \nu}{\sin \kappa} Y_{n-1}^2 \\
Y_n &= (\cos \kappa) Y_{n-1} + (\sin \kappa) P_{Y_{n-1}} + \lambda' X_{n-1} Y_{n-1} \\
P_{Y_n} &= -(\sin \kappa) Y_{n-1} + (\cos \kappa) P_{Y_{n-1}} + \lambda' (\operatorname{ctn} \kappa) X_{n-1} Y_{n-1}
\end{aligned}\right\} \quad (4)$$

This conveniently simple form for the transformation is thus seen to be inherently as general as the original form (1) and will serve as the basis of the analysis to follow.

3. Analysis Concerning the Onset of Y-Growth:

A. Method:

If we direct our attention to cases in which the axial-amplitude is initially very small, we may analyze the transformation equations in the spirit of Walkinshaw. The Y^2 terms are accordingly ignored in the recursion relations for the radial motion, whereupon the radial motion becomes represented by linear difference equations whose solution may be entered as a prescribed function of n into the axial equations. It is recognized, of course, that this procedure destroys the Hamiltonian form of the equations treated and precludes drawing in this way any inferences concerning the eventual character of the motion when Y may have grown to large amplitudes.

Proceeding to ignore the Y^2 term in the X and P_X equations, the solution for the radial motion becomes

$$X_n = (\cos n\nu) X_0 + (\sin n\nu) P_{X_0} .$$

This solution, when inserted into the remaining (axial) equations, then gives

$$Y_n = \left\{\cos\kappa + \lambda' \left[(\cos (n-1)\nu) X_0 + (\sin (n-1)\nu) P_{X_0} \right]\right\} Y_{n-1} + (\sin\kappa) P_{Y_{n-1}}$$

$$P_{Y_n} = \left\{-\sin\kappa + \lambda' \operatorname{ctn}\kappa \left[(\cos (n-1)\nu) X_0 + (\sin (n-1)\nu) P_{X_0} \right]\right\} Y_{n-1} + (\cos\kappa) P_{Y_{n-1}},$$

which, it may be noted, is a transformation with determinant unity. The two equations just written may, for the present purposes, be conveniently replaced by a second-order recursion relation involving only the quantities Y_j :

$$Y_{n+1} - \left\{2(\cos\kappa) + \lambda' \left[(\cos n\nu) X_0 + (\sin n\nu) P_{X_0} \right]\right\} Y_n + Y_{n-1} = 0.$$

Since the expression within the square brackets may be interpreted as the radial displacement, it is natural to replace it by A cos $(n\nu + \epsilon)$, in which A represents the amplitude of the (prescribed) radial motion and in which the phase-shift ϵ may be ignored for reasons of convenience. We accordingly direct our attention to the equation

$$Y_{n+1} - \left[2\cos\kappa + \lambda' A \cos n\nu\right] Y_n + Y_{n-1} = 0.$$

B. Solution for Threshold by Use of Corresponding Differential Equation:

It is informative to note that, if κ and $\lambda' A$ are taken as small, the equation just obtained at the end of the preceding subsection may be nicely approximated by a Mathieu differential equation of a type similar to that encountered in other treatments of y-growth. We note that

$$\frac{d^2 Y}{dn^2} \cong Y_{n+1} - 2Y_n + Y_{n-1}$$

and obtain

$$\frac{d^2Y}{dn^2} + \left[2(1-\cos\kappa) - \lambda' A\cos\nu n\right]Y \doteq 0$$

$$\frac{d^2Y}{dn^2} + \left[\kappa^2 - \lambda' A\cos\nu n\right]Y \doteq 0$$

or, with $\nu n \equiv 2\tau$,

$$\frac{d^2Y}{d\tau^2} + \left[\left(\frac{2\kappa}{\nu}\right)^2 - \frac{4\lambda' A}{\nu^2}\cos 2\tau\right]Y = 0.$$

The stability boundaries pertinent to the $\sigma_x = 2\sigma_y$ resonance ($\nu = 2\kappa$) are then, for $4\lambda' A/\nu^2$ small, of course given approximately by

$$\frac{2\lambda' A}{\nu^2} = \left|1 - \left(\frac{2\kappa}{\nu}\right)^2\right|$$

or

$$A = \frac{1}{2\lambda'}\left|\nu^2 - (2\kappa)^2\right|.$$

In terms of the quantities involved in our original transformation (1),

$$\begin{aligned}\text{amplitude of } x &= A/\alpha_x \\ &= \frac{1}{2\alpha_x\lambda'}\left|\nu^2 - (2\kappa)^2\right| \\ &= \frac{1}{2\lambda}\left|\nu^2 - (2\kappa)^2\right|.\end{aligned}$$

C. Threshold of Difference Equations:

It would be a more consistant procedure to derive directly the stability limits for the difference equations, without recourse to any allegedly-similar differential equation. It appears that this may be done by a variational method which closely parallels the method whereby we have elsewhere estimated stability limits for diverse Hill equations.

We imagine that ν is commensurate with the interval covered by the transformation, in that a whole number of radial oscillations will fit into some whole number of transformation intervals. For convenience, then, we write

$$p\nu = m(2\pi), \quad \text{with } p, m \text{ integers } (p \text{ even}).$$

By employing the concept that periodic solutions of the difference equations correspond to stability boundaries, we then consider

$$Y_{j+1} - \left[2\cos\kappa + \lambda' A\left(\cos j\,\frac{2m\pi}{p}\right)\right] Y_j + Y_{j-1} = 0$$

with $\quad Y_{j+p} = Y_j .$

(Solutions conforming to the aforementioned boundary condition are thus periodic in the interval $\Delta n = p$.)

The recursion equations written above are those which formally result from minimizing* the expression

$$\begin{aligned} S = {} & Y_0 Y_1 + Y_1 Y_2 + \cdots + Y_{j-1} Y_j + Y_j Y_{j+1} + \cdots + Y_{p-2} Y_{p-1} + Y_{p-1} Y_0 \\ & - \tfrac{1}{2}\left[2\cos\kappa + \lambda' A\right] Y_0^{\,2} \\ & - \tfrac{1}{2}\left[2\cos\kappa + \lambda' A\cos\frac{2m\pi}{p}\right] Y_1^{\,2} \\ & - \tfrac{1}{2}\left[2\cos\kappa + \lambda' A\cos\left(2\,\frac{2m\pi}{p}\right)\right] Y_2^{\,2} \\ & \cdots \\ & - \tfrac{1}{2}\left[2\cos\kappa + \lambda' A\cos\left(j\,\frac{2m\pi}{p}\right)\right] Y_j^{\,2} \\ & \cdots \\ & - \tfrac{1}{2}\left[2\cos\kappa + \lambda' A\cos\left((p-1)\,\frac{2m\pi}{p}\right)\right] Y_{p-1}^{\,2} . \end{aligned}$$

The connection between κ, ν and A at the stability boundaries can then be sought by the introduction of suitable trial solutions into S. For the purpose of this report it may be sufficient to consider, in turn, the simple forms

$$Y_j = B_1 \cos j\,\frac{\pi m}{p}$$

---

* A rigorous development of this method might better regard the "minimization" as causing a sum to be stationary subject to an auxiliary (isoperimetric) condition. The use of a Lagrange multiplier should then result in the equations with which we are concerned here.

and, alternatively

$$Y_j = C_1 \sin j \frac{\pi m}{p},$$

which represent the dominant terms of solutions appropriate in the neighborhood of the $\sigma_x = 2\sigma_y$ resonance.

With the first of these trial solutions, S becomes given by

$$(1/p)S = \left[\tfrac{1}{2} \cos \frac{\pi m}{p} - \tfrac{1}{2} \cos \kappa - \tfrac{1}{8} \lambda' A\right] B_1^2$$

and is "stationary" (for $B_1 \neq 0$) when

$$A = \frac{4}{\lambda'} \left[\cos \frac{\pi m}{p} - \cos \kappa\right];$$

similarly, with the second trial solution,

$$(1/p)\, S = \left[\tfrac{1}{2} \cos \kappa - \tfrac{1}{2} \cos \frac{\pi m}{p} - \tfrac{1}{8} \lambda' A\right] C_1^2$$

and

$$A = \frac{4}{\lambda'} \left[\cos \kappa - \cos \frac{\pi m}{p}\right].$$

Recalling that $\pi m/p = \nu/2$, we thus find the stability boundaries to be approximately located at

$$A \doteq \frac{4}{\lambda'} \left|\cos \kappa - \cos(\nu/2)\right|$$
$$= \frac{8}{\lambda'} \left|\sin^2(\nu/4) - \sin^2(\kappa/2)\right|,$$

or

amplitude of $x = \dfrac{8}{\lambda} \left|\sin^2(\nu/4) - \sin^2(\kappa/2)\right|$.*

With κ small one notes that this result for the threshold reduces to that obtained from consideration of a differential equation (cited at the end of sub-section B):

amplitude of $x \cong \dfrac{1}{2\lambda} \left|\nu^2 - (2\kappa)^2\right|$.

---

* In terms of the quantities $\cos \nu$ and $\cos \kappa$ most directly available from the original transformation, this result may be written perhaps most conveniently for calculation as

amplitude of $x = \dfrac{4}{\lambda} \left|\sqrt{\dfrac{1+\cos\nu}{2}} - \cos \kappa\right|$.

4. Estimate of Lapse-Rate:

An estimate for the lapse-rate to be expected when the initial radial amplitude is above threshold may be readily obtained by reference to the differential equation cited in Section 3B. The general procedure for obtaining such an estimate has been outlined by McLachlan ["Theory and Application of Mathieu Functions" (Claredon Press, Oxford, 1947), Sects. 4.90 - 4.91] and has been applied in previous discussions of y-growth.

In this way the lapse-rate associated with the Mathieu equation cited is found to be

$$(\lambda'/\nu^2)\sqrt{A^2 - A_{thr.}^2} \quad \text{nepers per unit increment of } \tau\,,$$

or

$$\frac{\lambda'}{2\nu}\sqrt{A^2 - A_{thr.}^2} \quad \text{nepers per iteration.}$$

In terms of the amplitude "a" for our initial variable "x", the corresponding lapse-rate is

$$\frac{\lambda}{2\nu}\sqrt{a^2 - a_{thr.}^2} \quad \text{nepers per iteration}$$

or

$$0.21715\,(\lambda/\nu)\sqrt{a^2 - a_{thr.}^2} \quad \text{decades per iteration.}$$

A procedure parallel to that outlined by McLachlan, if applied to the difference equations, suggests a lapse rate which, when small, is

$$\frac{\lambda}{4\sin(\nu/2)}\sqrt{a^2 - a_{thr.}^2} \quad \text{nepers per iteration}$$

or

$$0.10857\,\frac{\lambda}{\sin(\nu/2)}\sqrt{a^2 - a_{thr.}^2} \quad \text{decades per iteration.}$$

This formula, which for ν small reduces to the result found for the differential equation, is presumably preferable for predicting the lapse-rate developed by the transformation.

For hand calculations we write

$$\text{Lapse-Rate} = \frac{\lambda}{4}\frac{\sqrt{a^2 - a_{thr.}^2}}{\sqrt{\frac{1}{2}(1-\cos v)}} \quad \text{nepers per iteration}$$

$$= 0.15355\,\lambda \frac{\sqrt{a^2 - a_{thr.}^2}}{\sqrt{1-\cos v}} \quad \text{decades per iteration.}$$

5. Generating Function:

The transformation (4) may be written

$$X_n = (\sec v)X_{n-1} + (\tan v)P_{X\,n}$$

$$P_{X_{n-1}} = (\tan v)X_{n-1} + (\sec v)P_{X\,n} - (\lambda'/2)(\csc \kappa)Y_{n-1}^2$$

$$Y_n = (\sec \kappa)Y_{n-1} + (\tan \kappa)P_{Y_n}$$

$$P_{Y_{n-1}} = (\tan \kappa)Y_{n-1} + (\sec \kappa)P_{Y_n} - \lambda'(\csc \kappa)X_{n-1}Y_{n-1}.$$

These relations may be derived from a generating function

$$W(P_{X\,n}, P_{Y_n}; X_{n-1}, Y_{n-1})$$

$$= \tfrac{1}{2}(\tan v)X_{n-1}^2 + (\sec v)X_{n-1}P_{X\,n} + \tfrac{1}{2}(\tan v)P_{X\,n}^2$$

$$- (\lambda'/2)(\csc \kappa)X_{n-1}Y_{n-1}^2$$

$$+ \tfrac{1}{2}(\tan \kappa)Y_{n-1}^2 + (\sec \kappa)Y_{n-1}P_{Y_n} + \tfrac{1}{2}(\tan \kappa)P_{Y_n}^2,$$

employing

$$X_n = \partial W/\partial P_{X_n} \qquad Y_n = \partial W/\partial P_{Y_n}$$

$$P_{X_{n-1}} = \partial W/\partial X_{n-1} \qquad P_{Y_{n-1}} = \partial W/\partial Y_{n-1}.$$

It is possible that this generating function will be found of use in the further application of dynamical theory to transformations reduceable to the form represented by equations (4).

6. The Inverse Transformation:

The inverse of transformation (4) is found to be

$$X_{n-1} = (\cos v)X_n - (\sin v)P_{X\,n}$$

(continued)

$$P_{X_{n-1}} = (\sin v) X_n + (\cos v) P_{X_n} - (\lambda'/2)(\csc \kappa)[(\cos \kappa) Y_n - (\sin \kappa) P_{Y_n}]^2$$

$$Y_{n-1} = (\cos \kappa) Y_n - (\sin \kappa) P_{Y_n}$$

$$P_{Y_{n-1}} = (\sin \kappa) Y_n + (\cos \kappa) P_{Y_n}$$
$$- \lambda'(\csc \kappa)[(\cos v) X_n - (\sin v) P_{X_n}][(\cos \kappa) Y_n - (\sin \kappa) P_{Y_n}].$$

As with the forward transformation, this inverse transformation is again a rational algebraic transformation of degree not exceeding two. It would appear that transformations of this degree could be synthesized so that a closer similarity of form would obtain between the direct and inverse forms.

7. Computational Example:

A. Discussion:

A transformation equivalent in form to (4) has been run on the I.B.M.-704 computer by aid of the ALGYTEE program. Denoting the variables employed by the computer as ρ, p_ρ, Ψ, and p_Ψ, the equations directly iterated (Runs 10-18) were

$$\rho_n = -.128 \rho_{n-1} + 1.744 p_{\rho_{n-1}} + .11834784 \Psi_{n-1}^2$$

$$p_{\rho_n} = -.564 \rho_{n-1} - .128 p_{\rho_{n-1}} - .00868608 \Psi_{n-1}^2$$

$$\Psi_n = .74 \Psi_{n-1} + 2.60 p_{\Psi_{n-1}} + .78 \rho_{n-1} \Psi_{n-1}$$

$$p_{\Psi_n} = -.174 \Psi_{n-1} + .74 p_{\Psi_{n-1}} + .222 \rho_{n-1} \Psi_{n-1}.$$

These equations may be put into the form (1) [see footnote, section 2] by the substitution (change of scale)

$$\rho_j = x_j \qquad \Psi_j = y_j / \sqrt{.4524}$$
$$p_{\rho_j} = p_{x_j} \qquad p_{\Psi_j} = p_{y_j} / \sqrt{.4524}$$

to become of the Hamiltonian form:

$$x_n = -.128 x_{n-1} + 1.744 p_{x_{n-1}} + .2616 y_{n-1}^2$$

$$p_{x_n} = -.564 x_{n-1} - .128 p_{x_{n-1}} - .0192 y_{n-1}^2$$

$$y_n = .74\, y_{n-1} + 2.60\, p_{y_{n-1}} + .78\, x_{n-1}\, y_{n-1}$$
$$p_{y_n} = -.174\, y_{n-1} + .74\, p_{y_{n-1}} + .222\, x_{n-1}\, y_{n-1},$$

with $\lambda = .78$, $\cos \nu = -.128$, and $\cos \kappa = .74$.

From the results of Section 3C we expect the threshold x-amplitude for this problem to be

$$a_{thr.} = \frac{4}{0.78}\left[0.74 - \sqrt{0.436}\right]$$
$$= 0.41 .$$

The computational results to be reported suggest

$$a_{thr.} = 0.388 \cong 0.39$$

for this transformation, affording what may be regarded as a satisfactory check of the theory. (The approximate theoretical result, obtained from a differential equation in the limiting case of small κ, is $a_{thr.} = 0.455$, in somewhat poorer agreement with the computational result.)

Likewise, for the lapse-rate, the results at the end of Section 4 suggest

$$\frac{0.15355 \times 0.78}{\sqrt{0.872}}\sqrt{a^2 - a_{thr.}^{\;2}} \quad \text{decades per iteration}$$

or $\quad 0.12826\sqrt{a^2 - 0.1505} \quad$ decades per iteration

(to employ the computational result for the threshold amplitude). We tabulate below the lapse-rates calculated from this last formula and the corresponding values observed from the computations. It may be noted that the form of the theoretical equation suggests that the square of the lapse-rate will grow linearly with a^2, for values of $a > a_{thr.}$, a prediction which appears to be substantiated by the computations. The theoretical and computational results for $d(\mu^2)/da^2$ are, respectively, 0.016 and 0.014 (decades/iteration)^2.

x_o	$\lvert x_o - a_{thr.} \rvert$	Lapse-Rate (decades per iteration)	
		Calc. from Theory	From IBM Computations
-0.4	0.01	0.012	0.0116
-0.6	0.21	0.059	0.055
-0.8	0.41	0.09	0.084
-1.0	0.61	0.12	0.11

B. Method:

The computer printed ρ, Ψ, p_ρ, and p_Ψ after 16, 17, 18, 19, and 20 iterations, after 36, 37, 38, 39, and 40 iterations, etc. through 1200 iterations for each of 9 runs. In each run, $\Psi_o = 1.0 \times 10^{-4}$, $p_{\rho_o} = 0$, and $p_{\Psi_o} = 0$. The initial values of ρ for the several runs were -0.1, -0.2, -0.3, -0.4, -0.6, -0.8, -1.0, -1.2, and -1.4. An artificial limit of 64.0 was imposed on all quantities. As shown on the accompanying semi-logarithmic plot, the first three runs showed no evidence of Ψ-growth, the next two grew exponentially for three or four decades and then "turned over" to perform apparently stable oscillations of Ψ-amplitude, while the remaining four runs appeared unstable. In constructing the plot, the amplitude was estimated simply as the maximum Ψ appearing in each group of five consecutive printed iterations.

Graphs depicting the lapse-rate, as obtained from the aforementioned plot, are also shown.

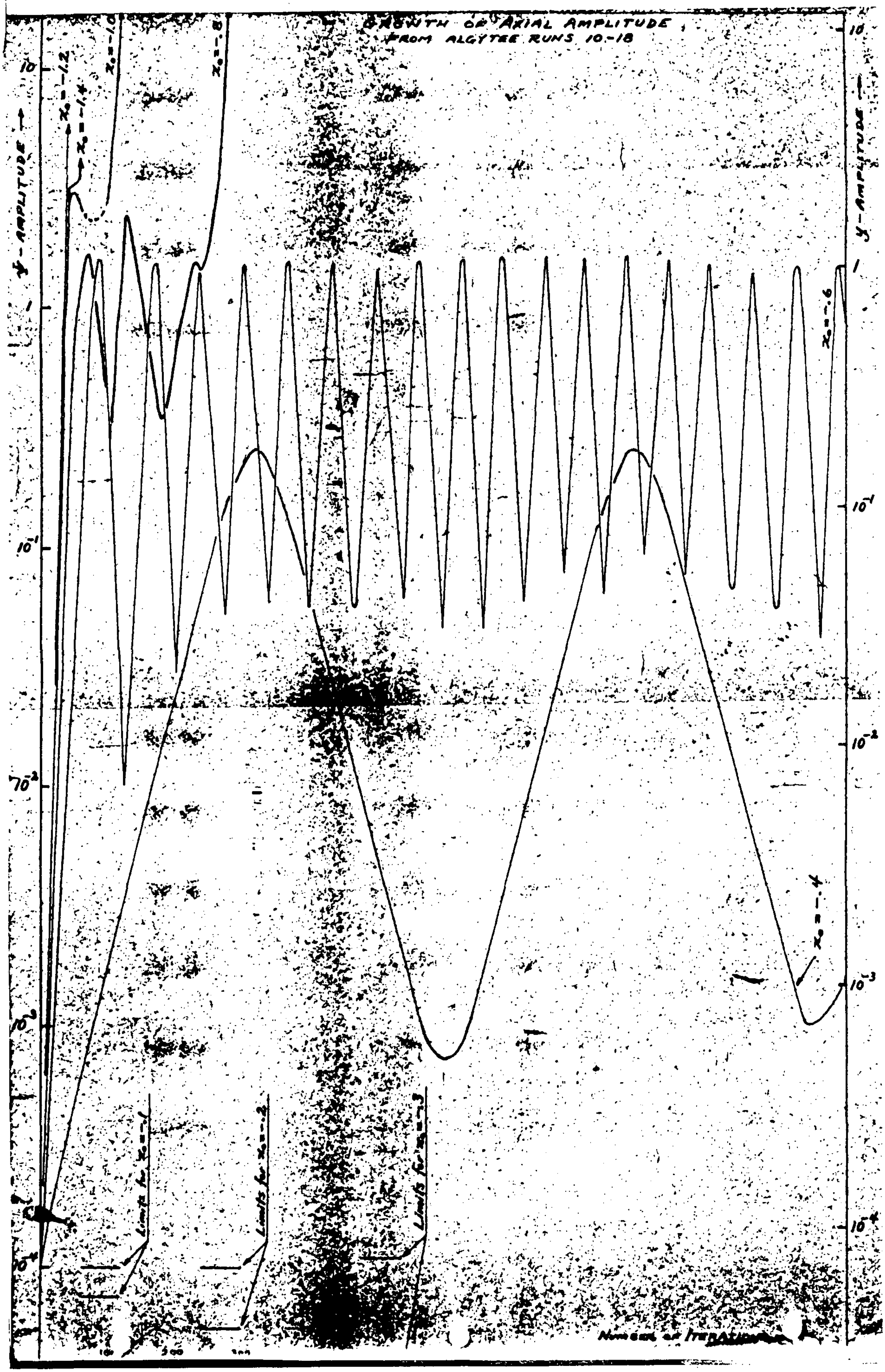
GROWTH OF AXIAL AMPLITUDE, FROM ALGYTEE RUNS 10-18
y-AMPLITUDE
$x_0=-1.2$
$x_0=-1.4$
$x_0=-1.0$
$x_0=-.8$
$x_0=-.6$
$x_0=-.4$
Limits for $x_0=-.1$
Limits for $x_0=-.2$
Limits for $x_0=-.3$
Number of ITERATIONS
10
1
10^{-1}
10^{-2}
10^{-3}
10^{-4}
100
200
300

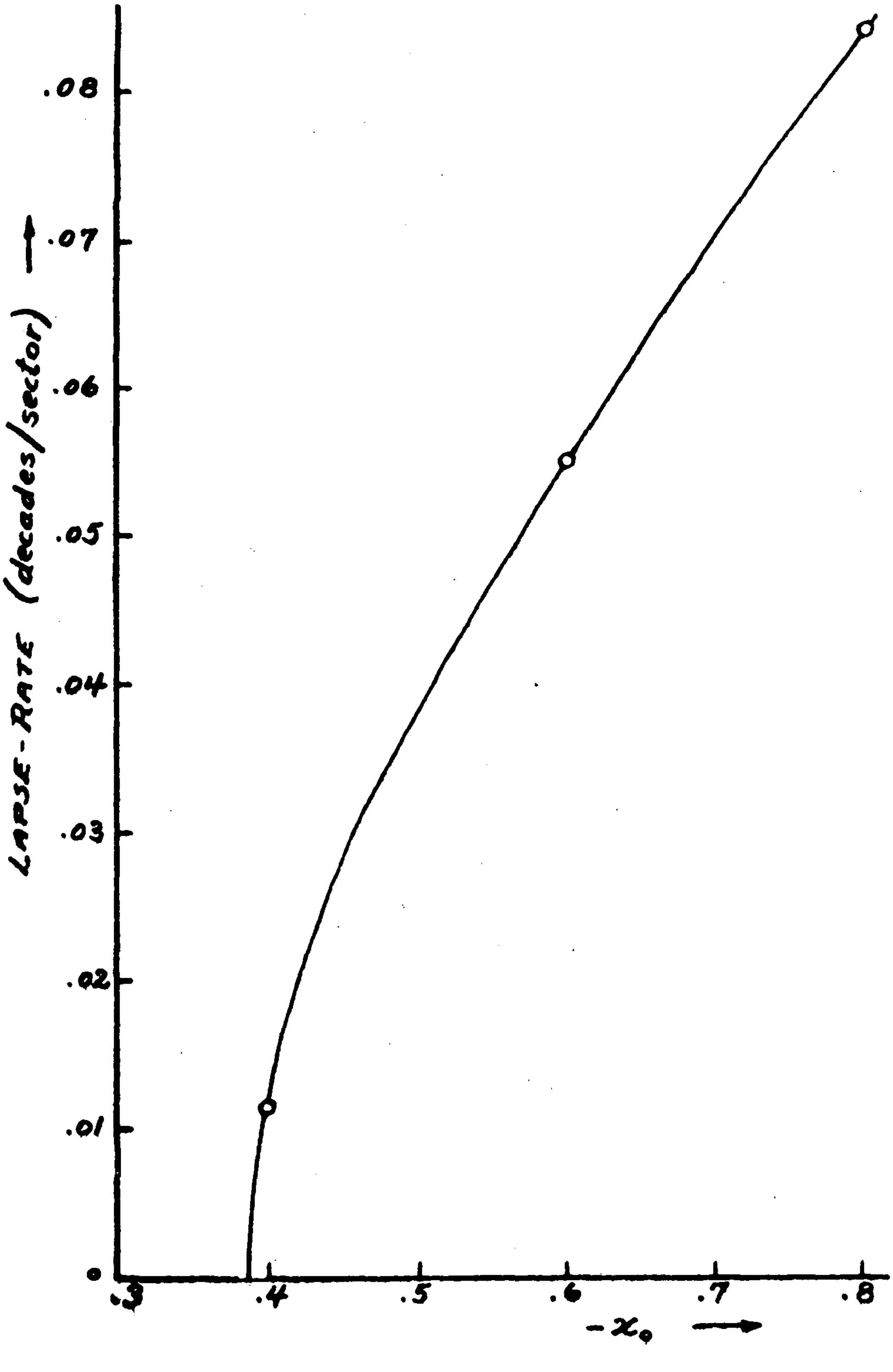

Fig. 2

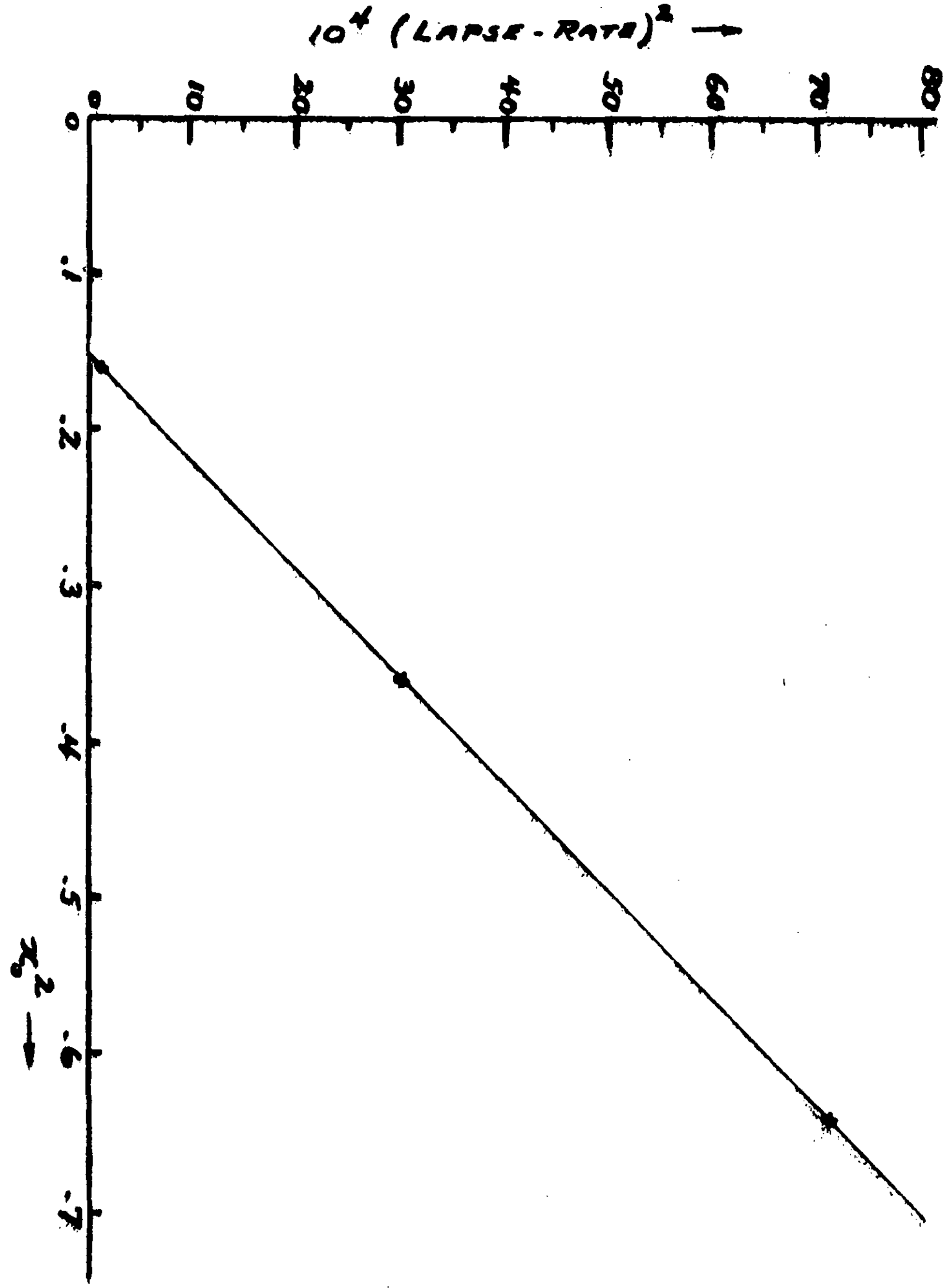

Fig. 3

CORRECTION - To MURA-246 (Int.)

"CONCERNING THE y-GROWTH PHENOMENON

EXHIBITED BY ALGEBRAIC TRANSFORMATIONS"

1. We have detected a slight numerical error in the calculations to an example given in Section 7A of MURA-246 (Int.). On p. 13, the expected lapse-rate should read

$$\frac{0.15355 \times 0.78}{\sqrt{1.128}} \sqrt{a^2 - a_{thr.}^2} \quad \text{decades per iteration}$$

or $0.11277 \sqrt{a^2 - 0.1505}$ decades per iteration when the computational result for the threshold amplitude is employed.

2. The theoretical and computational results for $d(\mu^2)/d(a^2)$ accordingly are 0.013 and 0.014 (decades/iteration)^2, respectively.

3. The table on p. 14 should read

x_0	$\lvert x_0 - a_{thr.} \rvert$	Lapse-Rate (decades per iteration) Calc. from Theory	Lapse-Rate (decades per iteration) From IBM Computations
- 0.4	0.01	0.011	0.0116
- 0.6	0.21	0.052	0.055
- 0.8	0.41	0.079	0.084
- 1.0	0.61	0.104	0.11

4. Similar results, giving a computational value of $d(\mu^2)/d(a^2)$ just slightly greater than the theoretical value, have also been obtained in subsequent computations with a similar transformation for which $\cos\nu = -0.125$, $\cos\kappa = 0.75$, and $\lambda = 1$.

L. Jackson Laslett
March 25, 1957

MURA-247
Internal

MIDWESTERN UNIVERSITIES RESEARCH ASSOCIATION *
2203 University Avenue - Madison, Wisconsin

SUPPLEMENTAL NOTE CONCERNING THE ALGEBRAIC TRANSFORMATIONS OF MURA - 246 (Int.)

L. Jackson Laslett**

March 18, 1957

ABSTRACT:

It is shown that the algebraic transformations of MURA - 246 (Int.) may be written in a form which more directly shows symmetry between the form of the forward and inverse transformation.

* Supported by Contract AEC #AT (11-1)-384

** On leave from Iowa State College, Ames, Iowa

1. In MURA-246 (Int.) the writer introduced and discussed second-degree algebraic transformations, capable of exhibiting y-growth, which were evidently able to represent certain features of the differential equations previously used to represent particle motion in FFAG accelerators. In Section 6 of that report the inverse transformation was presented and it was noted to be of a form superficially somewhat different from the original forward transformation. It is the purpose of the present note to indicate that this disparity of form is more apparent than real.

2. A simple change of variables given by a linear transformation of the form

$$
\begin{aligned}
u_j &= (\cos\beta)\,\underline{X}_j + (\sin\beta)\,P_{\underline{X}_j} \\
p_{u_j} &= -(\sin\beta)\,\underline{X}_j + (\cos\beta)\,P_{\underline{X}_j} \\
v_j &= (\cos\gamma)\,Y_j + (\sin\gamma)\,P_{Y_j} \\
p_{v_j} &= -(\sin\gamma)\,Y_j + (\cos\gamma)\,P_{Y_j}
\end{aligned}
$$

when introduced into transformation (4) of MURA-246 (Int.), converts the latter into

$$
\begin{aligned}
u_n = {} & (\cos\nu)\,u_{n-1} + (\sin\nu)\,p_{u_{n-1}} \\
& + \frac{\lambda'}{2}\,\frac{\sin(\nu+\beta)}{\sin\kappa}\Big[(\cos\gamma)\,v_{n-1} - (\sin\gamma)\,p_{v_{n-1}}\Big]^2
\end{aligned}
$$

$$
\begin{aligned}
p_{u_n} = {} & -(\sin\nu)\,u_{n-1} + (\cos\nu)\,p_{u_{n-1}} \\
& + \frac{\lambda'}{2}\,\frac{\cos(\nu+\beta)}{\sin\kappa}\Big[(\cos\gamma)\,v_{n-1} - (\sin\gamma)\,p_{v_{n-1}}\Big]^2
\end{aligned}
$$

$$
\begin{aligned}
v_n = {} & (\cos\kappa)\,v_{n-1} + (\sin\kappa)\,p_{n-1} \\
& + \lambda'\,\frac{\sin(\kappa+\gamma)}{\sin\kappa}\Big[(\cos\beta)\,u_{n-1} - (\sin\beta)\,p_{u_{n-1}}\Big]\Big[(\cos\gamma)\,v_{n-1} - (\sin\gamma)\,p_{v_{n-1}}\Big]
\end{aligned}
$$

$$
\begin{aligned}
p_{v_n} = {} & -(\sin\kappa)\,v_{n-1} + (\cos\kappa)\,p_{v_{n-1}} \\
& + \lambda'\,\frac{\cos(\kappa+\gamma)}{\sin\kappa}\Big[(\cos\beta)\,u_{n-1} - (\sin\beta)\,p_{u_{n-1}}\Big]\Big[(\cos\gamma)\,v_{n-1} - (\sin\gamma)\,p_{v_{n-1}}\Big]
\end{aligned}
$$

and the inverse transformation becomes

$$u_{n-1} = (\cos\nu)u_n - (\sin\nu)p_{u_n} - \frac{\lambda'}{2}\frac{\sin\beta}{\sin\kappa}\left[\cos(\kappa+\gamma)v_n - \sin(\kappa+\gamma)p_{v_n}\right]^2$$

$$p_{u_{n-1}} = (\sin\nu)u_n + (\cos\nu)p_{u_n} - \frac{\lambda'}{2}\frac{\cos\beta}{\sin\kappa}\left[\cos(\kappa+\gamma)v_n - \sin(\kappa+\gamma)p_{v_n}\right]^2$$

$$\begin{aligned} v_{n-1} = {} & (\cos\kappa)v_n - (\sin\kappa)p_{v_n} \\ & - \lambda'\frac{\sin\gamma}{\sin\kappa}\left[\cos(\nu+\beta)u_n - \sin(\nu+\beta)p_{u_n}\right]\left[\cos(\kappa+\gamma)v_n - \sin(\kappa+\gamma)p_{v_n}\right] \end{aligned}$$

$$\begin{aligned} p_{v_n} = {} & (\sin\kappa)v_n + (\cos\kappa)p_{v_n} \\ & - \lambda'\frac{\cos\gamma}{\sin\kappa}\left[\cos(\nu+\beta)u_n - \sin(\nu+\beta)p_{u_n}\right]\left[\cos(\kappa+\gamma)v_n - \sin(\kappa+\gamma)p_{v_n}\right] \end{aligned}$$

3. We accordingly may emphasis the symmetry between direct and inverse transformations of the type under consideration by choosing $\beta = -\nu/2$ **and** $\gamma = -\kappa/2$.

One than obtains

$$\begin{aligned} u_n = {} & (\cos\nu)u_{n-1} + (\sin\nu)p_{u_{n-1}} \\ & + (\mu/2)(\sin\nu/2)\left[(\cos\kappa/2)v_{n-1} + (\sin\kappa/2)p_{v_{n-1}}\right]^2 \end{aligned}$$

$$\begin{aligned} p_{u_n} = {} & -(\sin\nu)u_{n-1} + (\cos\nu)p_{u_{n-1}} \\ & + (\mu/2)(\cos\nu/2)\left[(\cos\kappa/2)v_{n-1} + (\sin\kappa/2)p_{v_{n-1}}\right]^2 \end{aligned}$$

$$\begin{aligned} v_n = {} & (\cos\kappa)v_{n-1} + (\sin\kappa)p_{v_{n-1}} \\ & + \mu(\sin\kappa/2)\left[(\cos\nu/2)u_{n-1} + (\sin\nu/2)p_{u_{n-1}}\right]\left[(\cos\kappa/2)v_{n-1} + (\sin\kappa/2)p_{v_{n-1}}\right] \end{aligned}$$

$$\begin{aligned} p_{v_n} = {} & -(\sin\kappa)v_{n-1} + (\cos\kappa)p_{v_{n-1}} \\ & + \mu(\cos\kappa/2)\left[(\cos\nu/2)u_{n-1} + (\sin\nu/2)p_{u_{n-1}}\right]\left[(\cos\kappa/2)v_{n-1} + (\sin\kappa/2)p_{v_{n-1}}\right] \end{aligned}$$

and

$$\begin{aligned} u_{n-1} = {} & (\cos\nu)u_n - (\sin\nu)p_{u_n} \\ & + (\mu/2)(\sin\nu/2)\left[(\cos\kappa/2)v_n - (\sin\kappa/2)p_{v_n}\right]^2 \end{aligned}$$

$$\begin{aligned} p_{u_{n-1}} = {} & (\sin\nu)u_n + (\cos\nu)p_{u_n} \\ & - (\mu/2)(\cos\nu/2)\left[(\cos\kappa/2)v_n - (\sin\kappa/2)p_{v_n}\right]^2 \end{aligned}$$

$$v_{n-1} = (\cos\kappa)v_n - (\sin\kappa)p_{v_n}$$
$$+\mu(\sin\kappa/2)[(\cos\nu/2)u_n - (\sin\nu/2)p_{u_n}][(\cos\kappa/2)v_n - (\sin\kappa/2)p_{v_n}]$$

$$p_{v_{n-1}} = (\sin\kappa)v_n + (\cos\kappa)p_{v_n}$$
$$-\mu(\cos\kappa/2)[(\cos\nu/2)u_n - (\sin\nu/2)p_{u_n}][(\cos\kappa/2)v_n - (\sin\kappa/2)p_{v_n}]$$

$$\text{with } \mu \equiv \lambda'/(\sin\kappa)$$

It is evident that, in this form, the inverse transformation differs from the direct only by a reversal of sign of ν, κ, and μ

4. It is perhaps worth noting that, according to the foregoing transformation,

$$(\cos\nu/2)u_{n-1} + (\sin\nu/2)p_{u_{n-1}} = (\cos\nu/2)u_n - (\sin\nu/2)p_{u_n}.$$

and

$$(\cos\kappa/2)v_{n-1} + (\sin\kappa/2)p_{v_{n-1}} = (\cos\kappa/2)v_n - (\sin\kappa/2)p_{v_n}.$$

MURA-248
Internal

MIDWESTERN UNIVERSITIES RESEARCH ASSOCIATION+
2203 University Avenue - Madison, Wisconsin

STABILITY LIMIT IN SPIRAL SECTOR STRUCTURES NEAR $\sigma_x = \frac{2\pi}{4}$

L. J. Laslett* and A. M. Sessler**

March 18, 1957

Renewed interest in the "handy formulas", stimulated by the possibility of applying them to the study of imperfection resonances, may make the following simple derivation of a stability limit near $\sigma_x = \frac{2\pi}{4}$ of general interest.

We start with the equation describing motion about the forced orbit in a spiral sector accelerator,

$$u'' + \left[k+1 - \frac{f^2}{2\omega^2 N^2} + \frac{f}{\omega}\cos N\theta\right]u = \frac{1}{2}\frac{f}{\omega^2}\sin N\theta\, u^2 + \frac{1}{6}\frac{f^3}{\omega^3}\cos N\theta\, u^3$$

where only the dominant terms have been retained.[1]

In the neighborhood of $\sigma_x = \frac{2\pi}{4}$ we may keep only the resonant terms, or:

$$u'' + \nu_x^2 u = \frac{1}{6}\frac{f}{\omega^3}\cos N\theta\, u^3$$

where ν_x^2 is the x-tune, and approximately:

$$\nu_x^2 = k+1$$

A trial function is now employed and solution is obtained by the method of harmonic balance.

Let $$x = A\sin\left(\frac{N\theta}{4} + \epsilon\right), \text{ then:}$$

$$\left(\nu_x^2 - \frac{N^2}{16}\right)A\sin\left(\frac{N\theta}{4} + \epsilon\right) = \frac{1}{6}\frac{fA^3}{\omega^3}\cos N\theta \sin^3\left(\frac{N\theta}{4} + \epsilon\right)$$

$$= \frac{1}{6}\frac{fA^3}{\omega^3}\left\{\frac{3}{8}\sin\left(\frac{5N\theta}{4} + \epsilon\right) + \frac{3}{8}\sin\left(-\frac{3N\theta}{4} + \epsilon\right) - \frac{1}{8}\sin\left(\frac{7N\theta}{4} + 3\epsilon\right) - \frac{1}{8}\sin\left(-\frac{N\theta}{4} - 3\epsilon\right)\right\}$$

+Supported by Contract AEC #AT (11-1)-384

* On leave from Iowa State College, Ames, Iowa

** Ohio State University, Columbus, Ohio

[1] F. T. Cole MURA Report #95

by harmonic balance:

$$\left(\nu_x^2 - \frac{N^2}{16}\right) A \sin\left(\frac{N\theta}{4} + \epsilon\right) = + \frac{fA^3}{48\omega^3} \sin\left(\frac{N\theta}{4} + 3\epsilon\right)$$

Thus if

$$\left(\nu_x^2 - \frac{N^2}{16}\right) > 0 \qquad \epsilon = 0$$

$$\left(\nu_x^2 - \frac{N^2}{16}\right) < 0 \qquad \epsilon = \frac{\pi}{2}$$

and in either case.

$$\frac{fA^2}{48\omega^3} = \left|\nu_x^2 - \frac{N^2}{16}\right| \quad \text{or} \quad A = \sqrt{\frac{48\omega^3}{f}} \left|\nu_x^2 - \frac{N^2}{16}\right|^{\frac{1}{2}}$$

It might be remarked that this method is the very same as that used previously to obtain the stability limit near $\sigma_x = \frac{2\pi}{3}$.[2]

This result is, of course, the same as that obtained by Parzen by his more sophisticated techniques.[3]

[2] L. J. Laslett and A. M. Sessler, MURA Notes, 6/1/56.

[3] G. Parzen, Non-Linear Resonances in Alternating Gradient Accelerators, MURA-200

MURA-252
Internal

MIDWESTERN UNIVERSITIES RESEARCH ASSOCIATION+

2203 University Avenue, Madison, Wisconsin

APPROXIMATE SOLUTIONS TO THE MATHIEU EQUATION

L. Jackson Laslett* and A. M. Sessler**

April 10, 1957

ABSTRACT: Floquet solutions and the coefficients of a trigonometric series representing such solutions were obtained computationally for the Mathieu equation

$$y'' + (A + B\cos 2t)y = 0$$

for representative cases with $B = 1.5$ or 1.0 and $0 < \sigma < \pi$. Algebraic formulas, in good agreement with the computational results, are given for the important coefficients in the series expansion.

+ Supported by Contract AEC #AT (11-1)-384

* On leave of absence from Iowa State College, Ames, Iowa

** Ohio State University

I. INTRODUCTION

For analytic work concerning the motion of particles in a cyclic accelerator, as in the study of imperfections when 2ν has values near an integer, solutions to the Mathieu equation may be required which remain accurate when σ is near π. Results which appear to describe such solutions adequately are presented here, for convenient reference in future work, although it is recognized that essentially the same problem has received considerable attention previously by other workers,[1-6] motivated either by accelerator problems or by an interest in solid-state physics.

The present report consists of two parts: Firstly, the Floquet solution of the Mathieu equation is obtained in representative cases and analysized in a series of cosine functions by means of digital computation (MURA I.B.M. "DUCK-ANSWER" and "FORANAL" programs). The adequacy of retaining only a limited number of terms in this expansion is examined. Secondly, algebraic expressions for the coefficients in such an expansion are obtained by harmonic balance and compared with the coefficients given by digital computation.

The differential equation with which we shall be concerned throughout the report is written

$$y'' + [A + B \cos Nt]y = 0, \tag{1}$$

with N = 2 and with representative values of the constants considered to be

B = 1.0 or 1.5

A such that $0 < \sigma < \pi$.

Expansion of the <u>even</u> Floquet solution ($y_o = 1$, $y_o' = 0$) in the form

$$y = g_o \cos \nu t + \sum_{m=1} \left[f_m \cos (mN - \nu)t + g_m \cos (mN + \nu)t \right] \tag{2a}$$

$$= g_o \cos \nu t + \sum_{m=1} \left[(f_m + g_m) \cos mNt \cos \nu t + (f_m - g_m) \sin mNt \sin \nu t \right] \tag{2b}$$

is specifically treated, from which the general solution may be written by replacing ν t with $\nu t + \epsilon$:

$$y = g_o \cos (\nu t + \epsilon) + \sum_{m=1} \left\{ f_m \cos\left[(mN - \nu)t - \epsilon\right] + g_m \cos\left[(mN + \nu)t + \epsilon\right] \right\}. \tag{2c}$$

Note that, with N=2, ν represents σ/π. In terms of this notation it may also be noted that the matrix which carries the solution ($\begin{smallmatrix} y \\ y' \end{smallmatrix}$) between $t = 0$ and $t = 2\pi/N$ is $\begin{pmatrix} M_{11} & M_{12} \\ M_{21} & M_{22} \end{pmatrix}$

$$= \begin{pmatrix} \cos \sigma & \dfrac{g_o + \sum_{m=1} (f_m + g_m)}{\nu g_o - \sum_{m=1} \left[(mN - \nu) f_m - (mN + \nu) g_m \right]} \sin \sigma \\ \dfrac{\nu g_o - \sum_{m=1} \left[(mN - \nu) f_m - (mN + \nu) g_m \right]}{g_o + \sum_{m=1} (f_m + g_m)} \sin \sigma & \cos \sigma \end{pmatrix}.$$

II. COMPUTATIONAL RESULTS:

A series of DUCK-ANSWER solutions to the equation $y'' + (A + B\cos 2t)y = 0$ were obtained with B = 1.5 and with B = 0. Values of A were chosen which were intended to lead to values of σ/π close to simple rational fractions in the range between 0 and 1. From the computational solutions, $M_{11} = M_{22} = \cos\sigma$ (and, hence, σ/π) could be determined, as could also the remaining matrix-elements M_{12} and M_{21}. These results are summarized in the accompanying table.

Taking as a guide the nearest simple rational fraction which would serve to represent σ/π in each case, an interval of t was found within which the solution was substantially periodic. The solution within such an interval was then subjected to Fourier analysis, by the FORANAL program, to yield the coefficients of a cosine series representing the solution. The coefficients so obtained are given in tabular form below and serve as the basis for the curves denoted "Digital" on the graphs appended to this report.

From the results of these computations - - considered representative of particle motion in a spirally-ridged FFAG accelerator with sinusoidally varying median-plane field -- it appears that the coefficients g_2 and certainly f_3 are quite small. One measure of the adequacy of the previous coefficients to describe the solution is provided by a comparison, given in tabular form below (for the case B = 1.5 and $\sigma = 0.889\pi$), of the actual solution with that computed from a limited number of coefficients. A more sensitive test, which may be relevant only in certain applications, is a comparison of the actual computed matrix-element M_{12} with that given by retaining only the first few terms of the series. The result of such a comparison, for a few representative cases, is also tabulated below. The conclusion may be drawn that the retention of 4 or 5 terms (through f_2 or, possibly, through g_2) affords a quite good representation of the Floquet solution in the cases considered. In the following section, therefore, we direct our attention to formulating algebraic expressions suitable for calculating the relative coefficients f_1/g_0 .... g_2/g_0.

III. ALGEBRAIC EVALUATION OF COEFFICIENTS:

We seek the even solution of

$$y'' + [A + B\cos Nt]\,y = 0 \tag{1}$$

in the approximate form

$$\begin{aligned} y = {} & g_0 \cos \nu t \\ & + f_1 \cos(N-\nu)t + g_1 \cos(N+\nu)t \\ & + f_2 \cos(2N-\nu)t + g_2 \cos(2N \mp \nu)t \, . \end{aligned} \tag{2}$$

By application of harmonic balance the following set of five algebraic equations is obtained:

$$\begin{aligned} A - \nu^2 + (B/2)(F_1 + G_1) &= 0 \\ [A - (N-\nu)^2]F_1 + (B/2)(1 + F_2) &= 0 \\ [A - (N+\nu)^2]G_1 + (B/2)(1 + G_2) &= 0 \\ [A - (2N-\nu)^2]F_2 + (B/2)\,F_1 &= 0 \\ [A - (2N+\nu)^2]G_2 + (B/2)\,G_1 &= 0 \, , \end{aligned} \tag{3}$$

where $F_{1,2}$ and $G_{1,2}$ denote respectively $f_{1,2}/g_0$ and $g_{1,2}/g_0$.

From these simultaneous equations it follows that

$$F_1 \equiv f_1/g_0 = \frac{B}{2\left[-A+(N-\nu)^2 - \dfrac{B^2}{4[-A+(2N-\nu)^2]}\right]}$$

$$G_1 \equiv g_1/g_0 = \frac{B}{2\left[-A+(N+\nu)^2 - \dfrac{B^2}{4[-A+(2N+\nu)^2]}\right]}$$

$$F_2 \equiv f_2/g_0 = \frac{B}{2[-A+(2N-\nu)^2]}\left(\frac{f_1}{g_0}\right)$$

$$G_2 \equiv g_2/g_0 = \frac{B}{2[-A+(2N+\nu)^2]}\left(\frac{g_1}{g_0}\right),$$

(4)

provided the frequency satisfies

$$\nu^2 = A + \frac{B^2}{4\left[-A+(N-\nu)^2 - \dfrac{B^2}{4[-A+(2N-\nu)^2]}\right]} + \frac{B^2}{4\left[-A+(N+\nu)^2 - \dfrac{B^2}{4[-A+(2N+\nu)^2]}\right]}.$$

(5)

It is noted that in some applications, when $\nu \ll N$, equation (5) and the first two of equations (4) may be replaced by

$$\nu^2 \doteq A + \frac{B^2}{2N^2}$$

$$f_1/g_0 \doteq \frac{B}{2N(N-2\nu)} \cong \frac{B}{2N^2}(1 + 2\nu/N)$$

$$g_1/g_0 \doteq \frac{B}{2N(N+2\nu)} \cong \frac{B}{2N^2}(1 - 2\nu/N), \qquad (6)$$

equations of this latter form having been employed previously[5] for the study of resonances in spirally-ridged accelerators when ν is small.

The use of equations (4) in analytic work does not appear significantly more troublesome than use of equations (6) if the value of A associated with ν is known from tables[7,8] or available from orientation runs with the digital computer. The accuracy of equations (4), as contrasted with that of the simpler relations (6) $f_1/g_0 \doteq \frac{B}{[2N(N-2\nu)]}$ and $g_1/g_0 \doteq \frac{B}{[2N(N+2\nu)]}$, is indicated by the comparison with results of digital computation given by the graphs appended to this report. (In calculating values of the coefficients used to construct these graphs, values of ν associated with the parameters A and B were obtained from the digital computations.) It appears, moreover, that numerical solution of equation (5) for ν in terms of the parameters A, B, and N will yield values in agreement with those obtained by digital computation to engineering accuracy, or to better than 0.2 percent for values of σ as high as 0.93π.

Commencing with recursion relations which are basically those employed in the present report, to the number of terms retained, Slater[6] obtains algebraic expressions for the coefficients F_i, G_i in terms of B and σ/π <u>alone.</u> Possibly because of the steps taken to eliminate the parameters A, however, convergence difficulties seem to be encountered when σ is near π .

IV. ACKNOWLEDGEMENTS:

The writers wish to thank Mr. Mills, Mr. Morton, and Mr. Westlund, who assisted in the numerical work.

V. REFERENCES:

1. A Spiral-Ridged Bevatron, W. Walkinshaw, A.E.R.E. Harwell (1956).

2. Expansions of the Characteristic Exponent and Solutions..., Nils Vogt-Nilsen, MURA Report-118 (May, 1956).

3. Approximations for Linear Betatron Oscillations, Adler and Baroncini, Nuovo Cimento (10) 4, 959-74 (1956).

4. Non-Linear Resonances in the Radial Equation, G. Parzen, MURA Report-200 (October 12, 1956).

5. Concerning Resonances in the Spirally-Ridged FFAG Accelerator, Laslett and Sessler, MURA Report in preparation -- Appendix II.

6. Soluble Problem in Energy Bands, J. C. Slater, Physical Review 87, 807-835 (September 1, 1952), Sect. 2.
For the case N = 2, our notation may be related to that of Slater as follows: His variables u and w are identified with our y and t, the parameters a and s with our A and 2B, his g_0 with our σ/π, and $v(g_0 \mp 2m)$ with our F_m and G_m, respectively.

7. MURA Tables No. 5 and accompanying graphs, Laslett, Snyder, and Hutchinson (April 20, 1955).

8. MURA Tables No. 6, Belford, Laslett, and Snyder, (April 3, 1956).

LINEAR EQUATIONS FOR WHICH FLOQUET SOLUTIONS OBTAINED

$$y'' + (A + B \cos 2t) y = 0$$

Run Nos.		Params.		Matrix Elements			σ/π *	
DUCK-ANS.	FOR-ANAL	B	A	M_{21}	M_{12}	$M_{11}=M_{22}$ = cos σ	From cos σ	Nominal
779	30	1.5	.1782	-.010 328	4.1584	-.978 291	.933 557	14/15
780	34		.1648	-.027 410	4.2329	-.940 199	.889 362	8/9
781	37		.1514	-.043 702	4.3085	-.900 950	.857 129	6/7
782	38		.1216	-.076 968	4.4800	-.809 434	.800 226	4/5
783	39		.0904	-.107 163	4.6646	-.707 195	.750 040	3/4
784	40		.0327	-.149 384	5.0202	-.500 067	.666 691	2/3
785	41		-.0352	-.173 818	5.4628	-.224 636	.572 119	4/7
786	42		-.0850	-.172 270	5.8048	+.0004918	.499 843	1/2
787	43		-.1470	-.144 598	6.2520	.309 801	.399 737	2/5
788	44		-.1823	-.114 921	6.5175	.501 004	.332 964	1/3
789	45		-.2170	-.075 130	6.7864	.700 100$_5$	.253 139	1/4
790	46		-.2330	-.053 061	6.9131	.795 728$_4$	.207 088	1/5 †
779	50	1.0	.450	-.028 369	2.3618	-.965 918	.916 658	11/12
780	54		.430	-.054 616	2.4415	-.930 942	.881 012	8/9 †
781	57		.411	-.078 378	2.5188	-.895 869	.853 446	6/7 †
782	58		.368	-.127 621	2.6993	-.809 637	.800 336	4/5
783	59		.323	-.171 786	2.8967	-.708 788	.750 758	3/4
784	60		.244	-.228 507	3.2654	-.503 814	.668 070	2/3
785	61		.180	-.252 125	3.5856	-.309 811	.600 266	3/5
786	62		.092	-.246 364	4.0590	+.001 299$_4$	.499 586	1/2
787	63		.017	-.201 068	4.4945	.310 321	.399 563	2/5
788	64		-.025	-.157 353	4.7518	.502 277$_5$	.332 496	1/3
789	65		-.065	-.102 323	5.0062	.698 389	.253 901	1/4
790	66		-.086	-.067 892	5.1435	.806 719	.201 241	1/5

* With N = 2, $\nu = \sigma/\pi$

† Approx.

Unnormalized FORANAL Coefficients For

$$y = g_0 \cos \nu\tau + \sum_{m=1} \left[f_m \cos(mN-\nu)\tau + g_m \cos(mN+\nu)\tau \right]^{*}$$

$$= g_0 \cos \nu\tau + \sum_{m=1} \left[(f_m+g_m) \cos mN\tau \cos \nu\tau + (f_m-g_m) \sin mN\tau \sin \nu\tau \right]$$

with $y(0) = 1$

FOR-ANAL NO.	NOM-INAL ν	g_0	f_1	g_1	f_2	g_2	f_3
30	14/15	.5000	.4173	.0446	.0340	~ .002 ‡	~ .002 ‡
34	8/9	.5260	.3903	$.0483_5$	$.0308_3$	$.0015_2$	.0009
37	6/7	.5449	.3726	$.0516_6$	.02880	.00164	.00082
38	4/5	$.5744_6$	.34116	.05599	.02533	.00183	.00070
39	3/4	.59808	.31626	.06023	.02269	.00201	.00062
40	2/3	.63147	.27953	.06715	.01896	.00232	.00050
41	4/7	.6616	.2445	.0749	.01555	.00267	.00038
42	1/2	.6796	$.2226_6$	.08082	.01356	.00299	.00034
43	2/5	.6988	.1968	.08918	.01128	.00344	.00027
44	1/3	$.740_4$	$.159_6$	$.083_4$	.010	.006	in noise
45	1/4	.721	.167	.103	.0087	.0042	~ .0002
46	1/5 †	.73	.16	.11	.008	.004	- - -
50	11/12	.5488	.3942	~ .035 ‡	~ .022 ‡		
54	8/9 †	.5850	.3794	.0373	.0208	.0009	.0005
57	6/7 †	.60	.35	$.04_9$	$.02_{75}$	- - -	- -
58	4/5	.6363	.3038	$.0426_2$	$.0153_8$	.00093	.00028
59	3/4	.665	$.273_3$	$.045_9$	.0133	.0010	.0002
60	2/3	.7034	$.232_3$	.0512	.0106	$.0011_4$	.00015
61	3/5	$.727_2$	$.206_7$	$.0553_4$	.00908	$.0013_1$	— —
62	1/2	$.753_4$	.1763	$.0613_3$	.00728	.00153	.00013
63	2/5	$.771_6$	.1530	$.0673_7$	.00593	.00175	.00010
64	1/3	.780	.1402	$.0715_5$	.00524	.00192	~ .0001
65	1/4	.793	.127	.077	.00441	.00206	- -
66	1/5	.795	.120	$.080_9$	.00410	.00228	- -

* In general $\nu\tau$ may be replaced by $\nu\tau + \epsilon$

† Approx.

Est. (not fm. Foranal)

COMPARISON OF CALCULATED AND TRUE EVEN FLOQUET SOLUTION

FOR MATHIEU EQUATION $y'' + (A + B \cos 2t) y = 0$

WITH B = 1.5 and $\sigma = 0.889\pi$

t/π (Sectors)	Calculated y: $y(g_0, f_1, g_1)$	Calculated y: $y(g_0, f_1, g_1, f_2)$	True y Duck-Ans Run 780
0	.9647	.9955	1.0000
1/8	.8683	.8788	.8800
1/4	.6226	.5991	.5989
3/8	.3173	.2907	.2938
1/2	.0152	.0206	.0213
5/8	-.2755	-.2452	-.2470
3/4	-.5592	-.5438	-.5420
7/8	-.7961	-.8158	-.8146
1	-.9065	-.9355	-.9379
1-1/8	-.8367	-.8361	-.8357
1-1/4	-.6112	-.5822	-.5808
1-3/8	-.3208	-.3406	-.3030
1-1/2	-.0437	-.0591	-.0597
1-5/8	.2006	.1703	.1718
1-3/4	.4281	.4228	.4210
1-7/8	.6276	.6543	.6523
2	.7390	.7625	.7636
2-1/8	.7030	.6925	.6915
2-1/4	.5259	.4951	.4932
2-3/8	.2855	.2750	.2761
2-1/2	.0670	.0905	.0910
2-5/8	-.1015	-.0748	-.0781
2 3/4	-.2455	-.2508	-.2496
2-7/8	- 3834	-.4138	-.4119
3	-.4824	-.4977	-.4981
3-1/8	-.4851	-.4653	-.4646
3 1/4	-.3773	-.3483	-.3466
3 3/8	-.2158	-.2158	-.2161
3-1/2	-.0821	-.1111	-.1114
3-5/8	-.0099	-.0297	-.0288
3-3/4	.0332	.0485	.0484
3-7/8	.0930	.1233	.1222
4	.1675	.1729	.1729
4-1/8	.2086	.1820	.1820
4-1/4	.1831	.1595	.1586
4-3/8	.1201	.1307	.1302
4-1/2	.0874	.0874	.1185

CALCULATED AND COMPUTED MATRIX-ELEMENT M_{12}

Duck-Ans. Run No.	Foranal Run No.	B	ν	M_{12} Calc. fm. 3 Terms	Calc. fm. 4 Terms	Calc. fm. 5 Terms	From I. B. M. Computations
780	34	1.5	.889362	1.8878	4.3391	3.9684	4.2329
781	37		.857129	2.2272	4.4057	4.0819	4.3085
789	45		.253139	5.7592	7.9081	6.6296	6.7864
780	54	1.0	.881012	1.8442	2.7978	2.7111	2.4415
788	64		.332496	4.4561	4.9766	4.7577	4.7518
789	65		.253901	4.6595	5.2460	4.9400	5.0062
790	66		.201241	4.8153	5.5416	5.0963	5.1435

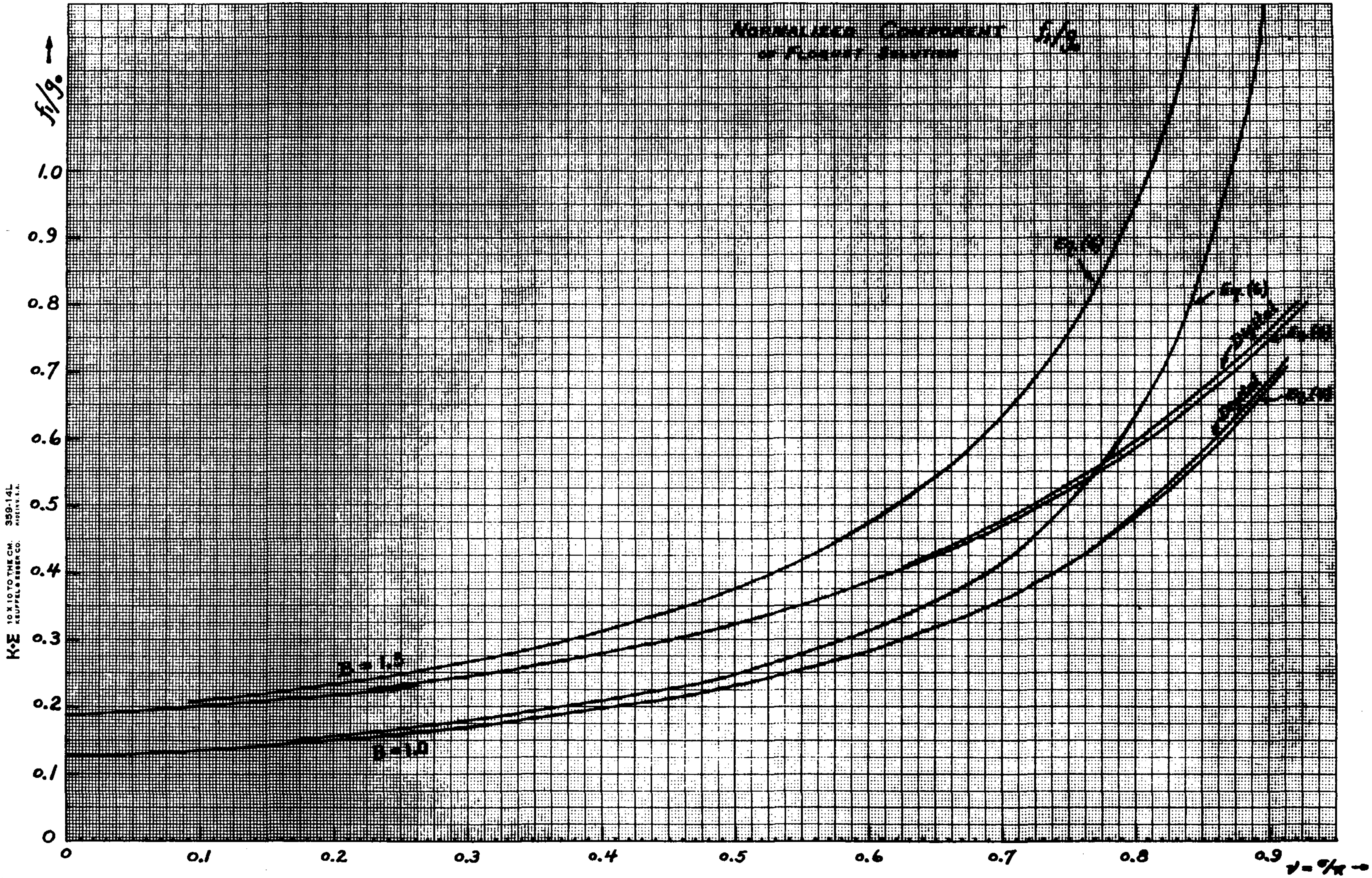

NORMALIZED COMPONENT f_1/g_0
OF FLOQUET SOLUTION
f_1/g_0
0
0.1
0.2
0.3
0.4
0.5
0.6
0.7
0.8
0.9
1.0
B = 1.5
B = 1.0
$\nu = \sigma/\pi$
K·E 10 X 10 TO THE CM. 359-14L
KEUFFEL & ESSER CO.

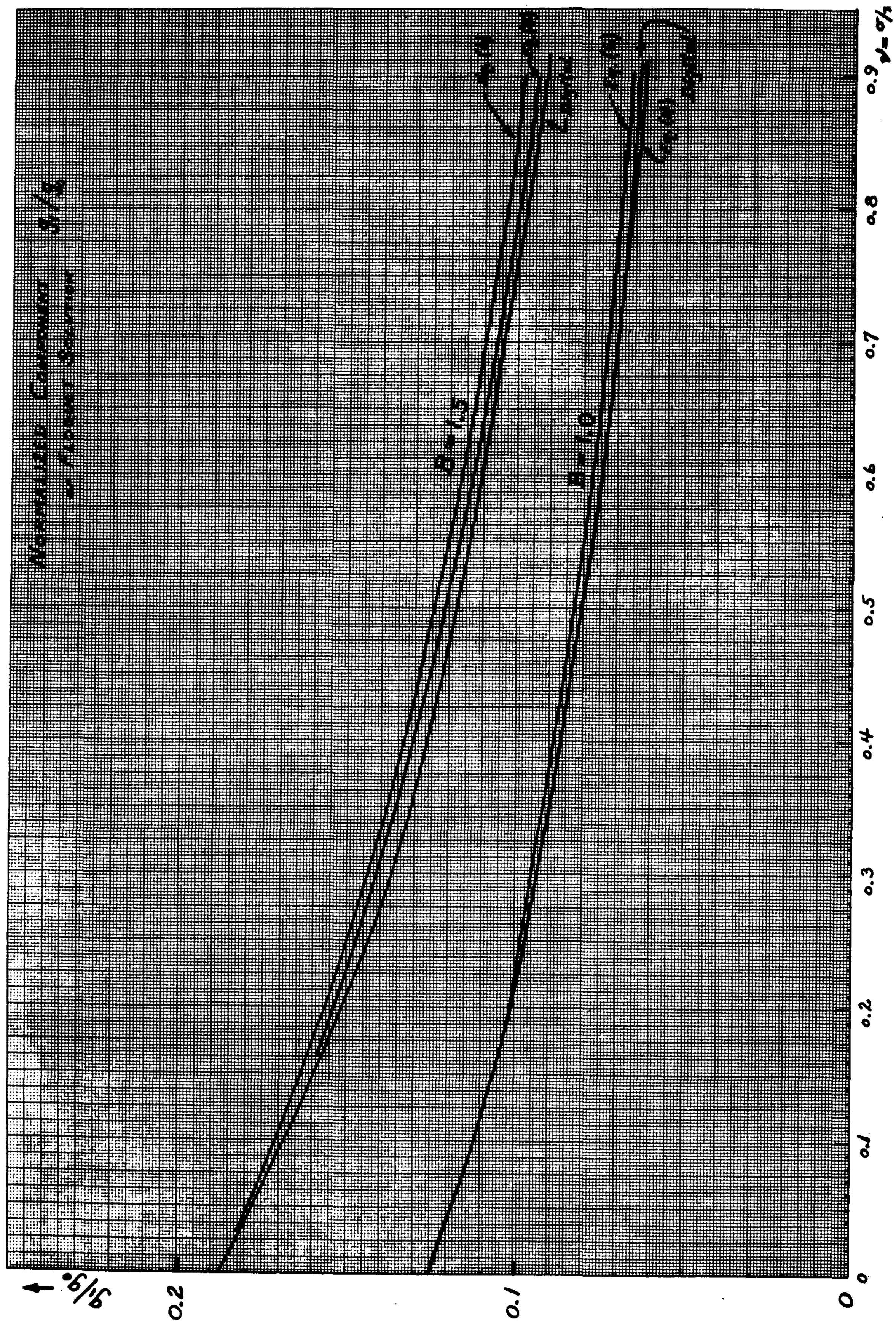
NORMALIZED COMPONENT
B = 1.5
B = 1.0
0.2
0.1
0
0
0.1
0.2
0.3
0.4
0.5
0.6
0.7
0.8
0.9

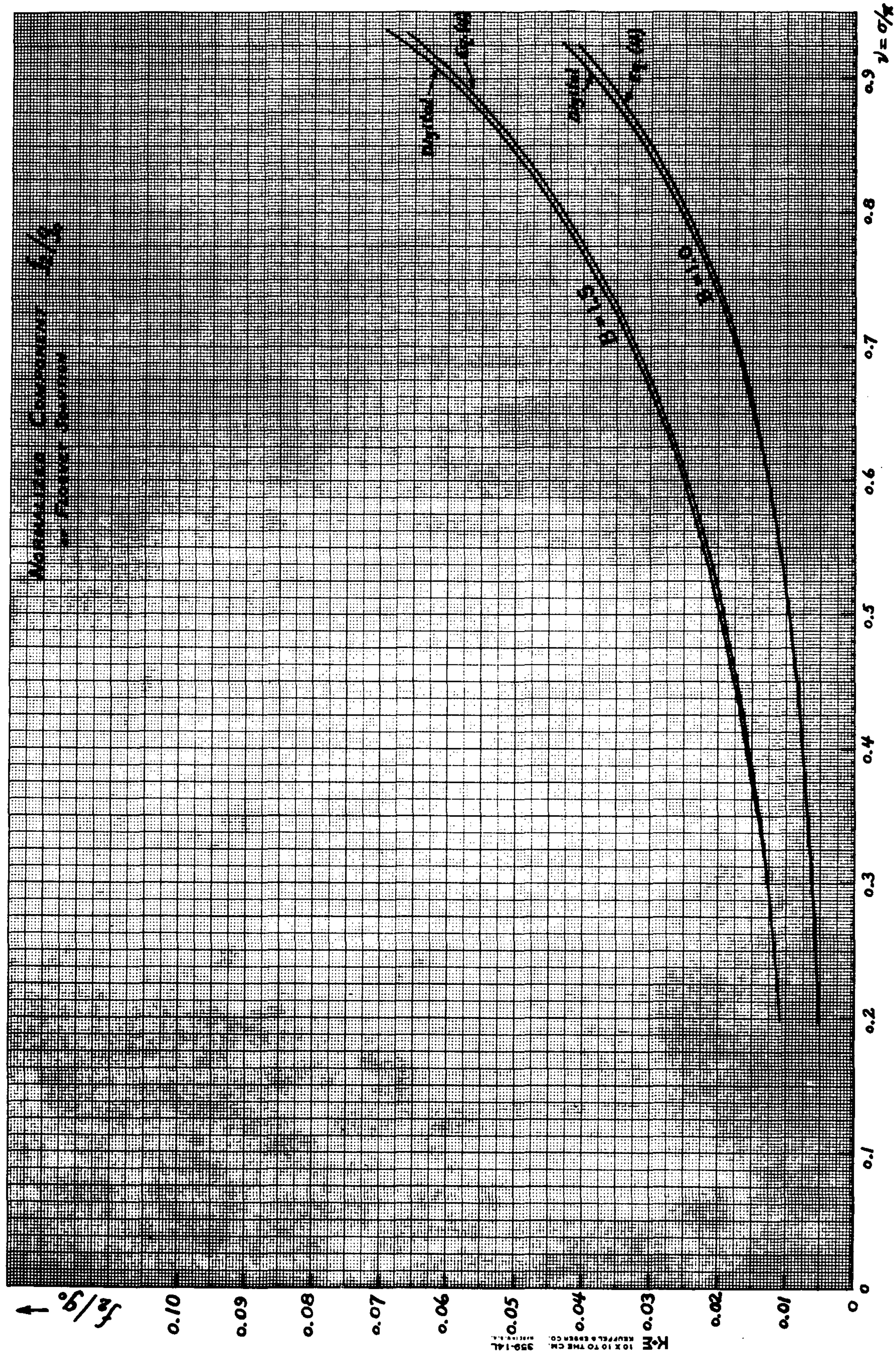

0
0.01
0.02
0.03
0.04
0.05
0.06
0.07
0.08
0.09
0.10
0.1
0.2
0.3
0.4
0.5
0.6
0.7
0.8
0.9
B=1.5
B=1.0
Digital
Digital

4

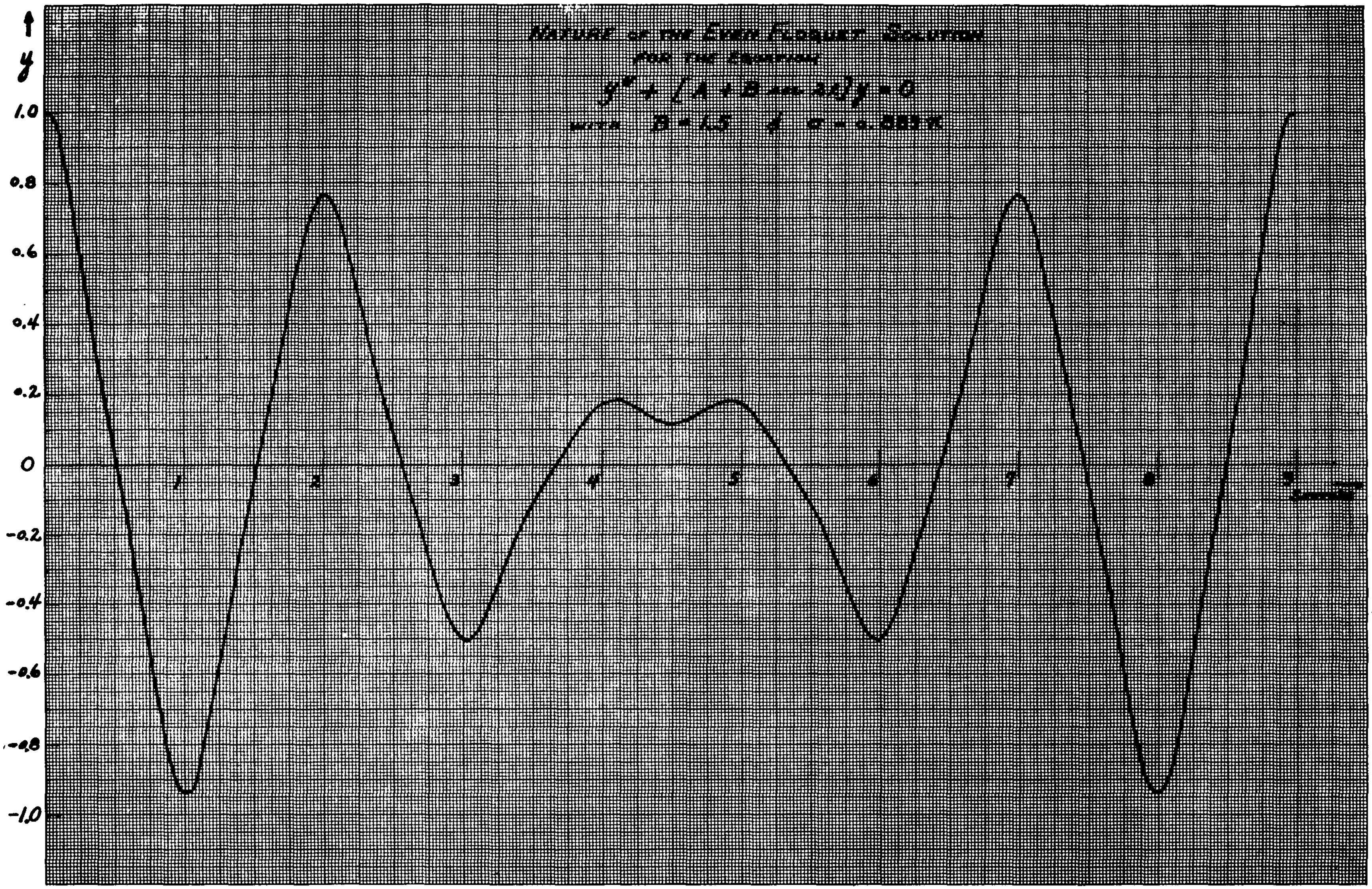

Nature of the Even Floquet Solution
for the Equation
$y'' + (A + B \cos 2z) y = 0$
with $B = 1.5$
y
1.0
0.8
0.6
0.4
0.2
0
-0.2
-0.4
-0.6
-0.8
-1.0
1
2
3
4
5
6
7
8
9

MURA-443
Distribution List UC 28

MIDWESTERN UNIVERSITIES RESEARCH ASSOCIATION*

2203 University Avenue, Madison, Wisconsin

THE NON-LINEAR COUPLING RESONANCE $2\nu_y - \nu_x = 1$

L. Jackson Laslett**

January 2, 1959

ABSTRACT

Computational results, obtained with the DUCK-ANSWER program and pertaining to the $2\nu_y - \nu_x = 1$ resonance, are reported for two examples of coupled Hamiltonian differential equations. Each of the examples contains a term involving $x \cdot y$ (with a periodic coefficient) in the y-equation. The width of the resonance appears in each case to be roughly proportional to the first power of the x-amplitude. Results are also presented to show the effect, on the y-motion, of traversing the $2\nu_y - \nu_x = 1$ resonance, at various rates.

A rough analytic examination of the second set of equations is also given. Comparisons with the computational results suggest the theory to be semi-quantitatively valid.

*AEC Research and Development Report. Research supported by the Atomic Energy Commission, Contract No. AT (11-1) 384.

**Department of Physics and Institute for Atomic Research, Iowa State College, Ames, Iowa.

I. MOTIVATION:

The character of the solutions to non-linear coupled differential equations, for oscillation frequencies in the neighborhood of certain non-linear coupling resonances, has been reported previously in a number of MURA reports[1†] and by members of the Harwell group.[2] Recently there has been interest in the $2\nu_y - \nu_x = 1$ resonance, since (i) the proposed operating point for the ANL 12.5 Gev accelerator[3] lies close to this resonance and (ii) it may be necessary to traverse this resonance when employing the Hammer-Bureau method[4, 5] of beam extraction from a conventional betatron or synchrotron.

Two systems of coupled differential equations have, accordingly, been studied by means of the MURA IBM 704 DUCK-ANSWER[6] computational program. Although neither of these systems may represent closely the physical situations mentioned above, it was felt that the results would be of interest as illustrative of effects attributable to the $2\nu_y - \nu_x = 1$ resonance. Attention has been focused on the growth of y-amplitude (axial-amplitude) rather than on the possible eventual "turn-over" of the y-growth, axial limitations of aperture frequently making turn-over of somewhat secondary interest. To simplify the study, only those non-linear terms were introduced which would be required to give a Hamiltonian system of equations capable of responding directly to the resonance in question and first-derivative terms were omitted.

A guide to the magnitude of the y-oscillation amplitude was obtained by computing the quantity[7]

$$K_y \equiv \left[y^2 + (\zeta_y / \xi_y)\, p_y^2\right]^{1/2},$$

which should be an invariant for small-amplitude oscillations.

---

† References are given in Section VI.

II. THE EQUATIONS STUDIED

The equations employed in this study were the following:

SET I.

$$d^2x/d\theta^2 + (0.536 - 1.8 \cos 8\theta - 0.075 \cos\theta)\, x = -(0.025 \cos\theta)\, y^2$$

$$d^2y/d\theta^2 + (-160\, S_2 + 1.2 \cos 8\theta + 0.050 \cos\theta)\, y = -2\,(0.025 \cos\theta)\, x \cdot y\,,$$

which wereput into a form suitable for use of the DUCK-ANSWER program by the transformation $4\theta = \tau$:

$$d^2x/d\tau^2 = 10\,(-0.00335 + 0.01125 \cos 2\tau + 0.00046875 \cos \frac{6\tau}{24})\, x + (-0.0015625 \cos \frac{6\tau}{24})\, y^2$$

$$d^2y/d\tau^2 = 10\,(S_2 - 0.0075 \cos 2\tau - 0.0003125 \cos \frac{6\tau}{24})\, y + 2\,(-0.0015625 \cos \frac{6\tau}{24})\, x \cdot y\,.$$

The constant coefficient S_2 was adjusted to obtain small-amplitude y-oscillation frequencies located as desired in the neighborhood of the $2\nu_y - \nu_x = 1$ resonance.

SET II.

$$d^2x/d\theta^2 + (-2.5\, S_1 - 0.063 \cos\theta)\, x = (-0.0825 - 0.105 \cos\theta)\,(x^2 - y^2)$$

$$d^2y/d\theta^2 + (-2.5\, S_2 + 0.063 \cos\theta)\, y = 2\,(0.0825 + 0.105 \cos\theta)\, x \cdot y,$$

which were transformed by the substitution $\theta = 2\tau$ to obtain the working equations:

$$d^2x/d\tau^2 = 10\,(S_1 + 0.0252 \cos 2\tau)\, x + (-0.33 - 0.42 \cos 2\tau)\,(x^2 - y^2)$$

$$d^2y/d\tau^2 = 10\,(S_2 - 0.0252 \cos 2\tau)\, y + 2\,(0.33 + 0.42 \cos 2\tau)\, x \cdot y\,.$$

In this case the constant coefficients S_1 and S_2 were adjusted together, in concordance with the relation $S_1 + S_2 = -0.4036$, to obtain desired operating points in the neighborhood of the $2\nu_y - \nu_x = 1$ resonance.

In connection with this set of equations it was also of interest to traverse the resonance "dynamically"--i.e., during the course of a run. This could be accomplished by introducing, in effect, a secular change in the coefficients S_1 and S_2. Specifically, the factors $S_1 + 0.0252 \cos 2\tau$ and $S_2 - 0.0252 \cos 2\tau$ in the last equations were then supplemented, respectively, by

$$B_1 \cos\left(\frac{4\tau}{16384} + \frac{\pi}{2}\right) \text{ and } B_2 \cos\left(\frac{4\tau}{16384} + \frac{\pi}{2}\right),$$

where the coefficients B_1 and B_2 are related to the rate-of-change of the "field-index," n, substantially by

$$B_1 \cong -3300 \ dn/d\theta \text{ and } B_2 \cong +3300 \ dn/d\theta .$$

The location of the working points, in relation to the $2\nu_y - \nu_x = 1$ resonance line, for these two sets of equations is indicated in Fig. 1. Inferences drawn from the computational results for the amount of non-linearity introduced in these equations may, of course, be re-interpreted for other magnitudes of non-linearity (of the same form) by "scaling" the dependent variables--i.e., by use of the transformation $x = \alpha X$, $y = \alpha Y$, which has the effect of increasing the relative amount of non-linearity by the factor α.

III. RESULTS FOR THE EQUATIONS OF SET I:

A. The Oscillation Frequencies:

The frequencies of small-amplitude oscillations were determined for the equations of Set II (for various values of the parameter S_2) by preliminary orientation runs in which the non-linear (coupling) terms were suppressed. The results are shown below in Table I.

TABLE I

Oscillation Frequencies for Equations of Set I

$\nu_x = 0.7483$

S_2	$-160\ S_2$	$2\nu_y - \nu_x$
-0.005235	0.8376	1.0938
-0.005075	0.8120	1.0664
-0.004995	0.7992	1.0515
-0.004915	0.7864	1.0379
-0.004835	0.7736	1.0235
-0.004755	0.7608	1.0090
-0.004675	0.7480	0.9943
-0.004595	0.7352	0.9796
-0.004515	0.7224	0.9646
-0.004355	0.6968	0.9344
-0.004195	0.6712	0.9036

B. The Examination of y-Growth:

For each of the frequencies listed in Table I, runs were made with a small initial y-amplitude (0.001) and various initial x-amplitudes, in an effort to find y-growth characteristic of the coupling resonance. When such growth was observed, "the lapse-rate" denoting the rate of exponential growth was measurable from a semi-logarithmic plot of K_y vs τ/π and could be conveniently expressed as decades per $\Delta\tau = \pi$. Since $\tau = 4\,\theta$, the lapse-rate so determined may also be regarded as expressed in "decades per octant."

The results of these runs are summarized in Table II and portrayed in the form of an altitude chart in Fig. 2. In the figure each notch corresponds to a lapse-rate of 0.005 decades per octant As mentioned in Section II, the results could be re-interpreted for other strengths of the non-linearity by suitable scaling of the dependent variables.

TABLE II

Lapse-Rate for Equations of Set I

Lapse-rates are given in decades per octant

$\nu_x = 0.7483$

S_2	$2\nu_y - \nu_x$	x_0			
		7.0	4.4	2.2	0.7
-0.005235	1.094	Throb-factor 5.8			
-0.005075	1.066	0.010_1	Throb-factor 4.37		
-0.004995	1.052		0.0062		
-0.004915	1.038			0.0028	
-0.004835	1.024	0.0141	0.0089	0.0043	
-0.004755	1.009	0.0143		0.0048	
-0.004675	0.994	0.0144	0.0091	0.0048	0
-0.004595	0.980	0.0136		0.003	
-0.004515	0.965	0.0123	0.0065	0	
-0.004355	0.934	0.0071_5	0		
-0.004195	0.904	0			

IV. RESULTS FOR THE EQUATIONS OF SET II:

A. Results with no Secular Change.

As with the equations of Set I the frequencies of small-amplitude oscillations were determined for the equations of Set II by short orientation runs with the non-linear terms suppressed. With the non-linear terms present a search was made to find y-growth, again using a small initial y-amplitude (0.00001) and various initial x-amplitudes. When y-growth was seen to be present, it was followed through a few decades--in every case through more than one decade save for those runs with x_o equal to 0.01 or to 0.005--and the lapse-rate determined. For the equations of Set II, in which $\theta = 2\tau$, the lapse-rate is conveniently expressed in decades per $\Delta\tau = \pi$ or, equivalently, as decades per revolution.

The results, giving the lapse-rate for various values of the parameters S_1 and S_2 together with the associated frequencies for small-amplitude oscillations, are listed in Table III. The lapse-rates are also shown in Fig. 3 in the form of an altitude chart, with each notch corresponding to a lapse-rate of 0.02 decades per revolution.

B. Results with Secular Change:

As remarked in Section II, the motion characterized by the equations of Set II could be caused to traverse the $2\nu_y - \nu_x = 1$ resonance by introduction of the terms $B_{1 \text{ or } 2} \cos\left(\frac{4\tau}{16384} + \frac{\pi}{2}\right)$, with $B_1 = -B_2$. These terms, in effect, are equivalent to a slow (substantially linear) secular change of the coefficients S_1 and S_2 and produce a change of the small-amplitude oscillation frequencies simulating a linear change of the field-index, n:

$$dn/d\theta \cong B_2/3300 .$$

The values of S_1 and S_2 actually used throughout this series were -0.1618 and -0.2418, respectively, corresponding to initial oscillation frequencies $\nu_x = 0.6334$ and $\nu_y = 0.7765$, with $2\nu_y - \nu_x = 0.9196$ [Table III].

TABLE

OSCILLATION FREQUENCIES AND LAPSE-RATES FOR EQUATIONS OF SET II

Lapse-Rates are given in decades per revolution $S_1 + S_2 = -0.4036$

S_1	S_2	ν_x	ν_y	$2\nu_y - \nu_x$	x_0 0.50	0.25	0.10	0.050	0.025	0.010	0.005
0.1618	-0.2418	0.6334	0.7765	0.9196	throb-factor						
0.1525	-0.2511	0.6143	0.7914	0.9685	2.5 or 2.6						
0.1505	-0.2531	0.6101	0.7946	0.9791	0.0175	throb -factor					
0.1495	-0.2541	0.6080	0.7962	0.9844		2.5					
0.1485	-0.2551	0.6058	0.7977	0.9896	0.0287	0.0086					
0.1475	-0.2561	0.6037	0.7993	0.9948		0.0141					
0.1470	-0.2566	0.6027	0.8001	0.9975			0.0052				
0.1465	-0.2571	0.6016	0.8009	1.0001	0.0306	0.0156	0.0062	0.0031	0.0016	0.0006_2	0.00038
0.1460	-0.2576	0.6005	0.8017	1.0028			0.0046				
0.1455	-0.2581	0.5994	0.8024	1.0054		0.0127					
0.1445	-0.2591	0.5972	0.8040	1.0107	0.0241	0.0044					
0.1435	-0.2601	0.5950	0.8055	1.0160		O					
0.1425	-0.2611	0.5928	0.8071	1.0213	O						
0.1408	-0.2628	0.5891	0.8097	1.0304							
0.1405	-0.2631	0.5884	0.8102	1.0320	O						
0.1268	-0.2768	0.5561	0.8311	1.1061							
0.1233	-0.2803	0.5469	0.8364	1.1258							
0.1198	-0.2838	0.5370	0.8416	1.1462							
0.1124	-0.2912	0.5000	0.8525	2.2050							

In all the runs made employing this secular change of parameters, the initial y-amplitude was, as before, taken as quite small (0.00001). It would be expected that the factor by which the y-amplitude is increased by traversal of the resonance would depend in a somewhat accidental way upon the phase with which the oscillations enter the region of instability--in most of the work reported here the initial amplitude of x-oscillation was obtained by taking $x_o = 0.50$, $p_{x_o} \equiv [dx/d\tau]_o = 0$ or $x_o = 0$, $p_{x_o} = 0.51$ (each corresponding to an initial amplitude 0.50), or by $x_o = 0.25$, $p_{x_o} = 0$ or $x_o = 0$, $p_{x_o} = 0.255$ (corresponding to an initial amplitude 0.25). The rates of secular change which were employed are listed in Table IV.

TABLE IV

Values of the Coefficients B_1 and B_2, Introduced to Represent a Secular Change of Frequency, and the Corresponding Rate-of-Change of Field-Index

B_1	B_2	Approx. $dn/d\theta$
-0.0990	0.0990	0.000 030
-0.1452	0.1452	0.000 044
-0.2145	0.2145	0.000 065
-0.3168	0.3168	0.000 096
-0.462	0.462	0.000 140
-0.66	0.66	0.000 200
-0.99	0.99	0.000 300

The results of such runs are shown in Figs. 4-10. Although traversal of the resonance $2\nu_y - \nu_x = 1$ is seen to have a material effect on the amplitude of the y-oscillations, normally increasing the amplitude by a substantial factor, the magnitude of the effect is seen to depend considerably upon the phase (of the x-oscillations in this case) at the start of the run and in some cases a decrease of y-amplitude is seen to result [Figs. 9 and 10]. In some of the runs, specifically those with the more rapid secular changes, the computations continued for a sufficient number of revolutions to carry the operating point to the neighborhood of $\sigma_x = \pi (\nu_x = 1/2)$--in such cases, of course, the x-motion would be expected to experience instability and, through coupling with the y-motion, exert a pronounced influence on the latter. In an auxiliary investigation,[8] however, no resonances leading to y-growth were detected in the interval between $2\nu_y - \nu_x = 1$ and $\nu_x = 1/2$ for the simple equations of Set II (as was to be expected).

Since, as noted above, the effect on the y-amplitude of traversing the coupling resonance will necessarily depend markedly upon the initial phases of the oscillatory motion, the results depicted in Fig. 7 [$B_1 = -0.3168$, $B_2 = 0.3168$; $dn/d\theta \cong 0.000\,096$] were supplemented by sixty additional runs to give what it was hoped would be a representative selection of initial phases for both the x- and the y-motion. As before, the initial values corresponded to an initial x-amplitude of either 0.50 or 0.25. From the results of this survey (summarized in Appendix I), it was felt that the following factors represent a fair estimate of the amount of growth which may be obtained with this rate of traversal of the $2\nu_y = \nu_x = 1$ resonance (cf. Fig. 13):

For an initial x-amplitude of 0.50, growth by a factor 18 or 1.25 decade;

For an initial x-amplitude of 0.25, growth by a factor 3.3 or 0.52 decade.

V. APPROXIMATE ANALYTIC TREATMENT:

A. The Case of No Secular Change:

It may be of interest to attempt an analytic treatment of the equations of Set II along the lines previously employed[9] in examination of other coupling resonances, although the accuracy of such theoretical results may suffer in the present instance because the oscillation frequencies are sufficiently high that both σ_x and σ_y lie rather close to π. The method[10] basically assumes the x-motion to be prescribed, unaffected by coupling with the relatively small y-motion, and this solution when substituted into the y-equation thus gives a differential equation linear in the single dependent variable y.

Since we are here attempting no more than an approximate treatment of the $2\nu_y - \nu_x = 1$ resonance, it apparently is sufficient to employ a simplified form of the y-equation

$$\frac{d^2y}{d\theta^2} + \left[\nu_y^2 + (d/2)(\cos\theta)\, x\right] y = 0,$$

where d = -0.42 in the computations reported above (Section IV). If a simple representation of the x-motion,

$$x = A_x \cos \nu_x \theta ,$$

is now employed, one obtains

$$\frac{d^2y}{d\theta^2} + \left[\nu_y^2 + (A_x\, d/2)(\cos \nu_x \theta)(\cos\theta)\right] y = 0$$

or

$$\frac{d^2y}{d\theta^2} + \left[\nu_y^2 + (A_x\, d/4)\cos(1+\nu_x)\theta + (A_x\, d/4)\cos(1-\nu_x)\theta\right] y = 0.$$

For purposes of studying the $2\nu_y - \nu_x = 1$ resonance, we may ignore the last term in the coefficient of y and consider the simple Mathieu equation

$$\frac{d^2y}{d\theta^2} + \left[\nu_y^2 + (A_x\, d/4)\cos(1 + \nu_x)\,\theta\right] y = 0.$$

(1.) This last equation has, as is well known, the stability boundaries [cf. Ref. 9, Appendix IB, C]:

$$-\left|\frac{A_x d}{2}\right| < (2\,\nu_y)^2 - (1 + \nu_x)^2 < \left|\frac{A_x d}{2}\right| ,$$

leading to a full-width for the resonance which may be conveniently expressed as

$$\Delta\left[2\,\nu_y - \nu_x - 1\right] = \frac{|A_x d|}{2\,\nu_y + \nu_x + 1} .$$

Numerically, for the problem at hand, this becomes

$$W \doteq \frac{0.42}{3.2}\, A_x$$

$$= 0.131\, A_x ,$$

where W denotes the full-width of the resonance in units of $2\,\nu_y - \nu_x$.

We may compare this theoretical width with that estimated from the computational results of Section IV A, as is done in Table V below.

TABLE V

Comparison of the Theoretical and Computational Width for the Resonance $2\,\nu_y - \nu_x = 1$

The Table gives the widths in units of $2\,\nu_y - \nu_x$

d = -0.42 $\qquad \nu_x \cong 0.6016,\ \nu_y \cong 0.8008$

A_x	0.50	0.25	0.10
$W_{theor.}$	0.066	0.033	0.013
$W_{obs.}$	0.051	0.029	0.012

(2.) The lapse-rate characterizing y-growth in the unstable region may also be estimated for the Mathieu equation cited earlier, by reference to methods used previously [cf. Ref. 9, Appendix IV]. One obtains

$$\mu = \frac{|d|}{8} \frac{\sqrt{A_x^2 - A_{thr.}^2}}{1 + \nu_x} \doteq \frac{1}{4}\sqrt{W^2 - 4q^2} \text{ nepers/radian of } \theta ,$$

where q denotes $2\nu_y - \nu_x - 1$ and $A_{thr.}$ the threshold amplitude,

$$\mu_{Max.} = \frac{|d|}{8} \frac{A_x}{1 + \nu_x} \doteq \frac{W}{4} \text{ nepers/radian of } \theta .$$

If, for convenience, we convert these results to decades per revolution (through multiplication by $2\pi \log e \doteq 2.72875$) and insert the appropriate constants for the problem at hand (when required), we obtain

$$\mu = 0.089\sqrt{A_x^2 - A_{thr.}^2} \doteq 0.68\sqrt{W^2 - 4q^2} \text{ decades/revolution of } \theta$$

and

$$\mu_{Max.} = 0.089\, A_x \doteq 0.68\, W \text{ decades/revolution of } \theta .$$

The formula for $\mu_{Max.}$ may be compared with the computational results, summarized in Table III, for $2\nu_y - \nu_x = 1.0001$, which corresponds closely to the resonant condition and for which the lapse-rates attain nearly their maximum values. This comparison is given in Table VI.

TABLE VI

Comparison of Theoretical and Observed Lapse-Rates.
Lapse-rates are given in decades/revolution.

$S_1 = -0.1465$, $S_2 = -0.2571$ $\nu_x = 0.6016$, $\nu_y = 0.8009$, $2\nu_y - \nu_x = 1.0001$

A_x	0.50	0.25	0.10	0.050	0.025	0.010	0.005
μ Calculated from A_x	0.045	0.022	0.0089	0.0045	0.0022	0.0009	0.0004
μ Calculated from $W_{obs.}$	0.035	0.020	0.0082				
$\mu_{obs.}$ from Computer	0.0306	0.0156	0.0062	0.0031	0.0016	0.0006	0.0004

From the comparisons shown we infer that the simple theory outlined in this section appears to provide a semi-quantitative account of the effects of the resonance, in the absence of secular change, although the widths for the resonance and the associated lapse-rates appear to be somewhat greater than observed from the computational results.

B. Effect of Traversal of Resonance:

It is tempting to employ the foregoing theoretical results to estimate the possible increase of y-amplitude when traversing the $2\nu_y - \nu_x = 1$ resonance. The results of such an attempt certainly cannot be expected to be of high accuracy, in part because of the approximate character of the preceding analysis and in part because of a certain amount of adiabatic amplitude-change (which we shall ignore) before reaching the resonance, but perhaps primarily because the situation with secular change is in a sense different and the net effect upon the y-motion will certainly (as we have seen) depend markedly on the phases of the respective oscillations.

From the results of the preceding sub-section, we estimate the growth of y-amplitude which can result from traversal of the $2\nu_y - \nu_x = 1$ resonance to be, if the ascending exponential solution dominates,

$$\text{Growth} = \int \frac{\sqrt{W^2 - 4q^2}}{4}\, d\theta \qquad \text{nepers, with the integral taken through the resonance}$$

$$= \frac{1}{4\left|\frac{dq}{d\theta}\right|} \int_{W/2}^{W/2} \sqrt{W^2 - 4q^2}\; dq$$

$$= \frac{W^2}{4\left|\frac{dq}{d\theta}\right|} \int_0^1 \sqrt{1 - \xi^2}\; d\xi$$

$$= \frac{\pi}{16} \frac{W^2}{\left|\frac{dq}{d\theta}\right|} \quad \text{nepers,}$$

where, as before, q denotes $2\nu_y - \nu_x - 1$. From the observed dependence of ν_x and ν_y on the parameters S_1 or S_2 (Table III), and from the rate at which the coefficients B_1 and B_2 in effect modify S_1 and S_2, one finds for the equations of Set II (with $B_1 = -B_2$),

$$\left|\frac{dq}{d\theta}\right| \cong \frac{5.3}{8192} \left| B_1 \right|$$

and

$$\begin{aligned} \text{Growth} &= \frac{\pi}{16} \; \frac{8192}{5.3} \; \frac{W^2}{|B_1|} \text{ nepers} \\ &= 303.5 \; \frac{W^2}{|B_1|} \text{ nepers} \\ &= 132 \; \frac{W^2}{|B_1|} \text{ decades,} \end{aligned}$$

W being the full-width of the resonance, for the x-amplitude under consideration, measured in units of $2\nu_y - \nu_x$.

In particular, for the case $B_1 = -0.3168$, $B_2 = 0.3168$,

$$\text{Growth} = 416 \; W^2 \text{ decades.}$$

If we employ the observed widths of the resonance (Table V) for the x-amplitudes 0.50 and 0.25, we then expect

For $x_o = 0.50$, Growth of 1.08 decades (factor 12);

For $x_o = 0.25$, Growth of 0.35 decades (factor 2.2).

[If the theoretical values of W were employed, the expected growth would be somewhat larger--1.81 and 0.45 decades, or factors of 65 and 2.8, respectively.] As noted in Section IV B, the corresponding figures estimated from actual computational runs (32 runs for each x-amplitude) were

For $x_o = 0.50$, Growth of 1.25 decades (factor 18);

For $x_o = 0.25$, Growth of 0.52 decades (factor 3.3).

VI. REFERENCES AND NOTES:

[1]For example, MURA-263, 295, 319, 320, 365, and 379.

[2]See, for example, A. E. R. E. T/R 2342.

[3]Argonne National Laboratory, Particle Accelerator Division Summary Report ANL-5630 (April-September 1956)--Section III.

[4]C. L. Hammer and A. J. Bureau, Rev Sci. Inst. 26, 594, 598 (June, 1955).

[5]C. L. Hammer and L. J. Laslett, Proceedings of the Second International Conference on the Peaceful Uses of Atomic Energy, Geneva, Switzerland (September, 1958)--Paper A/Conf. 15/P/726.

[6]J. N. Snyder, Internal MURA Reports (IBM Programs 75 and 77) 237 and 238 (February-March, 1957).

[7]L. Jackson Laslett, MURA Report 206 (November 21, 1956).

[8]In an investigation to see whether any resonances leading to y-growth could be detected for the equations of Set II in the interval between $2\nu_y - \nu_x = 1$ and $\nu_x = 1/2$, the initial x-amplitude was determined by taking $x_o = 0.50$ and, as before, the value $y_o = 10^{-5}$ was employed. The values used for the constants S_1, S_2, and estimates of the corresponding small-amplitude oscillation frequencies are listed below $[S_1 + S_2 = -0.4036]$.

S_1	S_2	ν_x(est.)	ν_y (est.)
-0.1380	-0.2656	0.583	0.814
-0.1355	-0.2681	0.577	0.818
-0.1330	-0.2706	0.571	0.822
-0.1305	-0.2731	0.575	0.825_5
-0.1280	-0.2756	0.559	0.829
-0.1255	-0.2781	0.553	0.833
-0.1230	-0.2806	0.546	0.837
-0.1205	-0.2831	0.539	0.840_5
-0.1180	-0.2856	0.531	0.844
-0.1155	-0.2881	0.52_3	0.848
-0.1130	-0.2906	0.51_0	0.852

As expected, with the coupling terms employed in the equations of Set II, no evidence of any coupling resonance was seen in this interval. For the two runs for which the coefficients were those listed in the last two lines of the preceding Table, however, x-instability for the x-amplitude employed (0.50) rapidly became apparent, attributable to the proximity to the $\sigma_x = \pi$ ($\nu_x = 1/2$) resonance (Figs. 11 and 12).

[9]Esp. L. Jackson Laslett and A. M. Sessler, MURA-263 (May 6, 1957).

[10]The procedure in principle thus parallels that suggested by W. Walkinshaw for analysis of the $2\nu_y - \nu_x = 0$ resonance--W. Walkinshaw, "A Spiral Ridged Bevatron," A. E. R. E., Harwell (1956).

APPENDIX I

Data Illustrating Growth in Traversal of Resonance

$dn/d\theta = 0.000\ 096$

$|A_x| = 0.50$

x_o	p_{x_o}	y_o	p_{y_o}	Growth Factor For Successive Maxima and Minima After Traversing Resonance				Geom. Mean of Middle Two Factors
.5	0	.00001	0	17.657	8.920	15.646	9.703	11.81
.354	.361			10.838	5.774	9.706	6.135	7.49
0	.51			3.146	1.661	2.709	1.769	2.12
-.354	.361			7.537	3.774	6.475	4.249	4.94
-.5	0			18.725	9.598	16.635	9.694	4.00
-.354	-.361			22.034	11.883	19.607	11.970	15.26
0	-.51			23.547	12.456	20.180	13.902	15.85
.354	-.361			23.390	11.906	20.104	12.619	15.47
.5	0	.00000 7101	.0000 11999	23.606	11.923	20.911	12.965	15.79
.354	.361			23.937	12.762	21.408	13.533	16.53
0	.51			18.128	9.586	14.962	10.585	11.98
354	.361			10.203	5.084	8.800	5.753	6.69
.5	0			0.378	0.183	0.325	0.235	0.24
-.354	-.361			7.552	4.016	6.708	4.121	5.19
0	-.51			14.729	7.826	12.671	8.713	9.96
.354	-.361			22.651	11.539	19.476	12.238	14.99
.5	0	0	.0000 16999	15.724	7.927	13.917	8.638	10.50
.354	.361			23.303	12.424	20.849	13.178	16.09
0	.51			23.565	12.468	20.143	13.760	15.85
-.354	.361			22.182	11.056	19.161	12.517	14.55
-.5	0			18.154	9.301	16.108	9.388	12.24
-.354	-.361			10.980	5.916	9.773	5.969	7.60
0	-.51			3.044	1.621	2.639	1.810	2.07
.354	-.361			8.504	4.365	7.331	4.656	5.66
.5	0	-.00000 7101	.0000 11999	2.136	1.068	1.883	1.178	1.42
.354	.361			8.469	4.519	7.622	4.816	5.87
0	.51			14.636	7.756	12.558	8.265	9.87
-.354	.361			21.19[illegible]	10.570	18.300	11.961	13.91
-.5	0			26.199	13.425	23.245	13.547	17.67 ←
-.354	-.361			23.184	12.523	20.631	12.587	16.07
0	-.51			18.088	9.560	15.494	10.675	12.17
354	-.361			10.497	5.346	9.025	5.681	6.95

$|A_x| = 0.25$

x_o	p_{x_o}	y_o	p_{y_o}	Growth Factor For Successive Maxima and Minima After Traversing Resonance				Geom. Mean of Middle Two Factors
.25	0	.00001	0	3.899	2.759	3.681	2.843	3.187
.177	.1805			4.010	2.857	3.745	2.945	3.271
0	.255			3.615	2.497	3.291	2.590	2.867
-.177	.1805			2.625	1.851	2.459	1.949	2.133
-.25	0			1.338	0.922	1.234	0.960	1.067
-.177	-.1805			0.561	0.419	0.541	0.436	0.476
0	-.255			2.045	1.478	1.917	1.510	1.683
.177	-.1805			3.280	2.293	2.988	2.409	2.618
.25	0	.00000 7101	.0000 11999	2.031	1.402	1.877	1.510	1.622
.177	.1805			3.285	2.348	3.070	2.412	2.685
0	.255			3.969	2.802	3.667	2.846	3.205
-.177	.1805			4.074	2.840	3.774	3.020	3.274
-.25	0			3.579	2.491	3.314	2.601	2.873
-.177	-.1805			2.591	1.808	2.395	1.823	2.081
0	-.255			1.310	0.905	1.191	0.945	1.038
177	-.1805			0.526	0.381	0.513	0.405	0.442
.25	0	0	.0000 16999	1.331	0.921	1.229	0.934	1.064
.177	.1805			0.590	0.442	0.567	0.455	0.501
0	.255			1.999	1.461	1.915	1.472	1.673
-.177	.1805			3.259	2.255	2.986	2.409	2.595
-.25	0			3.975	2.761	3.669	2.881	3.183
-.177	-.1805			4.007	2.863	3.754	2.843	3.278
0	-.255			3.565	2.491	3.285	2.607	2.861
.177	-.1805			2.686	1.833	2.435	1.958	2.113
.25	0	-.00000 7101	.0000 11999	3.568	2.529	3.361	2.569	2.915
.177	.1805			2.584	1.810	2.406	1.885	2.087
0	.255			1.341	0.908	1.204	0.980	1.046
-.177	.1805			0.314	0.491	0.369	0.483	0.426
-.25	0			2.025	1.440	1.900	1.493	1.654
-.177	-.1805			3.204	2.325	3.052	2.322	2.664
0	-.255			3.931	2.753	3.626	2.892	3.159
.177	-.1805			4.153	2.849	3.768	3.038	3.276

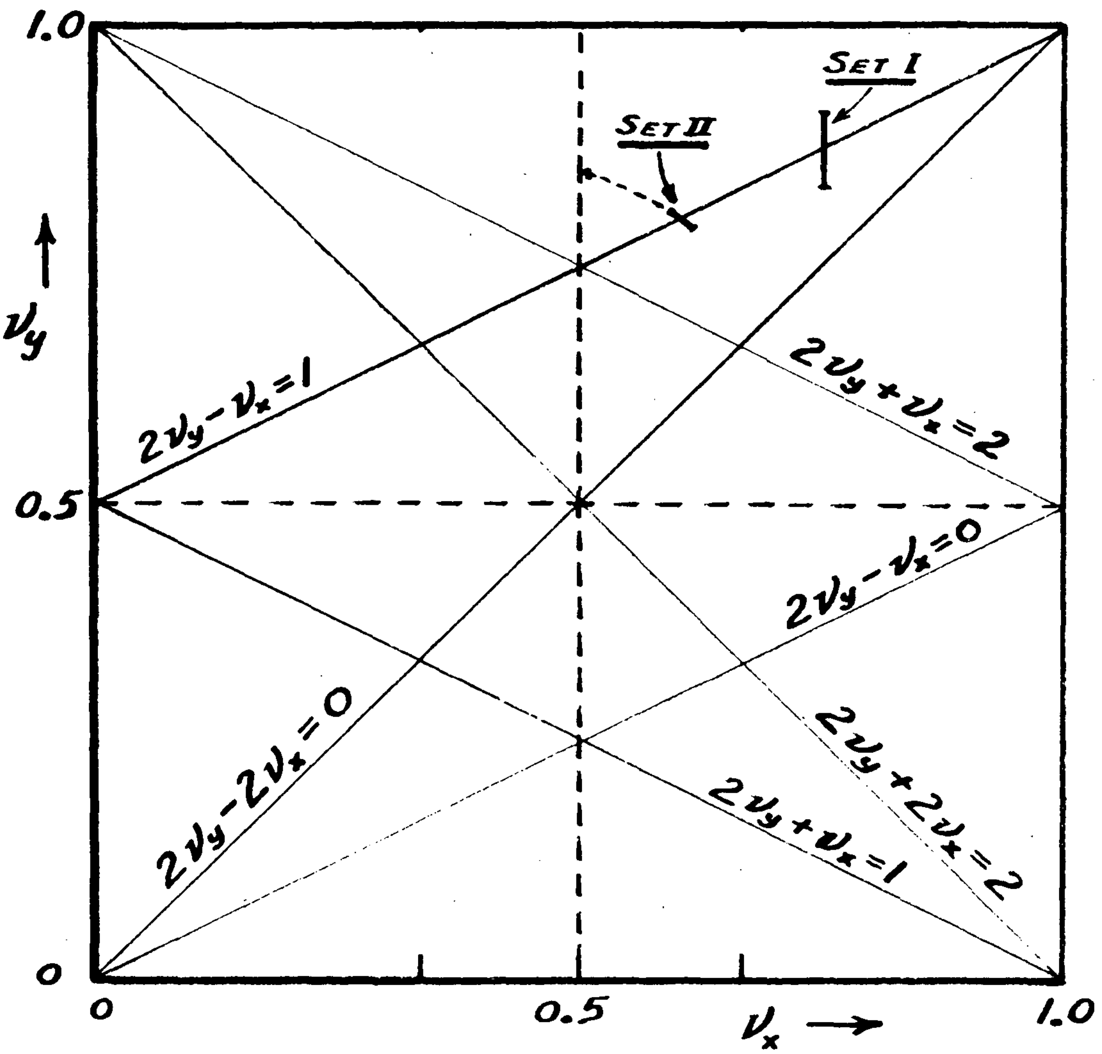

Fig. 1. Frequency diagram, showing location of the working points used in computational study of the equations of Sets I and II.

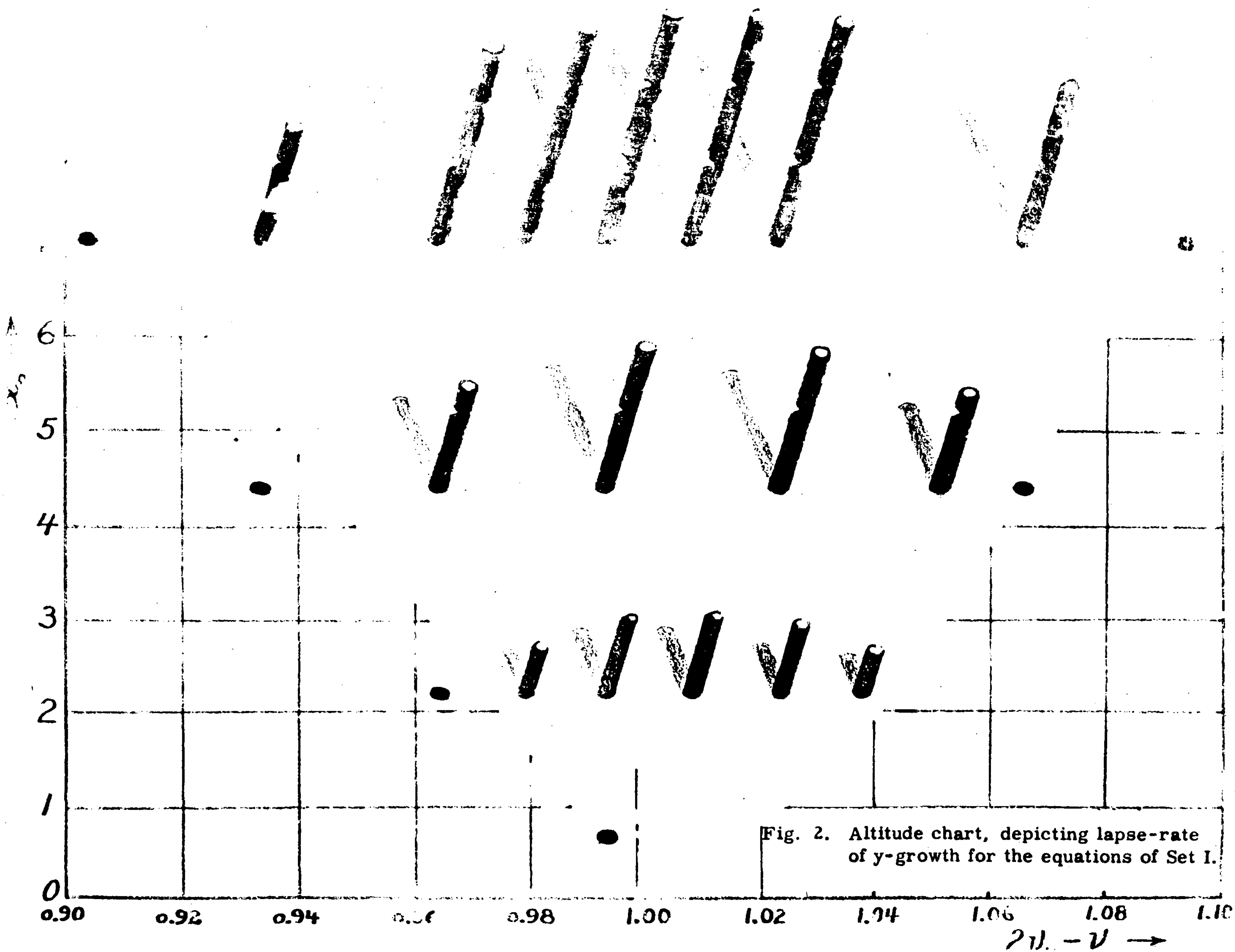

Fig. 2. Altitude chart, depicting lapse-rate of y-growth for the equations of Set I.

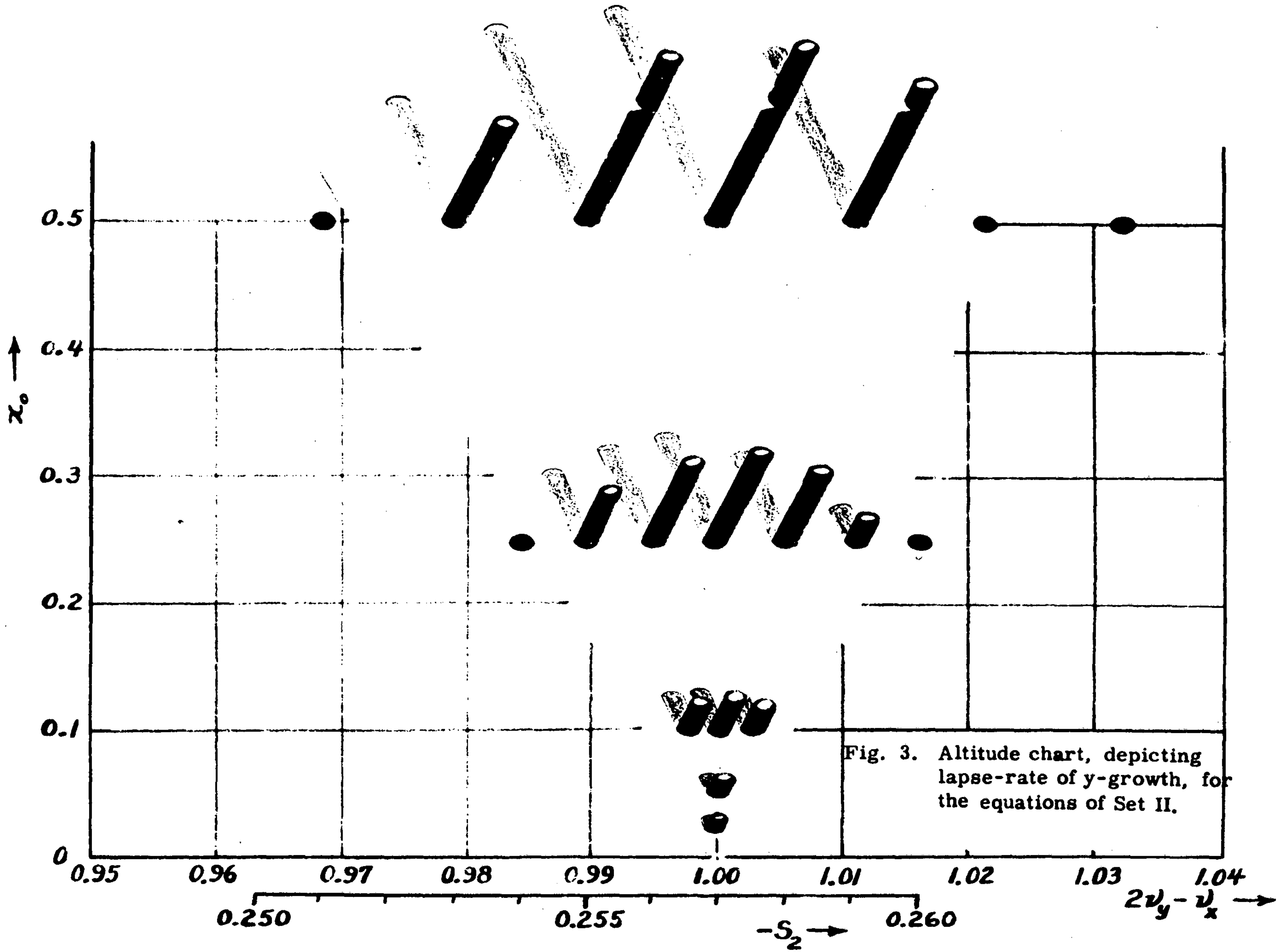

Fig. 3. Altitude chart, depicting lapse-rate of y-growth, for the equations of Set II.

Fig. 4. Variation of y-amplitude during traversal of resonance.

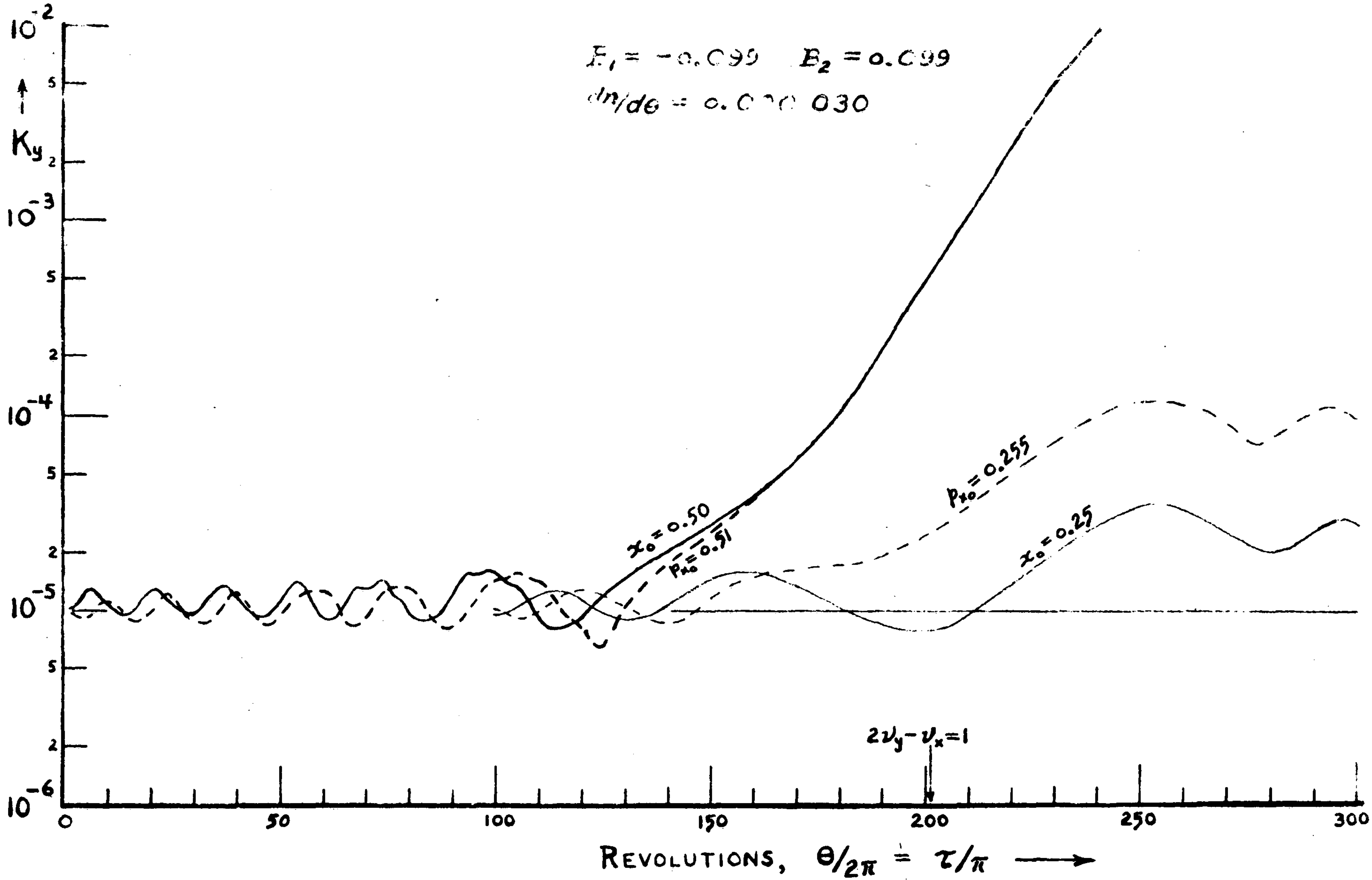

Fig. 5. Variation of y-amplitude during traversal of resonance.

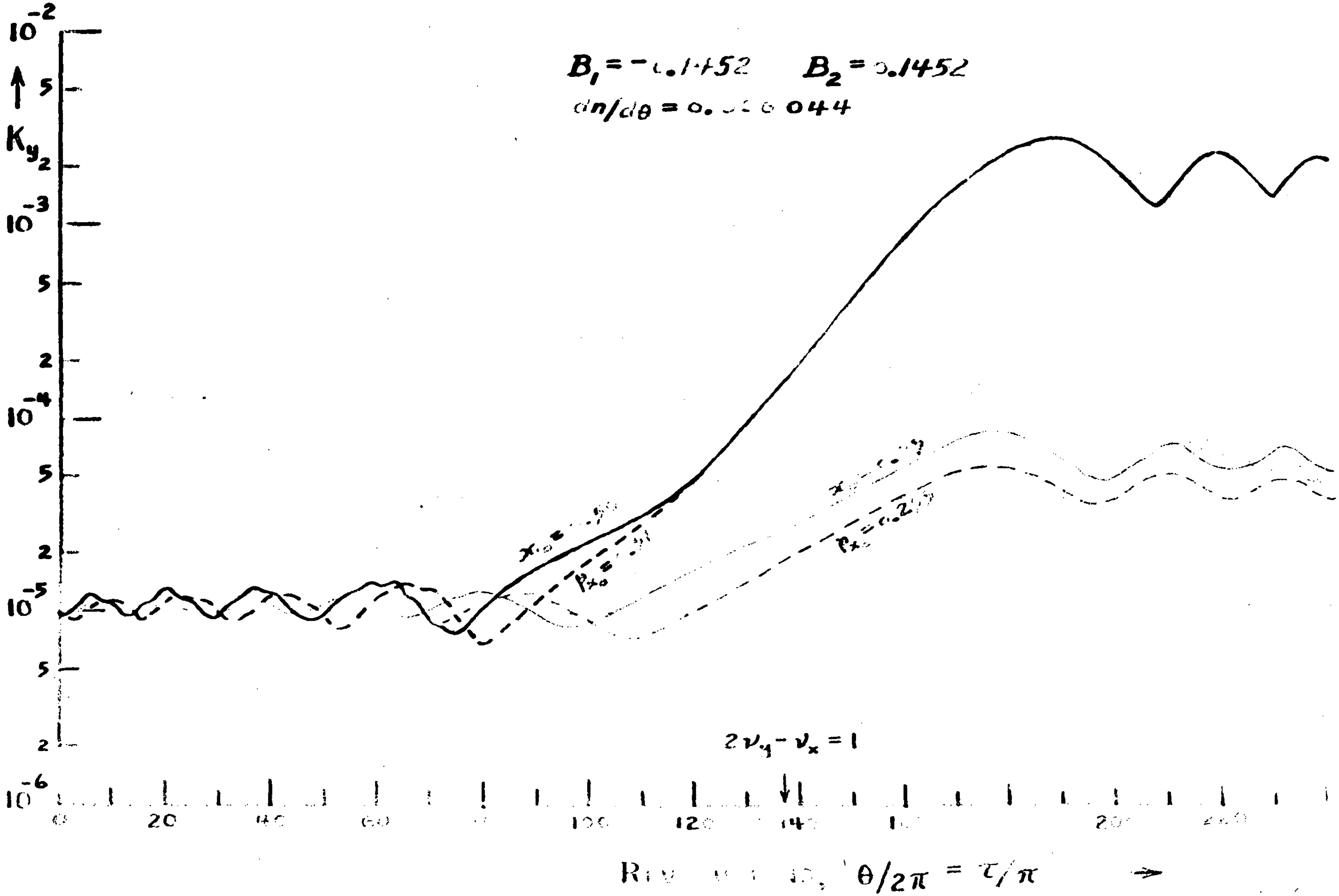

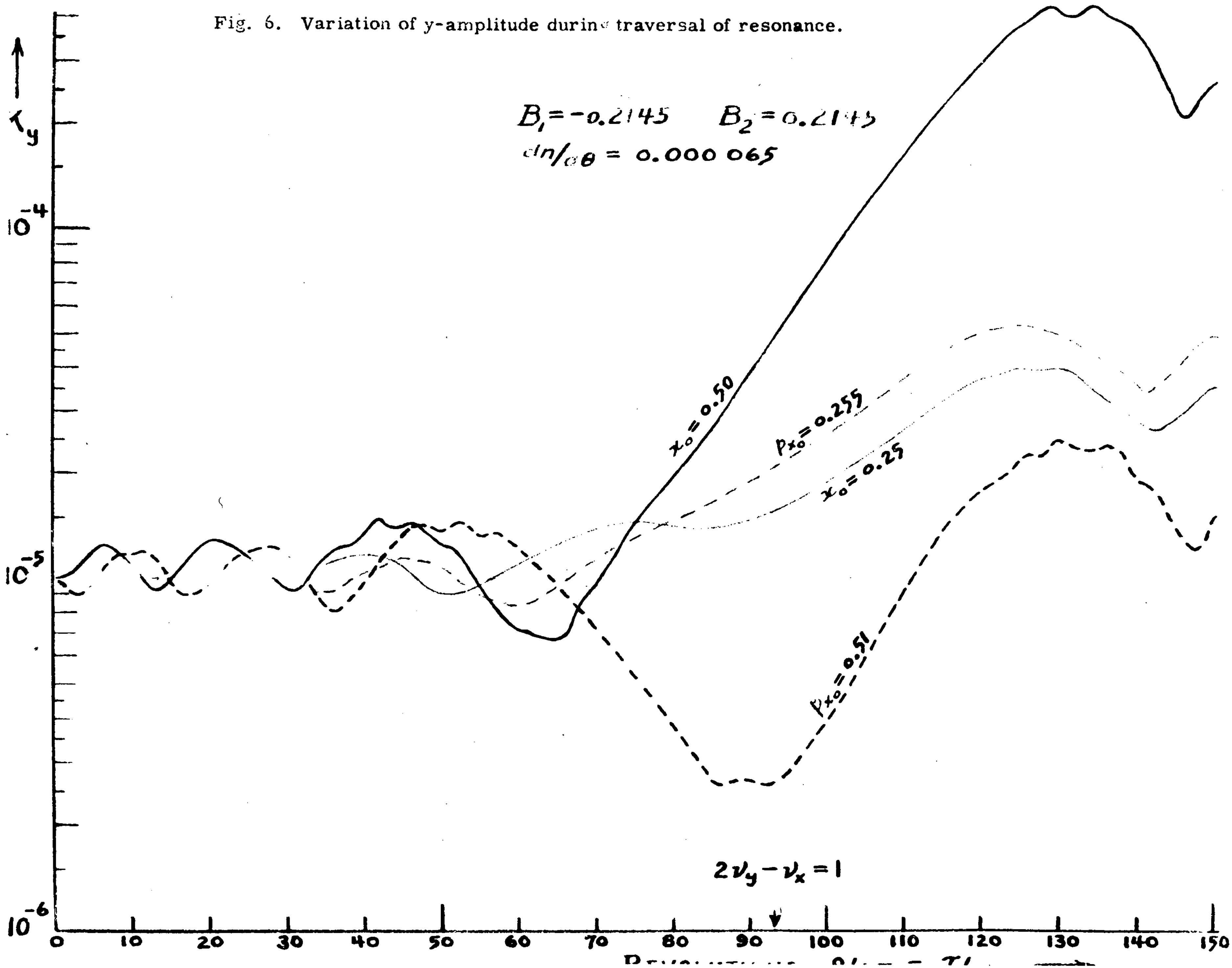

Fig. 6. Variation of y-amplitude during traversal of resonance.

Fig. 7. Variation of y-amplitude during aversal of resonance.

$B_1 = -0.3168 \quad B_2 = 0.3168$
$dn/d\theta = 0.000\,096$

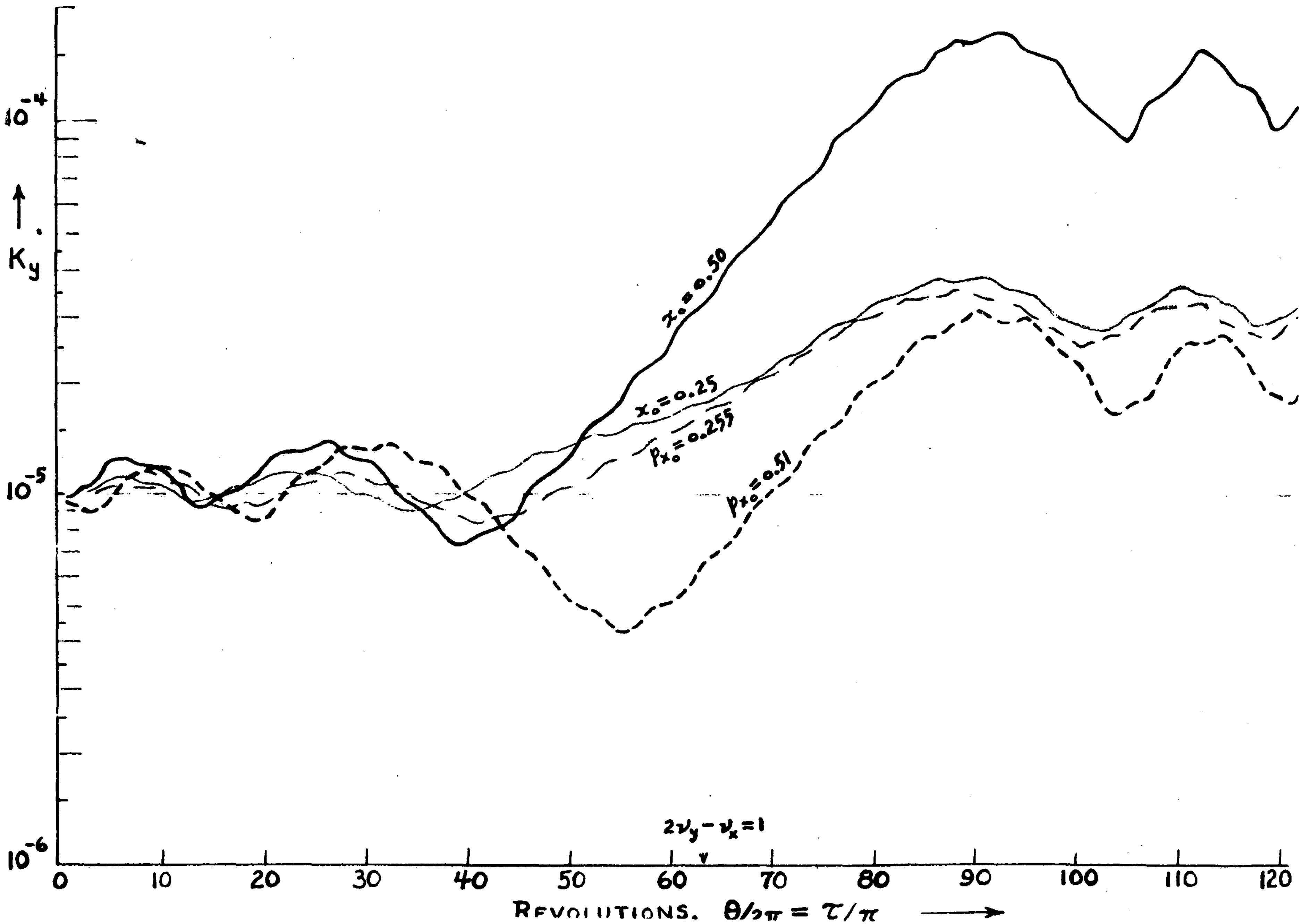

1-378

Fig. 8. Variation of y-amplitude durin_ raversal of resonance.

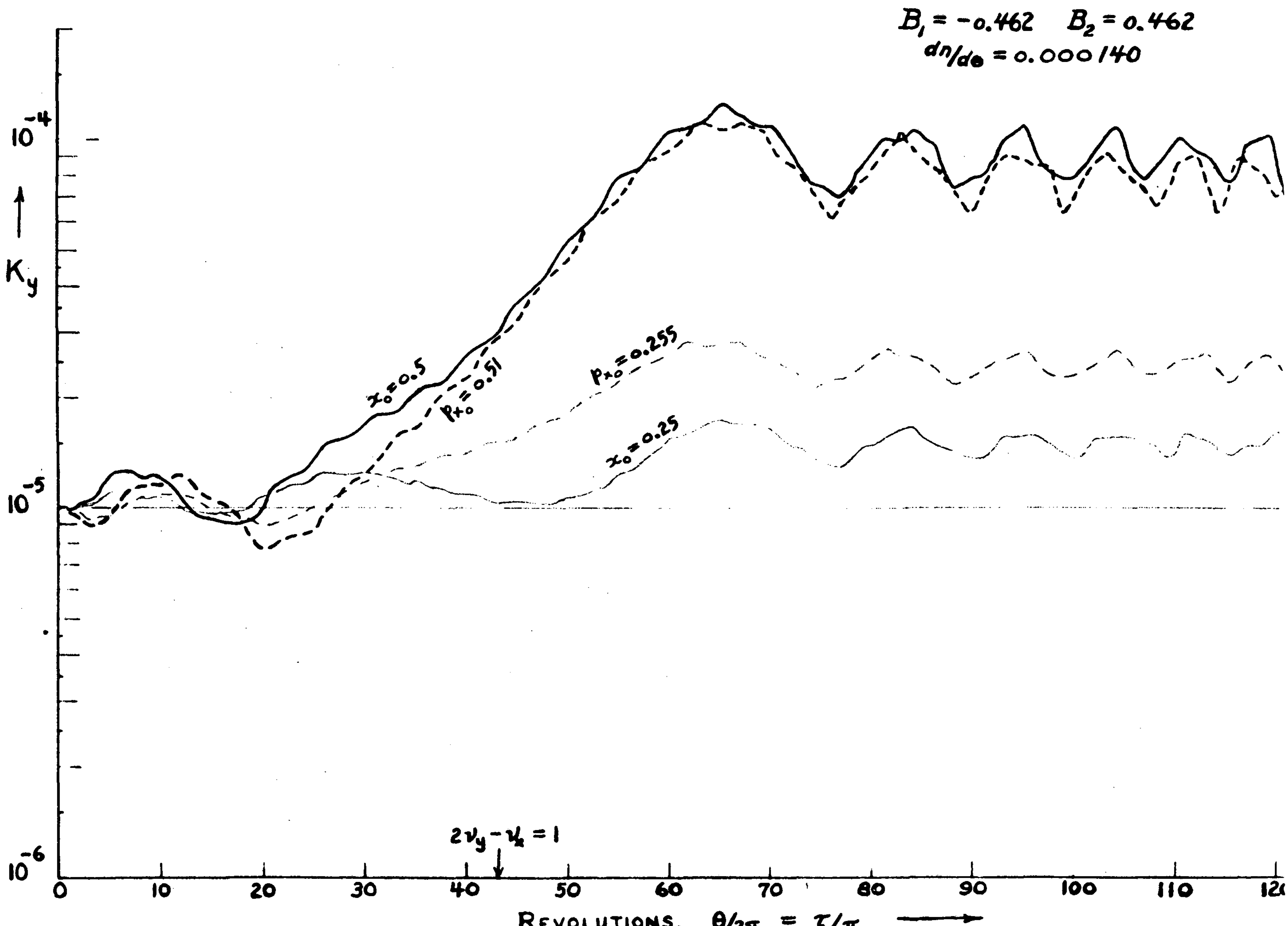

1-379

Fig. 9. Variation of y-amplitude during trav ;al of resonance.

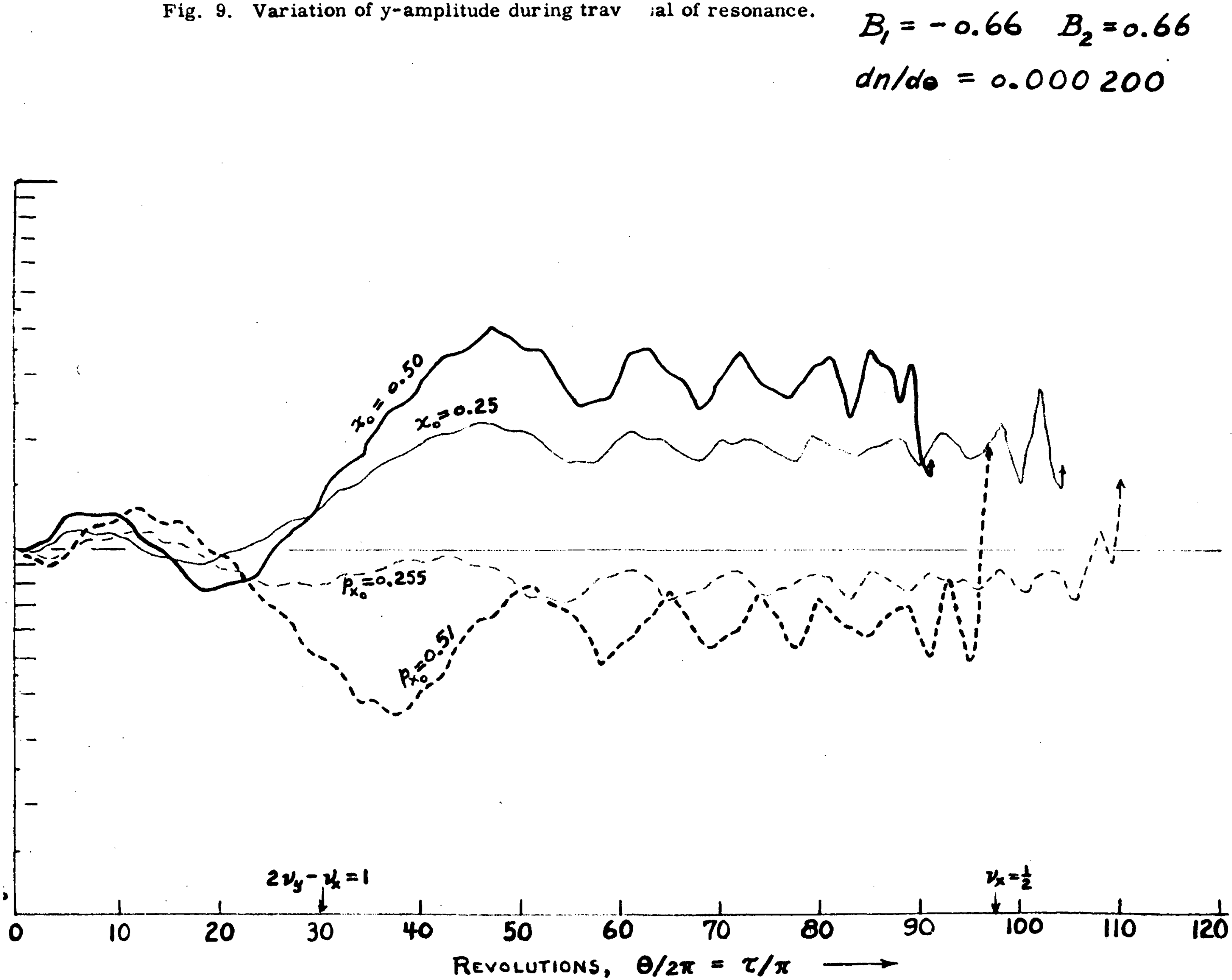

Fig. 10. Variation of y-amplitude during traversal of resonance. $B_1 = -0.99$ $B_2 = 0.99$ $dn/d\theta = 0.000300$

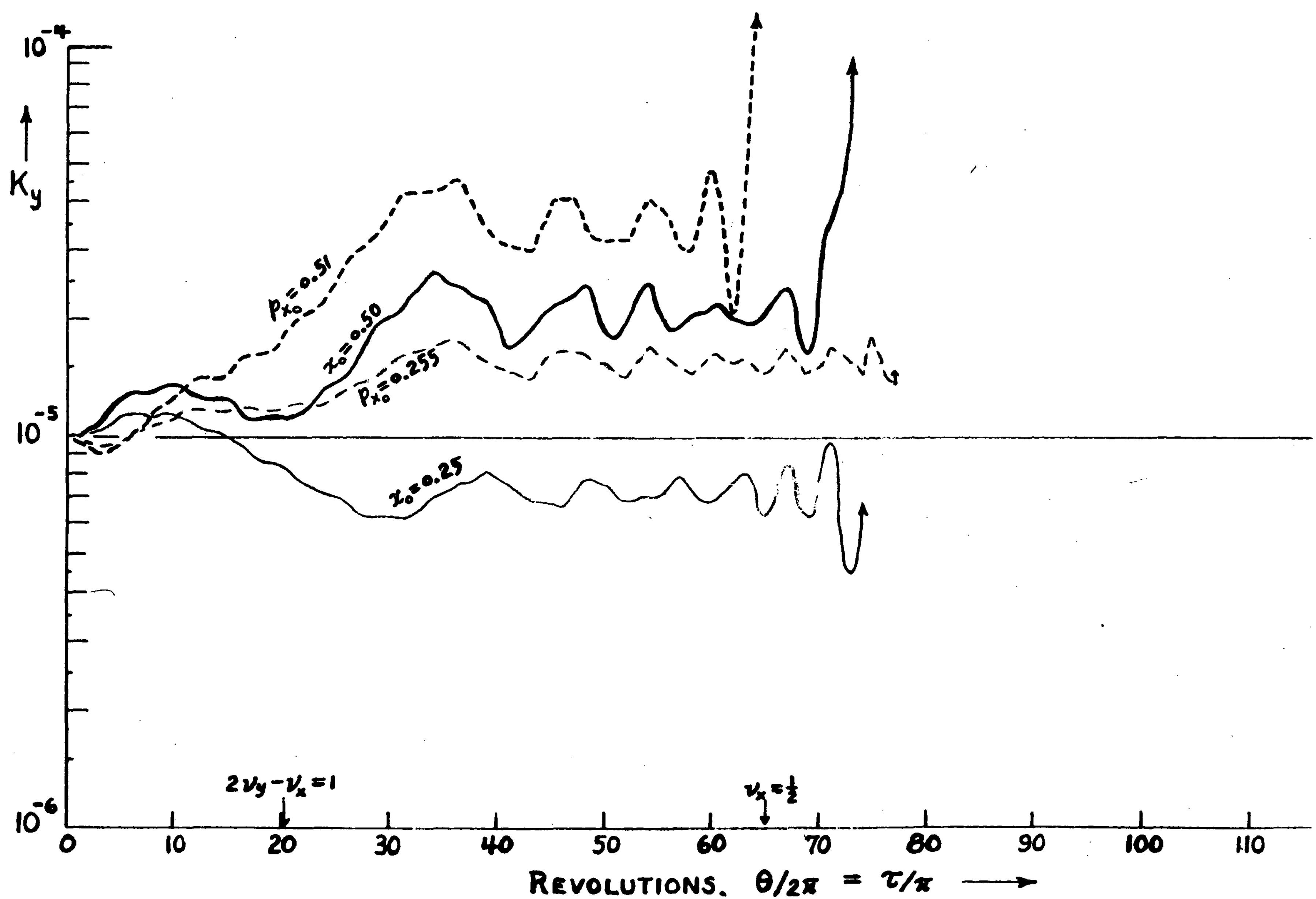

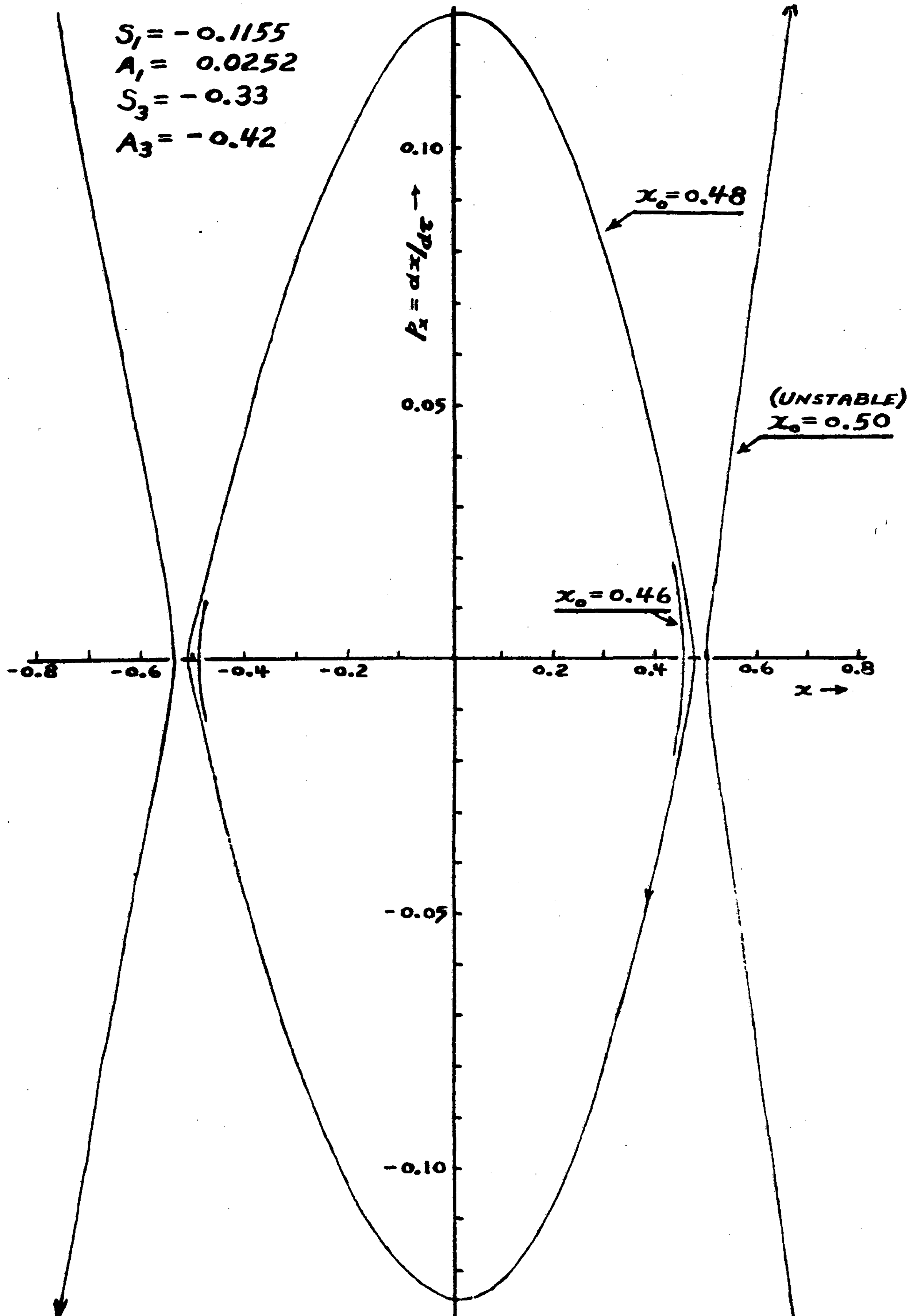

Fig. 11. Phase-plots for uncoupled radial motion at $\theta = 0$, mod. 2π.
$\nu_{x_o} \doteq 0.52_3$

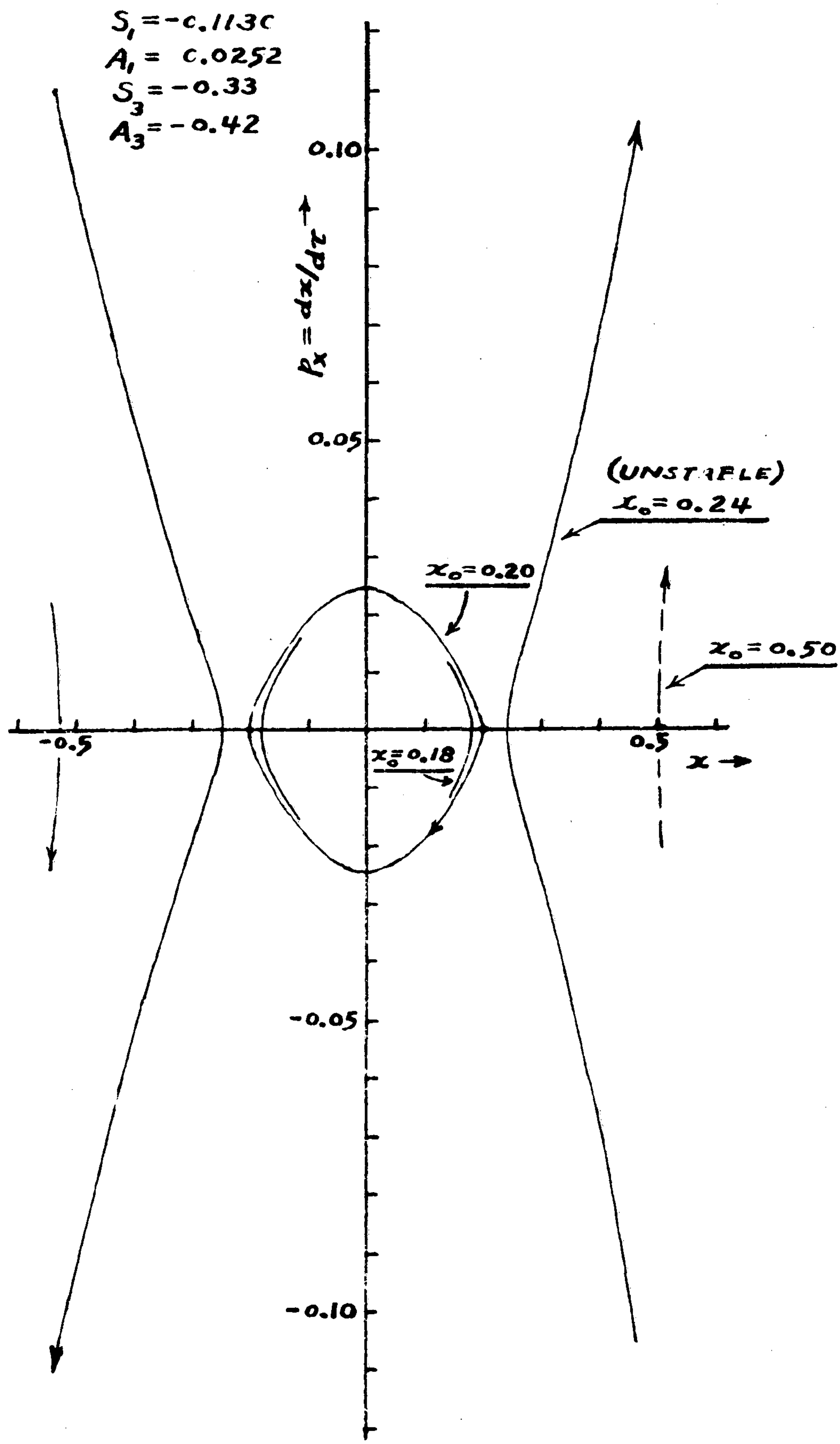

Fig. 12. Phase-plots for uncoupled radial motion at $\theta = 0$, mod. 2π. $\nu_x \doteq 0.51_0$

Example: [$dn/d\theta = 0.000\,096$. $x_0 = 0.5$]

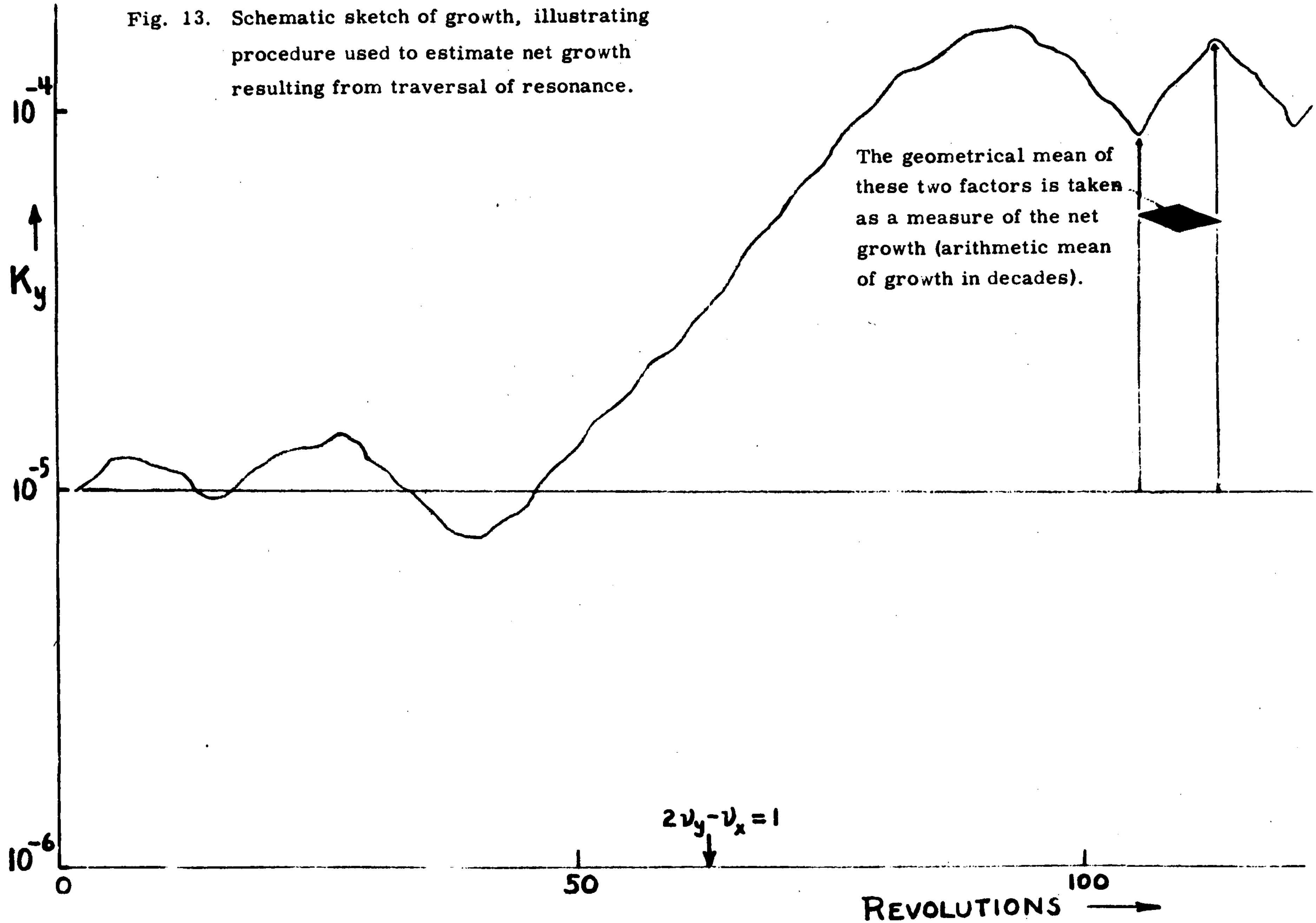

Fig. 13. Schematic sketch of growth, illustrating procedure used to estimate net growth resulting from traversal of resonance.

MURA-444
Internal Report

MIDWESTERN UNIVERSITIES RESEARCH ASSOCIATION*

2203 University Avenue, Madison, Wisconsin

ON THE SPIRAL ORBIT SPECTROMETER

L. Jackson Laslett**

January 27, 1959

ABSTRACT

The characteristics of orbits in the median plane of a spiral orbit spectrometer are briefly examined from the viewpoint of phase-plots similar to those used in accelerator theory. The characteristics of the spiral orbit spectrometer may be suggestive of injection methods which would prove useful in accelerator design.

*AEC Research and Development Report. Research supported by the Atomic Energy Commission, Contract No. AEC AT(11-1)384.

**Department of Physics and Institute for Atomic Research, Iowa State College, Ames, Iowa.

I. INTRODUCTION

The ingenious spiral orbit spectrometer has been described[1-7†] and analyzed[1, 3-5] in a series of published papers and its experimental use reported[8, 9] for the study of μ^+ meson decay. The instrument employs an axially-symmetric magnetic field characterized by a vector potential $(A\hat{e}_\theta)$ having a stationary value at a radius (r_σ) such that Br at that radius is equal to the magnetic rigidity of the particles. Particles with this magnetic rigidity, or momentum, emitted from a source on the axis then describe orbits which approach (asymptotically) a circle of radius r_σ while particles of lower momentum do not reach this radius and particles of larger momentum cross the circle quickly. The field-configuration thus appears well suited for the selection, with good resolution and large solid angle, of particles of the selected momentum -- particularly if a directional detector is used.

Although a source on the axis may not be realized exactly in practice and the particles which are emitted with initial conditions suitable for approaching the circle of convergence thus (even assuming the mechanical momentum to be correct) in a sense constitute a set of measure zero, the orbit characteristics may be of interest (beyond the spectrometer application) in suggesting effective means for injection into particle accelerators. The spectrometer characteristics have been calculated in some detail in the references cited (esp. ref. 3), but it may be useful here to describe the radial motion (in the median plane) briefly in a way which parallels the viewpoint frequently adopted for the examination of orbits

† References are given in Section IV.

in particle accelerators. Radial phase-plane plots may then be examined, in analogy with the procedure used in accelerator design. The magnetic field, as a function of radius, is normally bell-shaped and axial focusing may be expected [see, F. ex., eq. (43) of ref. 3.]

II. THE ORBITS IN THE MEDIAN PLANE

Employing polar coordinates (r, θ) the trajectories in the median plane may be obtained from the "space Lagrangian" (principle of Least Action)

$$L = \sqrt{r^2 + r'^2} + \frac{e}{p} \, r \, A(r) \qquad \text{[emu or MKS,]} \tag{1}$$

where $A(r)$ represents the vector potential, e and p the charge and mechanical momentum of the particle, and a prime denotes differentiation with respect to θ. It is convenient to normalize the argument of the vector potential so that it may be expressed in terms of a normalized function $a(x)$ as follows:

$$A(r) = - \frac{p_o}{e} \, a\,(r/r_o), \tag{2}$$

where $\quad a(1) = 1 \qquad$ (3a)

and $\quad a'(1) = 0. \qquad$ (3b)

[Thus at $x \equiv r/r_o = 1$ the vector potential is stationary and, at this point, $|Br| = |p_o/e|$; hence a possible orbit of a particle with mechanical momentum p_o is the circle $r = r_o$.]

We thus write

$$L = \sqrt{r^2 + r'^2} - \frac{1}{1 + \epsilon} \, r \, a(r/r_o)$$

$$= r_o \left\{ \sqrt{x^2 + x'^2} - \frac{1}{1 + \epsilon} \, x \, a(x) \right\} , \tag{4}$$

where $x \equiv r/r_o$ and $\epsilon \equiv p/p_o - 1$. One may then employ in what follows the simple Lagrangian

$$\mathcal{L} = \sqrt{x^2 + x'^2} - \frac{1}{1+\epsilon}\, x\, a(x). \tag{5}$$

From the Lagrangian (5) one obtains

$$P = \frac{\partial \mathcal{L}}{\partial x'} = x' / \sqrt{x^2 + x'^2} = r' / \sqrt{r^2 + r'^2} = \cos\alpha, \text{ or} \tag{6a}$$

$$x' = Px / \sqrt{1 - P^2} \tag{6b}$$

$$\sqrt{1 - P^2} = x / \sqrt{x^2 + x'^2} = r / \sqrt{r^2 + r'^2} = \sin\alpha, \tag{6c}$$

where α denotes the angle between the direction of motion and the radius vector;

$$P' = + \frac{\partial \mathcal{L}}{\partial x} = x / \sqrt{x^2 + x'^2} - \frac{1}{1+\epsilon} \frac{\partial}{\partial x}\left[x\, a(x)\right]. \tag{7}$$

The corresponding Hamiltonian is

$$\begin{aligned} \mathcal{H} &= Px' - \mathcal{L} \\ &= -x\sqrt{1 - P^2} + \frac{1}{1+\epsilon}\, x\, a(x), \end{aligned} \tag{8}$$

and will be a constant of the motion. Again from $\mathcal{H}$ the equations for the trajectory may be obtained:

$$x' = \frac{\partial \mathcal{H}}{\partial P} = Px / \sqrt{1 - P^2} \tag{9a}$$

$$P' = - \frac{\partial H}{\partial x} = \sqrt{1 - P^2} - \frac{1}{1+\epsilon} \frac{\partial}{\partial x}\left[x\, a(x)\right], \tag{9b}$$

as before.

The geometrical interpretation of P, the canonical momentum conjugate to x, as the cosine of the angle between the direction of motion and the radius vector is noted; one also sees [from (9b)] that one can have P identically zero ($x' \equiv 0$, corresponding to motion on a circle) at $x = 1$ for $\epsilon = 0$, since $\left\{\partial/\partial x \left[x\, a(x)\right]\right\}_{x=1} = 1$.

For a specific illustration of the features of the trajectories, as described by the foregoing equations, one may consider a bell-shaped magnetic field for which the vector potential has the simple form

$$a(x) = \frac{2x}{1 + x^2}, \tag{10}$$

for which, as desired, $a(1) = 1$ and $a'(1) = 0$. The general nature of the median-plane magnetic field, B, implied by this vector potential is indicated in Table I.

TABLE I

CHARACTER OF MAGNETIC FIELD DESCRIBED BY $a(x) = 2x/(1+x^2)$

Radius x	Field $-(er_o/p_o)\,B$	Field Times Radius $-(e/p_o)\,rB = -x\left[(er_o/p_o)\,B\right]$
0	4	0
0.2955 9774	3.382 9758	1
1	1	1

It is noted that the radii represented by each of the last two lines of this table correspond to possible circular motion of a particle with mechanical momentum p_o.

The invariant phase curves, in the x, P-plane, are given by $\mathcal{H}$ = constant. With a(x) as given by eq. (10), such phase curves are illustrated[10] in Fig. 1 for $\epsilon = 0$ $(p = p_o)$. It is noted that the axis of the spectrometer $(x = 0)$ corresponds to $\mathcal{H} = 0$ and that the curve $\mathcal{H} = 0$ passes through the point (1, 0), so that particles emitted from the axis with $p = p_o$ may approach the circle $r = r_o$, albeit requiring a logarithmically infinite time (as we shall see) to reach this radius. The dotted lines in Fig. 1 which connect branches of phase curves for which h > o evidently correspond to retrograde motion, for which the motion in time is backward in θ and $\sqrt{1 - P^2} = \sin\alpha$ should be taken as negative.

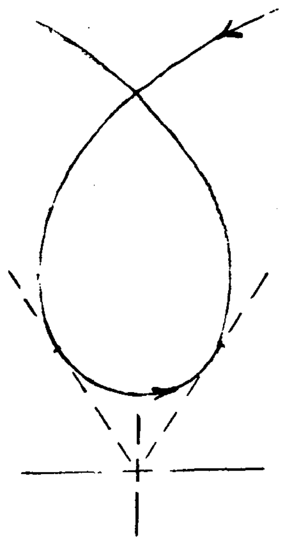

The situation for particles of somewhat larger momentum ($\epsilon > 0$) is illustrated in Fig. 2 and for particles of momentum smaller than p_o ($\epsilon < 0$) is shown in Fig. 3.

III. CORRELATION OF PHASE POINTS WITH θ OR t

The progress of the motion along the phase curves, such as those shown in Fig. 1, may be indicated by noting values of θ along such a curve. The progress of θ is given by

$$\begin{aligned} \Delta\theta &= \int_{x_1}^{x} \frac{dx}{x'} \\ &= \int_{x_1}^{x} \frac{\sqrt{1 - P^2}}{Px}\, dx \end{aligned} \qquad (11)$$

[cf eq. (15) of ref. 3], where P(x) is given in terms of the parameter $\mathcal{H}$ by eq. (8). Near the circle of convergence (1, 0) for $\epsilon = 0$ and $\mathcal{H} = 0$ the quantity P approaches zero in such a way that θ becomes infinite as x approaches unity; thus, for $\epsilon = 0$ and $\mathcal{H} = 0$,

$$P = \frac{1 - x^2}{1 + x^2}$$

$$\theta(x) - \theta(0) = \int_0^x \frac{2}{1 - x^2} \, dx$$

$$= \ln \frac{1 + x}{1 - x} = 2 \tanh^{-1} x. \qquad (12)$$

For other phase curves the progress of θ may perhaps be most conveniently found by numerical integration, aided by analytic integration of asymptotic forms applicable in the neighborhood of $P = 0$.

The progress may also be noted in terms of time, by noting

$$\Delta t = \frac{r_o}{v} \int_{x_1}^{x} \frac{dx}{P} \, .$$

Again for $\epsilon = 0$ and $\mathcal{H} = 0$, a logarithmic infinity is obtained in approaching the point (1, 0); specifically with the form of field considered here and for $\epsilon = 0$, $\mathcal{H} = 0$,

$$t(x) - t(0) = \frac{r_o}{v} \int_{x_1}^{x} \frac{1 + x^2}{1 - x^2} \, dx$$

$$= \frac{r_o}{v} \left[\ln \frac{1 + x}{1 - x} - x \right] = \frac{r_o}{v} \left[2 \tanh^{-1} x - 1 \right]. \qquad (13)$$

In Fig. 4 the curves $\mathcal{H} = 0$ and $\mathcal{H} = -.025$ of Fig. 1 ($\epsilon = 0$) have been approximately labeled with values of θ, fixing arbitrarily the relative positions of the points $\theta = 0$ on the two curves. As θ, the independent variable of our formulation, increases, phase points located between these two curves will progress as indicated and one may expect the area occupied by such points to be conserved. The progress of points with <u>time</u>, however, may be of somewhat greater interest and in Fig. 5 an attempt is made to attach time labels to the curves $\mathcal{H} = 0$ and $\mathcal{H} = -.025$ of Fig. 1. It does not appear that the region occupied by points in an x, P phase plot, when observed at a time common to all such particles, should be conserved. From Fig. 5 it is at any rate apparant that a certain accumulation of points in the neighborhood of the equilibrium circle (x = 1) is obtained.

IV. REFERENCES AND NOTES

1. G. Miyamoto, Proc. Phys. - Math. Soc. Japan [Nihon Sugaku - Buturigakukai Kaisi] 17, 557 (1943) -- in Japanese. The present writer is indebted to Dr. R. Sagane for his courtesy in providing reprints of this and some of the following references, with English translations of references 1 and 3.

2. R. Sagane, G. Miyamoto, K. Nakamura, and Takechi, Proc. Phys. - Math. Soc. Japan 25, 274 (1943).

3. G. Iwata, G. Miyamoto, and M. Kotani, Jour. Phys. Soc. Japan [Nihon Buturigakukai Kaisi] 2, 1 (1947) -- in Japanese.

4. M. Sakai, Jour. Phys. Soc. Japan 5, 178 (1950).

5. M. Sakai, Jour. Phys. Soc. Japan 5, 184 (1950).

6. G. Miyamoto, Proc. Phys. -Math. Soc. Japan 24, 676(L) (1942).

7. G. Miyamoto, Jour. Phys. Soc. Japan 6, 68 (1951). This reference concerns a spectrometer with two circles of convergence.

8. R. Sagane and P. C. Giles, Phys. Rev. 81, 653 (A) (February 15, 1951). This reference is an abstract of a paper presented before the Los Angeles meeting of the American Physical Society (December 29, 1950).

9. R. Sagane, W. L. Gardner, and H. W. Hubbard, Phys. Rev. 82, 557 (L) (May 15, 1951).

10. The writer is happy to acknowledge the assistance of Mr. Bob Clark, of the MURA Laboratory, in preparing the figures for this report.

11. It has been pointed out by Dr. D. Judd (private communication, 1959) that the "space Hamiltonian" which we have employed is essentially $-p_{\theta}$; i.e., the negative of the canonical momentum conjugate to θ, which of course is a constant of the motion in the present problem. This process of changing from the independent variable t of a true Hamiltonian to the variable θ (which may be demonstrated generally

by use of Hamilton's principle), and the distinction between observation of phase points projected in the r, p_r-plane at a common θ or at a common time, is illustrated by the following artificial example:

Consider the Hamiltonian

$$H(x, \theta; p_x, p_\theta; t) = \frac{1}{x}\left(p_\theta + \frac{1}{2} p_x^{2}\right).$$

For this Hamiltonian the equations of motion in time are, of course,

$$\dot{\theta} = \partial H/\partial p_\theta \qquad \dot{p}_\theta = -\frac{\partial H}{\partial \theta}$$

$$= \frac{1}{x}\ ; \qquad = 0, \quad \text{or } p_\theta = \text{const.};$$

$$\dot{x} = \partial H/\partial p_x \qquad \dot{p}_x = -\frac{\partial H}{\partial x}$$

$$= p_x/x\ ; \qquad = \frac{p_\theta + \frac{1}{2} p_x^2}{x^2} = \frac{H}{x}\ ; \text{ and } H = \text{const.}$$

From these equations it follows that the derivatives with respect to θ are

$$x' = p_x$$

$$p_x' = H, \qquad \text{with solutions} \quad p_x = p_{x_o} + H\theta$$

$$x = x_o + p_{x_o}\theta + \frac{1}{2} H\theta^2,$$

and the functional determinant, $\partial(x, p_x)/\partial(x_o, p_{xo})$, with the partial derivatives evaluated with θ held constant is, of course, unity, independent of θ:

$$\frac{\partial(x, p_x)}{\partial(x_o, p_{xo})} \equiv \begin{vmatrix} \frac{\partial x}{\partial x_o} & \frac{\partial p_x}{\partial x_o} \\ \frac{\partial x}{\partial p_{x_o}} & \frac{\partial p_x}{\partial p_{x_o}} \end{vmatrix} = \begin{vmatrix} 1 & 0 \\ \theta & 1 \end{vmatrix} = 1.$$

The time, t, is given in terms of θ by

$$dt = x\, d\theta$$

$$= \left(x_o + p_{x_o}\theta + \frac{1}{2} H\theta^2\right) d\theta,$$

$$t - t_o = \left(x_o\theta + \frac{1}{2} p_{x_o}\theta^2 + \frac{1}{6} H\theta^3\right).$$

In concordance with Judd's observations, the equations for x' and p_x' may be obtained by writing

$$\mathcal{H}(x, t; p_x, -H; \theta) = -p_\theta$$
$$= -xH + \frac{1}{2} p_x^2 ,$$

from which

$$\frac{\partial x}{\partial \theta} = \frac{\partial \mathcal{H}}{\partial p_x} = p_x \qquad \frac{\partial p_x}{\partial \theta} = \frac{\partial \mathcal{H}}{\partial x} = H$$

$$\frac{\partial t}{\partial \theta} = \frac{\partial \mathcal{H}}{\partial (-H)} = x \qquad \frac{\partial (-H)}{\partial \theta} = -\frac{\partial \mathcal{H}}{\partial t} = 0$$

as before.

If, for simplicity, we consider the particular solutions for which $H = 0$,

$$p_x = p_{x_o} \qquad x = x_o + p_{x_o}\theta ,$$

$$\theta = \frac{-x_o + \sqrt{x_o^2 + 2p_{x_o}(t - t_o)}}{p_{x_o}} , \qquad x = \sqrt{x_o^2 + 2p_{x_o}(t - t_o)} .$$

If we form the functional determinant $\partial(x, p_x) / \partial(x_o, p_{x_o})$ from these solutions, performing the partial differentiation with t held fixed, we obtain

$$\frac{\partial(x, p_x)}{\partial(x_o, p_{x_o})} \equiv \begin{vmatrix} \frac{\partial x}{\partial x_o} & \frac{\partial p_x}{\partial x_o} \\ \frac{\partial x}{\partial p_{x_o}} & \frac{\partial p_x}{\partial p_{x_o}} \end{vmatrix} = \begin{vmatrix} \frac{x_o}{\sqrt{x_o^2 + 2p_{x_o}(t - t_o)}} & 0 \\ \frac{t - t_o}{\sqrt{x_o^2 + 2p_{x_o}(t - t_o)}} & 1 \end{vmatrix} =$$

$$\frac{x_o}{\sqrt{x_o^2 + 2p_{x_o}(t - t_o)}} = \frac{x_o}{x} ;$$

this expression clearly will <u>not</u> in general be equal to unity.

The writer is indebted to Dr. B. C. Carlson and Dr. F. T. Cole for helpful general discussions concerning such specialized phase plots and in particular for remarks leading to the following summary:

This example illustrates a general situation of some interest. If one takes a group of particles governed by a Hamiltonian and projects the region occupied by these particles on a subspace of the total phase space, the area occupied by these particles on this subspace may or may not be constant as the motion develops, depending on the way in which the initial conditions of the particle are chosen.

Consider a system of two degrees of freedom governed by the Hamiltonian $H\,(r,\ p_r;\ \theta,\ p_\theta;\ t)$, where H is independent of θ, as in the example above. Then p_θ is a constant of the motion and if we consider a group of particles with the same p_θ, but different values of r and p_r and observe the progress of the system in time, the area projected on the $r - p_r$ plane by the particles will be constant in time, since effectively $H = H\,(r,\ p_r;\ t)$. Geometrically, all the phase space points representing the particles lie at all times on the hyperplane p_θ = const. normal to the $r - p_r$ plane in the four-dimensional phase space.

If, however, as a second example we choose a group of initial conditions with the same H and differing values of p_θ, the functional dependence of $H\,(r,\ p_r;\ t)$ varies from particle to particle, so that all particles are not governed by the same Hamiltonian. Area in the $r - p_r$ plane is <u>not</u> conserved in time.

The same problem can be viewed with θ as independent variable; the "Hamiltonian" is $-p_\theta = h(r, p_r; t, -H; \theta)$. If H is independent of t, it is a constant of the motion, and plays the same role as p_θ did when H was the Hamiltonian. A group of particles with the same H, but different values of p_θ (as in the second example) will have the same Hamiltonian $h(r, p_r, \theta)$ governing the motion and the area in the $r - p_r$ plane will be constant in θ. It goes almost without saying that Liouville's Theorem, which is concerned with the total phase space volume, is conserved in all cases.

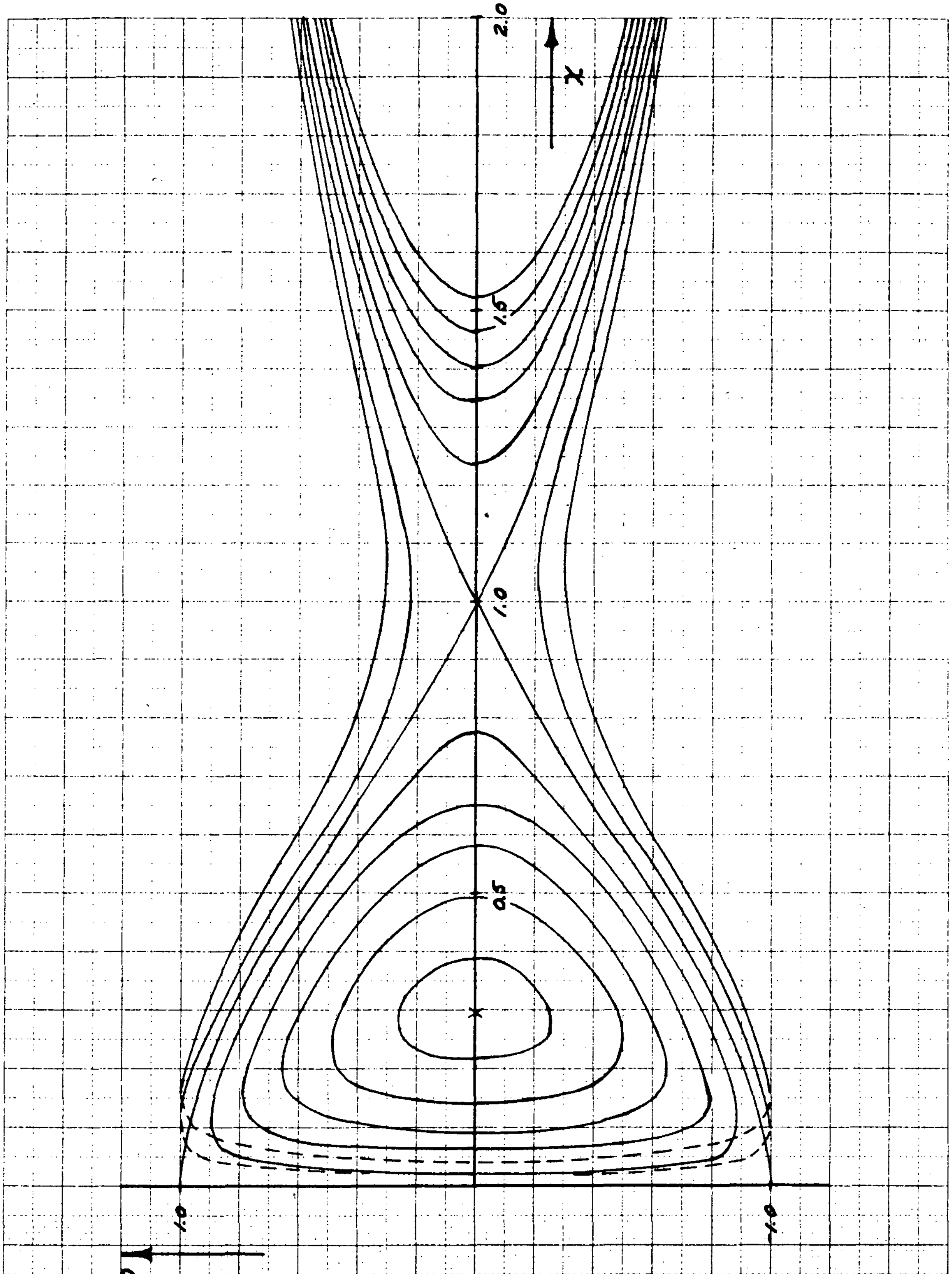

Fig. 1. $\epsilon = 0.$

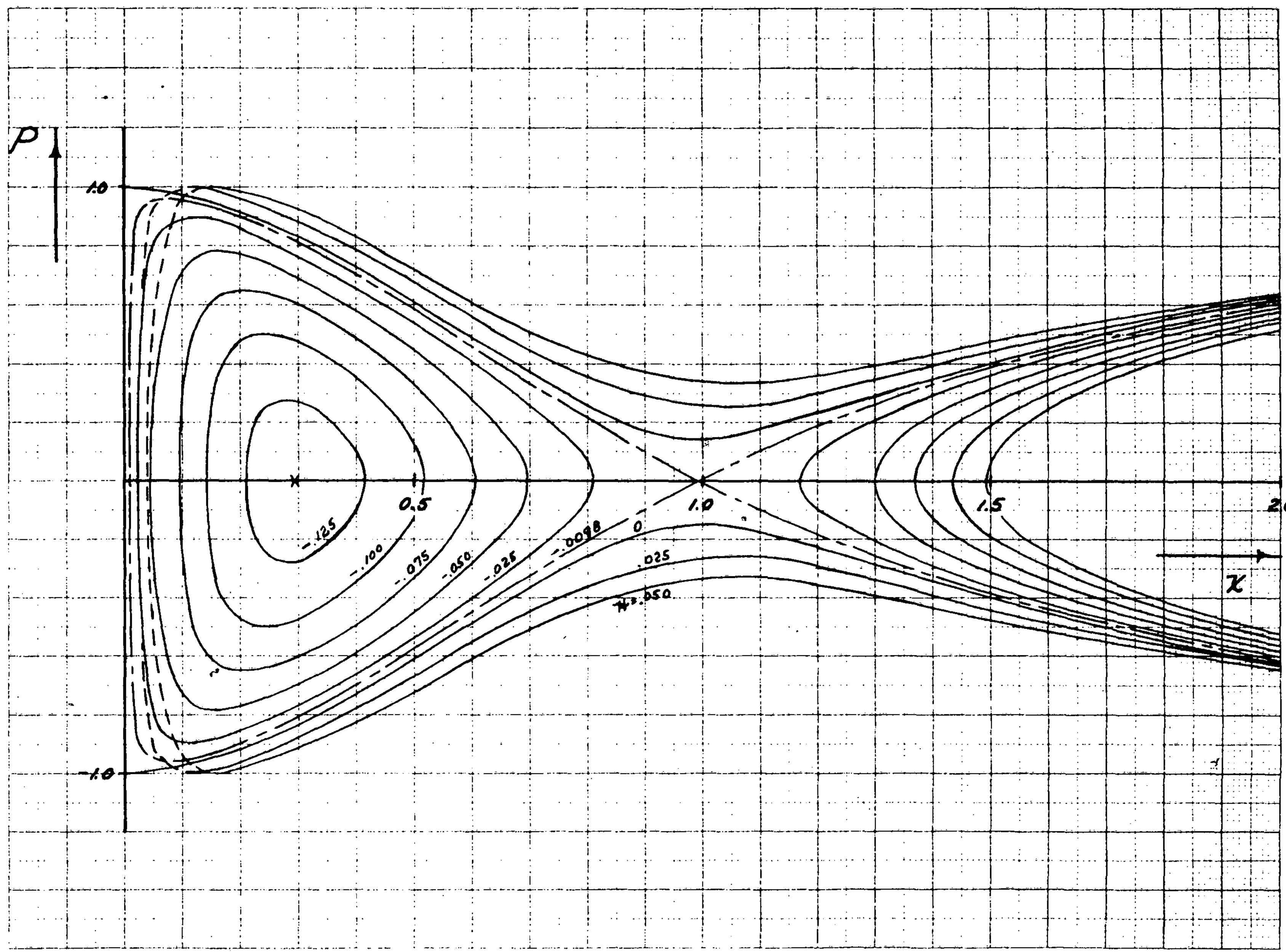

Fig. 2. ϵ = .01 Separatrix at x = 0.99

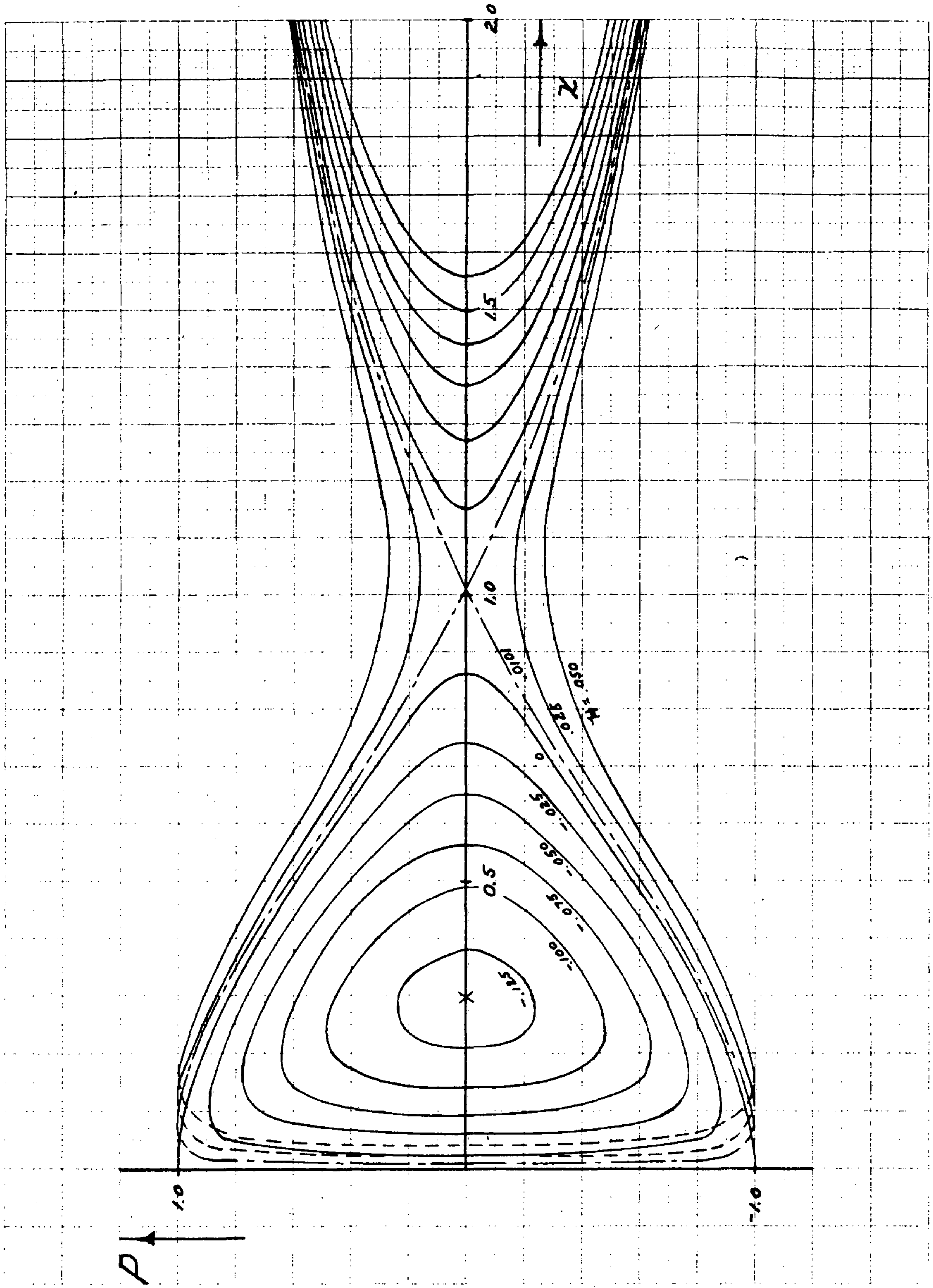

Fig. 3. ϵ =-.01 Separatrix at x = 1.01

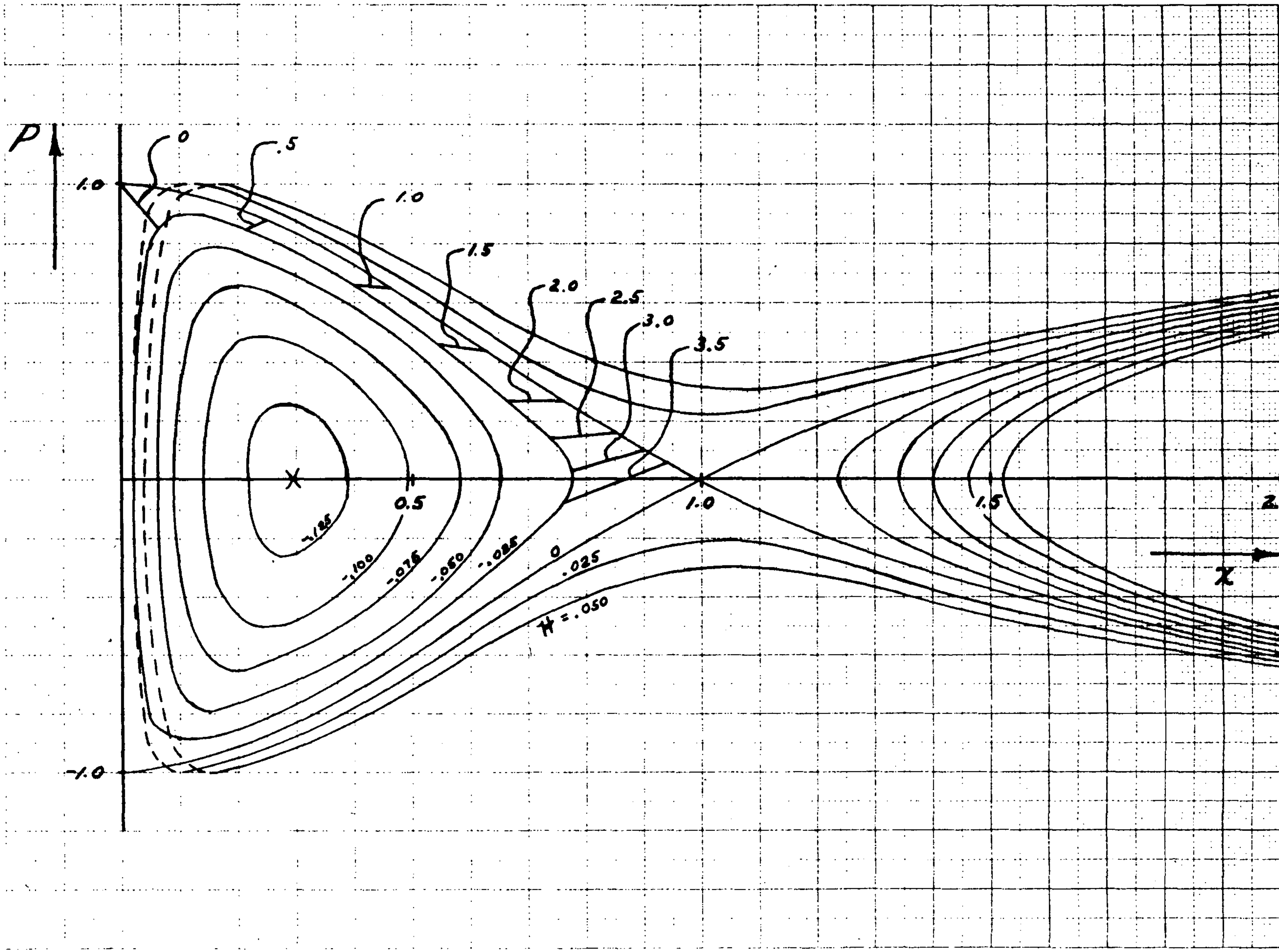

Fig. 4. $\epsilon = 0$. x, P phase plot for $\epsilon = 0$, with the progress of points in θ noted approximately for $\theta = 0, 0.5, \ldots 3.5$. The starting points, or relative values for the origin of θ, are arbitrarily chosen for the two curves $\mathcal{H} = 0$ and $\mathcal{H} = -0.025$.

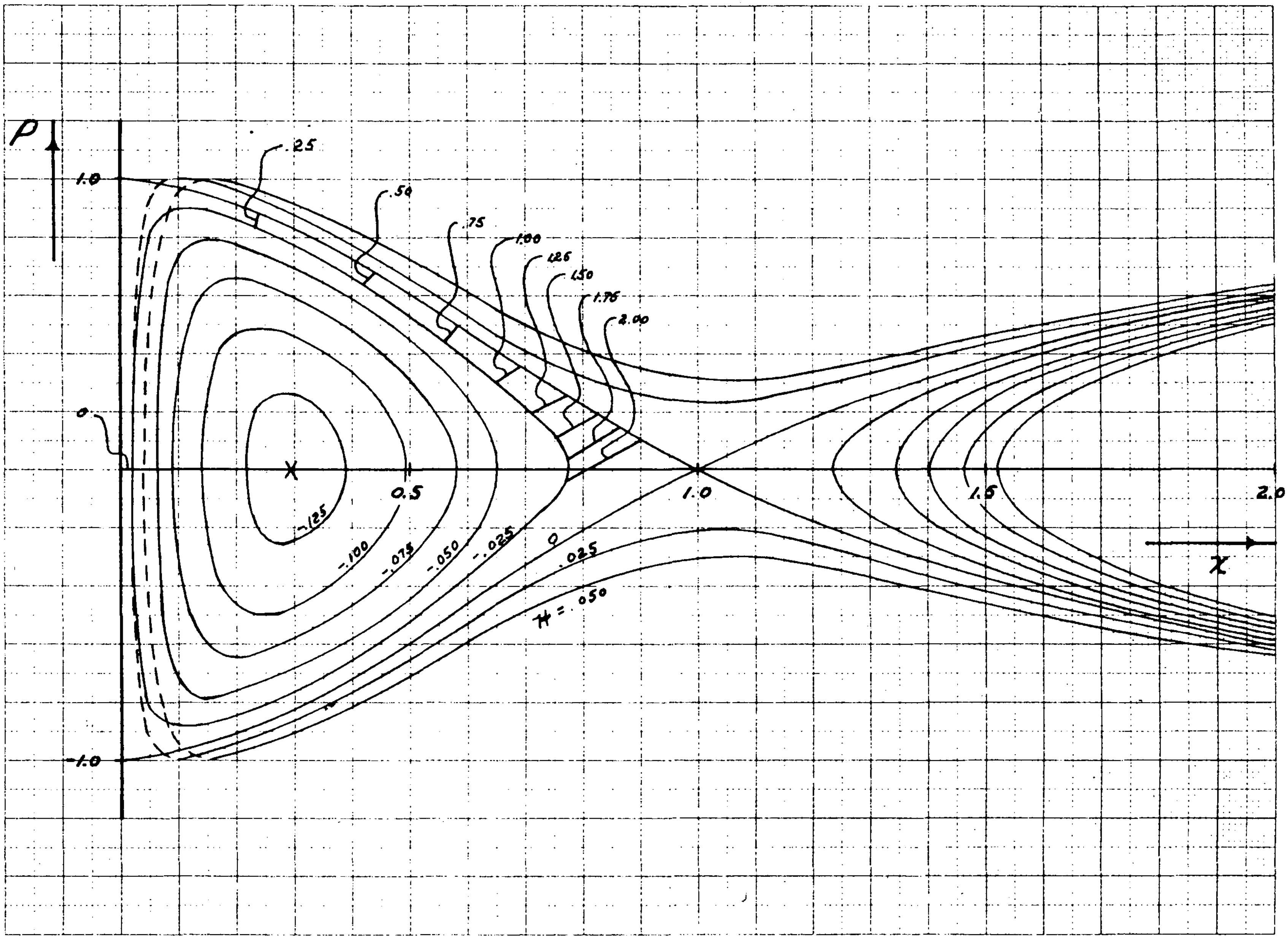

Fig. 5. $\epsilon = 0$. x, P phase plot for $\epsilon = 0$, with the progress of points in time noted approximately for $(v/r_o)t = 0,\ 0.25,\ \ldots 2.00$.

MURA-452
Distribution List UC-28

MIDWESTERN UNIVERSITIES RESEARCH ASSOCIATION*

2203 University Avenue, Madison, Wisconsin

CONCERNING THE $\nu/N \longrightarrow 1/3$ RESONANCE, I

APPLICATION OF A VARIATIONAL PROCEDURE AND OF THE MOSER METHOD TO THE EQUATION

$$\frac{d^2v}{dt^2} + \left(\frac{2\nu}{N}\right)^2 v + \frac{1}{2}(\sin 2t)\, v^2 = 0$$

L. Jackson Laslett**

April 13, 1959

ABSTRACT

As an introduction to certain non-linear dynamical problems in which the 1/3-resonance plays a dominant role, the stability boundary for the equation

$$\frac{d^2v}{dt^2} + \left(\frac{2\nu}{N}\right)^2 v + \frac{1}{2}(\sin 2t)\, v^2 = 0$$

has been studied analytically and by digital computation. Use of a relatively simple trial function in a variational procedure or with harmonic balance is shown to lead to simultaneous algebraic equations, for the coefficients in the trial function, whose solution affords a good estimate of the unstable fixed points. Application of the Moser method of solution is also carried through in detail, to include terms of the order $(\nu/N - 1/3)^2$, and the results compared with computer data for various values of ν/N.

*AEC Research and Development Report. Research supported by the Atomic Energy Commission, Contract No. AEC AT(11-1)-384.

**Department of Physics and Institute for Atomic Research, Iowa State College.

A. MOTIVATION

Simple applications of a variational method or of harmonic balance have been used previously[1*] to obtain "handy formulas" to indicate the stability limits for certain non-linear differential equations, with periodic coefficients occurring in the theory of cyclic accelerators. The applicability of the method described by Moser[2] has also been recognized and it may be noted that this latter method affords the opportunity of obtaining more detailed information concerning the solutions, since the previous methods are most simply applicable to the special problem of determining the unstable equilibrium solution, whose period is a multiple of that for the periodic coefficients in the differential equation.

Work currently in progress[3] concerning the possible practicality of injection into FFAG accelerators with a "field bump" deliberately introduced, with a period which is some integral multiple of the basic period of the unperturbed structure, has made it desirable to re-examine the analytic methods, in comparison with computational results, and to attempt to obtain analytic formulas of accuracy adequate to provide quantitatively useful orientation for detailed computational studies.

In the present report we develop analytic methods, which are compared with computational results, for solutions--particularly at the stability limit--to a simple type of differential equation for which the stability limit is determined by the one-third resonance ($\nu/N \longrightarrow 1/3$). The application of these methods in the present case has been felt to be fruitful and later reports may make use of similar methods in more complicated situations.

---

*References are given in Section E.

B. THE DIFFERENTIAL EQUATION EMPLOYED

In the theory of spirally-ridged FFAG accelerators the radial betatron motion, about the stable equilibrium orbit, may be convenienty represented by[4]

$$d^2u/d\theta^2 + \left[a + b \cos N\theta\right]u = b_1 (\theta)\, u^2/2 + \cdots , \tag{1}$$

where u denotes the departure from the stable equilibrium orbit, in units of the radius,

$$b \cong f/w\ , \text{ and} \tag{2a}$$

$$b_1 (\theta) \cong - (f/w^2) \sin N\theta\ . \tag{2b}$$

By introducing the scaled variables

$$t = (N/2)\, \theta\ , \tag{3a}$$

$$v = 4 \frac{f}{w N^2} \frac{u}{w}\ , \tag{3b}$$

eqn. (1) assumes the form

$$d^2v/dt^2 + 4\left[\frac{a}{N^2} + \frac{f}{w N^2} \cos 2t\right] v + \frac{1}{2} (\sin 2t)\, v^2 = 0. \tag{4}$$

Although it is possible by a suitable transformation to remove the alternating-gradient feature of the linear term,[5] it is frequently convenient, in the interests of simplicity, to replace[6] the A-G coefficient by $(2\nu/N)^2$. The equation which results is, then,

$$d^2v/dt^2 + (2\nu/N)^2\, v + (1/2)(\sin 2t)\, v^2 = 0. \tag{5}$$

It is this equation with which we shall work in the present report, being concerned in particular with the limiting-amplitude solution, governed by the one-third resonance ($\nu/N \rightarrow 1/3$). Results of a variational solution (or equivalently, of harmonic balance) and of application of the Moser procedure will be presented in Sections C and D, respectively, and compared with computational results.

Illustrative machine parameters might be

$$f = 1/4, \quad N = 33, \quad k \cong 79, \quad 1/w \cong 1252,$$

for which

$$k/N^2 = 0.0729, \quad \frac{f}{w N^2} = 0.2875,$$

and, from the approximate equations of motion, the frequencies of the small-amplitude (A-G) radial and axial oscillations are respectively such that

$$2\nu_x/N \equiv \sigma_x/\pi = 0.5994, \quad 2\nu_y/N \equiv \sigma_y/\pi = 0.1983;$$

in some of the work to follow the case $2\nu_x/N = 0.6$ will be specifically considered.

C. THE VARIATIONAL METHOD

1. Analytic Development

The unstable equilibrium orbit, or the associated "fixed points" characterizing the limiting-amplitude solution of eqn. (5),

$$d^2v/dt^2 + (2\nu/N)^2 v + (1/2)(\sin 2t) v^2 = 0, \tag{5}$$

may be sought by insertion of a trial function of suitable form into the variational statement

$$\delta \left[\langle (dv/dt)^2 \rangle - (2\nu/N)^2 \langle v^2 \rangle - (1/3) \langle v^3 \sin 2t \rangle \right] = 0. \tag{6}$$

We shall employ here the relatively simple three-term trial function

$$v \cong A_1 \sin 2t/3 + A_2 \sin 2t + A_3 \sin 10t/3, \tag{7}$$

in which the form of the last two terms may be suggested by insertion of the first term into the differential equation (5) and considerations of harmonic balance.

By insertion of the trial function (7) into the variational statement (6), or by harmonic balance in the differential equation (5), the following three simultaneous non-linear algebraic equations are obtained:

$$\left[\frac{4}{9} - \left(\frac{2\nu}{N}\right)^2\right] A_1 + \frac{1}{8} A_1^2 - \frac{1}{2} A_1 A_2 + \frac{1}{4} A_1 A_3 - \frac{1}{4} A_2 A_3 = 0 \tag{8a}$$

$$\left[4 - \left(\frac{2\nu}{N}\right)^2\right] A_2 - \frac{1}{4} A_1^2 - \frac{3}{8} A_2^2 - \frac{1}{4} A_1 A_3 - \frac{1}{4} A_3^2 = 0 \tag{8b}$$

$$\left[\frac{100}{9} - \left(\frac{2\nu}{N}\right)^2\right] A_3 + \frac{1}{8} A_1^2 - \frac{1}{4} A_1 A_2 - \frac{1}{2} A_2 A_3 = 0 . \tag{8c}$$

A systematic solution of eqns. (8a-c) in ascending powers of $\epsilon \equiv (4/9) - (2\nu/N)^2$ may be obtained, but for operation an appreciable distance away from the $\nu/N \rightarrow 1/3$ resonance--i.e., when ϵ is not very small--it may be considered more satisfactory to solve these equations numerically.

For the case $2\nu/N = 0.6$, a direct numerical solution of eqns. (8a-c) leads to the values

$$A_1 = -0.5751_{517}$$

$$A_2 = +0.0229_{394}$$

$$A_3 = -0.0041_{574} ,$$

so that the approximate solution

$$v \cong -0.5751_{517} \sin 2t/3 + 0.0229_{394} \sin 2t - 0.0041_{574} \sin 10t/3, \tag{9a}$$

$$dv/dt \cong -0.3834_{345} \cos 2t/3 + 0.0458_{788} \cos 2t - 0.0138_{58} \cos 10t/3 \tag{9b}$$

is obtained.

An algebraic solution of eqns. (8a-c) in ascending powers of $\epsilon \equiv 4/9 - (2\nu/N)^2$ leads to the series

$$A_1 = -8\epsilon \Big[1 - 2\left(\frac{4}{P} + \frac{1}{Q}\right)\epsilon + 4\left(\frac{32}{P^2} + \frac{11}{PQ} + \frac{2}{Q^2}\right)\epsilon^2 - 4\left(\frac{652}{P^3} + \frac{292}{P^2Q} + \frac{79}{PQ^2} + \frac{10}{Q^3}\right)\epsilon^3 + 4\left(\frac{14912}{P^4} + \frac{8294}{P^3Q} + \frac{2808}{P^2Q^2} + \frac{577}{PQ^3} + \frac{56}{Q^4}\right)\epsilon^4 + \cdots \Big] \tag{10a}$$

$$A_2 = \frac{16\epsilon^2}{P}\Big[1 - \left(\frac{16}{P} + \frac{3}{Q}\right)\epsilon + \left(\frac{326}{P^2} + \frac{100}{PQ} + \frac{15}{Q^2}\right)\epsilon^2 - 4\left(\frac{1864}{P^3} + \frac{785}{P^2Q} + \frac{188}{PQ^2} + \frac{21}{Q^3}\right)\epsilon^3 + \ldots\Big] \tag{10b}$$

$$A_3 = -\frac{8\epsilon^2}{Q}\Big[1 - 4\left(\frac{3}{P} + \frac{1}{Q}\right)\epsilon + 4\left(\frac{56}{P^2} + \frac{27}{PQ} + \frac{5}{Q^2}\right)\epsilon^2 - 4\left(\frac{1234}{P^3} + \frac{744}{P^2Q} + \frac{219}{PQ^2} + \frac{28}{Q^3}\right)\epsilon^3 + \ldots \tag{10c}$$

where

$$\epsilon \equiv \frac{4}{9} - \left(\frac{2\nu}{N}\right)^2$$

$$P \equiv 4 - \left(\frac{2\nu}{N}\right)^2$$

$$Q \equiv \frac{100}{9} - \left(\frac{2\nu}{N}\right)^2 .$$

In the case considered previously, in which $2\nu/N = 0.6$, so that $\epsilon = 19/225 = 0.08444\cdots$, the series (10a-c) appear to converge rather slowly. Evaluation of the terms listed would suggest

$$A_1 = -0.6755\,555\left[1 - 0.2013\,012 + 0.0774\,000 - 0.0379\,715 + 0.0209\,305 + \cdots\right]$$

$$\cong -0.6755\,555 \times 0.8590\,578 = -0.5803\,413,$$

$$A_2 = +0.0313\,445\left[1 - 0.3947\,478 + 0.1945\,985 - 0.1074\,831 + \cdots\right]$$

$$\cong +0.0313\,445 \times 0.6923\,676 = +0.0217\,019,$$

$$A_3 = -0.0053\,061\left[1 - 0.3098\,062 + 0.1414\,688 - 0.0755\,171 + \cdots\right]$$

$$\cong -0.0053\,061 \times 0.7561\,455 = -0.0040\,122.$$

As was just mentioned, it is seen that the convergence of the expressions for A_1, A_2, and A_3 is quite slow in this example, each term being roughly minus 50 or 55 percent of the term before it, and only about two-figure accuracy is obtained* for the solution of the algebraic equations in this case without extension of the series to include terms beyond those shown here. The convergence, of course, would be markedly better if one were, say, one-third as far from the resonant frequency as was the case in the example considered here.

It may be noted in passing that retention of only the leading term in A_1 leads to

$$\text{Ampl. of } v \cong 8\,|\epsilon| = 8\left|(4/9) - (2\nu/N)^2\right|, \tag{11a}$$

or

$$\text{Ampl. of } u \cong (2\,w^2 N^2/f)\left|(4/9) - (2\nu/N)^2\right| = (8\,w^2/f)\left|(N/3)^2 - \nu^2\right|, \tag{11b}$$

in agreement with the "handy formula" previously cited.[1]

*Cf. the results of the numerical solution which led to eqns. (9a, b).

2. Computational Results

(a) The coefficients of the trial function: For comparison with the solution (9a, b) which was found in sub-section 1 by a variational method, the unstable equilibrium solution (period $\Delta t = \pi/3$) of eqn. (5) was found computationally for $2\nu/N = 0.6$ by means of the DUCK-ANSWER program[7] and subjected to Fourier analysis by aid of the FORANAL program.[8] The result of this computational work is given below:

$$\begin{aligned} v = &- 0.575116 \sin 2t/3 + 0.022944 \sin 2t \\ &- 0.004159 \sin 10t/3 + 0.000182 \sin 14t/3 \\ &- 0.000019 \sin 6t + \cdots , \end{aligned} \tag{12a}$$

$$\begin{aligned} dv/dt = &- 0.383411 \cos 2t/3 + 0.045888 \cos 2t \\ &- 0.013865 \cos 10t/3 + 0.000851 \cos 14t/3 \\ &- 0.000116 \cos 6t + \cdots . \end{aligned} \tag{12b}$$

It is seen that the coefficients found for the first three terms of v and dv/dt check quite closely the results obtained by hand calculation in sub-section 1 [eqns. (9a, b)] and that the remaining coefficients are relatively small.

(b) Coordinates of fixed points: The predicted coordinates of the unstable fixed points for $t = 0$ (mod. π), or alternatively for $t = \frac{3\pi}{4}$ (mod. π), may be obtained by substitution of these values into the expressions of eqns. (9a, b). The results in the first case, then, refer to solutions of

$$d^2v/dt^2 + (2\nu/N)^2 v + (1/2)(\sin 2t) v^2 = 0 \qquad \text{at } t = 0, \text{ mod. } \pi ,$$

and in the second case to

$$d^2v/d\tau^2 + (2\nu/N)^2 v - (1/2)(\cos 2\tau) v^2 = 0 \quad \text{at } \tau = t - 3\pi/4 = 0, \text{ mod. } \pi$$

which are examples for which computer information has been obtained.

The results are summarized in Table I. The agreement between the results of eqns. (9a, b) and the computational values is seen to be quite good in these examples.

TABLE I

COORDINATES OF UNSTABLE FIXED POINTS, AS CALCULATED FROM EQNS. (9a, b) AND AS OBTAINED FROM COMPUTER RESULTS

t	From Eqns. (9a, b)		From Computer*	
	v	dv/dt	v	dv/dt
0,	0	- 0.3514	0	- 0.3506
mod. π	$\pm$ 0.4945	0.2445	$\pm$ 0.4943	0.2440
$3\pi/4$,	- 0.6022	0	- 0.6024	0
mod. π	0.2667	$\mp$ 0.3201	0.2668	$\mp$ 0.3207

D. THE MOSER PROCEDURE

1. Outline of Method

The differential equation (5), with which we are concerned in the present report, may be derived from the Hamiltonian

$$H = (1/2)\, p^2 + (1/2)\,(2\,\nu/N)^2\, v^2 + (1/6)\,(\sin 2\,t)\, v^3\,, \tag{13}$$

with $p \equiv dv/dt$. It is the purpose of the work to transform the variables (v, p) in such a way that the time-dependence is removed from the cubic term in H; the resultant Hamiltonian through terms of this order (and including the time-independent part of the terms of next higher order) may

*In much of the computational work the variables actually employed were $v/1.15$ and $(dv/dt)/1.15$, representing respectively u/w and $(2/N)(du/d\theta)/w$ when $\frac{4\,f}{w\,N^2} = 1.15$. To avoid complexity, however, the results are presented here in terms of the variable v which is employed in the analysis of the present report.

then be taken as an approximate constant of the motion, from which invariant phase curves can be constructed and values of fixed points determined.

The work first will be outlined in terms of complex variables ($\zeta_0, \bar{\zeta}_0$; $\zeta_1, \bar{\zeta}_1$) of the sort introduced by Moser,[2] and secondly will be carried out in a way which may be somewhat simpler for the present purposes, using quantities akin to angle-action variables. The use of these two methods may be of some inherent interest and serves to check the algebraic work.

2. Use of ζ , $\bar{\zeta}$ Variables

(a) The forward transformations: Commencing with the Hamiltonian (13), which is expressed in terms of v, p, and t, a first transformation is made to variables ζ_0 , $\bar{\zeta}_0$ which are complex conjugate quantities (with v and p real) but which are to be regarded as independent for the purposes of Hamiltonian theory, with ζ_0 playing the role of a coordinate and $\bar{\zeta}_0$ representing the canonically-conjugate momentum. ζ_0 and $\bar{\zeta}_0$ are defined in terms of v and p as follows:

$$\zeta_0 = (\nu/N)^{1/2}\left[v + \frac{i}{2}\frac{N}{\nu}\, p\right] \tag{14a}$$

$$\bar{\zeta}_0 = (\nu/N)^{1/2}\left[v - \frac{i}{2}\frac{N}{\nu}\, p\right], \tag{14b}$$

and, correspondingly,

$$v = (1/2)\,(N/\nu)^{1/2}\left[\zeta_0 + \bar{\zeta}_0\right] \tag{14c}$$

$$p = -\,i\,(\nu/N)^{1/2}\left[\zeta_0 - \bar{\zeta}_0\right]. \tag{14d}$$

It is noted that the functional determinant is

$$\frac{\partial(\zeta_0, \bar{\zeta}_0)}{\partial(v,\ p)} = -\,i\,, \tag{15}$$

but that one can write

$$p\,dv = +\,i\,(\xi_0\,d\,\xi_0) + \text{perfect differential;} \tag{16}$$

hence, although the transformation from v, p to ξ_0, $\bar{\xi}_0$ is strictly not canonical, the pair ξ_0, $\bar{\xi}_0$ may be regarded as canonically-conjugate in association with the Hamiltonian

$$\Omega_0 = -\,i\,H \tag{17a}$$

$$= -\,i\,(2\nu/N)\,\xi_0\bar{\xi}_0 - (i/48)\,(N/\nu)^{3/2}\,(\sin 2\,t)\,(\xi_0+\bar{\xi}_0)^3\,. \tag{17b}$$

A canonical transformation from ξ_0, $\bar{\xi}_0$ to ξ_1, $\bar{\xi}_1$ is now performed by means of a generating function $F_1(\xi_0, \bar{\xi}_1)$. The generating function is so chosen as to remove from the Hamiltonian all time-dependence in the cubic term, save that associated with the resonance $\nu/N \rightarrow 1/3$, the coefficients of the transformation thus remaining finite as the resonance is approached; supplementary fourth-order terms are also included in the generating function in order that, to the order that the work is carried, the new variables ξ_1, $\bar{\xi}_1$ conveniently will be complex conjugates.[9] The generating function selected is

$$F_1(\xi_0,\bar{\xi}_1) = \xi_0\bar{\xi}_1 - (i/48)(N/\nu)^{3/2}\left[\Phi_0\xi_0^3 + \Phi_1\xi_0^2\bar{\xi}_1 + \Phi_2\xi_0\bar{\xi}_1^2 + \Phi_3\bar{\xi}_1^3\right]$$
$$+\,(1/1152)(N/\nu)^3\left[\Psi_0\xi_0^4 + \Psi_1\xi_0^3\bar{\xi}_1 + \Psi_2\xi_0^2\bar{\xi}_1^2 + \Psi_3\xi_0\bar{\xi}_1^3 + \Psi_4\bar{\xi}_1^4\right], \tag{18}$$

where Φ_0, $\cdots$ are taken as periodic solutions of the differential equations

$$i\,(d\Phi_0/dt) + 3\,(2\nu/N)\Phi_0 - (1/2)\,e^{-2\,it} = 0 \tag{19a}$$

$$i\,(d\Phi_1/dt) + (2\nu/N)\Phi_1 + (3/2)\,(e^{2\,it} - e^{-2\,it}) = 0 \tag{19b}$$

$$i\,(d\Phi_2/dt) - (2\nu/N)\Phi_2 + (3/2)\,(e^{2\,it} - e^{-2\,it}) = 0 \tag{19c}$$

$$i\,(d\Phi_3/dt) - 3\,(2\nu/N)\Phi_3 + (1/2)\,e^{2\,it} = 0, \tag{19d}$$

namely

$$\Phi_0 = \frac{1}{4\left[1 + 3\nu/N\right]}\, e^{-2it} \tag{20a}$$

$$\Phi_1 = \frac{3}{4\left[1 - \nu/N\right]}\, e^{2it} + \frac{3}{4\left[1 + \nu/N\right]}\, e^{-2it} \tag{20b}$$

$$\Phi_2 = \frac{3}{4\left[1 + \nu/N\right]}\, e^{2it} + \frac{3}{4\left[1 - \nu/N\right]}\, e^{-2it} = \Phi_1^{*} \tag{20c}$$

$$\Phi_3 = \frac{1}{4\left[1 + 3\nu/N\right]}\, e^{2it} = \Phi_0^{*}\ , \tag{20d}$$

and where

$$\Psi_0 = -(3/4)\Phi_0\Phi_1 \tag{21a}$$

$$\Psi_1 = -(3/2)\Phi_0\Phi_2 \quad -(1/2)\Phi_1^2 \tag{21b}$$

$$\Psi_2 = -(9/4)\Phi_0\Phi_3 \quad -(5/4)\Phi_1\Phi_2 \tag{21c}$$

$$\Psi_3 = -(3/2)\Phi_1\Phi_3 \quad -(1/2)\Phi_2^2 \quad = \Psi_1^{*} \tag{21d}$$

$$\Psi_4 = -(3/4)\Phi_2\Phi_3 \quad = \Psi_0^{*} \tag{21e}$$

The transformation equations then read

$$\bar\xi_0 = \partial F_1/\partial \xi_0 = \bar\xi_1 - (i/48)(N/\nu)^{3/2}\left[3\Phi_0\xi_0^2 + 2\Phi_1\xi_0\bar\xi_1 + \Phi_2\bar\xi_1^2\right] + (1/1152)(N/\nu)^3\left[4\Psi_0\xi_0^3 + 3\Psi_1\xi_0^2\bar\xi_1 + 2\Psi_2\xi_0\bar\xi_1^2 + \Psi_3\bar\xi_1^3\right] \tag{22a}$$

$$\xi_1 = \partial F_1/\partial \bar\xi_1 = \xi_0 - (i/48)(N/\nu)^{3/2}\left[\Phi_1\xi_0^2 + 2\Phi_2\xi_0\bar\xi_1 + 3\Phi_3\bar\xi_1^2\right] + (1/1152)(N/\nu)^3\left[\Psi_1\xi_0^3 + 2\Psi_2\xi_0^2\bar\xi_1 + 3\Psi_3\xi_0\bar\xi_1^2 + 4\Psi_4\bar\xi_1\right] \tag{22b}$$

and

$$\Omega_1 = \Omega_0 + \partial F_1/\partial t$$

$$= \Omega_0 - (i/48)(N/\nu)^{3/2}\left[\Phi_0'\xi_0^3 + \Phi_1'\xi_0^2\bar\xi_1 + \Phi_2'\xi_0\bar\xi_1^2 + \Phi_3'\bar\xi_1^3\right.$$

$$+ (1/1152)(N/\nu)^3\left[\Psi_0'\xi_0^4 + \Psi_1'\xi_0^3\bar\xi_1 + \Psi_2'\xi_0^2\bar\xi_1^2 + \Psi_3'\xi_0\bar\xi_1^3 + \Psi_4'\bar\xi_1^4\right], \tag{23}$$

with primes denoting differentiation with respect to t. It is now necessary, of course, to solve eqns. (22a, b) algebraically with sufficient accuracy that eqn. (23) for Ω_1 may be expressed explicitly in terms of the new variables $\xi_1, \bar{\xi}_1$.

The algebraic steps leading to the expression of Ω_1 in terms of $\xi_1, \bar{\xi}_1$ are detailed in Appendix A, with the result

$$\Omega_1 = -i\,(2\nu/N)\,\xi_1\bar{\xi}_1 - (1/96)(N/\nu)^{3/2}\left[e^{2it}\xi_1^3 - e^{-2it}\bar{\xi}_1^3\right] - \alpha\,\frac{i}{2048}\,(N/\nu)^3\,\xi_1^2\,\bar{\xi}_1^2 \tag{24}$$

where

$$\alpha \equiv 6\,\frac{\nu/N}{1-(\nu/N)^2} - \frac{1}{1+3\nu/N} \tag{25}$$

and where we have only retained in the quartic term that part which involves $\xi_1^2\,\bar{\xi}_1^2$ and which is independent of t.[10]

It is now convenient to introduce variables γ and J, to play the roles of coordinate and momentum, defined as

$$\gamma \equiv \frac{1}{2i}\,\ln(\bar{\xi}_1/\xi_1) \tag{26a}$$

$$J \equiv \xi_1\,\bar{\xi}_1 \quad , \tag{26b}$$

so that, correspondingly,

$$\xi_1 = J^{1/2}\,e^{-i\gamma} \tag{27a}$$

$$\bar{\xi}_1 = J^{1/2}\,e^{i\gamma} \quad . \tag{27b}$$

In this case the functional determinant is

$$\frac{\partial(\gamma, J)}{\partial(\xi_1, \bar{\xi}_1)} = i \tag{28}$$

and

$$\begin{aligned}\bar{\xi}_1\,d\xi_1 &= -\,i\,J\,d\gamma + \tfrac{1}{2}\,dJ \\ &= -\,i\,J\,d\gamma + \text{perfect differential,}\end{aligned} \tag{29}$$

so the new variables γ , J may be referred to the Hamiltonian

$$H_1 = i\Omega_1 . \tag{30}$$

It is noted that the functional determinant of the over-all transformation from v, p to γ , J is

$$\frac{\partial(\gamma, J)}{\partial(v, p)} = \frac{\partial(\gamma, J)}{\partial(\xi_1, \bar{\xi}_1)} \frac{\partial(\xi_1, \bar{\xi}_1)}{\partial(\xi_0, \bar{\xi}_0)} \frac{\partial(\xi_0, \bar{\xi}_0)}{\partial(v, p)} = (i)(1)(-i) = 1, \tag{31}$$

so that the pair γ , J may be regarded as canonically related to the original pair v, p.

From the expression (24) for Ω_1 and the relation (30) which connects H_1 with Ω_1 , we immediately find

$$H_1 = (2\nu/N)\, J - (1/48)\, (N/\nu)^{3/2}\, J^{3/2} \sin (3\gamma - 2t) + (\alpha/2048)\, (N/\nu)^3\, J^2 . \tag{32}$$

A final canonical transformation to variables $\bar{\gamma}$, $\bar{J}$, defined by the generating function

$$F_2(\gamma , \bar{J}) = \bar{J}(\gamma - \tfrac{2}{3} t) , \tag{33}$$

leads to

$$J = \partial F_2/\partial\gamma = \bar{J} \tag{34a}$$

$$\bar{\gamma} = \partial F_2/\partial\bar{J} = \gamma - \tfrac{2}{3} t \tag{34b}$$

and

$$\begin{aligned} H_2 &= H_1 + \partial F/\partial t \\ &= H_1 - \tfrac{2}{3}\bar{J} \\ &= -\left(\frac{2}{3} - \frac{2\nu}{N}\right)\bar{J} - \frac{1}{48}\left(\frac{N}{\nu}\right)^{3/2} (\bar{J})^{3/2} \sin 3\bar{\gamma} \\ &\quad + \frac{\alpha}{2048}\left(\frac{N}{\nu}\right)^3 (\bar{J})^2 . \end{aligned} \tag{35}$$

By a sequence of transformations between the pairs of variables

Coordinate	Momentum
ν	p
ξ_0	$\bar{\xi}_0$
ξ_1	$\bar{\xi}_1$
γ	J
$\bar{\gamma}$	$\bar{J}$

we are thus led to a Hamiltonian H_2 [eqn (35)] from the first two terms of which the independent variable t has been entirely removed and in the last term of which we have retained the t-independent part * The retention of the last term in this form is believed to be desirable, since it can exert a significant influence on the J-dependence (or amplitude-dependence) of the oscillation frequency.[10] To the degree of approximation considered here, then, we take H_2 in the form expressed by eqn (35) to be a constant of the motion. In this spirit invariant phase curves of the problem are determined.

<u>(b) The separatrix:</u> The assumed constancy of H_2 means that for any particular value of t and points homologous thereto (t taken modulo π), the quantity

$$-\left(\frac{2}{3} - \frac{2\nu}{N}\right) J - \frac{1}{48}\left(\frac{N}{\nu}\right)^{3/2} J^{3/2} \sin(3\gamma - 2t) + \frac{\alpha}{2048}\left(\frac{N}{\nu}\right)^{3} J^{2} = H_2 \quad (36)$$

is constant If we introduce for convenience the scaled quantities

---

*A little reflection will show that only that part of the quartic terms in Ω_1 which have been retained in (24) make a t-independent contribution to the final H_2.

$$\xi^2 = \frac{1}{(48)^2\ (2/3 - 2\,\nu/N)^2\ (\nu/N)^3}\ J \tag{37a}$$

$$\mathcal{K} = -\frac{1}{(48)^2\ (2/3 - 2\,\nu/N)^3\ (\nu/N)^3}\ H_2 \tag{37b}$$

and

$$\lambda = (2/3 - 2\,\nu/N)\alpha$$

$$= (\frac{2}{3} - \frac{2\,\nu}{N})\left[6\,\frac{\nu/N}{1-(\nu/N)^2} - \frac{1}{1+3\,\nu/N}\right],^{*} \tag{37c}$$

eqn. (36) assumes the more concise form

$$\xi^2 + \xi^3 \sin(3\gamma - 2\,t) - (9\lambda/8)\,\xi^4 = \mathcal{K}. \tag{38}$$

The fixed points for the motion, in particular, are characterized by expression (38) being stationary with respect to γ and ξ. For the unstable fixed points associated with the separatrix between stable and unstable regions, we take γ as having values for which**

$$\sin(3\gamma - 2\,t) = -1 \tag{39a}$$

$$[\gamma = -\pi/6 + 2\,t/3,\ \text{mod.}\ 2\pi/3] \tag{39b}$$

and ξ to be the root ξ_1, near 2/3, of the quadratic equation

$$(9\lambda/2)\,\xi^2 + 3\,\xi - 2 = 0: \tag{40}$$

$$\xi_1 = \frac{\sqrt{1+4\lambda} - 1}{3\lambda} \tag{41a}$$

$$\doteq \frac{2}{3}\left[1 - \lambda + 2\lambda^2 - 5\lambda^3 + 14\lambda^4 - \cdots\right]. \tag{41b}$$

---

*For $\nu/N = 0.3$, $\alpha = 1.451706$, $\lambda = 0.0967804$, and $(9/8)\lambda = 0.108878$.

**With this choice of sign for $\sin(3\gamma - 2\,t)$, the value of ξ which we select is positive.

In the work to follow it will be convenient to employ a quantity, normally near unity,* which we denote as η_1 :

$$\eta_1 = \frac{3}{2}\xi_1 \tag{42a}$$

$$= \frac{\sqrt{1 + 4\lambda} - 1}{2\lambda} \tag{42b}$$

$$\doteq 1 - \lambda + 2\lambda^2 - 5\lambda^3 + 14\lambda^4 - \cdots , \tag{42c}$$

λ being defined by eqn. (37c). The associated value of K is**

$$K_1 = \xi_1^2 - \xi_1^3 - (9\lambda/8)\xi_1^4 \tag{43a}$$

$$= \xi_1^2 (2 - \xi_1)/4 \tag{43b}$$

$$= \frac{4}{27}\,\frac{\eta_1^2 (3 - \eta_1)}{2} . \tag{43c}$$

Associated with this value of K there is a value of ξ, which we denote by ξ_2 and which is normally roughly $\xi_1/2$, which corresponds to setting $\sin(3\gamma - 2t) = +1$ in eqn. (38); if we write $\eta_2 = \frac{3}{2}\xi_2$, in analogy to eqn. (42a), η_2 will be roughly 1/2.***

In summary, then

$$J^{1/2} = 64\,(1/3 - \nu/N)\,(\nu/N)^{3/2}\,\eta \tag{44}$$

[cf. eqn. (37a)]; points on a particular phase curve specified by its value of K, are then obtained by use of values of γ and J which are mutually consistent with K through eqn. (36) or (38), evaluation of the corresponding values of ξ_1, $\bar{\xi}_1$, and finally proceeding back through the transformations to obtain the associated values of v and p. Without continuation

---

*For $\nu/N = 0.3$, $\xi_1 = 0.61225$ and $\eta_1 = 0.918374$.

**For $\nu/N = 0.3$, $K_1 = 0.130049$.

***For $\nu/N = 0.3$, the value ξ_2 corresponding to $K_1 = 0.130049$ is $\xi_2 = 0.31570$ and $\eta_2 = 0.47355$.

of the analysis beyond the transformations described here, it is pointless to express the results to terms beyond those which are second order in the quantity $(1/3 - \nu/N)$.

We give below, in Table II, such values of ξ_1, $\bar{\xi}_1$, for the two types of locations considered in the examples of Section C 2 b, namely $t = 0 \pmod{\pi}$ and $t = 3\pi/4 \pmod{\pi}$.

(c) The reverse transformation to the original variables: For evaluation of ξ_0, $\bar{\xi}_0$, and hence of v, p, we now make use of the transformation equations previously exhibited. Since, by eqns. (14a, b), the quantities required for evaluating v and p are explicitly $\xi_0 + \bar{\xi}_0$ and $\xi_0 - \bar{\xi}_0$, respectively, we make use of eqn. (A4) of Appendix A,

$$\xi_0 + \bar{\xi}_0 \doteq \xi_1 + \bar{\xi}_1 + (i/48)(N/\nu)^{3/2}\left[(-3\Phi_0 + \Phi_1)\xi_1^2 + (-2\Phi_1 + 2\Phi_2)\xi_1\bar{\xi}_1 + (-\Phi_2 + 3\Phi_3)\bar{\xi}_1^2\right], \tag{45}$$

and the corresponding expression

$$\xi_0 - \bar{\xi}_0 \doteq \xi_1 - \bar{\xi}_1 + (i/48)(N/\nu)^{3/2}\left[(3\Phi_0 + \Phi_1)\xi_1^2 + (2\Phi_1 + 2\Phi_2)\xi_1\bar{\xi}_1 + (\Phi_2 + 3\Phi_3)\bar{\xi}_1^2\right] \tag{46}$$

obtained by subtraction of eqns. (A1) and (A2). It is a matter then of straight-forward algebra to evaluate $\Phi_0, \ldots, \Phi_3$ for the value of t which is of interest, to evaluate $\xi_0 \pm \bar{\xi}_0$ from the previously written ξ_1, $\bar{\xi}_1$ (e. g., those listed in Table II), and thus determine v, p. The results, for the cases to which Table II pertains, are given in Table III.

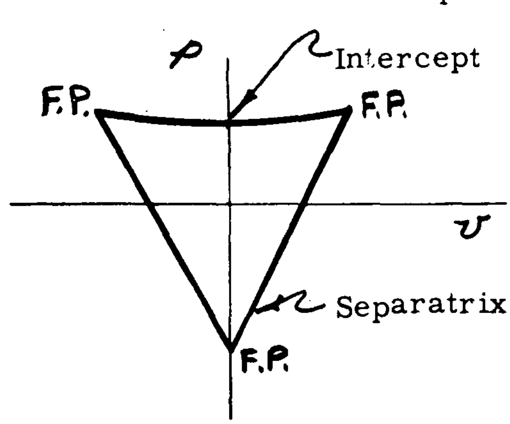

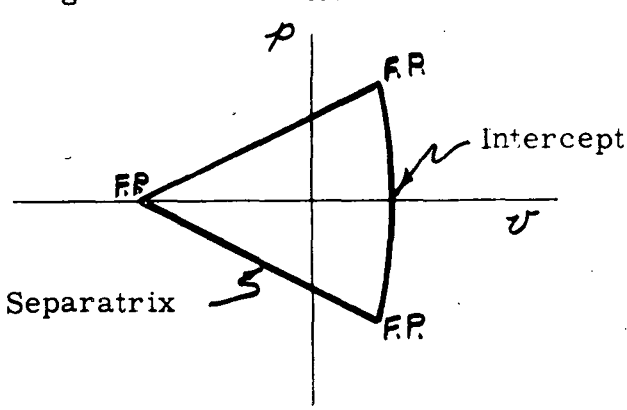

TABLE II

VALUES OF $\mathfrak{z}_1$ AND $\bar{\mathfrak{z}}_1$ CORRESPONDING TO THE SEPARATRIX OF EQUATION (5) FOR $t = 0$ (mod. π) AND FOR $t = 3\pi/4$ (mod. π)

The first lines apply to the unstable fixed points; the last line refers to the intercept of the separatrix with the symmetry axis of the v, p diagram.

ξ	γ	For $t = 0$, mod. π: $\mathfrak{z}_1$	For $t = 0$, mod. π: $\bar{\mathfrak{z}}_1$	For $t = 3\pi/4$, mod. π: $\mathfrak{z}_1$	For $t = 3\pi/4$, mod. π: $\bar{\mathfrak{z}}_1$
ξ_1	$-\frac{\pi}{6}+\frac{2t}{3}$	$32(\sqrt{3}+i)\left(\frac{1}{3}-\frac{\nu}{N}\right)\left(\frac{\nu}{N}\right)^{3/2}\eta_1$	$32(\sqrt{3}-i)\left(\frac{1}{3}-\frac{\nu}{N}\right)\left(\frac{\nu}{N}\right)^{3/2}\eta_1$	$32(1-\sqrt{3}\,i)\left(\frac{1}{3}-\frac{\nu}{N}\right)\left(\frac{\nu}{N}\right)^{3/2}\eta_1$	$32(1+\sqrt{3}\,i)\left(\frac{1}{3}-\frac{\nu}{N}\right)\left(\frac{\nu}{N}\right)^{3/2}\eta_1$
	$-\frac{5\pi}{6}+\frac{2t}{3}$	$-32(\sqrt{3}-i)\left(\frac{1}{3}-\frac{\nu}{N}\right)\left(\frac{\nu}{N}\right)^{3/2}\eta_1$	$-32(\sqrt{3}+i)\left(\frac{1}{3}-\frac{\nu}{N}\right)\left(\frac{\nu}{N}\right)^{3/2}\eta_1$	$32(1+\sqrt{3}\,i)\left(\frac{1}{3}-\frac{\nu}{N}\right)\left(\frac{\nu}{N}\right)^{3/2}\eta_1$	$32(1-\sqrt{3}\,i)\left(\frac{1}{3}-\frac{\nu}{N}\right)\left(\frac{\nu}{N}\right)^{3/2}\eta_1$
	$\frac{\pi}{2}+\frac{2t}{3}$	$-64\,i\left(\frac{1}{3}-\frac{\nu}{N}\right)\left(\frac{\nu}{N}\right)^{3/2}\eta_1$	$64\,i\left(\frac{1}{3}-\frac{\nu}{N}\right)\left(\frac{\nu}{N}\right)^{3/2}\eta_1$	$-64\left(\frac{1}{3}-\frac{\nu}{N}\right)\left(\frac{\nu}{N}\right)^{3/2}\eta_1$	$-64\left(\frac{1}{3}-\frac{\nu}{N}\right)\left(\frac{\nu}{N}\right)^{3/2}\eta_1$
ξ_2	$-\frac{\pi}{2}+\frac{2t}{3}$	$64\,i\left(\frac{1}{3}-\frac{\nu}{N}\right)\left(\frac{\nu}{N}\right)^{3/2}\eta_2$	$-64\,i\left(\frac{1}{3}-\frac{\nu}{N}\right)\left(\frac{\nu}{N}\right)^{3/2}\eta_2$	$64\left(\frac{1}{3}-\frac{\nu}{N}\right)\left(\frac{\nu}{N}\right)^{3/2}\eta_2$	$64\left(\frac{1}{3}-\frac{\nu}{N}\right)\left(\frac{\nu}{N}\right)^{3/2}\eta_2$

TABLE III

VALUES OF v AND p CORRESPONDING TO THE SEPARATRIX OF EQUATION (5) FOR $t = 0$ (mod. π) AND FOR $t = 3\pi/4$ (mod. π)

The first lines in each group give the coordinates of the unstable fixed points; the last line refers to the intercept of the separatrix on the axis of symmetry.

t	v	p
$t = 0$, mod. π	$\pm 32\sqrt{3}\left(\frac{1}{3}-\frac{\nu}{N}\right)\left(\frac{\nu}{N}\right)\eta_1\left[1-\left(\frac{2}{1-\nu^2/N^2}-\frac{1}{1+3\nu/N}\right)\left(\frac{1}{3}-\frac{\nu}{N}\right)\eta_1\right]$	$64\left(\frac{1}{3}-\frac{\nu}{N}\right)\left(\frac{\nu}{N}\right)^2\eta_1\left[1+\left(\frac{10}{1-\nu^2/N^2}+\frac{1}{1+3\nu/N}\right)\left(\frac{1}{3}-\frac{\nu}{N}\right)\eta_1\right]$
	0	$-128\left(\frac{1}{3}-\frac{\nu}{N}\right)\left(\frac{\nu}{N}\right)^2\eta_1\left[1-\left(\frac{2}{1-\nu^2/N^2}-\frac{1}{1+3\nu/N}\right)\left(\frac{1}{3}-\frac{\nu}{N}\right)\eta_1\right]$
	0	$128\left(\frac{1}{3}-\frac{\nu}{N}\right)\left(\frac{\nu}{N}\right)^2\eta_2\left[1+\left(\frac{2}{1-\nu^2/N^2}-\frac{1}{1+3\nu/N}\right)\left(\frac{1}{3}-\frac{\nu}{N}\right)\eta_2\right]$
$t = 3\pi/4$, mod. π	$32\left(\frac{1}{3}-\frac{\nu}{N}\right)\left(\frac{\nu}{N}\right)\eta_1\left[1-\left(\frac{10\,\nu/N}{1-\nu^2/N^2}+\frac{1}{1+3\nu/N}\right)\left(\frac{1}{3}-\frac{\nu}{N}\right)\eta_1\right]$	$\mp 64\sqrt{3}\left(\frac{1}{3}-\frac{\nu}{N}\right)\left(\frac{\nu}{N}\right)^2\eta_1\left[1+\frac{2\,\nu/N}{1-\nu^2/N^2}-\frac{1}{1+3\nu/N})\left(\frac{1}{3}-\frac{\nu}{N}\right)\eta_1\right]$
	$-64\left(\frac{1}{3}-\frac{\nu}{N}\right)\left(\frac{\nu}{N}\right)\eta_1\left[1+\left(\frac{2\,\nu/N}{1-\nu^2/N^2}-\frac{1}{1+3\nu/N}\right)\left(\frac{1}{3}-\frac{\nu}{N}\right)\eta_1\right]$	0
	$64\left(\frac{1}{3}-\frac{\nu}{N}\right)\left(\frac{\nu}{N}\right)\eta_2\left[1-\left(\frac{2\,\nu/N}{1-\nu^2/N^2}-\frac{1}{1+3\nu/N}\right)\left(\frac{1}{3}-\frac{\nu}{N}\right)\eta_2\right]$	0

Since the foregoing results have not been carried consistently beyond terms of order $\left(\frac{1}{3}-\frac{\nu}{N}\right)^2$, it may be considered sufficient to replace the coefficients of $\left(\frac{1}{3}-\frac{\nu}{N}\right)$ in the lastterm of the correction factors by the value which these coefficients assume as $\nu/N \rightarrow 1/3$. Thus the correction factor for the value of v given in the first line of Table III might be consistently written as $[1 - (7/4)(1/3 - \nu/N)]$. Indeed, since $\eta_1 \cong 1 - \lambda \cong 1 - (7/2)(1/3 - \nu/N)$, the factor η_1 outside the square bracket might be replaced by unity and a composite correction factor $[1 - (21/4)(1/3 - \nu/N)$ employed in this case.* Although this contention cannot be gainsaid, we elect, however to leave our results in the form summarized in Table III, being guided, in part, by some computational results pertaining to the case $t = 0$, mod. π [Sect. D 4].

*Also $\eta_2 \cong (1/2)(1 - 5\lambda/8)$.

3. Use of Quantities Akin to Angle-Action Variables

(a) The forward transformations: We commence again with the Hamiltonian of eqn. (13),

$$H = (1/2)\, p^2 + (1/2)\, (2\,\nu/N)^2\, v^2 + (1/6)\, (\sin 2\,t)\, v^3 , \qquad (13)$$

and make a series of canonical transformations from the conjugate pair v, p to γ_0, J_0 ; γ_1, J_1 ; and γ_2, J_2. The first transformation is defined by the generating function

$$G_0\,(v, \gamma_0) = (\nu/N)\, v^2 \operatorname{ctn} \gamma_0 , \qquad (47)$$

so that

$$p = \partial G_0/\partial v = (2\,\nu/N)\, v \operatorname{ctn} \gamma_0 \qquad (48a)$$

$$J_0 = -\,\partial G_0/\partial \gamma = (\nu/N)\, v^2 \csc^2 \gamma_0 \quad ; \qquad (48b)$$

thus

$$\operatorname{ctn} \gamma_0 = \frac{N}{2\nu}\,\frac{p}{v} \qquad (49a)$$

$$J_0 = \frac{1}{2}\left(\frac{N}{2\nu}\right) p^2 + \frac{1}{2}\left(\frac{2\nu}{N}\right) v^2 , \qquad (49b)$$

$$v = (N/\nu)^{1/2}\, J_0^{1/2} \sin \gamma_0 \qquad (49c)$$

$$p = 2\,(\nu/N)^{1/2}\, J_0^{1/2} \cos \gamma_0 \quad , \qquad (49d)$$

and the new Hamiltonian is

$$\begin{aligned} K_0 &= H + \partial G_0/\partial t \\ &= H \\ &= 2\,(\nu/N)\, J_0 + (1/6)\,(N/\nu)^{3/2}\, J_0^{3/2} \sin^3 \gamma_0 \ \sin 2\,t \\ &= 2\,(\nu/N)\, J_0 + (1/48)\,(N/\nu)^{3/2}\, J_0^{3/2} \big[3 \cos(\gamma_0 - 2\,t) \\ &\qquad - 3 \cos(\gamma_0 + 2t) + \cos(3\gamma_0 + 2\,t) - \cos(3\,\gamma_0 - 2\,t)\big] , \end{aligned} \qquad (50)$$

In analogy to the procedure followed in Section D 2 in formulating the transformation from ξ_0, $\bar{\xi}_0$ to ξ_1, $\bar{\xi}_1$, we now introduce a second generating function

$$G_1(\gamma_1, J_1) = J_1 \cdot \gamma_0 + (1/96)(N/\nu)^{3/2} J_1^{3/2} \left[3\frac{\sin(\gamma_0 - 2t)}{1 - \nu/N} + 3\frac{\sin(\gamma_0 + 2t)}{1 + \nu/N} - \frac{\sin(3\gamma_0 + 2t)}{1 + 3\nu/N} \right], \quad (51)$$

so that

$$J_0 = \partial G_1 / \partial \gamma_0$$
$$= J_1 + (1/32)(N/\nu)^{3/2} J_1^{3/2} \left[\frac{\cos(\gamma_0 - 2t)}{1 - \nu/N} + \frac{\cos(\gamma_0 + 2t)}{1 + \nu/N} - \frac{\cos(3\gamma_0 + 2t)}{1 + 3\nu/N} \right] \quad (52a)$$

$$\gamma_1 = \partial G_1 / \partial J_1$$
$$= \gamma_0 + (1/64)(N/\nu)^{3/2} J_1^{1/2} \left[3\frac{\sin(\gamma_0 - 2t)}{1 - \nu/N} + 3\frac{\sin(\gamma_0 + 2t)}{1 + \nu/N} - \frac{\sin(3\gamma_0 + 2t)}{1 + 3\nu/N} \right], \quad (52b)$$

and

$$K_1 = K_0 + \partial G_1 / \partial t$$
$$= K_0 + (1/48)(N/\nu)^{3/2} J_1^{3/2} \left[-3\frac{\cos(\gamma_0 - 2t)}{1 - \nu/N} + 3\frac{\cos(\gamma_0 + 2t)}{1 + \nu/N} - \frac{\cos(3\gamma_0 + 2t)}{1 + 3\nu/N} \right] \quad (53)$$

The new Hamiltonian, K_1, can be expressed in terms of the new variables γ_1, J_1 without much difficulty [Appendix B], with the result

$$K_1 = 2(\nu/N) J_1 - (1/48)(N/\nu)^{3/2} J_1^{3/2} \cos(3\gamma_1 - 2t)$$
$$+ (1/2048)(N/\nu)^3 J_1^2 \left[\frac{6\nu/N}{1 - \nu^2/N^2} - \frac{1}{1 + 3\nu/N} \right], \quad (54)$$

in which we have retained[10] only terms independent of t and of γ_1 in the term involving J_1^2.

It now only remains to introduce a third generating function,

$$G_2(\gamma_1, J_2) = J_2(\gamma_1 - \tfrac{2}{3} t), \tag{55}$$

which effects the transformation

$$J_1 = \partial G_2/\partial\gamma_1 = J_2 \tag{56a}$$

$$\gamma_2 = \partial G_2/\partial J_2 = \gamma_1 - \tfrac{2}{3} t \tag{56b}$$

with

$$\begin{aligned} K_2 &= K_1 + \partial G_2/\partial t \\ &= K_1 - \tfrac{2}{3} J_2 \\ &= -(2/3 - 2\nu/N) J_2 - (1/48)(N/\nu)^{3/2} J_2^{3/2} \cos 3\gamma_2 \\ &\qquad + (\alpha/2048)(N/\nu)^3 J_2^2, \end{aligned} \tag{57}$$

where, as previously,

$$\alpha \equiv \frac{6\nu/N}{1-\nu^2/N^2} - \frac{1}{1+3\nu/N} \qquad \left[\underline{\text{cf.}}\ \text{eqn. (25)}\right]$$

and t-dependent terms have been omitted[10] from the term involving J_2^2 .

This final Hamiltonian K_2, as expressed by eqn. (57) and which we shall take to be substantially a constant of the motion, is seen to be identical in form to the Hamiltonian H_2 of eqn. (35), as developed in Section D 2 save that the sine function is here fortuitously replaced by the cosine. It remains to perform with the present variables the reverse transformations required to carry particular values of γ_2 , J_2 back to the original quantities v, p--both the forward transformation and the reverse transformation which follows, however, appear to be somewhat simpler algebraically than the corresponding steps required with the ξ , $\bar{\xi}$ variables.

(b. The separatrix: To initiate the reverse transformation in this case, we shall focus our attention as before [Section D 2 b] on the particular salient points of the separatrix:*

For the Fixed Points

$$\gamma_1 = \begin{cases} \pi/3 + 2t/3, \\ -\pi/3 + 2t/3, \\ \pi + 2t/3, \end{cases} \quad \text{with } J_1^{1/2} = 64\,(1/3 - \nu/N)(\nu/N)^{3/2}\,\eta_1 \; ; \tag{58}$$

For the Intercept of the Separatrix

$$\gamma_1 = 0 + \frac{2t}{3}, \qquad \text{with } J_1^{1/2} = 64\,(1/3 - \nu/N)\,(\nu/N)^{3/2}\,\eta_2 \; . \tag{59}$$

(c) The reverse transformation to the original variables: For evaluation of the original variables v, p one notes from eqns. (49c, d) that the quantities explicitly required are $\sin\gamma_0$ and $\cos\gamma_0$, in addition to $J_0^{1/2}$. To the degree of accuracy with which we are concerned in the present work, it is sufficient for this purpose to refer to eqn. (52b) and write

$$\begin{aligned} \sin\gamma_0 &\doteq \sin\gamma_1 - (\cos\gamma_1)(\gamma_1 - \gamma_0) \\ &\doteq \sin\gamma_1 - \frac{\cos\gamma_1}{64}\left(\frac{N}{\nu}\right)^{3/2} J_1^{1/2}\left[3\frac{\sin(\gamma_1 - 2t)}{1 - \nu/N} + 3\frac{\sin(\gamma_1 + 2t)}{1 + \nu/N} - \frac{\sin(3\gamma_1 + 2t)}{1 + 3\nu/N}\right] \end{aligned} \tag{60a}$$

and

$$\begin{aligned} \cos\gamma_0 &\doteq \cos\gamma_1 + (\sin\gamma_1)(\gamma_1 - \gamma_0) \\ &\doteq \cos\gamma_1 + \frac{\sin\gamma_1}{64}\left(\frac{N}{\nu}\right)^{3/2} J_1^{1/2}\left[3\frac{\sin(\gamma_1 - 2t)}{1 - \nu/N} + 3\frac{\sin(\gamma_1 + 2t)}{1 + \nu/N} - \frac{\sin(3\gamma_1 + 2t)}{1 + 3\nu/N}\right], \end{aligned} \tag{60b}$$

*Because of the presence of $\cos 3\gamma_2$ in eqn. (57), in contrast to the presence of $\sin 3\bar{\gamma}$ in eqn. (35), the values of γ_2 which are of interest here may be related to the corresponding values of $\bar{\gamma}$ by $\gamma_2 = \bar{\gamma} + \pi/2$, or, similarly, $\gamma_1 = \gamma + \pi/2$. This distinction between γ_2 and $\bar{\gamma}$ of course could have been avoided by introduction of a phase shift in the generating function G_2.

while obtaining $J_o^{1/2}$ by [cf. eqn. (52a)]

$$J_o^{1/2} \doteq J_1^{1/2}\left\{1 + \frac{1}{64}\left(\frac{N}{\nu}\right)^{3/2} J_1^{1/2}\left[\frac{\cos(\gamma_1 - 2t)}{1-\nu/N} + \frac{\cos(\gamma_1 + 2t)}{1+\nu/N} - \frac{\cos(3\gamma_1 + 2t)}{1+3\nu/N}\right]\right\}. \quad (60c)$$

Thus for $t = 0$ and $\gamma_1 = \pm \pi/3$, eqns. (60a-c) give

$$\sin\gamma_0 = \pm\frac{\sqrt{3}}{2}\left[1 - \frac{3}{1-\nu^2/N^2}\left(\frac{1}{3}-\frac{\nu}{N}\right)\eta_1\right],$$

$$\cos\gamma_0 = \frac{1}{2}\left[1 + \frac{9}{1-\nu^2/N^2}\left(\frac{1}{3}-\frac{\nu}{N}\right)\eta_1\right],$$

and

$$J_o^{1/2} = 64\left(\frac{1}{3}-\frac{\nu}{N}\right)\left(\frac{\nu}{N}\right)^{3/2}\eta_1\left[1 + \left(\frac{1}{1-\nu^2/N^2} + \frac{1}{1+3\nu/N}\right)\left(\frac{1}{3}-\frac{\nu}{N}\right)\eta_1\right],$$

so that, by eqns. (49c, d), the fixed point coordinates

$$v = \pm 32\sqrt{3}\left(\frac{1}{3}-\frac{\nu}{N}\right)\left(\frac{\nu}{N}\right)\eta_1\left[1 - \left(\frac{2}{1-\nu^2/N^2} - \frac{1}{1+3\nu/N}\right)\left(\frac{1}{3}-\frac{\nu}{N}\right)\eta_1\right]$$

$$p = 64\left(\frac{1}{3}-\frac{\nu}{N}\right)\left(\frac{\nu}{N}\right)^2\eta_1\left[1 + \left(\frac{10}{1-\nu^2/N^2} + \frac{1}{1+3\nu/N}\right)\left(\frac{1}{3}-\frac{\nu}{N}\right)\eta_1\right]$$

are obtained. Similarly for the next case in the list (58), with $t = 0$ and $\gamma_1 = \pi$,

$$\sin\gamma_0 = 0$$

$$\cos\gamma_0 = -1$$

$$J_o^{1/2} = 64\left(\frac{1}{3}-\frac{\nu}{N}\right)\left(\frac{\nu}{N}\right)^{3/2}\eta_1\left[1 - \left(\frac{2}{1-\nu^2/N^2} - \frac{1}{1+3\nu/N}\right)\left(\frac{1}{3}-\frac{\nu}{N}\right)\eta_1\right],$$

so that

$$v = 0$$

$$p = -128\left(\frac{1}{3}-\frac{\nu}{N}\right)\left(\frac{\nu}{N}\right)^2\eta_1\left[1 - \left(\frac{2}{1-\nu^2/N^2} - \frac{1}{1+3\nu/N}\right)\left(\frac{1}{3}-\frac{\nu}{N}\right)\eta_1\right].$$

In this same way one finds complete agreement with all the results listed in Table III.

(d) The unstable equilibrium orbit: The procedure just followed can, of course, be employed in general to provide, as a function of t, the equation of the unstable equilibrium orbit, which is represented (mod. π) by fixed points as listed in sub-section (b).

For the unstable equilibrium orbits, in particular, the Hamiltonian equations which follow from K_2 [eqn. (57)] permit γ_2 and J_2 to be constant, with, let us say,

$$\gamma_2 = \pi \qquad \text{and} \quad J_2^{1/2} = 64\,(1/3 - \nu/N)\,(\nu/N)^{3/2}\,\eta_1 \quad [\underline{\text{cf.}}\ \text{(b)}].$$

Then

$$\gamma_1 = \gamma_2 + \frac{2\,t}{3} \tag{61a}$$

$$\quad = \pi + \frac{2\,t}{3}\ ,$$

$$J_1^{1/2} = J_2^{1/2}$$

$$= 64\,(1/3 - \nu/N)\,(\nu/N)^{3/2}\,\eta_1 \qquad [\underline{\text{cf.}}\ \text{eqns. (58)}]\ . \tag{61b}$$

By making use of eqns. (60a-c), in conjunction with eqn. (49c), the equation for the unstable equilibrium orbit, v(t), is then found to be

$$v(t) = -64\left(\frac{1}{3} - \frac{\nu}{N}\right)\left(\frac{\nu}{N}\right)\eta_1\left\{\sin\frac{2\,t}{3} - \left[\frac{\sin 2\,t/3}{1 - \nu/N} + 4\,\frac{(\nu/N)\sin 2\,t}{1 - \nu^2/N^2} - \left(\frac{1}{1+\nu/N} - \frac{1}{1+3\nu/N}\right)\sin\frac{10\,t}{3}\right]\left(\frac{1}{3} - \frac{\nu}{N}\right)\eta_1\right\}\ , \tag{62}$$

through quantities of the order of $(1/3 - \nu/N)^2$. The expression (62) is seen to contain circular functions of argument 2 t/3, 2 t, and 10 t/3, as was the case for the trial function (7) employed in the variational treatment of Section C. By substitution of particular values of t, the specific values of v for the fixed points listed in Table III may be obtained.

It may be noted, however, that differentiation of (62), which results in

$$p \equiv dv/dt = -128\left(\frac{1}{3}-\frac{\nu}{N}\right)\left(\frac{1}{3}-\frac{\nu}{N}\right)\eta_1\left\{\cos\frac{2t}{3}-\left[\frac{\cos 2t/3}{1-\nu/N}+12\frac{(\nu/N)\cos 2t}{1-\nu^2/N^2}\right.\right.$$
$$\left.\left.-5\left(\frac{1}{1+\nu/N}-\frac{1}{1+3\nu/N}\right)\cos\frac{10t}{3}\right]\left(\frac{1}{3}-\frac{\nu}{N}\right)\eta_1\right\}, \qquad (63)$$

does not lead exactly to the specific forms listed in Table III, although the forms become coincident through $(1/3 - \nu/N)^2$ when $\left(\frac{1}{3}-\frac{\nu}{N}\right)$ is expanded as $\left(\frac{\nu}{N}\right)^2\left[1 + 3(1/3 - \nu/N)\right]$. An expression for p may be obtained directly from eqn. (49d) of course, just as eqn. (62) was obtained from eqn. (49c), with the result

$$p = -128\left(\frac{1}{3}-\frac{\nu}{N}\right)\left(\frac{\nu}{N}\right)^2\eta_1\left\{\cos\frac{2t}{3}+\left[\frac{\cos 2t/3}{1-\nu/N}-4\frac{\cos 2t}{1-\nu^2/N^2}\right.\right.$$
$$\left.\left.+\left(\frac{1}{1+\nu/N}+\frac{1}{1+3\nu/N}\right)\cos\frac{10t}{3}\right]\left(\frac{1}{3}-\frac{\nu}{N}\right)\eta_1\right\}, \qquad (64)$$

from which the "momenta" for the fixed points listed in Table III follow for the special cases.

4. Computational Results

(a) The unstable equilibrium orbit: To establish a connection with Section C, in which the results of the variational method were presented, we note first that for $\nu/N = 0.3$ eqn. (62) leads to the unstable equilibrium orbit as given by

$$v(t) = -0.56206 \sin 2t/3 + 0.02373 \sin 2t - 0.00437 \sin 10t/3, \qquad (65)$$

while the alternative forms for p [eqn. (63), obtained by differentiation of eqn. (62), or eqn. (64), obtained directly from δ_2, J_2] are

$$p \equiv \frac{dv}{dt} = -0.37470 \cos 2t/3 + 0.04745 \cos 2t - 0.01457 \cos 10t/3 \qquad (66)$$

or

$$p = -0.36808 \cos 2t/3 + 0.04745 \cos 2t - 0.01399 \cos 10t/3 . \qquad (67)$$

These expressions may be compared with the Fourier analysis of computer results for this case, as given by eqns. (12a, b) of Section C 2. There is, of course, no fundamental basis for choosing between formulas (66) and (67) since, as noted previously, eqns. (63) and (64) are identical through terms in $(1/3 - \nu/N)^2$. It is in any event clear that the present results differ by a few percent from the computer results for $\nu/N = 0.3$.

(b) The fixed points: The results presented in Table III for the unstable fixed points at $t = 0$ (mod. π) and at $t = 3\pi/4$ (mod. π) have been subjected to computational checks for $\nu/N = 0.3$ and for $\nu/N = 0.3275$. Computational data pertaining to the fixed points at $t = 0$ (mod. π) have also been obtained for a series of values of ν/N, ranging from 0.30 to 0.36, in order to exhibit the dependence of the accuracy on the proximity to the $\nu/N \to 1/3$ resonance. We present these results below, to be followed in the suceeding sub-section by data for $\nu/N = 0.3$ which pertain to the "intercept" of the separatrix on the symmetry axis of the phase diagrams.

The coordinates of the fixed points, as calculated by the expressions listed in Table III, are compared with computer results for $\nu/N = 0.3$ in Table IV. The agreement with the computer results is seen to be poorer in Table IV than was obtained by the variational method summarized in Table I for $\nu/N = 0.3$.

TABLE IV

COORDINATES OF UNSTABLE FIXED POINTS,
AS CALCULATED FROM THE EXPRESSIONS OF TABLE III
AND AS OBTAINED FROM COMPUTER RESULTS

$\nu/N = 0.3$

t	From expressions of Table III		From Computer	
	v	p	v	p
0,	0	- 0.33461	0	- 0.3506
mod. π	$\pm$ 0.48297	0.23849	$\pm$ 0.4943	0.2440
$3\pi/4$,	- 0.59015	0	- 0.6024	0
mod. π	0.25949	$\mp$ 0.30665	0.2668	$\mp$ 0.3207

To illustrate results applying to operation nearer the $\nu/N \rightarrow 1/3$ resonance, the coordinates of the fixed points, as calculated by the expressions listed in Table III, are similarly compared in Table V with computer results for $\nu/N = 0.3275$.

TABLE V

COORDINATES OF UNSTABLE FIXED POINTS,
AS CALCULATED FROM THE EXPRESSIONS OF TABLE III
AND AS OBTAINED FROM COMPUTER RESULTS

$\nu/N = 0.3275$

t	From expressions of Table III		From Computer	
	v	p	v	p
0,	0	- 0.07778	0	- 0.07793
mod. π	$\pm$ 0.10284	0.04191	$\pm$ 0.10295	0.04195
$3\pi/4$,	- 0.12009_5	0	- 0.12021	0
mod. π	0.05854	$\mp$ 0.06812	0.05861	$\pm$ 0.06825

As is to be expected, the agreement in this case, with $\nu/N = 0.3275$, is considerably better than for the case $\nu/N = 0.3$ for which the results were described previously in Table IV.

As was mentioned earlier, it is of interest to examine the analytic results, in comparison with computer data, for various values of ν/N. The results of such a comparison, for $t = 0 \pmod{\pi}$ and ν/N in the range 0.30 to 0.36 are summarized below in Table VI,* in which the formulas used to obtain the theoretical results are those of Table III. The data are presented graphically in Figs. 1 through 3, and the percentage of error in the theoretical results is shown in Fig. 4.

A detailed numerical examination of the computer data summarized in Table VI (forming, for example, such quantities as

$$\frac{1}{\nu/N - 1/3}\left[\frac{p}{128\,(\nu/N)^2\,(\nu/N - 1/3)\,\eta_1} - 1\right]$$

and

$$\frac{1}{\nu/N - 1/3}\left[\frac{p}{128\,(\nu/N)^2\,(\nu/N - 1/3)} - 1\right]$$

for the various values of ν/N employed and noting that these quantities respectively approach 7/4 and 21/4 as $\nu/N \rightarrow 1/3$)suggests that the theory has, in fact, been carried correctly through terms of second order in $\nu/N - 1/3$. The correctness of this conclusion may, in fact, be immediately apparent from the second order dependence of the relative error on $\nu/N - 1/3$ in the graphs of Fig. 4.

*I am indebted to Mr. Igor Sviatoslavsky for assistance in performing some of the calculations necessary in the processing of these data.

TAB VI

COORDINATES OF UNSTABLE FIXED POINTS,
AS CALCULATED FROM THE EXPRESSIONS OF TABLE III AND AS OBTAINED FROM COMPUTER RESULTS

$t = 0 \ (\mathrm{mod.}\ \pi)$

ν/N	Fixed Point on Symmetry Axis			Fixed Points to right and left of Symmetry Axis					
	p formula	p computer	Error %	± v formula	± v computer	Error %	p formula	p computer	Error %
0.300	-0.33461	-0.35065	-4.57	±0.48297	±0.49430	-2.29	+0.23849	+0.24398	-2.25
0.305	-0.29897	-0.30971	-3.47	±0.42445	±0.43205	-1.76	+0.20384	+0.20731	-1.67
0.310	-0.25895	-0.26554	-2.48	±0.36171	±0.36638	-1.27	+0.16850	+0.17049	-1.17
0.315	-0.21416	-0.21768	-1.62	±0.29439	±0.29689	-0.84	+0.13262	+0.13361	-0.74
0.320	-0.16408	-0.16558	-0.91	±0.22202	±0.22310	-0.48	+0.09639	+0.09678	-0.40
0.3225	-0.13688	-0.13774	-0.62	±0.18379	±0.18440	-0.33	+0.07822	+0.07843	-0.27
0.325	-0.10815	-0.10856	-0.38	±0.14409	±0.14439	-0.21	+0.06004	+0.06014	-0.16
0.3275	-0.07778	-0.07793	-0.20	±0.10284	±0.10295	-0.11	+0.04191	+0.04195	-0.08
0.33	-0.04568	-0.04571	-0.08	±0.05994	±0.05997	-0.05	+0.02386	+0.02387	-0.04
0.3325	-0.01174	-0.01176	---	±0.01529	±0.01531	---	+0.00594	+0.00595	---
0.340	+0.10237	+0.10269	-0.30	±0.13038	±0.13060	-0.17	-0.04649	-0.04654	-0.10
0.345	+0.19025	+0.19226	-1.04	±0.23878	±0.24027	-0.62	-0.07963	-0.07987	-0.31
0.350	+0.28943	+0.29655	-2.40	±0.35808	±0.36341	-1.47	-0.11042	-0.11106	-0.57
0.355	+0.40211	+0.42186	-4.68	±0.49047	±0.50549	-2.97	-0.13781	-0.13883	-0.74
0.360	+0.53130	+0.58071	-8.51	±0.63906	±0.67734	-5.65	-0.1603	-0.16070	(-0.25)

(c) The intercept: The intercept of the separatrix on the symmetry axis, for which formulas have been given in Table III, is somewhat more tedious to determine computationally than the location of the fixed points. Computational estimates of the intercept have been obtained, however, for $\nu/N = 0.3$ at $t = 0$ (mod. π) and at $t = 3\pi/4$ (mod. π). The comparison of the theoretical and computational intercepts for these cases is given in Table VII.

TABLE VII

LOCATION OF THE INTERCEPT ON THE AXIS OF SYMMETRY, $\nu/N = 0.3$

t (mod. π)	LOCATION OF INTERCEPT From Table III	From Computer	Relative Error %
0	p = 0.1886	0.191	2
$3\pi/4$	v = 0.3024	0.308	2

E REFERENCES

1. Cf L J Laslett and A M Sessler, MURA-248 (1957)

2. Jürgen Moser, Nach Gött Akad (Math -Phys Kl) Nr 6, 87-120 (1955)

3. MURA General Conference (Feb 28, 1959)--presentation of ideas previously suggested by K Symon in internal discussions

4. F T Cole, MURA/FTC-3 (1956) In the present work the sign of $b_1(\theta)$ has been changed from that appearing in Dr Cole's report--see footnote p 6 of MURA-263

5. E D Courant and H S Snyder, Annals of Physics 3, No. 1, 1-48 (January 1958)--Section 4a, esp. eqns. (4 4) and (4 5), p. 18

6. This simplification is in the spirit of the "smooth approximation"--K R Symon, KRS (MURA)-1 (1954); K R. Symon, et al., Phys Rev. 103, 1837 (1956), Appendix A

7. J N Snyder, DUCK-ANSWER (I. B M. Program 75), MURA-237 (1957)

8. J N Snyder, FORANAL (I B M Program 52), MURA-228 (1957), John McNall, DUCKNALL (I B M Program 219), MURA-438 (1958)

9. This consideration concerning the complex conjugate feature of the new variables has been pointed out by H Meier, MURA-387 (1958)

10. The preferential retention of the constant part of the coefficient of J^2 appears to be consistent with ideas emphasized by P Sturrock, Annals of Physics 3 No 2, 113-189 (February, 1958) I am indebted to Mr Meier, Dr Cole, and Dr Symon for discussions concerning this feature of the procedure

APPENDIX A

EXPRESSION OF Ω_1 EXPLICITLY IN TERMS OF ξ_1, $\bar{\xi}_1$

An iterative solution of eqn. (22b) for ξ_0 (ξ_1 , $\bar{\xi}_1$) leads to

$$\begin{aligned}
\xi_0 = \xi_1 &+ (i/48)\,(N/\nu)^{3/2}\left[\Phi_1 \xi_1^2 + 2\Phi_2 \xi_1 \bar{\xi}_1 + 3\Phi_3 \bar{\xi}_1^2\right] \\
&- (1/1152)\,(N/\nu)^3\left[(\Phi_1^2 + \psi_1)\,\xi_1^3 + (3\Phi_1\Phi_2 + 2\psi_2)\,\xi_1^2\bar{\xi}_1 + (3\Phi_1\Phi_3 + 2\Phi_2^2 + 3\psi_3)\,\xi_1\bar{\xi}_1^2 + (3\Phi_2\Phi_3 + 4\psi_4)\,\bar{\xi}_1^3\right] \\
= \xi_1 &+ (i/48)\,(N/\nu)^{3/2}\left[\Phi_1 \xi_1^2 + 2\Phi_2 \xi_1\bar{\xi}_1 + 3\Phi_3 \bar{\xi}_1^2\right] \\
&+ (1/1152)\,(N/\nu)^3\left[\left((3/2)\Phi_0\Phi_2 - (1/2)\Phi_1^2\right)\xi_1^3 + \left((9/2)\Phi_0\Phi_3 - (1/2)\Phi_1\Phi_2\right)\xi_1^2\bar{\xi}_1 + \left((3/2)\Phi_1\Phi_3 - (1/2)\Phi_2^2\right)\xi_1\bar{\xi}_1^2\right], \qquad \text{(A1)}
\end{aligned}$$

in which the cubic term has been simplified by elimination of ψ_1 , $\cdots$ through use of eqns. (2b-e). Solution of eqn. (22a) for $\bar{\xi}_0$ (ξ_1 , $\bar{\xi}_1$) similarly gives

$$\begin{aligned}
\bar{\xi}_0 = \bar{\xi}_1 &- (i/48)\,(N/\nu)^{3/2}\left[3\Phi_0 \xi_1^2 + 2\Phi_1 \xi_1\bar{\xi}_1 + \Phi_2 \bar{\xi}_1^2\right] \\
&+ (1/1152)\,(N/\nu)^3\left[(3\Phi_0\Phi_1 + 4\psi_0)\,\xi_1^3 + (6\Phi_0\Phi_2 + \Phi_1^2 + 3\psi_1)\,\xi_1^2\bar{\xi}_1 + (9\Phi_0\Phi_3 + 2\Phi_1\Phi_2 + 2\psi_2)\,\xi_1\bar{\xi}_1^2 + (3\Phi_1\Phi_3 + \psi_3)\,\bar{\xi}_1^3\right] \\
= \bar{\xi}_1 &- (i/48)\,(N/\nu)^{3/2}\left[3\Phi_0 \xi_1^2 + 2\Phi_1 \xi_1\bar{\xi}_1 + \Phi_2 \bar{\xi}_1^2\right] \\
&+ (1/1152)\,(N/\nu)^3\left[\left((3/2)\Phi_0\Phi_1 - (1/2)\Phi_1^2\right)\xi_1^2\bar{\xi}_1 + \left((9/2)\Phi_0\Phi_3 - (1/2)\Phi_1\Phi_2\right)\xi_1\bar{\xi}_1^2 + \left((3/2)\Phi_1\Phi_3 - (1/2)\Phi_2^2\right)\bar{\xi}_1^3\right]. \qquad \text{(A2)}
\end{aligned}$$

It may be noted that, since $\Phi_2 = \Phi_1^*$ and $\Phi_3 = \Phi_0^*$ [eqns. (20c, d)], eqns. (A1, 2) are consistent with the statement that ξ_1 , $\bar{\xi}_1$ form a complex conjugate pair to this order.

Forming the product of eqns. (A1, 2) then leads, through fourth order terms, to

$$\begin{aligned}
\xi_0\bar{\xi}_0 = \xi_1\bar{\xi}_1 &+ (i/48)\,(N/\nu)^{3/2}\left[-3\Phi_0\xi_1^3 - \Phi_1\xi_1^2\bar{\xi}_1 + \Phi_2\xi_1\bar{\xi}_1^2 + 3\Phi_3\bar{\xi}_1^3\right] \\
&+ (1/768)\,(N/\nu)^3\left[\Phi_0\Phi_1\xi_1^4 + 4\Phi_0\Phi_2\xi_1^3\bar{\xi}_1 + (9\Phi_0\Phi_3 + \Phi_1\Phi_2)\,\xi_1^2\bar{\xi}_1^2 + 4\Phi_1\Phi_3\xi_1\bar{\xi}_1^3 + \Phi_2\Phi_3\bar{\xi}_1^4\right]. \qquad \text{(A3)}
\end{aligned}$$

In addition

$$\xi_0+\bar{\xi}_0=\xi_1+\bar{\xi}_1+(i/48)(N/\upsilon)^{3/2}\left[(-3\Phi_0+\Phi_1)\xi_1^2+(-2\Phi_1+2\Phi_2)\xi_1\bar{\xi}_1+(-\Phi_2+3\Phi_3)\bar{\xi}_1^2\right.$$

$$+ \text{ terms of third order}, \tag{A4}$$

so that

$$\begin{aligned}(\xi_0+\bar{\xi}_0)^3 &= \xi_1^3+3\xi_1^2\bar{\xi}_1+3\xi_1\bar{\xi}_1^2+\bar{\xi}_1^3\\ &+(i/16)(N/\upsilon)^{3/2}\left[(-3\Phi_0+\Phi_1)\xi_1^4+(-6\Phi_0+2\Phi_2)\xi_1^3\bar{\xi}_1+(-3\Phi_0-3\Phi_1+3\Phi_2+3\Phi_3)\xi_1^2\bar{\xi}_1^2+(-2\Phi_1+6\Phi_3)\xi_1\bar{\xi}_1^3+(-\Phi_2+3\Phi_3)\bar{\xi}_1^4\right].\end{aligned} \tag{A5}$$

Finally, the expression for $\partial F_1/\partial t$, which appears as a function ξ_0, $\bar{\xi}_1$ in eqn. (23), assumes the form

$$\begin{aligned}\partial F/\partial t = &-(i/48)(N/\upsilon)^{3/2}\left[\Phi_0'\xi_1^3+\Phi_1'\xi_1^2\bar{\xi}_1+\Phi_2'\xi_1\bar{\xi}_1^2+\Phi_3'\bar{\xi}_1^3\right]\\ &+(1/2304)(N/\upsilon)^3\left[(3\Phi_0'\Phi_1+2\Psi_0')\xi_1^4+(6\Phi_0'\Phi_2+2\Phi_1'\Phi_1+2\Psi_1')\xi_1^3\bar{\xi}_1\right.\\ &\quad\left.+(9\Phi_0'\Phi_3+4\Phi_1'\Phi_2+\Phi_2'\Phi_1+2\Psi_2')\xi_1^2\bar{\xi}_1^2+(6\Phi_1'\Phi_3+2\Phi_2'\Phi_2+2\Psi_3')\xi_1\bar{\xi}_1^3+(3\Phi_2'\Phi_3+2\Psi_4')\bar{\xi}_1^4\right]\\ = &-(i/48)(N/\upsilon)^{3/2}\left[\Phi_0'\xi_1^3+\Phi_1'\xi_1^2\bar{\xi}_1+\Phi_2'\xi_1\bar{\xi}_1^2+\Phi_3'\bar{\xi}_1^3\right]\\ &+(1/1536)(N/\upsilon)^3\left[(\Phi_0'\Phi_1-\Phi_0\Phi_1')\xi_1^4+2(\Phi_0'\Phi_2-\Phi_0\Phi_2')\xi_1^3\bar{\xi}_1+(3\Phi_0'\Phi_3+\Phi_1'\Phi_2-\Phi_1\Phi_2'-3\Phi_0\Phi_3')\xi_1^2\bar{\xi}_1^2\right.\\ &\quad\left.+2(\Phi_1'\Phi_3-\Phi_1\Phi_3')\xi_1\bar{\xi}_1^3+(\Phi_2'\Phi_3-\Phi_2\Phi_3')\bar{\xi}_1^4\right]\end{aligned} \tag{A6}$$

in terms of the variables ξ_1, $\bar{\xi}_1$.

Accordingly, the Hamiltonian Ω_1 becomes

$$
\begin{aligned}
\Omega_1 &= \Omega_0 + \partial F_1/\partial t \\
&= -i\,(2\upsilon/N)\,\xi_0\bar{\xi}_0 - (1/96)(N/\upsilon)^{3/2}(e^{2it}-e^{-2it})(\xi_0+\bar{\xi}_0)^3 + \partial F_1/\partial t \\
&= -i\,(2\upsilon/N)\,\xi_1\bar{\xi}_1 \\
&\quad -\frac{1}{48}\left(\frac{N}{\upsilon}\right)^{3/2}\left\{
\begin{aligned}
&[i\Phi_0' + 6(\upsilon/N)\Phi_0 + (1/2)(e^{2it}-e^{-2it})]\,\xi_1^3 \\
&+[i\Phi_1' + 2(\upsilon/N)\Phi_1 + (3/2)(e^{2it}-e^{-2it})]\,\xi_1^2\bar{\xi}_1 \\
&+[i\Phi_2' - 2(\upsilon/N)\Phi_2 + (3/2)(e^{2it}-e^{-2it})]\,\xi_1\bar{\xi}_1^2 \\
&+[i\Phi_3' - 6(\upsilon/N)\Phi_3 + (1/2)(e^{2it}-e^{-2it})]\,\bar{\xi}_1^3
\end{aligned}\right\} \\
&\quad -\frac{i}{1536}\left(\frac{N}{\upsilon}\right)^{3}\left\{
\begin{aligned}
&\left(\begin{aligned}&[i\Phi_0' + 6(\upsilon/N)\Phi_0 + (1/2)(e^{2it}-e^{-2it})]\Phi_1 \\ &-[i\Phi_1' + 2(\upsilon/N)\Phi_1 + (3/2)(e^{2it}-e^{-2it})]\Phi_0 - (1/2)(3\Phi_0-\Phi_1)(e^{2it}-e^{-2it})\end{aligned}\right)\xi_1^4 \\
&+\left(\begin{aligned}&2[i\Phi_0' + 6(\upsilon/N)\Phi_0 + (1/2)(e^{2it}-e^{-2it})]\Phi_2 \\ &-2[i\Phi_2' - 2(\upsilon/N)\Phi_2 + (3/2)(e^{2it}-e^{-2it})]\Phi_0 - (3\Phi_0-\Phi_2)(e^{2it}-e^{-2it})\end{aligned}\right)\xi_1^3\bar{\xi}_1 \\
&+\left(\begin{aligned}&3[i\Phi_0' + 6(\upsilon/N)\Phi_0 + (1/2)(e^{2it}-e^{-2it})]\Phi_3 \\ &+[i\Phi_1' + 2(\upsilon/N)\Phi_1 + (3/2)(e^{2it}-e^{-2it})]\Phi_2 \\ &-[i\Phi_2' - 2(\upsilon/N)\Phi_2 + (3/2)(e^{2it}-e^{-2it})]\Phi_1 \\ &-3[i\Phi_3' - 6(\upsilon/N)\Phi_3 + (1/2)(e^{2it}-e^{-2it})]\Phi_0 - (3/2)(\Phi_0+\Phi_1-\Phi_2-\Phi_3)(e^{2it}-e^{-2it})\end{aligned}\right)\xi_1^2\bar{\xi}_1^2 \\
&+\left(\begin{aligned}&2[i\Phi_1' + 2(\upsilon/N)\Phi_1 + (3/2)(e^{2it}-e^{-2it})]\Phi_3 \\ &-2[i\Phi_3' - 6(\upsilon/N)\Phi_3 + (1/2)(e^{2it}-e^{-2it})]\Phi_1 - (\Phi_1-3\Phi_3)(e^{2it}-e^{-2it})\end{aligned}\right)\xi_1\bar{\xi}_1^3 \\
&+\left(\begin{aligned}&[i\Phi_2' - 2(\upsilon/N)\Phi_2 + (3/2)(e^{2it}-e^{-2it})]\Phi_3 \\ &-[i\Phi_3' - 6(\upsilon/N)\Phi_3 + (1/2)(e^{2it}-e^{-2it})]\Phi_2 - (1/2)(\Phi_2-3\Phi_3)(e^{2it}-e^{-2it})\end{aligned}\right)\bar{\xi}_1^4
\end{aligned}\right\},
\end{aligned}
$$

which, by virtue of eqns. (19a-d), reduces to*

$$
\begin{aligned}
\Omega_1 = {} & -i(2\nu/N)\xi_1\bar{\xi}_1 - (1/96)(N/\nu)^{3/2}\left[e^{2it}\xi_1^3 - e^{-2it}\bar{\xi}_1^3\right] \\
& - \frac{i}{3072}\left(\frac{N}{\nu}\right)^3 \left\{ \begin{aligned}
& \left[-3\Phi_0(e^{2it}-e^{-2it}) + \Phi_1(2e^{2it}-e^{-2it})\right]\xi_1^4 \\
& + \left[-6\Phi_0(e^{2it}-e^{-2it}) + 2\Phi_2(2e^{2it}-e^{-2it})\right]\xi_1^3\bar{\xi}_1 \\
& + \left[-3\Phi_0(e^{2it}-2e^{-2it}) - 3\Phi_1(e^{2it}-e^{-2it}) \right. \\
& \qquad \left. + 3\Phi_2(e^{2it}-e^{-2it}) + 3\Phi_3(2e^{2it}-e^{-2it})\right]\xi_1^2\bar{\xi}_1^2 \\
& + \left[-2\Phi_1(e^{2it}-2e^{-2it}) + 6\Phi_3(e^{2it}-e^{-2it})\right]\xi_1\bar{\xi}_1^3 \\
& + \left[-\Phi_2(e^{2it}-2e^{-2it}) + 3\Phi_3(e^{2it}-e^{-2it})\right]\bar{\xi}_1^4
\end{aligned} \right\}. \qquad \text{(A7)}
\end{aligned}
$$

With respect to the quartic terms, use will be made in particular[10] of that part of the coefficient of $\xi_1^2\bar{\xi}_1^2$ which is independent of t --this specific contribution to Ω_1 is

$$
-\frac{i}{2048}\left(\frac{N}{\nu}\right)^3\left[6\,\frac{\nu/N}{1-(\nu/N)^2} - \frac{1}{1+3\nu/N}\right]\xi_1^2\bar{\xi}_1^2 ,
$$

as is readily found by use of eqns. (20a-d) for the functions Φ_0, Φ_1, Φ_2, and Φ_3.

---

*It was to effect this specific reduction of the cubic term that the quantities $\Phi_0, \cdots \Phi_3$ were required to satisfy eqns. (19a-d).

APPENDIX B

EXPRESSION OF K_1 EXPLICITLY IN TERMS OF γ_1, J_1

The Hamiltonian K_1 as given by eqn. (53), with K_o represented by eqn. (50) and the dynamical variables by eqns. (52a, b), may be expressed

$$
\begin{aligned}
K_1 = {} & 2\,(\nu/N)\,J_1 + (1/48)\,(N/\nu)^{1/2}\,J_1^{3/2}\left[3\,\frac{\cos(\gamma_0 - 2t)}{1 - \nu/N} + 3\,\frac{\cos(\gamma_0 + 2t)}{1 + \nu/N} - 3\,\frac{\cos(3\gamma_0 + 2t)}{1 + 3\nu/N}\right] \\
& + (1/48)\,(N/\nu)^{3/2}\left\{J_1^{3/2} + (3/64)\,(N/\nu)^{3/2}\,J_1^{2}\left[\frac{\cos(\gamma_0 - 2t)}{1 - \nu/N} + \frac{\cos(\gamma_0 + 2t)}{1 + \nu/N} - \frac{\cos(3\gamma_0 + 2t)}{1 + 3\nu/N}\right]\right\} \times \\
& \qquad \times \left\{3\cos(\gamma_0 - 2t) - 3\cos(\gamma_0 + 2t) + \cos(3\gamma_0 + 2t) - \cos(3\gamma_0 - 2t)\right\} \\
& + (1/48)\,(N/\nu)^{3/2}\,J_1^{3/2}\left[-3\,\frac{\cos(\gamma_0 - 2t)}{1 - \nu/N} + 3\,\frac{\cos(\gamma_0 + 2t)}{1 + \nu/N} - \frac{\cos(3\gamma_0 + 2t)}{1 + 3\nu/N}\right] \\
= {} & 2(\nu/N)\,J_1 + (1/48)(N/\nu)^{3/2}\,J_1^{3/2}\left\{\left[3\,\frac{\cos(\gamma_0 - 2t)}{1 - \nu/N} + 3\,\frac{\cos(\gamma_0 + 2t)}{1 + \nu/N} - 3\,\frac{\cos(3\gamma_0 + 2t)}{1 + 3\nu/N}\right]\cdot\left(\frac{\nu}{N}\right)\right. \\
& \qquad + 3\cos(\gamma_0 - 2t) - 3\cos(\gamma_0 + 2t) + \cos(3\gamma_0 + 2t) - \cos(3\gamma_0 - 2t) \\
& \qquad \left. - 3\,\frac{\cos(\gamma_0 - 2t)}{1 - \nu/N} + 3\,\frac{\cos(\gamma_0 + 2t)}{1 + \nu/N} - \frac{\cos(3\gamma_0 + 2t)}{1 + 3\nu/N}\right\} \\
& + (1/1024)(N/\nu)^{3/2}\,J_1^{2}\left[\frac{3}{2}\,\frac{1}{1 - \nu/N} - \frac{3}{2}\,\frac{1}{1 + \nu/N} - \frac{1}{2}\,\frac{1}{1 + 3\nu/N}\right. \\
& \qquad \left.\text{plus terms of argument } 4t,\ 2\gamma_0,\ 4\gamma_0,\ 6\gamma_0,\ 2\gamma_0 \pm 4t,\ 4\gamma_0 \pm 4t,\ 6\gamma_0 + 4t\right] .
\end{aligned}
\tag{B1}
$$

By the nature of the transformation, as determined by the selected generating function G_1, the coefficient of $J_1^{3/2}$ is such that a considerable cancellation is seen to be possible. Those terms in the coefficient of J_1^2 which involve t and/or γ_0 will be ignored, since, to the order to which the analysis is to be carried, they will not contribute t-independent terms to the Hamiltonian which results from the final transformation.[10]

In view of the remarks just made, K_1 is taken to be effectively

$$K_1 = 2\,(\nu/N)\,J_1 - (1/48)\,(N/\nu)^{3/2}\,J_1^{3/2}\cos(3\gamma_0 - 2t)$$
$$+ (1/2048)\,(N/\nu)^3\,J_1^2\left[\frac{6\,\nu/N}{1-\nu^2/N^2} - \frac{1}{1+3\,\nu/N}\right]. \qquad \text{(B2)}$$

1-441 Since [cf. eqn. (52b)] the variable γ_0 differs from γ_1 by terms of order $J_1^{1/2}$, we may expect that substitution for γ_0 in the second term of eqn. (B2) will contribute additional terms to the coefficient of J_1^2; this substitution, however, will not introduce terms other than those of the form which already have been ignored in the coefficient of J_1^2 and we therefore write, finally,

$$K_1 = 2\,(\nu/N)\,J_1 - (1/48)\,(N/\nu)^{3/2}\,J_1^{3/2}\cos(3\gamma_1 - 2t)$$
$$+ (1/2048)\,(N/\nu)^3\,J_1^2\left[\frac{6\,\nu/N}{1-\nu^2/N^2} - \frac{1}{1+3\,\nu/N}\right]. \qquad \text{(B3)}$$

The last factor appearing in the J_1^2 term will be recognized as the parameter denoted by α in the text [eqn. (25)].

Fig. 1

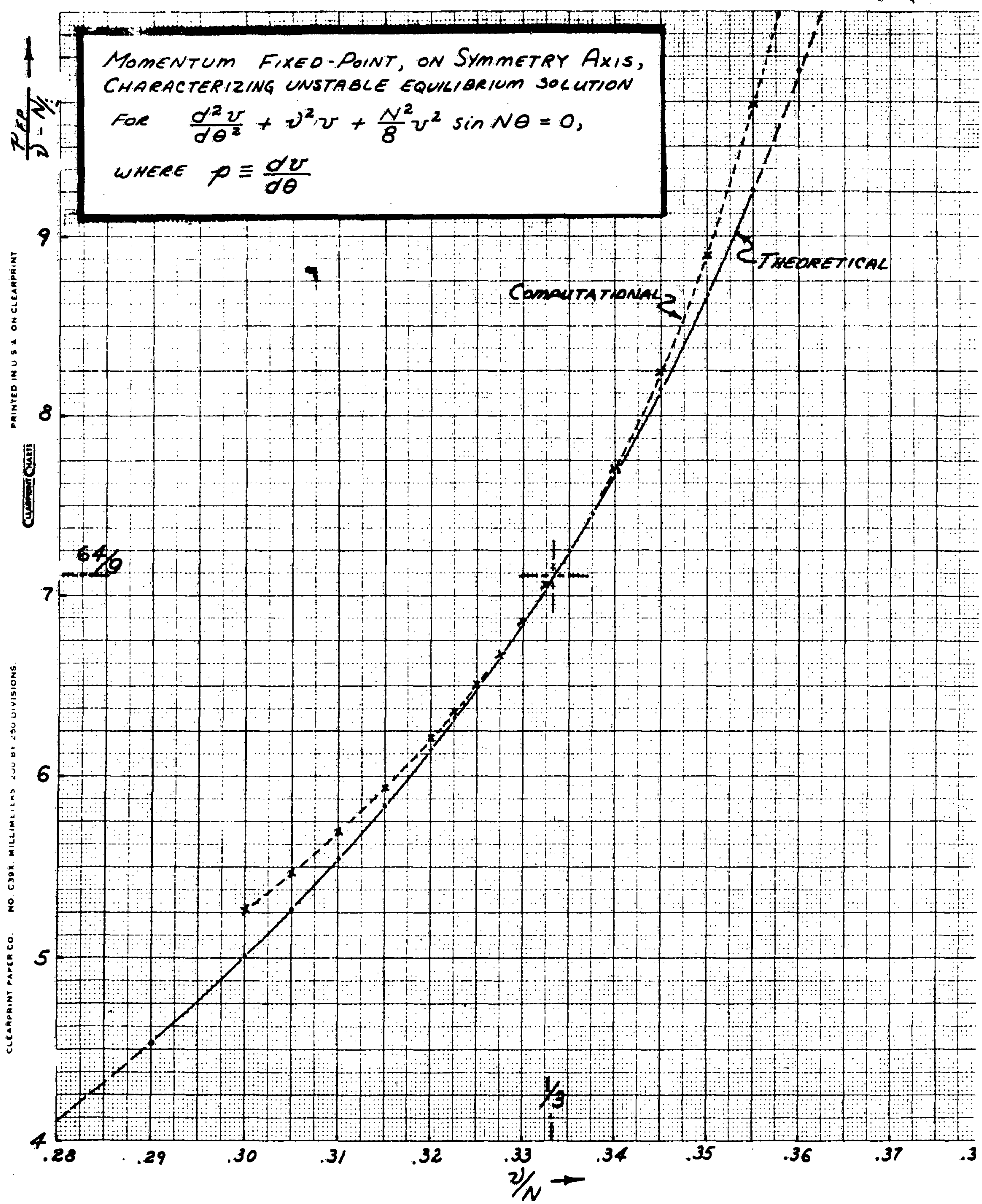

MOMENTUM FIXED-POINT, ON SYMMETRY AXIS, CHARACTERIZING UNSTABLE EQUILIBRIUM SOLUTION
FOR $\frac{d^2 v}{d\theta^2} + \nu^2 v + \frac{N^2}{8} v^2 \sin N\theta = 0$,
WHERE $p \equiv \frac{dv}{d\theta}$
THEORETICAL
COMPUTATIONAL
$\frac{p_{EP}}{\nu - N/3}$
64/9
1/3
ν/N
4
5
6
7
8
9
.28
.29
.30
.31
.32
.33
.34
.35
.36
.37
.3
CLEARPRINT PAPER CO. NO. C39X MILLIMETERS 200 BY 250 DIVISIONS
CLEARPRINT CHARTS
PRINTED IN U.S.A. ON CLEARPRINT

FIG. 2

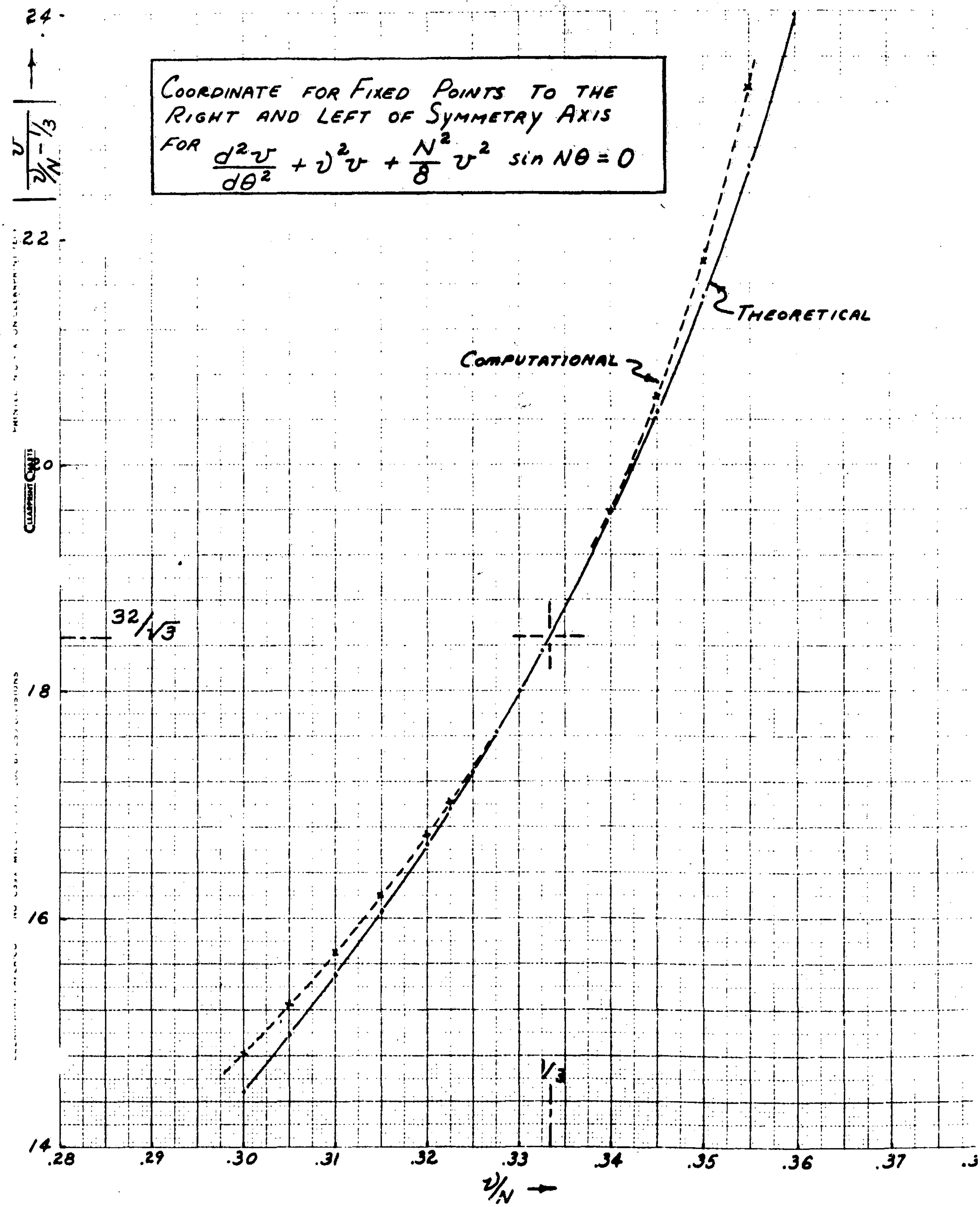
COORDINATE FOR FIXED POINTS TO THE RIGHT AND LEFT OF SYMMETRY AXIS FOR $\frac{d^2v}{d\theta^2} + \nu^2 v + \frac{N^2}{8} v^2 \sin N\theta = 0$
THEORETICAL
COMPUTATIONAL
$32/\sqrt{3}$
$1/3$
$\frac{v}{\nu/N - 1/3}$
ν/N
24
22
20
18
16
14
.28
.29
.30
.31
.32
.33
.34
.35
.36
.37

FIG. 5

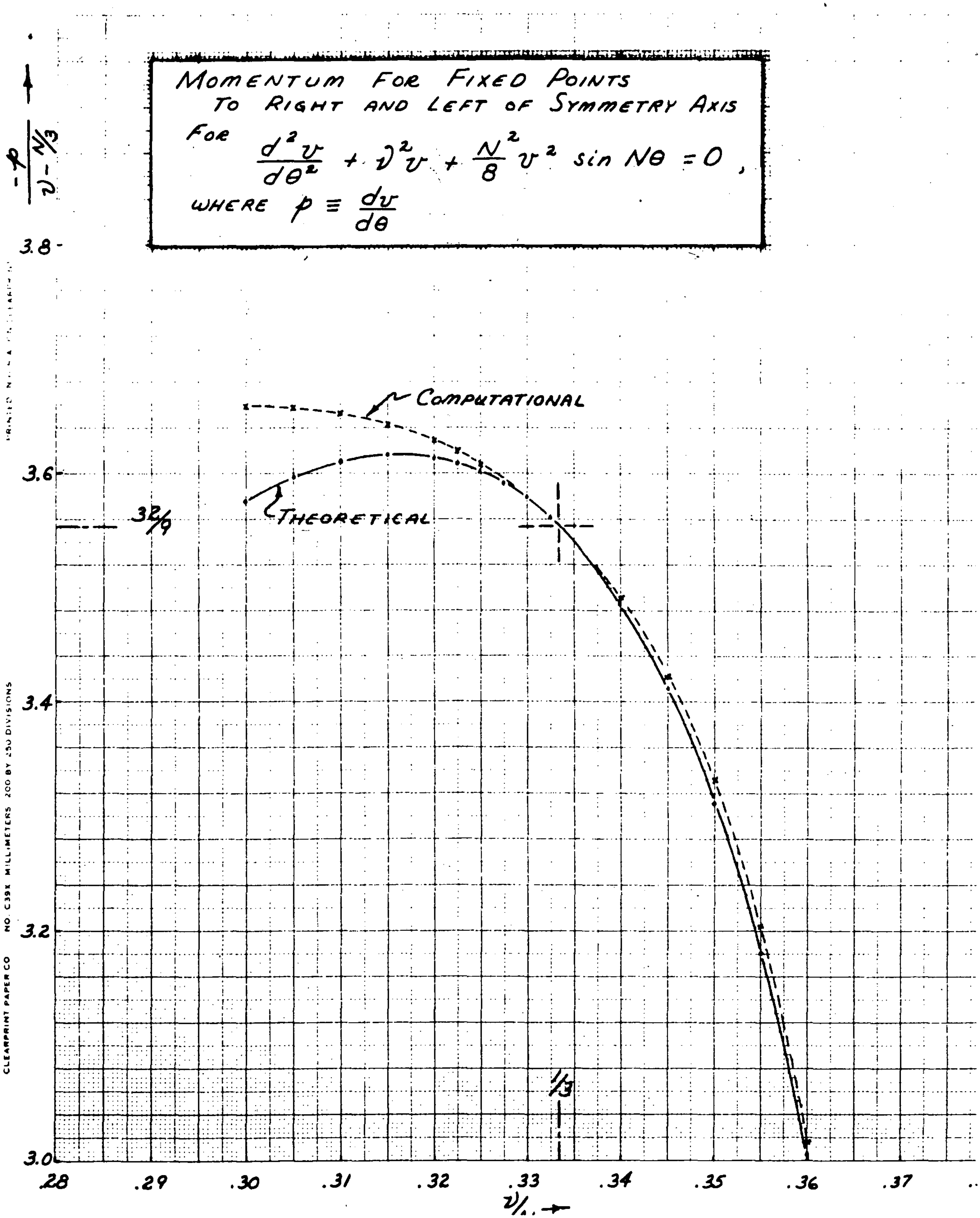
MOMENTUM FOR FIXED POINTS
TO RIGHT AND LEFT OF SYMMETRY AXIS
FOR $\frac{d^2v}{d\theta^2} + \nu^2 v + \frac{N^2}{8} v^2 \sin N\theta = 0$,
WHERE $p \equiv \frac{dv}{d\theta}$
$\frac{-p}{v - N/3}$
3.8
3.6
3.4
3.2
3.0
32/9
COMPUTATIONAL
THEORETICAL
1/3
.28
.29
.30
.31
.32
.33
.34
.35
.36
.37
$v/_{\Lambda}$
CLEARPRINT PAPER CO NO. C39X MILLIMETERS 200 BY 250 DIVISIONS

FIG. 4

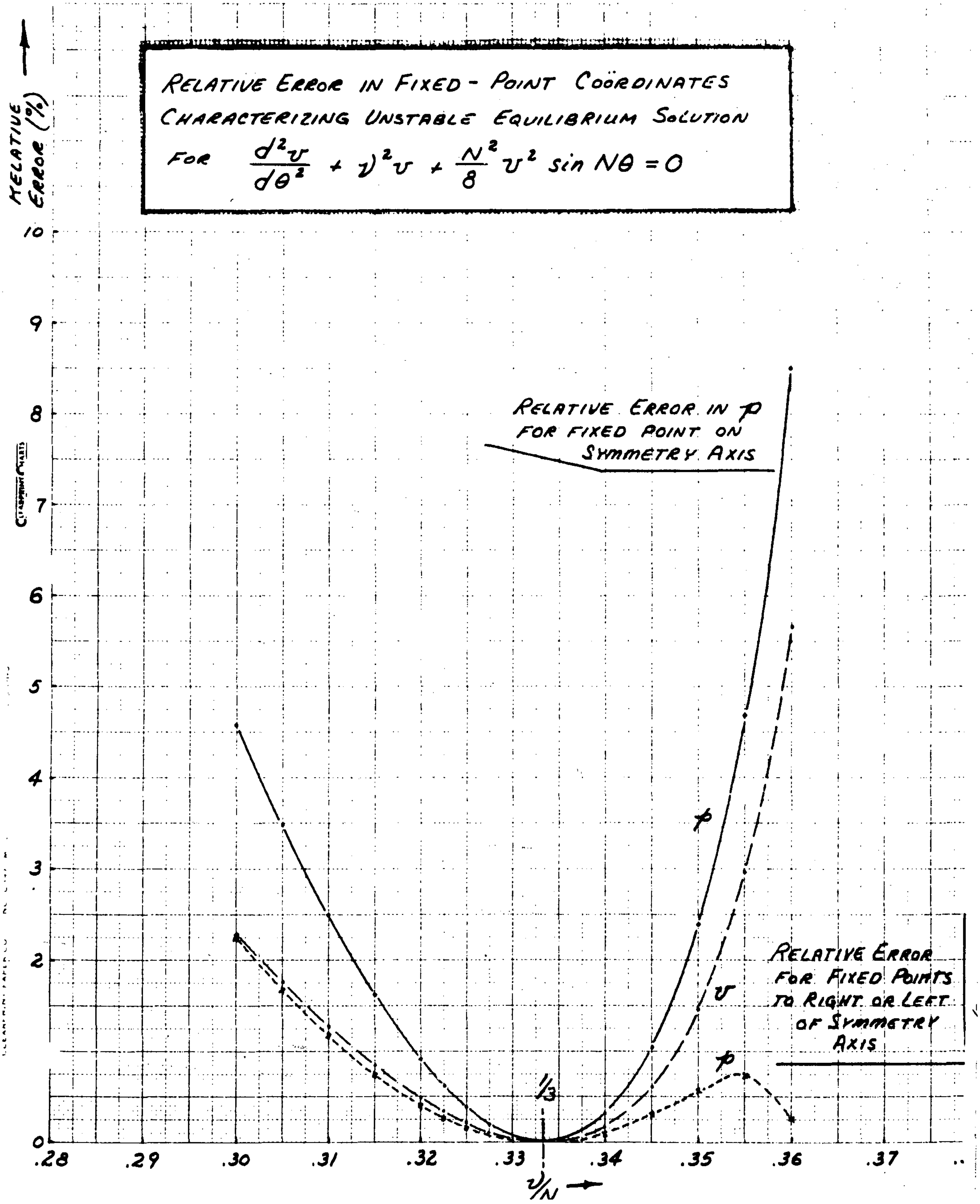
RELATIVE ERROR IN FIXED-POINT COÖRDINATES
CHARACTERIZING UNSTABLE EQUILIBRIUM SOLUTION
FOR $\frac{d^2 v}{d\theta^2} + \nu^2 v + \frac{N^2}{8} v^2 \sin N\theta = 0$
RELATIVE ERROR (%)
10
9
8
7
6
5
4
3
2
0
.28
.29
.30
.31
.32
.33
.34
.35
.36
.37
ν/N
1/3
RELATIVE ERROR IN p FOR FIXED POINT ON SYMMETRY AXIS
p
v
p
RELATIVE ERROR FOR FIXED POINTS TO RIGHT OR LEFT OF SYMMETRY AXIS

MURA-459
Distribution List UC 28

MIDWESTERN UNIVERSITIES RESEARCH ASSOCIATION*

2203 University Avenue, Madison, Wisconsin

CONCERNING THE $\nu/N \longrightarrow 1/3$ RESONANCE, II

APPLICATION OF A VARIATIONAL PROCEDURE AND OF THE MOSER METHOD TO THE EQUATION

$$\frac{d^2v}{dt^2} + \left(\frac{2\nu}{N}\right)^2 v + \frac{1}{2}\left[\sum_{m=1} b_m \sin 2mt\right] v^2 = 0$$

L. Jackson Laslett**

May 20, 1959

ABSTRACT

As a continuation of an earlier report pertaining to the $\nu/N \longrightarrow 1/3$ resonance, the stability boundary for the equation

$$\frac{d^2v}{dt^2} + \left(\frac{2\nu}{N}\right)^2 v + \frac{1}{2}\left[\sum_{m=1} b_m \sin 2mt\right] v^2 = 0$$

has been studied analytically and (for $b_1 = 1$, $b_3 = 3/4$, $b_5 = 1/2$) by digital computation. A relatively simple trial function,

$$v = \sum_{m=1}\left\{A_m \sin(2m - 4/3)t + B_m \sin 2mt + C_m \sin(2m + 4/3)t\right.$$

is employed in a variational procedure or with harmonic balance to obtain an estimate of the unstable equilibrium (periodic) solution and associated fixed points. Application of the Moser method of solution is also carried through, to include terms of order $(\nu/N - 1/3)^2$. The results are compared with computational data for $\nu/N = 0.3267$, 0.33, 0.3367, and 0.34.

*AEC Research and Development Report. Research supported by the Atomic Energy Commission, Contract No. AEC AT(11-1)-384.

**Department of Physics and Institute for Atomic Research, Iowa State College.

A. MOTIVATION

In a previous report,[1*] hereinafter designated as I, a study was made of the differential equation

$$\frac{d^2v}{dt^2} + (2\nu/N)^2 v + (1/2)(\sin 2t) v^2 = 0, \tag{1}$$

with particular attention to the limiting-amplitude solution governed by the one-third resonance ($\nu/N \rightarrow 1/3$). As was pointed out in I, if the coefficient of the linear term in (1) had not been constant but involved a periodic function of the independent variable t, it would be possible[2] to remove this t-dependence by a suitable transformation. Such a transformation, however, has the effect that the quadratic term becomes more complicated than in eqn. (1). As an extension of the results of I, we therefore consider in the present report the equation

$$\frac{d^2v}{dt^2} + (2\nu/N)^2 v + (1/2)\left[\sum_{m=1} b_m \sin 2mt\right] v^2 = 0, \tag{2}$$

with $b_1 \neq 0$.

As before,[1] results of a variational solution and of application of the Moser procedure[3] will be presented and compared with computational results. In particular we shall be concerned with the limiting-amplitude solution governed by the one-third resonance, and undertake to carry the analysis consistently through terms of order $(\nu/N - 1/3)^2$.

---

*References are given in Section E.

B. THE VARIATIONAL METHOD

The unstable equilibrium orbit, or the associated "fixed points" characterizing the limiting-amplitude solution of eqn. (2),

$$\frac{d^2v}{dt^2} + (2\,\nu/N)^2\, v + (1/2)\left[\sum_{m=1} b_m \sin 2\,m\,t\right] v^2 = 0,$$

may be sought by insertion of a suitable trial function into the variational statement

$$\delta\left\{\langle (dv/dt)^2\rangle - (2\,\nu/N)^2\langle v^2\rangle - (1/3)\sum_{m=1} b_m \langle v^3 \sin 2\,m\,t\rangle\right\} = 0. \quad (3)$$

We shall employ here the trial function

$$v = A_1 \sin 2\,t/3 + B_1 \sin 2\,t + C_1 \sin 10\,t/3$$
$$+ \sum_{m=2}\left[A_m \sin(2\,m - 4/3)\,t + B_m \sin 2\,m\,t + C_m \sin(2\,m + 4/3)\,t\right], \quad (4$$

in which the first term is the dominant one and the remaining terms are then of a form suggested by considerations of harmonic balance.

In the substitution of the trial function (4) into the variational statement (3), only those terms need be retained which will contribute terms of order no higher than $(\nu/N - 1/3)^2$ to the solution--to this accuracy it is then sufficient to retain (cubic) terms in $\langle v^3 \sin 2\,m\,t\rangle$ which involve A_1 squared or cubed. With this approximation the variational statement (3) then becomes (on multiplication of (3) by 72):

$$16\left[1 - 9\,(\nu/N)^2\right]A_1^2 + 16\left[9 - 9\,(\nu/N)^2\right]B_1^2 + 16\left[25 - 9\,(\nu/N)^2\right]C_1^2$$
$$+ 16\sum_{m=2}\left\{\left[(3\,m-2)^2 - 9\,(\nu/N)^2\right]A_m^2 + \left[(3\,m)^2 - 9\,(\nu/N)^2\right]B_m^2 + \left[(3\,m+2)^2 - 9\,(\nu/N)^2\right]C_m^2\right\}$$
$$+ 9\,b_1\left[A_1^3/3 - 2\,A_1^2 B_1 + A_1^2 C_1\right]$$
$$+ 9\sum_{m=2} b_m\left[A_1^2\,(A_m - 2\,B_m + C_m)\right] \text{ to be stationary.} \quad (5)$$

By performing the appropriate differentiations of the algebraic form (5) the simultaneous algebraic equations for the coefficients of the trial function are then obtained directly:

$$32\left[1 - 9\,(\nu/N)^2\right] A_1 + 9\, b_1 \left[A_1^2 - 4\, A_1\, B_1 + 2\, A_1\, C_1\right]$$
$$+ 18 \sum_{m=2} b_m\, A_1\, (A_m - 2\, B_m + C_m) = 0 \qquad (6a)$$

$$32\left[9 - 9\,(\nu/N)^2\right] B_1 - 18\, b_1\, A_1^2 = 0 \qquad (6b)$$

$$32\left[25 - 9\,(\nu/N)^2\right] C_1 + 9\, b_1\, A_1^2 = 0 \qquad (6c)$$

$$\left.\begin{aligned} &32\left[(3\,m - 2)^2 - 9\,(\nu/N)^2\right] A_m + 9\, b_m\, A_1^2 = 0 &(6d)\\ &32\left[(3\,m)^2 - 9\,(\nu/N)^2\right] B_m - 18\, b_m\, A_1^2 = 0 &(6e)\\ &32\left[(3\,m + 2)^2 - 9\,(\nu/N)^2\right] C_m + 9\, b_m\, A_1^2 = 0\,. &(6f)\end{aligned}\right\}\; m \geqslant 2$$

In solution of eqns. (6a-f), one may first express B_1, C_1, A_m, ... in terms of A_1 by means of eqns. (6b-f) and substitute the results into eqn. (6a) to obtain an equation involving the unknown A_1 alone. An approximate solution of this last-named equation, valid through terms of order $(\nu/N - 1/3)^2$, may then be obtained and the remaining coefficients (B_1, C_1, A_m, ...) determined [Appendix A]. We thus find

$$A_1 = -\frac{64}{3\, b_1}\,(1/3 - \nu/N)\left\{1 - 8\left[1 + \sum_{m=2}\left(\frac{b_m}{b_1}\right)^2 \frac{9\, m^2 - 5}{(m^2 - 1)(9\, m^2 - 1)}\right](1/3 - \nu/N)\right\} \qquad (7a)$$

$$B_1 = \frac{32}{b_1}\,(1/3 - \nu/N)^2 \qquad (7b)$$

$$C_1 = -\frac{16}{3\, b_1}\,(1/3 - \nu/N)^2 \qquad (7c)$$

$$\left.\begin{aligned} &A_m = -\frac{128}{3\, b_1}\,\frac{b_m/b_1}{(m-1)\,(3\,m-1)}\,(1/3 - \nu/N)^2 &(7d)\\ &B_m = \frac{256}{b_1}\,\frac{b_m/b_1}{9\,m^2 - 1}\,(1/3 - \nu/N)^2 &(7e)\\ &C_m = -\frac{128}{3\, b_1}\,\frac{b_m/b_1}{(m+1)\,(3\,m+1)}\,(1/3 - \nu/N)^2 &(7f)\end{aligned}\right\}\; m \geqslant 2$$

These coefficients, when employed in the trial function (4), provide us with an approximate representation of the unstable equilibrium orbit in the form of a trigonometric series.

From the foregoing results for the unstable equilibrium orbit, the coordinates of the fixed points may be obtained, as desired. Thus, at $t = 0$, one finds

$$v = 0 \tag{8a}$$

$$\begin{aligned} p_v \equiv \frac{dv}{dt} &= \frac{2}{3} A_1 + 2 B_1 + \frac{10}{3} C_1 \\ &\quad + \sum_{m=2} \left[\frac{2}{3} (3m - 2) A_m + 2m B_m + \frac{2}{3} (3m + 2) C_m \right] \\ &= -\frac{128}{9 b_1} \left(\frac{1}{3} - \frac{\nu}{N} \right) \left\{ 1 - \left[\frac{45}{4} - 8 \sum_{m=2} \frac{2m (b_m/b_1) - (9m^2 - 5)(b_m/b_1)^2}{(m^2 - 1)(9m^2 - 1)} \right] \left(\frac{1}{3} - \frac{\nu}{N} \right) \right\}. \end{aligned} \tag{8b}$$

From the experience reported previously in I (Section C of reference 1) it may be expected that the accuracy of these results, being carried only through second order terms, will be somewhat limited unless $\left| \frac{1}{3} - \frac{\nu}{N} \right|$ is small; reasonable accuracy might be expected, however, if $\left| \frac{1}{3} - \frac{\nu}{N} \right|$ were, say, as small as 0.01. A comparison of the analytic results with digital computations will be presented later in this report (Sect. D). We turn next to the applications of the analytic method of Moser to eqn. (2).

C. THE MOSER PROCEDURE

1. The Forward Transformations

In this section we undertake to treat eqn. (2) by the Moser procedure,[3] in a manner paralleling that presented in Sect. D 3 of I.[1] Our basic equation, eqn. (2), follows from the Hamiltonian

$$H = (1/2)\, p^2 + (1/2)\, (2\,\nu/N)^2\, v^2 + (1/6) \left[\sum_{m=1} b_m \sin 2\, m\, t\right] v^3, \tag{9}$$

which we now subject to a series of canonical transformations designed to eliminate the t-dependence from the cubic term in (9).

We commence by employing the generating function

$$G_o\,(v,\ \gamma_o) = (\nu/N)\, v^2 \operatorname{ctn} \gamma_o\ , \tag{10}$$

so that

$$p = \partial G_o/\partial v = (2\,\nu/N)\, v \operatorname{ctn} \gamma_o \tag{11a}$$

$$J_o = -\,\partial G_o/\partial \gamma_o = (\nu/N)\, v^2 \csc^2 \gamma_o\ ; \tag{11b}$$

thus

$$\operatorname{ctn} \gamma_o = \frac{N}{2\nu}\,\frac{p}{v} \tag{12a}$$

$$J_o = \frac{1}{2}\left(\frac{N}{2\nu}\right) p^2 + \frac{1}{2}\left(\frac{2\nu}{N}\right) v^2\ , \tag{12b}$$

$$v = (N/\nu)^{1/2}\, J_o^{1/2} \sin \gamma_o \tag{12c}$$

$$p = 2\,(\nu/N)^{1/2}\, J_o^{1/2} \cos \gamma_o\ , \tag{12d}$$

and the new Hamiltonian is

$$\begin{aligned} K_o &= H + \partial G_o/\partial t \\ &= H \\ &= 2\,(\nu/N)\, J_o + (1/6)(N/\nu)^{3/2}\, J_o^{3/2} \sin^3 \gamma_o \sum_{m=1} b_m \sin 2\, m\, t \\ &= 2\,(\nu/N)\, J_o \\ &\quad + (1/48)(N/\nu)^{3/2} J_o^{3/2} \sum_{m=1} b_m \begin{bmatrix} 3 \cos(\gamma_o - 2\, m\, t) - 3 \cos(\gamma_o + 2\, m\, t) \\ + \cos(3\,\gamma_o + 2\, m\, t) - \cos(3\gamma_o - 2\, m\, t) \end{bmatrix}, \end{aligned} \tag{13}$$

with γ_o and J_o constituting respectively the new coordinate and momentum.

We now select as a second generating function

$$G_1(\gamma_o, J_1) = J_1 \cdot \gamma_o + \frac{1}{96}\left(\frac{N}{\nu}\right)^{3/2} J_1^{3/2} \left\{ \begin{array}{l} b_1 \left[3\,\frac{\sin(\gamma_o - 2t)}{1 - \nu/N} + 3\,\frac{\sin(\gamma_o + 2t)}{1 + \nu/N} - \frac{\sin(3\gamma_o + 2t)}{1 + 3\nu/N} \right] \\ + \sum\limits_{m=2} b_m \left[\begin{array}{l} 3\,\frac{\sin(\gamma_o - 2mt)}{m - \nu/N} + 3\,\frac{\sin(\gamma_o + 2mt)}{m + \nu/N} \\ - \frac{\sin(3\gamma_o - 2mt)}{m - 3\nu/N} - \frac{\sin(3\gamma_o + 2mt)}{m + 3\nu/N} \end{array} \right] \end{array} \right\}, \tag{14}$$

so that

$$\begin{aligned} J_o &= \partial G_1 / \partial \gamma_o \\ &= J_1 + \frac{1}{32}\left(\frac{N}{\nu}\right)^{3/2} J_1^{3/2} \left\{ \begin{array}{l} b_1 \left[\frac{\cos(\gamma_o - 2t)}{1 - \nu/N} + \frac{\cos(\gamma_o + 2t)}{1 + \nu/N} - \frac{\cos(3\gamma_o + 2t)}{1 + 3\nu/N} \right] \\ + \sum\limits_{m=2} b_m \left[\begin{array}{l} \frac{\cos(\gamma_o - 2mt)}{m - \nu/N} + \frac{\cos(\gamma_o + 2mt)}{m + \nu/N} \\ - \frac{\cos(3\gamma_o - 2mt)}{m - 3\nu/N} - \frac{\cos(3\gamma_o + 2mt)}{m + 3\nu/N} \end{array} \right] \end{array} \right\} \end{aligned} \tag{15a}$$

$$\begin{aligned} \gamma_1 &= \partial G_1 / \partial J_1 \\ &= \gamma_o + \frac{1}{64}\left(\frac{N}{\nu}\right)^{3/2} J_1^{1/2} \left\{ \begin{array}{l} b_1 \left[3\,\frac{\sin(\gamma_o - 2t)}{1 - \nu/N} + 3\,\frac{\sin(\gamma_o + 2t)}{1 + \nu/N} - \frac{\sin(3\gamma_o + 2t)}{1 + 3\nu/N} \right] \\ + \sum\limits_{m=2} b_m \left[\begin{array}{l} 3\,\frac{\sin(\gamma_o - 2mt)}{m - \nu/N} + 3\,\frac{\sin(\gamma_o + 2mt)}{m + \nu/N} \\ - \frac{\sin(3\gamma_o - 2mt)}{m - 3\nu/N} - \frac{\sin(3\gamma_o + 2mt)}{m + 3\nu/N} \end{array} \right] \end{array} \right\}, \end{aligned} \tag{15b}$$

and

$$\begin{aligned} K_1 &= K_o + \partial G_1 / \partial t \\ &= K_o + \frac{1}{48}\left(\frac{N}{\nu}\right)^{3/2} J_1^{3/2} \left\{ \begin{array}{l} b_1 \left[-3\,\frac{\cos(\gamma_o - 2t)}{1 - \nu/N} + 3\,\frac{\cos(\gamma_o + 2t)}{1 + \nu/N} - \frac{\cos(3\gamma_o + 2t)}{1 + 3\nu/N} \right] \\ + \sum\limits_{m=2} b_m \left[\begin{array}{l} -3\,\frac{\cos(\gamma_o - 2mt)}{1 - \nu/mN} + 3\,\frac{\cos(\gamma_o + 2mt)}{1 + \nu/mN} \\ + \frac{\cos(3\gamma_o - 2mt)}{1 - 3\nu/mN} - \frac{\cos(3\gamma_o + 2mt)}{1 + 3\nu/mN} \end{array} \right] \end{array} \right\}. \end{aligned} \tag{16}$$

It is now in order, of course, to express the new Hamiltonian, K_1, explicitly in terms of γ_1 and J_1. As a first step, substitution of J_o, as given by eqn. (15a), into K_o, as given by eqn. (13), results (after considerable simplification) in eqn. (16) assuming the following form, through terms of order J_1^2:

$$K_1 = 2(\nu/N)\,J_1 - \frac{b_1}{48}\left(\frac{N}{\nu}\right)^{3/2} J_1^{3/2} \cos(3\gamma_o - 2t)$$
$$+ \frac{b_1^2}{2048}\left(\frac{N}{\nu}\right)^3 J_1^2 \left\{ \frac{6\,\nu/N}{1-\nu^2/N^2} - \frac{1}{1+3\,\nu/N} + \frac{6\nu}{N}\sum_{m=2}\left(\frac{b_m}{b_1}\right)^2 \left[\frac{1}{m^2-\nu^2/N^2} + \frac{1}{m^2 - 9\,\nu^2/N^2}\right] + \sum_{m=1}\frac{b_m b_{m+2}}{b_1^2}\left[\frac{1}{m+3\,\nu/N} - \frac{1}{m+2-3\,\nu/N}\right]\cos 2(3\gamma_o - 2t) + \text{terms which are neither constant, nor involve circular functions of an argument which is a multiple of } 3\gamma_o - 2t \right\} \quad (17)$$

It can be seen that the introduction of γ_1 in place of γ_o in eqn. (17) need not change the form of this result, since the substitution, based on eqn. (15b), which is involved in expressing $\cos(3\gamma_o - 2t)$ in terms of γ_1 does not introduce into the J_1^2 term any terms of the form which we have elected to retain. It may moreover be noted that there is little point to retaining the last term in eqn. (17), involving the cross products $b_m b_{m+2}$, since, to this order, $3\,\nu/N$ may here be set equal to unity with the result that the term in question vanishes. In this spirit, and in the interest of simplicity, we therefore write

$$K_1 = 2(\nu/N)\,J_1 - \frac{b_1}{48}\left(\frac{N}{\nu}\right)^{3/2} J_1^{3/2}\cos(3\gamma_1 - 2t) + \alpha\,\frac{b_1^2}{2048}\left(\frac{N}{\nu}\right)^3 J_1^2, \quad (18)$$

where

$$\alpha \equiv \frac{6\,\nu/N}{1-\nu^2/N^2} - \frac{1}{1+3\,\nu/N}$$

$$+\,6\,\frac{\nu}{N}\sum_{m=2}\left(\frac{b_m}{b_1}\right)^2\left[\frac{1}{m^2-\nu^2/N^2}+\frac{1}{m^2-9\,\nu^2/N^2}\right] \qquad (19)$$

[cf. eqn. (25) of I] and in which t-dependent terms have deliberately been omitted from the J_1^2 term of K_1.

For the final transformation we now, as in I, introduce the third generating function

$$G_2(\gamma_1, J_2) = J_2\cdot(\gamma_1 - \tfrac{2}{3}t), \qquad (20)$$

which effects the transformation

$$J_1 = \partial G_2/\partial\gamma_1 = J_2 \qquad (21a)$$

$$\gamma_2 = \partial G_2/\partial J_2 = \gamma_1 - \tfrac{2}{3}t \qquad (21b)$$

with

$$\begin{aligned} K_2 &= K_1 + \partial G_2/\partial t \\ &= K_1 - \tfrac{2}{3}J_2 \\ &= -2\left(\frac{1}{3}-\frac{\nu}{N}\right)J_2 - \frac{b_1}{48}\left(\frac{N}{\nu}\right)^{3/2}J_2^{3/2}\cos 3\gamma_2 + \alpha\,\frac{b_1^2}{2048}\left(\frac{N}{\nu}\right)^3 J_2^2 \end{aligned} \qquad (22)$$

and in which α is given by eqn. (19). K_2, which, as written, is independent of t, is now to be regarded as substantially a constant of the motion.

2. The Separatrix and Fixed Points

The expression (22) for K_2, which we take to be a constant of the motion, is virtually identical in form to eqn. (57) of I [Section D 3 of reference 1] and the succeeding step thus will parallel the corresponding work in I, save that the values of J_2 (= J_1) will contain a factor $1/b_1^2$ and χ_- is to be interpreted in the manner of eqn. (19).

The fixed points, corresponding to the unstable equilibrium orbit, are characterized by K_2 being stationary; i.e., by

$$\cos 3\gamma_2 = -1 \tag{23a}$$

$$\gamma_2 = \pm \pi/3, \pi \tag{23b}$$

$$\gamma_1 = \pm \pi/3 + 2t/3, \quad \pi + 2t/3 \tag{23c}$$

and

$$J_1^{1/2} = J_2^{1/2} = \frac{64}{b_1}\left(\frac{1}{3} - \frac{\nu}{N}\right)\left(\frac{\nu}{N}\right)^{3/2}\eta_1 , \tag{24}$$

where

$$\eta_1 = \frac{\sqrt{1 + 8\alpha\;(1/3 - \nu/N)} - 1}{4\alpha\;(1/3 - \nu/N)} \tag{25a}$$

$$= 1 - 2\alpha\,(1/3 - \nu/N) + \cdots . \tag{25b}$$

Other points on the separatrix are determined by eqn. (22), with K_2 given the value [implied by eqns. (23a) and (24)]

$$K_2 = -\frac{8192}{3b_1^2}\left(\frac{\nu}{N}\right)^3\left(\frac{1}{3} - \frac{\nu}{N}\right)^3 \frac{\eta_1^2\,(3 - \eta_1)}{2} . \tag{26}$$

3. The Inverse Transformation

To obtain an expression for the unstable equilibrium orbit in terms of the original dependent variable, v, we perform the inverse transformation from γ_1, J_1, making use of eqn. (24) and (say) setting $\gamma_1 = \pi + 2t/3$ [cf. eqn. (23c)]. We thus write

$$J_o^{1/2} \doteq J_1^{1/2}\left[1 - \frac{b_1}{64}\left(\frac{N}{\nu}\right)^{3/2} J_1^{1/2} \cdot R\right] \tag{27a}$$

$$\sin\gamma_o \doteq \sin\gamma_1 - (\cos\gamma_1)(\gamma_1 - \gamma_o)$$

$$\doteq \sin\gamma_1 + \frac{b_1\cos\gamma_1}{64}\left(\frac{N}{\nu}\right)^{3/2} J_1^{1/2} \cdot S \tag{27b}$$

and

$$\cos \gamma_o \doteq \cos \gamma_1 + (\sin \gamma_1)(\gamma_1 - \gamma_o)$$
$$\doteq \cos \gamma_1 - \frac{b_1 \sin \gamma_1}{64}\left(\frac{N}{\nu}\right)^{3/2} J_1^{1/2} \cdot S, \qquad (27c)$$

where

$$R \equiv \frac{\cos 4t/3}{1 - \nu/N} + \frac{\cos 8t/3}{1 + \nu/N} - \frac{\cos 4t}{1 + 3\nu/N}$$
$$+ \sum_{m=2} \frac{b_m}{b_1}\left[\frac{\cos (2/3)(3m-1)t}{m - \nu/N} + \frac{\cos (2/3)(3m+1)t}{m + \nu/N} - \frac{\cos 2(m-1)t}{m - 3\nu/N} - \frac{\cos 2(m+1)t}{m + \nu/N}\right] \qquad (27d)$$

and

$$S \equiv -3\frac{\sin 4t/3}{1 - \nu/N} + 3\frac{\sin 8t/3}{1 + \nu/N} - \frac{\sin 4t}{1 + 3\nu/N}$$
$$+ \sum_{m=2} \frac{b_m}{b_1}\left[-3\frac{\sin (2/3)(3m-1)t}{m - \nu/N} + 3\frac{\sin (2/3)(3m+1)t}{m + \nu/N} + \frac{\sin 2(m-1)t}{m - 3\nu/N} - \frac{\sin 2(m+1)t}{m + 3\nu/N}\right]. \qquad (27e)$$

Accordingly [cf. eqn. (12c)]

$$v = (N/\nu)^{1/2} J_o^{1/2} \sin \gamma_o$$
$$= -(N/\nu)^{1/2} J_1^{1/2}\left[1 - \left(\frac{1}{3} - \frac{\nu}{N}\right)\eta_1 \cdot R\right]\left[\sin 2t/3 + \left(\frac{1}{3} - \frac{\nu}{N}\right)\eta_1 (\cos 2t/3)\, S\right]$$

$$= -\frac{64}{b_1}\left(\frac{1}{3} - \frac{\nu}{N}\right)\left(\frac{\nu}{N}\right)\eta_1 \left\{ \begin{array}{l} \sin 2t/3 \\ -\left[\begin{array}{l} \dfrac{\sin 2t/3}{1 - \nu/N} + \dfrac{4(\nu/N)\sin 2t}{1 - \nu^2/N^2} - \left(\dfrac{1}{1 + \nu/N} - \dfrac{1}{1 + 3\nu/N}\right)\sin 10t/3 \\ + \sum_{m=2} \dfrac{b_m}{b_1} \left\{ \begin{array}{l} \left(\dfrac{1}{m - \nu/N} - \dfrac{1}{m - 3\nu/N}\right)\sin (2/3)(3m-2)t \\ + \dfrac{4(\nu/N)\sin 2mt}{m^2 - \nu^2/N^2} \\ -\left(\dfrac{1}{m + \nu/N} - \dfrac{1}{m + 3\nu/N}\right)\sin (2/3)(3m+2)t \end{array} \right\} \end{array} \right] \left(\dfrac{1}{3} - \dfrac{\nu}{N}\right)\eta_1 \end{array} \right\}; \qquad (28a)$$

similarly [cf. eqn. (12d)]

$$p = 2\,(\nu/N)^{1/2} J_0^{1/2} \cos \gamma_0$$

$$= -\,2\,(\nu/N)^{1/2} J_1^{1/2}\left[1 - \left(\frac{1}{3} - \frac{\nu}{N}\right)\eta_1 \cdot R\right]\left[\cos 2\,t/3 - \left(\frac{1}{3} - \frac{\nu}{N}\right)\eta_1 \left(\sin \frac{2\,t}{3}\right) S\right]$$

$$= -\frac{128}{b_1}\left(\frac{1}{3} - \frac{\nu}{N}\right)\left(\frac{\nu}{N}\right)^2 \eta_1 \left\{ \begin{array}{l} \cos 2\,t/3 \\ + \left[\begin{array}{l} \left(\dfrac{\cos 2t/3}{1 - \nu/N} - \dfrac{4\cos 2t}{1 - \nu^2/N^2}\right) + \left(\dfrac{1}{1 + \nu/N} + \dfrac{1}{1 + 3\nu/N}\right)\cos 10t/3 \\ + \sum\limits_{m=2} \dfrac{b_m}{b_1} \left\{ \begin{array}{l} \left(\dfrac{1}{m - \nu/N} + \dfrac{1}{m - 3\,\nu/N}\right)\cos\,(2/3)\,(3\,m - 2)t \\ -\ \dfrac{4\,m \cos 2\,m\,t}{m^2 - \nu^2/N^2} \\ + \left(\dfrac{1}{m + \nu/N} + \dfrac{1}{m + 3\,\nu/N}\right)\cos\,(2/3)\,(3\,m + 2)t \end{array} \right\} \end{array} \right] \left(\frac{1}{3} - \frac{\nu}{N}\right)\eta_1 \end{array} \right\} \tag{28b}$$

For comparison with the results of Section B, we may first examine the coefficient of $\sin 2\,t/3$ in the expression for v shown in eqn. (28a), making certain simplifications consistent with retention of terms through those of order $\left(\frac{1}{3} - \frac{\nu}{N}\right)^2$. This coefficient is

$$A_1 = -\frac{64}{b_1}\left(\frac{1}{3} - \frac{\nu}{N}\right)\left(\frac{\nu}{N}\right)\eta_1 \left[1 - \frac{1/3 - \nu/N}{1 - \nu/N}\,\eta_1\right] \tag{29a}$$

$$\doteq -\frac{64}{b_1}\left(\frac{1}{3} - \frac{\nu}{N}\right)\left(\frac{\nu}{N}\right)\left[1 - \left(2\,\alpha + \frac{1}{1 - \nu/N}\right)\left(\frac{1}{3} - \frac{\nu}{N}\right)\right] \tag{29b}$$

$$\doteq -\frac{64}{b_1}\left(\frac{1}{3} - \frac{\nu}{N}\right)\left(\frac{\nu}{N}\right)\left[1 - \left(2\,\alpha + \frac{3}{2}\right)\left(\frac{1}{3} - \frac{\nu}{N}\right)\right] \tag{29c}$$

$$\doteq -\frac{64}{3\,b_1}\left(\frac{1}{3} - \frac{\nu}{N}\right)\left[1 - \left(2\,\alpha + \frac{9}{2}\right)\left(\frac{1}{3} - \frac{\nu}{N}\right)\right] \tag{29d}$$

and, with

$$\alpha \doteq 7/4 + 4\sum_{m=2}\left(\frac{b_m}{b_1}\right)^2 \frac{9\,m^2 - 5}{(9\,m^2 - 1)\,(m^2 - 1)} \qquad \text{[cf. eqn. (19)]}, \tag{30}$$

$$A_1 \doteq -\frac{64}{3\,b_1}\left(\frac{1}{3}-\frac{\nu}{N}\right)\left\{1-8\left[1+\sum_{m=2}\left(\frac{b_m}{b_1}\right)^2 \frac{9\,m^2-5}{(m^2-1)(9\,m^2-1)}\right]\left(\frac{1}{3}-\frac{\nu}{N}\right)\right\}, \tag{29e}$$

in agreement with the expression given as eqn. (7a). A similar reduction of the coefficient of $\cos 2\,t/3$ in the expression (28b) for p leads to a quantity which is $2/3$ of formula (29e) for A_1, as it of course should since $p = dv/dt$.

Similar reductions of the remaining (second order) terms in the trigonometric series for v and p, as given by eqns. (28a, b), leads to the coefficients listed below in Table I.

TABLE I

COEFFICIENTS OF SECOND ORDER TERMS IN THE TRIGONOMETRIC SERIES FOR v AND p, FROM EQUATIONS 28a AND 28b.

Argument	Sine Coefficient in v	Cosine Coefficient in p
$2\,t$	$+\frac{32}{b_1}\left(\frac{1}{3}-\frac{\nu}{N}\right)^2$	$+\frac{64}{b_1}\left(\frac{1}{3}-\frac{\nu}{N}\right)^2$
$10\,t/3$	$-\frac{16}{3\,b_1}\left(\frac{1}{3}-\frac{\nu}{N}\right)^2$	$-\frac{160}{9\,b_1}\left(\frac{1}{3}-\frac{\nu}{N}\right)^2$
$(2/3)(3m-2)t$	$-\frac{128\,b_m}{3\,b_1^2}\frac{1}{(m-1)(3\,m-1)}\left(\frac{1}{3}-\frac{\nu}{N}\right)^2$	$-\frac{256\,b_m}{9\,b_1^2}\frac{3\,m-2}{(m-1)(3\,m-1)}\left(\frac{1}{3}-\frac{\nu}{N}\right)^2$
$2\,m\,t$	$+\frac{256\,b_m}{b_1^2}\frac{1}{9\,m^2-1}\left(\frac{1}{3}-\frac{\nu}{N}\right)^2$	$+\frac{512\,b_m}{b_1^2}\frac{m}{9\,m^2-1}\left(\frac{1}{3}-\frac{\nu}{N}\right)^2$
$(2/3)(3m+2)t$	$-\frac{128\,b_m}{3\,b_1^2}\frac{1}{(m+1)(3\,m+1)}\left(\frac{1}{3}-\frac{\nu}{N}\right)^2$	$-\frac{256\,b_m}{9\,b_1^2}\frac{3\,m+2}{(m+1)(3\,m+1)}\left(\frac{1}{3}-\frac{\nu}{N}\right)^2$.

The coefficients listed here for the terms appearing in eqn. (28a) for v are immediately seen to be concordant with the coefficients of the trial function of Section B, as listed in eqns. (7b-f). Similarly the coefficients listed for p are seen to be related to those given for v in a way consistent with $p = dv/dt$.

Coordinates of fixed points may of course be obtained directly from eqns. (28a, b). Thus, for one of the fixed points at $t = 0$ one finds

$$v = 0 \tag{31a}$$

$$p = -\frac{128}{b_1}\left(\frac{1}{3}-\frac{\nu}{N}\right)\left(\frac{\nu}{N}\right)^2\eta_1\left\{1-\left[\begin{array}{l}\dfrac{2}{1-\nu^2/N^2}-\dfrac{1}{1+3\,\nu/N}\\ -2\sum\limits_{m=2} m\dfrac{b_m}{b_1}\left(\dfrac{1}{m^2-9\nu^2/N^2}-\dfrac{1}{m^2-\nu^2/N^2}\right)\end{array}\right]\left(\frac{1}{3}-\frac{\nu}{N}\right)\eta_1\right\}. \tag{31b}$$

This expression (31b) for p may be somewhat simplified if various reductions are made by aid of $\eta_1 \cong 1 - 2\alpha\left(\frac{1}{3}-\frac{\nu}{N}\right)$, use of eqn. (30), and the approximation $(\nu/N)^2 \cong \frac{1}{9}\left[1-6\left(\frac{1}{3}-\frac{\nu}{N}\right)\right]$:

$$\begin{aligned} p &\doteq -\frac{128}{b_1}\left(\frac{1}{3}-\frac{\nu}{N}\right)\left(\frac{\nu}{N}\right)^2\eta_1\left\{1-\left[\frac{7}{4}-16\sum_{m=2}\frac{m\,(b_m/b_1)}{(m^2-1)(9\,m^2-1)}\right]\left(\frac{1}{3}-\frac{\nu}{N}\right)\right\}\\ &\doteq -\frac{128}{b_1}\left(\frac{1}{3}-\frac{\nu}{N}\right)\left(\frac{\nu}{N}\right)^2\left\{1-\left[\frac{21}{4}-8\sum_{m=2}\frac{2m(b_m/b_1)-(9m^2-5)(b_m/b_1)^2}{(m^2-1)\,(9\,m^2-1)}\right]\left(\frac{1}{3}-\frac{\nu}{N}\right)\right\}\\ &\doteq -\frac{128}{9\,b_1}\left(\frac{1}{3}-\frac{\nu}{N}\right)\left\{1-\left[\frac{45}{4}-8\sum_{m=2}\frac{2\,m\,(b_m/b_1)-(9\,m^2-5)\,(b_m/b_1)^2}{(m^2-1)\,(9\,m^2-1)}\right]\left(\frac{1}{3}-\frac{\nu}{N}\right)\right\},\end{aligned} \tag{31b'}$$

which is in agreement with the result (8b) found in Section B. The other unstable fixed points associated with this value of t likewise may be obtained, by the substitution of $t = \pm\pi$ in eqns. (28a, b):

$$v = \mp\frac{32\sqrt{3}}{b_1}\left(\frac{1}{3}-\frac{\nu}{N}\right)\left(\frac{\nu}{N}\right)\eta_1\left\{1-\left[\begin{array}{l}\dfrac{2}{1-\nu^2/N^2}-\dfrac{1}{1+3\,\nu/N}\\ -2\sum\limits_{m=2} m\dfrac{b_m}{b_1}\left(\dfrac{1}{m^2-9\,\nu^2/N^2}-\dfrac{1}{m^2-\nu^2/N^2}\right)\end{array}\right]\left(\frac{1}{3}-\frac{\nu}{N}\right)\eta_1\right\} \tag{32a}$$

$$\doteq \mp \frac{32\sqrt{3}}{b_1}\left(\frac{1}{3}-\frac{\nu}{N}\right)\left(\frac{\nu}{N}\right)\eta_1\left\{1-\left[\frac{7}{4}-16\sum_{m=2}\frac{b_m}{b_1}\frac{m}{(m^2-1)(9m^2-1)}\right]\left(\frac{1}{3}-\frac{\nu}{N}\right)\right\}$$

$$\doteq \mp \frac{32\sqrt{3}}{b_1}\left(\frac{1}{3}-\frac{\nu}{N}\right)\left(\frac{\nu}{N}\right)\left\{1-\left[\frac{21}{4}-8\sum_{m=2}\frac{2m(b_m/b_1)-(9m^2-5)(b_m/b_1)^2}{(m^2-1)(9m^2-1)}\right]\left(\frac{1}{3}-\frac{\nu}{N}\right)\right\}$$

$$\doteq \mp \frac{32\sqrt{3}}{3b_1}\left(\frac{1}{3}-\frac{\nu}{N}\right)\left\{1-\left[\frac{33}{4}-8\sum_{m=2}\frac{2m(b_m/b_1)-(9m^2-5)(b_m/b_1)^2}{(m^2-1)(9m^2-1)}\right]\left(\frac{1}{3}-\frac{\nu}{N}\right)\right\}, \tag{32a'}$$

$$p=\frac{64}{b_1}\left(\frac{1}{3}-\frac{\nu}{N}\right)\left(\frac{\nu}{N}\right)^2\eta_1\left\{1+\left[\frac{10}{1-\nu^2/N^2}+\frac{1}{1+3\nu/N}+2\sum_{m=2}m\frac{b_m}{b_1}\left(\frac{5}{m^2-\nu^2/N^2}+\frac{1}{m^2-9\nu^2/N^2}\right)\right]\left(\frac{1}{3}-\frac{\nu}{N}\right)\eta_1\right\} \tag{32b}$$

$$\doteq \frac{64}{b_1}\left(\frac{1}{3}-\frac{\nu}{N}\right)\left(\frac{\nu}{N}\right)^2\eta_1\left\{1+\left[\frac{47}{4}+4\sum_{m=2}m\frac{b_m}{b_1}\frac{27m^2-23}{(m^2-1)(9m^2-1)}\right]\left(\frac{1}{3}-\frac{\nu}{N}\right)\right\}$$

$$\doteq \frac{64}{b_1}\left(\frac{1}{3}-\frac{\nu}{N}\right)\left(\frac{\nu}{N}\right)^2\left\{1+\left[\frac{33}{4}+4\sum_{m=2}\frac{m(27m^2-23)(b_m/b_1)-2(9m^2-5)(b_m/b_1)^2}{(m^2-1)(9m^2-1)}\right]\left(\frac{1}{3}-\frac{\nu}{N}\right)\right\}$$

$$\doteq \frac{64}{9b_1}\left(\frac{1}{3}-\frac{\nu}{N}\right)\left\{1+\left[\frac{9}{4}+4\sum_{m=2}\frac{m(27m^2-23)(b_m/b_1)-2(9m^2-5)(b_m/b_1)^2}{(m^2-1)(9m^2-1)}\right]\left(\frac{1}{3}-\frac{\nu}{N}\right)\right\}. \tag{32b'}$$

The reduced forms (32a') and (32b') agree with the value of the trial function of Section B and its derivative at $t = \pm\pi$, namely $v = \pm(\sqrt{3}/2)\sum_{m=1}(A_m - C_m)$ and $dv/dt = -(1/3)\sum_{m=1}\left[(3m-2)A_m - 6mB_m + (3m+2)C_m\right]$, when the coefficients are taken as given by eqns. (7a-f).

The coefficients of the trigonometric development of the unstable equilibrium orbit, and particular fixed-point coordinates, are thus seen to agree, through terms in $\left(\frac{1}{3}-\frac{\nu}{N}\right)^2$, when obtained by the variational method or by the Moser procedure. In the following Section we present some computational checks of these results.

D. COMPUTATIONAL CHECKS

The analytic results of Sections B and C for the limiting-amplitude solution of eqn. (2), for which the solution was carried through terms of order $(\nu/N - 1/3)^2$, have been subjected to computational checks[4] for a series of examples in which

$$b_1 = 1, \quad b_3 = 3/4, \quad \text{and} \quad b_5 = 1/2, \tag{33}$$

and in which ν/N successively assumed the values

0.3267,

0.33,

0.3367, and

0.34.

The computational results for the trigonometric representation of the unstable equilibrium orbit, and for the coordinates (v, p) of the fixed points corresponding to t = 0, were compared with the results of the analytic work, both in the form obtained directly from application of the Moser method and in the simplified, or "reduced", forms in which the results also could be expressed. A particularly decisive test of the results might be afforded by examining explicitly the coefficient of $(\nu/N - 1/3)^2$ in the results--thus by forming

$$\frac{1 - \dfrac{9\,b_1}{128}\,\dfrac{(-p)}{\dfrac{1}{3} - \dfrac{\nu}{N}}}{\dfrac{1}{3} - \dfrac{\nu}{N}}$$

one might expect to obtain a result which would approach

$$\frac{45}{4} - 8\sum_{m=2} \frac{2\,m\,(b_m/b_1) - (9\,m^2 - 5)\,(b_m/b_1)^2}{(m^2 - 1)\,(9\,m^2 - 1)} \doteq 11.80$$

as $\nu/N \rightarrow 1/3$ [cf. eqn. (31b')]. From such tests it appeared that the coefficients of interest were approximately of the size expected but assumed limiting values which depended appreciably on the Runge-Kutta interval employed in the computations--thus with $N_{RK} = 64$ (requiring runs of length $N_E = 960$ Runge-Kutta steps), the limiting value of

$$\frac{1 - \frac{9\,b_1}{128}\,\frac{(-p)}{\frac{1}{3} - \frac{\nu}{N}}}{\frac{1}{3} - \frac{\nu}{N}}$$

appeared to be about 11.7. In the results reported below, the computational results are taken primarily from runs made with $N_{RK} = 64$.

In Table II we list the Fourier coefficients of the unstable equilibrium orbit for the cases studied. For each argument listed, the first line gives the value of the coefficient expected from the results of the Moser theory [eqns. (28a, b)]; the second line gives the value obtained from the reduced forms [see eqn. (29e) and Table I]; and the third line gives the coefficients obtained computationally.

In Table III we similarly list the fixed-point coordinates, for $t = 0$. The agreement between the analytic and computational results, as illustrated by Table II and Table III, is felt to be completely satisfactory.

TABLE II

FOURIER COEFFICIENTS IN [illegible] STABLE EQUILIBRIUM ORBIT

$b_1 = 1$ $b_3 = 3/4$ $b_5 = 1/2$

Argument	Sine Coefficient in v				Cosine Coefficient in p			
	ν/N				ν/N			
	0.3267	0.3300	0.3367	0.3400	0.3267	0.3300	0.3367	0.3400
2 t/3	-.133 9152 [a]	-.069 1337	+.073 9787	+.150 9863	-.089 1973 [a]	-.046 0785	+.049 3068	+.100 5561
	-.133 4186 [b]	-.069 0676	+.073 9068	+.150 3963	-.088 9457 [b]	-.046 0451	+.049 2712	+.100 2642
	-.134 1$_{351}$ [c]	-.069 1$_{799}$	+.073 9$_{996}$	+.151 3$_{083}$	-.089 4$_{23}$ [c]	-.046 1$_{20}$	+.049 3$_{33}$	+.100 8$_{72}$
2 t	+.001 2792	+.000 3385	+.000 3818	+.001 5780	+.002 5584	+.000 6771	+.000 7637	+.003 1561
	+.001 4080	+.000 3556	+.000 3627	+.001 4222	+.002 8161	+.000 7111	+.000 7254	+.002 8444
	+.001 25$_{94}$	+.000 33$_{57}$	+.000 38$_{59}$	+.001 61$_{75}$	+.002 51$_{9}$	+.000 67$_{1}$	+.000 77$_{2}$	+.003 23$_{5}$
10 t/3	-.000 2175	-.000 0570	-.000 0630	-.000 2578	-.000 7192	-.000 1892	-.000 2109	-.000 8662
	-.000 2347	-.000 0593	-.000 0605	-.000 2370	-.000 7822	-.000 1975	-.000 2015	-.000 7901
	-.000 210$_{1}$	-.000 056$_{0}$	-.000 064$_{3}$	-.000 269$_{3}$	-.000 70$_{0}$	-.000 18$_{7}$	-.000 21$_{4}$	-.000 89$_{8}$
14 t/3	-.000 0794	-.000 0211	-.000 0240	-.000 0994	-.000 3724	-.000 0987	-.000 1115	-.000 4611
	-.000 0880	-.000 0222	-.000 0227	-.000 0889	-.000 4107	-.000 1037	-.000 1058	-.000 4148
	-.000 078$_{5}$	-.000 020$_{9}$	-.000 024$_{1}$	-.000 101$_{3}$	-.000 36$_{7}$	-.000 09$_{8}$	-.000 11$_{3}$	-.000 47$_{3}$
6 t	+.000 0964	+.000 0254	+.000 0286	+.000 1178	+.000 5782	+.000 1527	+.000 1714	+.000 7069
	+.000 1056	+.000 0267	+.000 0272	+.000 1067	+.000 6336	+.000 1600	+.000 1632	+.000 6400
	+.000 094$_{7}$	+.000 025$_{2}$	+.000 028$_{9}$	+.000 121$_{0}$	+.000 56$_{8}$	+.000 15$_{1}$	+.000 17$_{3}$	+.000 72$_{6}$
22 t/3	-.000 0324	-.000 0085	.000 0095	-.000 0390	-.000 2365	-.000 0623	-.000 0697	-.000 2869
	-.000 0352	-.000 0089	-.000 0091	-.000 0356	-.000 2581	-.000 0652	-.000 0665	-.000 2607
	-.000 031$_{8}$	-.000 008$_{4}$	-.000 009$_{6}$	-.000 039$_{9}$	-.000 23$_{4}$	-.000 06$_{2}$	-.000 07$_{0}$	-.000 29$_{3}$
26 t/3	-.000 0152	-.000 0040	-.000 0045	-.000 0188	-.000 1322	-.000 0350	-.000 0394	-.000 1625
	.000 0168	-.000 0042	.000 0043	-.000 0169	-.000 1453	-.000 0367	.000 0374	-.000 1467
	-.000 014$_{8}$	.000 003$_{9}$	.000 004$_{6}$	.000 019$_{5}$	-.000 12$_{8}$	-.000 03$_{4}$	-.000 04$_{0}$	-.000 16$_{9}$
10 t	+.000 0230	+.000 0061	+.000 0068	+.000 0280	+.000 2295	+.000 0606	+.000 0680	+.000 2804
	+.000 0251	+.000 0063	+.000 0065	+.000 0254	+.000 2514	+.000 0635	+.000 0648	+.000 2540
	+.000 022$_{5}$	+.000 006$_{0}$	+.000 006$_{9}$	+.000 028$_{8}$	+.000 22$_{5}$	+.000 06$_{0}$	+.000 06$_{9}$	+.000 28$_{8}$
34 t/3	.000 0090	-.000 0024	.000 0026	-.000 0109	.000 1014	-.000 0267	-.000 0299	-.000 1233
	-.000 0098	-.000 0025	.000 0025	-.000 0099	-.000 1108	-.000 0280	-.000 0285	-.000 1119
	.000 009$_{0}$	-.000 002$_{3}$	-.000 002$_{6}$	-.000 010$_{9}$	-.000 10$_{3}$	-.000 02$_{7}$	-.000 03$_{0}$	-.000 12$_{3}$

(a)Eqn. (28a)
(b)Reduced forms(29e), et seq.
(c)Computational

(a)Eqn. (28a)
(b)Reduced forms
(c)Computational

TABLE III

FIXED POINT COORDINATES

($t = 0$, mod. 2π)

	$b_1 = 1$	$b_3 = 3/4$	$b_5 = 1/2$
ν/N	On Symmetry Axis	To Right and Left of Symmetry Axis	
	p	v	p
0.3267	-.087 393[a]	$\mp$.115 832[a]	+.048 746[a]
	-.086 955[b]	$\mp$.115 396[b]	+.049 029[b]
	-.087 64[c]	$\mp .116\ 0_{40}$[c]	$+.048\ 7_{94}$[c]
0.33	-.045 600	$\mp$.059 834	+.024 136
	-.045 542	$\mp$.059 777	+.024 173
	-.045 65	$\mp .059\ 8_{92}$	$+.024\ 1_{53}$
0.3367	+.049 849	$\pm$.064 108	-.023 420
	+.049 784	$\pm$.064 043	-.023 462
	+.049 87	$\pm .064\ 1_{12}$	$-.023\ 4_{13}$
0.34	+.102 799	$\pm$.130 922	-.045 185
	+.102 275	$\pm$.130 396	-.045 530
	+.103 16	$\pm .131\ 2_{00}$	$-.045\ 2_{04}$

(a) Eqn. (31b)	(a) Eqn. (32a)	(a) Eqn. (32b)
(b) Eqn. (31b')	(b) Eqn. (32a')	(b) Eqn. (32b')
(c) Computed	(c) Computed	(c) Computed

E. REFERENCES

1. L. Jackson Laslett, MURA-452 (April 13, 1959), hereinafter designated as I.

2. E. D. Courant and H. S. Snyder, Annals of Physics 3, No. 1, 1-48 (January, 1958)--Section 4a, esp. eqns. (4.4) and (4.5), p. 18.

3. Jürgen Moser, Nach. Gött. Akad. (Math.-Phys. Kl.) Nr. 6, 87-120 (1955).

4. The computational work was performed with the MURA IBM 704, by means of the DUCK-ANSWER program [J. N. Snyder, (IBM Program 75), MURA-237 (1957)], with the independent variable, τ, of the program identified as $\tau = 5t$ and with the dependent variable (ρ or ψ) usually identified as 10 times the dependent variable (v) of eqn. (2). Accordingly, dv/dt is then represented by $0.5\, d\rho/d\tau$ or $0.5\, d\psi/d\tau$. The coefficients of the program are then taken to be

$$S_1 = S_2 = -0.016\,(\nu/N)^2,$$
$$A_3 = A_{15} = 0.001,$$
$$B_2 = B_{15} = 0.002,$$
$$C_3 = C_{15} = 0.0015,$$

with $N_1 = 10$, $N_2 = 5$, and $\alpha_3 = \alpha_{15} = \beta_3 = \beta_{15} = \gamma_3 = \gamma_{15} = 0.5$. If one selects $N_{RK} = 64$, a computational run through an interval $\Delta t = 3\pi$ requires a total of $N_E = 960$ Runge-Kutta integration steps. For Fourier analysis of the results of a DUCK-ANSWER computation, the DUCKNALL program was employed [John McNall, (IBM Program 219), MURA-438 (1958)], this program constituting basically an incorporation into the DUCK-ANSWER program of the FORANAL program [J. N. Snyder, (IBM Program 52), MURA-228 (1957)].

APPENDIX A

SOLUTION OF EQNS. 6a-f FOR THE COEFFICIENTS OF THE TRIAL FUNCTION

From eqns. (6b-f) we immediately obtain

$$B_1 = (1/16)\, b_1 A_1^2 \left[1 - (\nu/N)^2\right]^{-1} \tag{A-1a}$$

$$C_1 = -(9/32)\, b_1 A_1^2 \left[25 - 9\,(\nu/N)^2\right]^{-1} \tag{A-1b}$$

$$\left.\begin{aligned} A_m &= -\,(9/32)\, b_m A_1^2 \left[(3\,m-2)^2 - 9\,(\nu/N)^2\right]^{-1} && \text{(A-1c)}\\ B_m &= (9/16)\, b_m A_1^2 \left[(3\,m)^2 - 9\,(\nu/N)^2\right]^{-1} && \text{(A-1d)}\\ C_m &= -\,(9/32)\, b_m A_1^2 \left[(3\,m+2)^2 - 9\,(\nu/N)^2\right]^{-1}. && \text{(A-1e)} \end{aligned}\right\} \quad m \geqslant 2$$

By insertion of the expressions (A-1a-e) into eqn. (6a), and rejection of the trivial root $A_1 = 0$, the quadratic equation for A_1 is obtained:

$$32\left[1 - 9\,(\nu/N)^2\right] + 9\, b_1 A_1 - 9\, b_1^2 A_1^2 \left[\frac{1/4}{1-(\nu/N)^2} + \frac{9/16}{25 - 9\,(\nu/N)^2}\right]$$
$$-\frac{81}{16} A_1^2 \sum_{m=2} b_m^2 \left[\frac{1}{(3\,m-2)^2 - 9\,(\nu/N)^2} + \frac{4}{(3\,m)^2 - 9\,(\nu/N)^2} + \frac{1}{(3\,m+2)^2 - 9\,(\nu/N)^2}\right] = 0 \tag{A-2}$$

An approximate solution of eqn. (A-2) then gives

$$A_1 = -\frac{32}{9b_1}\left[1 - 9(\nu/N)^2\right]\left[1 - \frac{32}{81}\left\{9\left[\frac{1/4}{1-(\nu/N)^2} + \frac{9/16}{25-9\,(\nu/N)^2}\right] + \frac{81}{16}\sum_{m=2}\left(\frac{b_m}{b_1}\right)^2\left[\frac{1}{(3m-2)^2-9(\nu/N)^2} + \frac{4}{(3m)^2-9(\nu/N)^2} + \frac{1}{(3m+2)^2-9(\nu/N)^2}\right]\right\}\left[1 - 9\,(\nu/N)^2\right]\right]$$

$$= -\frac{32}{b_1}\left[\frac{1}{9} - \left(\frac{\nu}{N}\right)^2\right]\left[1 - 9\left\{\frac{8/9}{1-(\nu/N)^2} + \frac{2}{25 - 9\,(\nu/N)^2} + 2\sum_{m=2}\left(\frac{b_m}{b_1}\right)^2\left[\frac{1}{(3m-2)^2-9(\nu/N)^2} + \frac{4}{(3m)^2-9(\nu/N)^2} + \frac{1}{(3m+2)-9(\nu/N)^2}\right]\right\}\left[\frac{1}{9} - \left(\frac{\nu}{N}\right)^2\right]\right].$$

$$\cong -\frac{32}{b_1}\left[\frac{1}{9}-\left(\frac{\nu}{N}\right)^2\right]\left[1-9\left\{\frac{13}{12}+2\sum_{m=2}\left(\frac{b_m}{b_1}\right)^2\left[\frac{1}{(3m-2)^2-1}+\frac{4}{(3m)^2-1}+\frac{1}{(3m+2)^2-1}\right]\right\}\left[\frac{1}{9}-\left(\frac{\nu}{N}\right)^2\right]\right]$$

$$\cong -\frac{64}{3b_1}\left(\frac{1}{3}-\frac{\nu}{N}\right)\left[1-\frac{3}{2}\left(\frac{1}{3}-\frac{\nu}{N}\right)\right]\left[1-6\left\{\frac{13}{12}+\frac{4}{3}\sum_{m=2}\left(\frac{b_m}{b_1}\right)^2\frac{9m^2-5}{(m^2-1)(9m^2-1)}\right\}\left(\frac{1}{3}-\frac{\nu}{N}\right)\right]$$

$$\cong -\frac{64}{3b_1}\left(\frac{1}{3}-\frac{\nu}{N}\right)\left[1-8\left\{1+\sum_{m=2}\left(\frac{b_m}{b_1}\right)^2\frac{9m^2-5}{(m^2-1)(9m^2-1)}\right\}\left(\frac{1}{3}-\frac{\nu}{N}\right)\right], \qquad \text{(A-3a)}$$

in which ν/N has been replaced by 1/3 in terms such that a simplification could thereby be achieved consistent with the objective of retaining accuracy through order $(1/3 - \nu/N)^2$. To this same order we also obtain, by substitution of $A_1 \cong -\frac{64}{3b_1}\left(\frac{1}{3}-\frac{\nu}{N}\right)$ into eqns. (A-1a-e) in turn,

$$B_1 = \frac{32}{b_1}\left(\frac{1}{3}-\frac{\nu}{N}\right)^2 \qquad \text{(A-3b)}$$

$$C_1 = -\frac{16}{3b_1}\left(\frac{1}{3}-\frac{\nu}{N}\right)^2 \qquad \text{(A-3c)}$$

$$A_m = -\frac{128}{b_1}\frac{b_m/b_1}{(3m-2)^2-1}\left(\frac{1}{3}-\frac{\nu}{N}\right)^2 = -\frac{128}{3b_1}\frac{b_m/b_1}{(m-1)(3m-1)}\left(\frac{1}{3}-\frac{\nu}{N}\right)^2 \qquad \text{(A-3d)}$$

$$B_m = \frac{256}{b_1}\frac{b_m/b_1}{(3m)^2-1}\left(\frac{1}{3}-\frac{\nu}{N}\right)^2 = \frac{256}{b_1}\frac{b_m/b_1}{9m^2-1}\left(\frac{1}{3}-\frac{\nu}{N}\right)^2 \qquad m \geq 2 \qquad \text{(A-3e)}$$

$$C_m = -\frac{128}{b_1}\frac{b_m/b_1}{(3m+2)^2-1}\left(\frac{1}{3}-\frac{\nu}{N}\right)^2 = -\frac{128}{3b_1}\frac{b_m/b_1}{(m+1)(3m+1)}\left(\frac{1}{3}-\frac{\nu}{N}\right)^2. \qquad \text{(A-3f)}$$

It is these equations which have been taken as eqns. (7a-f) in the main body of the text. The results for the special case $b_m = 0$ ($m \geq 2$) can be seen to be consistent, through order ϵ^2, with equations (10a-c) of I [Section C 1 of refereeence 1].

MIDWESTERN UNIVERSITIES RESEARCH ASSOCIATION*
2203 University Avenue, Madison, Wisconsin

CONCERNING THE $\nu/N \rightarrow 1/3$ RESONANCE, III

Use Of The Moser Method To Estimate The Rotation Number, As A Function Of Amplitude, For The Equation

$$\frac{d^2v}{dt^2} + \left(\frac{2\nu}{N}\right)^2 v + \frac{1}{2}\,(\sin 2t)\, v^2 = 0$$

L. Jackson Laslett**

May 28, 1959

ABSTRACT

The Moser method of analysis, as applied through terms of order $(\nu/N - 1/3)^2$ in an earlier report, is here employed to determine the variation of rotation number (or "tune") with amplitude for solutions of the non-linear differential equation given in the title. The result is given in terms of a complete elliptic integral of the first kind, with a modulus determined by the roots of a quartic equation. The rotation number is thus calculable in terms of an amplitude characterized by the value of the Moser t-independent Hamiltonian and this in turn may be related to some desired salient dimension of the phase curve of interest. This result, although by no means as convenient for hand calculation as the handy formulas sometimes employed for this purpose, is found to give results in very good agreement with numerical computations for a problem in which the small-amplitude frequency corresponds to $\nu/N = 0.3$. As is typical, the rotation number in this example departs initially from its small-amplitude value (0.3) by an amount proportional to the square of the oscillation amplitude and only near the stability limit undergoes a rapid variation to attain the value 1/3. The area enclosed by the phase curves, most specifically by the separatrix, is also briefly examined.

* AEC Research and Development Report. Research supported by the Atomic Energy Commission, Contract No. AEC AT(11-1)-384.

** Department of Physics and Institute for Atomic Research, Iowa State College, Ames, Iowa.

A. INTRODUCTION

In an earlier report,[1,*] hereinafter denoted as I, a differential equation of the form

$$\frac{d^2v}{dt^2} + \left(\frac{2\nu}{N}\right)^2 v + \frac{b_1}{2} (\sin 2t) v^2 = 0 \tag{1}$$

was discussed, the dependent variable v being so scaled, for convenience, that $b_1 = 1$:

$$\frac{d^2v}{dt^2} + \left(\frac{2\nu}{N}\right)^2 v + \frac{1}{2} (\sin 2t)\, v^2 = 0. \tag{2}$$

In that report[1] the Moser method[2] of solution was applied to eqn. (2), through terms of order $(\nu/N - 1/3)^2$, to obtain an approximate t-independent Hamiltonian

$$K_2 = -2\delta J_2 - (1/48)(N/\nu)^{3/2} J_2^{3/2} \cos 3\gamma_2$$

$$+ (\alpha/2048)(N/\nu)^3 J_2^2 \quad , \tag{3a}^{**}$$

with

$$\alpha = \frac{6\nu/N}{1-(\nu/N)^2} - \frac{1}{1+3\nu/N} \tag{3b}^{***}$$

and

$$\delta \equiv 1/3 - \nu/N \quad , \tag{3c}$$

the expression K_2 thus representing an approximate constant of the motion.

In I the results of the analysis were specifically applied to examine the character of the limiting amplitude solution of eqn. (2), resulting from the $\nu/N \rightarrow 1/3$ resonance--in the present report we apply the results of the same general analysis to examine the dependence of the "rotation number" on amplitude.

The Hamiltonian K_2 [eqn. (3a)] was obtained in Sec. D3 of I by a series of canonical transformations.

---

*References are given in Section D.

**Eqn. (57) of I.

***Eqn. (25) of I.

Coordinate	Momentum
v	p
γ_o	J_o
γ_1	J_1
γ_2	J_2

in which $\quad \gamma_2 \equiv \gamma_1 - \frac{2}{3}t \cong \gamma_o - \frac{2}{3}t$ (4a)*

and $\quad J_2 \equiv J_1 \cong J_o$. (4b)**

with

$$v = (N/\nu')^{1/2} J_o^{1/2} \sin \gamma_o \tag{5a}$$***

and

$$p = 2(\nu/N)^{1/2} J_o^{1/2} \cos \gamma_o . \tag{5b}$$****

Phase plots of solutions to eqn. (2), plotted in v, p-space at $t = 3\pi/4$, mod. π , show a transition in form from elliptical to roughly triangular curves (as illustrated) as the amplitude approaches the stability limit.

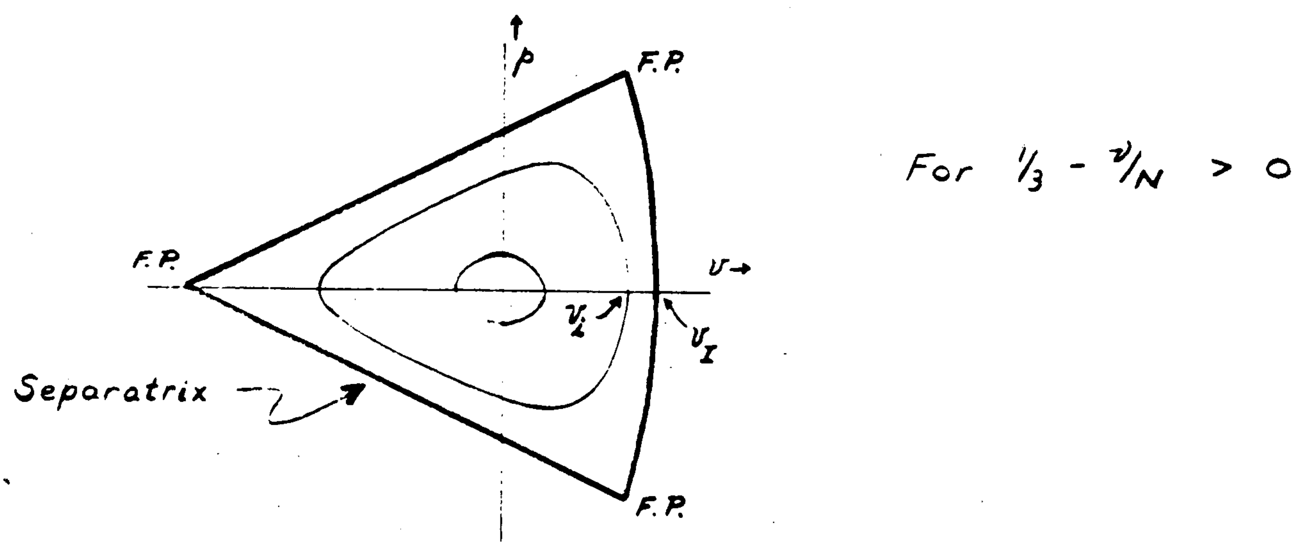

*Eqns. (56b) and (52b) of I.

**Eqns. (56a) and (52a) of I.

***Eqns. (49c) of I.

****Eqn. (49d) of I.

Operationally, the amplitude may be characterized by the intercept v_1 (see sketch), with v_I then serving to denote the value of this intercept for the separatrix. The corresponding values of J_2 or J_1 may be similarly designated. In the present report we shall examine analytically the dependence of the rotation number on $(J_2)_1$ and hence on v_1/v_I, specifically for a case in which the small-amplitude frequency is characterized by $\nu/N = 0.3$, and compare the results of this analysis with corresponding results obtained from computer solutions. A brief examination will also be made of the area enclosed by particular phase curves, in specific limiting cases.

B. THE ROTATION NUMBER

1. Analytic

To illustrate the procedure to be followed in obtaining a rotation number to characterize a particular solution, we may first note that, due to the non-linear character of the differential equation [eqn. (2)], J_2 is not a constant of the motion but is governed by the following differential equation:

$$dJ_2/dt = -\partial K_2/\partial\gamma_2$$

$$= -(1/16)(N/\nu)^{3/2} J_2^{\ 3/2} \sin 3\gamma_2, \tag{6}$$

and $d\gamma_2/dt$ is similarly given by $\partial K_2/\partial J_2$. In the course of integration of dJ_2/dt, J_2 may go from an extreme value (say a minimum value) corresponding to its value $(J_2)_i \equiv a$ at the intercept v_i to a second extreme value (say its maximum value) b in an interval $\Delta t = T$. The corresponding changes of the variables of interest are then as listed below:

Δt	$J_2 = J_1$	γ_2	$\Delta\gamma_1$
0	a	0	0
T	b	$-\pi/3$	$2T/3 - \pi/3$

A frequency of revolution may then be taken as

$$\nu' = \Delta\gamma_1 / T$$
$$= \frac{2}{3} - \frac{\pi}{3T}$$

or, since we consider $N = 2$ in eqns. (1) or (2), a "rotation number" introduced as

$$\frac{\nu'}{N} = \frac{1}{3} - \frac{\pi}{6T} \,. \tag{7}$$

This quantity, ν'/N, will be seen to vary from the small-amplitude value, ν/N, to 1/3 as the amplitude increases to the value corresponding to the stability limit.

The differential equation (6) may be integrated by making use of the constancy of K_2 [given by eqn. (3a)] to eliminate γ_2:

$$dJ_2/dt = -\partial K_2/\partial\gamma_2$$
$$= -(1/16)(N/\nu)^{3/2} J_2^{3/2} \sin 3\gamma_2$$
$$= \frac{1}{16}\left(\frac{N}{\nu}\right)^{3/2}\sqrt{J_2^3 - 2304\left(\frac{\nu}{N}\right)^3\left[-K_2 - 2\delta\cdot J_2 + \frac{\alpha}{2048}\left(\frac{N}{\nu}\right)^3 J_2^2\right]^2}\,; \tag{8a}$$

$$T = 16\left(\frac{\nu}{N}\right)^{3/2}\int_a^b \frac{dJ_2}{\sqrt{J_2^3 - 2304\left(\frac{\nu}{N}\right)^3\left[\frac{\alpha}{2048}\left(\frac{N}{\nu}\right)^3 J_2^2 - 2\delta\cdot J_2 - K_2\right]^2}}$$

$$= \frac{2^{11}}{3\alpha}\left(\frac{\nu}{N}\right)^3\int_a^b \frac{dJ_2}{\sqrt{\begin{aligned}&-J_2^4 + \left(\frac{2^7}{3\alpha}\right)^2\left(\frac{\nu}{N}\right)^3\left[1 + \frac{9}{2}\alpha\cdot\delta\right]J_2^3 + \left[\frac{2^{12}K_2}{\alpha}\left(\frac{\nu}{N}\right)^3\right. \\ &\left. - \left(\frac{2^{12}\delta}{\alpha}\right)^2\left(\frac{\nu}{N}\right)^6\right]J_2^2 - \left(\frac{2^{12}}{\alpha}\right)^2\left(\frac{\nu}{N}\right)^6\delta\cdot K_2 J_2 \\ &- \left(\frac{2^{11}}{\alpha}\right)^2\left(\frac{\nu}{N}\right)^6 K_2^2\end{aligned}}}\,. \tag{8b}$$

In the particular case that $\nu/N = 0.3$, $\delta = 1/3 - 0.3 = 1/30$ and $\alpha = 1.4517_{06}$ *

eqn. (8b) above then assumes the form

$$T = 12.696\,785\,71 \int_a^b \frac{dJ_2}{\sqrt{\begin{array}{l} -J_2^4 + 28.401\,684\,09\,J_2^3 \\ + (76.180\,714\,27\,K_2 - 6.448\,334\,695)J_2^2 \\ - 193.450\,0409\,K_2J_2 - 1450.875\,307\,K_2^2 \end{array}}} \qquad (8c)$$

$$= 12.696\,785\,71 \int_a^b \frac{dJ_1}{\sqrt{(J_1 - a)(b - J_1)(c - J_1)(d - J_1)}} \qquad (8c')$$

$$= \frac{25.393\,571\,42}{\sqrt{(c - a)(d - b)}}\ \mathbf{K}(k)\,, \qquad (8c'')$$

where a, b, c, d represent the roots of the equation obtained by setting the denominator of the integrand in eqn. (8c) equal to zero ($a < b < c < d$),

$$k = \sqrt{\frac{(b - a)(d - c)}{(c - a)(d - b)}}\ , \qquad (8d)$$

and $\mathbf{K}(k)$ denotes the complete elliptic integral of the first kind (modulus k).[3] The values of T computed from eqn. (8c'') may then be substituted into eqn. (7) to obtain the estimated rotation number, ν'/N, for this case.

2. Comparison with Computational Results

In applying the results of the previous sub-section, the value $a = (J_2)_1 = (J_1)_i$ may be related to a corresponding value of J_o by aid of eqn. (52) of I and thence directly to the intercept coordinate, v_i. The quantities $(v_i/v_I)^2$ and $(J_1)_i/(J_1)_I$ will, of course, be roughly proportional to one another. The root "a" will have the value

*From Eqn. (3b), or from p. 16 of I.

$(J_1)_i$; for small $(J_1)_i$ the roots a and b each approach zero, while for $(J_1)_i$ near the limiting value $(J_1)_I$ the roots b and c each approach 0.103 6384 and a = 0.027 5557.

The results for a series of selected values of $(J_1)_i$ are listed in Table I. For small values, the modulus k varies directly as $(J_1)_i^{3/4}$, being approximately equal to $4(J_1)_i^{3/4}$ - - see Fig. 1. Observed rotation numbers from a series of computer runs, made with the MURA I. B. M. - 704 computer by use of the DUCK-ANSWER program,[4] were obtained from examination of suitably numbered points on phase plots of the output data - - see Fig. 2. - - and are included in Table I. The results are expressed in terms of v_i/v_I, or $(v_i/v_I)^2$, using the value of v_I reported previously in I.[1]

The variation of rotation number with "amplitude" (or amplitude squared) is, finally, depicted in Fig. 3, in which the curve has been drawn to pass through the calculated values listed in Table I and the circles represent the results obtained from the machine computations. The agreement between the calculated curve and the computer results is seen to be close.[5]

Since the enclosed phase-space area is proportional to K_2, to a reasonable approximation, an effective average value of ν'/N may be taken as given by $\int (\nu'/N)\, dK_2 / \int dK_2$ - - i.e., by an average of ν'/N sampled in equal intervals of K_2. For the case considered, there thus results the effective value

$$\langle \nu'/N \rangle \cong 0.306 \, . \tag{9}$$

TABLE I
CALCULATED AND OBSERVED VALUES OF ν'/N

v_i/v_I	$(v_i/v_I)^2$	$(J_1)_i^{1/2}$	$(J_1)_i$	-10^3K_2	a, b, c, d	$k^{(*)}$	K	T	ν/N Calc.	ν'/N Obs.
0	0	0	0	0	0 0 .228 8851 28.172 7990	0	$\pi/2 =$ 1.5708	$10\pi/2 =$ 15.708	$1/3 - 1/30$ $= 0.3$	0.3
$\frac{.050}{.268} = .186\ 567$	0.3481	.030 918	.000 9559	0.06745	.000 9559 .001 0797 .227 0228 28.172 6257	.02331	1.5710	15.808	0.3002	0.3002
$\frac{.100}{.268} = .373\ 134$	.13923	.061 860	.003 8267	0.28474	.003 8267 .004 9413 .220 8204 28.172 0957	.07139	1.5728	16.155	0.3009	0.3010
.5427	.2945	.09	.0081	0.63071	.008 1 .012 0251 .210 3242 28.171 2348	.13883	1.5784	16.796	0.3022	---
$\frac{.150}{.268} = .559\ 701$	.31327	.092 826	.008 6167	0.67391	.008 6167 .012 9909 .208 9491 28.171 1274	.14725	1.5794	16.886	0.3023	0.3023
$\frac{.200}{.268} = .746\ 269$	.55692	.12382	.015 3314	1.25661	.015 3314 .028 0399 .188 5344 28.169 7784	.27010	1.6007	18.411	0.3049	0.3051
.7534	.5676	.125	.015 625	1.28289	.015 6250 .028 9322 .187 5105 28.169 6164	.27746	1.6024	18.502	0.3050	---
$\frac{.250}{.268} = .932\ 836$	.87018	.15483	.023 972	2.05366	.023 972 .060 689 .149 319 28.167 704	.54037	1.7093	23.125	0.3107	0.3111

TABLE 1
(continued)

v_i/v_I	$(v_i/v_I)^2$	$(J_1)_i^{1/2}$	$(J_1)_i$	$-10^3 K_2$	a, b, c, d	k(*)	κ	T	ν'/N Calc.	ν'/N Obs.
.9640	.9293	.16	.025 6	2.20878	.025 600 .071 529 .137 236 28.167 319	.64067	1.7849	25.593	0.3129	- - -
1	1	.166	.027 556	2.39707	.027 5557 .103 6384 .103 6384 28.166 8515	1	∞	∞	$\frac{1}{3}$	$\frac{1}{3}$

(*)For small $(J_1)_i$, k is proportional to $(J_1)_i^{3/4}$, being approximately $4(J_1)_i^{3/4}$.

C. THE PHASE SPACE AREA

1. Analytic Introduction

It may be of some interest to inquire concerning the area, S, in phase space included within a curve of constant K_2, taking, as before, K_2 as given in eqn. (3a). We thus investigate

$$S \equiv \oint p\, dv = 6\int_0^{\pi/3} J_2\, d\gamma_2 , \qquad (10)$$

with K_2 given in terms of J_2 ($=J_1$) and γ_2 by [from eqn. (3a) with $\nu/N = 0.3$]

$$K_2 = -\frac{1}{15} J_2 - 0.126\,787\,629\, J_2^{3/2} \cos 3\gamma_2 + 0.026\,253\,363\,72\, J_2^2 . \qquad (11)$$

Equation (11) may be used to eliminate γ_2 from eqn. (10), with the result (written in terms of J_1)

$$S = 38.090\,35713 \int_a^b \frac{-3K_2 - (1/15)\, J_1 - 0.026\,253\,363\,72\, J_1^2}{\sqrt{(J_1 - a)(b - J_1)(c - J_1)(d - J_1)}}\, dJ_1 , \qquad (12)$$

where a, b, c, d have the same meaning as before [i.e., in connection with eqn. (8c')].

If one were to undertake to evaluate the integral of eqn. (12) directly, it appears that the (complete) elliptic integral of the third kind would appear[6] and we shall not further pursue this matter with such generality here. The character of the integral, and hence the value of the area S may, however, be examined with some interest in the case (i) that K_2 is small and (ii) in the case that $K_2 = (K_2)_I$, corresponding to the separatrix which encloses the entire stable area of phase space.

(i) For K_2 small, the numerator of the integrand in eqn. (12) is approximately $-3K_2 - (1/15)\, J_2$ or $(2/15)\, J_1$, and is approximately constant, while $\sqrt{(c - J_2)(d - J_2)} \cong \sqrt{cd} = 2.539\,357$ [*cf.* Table I]. Accordingly, in this limit, we may write eqn. (12) as

$$S \doteq 2\langle J_1\rangle \int_a^b \frac{dJ_1}{\sqrt{(J_1 - a)(b - J_1)}}$$

$$= 2\pi(J_1) \qquad \text{(by an elementary integration)}$$

$$= 2\pi J_o$$

$$= 2\pi(\nu/N)\, v_i^2 \qquad \text{[by eqn. (5a)]} \quad . \tag{13}$$

This result is immediately seen to be correct, for the area enclosed within an elliptical phase curve of semi-axes v_i, $2(\nu/N)\, v_i$ [cf. eqn. (5b)], and thus, to a degree, constitutes a check of eqn. (12).

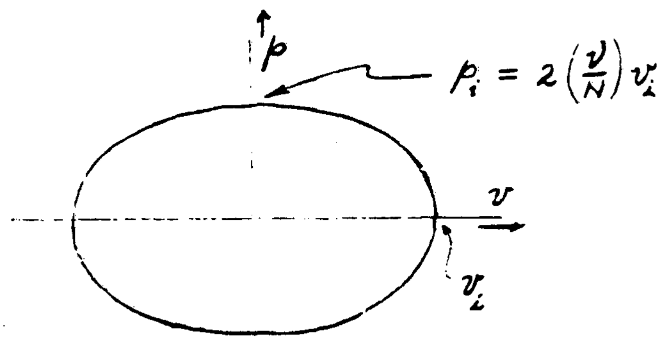

(ii) When K_2 assumes the value $(K_2)_I$ characterizing the separatrix, b = c and the numerator of the integrand in eqn. (12) moreover may be factored to give us

$$S = \int_a^b \frac{(b - J_1)(J_1 + 2.642\,995)\, dJ_1}{\sqrt{(J_1 - a)(b - J_1)(c - J_1)(d - J_1)}} \quad , \text{ with } c = b$$

$$= \int_a^b \frac{J_1 + 2.642\,995}{\sqrt{(J_1 - a)(d - J_1)}}\, dJ_1$$

$$= \left[(5.28599 + a + d)\tan^{-1}\sqrt{\frac{J_1 - a}{d - J_1}} - \sqrt{(J_1 - a)(d - J_1)}\right]_a^b$$

$$= (5.28599 + a + d)\tan^{-1}\sqrt{\frac{b - a}{d - b}} - \sqrt{(b - a)(d - b)}$$

$$= 0.2805 \quad , \tag{14}$$

by use of the values a = 0.027 5557, b = c = 0.103 6384, and d = 28.166 8515 listed in Table I.

2. Computer Result for Area Within Separatrix

From computer results obtained in connection with the work reported previously in I, one finds (after scaling of those results so as to apply to the case $b_1 = 1$ under consideration here) that the area enclosed within the separatrix (estimated from the original plot in the v, p-plane) is approximately

$$S_{computer} \cong 0.296. \tag{15}$$

This area is some 5 or 6 percent greater than that suggested by the analytic result, eqn. (14), as might be expected in view of the observation that the computer values for salient coördinates and momenta on the separatrix were found correspondingly to be a few percent greater than the values derived from the Moser theory employed here [see, f. ex., Table IV or the first line of Table VI in I].

Finally, it may be noted in closing that if the small-amplitude result,

$$\begin{aligned} S &\doteq 2\pi\left[15(-K_2)\right] \\ &= 30\pi(-K_2) , \qquad \left[\text{for } K_2 \text{ small}\right] \end{aligned} \tag{16}$$

of eqn. (13) had been applied in this form to the large value $K_2 = -0.002397$ which corresponds to the separatrix, one would have obtained the result

$$S = 0.2259 \quad ;$$

the value obtained in this way thus would have been some 20 percent lower than that calculated by eqn. (14).

D. REFERENCES AND NOTES

1. L. Jackson Laslett, MURA-452 (April 13, 1959), hereinafter denoted by I.

2. Jürgen Moser, Nach. Gött. Akad. (Math. - Phys. Kl.) Nr. 6, 87-120 (1955).

3. Cf. B. O. Peirce "A Short Table of Integrals", Ed. 3 (Ginn and Company, Boston, Massachusetts), Formula 552, p. 70.

4. J. N. Snyder, DUCK-ANSWER (I.B.M. Program 75), MURA-237 (1957). In the actual use of this program for the work reported here, the coefficient b_1 in eqn. (1) was given the value 1.15; the computational values of v and p, accordingly, each required multiplication by the factor 1.15 to bring them into agreement with the quantities employed in the analytic work presented here.

5. Although the analytic approach outlined in the present report is of interest as an illustration of the applicability of Moser methods, and the results appear to be quantitatively quite accurate, the results obtained here [eqn. (8c"), etc.] cannot be regarded as particularly convenient for numerical evaluation. It therefore may be of interest to recall, as Dr. G. Parzen has kindly pointed out (private communication, 27 May 1959), that a "handy formula" has been proposed to describe the variation of "tune" in cases such as we consider here. One form of this formula is such that one would write for the present problem

$$(\nu'/N)^2 \doteq (1/3)^2 - \left[(1/3)^2 - (\nu/N)^2\right] \sqrt{1 - (A/A_I)^2} \quad , \qquad (17)$$

where A and A_I respectively denote the "amplitudes" of the actual oscillation and of the limiting stable motion. In the present instance we might, perhaps somewhat arbitrarily, identify A^2 as proportional to K_2 and write

$$(\nu'/N)^2 \cong (1/3)^2 - \left[(1/3)^2 - (0.3)^2\right] \sqrt{1 - K_2/(K_2)_I} \quad . \qquad (18)$$

We now may make a comparison, presented below, of (i) the results derived in the body of the text, (ii) the prediction of the handy formula noted here, and (iii) the rotation number derived from the computer results:

$K_2/(K_2)_I$	ν'/N		
	Formula of text	Handy formula	Computer
0	.3	.3	.3
.028 139	.3002	.3005	.3002
.118 786	.3009	.3021	.3010
.281 137	.3023	.3053	.3023
.524 226	.3049	.3107	.3051
.856 737	.3107	.3211	.3111
1	1/3	1/3	1/3

Although the handy formula certainly represents correctly the general trend of ν'/N, it appears to be somewhat inferior quantitatively, at least as applied here, to the more elaborate result given in the text.

6. See, f. ex., W. Gröbner and N. Hofreiter, "Integraltafel", Ed. 2 (Springer, Vienna, 1957) in regard to integrals such as they denote by $\int \frac{x^n}{y} dx$, $n \gg 1$ [as in Pt. I, Indef. Int., Sect. 244, pp. 81 ff].

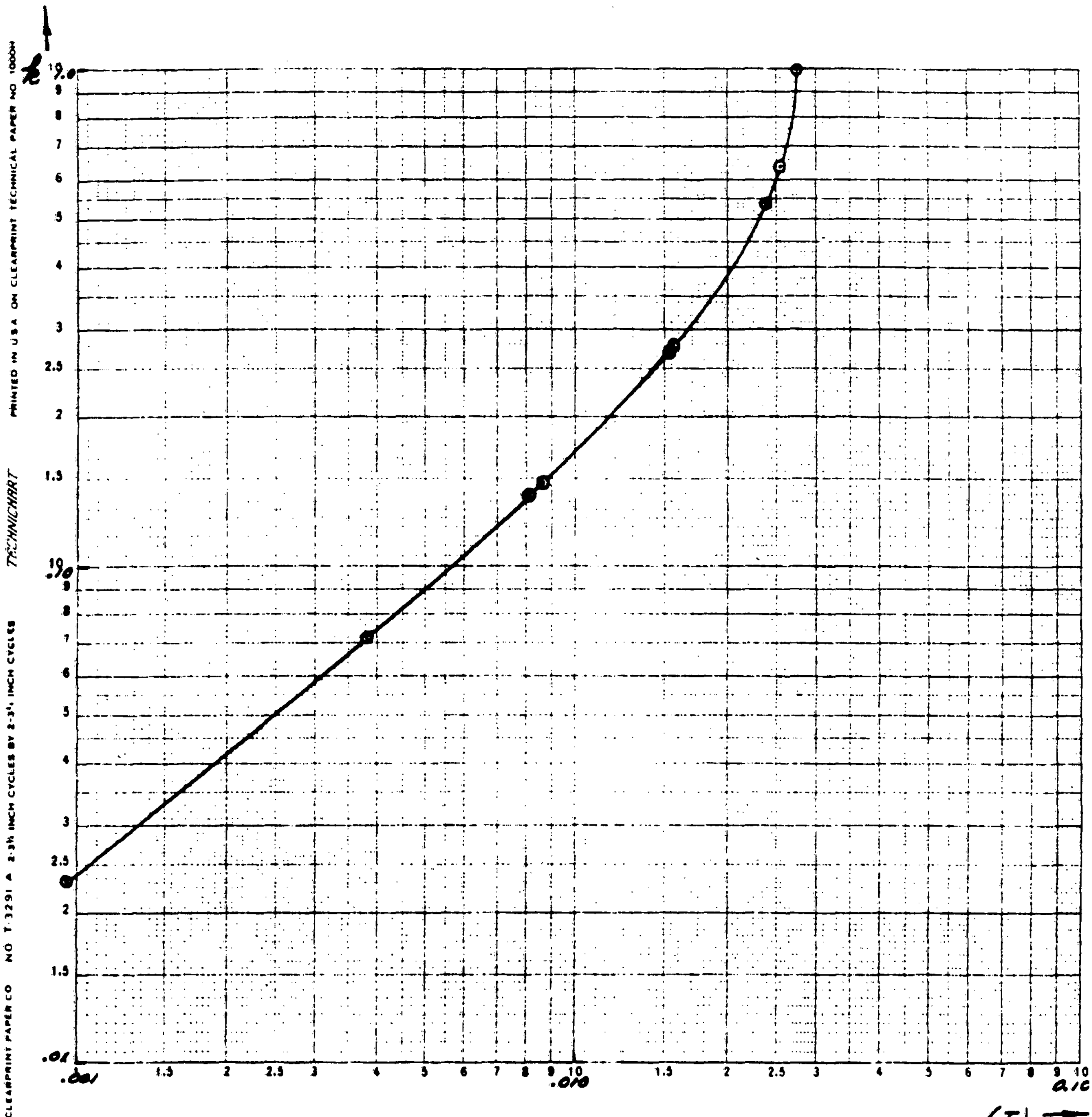

k
(J₁)ᵢ
.001
.010
0.10
.01
1.0
CLEARPRINT PAPER CO. NO. T-3291 A 2-3½ INCH CYCLES BY 2-3½ INCH CYCLES
TECHNICHART
PRINTED IN U.S.A. ON CLEARPRINT TECHNICAL PAPER NO. 1000H

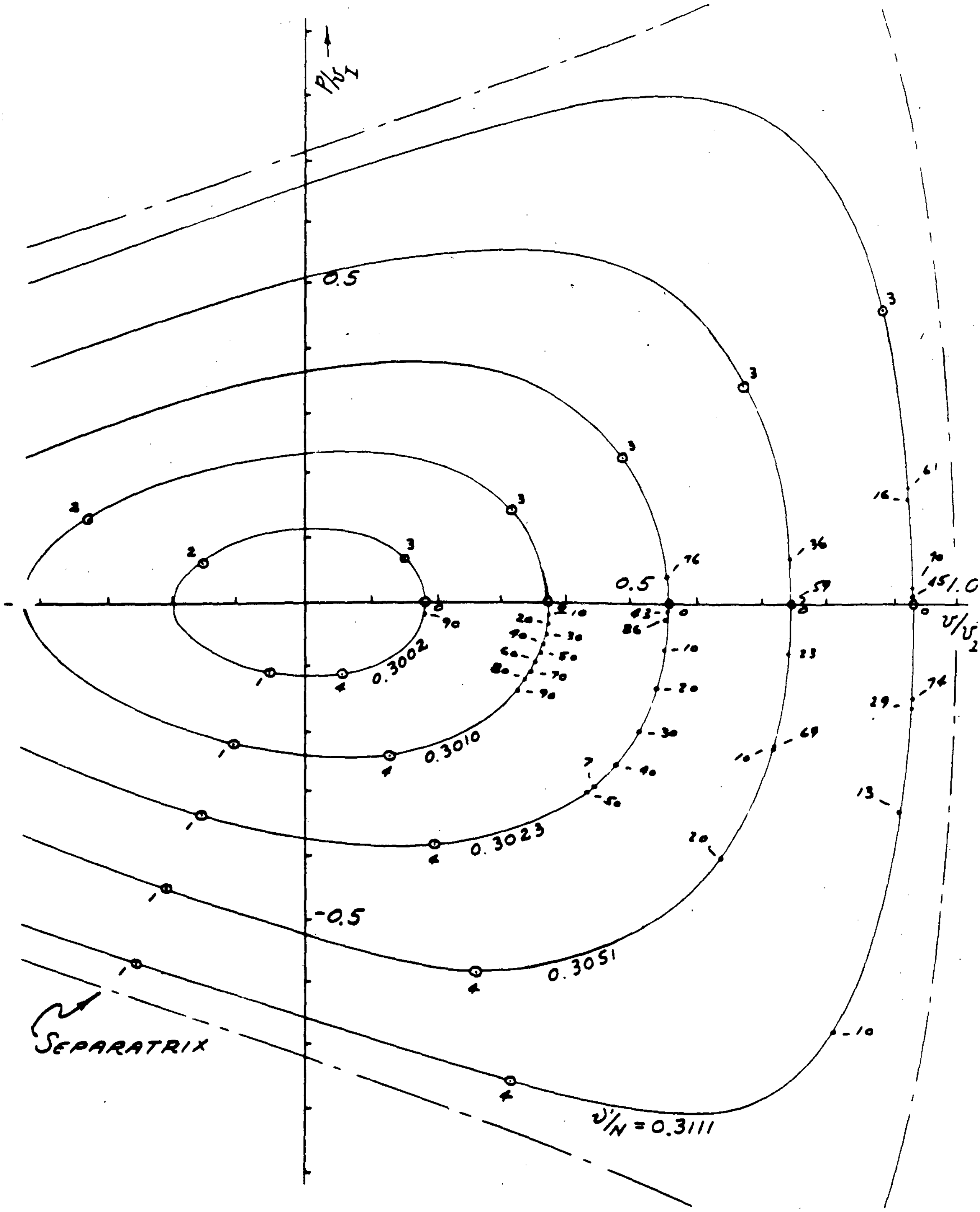
p/σ_I
0.5
-0.5
0.5
1.0
υ/υ_2
0.3002
0.3010
0.3023
0.3051
υ'/N = 0.3111
SEPARATRIX

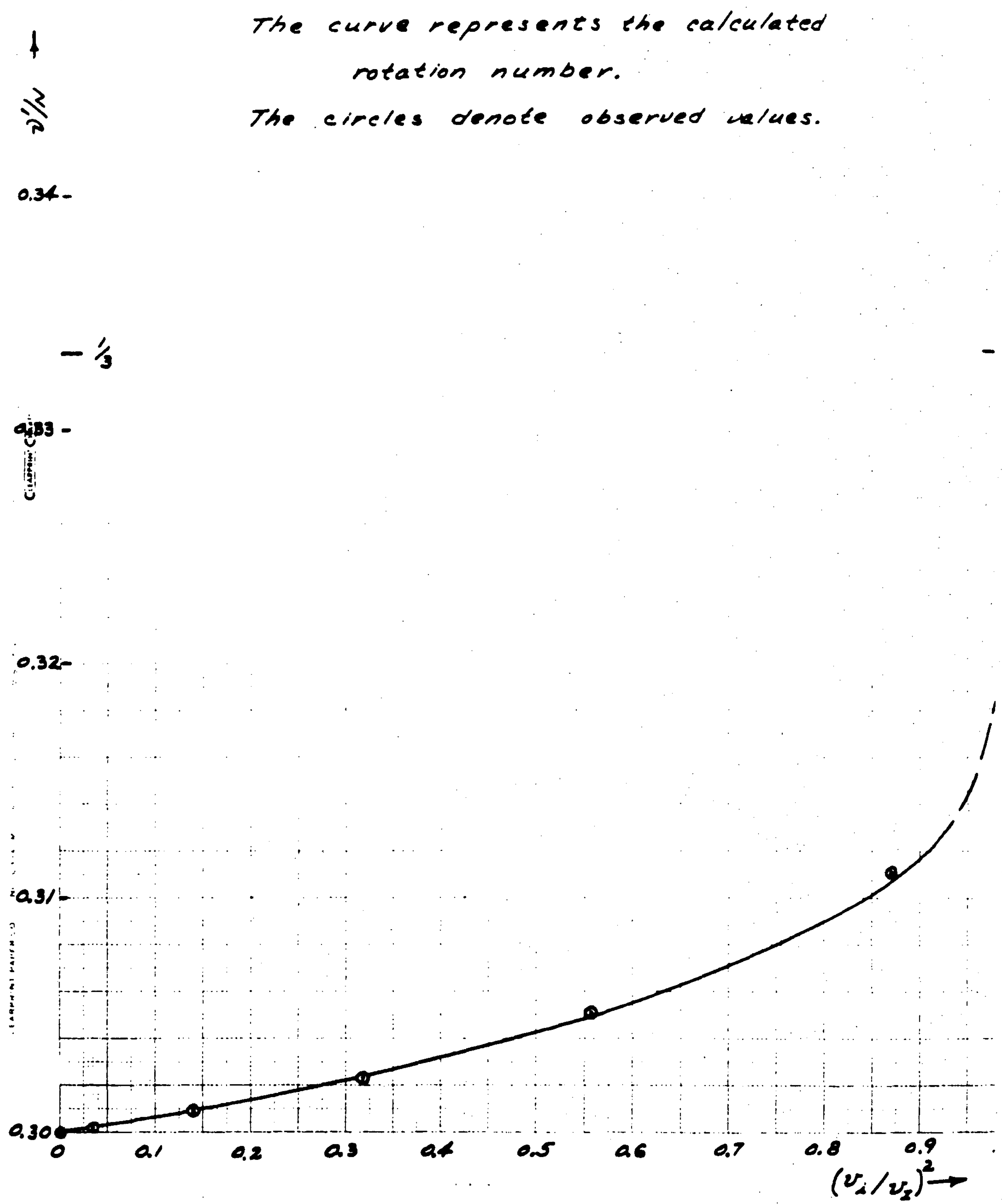

The curve represents the calculated rotation number.
The circles denote observed values.
ν'/ν
0.34
1/3
0.33
0.32
0.31
0.30
0
0.1
0.2
0.3
0.4
0.5
0.6
0.7
0.8
0.9
$(v_i/v_s)^2$

MURA-463
Distribution List UC28

MIDWESTERN UNIVERSITIES RESEARCH ASSOCIATION*

2203 University Avenue, Madison, Wisconsin

CONCERNING THE $\nu/N \longrightarrow 1/3$ RESONANCE, IV
THE LIMITING-AMPLITUDE SOLUTION OF THE EQUATION

$$\frac{d^2u}{d\phi^2} + (a + b \cos 2\phi)\, u + \frac{B_1}{2} (\sin 2\phi)\, u^2 = 0$$

L. Jackson Laslett**

June 3, 1959

ABSTRACT

The equation shown in the title is reduced, by the transformations

$$v = \sqrt{\frac{N}{2\nu\beta}}\; u \quad \text{and} \quad t = \frac{N}{2\nu} \int_0^{\phi} \frac{d\phi}{\beta} \;, \text{ to the form}$$

$$\frac{d^2v}{dt^2} + \left(\frac{2\nu}{N}\right)^2 v + \frac{1}{2} \left[\sum_{m=1} b_m (\sin 2mt)\right] v^2 = 0 .$$

Use is made of the results of an earlier report, in which the characteristics of the limiting-amplitude solution of this latter equation were obtained by a variational procedure and by application of the Moser method, to obtain corresponding information concerning the solution $u(\phi)$ of the first equation. The analytic work is carried through terms of order $(1/3 - \nu/N)^2$ and applied to an example in which

$a = 0.1262875 \qquad b = 1.15$

$\nu/N = 0.2997 \qquad B_1 = 1.$

Comparisons with the results of direct digital computation for this example indicate the results of the analytic theory are within a few (2 to 4) percent of computed values.

*AEC Research and Development Report. Research supported by the Atomic Energy Commission Contract No. AEC AT(11-1)-384.

**Department of Physics and Institute for Atomic Research, Iowa State College, Ames Iowa.

A. INTRODUCTION

In a previous report,[1*] hereinafter designated as I, the characteristics of the differential equation

$$\frac{d^2v}{dt^2} + (2\,\nu/N)^2\, v + (1/2)\,(\sin 2\,t)\, v^2 = 0 \tag{1}$$

were investigated, in particular at the stability boundary, both by a variational method and by application of the Moser procedure. These results were extended in a second report,[2] denoted by II, to describe similarly the results for the limiting-amplitude solutions of the equation

$$\frac{d^2v}{dt^2} + (2\,\nu/N)^2\, v + (1/2)\left[\sum_{m=1} b_m \sin 2\,mt\right] v^2 = 0\,, \tag{2}$$

the work being carried through terms of order $(\nu/N - 1/3)^2$.

It was pointed out in I that if the coefficient of v in eqn. (1) had contained an alternating-gradient (A-G) term, it would have been possible to transform the equation, through a suitable introduction of new variables, so as to remove the A-G character of the linear term. In the present report we undertake to apply this technique to the equation

$$\frac{d^2u}{d\phi^2} + (a + b\cos 2\,\phi)\, u + (B_1/2)\,(\sin 2\,\phi)\, u^2 = 0\,, \tag{3}$$

and, by subsequent use of the results of II, then to examine the nature of the limiting-amplitude solutions for a particular example with a small-amplitude oscillation frequency given by $\nu/N = 0.2997$.

B. ELIMINATION OF THE A-G ASPECT OF THE LINEAR COEFFICIENT

We commence with eqn. (3), written above, and, for convenience in executing the transformations, note that it may be associated with the

*References are given in Section E.

Lagrangian

$$L_o\,(du/d\phi,\ u,\ \phi)$$

$$= (1/2)\,(du/d\phi)^2 - (1/2)\,k\,(\phi)\,u^2 - (B_1/6)\,(\sin 2\phi)\,u^3\,, \tag{4a}$$

in which

$$k\,(\phi) \equiv a + b\cos 2\phi\,. \tag{4b}$$

The transformation to follow then makes use of the constant $2\nu/N$, where $2\pi\nu/N\ (\equiv \sigma)$ represents the change in phase of the solutions of the linearized eqn. (3) when $\Delta\phi = \pi$ and also employs the function $\beta(\phi)$ commonly employed in the theory of A-G accelerators.[3, 4] We then introduce the variables[5]

$$v = \sqrt{\frac{N}{2\nu\beta}}\ u \tag{5a}$$

$$t = \frac{N}{2\nu}\int_0^{\phi}\frac{d\phi}{\beta}\ , \tag{5b}$$

the transformation of the independent variable being such that in an interval $\Delta\phi = \pi$ [i.e. in one period of the coefficients of eqn. (3)], $\Delta t = \frac{N\sigma}{2\nu} = \pi$ and the period in terms of t accordingly is the same as in terms of ϕ.

The Lagrangian in terms of the new variables is taken to be

$$\begin{aligned} L_1\,(dv/dt,\ v;\ t) &= \frac{2\nu\beta}{N}\,L_o \\ &= \frac{1}{2}\left(\frac{dv}{dt}\right)^2 + \frac{\nu}{N}\,\frac{d\beta}{dt}\,v\,\frac{dv}{dt} \\ &+ \frac{1}{2}\left[\left(\frac{\nu}{N}\right)^2\left(\frac{d\beta}{d\phi}\right)^2 - \frac{k}{2}\left(\frac{2\nu\beta}{N}\right)^2\right]v^2 \\ &- \frac{B_1}{6}\left(\frac{2\nu\beta}{N}\right)^{5/2}(\sin 2\phi)\,v^3\,. \end{aligned} \tag{6}$$

The Lagrangian (6) is then modified by subtraction of a perfect differential to eliminate the term containing $v \frac{dv}{dt}$

$$
\begin{aligned}
L_2 (dv/dt, v, t) &= L_1 - \frac{d}{dt}\left[\frac{\nu}{2N} \frac{d\beta}{d\phi} v^2\right] \\
&= \frac{1}{2}\left(\frac{dv}{dt}\right)^2 - \frac{1}{2}\left(\frac{2\nu}{N}\right)^2\left[\frac{\beta}{2} \frac{d^2\beta}{d\phi^2} - \frac{1}{4}\left(\frac{d\beta}{d\phi}\right)^2 + k\beta^2\right] v^2 \\
&\quad - \frac{B_1}{6}\left(\frac{2\nu\beta}{N}\right)^{5/2} (\sin 2\phi)\, v^3 \\
&= \frac{1}{2}\left(\frac{dv}{dt}\right)^2 - \frac{1}{2}\left(\frac{2\nu}{N}\right)^2 v^2 - \frac{B_1}{6}\left(\frac{2\nu\beta}{N}\right)^{5/2} (\sin 2\phi)\, v^3 \qquad (7)
\end{aligned}
$$

the last reduction being accomplished by virtue of the relation[6]

$$\frac{\beta}{2} \frac{d^2\beta}{d\phi^2} - \frac{1}{4}\left(\frac{d\beta}{d\phi}\right)^2 + k\beta^2 = 1 . \qquad (8)$$

The differential equation which follows from the Lagrangian (7) is seen to be

$$\frac{d^2v}{dt^2} + \left(\frac{2\nu}{N}\right)^2 v + \frac{B_1}{2}\left(\frac{2\nu\beta}{N}\right)^{5/2} (\sin 2\phi)\, v^2 = 0 \qquad (9)$$

and the associated Hamiltonian is

$$H = \frac{1}{2} p^2 + \frac{1}{2}\left(\frac{2\nu}{N}\right)^2 v^2 + \frac{B_1}{6}\left(\frac{2\nu\beta}{N}\right)^{5/2} (\sin 2\phi)\, v^3 \qquad (10)$$

with $p = dv/dt$. Accordingly, if one makes the expansion

$$B_1\left(\frac{2\nu\beta}{N}\right)^{5/2} (\sin 2\phi) = \sum_{m=1} b_m (\sin 2mt) , \qquad (11)$$

these results (9) and (10) are in the form treated in II. We proceed then to an application of this analysis to a specific example in which, for comparison, computational solutions are available for the original differential equation. Specifically, we shall take

$$a = 0.126\,2875, \tag{12a}$$

$$b = 1.15 \quad \text{and} \tag{12b}$$

consider as in [1] the dependent variable to be so scaled that

$$B_1 = 1. \tag{12c}$$

The value of ν/N which is implied by this particular selection of values for a and b may be estimated analytically[7] obtained from available tables,[4] or determined by a direct computation--in the present example we find

$$\nu/N = 0.2997 \tag{12d}$$

or substantially 0.3.

C. THE EXPANSION INVOLVING β

The function $\beta(\phi)$ may be estimated analytically,[7] obtained from tabulated[4] values of $\beta \cdot (\sin\sigma)$, or found by direct computation. In the present instance, with the governing parameters given by (12a, b), $\beta(\phi)$ itself may be represented by the expansion[8] (see Fig. 1)

$$\begin{aligned} \frac{2\nu}{N}\beta = 1.3956 \Big[1 &+ 0.741\,13 \cos 2\phi \\ &+ 0.083\,56 \cos 4\phi \\ &+ 0.004\,54 \cos 6\phi + \cdots \Big]. \end{aligned} \tag{13}$$

It may be of interest to note in passing that the analytic results of reference 7 suggest that in the present case the quantity $\frac{2\nu}{N}\beta$ ranges between the maximum and minimum values (at $\phi = 0$ and at $\phi = \pi/2$, respectively) 2.539 and 0.474, while the values obtained by a direct computation are substantially 2.552 and 0.472.

In the present work we require the expansion of $B_1\left(\frac{2\nu\beta}{N}\right)^{5/2} \sin 2\phi$, as a trigonometric series in the variable t, with t related to ϕ by eqn. (5b).

The coefficients[8] of this expansion, (11), are as listed in Table I.

TABLE I

COEFFICIENTS, b_m, OF sin 2 m t IN THE EXPANSION (11)

$a = 0.126\ 2875$ $\qquad$ $b = 1.15$ $\qquad$ $B_1 = 1$

m	b_m
1	1.0645
2	1.3531
3	1.2396
4	0.9878
5	0.7278
6	0.5100
7	0.3450
8	0.2274
9	0.1470
$\geqslant 10$	< 0.01

These tabulated values may be employed, in application of the results given in II, to an examination of the expected limiting-amplitude solution to eqn. (3). The scale distortion in passing from the variable ϕ to the variable t is instrumental in effecting a pronounced peak in a plot of the (odd) function $\left(\frac{2\nu}{N}\beta\right)^{5/2} \sin 2\phi$ vs. t (Fig. 2), with a consequent enhancement of the higher-order Fourier coefficients b_m; the effect of the higher-order coefficients on the salient features of the phase plots, however, would not be expected to be great.

D. COMPARISON WITH COMPUTATIONAL RESULTS

For comparison with available computer results we apply the procedure outlined above to the specific case for which* $a = 0.126\,2875$

$$b = 1.15$$

$$(\nu/N = 0.2997)$$

$$B_1 = 1,$$

particularly with respect to the location of the unstable fixed points which characterize the unstable equilibrium orbit at $t = 0$. In terms of the notation of II, then, we have

$$1/3 - \nu/N = 0.0336\,3333\ldots = 1.009/30\,, \tag{14a}$$

$$\alpha = 3.975\,962\,, \quad \text{and} \tag{14b}$$

$$\eta_1 = 0.8201\,1582\,, \tag{14c}$$

making use of the values of b_m ($m \leq 9$) listed in Table I.

1. Location of Unstable Fixed Points

For the fixed point on the symmetry axis (at $t = 0$) we calculate**

$$v = 0 \tag{15a}$$

$$p = -\frac{128}{b_1}\left(\frac{1}{3}-\frac{\nu}{N}\right)\left(\frac{\nu}{N}\right)^2\eta_1\left\{1-\left[\begin{array}{l}\dfrac{2}{1-\nu^2/N^2}-\dfrac{1}{1+3\,\nu/N}\\ -2\displaystyle\sum_{m=2} m\,\frac{b_m}{b_1}\left(\frac{1}{m^2-9\nu^2/N^2}-\frac{1}{m^2-\nu^2/N^2}\right)\end{array}\right]\left(\frac{1}{3}-\frac{\nu}{N}\right)\eta_1\right\} \tag{15b}$$

to obtain

$$v = 0 \tag{15a'}$$

$$p = -0.2874\,. \tag{15b'}$$

---

*Eqns. (12 a - d).

**Eqns. (31a, b) of II.

again making use of the values of b_m ($m \leq 9$) in Table I. Similarly, for the fixed points situated to the right and left of the symmetry axis (for $t = 0$) we calculate*

$$v = \mp \frac{32\sqrt{3}}{b_1}\left(\frac{1}{3} - \frac{\nu}{N}\right)\left(\frac{\nu}{N}\right)\eta_1\left\{1 - \left[\begin{array}{l}\dfrac{2}{1 - \nu^2/N^2} - \dfrac{1}{1 + 3\,\nu/N} \\ -2\sum\limits_{m=2} m\,\dfrac{b_m}{b_1}\left(\dfrac{1}{m^2 - 9\,\nu^2/N^2} - \dfrac{1}{m^2 - \nu^2/N^2}\right)\end{array}\right]\left(\frac{1}{3} - \frac{\nu}{N}\right)\eta_1\right\} \quad (16a)$$

$$p = +\frac{64}{b_1}\left(\frac{1}{3} - \frac{\nu}{N}\right)\left(\frac{\nu}{N}\right)^2\eta_1\left\{1 + \left[\begin{array}{l}\dfrac{10}{1 - \nu^2/N^2} + \dfrac{1}{1 + 3\,\nu/N} \\ +\,2\sum m\,\dfrac{b_m}{b_1}\left(\dfrac{5}{m^2 - 9\,\nu^2/N^2} + \dfrac{1}{m^2 - \nu^2/N^2}\right)\end{array}\right]\left(\frac{1}{3} - \frac{\nu}{N}\right)\eta_1\right\}, \quad (16b)$$

to obtain

$$v = \mp\, 0.4153 \quad (16a')$$

$$p = +\, 0.2759\,. \quad (16b')$$

To transform the quantities v, p, found above, to the quantities u, $P \equiv du/d\phi$, which pertain to eqn. (3) and which essentially constitute the working variables in the computational work, we note from eqns. (5a, b) that

$$u = \sqrt{\frac{2\,\nu\beta}{N}}\quad v = 1.5975\ v \quad (17a)$$

and

---

*Eqns. (32a, b) of II.

$$P = \frac{du}{d\phi} = \frac{d}{d\phi}\left(\sqrt{\frac{2\nu\beta}{N}}\; v\right)$$

$$= \frac{\nu}{N}\sqrt{\frac{N}{2\nu\beta}}\;\frac{d\beta}{d\phi}\; v + \sqrt{\frac{N}{2\nu\beta}}\;\frac{dv}{dt}$$

$$= \frac{p}{1.5975} \tag{17b}$$

when (as here at $t = 0$, $\phi = 0$) $\frac{2\nu\beta}{N} = 2.552$ and $d\beta/d\phi = 0$ (Fig. 1).

The resulting predicted fixed-point coordinates and the corresponding values obtained from digital computation are presented in Table II. The latter values were obtained with the MURA IBM 704 computer, by use of the DUCK-ANSWER[9] program. A phase plot, obtained from the computational results for $\phi = 0$ (mod. π) is given in Fig. 3.

TABLE II

COORDINATES OF UNSTABLE FIXED POINTS AT $\phi = 0$,
As Obtained from the Analysis of this Report and from Computer Results

$a = 0.125\,2875$ $\quad b = 1.15$ $\quad \nu/N = 0.2997$ $\quad B_1 = 1$

FIXED POINT	From Analysis		From Computer	
	u	$P \equiv du/d\phi$	u	$P \equiv du/d\phi$
On Symm. Axis	0	-0.1799	0	-0.1866
R and L of Symm. Axis	$\mp$ 0.6634	+0.1727	$\mp$0.6866	+0.1765

It is noted from Table II that the values found by use of our formulas are some two to four per cent less in magnitude than those given by the computer--a situation similar to that shown in Table VI of I for an example with $\nu/N = 0.3$.

2. Representation of the Unstable Equilibrium Orbit

Our application of the results of II to eqn. (9) gives us, of course, a trigonometric (sine) series for v(t), from which, for example, eqn. (16a) would follow. In the present example the pertinent coefficients for such a development of v(t), and the similar (cosine) coefficients calculated separately for p(t) by the expressions in II with which our present eqns. (15b) and (16b) are consistent, are listed in Table III (by use of Table I, considering $m \leq 9$).

TABLE III

COEFFICIENTS FOR A TRIGONOMETRIC EXPANSION OF v(t) AND p(t)
$m \leq 9$

Argument	m	Sine Coefficient in v	Cosine Coefficient in p
2 t/3	1	-0.477 435	-0.309 642
2 t	1	+0.018 056	+0.036 113
8 t/3	2	-0.005 580	-0.015 631
10 t/3	1	-0.003 329	-0.010 649
4 t	2	+0.005 343	+0.021 370
14 t/3	3	-0.001 687	-0.008 098
16 t/3	2	-0.001 567	-0.008 145
6 t	3	+0.002 148	+0.012 887
20 t/3	4	-0.000 665	-0.004 520
22 t/3	3	-0.000 744	-0.005 354
8 t	4	+0.000 959	+0.007 668
26 t/3	5	-0.000 291	-0.002 565
28 t/3	4	-0.000 362	-0.003 330
10 t	5	+0.000 451	+0.004 511
32 t/3	6	-0.000 135	-0.001 462
34 t/3	5	-0.000 180	-0.002 012
12 t	6	+0.000 219	+0.002 631
38 t/3	7	-0.000 065	-0.000 834
40 t/3	6	-0.000 091	-0.001 196
14 t	7	+0.000 109	+0.001 525
44 t/3	8	-0.000 032	-0.000 475
46 t/3	7	-0.000 046	-0.000 702
16 t	8	+0.000 055	+0.000 879
50 t/3	9	-0.000 016	-0.000 271
52 t/3	8	-0.000 024	-0.000 409
18 t	9	+0.000 028	+0.000 505
58 t/3	9	-0.000 012	-0.000 237

The conversion of $v(t)$ to $u(\phi)$ would appear to be rather tedious, involving as it does both the factor $1/\beta$ and the non-linear relation between the independent variables t and ϕ. It is of interest to note from Table III, however, that $v(t)$ itself evidently should be rather well represented by its first one or two coefficients*--say by

$$v(t) \cong -0.477_{435} \sin 2t/3 + 0.018_{056} \sin 2t . \tag{18}$$

If a table of values of $u = \sqrt{\frac{2\nu\beta}{N}}\, v$, vs. ϕ, is constructed by hand computation, one finds that eqn. (18) suggests $u(\phi)$ should have a representation[8] in which the leading terms are roughly

$$u(\phi) \cong -0.533_9 \sin\frac{2\phi}{3} + 0.177_2 \sin\frac{4\phi}{3} + 0.015_5 \sin 2\phi - 0.040_0 \sin\frac{8\phi}{3} + \cdots \quad ; \tag{19}$$

this result, eqn. (19), may be compared with the direct computer analysis[10] of the limiting-amplitude solution for eqn. (3), namely (with $B_1 = 1$):

$$u(\phi) = -0.55231 \sin\frac{2\phi}{3} + 0.18429 \sin\frac{4\phi}{3} + 0.02167 \sin 2\phi - 0.04919 \sin\frac{8\phi}{3} + 0.00575 \sin\frac{10\phi}{3} + 0.00283 \sin 4\phi - 0.00140 \sin\frac{14\phi}{3} + \cdots . \tag{20}$$

As with the data of Table II, it is seen that the major calculated coefficients in the representation (19) are some three or four per cent less than the corresponding directly-computed values shown in eqn. (20).

---

*Cf. the result of the numerical solution of eqns. (8a - c) in Sect. C 1 of I, or the computer results given by eqn. (12a) of that report ($\nu = 0.3$).

E. REFERENCES AND NOTES

1. L. Jackson Laslett, MURA-452 (April 13 1959), herein designated as I.
2. L. Jackson Laslett MURA-459 (May 20, 1959) herein designated as II.
3. β is a characteristic of the linearized eqn. (3) such that, in the notation employed in the Belford tables,[4] $\beta = M_{12}/\sin \sigma = 1/\Phi'$, where Φ is the "phase function."
4. G. Belford, L. Jackson Laslett, and J. N. Snyder, "Table Pertaining to Solutions of a Hill Equation," MURA Notes (April 3, 1956).
5. Cf. E. D. Courant and H. S. Snyder, Annals of Physics 3, 1-48 (January, 1958); eqns. (4.4) and (4.5), p. 18.
6. This relation (8) is implied by results appearing in
   (i) L. Jackson Laslett, MURA Notes (28 October 1954);
   (ii) L. Jackson Laslett, MURA-206 (November 21, 1956)--Appendix A; or
   (iii) Reference 5, Section 3(a).
7. L. Jackson Laslett and A. M. Sessler, MURA-252 (April 10, 1957). In this report an approximate solution of the linear (A-G) equation is given in terms of circular functions, explicitly those of argument $\nu\theta$, $(N \pm \nu)\theta$, and $(2N \pm \nu)\theta$, with $N\theta$ representing 2ϕ.
8. The Fourier expansion of tabulated function values is aided by use of the FORANAL program-- J. N. Snyder, FORANAL (IBM Program 52), MURA-228 (1957).
9. J. N. Snyder, DUCK-ANSWER (IBM Program 75), MURA-237 (1957). In the actual computations the value of B_1 was 1.15; the computer results for u and $du/d\phi$, accordingly, were multiplied by the factor 1.15 to obtain the values cited in the present report.
10. John McNall, DUCKNALL (IBM Program 219), MURA-438 (1958).

Fig. 1

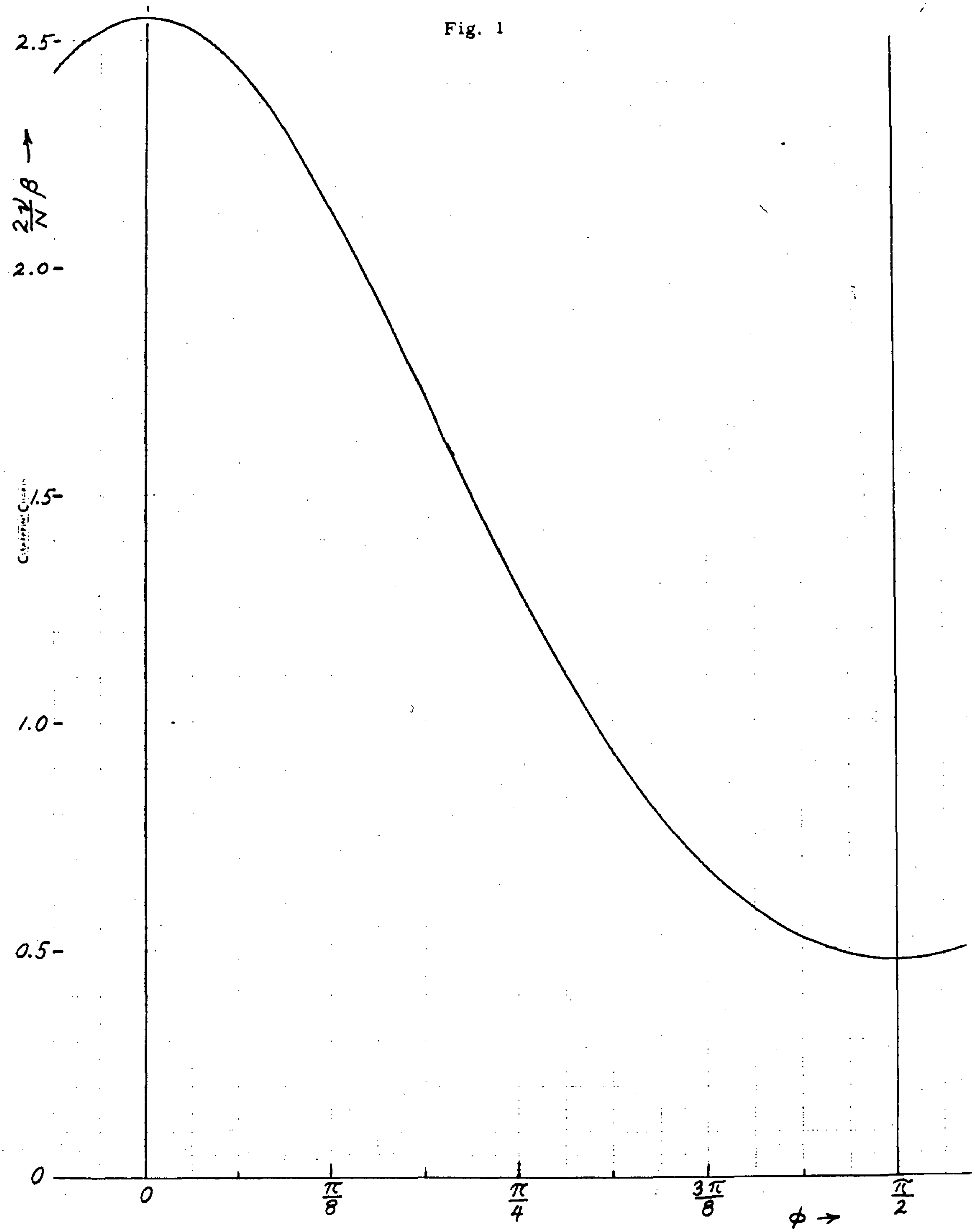

$2\nu/N\beta \rightarrow$
2.5
2.0
1.5
1.0
0.5
0
0
$\frac{\pi}{8}$
$\frac{\pi}{4}$
$\frac{3\pi}{8}$
$\frac{\pi}{2}$
$\phi \rightarrow$

Fig. 2

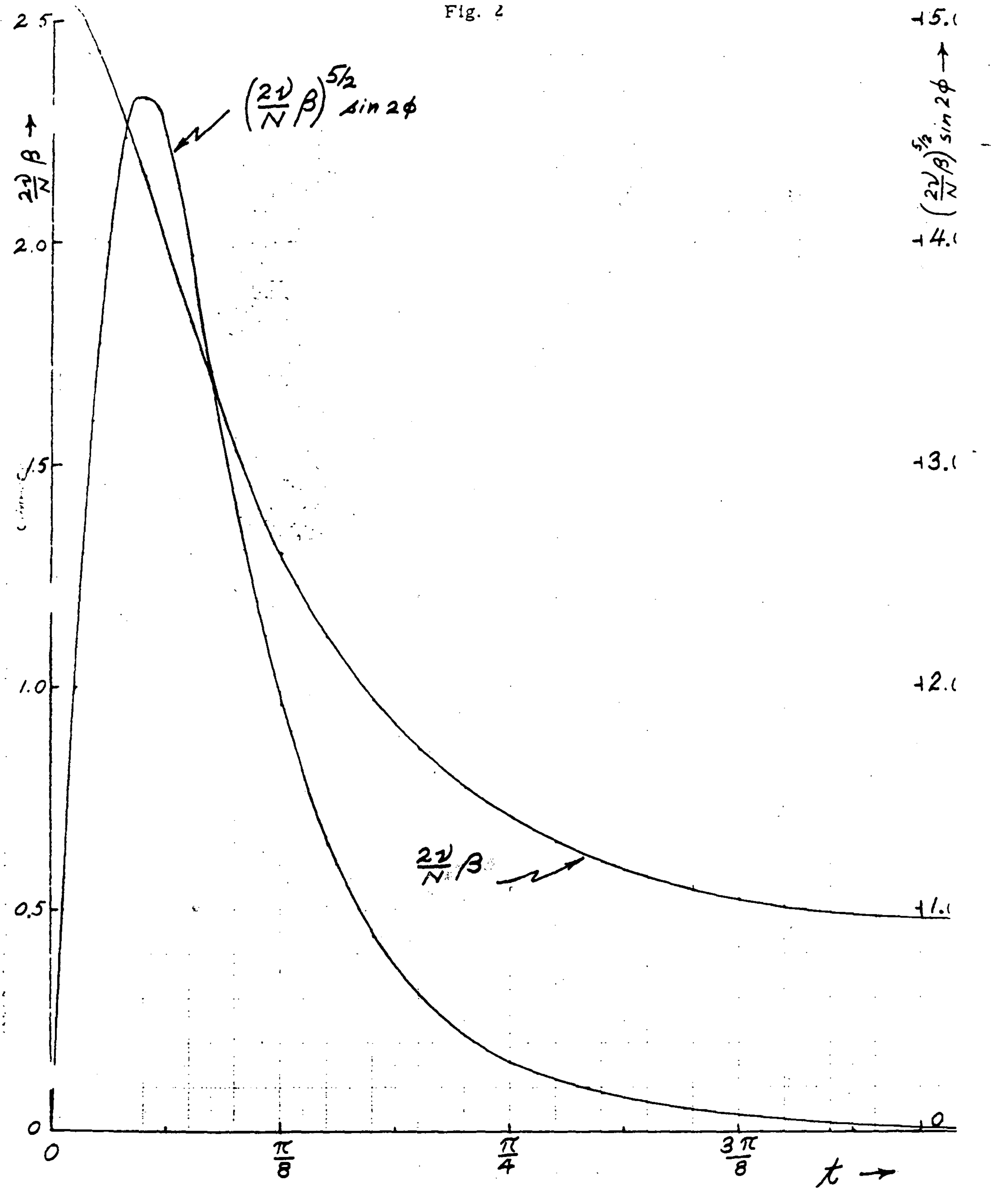

2.5
2.0
1.5
1.0
0.5
0
$\frac{2\nu}{N}\beta$ →
$\left(\frac{2\nu}{N}\beta\right)^{5/2}\sin 2\phi$
$\frac{2\nu}{N}\beta$
5.0
4.0
3.0
2.0
1.0
0
$\left(\frac{2\nu}{N}\beta\right)^{5/2}\sin 2\phi$ →
0
$\frac{\pi}{8}$
$\frac{\pi}{4}$
$\frac{3\pi}{8}$
t →

Fig. 3

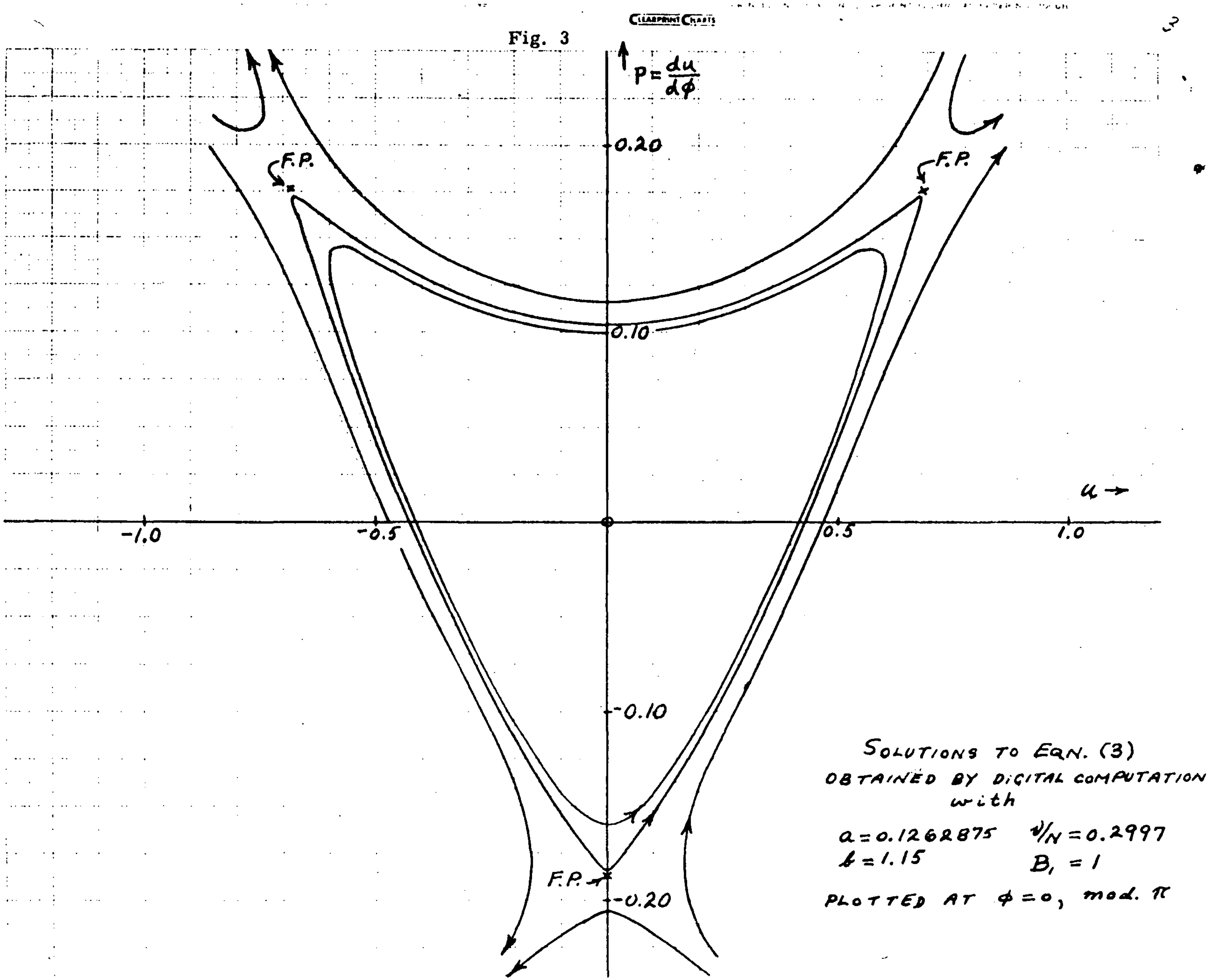

CLEARPRINT CHARTS
$p = \frac{du}{d\phi}$
0.20
0.10
-0.10
-0.20
$u \rightarrow$
-1.0
-0.5
0.5
1.0
F.P.
F.P.
F.P.
SOLUTIONS TO EQN. (3)
OBTAINED BY DIGITAL COMPUTATION with
a = 0.1262875 ν/N = 0.2997
b = 1.15 B₁ = 1
PLOTTED AT φ = 0, mod. π

MURA-490
Distribution List UC 28

MIDWESTERN UNIVERSITIES RESEARCH ASSOCIATION*
2203 University Avenue, Madison, Wisconsin

CONCERNING THE $\nu/N \longrightarrow 1/3$ RESONANCE, IV A
A TRIAL FUNCTION FOR THE LIMITING-AMPLITUDE SOLUTION OF

$$\frac{d^2u}{d\phi^2} + (a + b\cos 2\phi)\, u + \frac{B_1}{2} (\sin 2\phi)\, u^2 = 0$$

L. Jackson Laslett**

June 17, 1959

ABSTRACT

For comparison with the results given in an earlier report, use of a trial function for the limiting-amplitude solution of the equation given in the title is illustrated for an example in which

$a = 0.1262875$	$b = 1.15$
$\nu/N = 0.2997$	$B_1 = 1.$

The trial function employed sine functions of argument $2\phi/3$, $4\phi/3$, 2ϕ, $8\phi/3$, and $10\phi/3$. The coefficient found for the dominant term appeared to be within one-tenth of a per cent of the computer result and the spatial fixed-point coordinate (for the unstable fixed points situated to the right and left of the symmetry axis at $\phi = 0$, mod. π) within 0.2 per cent; the corresponding fixed-point momentum is found to be somewhat less accurate, due to the enhanced contributions of error from the higher-frequency terms, the error being roughly 3% in this example.

*AEC Research and Development Report. Research supported by the Atomic Energy Commission, Contract No. AEC AT (11-1)-384.

**Department of Physics and Institute for Atomic Research, Iowa State College, Ames, Iowa.

A. INTRODUCTION

In a previous report[1*] solutions to the differential equation

$$\frac{d^2u}{d\phi^2} + (a + b \cos 2\phi) u + \frac{B_1}{2} (\sin 2\phi) u^2 = 0 \qquad (1)$$

were studied by the Moser method, after use of a suitable transformation to eliminate the alternating-gradient (A-G) character of the linear term. The limiting-amplitude solution was examined in this way for a particular example and the results compared with corresponding computer information.

Recently an interest has been expressed[2] in the use of a variational or harmonic-balance method to estimate the limiting-amplitude solution of eqn. (1), in a way which would parallel closely the application of this method in other papers[3] of this series and in earlier reports.[4] In the present report we apply this method to eqn. (1) and illustrate the results for the example which was previously employed in reference 1.

B. THE VARIATIONAL METHOD

As in earlier work,[3,4] the differential equation is replaced by a variational statement for purposes of determining the (periodic) unstable equilibrium orbit. In the case of eqn. (1), this statement is

$$\delta \left[\langle (u')^2 \rangle - a \langle u^2 \rangle - b \langle u^2 \cos 2\phi \rangle - (B_1/3) \langle u^3 \sin 2\phi \rangle \right] = 0, \qquad (2)$$

the prime denoting differentiation with respect to ϕ and the symbol $\langle\ \rangle$ denoting that the function embraced is to be averaged over one or more periods. The coefficient B_1 of eqn. (1) may, of course, be made unity by suitable scaling of the dependent variable u.

*References are given in Section D.

In selecting an adequate, but reasonably simple, trial function we note first that the dominant term in a development of the periodic solution controlled by the $\nu/N \rightarrow 1/3$ resonance would be expected to be of the form $A_1 \sin 2\phi/3$, the sine function being selected because of the predictable symmetry of the phase plots (at $\phi = 0$, mod. π) about the vertical axis. Because of the nature of the coefficient of the linear term in eqn. (1), this dominant term should be supplemented[5] by terms of argument $4\phi/3$ and $8\phi/3$, while the non-linear term suggests[3] supplementary terms of argument 2ϕ and $10\phi/3$. We select, therefore, the five-term trial function

$$u = A_1 \sin 2\phi/3 + A_2 \sin 4\phi/3 + A_3 \sin 2\phi + A_4 \sin 8\phi/3 + A_5 \sin 10\phi/3. \tag{3}$$

Substitution of the trial function (3) into the variational statement (2) leads to

$$\begin{aligned}\delta \Big\{ &(1/2)\left[(2/3)^2 - a\right] A_1^2 + (1/2)\left[(4/3)^2 - a\right] A_2^2 + (1/2)\left[(2)^2 - a\right] A_3^2 \\ &\qquad + (1/2)\left[(8/3)^2 - a\right] A_4^2 + (1/2)\left[(10/3)^2 - a\right] A_5^2 \\ &+ (b/2)\, A_1A_2 - (b/2)\, A_1A_4 - (b/2)\, A_2A_5 \\ &+ (1/24)\, A_1^3 - (1/4)\, A_1^2 A_3 + (1/8)\, A_1^2 A_5 \\ &- (1/8)\, A_1A_2^2 - (1/4)\, A_1A_2A_4 - (1/4)\, A_1A_3A_5 \\ &- (1/4)\, A_2^2A_3 - (1/4)\, A_2A_3A_4 - (1/4)\, A_2A_4A_5 \\ &- (1/8)\, A_3^3 - (1/4)\, A_3A_4^2 - (1/4)\, A_3A_5^2 - (1/8)\, A_4^2A_5 \Big\} = 0, \end{aligned} \tag{4}$$

where, for simplicity, we have set $B_1 = 1$.

By making the appropriate differentiations of eqn. (4), one then obtains the simultaneous non-linear algebraic equations

$$\left[(2/3)^2 - a\right] A_1 + \frac{b}{2} A_2 - \frac{b}{2} A_4 + \frac{1}{8} A_1^2 - \frac{1}{2} A_1A_3 + \frac{1}{4} A_1A_5 - \frac{1}{8} A_2^2 - \frac{1}{4} A_2A_4 - \frac{1}{4} A_3A_5 = 0$$

$$\left[(4/3)^2 - a\right] A_2 + \frac{b}{2} A_1 - \frac{b}{2} A_5 - \frac{1}{4} A_1A_2 - \frac{1}{4} A_1A_4 - \frac{1}{2} A_2A_3 - \frac{1}{4} A_3A_4 - \frac{1}{4} A_4A_5 = 0$$

$$\left[(2)^2 - a\right] A_3 - \frac{1}{4} A_1^2 - \frac{1}{4} A_1A_5 - \frac{1}{4} A_2^2 - \frac{1}{4} A_2A_4 - \frac{3}{8} A_3^2 - \frac{1}{4} A_4^2 - \frac{1}{4} A_5^2 = 0$$

$$\left[(8/3)^2 - a\right] A_4 - \frac{b}{2} A_1 - \frac{1}{4} A_1A_2 - \frac{1}{4} A_2A_3 - \frac{1}{4} A_2A_5 - \frac{1}{2} A_3A_4 - \frac{1}{4} A_4A_5 = 0$$

$$\left[(10/3)^2 - a\right] A_5 - \frac{b}{2} A_2 + \frac{1}{8} A_1^2 - \frac{1}{4} A_1A_3 - \frac{1}{4} A_2A_4 - \frac{1}{2} A_3A_5 - \frac{1}{8} A_4^2 = 0, \qquad (5)$$

which serve to determine the coefficients $A_1, \cdots A_5$.

C. NUMERICAL EXAMPLE

In the specific case taken as an example in reference 1, for which

$$a = 0.1262875 \qquad b = 1.15$$

$$\nu/N = 0.2997 \qquad B_1 = 1,$$

an approximate numerical solution of eqns. (5) leads to coefficients such that the trial solution assumes the form:

$$u = -0.5520 \sin 2\phi/3 + 0.1840 \sin 4\phi/3 + 0.0213 \sin 2\phi - 0.0497 \sin 8\phi/3 + 0.0057 \sin 10\phi/3 . \qquad (6)$$

This result may be compared with the Fourier analysis of the limiting-amplitude solution given by direct computational integration[1, 6] of eqn. (1), namely

$$u = -0.55231 \sin 2\phi/3 + 0.18429 \sin 4\phi/3 + 0.02167 \sin 2\phi - 0.04919 \sin 8\phi/3 + 0.00575 \sin 10\phi/3 + 0.00283 \sin 4\phi - 0.00140 \sin 14\phi/3 + \cdots . \qquad (7)$$

From comparison of eqns. (6) and (7) it is noted that the coefficients given in (6) agree through three decimal places with the computational result and the coefficient of the dominant sin $2\phi/3$ term is within one-tenth of one per cent of the value found computationally. From eqn. (6) the spatial fixed-point coordinate (for the unstable fixed points situated to the right and left of the symmetry axis at $\phi = 0$ mod. π) is obtainable within 0.2 per cent [cf. Table II of reference 1]. The corresponding fixed-point momenta are found to be somewhat less accurate, due to the enhanced contributions of error from the higher-frequency terms--including those omitted from eqn. (6)--the error being of the order of 3% in this example.

In summary, it appears that the use of a trial function of the form given in eqn. (3) permits one to obtain a reasonably accurate representation of the periodic solution to eqn. (1) with rather better accuracy and somewhat less complexity than by employing the methods outlined in reference 1. These latter more general methods, however, do of course permit additional features of solutions to equation (1) to be estimated analytically.

D. REFERENCES

1. L. Jackson Laslett, MURA-463 (June 3, 1959).
2. F. T. Cole, private communication (June 16, 1959).
3. L. Jackson Laslett, MURA-452 (April 13, 1959).

   L. Jackson Laslett, MURA-459 (May 20, 1959).
4. Cf. L. J. Laslett and A. M. Sessler, MURA-248 (1957).
5. Cf. L. Jackson Laslett and A. M. Sessler, MURA-252 (1957).
6. Integration of the differential equation (1) was accomplished with the MURA IBM 704 computer, by aid of the DUCK-ANSWER computational program [J. N. Snyder (IBM Program 75), MURA-237 (1957)]. Fourier analysis of periodic solutions is aided by use of the DUCKNALL program [John McNall (IBM Program 219), MURA-438 (1958)], which is based on the earlier FORANAL program [J. N. Snyder (IBM Program 52), MURA-228 (1957)].

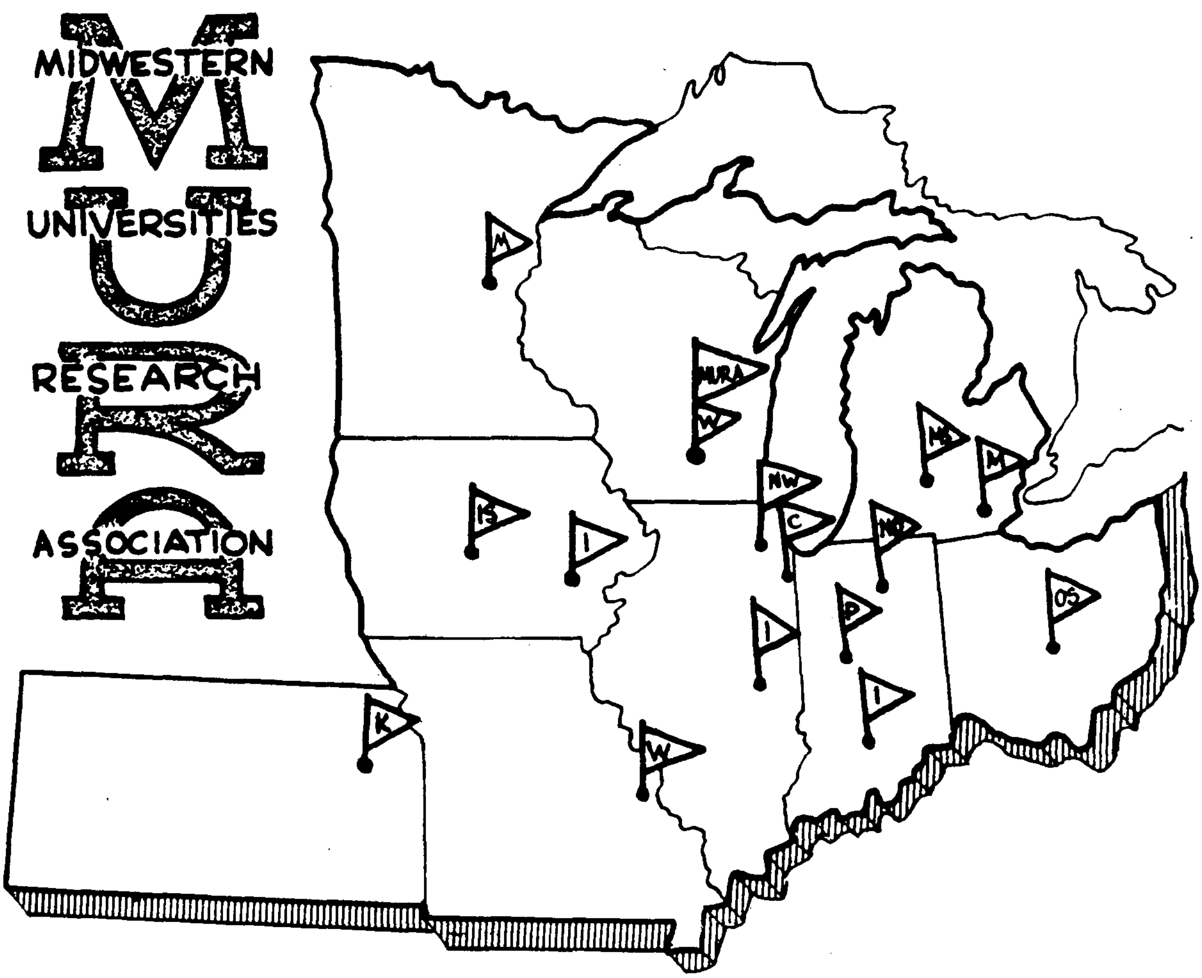

CONCERNING THE $\nu/N \rightarrow 1/3$ RESONANCE, V

ANALYSIS OF THE EQUATION

$$\frac{d^2v}{ds^2} + \left(\frac{2\nu}{N}\right)^2 v - \frac{b}{2}(\cos 2s)\, v^2 - \lambda \left(\cos \frac{2s}{3}\right) = 0$$

L. Jackson Laslett and Seymour J. Wolfson

REPORT NUMBER 497

MURA-497
Distribution List UC 28

MIDWESTERN UNIVERSITIES RESEARCH ASSOCIATION*
2203 University Avenue, Madison, Wisconsin

CONCERNING THE $\nu/N \rightarrow 1/3$ RESONANCE, V

ANALYSIS OF THE EQUATION

$$\frac{d^2v}{ds^2} + \left(\frac{2\nu}{N}\right)^2 v - \frac{b}{2}(\cos 2s)\, v^2 - \lambda\left(\cos\frac{2s}{3}\right) = 0$$

L. Jackson Laslett** and Seymour J. Wolfson***

August 17, 1959

ABSTRACT

An analytic and computational study has been made of the equation given in the title, specifically for the fixed points in the case $\nu/N = 0.3$, $b = 1.15$, and λ usually equal to 0.006. The equilibrium orbits and the fixed points are found to be obtainable quite accurately by a variational method or by use of harmonic balance if a numerical solution of the simultaneous algebraic equations for the coefficients of the trial function is performed. A straightforward application of the Moser procedure is seen to involve as a first step the elimination of the stable forced equilibrium motion--as is given by the appropriate trial-function solution--and the new differential equation is then found to involve an s-dependent (A-G) coefficient for the linear term. The solution is carried through, by continuation of the Moser method to the same order as in previous reports of this series, aided where appropriate by numerical work for the particular example considered. An alternative, and considerably simpler, analytic method similar to the Moser procedure is also examined and is found to lead to results of reasonable accuracy without requiring extensive numerical work. This last method also permits one to estimate without great effort the critical value of λ at which the stable fixed point and one of the unstable fixed points become coincident.

*Research supported by the Atomic EnergyCommission, Contract No. AT(11-1)-384.
**Department of Physics and Institute for Atomic Research, Iowa State University.
***Summer participant from Wayne State University, Detroit, Michigan.

CONTENTS

A MOTIVATION

Computer studies, to be reported in detail elsewhere, have been in progress to examine the regions of phase space from which injected particles may be captured into a stable region when a secularly-changing perturbation (decreasing field bump) is applied to an FFAG structure characterized, under certain simplifying assumptions, by a simple non-linear differential equation whose stability limits are determined by the $\nu/N \longrightarrow 1/3$ resonance. In parallel with the computer studies an analytic investigation has been made of unperturbed differential equations, similar to that employed in the computer work, and the results summarized in a series of MURA reports.[1, 2, 3*] It is the purpose of the present report to investigate in a somewhat similar way the character of solutions--particularly of the limiting-amplitude solutions--to an equation of this same form but containing a static perturbation (field bump free of secular change).

B. PROCEDURE

The differential equation which which we shall be concerned in the present report will be taken to be[4]

$$\frac{d^2v}{ds^2} + \left(\frac{2\nu}{N}\right)^2 v - \frac{b}{2}(\cos 2s)\, v^2 - \lambda \cos\frac{2s}{3} = 0. \qquad (1)$$

If one visualizes the application of the Moser procedure[5] to Eq. (1) in the spirit of previous reports in this series[1, 2, 3] one realizes that the first step which it

*References are given in Section I at the end of this report.

would be natural to undertake would be the removal of the forcing term $-\lambda \cos \frac{2s}{3}$, from Eq. (1).* This step which may be regarded as making a transformation of the dependent variable so as to measure displacements from the stable (forced) equilibrium orbit, appears to require, then, determination of this periodic solution (period 3π) by harmonic balance or some similar method. It may be remarked that the very steps which are then employed to determine this stable equilibrium orbit are substantially those which also can serve to give unstable equilibrium orbits and hence, to a degree, may provide the solution to the questions of major interest with respect to Eq. (1).

The elimination of the forcing term from Eq. (1) results, by this procedure, in the new differential equation containing a s-dependent (A-G) coefficient for the linear term, thus removing any simplification which it might have been supposed would result from selection of the simple non-AG coefficient for v in Eq. (1). A continuation of the analysis would then require removal of this A-G feature from the linear term, by a transformation of the dependent and independent variables through use of the function $\beta(s)$, in a manner paralleling that illustrated in a previous report.[3] Following completion of such preliminary steps it should then be possible to proceed with the Moser method, as it was applied in reference 2, to obtain results which may be interpreted in terms of the original variables after application of the appropriate reverse transformations.

It can be remarked, if one may anticipate, that the preliminary steps mentioned above can typically be performed with acceptable accuracy more

*The writer is indebted to Dr. F. T. Cole for discussions concerning the straightforward method of applying the Moser procedure to equations of the form of Eq. (1).

satisfactorily by numerical solution of the algebraic equations, which serve to specify the coefficients of the various functions which are required, than is possible conveniently by purely algebraic means. In view of this situation it is understandably difficult to expect that one can obtain satisfactory final results in a simple closed algebraic form.

In what follows we undertake to carry through the analytical procedure outlined above for a specific example, using numerical solutions of algebraic equations where desirable but attempting also to note approximate handy formulas which may serve to indicate roughly the magnitude of the quantities with which we are concerned. As a second undertaking, we also attempt to follow, in Section H, a somewhat less logical procedure which, it is hoped, may have some merit in circumventing the inconveniences mentioned above.

C. THE FORCED MOTION
(Stable Equilibrium Orbit)

The solution of equation (1) which describes the forced motion, or stable equilibrium orbit, may be sought by harmonic balance or by application of a variational procedure similar to that employed to find the periodic (unstable) solution to the equations of references 1 *et seq*. We thus replace Eq. (1) by the variational statement

$$\delta\left[\langle (dv/ds)^2\rangle - (2\nu/N)^2\langle v^2\rangle + (b/3)\langle v^3\cos 2s\rangle + 2\lambda\langle v\cos\frac{2s}{3}\rangle\right] = 0, \tag{2}$$

in which the symbol $\langle\,\rangle$ denotes that the average value of the embraced quantity is to be taken. For the present purpose a trial function of the form

$$v = A_1\cos 2s/3 + A_2\cos 2s + A_3\cos 10s/3 \tag{3}$$

is substituted into Eq. (2) to obtain

$$\delta\left\{\frac{1}{2}\left[\frac{4}{9}-\left(\frac{2\nu}{N}\right)^2\right]A_1^2+\frac{1}{2}\left[4-\left(\frac{2\nu}{N}\right)^2\right]A_2^2+\frac{1}{2}\left[\frac{100}{9}-\left(\frac{2\nu}{N}\right)^2\right]A_3^2\right.$$
$$+\frac{b}{24}A_1^3+\frac{b}{4}A_1^2A_2+\frac{b}{4}A_1A_2A_3+\frac{b}{8}A_1^2A_3$$
$$\left.+\frac{b}{8}A_2^3+\frac{b}{4}A_2A_3^2+\lambda A_1\right\}=0, \tag{4}$$

or

$$\left[\frac{4}{9}-\left(\frac{2\nu}{N}\right)^2\right]A_1+\frac{b}{8}A_1^2+\frac{b}{2}A_1A_2+\frac{b}{4}A_1A_3+\frac{b}{4}A_2A_3=-\lambda \tag{5a}$$

$$\left[4-\left(\frac{2\nu}{N}\right)^2\right]A_2+\frac{b}{4}A_1^2+\frac{3b}{8}A_2^2+\frac{b}{4}A_1A_3+\frac{b}{4}A_3^2=0 \tag{5b}$$

$$\left[\frac{100}{9}-\left(\frac{2\nu}{N}\right)^2\right]A_3+\frac{b}{8}A_1^2+\frac{b}{4}A_1A_2+\frac{b}{2}A_2A_3=0\,. \tag{5c}$$

Equations (5a-c) admit, of course, the solution $A_1 = A_2 = A_3 = 0$ when $\lambda = 0$, corresponding to the equilibrium orbit $v \equiv 0$ which applies in that case; with λ not necessarily zero, the corresponding solution is such that

$$A_1 \cong -\frac{\lambda}{4/9-(2\nu/N)^2}\,, \tag{6a}$$

with

$$A_2 \cong -\frac{b}{4}\,\frac{1}{4-(2\nu/N)^2}\,A_1^2 \tag{6b}$$

and

$$A_3 \cong -\frac{b}{8}\,\frac{1}{100/9-(2\nu/N)^2}\,A_1^2\,. \tag{6c}$$

Somewhat more satisfactory results than can be obtained conveniently from Eqs. (5a-c) by algebraic means are obtainable numerically--in the particular case that

$$\nu/N = 0.3 \tag{7a}$$

$$b = 1.15 \tag{7b}$$

$$\lambda = 0.006 \tag{7c}$$

we find values of A_1, A_2, A_3 such that

$$v = -0.0831620 \cos 2s/3 - 0.0005469 \cos 2s - 0.0000937 \cos 10s/3, \qquad (8a)$$

while a computer investigation[6] leads to the result

$$v = -0.083160_4 \cos 2s/3 - 0.000546_7 \cos 2s - 0.000093_7 \cos 10s/3. \qquad (8b)$$

The corresponding location of the stable fixed point, for $s = 0$ (mod. 3π), is at

$$v = -.083802_6 \quad \text{from Eq. (8a)}$$

and at

$$v = -.083802_3 \quad \text{from direct computer studies.}$$

The results of the numerical solution of Eqs. (5a-c) are thus found to be in excellent agreement with the computer results, while the stable fixed point computed from the simple forms (6a-c) would be $-.07105 - .00040 - .00007 = -.07152$, or about 85% of the correct value.

D. LIMITING-AMPLITUDE SOLUTIONS
(Unstable Periodic Orbits)

1.

In addition to the solution of Eqs. (5a-c) discussed in the previous section, these equations admit a second solution--a solution with which the unstable fixed point lying on the symmetry axis of the phase plot (for $s = 0$, mod. 3π) is associated. The coefficients given by this second solution have values given roughly by

$$A_1 \cong \frac{-8\left[\frac{4}{9} - \left(\frac{2\nu}{N}\right)^2\right]}{b} + \frac{\lambda}{\frac{4}{9} - \left(\frac{2\nu}{N}\right)^2} \qquad (9a)$$

(in which the first term should represent the value of A_1 for $\lambda = 0$), and

$$A_2 \cong - \frac{b}{4} \frac{1}{4 - (2\nu/N)^2} A_1^2 \tag{9b}$$

$$A_3 \cong - \frac{b}{8} \frac{1}{100/9 - (2\nu/N)^2} A_1^2 , \tag{9c}$$

[as in (6b, c)].

A numerical solution of Eqs. (5a-c), for the parameters taken previously [Eqs. (7a-c)], leads to the solution (unstable periodic orbit)

$$v = - 0.426294 \cos 2 s/3 - 0.014466 \cos 2 s - 0.002597 \cos 10 s/3, \tag{10a}$$

whereas a computer investigation leads to the result

$$v = - 0.426274 \cos 2 s/3 - 0.014468 \cos 2 s - 0.002598 \cos 10 s/3$$
$$- 0.000098 \cos 14 s/3 - 0.000010 \cos 18 s/3 - \cdots . \tag{10b}$$

The corresponding fixed-point location (for $s = 0$, mod. 3π) is

$v = - 0.443357$ from Eq. (10a)

and

$v = - 0.443449$ from direct computer studies.

With a stronger perturbation (larger λ) this unstable fixed point and the stable fixed point will approach one another.

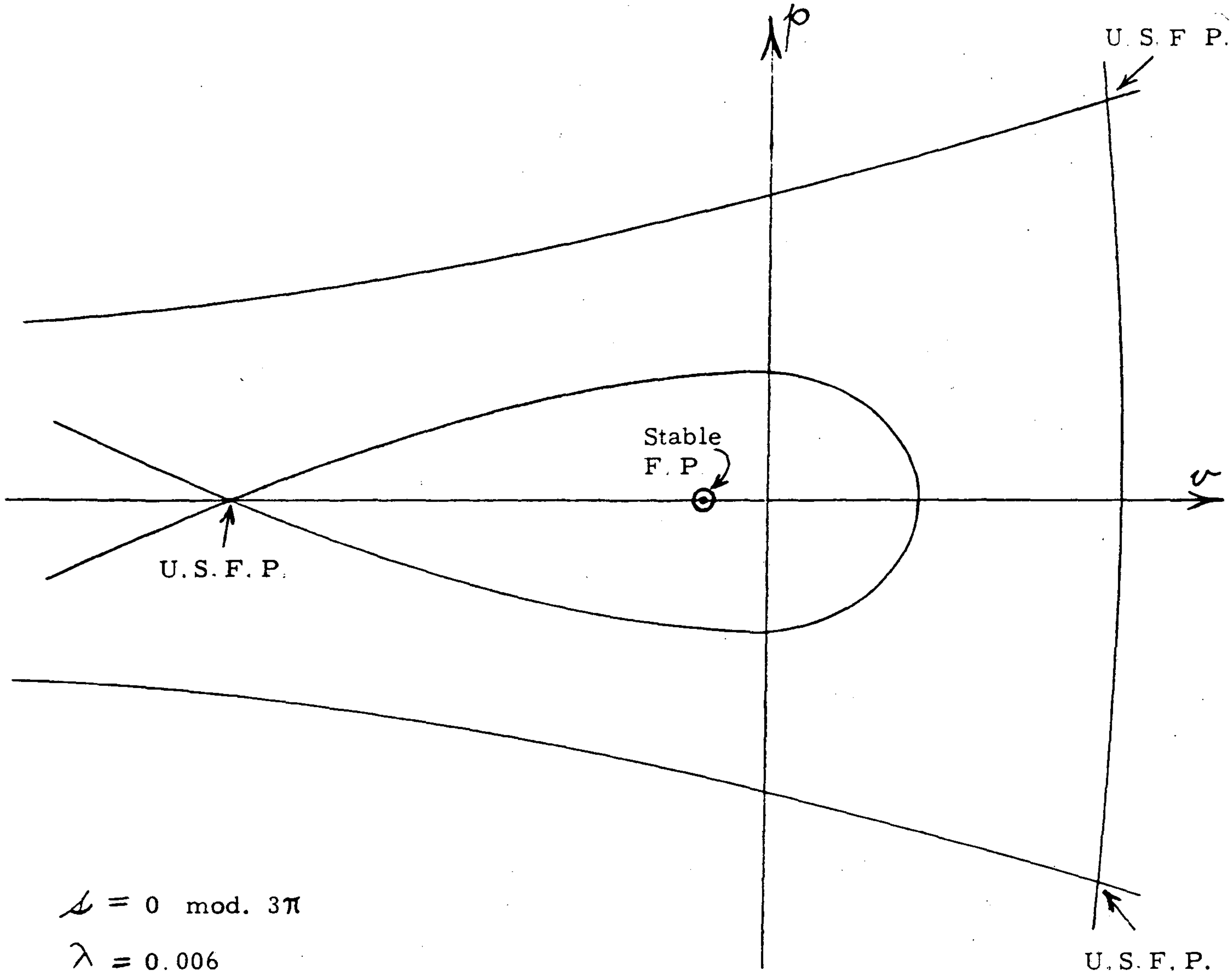

2.

To determine in this same way the locations of the other unstable fixed points--those situated above and below the symmetry axis of the $s = 0$, mod. 3π, phase plot-- a trial function more general than that shown in

Eq (3) must be employed.* For this purpose we may employ the periodic trial function

$$v = A_1 \cos 2\, s/3 + A_2 \cos 2\, s + A_3 \cos 10\, s/3$$
$$\pm\, (B_1 \sin 2\, s/3 + B_2 \sin 2\, s + B_3 \sin 10\, s/3) \tag{11}$$

which, upon introduction into the variational statement (2) leads to

$$\delta \Big\{ \tfrac{1}{2}\left[\tfrac{4}{9} - \left(\tfrac{2\nu}{N}\right)^2\right](A_1^2 + B_1^2) + \tfrac{1}{2}\left[4 - \left(\tfrac{2\nu}{N}\right)^2\right](A_2^2 + B_2^2) + \tfrac{1}{2}\left[\tfrac{100}{9} - \left(\tfrac{2\nu}{N}\right)^2\right](A_3^2 + B_3^2)$$
$$+ \tfrac{b}{24} A_1^3 + \tfrac{b}{4} A_1^2 A_2 + \tfrac{b}{8} A_1^2 A_3 + \tfrac{b}{4} A_1 A_2 A_3 + \tfrac{b}{8} A_2^3 + \tfrac{b}{4} A_2 A_3^2$$
$$- \tfrac{b}{8} A_1 B_1^2 + \tfrac{b}{4} A_1 B_1 B_3 + \tfrac{b}{4} A_1 B_2 B_3$$
$$+ \tfrac{b}{4} A_2 B_1^2 - \tfrac{b}{4} A_2 B_1 B_3 + \tfrac{b}{4} A_2 B_3^2 - \tfrac{b}{8} A_2 B_2^2$$
$$- \tfrac{b}{8} A_3 B_1^2 + \tfrac{b}{4} A_3 B_1 B_2 + \lambda A_1 \Big\} \quad 0 \tag{12}$$

or

$$\left[\tfrac{4}{9} - \left(\tfrac{2\nu}{N}\right)^2\right] A_1 + \tfrac{b}{8} A_1^2 + \tfrac{b}{2} A_1 A_2 + \tfrac{b}{4} A_1 A_3 + \tfrac{b}{4} A_2 A_3$$
$$- \tfrac{b}{8} B_1^2 + \tfrac{b}{4} B_1 B_3 + \tfrac{b}{4} B_2 B_3 \quad -\lambda \tag{13a}$$

$$\left[4 - \left(\tfrac{2\nu}{N}\right)^2\right] A_2 + \tfrac{b}{4} A_1^2 + \tfrac{b}{4} A_1 A_3 + \tfrac{3b}{8} A_2^2 + \tfrac{b}{4} A_3^2$$
$$+ \tfrac{b}{4} B_1^2 - \tfrac{b}{4} B_1 B_3 + \tfrac{b}{8} B_2^2 + \tfrac{b}{4} B_3^2 \quad 0 \tag{13b}$$

---

*It may be noted that, in contrast to cases discussed in previous reports (e.g., ref 1), the basic period of the coefficients in the differential equation is 3π when the perturbation is present and the locations of the various fixed points are no longer obtainable from a single periodic solution by substitution in turn of values of the independent variable differing by π from one another

$$\left[\frac{100}{9} - \left(\frac{2\nu}{N}\right)^2\right] A_3 + \frac{b}{8} A_1^2 + \frac{b}{4} A_1 A_2 + \frac{b}{2} A_2 A_3 - \frac{b}{8} B_1^2 + \frac{b}{4} B_1 B_2 = 0 \qquad (13c)$$

$$\left[\frac{4}{9} - \left(\frac{2\nu}{N}\right)^2\right] B_1 - \frac{b}{4} A_1 B_1 + \frac{b}{4} A_1 B_3 + \frac{b}{2} A_2 B_1 - \frac{b}{4} A_2 B_3 - \frac{b}{4} A_3 B_1 + \frac{b}{4} A_3 B_2 = 0 \qquad (13d)$$

$$\left[4 - \left(\frac{2\nu}{N}\right)^2\right] B_2 + \frac{b}{4} A_1 B_3 + \frac{b}{4} A_2 B_2 + \frac{b}{4} A_3 B_1 = 0 \qquad (13e)$$

$$\left[\frac{100}{9} - \left(\frac{2\nu}{N}\right)^2\right] B_3 + \frac{b}{4} A_1 B_1 + \frac{b}{4} A_1 B_2 - \frac{b}{4} A_2 B_1 + \frac{b}{2} A_2 B_3 \doteq 0 . \qquad (13f)$$

Possible solutions of Eqs. (13a-f) are of course given by $B_1 = B_2 = B_3 = 0$ with A_1, A_2, A_3 then being solutions of Eqs. (5a-c); the new results which are obtained by admitting the case in which not all the coefficients B_i vanish will have, very roughly,

$$A_1 \cong \frac{4\left[\frac{4}{9} - \left(\frac{2\nu}{N}\right)^2\right]}{b} \qquad (14a)$$

$$B_1 \cong \frac{4\sqrt{3}\left[\frac{4}{9} - \left(\frac{2\nu}{N}\right)^2\right]}{b} \sqrt{1 + \frac{b\lambda}{6\left[\frac{4}{9} + \left(\frac{2\nu}{N}\right)^2\right]^2}} \qquad (14b)$$

$$\cong \frac{4\sqrt{3}\left[\frac{4}{9} - \left(\frac{2\nu}{N}\right)^2\right]}{b} + \frac{1}{\sqrt{3}} \frac{\lambda}{\left[\frac{4}{9} - \left(\frac{2\nu}{N}\right)^2\right]} \qquad (14b')$$

A numerical solution of Eqs. (13a-f). again for the parameters specified by Eqs. (7a-c), suggests a solution

$$v = 0.244637 \cos 2s/3 - 0.022431 \cos 2s + 0.002307 \cos 10s/3$$
$$\pm (0.470329 \sin 2s/3 - 0.000021 \sin 2s - 0.003362 \sin 10s/3), \qquad (15a)$$

while a computer investigation gives the corresponding result

$$v = 0.244624 \cos 2\, s/3 - 0.022434 \cos 2\, s + 0.002309 \cos 10\, s/3$$
$$+ 0.000087 \cos 14\, s/3 - 0.000020 \cos 6\, s + \cdots$$
$$\pm (0.0470300 \sin 2\, s/3 - 0.000021 \sin 2\, s - 0.003365 \sin 10\, s/3$$
$$+ 0.000168 \sin 14\, s/3 - 0.000002 \sin 6\, s + \cdots) \qquad (15b)$$

The corresponding fixed-point coordinates (for $s = 0$, mod. 3π) are

$$\left.\begin{aligned} v &= 0.224513 \\ p &= \pm\, 0.3023 \end{aligned}\right\} \quad \text{from Eq. (15a)}$$

and

$$\left.\begin{aligned} v &= 0.224566 \\ p &= \pm\, 0.3030 \end{aligned}\right\} \quad \text{from direct computer studies.}$$

The methods described in this section evidently are able to give a good representation of the unstable periodic solutions for the differential equation (1). For the present, however, we shall regard this section as a diversion and proceed with the results of Section C to effect a removal of the forcing term from (1) and so permit a continuation of the analysis in the manner outlined in Section B.

E. REMOVAL OF FORCING TERM AND DETERMINATION OF β (s)

1.

If we denote by v_s the stable periodic orbit resulting from the forcing term $- \lambda \cos \frac{2\,s}{3}$ in Eq. (1), with v_s taken as well given by expressions presented in Section C [e.g., Eq. (3), with coefficients as illustrated in Eqs. (8a, b)], we may write

$$v = v_s + q \qquad (16)$$

and transform Eq. (1) to the form

$$\frac{d^2q}{ds^2} + \left[\left(\frac{2\nu}{N}\right)^2 - b\,(\cos 2\,s)\,v_s\right] q - \frac{b}{2}\,(\cos 2\,s)\,q^2 = 0 \tag{17a}$$

or, making use of (3),

$$\frac{d^2q}{ds^2} + \left[\left(\frac{2\nu}{N}\right)^2 - \frac{bA_2}{2} - b\,\frac{A_1 + A_3}{2}\cos\frac{4\,s}{3} - b\,\frac{A_1}{2}\cos\frac{8\,s}{3} - b\,\frac{A_2}{2}\cos 4\,s - b\frac{A_3}{2}\cos\frac{16\,s}{3}\right] q$$
$$- \frac{b}{2}\,(\cos 2\,s)\,q^2 = 0 \tag{17b}$$

in which the terms of primary importance in the coefficient of q would normally be

$$\left(\frac{2\nu}{N}\right)^2 - \frac{bA_2}{2}\,, \quad -\frac{b\,A_1}{2}\cos\frac{4\,s}{3}\,, \text{ and } -\frac{b\,A_1}{2}\cos\frac{8\,s}{3}\,.$$

With the coefficients of v_s found in Section C by numerical methods [cf. Eq. (8a)], for the parameters specified by Eqs. (7a-c), the differential equation (17b) for q becomes

$$\frac{d^2q}{ds^2} + \left[0.3603\,145 + 0.0478\,720\cos\frac{4\,s}{3} + 0.0478\,182\cos\frac{8\,s}{3}\right.$$
$$\left. + 0.0003\,145\cos 4\,s + 0.0000\,539\cos\frac{16\,s}{3}\right] q$$
$$- 0.575\,(\cos 2\,s)\,q^2 = 0. \tag{18}$$

2.

It is of some interest to estimate the small-amplitude oscillation frequency ν_λ for Eq. (18), and it is necessary for what follows to describe the variation of the function β which characterizes the solutions of the linearized equation. To this end it is convenient to introduce a change of scale for the independent variable,

$$\tau = \frac{2}{3}\,s \tag{19}$$

and consider the linearized equation

$$\frac{d^2q}{d\tau^2} + (a + b \cos 2\tau + c \cos 4\tau)\, q \doteq 0 \tag{20}$$

with, in the case corresponding to Eq. (18),

$$a = 0.810\,708 \tag{21a}$$

$$b = 0.107\,712 \tag{21b}$$

$$c = 0.107\,591 \tag{21c}$$

(the coefficients of the higher-order terms, $\cos 6\tau$ and $\cos 8\tau$, being ignored).

(i) It is tempting to attempt to estimate the oscillation frequency for Eq. (20) by means of the "smooth approximation"--since the value of ν_λ for Eq. (18) is not very far from $\frac{2}{3}$ and hence the corresponding value, ν', for Eq (20) not far from unity (σ' near π), however, this method would be inappropriate A possible, relatively quick, estimate may be obtained by reference to available ILLIAC tables[7] from which one finds

$$\cos \nu'\pi \cong \cos \sqrt{a}\,\pi - 0.36\, b^2 - 0.022\, c^2 \tag{22}$$

for b and c small, $\sqrt{a}$ in the neighborhood of 0.9, and with ν' denoting $\frac{3}{2}\nu_\lambda$ in the present application. With the particular coefficients of interest here [Eqs. (21a-c)], the expression (22) gives $\nu' = 0.9051$, or $\nu_\lambda = 0.6034$, in complete agreement with the value found by direct computation[4, 6a] for $\lambda = 0.006$. Alternatively, a somewhat less arbitrary estimate may be made in connection with an examination of the range of variation of β, to be discussed below.

(ii) The differential equation (20) is of the form

$$\frac{d^2q}{d\tau^2} + (a + b \cos N\tau + c \cos 2N\tau)\, q = 0, \tag{20'}$$

with N = 2. As has been noted previously,[8] a rather accurate solution may be found by use of the trial function

$$q = g_0 \cos \nu'\tau + f_1 \cos (N - \nu')\tau + g_1 \cos (N + \nu')\tau + f_2 \cos (2N - \nu')\tau + g_2 \cos (2N + \nu')\tau \tag{23}$$

and use of harmonic balance.* There results in this way the algebraic equations

$$a - \nu'^2 + \frac{b}{2}(f_1 + g_1) + \frac{c}{2}(f_2 + g_2) = 0 \tag{24a}$$

$$\left[a - (N - \nu')^2\right] f_1 + \frac{b}{2}(1 + f_2) + \frac{c}{2} g_1 = 0 \tag{24b}$$

$$\left[a - (N + \nu')^2\right] g_1 + \frac{b}{2}(1 + g_2) + \frac{c}{2} f_1 = 0 \tag{24c}$$

$$\left[a - (2N - \nu')^2\right] f_2 + \frac{b}{2} f_1 + \frac{c}{2} = 0 \tag{24d}$$

$$\left[a - (2N + \nu')^2\right] g_2 + \frac{b}{2} g_1 + \frac{c}{2} = 0 . \tag{24e}$$

Guided by prior knowledge of at least an approximate value of ν' a numerical solution of Eqs. (24a-e) is readily obtained, leading in the present case [coefficients given by Eqs. (21a-c)] to

$$f_1 = 0.1408\,59 \tag{25a}$$

$$g_1 = 0.0080\,69 \tag{25b}$$

$$f_2 = 0.0070\,01 \tag{25c}$$

$$g_2 = 0.0023\,3\dot{3} \tag{25d}$$

and

$$\nu' \doteq 0.9051 \qquad (\nu_\lambda \doteq 0.6034) . \tag{25e}$$

The extreme values of $\nu'\beta(\tau)$, and hence of the quantity $\nu_\lambda\beta(s)$ for Eq. (18), are given by[8]

$$\left[\nu_\lambda \beta\right] = \frac{1 \pm (f_1 + g_1) + (f_2 + g_2)}{1 \mp \left[\left(\frac{N}{\nu'} - 1\right) f_1 - \left(\frac{N}{\nu'} + 1\right) g_1\right] - \left[\left(\frac{2N}{\nu'} - 1\right) f_2 - \left(\frac{2N}{\nu'} + 1\right) g_2\right]} , \tag{26}$$

*We here omit, for simplicity, the phase shift (denoted by ϵ in ref. 8) which permits one to form in this way a general solution.

the upper and lower signs referring respectively to s = 0 (τ = 0) and s = 3π/4 (τ = π/2)--the range of values for $\nu_\lambda \beta$ suggested by the numerical values of f_1 etc. given in Eqs. (25a-e) is, then

$$0.759 \leqslant \nu_\lambda \beta \leqslant 1.372 . \tag{27a}$$

These limits, (27a), are within a few tenths of a percent of the computational values.

$$0.7578 \leqslant \nu_\lambda \beta \leqslant 1.3755 . \tag{27b}$$

It appears to be quite tedious to derive $\nu' \beta (\tau)$ as a function of τ from the solution q (τ) as expressed by Eq. (23)--on the supposition that the variation is a pure cosine function; however, one might write roughly

$$\nu_\lambda \beta \cong 1.066 + 0.306 \cos 4 s/3. \tag{28a}$$

A corresponding very approximate formula, based on taking $f_1 \cong \dfrac{b}{8(1 - \nu')}$ and ignoring g_1, · · · , might be written

$$\nu_\lambda \beta \cong 1 + \frac{b}{4(1 - \nu')} \cos 4 s/3 \quad \text{or} \quad 1 + \frac{b}{2(1 - a)} \cos 4 s/3 \tag{28b}$$

which, in the present example, would lead to

$$\nu_\lambda \beta \cong 1 + 0.284 \cos 4 s/3 \tag{28b'}$$

A more satisfactory evaluation of the functional dependence of may be sought by reference to the differential equation which is satisfied by β :*

$$\frac{\beta}{2} \frac{d^2 \beta}{d \tau^2} - \frac{1}{4}\left(\frac{d\beta}{d\tau}\right)^2 + (a + b \cos 2\tau + c \cos 4\tau)\beta^2 = 1 . \tag{29}$$

A functional dependence

$$\beta = A + B \cos 2\tau + C \cos 4\tau \tag{30}$$

*Cf. Eq. (8) of reference 3

may be inserted into Eq (29) and the coefficients adjusted by harmonic balance to obtain the set of simultaneous equations

$$a A^2 - \frac{6 - 2a - c}{4} B^2 - (6 - \frac{a}{2}) C^2 + b A B + \frac{b}{2} B C + c A C = 1 \quad (31a)$$

$$- 2 (1 - a - \frac{c}{2}) A B - (7 - a - c) B C + b (A^2 + \frac{3}{4} B^2 + \frac{1}{2} C^2 + A C) = 0 \quad (31b)$$

$$- 2 (4 - a) A C - \frac{1 - a - c}{2} B^2 + b (A B + B C) + c A^2 + \frac{3}{4} c C^2 = 0 . \quad (31c)$$

For the parameters a, b, c as given by Eqs. (21a-c), a numerical solution of Eqs. (31a-c) leads to

$$A \doteq 1.1536 \quad (32a)$$

$$B = 0.3365 \quad (32b)$$

$$C = 0.024\dot{7} ; \quad (32c)$$

substitution of these values into the expression (30) and multiplication by ν' (= 0.9051)* leads to the result

$$\nu/\beta = 1.044 + 0.305 \cos 4 s/3 + 0.022 \cos 8 s/3 . \quad (33a)$$

The results of a computer analysis of this case leads to

$$\nu/\beta = 1.045\,01 + 0.307\,35 \cos 4 s/3 + 0.021\,56 \cos 8 s/3$$

$$+ 0.001\,51 \cos 4 s + 0.000\,06_6 \cos 16 s/3 , \quad (33b)$$

with which the numerical result (33a) is in reasonable agreement.

F. ELIMINATION OF THE A-G COEFFICIENT FROM THE LINEAR TERM AND CONTINUATION OF THE MOSER METHOD

1.

For continuation of the analysis of Eq. (18), it is convenient to introduce the independent variable

*By use of the values (32a-c) in connection with Eq. (30), a value of ν' could be estimated from this solution for β by forming $\nu' = \langle 1/\beta \rangle$.

$$t = \tau/2 = s/3 \qquad (34)$$

to obtain

$$\frac{d^2q}{dt^2} + 4\,(a + b\cos 4\,t + c\cos 8\,t + \cdots)\,q - 5.175\,(\cos 6\,t)\,q^2 = 0. \qquad (35)$$

As in an example presented previously [Sect. B of ref. 3], the transformation[9]

$$Q = q/\sqrt{\nu\beta} \qquad (36a)$$

$$T = \int_0^t \frac{dt}{\nu\beta} \qquad (36b)$$

enables one to eliminate the A-G aspect of the coefficient of the linear term in Eq. (34), to obtain:

$$\frac{d^2Q}{dT^2} + \nu''^2\,Q - 5.175\,(\nu\beta)^{5/2}\,(\cos 6\,t)\,Q^2 = 0\,, \qquad (37)$$

in which $\nu'' = 2\,\nu' = 2\,(0.9051) = 1.8102$. The variables t and T become equal at $t = 0$, $\pi/4$, $\pi/2$, $3\pi/4$, π, etc. The quantity $(\nu\beta)^{5/2}\cos 6\,t$, if expressed[6b, 10] in terms of T (Fig. 1), permits Eq. (37) to be written

$$\frac{d^2Q}{dT^2} + 3.2768\,Q - \Big[1.03504\cos 2\,T + 5.41441\cos 6\,T + 3.05511\cos 10\,T + 1.26600\cos 14\,T + 0.46114\cos 18\,T + 0.15573\cos 22\,T + 0.04940\cos 26\,T + 0.01441\cos 30\,T + \cdots\Big]\,Q^2 = 0\,. \qquad (38)$$

It may be helpful to note that, with ν'' near 2, the oscillations will have a phase change of about 2π in one period of the term $1.03504\cos 2\,T$ (as for an integral resonance) and a phase change near $2\pi/3$ in one period of the (larger) term $5.41441\cos 6\,T$ (third-integral resonance). Accordingly, as we shall indicate in the work to follow, in undertaking to remove by the Moser method[5] the T-dependence from the Hamiltonian associated with Eq. (38) special attention must be given both to terms stemming from the $\cos 2\,T$ term above and to those stemming from $\cos 6\,T$, in order to avoid potentially-resonant denominators.

Solutions for the unstable equilibrium orbits associated with Eq. (38) could, of course, be sought by harmonic balance, although this procedure would be of value only as a check of the preceding work since the original equation [Eq. (1)] was already treated satisfactorily by this method in earlier sections (Sects. C and D). Thus one solution of Eq. (38) may be sought in the form

$$Q = C_1 \cos 2T + C_2 \cos 6T + C_3 \cos 10T ,$$

in which, approximately,

$$A_1 = -0.29519, \; A_2 = -0.01036, \text{ and } A_3 = -0.00303;$$

accordingly the corresponding fixed point for Q (at $T = 0$) is at $Q = -0.30858$, $q = \sqrt{2\beta}\, Q = 1.17282 \cdot (-0.30858) = -0.36191$, and $v = v_s + q = -0.08380 - 0.36191 = -0.44571$, which is in error by about one-half of one percent of the computer fixed point. As a further check, a direct computational determination of the unstable fixed points for Eq. (38) was made, retaining just the first four cosine terms in the coefficient of Q^2; the values of (Q, P) found in this way were $(-0.307_{29}, 0)$ and $(0.263, \pm 1.064)$, which correspond to values of (v, p) which are $(-0.444_{20}, 0)$ and $(0.224_{65}, \pm 0.3024_{05})$ and thus are in good agreement with the results $(-0.44345, 0)$ and $(0.2246, \pm 0.3030)$ reported previously (Sect. D) from direct computer studies of Eq. (1).

In the subsection to follow we continue with the Moser procedure, which is of greater versatility than the harmonic-balance methods of Sects. C and D, applying the Moser method to Eq. (38) and then deducing in particular the fixed points in this way.

The Hamiltonian associated with Eq. (38) is

$$H = \frac{1}{2} P^2 + \frac{1}{2} \nu''^2 Q^2 - \frac{1}{3} (b_1 \cos 2T + b_2 \cos 6T + \cdots + b_j \cos 2(2j-1)T + \cdots) Q^3 \tag{39}$$

where P denotes dQ/dT, $\nu'' = 1.8102$, $b_1 = 1.03504$, $b_2 = 5.41441$, etc. As in previous reports,[1-3] we now employ the generating function

$$G_o(Q, \gamma_o) = (\nu''/2) Q^2 \operatorname{ctn} \gamma_o \tag{40}$$

to effect the transformation

$$P = \partial G_o / \partial Q = \nu'' Q \operatorname{ctn} \gamma_o \tag{41a}$$

$$J_o = - \partial G_o / \partial \gamma_o = (\nu''/2) Q^2 \csc^2 \gamma_o ; \tag{41b}$$

thus

$$\operatorname{ctn} \gamma_o = \frac{1}{\nu''} \frac{P}{Q} \tag{42a}$$

$$J_o = \frac{1}{2\nu''} P^2 + \frac{\nu''}{2} Q^2 \tag{42b}$$

$$Q = (2/\nu'')^{1/2} J_o^{1/2} \sin \gamma_o \tag{42c}$$

$$P = (2\nu'')^{1/2} J_o^{1/2} \cos \gamma_o , \tag{42d}$$

and the new Hamiltonian is

$$\begin{aligned} K_o &= H + \partial G_o / \partial T \\ &= H \\ &= \nu'' J_o - \frac{1}{3} \left(\frac{2}{\nu''}\right)^{3/2} J_o^{3/2} \sin^3 \gamma_o \sum_{j=1} b_j \cos 2(2j-1)T \end{aligned}$$

$$= \nu'' J_o - \frac{1}{24} \left(\frac{2}{\nu''}\right)^{3/2} J_o^{3/2} \sum_{j=1} b_j \left\{ \begin{array}{l} 3\sin\left[\gamma_o + 2(2j-1)T\right] + 3\sin\left[\gamma_o - 2(2j-1)T\right] \\ -\sin\left[3\gamma_o + 2(2j-1)T\right] - \sin\left[3\gamma_o - 2(2j-1)T\right] \end{array} \right\}. \tag{43}$$

As a second generating function we next employ

$$G_1(\gamma_0, J_1) = J_1 \cdot \gamma_0 - \frac{1}{24}\left(\frac{2}{\nu''}\right)^{3/2} J_1^{3/2} \sum_{j=1} b_j \left\{ \begin{array}{l} 3\,\dfrac{\cos[\gamma_0 + 2(2j-1)T]}{\nu'' + 2(2j-1)} + 3(1-\delta_j^1)\,\dfrac{\cos[\gamma_0 - 2(2j-1)T]}{\nu'' - 2(2j-1)} \\ -\dfrac{\cos[3\gamma_0 + 2(2j-1)T]}{3\nu'' + 2(2j-1)} - (1-\delta_j^2)\,\dfrac{\cos[3\gamma_0 - 2(2j-1)T]}{3\nu'' - 2(2j-1)} \end{array} \right\}, \quad (44)$$

in which the Kronecker delta, δ_j^1 or δ_j^2, serves to eliminate terms which, with j = 1 or j = 2, would lead to terms with potentially-resonant denominators. The transformation equations which result from the generating function $G_1(\gamma_0, J_1)$ are

$$J_0 = \partial G_1 / \partial \gamma_0$$

$$= J_1 + \frac{1}{8}\left(\frac{2}{\nu''}\right)^{3/2} J_1^{3/2} \sum_{j=1} b_j \left\{ \begin{array}{l} \dfrac{\sin[\gamma_0 + 2(2j-1)T]}{\nu'' + 2(2j-1)} + (1-\delta_j^1)\,\dfrac{\sin[\gamma_0 - 2(2j-1)T]}{\nu'' - 2(2j-1)} \\ -\dfrac{\sin[3\gamma_0 + 2(2j-1)T]}{3\nu'' + 2(2j-1)} - (1-\delta_j^2)\,\dfrac{\sin[3\gamma_0 - 2(2j-1)T]}{3\nu'' - 2(2j-1)} \end{array} \right\} \quad (45a)$$

$$\gamma_1 = \partial G_1 / \partial J_1$$

$$= \gamma_0 - \frac{1}{16}\left(\frac{2}{\nu''}\right)^{3/2} J_1^{1/2} \sum_{j=1} b_j \left\{ \begin{array}{l} 3\,\dfrac{\cos[\gamma_0 + 2(2j-1)T]}{\nu'' + 2(2j-1)} + 3(1-\delta_j^1)\,\dfrac{\cos[\gamma_0 - 2(2j-1)T]}{\nu'' - 2(2j-1)} \\ -\dfrac{\cos[3\gamma_0 + 2(2j-1)T]}{3\nu'' + 2(2j-1)} - (1-\delta_j^2)\,\dfrac{\cos[3\gamma_0 - 2(2j-1)T]}{3\nu'' - 2(2j-1)} \end{array} \right\}, \quad (45b)$$

with the new Hamiltonian

$$K_1 = K_0 + \partial G_1 / \partial T$$

$$= \nu'' J_1 + \frac{1}{4}\left(\frac{2}{\nu''}\right)^{1/2} J_1^{3/2} \sum_{j=1} b_j \left\{ \begin{array}{l} \dfrac{\sin[\gamma_0 + 2(2j-1)T]}{\nu'' + 2(2j-1)} + (1-\delta_j^1)\,\dfrac{\sin[\gamma_0 - 2(2j-1)T]}{\nu'' - 2(2j-1)} \\ -\dfrac{\sin[3\gamma_0 + 2(2j-1)T]}{3\nu'' + 2(2j-1)} - (1-\delta_j^2)\,\dfrac{\sin[3\gamma_0 - 2(2j-1)T]}{3\nu'' - 2(2j-1)} \end{array} \right\}$$

$$
-\frac{1}{24}\left(\frac{2}{\nu''}\right)^{3/2}\left[J_1^{3/2}+\frac{3}{16}\left(\frac{2}{\nu''}\right)^{3/2}J_1^{2}\sum_{j=1}b_j\left\{\begin{array}{l}\dfrac{\sin[\gamma_0+2(2j-1)T]}{\nu''+2(2j-1)}+(1-\delta_j^1)\dfrac{\sin[\gamma_0-2(2j-1)T]}{\nu''-2(2j-1)}\\[2ex]-\dfrac{\sin[3\gamma_0+2(2j-1)T]}{3\nu''+2(2j-1)}-(1-\delta_j^2)\dfrac{\sin[3\gamma_0-2(2j-1)T]}{3\nu''-2(2j-1)}\end{array}\right\}\right]
$$

$$
\times\sum_{j=1}b_j\left\{\begin{array}{l}3\sin[\gamma_0+2(2j-1)T]+3\sin[\gamma_0-2(2j-1)T]\\-\sin[3\gamma_0+2(2j-1)T]-\sin[3\gamma_0-2(2j-1)T]\end{array}\right\}
$$

$$
+\frac{1}{24}\left(\frac{2}{\nu''}\right)^{3/2}J_1^{3/2}\sum_{j=1}2(2j-1)b_j\left\{\begin{array}{l}3\dfrac{\sin[\gamma_0+2(2j-1)T]}{\nu''+2(2j-1)}-3(1-\delta_j^1)\dfrac{\sin[\gamma_0-2(2j-1)T]}{\nu''-2(2j-1)}\\[2ex]-\dfrac{\sin[3\gamma_0+2(2j-1)T]}{3\nu''+2(2j-1)}+(1-\delta_j^2)\dfrac{\sin[3\gamma_0-2(2j-1)T]}{3\nu''-2(2j-1)}\end{array}\right\}
$$

$$
=\nu''J_1+\frac{1}{24}\left(\frac{2}{\nu''}\right)^{3/2}J_1^{3/2}\left[b_2\sin 3(\gamma_0-2T)-3b_1\sin(\gamma_0-2T)\right]
$$

$$
-\frac{1}{16\nu''^3}J_1^2\sum_{j=1}b_j\left\{\begin{array}{l}\dfrac{\sin[\gamma_0+2(2j-1)T]}{\nu''+2(2j-1)}+(1-\delta_j^1)\dfrac{\sin[\gamma_0-2(2j-1)T]}{\nu''-2(2j-1)}\\[2ex]-\dfrac{\sin[3\gamma_0+2(2j-1)T]}{3\nu''+2(2j-1)}-(1-\delta_j^2)\dfrac{\sin[3\gamma_0-2(2j-1)T]}{3\nu''-2(2j-1)}\end{array}\right\}
$$

$$
\times\sum_{j=1}b_j\left\{\begin{array}{l}3\sin[\gamma_0+2(2j-1)T]+3\sin[\gamma_0-2(2j-1)T]\\-\sin[3\gamma_0+2(2j-1)T]-\sin[3\gamma_0-2(2j-1)T]\end{array}\right\}. \qquad (46)
$$

To continue the work beyond this point, K_1, as expressed by Eq. (46) should be written in terms of γ_1 and a final transformation then made[1-3] to new variables, $\gamma_2 = \gamma_1 - 2T$ and $J_2 = J_1$ with the aim of obtaining a new Hamiltonian which is substantially independent of T It would be the intention to keep in the J_2^2 term, which is in a sense regarded as a correction term only terms which are constant or possibly functions of γ_2 (i.e., circular functions with arguments which are multiples of $\gamma_2 = \gamma_1 - 2T$ and hence are T-independent). Since by Eq. (45b), the difference between γ_1 and γ_0 is of order $J_1^{1/2}$, γ_0 may simply be replaced by γ_1 in the J_1^2 terms of Eq. (46). The distinction between γ_1 and γ_0 in the term involving $J_1^{3/2}\left[b_2 \sin 3(\gamma_0 - 2T) - 3b_1 \sin(\gamma_0 - 2T)\right]$ does not appear to introduce into the J_1^2 term any terms of the form which we elect to retain. Considerable complexity arises, however, in evaluating in this same sense the product of the two sums which appear in the J_1^2 term of Eq. (46), since numerous cross products occur which involve circular functions with arguments that are multiples of $\gamma_2 = \gamma_1 - 2T$.

The J_1^2 term of Eq. (46) includes, then firstly the constant terms $\dfrac{\alpha' b_2^2}{192\,\nu''^3} J_1^2$, where α' denotes

$$\alpha' = -\frac{1 + (3b_1/b_2)^2}{\frac{\nu''}{2} + 1} + 36\,\nu'' \sum_{j=1} \left(\frac{b_j}{b_2}\right)^2 \left\{ \frac{1 - \delta_j^1}{\left[2(2j-1)\right]^2 - \nu''^2} + \frac{1 - \delta_j^2}{\left[2(2j-1)\right]^2 - (3\nu'')^2} \right. \tag{47a}$$

$$= +1.75516 \quad \text{(in our example).} \tag{47b}$$

There are, in addition, cross terms which involve circular functions of arguments that are multiples of $\gamma_2 = \gamma_1 - 2T$, of which we write those depending on b_2 in combination with b_1 or b_3 as $\dfrac{b_2^2}{192\,\nu''^3} J_1^2 F(\gamma_2)$, with

$$F(\gamma_2) = -6\left\{\frac{b_3}{b_2}\left[\frac{1}{6-\nu''} + \frac{3}{10-3\nu''} - \frac{3}{6+\nu''} + \frac{3}{10-\nu''} - \frac{3}{6+3\nu''} - \frac{1}{10+\nu''}\right]\cos 2\gamma_2\right.$$

$$-\frac{b_1}{b_2}\left[\frac{3}{2+\nu''} - \frac{3}{6-\nu''} + \frac{3}{2+3\nu''} + \frac{1}{6+\nu''}\right]\cos 2\gamma_2$$

$$\left.+\frac{b_1}{b_2}\left[\frac{3}{3\nu''-2} - \frac{1}{6-\nu''}\right]\cos 4\gamma_2\right\} \tag{48a}$$

$$= -1.10355 \cos 2\gamma_2 - 0.72926 \cos 4\gamma_2 \quad \text{(in our example)}. \tag{48b}$$

We accordingly take

$$K_1 = \nu'' J_1 + \frac{1}{24}\left(\frac{2}{\nu''}\right)^{3/2} J_1^{3/2}\left[b_2 \sin 3(\gamma_1 - 2T) - 3 b_1 \sin(\gamma_1 - 2T)\right]$$

$$+ \frac{b_2^2\left[\alpha' + F(\gamma_1 - 2T)\right]}{192\,\nu''^3} J_1^2 \;. \tag{49}$$

For the final transformation we now, of course, employ the simple generating function

$$G_2(\gamma_1, J_2) = J_2 \cdot (\gamma_1 - 2T), \tag{50}$$

so that

$$J_1 = \partial G_2/\partial \gamma_1 = J_2 \tag{51a}$$

$$\gamma_2 = \partial G_2/\partial J_2 = \gamma_1 - 2T \tag{51b}$$

and

$$
\begin{aligned}
K_2 &= K_1 + \partial G_2 / \partial T \\
&= K_1 - 2 J_1 \\
&= (\nu'' - 2) J_2 + \frac{1}{24}\left(\frac{2}{\nu''}\right)^{3/2} J_2^{3/2} (b_2 \sin 3\gamma_2 - 3 b_1 \sin \gamma_2) \quad (52a) \\
&\qquad + \frac{b_2^2 [\alpha' + F(\gamma_2)]}{192\, \nu''^3} \; J_2^2 \; .
\end{aligned}
$$

Since K_2, as expressed by Eq. (52a), is so written as to be T-independent, we take K_2 to be a constant of the motion. In our present example this invariant is

$$
\begin{aligned}
K_2 &= -0.1898\, J_2 + 0.048389\, (5.41441 \sin 3\gamma_2 - 3.10512 \sin \gamma_2)\, J_2^{3/2} \\
&\quad + [0.045179 - 0.028406 \cos 2\gamma_2 - 0.018772 \cos 4\gamma_2]\, J_2^2 \; . \qquad (52b)
\end{aligned}
$$

G. THE FIXED POINTS
[In Particular For T = 0]

1.

The fixed points associated with the Hamiltonian K_2 of Eq. (52a) are given by points which simultaneously satisfy

$$\partial K_2 / \partial \gamma_2 = 0 \qquad \underline{\text{and}} \qquad \partial K_2 / \partial J_2 = 0 \, , \qquad (53a, b)$$

so that K_2 is stationary. If it were not for the presence of the function $F(\gamma_2)$, the first condition would be met when

$$\cos \gamma_2 = 0 \qquad \underline{\text{or}} \text{ when } \qquad 4 \cos^2 \gamma_2 - 3 = \frac{b_1}{b_2} \, . \qquad (54a, b)$$

The two roots in addition to the root $\gamma_2 = 270^\circ$ appear to be shifted by about 5/3 degree by inclusion of the function $F(\gamma_2)$ in the calculation, and the value of $J_2^{1/2}$ which corresponds to these latter roots increased by about 3 percent. Estimates of these solutions to Eqs. (53a, b) are given in Table I,*

*The roots chosen here are selected so that, with $\nu'' < 2$, $J_2^{1/2}$ will be positive. At T = 0 the values of γ_1 will be identical with γ_2 [Eq. (51b)].

together with the associated values of K_2, which are now necessarily not all the same.

TABLE I

Values of γ_2, J_2 for which the Hamiltonian K_2 can be Stationary
$(b_1/b_2 = 1.03504/5.41441)^2$

Root	γ_2	$3\gamma_2$	$J_2^{1/2}$	J_2	K_2
1	-90°	-270°	0.291 84	0.0851 68	-0.0055 21
2, 3	$28^\circ.41$ $151^\circ.59$	$85^\circ.23$ $454^\circ.77$	0.579 58	0.335 915	-0.0226 50

It will be recalled that $J_1 = J_2$ and, for $T = 0$, $\gamma_1 = \gamma_2$. In the following subsection we make the inverse transformations necessary to express these results in terms of the original variables, specifically for $T = 0$ $(s = 0)$.

2

For the assumed value of T, namely $T = 0$ in the present case, the values of γ_2 $(= \gamma_1)$ and J_2 $(= J_1)$ may be transformed to corresponding values of γ_0, J_0 by means of Eqs. (45a, b). This transformation is least laborious in the case designated as "Root 1" in Table I, since, for that case, $\gamma_0 = \gamma_1$ $(= 270^\circ)$. Once the desired values of γ_0, J_0 are obtained, Q and P $(= dQ/dT)$ follow immediately from Eqs. (42c, d). Since, at $T = 0$, $\nu\beta = 1.3755$ and $d(\nu\beta)/dt = 0$, one next may evaluate

$$q = \sqrt{\nu\beta}\, Q = 1.17282\, Q \tag{55a}$$

$$dq/dt = (1/\sqrt{2\beta})\, dQ/dT = P/\sqrt{2\beta} = P/1.17282.^{*} \tag{55b}$$

Finally, of course,

$$v = v_s + q = -0.08380_2 + q \quad \left[\text{from Eq. (16)}\right] \tag{56a}$$

and

$$p \equiv \frac{dv}{ds} = \frac{1}{3}\frac{dq}{dt}, \tag{56b}$$

since $t = s/3$ [Eq. (34)] and $dv_s/ds = 0$ at $s = 0$. In this way we estimate the values listed in Table II.

TABLE II

Values Leading to Fixed-Point Coordinates
($T = 0$, $s = 0$)

Root	γ_0	$J_0^{1/2}$	Q	P	q	dq/dt	v	p=dv/ds
1	-90°	0.29265	-0.30761	0	-0.36077	0	-0.44457	0
2, 3	$25^\circ.11$ $154^\circ.89$	0.5665	0.2527	± 0.9761	0.2964	± 0.8323	0.2126	± 0.2774

The true values for the coordinates v, p of the unstable fixed points, as given by the computer, are (Sect. D)

$$v = -0.44345, \qquad p = 0,$$

$$v = 0.2245, \qquad p = \pm 0.3030;$$

it is seen, accordingly, that the present "analytic" method gives (as Root 1) the location of the unstable fixed point which lies on the v-axis with an accuracy considerably better than 1 %, but that the values of v and p for the other unstable fixed points are respectively smaller than the correct values by $5\frac{1}{2}$ and

---

*Cf. Eqs (17a, b) of ref. 3.

$8\frac{1}{2}$ %. These analytic results were not materially affected by a refinement of the function F (γ_2) [Eq. (48b)], which enters in Eqs. (52a, b), through inclusion of terms involving b_3b_4 in the coefficient of cos 2 γ_2 and terms involving $b_1\ b_3$ and $b_2\ b_4$ in the coefficient of cos 4 γ_2 .

H. ALTERNATIVE, SIMPLIFIED, ANALYTIC METHOD

The analytic method of the previous sections, in which it was attempted to follow the Moser procedure in an orderly fashion, clearly involved considerable complexity in the details of the calculations. It was necessary, firstly, to undertake some numerical work in order to estimate adequately the stable solution for the forced motion. Subsequently, once the forcing term was removed from the equation of motion, additional labor was required because the new differential equation then contained an A-G coefficient for the linear term. Because of these complications, it would seem difficult to arrive at useful formulas by following the methodology on which our numerical work was based and, accordingly, it is of interest to explore a somewhat less straightforward, but simplified, analytical procedure.

In this second method the effect of the forcing term will only be eliminated immediately by subtraction of that part which would result from consideration of the linear terms of Eq. (1). In the subsequent work, terms of order $\lambda\ J_1^{3/2}$ and $\lambda^2\ J_1$ in the Hamiltonian will be neglected, in comparison to the $J_1^{3/2}$ term and the constant part of J_1^2 term, since λ may in a sense be regarded as a perturbation. Information concerning the stable equilibrium orbit, as well as pertaining to the unstable equilibrium orbits and other features of the motion, should then result from the analysis.

1.

We commence, therefore, with the differential equation (1), for which the Hamiltonian has the form

$$h = \frac{1}{2} p^2 + \frac{1}{2}\left(\frac{2\nu}{N}\right)^2 v^2 - (b/6)(\cos 2s) v^3 - \lambda \left(\cos \frac{2s}{3}\right) v . \tag{57}$$

For the initial transformation, to quantities akin to angle-action variables, we employ the generating function

$$F_o(v, \gamma_o) = \frac{\nu}{N}\left[v + \frac{\lambda}{\frac{4}{9} - \left(\frac{2\nu}{N}\right)^2} \cos\frac{2s}{3}\right]^2 \operatorname{ctn}\gamma_o + \frac{2}{3}\,\frac{\lambda}{\frac{4}{9} - \left(\frac{2\nu}{N}\right)^2}\left(\sin\frac{2s}{3}\right) v + f(s) , \tag{58}$$

where f (s) would be selected to obviate the need to include in the new Hamiltonian terms which only involve the independent variable and hence play no significant rôle. The resultant transformation is

$$p = \partial F_o/\partial v = \frac{2\nu}{N}\left[v + \frac{\lambda}{\frac{4}{9} - \left(\frac{2\nu}{N}\right)^2}\cos\frac{2s}{3}\right]\operatorname{ctn}\gamma_o + \frac{2}{3}\,\frac{\lambda}{\frac{4}{9} - \left(\frac{2\nu}{N}\right)^2}\sin\frac{2s}{3} \tag{59a}$$

$$J_o = -\partial F_o/\partial\gamma_o = \frac{\nu}{N}\left[v + \frac{\lambda}{\frac{4}{9} - \left(\frac{2\nu}{N}\right)^2}\cos\frac{2s}{3}\right]^2 \csc^2\gamma_o ; \tag{59b}$$

so that

$$\operatorname{ctn}\gamma_o = \frac{N}{2\nu}\,\frac{p - \frac{2}{3}\,\frac{\lambda}{\frac{4}{9} - \left(\frac{2\nu}{N}\right)^2}\sin\frac{2s}{3}}{v + \frac{\lambda}{\frac{4}{9} - \left(\frac{2\nu}{N}\right)^2}\cos\frac{2s}{3}} \tag{60a}$$

$$J_o = \frac{N}{4\nu}\left[p - \frac{2}{3}\,\frac{\lambda}{\frac{4}{9} - \left(\frac{2\nu}{N}\right)^2}\sin\frac{2s}{3}\right]^2 + \frac{\nu}{N}\left[v + \frac{\lambda}{\frac{4}{9} - \left(\frac{2\nu}{N}\right)^2}\cos\frac{2s}{3}\right]^2 , \tag{60b}$$

$$v = \left(\frac{N}{\nu}\right)^{1/2} J_o^{1/2} \sin \gamma_o - \frac{\lambda}{\frac{4}{9} - \left(\frac{2\nu}{N}\right)^2} \cos \frac{2s}{3} \tag{60c}$$

$$p = 2\left(\frac{\nu}{N}\right)^{1/2} J_o^{1/2} \cos \gamma_o + \frac{2}{3} \frac{\lambda}{\frac{4}{9} - \left(\frac{2\nu}{N}\right)^2} \sin \frac{2s}{3}, \tag{60d}$$

and the new Hamiltonian is found to be (after some intermediate algebraic work)

$$\begin{aligned} H_o &= h + \partial F_o / \partial s \\ &= 2\frac{\nu}{N} J_o + \frac{b}{48}\left(\frac{N}{\nu}\right)^{3/2} J_o^{3/2} \begin{bmatrix} \sin(3\gamma_o + 2s) + \sin(3\gamma_o - 2s) \\ - 3\sin(\gamma_o + 2s) - 3\sin(\gamma_o - 2s) \end{bmatrix} \\ &\quad + \frac{b}{16}\frac{N}{\nu} \frac{\lambda}{\frac{4}{9} - \left(\frac{2\nu}{N}\right)^2} J_o \begin{bmatrix} 2\cos\frac{8s}{3} + 2\cos\frac{4s}{3} \\ - \cos(2\gamma_o + \frac{8s}{3}) - \cos(2\gamma_o - \frac{8s}{3}) \\ - \cos(2\gamma_o + \frac{4s}{3}) - \cos(2\gamma_o - \frac{4s}{3}) \end{bmatrix} \\ &\quad + \frac{b}{16}\left(\frac{N}{\nu}\right)^{1/2} \frac{\lambda^2}{\left[\frac{4}{9} - \left(\frac{2\nu}{N}\right)^2\right]^2} J_o^{1/2} \begin{bmatrix} - 2\sin(\gamma_o + 2s) - 2\sin(\gamma_o - 2s) \\ - \sin(\gamma_o + \frac{10s}{3}) - \sin(\gamma_o - \frac{10s}{3}) \\ - \sin(\gamma_o + \frac{2s}{3}) - \sin(\gamma_o - \frac{2s}{3}) \end{bmatrix}. \end{aligned} \tag{61}$$

[The nature of the transformation and its effectiveness in removing completely the coupling term from the <u>linearized</u> differential equation (1) may be evident from Eqs. (60a) and (61). The general character of the Hamiltonian H_o of (61) is seen to correspond to that given for K_o by Eq. (50) of ref. 1(p. 21), noting that, in ref. 1, $b = 1$ and that for our present $- \cos 2s$ the function $\sin 2t$ is employed in the v^2 term of the differential equation.]

Paralleling previous work,[1] we now make the next transformation by use of the generating function

$$F_1(\gamma_0, J_1) = J_1 \cdot \gamma_0 + \frac{b}{96}\left(\frac{N}{\nu}\right)^{3/2} J_1^{3/2} \left[\frac{\cos(3\gamma_0 + 2s)}{1 + 3\nu/N} - 3\frac{\cos(\gamma_0 + 2s)}{1 + \nu/N} + 3\frac{\cos(\gamma_0 - 2s)}{1 - \nu/N} \right]; \tag{62}$$

so that

$$J_0 = \partial F_1/\partial\gamma_0 = J_1 + \frac{b}{32}\left(\frac{N}{\nu}\right)^{3/2} J_1^{3/2} \left[-\frac{\sin(3\gamma_0 + 2s)}{1 + 3\nu/N} + \frac{\sin(\gamma_0 + 2s)}{1 + \nu/N} - \frac{\sin(\gamma_0 - 2s)}{1 - \nu/N} \right] \tag{63a}$$

$$\gamma_1 = \partial F_1/\partial J_1 = \gamma_0 + \frac{b}{64}\left(\frac{N}{\nu}\right)^{3/2} J_1^{1/2} \left[\frac{\cos(3\gamma_0 + 2s)}{1 + 3\nu/N} - 3\frac{\cos(\gamma_0 + 2s)}{1 + \nu/N} + 3\frac{\cos(\gamma_0 - 2s)}{1 - \nu/N} \right], \tag{63b}$$

and

$$\begin{aligned} H_1 &= H_0 + \partial F_1/\partial s \\ &= H_0 + \frac{b}{48}\left(\frac{N}{\nu}\right)^{3/2} J_1^{3/2} \left[-\frac{\sin(3\gamma_0 + 2s)}{1 + 3\nu/N} + 3\frac{\sin(\gamma_0 + 2s)}{1 + \nu/N} + 3\frac{\sin(\gamma_0 - 2s)}{1 - \nu/N} \right] \\ &\cong 2\frac{\nu}{N} J_1 + \frac{b}{48}\left(\frac{N}{\nu}\right)^{3/2} J_1^{3/2} \sin(3\gamma_1 - 2s) \\ &\quad + \frac{b^2}{2048}\left(\frac{N}{\nu}\right)^3 J_1^2 \left[\frac{6\,\nu/N}{1 - \nu^2/N^2} - \frac{1}{1 + 3\nu/N} \right] \\ &\quad - \frac{b}{16}\,\frac{N}{\nu}\,\frac{\lambda}{\frac{4}{9} - \left(\frac{2\nu}{N}\right)^2} J_1 \cos\left(2\gamma_1 - \frac{4s}{3}\right) \\ &\quad - \frac{b}{16}\left(\frac{N}{\nu}\right)^{1/2} \frac{\lambda^2}{\left[\frac{4}{9} - \left(\frac{2\nu}{N}\right)^2\right]^2} J_1^{1/2} \sin\left(\gamma_1 - \frac{2s}{3}\right). \end{aligned} \tag{64}$$

in which the last result follows after some algebraic simplification and as a result of neglecting terms of the order $\lambda J_1^{3/2}$ $\lambda^2 J_1$ and terms which do not involve circular functions which are multiples of $(\gamma_1 - 2s/3)$-- [cf Eq. (54) of ref. 1 (p. 22)]

For the final transformation we employ as in previous work the generating function

$$F_2(\gamma_1, J_2) = J_2 \cdot (\gamma_1 - \frac{2s}{3}); \tag{65}$$

so that

$$J_1 = \partial F_2/\partial \gamma_1 = J_2 \tag{66a}$$

$$\gamma_2 = \partial F_2/\partial J_2 = \gamma_1 - \frac{2s}{3} \tag{66b}$$

and

$$\begin{aligned} H_2 &= H_1 + \partial F_2/\partial s \\ &= H_1 - \frac{2}{3} J_2 \\ &= 2\left(\frac{\nu}{N} - \frac{1}{3}\right) J_2 + \frac{b}{48}\left(\frac{N}{\nu}\right)^{3/2} J_2^{3/2} \sin 3\gamma_2 + \frac{b^2 \alpha}{2048}\left(\frac{N}{\nu}\right)^3 J_2^2 \\ &\quad - \frac{b}{16}\frac{N}{\nu}\frac{\lambda}{\frac{4}{9} - \left(\frac{2\nu'}{N}\right)^2} J_2 \cos 2\gamma_2 \\ &\quad - \frac{b}{16}\left(\frac{N}{\nu}\right)^{1/2}\frac{\lambda^2}{\left[\frac{4}{9} - \left(\frac{2\nu}{N}\right)^2\right]^2} J_2^{1/2} \sin \gamma_2 \end{aligned} \tag{67}$$

[cf Eq. (57) of ref. 1 (p 23)] where

$$\alpha = \frac{6\nu/N}{1 - \nu^2/N^2} - \frac{1}{1 + 3\nu'/N}$$

[cf. Eq. (25) of ref. 1 (pp. 13, 23)] The Hamiltonian H_2, in the form written, is independent of s and will be taken as a constant of the motion

To obtain the fixed points, in particular, we may take the Hamiltonian H_2 to be stationary, as given by setting the partial derivatives $\partial H_2/\partial \gamma_2$ and $\partial H_2/\partial J_2$ each equal to zero; specifically,

$$\frac{b}{16}\left(\frac{N}{\nu}\right)^{3/2} J_2^{3/2} \cos 3\gamma_2 + \frac{b}{8}\left(\frac{N}{\nu}\right)\frac{\lambda}{\frac{4}{9}-\left(\frac{2\nu}{N}\right)^2} J_2 \sin 2\gamma_2 - \frac{b}{16}\left(\frac{N}{\nu}\right)^{1/2}\frac{\lambda^2}{\left[\frac{4}{9}-\left(\frac{2\nu}{N}\right)^2\right]^2} J_2^{1/2}\cos\gamma_2 = 0 \tag{69a}$$

and

$$2\left(\frac{\nu}{N}-\frac{1}{3}\right)+\frac{b}{32}\left(\frac{N}{\nu}\right)^{3/2} J_2^{1/2} \sin 3\gamma_2 + \frac{b^2\alpha}{1024}\left(\frac{N}{\nu}\right)^3 J_2$$
$$-\frac{b}{16}\frac{N}{\nu}\frac{\lambda}{\frac{4}{9}-\left(\frac{2\nu}{N}\right)^2}\cos 2\gamma_2 - \frac{b}{32}\left(\frac{N}{\nu}\right)^{1/2}\frac{\lambda^2}{\left[\frac{4}{9}-\left(\frac{2\nu}{N}\right)^2\right]^2} J_2^{-1/2}\sin\gamma_2 = 0. \tag{69b}$$

Two roots of interest for Eq. (69a, b), corresponding to the stable and unstable fixed points which lie on the v-axis of the phase plot for $s = 0 \pmod{3\pi}$, are obtained by taking $\gamma_2 = -90^\circ$ and J_2 as satisfying

$$2\left(\frac{\nu}{N}-\frac{1}{3}\right)+\frac{b}{32}\left(\frac{N}{\nu}\right)^{3/2} J_2^{1/2} + \frac{b^2\alpha}{1024}\left(\frac{N}{\nu}\right)^3 J_2$$
$$+\frac{b}{16}\frac{N}{\nu}\frac{\lambda}{\frac{4}{9}-\left(\frac{2\nu}{N}\right)^2} + \frac{b}{32}\left(\frac{N}{\nu}\right)^{1/2}\frac{\lambda^2}{\left[\frac{4}{9}-\left(\frac{2\nu}{N}\right)^2\right]^2} J_2^{-1/2} = 0\,, \tag{70}$$

in which the term of order J_2 is comparatively small--for small λ one root, in fact, may be estimated roughly by consideration of just the constant term and that involving $J_2^{-1/2}$, while the other is given roughly by use of just the constant term and that which involves $J_2^{1/2}$. Numerically, for

$\nu/N = 0.3$, $\quad b = 1.15$, $\quad$ and $\quad \lambda = 0.006$, Eq. (70) becomes

$$0.06944\, J_2 + 0.21871\, J_2^{1/2} - 0.04964 + 0.00033124\, J_2^{-1/2} = 0\,, \qquad (70')$$

with roots for $J_2^{1/2}$ given by 0.006881_5 and 0.2061_5. The remaining roots of interest similarly involve simultaneous solution of Eqs. (69a, b) for values of γ_2 near 30^o or the supplementary angle 150^o. To obtain the corresponding v, p coordinates of the fixed points, at s = 0 (mod. 3π), one must next transform γ_2 (= γ_1 for s = 0) and J_2 (= J_1) to γ_0 , J_o and thence to v, p by use of Eqs. (63a, b) and (60c, d).

It may be noted in passing that the two roots of Eq. (70) become coincident for a critical value of λ given approximately by

$$\lambda_c \cong \frac{64}{b}\left(\frac{1}{3} - \frac{\nu}{N}\right)^2 \left(\frac{1}{3} + \frac{\nu}{N}\right) \frac{\nu}{N} \qquad (71)$$

$$= 0.01175\,,$$

for $\nu/N = 0.3$ and b = 1.15; a more accurate numerical estimate, again based on Eq. (70), gives

$$\lambda_c = 0.01168\,,$$

with

$$J_2^{1/2} = 0.0740_4\,,$$

from which one finds, by Eq. (63a),

$$J_o^{1/2} = 0.07412$$

and, by Eqs. (60c, d),

$$v_c = -\left(\frac{10}{3}\right)^{1/2} (0.07412) - \frac{0.01168}{\frac{4}{9} - \frac{36}{100}}$$

$$= -\ 0.13532 - 0.13832$$

$$= -\ 0.2736_4\,,$$

$$p_c = 0\,.$$

The correct values for this confluent situation, as obtained by direct digital computation,[4] are

$$\lambda_c = 0.01136\ ,$$

$$v_c = -\ 0.2650\ ,$$

$$p_c = 0\ ;$$

so that our estimates for λ_c and v_c are evidently some 3% larger, in relative magnitude, than the correct values.[11]

Returning to our example with $\lambda = 0.006$, the fixed-point coordinates found by the present method of analysis are as summarized in Table III.

TABLE III

Estimated Fixed-Point Coordinates at $s = 0$, mod. 3π

$\nu/N = 0.3$ $\qquad$ $b = 1.15$ $\qquad$ $\lambda = 0.006$

Root	Calculated Values						Computer Results		Relative Error	
	γ_2	J_2	γ_o	J_o	v	p	v	p	ϵ_v	ϵ_p
Stable	-90^o	0.006881_5	-90^o	0.006882_2	-0.08361_8	0	-0.083802	0	-0.22%	--
1	-90^o	0.2061_5	-90^o	0.2067_6	-0.4485_5	0	-0.44345	0	+1.15%	--
2, 3	$34^{\circ}.20_6$ $145^{\circ}.79_4$	0.312_{69}	$31^{\circ}.24$ $148^{\circ}.76$	0.303_3	0.216_1	$\pm 0.284_1$	0.2246	± 0.3030	-4 %	-6

The results obtained by the present simplified method not only are far more easily obtainable but appear to be of as good accuracy as those previously summarized in Table II (Sect. G).

I. REFERENCES AND NOTES

1. L. Jackson Laslett, MURA-452 (April 13, 1959).

2. L. Jackson Laslett, MURA-459 (May 20, 1959).

3. L. Jackson Laslett, MURA-463 (June 3, 1959).

4. In the main series of computer studies the differential equation was regarded as of the form

$$\frac{d^2v}{d\tau^2} + \left(\frac{2\nu}{N}\right)^2 v + \frac{b}{2} (\sin 2\tau)\, v^2 - \lambda \cos\left(\frac{2\tau}{3} + \frac{\pi}{6}\right) = 0 \quad \text{and}$$

attention was directed in particular to phase plots made at $\tau = 2.75\pi$, mod 3π. The translation of independent variable given by setting $s = \tau - 2.75\pi$ transforms this form of the equation to

$$\frac{d^2v}{ds^2} + \left(\frac{2\nu}{N}\right)^2 v - \frac{b}{2} (\cos 2s)\, v^2 - \lambda \cos \frac{2s}{3} = 0,$$

with the corresponding phase plots pertaining to $s = 0$, mod. 3π. It is this latter equation which we have introduced as Eq. (1) of the text. In the computational work ν/N was taken as 0.3, $b = 1.15$, and λ covered positive values extending through the critical value $\lambda_c = 0.01136$. Some simplification is possible, of course, by introduction of the scaled quantities $V = bv$ and $\mu = b\lambda$, in terms of which the differential equation becomes

$$\frac{d^2V}{ds^2} + \left(\frac{2\nu}{N}\right)^2 V - \frac{1}{2} (\cos 2s)\, V^2 - \mu \cos \frac{2s}{3} = 0.$$

5. Jürgen Moser, Nach. Gött. Akad. (Math.-Phys. Kl.) IIa, #6, 87-120 (1955).

6. The computational work was done with the MURA IBM 704 computer, by aid of the following programs:

(a) J. N. Snyder, DUCK-ANSWER (IBM Program 75), MURA-237 (1957);

(b) J. N. Snyder, FORANAL (IBM Program 52), MURA-228 (1957); and

(c) John McNall, DUCKNALL (IBM Program 219), MURA-438 (1958).

7. L. Jackson Laslett, MURA Notes (20 April 1955) [MURA Tables, Book 1B, Table 5].

8. L. Jackson Laslett and A. M. Sessler, MURA-252 (1957).

9. Cf. E. D. Courant and H. S. Snyder, Annals of Physics 3, No. 1, 1-48 (January, 1958)--Sect. 4a, esp. Eqs. (4. 4) and (4. 5), p. 18.

10. The computer solution for ν/β was employed in forming this transformation, since the data were available in tabular form convenient for proceeding with the calculation. Values of $(\nu/\beta)^{5/2}$ cos 6 t, at equally spaced values of T, were then prepared and presented to the FORANAL program[6b] for Fourier analysis.

11. An alternative method for obtaining a formula similar to Eq. (71), to afford an approximate estimate of λ_c, has also been reported [L. Jackson Laslett and K. R. Symon, "Computational Results Pertaining to Use of a Time-Dependent Magnetic Field Perturbation to Implement Injection or Extraction in a FFAG Synchrotron," Paper submitted for inclusion in the Proceedings of the Second CERN Symposium on High Energy Accelerators, Genève, 1959]. In this method we note from Eqs. (6a) [Sect. C] and (9a) [Sect. D] that, for small λ, the locations of the two fixed points with which we are concerned may be estimated by

$$v_1(\lambda) \cong -\frac{\lambda}{4/9 - (2\nu/N)^2} \qquad (72a)$$

$$v_2(\lambda) \cong v_2(\lambda = 0) + \frac{\lambda}{4/9 - (2\nu/N)^2} . \qquad (72b)$$

A parabolic fit, tangent to the lines (11a, b) at $\lambda = 0$, may be obtained by writing

$$\lambda \cong \frac{v \cdot [v - v_2(\lambda = 0)]}{v_2(\lambda = 0)} \cdot [4/9 - (2\nu/N)^2] , \tag{73}$$

for which the maximum value of λ ;

$$\lambda_c = \frac{1}{4} \cdot [4/9 - (2\nu/N)^2] \cdot [-v_2(\lambda = 0)] , \tag{74a}$$

is attained at

$$v_c = \frac{1}{2} v_2 (\lambda = 0) . \tag{74b}$$

With $2\nu/N = 0.6$ and $-v_2(\lambda = 0) = 0.5238$ [from computational results cited in ref. 1, after division by b = 1.15], Eqs. (74a, b) suggest

$$\lambda_c = 0.01106$$

$$v_c = -0.2619 ,$$

which may be compared with the computational results cited in the text, namely

$$\lambda_c = 0.01136$$

$$v_c = -0.2650 .$$

ERAN-72-B
pp 1-8, 55 only

ON THE PASSAGE OF A BEAM THROUGH A CAVITY,*
INCLUDING ANALYTIC NOTES OF A.M. SESSLER

L. Jackson Laslett

Lawrence Radiation Laboratory
University of California
Berkeley, California

April 20, 1970

I. Introduction and General Principles

A particle beam may be sent through an R.F. cavity with the object of attaining a time-varying deflection or, alternatively, of obtaining an energy spread. It can be shown that these two effects are related, and one may be distressed to obtain one of the effects when interested only in obtaining the other.

As an example of the relationship mentioned above, one may consider three trajectories that pass through a cavity that extends from z_a to z_b. All three rays will be taken to enter with the same energy and to be parallel (e.g., normal incidence). The first ray (#1) will be regarded as the reference ray. The second ray will be supposed to emerge at the same time as #1, but with a transverse displacement δx and an energy that differs by δE from the emergent energy of the reference ray. The

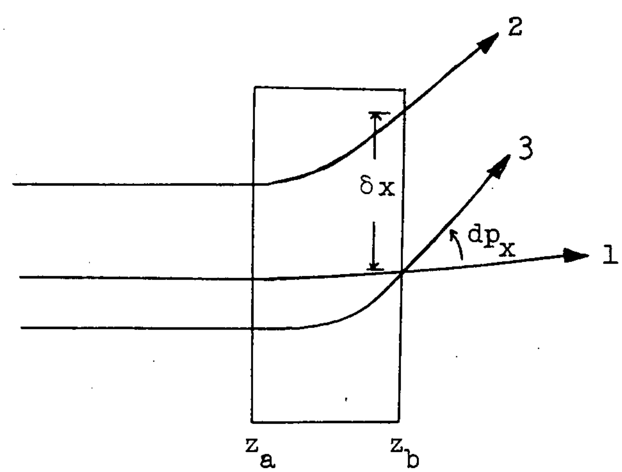

* Work supported by the U.S. Atomic Energy Commission.

third ray will be supposed to emerge at the same point as #1, but later by a time interval dt. For this to occur, in the presence of time-varying forces within the cavity, the third ray may follow a trajectory that differs from that of the reference ray and the emergent transverse momenta accordingly may differ by dp_x . It then can be shown that, provided only that the particle motion within the cavity is governed by Hamiltonian dynamics,

$$\frac{dp_x}{dt} = - \frac{\delta E}{\delta x} \; ; \tag{1}$$

i.e., the scanning-rate and the energy-dispersion are directly related in the manner indicated by Eqn. (1).

The reasoning leading to Eqn. (1) has been outlined by Fowler and Good[1*] in connection with a beam sweeper, and was based on application of the bilinear covariant of Whittaker.[2] In this type of application it is useful to consider the motion as governed by a "space Hamiltonian," in which a distance coördinate (e.g., z) plays the rôle of independent variable and the negative of the momentum conjugate to this coördinate then serves as the Hamiltonian function. In such a formulation the time t acts as a generalized coördinate, and the conjugate "momentum" then is the negative of the usual Hamiltonian or, in this instance, the negative of the particle energy. One then notes that the evolution of a Hamiltonian system[**] effects a canonical transformation of the dynamical variables, so that the invariants of a canonical transformation can be applied to these variables.

Because the derivation of Eqn. (1) through use of the bilinear covariant has been treated elsewhere,[1] it may be of interest here to indicate how this result might alternatively have been demonstrated by appeal to the Fundamental Poisson-Bracket Relations.[3] Thus, supposing a space Hamiltonian to be employed, we may in the present application consider x, p_x and $t, -E$ to constitute two conjugate coördinate-momentum pairs. Suppose we now pass to differential quantities about some possible trajectory (but omit, for brevity, the differential symbol)

---

* References are listed in Sect. IV.

** I.e., the evolution from one definite value of the independent variable to a second definite value of this quantity.

and linearize the transformation that carries a particle from $z = z_a$ to $z = z_b$; we then may write

$$\begin{pmatrix} x \\ p_x \\ t \\ -E \end{pmatrix}_{z_b} = \begin{pmatrix} T_{1,1} & T_{1,2} & T_{1,3} & T_{1,4} \\ T_{2,1} & T_{2,2} & T_{2,3} & T_{2,4} \\ T_{3,1} & T_{3,2} & T_{3,3} & T_{3,4} \\ T_{4,1} & T_{4,2} & T_{4,3} & T_{4,4} \end{pmatrix} \begin{pmatrix} x \\ p_x \\ t \\ -E \end{pmatrix}_{z_a} , \tag{2a}$$

or, for the inverse transformation,

$$\begin{pmatrix} x \\ p_x \\ t \\ -E \end{pmatrix}_{z_a} = \begin{pmatrix} \tilde{T}_{1,1} & \tilde{T}_{1,2} & \tilde{T}_{1,3} & \tilde{T}_{1,4} \\ \tilde{T}_{2,1} & \tilde{T}_{2,2} & \tilde{T}_{2,3} & \tilde{T}_{2,4} \\ \tilde{T}_{3,1} & \tilde{T}_{3,2} & \tilde{T}_{3,3} & \tilde{T}_{3,4} \\ \tilde{T}_{4,1} & \tilde{T}_{4,2} & \tilde{T}_{4,3} & \tilde{T}_{4,4} \end{pmatrix} \begin{pmatrix} x \\ p_x \\ t \\ -E \end{pmatrix}_{z_b} . \tag{2b}$$

The fundamental Poisson-Bracket relations are (in Goldstein's[3] notation)

$$[q_i, q_j] = 0, \qquad [p_i, p_j] = 0, \qquad \text{and} \qquad [q_i, p_j] = \delta_{i,j}, \tag{3}$$

where $\delta_{i,j}$ is the Kronecker δ-symbol; these necessary and sufficient conditions for a canonical transformation impose six conditions on the matrix elements $T_{i,j}$ of the transformation (2a)* -- or on the coefficients $\tilde{T}_{i,j}$ of the inverse transformation (2b). Thus, in particular, the condition $[p_{x_a}, -E_a] = 0$ imposes the relation

$$\tilde{T}_{2,1}\,\tilde{T}_{4,2} - \tilde{T}_{2,2}\,\tilde{T}_{4,1} + \tilde{T}_{2,3}\,\tilde{T}_{4,4} - \tilde{T}_{2,4}\,\tilde{T}_{4,3} = 0. \tag{4}$$

---

* With 6 significant relations imposed on the 16 coefficients $T_{i,j}$, the number of free parameters for the linear (homogeneous) transformations (2a) becomes 10. It may be noted that if such a transformation were to be considered as arising from a homogeneous quadratic generating function of 4 variables, the number of terms (with arbitrarily assignable coefficients) in such a generating function would be $\frac{4(4+1)}{2} = 10$ -- in agreement with the above.

With reference now to the specific problem considered initially, the fact that the incident rays are taken to have the same direction and the same energy requires that

$$0 = \tilde{T}_{2,1}x_b + \tilde{T}_{2,2}\, p_{x_b} + \tilde{T}_{2,3}\, t_b + \tilde{T}_{2,4}\, (-E_b) \tag{5a}$$

and

$$0 = \tilde{T}_{4,1}x_b + \tilde{T}_{4,2}\, p_{x_b} + \tilde{T}_{4,3}\, t_b + \tilde{T}_{4,4}\, (-E_b). \tag{5b}$$

For ray #2 it is understood that there is to be no time differential (with respect to #1), so from Eqns. (5a,b) we have for this ray

$$\tilde{T}_{2,1}\, x_b + \tilde{T}_{2,2}\, p_{x_b} + \tilde{T}_{2,4}\, (-E_b) = 0 \tag{6a}$$

and

$$\tilde{T}_{4,1}\, x_b + \tilde{T}_{4,2}\, p_{x_b} + \tilde{T}_{4,4}\, (-E_b) = 0, \tag{6b}$$

from which elimination of p_{x_b} yields

$$(\tilde{T}_{2,1}\,\tilde{T}_{4,2} - \tilde{T}_{4,1}\,\tilde{T}_{2,2})x_b + (\tilde{T}_{2,4}\,\tilde{T}_{4,2} - \tilde{T}_{4,4}\,\tilde{T}_{2,2})(-E_b) = 0 \tag{7a}$$

or, recalling that the variables x_b and E_b are actually differentials,

$$-\left.\frac{\delta E}{\delta x}\right|_b = \frac{\tilde{T}_{2,1}\,\tilde{T}_{4,2} - \tilde{T}_{2,2}\,\tilde{T}_{4,1}}{\tilde{T}_{2,2}\,\tilde{T}_{4,4} - \tilde{T}_{2,4}\,\tilde{T}_{4,2}} \; . \tag{7b}$$

Likewise, for ray #1, the (differential) transverse coördinate is to vanish, so for this ray Eqns. (5a,b) become

$$\tilde{T}_{2,2}\, p_{x_b} + \tilde{T}_{2,3}\, t_b + \tilde{T}_{2,4}\, (-E_b) = 0 \tag{8a}$$

and

$$\tilde{T}_{4,2}\, p_{x_b} + \tilde{T}_{4,3}\, t_b + \tilde{T}_{4,4}\, (-E_b) = 0, \tag{8b}$$

so that, on elimination of $-E_b$,

$$(\tilde{T}_{2,2}\,\tilde{T}_{4,4} - \tilde{T}_{4,2}\,\tilde{T}_{2,4})p_{x_b} + (\tilde{T}_{2,3}\,\tilde{T}_{4,4} - \tilde{T}_{4,3}\,\tilde{T}_{2,4})t_b = 0 \tag{9a}$$

or

$$\frac{dp_{x_b}}{dt_b} = \frac{\tilde{T}_{2,4}\,\tilde{T}_{4,3} - \tilde{T}_{2,3}\,\tilde{T}_{4,4}}{\tilde{T}_{2,2}\,\tilde{T}_{4,4} - \tilde{T}_{2,4}\,\tilde{T}_{4,2}} \; . \tag{9b}$$

The expressions on the right-hand sides of Eqns. (7b) and (9b) are seen to have identical denominators, and the numerators are equal by virtue of Eqn. (4). We thus in this way have verified the correctness of the relation $\delta E/\delta x = -dp_x/dt$ that was cited as Eqn. (1). A similar approach, again making reference to the fundamental Poisson-bracket relations, might prove useful for establishing other relationships that could be of interest for a dynamical system.

II. Example of a Specific Transformation to Represent Passage through an R-F Cavity

We present here a specific Hamiltonian transformation intended to describe the essential features of particle motion through an R-F cavity whose thickness s is sufficiently small that transit-time effects can be neglected. Energy will be measured in terms of a nominal injection energy (total energy) $mc^2 = \gamma m_o c^2$, time will be measured as $\tau = ct$, and the motion will be treated as ultra-relativistic ($v \approx c$). With a simple standing-wave mode in a two-dimensional cavity of half-width **a**, the fields may be taken to be of the form

$$E_z(x,t) = E_o \cos\frac{x}{\bar{\lambda}} \cos\frac{\tau}{\bar{\lambda}} \tag{10a}$$

$$B_y(x,t) = -E_o \sin\frac{x}{\bar{\lambda}} \sin\frac{\tau}{\bar{\lambda}} \tag{10b}$$

where $a = \lambda/4,\ 3\lambda/4,\ 5\lambda/4$, or etc. (with $\lambda = 2\pi\bar{\lambda}$), and we may consider use of the transformation

$$\begin{aligned} x &= x_o + \frac{p_x + p_{x_o}}{2} s - \frac{qs^2}{2mc^2} B_y(x_o, t_o) \\ &= x_o + p_{x_o} s - \frac{qs^2}{mc^2} B_y(x_o, t_o) \\ &= x_o + p_{x_o} s + F_o s \sin\frac{x_o}{\bar{\lambda}} \sin\frac{\tau_o}{\bar{\lambda}} , \end{aligned} \tag{11a}$$

$$\begin{aligned} p_x &= p_{x_o} - \frac{qs^2}{mc^2} B_y(x_o, t_o) \\ &= p_{x_o} + F_o \sin\frac{x_o}{\bar{\lambda}} \sin\frac{\tau_o}{\bar{\lambda}} , \end{aligned} \tag{11b}$$

$$t = t_o + s/c \qquad \text{or} \qquad \tau = \tau_o + s, \tag{11c}$$

and

$$\text{Energy increment} = q\,s\,E_z(x_o,\ t_o)$$

or

$$W = W_o + F_o \cos\frac{x_o}{\bar{\lambda}} \cos\frac{\tau_o}{\bar{\lambda}}, \tag{11d}$$

where $F_o = \dfrac{qE_o s}{mc^2}$ and $W = \dfrac{\text{Energy}}{mc^2}$. With x, p_x and $\tau, -W$ regarded as conjugate coördinate-momentum pairs, the transformation equations (11a-d) will be found to fulfill all the required Poisson-bracket relationships (3) and hence may be adequate for revealing the salient features in the motion of fast particles through such a cavity.*

As a numerical example, it may be of interest to consider a situation of the type just described in which all particles enter with the nominal energy ($W = 1$) and the center of the incident beam falls at the point $x = \lambda/4$ (where the spatial gradient of the electric field component E_z has its maximum magnitude and where the magnetic field then perforce will attain its maximum value). The distribution of transverse displacement (x_o) and slope (p_{x_o}) about such a central ray will be taken to be that contained within an ellipse in x, p_x-phase space of widths $\delta x_o = \pm\ 0.5$ cm, $\delta p_{x_o} = \pm\ 0.05$ radian [emittance area, $\pi(\delta x_o)(\delta p_{x_o}) = 0.07854$ cm·radian = 78.54 milliradian·cm]. The wave-length associated with the electrical excitation of the cavity will be chosen to be $\lambda = 10.8$ cm ($\bar{\lambda} = 1.71887$ cm), so that the incident beam is centered at $x_o = 2.7$ cm, F_o is taken to be 0.04, and $s = 2.0$ cm.

Under the conditions just specified, one expects that the particles would gain or lose energy up to the maximum amount of 0.0115 (mc^2) -- *i.e.*, ± 1.15% -- [since $0.04 \sin(0.5\ \text{cm}/\bar{\lambda}) \cong 0.04 \sin(16.7\ \text{deg.}) = 0.04 \times 0.287 = 0.0115$] and other particles could experience deflections of as much as ± 40 milliradian. The initial conditions for eight representative particles are

---

* Direct differentiation of Eqns. (11b) and (11d) will be seen immediately to lead to a result that is consistent with the general relation expressed by Eqn. (1).

shown on the first of the following figures. This is followed by a sequence of similar diagrams* showing the emergent values of x and p_x when transit of the cavity is considered to occur, in turn, at the following times (30-degree intervals of electrical phase):

$$\tau_o: \ 0,\ 0.9 \doteq \lambda/12,\ \cdots\ 9.9 = 11\lambda/12.$$

Adjacent to the points plotted on these latter diagrams are given, in parentheses, the values of W on emergence so that one thereby obtains the factor by which the initial total energy is modified in each case by traversal of the cavity.

It is seen that, as expected, values of W that cover the range 0.9885 to 1.0115 are produced on traversing the cavity at $\tau_o = 0$ and at $\tau_o = \lambda/2$. Extreme slopes of ± 0.09 are found to occur at $\tau_o = \lambda/4$ and $\tau_o = 3\lambda/4$, respectively -- a change of ±0.04 from the limiting values of p_x in the incident beam. In addition to this additional deflection, some increased displacements of course may be expected when $s \neq 0$. From the complete set of graphs it is seen that in this example there is an approximate doubling of the area of x,p_x phase-space required to contain the beam.

The transformations introduced here have been employed in work associated with A.M. Sessler and G.R. Lambertson for an analytic examination of the cavity effects -- see below. The results seem to be consistent with the work reported here and suggest that the mode of operation just considered may be unattractive unless a beam of large emittance (but suitable brightness) is available, or unless cavity operation at considerably shorter wave-lengths is feasible. For this reason it has been suggested that some attention should be devoted to the possibility of passing the beam through the cavity in the neighborhood of $x_o = 0$, where the electric field is strong but the magnetic field is zero. Since in this case all particles traversing the cavity at the same moment would experience virtually the same change of energy, special attention should then be directed to the possible subsequent "bunching" of such a beam in the transport line or, more likely, in the compressor itself. Such a continuation

---

* Numerical values obtained by aid of the BRF teletype program ESPCY, a modification of ENSPR that automatically generated the sequential initial values employed in this series.

of the work possibly would be aided, or at least illustrated, by numerical work that could be performed with teletype programs similar to that used for the numerical work reported in this Section.

IV. REFERENCES

1. T. K. Fowler and W. M. Good, Nucl. Instr. and Methods 7, 245-252 (1960). See also an internal CERN report by B. Montague (CERN, Geneva, Switzerland). The technique has been discussed by Andre Lanzaro in an ERA Seminar at this Laboratory.

2. E. T. Whittaker, "Analytical Dynamics" (Dover, New York, 1944), §§ 127-128, p. 296 ff.

3. E. T. Whittaker (op. cit.) § 131, p. 300; H. Goldstein, "Classical Mechanics" (Addison-Wesley, Reading, Massachusetts, 1950), § 8-4, p. 250 ff -- esp. Eqns. (8-47, a-c), p. 253.

4. Program "RFCAV," remotely submitted by teletype to the LRL CDC-6600 computer.

Submitted to
Nuclear Instruments and Methods

UCRL-20143
ERAN-118

BETATRON AMPLITUDE GROWTH UPON TRAVERSING RESONANCES DURING THE COMPRESSION CYCLE OF AN ELECTRON RING ACCELERATOR†

L. J. Laslett and W. A. Perkins

Lawrence Radiation Laboratory
University of California
Berkeley, California

May 21, 1971

Abstract

In an electron ring accelerator electrons are often injected into a magnetic field with index $n = -(r/B_z)(dB_z/dr)$ of about 0.5. For extraction and axial acceleration of the ring, n must approach zero and several betatron resonances are crossed. Following particles on a computer through simulated fields (which approximate measured experimental fields) has elucidated which resonances are important and which magnetic field perturbations cause large growth for a particular geometry and coil-energizing sequence. Analytical formulas for resonance growth also have been derived and checked against the computer calculations. These equations indicate the important driving terms of the field and are convenient for estimating the expected growth on traversing a resonance. Resonances at $n = 0.5$, 0.36, 0.25, and 0.20 have been investigated.

1. Introduction

Betatron amplitude growth has been observed under certain conditions during the compression cycle of an electron ring accelerator [1,2].

† Work supported by the U.S. Atomic Energy Commission.

1-559

To better understand this phenomenon, and to be able to predict betatron-amplitude growth in future experiments, we undertook computer and analytical calculations pertaining to the device of ref. 2). In previous work with betatron resonances analytic[3-5] and some limited computer calculations[6] have been performed for other geometries. For an electron ring accelerator, the electrons typically are injected with a magnetic field index $n = (-r/B_z)(dB_z/dr)$ of about 0.5, and then during the compression cycle n decreases to ≈ 0.1.

Betatron resonant growth can occur when the radial oscillation frequency of an electron divided by its gyrofrequency, ν_r, or the axial oscillation frequency, divided by its gyrofrequency, ν_z, is a simple fraction, or when the ν_r and ν_z values are connected by simple integral relations. The quantities ν_r and ν_z are also called the radial and axial betatron tunes, and they are approximately related to the field gradient index n by

$$\nu_r^2 = 1 - n,$$

$$\nu_z^2 = n. \tag{1}$$

A particular resonance is designated by an equation of the form

$$k\nu_r + \ell\nu_z = m, \tag{2}$$

where k, ℓ, and m are positive or negative integers. In eq. (2) m indicates the harmonic order of the magnetic field's azimuthal variation that drives the resonance (see section 4). Important resonances arise when k, ℓ, and m are small, and if the magnetic field has median-plane symmetry, only resonances with even ℓ can occur.

We have investigated the following potentially dangerous resonances:

$$2\nu_r - 2\nu_z = 0, \quad \text{at} \quad n = 0.5;$$
$$\nu_r + 2\nu_z = 2, \quad \text{at} \quad n = 0.36;$$
$$2\nu_z = 1, \text{ at } \quad n = 0.25;$$
$$\nu_r - 2\nu_z = 0, \text{ at } \quad n = 0.20. \tag{3}$$

Presumably less important, and hence not included in eqs. (3), are higher-order resonances and those occurring in fields with non-median-plane symmetry. Unless the magnetic field has large higher harmonic components, the growth will be greatest on the lower-order resonances. With regard to resonances that arise only in the absence of median-plane symmetry, electron ring compressors are designed with due consideration to median-plane symmetry, and magnetic measurements indicate that deviation from this symmetry is small.

In sections 2 and 3 we discuss the computer method of calculating betatron growth by simulating the experimental magnetic fields. Then, in section 4 the analytic method is discussed, in which growth is calculated from certain parameters that characterize the radial and (possible) azimuthal variations of the magnetic field and can be determined from the magnetic measurements. (Often these field parameters can be estimated from simple calculations.) After determining these field variations, one can use the convenient analytic formulas given in section 4 to predict the growth for each resonance. The growth rates calculated from these formulas when compared with the computer calculations have agreed typically within 30% and in the worst case within a factor of 2.

2. Computer Simulation of the Experimental Magnetic Field

To compute the effect of a betatron resonance on a particle, one must simulate closely the driving terms of the actual magnetic field.

It is convenient to separate the magnetic field into two parts: (a) an azimuthally symmetric field and (b) an azimuthally varying (perturbation) field (if it is of significant magnitude). Note that a non-symmetric field is not required to actuate a homogeneous ($m = 0$) resonance. For each particular calculation two arrays are stored in the computer. One array contains the axial and radial magnetic field components (B_z, B_r) for the symmetric field and the other array is used to calculate the nonsymmetric field (B_z, B_r, B_θ).

The computational results reported in this paper were obtained for fields intended to simulate those present in the compression experiments reported in ref. 2).

2.1 Symmetric Field

The experimental apparatus for forming rings usually contains three or four sets of compression coils (see fig. 1 of ref.2). The coils of ref.2) have many turns of copper windings. If the particle is 20 cm or further from the coil, the windings can be accurately simulated by infinitesimal circular current loops. The fields from these loops can then be calculated by integration of the Biot-Savart law[7]. If the particle is closer than about 20 cm to the coil, however, the helical nature and crossover region of the windings can alter the magnetic field; see section 2.2.

The coils in the apparatus of ref. 2) were pulsed, so that the currents used in the program could be taken from those measured experimentally with Rogowski belts. Alternatively they could be calculated from knowledge of the voltages and capacity of the capacitor banks, and the inductance, mutual inductance, and resistances of the coil system. Both methods gave essentially the same result, so the latter method usually was used.

Because of the pulsed nature of the fields, the magnetic field from one coil could induce eddy currents in the copper turns (whether shorted or unshorted) of another coil. For a shorted loop, the current induced in the complete circuit can be calculated in a rather direct manner. However, the induced eddy currents due to the physical presence of the copper even when the coil is open must also be included. This was taken into account in computation of the symmetric field by means of simulation circuits comprised of two adjacent current loops with current in opposite directions. The currents in these loop pairs (which were driven by the active coils) were calculated in the program after parameters, such as the mutual inductances to the main coils, were adjusted so that the resulting magnetic field gradients were in agreement with measured values.

The calculated symmetric magnetic field agreed very well with measured field, the difference being less than 2%.

2.2 Azimuthally Varying Fields

Azimuthal variations of magnetic fields arise from two sources: (a) asymmetric coil construction or location, (b) eddy currents in metal that is nonazimuthally symmetric and in spatially localized ferromagnetic material.

The coils were placed very accurately with regard to center and tilt, and the possible field perturbation from this effect was estimated to be small. The effect of coil leads was also calculated. This introduced a field asymmetry of only 0.1% in the midplane B_z.

Coil Sets 1B, 2, and 3 (see fig. 1 of ref. 2) were wound with a threefold symmetry in their crossovers (inner radius to outer radius). This minimized first and second harmonic perturbations but introduced

a third harmonic variation. The magnitude of this effect was calculated for a current element with the geometry of the crossover conductor, and the resultant axial field was 0.5 to 1% of the total symmetric field. During the first stage of compression only Coil Sets 1A and 1B were energized, but eddy currents in the unshorted copper crossovers of Coil Sets 2 and 3 produced field perturbations of the same magnitude as those arising from the normal currents in the crossovers in Coil Set 1B.

Eddy currents in the copper-iron injection snout[2], the stainless steel flanges, probe housing, etc. gave rise to large peripheral bumps in the magnetic field. Fig. 1 shows the azimuthal variation of the axial field component in the median plane for two radii at the time of injection. Similar data were obtained as a function of time for several radii from 11 cm to 19 cm. Also direct midplane measurements of $(\Delta B_z/\Delta r)$ were made.

The third harmonic component was described by the calculated field contribution from the crossovers. In addition, four circular current loops (and a bias field) were used to simulate the peripheral bumps. The radius and location of each loop were chosen to fit the width and radial variation of the measured bump. The currents in the four simulation loops were determined as a function of time by a least-squares fit of the calculated fields $B_z(r, \theta, z = 0, t)$ to the measured midplane fields. A typical example of such a calculated field at injection time for $R = 19$ cm is shown in fig. 2. At injection time the guide field was typically 700 G.

The compressor was designed to have median-plane symmetry in its magnetic field during the compression cycle. Although Coil Set 3 was mechanically unsymmetric, the turn-to-turn spacing in the short coil of the pair was made larger so that the total field had reasonably good median-plane symmetry. Measurement of B_r indicated that the deviations from median-plane symmetry were small. Therefore, in the calculations it was assumed that B_r and B_θ are zero on the median plane. For convenience, a midplane array of $B_z(r, \theta, z = 0, t_1)$ was stored in the computer for the orbit code to calculate resonant growth near a time t_1. If B_z on the midplane is known, $\underset{\sim}{B}$ can be calculated for small (z/r) by the expansion equations

$$B_z(z) = B_z\Big|_{z=0} - \frac{z^2}{2r^2}\left\{ r\frac{\partial B_z}{\partial r}\Big|_{z=0} + r^2\frac{\partial^2 B_z}{\partial r^2}\Big|_{z=0} + \frac{\partial^2 B_z}{\partial \theta^2}\Big|_{z=0}\right\},$$

$$B_r(z) = z\frac{\partial B_z}{\partial r}\Big|_{z=0} ,$$

$$B_\theta(z) = \frac{z}{r}\frac{\partial B_z}{\partial \theta}\Big|_{z=0} . \qquad (4)$$

Most of the calculations were done neglecting the higher-order second term of B_z, as this simplification was found not to affect the results for those cases that were compared.

Another method of handling the azimuthally asymmetric field was to make a least-squares fit of the data (B_z and $\Delta B_z/\Delta r$) to Fourier series. For a particular time (when the resonance is crossed) arrays $(C_m^B, S_m^B, C_m^P, S_m^P)$ of Fourier coefficients (vs. r) are stored in the computer for use by the orbit code. The components of the asymmetry field are calculated from the arrays as follows:

1-562

$$B_z(r,z,\theta) = \sum_m \left\{\left(1 + \frac{m^2z^2}{2r^2}\right)\left[C_m^B(r)\cos m\theta + S_m^B(r)\sin m\theta\right]\right\}$$

$$- \frac{z^2}{2r}\sum_m\left[\left\{\frac{d}{dr}C_m^P(r)\right\}\cos m\theta + \left\{\frac{d}{dr}S_m^P(r)\right\}\sin m\theta\right] ,$$

$$B_r(r,z,\theta) = \frac{z}{r}\sum_m\left[C_m^P(r)\cos m\theta + S_m^P(r)\sin m\theta\right] ,$$

$$B_\theta(r,z,\theta) = \frac{z}{r}\sum_m m\left[S_m^B(r)\cos m\theta - C_m^B(r)\sin m\theta\right] , \qquad (5)$$

where C_m^B and S_m^B are the Fourier coefficients determined from the midplane B_z measurements. The coefficients C_m^P and S_m^P represent respectively $r\frac{\partial}{\partial r}C_m^B$ and $r\frac{\partial}{\partial r}S_m^B$, and are determined directly from the midplane $\Delta B_z/\Delta r$ measurements.

3. Computer and Some Experimental Results for Betatron Amplitude Growth

A typical calculated compression cycle is plotted in fig. 3 to indicate how the radius R, magnetic field B, kinetic energy T, and magnetic field index n vary with time. The variation with time of n at the location of the closed orbit (as on fig. 3) we will call the "n trajectory." Trajectories similar to this could be calculated for any set of parameters used in the experiment.

The n value at the location of the closed orbit could be shifted experimentally by putting a small current through a coil set which by itself would cause a large value of n at that location. For example, a small capacitor (of an n-shifter circuit) could be discharged through Coil Set 1B (see fig. 1 of ref. 2) to shift the n trajectory at large radius.

By use of the exact relativistic equations of motion and a simulated magnetic field for which the characteristics were adjusted to fit the experimental conditions, the resulting particle motion was determined by numerical integration. To obtain a scan of the total interesting region of n, particles were injected with different energies at various appropriate radii into a magnetic field that was constant with time. They were injected with an axial amplitude of 0.1 cm and a radial amplitude of roughly 2 cm. The resulting axial amplitude growth rate for the particles is plotted in fig. 4. The computer results thus demonstrate directly that there are regions of growth near $n = 0.20$, 0.25, 0.36, and 0.50. The peaks are not exactly centered about these n values, because the axial motion is modified by radial motion of appreciable amplitude. If the same calculations are performed for an azimuthally symmetric field, the $n = 0.25$ and $n = 0.36$ peaks disappear, but the $n = 0.20$ and $n = 0.5$ peaks remain.

That these results have physical significance is demonstrated in fig. 5, which depicts the experimental results for a compression cycle during which n was rapidly swept over a large range. (This result was obtained with an experimental apparatus similar to that of ref. 1 .) The X-ray signal is due to electrons striking an obstacle at 1.7 cm from the median plane and so is indicative of the acquisition of considerable axial amplitude. The value of n versus time was determined by a computer calculation and is accurate only to about 0.03. Thus, experimentally, there appear to be axial losses near $n = 0.5$, 0.25, and 0.20, in qualitative agreement with the computer calculations. (Axial growth near $n = 0.36$ has been observed for other conditions, but apparently it was too small to be observed in this case.)

The phenomenon of interest here in each case evidently is basically that which was treated in ref. 4). Briefly, in any resonant region an initially small axial amplitude exhibits an exponential growth, at least until quite large amplitudes are attained. The rate of this growth is dependent upon the proximity of n to the resonant value, and, in the case of coupling resonances, is dependent upon the amount by which the initial radial amplitude exceeds a certain threshold value.

To determine the total growth that would be expected in the operation of a compressor, it is necessary to traverse the resonance in the course of the computation. To simplify the calculation, the arrays for the symmetric and azimuthally asymmetric fields are stored in the computer for approximately the time at which a particular resonance is crossed. Then the symmetric magnetic field and the particle energy are varied with time at the same rate as they change during compression.

3.1 $2\nu_r - 2\nu_z = 0$ ($n = 0.50$) Resonance

This resonance occurs in the absence of azimuthal bumps, and is driven by nonlinearities of the field $(\partial^2 B_z/\partial r^2)$, $(\partial^3 B_z/\partial r^3)$, etc. This was shown in the computer calculations by runs with and without azimuthal bumps and with several different values of $(\partial^2 B_z/\partial r^2)$ and $(\partial^3 B_z/\partial r^3)$.

An example of crossing this resonance during the experiment[2] is shown in fig. 6. The x-ray signal is due to an axial loss of electrons when the n trajectory crossed $n = 0.5$. By moving the ring into a probe at smaller radius it was determined that about 1/3 of the electrons were lost on this resonance.

A computer simulation of traversing this resonance is shown in fig. 7. The particle is followed for only the few microseconds during which the resonance is traversed. The variation of n with number of revolutions (or time) is shown at the top of fig. 7. The time for one revolution is about 3.5 nsec.

Since the particle's position is not always printed out for its maximum axial or radial excursion, it is convenient to take for the axial and radial amplitudes the quantities

$$A_z = [(p_z/m_0\gamma\omega_{ce})^2/n + z^2]^{1/2} \tag{6}$$

and

$$A_r = [(p_r/m_0\gamma\omega_{ce})^2/(1-n) + (r - R)^2]^{1/2}, \tag{7}$$

where p_z and p_r are the momentum components, m_0 is the electron rest mass, γ is the ratio of total mass to rest mass, ω_{ce} is the gyrofrequency, and R is the radius of the closed orbit. By tracking particles in a constant magnetic field, R can be determined for a given electron energy. However, in traversing a resonance, R changes with time. Since $R \approx r_{ave}$ and r_{ave} is easier to obtain in the computer calculation, r_{ave} was used for most of the calculations of A_r. The initial radial and axial betatron amplitudes were chosen, for this calculation, to be 1.5 cm and 0.1 cm, respectively (see fig. 7). As one can see, the axial amplitude grows while the radial amplitude decreases. Several different initial phases were tried with similar results. Also the initial radial amplitude was varied, and in each case the axial amplitude grew to equal the initial radial amplitude. Because of the multiturn injection process, the initial radial amplitudes are 2 to 3 cm, and particles strike the walls if the axial

1-564

amplitudes grow to greater than about 2 cm. Thus this resonance growth at $n = 0.5$ explains the X-ray signals of fig. 6.

If a particle is injected into a constant magnetic field in the middle of the resonance, the axial and radial amplitudes continuously exchange maxima and minima, as shown in fig. 8. From these and other computer calculations an approximate rule for the relationship between axial and radial amplitudes was obtained,

$$A_z^2 + A_r^2 \approx \text{const.} \tag{8}$$

This rule seems to fit very well for small and moderate amplitudes. However, if the amplitudes become extreme, the rule breaks down. The maximum growth rate was shown to be approximately proportional to A_r^2.

3.2 $\nu_r - 2\nu_z = 0$ ($n = 0.20$) Resonance

This resonance at $n = 0.2$ is often referred to as the Walkinshaw resonance[3]. It has many similarities to the $(2\nu_r - 2\nu_z = 0)$ resonance discussed in 3.1. This resonance also can be driven by nonlinearities of the magnetic field in the absence of azimuthal variations.

The relationship between axial and radial amplitudes for this resonance is[5]

$$A_z^2 + 4A_r^2 \approx \text{const}, \tag{9}$$

for small and moderate amplitudes. This is demonstrated by the computational results, plotted in fig. 9, for particle motion in a constant magnetic field for which n has the resonant value 0.2. The maximum growth rate is approximately proportional to A_r.

3.3 $2\nu_z = 1$ ($n = 0.25$) Resonance

This resonance was shown to be driven by azimuthal asymmetries of the magnetic field. It was further shown by decomposing the field into its Fourier components that just first harmonic variations drive this resonance. Calculations were done for several initial values of A_r with no indication that the growth rate depends on A_r.

3.4 $\nu_r + 2\nu_z = 2$ (n = 0.36) Resonance

This resonance was shown to be driven by azimuthal asymmetries of the magnetic field. It was further shown by decomposing the field into its Fourier components that second harmonic variations account for more than 80% of the observed growth rate in typical cases. Also, the growth rate was shown to be roughly proportional to A_r.

In determining the total growth developed in traversing this resonance it was particularly important to start particles with several different phases. The sensitivity of the accumulated growth to the initial phase of the axial motion may be attributed to the fact that this resonance is inhomogeneous ($m \neq 0$) and involves a coupling effect from the radial motion. (The choice of the otherwise arbitrary origin of the angular coordinate θ cannot be used effectively in such cases to eliminate the apparent significance of phase differences between radial motion, axial motion, and the field perturbations.) Some particles have an increase in betatron amplitude, whereas other particles have a decrease. In fig. 10 the axial momentum p_z and position z are plotted for 24 particles (with different initial phases) for different times as the resonance is traversed. "T" refers to the number of revolutions (gyroperiods). One notes from fig. 10 that the elongation of the phase-space ellipses means that, after the resonance has been traversed, most particles have a larger axial betatron amplitude whereas some particles have a smaller axial amplitude.

4. Analytical Formulas for Four Resonances

The derivations of the analytical expressions for the growth rate, total growth, and width are given in Appendix A for the resonances described in section 3. The results of these calculations are given below. For the $2\nu_z + \nu_r = 2$ (n = 0.36) resonance and the $2\nu_z = 1$ (n = 0.25) resonance it was assumed that the midplane magnetic field had the form

$$B_z = B_0(r) + \sum_m [C_m(r,t) \cos m\theta + S_m(r,t) \sin m\theta]. \qquad (10)$$

The resonances do not always occur exactly at the expected value of n (see fig. 4) because of the modification of the axial equation by radial motion of appreciable amplitude.

4.1 $2\nu_r - 2\nu_z = 0$ (n = 0.50) Resonance

Let

$$b'' = \frac{R^2}{B_0} \left. \frac{\partial^2 B_z(r,t)}{\partial r^2} \right|_{r=R},$$

$$b''' = \frac{R^3}{B_0} \left. \frac{\partial^3 B_z(r,t)}{\partial r^3} \right|_{r=R}, \qquad (11)$$

where R and t are the radius and time at which the resonance is crossed. Then the maximum growth rate, total growth, growth factor, and full width of the resonance are given by

$$M = \text{Maximum Growth Rate} = \frac{0.020\, A_r^2}{R^2} \left| 3 + 20b'' - 56b''^2 - 12b''' \right| \quad \text{(decades/rev)}, \qquad (12)$$

$$G = \text{Total Growth} = \frac{1.6 \times 10^{-4} A_r^{\,4}}{R^4} \; \frac{[3 + 20b'' - 56b''^2 - 12b''']^2}{|dn/d(rev)|} \quad \text{(decades)}, \tag{13}$$

$$\text{Growth Factor} = 10^G, \tag{14}$$

and

$$\Delta n = 0.52\ M, \tag{15}$$

where A_r is the radial betatron amplitude given by eq. (7), and dn/d(rev) (the change in n per revolution) measures the rate at which the resonance is crossed. Thus for a given initial axial betatron amplitude, the predicted axial betatron amplitude after traversing the resonance is given by

$$A_z(\text{final}) = 10^G\ A_z\ (\text{initial}). \tag{16}$$

If the value for the final A_z [calculated by eq. (16)] is greater than A_r, then, in general, the limitations on growth given in eq. (8) will apply.

To minimize the growth caused by traversing this resonance one wishes to minimize the quantity $(3 + 20b'' - 56b''^2 - 12b''')$. Fig. 11 shows the curve of the equation

$$3 + 20b'' - 56b''^2 - 12b''' = 0. \tag{17}$$

This relation between b" and b"' for minimum growth was checked with a computer code using approximate equations of motion, and the four points obtained by minimizing growth for a given b" are also plotted in fig. 11. Results with exact particle trajectories were also consistent with this curve.

4.2 $\nu_r - 2\nu_z = 0$ (n = 0.20) Resonance

Here one has

$$M = \text{Maximum Growth Rate} = \frac{1.5 A_r}{R}\,|b''| \quad \text{(decades/rev)}, \tag{18}$$

$$G = \text{Total Growth} = \frac{0.96}{|dn/d(rev)|} \left(\frac{A_r b''}{R}\right)^2 \quad \text{(decades)}, \tag{19}$$

$$\text{Growth Factor} = 10^G, \tag{20}$$

and

$$\Delta n = 0.52\ M. \tag{21}$$

If the value for the final A_z [calculated by eq. (16)] is greater than $2A_r$, then, in general, the limitations on growth given in eq. (9) will apply.

4.3 $2\nu_z = 1$ (n = 0.25) Resonance

Let

$$C'_m(r,t) = r\,\frac{\partial C_m(r,t)}{\partial r}, \qquad S'_m(r,t) = r\,\frac{\partial S_m(r,t)}{\partial r}, \tag{22}$$

and

$$K = \frac{1}{B_0}\left\{[2C_1(r,t) - C'_1(r,t)]^2 - [2S_1(r,t) - S'_1(r,t)]^2\right\}^{1/2}, \tag{23}$$

where C_m, S_m, and B_0 are defined by eq. (10). Then,

$$M = \text{Maximum Growth Rate} = 1.4\ K \quad \text{(decades/rev)}, \tag{24}$$

$$G = \text{Total Growth} = \frac{1.1\ K^2}{|dn/d(rev)|} \quad \text{(decades)}, \tag{25}$$

$$\text{Growth Factor} = 10^G \tag{26}$$

and

$$\Delta n = 0.73\ M. \tag{27}$$

4.4 $\nu_r + 2\nu_z = 2$ (n = 0.36) Resonance

Let

$$C_m'' = \frac{\partial}{\partial r}\left[r^2 \ \frac{\partial C_m(r,t)}{\partial r}\right] ,$$

$$S_m'' = \frac{\partial}{\partial r}\left[r^2 \ \frac{\partial S_m(r,t)}{\partial r}\right] , \tag{28}$$

and

$$L = \frac{1}{2B_0}\left[(C_2'')^2 + (S_2'')^2\right]^{1/2} , \tag{29}$$

where C_m, S_m and B_0 are defined by eq. (10). Then

$$M = \text{Maximum Growth Rate} = 1.1 \ \frac{A_r}{R}\left|L\right| \quad \text{(decades/rev)}, \tag{30}$$

$$G = \text{Total Growth} = \frac{1.4 \ A_r^2 L^2}{R^2 \left|dn/d(rev)\right|} \quad \text{(decades)}, \tag{31}$$

$$\text{Growth Factor} = 10^G \tag{32}$$

and

$$\Delta n = 1.4 \ M. \tag{33}$$

It should be noted that the formulas above apply for the particle with the maximum growth on the phase-space ellipse (see fig. 10).

5. Discussion

To understand the resonant growth behavior observed in experiments during the compression phase of an electron ring accelerator, computer and analytical calculations have been performed for conditions similar to those in the experiment of ref. 2). At low intensity, when only single-particle effects should be important, the calculations agree

qualitatively with the experimental results. At high intensity some energy spreading occurs that broadens the time at which different particles cross the resonance. This makes it more difficult to compare the experimental and computer results, but even in these cases they seem to be consistent.

The calculations have also elucidated the driving terms for each resonance. Thus, if a particular resonance causes large growth one can try to reduce the field variation driving that resonance. For the n = 0.5 and n = 0.2 resonances one could add extra coils to adjust b" and b"' at the time the resonance is crossed. Changing the coil spacing or energizing the coils in a different sequence also can affect b" and b"'. For the n = 0.36 and n = 0.25 resonances the significant perturbations are greatest near the periphery of the chamber. By use of an n-shifter circuit these resonances can be crossed at smaller radii where the perturbations are smaller. If the magnetic-field bumps are still too large, one can remove various components from or add them to the simulated field in a computational program until satisfactory growth is obtained. Then one could remove these same components from (or add them to) the real experimental apparatus.

Looking at the formulas for "total growth" one notes that the total growth is proportional to the factor $1/\left|dn/d(rev)\right|$. Thus if a resonance can be crossed more rapidly this, in general, will reduce the growth, particularly since it appears in the exponent of the "growth factor." This will work well if the growth is not too large. For the n = 0.5 and n = 0.2 resonances, if the growth is so large that it is already limited only by the initial radial betatron amplitude, a small change in the speed of crossing the resonance may not reduce the final axial amplitudes.

ACKNOWLEDGMENTS

We are very appreciative for the use of the results of magnetic measurement performed by J. M. Peterson and J. B. Rechen. We are very thankful to A. C. Paul for a modified version of his orbit code and to D. R. George for his help in cataloging the measured and computed data. Helpful discussions with J. M. Peterson, A. M. Sessler, D. Keefe, and G. R. Lambertson are gratefully acknowledged.

APPENDIX A

Derivation of Analytical Formulas of Section 4

These calculations are directed to the occurrence of a substantial exponential growth of axial amplitude when the radial amplitude is sufficiently great. The axial amplitude is assumed to be small initially, consequently the axial motion can be characterized by a linear differential equation in which the radial motion may be regarded as a prescribed function.

The general procedure for deriving the analytical formulas is

(a) Determine the radial and axial equations of motion for a particle in the magnetic field.

(b) Determine an appropriate expression for the magnetic field which contains the relevant driving terms for the particular resonance under consideration. Then put this magnetic field into the equations of motion of (a).

(c) Make reasonable approximations to obtain a simple expression for the radial coordinate with the axial coordinate ignored. Then insert this expression into the axial equation of motion.

(d) After confirming that the axial equation has the form of a Hill or Mathieu equation, obtain a simple approximate solution.

(e) Using this solution, determine the width of the stop band of the resonance, the maximum growth rate, and the total growth.

We obtain the equations of motion from the Principle of Least Action,

$$\delta \int (\underset{\sim}{p} - e\underset{\sim}{A}) \cdot d\underset{\sim}{s} = 0, \qquad \text{(A1)}$$

where $\underset{\sim}{p}$ is the mechanical momentum and $\underset{\sim}{A}$ is the vector potential.

Since $d\underset{\sim}{s} = (r'\hat{e}_r + z'\hat{e}_z + r\hat{e}_\theta)d\theta$ (where the primes indicate differentiation with respect to θ), eq. (A1) can be expressed as

$$\delta \int \{ p[r^2 + r'^2 + z'^2]^{\frac{1}{2}} - e[rA_\theta + r'A_r + z'A_z]\} \, d\theta = 0 . \qquad \text{(A2)}$$

In the median plane, the radial variation of (A2) gives the familiar trajectory equation,

$$\frac{d}{d\theta}\left[\frac{pr'}{(r^2 + r'^2)^{\frac{1}{2}}}\right] - \frac{pr}{(r^2 + r'^2)^{\frac{1}{2}}} + e\left(\frac{\partial(rA_\theta)}{\partial r} - \frac{\partial A_r}{\partial \theta}\right) = 0, \qquad \text{(A3)}$$

or

$$\frac{d}{d\theta}\left[\frac{pr'}{(r^2 + r'^2)^{\frac{1}{2}}}\right] = \frac{pr}{(r^2 + r'^2)^{\frac{1}{2}}} - erB_z .$$

For $r' \ll r$ this can be written as the simplified approximate equation

$$r'' - r + er^2 B_z/p = 0. \qquad \text{(A4)}$$

Considering the axial variation of (A2) results in

$$\frac{d}{d\theta}\left[\frac{pz'}{(r^2 + r'^2 + z'^2)^{\frac{1}{2}}}\right] - er\left(\frac{1}{r}\frac{\partial A_z}{\partial \theta} - \frac{\partial A_\theta}{\partial z}\right) + er'\left(\frac{\partial A_r}{\partial z} - \frac{\partial A_z}{\partial r}\right) = 0,$$

or (A5)

$$\frac{d}{d\theta}\left[\frac{pz'}{(r^2 + r'^2 + z'^2)^{\frac{1}{2}}}\right] = erB_r - er'B_\theta ,$$

which similarly may be approximated as

$$z'' - er^2 B_r/p = 0. \qquad \text{(A6)}$$

1. $\underline{\nu_r - 2\nu_z = 0 \ (n = 0.20) \text{ Resonance}}$

Because the relation between the oscillation frequencies is homogenous [it has the form of eq. (2) with $m = 0$], azimuthal field variations are not required for excitation of this resonance, and it therefore is appropriate to focus attention instead on the effect of nonlinearity in the magnetic field.

Let

$$x = \frac{r-R}{R}$$

and (A7)

$$y = \frac{z}{R} .$$

Expanding the magnetic field about $r = R$ and $z = 0$, with B_z symmetric with respect to the median plane, and using Maxwell's equation, we obtain

$$B_z = B_0 \, [1 - nx + \tfrac{1}{2}b'' \, (x^2 - y^2)] \; , \qquad \text{(A8)}$$

$$B_r = B_0 \, [- ny + b''xy] \; , \qquad \text{(A9)}$$

where b'' is given by eq. (11). Curvature effects have been neglected in (A8) and (A9), and these field components satisfy the curl condition $\frac{\partial B_z}{\partial x} = \frac{\partial B_r}{\partial y}$ and the divergence condition $\nabla\cdot\underset{\sim}{B} \approx \frac{1}{R}\left[\frac{\partial B_r}{\partial x} + \frac{\partial B_z}{\partial y}\right] = 0.$

Substituting (A8) and (A9) into (A4) and (A6) and neglecting higher-order terms results in

$$x'' + (1-n)x - \tfrac{1}{2}b''(y^2-x^2) = 0 \tag{A10}$$

and

$$y'' + ny - b''xy = 0\ , \tag{A11}$$

where we have used eq. (A7) and $p = eRB_0$.

We adopt the viewpoint of Walkinshaw[3] and treat the x motion as a prescribed motion unaffected by coupling effects. This non-Hamiltonian approach appears to be entirely justified when one is examining the onset of y growth from initial amplitudes that are quite small.

In this spirit one writes eq. (A11) as

$$y'' + (\nu_y^2 - b''x)y = 0 \tag{A12}$$

and introduces† $x = A_x \cos \nu_x\theta$ to obtain the Mathieu equation

$$y'' + (\nu_y^2 - b''A_x \cos \nu_x\theta)y = 0, \tag{A13}$$

where $\nu_x^2 = 1-n$ and $\nu_y^2 = n$.

The relevant "stop band" for this equation, within which growth ultimately will occur for all non zero initial conditions (save for a set of measure zero) is defined by the inequalities††

† An additional phase constant in the expression for x would clearly be inconsequential in this case, as it would correspond to no more than a translation of the origin of θ.

†† See ref. 4), esp. eqs. (2.7) and (2.9), p. 1237. These expressions are, of course, merely the leading terms of well-known series developments for the eigenvalues associated with the eigenfunctions ce_1 and se_1 of the Mathieu equation [cf. Whittaker and Watson, Modern Analysis (Cambridge University Press, London and New York, 1927), Sect. 19.3]. The phase shift of these solutions, per period of the coefficient of y, is π (and hence $\nu_y \approx \nu_x/2$).

$$\frac{\nu_x^2}{4} - \left|\frac{b''A_x}{2}\right| < \nu_y^2 < \frac{\nu_x^2}{4} + \left|\frac{b''A_x}{2}\right| \ ; \tag{A14}$$

i.e., by †

$$\left|\nu_x^2 - (2\nu_y)^2\right| < 2\left|b''A_x\right| \ , \tag{A15}$$

or

$$|A_x| > A_{thr} = \frac{\left|\nu_x^2 - (2\nu_y)^2\right|}{2|b''|} . \tag{A16}$$

The quantity A_{thr} defined by eq. (A16) thus constitutes a threshold amplitude of radial motion above which axial growth will be expected to occur.

Within the stop-band just defined one expects a lapse rate μ, for the amplitude of the exponentially growing solution of the Mathieu equation (A13), given by††

$$\mu \approx \left\{ \frac{\left[\nu_y^2 - \left(\frac{\nu_x}{2}\right)^2 - \frac{1}{2}b''A_x\right]\left[\left(\frac{\nu_x}{2}\right)^2 - \frac{1}{2}b''A_x - \nu_y^2\right] < c^2 > < s^2 >}{4 < -sc' > < cs' >} \right\}^{1/2} . \tag{A17}$$

For the eigenfunctions $c(\theta)$ and $s(\theta)$, it is convenient merely to take $\cos \nu_y\theta$ and $\sin \nu_y\theta$ respectively, resulting in

$$\frac{\langle c^2\rangle \langle s^2\rangle}{\langle -sc'\rangle \langle cs'\rangle} \approx \frac{1}{\nu_y^2} . \tag{A18}$$

Then,

$$\mu = \frac{|b''|}{4\nu_y}(A_x^2 - A_{thr}^2)^{1/2} \text{ neper per radian of } \theta . \tag{A19}$$

† Cf. section IIIA of ref. 4, especially eqs. (3.4) and (3.5), pp. 1241-1242, with $a = \nu_y^2$, $b = c = 0$, and $d = -b''A_x$.

†† Ref. 4, section IID, especially eq. (2.58), p. 1240.

Writing $A_x = A_r/R$ and $\nu_y \approx \sqrt{0.2}$, with $A_{thr} = 0$, we obtain the maximum growth rate

$$M = \frac{\pi}{\sqrt{0.8}\ \ln 10}\ \frac{A_r}{R}\left|b''\right| \quad \text{decades/rev} \ . \tag{A20}$$

In passage through the resonance there is an accumulated growth that can be estimated by use of eq. (A17), which is conveniently rewritten as

$$\mu = \left[(2b''A_x - 1 + 5n)(2b''A_x + 1 - 5n)\right]^{1/2}/(8\sqrt{0.2}) . \tag{A21}$$

In passage through the resonance, n increases from its value

$$n_1 = \frac{1 - 2\left|b''\right|A_x}{5} \tag{A22}$$

at one edge of the stop band to

$$n_2 = \frac{1 + 2\left|b''\right|A_x}{5} \tag{A23}$$

at the other. On the assumption that the growth is not so great that turnover has occurred or is approached, the y amplitude is expected to grow by the factor $\exp \int_{n=n_1}^{n=n_2} \mu d\theta$. If the resonance is traversed at a constant rate of change of $n \left[\frac{dn}{d\theta} = \text{const.}; \text{ or } \frac{dn}{d\theta} = \frac{1}{2\pi}\frac{dn}{d(\text{rev})}\right.$, where $\frac{dn}{d(\text{rev})}$ is the rate of change of n per revolution and is treated as a $\left.\text{constant}\right]$, one has

$$\int_{n=n_1}^{n=n_2} \mu d\theta = \frac{1}{\left|\frac{dn}{d\theta}\right|}\int_{n_1}^{n_2} \mu dn = \frac{2\pi}{\left|\frac{dn}{d(\text{rev})}\right|}\int_{n_1}^{n_2} \mu dn$$

$$= \frac{2\pi}{\left|\frac{dn}{d(\text{rev})}\right|}\int_{n_1}^{n_2} \frac{5\sqrt{(n-n_1)(n_2-n)}}{8\sqrt{0.2}}\, dn = \frac{(\pi^2/4)(5/4)^{3/2}(n_2-n_1)^2}{\left|dn/d(\text{rev})\right|}$$

$$= \frac{\pi^2}{2\sqrt{5}}\ \frac{b''^2 A_x^2}{\left|dn/d(\text{rev})\right|} \quad \text{nepers,} \tag{A24}$$

or the total growth is

$$G = \frac{\pi^2}{2\sqrt{5}\ \ln 10}\ \frac{1}{\left|dn/d(\text{rev})\right|}\left(\frac{A_r b''}{R}\right)^2 \quad \text{decades.} \tag{A25}$$

The width of the resonance is

$$\Delta n = \left|n_2 - n_1\right| = \frac{4A_r}{5R}\left|b''\right| = \frac{8\sqrt{0.2}\ \ln 10}{5\pi}\ M \approx 0.52\ M. \tag{A26}$$

2. $2\nu_r - 2\nu_z = 0$ ($n = 0.50$) Resonance

Here also the relation between the oscillation frequencies is homogeneous, and it again is appropriate to focus attention on the effect of nonlinearity in the magnetic field.

The resonance $2\nu_r - 2\nu_z = 0$ is of higher order than most of the coupling resonances to which attention has been given, leading, for example, to a predicted "stop-band width" that is proportional to the square rather than to the first power of the radial amplitude. Special care must be taken, therefore, not to omit effects whose consequences would be of the same order as those treated in the analysis, and the algebraic work correspondingly is tedious. The analysis presented below has, however, been subjected to some computational checks and is believed to constitute an adequate semiquantitative description of the axial growth that can arise from the $2\nu_r = 2\nu_z$ resonance.

The magnetic field can be adequately described by means of an azimuthally directed vector-potential function that is developed in terms of the coordinates x and y as†

$$\frac{rA_\theta}{R^2B_0} = \frac{2x + x^2}{2} - \frac{3x^2 + 2x^3}{6}n + \frac{4x^3 + 3x^4}{24}b'' + \frac{5x^4 + 4x^5}{120}b'''$$

$$+ \frac{1 + x}{2}\,(n - xb'' - \tfrac{1}{2}x^2b''')y^2. \qquad \text{(A27)}$$

Here n is the field index, and b'', b''' are constants that have been evaluated at the (circular) equilibrium orbit of radius R [see eqs. (11)]. The differential equation for uncoupled radial motion (A3) with use of this vector potential is

$$\frac{d}{d\theta}\left[\frac{x'}{\sqrt{(1+x)^2 + x'^2}}\right] - \frac{1+x}{\sqrt{(1+x)^2+x'^2}} + (1+x)\left[1 - nx + \frac{1}{2}\,b''x^2 + \frac{1}{6}\,b'''x^3\right] = 0, \qquad \text{(A28)}$$

where x' denotes $dx/d\theta$ and we have set $p = eRB_0$.

To provide in full measure the required alternating terms in the equation for axial motion, it is necessary to obtain a solution for x

†The expression given for rA_θ/R^2B_0 can be extended to a more consistent form by the addition of the term

$$\frac{1}{24(1+x)}\left(n + b'' + \frac{2 + 6x + 3x^2}{2}\,b'''\right) y^4;$$

such a term is not required for the present analysis, however, since only linear forces are included in the differential equation for axial motion used here.

that is valid through terms proportional to the square of the radial-oscillation amplitude. Terms proportional to x'^2 in the differential equation thus properly should not be ignored. A suitable solution, obtainable by harmonic balance, is of the form[8]

$$x = P_0 + P_1 \cos \nu_x\theta + P_2 \cos 2\nu_x\theta \qquad \text{(A29)}$$

(an inconsequential arbitrary phase constant being ignored), with

$$P_0 = (3C_2 + \tfrac{1}{4})A_x^{\,2}, \quad P_1 = A_x, \quad P_2 = -\,(C_2 - \tfrac{1}{12})A_x^{\,2} \qquad \text{(A30)}$$

and

$$\nu_x^2 = 1 - n - (15\,C_2^2 + \tfrac{5}{4}\,C_2 + \tfrac{3}{4}\,C_3 - \tfrac{11}{96}\,)\,A_x^2; \qquad \text{(A31)}$$

here $C_2 = -\,(2-4n + b'')/6$ and $C_3 = (6n - 6b'' - b''')/6$, and these coefficients are approximately equal to $-\frac{1}{6}\,b''$ and $\frac{1}{2} - b'' - \frac{1}{6}\,b'''$, respectively, for $n \approx \frac{1}{2}$.

The linearized differential equation that describes small-amplitude axial excursions is obtained from eq. (A5):

$$\frac{d}{d\theta}\left[\frac{y'}{\sqrt{(1+x)^2 + x'^2}}\right] + (1+x)(n - b''x - \tfrac{1}{2}\,b'''x^2)y = 0, \qquad \text{(A32)}$$

with $y' = dy/d\theta$. The quantity $\left[(1+x)^2 + x'^2\right]^{-\frac{1}{2}}$ may now be expanded through terms of order x^2 or x'^2 and the solution previously given for x substituted into this equation to obtain a result of the form

$$\frac{d}{d\theta}[(1+\alpha_2+\beta_2\cos \nu_x\theta+\gamma_2\cos 2\nu_x\theta)y'] + (\alpha_0+\beta_0\cos \nu_x\theta+\gamma_0\cos 2\nu_x\theta)y = 0, \qquad \text{(A33)}$$

where

$$\alpha_2 = (\tfrac{1}{8} + \tfrac{1}{2}b'')A_x^2\,, \quad \beta_2 = -A_x\,, \quad \gamma_2 = (\tfrac{13}{24} - \tfrac{1}{6}b'')A_x^2\,,$$

$$\alpha_0 = n + (\tfrac{1}{8} - b'' + \tfrac{1}{2}b''^2 - \tfrac{1}{4}b''')A_x^2, \quad \beta_0 = (n-b'')A_x,$$

$$\gamma_0 = (\tfrac{1}{24} - \tfrac{1}{2}b'' - \tfrac{1}{6}b''^2 - \tfrac{1}{4}b''')A_x^2\,. \tag{A34}$$

The differential equation (A33) can be regarded as a generalized Hill equation, for which we may seek eigenvalues α_0 that permit periodic solutions with a basic frequency (ν_y) equal to ν_x. It will be recognized that with regard to the coefficient γ_0 such solutions would be analogous to the solutions se_1 and ce_1 that occur at the boundaries of the first stop band for the Mathieu equation, whereas with respect to the coefficient β_0 they are analogous to the functions se_2 and ce_2 associated with the second stop band of the Mathieu equation. Because β_0 is directly proportional to A_x and γ_0 is proportional to A_x^2, one thus may expect that the influence of each of these terms will be to generate a stop band whose width is proportional to A_x^2.

By the use, in turn, of trial functions of the form $D_1 \sin \nu_x\theta + D_2 \sin 2\nu_x\theta$ and $E_0 + E_1 \cos \nu_x\theta + E_2 \cos 2\nu_x\theta$, the procedure of harmonic balance leads respectively to the following estimates for the corresponding eigenvalues:

$$\alpha_{0,1} = \nu_x^2 - \left(\tfrac{5}{32} - \tfrac{11}{24}b'' + \tfrac{1}{4}b''^2 + \tfrac{1}{8}b'''\right)A_x^2\,,$$

$$\alpha_{0,2} = \nu_x^2 - \left(\tfrac{7}{32} - \tfrac{1}{24}b'' - \tfrac{11}{12}b''^2 - \tfrac{1}{8}b'''\right)A_x^2\,, \tag{A35}$$

or, after the expression given in Eq. (A31) for ν_x^2 is inserted,

$$\alpha_{0,1} = 1 - n - \left(\tfrac{5}{12} - \tfrac{17}{12}b'' + \tfrac{2}{3}b''^2\right)A_x^2\,,$$

$$\alpha_{0,2} = 1 - n - \left(\tfrac{23}{48} - b'' - \tfrac{1}{2}b''^2 - \tfrac{1}{4}b'''\right)A_x^2\,. \tag{A36}$$

Finally, noting that

$$\alpha_0 = n + \left(\tfrac{1}{8} - b'' + \tfrac{1}{2}b''^2 - \tfrac{1}{4}b'''\right)A_x^2\,, \tag{A37}$$

we obtain the estimated stability boundaries

$$n_1 = \frac{1}{2} - \frac{13 - 58b'' + 28b''^2 - 6b'''}{48}A_x^2\,, \tag{A38}$$

$$n_2 = \frac{1}{2} - \frac{29 - 96b'' - 24b'''}{96}A_x^2\,, \tag{A39}$$

with a central value

$$n_c = \frac{1}{2} - \frac{55 - 212b'' + 56b''^2 - 36b'''}{192}A_x^2 \tag{A40}$$

and a width

$$\Delta n = |n_2 - n_1| = \frac{|3 + 20b'' - 56b''^2 - 12b'''|}{96}A_x^2\,. \tag{A41}$$

Within the stop band bounded by the eigenvalues $\alpha_{0,1}$ and $\alpha_{0,2}$ one expects† that the growth rate of an exponentially increasing solution (formed approximately as $e^{\mu\theta}$ times a linear combination of

† See ref. 4, especially Sect. IID, p. 1240.

the periodic eigenfunctions associated with the boundaries of this stop band) will be given approximately by

$$\mu = \left(\frac{(\alpha_0-\alpha_{0,1})(\alpha_{0,2}-\alpha_0)}{4\nu_x^2}\right)^{\frac{1}{2}} = \left[0.5(\alpha_0-\alpha_{0,1})(\alpha_{0,2}-\alpha_0)\right]^{\frac{1}{2}} \text{ nepers/radian.} \qquad (A42)$$

By use of the expressions previously given for α_0, $\alpha_{0,1}$, and $\alpha_{0,2}$, this characteristic exponent becomes

$$\mu = \left[2(n-n_1)(n_2-n)\right]^{\frac{1}{2}} \text{ nepers/radian,} \qquad (A43)$$

with a maximum growth rate of

$$M = \frac{\sqrt{2}\,\pi}{96 \ln 10}\left|3 + 20b'' - 56b''^2 - 12b'''\right|\left(\frac{A_r}{R}\right)^2 \text{ decades/rev.} \qquad (A44)$$

The total growth in traversing the resonance is

$$G = \int_{n=n_1}^{n_2}\mu d\theta = \frac{\pi^2\sqrt{2}}{36864 \ln 10}\,\frac{(3+20b''-56b''^2-12b''')^2}{|dn/d(\text{rev.})|}\left(\frac{A_r}{R}\right)^4 \text{ decades.} \qquad (A45)$$

The proportionality of this result to A_r^4, being characteristic of traversal of a second-order resonance, is noteworthy.

3. $2\nu_z = 1 (n = 0.25)$ Resonance

We represent the magnetic field components by expressions that contain azimuthal variations but are carried only through first-order terms in x, y. The radial motion in this case contains a flutter that arises from closed-orbit distortions produced by the azimuthal variation

of B_z, and this flutter is introduced into the axial equation through the factor $r^2[= R^2(1+2x + \cdots)]$ of eq. (A4). In principle a term of similar order would arise from the inclusion of the second-order term $B_0 b''\cdot xy$ in B_r, but normally the contribution of this additional term is relatively small. We accordingly write

$$B_z = B_0(1-nx) + C_m^B \cos m\theta + S_m^B \sin m\theta + (C_m^P \cos m\theta + S_m^P \sin m\theta)\,x \qquad (A46)$$

and

$$B_r = -\,n B_0 y + (C_m^P \cos m\theta + S_m^P \sin m\theta)y, \qquad (A47)$$

where

$$C_m^P = \left[r\,\frac{dC_m^B(r)}{dr}\right], \qquad S_m^P = \left[r\,\frac{dS_m^B(r)}{dr}\right], \qquad (A48)$$

with the coefficients C_m^B, S_m^B, C_m^P, S_m^P evaluated at $r = R$.

The resonance $2\nu_z = 1$ has the form of eq. (2) with $m = 1$, indicating that first harmonic variations in the azimuthal field are important. Substituting the magnetic field of eqs. (A46) and (A47), with m = 1, into eqs. (A4) and (A6) and neglecting higher-order terms in x and y results in

$$x'' + (1-n)x + x[(C_1^P + 2C_1^B)\cos\theta + (S_1^P + 2S_1^B)\sin\theta]/B_0 = -(C_1^B\cos\theta + S_1^B\sin\theta)/B_0, \qquad (A50)$$

$$y'' + (1+2x)ny - (C_1^P\cos\theta + S_1^P\sin\theta)\,(y/B_0) = 0. \qquad (A51)$$

In a low order of approximation, we write the solution to (A50) as

$$x \approx \frac{C_1^{\,B} \cos\theta + S_1^{\,B} \sin\theta}{nB_0} . \tag{A52}$$

Substituting (A52) into (A51), we obtain

$$y'' + ny + [(2C_1^{\,B} - C_1^{\,P}) \cos\theta \quad + (2S_1^{\,B} - S_1^{\,P}) \sin\theta]\, y/B_0 = 0 . \tag{A53}$$

Thus we may consider the Hill equation

$$y'' + (n + K \cos\theta)y = 0, \tag{A54}$$

where

$$K = \frac{1}{B_0} [(2C_1^{\,B} - C_1^{\,P})^2 + (2S_1^{\,B} - S_1^{\,P})^2]^{\frac{1}{2}}. \tag{A55}$$

From (A54) we obtain a lapse rate†

$$\left[\frac{(n-n_1)(n_2-n) < c^2 > < s^2 >}{4 < -sc' > < cs' >} \right]^{\frac{1}{2}} = [(n-n_1)(n_2-n_1)]^{1/2} \tag{A56}$$

within the $\nu_z = \frac{1}{2}$ stop band. Also††

$$n_1 = 0.25 - K/2,$$

$$n_2 = 0.25 + K/2. \tag{A57}$$

† Ref. 4, section IID, especially eq. (2.58), p. 1240.

†† See ref. 4, especially eq. (2.60), p. 1241.

Thus the maximum growth rate is

$$M = K/2 \quad \text{nepers/radian} \tag{A58}$$

or

$$M = \frac{\pi K}{\ln 10} \quad \text{decades/rev}, \tag{A59}$$

and the width of the stop band is

$$\Delta n = n_2 - n_1 = K = \frac{\ln 10}{\pi} M \approx 0.73\ M. \tag{A60}$$

The total growth upon traversing this resonance is

$$G = \int_{n=n_1}^{n_2} \mu d\theta = \frac{\pi^2}{4 \ln 10} \frac{K^2}{|dn/d(\text{rev})|} \quad \text{decades}. \tag{A61}$$

4. $\nu_r + 2\nu_z = 2$ ($n = 0.36$) Resonance

This resonance has the form of eq. (2) with $m = 2$, indicating that second harmonic azimuthal variations in the field are important for its excitation. In order to allow fully for coupling of free radial oscillations into the axial equation as a first-order perturbation, it is appropriate to develop the B_r component of magnetic field to such an order that eq. (A47) is supplemented by a term proportional to xy. Accordingly, if the B_r component is taken to be given as in eq. (A47) to lowest order by $(1/z)B_r(r,\theta) = (1/r)\xi(r,\theta)$ [where $\xi(r,\theta) = r\, \partial B_z/\partial r = - n(r,\theta)B_z(r,\theta)$ for $z = 0$], one writes

$$\frac{B_r(r,\theta)}{z} \doteq \frac{\varepsilon(r,\theta)}{r}\bigg|_{r=R} + \frac{\partial\left(\frac{\varepsilon(r,\theta)}{r}\right)}{\partial r}\Bigg|_{r=R} (r-R) \qquad \text{(A62)}$$

or

$$\begin{aligned} r^2B_r(r,\theta) &\doteq R^2(1+2x+\cdots)\Bigg\{\left[-nB_0 + C_2{}^P\Big|_R \cos 2\theta + S_2{}^P\Big|_R \sin 2\theta\right] y \\ &\quad + \left[b''B_0 + R^2\left(\frac{d(C_2{}^P/r)}{dr}\bigg|_R \cos 2\theta + \frac{d(S_2{}^P/r)}{dr}\bigg|_R \sin 2\theta\right)\right] xy\Bigg\} \\ &\doteq R^2\Bigg\{\left[-nB_0 + C_2{}^P\Big|_R \cos 2\theta + S_2{}^P\Big|_R \sin 2\theta\right] y \\ &\quad + \left[(b''-2n)B_0 + \frac{d(rC_2{}^P)}{dr}\bigg|_R \cos 2\theta + \frac{d(rS_2{}^P)}{dr}\bigg|_R \sin 2\theta\right] xy\Bigg\}. \qquad \text{(A63)} \end{aligned}$$

Insertion of this expression (A63) for r^2B_r into the differential equation for axial motion, $y'' - \frac{r^2B_r}{R^2B_0} = 0$ [cf. (A6)], then yields

$$\begin{aligned} &y'' + \left[n - \frac{1}{B_0}\left(C_2{}^P\Big|_R \cos 2\theta + S_2{}^P\Big|_R \sin 2\theta\right)\right] y \\ &\quad + \left[2n - b'' - \frac{1}{B_0}\left(\frac{d(rC_2{}^P)}{dr}\bigg|_R \cos 2\theta + \frac{d(rS_2{}^P)}{dr}\bigg|_R \sin 2\theta\right)\right] xy = 0. \end{aligned} \qquad \text{(A64)}$$

For the coupling resonance $2\nu_z + \nu_r = 2$ of present interest we now may ignore the constant term $2n - b''$ in the coefficient of xy in (A64); likewise the alternating component in the coefficient of y does not play a direct role in exciting this resonance, and recognition of this alternating component can be given through use of a $\nu_y{}^2$ whose value is slightly displaced from n.

Recognizing that the absolute phase of the perturbation is of no importance, the equation for axial motion [eq. (A64)] therefore can be taken to be of the form

$$y'' + (\nu_y{}^2 - 2\,L\,x \sin 2\theta)\,y = 0, \qquad \text{(A65)}$$

where

$$L = \frac{1}{2B_0}\left\{\left[\frac{d(rC_2^P)}{dr}\bigg|_R\right]^2 + \left[\frac{d(rS_2^P)}{dr}\bigg|_R\right]^2\right\}^{1/2}. \qquad \text{(A66)}$$

With the radial oscillations written simply as $x \doteq A_x \sin \nu_x\theta$, eq. (A65) then becomes

$$y'' + \{\nu_y{}^2 + A_xL[\cos(2+\nu_x)\theta - \cos(2-\nu_x)\theta]\}y = 0. \qquad \text{(A67)}$$

Equation (A67) may be regarded as a Hill equation [especially if we artificially suppose ν_x and $m(=2)$ to be commensurate in some, possibly large, interval]. Noting that eq. (A67) has the form of eq. (2.45) of ref. 4 (taking the lower sign) with

$$\begin{aligned} a &= \nu_y{}^2 \approx n, \\ c &= -2A_xL, \\ \nu_0 &= 2-\nu_x, \\ q &= 2/\nu_0, \\ b &= d = 0, \end{aligned} \qquad \text{(A68)}$$

we conclude the estimated width of the resonance indicated by the stability boundaries is†

---

† Ref. 4, especially eq. (2.50), p. 1240.

$$\left|(2\nu_y)^2 - (2-\nu_x)^2\right| = 2\left|LA_x\right| . \tag{A69}$$

If the threshold amplitude is taken to be

$$A_{thr} = 2\,\frac{\left|\nu_y^2 - \left(\frac{2-\nu_x}{2}\right)^2\right|}{|L|} , \tag{A70}$$

then the lapse rate is expected to be†

$$\mu = \left\{\left[\nu_y^2 - \left(\frac{2-\nu_x}{2}\right)^2 + \frac{1}{2}\left|LA_x\right|\right]\left[\left(\frac{2-\nu_x}{2}\right)^2 + \frac{1}{2}\left|LA_x\right| - \nu_y^2\right]\right\}^{1/2} \Big/ 2\nu_y \tag{A71}$$

or

$$\mu = \frac{|L|}{4\nu_y} \quad (A_x^2 - A_{thr}^2)^{1/2} \text{ nepers per radian of } \theta . \tag{A72}$$

The maximum growth rate is thus

$$M = \frac{5\pi |L|}{6 \ln 10} \left(\frac{A_r}{R}\right) \text{ decades/rev,} \tag{A73}$$

and the total growth is

$$G = \frac{\pi^2}{3(\ln 10)\left|dn/d(rev)\right|} \left(\frac{LA_r}{R}\right)^2 \text{ decades} \tag{A74}$$

with a resonance width of

$$\Delta n = \frac{8|L|}{5} \left(\frac{A_r}{R}\right) = \frac{48 \ln 10}{25\,\pi} \; M \approx 1.4 \; M . \tag{A75}$$

† Ref. 4, section IID, especially eq. (2.58), p. 1240.

1-577

REFERENCES

1. D. Keefe, G. R. Lambertson, L. J. Laslett, W. A. Perkins, J. M. Peterson, A. M. Sessler, R. W. Allison, Jr., W. W. Chupp, A. U. Luccio, and J. B. Rechen, Phys. Rev. Letters <u>22</u> (1969) 558.

2. D. Keefe, W. W. Chupp, A. A. Garren, G. R. Lambertson, L. J. Laslett, A. U. Luccio, W. A. Perkins, J. M. Peterson, J. B. Rechen, and A. M. Sessler, Experiments on Forming, Compressing and Extracting Electron Rings for the Collective Acceleration of Ions (Lawrence Radiation Laboratory Report UCRL-20144, 1970) to be published in Nucl. Instr. and Methods.

3. W. Walkinshaw, A Spiral Ridged Bevatron, A.E.R.E. Report, Harwell, 1956 (unpublished).

4. L. J. Laslett and A. M. Sessler, Rev. Sci. Instr. <u>32</u> (1961) 1235.

5. A. A. Garren, D. L. Judd, L. Smith, and H. A. Willax, Nucl. Instr. and Meth. <u>18</u>, <u>19</u>, (1962) 525.

6. A. C. Paul, Study of the Regenerative Extractor of the Berkeley 184-Inch Synchrocyclotron, UCRL-18211, April, 1968 (unpublished).

7. W. R. Smythe, <u>Static and Dynamic Electricity</u>, 2nd ed., (McGraw-Hill Book Co., New York, 1950) Sect. 7.14, Eq. (1), p. 275.

8. L. J. Laslett, On an Analytic Solution for Radial Motion When x' Terms Are Included, Lawrence Radiation Laboratory Report ERAN-102, August 1970 (unpublished).

FIGURE CAPTIONS

Fig. 1. The variation of the z component of magnetic field as a function of the azimuthal angle for radii of 18.5 cm and 13 cm at the time of injection.

Fig. 2. Comparison of measured and simulated azimuthally varying fields for a radius of 19 cm at the time of injection.

Fig. 3. The radius of the closed orbit (R), the kinetic energy (T) of the electrons, the magnetic field (B), and the magnetic field index (n) at the location of the closed orbit, as functions of time during the compression of the electron ring for a typical compression cycle.

Fig. 4. Growth rate of axial betatron amplitude for particles injected into a magnetic field that is constant in time, for different values of n (different radii and kinetic energies).

Fig. 5. X-ray signal (due to electrons striking an axial obstacle 1.7 cm from the median plane) as a function of time during a compression cycle in which n at the location of the ring is swept rapidly with the aid of n-shifter circuits; n is determined by calculation and is accurate only to about 0.03.

Fig. 6. X-ray signal showing electron loss on traversal of n = 0.5 resonance.

Fig. 7. Radial and axial betatron amplitudes versus time (number of revolutions) as the n = 0.5 resonance is traversed by a particle in the computer calculation. The initial radial and axial betatron amplitudes are 1.5 cm and 0.1 cm respectively. The upper graph shows how n is varying during this time.

Fig. 8. Radial and axial betatron amplitudes versus time (number of revolutions) for a particle in a constant magnetic field in the middle of the n = 0.5 resonance.

Fig. 9. Radial and axial betatron amplitudes versus time (number of revolutions) for a particle in a constant magnetic field in the middle of the n = 0.2 resonance.

Fig. 10. P_z-z phase-space ellipse as the n = 0.36 resonance is traversed. T refers to the number of revolutions.

Fig. 11. Relation between b" and b"' for vanishing growth rate from eq. (17). The circled points represent a computer check of the analytical formula.

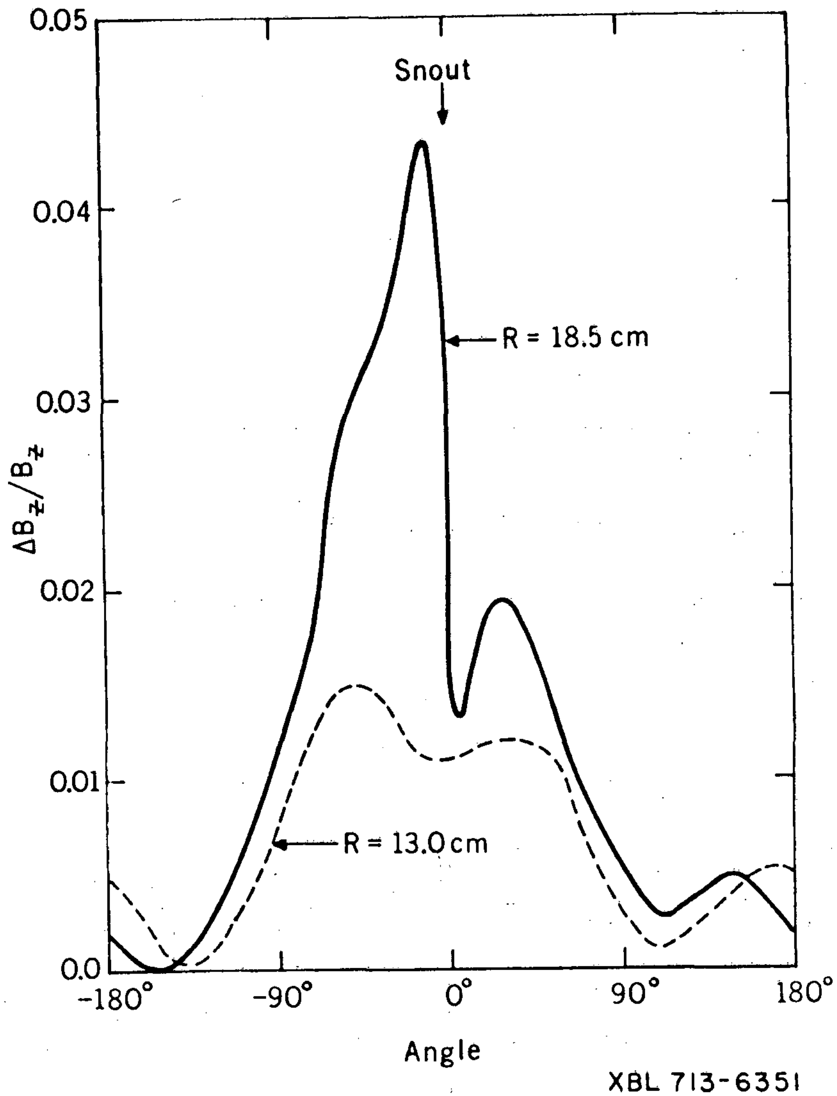

Figure 1

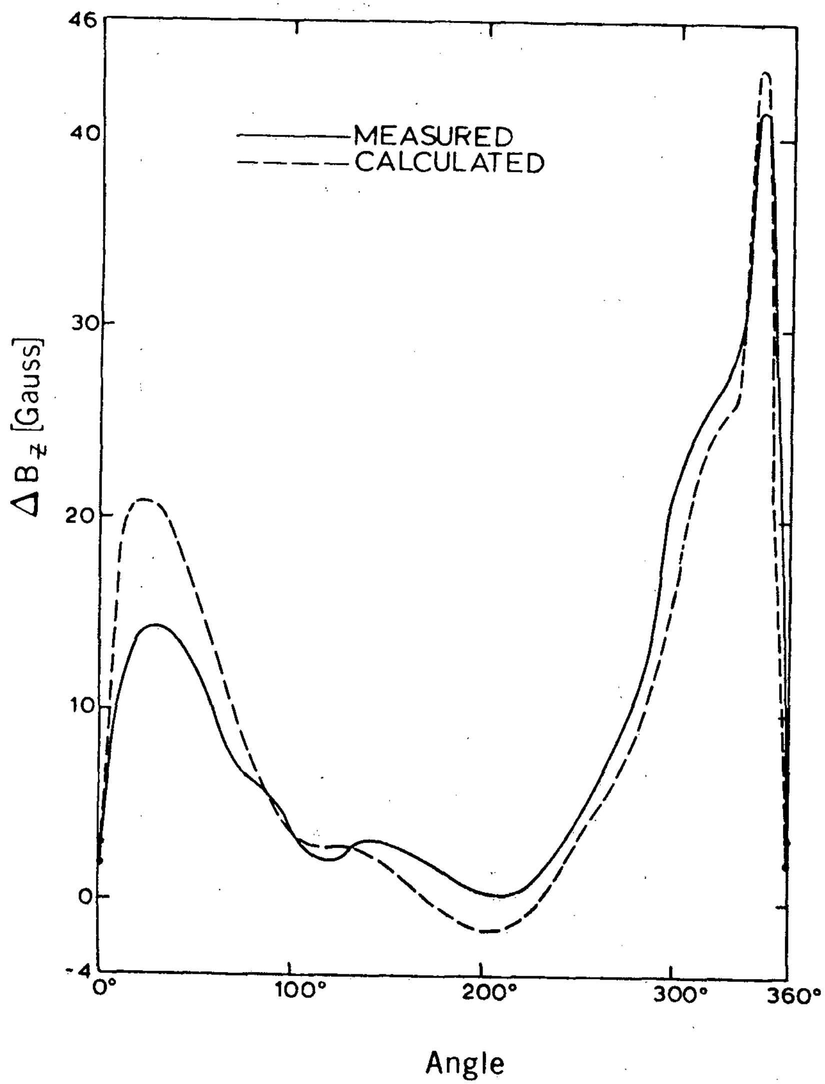

Figure 2

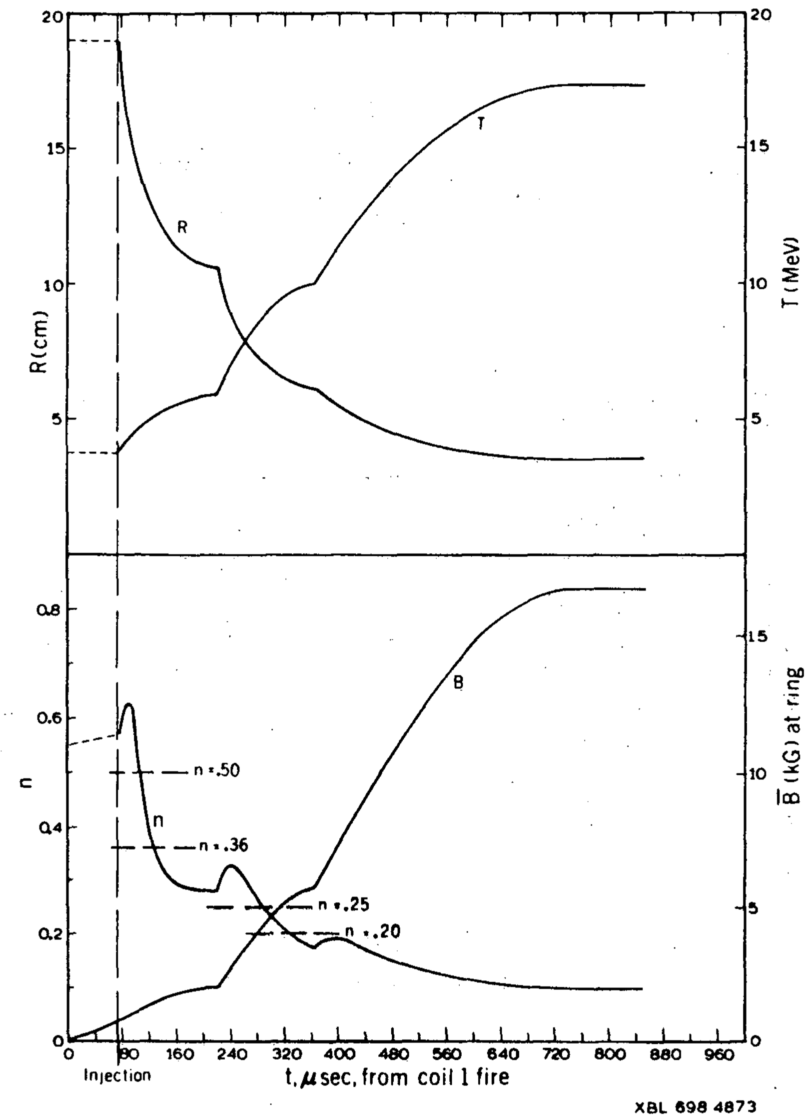

Figure 3

1-579

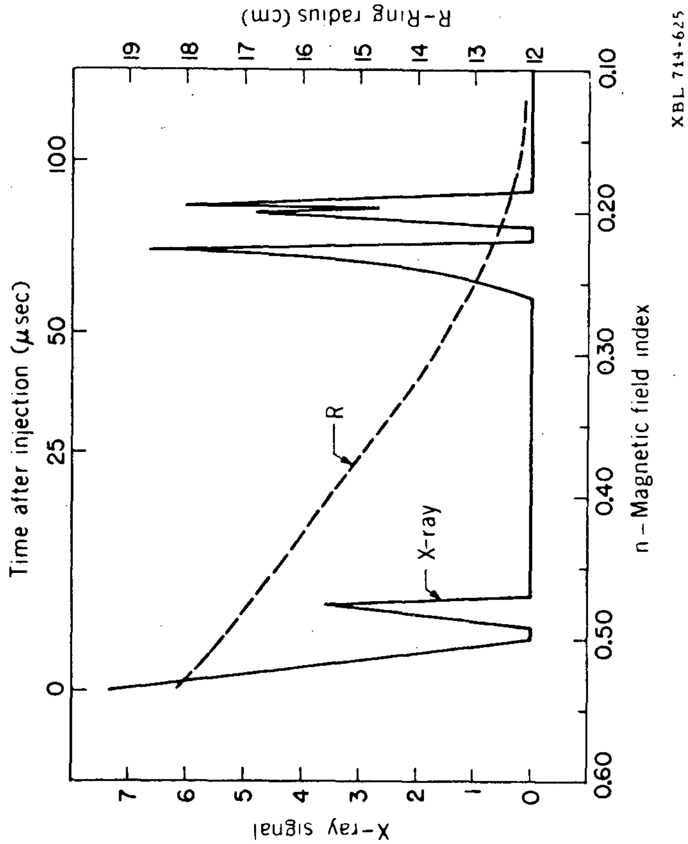

Figure 5

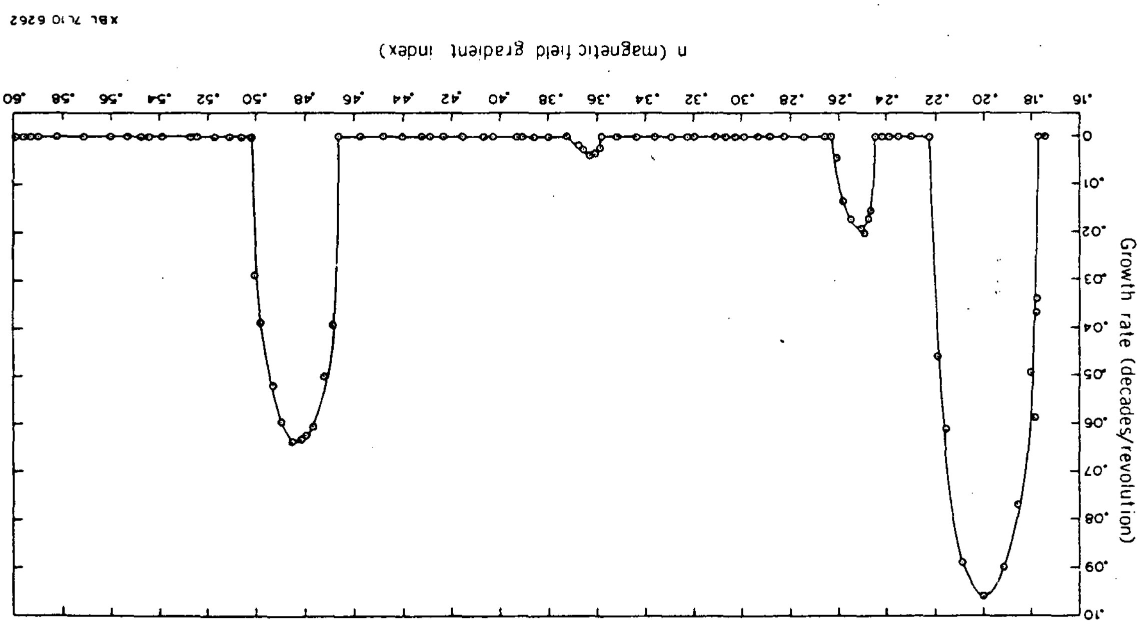

Figure 4

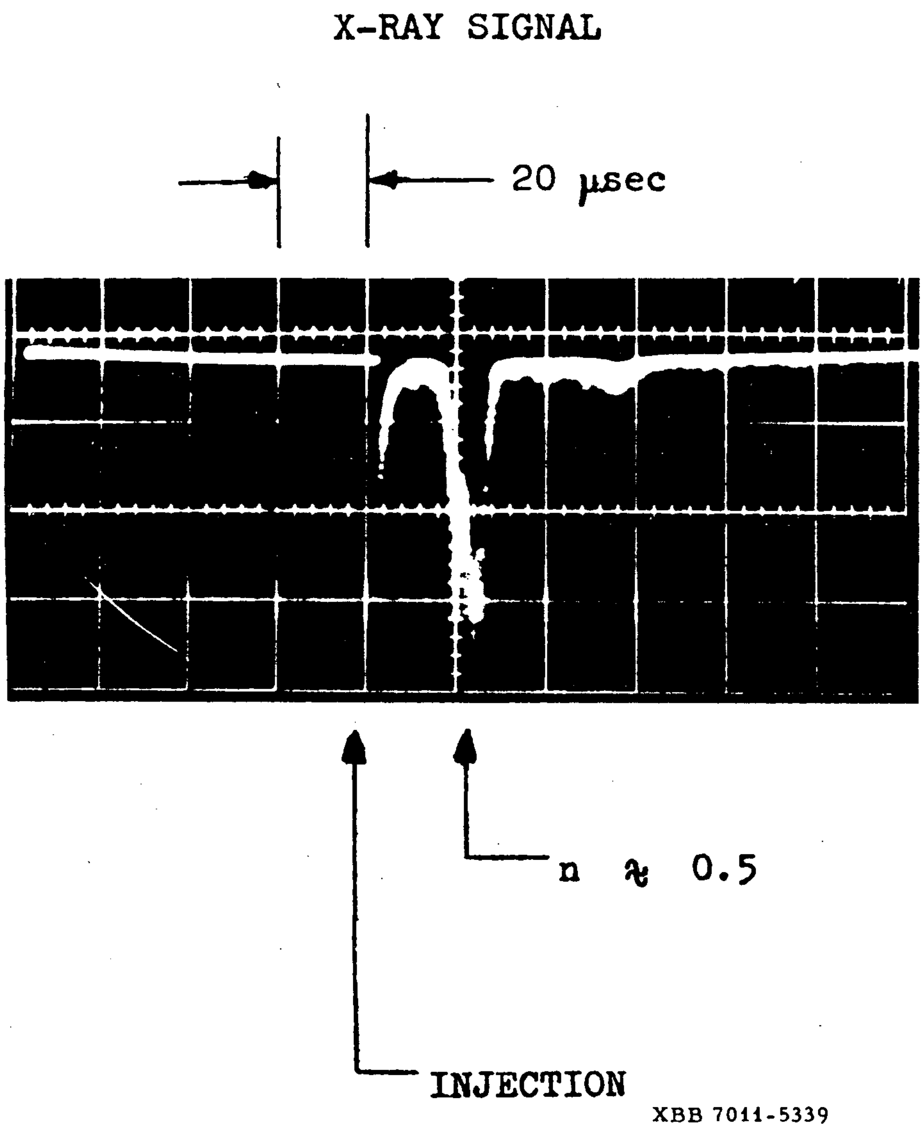

Figure 6

1-581

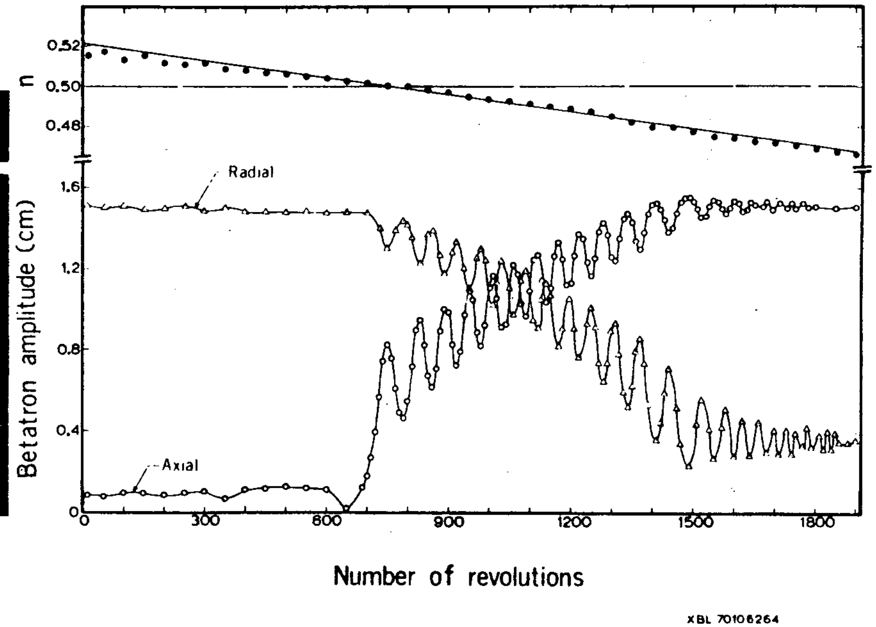

Figure 7

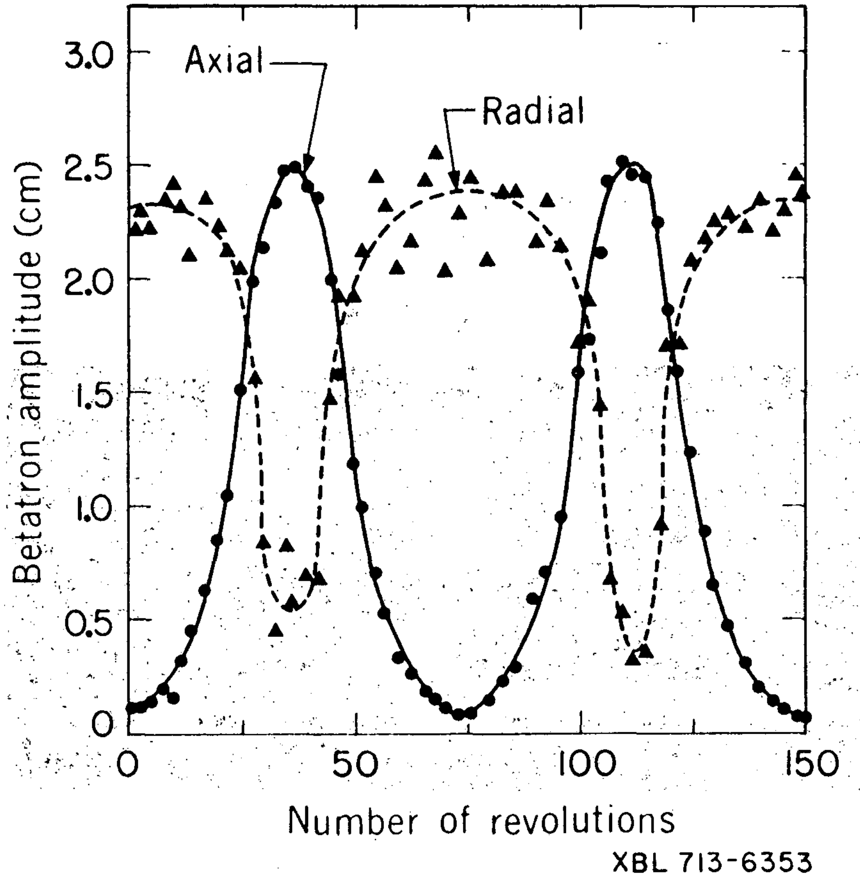

Figure 8

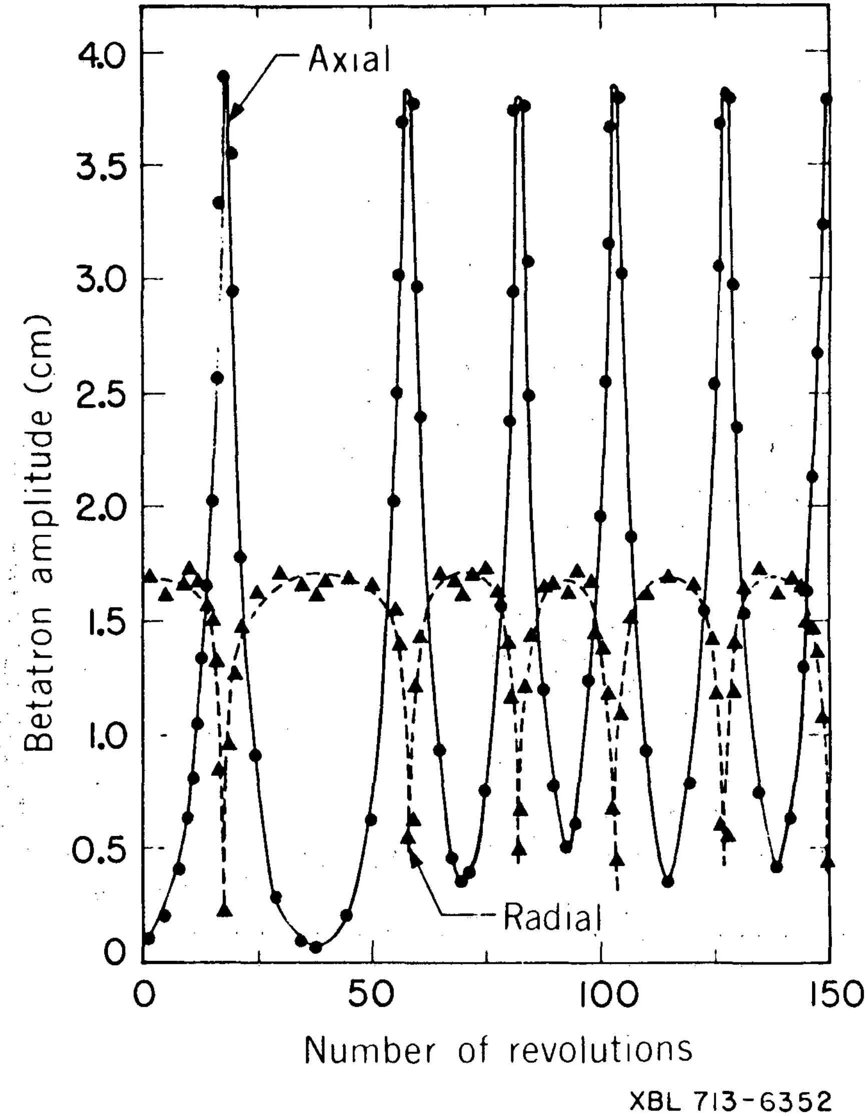

Figure 9

1-582

1-583

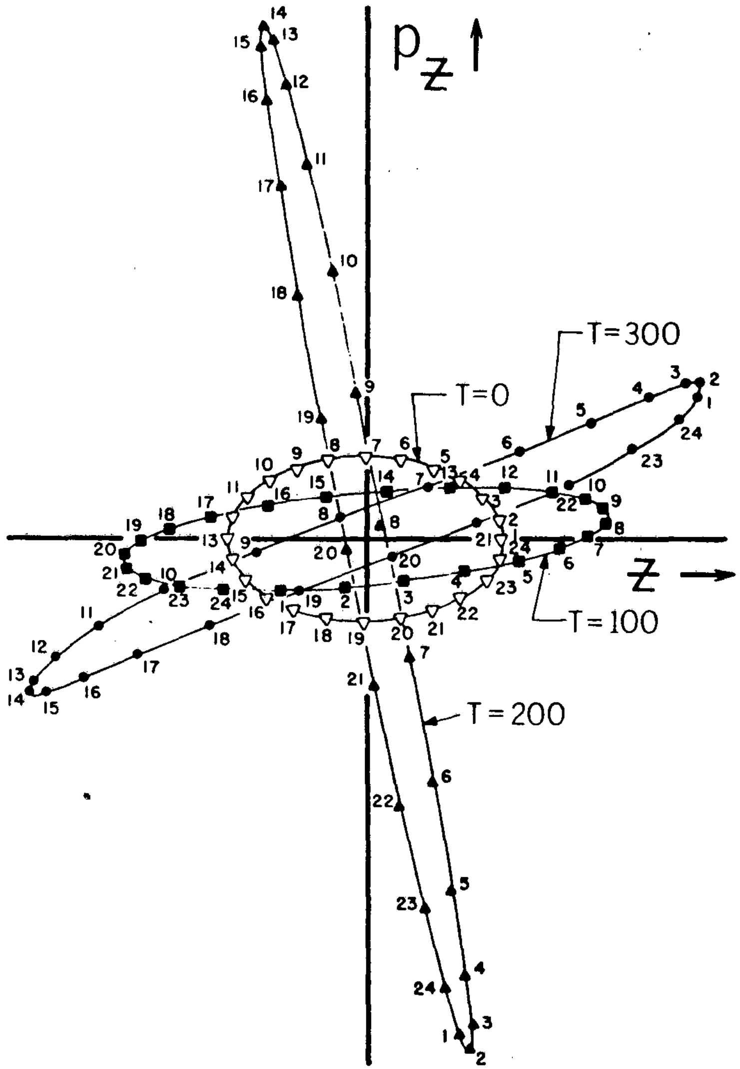

XBL 713-6355

Figure 10

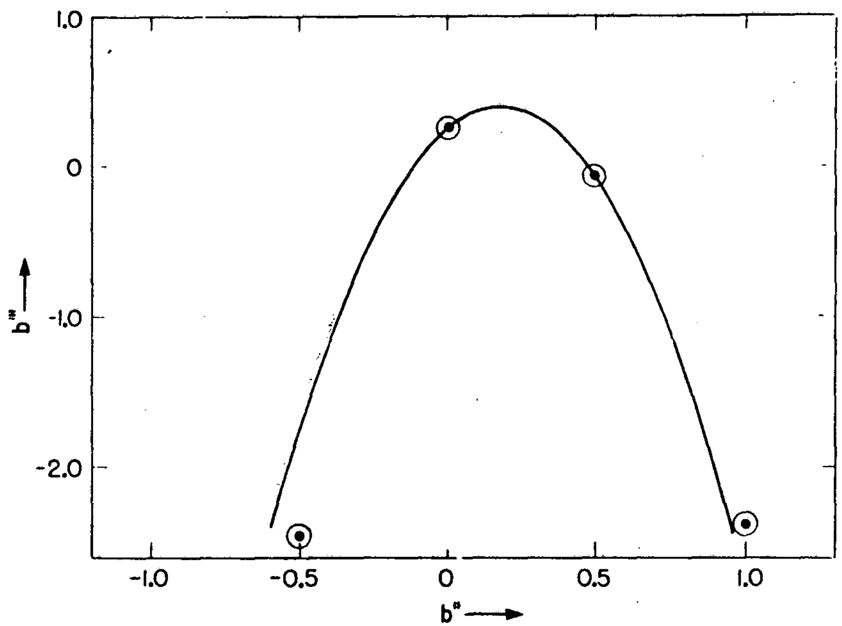

XBL 713-6354

Figure 11

2

Magnets and Magnetic Fields

TEST OF LASLETT BOUNDARY WITH WINDOW FRAME CURRENT REGION.

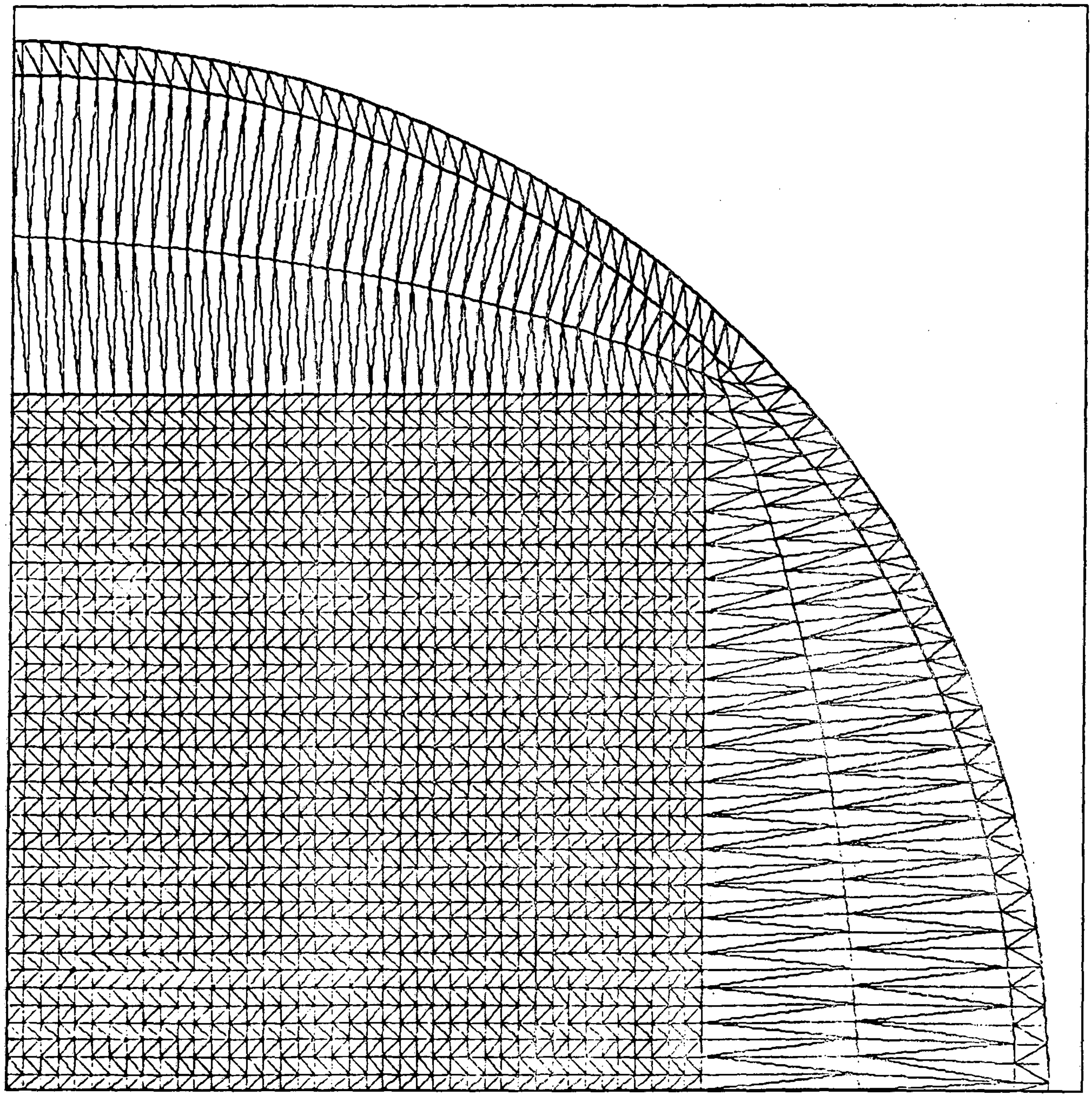

ACCELERATOR DEVELOPMENT DEPARTMENT

BROOKHAVEN NATIONAL LABORATORY
Associated Universities, Inc.
Upton, L. I., N. Y.

SOME ASPECTS OF SEARCH COIL DESIGN

L. J. Laslett*

July 5, 1954

* On leave from the Ames Laboratory of the AEC, Iowa State College, to represent the Mid-Western University Research Association.

The preparation of the present notes has been motivated by the importance of magnetic field measurements in the design of a high-energy alternate-gradient proton synchrotron at the Brookhaven National Laboratory. The report consists of five parts.

I. Review of Garrett's Theory for Axially-Symmetric Search Coils

II. Theory for Two-Dimensional Search Coils

III. Estimate of Some Errors in Search Coil Measurements

IV. Measurement of Field-"Gradients" with Axially-Symmetric Search Coils

V. Measurement of Field-"Gradients" with Two-Dimensional Search Coils

VI. Reference and Notes

A summary of this material was presented to the ADD Magnet Group on July 2, 1954 and is reported here for convenient reference by those participating in the magnet program.

PART I

Review of Garrett's Theory for Axially-Symmetric Search Coils

1. Introduction

The design of flux-coils for measurement of magnetic fields is materially aided by the use of theoretical results contained in a series of two papers by Garrett.[1,2] Since we shall make frequent use of the results of Garrett's work, it is convenient to make available here a summary of that portion of Garrett's theory which pertains to search-coil design.[2] We shall endeavor to adhere to Garrett's notation throughout.

2. Method of Approach

We shall be concerned with coil systems possessing an axis of symmetry, but which may be used for measurements of magnetic fields free of any special symmetry restrictions. Spherical polar coordinates are used, with x designating distance along the polar axis and θ, α the colatitude angles of field points or points on the coil system.

It is found useful to note that the response of a search coil to axial derivatives of an external applied field is related to the nature of the exterior field which would be generated by current in the search coil. The scalar magnetic potential generated externally by a current i (e.s.u.) in the coil is written

$$V_{coil} = 2\pi\,(i/c) \sum \frac{p_n}{n+1} \left(\frac{r_o}{r}\right)^{n+1} P_n(\cos\theta),$$

where r_o is a constant length introduced for dimensional convenience. It may then be shown [3] that the response of the search coil, when situated in an applied external magnetic field characterized by a scalar potential V_o, is given by the flux linkages

$$\Phi = \sum \Phi_n,$$

where

$$\Phi_n = -2\pi p_n\, r_o^{\,n+1}\, V_o^{(n)} / (n+1)!$$

and

$$V_o^{(n)} \equiv d^n V_o/dx^n \text{ evaluated at the origin.}$$

For a coil intended to measure flux-density at a point it is thus desirable that p_3 shall vanish (the coefficients

p_n normally vanishing automatically for n even, due to symmetry in the coil construction), and the vanishing of additional coefficients p_5, ... would be a beneficial refinement. [We note that in the special case of a two-dimensional field $V_o(x, \xi)$, the derivative associated with p_3 may be written $V_o^{(3)} \equiv d^3V_o/dx^3 = -(d^2/d\xi^2)(dV_o/dx) = d^2H_{axial}/d\xi^2$.]

3. Evaluation of the Coefficients P_n

(i) For a current loop ----The exterior magnetic potential from a current loop (f_j) is readily shown to be given on the axis by

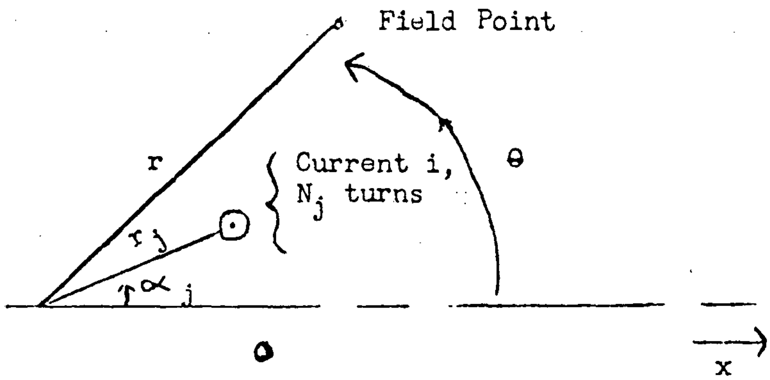

$$V_{axis}(f_j) = N_j\,(i/c)\,(\text{solid angle subtended by the coil})$$

$$= 2\pi N_j\,(i/c)\left[1 - \frac{r - r_j\cos\alpha_j}{|\bar{r} - \bar{r}_j|}\right]$$

$$= 2\pi N_j\,(i/c)\left\{1 - \left[1 - \left(\frac{r_j}{r}\right)\cos\alpha_j\right]\left[P_o + \left(\frac{r_j}{r}\right)P_1 + \left(\frac{r_j}{r}\right)^2 P_2 + \ldots\right]\right\}$$

$$= 2\pi N_j\,(i/c)\sum_n \left(\frac{r_j}{r}\right)^{n+1}(\cos\alpha_j\,P_n - P_{n+1})$$

$$\doteq 2\pi N_j\,(i/c)\sum_n \left(\frac{r_j}{r}\right)^{n+1}\frac{\sin^2\alpha_j}{n+1}\,P_n'(\cos\alpha_j)\;;$$

hence, generally,

$$V\,(f_j) = 2\pi N_j\ (i/c)\ \sum_n \frac{\sin^2\alpha_j\ P_n'(\cos\alpha_j)}{n+1}\left(\frac{r_j}{r}\right)^{n+1} P_n\,(\cos\theta), \text{ and}$$

$$p_n\,(f_j) = N_j\ \sin^2\alpha_j\ \ P_n'\,(\cos\alpha_j)\,\left(\frac{r_j}{r_o}\right)^{n+1}.$$

(ii) For a solenoid ----For a solenoid which is thin radially (cylindrical current sheet) and is formed of N_k' turns/cm, the exterior magnetic potential and the associated coefficients $p_n(s)$ may be obtained by integration of the result for a current loop. We note that[4]

$$\frac{d}{dx}\left[r^{n+2}\ \sin^2\alpha\, P_{n+1}'\ (\cos\alpha)\right] \equiv (n+2)\ r^{n+1}\ \sin^2\alpha\, P_n'\ (\cos\alpha)$$

and obtain

$$p_n(s) = \frac{r_o}{n+2}\ \sum_k\ N_k'\ \ \sin^2\alpha_k\ \ P'_{n+1}\,(\cos\alpha_k)\,\left(\frac{r_k}{r_o}\right)^{n+2},$$

N_k' being given opposite sign at the two ends of the solenoid.

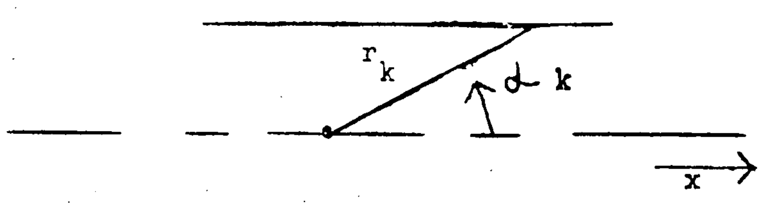

(iii) <u>For a coil</u> ----The exterior magnetic potential from an extended coil, with N''_ℓ turns per cm^2, is obtained by an additional integration.

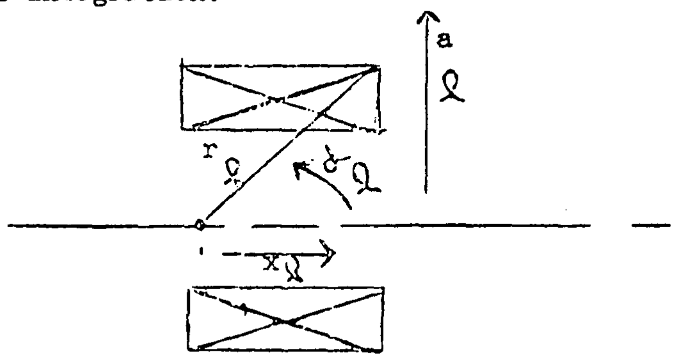

Garrett [2] discusses a systematic procedure for this integration, which we may check directly for the coefficient $p_3(c)$ in the case of a winding with rectangular cross-section:

from (ii) $$p_3(c) = \frac{r_o}{5} \sum N'_k \sin^2\alpha_k \, P'_4(\cos\alpha_k) \left(\frac{r_k}{r_o}\right)^5$$

$$= r_o \sum N'_k \left(\frac{x_\ell}{x_o}\right)^5 \frac{\sin^2\alpha_k}{\cos^5\alpha_k} \left(\frac{7}{2}\cos^3\alpha_k - \frac{3}{2}\cos\alpha_k\right);$$

$$p_3(c) = \frac{N''}{N'} \int p_3(s)\, da$$

$$= \frac{N''}{N'} \int p_3(s) \frac{x_k \, d\alpha_k}{\cos^2\alpha_k}$$

$$= r_o^2 \sum_\ell N''_\ell \left(\frac{x_\ell}{r_o}\right)^6 \int \left[\frac{7}{2}\frac{\sin^2\alpha}{\cos^4\alpha} - \frac{3}{2}\frac{\sin^2\alpha}{\cos^6\alpha}\right] d\alpha$$

$$= \frac{r_o^2}{30} \sum_\ell N'_\ell \left(\frac{x_\ell}{r_o}\right)^6 \left[20\tan^3\alpha_\ell - 9\tan^5\alpha_\ell\right],$$

or, in Garrett's form,

$$p_3\ (c) = \frac{r_o^2}{5 \times 6} \sum_{\ell} N''_{\ell} \left(\frac{x_\ell}{r_o}\right)^3 \left[\left(\frac{a_\ell}{r_o}\right)^3 (20 - 9 \tan^2 \alpha_\ell)\right],$$

since $x_\ell / a_\ell = 1/\tan \alpha_\ell$.

Garrett (Table I, Ref. 2) gives the coefficients A_n, B_{no}, B_{n2}, ... (for $n \leq 11$) in the general expression

$$p_n\ (c) = \frac{r_o^2}{(n+2)\ (n+3)} \sum_{\ell} N''_{\ell} \left(\frac{x_\ell}{r_o}\right)^n \left(\frac{a_\ell}{r_o}\right)^3 \frac{B_{no} - B_{n2} \tan^2 \alpha_\ell + \ldots}{A_n};$$

this table is given below for convenient reference. The sign of N''_{ℓ} alternates as one proceeds with the summation around the boundary of the rectangular winding.

TABLE I

COEFFICIENTS FOR THICK-SOLENOID CONSTANTS p_n, APPEARING IN THE EXPRESSION

$$p_n\ (c) = \frac{r_o^2}{(n+2)\ (n+3)} \sum_{\ell} N''_{\ell} \left(\frac{x_\ell}{r_o}\right)^n \left(\frac{a_\ell}{r_o}\right)^3 \frac{B_{no} - B_{n2} \tan^2 \alpha_\ell + \ldots}{A_n}$$

n	A_n	B_{no} (+)	B_{n2} (−)	B_{n4} (+)	B_{n6} (−)	B_{n8} (+)	B_{n10} (−)	C
0	1	(1)*						
1	1	4						
2	2	20	(3)*					2*
3	1	20	9					

Table I (continued)

n	A_n	B_{no} +	B_{n2} −	B_{n4} +	B_{n6} −	B_{n8} +	B_{n10} −	C
4	8	280	252	(15)*				4*
5	1	56	84	15				
6	16	1344	3024	1080	(35)*			24*
7	8	960	3024	1800	175			
8	128	21120	88704	79200	15400	(315)*		88*
9	32	7040	38016	47520	15400	945		
10	256	73216	494208	823680	400400	49140	(693)*	52*
11	128	46592	384384	823680	560560	114660	4851	

*Coefficients of terms free from powers of x. Omit in most cases, i.e., when the sources occur in pairs of opposite sign for each value of "a". In such cases, simplify by isolating the factor C, common to the remaining coefficients.

Thus $p_o = \sum \frac{N''a^3}{6\ r_o}$, $p_1 = \sum \frac{N''}{12\ r_o} \ \frac{4.x.a^3}{r_o}$,

$p_2 = \sum \frac{N''}{20\ r_o} \ \frac{x^2.a^3}{r_o^2} \left[\frac{20-3\ (a/x)^2}{2}\right]$, ...

4. Applications

(i) Expanded Solenoidal Coils ----The result indicated for p_3 (c) serves to guide the design of "fourth-order" solenoidal coils intended for field measurements, and evidently forms the basis whereby the relative dimensions of the various "expanded dipole" solenoidal coils listed in Garrett's Table IX[2] are obtained.

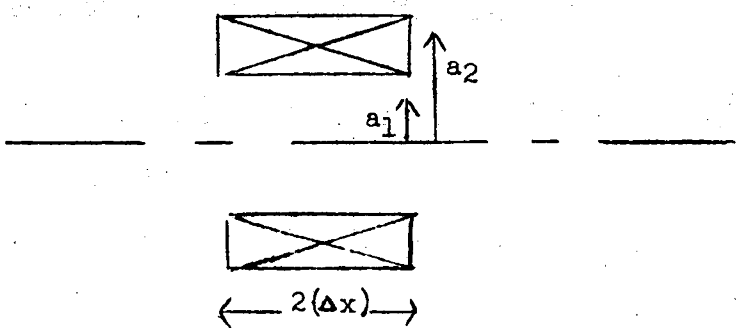

We require specifically in this case that, for p_3 (c) to vanish,

$$a_1^3\left[20-9\,(a_1/\Delta x)^2\right] = a_2^3\left[20-9\,(a_2/\Delta x)^2\right] .$$

Explicitly,

$$\Delta x = \sqrt{\frac{9}{20}\,\frac{a_2^5 - a_1^5}{a_2^3 - a_1^3}} ,$$

or

$$\frac{\Delta x}{a_2} = \sqrt{\frac{9}{20}\,\frac{1 - (a_1/a_2)^5}{1 - (a_1/a_2)^3}}$$

$$= 0.67082\sqrt{\frac{1 - (a_1/a_2)^5}{1 - (a_1/a_2)^3}} .$$

We give in Table II some numerical results, which include the values tabulated by Garrett.[2]

TABLE II

RELATIVE DIMENSIONS OF EXPANDED DIPOLE SOLENOIDS

a_1/a_2	$\Delta x/a_2$	a_1/a_2	$\Delta x/a_2$	a_1/a_2	$\Delta x/a_2$
0	0.67082	0.4	0.68982	0.8	0.78738
0.1	0.67115	0.5	0.70584	0.9	0.82462
0.2	0.67341	0.6	0.72756	1.0	0.86603
0.3	0.67924	0.7	0.75486		

(ii) Expanded Helmholtz Pairs ----The vanishing of p_3 (c) similarly forms the basis of determining the relative dimensions of the expanded Helmholtz coil-pairs listed in Garrett's Table IX.[2] In this case the condition to be met has the form

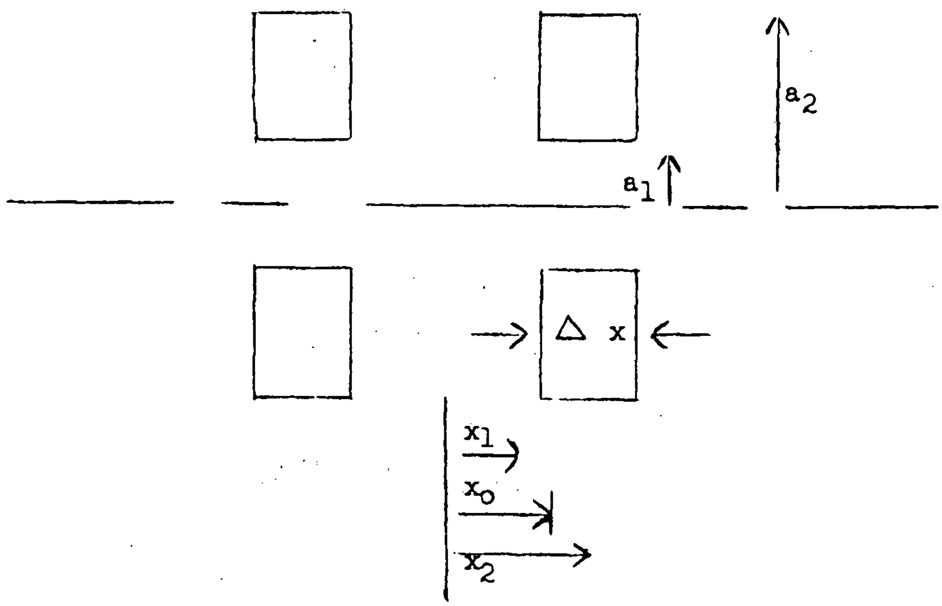

$$\frac{15p_3r_o^4}{N''} \equiv x_2^3\, a_2^3 \left[20-9\left(\frac{a_2}{x_2}\right)^2\right] - x_2^3\, a_1^3 \left[20-9\left(\frac{a_1}{x_2}\right)^2\right]$$

$$+ x_1^3\, a_1^3 \left[20-9\left(\frac{a_1}{x_1}\right)^2\right] - x_1^3\, a_2^3 \left[20-9\left(\frac{a_2}{x_1}\right)^2\right] = 0,$$

which may be rewritten

$$\frac{x_2^3 - x_1^3}{x_2 - x_1} = \frac{9}{20}\,\frac{a_2^5 - a_1^5}{a_2^3 - a_1^3}$$

or in the equivalent forms

$$x_1^2 + x_1x_2 + x_2^2 \equiv 3x_1^2 + 3x_1\,\Delta x + (\Delta x)^2 \equiv 3x_2^2 - 3x_2\,\Delta x + (\Delta x)^2$$
$$\equiv 3x_o^2 + (\Delta x/2)^2 = \frac{9}{20}\,\frac{a_2^5 - a_1^5}{a_2^3 - a_1^3} \quad .$$

[The result of the preceding subsection thus constitutes a special case of this result, with $x_1 = 0$.]

(iii) Quadrupole Pair ----If the members of the coil-pair above are connected in opposition, a quadrupole coil results, for which the relative dimensions should be selected so that $p_4 = 0$. Thus

$$\frac{42p_4r_o^5}{N''} \equiv \left[x_2^2\, a_2^3\,(70x_2^2 - 63a_2^2) - x_2^2 a_1^3\,(70x_2^2 - 63a_1^2)\right.$$
$$\left. + x_1^2 a_1^3\,(70x_1^2 - 63a_1^2) - x_1^2 a_2^3\,(70x_1^2 - 63a_2^2)\right]$$

$$= 70\,(x_2^4 - x_1^4)\,(a_2^3 - a_1^3) - 63\,(x_2^2 - x_1^2)\,(a_2^5 - a_1^5) = 0,$$

or

$$x_1^2 + x_2^2 = \frac{9}{10} \frac{a_2^5 - a_1^5}{a_2^3 - a_1^3} .$$

(iv) Higher Order Coils ----The coefficients of section 3 (iii) are also convenient in the design of dipole coils of higher order accuracy. Thus Garrett has exhibited [2] the relative dimensions of a coil for which both p_3 and p_5 vanish, and for which p_7 is very small,

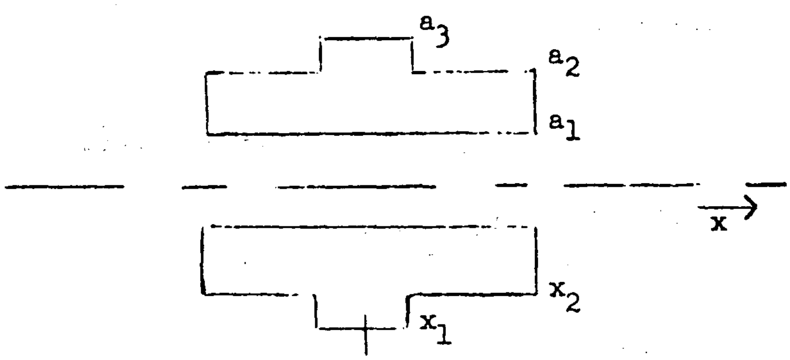

so that p_9 and p_{11} represent the dominant coefficients beyond p_1:

$$x_1 : x_2 : a_1 : a_2 : a_3 = 0.45735 : 0.82148 : 0.35 : 0.704545 : 1 .$$

5. Definition of Theoretical Error Coefficients, Sensitivity, and Efficiency

We summarize here, for completeness, the definitions of quantities introduced by Garrett [2] to characterize the comparative merit of various coil designs. The quantities defined are listed in Table III at the end of this section.

(i) Error Coefficients, ϵ_e ----For dipole coils, intended for the measurement of H_x, the desired signal is proportional to p_1 and, with an ideal winding, the extraneous signal may be expected to arise from the first subsequent non-vanishing coefficient, p_{e+1} (e being even). The error coefficient for such coils is defined as $\epsilon_e \equiv p_{e+1}/p_1$. Similarly for quadrupole coils, the coefficient ϵ_e is taken as p_{e+2}/p_2, again with e even. The importance of an error coefficient of given magnitude will, of course, depend upon the character of the magnetic field under study, in that (see section 2)

$$\frac{\Phi_{n'}}{\Phi_n} = r_o^{\,n'-n} \frac{(n+1)!}{(n'+1)!} \frac{p_{n'}}{p_n} \frac{V_o^{(n')}}{V_o^{(n)}} .$$

For the dipole coils discussed in sections 4 (i) and 4 (ii) the error coefficient of interest is thus $\epsilon_4 = p_5/p_1$. For the expanded solenoids one readily finds

$$p_1\ (c) = \sum \frac{N_\ell''}{3} \quad \frac{x_\ell \cdot a_\ell^3}{r_o^2} = \frac{2}{3} N'' \frac{\Delta x}{r_o^2} \left[a_2^3 - a_1^3\right]$$

and (with the aid of Garrett's table, reproduced as Table I above)

$$p_5\ (c) = \frac{r_o^2}{7x8} \sum_l N''_l \left(\frac{x_l}{r_o}\right)^5 \left(\frac{a_l}{r_o}\right)^3 \left[56-84 \tan^2 \alpha_l + 15 \tan^4 \alpha_l\right]$$

$$= \frac{N''}{28} \frac{(\Delta x)^5}{r_o^6} \left\{ a_2^3 \left[56-84\ (a_2/\Delta x)^2 + 15\ (a_2\ /\Delta x)^4\right] \right.$$

$$\left. -a_1^3 \left[56-84\ (a_1/\Delta x)^2 + 15\ (a_1/\Delta x)^4\right] \right\}.$$

By way of example, one thus finds for coil "H" (Table IX, ref. 2).

$$p_1\ (c) = \frac{2}{3}\ N''\ \frac{a_2^4}{r_o^2}\ \ (0.67924) \left[1-(0.3)^3\right]$$

$$= 0.4406\ (a_2^4\ /r_o^2)\ \ N'' \qquad \text{and}$$

$$p_5\ (c) = \frac{N''}{28} \frac{a_2^8}{r_o^6}\ \ (0.67924)^5 \left\{ \left[56-84\ \left(\frac{1}{.67924}\right)^2 + 15\ \left(\frac{1}{.67924}\right)^4\right] \right.$$

$$\left. -(0.3)^3 \left[56-84\ \left(\frac{0.3}{.67924}\right)^2 + 15\ \left(\frac{0.3}{.67924}\right)^4\right] \right\}$$

$$= -\ 0.2927\ (a_2^8/r_o^6)\ \ N'';$$

hence, in this case,

$$\epsilon_4 = -\ 0.664\ (a_2^4/r_o^4)$$

and $$\frac{\Phi_5}{\Phi_1} = -\,0.664\,\frac{2!}{5!}\,\frac{a_2^4\,V_o^{(5)}}{V_o^{(1)}}$$

$$= -\,0.011\,\frac{a_2^4\,V_o^{(5)}}{V_o^{(1)}}\,.$$

(ii) <u>Alternate Specification of Error</u> ---- The error in measurement associated with a given error coefficient is, as Garrett [2] has emphasized, dependent upon the type of field in which the search coil is situated. It is therefore considered of interest to specify the performance of a dipole search coil by stating how large the dimensions of a standard field coil must be if the search coil is to measure the resulting field with an accuracy taken (arbitrarily) as 1 percent.

The standard field coil is taken to be a single circular loop concentric with the search coil and its radius designated as a_{o1}.

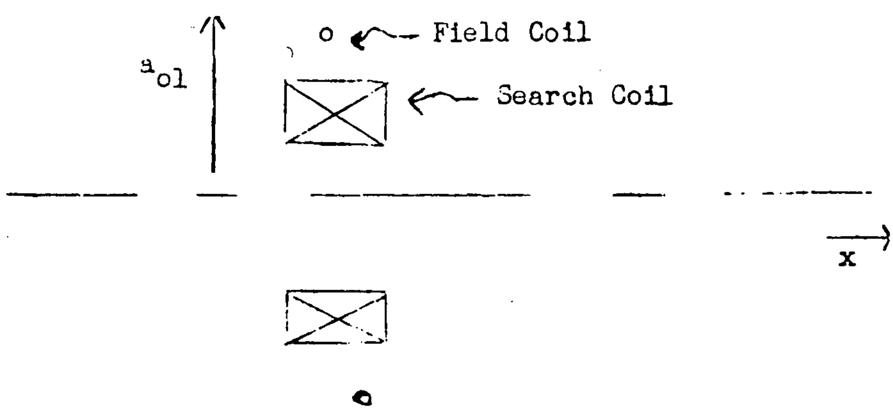

It is then required that

$$\frac{1}{100} = \left| \frac{\Phi_{e+1}}{\Phi_1} \right| .$$

Since it is readily shown that the central field of the search coil is such that

$$\left. \frac{d^n H_x}{dx^n} \right|_o = 2\pi \ (i/c) \ \frac{(n+1)! \ P_n \ (0)}{a_{o1}^{\ n}},$$

we have the condition

$$\frac{1}{100} = (r_o)^e \ \frac{2!}{(e+2)!} \left| \frac{P_{e+1}}{P_1} \right| \frac{V_o \ (e+1)}{V_o \ (1)}$$

$$= \frac{2}{e+2} \left| \epsilon_e \right| \ P_e \ (0) \ (\frac{r_o}{a_{o1}})^e,$$

or $$(\frac{a_{o1}}{r_o})^e = \frac{200}{e+2} \left| \epsilon_e \right| \ P_e \ (0).$$

An analogous expression may be employed for quadrupole coils:

$$(\frac{a_{o1}}{r_o})^e = \frac{600}{(e+2)\ (e+3)} \left| \epsilon_e \right| \ P_e \ (0).$$

As an example, we have for the dipole coil "H" considered previously,

$$\left(\frac{a_{o1}}{r_o}\right)^4 = \frac{200}{6} \cdot \frac{3}{8} \cdot (0.664)\ (a_2/r_o)^4 \text{ ,} \qquad \text{or}$$

$$(a_{o1}/a_2)^4 = 8.30 \qquad \text{and}$$

$(a_{o1}/a_2) = 1.70$, as stated by Garrett.

(iii) Specification of Sensitivity ----The sensitivity of any particular dipole coil arrangement is defined with reference to an ideal standard spherical winding. The standard consists of harmonic windings, of the same maximum turn density N" as the coil, situated within a radius r_f. The value of the coefficient p_1 for this standard is: [5]

$$p_1 \text{ (std.)} = \frac{4}{15}\ (r_f^{\,4}/r_o^{\,2})N''$$

and a measure of sensitivity is the value of r_f for which the coefficient p_1 of the standard and of the coil are equal.

Similarly, for quadrupole coils, a theoretical standard winding is conceived for which

$$p_2 \text{ (std.)} = \frac{8}{25}\ (r_5^{\,5}/r_o^{\,3})N''.$$

Normalized sensitivities, which take account of the magnitude of the error coefficient of a given coil may also be introduced:

$$S_1\,(\epsilon_e) \propto \left(\frac{r_f}{r_o}\right)^4 \frac{1}{|\epsilon_e|^{4/e}}\,, \text{ for dipole coils;}$$

$$S_2\,(\epsilon_e) \propto \left(\frac{r_s}{r_o}\right)^5 \frac{1}{|\epsilon_e|^{5/e}}\,, \text{ for quadrupole coils.}$$

Returning, by way of example, to coil "H",

$$p_1 = 0.4406\ (a_2^4/r_o^2)\ N'', \qquad \text{so}$$

$$r_f/a_2 = \sqrt[4]{\frac{15}{4} \times 0.4406}$$

$$= 1.13.$$

Since, as shown previously, the error coefficient for this coil is

$$\epsilon_4 = -\,0.664\ a_2^4/r_o^4,$$

$$S_1\,(\epsilon_4) \propto [1.13\ (a_2/r_o)]^4 \Big/ [0.664\ (a_2/r_o)^4]\,,$$

or, with the constant of proportionality arbitrarily selected as 0.37 (as was done by Garrett[2] for convenience in the comparison of the coils listed in his Table IX),

$$S_1\,(\epsilon_4) = 0.37 \times (1.13)^4/0.664 = 0.91.$$

(iv) Efficiency ----In addition, the efficiency or economy in the utilization of turns is considered to be of interest. This feature is evaluated for dipole coils by determining first the radius, $\hat{a}$, of a single-turn loop with current Ni having the same moment (or same $p_1 i$) as the search coil in question. Accordingly, $p_1 = N_f \left(\frac{\hat{a}}{r_o}\right)^2 = N''A \left(\frac{\hat{a}}{r_o}\right)^2$, or $\hat{a}^2 = \frac{p_1 r_o^2}{N''A}$, where A is the area occupied by the search coil winding.

An analogous dimension $\hat{r}$ is introduced for quadrupole coils:

$$\hat{r}^3 = \frac{\sqrt{3}}{2} \frac{p_2 r_o^3}{N''A} .$$

Normalized efficiencies, involving the error coefficients, are also introduced:

$$E_1 (\epsilon_e) \propto \left(\frac{\hat{a}}{r_o}\right)^2 \frac{1}{|\epsilon_e|^{2/e}} , \text{ for dipole coils;}$$

$$E_2 (\epsilon_e) \propto \left(\frac{\hat{r}}{r_o}\right)^3 \frac{1}{|\epsilon_e|^{3/e}} , \text{ for quadrupole coils.}$$

Again for coil "H", with

$$p_1 = 0.4406 \; (a_2^4/r_o^2) \; N'', \quad A = 0.951 a_2^2, \text{ and}$$

$$|\epsilon_4| = 0.664 \; (a_2/r_o)^4 \text{, one finds}$$

$$(\hat{a}/r_o)^2 = 0.463 \; (a_2/r_o)^2 \qquad \text{and,}$$

with a constant of proportionality taken as 1.44,

$$E_1\ (\epsilon_4) = 1.44 \times 0.463 \Big/ \sqrt{0.664} = 0.82.$$

(v) Summary ----The quantities defined in this section are summarized in Table III. The normalized coefficients are useful for comparing different designs of coils of the same order.

TABLE III

SUMMARY OF DEFINITIONS OF THEORETICAL ERROR COEFFICIENTS, SENSITIVITY, AND EFFICIENCY

	Dipole Coils
Error Coefficient:	$\epsilon_e = p_e + 1 / p_1$
Radius of Standard Source:	$(a_{o1}/r_o)^e = \frac{200}{e+2} \lvert\epsilon_e\rvert \ P_e^{(o)}$
Sensitivity	
Radius of Standard Coil:	$(r_f/r_o)^4 = \frac{15}{4} \frac{p_1}{N'' r_o^2}$
Normalized Sensitivity	$S_1\ (\epsilon_e) \propto (r_f/r_o)^4 \lvert\epsilon_e\rvert^{-4/e}$
	$\propto \frac{p_1}{N'' r_o^2} \left[\frac{p_1}{p_e + 1}\right]^{4/e}$
Efficiency	
Radius of Standard Winding:	$\left(\frac{\hat{a}}{r_o}\right)^2 = \frac{p_1}{N'' A}$
Normalized Efficiency:	$E_1\ (\epsilon_e) \propto \left(\frac{\hat{a}}{r_o}\right)^2 \lvert\epsilon_e\rvert^{-2/e}$
	$\propto \frac{p_1}{N'' A} \left[\frac{p_1}{p_e + 1}\right]^{2/e}$
Alternative Figure-of-Merit:	$\left(\frac{\hat{a}}{a_{o1}}\right)^2$

Table III (continued)

	Quadrupole Coils
Error Coefficient:	$\epsilon_e = p_e + 2 / p_2$
Radius of Standard Source:	$(a_{o1}/r_o)^e = \frac{600}{(e+2)(e+3)} \lvert \epsilon_e \rvert P_e$ (0)
Sensitivity	
Radius of Standard Coil:	$(r_s/r_o)^5 = \frac{25}{8} \frac{p_2}{N'' r_o^2}$
Normalized Sensitivity:	$S_2 (\epsilon_e) \propto (\frac{r_s}{r_o})^5 \lvert \epsilon_e \rvert^{-5/e}$
	$\propto \frac{p_2}{N'' r_o^2} \left[\frac{p_2}{p_e + 2} \right]^{5/e}$
Efficiency	
Radius of Standard Winding:	$(\frac{\hat{r}}{r_o})^3 = \frac{\sqrt{3}}{2} \frac{p_2}{N'' A}$
Normalized Efficiency:	$E_2 (\epsilon_e) \propto (\frac{\hat{r}}{r_o})^3 \lvert \epsilon_e \rvert^{-3/e}$
	$\propto \frac{p_2}{N'' A} \left[\frac{p_2}{p_e + 2} \right]^{3/e}$
Alternative	
Figure-of-Merit:	$(\frac{\hat{r}}{a_{o1}})^3$

PART II

Theory For Two-Dimensional Search Coils

1. Introduction

The analysis of the behavior of long coils, as may be used for measurement of two-dimensional magnetic fields is notably simpler than the analysis of axially-symmetric coil systems.[6] From the standpoint of convenience it appears desirable, however, to treat the two-dimensional case in a manner analogous to that employed in Part I.

2. Notation and General Relationships

We select the normal to the plane of the coil as the axis of plane polar coordinates, with x designating distance measured along this axis. Coordinates r, θ designate a field point and r_j, α_j the location of a coil.

We express the exterior magnetic scalar potential generated by a current of i e.s.u. in the coil by

$$V_{coil} = 2\ (i/c)\sum \frac{p_n}{n} \left(\frac{r_o}{r}\right)^n \cos n\theta\ ,$$

the constant r_o again being introduced solely for reasons of dimensional convenience. A reciprocity relation then permits [7] us to write the flux linkages per unit length between the coil and an external applied field characterized by the potential V_o as

$$\Phi = \sum \Phi_n,$$

with $$\Phi_n = -\frac{p_n}{n!} r_o^{\,n} V_o^{(n)}.$$

and $$V_o^{(n)} \equiv d^n V_o/dx^n \text{ evaluated at the origin.}$$

3. Evaluation of the coefficients p_n

(i) For a two-dimensional current loop ----The exterior

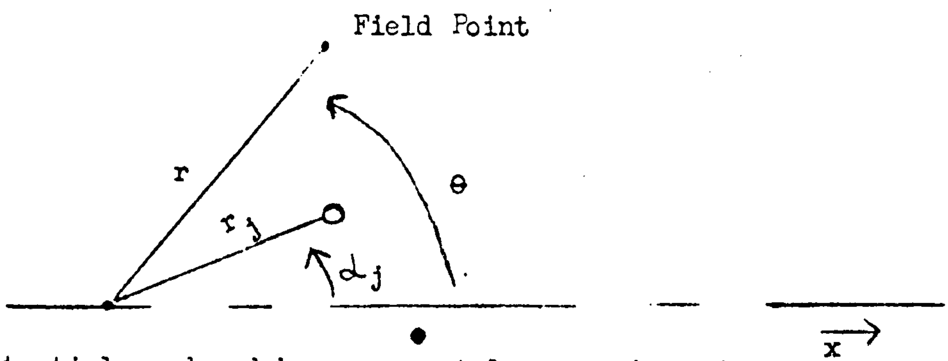

potential produced by a current loop may be written

$$V(f_j) = 4N_j \,(i/c) \sum \frac{\sin n\alpha_j}{n} \left(\frac{r_j}{r}\right)^n \cos n\theta;$$

hence

$$p_n(f_j) = 2N_j \sin n\alpha_j \left(\frac{r_j}{r_o}\right)^n.$$

(ii) For a layer-coil ----For a coil of finite extent in the x-direction, and which contains N_k' turns/cm, the exterior potential and the associated coefficients $p_n(s)$ may be found by integrating the preceding result, to obtain

$$p_n\,(s) = 2\,\frac{r_o}{n+1}\sum_k N_k'\,\sin\,(n+1)\alpha_k\,\left(\frac{r_k}{r_o}\right)^{n+1},$$

N_k' being given opposite sign at the ends of the layer.

(iii) For a coil ----For a coil with windings occupying a rectangular cross-section and with N_ℓ'' turns/cm^2 one similarly finds by a second integration

$$p_n\,(c) = -2\,\frac{r_o^2}{(n+1)\,(n+2)}\sum_\ell N_\ell''\,\cos\,(n+2)\alpha_\ell\,\left(\frac{r_\ell}{r_o}\right)^{n+2}.$$

The summation again extends over the corners of the winding, with N_ℓ'' alternating in sign.

For convenience in computation, this last result is rewritten.

$$p_n\,(c) = \frac{2}{(n+1)\,(n+2)\,r_o^n}\,\times$$

$$\times\sum_\ell N_\ell''\left[-x_\ell^{\,n+2} + \frac{(n+2)\,(n+1)}{2!}\,x_\ell^n\,a_\ell^2 - \frac{(n+2)\,(n+1)\,n\,(n-1)}{4!}\,x_\ell^{n-2}\,a_\ell^4\,\ldots\right],$$

the first term within the brackets normally dropping out when the summation is taken.

4. Applications

(i) For an "Expanded Dipole Sheet" ----For a coil with windings of rectangular cross-section (half-width in direction normal to plane, Δx; half-widths in plane, a_1 and a_2),

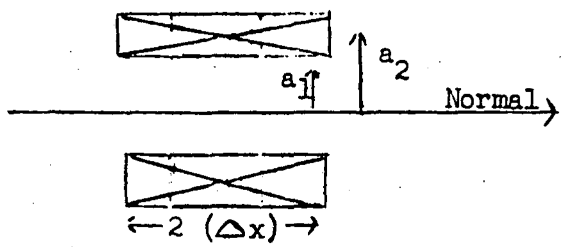

intended for field-strength measurements, the dominant coefficient is

$$p_1 = 2\,\frac{\Delta x\,(a_2^2 - a_1^2)}{r_o}\,N''$$

and we seek to make the coefficient

$$p_3 = \frac{\Delta x\,(a_2^2 - a_1^2)\left[2\,(\Delta x)^2 - (a_2^2 + a_1^2)\right]}{r_o^3}\,N'' \text{ vanish.}$$

This latter condition requires that

$$\Delta x = \sqrt{\frac{a_2^2 + a_1^2}{2}}\,.$$

(ii) For a Quadrupole Coil ----For a quadrupole pair

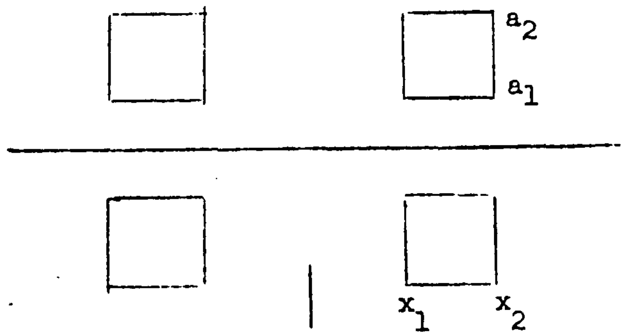

one finds the value of the dominant coefficient to be

$$p_2 = 2 \frac{(x_2^2 - x_1^2)\ (a_2^2 - a_1^2)}{r_o^2}\ N''.$$

The dimensions should be so selected that

$$p_4 = 2 \frac{(x_2^4 - x_1^4)\ (a_2^2 - a_1^2) - (x_2^2 - x_1^2)\ (a_2^4 - a_1^4)}{r_o^4}\ N''$$

$$= 2 \frac{(x_2^2 - x_1^2)\ (a_2^2 - a_1^2) \left[(x_2^2 + x_1^2) - (a_2^2 + a_1^2) \right]}{r_o^4}\ N'' \text{ will vanish.}$$

This latter condition requires that

$$x_2 = \sqrt{a_2^2 + a_1^2 - x_1^2}\ .$$

5. <u>Definitions of Theoretical Error Coefficients, Normalized Sensitivity, and Normalized Efficiency</u>

(i) <u>Error Coefficients</u> ----As in Part I, we may define

$$\epsilon_e = p_e + 1/p_1 \qquad \text{for dipole coils}$$

and

$$\epsilon_e = p_e + 2/p_2 \qquad \text{for quadrupole coils.}$$

(ii) Sensitivity ----We likewise define the normalized sensitivity as

$$S_1\ (\epsilon_e) \propto \frac{p_1}{N''\ r_o^2} \left|\frac{1}{\epsilon_e}\right|^{3/e} = \frac{p_1}{N''\ r_o^2} \left[\frac{p_1}{p_e + 1}\right]^{3/e} \quad \text{for dipole coils}$$

$$\text{and} \quad S_2\ (\epsilon_e) \propto \frac{p_2}{N'' r_o^2} \left|\frac{1}{\epsilon_e}\right|^{4/e} = \frac{p_2}{N''\ r_o^2} \left[\frac{p_2}{p_e + 2}\right]^{4/e} \quad \text{for quadrupole coils.}$$

These normalized sensitivities may be of interest for comparing the performance of proposed coils of various relative dimensions. Save for higher order coils, one has normally $e = 4$.

(iii) Efficiency ----Similarly, as a measure of economy in the utilization of turns, one defines the normalized efficiences

$$E_1\ (\epsilon_e) \propto \frac{p_1}{N''A} \left|\frac{1}{\epsilon_e}\right|^{1/e} = \frac{p_1}{N''A} \left[\frac{p_1}{p_e + 1}\right]^{1/e} \quad \text{for dipole coils}$$

$$\text{and} \quad E_2\ (\epsilon_e) \propto \frac{p_2}{N''A} \left|\frac{1}{\epsilon_e}\right|^{2/e} = \frac{p_2}{N''A} \left[\frac{p_2}{p_e + 2}\right]^{2/e} \quad \text{for quadrupole coils,}$$

with A representing the cross-sectional area occupied by the windings.

PART III

Estimate of Some Errors in Search Coil Measurements

1. Introduction

For field measurements, as in magnet model work, dipole search coils are employed and, if "fourth order," are designed so that p_3 vanishes. It is of interest to estimate in a particular case the actual magnitude of the errors to be expected, with fields of the type under investigation, (i) from the theoretical contribution Φ_5 and (ii) from a possible Φ_3 term arising from imperfect coil construction.

2. Estimate of the Value of the Coefficient p_3 which may arise from Constructional Errors

(i) From errors in the overall dimensions ----For an expanded solenoid, as discussed in Part I, 4 (i), the coefficient p_3 has the form

$$p_3 = \frac{1}{30\, r_o^4} \sum' N''_{\ell} \left[20\, x_{\ell}^3\, a_{\ell}^3 - 9 . x . a_{\ell}^5 \right]$$

$$= \frac{N''}{15\, r_o^4} (20\, x^3\, a_2^3 - 20\, x^3\, a_1^3 - 9xa_2^5 + 9xa_1^5),$$

where, for simplicity, x is used in place of Δx to designate the half-width of the coil. We now assign errors to the dimensions x_{ℓ}, a_{ℓ}, such as might arise from inaccuracy in machining, incorrect allowance for wire diameter, or looseness in winding.

If we assume the dimensions of the coil corners to be in error symmetrically, but otherwise independent, by an RMS value δ,

$$\Delta p_3 = \pm \frac{N''}{15\, r_o^4} \left\{ \left[60\, x^2\, (a_2^3 - a_1^3) - 9\, (a_2^5 - a_1^5)\right]^2 + \left[60\, x^3\, a_2 - 45\, x a_2^4\right]^2 + \left[60\, x^3\, a_1^2 - 45\, x a_1^4\right]^2 \right\}^{1/2} \cdot \delta$$

$$= \pm \frac{N''}{5\, r_o^4} \Big[400\, x^6\, (a_2^4 - a_1^4) - 200\, x^4\, (a_2^6 + 4 a_2^3\, a_1^3 + a_1^6) + 3x^2\, (35\, a_2^8 + 40\, a_2^5\, a_1^3 + 40\, a_2^3\, a_1^5 + 35\, a_1^8) + 9\, (a_2^5 - a_1^5)^2\Big]^{1/2} \cdot \delta$$

(ii) <u>From errors in individual loops</u> ----It may also be of interest to inquire concerning the error which would arise to generate a non-vanishing coefficient p_3 if a coil of the intended dimensions were formed by winding N single-turn loops, each subject to an independent statistical error in "x" and "a" (again with an RMS error designated as δ).

For this case we may begin with the expression for the coefficient associated with a single turn and write

$$p_3 = \sum N_j \sin^2\alpha_j \; P_3'(\cos\alpha_j) \left(\frac{r_j}{r_o}\right)^4$$

$$= \sum \frac{N_j}{r_o^4} \left[6\, x^2\, y^2 - \tfrac{3}{2}\, y^4\right] , \qquad \text{so}$$

$$\Delta p_3 = \pm \frac{\sqrt{N}}{r_o^4} \left\langle (12.x.y^2)^2 + (12\, x^2\, y - 6\, y^3)^2 \right\rangle_{A_v}^{1/2} .\delta$$

$$= \pm \frac{6 \sqrt{N}\ \delta}{r_o^4} \left\langle y^6 + 4\, x^4\, y^2 \right\rangle_{A_v}^{1/2}$$

$$= \pm \frac{6 \sqrt{N}\ \delta}{r_o^4} \left[\frac{(1/7)\ (a_2^7 - a_1^7) + (4/15)\ x^4\ (a_2^3 - a_1^3)}{a_2 - a_1} \right]^{1/2}$$

3. Numerical Values

In the case of a coil for which $x = 0.67924a_2$ and $a_1 = 0.3\ a_2$, so that ideally $p_3 = 0$ (see Table I), our first estimate gives

$$\left.\begin{aligned} \Delta p_3 &= \pm\, 1.43\ N'' \frac{a_2^5\ .\delta}{r_o^4} \\ &= \pm\, 1.47\ N \frac{a_2^3\ .\delta}{r_o^4} \end{aligned}\right\} , \quad \begin{aligned} &\text{from section 3 (i), with} \\ &A = 2\text{x}0.67924\text{x}0.7a_2^2, \end{aligned}$$

and the second estimate gives

$$\Delta p_3 = \pm\, 3.2\ \sqrt{N}\ \frac{a_2^3\ .\delta}{r_o^4}, \text{ from section 3 (ii).}$$

It is noted that the first estimate exceeds the second for multi-turn coils ($N > 5$), the same value of δ being considered in each case, and we shall therefore employ the first estimate in what follows.

For the type of coil considered here we also have (see section I, 5 (i)):

$$p_1 = 0.4406\ N'' \frac{a_2^4}{r_o^2} \quad \text{and}$$

$$p_5 = -\ 0.2927\ N'' \frac{a_2^8}{r_o^6}\ .$$

The flux contributions of interest are, in a two-dimensional field V (x, ξ):

$$\Phi_1 \equiv -2\pi p_1\, r_o^2\, V_o^{(1)}/2 \quad = 2\pi r_o^2 . \frac{p_1}{2} . H_x,$$

$$\Phi_3 \equiv -2\pi p_3\, r_o^4\, V_o^{(3)}/24 \quad = -2\pi r_o^4 . \frac{p_3}{24} . H_x^{(2)}, \quad \text{and}$$

$$\Phi_5 \equiv -2\pi p_5\, r_o^6\, V_o^{(5)}/720 \quad = 2\pi r_o^6 . \frac{p_5}{720} . H_x^{(4)},$$

where $H_x^{(n)} \equiv \frac{d^n H_x}{d\xi^n}$ at $x = \xi = o$;

thus the relevant possible errors are

$$\Phi_3/\Phi_1 = \frac{r_o^2}{12} \frac{p_3}{p_1} \frac{H_x^{(2)}}{H_x} = \pm\ 0.27\ a_2 . \delta .\ \left(\frac{H_x^{(2)}}{H_x}\right) \text{ and}$$

$$\Phi_5/\Phi_1 = \frac{r_o^4}{360} \frac{p_5}{p_1} \frac{H_x^{(4)}}{H_x} = -\ 0.00185\ a_2^4\ \left(\frac{H_x^{(4)}}{H_x}\right).$$

If we consider that within the region of interest in the magnet model, $H_x^{(2)}/H_x$ may become as large as 0.2 in $^{-2}$ and

$H_x^{(4)}/H_x$ possibly as large as 0.2 in $^{-4}$ in magnitude, while the dimension a_2 of the search coil is taken as 0.25 inch and δ estimated as 0.003 inch,

$$\left| \Phi_3/\Phi_1 \right| \cong 0.004 \times 10^{-2} = \frac{1}{250} \text{ of 1 percent and}$$

$$\left| \Phi_5/\Phi_1 \right| \cong 0.000145 \times 10^{-2} = \frac{1}{7000} \text{ of one percent.}$$

It is suggested, therefore, that the error introduced by incomplete attainment of the ideal coil configuration may in practice be the greater of the two errors considered.

PART IV

Measurement of Field-"Gradients" with Axially-Symmetric Search Coils

1. Introduction

We consider here the measurement of field gradients in two-dimensional magnetic fields by use of coil systems possessing an axis of symmetry. The two dimensional field will be regarded as having a plane of symmetry, so that it may be represented by the scalar magnetic potential V_o:

$$-V_o = H_o z + n_o H_o \frac{yz}{R} + \frac{H_o^{(2)}}{6}\left(3y^2 z - z^3\right) + \frac{H_o^{(3)}}{6}\left(y^3 z - z^3 y\right) + \frac{H_o^{(4)}}{120}\left(5y^4 z - 10y^2 z^3 + z^5\right) + \ldots,$$

where z designates the coordinate normal to the median plane, y is orthogonal to z, and $H_o^{(n)}$ represents $\frac{\partial^n H_z}{\partial y^n}$ evaluated at $y = z = o$, $\left[H_o^{(1)} = n_o H_o/R\right]$.

We examine in what follows two methods for measuring $H_o^{(1)}$: the use of a quadrupole coil system with its axis inclined at an angle of 45° to the median plane [8] and, secondly, the use of a pair of parallel dipole coils connected in opposition.

2. Use of an Oblique Quadrupole Coil

For a coil whose axis of symmetry is inclined at an angle Ψ with respect to the z direction it is convenient to introduce the transformation

$$y = x \sin\Psi + \xi \cos\Psi$$
$$z = x \cos\Psi - \xi \sin\Psi$$

to obtain

$$-V_o = H_o\,(x\cos\Psi - \xi\sin\Psi) + n_o H_o\left[\frac{1/2\,(x^2 - \xi^2)\sin 2\Psi + x\,\xi\cos 2\Psi}{R}\right]$$
$$- \frac{H_o^{(2)}}{6}\left[x^3\cos 3\Psi - 3\,x^2\,\xi\sin 3\Psi - 3\,x\,\xi^2\cos 3\Psi + \xi^3\sin 3\Psi\right] + \dots\,.$$

It then follows that

$$V_o^{(2)} \equiv \frac{\partial^2 V_o}{\partial x^2}\Bigg|_{x=0,\,\xi=0} = -\frac{n_o H_o}{R}\sin 2\Psi$$

and $\Phi_2 \equiv -2\pi p_2\, r_o^3\, V_o^{(2)}/6 = 2\pi\,\frac{p_2\, r_o^3}{6}\,\frac{n_o H_o}{R}\sin 2\Psi.$

The inclined coil-pair thus affords a means for measuring the desired gradient and, for $\Psi = 45°$; the flux-linkages assume the stationary value

$$\Phi_2\,(45^o) = 2\pi\,\frac{p_2\, r_o^3}{6}\,\frac{n_o H_o}{R}\,.$$

The total flux change will be twice this value if the coil is rotated from this position through an angle ($\Delta\Psi$) of 90 degrees. The design of such coils has been mentioned in section I, 5 (iii).

3. Use of a Pair of Dipole Coils

As an alternative, more obviously direct, means of measuring field gradient, a pair of axially symmetric search coils has been used,[9] oriented with their axies coinciding with the direction of the field or perpendicular to the median plane of the magnet. If each coil is regarded as measuring the value of the field at its center, the difference of the readings, divided by their axial separation, affords a measure of the field-gradient at the mid-point. As Haworth has pointed out, however, an error proportional to $H_o^{(3)}$ could thereby be introduced[10] with the coils individually measuring accurately the flux-densities at their respective centers. It is therefore appropriate to re-examine this arrangement to determine whether a suitable value, different from zero, can be found for the coefficient p_3 of the individual coils to compensate this error. It will be found that the coils can be so proportioned that in the two-dimensional field each responds sufficiently to the axial derivative $V_o^{(3)}$ that the error from $H_o^{(3)}$ is cancelled.

To investigate this possibility we locate the axies of the two coils at $y = \pm\delta$ and note that the net flux to which the pair responds is

$$\Phi = 2\pi \sum \frac{p_n \, r_o^{\,n+1}}{(n+1)!} \left\{ \left[-\frac{\partial^n V_o}{\partial z^n} \right]_{+\delta} - \left[-\frac{\partial^n V_o}{\partial z^n} \right]_{+\delta} \right\},$$

in which only the p_n with n odd enter for dipole coils. We next note, from the series of section 1, that, with $z = o$,

$$\left[-\frac{\partial V_o}{\partial z}\right]_{\pm\delta} = H_o + n_o H_o \frac{(\pm\delta)}{R} + \frac{H_o^{(2)}}{2} \delta^2 + \frac{H_o^{(3)}}{6} (\pm\delta)^3 + \frac{H_o^{(4)}}{24} \delta^4 + \ldots$$

and $$\left[-\frac{\partial^3 V_o}{\partial z^3}\right]_{\pm\delta} = - H_o^{(2)} - H_o^{(3)}.(\pm\delta) - \frac{H_o^{(4)}}{2} \delta^2 - \ldots \quad .$$

Hence $$\left[-\frac{\partial V_o}{\partial z}\right]_{+\delta} - \left[-\frac{\partial V_o}{\partial z}\right]_{-\delta} = n_o H_o \frac{2\delta}{R} + \frac{H_o^{(3)}}{6} .2\delta^3 + \ldots$$ and

$$\left[-\frac{\partial^3 V_o}{\partial z^3}\right]_{+\delta} - \left[-\frac{\partial^3 V_o}{\partial z^3}\right]_{-\delta} = - H_o^{(3)} (2\delta) - \ldots,$$

so that $$\Phi = 2\pi \left\{ \frac{p_1 r_o^2}{2!} \left[n_o H_o \frac{2\delta}{R} + \frac{H_o^{(3)}}{3} \delta^3 + \ldots \right] - \frac{p_3 r_o^4}{4!} H_o^{(3)} 2\delta + \ldots \right\} .$$

From the results of the preceding paragraph, the effect of $H_o^{(3)}$ on the measurement can be removed if one designs the coils, not so that p_3 vanishes, but in accord with the relation

$$p_3 / p_1 = 2\, \delta^2 / r_o^2 .$$

[It may be noted in passing that with such a set of coils connected in series-aiding, the condition for them to measure the field at the midpoint--the effect of $H_o^{(2)}$ being eliminated--would require $p_3/p_1 = 6\, \delta^2/r_o^2$.]

We consider, then, the effect of the condition just derived on the relative dimensions of coils of the expanded solenoid type. The coefficients for such coils are (section I, 3, esp. Table I):

$$p_1 = \frac{1}{3\, r_o^2} \sum N''_\ell\, x_\ell\, a_\ell^3 = \frac{2}{3}\, N'' \frac{(\Delta x)\left[a_2^3 - a_1^3\right]}{r_o^2}, \qquad \text{and}$$

$$p_3 = \frac{1}{30\, r_o^4} \sum N''_\ell\, x_\ell^3\, a_\ell^3 \left[20 - 9 \left(\frac{a_\ell}{x_\ell}\right)^2\right] = \frac{N''}{15}\, \frac{\Delta x\left[20\, (\Delta x)^2\, (a_2^3 - a_1^3) - 9\, (a_2^5 - a_1^5)\right]}{r_o^4}.$$

The requirement that $p_3/p_1 = 2\, \delta^2/r_o^2$ then reduces to the simple condition

$$\Delta x = \sqrt{\frac{9}{20}\, \frac{a_2^5 - a_1^5}{a_2^3 - a_1^3} + \delta^2}\,, \qquad \text{or}$$

$$\Delta x/a_2 = \sqrt{\frac{9}{20}\, \frac{1 - (a_1/a_2)^5}{1 - (a_1/a_2)^3} + \left(\frac{\delta}{a_2}\right)^2}\,,$$

which reduces when $\delta = o$ to the result of section I, 4 (i).

In Table IV below we give, for comparative purposes, sets of dimensions which satisfy the foregoing relation.

TABLE IV

DIMENSIONS OF AXIALLY-SYMMETRIC SEARCH COILS, TO BE USED IN PAIRS TO DETERMINE THE GRADIENT OF A TWO-DIMENSIONAL MAGNETIC FIELD

Inner Radius, a_1 :	0.075		0.075
Outer Radius, a_2 :	0.250		0.125
Semi-axial Separation, δ :	0	0.500	0.250
Overall Length, $2(\Delta x)$:	0.33962	1.05610	0.53206

PART V

Measurement of Field-"Gradients" with Two-Dimensional Search Coils

1. Introduction

We consider here the measurement of two-dimensional magnetic fields through the use of long coils, by means analogous to those described in Part IV. The potential describing the magnetic field may be used in the form given in sections IV, 1 and IV, 2.

2. Use of a Quadrupole Coil

For a long quadrupole coil-pair, centered on the median plane and oriented with its normal inclined at an angle Ψ with respect to the field direction, we have as before

$$V_o^{(2)} = -\frac{n_o H_o}{R} \sin 2\Psi.$$

Since $\Phi_2 = -\frac{p_2}{2} r_o^2 V_o^{(2)}$ (section II, 2), the flux to which the coil responds is substantially

$$\Phi_2 = \frac{p_2\, r_o^2}{2} \frac{n_o H_o}{2} \sin 2\Psi, \text{ per unit length.}$$

The inclined coil-pair thus affords a means for measuring the desired gradient and, for $\Psi = 45^\circ$, the flux-linkages per unit length assume the stationary value

$$\Phi_2 \quad (45^\circ) = \frac{p_2\, r_o^2}{2} \frac{n_o H_o}{R} \quad .$$

The design of a coil of this type has been mentioned in section II, 4 (ii).

3. Use of a Pair of Long Dipole Coils

We consider here the use of a pair of long dipole coils connected in series opposition. The normals to the planes of the coils are directed along the magnetic field, at right angles to the median plane, and the centers taken to be at $y = \pm\delta$.

The measured net flux, per unit length, is

$$\Phi = \sum \frac{p_n\, r_o^n}{n!} \left\{ \left[-\frac{\partial^n V_o}{\partial z^n} \right]_{+\delta} - \left[-\frac{\partial^n V_o}{\partial z^n} \right]_{-\delta} \right\}$$

and, with the values used previously for the differences of the derivatives (section IV, 3),

$$\Phi = p_1\, r_o \left[n_o H_o \frac{2\delta}{R} + \frac{H_o^{(3)}}{6} 2\delta^3 + \ldots \right] - \frac{p_3}{3!} r_o^3\, H_o^{(3)}\, 2\delta + \ldots \; .$$

To remove the effect of $H_o^{(3)}$ on the measurement we therefore require

$$p_3/p_1 = \delta^2/r_o^2 \; .$$

[It may also be noted in passing that with such a set of coils connected series-aiding, the condition for them best to measure the field midway between them is that $p_3/p_1 = 3\delta^2/r_o^2$.]

The coefficients p_1 and p_3, for coils whose windings occupy a rectangular cross-section, have been given in section II, 4 (i):

$$p_1 = 2\,\frac{\Delta x\,(a_2^2 - a_1^2)}{r_o}\quad N'',$$

$$p_3 = \frac{\Delta x\,(a_2^2 - a_1^2)\left[2\,(\Delta x)^2 - (a_2^2 + a_1^2)\right]}{r_o^3}\quad N''.$$

The requirement that $p_3/p_1 = \delta^2/r_o^2$ then reduces to the simple condition

$$\Delta x = \sqrt{\frac{a_2^2 + a_1^2}{2} + \delta^2}.$$

A possible set of values would be:

Inner Half-width, $a_1 = 0.075$

Outer Half-width, $a_2 = 0.125$

Semi-Separation of centers, $\delta = 0.250$

Overall Height, $2(\Delta x) = 0.54083$.

Since Δx is, by the equation cited, necessarily greater than δ, the rotation (individually) of the members of such a pair of coils for the measurement of a static magnetic field would involve mechanical interference. The use of the quadrupole pair may be preferred, therefore, in such cases.

PART VI

References and Notes

1. M. W. Garrett, "Axially Symmetric Systems for Generating and Measuring Magnetic Fields, Part I," Appl. Physics 22, No. 9, 1091-1107 (September 1951).

2. ________, sequel, Part II, available as a photostated manuscript.

3. Cf. ref. 2, eq. 2.27. One makes use of the exterior magnetic potential produced by a current i in the coil

$$V_{coil} = 2\pi\,(i/c) \sum \frac{p_n}{n+1} \left(\frac{r_o}{r}\right)^{n+1} P_n\,(\cos\theta).$$

In addition, one considers as an elementary source a magnetic pole of strength μ situated at r, θ. The flux from the pole is designated as Φ and one has the relationship

$$-\,(i/c)\,\Phi = \mu\,V_{coil}$$

by use of energy considerations. Accordingly Φ may be written

$$\Phi = \sum \Phi_n,$$

with

$$\Phi_n = -\,2\pi\mu\,\frac{p_n}{n+1}\left(\frac{r_o}{r}\right)^{n+1} P_n\,(\cos\theta).$$

For the particular special source assumed here, the potential at r_j, α_j, in the neighborhood of the coil is, however,

$$V_o = \mu/R$$
$$= \frac{\mu}{r} \sum_n \left(\frac{r_j}{r}\right)^n P_n \left(\cos\left(\theta - \alpha_j\right)\right).$$

At points x_5 on the axis of the coil

$$V_o \Big|_{axis} = \frac{\mu}{r} \sum \left(\frac{x_j}{r}\right)^n P_n \left(\cos \theta\right)$$

and the axial derivatives at the origin are given by

$$V_o^{(n)} \equiv \frac{\partial^n V_o}{\partial {x_j}^n}\Big|_o = \mu\, n\,!\, (1/r)^{n+1} P_n(\cos\theta).$$

Accordingly, Φ_n may be identified as

$$\Phi_n = -\, 2\pi \frac{p_n}{(n+1)!} r_o^{n+1} V_o^{(n)},$$

for this particular field or for any general applied field which may be regarded as established by the superposition of such monopole contributions. This is the result of Garrett,[2] cited in section I, 2.

4. This follows from the identity

$$P'_n - 2\,u\,P'_{n+1} + P'_{n+2} \equiv P_{n+1},$$

where u = cos ϑ represents the argument of the functions P, P'.

5. The standard coil has windings with <u>axial</u> density proportional to P'_1 (= sin ϑ) and thus an actual density proportional to $\sin^2 \vartheta$. Hence N_j = (N'' r dϑ dr) $\sin^2\vartheta$ and

$$P_1 = \iint N_j \sin^3\vartheta\,(r^2/r_o^2)\,d\sigma = \frac{N''}{r_o^2}\int_0^{r_f}\int_0^{\pi} r^3 \sin^5\vartheta\,dr\,d\vartheta$$
$$= \frac{4}{15}\,(r_f^4/r_o^2)\,N''.$$

6. Certain aspects of the measurement of two-dimensional magnetic fields are treated by W. C. Elmore and M. W. Garrett, Report of Princeton University Accelerator Design Group, WCE-MWG-1-53 (June 8, 1953); Rev. Sci. Instruments <u>25</u>, No. 5, 480-485 (May 1954). It is there pointed out that any potential or field-component satisfying Laplace's equation in three dimensions will have a z-average which satisfies Laplace's two-dimensional equation, if the average is taken between two points where the z-derivative of the quantity in question has equal values (for example, points where the z-derivative vanishes).

7. The reciprocity argument for long coils in a two-dimensional situation parallels that given for the axially-symmetric coils.[3] In this case we write the external magnetic potential arising from a current in the coil as

$$V_{coil} = 2\,(i/c)\sum \frac{p_n}{n}\left(\frac{r_o}{r}\right)^n \cos n\,\theta.$$

We consider a line-pole source, of strength μ per unit length, situated at r, θ and let Φ designate the consequent flux per unit length at the coil. We again write

$$-(1/c)\,\Phi = \mu\, V_{coil},$$

so that $$\Phi = \sum \Phi_n$$

with $$\Phi_n = -2\mu\, \frac{p_n}{n}\,(r_o/r)^n \cos n\,\theta.$$

The potential of the special line source assumed here is, however,

$$V_o = -\mu \ln R^2$$

and on the axis assumes the form

$$\left. V_o \right]_{axis} = -\mu \ln (r^2 - 2x_j\, r \cos \theta + x_j^{\,2}) = 2\mu \left[-\ln r + \sum \frac{1}{n}\,(x_j/r)^n \cos n\,\theta \right]$$

The axial derivatives of V_o at the origin are hence given by

$$V_o^{(n)} = \left. \frac{\partial^n V_o}{\partial x_j^{\,n}} \right|_o = 2\mu\,(n-1)!\,(1/r)^n \cos n\,\theta$$

and, accordingly, Φ_n may be identified as

$$\Phi_n = -\frac{p_n}{n!}\, r_o^{\,n}\, V_o^{(n)}$$

for this field or for a general composite field. This is the result stated in section II, 2.

8. The use of an oblique quadrupole coil has been suggested by Garrett and Elmore -- cf. ref. 6.

9. See reports of the Magnet Group, ADD.

10. L. J. Haworth, meeting of ADD (June 30, 1954). The relative error involved would be of the order $\frac{H_0(3)}{6H_0(1)}\left[\frac{\text{separation}}{2}\right]^2$.

LJL:mt
8/25/54

Distribution
ADD-B1

SUMMARY OF RESULTS

CONCERNING

DESIGN OF AXIALLY-SYMMETRIC SEARCH COILS

[Unrationalized e.m.u.] Ref.: M. W. Garrett

1a. The potential representing the field produced by a current i in the coil is expressed

$$V_{coil} = 2\pi i \sum \frac{p_n}{n+1} (r_o/r)^{n+1} P_n(\cos\theta) \quad ,$$

where r_o is a constant length introduced for dimensional convenience.

b. The flux-linkage when this coil is inserted in an external magnetic field characterized by the potential V_o is

$$\phi = \sum \phi_n \ ,$$

where $\phi_n = -2\pi p_n r_o^{n+1} V_o^{(n)} /(n+1)!$

and $V_o^{(n)} = \frac{d^n V_o}{dx^n}$ evaluated at the origin.

c. For a coil intended to measure flux-density at a point it is thus desirable that p_3 shall vanish, the coefficients p_n normally vanishing automatically for n even in such cases due to symmetry in the coil construction.

2a. For a current loop

$$p_n = N_j \sin^2\alpha_j P_n'(\cos\alpha_j) (r_j/r_o)^{n+1} \ .$$

b. For a solenoid

$$p_n = \frac{r_o}{n+2} \sum_k N_k' \sin^2\alpha_k P_{n+1}'(\cos\alpha_k) (r_k/r_o)^{n+2} \ ,$$

the linear turn-density N_k' being given opposite sign at the two ends of the solenoid.

c. For a coil

$$p_n = \frac{r_o^2}{(n+2)(n+3)} \sum_{\ell} N''_{\ell} (x_{\ell}/r_o)^n (a_{\ell}/r_o)^3 \frac{B_{no} - B_{n2}\tan^2\alpha_{\ell} + \dots}{A_n} \ ,$$

the turn-density N''_{ℓ} being given alternate signs as one proceeds with the summation around the boundary of the rectangular winding.

TABLE

COEFFICIENTS FOR THICK-SOLENOID CONSTANTS p_n

APPEARING IN THE EXPRESSION

$$p_n(c) = \frac{r_o^2}{(n+2)(n+3)} \sum N''(x/r_o)^n(a/r_o)^3 \frac{B_{no} - B_{n2}\tan^2\alpha + \dots}{A_n}$$

n	A_n	B_{no}	B_{n2}	B_{n4}	B_{n6}	B_{n8}	B_{n10}	C
0	1	(1)						
1	1	4						
2	2	20	(3)					2
3	1	20	9					
4	8	280	252	(15)				4
5	1	56	84	15				
6	16	1344	3024	1080	(35)			24
7	8	960	3024	1800	175			
8	128	21120	88704	79200	15400	(315)		88
9	32	7040	38016	47520	15400	945		
10	256	73216	494208	823680	400400	49140	(693)	52
11	128	46592	384384	823680	560560	114660	4851	

The values in parentheses represent coefficients of terms independent of x and hence will normally drop out of the summation. In such cases the quantity C may conveniently be factored out of the remaining coefficients.

Thus $p_o = \sum \frac{N''}{6} \frac{a^3}{r_o}$, $\quad p_1 = \sum \frac{N'' r_o^2}{12} \frac{4 \cdot x \cdot a^3}{r_o^4}$,

$$p_2 = \sum \frac{N'' r_o^2}{20} \frac{x^2 \cdot a^3}{r_o^5} \left[\frac{20 - 3(a/x)^2}{2} \right] ,$$

$$p_3 = \sum \frac{N'' r_o^2}{30} \frac{x^3 a^3}{r_o^6} \left[20 - 9(a/x)^2 \right] , \dots .$$

CERTAIN RELATIONS AMONG LEGENDRE FUNCTIONS

1. The following five recurrence formulas are cited by Whittaker and Watson (Sect. 15.31):

$$\text{I.}\quad P'_{n+1} - z\,P'_n = (n+1)\,P_n$$

$$\text{II.}\quad (n+1)\,P_{n+1} - (2n+1)\,z\,P_n + n\,P_{n-1} = 0$$

$$\text{III.}\quad z\,P'_n - P'_{n-1} = n\,P_n$$

$$\text{IV.}\quad P'_{n+1} - P'_{n-1} = (2n+1)\,P_n$$

$$\text{V.}\quad (z^2-1)\,P'_n = n\,z\,P_n - n\,P_{n-1}\,.$$

2. The following two identities were cited in connection with the discussion of search coil design:

A. Subtracting equation V from equation II,

$$(1-z^2)\,P'_n = (n+1)\,z\,P_n - (n+1)\,P_{n+1}\,,$$

or $$\frac{\sin^2\alpha}{n+1}P'_n(\cos\alpha) = \cos\alpha\,P_n(\cos\alpha) - P_{n+1}(\cos\alpha)\,.$$

B. By I, $(n+2)\,P_{n+1} = P'_{n+2} - z\,P'_{n+1}$;

by III, $(n+1)\,P_{n+1} = z\,P'_{n+1} - P'_n$;

hence, subtracting,

$$P_{n+1} = P'_{n+2} - 2\,z\,P'_{n+1} + P'_n\,.$$

3. We also wish to establish

$$\frac{d}{dx}\left[r^{n+2}\sin^2\alpha\,P'_{n+1}(\cos\alpha)\right] = (n+2)\,r^{n+1}\sin^2\alpha\,P'_n(\cos\alpha)\,,$$

where $r = a/\sin\alpha$, $x = a/\tan\alpha$, and "a" is constant.

To this end we note that

$$\frac{d}{dx} = \frac{d/d\alpha}{dx/d\alpha} = -\frac{1}{a}\sin^2\alpha\,\frac{d}{d\alpha} = -\frac{\sin\alpha}{r}\,\frac{d}{d\alpha}$$

and in particular, of course,

$$\frac{dr}{dx} = \cos\alpha\,.$$

Then $\frac{d}{dx}\left[r^{n+2}\sin^2\alpha\, P'_{n+1}\right]$

$$= (n+2)\sin^2\alpha\cos\alpha\; r^{n+1}\, P'_{n+1}$$

$$-\ \frac{\sin\alpha}{r}\, r^{n+1}\left(2\sin\alpha\cos\alpha\, P'_{n+1} - \sin^3\alpha\, P''_{n+1}\right)$$

$$= r^{n+1}\sin^2\alpha\left[(n+2)\cos\alpha\, P'_{n+1} - 2\cos\alpha\, P'_{n+1} + \sin^2\alpha\, P''_{n+1}\right]$$

$$= r^{n+1}\sin^2\alpha\left[(n+2)\cos\alpha\, P'_{n+1} - (n+1)(n+2)P_{n+1}\right]$$

by Legendre's differential equation

$$= (n+2)\, r^{n+1}\sin^2\alpha\left[\cos\alpha\, P'_{n+1} - (n+1)\, P_{n+1}\right]$$

$$= (n+2)\, r^{n+1}\sin^2\alpha\, P'_n\ , \quad \text{by III}\ .$$ Q.E.D.

4. We also cite, with respect to the Associated Legendre functions [cf. Jahnke u. Emde, Funktionentafeln, esp. p.114] :

$$(2n+1)\, z\, P_n^m = (n-m+1)\, P_{n+1}^m + (n+m)\, P_{n-1}^m \quad ,$$

$$(2n+1)\, z\, P_n^n = P_{n+1}^n\ .$$

MEMO 2 July 1954

To: K. Green

Fm: L. Jackson Laslett

Re: Use of reciprocity Relation in Garrett's Method of Analysis of Search-Coil Response.

Ref: M. W. Garrett, "Axially Symmetric Systems for Generating and Measuring Magnetic Fields, Part I", Jour. Appl. Physics 22, #9, 1091-1107 (September, 1951); sequel, Part II, available as a photostated manuscript.

1. At the 2 July 1954 meeting of the ADD Magnet Group you expressed an interest in the generality of the results inferred from a reciprocity principle in Garrett's analysis of search coil behavior. The following proof may therefore be of interest.

2. We consider a coil with axial symmetry, carrying a current of i (e.s.u.), and producing an exterior magnetic potential

$$V_{coil} = 2\pi(i/c) \sum \frac{p_n}{n+1} \left(\frac{r_o}{r}\right)^{n+1} P_n(\cos\theta) .$$

We now consider, as an elemental source, a magnetic pole of strength μ situated at r,0; the flux from this pole threading the coil is designated as ϕ and we have the relationship

$$-(i/c)\phi = \mu V_{coil}$$

by use of energy considerations.

Accordingly ϕ may be written as $\phi = \sum \phi_n$,

with $$\phi_n = -2\pi\mu \frac{p_n}{n+1} (r_o/r)^{n+1} P_n(\cos\theta) .$$

For the particular special source assumed in this case, the potential at ρ_j, α_j produced in the neighborhood of the coil by this point source is, however,

$$V_o = \mu/R$$
$$= \frac{\mu}{r} \sum_n \left(\frac{\rho_j}{r}\right)^n P_n(\cos(\theta - \alpha_j)),$$

[Smythe (Ed. II), Sect. 5.153]. At points x_j along the axis of the coil,

$$V_o\Big]_{axis} = \frac{\mu}{r} \sum (x_j/r)^n P_n(\cos\theta)$$

and the axial derivatives at the origin are given by

$$V_o^{(n)} \equiv \frac{\partial^n V_o}{\partial x_j^n}\Big]_o = \mu\, n!\,(1/r)^{n+1} P_n(\cos\theta) .$$

Accordingly, ϕ_n may be identified as

$$\phi_n = -2\pi \frac{p_n}{(n+1)!} r_o^{n+1} V_o^{(n)} ,$$

for this particular applied field or for any general applied field which may be regarded as established by the superposition of such multipole contributions. This is the result stated by Garrett.

3. A parallel argument may be advanced for long coils in a two-dimensional situation.

In this case we write the external magnetic potential as

$$V_{coil} = 2(i/c) \sum \frac{p_n}{n}\left(\frac{r_o}{r}\right)^n \cos n\theta .$$

We consider a line-pole source, of strength μ per unit length, situated at r,θ and let ϕ designate the flux per unit length through the source. The reciprocity relation then is again

$$-(1/c)\phi = \mu V_{coil}$$

and we may write

$$\phi = \sum \phi_n ,$$

with

$$\phi_n = -2\mu \frac{p_n}{n} (r_o/r)^n \cos n\theta .$$

The potential of the special line source assumed here is, however,

$$V_o = -\mu \ln R^2$$

and on the axis assumes the form

$$V_o\Big]_{axis} = -\mu \ln(r^2 - 2x_j r \cos\theta + x_j^2) ,$$

$$= 2\mu \left[-\ln r + \sum (1/n)(x_j/r)^n \cos n\theta\right].$$

The axial derivatives at the origin are hence given by

$$V_o^{(n)} \equiv \frac{\partial^n V_o}{\partial x_j^n} = 2\mu (n-1)!(1/r)^n \cos n\theta$$

and, accordingly, ϕ_n may be identified as

$$\phi_n = \frac{p_r}{n!} r_o^n V_o^{(n)}$$

for this field or for a general composite field.

4. It is noted that in the foregoing derivations the location of the source remains general.

BROOKHAVEN NATIONAL LABORATORY
Associated Universities, Inc.
Upton, L. I., N. Y.

COIL SYSTEMS FOR MEASUREMENT OF FIELD AND FIELD-GRADIENT IN TWO DIMENSIONAL MAGNETIC FIELDS

L. Jackson Laslett*

July 16, 1954

---

* On leave from the Ames Laboratory of the AEC, Iowa State College, to represent the Mid-Western University Research Association.

I. INTRODUCTION

1. Purpose:

In connection with the design and development of a high-energy alternate-gradient proton synchrotron at the Brookhaven National Laboratory, it is desired to measure in a pulsed model (and prototype) the ratio of field gradient to field intensity throughout the excitation cycle. It is hoped in these measurements to include a measurement of this ratio in the D.C. residual fields prevailing at the start of the cycle, preferably employing the same instrumentation. For purposes of computation it is presumed that the initial field and its time derivative will be of the order of 20 gauss and 10^4 gauss/sec, respectively, while the corresponding values for the gradient in a full-scale model will be 2 gauss/inch and 10^3 (gauss/inch)/sec.

It is the purpose of the present report to exhibit the characteristics of a few coil systems which have been given consideration for this work.

2. Basic Equations:

(i) Response: The response of dipole and quadrupole search coils has been discussed in an earlier report (LJL-1); we list here for convenience the applicable specific formulas:

(a) Axially-Symmetric Dipole Coil [Solenoid], of half-height Δx, turn density N'', and total turns N:

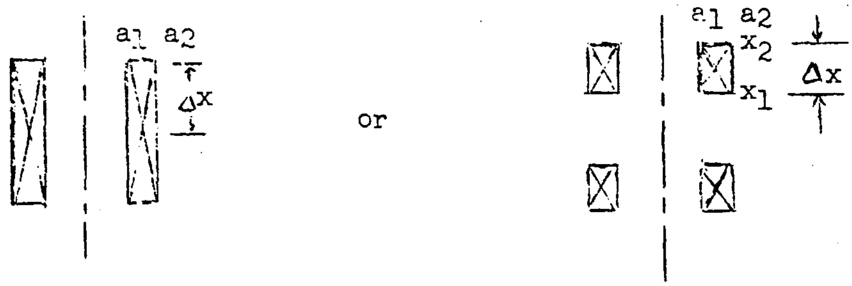

$$\phi_1 = 2\pi N'' \frac{\Delta x\,(a_2^3 - a_1^3)}{3} H \cos\psi$$

$$= \frac{\pi}{3} N \frac{a_2^3 - a_1^3}{a_2 - a_1} H \cos\psi$$

(b) Axially-Symmetric Quadrupole Pair, with N turns per coil:

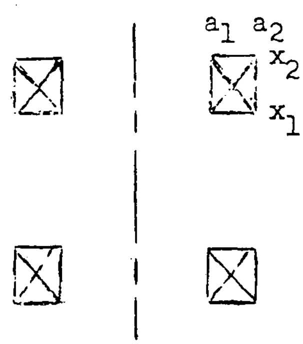

$$\phi_2 = \frac{\pi}{3} N'' (x_2^2 - x_1^2)(a_2^3 - a_1^3) \frac{dH}{dy} \sin 2\psi$$

$$= \frac{\pi}{3} N (x_2 + x_1) \frac{a_2^3 - a_1^3}{a_2 - a_1} \frac{dH}{dy} \sin 2\psi$$

(c) Long Dipole-Layer, of length s, with turn density N" or <u>total</u> turns N:

$$\phi_1 = 2N'' \Delta x \, (a_2^2 - a_1^2) \, s_{eff} \, H \cos \psi$$

$$= N \, (a_2 + a_1) \, s_{eff} \, H \cos \psi \, ,$$ where

$$s_{eff} = \frac{\langle a \, [s + 2(a - a_1)] \rangle}{\langle a \rangle}$$

$$= s - 2a_1 + 2\frac{\langle a^2 \rangle}{\langle a \rangle} = s + (a_2 - a_1) + \frac{1}{3} \frac{(a_2 - a_1)^2}{a_2 + a_1} \; .$$

(ii) Theoretically Optimum Dimensions:

(a) Axially-Symmetric Dipole Coil, if response to $\frac{d^3V}{dx^3}$ vanishes:

$$x_2^2 + x_1 x_2 + x_1^2 = \frac{9}{20} \frac{a_2^5 - a_1^5}{a_2^3 - a_1^3} \; .$$

(b) Long Dipole-Layer, if response to $\frac{d^3V}{dx^3}$ vanishes:

$$x_2^2 + x_1 x_2 + x_1^2 = \frac{1}{2} (a_2^2 + a_1^2) \; .$$

(c) Long Quadrupole-Combination, if response to $\frac{d^4V}{dx^4}$ vanishes:

$$x_2^2 + x_1^2 = a_2^2 + a_1^2 \; .$$

(iii) Modified Dimensions for Separated Difference Coils:

(a) Separated Axially-Symmetric Dipole Coils, of semi-axial spacing δ:

$$x_2^2 + x_1x_2 + x_1^2 = \frac{9}{20}\,\frac{a_2^5 - a_1^5}{a_2^3 - a_2^3} + \delta^2 .$$

(b) Separated Dipole-Layer Coils, in opposition:

$$x_2^2 + x_1x_2 + x_1^2 = \frac{1}{2}\,(a_2^2 + a_1^2) + \delta^2 .$$

(iv) Inductance Coefficients:

[Ref.: J. Hak, "Eisenlose Drosselspulen" -- K. F. Koehler Verlag, Leipzig (1938); Edwards Brothers, Inc., Ann Arbor, Michigan (1944).]

(a) Self-Inductance of Solenoidal Coil: It is convenient to use the expression $L = N^2\cdot(\text{mean diam.})\cdot\emptyset$ e.m.u., where $\emptyset$ is plotted in Figs. 20-22 by Hak, as a function of the parameters

$$\alpha = \frac{\text{axial dimension}}{\text{mean diameter}} \quad \text{and} \quad \rho = \frac{\text{radial thickness}}{\text{mean diameter}} .$$

(b) Mutual-Inductance of Coaxial Identical Solenoidal Coils: The mutual inductance of interest being comparatively small, it may be estimated roughly as $2\pi^2N^2\langle a\rangle^4/\langle \text{sep'n}\rangle^3$ e.m.u. or approximately by Hak's form $M = (\text{Diam.})\emptyset$, where (with the diameter ratio $\delta = 1$) $\emptyset$ may be found from Hak's Figs. 5-7 as a function of the parameter $\xi = \langle \text{sep'n}\rangle/\langle \text{diam.}\rangle$.

(c) Self-Inductance of Single Long Coil, of Rectangular Form:

$$L = 4N^2(c + d)\left[\ln \frac{2cd}{a+r} - \frac{c}{c+d}\ln(c + \sqrt{c^2 + d^2}) - \frac{d}{c+d}\ln(d + \sqrt{c^2 + d^2}) + 2\frac{\sqrt{c^2+d^2}}{c + d} - 0.5 + 0.447\frac{a+r}{c+d}\right],$$

with $a = x_2 - x_1$, $c = s + (a_2 - a_1)$, $d = a_2 + a_1$, and $r = a_2 - a_1$.

II. SYSTEM INVOLVING LONG COILS

1. Description:

The system designed here consists of a quadrupole coil pair, whose maximum transverse dimensions fall within a circle of 0.940" diameter, and a small coaxial dipole coil, each wound on forms whose length is taken as 4 inches. It is supposed that these coils may be rotated, about their longitudinal axis, to measure the ratio of magnitude and gradient in a static residual field and then used to investigate similarly the time-varying magnetic field of a dynamic model. If it is desired that the field measurements themselves be made at a fixed location, while the gradient measurements are taken at a series of other locations, the dipole coil (or a replica) may be divorced from the quadrupole pair and located as desired.

The dimensions selected for the coils are the following /see Drg. 1/:

Dipole Coil: $a_1 = 0.050''$

$a_2 = 0.080''$

$x = 0.0667''$ (half length);

Quadrupole Coils: $a_1 = 0.130''$

$a_2 = 0.300''$

$x_1 = \pm 0.170''$

$x_2 = \pm 0.279''$.

It will be observed that the dimensions of the dipole coil are such as to satisfy the relation of section I.2(ii-b) -- namely, $(0.0667)^2 = \frac{1}{2}[(0.080)^2 + (0.050)^2]$ -- so as to render the coil response insensitive to $\frac{d^3V}{dx^3}$ and thus give a theoretically precise measurement of the field strength at its center. Similarly the dimensions of the quadrupole pair are in accord with section I.2(ii-c) -- namely, $(0.279)^2 + (0.170)^2 = (0.300)^2 + (0.130)^2$ -- so that the response to $\frac{d^4V}{dx^4}$ is removed and an accurate measurement is made of $\frac{d^2V}{dx^2}$ and hence of the field-gradient $H^{(1)}$ in the median plane.

For estimation of coil response, the effective lengths of the coils are:

Dipole Coil: $4.000 + 0.030 + 0.0023 = 4.0323$ inches;

Quadrupole Coil: $4.000 + 0.170 + 0.0224 = 4.1924$ inches.

2. Turn-Density:

Based on the use of #40 B.&S. enameled wire, for which the Anaconda nominal diameter (over insulation) is

0.0034 inches and which is here taken (conservatively) as 0.0035 inches, we assign the following numbers of turns to the respective coils:

Dipole coil: $N = 0.80 \dfrac{0.030 \times 0.1134}{(0.0035)^2} \doteq 260$;

Each member of quadrupole pair:

$$N = 0.80 \frac{0.170 \times 0.109}{(0.0035)^2} \doteq 1200.$$

The factor 0.80 is introduced as an empirical factor to allow for unavoidable looseness in winding.

The resistance of the wire is taken as 1049 ohms per thousand feet or 0.0874 ohms per inch.

3. Performance:

The properties of these coils and their expected performance in the fields specified in the introduction will be found listed in Table I below:

[Note: The mutual inductance between the two parallel long rectangular coils, of similar form and size, is relatively small in the present instance and might be estimated as $M \doteq 2N^2(\text{Length})\left(\dfrac{\text{width}}{\text{separation}}\right)^2$; a more complete expression is given by Hak, which suggests that for the dimensions of interest here a reasonable approximation would be

$M \doteq 2N^2(\text{Length}) \ln\left[1 + \left(\dfrac{\text{width}}{\text{separation}}\right)^2\right]$ e.m.u.]

TABLE I

EXPECTED CHARACTERISTICS AND PERFORMANCE OF LONG COILS

	Dipole Coil
Resistance, R	$260(2 \times 4.13)(0.0874) = 188$ ohms
Approximate Inductance, L	$4.98(260)^2(4.16 \times 2.54)10^{-9} = 3.56 \times 10^{-3}$ henry
Response in Static Field*	$260(0.130 \times 4.0323)(2.54)^2\ 20 \times 10^{-8}$ $= (879 \times 10^{-8}) \times 20 = 0.176 \times 10^{-3}$ volt-sec
Response in Dynamic Field	$879 \times 10^{-8} \times 10^4 = 87.9 \times 10^{-3}$ volts
	Quadrupole Pair
Resistance, R	$2 \times 1200(2 \times 4.43)(0.0874) = 1860$ ohms
Approximate Inductance, $L = L_I + L_{II} - 2M$	$2[7.32(1200)^2(4.6 \times 2.54)10^{-9}]$ $-2[2(1200)^2(4.17 \times 2.54)\ \ln(1 + (\frac{0.430}{0.449})^2) \times 10^{-9}$ $= 0.25 - 0.04 = 0.21$ henry
Response in Static Field*	$1200(0.449 \times 0.430)(2.54)^2(4.1924)\ 2 \times 10^{-8}$ $= 0.125 \times 10^{-3}$ volt sec
Response in Dynamic Field	$1200(0.449 \times 0.430)(2.54)^2(4.1924)\ 10^3 \times 10^{-8}$ $= 62.6 \times 10^{-3}$ volts

* The dipole and quadrupole coils should preferably be flipped through angles ($\Delta\psi$) of 180° and 90° respectively, in order that the generated signals be insensitive to the angle of rotation, but the computed signals are taken to be one-half as great as those which would then result in order that they may serve as appropriate initial values for ensuing dynamic measurements.

III. SYSTEM EMPLOYING AXIALLY-SYMMETRIC COILS

1. Description:

We suggest here the use of five pairs of dipole coils for the gradient measurements. The two members of each pair are connected in series opposition to provide a measure of the gradient and the five pair, arranged longitudinally, are connected in series to augment the signal and to provide an average value for the gradient. For measurement of the field itself, a couple of additional dipole coils are used in a series aiding connection.

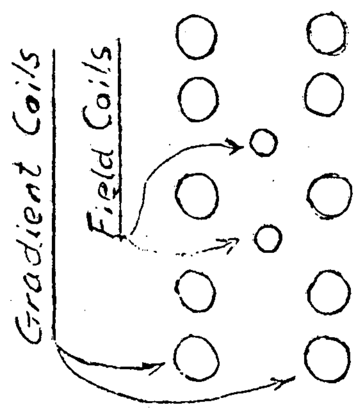

The dimensions selected for the coils are as follows [Drg. II]:

Dipole Coils: $a_1 = 0.186''$
$a_2 = 0.210''$
$\Delta x = 0.172''$ (half length);

Quadrupole Pair: $a_1 = 0.100''$, $x_1 = 0.320''$, $b = 0.600''$,
$a_2 = 0.250''$, $x_2 = 0.400''$, $\sqrt{x_2^2 + a_2^2} = 0.472''$.

It will be observed that the dimensions of the dipole coil are such as to satisfy the relation of section I.2(ii-a) -- namely, $(0.172)^2 = \frac{9}{20}\,\frac{(0.210)^5 - (0.186)^5}{(0.210)^3 - (0.186)^3}$ -- to remove the dependence upon $\frac{d^3V}{dx^3}$. Likewise, for any of the quadrupole pair, the relation of section I.2(iii-a) is satisfied --

namely,

$$(0.400)^2 + (0.400)(0.320) + (0.330)^2 = \frac{9}{20}\frac{(.250)^5-(.100)^5}{(.250)^3-(.100)^3} + (.600)^2$$

-- with the result that the gradient at the mid-point may be determined by use of this coil combination, independent of the second derivative of the flux-density.

2. Turn-Density:

As in section II.2, we consider the use of enameled #40 wire and assign the following numbers of turns to the coils:

Dipole coil: $N = 0.80 \frac{0.024 \times 0.344}{(0.0035)^2} = 540$;

One Member of Quadrupole Pair:

$$N = 0.80 \frac{0.150 \times 0.160}{(0.0035)^2} \doteq 1560$$

(i.e., 780 turns each on upper and on lower windings).

3. Performance:

The properties and expected performance of these coils are given in Table II below:

TABLE II

EXPECTED CHARACTERISTICS AND PERFORMANCE
OF COMBINED AXIALLY-SYMMETRIC COILS

	Dipole Coils
Total Resistance, R	$2[540(2\pi \times 0.198)(0.0874)]$ $= 117$ ohms
Approximate Inductance, L	$2[7.05(540)^2(0.396 \times 2.54)] \cdot 10^{-9}$ $= 4.13 \times 10^{-3}$ henry
Response in Static Field*	$2(\pi/3)(540)(0.1178)(2.54)^2 \times 20 \times 10^{-8}$ $= 0.172 \times 10^{-3}$ volt-sec
Response in Dynamic Field	$2(\pi/3)(540)(0.1178)(2.54)^2 \cdot 10^4 \times 10^{-8}$ $= 86 \times 10^{-3}$ volts
	Set of Quadrupole Pairs
Total Resistance, R	$10[1560(2\pi \times 0.175)(0.0874)]$ $= 1500$ ohms
Approximate Inductance, $L = L_I + L_{II} + 2M$	$10\{2[8.6(780)^2(0.350 \times 2.54)] \cdot 10^{-9} + 2[0.12(780)^2(0.350 \times 2.54)] \cdot 10^{-9}\}$ $= 10[(9.31 + 0.13) \cdot 10^{-3}] = 94.4 \times 10^{-3}$ henry
Response in Static Field*	$5(\pi/3)(1560)(0.0975)(2.54)^2(2 \times 1.2)\ 10^{-8}$ $= 0.124 \times 10^{-3}$ volt sec
Response in Dynamic Field	$5(\pi/3)(1560)(0.0975)(2.54)^2(10^3 \times 1.2)\ 10^{-8}$ $= 62 \times 10^{-3}$ volts

* For rotation of coils, in effect, through 90°, so that signals shall provide suitable initial values for the dynamic measurements.

4. Supplementary Comment:

Although the coil systems described in Parts II and III appear, at least at this stage, to meet the requirements set down for measurement of the dynamic magnet model, other possible coil systems should perhaps be considered. It may prove of advantage (in the sense of reducing self-inductance, simplifying the construction, etc.) to relax or withdraw the requirement of suppressing the effect of the higher order derivatives to which the coils might respond, if a more compact arrangement can thereby be achieved. Evaluation of the relative merits of such schemes would then require, of course, knowledge of the relative magnitudes of the various derivatives of the magnetic field. In addition, careful balancing electrically of the final coils would be required in order to insure that their performance is that expected theoretically. The use of the axially-symmetric coils may be preferable to the use of long coils from the standpoint of distributed capacity and, where applicable, the use of "bank winding" would be desirable.

IV. MULTI-COIL LAMBDA-METER

1. Purpose:

The use of a two coil bridge circuit to measure $\frac{1}{\langle H\rangle_{Av}} \frac{\Delta H}{\Delta y}$ has been proposed by Beth [RAB-1 (June 30, 1954)]. It may be desirable to modify this proposal in such a way as to eliminate the dependence of $\langle H\rangle_{Av}$ on $\frac{d^2H}{dy^2}$ and of $\frac{\Delta H}{\Delta y}$ on $\frac{d^3H}{dy^3}$ and so provide a more precise measurement of $\frac{1}{H}\frac{dH}{dy}$. The following sections, although not necessarily employing optimum dimensions, incorporate a suggestion of Snyder [AGS Magnet Group meeting, July 9, 1954] concerning the use of multiple coils and are intended to illustrate the possible use of the modified bridge method for measurement of $\frac{1}{H}\frac{dH}{dy}$ in a two-dimensional magnetic field.

2. Circuit:

The proposed circuit is illustrated schematically below, each of the outside coils being connected (as shown) in opposition to their immediate neighbor. The condition of

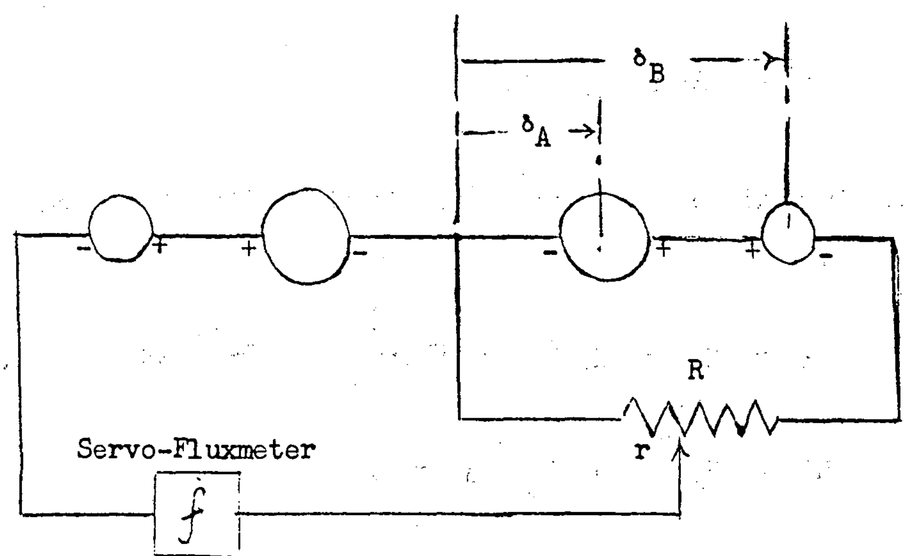

balance for the bridge is that

$$[\phi_A(-\delta_A) - \phi_B(-\delta_B)] = \frac{r}{R}[\phi_A(+\delta_A) - \phi_B(+\delta_B)], \qquad \text{or}$$

$$\frac{R-r}{R+r} = \frac{[\phi_A(+\delta_A) - \phi_A(-\delta_A)] - [\phi_B(+\delta_B) - \phi_B(-\delta_B)]}{[\phi_A(+\delta_A) + \phi_A(-\delta_A)] - [\phi_B(+\delta_B) + \phi_B(-\delta_B)]}.$$

3. Basic Equations:

We write the response of the individual coils as

$$\phi_A = b_A H + c_A H'' \qquad \text{and}$$

$$\phi_B = b_B H + c_B H'',$$

where $H'' \equiv \frac{d^2H}{dy^2}$ (at the center of the coil) and the coefficients b, c may (for axially-symmetric coils) be identified with the coefficients p_1, p_3 of LJL-1 (Part I):

$$b = 2\pi r_o^2 p_1 / 2,$$

$$c = -2\pi r_o^4 p_3 / 24.$$

We note, in addition, that the field in the median plane may be expanded

$$H = H_o + H_o^{(1)} + \frac{H_o^{(2)}}{2} y^2 + \frac{H_o^{(3)}}{6} y^3 + \ldots,$$

$$H'' = H_o^{(2)} + H_o^{(3)} y + \ldots.$$

The condition of balance for the bridge hence becomes

$$\frac{R - r}{R + r} \doteq \frac{(b_A\delta_A - b_B\delta_B)H_o^{(1)} + \left(\frac{b_A\delta_A^3 - b_B\delta_B^3}{6} + c_A\delta_A - c_B\delta_B\right)H_o^{(3)}}{(b_A - b_B)H_o + \left(\frac{b_A\delta_A^2 - b_B\delta_B^2}{2} + c_A - c_B\right)H_o^{(2)}}$$

It is seen, therefore, that it is desirable to arrange the constants of the coils so that

$$b_A\delta_A^3 - b_B\delta_B^3 + 6c_A\delta_A - 6c_B\delta_B = 0 \qquad \text{and}$$

$$b_A\delta_A^2 - b_B\delta_B^2 + 2c_A - 2c_B = 0 ,$$

whereupon

$$\frac{R - r}{R + r} \doteq \frac{b_A\delta_A - b_B\delta_B}{b_A - b_B}\,\frac{H_o^{(1)}}{H_o} ,$$

as is desired for a measurement of the relative gradient at a point.

4. Numerical Example:

We exhibit here the dimensions of a set of coils, all of the same turn-density N", meeting the conditions of section 3. Scaling of the dimensions would, of course, be permissible but no claim is laid to the relative dimensions being optimum in every respect.

We select $\delta_A = 0.500"$

and $\delta_B = 1.250"$.

We then take [Drg. III]

For Coil "A":

$a_1 = 0.810''$

$a_2 = 0.900''$

$x_1 = 0$

$x_2 = 0.080''$

$(\Delta x = 0.080'')$;

For Coil "B":

$a_1 = 0.100''$

$a_2 = 0.500''$

$x_1 = 0.448''$

$x_2 = 0.487''$

$(\Delta x = 0.039'')$.

The coil constants accordingly become (for N" expressed in turns/inch^2)

$$b_A = 2\pi \frac{r_o^{\,2} p_1(A)}{2} = 2\pi \frac{(a_2^{\,3} - a_1^{\,3})(\Delta x)}{3} N''$$

$$= 2\pi(2.54)^2 \frac{0.197559 \times 0.080}{3} N'' = 2\pi(2.54)^2 [0.005250] N'' \text{ cm}^2,$$

$$b_B = 2\pi(2.54)^2 \frac{0.124 \times 0.039}{3} N'' = 2\pi(2.54)^2 [0.001612] N'' \text{ cm}^2,$$

$$c_A = -2\pi \frac{r_o^{\,4} p_3(A)}{24} = -2\pi \frac{[20(\Delta x)^2 (a_2^{\,3} - a_1^{\,3}) - 9(a_2^{\,5} - a_1^{\,5})](\Delta x)}{360} N''$$

$$= -2\pi(2.54)^2 \frac{[20(0.080)^2 (0.197559) - 9(0.241812)](0.080)}{360} N''$$

$$= 2\pi(2.54)^2 [0.000478] N'' \text{ cm}^2 \text{in}^2$$ (for use with H" expressed in gauss/in^2),

$$c_B = -2\pi \frac{[20(x_2^2 + x_1 x_2 + x_1^2)(a_2^3 - a_1^3) - 9(a_2^5 - a_1^5)](\Delta x)}{360} N''$$

$$= -2\pi(2.54)^2 \frac{[20(0.65605)(0.124) - 9(0.03124)](0.039)}{360} N''$$

$$= -2\pi(2.54)^2 [0.0001458] N'' \text{ cm}^2 \text{in}^2 .$$

These values will be seen to satisfy reasonably well the conditions of section 3, so that

$$\frac{R-r}{R+r} \doteq \frac{(0.005250)(0.500) - (0.001612)(1.250)}{0.005250 - 0.001612} \frac{H_o^{(1)}}{H_o}$$

$$= \frac{0.002625 - 0.002015}{0.005250 - 0.001612} \frac{H_o^{(1)}}{H_o}$$

$$= \frac{0.000610}{0.003638} \frac{H_o^{(1)}}{H_o} = 0.168 \frac{H_o^{(1)}}{H_o} ,$$

the relative gradient $H_o^{(1)}/H_o$ being expressed in reciprocal inches. [Typically $H_o^{(1)}/H_o$ for a full-scale model of an AGS magnet-sector would be $\frac{1}{10}$ in^{-1}, so $\frac{R-r}{R+r} \doteq 0.0168$ or $r \doteq 0.967\,R$ in this example.]

V. EVALUATION OF POSSIBLE ERROR FROM INDUCTIVE EFFECTS

1. Purpose:

In the dynamic field measurements it is planned* first to combine the signals from the gradient coils and field coils in such a way that these signals nearly balance, then to introduce the resultant signal to a high-performance integrator, and finally to display the output on an oscilloscope against a raster of radial lines representing variations of n in parts per thousand. Due to the time-varying character of the measurement, it is important that the signals from the two

* cf. J. P. Palmer's presentation, ADD meeting, July 14, 1954.

sets of coils shall at every instant buck one another substantially as with steady state EMF's, regardless of inductive or capacitative effects.

In this section we shall undertake to analysize the rôle played by inductive effects alone and to estimate the magnitude of the errors which could thereby arise through the use of coil systems with characteristics similar to those described in Parts II and III of the present report. Examination of the influence of capacitative effects is deferred until later; it appears from the present analysis, however, that the inductive effects (which will predominate) should alone not introduce a serious error, despite the fairly high values for the inductance of small coils constructed so as to provide the desired induced signal strengths.

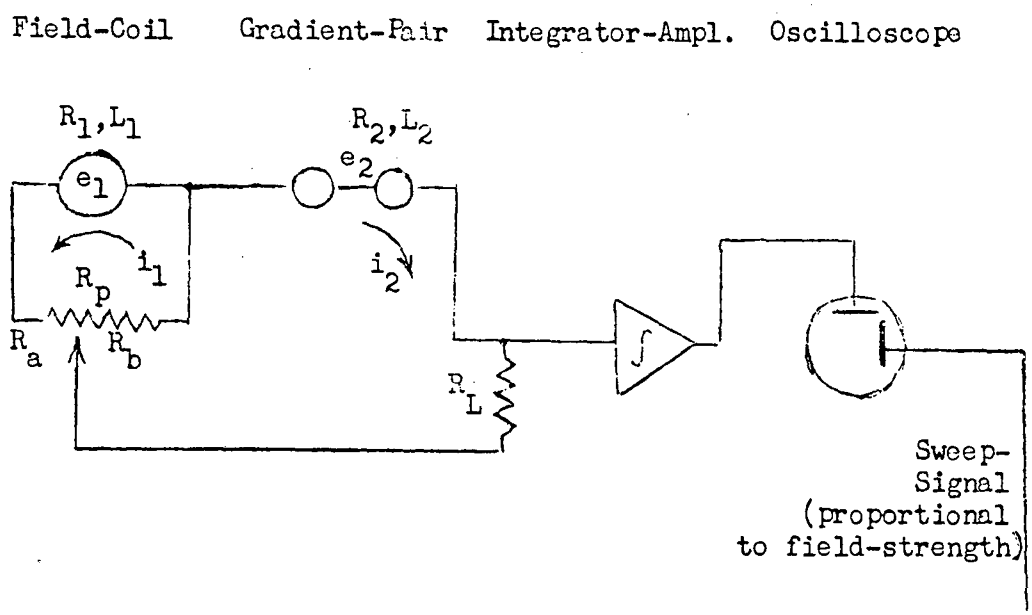

2. Basic Equations:

The basic loop equations for the circuit indicated are:

$$e_1 = L_1 \, di_1/dt + (R_1 + R_p)\, i_1 + R_b i_2 ,$$

$$e_2 = L_2 \, di_2/dt + R_b i_1 + (R_2 + R_L + R_b)\, i_2 .$$

Rather than solve these equations explicitly for i_2 as a function of time, we find it convenient first to integrate the equations and to solve for $\int i_2 \, dt$. The measured signal is proportional to

$$R_L \int i_2 \, dt = \frac{R_L}{D}\left\{ (R_1 + R_p)\int e_2 \, dt - R_b \int e_1 \, dt + \left[R_b L_1 i_1 - (R_1 + R_p) L_2 i_2 \right] \right\},$$

where $D = (R_1 + R_p)(R_2 + R_L + R_b) - R_b^{\,2}$

$$= (R_1 + R_p)(R_2 + R_L) + (R_1 + R_a) R_b .$$

[It will be found that the terms contained within the square brackets constitute the source of the error under investigation.]

3. Interpretation of Measured Signal:

We note that the signals from the field and gradient coils may be written

$$e_1 = k_1 (dB/dt) , \qquad e_2 = k_2 R_o (dB'/dt) ,$$

the prime disignating space differentiation. In addition

$$n = R_o B'/B .$$

We now introduce the quantity

$$n_d = \frac{k_1 R_b}{k_2\,(R_1 + R_p)} \quad ,$$

which will be seen to represent the value of n ideally giving zero output signal for the potentiometer setting adopted; the measured signal then may be written

$$R_L \int i_2 dt = \frac{R_L}{D}\left\{(R_1 + R_p)k_2(n - n_d)B + \left[R_b L_1 i_1 - (R_1 + R_p)L_2 i_2\right]\right\}.$$

If this output signal is interpreted in terms of an apparent n_{app} as

$$R_L \int i_2 dt = \frac{R_L}{D}\left\{(R_1 + R_p)k_2(n_{app} - n_d)B\right\}, \qquad \text{we have}$$

$$n_{app} - n = \frac{R_b L_1 i_1 - (R_1 + R_p)\,L_2 i_2}{(R_1 + R_p)\,k_2\,B} \qquad \text{or}$$

$$\frac{n_{app} - n}{n_d} = \frac{L_1 i_1 - \frac{R_1 + R_p}{R_b}\,L_2 i_2}{k_1\,B}$$

representing the error or relative error which inductive effects introduce into the measurement of n .

4. Estimation of the Error:

It is of interest to estimate the error contributions represented by the terms, involving i_1 and i_2, in the last equation of the preceding section. By reference to the original circuit, one may readily set an upper limit on i_1 :

$$i_1 < \frac{e_1}{R_1 + R_p} \quad ; \qquad \text{so} \quad \frac{L_1 i_1}{k_1 B} < \frac{L_1}{R_1 + R_p} \frac{dB/dt}{B} .$$

The maximum value of i_2 is considerably limited by the bucking feature of the potentiometer connection:

$$i_2 \leqslant \frac{(R_1 + R_p)e_2 - R_b e_1}{D}$$

$$= \frac{1}{D}\left\{(R_1 + R_p)k_2\left[d(nB)/dt - n_d(dB/dt)\right]\right\}$$

$$= \frac{k_1 R_b}{D}\left[\frac{d(nB)/dt}{n_d} - \frac{dB}{dt}\right]$$

$$= \frac{k_1 R_b}{D}\left[\frac{dn/dt}{n_d} B + \left(\frac{n}{n_d} - 1\right)\frac{dB}{dt}\right],$$

whereupon

$$\frac{(R_1 + R_p)L_2 i_2}{R_b k_1 B} \leqslant \frac{L_2}{R_2 + R_L + \frac{R_1 + R_a}{R_1 + R_p} R_b}\left[\frac{dn/dt}{n_d} + \left(\frac{n}{n_d} - 1\right)\frac{dB/dt}{B}\right] .$$

5. <u>Numerical Values</u>:

We consider that in a typical series of measurements we may establish the definite limits

$$\frac{dn/dt}{n_d} < 500 \times 10^{-2} = 5 ,$$

$$\frac{n}{n_d} - 1 < 10^{-2} , \qquad \text{and}$$

$$\frac{dB/dt}{B} < \frac{10^4}{20} = 500 .$$

We further consider circuit parameters, similar to the estimated values of Part III, as follows:

$L_1 = 4.13 \times 10^{-3}$ henry, $L_2 = 0.094$ henry,

$R_1 = 117$ ohms, $R_2 = 1500$ ohms,

$R_a = 750$ ohms, $R_b = 2250$ ohms, $R_p = 3000$ ohms, $R_L = 5000$ ohms.

With these values, the relative error from the effects of self-inductance would not exceed the following estimate:

$$\frac{n_{app} - n}{n_d} < \frac{4.13 \times 10^{-3}}{3117} \times 500 + \frac{0.094}{1500 + 5000 + 626}(5 + 5)$$

$$< 0.6625 \times 10^{-3} + 0.1319 \times 10^{-3}$$

$$< 0.8 \times 10^{-3}, \quad \text{or within one-tenth of one percent.}$$

Because of possible ringing effects, due to the presence of such inherent capacitances as are considered in Part VI, the currents i_1 and i_2 may have instantaneous values greater than the foregoing estimates and, over a short time interval, the relative error of the apparent n might appear larger than estimated here.

VI. ESTIMATE OF POSSIBLE ERRORS FROM COIL CAPACITANCE

1. Purpose and General Method:

As pointed out earlier, some error will be introduced in the dynamic field measurements by the self-capacitance of the several search coils. It is the purpose of the present sections to include this phenomenon in attempting to evaluate the errors of the measurement procedure.

The capacitative effects will, as is customary, be considered representable by an equivalent shunt capacitance across the combined inductance and resistance of the coil system. It is difficult accurately to estimate in advance the capacitance to be associated in this way with multi-layer coils such as are proposed here, although what may be regarded as an adequate formula for single-layer coils has been given by Palermo.*

---

* A. J. Palermo, Proc. I.R.E. 22, 897 (July, 1934). The result of this work has been quoted by J. Hak (op. cit.) and has been displayed in the form of an alignment chart by P. H. Massant in "Electronics for Engineers" (J. Markus and Vin Zeluff, Eds.), McGraw-Hill, Inc., N.Y., 1945.

The system of axially-symmetric flux-coils suggested in Part III may be expected to have a somewhat less prominent capacitance than would long coils of otherwise similar performance, due to the smaller E.M.F. per turn and the distributed character of the winding for the axial coils. Although the best estimates would undoubtedly result from measurements made on the coils themselves, we believe that the capacitance to be associated with the gradient coil system may be primarily that due to stray- or lead-capacity, while that for the field coils may run as high as a milli-microfarad. We propose, accordingly, to take the shunt capacity of the field-coil system as

$$C_1 = 960 \ \mu\mu\text{fds}$$

and that of the gradient coils as

$$C_2 = 10.5 \ \mu\mu\text{fds} ,$$

for which the nominal resonant frequencies would be, respectively,

$$f_1 = 80 \text{ KC} ,$$

$$f_2 = 160 \text{ KC} .$$

2. Basic Circuit Equations:

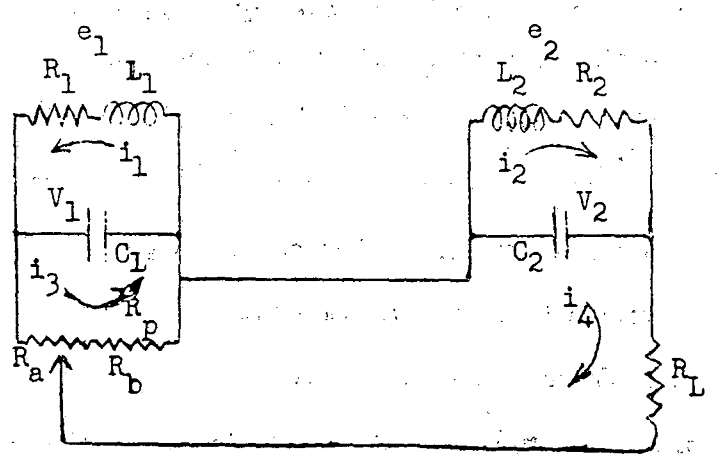

We write the basic loop equations for the equivalent circuit illustrated as

$$L_1(di_1/dt) + (1/C_1)\left[\int i_1 dt - \int i_3 dt\right] + R_1 i_1 = e_1$$

$$L_2(di_2/dt) + (1/C_2)\left[\int i_2 dt - \int i_4 dt\right] + R_2 i_2 = e_2$$

$$(1/C_1)\left[\int i_3 dt - \int i_1 dt\right] + i_3 R_p + i_4 R_b = 0$$

$$(1/C_2)\left[\int i_4 dt - \int i_2 dt\right] + i_4(R_L + R_b) + i_3 R_b = 0 .$$

By use of the last two equations to eliminate the capacitance terms, the first two equations may be written

$$(R_1 + R_p)\int i_3 dt + R_b\int i_4 dt = \int e_1 dt - L_1 i_1 - R_1\int (i_1 - i_3)dt$$

$$R_b\int i_3 dt + (R_2 + R_L + R_b)\int i_4 dt = \int e_2 dt - L_2 i_2 - R_2\int (i_2 - i_4)dt .$$

The measured output will then be proportional to

$$R_L\int i_4 dt = \frac{R_L}{D}\left\{(R_1 + R_p)\int e_2 dt - R_b\int e_1 dt + \left[R_b L_1 i_1 - (R_1 + R_p)L_2 i_2 + R_b R_1\int (i_1 - i_3)dt - (R_1 + R_p)R_2\int (i_2 - i_4)dt\right]\right\} .$$

3. <u>Interpretation of the Error</u>:

By the same methods as employed in Section V.3, we find

$$\frac{n_{app} - n}{n_d} = \frac{L_1 i_1 - \frac{R_1 + R_p}{R_b} L_2 i_2 + R_1\int (i_1 - i_3)dt - \frac{R_1 + R_p}{R_b} R_2\int (i_2 - i_4)dt}{k_1 B}$$

$$= \frac{\left[L_1 i_1 + R_1 C_1 V_1\right] - \frac{R_1 + R_p}{R_b}\left[L_2 i_2 + R_2 C_2 V_2\right]}{k_1 B} ,$$

where V_1 , V_2 represent the potentials across the capacitors C_1 , C_2.

4. Estimation of the Error:

The terms which explicitly involve L_1 and L_2 in the expression for error given in section 3 have been estimated in Part V -- it remains therefore to estimate the magnitudes of the terms which depend upon C_1 and C_2.

We suppose that $V_1 < 2e_1$, so that for the first term of interest

$$\frac{R_1 C_1 V_1}{k_1 B} < 2R_1 C_1 \frac{dB/dt}{B} .$$

We similarly suppose that $V_2 < 2e_2$, so that

$$\frac{R_1 + R_p}{R_b} \cdot \frac{R_2 C_2 V_2}{k_1 B} < 2R_2 C_2 \frac{dB/dt}{B} .$$

5. Numerical Values:

Considering, as stated in section 1, that

$$C_1 \cong 960 \ \mu\mu\text{fds},$$

$$C_2 \cong 10.5 \ \mu\mu\text{fds},$$

and the remaining constants are as stated in section V.5, we find that the foregoing contributions to the relative error of the n-measurement are:

From C_1: $2 \times 117 \times 0.96 \times 10^{-9} \times 500 = 0.112 \times 10^{-3}$ and

From C_2: $2 \times 1500 \times 10.5 \times 10^{-12} \times 500 = 0.016 \times 10^{-3}$.

It thus appears that if the capacitative effects have not been grossly underestimated the resultant errors will be negligible in gradient measurements of the type proposed.

It is hoped that more definitive information concerning the performance and errors of a coil system such as herein described will result from experimental tests now being undertaken in this Laboratory.

jl
7/20/54

Distribution
ADD-B1

BROOKHAVEN NATIONAL LABORATORY

DRG. I

BY L. J. L. DATE

SUBJECT LONG COILS

SHEET No. OF

CHKD. BY DATE

JOB No.

DEPT. OR PROJECT

Accelerator Development Department
Internal Report LJL-2

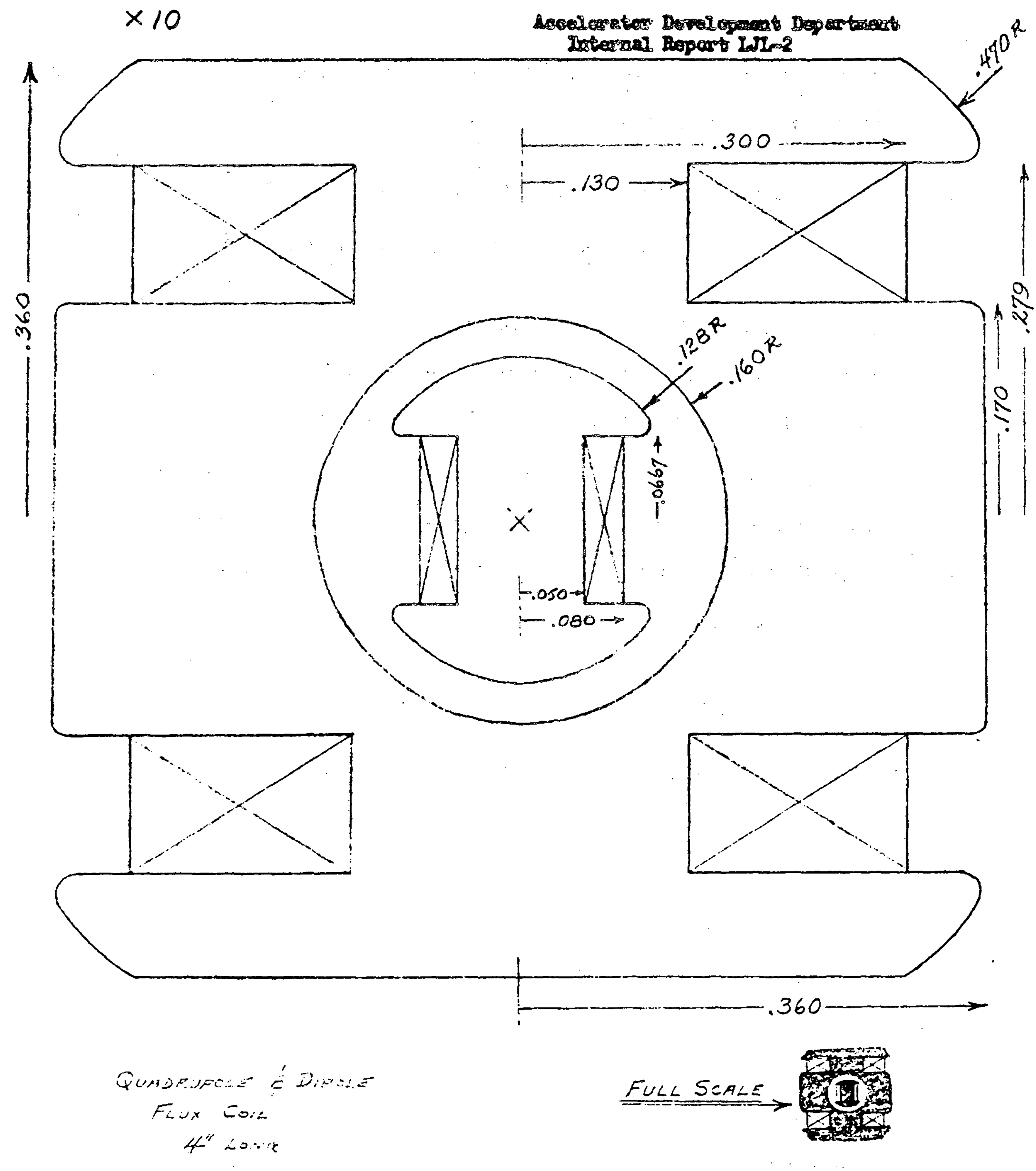

BROOKHAVEN NATIONAL LABORATORY

BY L.J.L. DATE ______ SUBJECT Axially-Symmetric Flux-Coils SHEET No. ______ OF ______

CHKD. BY ______ DATE ______ JOB No. ______

DEPT. OR PROJECT ______

Accelerator Development Department
Internal Report - LJL-2

FULL SCALE

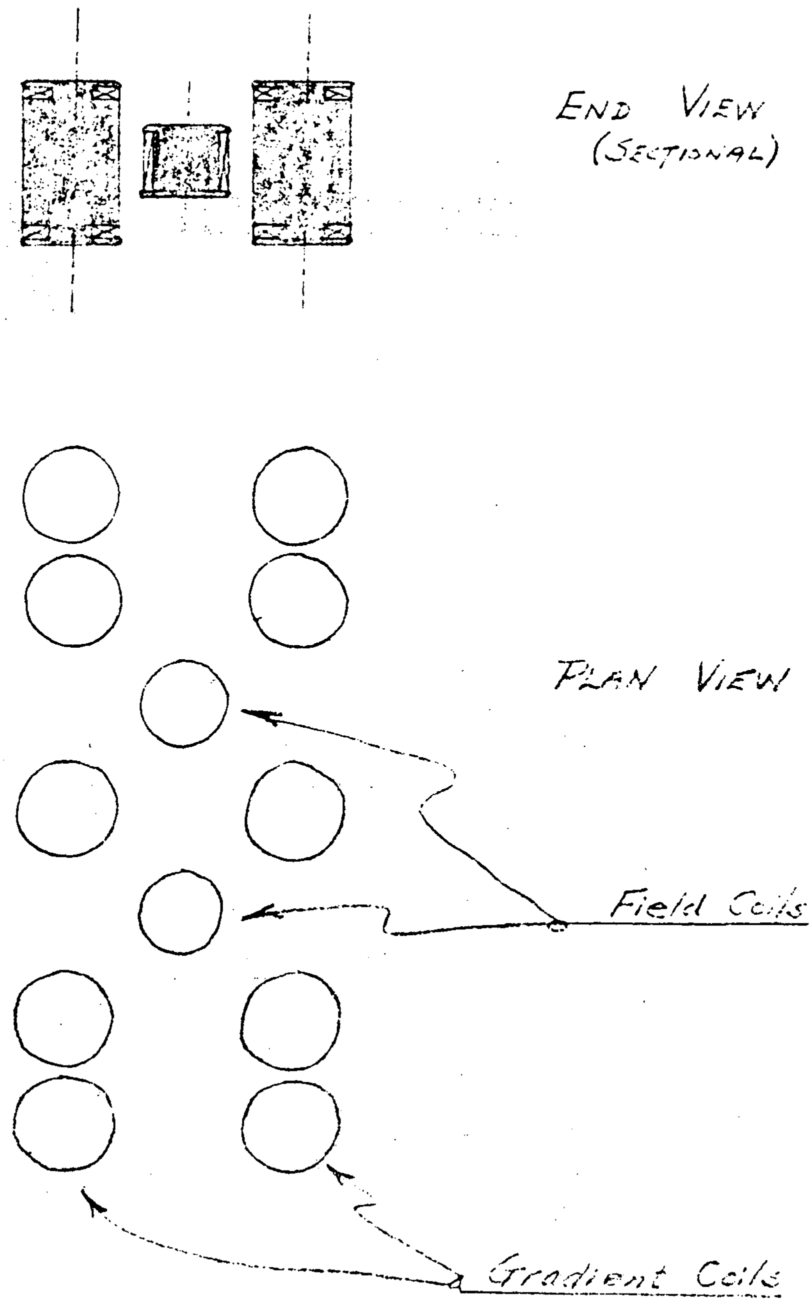

DRG. III.

BROOKHAVEN NATIONAL LABORATORY

BY L. J. L. DATE

CHKD. BY DATE

SUBJECT Coils for Multi-Coil Lambda-Meter

DEPT. OR PROJECT

SHEET No. OF

JOB No.

Accelerator Development Department
Internal Report LJL-2

FULL SCALE

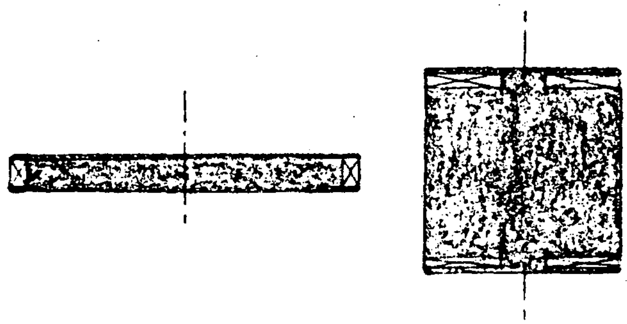

SECTIONAL VIEW

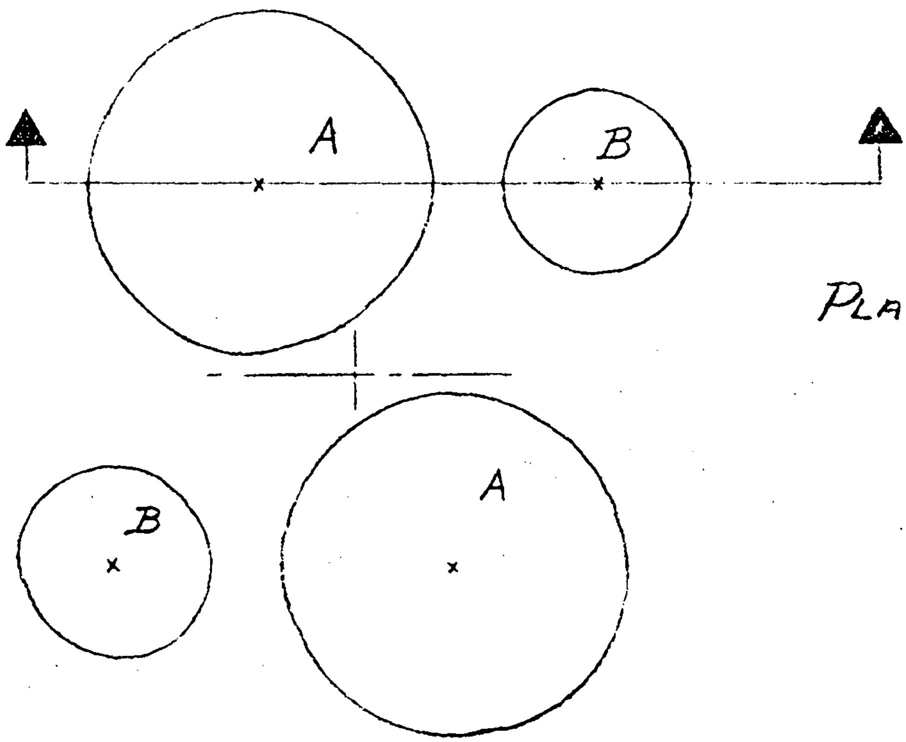

PLAN VIEW

ESCAR - 28
INTERIM REPORT

ON A BOUNDARY CONDITION APPLICABLE TO MAGNETOSTATIC RELAXATION COMPUTATIONS*

L. Jackson Laslett

November 5, 1975

CONTENTS

*Work assisted by the U.S. Energy Research and Development Administration.

ON A BOUNDARY CONDITION
APPLICABLE TO MAGNETOSTATIC RELAXATION COMPUTATIONS*

L. Jackson Laslett

INTRODUCTION

With the exception of methods that solve directly for the magnetization,[1] magnetostatic problems that involve a prescribed current distribution and ferromagnetic material customarily are solved by a relaxation procedure that employs as the working variable a potential function (scalar, vector -- or, selectively, a potential of one type in some regions and a potential of the other type in the remaining regions) from which the field components can be derived. In such cases it commonly is necessary to provide an "exterior" region -- that in principle should extend to infinity -- within which the relaxation evaluations of potential must be performed, although the character of the field in such regions may be of little or no interest.

Such exterior regions frequently (and perhaps usually) are processed on a coarse mesh -- which, although sometimes inconvenient, is both understandable and reasonable. A judgment then must be made whether to apply a Dirichlet or a Neumann type of boundary condition at the outer edge of this exterior region

[1] E.g., programs of the GFUN family, developed at the Rutherford Laboratory of the U.K. Atomic Energy Authority.

* Work assisted by the U.S. Energy Research and Development Administration.

(or possibly a Dirichlet condition along a portion of this edge and a Neumann condition along the remainder). In any case, however, this technique must be recognized as only approximate and as one that introduces into the problem a substantial number of additional mesh points on which the potential function must be processed by iteration of the relaxation algorithm.

It accordingly appears desirable to devise a boundary condition that could be applied on a boundary closely surrounding the region of physical significance and that would correctly describe the fact that no "sources" (current or magnetization) are present outside this boundary. In the following Section we propose a boundary condition of this type, that can be applied to process the values of potential on this boundary, while values in the interior are processed by a standard relaxation algorithm. In a subsequent Section we report briefly on tests that have been performed to check the performance of this proposed procedure in various two-dimensional situations. It will be immediately evident that the proposed procedure has an obvious analogue for application to electrostatic problems in which an exterior region can be taken to be free of charges[2] and of polarized matter.

---

[2] The analogy to the magnetostatic problem will be the most immediate if the total charge in the interior is zero -- since then, so to speak, there is no "charge at infinity" and the types of function admissible for expressing the potential function in the exterior region will be similar in the electrostatic and magnetostatic cases.

DERIVATION OF THE BOUNDARY CONDITION

If U and V are harmonic functions of position ($\nabla^2 U = 0$, $\nabla^2 V = 0$) that tend toward zero sufficiently rapidly as the field point approaches infinity and if $\hat{n}$ denotes an outward-drawn unit normal vector directed into the exterior source-free region from a closed inner boundary to this region,
then by application of Green's theorem one may write

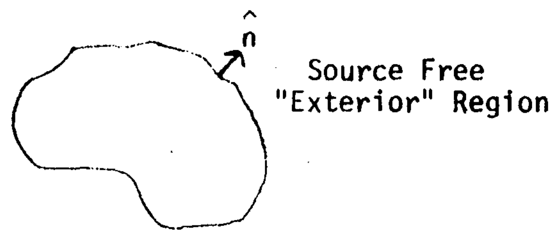

$$\int \left(V \frac{\partial U}{\partial n} - U \frac{\partial V}{\partial n}\right) ds = 0$$

in which the integration is taken over the boundary.

In the work to follow we shall let V represent the potential function (such as the vector potential of a two-dimensional magnetostatic problem), for which $\nabla^2 V = 0$ in the source-free exterior region, and we shall denote this function by A in the remainder of this work.

In the case of a two-dimensional situation in which the inner boundary to the exterior region is taken to be a circle, a natural choice for U would be any of the harmonic functions

$$r^{-m} \cos m\theta \,, \qquad r^{-m} \sin m\theta \qquad \text{(with m positive)},$$

plane polar coordinates being employed. In this case the unit normal is simply $\hat{n} = \hat{e}_r$ and the absence of exterior sources requires that

$$\oint \left(mA + a \frac{\partial A}{\partial r}\right) \cos m\theta \; d\theta = 0$$

and

$$\oint \left(mA + a \frac{\partial A}{\partial r}\right) \sin m\theta \; d\theta = 0$$

for every (positive) m, with a denoting the radius of the boundary circle.

Conditions of similar form can be obtained for two-dimensional situations in which one wishes to employ a different type of boundary curve -- that may more suitably enclose the region of physical interest. Such curves, and functions U, in fact may be conveniently suggested through the use of conformal transformations. Thus the transformation

$$x + iy = c \operatorname{Cosh} (u + iv),$$

For which

$$\left.\begin{aligned} x &= c \operatorname{Cosh} u \cos v \\ y &= c \operatorname{Sinh} u \sin v \end{aligned}\right\},$$

results in the curves of constant u forming a set of (confocal) ellipses, concentric with the origin, whose major semi-axes are c Cosh u (coincident with the x-axis) and c Sinh u (coincident with the y-axis). The variable v is a distorted analogue to the polar coordinate angle θ ($\tan\theta = \operatorname{Tanh} u \tan v$) and numerically covers the same range as θ in transversing successive quadrants. Selection of (harmonic) functions U of the form

$$e^{-mu} \cos mv, \qquad e^{-mu} \sin mv \qquad \text{(with m positive)}$$

then leads to the condition for no external sources to be present to be expressible as

$$\oint (mA + \frac{\partial A}{\partial u}) \cos mv \, dv = 0$$

and

$$\oint (mA + \frac{\partial A}{\partial u}) \sin mv \, dv = 0,$$

for every positive m, with the integration taken along a curve of constant u.

As another example, a quartic boundary curve may be formed through use of the transformation [3]

$$(x + iy)^2 = c^2 \text{ Cosh } (u + iv),$$

leading to curves of constant u that in Cartesian form are given by

$$\left[\frac{x^2 - y^2}{c^2 \text{ Cosh } u}\right]^2 + \left[\frac{2\,xy}{c^2 \text{ Sinh } u}\right]^2 = 1$$

Again with the functions

$$e^{-mu} \cos mv \quad \text{and} \quad e^{-mu} \sin mv$$

chosen for U, one obtains conditions of the same form as written in the preceding paragraph.

---

3 The transformation $(x + iy)^2 = c^2$ Cosh $(u + iv)$ leads to the explicit expressions

$$x = c\sqrt{\frac{\sqrt{\text{Cosh}^2 u - \sin^2 v} + \text{Cosh } u \cos v}{2}}$$

$$y = c\sqrt{\frac{\sqrt{\text{Cosh}^2 u - \sin^2 v} - \text{Cosh } u \cos v}{2}}$$

for the Cartesian coordinates. An <u>octant</u> is covered by $0 < v < \frac{\pi}{2}$, with $x = y$ when $v = \frac{\pi}{2}$.

For three-dimensional problems employing a scalar potential function V in the region near (and external to) a spherical boundary, the suitable set of harmonic functions U would appear to be the spherical-harmonics

$$r^{-(m+1)}\ P_m^{(\ell)}\ (\cos\ \theta)\ \begin{Bmatrix}\cos\\ \sin\end{Bmatrix}\ \ell\phi$$

and the integration would be over the surface of this spherical boundary. In order that the conditions cited to describe the absence of external sources be not only necessary but also sufficient, it would appear that in any of the cases one merely must specify that the functions U constitute a complete set of harmonic functions suitable for describing the potential function in the exterior region. In many applications certain symmetry properties of the problem under consideration will be recognized in formulation of the relaxation procedure and in such cases only functions of U that possess the appropriate symmetry need be explicitly considered.

APPLICATION

The detailed application of the principle stated to relaxation procedures on a finite mesh will, as has been noted, be influenced by the symmetry of the problems, and some specific choices with respect to procedure can result in some simplifications. We may best illustrate these points that arise in practice by considering a means of applying the foregoing principle to a two-dimensional situation in which the vector potential A will have the quadrant symmetry characteristic of a dipole magnet. The area of study in this case thus may be confined to the first quadrant, with A to be maintained at a value zero at all points on the y-axis and the derivative $\partial A/\partial y$ to vanish at all points on the x-axis.

In the situation just mentioned, values of A would be sought by a relaxation process applied on a mesh that should be terminated on a boundary arc, external to the sources and magnetic material present, that is of some convenient form such as a quarter-circle or quarter-ellipse. "Active" mesh points, on which the values of the vector potential will be subject to repeated revision, will be located on this arc. If N such points are present, it would be reasonable to employ only N suitable functions U in formulating the condition that no external sources are present and to construct a suitable finite-difference algorithm to describe the integral required for each of these functions. The values of $\partial U/\partial n$ that are required to construct the integrands similarly would be obtained from some finite difference algorithm that employs points on one or more nested arcs (also external to all sources) immediately inside the boundary, and it clearly would be convenient for such arcs to be related in a simple geometrical manner to the outer boundary arc -- thus, in the first examples cited, the arcs to be employed might constitute portions of concentric circles or of confocal ellipses with a separation Δr or Δu equal to a constant h. It seems indeed highly approporiate to employ just two such nested arcs and to perform the integration along a similar arc midway between them.

The integration algorithm and some of the subsequent work will be materially simplified if the points on the outer arc (and the points at which values of the integrand are estimated) are regularly spaced -- specifically, in these examples, taking θ or v as given by $(2k - 1) \frac{\pi}{4N}$, with $k = 1,2,...N$. Because of the quadrant symmetry assumed for the present discussion, appropriate forms for the function U would be

$$r^{-(2m-1)} \cos (2m-1)\theta \quad \text{or}$$

$$e^{-(2m-1)u} \cos (2m-1)v,$$

with $m = 1,2,...N$. The conditions to be applied then may be written

$$\sum_{k=1}^{N} \left[(2m-1)A + r \frac{\partial A}{\partial r} \right]_{\substack{r=a-h/2 \\ \theta=(2k-1)\frac{\pi}{4N}}} \cos \left((2m-1)(2k-1) \frac{\pi}{4N}\right) = 0$$

or

$$\sum_{k=1}^{N} \left[(2m-1)A + \frac{\partial A}{\partial u} \right]_{\substack{u=u_1 - h/2 \\ v= (2k-1) \frac{\pi}{2N}}} \cos \left((2m-1)(2k-1) \frac{\pi}{4N}\right) = 0$$

for the respective cases.

Both the function and the derivative can be estimated on the midway arc ($r = a - h/2$ or $u = u_1 - h/2$) by use of values of A on the two nested arcs mentioned earlier. Thus, if there are N such points on each of these arcs (disposed in the regular manner suggested above), one can simply write

$$A = \frac{A^{(b)} + A^{(i)}}{2}$$

and, for the derivative,

$$\frac{\partial A}{\partial r} = \frac{A^{(b)} - A^{(i)}}{h} \quad \text{or} \quad \frac{\partial A}{\partial u} = \frac{A^{(b)} - A^{(i)}}{h}$$

-- where the superscripts $^{(b)}$ and $^{(i)}$ refer respectively to the outer (boundary) arc and to the neighboring nested arc inside it. The conditions to be applied then become:

$$\sum_{k=1}^{N} \{[\tfrac{a}{h} + (m-1)]A_k^{(b)} - [\tfrac{a}{h} - m]A_k^{(i)}\} \cos\left((2m-1)(2k-1)\frac{\pi}{4N}\right) = 0$$

or

$$\sum_{k=1}^{N} \{[\tfrac{1}{h} + (m - \tfrac{1}{2})]A_k^{(b)} - [\tfrac{1}{h} - (m - \tfrac{1}{2})]\, A_k^{(i)}\} \cos\left((2m-1)(2k-1)\frac{\pi}{4N}\right) = 0$$

for the respective cases.

The equations just written can be solved for the $A_k^{(b)}$, with the result

$$A_k^{(b)} = \sum_{\ell=1}^{N} \left[\frac{2}{N} \sum_{m=1}^{N} \frac{\frac{a}{h} - m}{\frac{a}{h} + (m-1)} \cos\left((2m-1)(2k-1)\frac{\pi}{4N}\right)\cos\left((2m-1)(2\ell-1)\frac{\pi}{4N}\right)\right] A_\ell^{(i)}$$

(for circular arcs),

or

$$A_k^{(b)} = \sum_{\ell=1}^{N} \left[\frac{2}{N} \sum_{m=1}^{N} \frac{\frac{1}{h} - (m - \frac{1}{2})}{\frac{1}{h} + (m - \frac{1}{2})} \cos \left\{(2m-1)(2k-1) \frac{\pi}{4N}\right\} \cos \left\{(2m-1)(2\ell-1) \frac{\pi}{4N}\right\} \right] A_\ell^{(i)}$$

(for elliptical arcs).

Introducing a matrix $\mathcal{E}$, evaluated at the start of a run, with elements

$$\mathcal{E}_{k,\ell} = \frac{2}{N} \sum_{m=1}^{N} \frac{\frac{a}{h} - m}{\frac{a}{h} + (m-1)} \cos \left\{(2m-1)(2k-1) \frac{\pi}{4N}\right\} \cos \left\{(2m-1)(2\ell-1) \frac{\pi}{4N}\right\}$$

or

$$\mathcal{E}_{k,\ell} = \frac{2}{N} \sum_{m=1}^{N} \frac{\frac{1}{h} - (m - \frac{1}{2})}{\frac{1}{h} + (m - \frac{1}{2})} \cos \left\{(2m-1)(2k-1) \frac{\pi}{4N}\right\} \cos \left\{(2m-1)(2\ell-1)) \frac{\pi}{4N}\right\} ,$$

then the result for the $A_k^{(b)}$ is very simply expressed as

$$A_k^{(b)} = \sum_{\ell=1}^{N} \mathcal{E}_{k,\ell} A_\ell^{(i)} .$$

The result last given can be used (possibly with an under-relaxation or over-relaxation factor) to revise from time to time the values of the vector potential on the outer (boundary) arc. The conventional relaxation procedure will be used to process values at the remaining (interior) points, and in the course of this process sometimes will make use of the values residing at the points on the boundary.

Modification for a TRIM-type mesh: In constructing a triangular mesh, of the type used in TRIM[4] and similar programs, it apparently is convenient to employ only N-2 mesh points on the inner arc immediately adjacent to the outer (boundary) arc if N points are present on the latter. As we indicate below for circular arcs, in the case with quadrupole symmetry with points at $\theta = \theta_k = (2k-1)\frac{\pi}{4N}$ on the outer arc, this special feature is found to introduce no serious computations.

Again we may apply the condition expressing the absence of all external sources on an arc of radius $a - \frac{h}{2}$ and express the integral condition as a sum over values of A and its radial derivative at points for which $\theta = \theta_k$. A trigonometric development of the vector potential $A^{(i)}$ on the arc $r = a-h$ can be conveniently written in terms of values $A_\ell^{(i)}$ at $\theta = \theta_\ell = (2\ell-1)\frac{\pi}{4(N-2)}$, with $\ell = 1, 2, \ldots N-2$:

$$A^{(i)} = \frac{2}{N-2}\sum_{s=1}^{N-2}\sum_{\ell=1}^{N-2} A_\ell^{(i)} \cos\left((2s-1)(2\ell-1)\frac{\pi}{4(N-2)}\right)\cos\left((2s-1)\theta\right).$$

At polar angles identical to the θ_k, then, one may make use of the interpolated values

$$A_{\theta_k}^{(i)} = \frac{2}{N-2}\sum_{s=1}^{N-2}\sum_{\ell=1}^{N-2} A_\ell^{(i)} \cos\left((2s-1)(2\ell-1)\frac{\pi}{4(N-2)}\right)\cos\left((2s-1)(2k-1)\frac{\pi}{4N}\right).$$

In these terms, the condition

---

4 See John S. Colonias, "Particle Accelerator Design: Computer Programs", Academic press, New York, 1974; or see the original paper A.M. Winslow, "Numerical Solution of the Quasilinear Poisson Equation in a Non-uniform Triangular Mesh", J. Comput. Phys. 1, 149 172 (1966).

$$\sum_{k=1}^{N}\left[(2m-1)A+r\frac{\partial A}{\partial r}\right]_{\substack{r=a-\frac{h}{2}\\ \theta=(2k-1)\frac{\pi}{4N}}} \cos\left((2m-1)(2k-1)\frac{\pi}{4N}\right)=0 \qquad (m=1,2,\dots)$$

becomes

$$\sum_{k=1}^{N}\left\{(2m-1)\left[\frac{A_k^{(b)}}{2}+\frac{1}{N-2}\sum_{s=1}^{N-2}\sum_{\ell=1}^{N-2}A_\ell^{(i)}\cos\left((2s-1)(2\ell-1)\frac{\pi}{4(N-2)}\right)\cos\left((2s-1)(2k-1)\frac{\pi}{4N}\right)\right]\right.$$

$$\left.+\left(\frac{a}{h}-\frac{1}{2}\right)\left[A_k^{(b)}-\frac{2}{N-2}\sum_{s=1}^{N-2}\sum_{\ell=1}^{N-2}A_\ell^{(i)}\cos\left((2s-1)(2\ell-1)\frac{\pi}{4(N-2)}\right)\cos\left((2s-1)(2k-1)\frac{\pi}{4N}\right)\right]\right\}$$

$$\times\cos\left((2m-1)(2k-1)\frac{\pi}{4N}\right)=0,$$

or

$$\sum_{k=1}^{N}\left[\frac{a}{h}+(m-1)\right]A_k^{(b)}\cos\left((2m-1)(2k-1)\frac{\pi}{4N}\right)$$

$$=\sum_{k=1}^{N}\left[\frac{a}{h}-m\right]\frac{2}{N-2}\sum_{s=1}^{N-2}\sum_{\ell=1}^{N-2}A_\ell^{(i)}\cos\left((2s-1)(2\ell-1)\frac{\pi}{4(N-2)}\right)\cos\left((2s-1)(2k-1)\frac{\pi}{4N}\right)$$

$$\times\cos\left((2m-1)(2k-1)\frac{\pi}{4N}\right).$$

The summation over k may be explicitly performed in the expression on the right-hand side of this last equation, with the result:

$$\sum_{k=1}^{N}\left[\frac{a}{h}+(m-1)\right]A_k^{(b)}\cos\left((2m-1)(2k-1)\frac{\pi}{4N}\right)$$

$$=\frac{N}{N-2}\sum_{\ell=1}^{N-2}\left(\frac{a}{h}-m\right)A_\ell^{(i)}\cos\left((2m-1)(2\ell-1)\frac{\pi}{4(N-2)}\right),\text{ or zero if } m>N-2.$$

Finally, as a solution to this last equation, we write

$$A_k^{(b)} = \sum_{\ell=1}^{N-2} \left[\frac{2}{N-2} \sum_{m=1}^{N-2} \frac{\frac{a}{h} - m}{\frac{a}{h} + (m-1)} \cos\left((2m-1)(2k-1)\frac{\pi}{4N}\right) \cos\left((2m-1)(2\ell-1)\frac{\pi}{4(N-2)}\right)\right] A_\ell^{(i)}$$

--*i.e.*,

$$A_k^{(b)} = \sum_{\ell=1}^{N-2} \mathcal{E}_{k,\ell} \, A_\ell^{(i)} \, ,$$

where

$$\mathcal{E}_{k,\ell} = \frac{2}{N-2} \sum_{m=1}^{N-2} \frac{\frac{a}{h} - m}{\frac{a}{h} + (m-1)} \cos((2m-1)(2k-1)\frac{\pi}{4N}) \cos((2m-1)(2\ell-1)\frac{\pi}{4(N-2)}).$$

[This result is seen to be closely similar to that obtained earlier for the case of nested arcs containing an equal number of mesh points.]

Likewise, for revision of values of vector potential that may be required at $r=a$, $\theta=0$,[5] one may employ

$$A_{\theta=0}^{(b)} = \sum_{\ell=1}^{N} \mathcal{E}_{(o),\ell} \, A_\ell^{(i)} \, ,$$

[5] On a triangular mesh with $\partial A/\partial n = 0$ at $\theta = 0$, values of A at $r = a$, $\theta = 0$ may be required for relaxation of the potential values at a smaller radius (e.g., at $r = a - h$). The relation proposed in the text for $A_{\theta=0}^{(b)}$ constitutes, in effect, the extension to $\theta = 0$ ($k = 1/2$) of the trigonometric expression given for the $A_k^{(b)}$ ($k = 1, 2, \ldots N$).

where

$$\mathcal{E}_{(o),\ell} = \frac{2}{N-2} \sum_{m=1}^{N-2} \frac{\frac{a}{h} - m}{\frac{a}{h} + (m-1)} \cos((2m-1)(2\ell - 1) \frac{\pi}{4(N-2)}).$$

Results analogous to those just cited are clearly derivable for relaxation of a problem with quadrant symmetry on a triangular mesh with elliptical boundary arcs -- namely, with $A^{(b)}$ and $A^{(i)}$ respectively at $u = u_1$ or $u_1 - h$ and at $v = (2k-1)\frac{\pi}{4N}$ $(k = 1,2,N)$ or $(2\ell - 1)\frac{\pi}{4(N-2)}$ $(\ell = 1, 2, \ldots N-2)$,

$$A_k^{(b)} = \sum_{\ell=1}^{N-2} \mathcal{E}_{k,\ell} A_\ell^{(i)}$$

with

$$\mathcal{E}_{k,\ell} = \frac{2}{N-2} \sum_{m=1}^{N-2} \frac{\frac{1}{h} - (m-1/2)}{\frac{1}{h} + (m-1/2)} \cos((2m-1)(2k-1) \frac{\pi}{4N}) \cos(2m-1)(2\ell-1) \frac{\pi}{4(N-2)}$$

and

$$A_{v=0}^{(b)} = \sum_{\ell=1}^{N-2} \mathcal{E}_{(o),\ell} A_\ell^{(i)}$$

with

$$\mathcal{E}_{(o),\ell} = \frac{2}{N-2} \sum_{m=1}^{N-2} \frac{\frac{1}{h} - (m-1/2)}{\frac{1}{h} + (m-1/2)} \cos((2m-1)(2\ell-1) \frac{\pi}{4(N-2)}).$$

Cases with Half-Plane Symmetry

In a number of cases of practical interest (e.g., in the design of a combined-function magnet that serves both to bend and to focus or defocus particle trajectories) a half-plane symmetry may be present that can be exploited to advantage. Typically, if a vector potential is employed in such cases, the vector potential for a two-dimensional problem will be even about a line that we may take to be the x-axis ($\theta = 0,\pi$), and $\partial A/\partial n$ will be zero at all points on this line. To obtain a mathematically well-posed problem, whose solution is to be sought by relaxation methods, it will be desirable in such cases also to specify the value of the potential itself at some point of the relaxation mesh.

Given a circular or elliptical arc outside of which no sources are present, one then can assert under the circumstances just mentioned, that [6]

$$\int_0^\pi \left[(m-1)A + r\frac{\partial A}{\partial r}\right] \cos (m-1)\theta \, d\theta = 0$$

$$\text{or} \quad \int_0^\pi \left[(m-1)A + \frac{\partial A}{\partial u}\right] \cos (m-1)v \, dv = 0$$

on such an arc, for all $m \geqslant 1$.

---

6 It will be recognized that we have here adopted for the functions U (first introduced in our application of Green's theorem) functions of appropriate symmetry of the form

$$c_0, \ \frac{c_1}{r}\cos\theta, \ \frac{c_2}{r^2}\cos 2\theta, \ \ldots$$

$$\text{or} \qquad c_0, \ c_1 e^{-u}\cos v, \ c_2 e^{-2u}\cos 2v, \ \ldots$$

that would be appropriate for development of the potential in the exterior region, while excluding such functions as

$$\ell n\ r,\ r\cos\theta\ ,\ r^2\cos 2\theta,\ \ldots$$

or

$$u,\ e^u\cos v,\ e^{2u}\cos 2v,\ \ldots\ .$$

With N points on an outer arc and M (e.g., N-2) points on an adjacent inner arc, at

$$\theta = (2k-1)\frac{\pi}{2N}\quad (k = 1,2,\ldots N)\ \text{and}\ (2\ell-1)\frac{\pi}{2M}\quad (\ell = 1,2,\ldots M)$$

or

$$v = (2k-1)\frac{\pi}{2N}\ (k = 1,2,\ldots N)\ \text{and}\ (2\ell-1)\frac{\pi}{2M}\quad (\ell = 1,2,\ldots M)$$

for a half circle or half ellipse, we accordingly write

$$\left.\sum_{k=1}^{N}\left[(m-1)A + r\frac{\partial A}{\partial r}\right]\cos\left((m-1)\ (2k-1)\ \frac{\pi}{2N}\right)\right|_{\substack{r = a - \frac{h}{2} \\ \theta = (2k-1)\frac{\pi}{2N}}} = 0$$

or

$$\left.\sum_{k=1}^{N}\left[(m-1)A + \frac{\partial A}{\partial r}\right]\cos\left((m-1)(2k-1)\ \frac{\pi}{2N}\right)\right|_{\substack{u = u_1 - \frac{h}{2} \\ v = (2k-1)\frac{\pi}{2N}}} = 0$$

for m = 1, 2, ...

Then, by algebraic work entirely similar to that indicated previously, we obtain

$$A_k^{(b)} = \sum_{\ell=1}^{M}\mathcal{E}_{k,\ell}\ A_\ell^{(i)},$$

where

$$\mathcal{E}_{k,\ell} = \frac{2}{M}\sum_{m=1}^{M} f_m\ \frac{2\frac{a}{h} - m}{2\frac{a}{h} + (m-2)}\cos\left((m-1)(2k-1)\ \frac{\pi}{2N}\right)\cos\left((m-1)(2\ell-1)\ \frac{\pi}{2M}\right)$$

or

$$\mathcal{E}_{k,\ell} = \frac{2}{M} \sum_{m=1}^{M} f_m \frac{\frac{2}{h} - (m-1)}{\frac{2}{h} + (m-2)} \cos\left((m-1)(2k-1)\frac{\pi}{2N}\right) \cos\left((2m-1)(2\ell-1)\frac{\pi}{2M}\right),$$

where $f_m = 0.5$ for $m=1$ and $f_m = 1.0$ for $m>1$.

Values of $A^{(b)}$ at $\theta=0$ and $\theta=\pi$ could be obtained, if required, by respectively setting $k = 1/2$ or $k = N+1/2$ into these formulas.

Absence of Symmetry

In a two-dimensional problem in which no symmetry is present to be exploited, it would be appropriate to employ both cosine and sine functions in expressing the condition that no external sources are present beyond the boundary curves. We might employ $p = 2N$ points on the outermost curve and Q (taken to be even) points on an adjacent inner curve, taking (for a circular or elliptical boundary, respectively) mesh points with coordinates

$$r = a,\ \theta_k = (2k-1)\pi/p;\ r = a-h,\ \theta_\ell = (2\ell-1)\pi/Q$$

or

$$u = u_1,\ v_k = (2k-1)\pi/p;\ u = u_1 - h,\ v_\ell = (2\ell-1)\pi/Q.$$

The condition of no external sources would then be expressed, in these respective cases, as

$$\sum_{k=1}^{p} \left[(m-1)A + r\frac{\partial A}{\partial r}\right]_{\substack{r = a-h/2 \\ \theta = \theta_k}} \cos (m-1)\theta_k = 0$$

$$\text{and} \quad \sum_{m=1}^{p} \left[mA + r\frac{\partial A}{\partial r}\right]_{\substack{r = a-h/2 \\ \theta = \theta_k}} \sin m\theta_k = 0\ ;$$

or

$$\sum_{k=1}^{p} \left[(m-1)A + \frac{\partial A}{\partial u}\right]_{\substack{u = u_1 - h/2 \\ v = v_k}} \cos (m-1)\, v_k = 0$$

$$\text{and} \quad \sum_{m=1}^{p} \left[mA + \frac{\partial A}{\partial u} \right] \sin m\, v_k = 0 \qquad \begin{array}{l} u = u_1 - h/2 \\ v = v_k \end{array}$$

for positive values of m.

As in the case of half-plane symmetry discussed previously, one again should also specify the value of the potential itself at some point of the relaxation mesh.

These specifications then lead (after some algebraic work of a character similar to that indicated previously) to a result of the form

$$A_k^{(b)} = \sum_{\ell=1}^{Q} \mathcal{E}_{k,\ell}\, A_\ell^{(i)}$$

where

$$\mathcal{E}_{k,\ell} = \frac{1}{Q/2} \sum_{m=1}^{Q/2} \left[g_m \frac{T_m^{(c)}}{B_m^{(c)}} \cos\left((m-1)(2k-1)\frac{\pi}{p}\right) \cos\left((m-1)(2\ell-1)\frac{\pi}{Q}\right) + \frac{T_m^{(s)}}{B_m^{(s)}} \sin\left(m(2k-1)\frac{\pi}{p}\right) \sin\left(m(2\ell-1)\frac{\pi}{Q}\right) \right]$$

with $g_m = 0.5$ for m=1, $g_m = 1.0$ for m>1,

and, for a circular boundary

$$T_m^{(c)} = 2\frac{a}{h} - m \qquad B_m^{(c)} = 2\frac{a}{h} + (m-2)$$

$$T_m^{(s)} = 2\frac{a}{h} - (m+1) \qquad B_m^{(s)} = 2\frac{a}{h} + (m-1)\ ,$$

while for an elliptical boundary

$$T_m^{(c)} = \frac{2}{h} - (m-1) \qquad B_m^{(c)} = \frac{2}{h} + (m-1)$$

$$T_m^{(s)} = \frac{2}{h} - m \qquad B_m^{(s)} = \frac{2}{h} + m\ .$$

Tests

Several computational tests have been made of the principles discussed above, both with small special interactive programs executed through the LBL SESAME system and also by modification of the TRIM program for the CDC7600 computer. The interactive programs all employed a two-dimensional polar-coordinate mesh with the same number of mesh points per angular interval at every radius, while TRIM employed the customary triangular mesh with the number of mesh points at the periphery decreasing by 2 as one moves inward from one arc to the next. In all the interactive runs and in some of the TRIM runs the results obtained could be compared with known analytic results in order to verify that a good approximation was being obtained to the true solution.[7] The tests with TRIM, which are continuing, so far have been confined to cases of quadrant symmetry.

The early tests employed values of vector potential on three, rather than two, nested arcs (because of the choice of algorithm for estimating $\partial A/\partial n$), but subsequently some of the work was repeated so as to involve values on only two such arcs in the manner outlined earlier in this report. In all cases convergent solutions appeared to represent good approximations to the correct solution of the problem under consideration. The use of potential values on two, rather than three, nested arcs appeared to lead to results of even somewhat better accuracy and clearly represents a certain simplification.

The cases for which interactive computational trials were made were of the following types:

Quadrant symmetry, with circular boundary arcs,

Half-Plane symmetry, with eliptical boundary arcs.

Some attention was devoted to examining empirically, for these cases, the

---

[7] None of the interactive computations involved the presence of magnetic material.

advantages, with respect to rate of convergence, of over-relaxation.[8] It appeared that (as expected) over-relaxation was distinctly helpful when applied to the conventional relaxation procedure for the potential in the interior, but that then it was desirable to confine the over-relaxation parameter used for adjustment to the boundary values $A^{(b)}$ to moderate values (for example, to 1.5, or possibly less). A satisfactory procedure that may warrant adoption accordingly is one in which a common value is employed for the over-relaxation parameter used in each of these operations, but the boundary values are revised only on every other passage through the mesh.

As with any relaxation procedure, it is a delicate question how best to adjust the over-relaxation parameter, and further examination should be given to the suitability of the automatic adjustment procedure (now frequently employed with TRIM) when the boundary values are processed in the manner suggested in this note.

---

[8] In all the work, relaxation was of the Liebmann type, wherein new values are stored (over-writing old values) immediately, and are subsequently used whenever required. By an over-relaxation parameter (α) we mean the following:

$$\text{New Value} = \alpha \cdot (\text{Recommended Value}) + (1-\alpha)\cdot(\text{Old Value}).$$

Over-relaxation then consists in the use of values of this parameter that are greater than unity. [In some runs, after the relaxation had been considered to have progressed sufficiently far toward convergence, a few additional relaxation sweeps through the mesh would be made with the over-relaxation parameters set to unity.]

Acknowledgements

It is a pleasure to acknowledge the interest and encouragement of John C. Colonias and V. O. Brady in this work, and to record the invaluable assistance of Mr. Brady in adapting the TRIM program to permit making the tests that have been performed and are being continued. Initiation of the work was stimulated by magnet design problems that arose in connection with the ESCAR project at LBL, and appreciation is expressed to T. Elioff and G. R. Lambertson for their support.

CAPTIONS FOR FIGURES

Fig. 1 - Typical TRIM mesh for studying one quadrant of a proposed ESCAR dipole magnet. Note the extensive air region external to the iron.

Fig. 2 - TRIM mesh for the example of Fig. 1, after introduction of circular boundary arcs (external to the iron) whereon one applies the boundary conditions presented in the text.

Fig. 3 - An example employing a "window-frame" current distribution, with quadrant symmetry, with no magnetic material present -- so that the correct vector potential can be calculated analytically for test purposes. Circular boundary arcs, closely surrounding this current distribution, are shown whereon one applies the boundary conditions presented in the text. In this example the inner half-width and half-height of the window frame were each taken to be 31.0 units and the external half-width and half-height to be 41.0 units.

Fig. 4 - Detail of the warm-iron dipole-magnet design used to obtain the data recorded in Table II.

4532 29 SCARGOS V.BRADY
.453229 29 JAN 75 11.14
PLOT 29 JAN 75 12.01
.453229 11.15 11.14 29 JAN 75

FIGURE 1

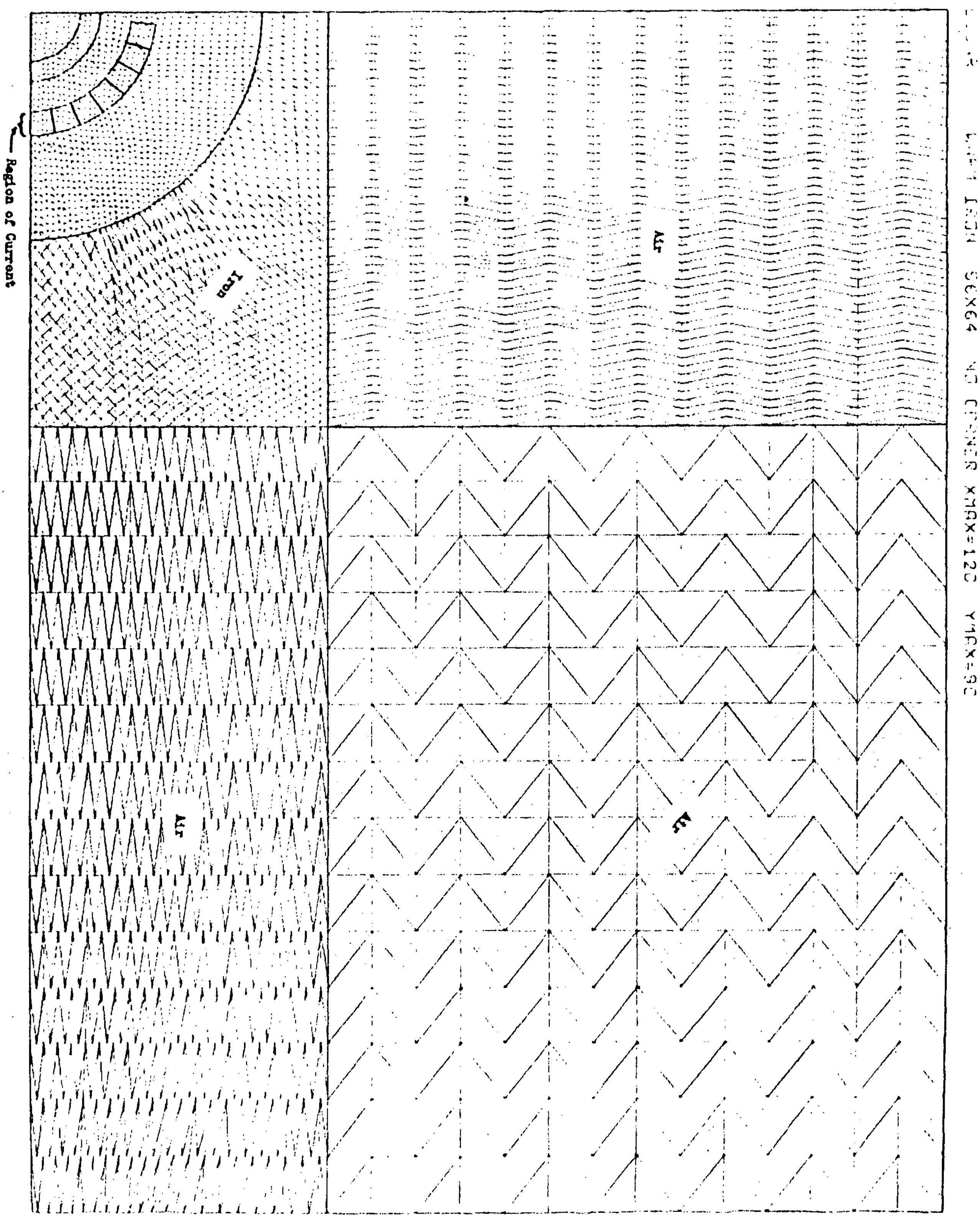

Figure 2

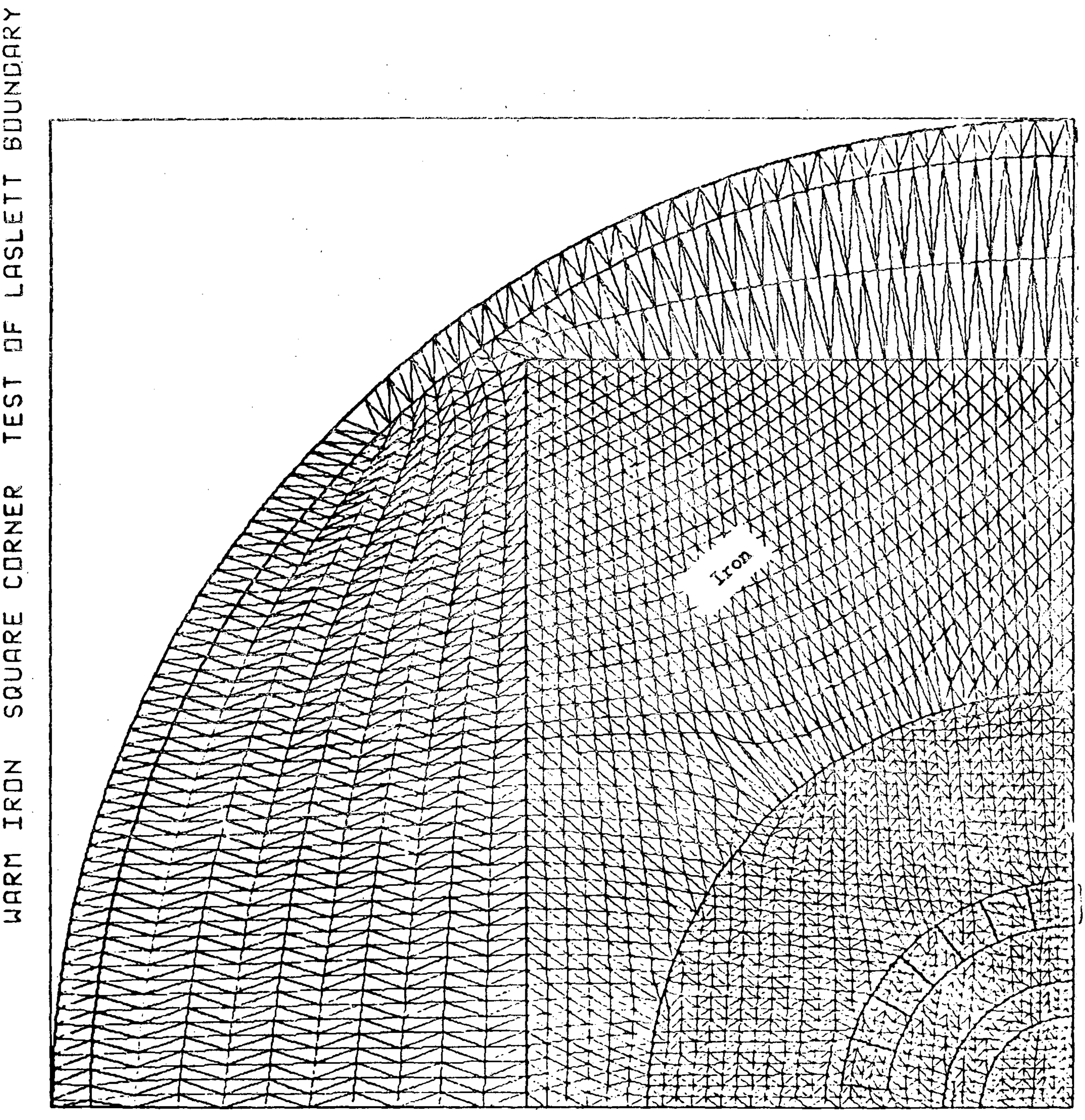

Figure 3

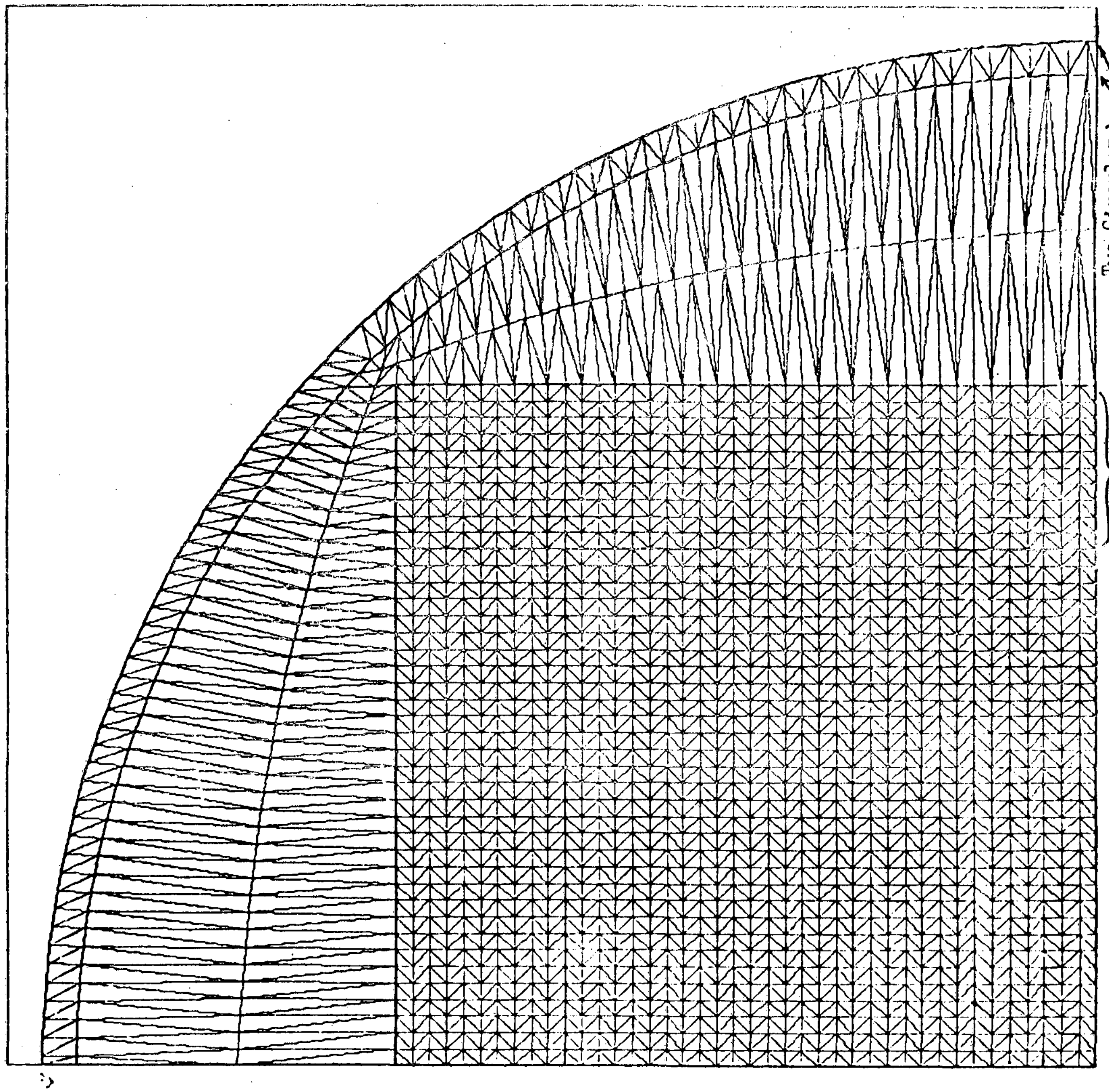

TEST OF LASLETT BOUNDARY WITH WINDOW FRAME CURRENT REGION.

Figure 4

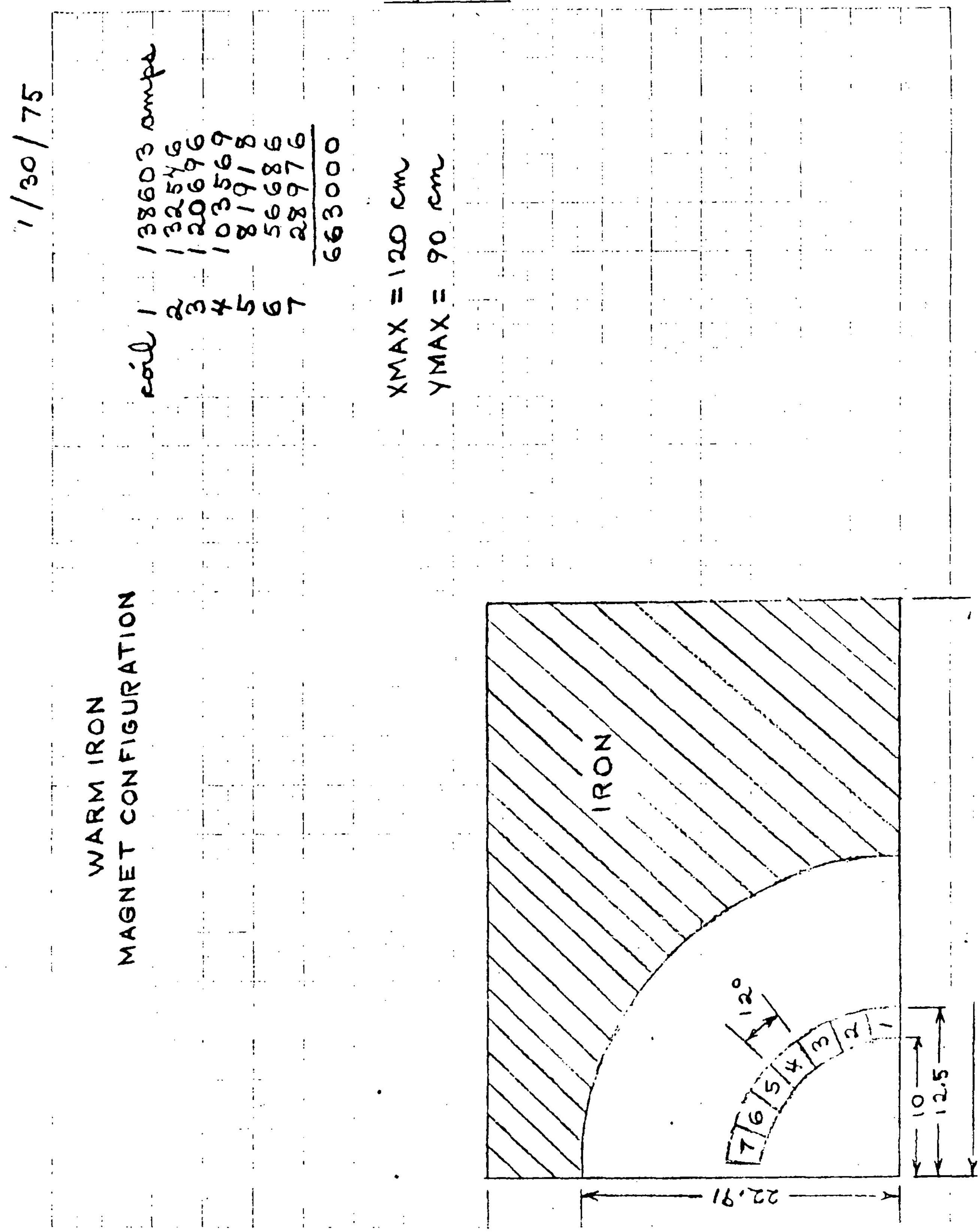
1/30/75
coil 1 138603 amps
2 132546
3 120696
4 103569
5 81918
6 56686
7 28976
663000
XMAX = 120 cm
YMAX = 90 cm
WARM IRON
MAGNET CONFIGURATION
IRON
12°
1
2
3
4
5
6
7
10
12.5
22.91

TABLE I --

Comparison of Numerical and Analytic Results for the Problem illustrated in Fig. 3

x	y	A, by relaxation	A, analytic
10.	0.	249.7	250.2
20.	0.	493.1	493.9
30.	0.	730.6	731.6
61.98276	0.	625.9	626.9
61.25426	9.47511	625.1	626.1
58.91443	19.26013	622.2	622.9
53.95623	30.50553	612.6	613.1
43.82843	43.82843	561.7	562.1
30.50553	53.95623	405.0	404.1
19.26013	58.91443	257.3	256.1
9.47511	61.25426	127.2	126.1
5.	5.	125.9	126.1
20.	20.	511.8	513.2
25.	25.	631.5	633.2
30.	30.	727.3	729.1

TABLE II --

Comparison of Values for Vector Potential

Obtained with conventional TRIM and modified TRIM for the dipole magnet of Figure 4.

x	y	Conventional TRIM*	Modified TRIM
10	0.	456684	456756
22.91	0.	401632	401841
41.52	0.	7113	8290
41.52	6.478	6381	7574
41.52	29.51	2515	3484
30.504	29.51	2631.5	3254.3
20.336	29.51	3920	4360
10.168	29.51	3097	3332
0.847	29.51	218	229

* A = 0 on outer boundary.

3

Electromagnetism – Image Forces in Presence of Boundaries, etc.

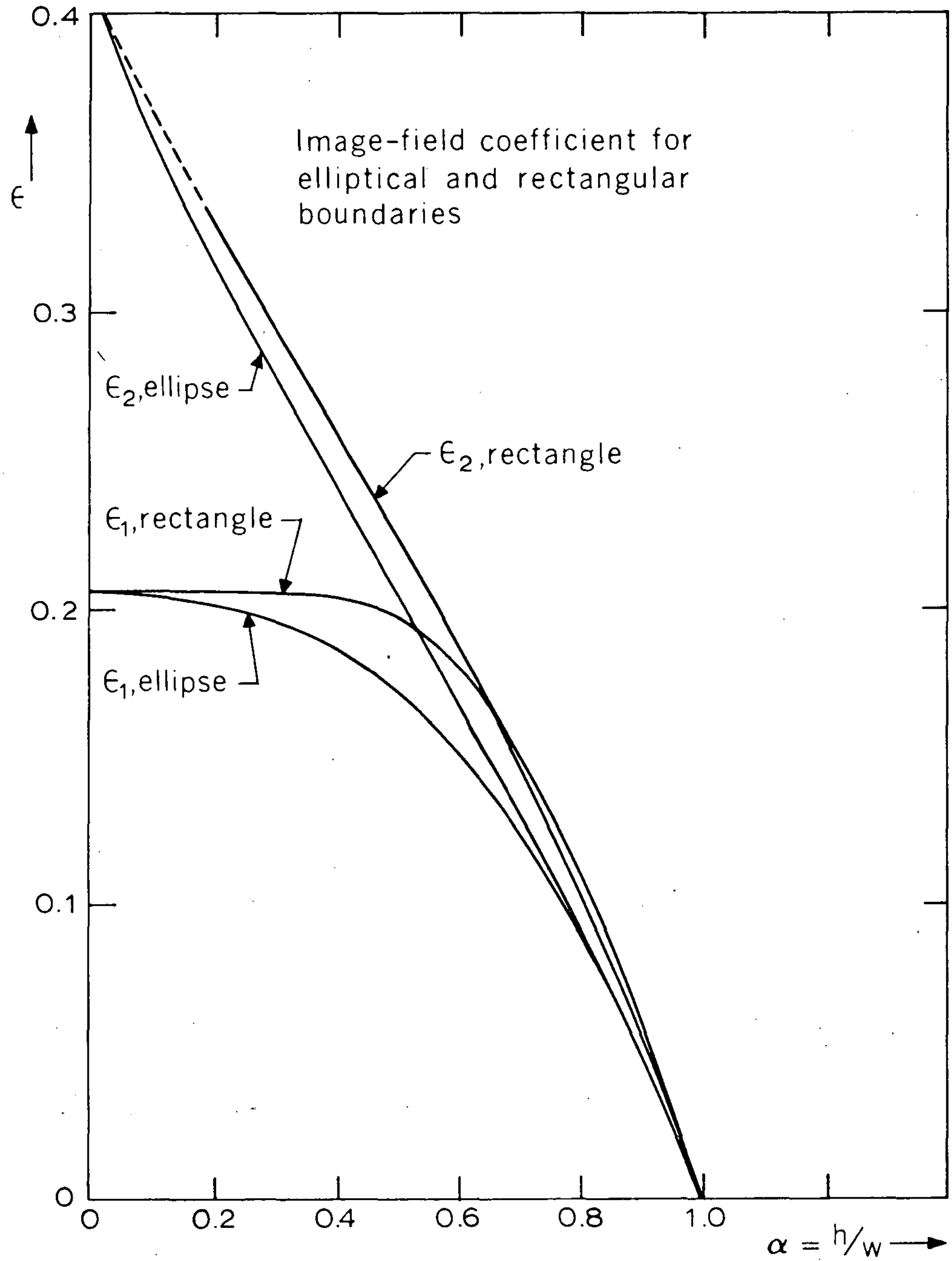
Image-field coefficient for
elliptical and rectangular
boundaries
ϵ
0.4
0.3
0.2
0.1
0
ϵ_2,ellipse
ϵ_2,rectangle
ϵ_1,rectangle
ϵ_1,ellipse
0
0.2
0.4
0.6
0.8
1.0
$\alpha = h/w$

Reprinted from AMERICAN JOURNAL OF PHYSICS, Vol. 26, No. 6, 402–403, September, 1958
Printed in U. S. A.

Field of a Linear Electrostatic Multipole

L. JACKSON LASLETT
Department of Physics and Institute for Atomic Research, Iowa State College, Ames, Iowa

ARFKEN[1] has recently emphasized the desirability of bringing the multipole concept emphatically to the attention of physics students. A specific examination of certain features of the field from a linear multipole may be of value, both in lending definiteness to the multipole picture and in affording an illustration of useful analytic techniques.

The generation of multipole potentials by *differentiation*[2] is a method of general utility. Thus, in terms of polar coordinates (r,θ), the electrostatic potential of a linear 2^n-pole is immediately seen[1,2] to be proportional to

$$(\partial^n/\partial z^n)(1/r)=(-1)^n n!P_n(\mu)/r^{n+1},$$

where $P_n(\mu)$ is the Legendre polynominal of order n and argument $\mu=\cos\theta$. The field-components accordingly are in the ratio

$$E_r:E_\theta=(n+1)P_n:\sin\theta P_n', \qquad (1)$$

and the equation describing the lines of force is determined by the condition

$$dr:rd\theta=E_r:E_\theta. \qquad (2)$$

With the field-components (1), the differential Eq. (2) may be integrated easily to obtain the explicit equation for a line of force

$$\int\frac{dr}{r}+\int\frac{(n+1)P_n}{(1-\mu^2)P_n'}d\mu=\text{const.}$$

$$\ln r-(1/n)\ln[(1-\mu^2)P_n']=\text{const.}$$

$$r^n=C\sin^2\theta P_n'(\cos\theta), \qquad (3)$$

the second integral being evaluated by subtituting for P_n the expression

$$P_n=[2\mu P_n'-(1-\mu^2)P_n'']/[n(n+1)] \qquad (4)$$

obtained from Legendre's equation.

A direct derivation of the foregoing equation for a line of force may be obtained alternatively by application of Gauss's law in a manner indicated by Smythe. For an array of collinear charges q_i arranged along the polar axis, Smythe[3] shows that the lines of force are described by the equation

$$\Sigma q_i\cos\theta_i=\text{const.} \qquad (5)$$

For a linear 2^n-pole of infinitesimal spatial extent the lines of force would then be given by

$$(\partial^n/\partial z^n)\cos\theta=\text{const.}$$
$$(\partial^n/\partial z^n)(z/r)=\text{const.}$$
$$n(\partial^{n-1}/\partial z^{n-1})(1/r)+z(\partial^n/\partial z^n)(1/r)=\text{const.}$$
$$(-1)^{n-1}(n!/r^n)P_{n-1}+(-1)^n(n!z/r^{n+1})P_n=\text{const.}$$
$$(1/r^n)[P_{n-1}-\mu P_n]=\text{const.}$$
$$(1-\mu^2)P_n'/r^n=\text{const.},[4]$$

or

$$r^n=C\sin^2\theta P_n'(\cos\theta)$$

as before [Eq. (3)]. Figure 1 illustrates the direction of lines of force from linear dipoles, quadrupoles, and octupoles.

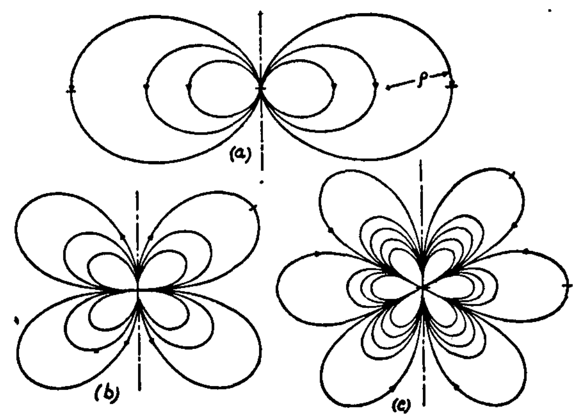

FIG. 1. Direction of lines of force from linear multipoles: (a) dipole, (b) quadrupole, (c) octupole.

It may be worthwhile to point out, however, that certain characteristics of the lines of force can be found without use of the equations for these curves in their integrated form. Thus, from Eqs. (1) and (2), the line of force will be perpendicular to the radius vector at polar angles for which

$$P_n(\cos\theta)=0. \qquad (6)$$

The radius-of-curvature ρ of the line of force can be found by differentiation of the unit-tangent with respect to arc-length. In particular, at a point such that the line of force is perpendicular to the radius vector

$$(1/\rho)\hat{\mathbf{e}}_n \equiv d\hat{\mathbf{e}}_t/ds = (1/r)d\hat{\mathbf{e}}_t/d\theta, \tag{7}$$

where $\hat{\mathbf{e}}_t$ and $\hat{\mathbf{e}}_n$ denote unit vectors which *at every point* are, respectively, tangent and normal to the curve. The unit-tangent may be expressed in terms of the field-components, E_r and E_θ, and the associated unit vectors, $\hat{\mathbf{e}}_r$ and $\hat{\mathbf{e}}_\theta$, taken, respectively, in the directions of increasing r and θ:

$$\hat{\mathbf{e}}_t = [E_r\hat{\mathbf{e}}_r + E_\theta\hat{\mathbf{e}}_\theta]/[E_r^2+E_\theta^2]^{\frac{1}{2}} = [(n+1)P_n\hat{\mathbf{e}}_r + \sin\theta P_n'\hat{\mathbf{e}}_\theta]/[(n+1)^2(P_n)^2 + \sin^2\theta(P_n')^2]^{\frac{1}{2}}. \tag{8}$$

The differentiation indicated by Eq. (7) is performed by the use of Eq. (8), noting that $d\hat{\mathbf{e}}_r/d\theta = \hat{\mathbf{e}}_\theta$ and $d\hat{\mathbf{e}}_\theta/d\theta = -\hat{\mathbf{e}}_r$. Following the differentiation one makes use of Eq. (6) to obtain the simple result

$$(1/\rho)\hat{\mathbf{e}}_n = -[(n+2)/r]\hat{\mathbf{e}}_r, \tag{9}$$

or

$$\rho = r/(n+2) \tag{10}$$

for the radius of curvature at points where the line of force is perpendicular to the radius vector.

In summary, the generation of multipole potentials by differentiation appears as a useful basic concept which affords a means of readily obtaining a simple equation describing the lines of force of a linear multipole. It is interesting to note, however, that certain features of the lines of force can be found without use of the equations for these curves in their integrated form.

[1] G. Arfken, Am. J. Phys. 25, 481 (1957).
[2] W. K. H. Panofsky and M. Phillips, *Classical Electricity and Magnetism* (Addison-Wesley Press, Cambridge, 1955), Sec. 1–7.
[3] W. R. Smythe, *Static and Dynamic Electricity* (McGraw-Hill Book Company, Inc., New York, 1950), second edition, Sec. 1.101.
[4] By the identity $(1-\mu^2)P_n' + n\mu P_n - nP_{n-1} = 0$; E. T. Whittaker and G. N. Watson, *A Course in Modern Analysis* (Cambridge University Press, New York, 1927), Sec. 15.21, Eq. (V), or reference 3, Sec. 5.154.

Reprinted from JOURNAL OF APPLIED PHYSICS, Vol. 37, No. 6, 2361–2363, May 1966

An Equivalent Distribution of Surface Currents for the Generation of a Prescribed Static Magnetic Field within the Enclosed Volume*

L. JACKSON LASLETT
Lawrence Radiation Laboratory and Department of Physics, University of California, Berkeley, California
(Received 12 January 1966)

It is shown how a specified static magnetic field within a given volume may be generated through use of a current distribution on the surface surrounding this volume. The surface distribution includes a distribution of magnetic moment (oriented tangential to the surface) that may be interpreted as a double-current layer, but no magnetic poles are introduced. No sources are required external to the surface and the exterior field will be zero.

IT is known[1,2] that the external sources of an electrostatic field that is specified within a closed surface S can be replaced by an equivalent distribution of charge and electric dipole moment on S (the so-called Green's equivalent stratum). With this replacement, the electric field external to S vanishes. It appears to be less well known whether an analogous distribution of surface currents may be found to replace the external sources of a static *magnetic* field, without employing magnetic poles or surface distributions for which no physical interpretation is evident.[3] It is shown here that there exists a current distribution on S that will produce the same magnetic field interior to S as is produced by the external sources (whether the external sources are formed by a current system or are imagined to be magnetic poles), and an explicit prescription is given for determining this current distribution.

The magnetic field $\mathbf{H}$ is considered as given within a closed surface S, together with an associated vector potential $\mathbf{A}$ so that $\nabla\times\mathbf{A}=\mathbf{H}$ and $\nabla\cdot\mathbf{A}=0$. Within S, $\nabla\cdot\mathbf{H}=0$ and $\nabla\times\mathbf{H}=4\pi\mathbf{J}$,[4] with $\mathbf{J}=0$ if no currents exist in the volume V interior to S. One may construct a new vector potential,

$$\mathbf{A}'\equiv\mathbf{A}+\nabla\Phi, \tag{1}$$

where Φ is specifically selected so that, at all points on S,

$$(\nabla\Phi)\cdot\hat{n}=-\mathbf{A}\cdot\hat{n}, \tag{2}$$

$\hat{n}$ being the outward-directed unit vector normal to the surface S. [Such a Φ may be assumed to exist. In particular, with the stipulation that $\nabla\cdot\mathbf{A}=0$ (so that $\int\int_S\mathbf{A}\cdot\hat{n}dS\equiv\int\int\int_V\nabla\cdot\mathbf{A}dv=0$), Φ may be taken as a solution of the Neumann problem in which $\nabla^2\Phi=0$ and boundary conditions of the second kind apply.] Accordingly, $\nabla\times\mathbf{A}'=\mathbf{H}$, and $\mathbf{A}'\cdot\hat{n}=0$ on S.

One now defines the vector

$$\mathbf{A}''\equiv\iiint_V\frac{\mathbf{J}}{r}dv+\frac{1}{4\pi}\iint_S\left\{\frac{\mathbf{H}\times\hat{n}}{r}+\frac{\mathbf{r}\times[\mathbf{A}'\times\hat{n}]}{r^3}\right\}dS \tag{3a}$$

$$=\iiint_V\frac{\mathbf{J}}{r}dv+\frac{1}{4\pi}\iint_S\left\{\frac{\mathbf{H}\times\hat{n}}{r}+\frac{\mathbf{r}\times[\mathbf{A}'\times\hat{n}]}{r^3}+\frac{\mathbf{r}}{r^3}(\mathbf{A}'\cdot\hat{n})\right\}dS \tag{3b}$$

that can serve as a suitable vector potential to give the field $\mathbf{H}$ within S. The vector $\mathbf{r}$ is to be understood as extending from the field point P to the surface element dS (Fig. 1), and the two forms given for Eq. (3) are equivalent because the factor $\mathbf{A}'\cdot\hat{n}$ that appears in the last term of Eq. (3b) is identically zero on all points of S.

The three surface integrals in Eq. (3b) can be transformed to volume integrals as follows:

$$\iint_S(\mathbf{H}/r)\times\hat{n}dS=\iiint_V(-[\nabla\times\mathbf{H}]/r+[\mathbf{r}\times\mathbf{H}]/r^3)dv$$

$$=-4\pi\iiint_V(\mathbf{J}/r)dv+\iiint_V[(\mathbf{r}/r^3)\times(\nabla\times\mathbf{A}')]dv; \tag{4a}$$

* Work assisted by the U. S. Atomic Energy Commission.

[1] Sir James Jeans, *The Mathematical Theory of Electricity and Magnetism* (Cambridge University Press, Cambridge, England, 1948), 5th ed., Secs. 204–206.

[2] W. R. Smythe, *Static and Dynamic Electricity* (McGraw-Hill Book Co., Inc., New York, 1939), 1st ed., Sec. 3.12.

[3] See, J. A. Stratton, *Electromagnetic Theory,* (McGraw-Hill Book Co., Inc., New York, 1941), 1st ed., Sec. 4.15 [esp. Eq. (14), in which the last term is difficult to interpret in physical terms, and Eq. (23) in which the last term represents (in rationalized mks units) the field of a distribution of magnetic poles].

[4] Unrationalized electromagnetic units are employed.

$$\iint_S [(\mathbf{r}/r^3)\times(\mathbf{A}'\times\hat{n})]dS=\iiint_V \{\mathbf{A}'\nabla\cdot(\mathbf{r}/r^3)+[(\mathbf{r}/r^3)\cdot\nabla]\mathbf{A}'-\nabla[(\mathbf{r}/r^3)\cdot\mathbf{A}']\}dv$$

$$=4\pi\mathbf{A}'+\iiint_V \{[(\mathbf{r}/r^3)\cdot\nabla]\mathbf{A}'-\nabla[(\mathbf{r}/r^3)\cdot\mathbf{A}']\}dv \tag{4b}$$

for P *interior* to S [since $\nabla\cdot(\mathbf{r}/r^3)$ may be identified with 4π times the Dirac delta function]; and

$$\iint_S (\mathbf{r}/r^3)(\mathbf{A}'\cdot\hat{n})dS=\iiint_V [(\mathbf{r}/r^3)(\nabla\cdot\mathbf{A}')+(\mathbf{A}'\cdot\nabla)(\mathbf{r}/r^3)]dv. \tag{4c}$$

By addition of Eqs. (4), expansion of $\nabla[(\mathbf{r}/r^3)\cdot\mathbf{A}']$, and use of $\nabla\times(\mathbf{r}/r^3)=0$, Eq. (3b) reduces to

$$\mathbf{A}''=\mathbf{A}'+\frac{1}{4\pi}\iiint_V \frac{\mathbf{r}}{r^3}(\nabla\cdot\mathbf{A}')dv. \tag{5}$$

The curl of the last term in Eq. (5), taken with respect to the coordinates of P, is found to vanish. It thus follows that

$$\nabla\times\mathbf{A}''=\nabla\times\mathbf{A}'=\mathbf{H}, \tag{6}$$

and $\mathbf{A}''$ will serve as a vector potential to describe the field $\mathbf{H}$ in the region interior to S.

From Eq. (3a), which served to define $\mathbf{A}''$, it is seen that this potential would arise from such currents $\mathbf{J}$ as may exist in the region interior to S, *supplemented by* the following surface distributions:

(i) a *surface current*

$$\mathbf{j}=(1/4\pi)[\mathbf{H}\times\hat{n}]\text{ abamp/cm} \tag{7a}$$

and

(ii) a *double layer of current*, visualized as formed of currents parallel and antiparallel to $\mathbf{A}'$ on the inner and outer surfaces of an infinitesimally thin shell, that is describable by a surface distribution of magnetic moment

$$\mathbf{p}=(1/4\pi)[\mathbf{A}'\times\hat{n}]\text{ abamp.} \tag{7b}$$

These surface distributions therefore may be employed in place of sources external to S. The surface-current distribution of Eq. (7a), when supplemented by volume currents $\mathbf{J}$ that terminate on leaving the interior region, are such that the steady-state equation of continuity is satisfied.

If the foregoing analysis is applied to evaluate $\mathbf{A}''$ at a point P *external* to S, subject to $\mathbf{A}'$ being characteristic of a field whose sources are confined to a finite region of space, Eqs. (4) still apply *except that* the term $4\pi\mathbf{A}'$ will be absent from Eq. (4b). In this case the term $\mathbf{A}'$ will be absent from Eq. (5) and the curl of $\mathbf{A}''$ will vanish. The current distribution stipulated in the preceding paragraph therefore produces no external field.

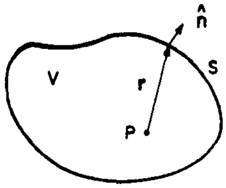

FIG. 1. The surface S to which the vector $\mathbf{r}$ is drawn from the field point P.

In examples for which the given vector potential is such that $\mathbf{A}\cdot\hat{n}=0$ on the boundary S, the scalar function Φ, of course, need not be introduced. Thus one may characterize a uniform interior field

$$\mathbf{H}=H_0\hat{e}_z=H_0[\cos\theta\hat{e}_r-\sin\theta\hat{e}_\theta]$$
$$=H_0[P_1(\cos\theta)\hat{e}_r-P_1^1(\cos\theta)\hat{e}_\theta] \tag{8}$$

with $\mathbf{J}=0$, by the vector potential

$$\mathbf{A}_1=\tfrac{1}{2}H_0(-y\hat{e}_x+x\hat{e}_y)=\tfrac{1}{2}H_0r\sin\theta\hat{e}_\phi$$
$$=\tfrac{1}{2}H_0rP_1^1(\cos\theta)\hat{e}_\phi, \tag{9}$$

in which the last forms shown in Eqs. (8) and (9) are expressed in spherical coordinates. If S is selected to be a sphere of radius a concentric with the origin of the coordinate system, the vector potential $\mathbf{A}_1$ is such that $\mathbf{A}_1\cdot\hat{n}=0$ on this surface and $\mathbf{A}'=\mathbf{A}_1$. Equations (7) then immediately give the surface distributions

$$\mathbf{j}=(H_0/4\pi)\sin\theta\hat{e}_\phi\quad\text{and}\quad\mathbf{p}=(H_0a/8\pi)\sin\theta\hat{e}_\theta \tag{10}$$

that will produce the specified uniform internal field. The form of the surface current $\mathbf{j}$ is such that this current alone will produce a uniform interior field[5]; the respective contributions to the internal field, due to the current and magnetic moment distributions of Eqs. (10), are in the ratio 2:1 and the individual contributions to the external field cancel.

Alternatively, if the field of Eq. (8) were characterized by the vector potential

$$\mathbf{A}_2=-H_0y\hat{e}_x=-H_0r(\sin^2\theta\sin\phi\cos\phi\hat{e}_r$$
$$+\sin\theta\cos\theta\sin\phi\cos\phi\hat{e}_\theta-\sin\theta\sin^2\phi\hat{e}_\phi); \tag{11}$$

[5] W. R. Smythe, Ref. 2, Sec. 7.051; *ibid* (1950), 2nd ed., Sec. 7.12.

$\mathbf{A}_2\cdot\hat{n}=-H_0a\sin^2\theta\sin\phi\cos\phi$ and one may take Φ as the (harmonic) function

$$\Phi=\tfrac{1}{2}H_0r^2\sin^2\theta\sin\phi\cos\phi \tag{12}$$

to satisfy Eq. (2). With this form for Φ,

$$\mathbf{A}_2'=\mathbf{A}_2+\nabla\Phi=\tfrac{1}{2}H_0r\sin\theta\hat{e}_\varphi=\mathbf{A}_1 \tag{13}$$

and Eqs. (7) lead to the expressions for $\mathbf{j}$ and $\mathbf{p}$ given before by Eqs. (10).

This work was begun as a result of stimulating conversations with my colleague, Dr. A. M. Sessler, concerning the possibility of realizing certain field configurations intended to reduce aberrations in beta-ray spectrometers.

A METHOD FOR STATIC-FIELD COMPRESSION

IN AN ELECTRON-RING ACCELERATOR*

L. Jackson Laslett and Andrew M. Sessler

Lawrence Radiation Laboratory
University of California
Berkeley, California

Summary

A review of methods for static-field compression of an electron ring is shown to suggest advantages for a method in which there is no axial acceleration or deceleration of the ring. In the method proposed here the static magnetic field itself is of such a character that the electrons are neither focused nor defocused in the axial direction. The integrity and movement of the ring through the compressor is controlled by a small traveling magnetic well. The feasibility of creating such a traveling well is discussed. and an example is presented of a current distribution capable of producing the static magnetic field of the compressor.

Introduction

In the original proposal of Veksler et al.,[1] the electron ring of an electron-ring accelerator (ERA) is compressed by a pulsed field from a large to a small radius and with an associated increase of electron energy. As Christofilos[2] and others[3,4,5,6] have noted, compression can be achieved (without an energy gain) in a static magnetic field. With acceleration divorced from the compression function, the need for large supplies of pulsed power is avoided, and increased repetition rates become possible--at the expense of a higher-energy injector.

The method proposed (independently) in Refs. 3, 4, 5, 6 is essentially the reverse of a normal magnetic expansion process.[7] In contrast to the situation during normal expansion, the ring will not hold ions during the compression process and hence will not be self-focused; accordingly, there are critical questions concerning the feasibility of achieving rings of small minor dimensions in a static-field compressor--in the face of an inherent energy spread and transverse emittance of the electron beam from the injector.

The method proposed by Christofilos (Ref. 2) has one or more alternating sections of axial acceleration and deceleration and therefore can provide focusing except within a short region between adjacent decelerating and subsequent accelerating sections. Such defocusing regions may not be serious if special methods are employed,[8] or if the crossing is sufficiently rapid.[2,8] However, as in the other static compressor proposals, the requirement of final rings with small minor dimensions seems to impose an almost unattainable demand on the energy spread of the injected beam (cf. Ref. 5).

We propose a static-field compressor in which there is no axial ring deceleration (or acceleration) and hence no very stringent sensitivity to initial energy spread. Furthermore, the fields of the static compressor are neither focusing or defocusing in the axial direction so that, with the addition of a small traveling magnetic well, transverse focusing can be maintained throughout the compression process, and the integrity of the ring maintained. A traveling magnetic pulse, matched to the repetition rate of an electron injector, can easily be attained in practice,[9] and thus can preserve the high pulse-rate advantage conceived for a static-field compressor. In addition, the continuous control of the electron ring may prove advantageous for the proper phasing of a compressed and loaded ring into an accelerating section.

In this paper we first discuss general aspects of the compressor static field and the associated traveling well. Subsequently, we give an example of a possible field configuration and coil arrangement. An appendix is devoted to describing the computational procedures employed in seeking practical designs. A schematic general view of the proposed compressor is given in Fig. 1.

The Static Field

In the design of the static compressor we have at our disposal the choice of the surface $r = r(z)$ on which the electron ring moves. Because the fields are static, the energy of an electron does not change during the compression process, and with no axial acceleration, the orbital component of momentum remains substantially constant for an electron on a circular (equilibrium) orbit. With the requirement that this orbit lie on a specified surface $r = r(z)$, it is necessary that

$$r(z)\cdot B_z[r(z),z] = \text{constant}. \qquad (1)$$

We also wish to impose the requirement that rings not be accelerated (or decelerated) in the z-direction. Since the force in the z-direction is proportional to B_r, we require--for all z included in the compression process--that

$$B_r[r(z),z] = 0. \qquad (2)$$

* This work was done under the auspices of the U. S. Atomic Energy Commission.

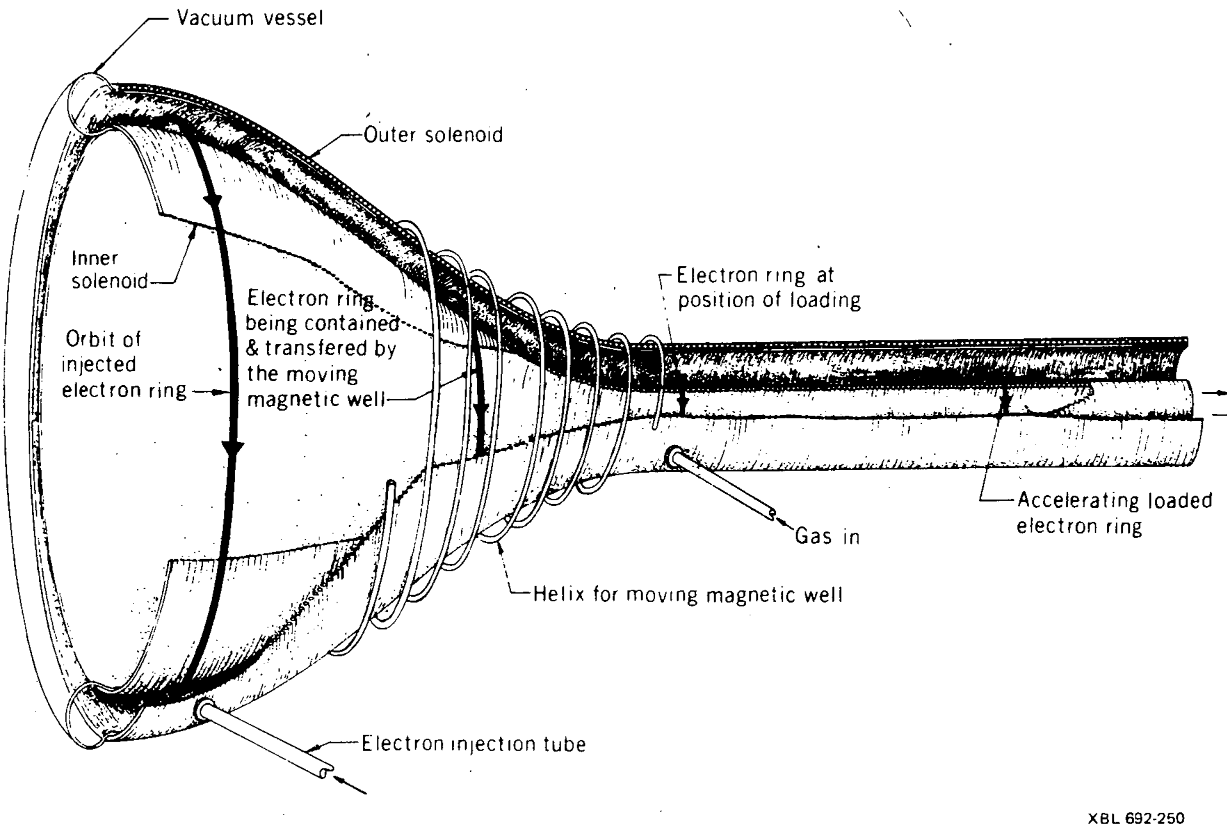

Fig. 1. Schematic view of the static compressor. Note the inner and outer coils. Injection is at the left, loading takes place just after compression, and a magnetic expansion unit is shown on the right. The traveling magnetic well is supplied by a current pulse on the (slow-wave) helix.

The specification of B_z and B_r on the surface $r = r(z)$ can be seen to be: (1) consistent with Maxwell's equations, and hence a permissible procedure; and (2) adequate to determine completely the field for points near the surface $r = r(z)$ (as an expansion in powers of the distance from the surface). Thus we find that, if R_0 is the (arbitrary) injection radius at which the field B_z takes the (arbitrary) value B_0, then

$$B_z(r,z) = \frac{B_0R_0}{r(z)}\left\{1 - \frac{[dr(z)/dz]^2[r - r(z)]}{r(z)[1 + [dr(z)/dz]^2]} + \cdots\right\} \tag{3}$$

and

$$B_r(r,z) = \frac{B_0R_0}{r^2(z)}\left\{\frac{[dr(z)/dz][r - r(z)]}{[1 + [dr(z)/dz]^2]} + \cdots\right\}, \tag{4}$$

through first order in $[r - r(z)]$. It is easy to verify that these first-order expressions satisfy (1) and (2), as well as the zero-order equations which follow from

$$\nabla \cdot \mathbf{B} = 0, \qquad \nabla \times \mathbf{B} = 0, \tag{5}$$

namely

$$\left[\frac{\partial B_r(r,z)}{\partial z} - \frac{\partial B_z(r,z)}{\partial r}\right]\Bigg|_{r=r(z)} = 0, \tag{6}$$

and

$$\left[\frac{B_r(r,z)}{r} + \frac{\partial B_r(r,z)}{\partial r} + \frac{\partial B_z(r,z)}{\partial z}\right]\Bigg|_{r=r(z)} = 0. \tag{7}$$

Focusing Properties of the Static Field

The focusing properties of the static field follow from the dynamical equations of motion for electrons in the field of Eqs. (3) and (4). At first thought one might argue that, since B_r is zero along the trajectory $r = r(z)$, the derivative of B_r in the z-direction is not zero, the field index n is nonvanishing, and the static field would necessarily have some focusing or defocusing effect. One recalls, however, that the usual derivation of focusing is special to situations with median-plane symmetry, which is not present in the static compressor. We have undertaken a detailed calculation (outlined below) of small-amplitude motion in the region of the equilibrium orbit $r = r(z)$. The general result is that the focusing involves two field indices. When we employ the fields of Eqs. (3) and (4) to determine the indices, we find that the static field determined by Eqs. (1) and (2) has the same focusing frequencies as a uniform field (namely one mode in neutral equilibrium).

Proceeding as we have, this result is certainly nonobvious; we are aware that such a simple conclusion probably can be obtained by a general consideration of our original (simple) field specifications. In lieu of such an argument, we burden the reader, in the remainder of this section, with details of the straightforward argument.

Starting from the principle of least action,

$$\delta \int (\underset{\sim}{p}_{mech} - \underset{\sim}{A})\cdot d\underset{\sim}{s} = 0 \tag{8}$$

(with the mechanical momentum measured in units of "magnetic rigidity"), one can conveniently derive the equations for a general particle trajectory. Keeping only first-order terms in the motion about the equilibrium orbit $r = r(z)$, one obtains

$$\frac{px''}{r(z) + x} - p + [r(z) + x]B_z(r,z) = 0 \tag{9a}$$

and

$$\frac{pz''}{r(z) + x} - [r(z) + x]B_r(r,z) = 0, \tag{9b}$$

where $p = r(z)B_z[r(z),z]$, $x = r - r(z)$, and the primes denote differentiation with respect to the azimuthal angle θ.

Expanding the fields about the equilibrium orbit, and employing Maxwell's equations to relate field derivatives, we may put the coupled equations in the form

$$x'' + (1 - n)x + \alpha z = 0 \tag{10a}$$

and

$$z'' + nz + \alpha x = 0, \tag{10b}$$

where the field indices n and α are defined by

$$n \equiv - \left[\frac{r}{B_z(r,z)}\ \frac{\partial B_z(r,z)}{\partial r}\right]\Bigg|_{r=r(z)}$$

$$n = - \left[\frac{r}{B_z(r,z)}\ \frac{\partial B_r(r,z)}{\partial z}\right]\Bigg|_{r=r(z)} \tag{11a}$$

and

$$\alpha \equiv \left[\frac{r}{B_z(r,z)}\ \frac{\partial B_z(r,z)}{\partial z}\right]\Bigg|_{r=r(z)},$$

$$\alpha = - \left[\frac{r}{B_z(r,z)}\ \frac{\partial B_r(r,z)}{\partial r}\right]\Bigg|_{r=r(z)}, \tag{11b}$$

with

$$B_r(r,z)\Big|_{r=r(z)} = 0 .$$

The characteristic frequencies of the system (10) are given by

$$\nu^2 = \frac{1}{2} \pm [(\tfrac{1}{2} - n)^2 + \alpha^2]^{1/2}, \tag{12}$$

and correspond to eigenmodes in which the r and z motion is mixed. From (3) and (4), and the definition of n and α [Eqs. (11a,b)], we find

$$n = \frac{[dr(z)/dz]^2}{\{1 + [dr(z)/dz]^2\}}, \tag{13a}$$

$$\alpha = - \frac{dr(z)/dz}{\{1 + [dr(z)/dz]^2\}}, \tag{13b}$$

and consequently, from (12), $\nu^2 = 0, 1$. These frequencies are the same as would be obtained in a uniform field (but now with some coupling of r and z motion corresponding to the pure-r and pure-z modes of the uniform field). One mode is on an integral resonance, and the other is in neutral equilibrium.

The Moving Magnetic Well

In order to control ring position along the trajectory $r = r(z)$, and also to supply axial focusing, a moving magnetic well must be added to the static field of the compressor. Because of the neutral equilibrium of the axial mode in the static field, only a modest strength is required for the moving field.

A number of possibilities have been suggested for creating the moving well; a particularly interesting proposal is to send a current pulse down a slow-wave structure. Dombrowski has considered a design involving a helix with a surrounding dielectric layer and an outer conducting sheath.[9] He finds that the dispersion of a current pulse can be made acceptably small, while the rather slow decrease of impedance with frequency is advantageous for matching into a modulated power supply. Details may be found in Ref. 9, but the conclusion is that a helix appears to be a practical solution to the problem of ring focusing and control.

Numerical Example

A practical compressor design consists of specifying coil radii, positions, and associated currents. The expansion of fields about the trajectory $r = r(z)$ (which was described above) could be used to generate fields at distances away from the trajectory; these fields could then be "terminated" by suitable current distributions in such a way as to require no further currents at greater distances. This procedure is not easy to follow. Furthermore, it is not clear in advance at what point singularities will appear in the expansion and thus dictate the location of currents. If these singularities are too close to the trajectory, $r = r(z)$, they would preclude adequate room for particle oscillations or adequate vacuum chamber width for pumping, and might force the windings to be inconveniently thin in order that intolerable field ripples be avoided.

In order, then, to demonstrate the feasibility of the compressor in cases of practical interest, we have resorted to digital computation. The computational studies were undertaken by Steven Sackett, and the procedures employed are described in the Appendix.

In Fig. 2 we present one numerical example which should suffice to show the practicality of the device. The compressor has a length of one meter; it accepts electrons at a radius of 57 cm and compresses them, by a factor of 7.8, to a radius of 7.3 cm. The separation between inner and outer coil surfaces is 8.0 cm. It can be seen that the required coil currents are smooth (the oscillations near the ends presumably can be removed by slight lengthening of the solenoid) and not excessive in magnitude.

Acknowledgments

We are indebted to Steven Sackett for development of the computer program which made possible the practical design studies. We are also indebted to him for agreeing to let us include here the material which constitutes the Appendix of this paper. We are grateful to Professor George Dombrowski for his interest in the problem of the moving magnetic well, and for his contributions to this subject. Finally, we acknowledge that this work was a result of N. C. Christofilos' stimulating lectures and remarks on the advantages of static compressors.

Appendix: Determination of Coil Currents*

Practical designs have been investigated by choosing (1) a desired compression surface $r = r(z)$, and (2) a desired set of coil locations. The currents which must be supplied to the coils to give the necessary compressor fields are then computed. Because of the linearity of Maxwell's equations, the problem reduces to solving the system of (linear) equations:

$$\sum_{j=1}^{n} B_{ij}^{(z)} I_j = B_{zi} ; \quad i = 1, \cdots m, \tag{A1}$$

$$\sum_{j=1}^{n} B_{ij}^{(r)} I_j = B_{ri} ; \quad i = 1, \cdots m , \tag{A2}$$

where $B_{ij}^{(z)}$ and $B_{ij}^{(r)}$ denote the z and r components, respectively, of the field at point i due to unit current in coil j, and the field components desired at point i are denoted by B_{zi} and B_{ri}.

A practical solution for the currents I_j may be obtained by taking $2m \geq n$ and obtaining the best fit to (A1, A2) in a least-squared sense, with the possibility of a relative weighting of the B_r equations compared with the B_z equations. This process will, in general, lead to currents that are not smoothly varying, or that are large in value. Consequently we require that the quantity to be minimized be supplemented by

$$w_0 \sum_{j=1}^{n} I_j^2 + w_1 \sum_{j=2}^{n} (I_{j-1} - I_j)^2 + w_2 \sum_{j=2}^{n-1} (I_{j-1} - I_{j+1})^2$$

$$+ w_3 \sum_{j=2}^{n-1} (I_{j-1} - 2I_j + I_{j+1})^2 , \tag{A3}$$

where the w_i are weighting factors.

The computational procedure consists of a reduction of the matrix equations, by orthogonal Householder transformations, followed by iterations which successively improve the least-squares fit.[10] The computer program first generates the fields to be fitted, B_i, and the matrix of coefficients, B_{ij} (employing the fields of infinitely thin wire loops); it then (using input values of weights and a convergence criterion) determines I_j. Since machine language is used, the speed is high. Output is numerical and also graphical.

---

* This Appendix was prepared by Steven Sackett.

In the example cited in the text, the orbit trajectory was taken to be a cosine curve with 100 fitting points between $z = 5$ cm and 95 cm. There were 200 coils located between $z = 0$ and $z = 100$ cm on two cosine curves separated by 8 cm. The B_r weighting factor was 5, $w_0 = 10^{-10}$, $w_1 = 0$, $w_2 = 10^{-12}$, and $w_3 = 10^{-9}$. (These values were seen, in some survey studies, to be effective.) The time to solve the problem was 14.8 seconds on a CDC 6600, and the total sums of squares of the relative errors in B_z and in B_r were respectively 8.4×10^{-6} and 7.3×10^{-6}.

References

1. V. I. Veksler et al., Proc. VI International Conference on High Energy Accelerators, Cambridge Electron Accelerator, Cambridge, 1967, p. 289.

2. N. C. Christofilos, Static Compression of Relativistic Electron Rings, Lawrence Radiation Laboratory Technical Note UCID-15378, September 17, 1968 (submitted to Phys. Rev. Letters).

3. E. M. McMillan, private communication (1967).

4. E. Keil, private communication (1968).

5. R. E. Berg, H. Kim, M. P. Reiser, and G. T. Zorn, Possibilities of Forming a Compressed Electron Ring in a Static Magnetic Field, University of Maryland Department of Physics Technical Report 918, November 1968 (submitted to Phys. Rev. Letters).

6. W. Hintz, private communication (1969).

7. See, for example, Symposium on Electron Ring Accelerators, Lawrence Radiation Laboratory Report UCRL-18103, 1968, p. 16.

8. N. C. Christofilos, private communication.

9. G. E. Dombrowski, Use of a Helix for Transport of Electron Rings Through Static Compression Fields, Lawrence Radiation Laboratory Technical Note ERAN-24, 1968 (unpublished).

10. G. Golup, "Numerical Methods for Solving Linear Least-Squares Problems," Numerische Math. 7, 3 (1965), p. 206-216.

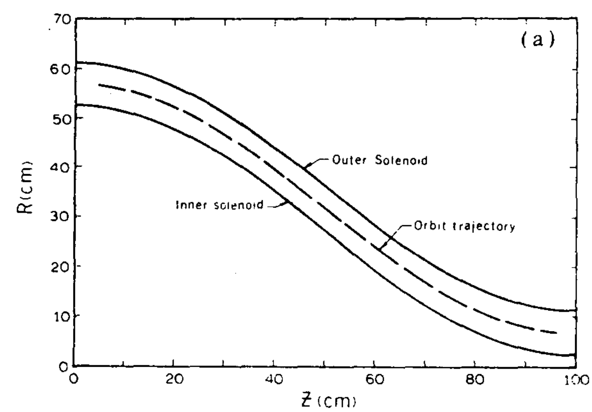

XBL 692-4462

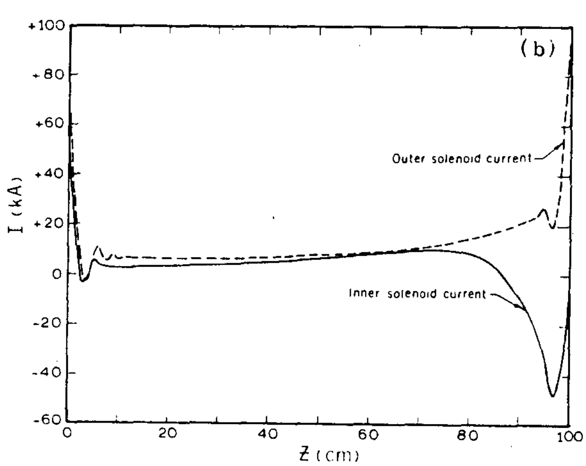

XBL 692-4463

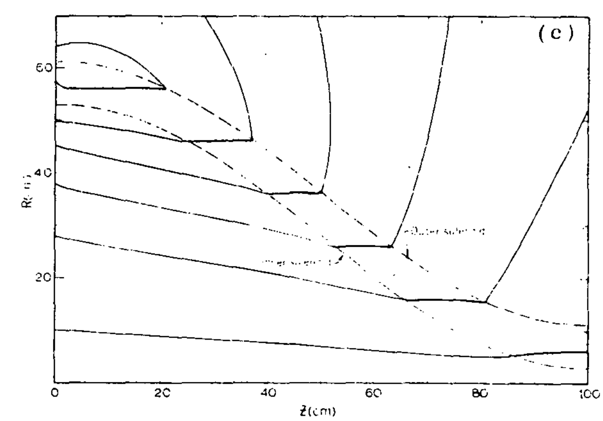

XBL 692-4494

Fig. 2. Static compressor having a compression ratio of 7.8:1. (a) Geometry of the coils and ring trajectory. (b) Currents required in each turn of two 100-turn solenoids (or, equivalently, the turn densities required for series-wound coils). The current values correspond to a field $B_z = 4.0$ kg at $r = 56.7$ cm; i.e. electron kinetic energy of 68.3 MeV. (c) "Flux plot" showing lines of force (the density of lines does not reflect field strength).

ON THE FOCUSSING EFFECTS ARISING FROM THE SELF FIELDS OF A TOROIDAL BEAM*

L. Jackson Laslett

Lawrence Radiation Laboratory
University of California
Berkeley, California

INTRODUCTION

The self fields of a toroidal beam were discussed in the ERA Proceedings (UCRL-18103, Papers ERAN 7-8), wherein simple approximate formulas were presented to describe the bias fields at the center of the beam, and computational results were reported to confirm the magnitude of these bias fields and to suggest values for the gradients of the self-field components.

A recent Soviet paper [I.N. Ivanov et al., JINR Report P9-4132 (1968)] has given identical formulas for the bias fields, together with similar formulas for the field gradients. The Soviet authors, moreover, indicate the effect of these self-field effects on the betatron-oscillation frequencies of individual particles in the beam, and it is evident that these oscillation frequencies can be markedly affected by the toroidal self-field effects when the parameters of the ring are similar to those that pertain to the Soviet electron-ring device (V. P. Sarantsev, private communication, March 1969).

Because of the potential interest in these effects, we review here the considerations that can lead to the analytic results cited in the Soviet report. It will be noted that analysis of this problem is complicated by the presence of the bias fields, E_r and B_z, that act to expand the ring and whose presence requires that the applied guide (and focussing) field be strengthened, or the particle energy be reduced, or that some combination of these actions be taken if the major orbit radius of the ring is to be maintained. The analysis also is complicated by the presence of electric, as well as magnetic self fields, whose dynamical effects must be evaluated.

The present notes are divided below into four sections, of which the first three in turn (I) derive the self fields of a toroidal beam, (II) discuss the general dynamical problem of small-amplitude oscillations in

* Work supported by the U. S. Atomic Energy Commission.

the presence of magnetic and electric fields, and (III) apply the dynamical results to obtain the implications of the self fields with respect to the incoherent oscillation frequencies of particles in the toroidal beam. This analysis does not take explicitly into account the possible presence of stationary ions in the beam, nor does it include the inherent non-toroidal space-charge forces that would be present with a straight beam. These latter effects, that have been treated by Teng for a uniform beam of elliptical cross-section [L. C. Teng, Argonne National Laboratory Report ANLAD-59 (1963)], introduce no bias terms and so present no complication -- they moreover often will be small in practice because of the strong $1 - \beta^2$ cancellation between the electric and magnetic forces of an unneutralized highly relativistic beam. A concluding section (IV) attempts to take into account partial neutralization of the beam by stationary ions, with the inclusion of direct self-field effects and of image terms that will arise from nearby conducting or dielectric cylinders. The present work will be concerned most specifically with a beam of highly relativistic identical particles distributed uniformly throughout the cross-section of a toroidal beam. For the limiting situation $\beta = 1$, we write $I_{emu} = \frac{Q_{esu}}{2\pi R}$.

I. THE SELF FIELDS OF A TOROIDAL BEAM

A. The Bias Fields

The scalar and vector potential functions of a filamentary charge-current ring can be expressed directly in terms of complete elliptic integrals [cf. W. R. Smythe, "Static and Dynamic Electricity," Sect. 7.10], and the corresponding potentials for a toroidal beam can then be expressed as definite integrals. Differentiation of such expressions then gives the components of the electric and magnetic fields, and further differentiation gives the gradients of these field components. Thus, for a ring of major radius R and an elliptical cross-section with semi-axes a,b:

$$E_r = \frac{Q}{\pi^2 abRr}\iint\left[K - \frac{(R+r'\sin\theta')^2 - r^2 + (z-r'\cos\theta')^2}{(R-r+r'\sin\theta')^2+(z-r'\cos\theta')^2}\,E\right]\frac{R+r'\cos\theta'}{\sqrt{(R+r+r'\sin\theta')^2+(z-r'\cos\theta')^2}}\,dS'$$

and

$$B_z = \frac{2I}{\pi ab}\iint\left[K + \frac{(R+r'\sin\theta')^2 - r^2 - (z-r'\cos\theta')^2}{(R-r+r'\sin\theta')^2+(z-r'\cos\theta')^2}\,E\right]\frac{1}{\sqrt{(R+r+r'\sin\theta')^2+(z-r'\cos\theta')^2}}\,dS',$$

where the parameter of the complete elliptic integrals E and K is

$$m = k^2 = \frac{4r(R + r'\sin\theta')}{(R + r + r'\sin\theta')^2 + (z - r'\cos\theta')^2}\ .$$

If we are interested in the bias fields at the center of the cross-section, where $r = R$ and $z = 0$, we note that

$$m = \frac{4R(R + r'\sin\theta')}{(2R + r'\sin\theta')^2 + r'^2\cos^2\theta'} = \frac{1 + \frac{r'}{R}\sin\theta'}{1 + \frac{r'}{R}\sin\theta' + (\frac{r'}{2R})^2}$$

and

$$m_1 = 1 - m = \frac{(\frac{r'}{2R})^2}{1 + \frac{r'}{R}\sin\theta' + (\frac{r'}{2R})^2} \cong (\frac{r'}{2R})^2\ .$$

Hence a critical term in each of the definite integrals is

$$K \cong \ln\frac{4}{k'} = \ln\frac{4}{\sqrt{m_1}} = \ln\frac{8R}{r'}\ .$$

Accordingly the dominant terms in E_r and B_z at $r = R$ and $z = 0$ are respectively, when the minor dimensions are small relative to R,

$$E_r \cong \frac{Q}{2\pi^2 abR^2}\iint K\, dS' \cong \frac{Q}{2\pi^2 abR^2}\iint \ln\frac{8R}{r'}\, dS'$$

and

$$B_z \cong \frac{I}{\pi abR}\iint K\, dS' \cong \frac{I}{\pi abR}\iint \ln\frac{8R}{r'}\, dS'\ .$$

The integral $\iint K\, dS'$ over the cross-section of the beam is readily evaluated (see the Appendix to this Section) and yields, as a dominant term,

$\iint K\, dS' \cong \pi ab \ln\frac{16R}{a+b} = \pi ab \ln\frac{8R}{\bar{b}}$, where $\bar{b} = \frac{a+b}{2}$ is the average minor radius of the beam. We thus obtain for the bias fields,

$$E_r \cong \frac{Q}{2\pi R^2}\ln\frac{8R}{\bar{b}} \qquad \text{and} \qquad B_z \cong \frac{I}{R}\ln\frac{8R}{\bar{b}}\ .$$

These results were checked reasonably well computationally, for a beam of circular cross-section with a ratio of major- to minor radius equal to 40, although the result of numerical integration gave a result for the <u>electric</u> field that was <u>only</u> 83 percent of the approximate analytic value.

B. The Field Gradients

For the "effective field," $F_r = E_r + B_z$ at the center of the beam, we similarly find, to the same order of approximation (with $I = \frac{Q}{2\pi R}$), the gradient

$$\frac{\partial F_r}{\partial r} \cong -\frac{Q}{\pi^2 abR^3} \iint \ln \frac{8R}{r'}\, dS' \cong -\frac{Q}{\pi R^3} \ln \frac{8R}{b},$$

which is $-\frac{1}{R}$ times the total bias field $F_r = E_r + B_z$ at the center of the beam.

From the result just found, one can immediately write the corresponding derivative $\partial F_z/\partial z$ through use of the divergence and curl conditions, where F_z denotes the effective axial field $E_z - B_r$.

$$\begin{aligned}
\frac{\partial F_z}{\partial z} = \frac{\partial E_z}{\partial z} - \frac{\partial B_r}{\partial z} &= \left(\nabla\cdot\vec{E} - \frac{E_r}{r} - \frac{\partial E_r}{\partial r}\right) - \left([\nabla\times\vec{B}]_\theta + \frac{\partial B_z}{\partial r}\right) \\
&= \nabla\cdot\vec{E} - [\nabla\times\vec{B}]_\theta - \left(\frac{E_r}{R} + \frac{\partial E_r}{\partial r} + \frac{\partial B_z}{\partial r}\right) \\
&= 4\pi(\rho - J) - \left(\frac{E_r}{R} + \frac{\partial F_r}{\partial r}\right) \\
&= -\frac{E_r}{R} - \frac{\partial F_r}{\partial r} \\
&= \left(-\frac{Q}{2\pi R^3} + \frac{Q}{\pi R^3}\right)\ln\frac{8R}{b} \\
&= \frac{Q}{2\pi R^3}\ln\frac{8R}{b},
\end{aligned}$$

a result that has half the magnitude and the opposite sign when compared to $\partial F_r/\partial r$.

Computationally, values of $\partial F_z/\partial z$ were found that were about 78 percent of the values expected from this simple analytic formula (for ratios of major to minor radii equal to 40 or to 10). The computational results for $\partial F_r/\partial r$ were somewhat less clear, although the average slopes of F_r across the beam were roughly in agreement with the formula given above for $\partial F_r/\partial r$ at the center.

C. Summary

With introduction of the notation employed by the Soviet workers, we have

Effective Bias Field:

$$eF_r)_o = \frac{m_o c^2 \gamma_\perp}{R}\mu P$$

Gradients:

$$e\,\partial F_r/\partial r = -\frac{m_o c^2 \gamma_\perp}{R^2}\mu P$$

$$e\,\partial F_z/\partial z = \frac{m_o c^2 \gamma_\perp}{2R^2}\mu P$$

where $\frac{m_o c^2 \gamma_\perp}{R}\mu P = \frac{Ne^2}{\pi R^2}\ln\frac{8R}{b} = \frac{Qe}{\pi R^2}\ln\frac{8R}{b}$.

Hence the effective radial and axial forces on a particle of the beam are

$$\mathcal{F}_r = \frac{m_o c^2 \gamma_1}{R}\left[\mu P - \frac{x}{R}\,\mu P\right] \qquad \text{and}$$

$$\mathcal{F}_z = \frac{m_o c^2 \gamma_1}{R}\,\frac{z}{R}\,\frac{\mu P}{2}, \qquad \text{where} \quad x = r - R,$$

in agreement with Eqns. (3.1) and (3.2) of the Soviet report.

APPENDIX

To evaluate $\iint K\,dS' \cong \iint \ln \frac{8R}{r'}\,dS'$, we may introduce the coördinates

$$\left.\begin{aligned} r'\cos\theta' &= x' = \xi\, a \cos\psi \\ r'\sin\theta' &= y' = \xi\, b \sin\psi \end{aligned}\right\} \quad \begin{aligned} &0 \leq \xi \leq 1 \\ &0 \leq \psi \leq 2\pi, \end{aligned}$$

with

$$r' = \sqrt{x'^2 + y'^2} = \xi\sqrt{a^2\cos^2\psi + b^2\sin^2\psi}$$

and

$$\frac{\partial(x', y')}{\partial(\xi, \psi)} = ab\,\xi.$$

Then

$$\iint K\,dS' = ab\int_{\xi=0}^{1}\int_{\psi=0}^{2\pi} \xi \ln \frac{8R}{\xi\sqrt{a^2\cos^2\psi + b^2\sin^2\psi}}\,d\xi\,d\psi$$

$$= 4ab\int_{\xi=0}^{1}\xi\,d\xi\int_{\psi=0}^{\pi/2}\left[\ln\left(\frac{8R}{a\xi}\right) - \frac{1}{2}\ln\left(1 - \frac{a^2-b^2}{a^2}\sin^2\psi\right)\right]d\psi$$

$$= 2\pi ab\int_{\xi=0}^{1}\xi \ln\frac{16R}{(a+b)\xi}\,d\xi$$

[see, for example, I. S. Gradshteyn and I. M. Ryzhik, "Table of Integrals, Series, and Products," Sect. 4.226(2), p. 528], and finally

$$\iint K\,dS' \cong \pi ab \ln \frac{16R}{a+b}$$

$$= \pi ab \ln \frac{8R}{\bar{b}}.$$

where $\bar{b} = \frac{a+b}{2}$.

II. DYNAMICAL CONSIDERATIONS

We are familiar with the focussing characteristics of a purely magnetostatic field and recognize that analysis of such phenomena is simplified by the fact that the magnetic field does no work on the particle. Thus, in particular, the speed and mass of a particle remain constant, and the dynamical behaviour is described in just the same way for a relativistic particle as for a classical (non-relativistic) particle -- save that the relativistic mass $m = m_0/\sqrt{1 - v^2/c^2}$ is employed to relate mechanical momentum to velocity.

The situation is different, however, for a charged particle in an electrostatic field -- or, more generally, for a particle acted upon by a conservative force derivable from a scalar potential function. In this case the focussing effect of the field will be distinctly different for non-relativistic (N-R) and for ultra-relativistic (U-R) particles. If we restrict our attention to fields with axial symmetry and that possess a median plane, the striking differences arise in evaluating the radial betatron-oscillation frequency, ν_r.

The equations for small-amplitude oscillation about a circular equilibrium orbit can be derived with confidence from general principles of analytical mechanics -- for example using the Routhian or, perhaps more directly, by employing the Principle of Least Action. It may be more informative, however, to attempt a simple, more physical treatment that proceeds directly from the force equation.

Particle in a Pure Magnetostatic Field

In the case of a pure magnetostatic field, one writes

$$m\ddot{r} = qvB_z + \frac{mv^2}{r},$$

in which m is the relativistic mass, and recalls that m and v^2 are constants of the motion. One may then make an expansion about a circle of radius r_o, writing $r = r_o + x$ to obtain

$$m\ddot{x} = qvB_{z_o}\left(1 + \left[\frac{r}{B_z}\frac{\partial B_z}{\partial r}\right]_o \cdot \frac{x}{r_o}\right) + \frac{mv^2}{r_o}\left(1 - \frac{x}{r_o}\right).$$

Then to obtain a homogeneous differential equation of motion, one sets $qvB_{z_o} = -\frac{mv^2}{r_o}$ and makes the identification $(r/B_z)(\partial B_z/\partial r) = -n$ to obtain

$$m\ddot{x} = m\frac{v^2}{r_o^2}(n - 1)\cdot x,$$

$$\ddot{x} + \omega^2(1 - n)x = 0,$$

or, with primes denoting differentiation with respect to θ,

$$x'' + (1 - n)x = 0,$$

whence

$$\nu_r^2 = 1 - n.$$

Particle in an Electrostatic Field

In the case of a charged particle moving in an electrostatic field, it is expedient to write the "centrifugal force" as $\omega(p_\theta/r)$, where p_θ is the mechanical angular momentum and constitutes a constant of the motion in this case. [In lowest order, moreover, we approximate $\frac{d}{dt}(m\dot{r})$ by $m\ddot{r}$.]

In the non-relativistic limit, $\omega \doteq \frac{p_\theta}{m_o r^2}$, while in the ultra-relativistic limit, $\omega \cong c/r$. Accordingly, one has in these limiting cases:

N-R:

$$m_o\ddot{r} = qE_r + \frac{p_\theta^2}{m_o r^3}$$

U-R:

$$m\ddot{r} = qE_r + \frac{p_\theta c}{r^2}$$

and, on expanding, obtains

N-R:

$$m_o\ddot{x} = qE_r\left(1+\left[\frac{r}{E_r}\frac{\partial E_r}{\partial r}\right]_o\frac{x}{r_o}\right) + \frac{p_\theta^2}{m_o r_o^3}\left(1 - 3\frac{x}{r_o}\right)$$

$$= \frac{p_\theta^2}{m_o r_o^4}(n_{elec} - 3)\cdot x$$

$$= m_o\frac{v^2}{r_o^2}(n_{elec} - 3)\cdot x$$

U-R:

$$m\ddot{x} = qE_r\left(1+\left[\frac{r}{E_r}\frac{\partial E_r}{\partial r}\right]_o\frac{x}{r_o}\right) + \frac{p_\theta c}{r_o^2}\left(1 - 2\frac{x}{r_o}\right)$$

$$= \frac{p_\theta c}{r_o^3}(n_{elec} - 2)\cdot x$$

$$= m\frac{c^2}{r_o^2}(n_{elec} - 2)\cdot x$$

or

N-R:

$$\ddot{x} + \omega^2(3 - n_{elec})\cdot x = 0$$

$$x'' + (3 - n_{elec})\cdot x = 0$$

$$\nu_r^2 = 3 - n_{elec}.$$

U-R:

$$\ddot{x} + \omega^2(2 - n_{elec})\cdot x = 0$$

$$x'' + (2 - n_{elec})\cdot x = 0$$

$$\nu_r^2 = 2 - n_{elec}.$$

[The non-relativistic result $\nu_r^2 = 3 - n_{elec}$ is familiar from celestial mechanics -- specifically, in an inverse-square central-force field: (i) $p_\theta^2/(2m_o r^2)$ is known to represent an equivalent centrifugal potential, so $p_\theta^2/(m_o r^3)$ represents the radial force arising from this centrifugal potential, and (ii) with $n = 2$, the result $\nu_r^2 = 3 - 2 = 1$ describes the closed character of elliptical orbits.]

A similar, but slightly more tedious analysis leads to the general result for the electrostatic case:

$$\underline{\underline{\nu_r^2 = (3 - \beta^2) - n_{elec}.}}$$

ok

Electrostatic and Magnetostatic Field

An analysis may be made in a similar spirit for the ultra-relativistic case when both magnetostatic and electrostatic fields are present. In this case the quantity p_θ that we take to be a constant of the motion is the dynamical angular momentum plus $\frac{q}{c}rA$, where A is the (azimuthally directed) vector potential from which the magnetic field can be derived. Hence the centrifugal force is written

$$\omega\frac{p_\theta - \frac{q}{c}rA}{r} = \frac{p_\theta - \frac{q}{c}rA}{r^2}c. \tag{1}$$

We thus write, as the radial equation of motion,

$$m\ddot{r} = qE_r + \frac{q}{c}\cdot c\cdot B_z + \frac{p_\theta - \frac{q}{c}rA}{r^2}c.$$

On expansion one obtains

$$m\ddot{r} = qE_{r_0} + q\left.\frac{\partial E_r}{\partial r}\right|_0 x + q\left.\frac{\partial B_z}{\partial r}\right|_0 x + \frac{p_\theta - \frac{q}{c}(rA)_0}{r_0^2}c\left(1 - 2\frac{x}{r_0}\right) - \frac{q}{r_0^2}\left.\frac{\partial(rA)}{\partial r}\right|_0 x.$$

The inhomogeneous terms on the right are removed by selecting

$$\frac{p_\theta - \frac{q}{c}(rA)_0}{r_0^2}c = -q(E_{r_0} + B_{z_0}) \tag{2}$$

(which physically balances the "centrifugal force" at the equilibrium orbit by the force arising at that radius from the electric and magnetic fields), with the result

$$m\ddot{x} = q\left.\frac{\partial E_r}{\partial r}\right|_0 x + q\left.\frac{\partial B_z}{\partial r}\right|_0 x + 2(E_{r_0} + B_{z_0})\frac{x}{r_0} - qB_{z_0}\frac{x}{r_0}$$

$$= q\,\frac{2E_{r_0} + B_{z_0} + \left[r\left(\frac{\partial E_r}{\partial r} + \frac{\partial B_z}{\partial r}\right)\right]_0}{r_0}\,x. \tag{3}$$

The expression given by Eqn. (1) on this page is equal, however, simply to the mechanical linear momentum (in the θ direction) times c/r; i.e., to mc^2/r. Our differential equation (3) thus, with the aid of (2), can be put into the form

$$m\ddot{x} = q\frac{mc^2}{r_0^2}\,\frac{2E_{r_0} + B_{z_0} + \left[r\left(\frac{\partial E_r}{\partial r} + \frac{\partial B_z}{\partial r}\right)\right]_0}{-q\left(E_{r_0} + B_{z_0}\right)}\,x$$

$$\ddot{x} = -\left(\frac{c}{r_0}\right)^2 \frac{2E_{r_0} + B_{z_0} + \left[r\left(\frac{\partial E_r}{\partial r} + \frac{\partial B_z}{\partial r}\right)\right]_0}{E_{r_0} + B_{z_0}}\,x$$

$$x'' + \frac{2E_{r_0} + B_{z_0} + \left[r\left(\frac{\partial E_r}{\partial r} + \frac{\partial B_z}{\partial r}\right)\right]_0}{E_{r_0} + B_{z_0}}\,x = 0$$

$$\nu_r^2 = \left.\frac{2E_r + B_z + r\left(\frac{\partial E_r}{\partial r} + \frac{\partial B_z}{\partial r}\right)}{E_r + B_z}\right|_0 = 1 + \left.\frac{E_r + r\left(\frac{\partial E_r}{\partial r} + \frac{\partial B_z}{\partial r}\right)}{E_r + B_z}\right|_0 .$$

Similarly, for the axial motion, we undertake an expansion of the force equation about the assumed median plane of symmetry:

$$m\ddot{z} = qE_z - \frac{q}{c}\cdot c\cdot B_r$$

$$= q\left.\frac{\partial E_z}{\partial z}\right|_0 z - q\left.\frac{\partial B_r}{\partial z}\right|_0 z$$

$$= q\frac{mc^2}{r_0}\,\frac{\left[\frac{\partial E_z}{\partial z} - \frac{\partial B_r}{\partial z}\right]_0}{-q(E_{r_0}+B_{z_0})}\,z$$

$$\ddot{z} = -\left(\frac{c}{r_0}\right)^2 \frac{\left[r\left(\frac{\partial E_z}{\partial z} - \frac{\partial B_r}{\partial z}\right)\right]_0}{E_{r_0} + B_{z_0}}\,z$$

$$z'' + \frac{\left[r\left(\frac{\partial E_z}{\partial z} - \frac{\partial B_r}{\partial z}\right)\right]_0}{E_{r_0} + B_{z_0}}\,z = 0$$

$$\nu_z^2 = \left.\frac{r\left(\frac{\partial E_z}{\partial z} - \frac{\partial B_r}{\partial z}\right)}{E_r + B_z}\right|_0 .$$

The result found for ν_r^2 will be seen to be consistent with the usual result (p.6) for a purely magnetostatic field and with that given on p. 7 for a pure electrostatic field in the ultra-relativistic limit.

As shown on the following pages in the Appendix to this Section, an analysis based on more general methods will also lead to these results for the frequencies of small-amplitude betatron oscillations.

APPENDIX

Derivation from a Routhian Function

The equations of motion may be derived from a Lagrangian function that contains the scalar and vector potential functions that respectively account for the electrostatic and magnetostatic fields ($\vec{A} = A(r,z)\hat{e}_\theta$):

$$\mathcal{L} = -m_o c^2 \sqrt{1 - \frac{\dot{r}^2 + \dot{z}^2 + r^2\dot{\theta}^2}{c^2}} + \frac{q}{c} r\dot{\theta} A(r,z) - qV(r,z).$$

The coordinate θ is a "cyclic" variable ($\partial\mathcal{L}/\partial\theta = 0$), so the conjugate momentum is a constant of the motion:

$$p_\theta \equiv \frac{\partial\mathcal{L}}{\partial\dot{\theta}} = \frac{m_o r^2\dot{\theta}}{\sqrt{1 - \frac{\dot{r}^2 + \dot{z}^2 + r^2\dot{\theta}^2}{c^2}}} + \frac{q}{c} r A(r,z)$$

from which

$$\dot{\theta} = \sqrt{\frac{1 - \frac{\dot{r}^2 + \dot{z}^2}{c^2}}{1 + \frac{(p_\theta - \frac{q}{c} rA)^2}{m_o^2 r^2 c^2}}} \cdot \frac{p_\theta - \frac{q}{c} rA}{m_o r^2} .$$

To benefit from the constancy of p_θ it is <u>not</u> correct to replace $\dot{\theta}$ in the Lagrangian by its expression in terms of p_θ and then to regard the result as a suitable Lagrangian function from which to obtain the r and z equations of motion. One can, however, form the Routhian [cf. Goldstein, "Classical Mechanics," Sect. 7-2] for this purpose. The Routhian is found, after some intermediate algebra, to be

$$\mathcal{R} \equiv \mathcal{L} - p_\theta\dot{\theta}$$

$$= -m_o c^2 \sqrt{\left[1 + \frac{(p_\theta - \frac{q}{c} rA)^2}{m_o^2 r^2 c^2}\right] \cdot \left[1 - \frac{\dot{r}^2 + \dot{z}^2}{c^2}\right]} - qV$$

$$\cong -\left(\frac{p_\theta c}{r} - qA\right)\left(1 - \frac{\dot{r}^2 + \dot{z}^2}{2c^2}\right) - qV \qquad \text{in the U-R limit.}$$

This function may be expanded about the circle of radius r_o, omitting derivatives that vanish because of the assumed median-plane symmetry:

$$\mathcal{R} \cong \left(\frac{p_\theta}{r_o} - qA_o\right)\frac{\dot{r}^2+\dot{z}^2}{2c^2} - \frac{p_\theta c}{r_o}\left(1 - \frac{x}{r_o} + \frac{x^2}{r_o^2}\right) + q\cdot\left[\begin{array}{l} A_o + \left.\frac{\partial A}{\partial r}\right|_o x + \frac{1}{2}\left.\frac{\partial^2 A}{\partial r^2}\right|_o x^2 + \frac{1}{2}\left.\frac{\partial^2 A}{\partial z^2}\right|_o z^2 \\ -V_o - \left.\frac{\partial V}{\partial r}\right|_o x - \frac{1}{2}\left.\frac{\partial^2 V}{\partial r^2}\right|_o x^2 - \frac{1}{2}\left.\frac{\partial^2 V}{\partial z^2}\right|_o z^2 \end{array}\right].$$

The radius r_o is to be chosen such that the first-order terms in x are absent from the Routhian, and this requires that

$$\frac{p_\theta c}{r_o^2} + q\left.\frac{\partial A}{\partial r}\right|_o - q\left.\frac{\partial V}{\partial r}\right|_o = 0,$$

or, since $\left.\frac{\partial A}{\partial r}\right|_o = B_{z_o} - \frac{A_o}{r_o}$ and $\left.\frac{\partial V}{\partial r}\right|_o = -E_{r_o}$, that $\frac{p_\theta c}{r_o^2} - q\frac{A_o}{r_o} = -q(B_{z_o} + E_{r_o})$.

Employing this result, noting that $\frac{\partial^2 A}{\partial r^2} = \frac{A}{r^2} - \frac{1}{r}\frac{\partial A}{\partial r} + \frac{\partial B_z}{\partial r}$, and dropping constant terms (that do not affect the equations of motion), the Routhian is expressible as

$$\mathcal{R} = -q\left(B_{z_o}+E_{r_o}\right)\frac{\dot{x}^2+\dot{z}^2}{2c^2}r_o + \left[-\frac{p_\theta c}{r_o^3} + \frac{q}{2}\left(\frac{A_o}{r_o^2} - \frac{1}{r_o}\left.\frac{\partial A}{\partial r}\right|_o + \left.\frac{\partial B_z}{\partial r}\right|_o + \left.\frac{\partial E_r}{\partial r}\right|_o\right)\right]x^2 + \frac{q}{2}\left[\left.\frac{\partial E_z}{\partial z}\right|_o - \left.\frac{\partial B_r}{\partial z}\right|_o\right]z^2$$

$$= -q\left(B_{z_o}+E_{r_o}\right)\frac{\dot{x}^2+\dot{z}^2}{2c^2}r_o + \frac{q}{2}\left[2\,\frac{B_{z_o}+E_{r_o}}{r_o} - \frac{1}{r_o}\left(\frac{A_o}{r_o} + \left.\frac{\partial A}{\partial r}\right|_o\right) + \left.\frac{\partial B_z}{\partial r}\right|_o + \left.\frac{\partial E_r}{\partial r}\right|_o\right]x^2 + \frac{q}{2}\left[\left.\frac{\partial E_z}{\partial z}\right|_o - \left.\frac{\partial B_r}{\partial z}\right|_o\right]z^2$$

$$= -q\left(B_{z_o}+E_{r_o}\right)\frac{\dot{x}^2+\dot{z}^2}{2c^2}r_o + \frac{q}{2}\left[\frac{B_{z_o}+2E_{r_o}}{r_o} + \left.\frac{\partial B_z}{\partial r}\right|_o + \left.\frac{\partial E_r}{\partial r}\right|_o\right]x^2 + \frac{q}{2}\left[\left.\frac{\partial E_z}{\partial z}\right|_o - \left.\frac{\partial B_r}{\partial z}\right|_o\right]z^2.$$

For convenience, the constant factor $-q(B_{z_0} + E_{r_0})/r_0$ may be divided out and the ratio r_0/c identified as $1/\omega$ to obtain the equivalent Routhian:

$$\mathcal{R} = \frac{1}{\omega^2}\frac{\dot{x}^2 + \dot{z}^2}{2} - \frac{\left[B_z + 2E_r + r\left(\frac{\partial B_z}{\partial r} + \frac{\partial E_r}{\partial r}\right)\right]_0 x^2 + \left[r\left(\frac{\partial E_z}{\partial z} - \frac{\partial B_r}{\partial z}\right)\right]_0 z^2}{2(B_z + E_r)_0} .$$

The resulting differential equations of motion then are:

$$\frac{1}{\omega^2}\ddot{x} + \left[\frac{B_z + 2E_r + r\left(\frac{\partial B_z}{\partial r} + \frac{\partial E_r}{\partial r}\right)}{B_z + E_r}\right]_0 \cdot x = 0 \qquad \frac{1}{\omega^2}\ddot{z} + \left[r\,\frac{\frac{\partial E_z}{\partial z} - \frac{\partial B_r}{\partial z}}{B_z + E_r}\right]_0 \cdot z = 0$$

$$x'' + \left[\frac{B_z + 2E_r + r\left(\frac{\partial B_z}{\partial r} + \frac{\partial E_r}{\partial r}\right)}{B_z + E_r}\right]_0 \cdot x = 0 \qquad z'' + \left[r\,\frac{\frac{\partial E_z}{\partial z} - \frac{\partial B_r}{\partial z}}{B_z + E_r}\right]_0 \cdot z = 0$$

and

$$\nu_r^2 = \left[\frac{B_z + 2E_r + r\left(\frac{\partial B_z}{\partial r} + \frac{\partial E_r}{\partial r}\right)}{B_z + E_r}\right]_0 \qquad \nu_z^2 = \left[\frac{r\left(\frac{\partial E_z}{\partial z} - \frac{\partial B_r}{\partial z}\right)}{B_z + E_r}\right]_0 .$$

$$= 1 + \left[\frac{E_r + r\left(\frac{\partial B_z}{\partial r} + \frac{\partial E_r}{\partial r}\right)}{B_z + E_r}\right]_0$$

From these results it is noted that

$$\nu_r^2 + \nu_z^2 = 1 + \left[\frac{E_r + r\left(\frac{\partial B_z}{\partial r} + \frac{\partial E_r}{\partial r}\right) + r\left(\frac{\partial E_z}{\partial z} - \frac{\partial B_r}{\partial z}\right)}{B_z + E_r}\right]_0$$

$$= 1 + \left[r\,\frac{\left(\frac{E_r}{r} + \frac{\partial E_r}{\partial r} + \frac{\partial E_z}{\partial z}\right) - \left(\frac{\partial B_r}{\partial z} - \frac{\partial B_z}{\partial r}\right)}{B_z + E_r}\right] = 1 + \left[r\,\frac{\nabla\cdot\vec{E} - [\nabla\times B]_\theta}{B_z + E_r}\right]_0$$

$$= 1 + 4\pi r\,\frac{\rho - J_\theta}{B_z + E_r}\bigg|_0 = 1 \quad \text{in the limit } \beta \to 1,$$

since then $J_{emu} \to \rho_{esu}$ (for an un-neutralized highly relativistic beam).

Alternative Dynamical Formulation -- Use of the Principle of Least Action

The Principle of Least Action may be written, for a charge q esu, as the variational statement:

$$\delta\int\left(\vec{p}+\frac{q}{c}\vec{A}\right)\cdot d\vec{s}=0 \qquad \text{or} \qquad \delta\int\left[p\,ds+\frac{q}{c}(\vec{A}\cdot\vec{ds})\right]=0,$$

where $$p=\sqrt{\left(p_0-\frac{qV}{c}\right)^2-(m_0c)^2},$$

p_0 being a constant (conservation of energy).

Thus

$$\delta\int\left[\sqrt{\left(p_0-\frac{qV}{c}\right)^2-(m_0c)^2}\;\sqrt{r^2+r'^2+z'^2}+\frac{q}{c}\,rA\right]d\theta=0.$$

This formulation is convenient, in that it leads directly to differential equations for the trajectory, rather than to equations that describe the motion in terms of time.

Radial Motion

Considering r motion only, then

$$\frac{d}{d\theta}\left[\frac{\sqrt{\left(p_0-\frac{qV}{c}\right)^2-(m_0c)^2}}{\sqrt{r^2+r'^2}}\,r'\right]-r\,\frac{\sqrt{\left(p_0-\frac{qV}{c}\right)^2-(m_0c)^2}}{\sqrt{r^2+r'^2}}$$
$$+\frac{q}{c}\,\frac{p_0-\frac{q}{c}V}{\sqrt{\left(p_0-\frac{q}{c}V\right)^2-(m_0c)^2}}\sqrt{r^2+r'^2}\,\frac{\partial V}{\partial r}-\frac{q}{c}\frac{\partial}{\partial r}(rA)=0$$

To avoid terms of order r'^2, etc., one may simplify and write

$$\frac{\sqrt{\left(p_0-\frac{qV}{c}\right)^2-(m_0c)^2}}{r}\,r''-\sqrt{\left(p_0-\frac{qV}{c}\right)^2-(m_0c)^2}$$
$$+\frac{q}{c}\,\frac{p_0-\frac{q}{c}V}{\sqrt{\left(p_0-\frac{q}{c}V\right)^2-(m_0c)^2}}\,r\frac{\partial V}{\partial r}-\frac{q}{c}\frac{\partial}{\partial r}(rA)=0.$$

In a highly-relativistic situation, moreover, namely for $p_0 \gg m_0c$, this last equation may be written

$$\left(p_0-\frac{qV}{c}\right)\frac{r''}{r}-\left(p_0-\frac{qV}{c}\right)+\frac{q}{c}\left(r\frac{\partial V}{\partial r}-\frac{\partial}{\partial r}(rA)\right)=0$$

or

$$r''-r+\frac{q}{c}\,r^2\cdot\frac{\frac{\partial V}{\partial r}-\frac{1}{r}\frac{\partial}{\partial r}(rA)}{p_0-\frac{qV}{c}}=0.$$

Suppose now we write $r = r_0 + x$

$$V = V(r_0) - E_{r_0}\cdot x - \frac{1}{2}(\partial E_r/\partial r)_0 x^2$$

$$\partial V/\partial r = - E_{r_0} - (\partial E_r/\partial r)_0\cdot x$$

and

$$\frac{1}{r}\frac{\partial}{\partial r}(rA) = B_{z_0} + (\partial B_z/\partial r)_0\cdot x\ .$$

Then

$$x'' - r_0 - x + \frac{q}{c}(r_0 + x)^2 \frac{-E_{r_0} - \left.\frac{\partial E_r}{\partial r}\right|_0 x - B_{z_0} - \left.\frac{\partial B_z}{\partial r}\right|_0 x}{p_0 - \frac{q}{c}V(r_0) + \frac{q}{c}E_{r_0}\cdot x} = 0.$$

For this equation to be satisfied by $x \equiv 0$, we must set $p_0 - \frac{q}{c}V(r_0) = -\frac{q}{c}r_0(E_r + B_z)_0$, whereupon one obtains

$$x'' - r_0 - x + \frac{(r_0 + x)^2}{r_0}\ \frac{E_{r_0} + \left.\frac{\partial E_r}{\partial r}\right|_0 x + B_{z_0} + \left.\frac{\partial B_z}{\partial r}\right|_0 x}{E_{r_0} + B_{z_0} - E_{r_0}\frac{x}{r_0}}$$

or, in first order,

$$x'' + \left[1 + \left.\frac{E_r + r\left(\frac{\partial E_r}{\partial r} + \frac{\partial B_z}{\partial r}\right)}{E_r + B_z}\right|_0\right] x = 0$$

Thus,

$$\nu_r^2 = 1 + \left.\frac{E_r + r\left(\frac{\partial E_r}{\partial r} + \frac{\partial B_z}{\partial r}\right)}{E_r + B_z}\right|_0 .$$

<u>Axial Motion</u>

Again from the variational statement representing the application of the Principle of Least Action to the present problem, one obtains for the z-motion (with $x = 0$):

$$\frac{d}{d\theta}\left[\frac{\sqrt{(p_0 - \frac{qV}{c})^2 - (m_0 c)^2}}{\sqrt{r^2 + r'^2 + z'^2}}\, z'\right] + \frac{q}{c}\frac{p_0 - \frac{q}{c}V}{\sqrt{(p_0 - \frac{qV}{c})^2 - (m_0 c)^2}}\sqrt{r^2 + r'^2 + z'^2}\ \frac{\partial V}{\partial z}$$

$$- \frac{q}{c}\, r\,\frac{\partial A}{\partial z} = 0,$$

or, to the order of accuracy required,

$$\left(p_0 - \frac{qV}{c}\right)\frac{z''}{r} + \frac{q}{c}\, r\left(\frac{\partial V}{\partial z} - \frac{\partial A}{\partial z}\right) = 0\ ;$$

i.e.,

$$z'' + \frac{q}{c}\, r^2\ \frac{\frac{\partial V}{\partial z} - \frac{\partial A}{\partial z}}{p_0 - \frac{qV}{c}} = 0.$$

We next write $V = V(r_o) - E_{z_o} \cdot z - \frac{1}{2}(\partial E_z/\partial z)_o \cdot z^2 = V(r_o) - \frac{1}{2}(\partial E_z/\partial z)_o \cdot z^2$

$$\partial V/\partial z = - E_{z_o} - (\partial E_z/\partial z)_o \cdot z = - (\partial E_z/\partial z)_o \cdot z$$

and $$\partial A/\partial z = - B_{r_o} - (\partial B_r/\partial z)_o \cdot z = - (\partial B_r/\partial z)_o \cdot z \,,$$

the last forms being written by virtue of the symmetry of the field with respect to the plane $z = 0$ where the ring is assumed to be situated. Finally, we set $p_o - \frac{q}{c} V(r_o) = - \frac{q}{c} r_o (E_r + B_z)_o$, as before (p. 14).

Thus we obtain

$$z'' + r_o \left. \frac{\frac{\partial E_z}{\partial z} - \frac{\partial B_r}{\partial z}}{E_r + B_z} \right|_o z = 0$$

and hence

$$\nu_z^2 = \left. \frac{r\left(\frac{\partial E_z}{\partial z} - \frac{\partial B_r}{\partial z}\right)}{E_r + B_z} \right|_o .$$

[Note: r_o denotes the radial coordinate of the actual center of the beam.]

III. APPLICATION TO THE ELECTRON RING

For a ring of total charge Q ($Q < 0$ for an electron ring), actual mean major radius R, average minor radius $\bar{b}$, and composed of particles moving with relativistic speeds ($\beta \cong 1$), the "bias fields" are (for Q in esu and $I = \frac{Q}{2\pi R}$ emu):

$$E_r^{ring} = \frac{Q}{2\pi R^2} \ln \frac{8R}{\bar{b}} \tag{1}$$

$$B_z^{ring} = \frac{I}{R} \ln \frac{8R}{\bar{b}} = \frac{Q}{2\pi R^2} \ln \frac{8R}{\bar{b}} \tag{2}$$

and the field "gradients" may be taken to be such that

$$R\left[\frac{\partial E_r^{ring}}{\partial r} + \frac{\partial B_z^{ring}}{\partial r}\right] = R\frac{\partial F_r^{ring}}{\partial r} = -\frac{Q}{\pi R^2} \ln \frac{8R}{\bar{b}} \tag{3}$$

$$R\left[\frac{\partial E_z^{ring}}{\partial z} - \frac{\partial B_r^{ring}}{\partial z}\right] = R\frac{\partial F_z^{ring}}{\partial z} = \frac{Q}{2\pi R^2} \ln \frac{8R}{\bar{b}}\,. \tag{4}$$

It is noted that if we form $\frac{1}{R}$ times the sum of Eqns (1), (3), and (4), we obtain zero, in consistency with the condition

$$\nabla\cdot\vec{E} - [\nabla\times\vec{B}]_\theta \equiv \left(\frac{E_r}{r} + \frac{\partial E_r}{\partial r} + \frac{\partial E_z}{\partial z}\right) - \left(\frac{\partial B_r}{\partial z} - \frac{\partial B_z}{\partial r}\right) = 4\pi\rho - 4\pi J_\theta = 0$$

for $\beta = 1$.

8/6

To compare with the Soviet work we introduce the notation of I. N. Ivanov et al. [JINR Report P9-4132] by writing

$$\mu P = \frac{|Qe|}{\pi R p c} \ln \frac{8R}{\bar{b}}$$

$$= \frac{|Q|}{\pi B_g R^2} \ln \frac{8R}{\bar{b}}\,,$$

where B_g denotes the magnitude of the total effective guide field, including self electric and magnetic fields as well as the externally applied magnetic field. Thus the bias fields may be written

$$E_r^{ring} = \pm B_g \frac{\mu P}{2}$$

$$B_z^{ring} = \pm B_g \frac{\mu P}{2}$$

and the field gradients as

$$R\left[\frac{\partial E_r^{ring}}{\partial r} + \frac{\partial B_z^{ring}}{\partial r}\right] = \mp B_g \mu P$$

$$R\left[\frac{\partial E_z^{ring}}{\partial z} - \frac{\partial B_r^{ring}}{\partial z}\right] = \pm B_g \frac{\mu P}{2},$$

for positive or negative charges respectively.

The guide field, and hence the applied field, will be negative for positive charges and currents, so

$$\mp B_g = B_a \pm B_g \mu P \quad \text{and hence} \quad B_a = \mp B_g (1 + \mu P) \text{ is the applied field.}$$

This applied field contributes the gradients

$$\frac{\partial B_z^{appl}}{\partial r} = \frac{\partial B_r^{appl}}{\partial z} = -B_a \frac{n}{R} = \pm B_g \frac{n(1 + \mu P)}{R}$$

that of course must be included in evaluating the focussing action of the total field.

Accordingly,

$$\nu_r^2 = 1 + \frac{E_r + R\left(\frac{\partial B_z}{\partial r} + \frac{\partial E_r}{\partial r}\right)}{B_z + E_r}$$

$$= 1 + \frac{E_r^{ring} + R\left(\frac{\partial B_z^{ring}}{\partial r} + \frac{\partial E_r^{ring}}{\partial r}\right) + R\,\frac{\partial B_z^{appl.}}{\partial r}}{\mp B_g}$$

$$= 1 - \frac{\mu P}{2} + \mu P - n(1 + \mu P)$$

$$= 1 - n(1 + \mu P) + \frac{\mu P}{2} \qquad (5a)$$

$$= (1 - n)(1 + \mu P) - \frac{\mu P}{2} \qquad (5b)$$

and

$$\nu_z^2 = \frac{R\left(\frac{\partial E_z}{\partial z} - \frac{\partial B_r}{\partial z}\right)}{B_z + E_r}$$

$$= \frac{R\left(\frac{\partial E_z^{ring}}{\partial z} - \frac{\partial B_r^{ring}}{\partial z}\right) - R\,\frac{\partial B_r^{appl.}}{\partial z}}{\mp B_g}$$

$$= -\frac{\mu P}{2} + n(1 + \mu P)$$

$$= n(1 + \mu P) - \frac{\mu P}{2}\,. \tag{6}$$

The results found for v_r^2 and v_z^2 agree with those given by the Soviet authors (cf. their Eqns. (4.7)). The results expressed by (5a) and by (6) appear reasonable, moreover, in that the effect of the focussing index n for the applied field is enhanced by the factor $1 + \mu P$, thereby taking account of the fact that this applied field must be strengthened by this factor (or the particle momentum correspondingly decreased) to compensate for the outwardly directed electric and magnetic forces that arise at the center of the beam from the self fields (bias fields) of the ring. The supplemental terms, $+\frac{\mu P}{2}$ in (5a) and $-\frac{\mu P}{2}$ in (6) then describe the inherent focussing characteristics (focussing for radial motion and defocussing for axial motion) of these self fields.

It is noted that, as expected (p. 12), $v_r^2 + v_z^2 = 1$ for the (highly relativistic) beam considered here.

IV. EFFECT OF "IMAGES" ON THE INCOHERENT (SINGLE-PARTICLE) "TUNE"

Images, if present, can act to shift the betatron-oscillation frequencies of individual particles oscillating in a given toroidal beam, and such effects may prove useful in the operation of an electron-ring device. The images may arise because of the presence of material cylinders external or internal to the beam (or from cylinders in both locations) – if the cylinders are conducting, they may be taken to impose the boundary conditions $E_t = 0$, $B_n = 0$ (A.C.-magnetic boundary condition) on the fields, whereas a dielectric cylinder of high specific inductive capacity may be regarded as essentially (although in principle only approximately) imposing on the electric field a boundary condition similar to that which applies at a conducting surface. A dielectric cylinder thus appears to provide a means (similar to the conducting "comb" employed by the Soviet workers) for separating the electric- and magnetic-image effects and so can result in avoiding the strong cancellation often occurring between forces of electric and of magnetic origin.

The image fields may be present both as additional "bias fields" and as fields whose "gradients" are of importance. They basically have the character of toroidal fields – just as for the direct self fields of the ring – but, with a separation of electric and magnetic boundary surfaces (or with ions present in the beam), toroidal effects may be of secondary importance in some cases of interest. In many cases, moreover, it may prove adequate to estimate the bias fields and gradients as if these quantities resulted from the proximity of a straight beam to a planar boundary.

The image fields of a charge-current ring in a cylindrical surface can be expressed in terms of integrals over modified Bessel functions (of order 0 or 1), and the relevant integrals evaluated numerically with the computer. Thus, for a conducting cylinder of radius T external to (but co-axial with) a ring beam of major radius r_0, it was shown in paper ERAC-38 of the 1968 ERA Symposium Proceedings that the electric field of the "images" could be expressed by the scalar potential function

$$V = -\frac{2}{\pi}\frac{Q}{r_0}\int_0^\infty \frac{K_0(Sx)}{I_0(Sx)}\, I_0(x)\, I_0\!\left(\frac{r}{r_0}x\right) \cos\frac{z}{r_0}x\; dx ,$$

where $S = T/r_0$ and a similar expression (involving the Bessel functions I_1, K_1) can be written for the vector potential of the magnetic image-field.

From such an analysis, the bias fields can be written

$$E_r = \frac{Q}{2\pi R^2} K = \pm K \cdot B_g \mu$$

$$B_z = \mp \beta \bar{L} B_g \mu ,$$

where approximately (for S near unity) the coefficients are such that

$$K \cong \frac{1}{S_E - 1} , \qquad \bar{L} \cong \frac{1}{S_m - 1} ,$$

as would be expected for a straight beam near a planar boundary. [Note, for an external cylinder, and a positive beam, E_r is radially outward and B_z is to the left (i.e., directed in the negative-z direction), as expected.]

Similarly, the gradients may be expressed so that

$$r_o \left(\frac{\partial E_r}{\partial r} + \beta \frac{\partial B_z}{\partial r} \right)_o = \left\{ -K + 4 \left[\frac{\epsilon_{1,E}}{(S_E - 1)^2} - \beta^2 \frac{\epsilon_{1,M}}{(S_m - 1)^2} \right] \right\} \frac{Q}{2\pi R^2}$$

$$= \pm B_g \left\{ -K + 4 \left[\frac{\epsilon_{1,E}}{(S_E - 1)^2} - \beta^2 \frac{\epsilon_{1,m}}{(S_m - 1)^2} \right] \right\} \mu$$

$$r_o \left(\frac{\partial E_z}{\partial z} - \beta \frac{\partial B_r}{\partial z} \right)_o = \mp 4 B_g \left[\frac{\epsilon_{1,E}}{(S_E - 1)^2} - \beta^2 \frac{\epsilon_{1,m}}{(S_m - 1)^2} \right] \mu ,$$

with $\epsilon_{1,E}$ and $\epsilon_{1,M}$ each approximately $\frac{1}{8}$, but with a strong cancellation avoided if the boundary surfaces for the electric and magnetic fields are such that $S_E \neq S_m$.

To pull all this together we may write (for a beam neutralized by a fraction f of stationary ions), including internal self fields that would be present with a straight beam (uniform density, radial and axial semi-axes a and b respectively, $\bar{b} = \frac{a + b}{2}$):

Bias Fields

$$E_r = \underset{\text{Toroid Term}}{(1-f)\frac{Q}{2\pi r_0^2}\ln\frac{8r_0}{\bar{b}}} + \underset{\text{Electrostatic - Image Term}}{(1-f)\frac{Q}{2\pi r_0^2}K}$$

$$= \pm B_g(1-f)\left[\frac{P}{2} + K\right]\mu$$

$$B_z = B_a \pm B_g\frac{\mu P}{2} \mp \beta \bar{L} B_g \mu$$

$$= B_a \pm B_g\left[\frac{P}{2} - \beta\bar{L}\right]\mu .$$

Gradients*

$$r_0\left(\frac{\partial E_r}{\partial r} + \beta\frac{\partial B_z}{\partial r}\right)_0 = \underset{\text{Applied Field}}{-n\beta B_a} \mp \underset{\text{Toroid}}{B_g(1-f)\mu P} \pm \underset{\text{Image}}{B_g\left\{-(1-f)K + 4\left[\frac{(1-f)\epsilon_{1,E}}{(S_E-1)^2} - \beta^2\frac{\epsilon_{1,m}}{(S_m-1)^2}\right]\right\}\mu} \pm \underset{\text{Internal (Teng)}}{B_g\frac{2r_0^2}{a\bar{b}}\left(\frac{1}{\gamma^2}-f\right)\mu}$$

$$= -n\beta B_a \pm B_g\left\{\frac{2r_0^2}{a\bar{b}}\left(\frac{1}{\gamma^2}-f\right) - (1-f)P - (1-f)K + 4\left[\frac{(1-f)\epsilon_{1,E}}{(S_E-1)^2} - \beta^2\frac{\epsilon_{1,m}}{(S_m-1)^2}\right]\right\}\mu$$

$$r_0\left(\frac{\partial E_z}{\partial z} - \beta\frac{\partial B_r}{\partial z}\right)_0 = n\beta B_a \pm B_g(1-f)\frac{\mu P}{2} \mp 4B_g\left[\frac{(1-f)\epsilon_{1,E}}{(S_E-1)^2} - \beta^2\frac{\epsilon_{1,m}}{(S_m-1)^2}\right]\mu \pm B_g\frac{2r_0^2}{b\bar{b}}\left(\frac{1}{\gamma^2}-f\right)\mu$$

$$= n\beta B_a \pm B_g\left\{\frac{2r_0^2}{b\bar{b}}\left(\frac{1}{\gamma^2}-f\right) + (1-f)\frac{P}{2} - 4\left[\frac{(1-f)\epsilon_{1,E}}{(S_E-1)^2} - \beta^2\frac{\epsilon_{1,m}}{(S_m-1)^2}\right]\right\}\mu ,$$

where B_a is the (Z-directed) applied magnetic field, and $n \equiv -\frac{r}{B_a}\frac{\partial B_a}{\partial r}$ is the field index of this applied field.

---

*See Note on the last page of this section.

The net guide field, and hence B_a, will be negative for positive charges and currents — hence

$$\mp \beta B_g = \beta B_a \pm B_g(1-f)\left[\frac{P}{2}+K\right]\mu \pm \beta B_g\left[\frac{P}{2}-\beta\bar{L}\right]\mu\,,$$

or, only retaining the factor β as different from unity in the combination $(1-f)K - \beta^2\bar{L}$,

$$B_a = \mp B_g\left\{1 + \left[\left(1-\frac{f}{2}\right)P + (1-f)K - \beta^2\bar{L}\right]\mu\right\}.$$

Then

$$\nu_r^2 = 1 + \frac{E_r + r_0\left(\frac{\partial E_r}{\partial r} + \beta\frac{\partial B_z}{\partial r}\right)_0}{B_{z_0} + E_{r_0}}$$

$$= 1 + \frac{\left[\begin{array}{l}\pm B_g(1-f)\left[\frac{P}{2}+K\right]\mu \pm n B_g\left\{1+\left[\left(1-\frac{f}{2}\right)P + (1-f)K - \beta^2\bar{L}\right]\mu\right\} \\ \pm B_g\left\{\frac{2r_0^2}{ab}\left(\frac{1}{\gamma^2}-f\right) - (1-f)P - (1-f)K + 4\left[\frac{(1-f)\epsilon_{1,E}}{(S_E-1)^2} - \beta^2\frac{\epsilon_{1,M}}{(S_m-1)^2}\right]\right\}\mu\end{array}\right]}{\mp B_g}$$

$$= 1-n - \left\{\frac{2r_0^2}{ab}\left(\frac{1}{\gamma^2}-f\right) - (1-f)\frac{P}{2} + 4\left[\frac{(1-f)\epsilon_{1,E}}{(S_E-1)^2} - \beta^2\frac{\epsilon_{1,m}}{(S_m-1)^2}\right] + n\left[\left(1-\frac{f}{2}\right)P + (1-f)K - \beta^2\bar{L}\right]\right\}\mu\,.$$

and

$$\nu_z^2 = \frac{r_0\left(\dfrac{\partial E_z}{\partial z} - \beta\dfrac{\partial B_r}{\partial z}\right)_0}{B_{z_0} + E_{r_0}}$$

$$= \frac{\left[\begin{array}{l} \overbrace{\mp nB_g \mp nB_g\left[\left(1-\frac{f}{2}\right)P + (1-f)K - \beta^2\bar{L}\right]\mu}^{n\,B_a} \\ \qquad \underbrace{\pm B_g\left\{\frac{2r_0^2}{b\bar{b}}\left(\frac{1}{\gamma^2}-f\right) + (1-f)\frac{P}{2} - 4\left[\frac{(1-f)\epsilon_{1,E}}{(S_E-1)^2} - \beta^2\frac{\epsilon_{1,m}}{(S_m-1)^2}\right]\right\}\mu}_{\text{from "gradient" terms}} \end{array}\right]}{\mp B_g}$$

$$= n + \left\{\begin{array}{c} -\frac{2r_0^2}{b\bar{b}}\left(\frac{1}{\gamma^2}-f\right) - (1-f)\frac{P}{2} + 4\left[\frac{(1-f)\epsilon_{1,E}}{(S_E-1)^2} - \beta^2\frac{\epsilon_{1,M}}{(S_m-1)^2}\right] \\ + n\left[\left(1-\frac{f}{2}\right)P + (1-f)K - \beta^2\bar{L}\right] \end{array}\right\}\mu,$$

where we recall $\bar{b} = \frac{a+b}{2}$.

It is noted from these expressions that

$$\nu_r^2 + \nu_z^2 = 1 - \frac{2r_0^2}{\bar{b}}\left(\frac{1}{a} + \frac{1}{b}\right)\left(\frac{1}{\gamma^2} - f\right)\mu$$

$$= 1 - \frac{4r_0^2}{ab}\mu\left(\frac{1}{\gamma^2} - f\right)$$

$$= 1 - \frac{2}{\pi}\,\frac{Q/(ab)}{B_g}\left(1 - f - \beta^2\right),$$

and so differs from unity only in the familiar way from the effect of the "direct" self fields acting in the region where $\nabla\cdot\vec{E}$ and $\nabla\times\vec{B}$ <u>do not vanish</u>.

If the image terms are discarded and if f is set equal to zero, one obtains from the above formulas for ν_r^2 & ν_z^2:

$$\nu_r^2 = 1 - n + \frac{\mu P}{2} - n\mu P - \frac{2\mu r_0^2}{a\bar{b}}\frac{1}{\gamma^2} = (1-n)(1+\mu P) - \left[\frac{4\mu r_0^2}{a(a+b)\gamma^2} + \frac{\mu P}{2}\right]$$

$$\nu_z^2 = n - \frac{\mu P}{2} + n\mu P - \frac{2\mu r_0^2}{b\bar{b}}\frac{1}{\gamma^2} = n(1+\mu P) - \left[\frac{4\mu r_0^2}{b(a+b)\gamma^2} + \frac{\mu P}{2}\right],$$

in agreement with the results presented by Eqs. (4.7) of the Soviet paper P9-4132 by I. N. Ivanov et al.

Note: The introduction of the fractional-neutralization coefficient f in with the μP terms is not entirely clear, since with $f \neq 0$, the strong cancellation between the effects of electric and magnetic field gradients is lost and the logarithmic term becomes dominated by the larger effects of a straight beam with $\beta \lessapprox 1$ but $f \neq 0$.

It is clear, however, that the factor (1-f) should be appended to the $B_g \frac{\mu P}{2}$ term in the bias electric field E_r and not to the $B_g \frac{\mu P}{2}$ term in the bias magnetic field B_z.

If we now write the μP terms in the gradients as follows:

$$r_o \left(\frac{\partial E_r}{\partial r} + \beta \frac{\partial B_z}{\partial r}\right)_o \cong - B_g (1-f) \mu P$$

and

$$r_o \left(\frac{\partial E_z}{\partial z} - \beta \frac{\partial B_r}{\partial z}\right)_o \cong + B_g (1-f) \frac{\mu P}{2},$$

we find that this procedure is consistent to the extent that then (for these terms only) we have, with $\beta = 1$:

$$\begin{aligned} E_r + r\left(\frac{\partial E_r}{\partial r} + \beta \frac{\partial B_z}{\partial r}\right) + r\left(\frac{\partial E_z}{\partial z} - \beta \frac{\partial B_r}{\partial z}\right) &\equiv r\left(\nabla\cdot\vec{E} - \beta[\nabla\times\vec{B}]_\theta\right) \\ &= B_g\left[(1-f)\frac{\mu P}{2} - (1-f)\frac{\mu P}{2}\right] = 0. \end{aligned}$$

This result for the fields of the beam itself is correct (for $\beta \doteq 1$), since then $\nabla\cdot\vec{E} - [\nabla\times\vec{B}]_\theta = 4\pi\left(\rho_{esu} - J_{emu}\right) \cong 0$ (for $\beta \doteq 1$).

On The Focussing Effects Arising From The Self Fields of a Toroidal Beam*

-- Sequel to ERAN-30 --

L. Jackson Laslett

Lawrence Berkeley Laboratory
University of California
Berkeley, California

October 26, 1972

The present report indicates a revision of results given in earlier notes [ERAN-30] for the oscillation frequencies of an electron in a partially neutralized electron-ring beam subject to toroidal self-field gradients. The need for this revision arises from the observation by Professor M. Reiser that the toroidal contribution to $\partial E_z/\partial z$ is small in comparison to the toroidal term in $\partial B_r/\partial z$ while the toroidal contributions to $\partial E_r/\partial r$ and $\partial B_z/\partial r$ are comparable. Some numerical computations are reported that appear to support this property of the toroidal field gradients.

* Work supported by the U.S. Atomic Energy Commission

CONTENTS

I. Motivation

Stimulated by a Soviet report by Ivanov et al.,[1] notes were prepared by the writer[2] for a Seminar talk in April 1969 concerning the self fields and self-field gradients of a toroidal beam and the focussing effects that arise from the action of these field quantities. The analysis to some degree was an extension of an earlier examination of self fields and self-field gradients as reported in the Proceedings of the 1968 LBL Symposium on Electron Ring Accelerators.[3]

The 1969 notes[2] attempted, in a final Section, to include the effect of partial neutralization of the electron ring beam by stationary ions having a similar (constant density) distribution throughout the cross-section of the beam. This adjustment of the equations for the betatron-oscillation frequencies admittedly was not done carefully, however, since at that stage of the analysis the electric and magnetic field gradients had been combined into quantities $\partial F_r/\partial r = \partial E_r/\partial r + \partial B_z/\partial r$ and $\partial F_z/\partial z = \partial E_z/\partial z - \partial B_r/\partial z$ (for highly-relativistic electrons).

M. Reiser recently has kindly forwarded to the writer an advanced copy of a report[4] in which he re-examines separately the electric and magnetic bias fields and field gradients of a toroidal beam and also evaluates the betatron-oscillation frequencies of electrons of arbitrary energy in a partially neutralized electron ring beam. Reiser's analytic estimates[4] of the field gradients at the center of the ring cross-section indicate that the neutralization factor $f = N_i/N_e$ was incorrectly introduced into the μP terms of the equations given for ν_r^2 and ν_z^2 in the 1969 notes.[2] We have undertaken, therefore, to re-examine these field gradients computationally, treating the electric- and magnetic-field gradients separately, in order to obtain some impression of the accuracy of the convenient simple analytic forms given by Reiser[4] for these quantites.

It is the purpose of the present report to summarize the results of this recent computational work, to indicate the comparison between these results and the simple analytic forms proposed by Reiser,[4] and to note the correction that should be applied to certain terms in the equations of the 1969 notes[2] if Reiser's forms[4] for the self-field gradients are adopted.

II. Equations for Fields and Field Gradients

A. Formulas for Computational Evaluation

The magnetic vector potential for a current-carrying loop has been given by Smythe[5] and an analogous similar expression may be similarly derived[6] for the electrostatic scalar potential of a ring charge of infinitesimal cross-section. The resulting magnetic and electric fields can be obtained from these potentials by differentiation and the resulting expressions integrated numerically over the cross-section of the beam to find the required field components produced by a ring beam. Finally, the desired field gradients can be obtained from these latter quantities by numerical differentiation.

Because considerable interest is attached to the difference between the fields and field gradients of a ring beam in comparison to those that arise from a straight beam, and because the integrations involve integrands with an (integrable) singularity, it is expedient to perform the numerical evaluations not only for the field quantities arising from a ring beam but also directly for the difference between these quantities and those for a straight beam (i.e., for the toroidal contributions).

We consider here a ring charge Q (e.s.u.) or ring current I (e.m.u.)

of major radius R and a circular cross-section of minor radius $b = R/L$. Field quantities will be evaluated either along a radial line passing through the center of the distribution, at $r = R + xb$, or along a line passing through the center of the distribution and parallel to the axis, at $z = yb$. A factor Δ present in the integrands will serve, if set equal to unity, to subtract off the contribution that a straight beam would make in the integral in question.

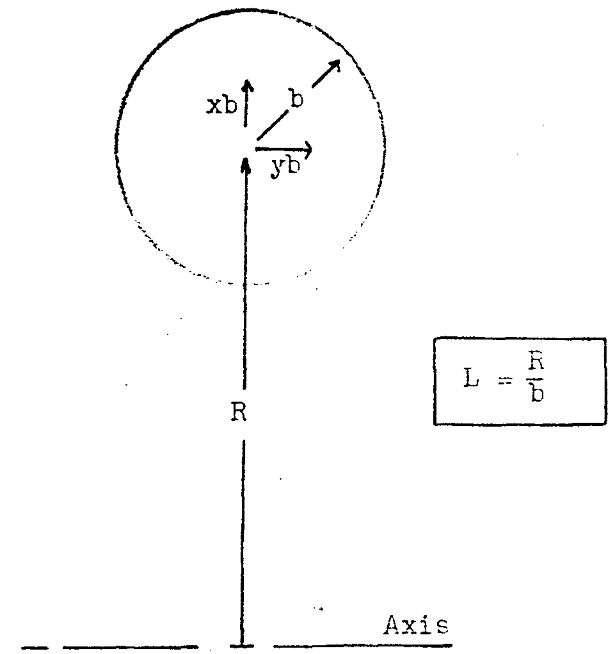

With m_1 denoting the complementary parameter[7] $(m_1 = k'^2 = 1 - k^2 = 1 - m)$ of the complete elliptic integrals K and E, then if

3-41

$$m_1 = \frac{x^2-2xx'\cos\theta'+x'^2}{4L^2+4L(x+x'\cos\theta') + x^2+2xx'\cos\theta'+x'^2} ,$$

$$\frac{\pi^2 b^2}{Q} E_r = \frac{2}{L}\int_{x'=0}^{1}\int_{\theta'=0}^{\pi}\left\{\frac{L+x'\cos\theta'}{(L+x)\sqrt{4L^2+4L(x+x'\cos\theta')+x^2+2xx'\cos\theta'+x'^2}}\left[K + \frac{2L(x-x'\cos\theta')+x^2-x'^2}{x^2-2xx'\cos\theta'+x'^2}E\right]\right.$$

$$\left. - \Delta\cdot\frac{x-x'\cos\theta'}{x^2-2xx'\cos\theta'+x'^2}\right\} x'dx'd\theta'$$

and

$$\frac{\pi b}{2I} B_z = 2 \int_{x'=0}^{1} \int_{\theta'=0}^{\pi} \left\{ \frac{1}{\sqrt{4L^2+4L(x+x'\cos\theta')+x^2+2xx'\cos\theta'+x'^2}} \left[K - \frac{2L(x-x'\cos\theta')+x^2-x'^2\cos 2\theta'}{x^2-2xx'\cos\theta'+x'^2} E \right] + \Delta \cdot \frac{x-x'\cos\theta'}{x^2-2xx'\cos\theta'+x'^2} \right\} x'dx'd\theta'.$$

Also, if

$$m_1 = \frac{y^2-2yx'\sin\theta'+x'^2}{4L^2+4Lx'\cos\theta'+y^2-2yx'\sin\theta'+x'^2} ,$$

then

$$\frac{\pi^2 b^2}{Q} E_z = \frac{1}{L} \int_{x'=0}^{1} \int_{\theta'=0}^{2\pi} \left[2 \frac{L+x'\cos\theta'}{\sqrt{4L^2+4Lx'\cos\theta'+y^2-2yx'\sin\theta'+x'^2}} E - \Delta \right] \cdot \frac{y-x'\sin\theta'}{y^2-2yx'\sin\theta'+x'^2} x'dx'd\theta'$$

and

$$\frac{\pi b}{2I} B_r = \int_{x'=0}^{1} \int_{\theta'=0}^{2\pi} \left\{ \frac{1}{L} \frac{1}{\sqrt{4L^2+4Lx'\cos\theta'+y^2-2yx'\sin\theta'+x'^2}} \left[\frac{2L^2+2Lx'\cos\theta'+y^2-2yx'\sin\theta'+x'^2}{y^2-2yx'\sin\theta'+x'^2} E - K \right] - \Delta \cdot \frac{1}{y^2-2yx'\sin\theta'+x'^2} \right\} (y-x'\sin\theta')x'dx'd\theta'.$$

B. Approximate Analytic Estimates

The approximate analytic estimates for the bias fields at the center of the cross-section are,[3,2,4] in the present notation,

$$\frac{\pi^2 b^2}{Q} E_r \cong \frac{\pi}{2L^2} \ln 8L$$

and

$$\frac{\pi b}{2I} B_z \cong \frac{\pi}{2L} \ln 8L,$$

where $L = R/b$. Similarly, for the field gradients expressed in the present notation, Reiser[4] proposes the expressions

$$\frac{\pi^2 b^3}{Q} \frac{\partial E_r}{\partial r} \cong -\frac{\pi}{2L^3} \ln 8L$$

$$\frac{\pi b^2}{2I} \frac{\partial B_z}{\partial r} \cong -\frac{\pi}{2L^2} \ln 8L$$

$$\frac{\pi^2 b^3}{Q} \frac{\partial E_z}{\partial z} = 0$$

and

$$\frac{\pi b^2}{2I} \frac{\partial B_r}{\partial z} \cong -\frac{\pi}{2L^2} \ln 8L$$

for the toroidal contributions that remain after subtraction of the values that would apply for a straight beam.

It may be noted that these last four expressions imply, for a highly relativistic beam $(I \cong \lambda = \frac{Q}{2\pi R})$,

$$\frac{\pi^2 b^3}{Q} \frac{\partial}{\partial r} [E_r + B_z] \cong - \frac{\pi}{L^3} \ln 8L$$

and

$$\frac{\pi^2 b^3}{Q} \frac{\partial}{\partial z} \left[E_z - B_r\right] \cong \frac{\pi}{2L^3} \ln 8L,$$

in agreement with results previously suggested[2] for $\partial F_r/\partial r$ and $\partial F_z/\partial z$. The self-consistency of the expressions suggested by Reiser[4] with respect to the conditions $\nabla \cdot \vec{E} = 0$ and $[\nabla \times \vec{B}]_\phi = 0$ for the toroidal contributions moreover may be checked, for the forms written above, by forming

$$\frac{1}{L} \left(\frac{\pi^2 b^2}{Q} E_r \right) + \frac{\pi^2 b^3}{Q} \frac{\partial E_r}{\partial r} + \frac{\pi^2 b^3}{Q} \frac{\partial E_z}{\partial z}$$

and

$$\frac{\pi b^2}{2I} \frac{\partial B_r}{\partial z} - \frac{\pi b^2}{2I} \frac{\partial B_z}{\partial r}$$

to obtain zero in each instance.

III. Computations

A. Method

Numerical evaluations of $E_r(r)$, $B_z(r)$, $E_z(z)$, $B_r(z)$ and of the associated derivatives at the center of the cross-section were made for $L = R/b = 40$ and for $L = 10$. The numerical integrations were performed simply by summation of values at the centers of cells (usually of width $\Delta x' = 1/200$, $\Delta\theta' = \pi/400$, although some check runs were made with $\Delta x' = 1/2000$ and with $\Delta\theta' = \pi/4000$ in the angular interval lying within $\pi/8$ of the singularity of the integrand). Because of the singularity of the integrand, the field points were always chosen to be at the corners of such cells, so that the singularity was not directly encountered. Field derivatives were estimated as the weighted average (weights +4/3 and -1/3) of slopes evaluated for points displaced by

$\Delta x = \pm\, 0.05$ and $\pm\, 0.10$ or by $\Delta y = 0.05$ and 0.10

with respect to the center of the cross-section. Consistency checks on the accuracy of the work are provided by noting how well the following identities, relating to div $\vec{E}$ and curl $\vec{B}$, are satisfied:

$$\frac{1}{L}\,\frac{\pi^2 b^2}{Q}\,E_r + \frac{\pi^2 b^3}{Q}\,\frac{\partial E_r}{\partial r} + \frac{\pi^2 b^3}{Q}\,\frac{\partial E_z}{\partial z} = \begin{cases} 2\pi/L & \text{for } \Delta = 0 \\ 0 & \text{for } \Delta = 1, \end{cases}$$

$$\frac{\pi b^2}{2I}\,\frac{\partial B_r}{\partial z} - \frac{\pi b^2}{2I}\,\frac{\partial B_z}{\partial r} = \begin{cases} 2\pi & \text{for } \Delta = 0 \\ 0 & \text{for } \Delta = 1. \end{cases}$$

B. The Bias Fields

The bias fields, as obtained computationally at the center of the cross-section for $L = 40$ and for $L = 10$, are given in the following table.

Also shown are the values suggested for these quantities by the simple analytic forms $\frac{\pi^2 b^2}{Q} E_r \cong \frac{\pi}{2L^2} \ln 8L$ and $\frac{\pi b}{2I} B_z \cong \frac{\pi}{2L} \ln 8L$.

$L = \frac{R}{b}$	$\frac{\pi^2 b^2}{Q} E_r$		$\frac{\pi b}{2I} B_z$	
	Computer	Analytic[(a)]	Computer	Analytic[(b)]
40	0.004681	0.005663	0.226518	0.226521
10	0.053065	0.068833	0.68811	0.68833

(a) $\frac{\pi}{2L^2} \ln 8L$ (b) $\frac{\pi}{2L} \ln 8L$

The analytic estimates for the magnetic bias field are thus seen to be in good agreement with the computational results, but the similar estimates for the bias electric field exceed the computational values by some 20 or 30 percent in these cases.

C. The Field Gradients

The field gradients, as obtained for the toroidal contributions ($\Delta = 1$, the gradients of a straight beam thus being removed) are similarly tabulated below.

$L = \frac{R}{b}$	$\frac{\pi^2 b^3}{Q} \frac{\partial E_r}{\partial r}$		$\frac{\pi b^2}{2I} \frac{\partial B_z}{\partial r}$	
	Computer	Analytic[a]	Computer	Analytic[b]
40	-0.0001417	-0.0001416	-0.003694	-0.005663
10	-0.00634	-0.00688	-0.04276	-0.06883

(a) $- \frac{\pi}{2L^3} \ln 8L$

(b) $- \frac{\pi}{2L^2} \ln 8L$

$L = \frac{R}{b}$	$\frac{\pi^2 b^3}{Q} \frac{\partial E_z}{\partial z}$		$\frac{\pi b^2}{2I} \frac{\partial B_r}{\partial z}$	
	Computer	Analytic	Computer	Analytic[c]
40	0.00002465	0	-0.003695	-0.005663
10	0.0010307	0	-0.04276	-0.06883

(c) $- \frac{\pi}{2L^2} \ln 8L$

The field derivatives can be seen to satisfy the conditions $\nabla \cdot \vec{E} = 0$ and $[\nabla \times \vec{B}]_\phi = 0$ acceptably well, the derivative $\partial E_z/\partial z$ is seen to be rather small, and $\partial E_r/\partial r$ is close to its analytic estimate. The magnitudes of the analytic estimates for the derivatives $\partial B_z/\partial r$ and $\partial B_r/\partial z$ of the magnetic field components, however, evidently exceed the computational values by some 50 to 60 percent in these examples.

IV. The Betatron Oscillation Frequencies for a Relativistic Electron Ring Beam

If we accept the conclusion that $\partial E_z/\partial z = 0$ for the toroidal component and also adopt the other convenient approximate analytic expressions cited above, we may proceed to estimate the betatron-oscillation frequencies for relativistic electrons ($\beta = v/c \cong 1$), neglecting any possible complications due to the "polarization" to which Reiser has called attention on p. 15 of his report.[4] As in our earlier work,[2] we may make use of the Soviet notation[1]

$$\mu = \frac{\nu}{\gamma} = \frac{N_e r_c}{2\pi R\gamma} \doteq \frac{|\dot{Q}e|}{2\pi Rpc} = \left|\frac{Q}{2\pi\ B_g\ R^2}\right|$$

for a highly relativistic electron of momentum p in a total "effective" (magnetic and electric) field B_g, and

$$P = 2\ \ln \frac{8R}{\bar{b}}$$

with[2]

$$\bar{b} = \frac{a + b}{2}\ .$$

The toroidal terms in the fields and field gradients then are, as noted,[4]

$$E_r = \frac{Q}{2\pi R^2}\ \ln \frac{8R}{\bar{b}} = \pm\frac{1}{2}\ B_g\ \mu P,$$

$$B_z = \frac{I}{R}\ \ln \frac{8R}{\bar{b}} = \frac{Q}{2\pi R^2} = \pm\frac{1}{2}\ B_g\ \mu P,$$

$$R\frac{\partial E_r}{\partial r} = \mp \frac{1}{2} B_g \mu P, \quad R\frac{\partial B_z}{\partial r} = \mp \frac{1}{2} B_g \mu P$$

$$R\frac{\partial E_z}{\partial z} = 0, \quad \text{and} \quad -R\frac{\partial B_r}{\partial z} = \pm\frac{1}{2} B_g \mu P$$

when no ions are present to effect some neutralization of the beam.

A fraction f of ions will act to reduce the electric fields, by a factor (1-f), while causing no change in the toroidal magnetic fields of the beam. We thus replace the equations written immediately above by

$$E_r = \pm \frac{1-f}{2} B_g \mu P, \qquad B_z = \pm\frac{1}{2} B_g \mu P,$$

$$R\frac{\partial E_r}{\partial r} = \mp \frac{1-f}{2} B_g \mu P, \qquad R\frac{\partial B_z}{\partial r} = \mp\frac{1}{2} B_g \mu P,$$

$$R\frac{\partial E_z}{\partial z} = 0, \qquad -R\frac{\partial B_r}{\partial z} = \pm\frac{1}{2} B_g \mu P,$$

and also write (using these supplemental bias fields) for the externally applied magnetic field the relation

$$B_a = \mp B_g\{1 + [(1 - \frac{f}{2})P + (1-f)K - \beta^2 \bar{L}]\mu\}$$

that was given on p. 22 of Ref. 2 (where K and $\bar{L}$ characterize possible electric and magnetic image fields as might arise from an image cylinder co-axial with the ring beam).[8,9]

We now proceed to re-do the analysis attempted in Ref. 2 to evaluate

$$\nu_r^{\,2} = 1 + \frac{E_r + R\left(\frac{\partial E_r}{\partial r} + \beta\frac{\partial B_z}{\partial r}\right)}{B_z + E_r}$$

and

$$\nu_z^{\,2} = \frac{R\left(\frac{\partial E_z}{\partial z} - \beta\frac{\partial B_r}{\partial z}\right)}{B_z + E_r},$$

where the expression $B_z + E_r$ that we have written in the denominator (for $\beta \doteq 1$) is the quantity $\mp B_g$. We substitute[8]

$$E_r = \pm B_g(1-f)\left[\frac{P}{2} + K\right]\ \mu$$

and[10]

$$R\left(\frac{\partial E_r}{\partial r} + \beta\frac{\partial B_z}{\partial r}\right) = \underbrace{-\,n\beta B_a}_{\text{Applied Field}} \ \underbrace{\pm\, B_g\,\frac{2R^2}{a\bar{b}}\left(\frac{1}{\gamma^2} - f\right)\mu}_{\text{Internal, for a straight beam}}$$

$$\underbrace{\mp\, B_g\left[\frac{1-f}{2} + \frac{1}{2}\right]\mu P}_{\text{toroidal terms}}$$

$$\underbrace{\pm\, B_g\left\{-(1-f)K + 4\left[(1-f)\frac{\epsilon_{1,E}}{(S_E-1)^2} - \beta^2\frac{\epsilon_{1,M}}{(S_M-1)^2}\right]\right\}\mu,}_{\text{image term}}$$

$$R\left(\frac{\partial E_z}{\partial z} - \beta\frac{\partial B_r}{\partial z}\right) = n\beta B_a \pm B_g\,\frac{2R^2}{b\bar{b}}\left(\frac{1}{\gamma^2} - f\right)\mu$$

$$\pm\,\frac{1}{2}\,B_g\,\mu P$$

$$\mp\, 4\,B_g\left[(1-f)\frac{\epsilon_{1,E}}{(S_E-1)^2} - \beta^2\frac{\epsilon_{1,M}}{(S_M-1)^2}\right]\mu.$$

We then obtain

$$\nu_r^2 = 1-n - \left\{ \frac{2R^2}{a\bar{b}} \left(\frac{1}{\gamma^2} - f \right) - \frac{P}{2} + 4 \left[\frac{(1-f)\epsilon_{1,E}}{(S_E-1)^2} - \beta^2 \frac{\epsilon_{1,M}}{(S_M-1)^2} \right] \right.$$

$$\left. + n \left[(1 - \frac{f}{2})P + (1-f)K - \beta^2 \bar{L} \right] \right\} \mu,$$

$$\nu_z^2 = n + \left\{ - \frac{2R^2}{b\bar{b}} \left(\frac{1}{\gamma^2} - f \right) - \frac{P}{2} + 4 \left[\frac{(1-f)\epsilon_{1,E}}{(S_E-1)^2} - \beta^2 \frac{\epsilon_{1,M}}{(S_M-1)^2} \right] \right.$$

$$\left. + n \left[(1 - \frac{f}{2})P + (1-f)K - \beta^2 \bar{L} \right] \right\} \mu,$$

where we have set $\beta \doteq 1$ throughout except in a few selected terms where a strong cancellation may occur when β is close to unity. The expressions written for ν_r^2 and ν_z^2 differ from those of Ref 2 in that the n-free terms $\pm \frac{1}{2} \mu P$ in these expressions no longer contain the factor (1-f) -- as a result of our recognizing Reiser's observation that the toroidal contributions to $R \left(\frac{\partial E_z}{\partial z} - \beta \frac{\partial B_r}{\partial z} \right)$ arise primarily from the magnetic term. The results just written for ν_r^2 and ν_z^2 thus agree, when image effects are ignored, with the results given by Reiser[4] when we set $\beta = 1$ and neglect terms proportional to the square of μP in his expressions. When, in addition, f is set equal to zero the results can be seen then to coincide with those given by Ivanov et al.[1] It may be noted, finally, that the complete expressions given for ν_r^2 and ν_z^2 are such that, as expected,

$$\nu_r^2 + \nu_z^2 = 1 - 4 \frac{\mu R^2}{ab} \left(\frac{1}{\gamma^2} - f \right)$$

and so differ from unity only in the familiar way from the effect of the "direct" self-fields acting in the region where they make non-vanishing contributions to $\nabla \cdot \vec{E}$ and $\nabla \times \vec{B}$.

V. Acknowledgements

It is a pleasure to express our appreciation to Professor Reiser for his kindness in sending us an advance copy of his report concerning toroidal space-charge effects and our thanks to Mrs. Barbara (Harold) Levine for assistance with the numerical work reported here.

VI. References and Notes

1. I.N. Ivanov et al., JINR Report P9-4132 (1968).

2. L. Jackson Laslett, ERAN-30 (Notes for a Seminar on Electron-Ring Accelerators, LBL, 15 April 1969).

3. L. Jackson Laslett, in Symposium on Electron Ring Accelerators (UCRL-18103, LBL, February 1968), papers ERAN 7-8, pp. 275-290.

4. M. Reiser,* "On the Equilibrium Orbit and Linear Oscillations of Charged Particles in Axisymmetric E x B Fields and Application to the Electron Ring Accelerator", Report IPP 0/14 (Max-Planck-Institut für Plasma Physik, Munich-Garching, July 1972).

5. William R. Smythe, "Static and Dynamic Electricity", Ed. 2 (McGraw-Hill Book Co., New York, 1950), Sect. 7.10, pp. 270-271.

6. With

$$m = k^2 = \frac{4r_{ring}\, r_{obs}}{(r_{ring} + r_{obs})^2 + (\Delta z)^2}$$

or

$$m_1 = k'^2 = \frac{(r_{ring} - r_{obs})^2 + (\Delta z)^2}{(r_{ring} + r_{obs})^2 + (\Delta z)^2},$$

$$V = \iint \frac{\rho_V\, dS'}{s} = 4 \iint (\rho_V\, dS') \frac{r_{ring}}{\sqrt{(r_{ring} + r_{obs})^2 + (\Delta z)^2}} K,$$

where ρ_V denotes the volume density of charge.

7. L.M. Milne-Thomson, "Elliptic Integrals", in "Handbook of Mathematical Functions" (Milton Abramowitz and Irene A. Stegun, Eds.), Ch. 17, p. 590 (Dover Publications, New York, 1965).

8. We take the electric and magnetic fields arising from an image cylinder of radius S·R to be, respectively,

$$E_r = \frac{Q_{net}}{2\pi R^2} K = \pm (1-f) K B_g \mu$$

---

* Dr. Reiser's report was written at Garching while he was on leave from the University of Maryland.

and

$$B_z = \mp \beta \bar{L} B_g \mu,$$

where approximately (for S near unity)[2]

$$K \cong \frac{1}{S_E - 1} \text{ and } \bar{L} \cong \frac{1}{S_M - 1}.$$

The total electrostatic field that contributes to equilibrium at the equilibrium radius then is[2]

$$E_r = \pm \frac{1-f}{2} B_g \mu P \pm (1-f)K B_g \mu = \pm B_g(1-f)\left[\frac{P}{2} + K\right] \mu,$$

and the corresponding total magnetic field is

$$B_z = B_a \pm \frac{1}{2} B_g \mu P \mp \beta \bar{L} B_g \mu = B_a \pm B_g\left[\frac{P}{2} - \beta \bar{L}\right]\mu.$$

9. The condition for equilibrium at the equilibrium radius R is written[2,8]

$$\mp \beta B_g = \beta B_a \pm B_g(1-f)\left[\frac{P}{2} + K\right]\mu$$
$$\pm \beta B_g\left[\frac{P}{2} - \beta \bar{L}\right]\mu ,$$

whence, if we retain the factor β as different from unity only in the combination $(1-f)K - \beta^2 \bar{L}$,

$$B_a = \mp B_g \{1 + [(1 - \frac{f}{2})P + (1-f)K - \beta^2 \bar{L}] \mu\} .$$

10. The image field gradients are written in terms of coefficients $\epsilon_{1,E}$ and $\epsilon_{1,M}$:[2]

$$E_r + R\frac{\partial E_r}{\partial r} = - R\frac{\partial E_z}{\partial z} \doteq 4 \frac{\epsilon_{1,E}}{(S_E-1)^2} \frac{Q_{net}}{2\pi R^2} = \pm 4(1-f)B_g \frac{\epsilon_{1,E}}{(S_E-1)^2} \mu$$

$$\beta R \frac{\partial B_z}{\partial r} = \beta R \frac{\partial B_r}{\partial z} \doteq - 4\beta^2 \frac{\epsilon_{1,M}}{(S_M-1)^2} \frac{Q}{2\pi R^2} = \mp 4\beta^2 B_g \frac{\epsilon_{1,M}}{(S_M-1)^2} \mu.$$

Normally $\epsilon_{1,E}$ and $\epsilon_{1,M}$ will each be approximately $\frac{1}{8}$.

DECAY OF IMAGE CURRENTS IN A PLANE GEOMETRY*

L. Jackson Laslett

Lawrence Radiation Laboratory
University of California
Berkeley, California

July 28, 1969

I. Introduction (Motivation)

The effect of eddy currents induced in an infinite plane conducting sheet (infinitely thin, with a surface resistivity $\rho_{\text{emu per square}}$)[1] has been elegantly solved by Maxwell[2] in terms of images that recede from the sheet with a speed $\frac{\rho}{2\pi}$. Since problems may arise in which the conducting boundary is not a plane sheet, it may be instructive to attempt to find Maxwell's solution for the plane sheet by other methods, for some particular type of source. Such an exercise may then facilitate (illuminate) the solution of additional problems of interest.

We consider below an example in which the magnetic field can be characterized by a vector potential with a single non-zero Cartesian component (A_z). The problem will be taken to be one in which there is no z dependence, and most specifically will be concerned with a case in which two long parallel wires run parallel to the sheet at $y = -(h \mp s/2)$ (with respect to the sheet at $y = 0$) and carry currents $\pm I_{emu}\,\hat{e}_z$ respectively. By taking the limit $s \to o$, while $Is \to P$, we simplify the source to a two-dimensional current loop of infinitesimal width.

As is customary[2] in this type of problem, displacement currents are regarded as ignorable.

II. Solution in the Spirit of Maxwell's Solution

For the specific case considered the vector potential of the isolated sources $\pm I(t)$ at $y = -(h \mp s/2)$ would be

$$- P(t) \frac{\partial}{\partial h} \left[\ln \frac{1}{x^2 + (y+h)^2} \right] = 2\,P(t) \frac{y+h}{x^2 + (y+h)^2} \text{ , where}$$

$P(t) = \underset{s \to o}{L} \left[I(t) \cdot s \right]$, for $s \to o$. We wish to write

$$A_z = 2\,P(t) \frac{y+h}{x^2 + (y+h)^2} + A^I\,(x, y; t),$$

where A^I denotes the vector potential of the eddy currents induced in the infinite plane conducting sheet (at $y = o$) and may be expected to be an even function of y.

Since the induced currents are of the amount (emu/cm)

$$- \frac{1}{\rho} \frac{\partial A_z}{\partial t} \bigg|_{y=o} ,$$

we require

$$- \frac{\partial A_z}{\partial y} \bigg|_{y=o^+} + \frac{\partial A_z}{\partial y} \bigg|_{y=o^-} = - \frac{4\pi}{\rho} \frac{\partial A_z}{\partial t} \bigg|_{y=o} ;$$

Since A^I is even in y, this may be written

$$2 \frac{\partial A^I}{\partial y} \bigg|_{y=o^+} = \frac{4\pi}{\rho} \left[2\,P'(t) \frac{h}{x^2 + h^2} + \frac{\partial A^I}{\partial t} \bigg|_{y=o} \right]$$

or

$$\left.\frac{\partial A^I}{\partial y}\right|_{y=o^+} = \frac{2\pi}{\rho}\left[2\,P'(t)\,\frac{h}{x^2+h^2} + \left.\frac{\partial A^I}{\partial t}\right|_{y=o}\right],$$

or

$$\left.\frac{\partial A^I}{\partial t}\right|_{y=o} - \frac{\rho}{2\pi}\left.\frac{\partial A^I}{\partial y}\right|_{y=o^+} = -\,2\,P'(t)\,\frac{h}{x^2+h^2}\,.$$

In addition, we of course require $\frac{\partial^2 A^I}{\partial x^2} + \frac{\partial^2 A^I}{\partial y^2} = 0 \; (y \neq o)$.

A solution for A^I in the Maxwell form is readily seen to be

$$A^I = -\,2\int_{-\infty}^{t} \frac{dP(\tau)}{d\tau}\,\frac{h + |y| + v\,(t-\tau)}{x^2 + [h + |y| + v\,(t-\tau)]^2}\,d\tau$$

with $v = \frac{\rho}{2\pi}$, for which A^I receives contributions only from values of $\frac{dP}{dt}$ that occur at times less than t. One thus may write:

$$A_z = 2\,P(t)\,\frac{y+h}{x^2+(y+h)^2} - 2\int_{-\infty}^{t} \frac{dP(\tau)}{d\tau}\,\frac{h + |y| + \frac{\rho}{2\pi}(t-\tau)}{x^2 + [h + |y| + \frac{\rho}{2\pi}(t-\tau)]^2}\,d\tau$$

$$= 2\,P(t)\left[\frac{y+h}{x^2+(y+h)^2} - \frac{|y|+h}{x^2+(|y|+h)^2}\right]$$

$$+\,2\left(\frac{\rho}{2\pi}\right)\int_{-\infty}^{t} P(\tau)\,\frac{[|y| + h + \frac{\rho}{2\pi}(t-\tau)]^2 - x^2}{\{[|y| + h + \frac{\rho}{2\pi}(t-\tau)]^2 + x^2\}^2}\,d\tau$$

[by partial integration]

$$= 2\,P(t)\left[\frac{y+h}{x^2+(y+h)^2} - \frac{|y|+h}{x^2+(|y|+h)^2}\right]$$

$$+ 2\left(\frac{\rho}{2\pi}\right)\int_0^\infty \frac{(|y|+h+\frac{\rho}{2\pi}\xi)^2 - x^2}{[(|y|+h+\frac{\rho}{2\pi}\xi)^2+x^2]^2}\; P(t-\xi)\,d\xi .$$

Thus for an abrupt step-function form of $P(t)$, in which P changes suddenly from zero to unity at $t = t_o$ — i.e., $P' = \delta(t - t_o)$ — the first form shown for A_z becomes

$$A_z = 2\left\{\frac{y+h}{x^2+(y+h)^2} - \frac{|y|+h+\frac{\rho}{2\pi}(t-t_o)}{x^2+[\,|y|+h+\frac{\rho}{2\pi}(t-t_o)]^2}\right\},\quad (t \geqslant t_o)$$

an expression which permits interpretation in terms of Maxwell's general result concerning images. In the present case we have images at $\mp [h + \frac{\rho}{2\pi}(t - t_o)]$ for supplementing the field at $y \gtrless o$, respectively, and hence each of these recedes from the sheet at the speed $\frac{\rho}{2\pi}$ cm/sec. The "dipole" image at $-[h + \frac{\rho}{2\pi}(t - t_o)]$, which contributes to giving the field in the region $y > o$, is of the opposite polarity to the given source (and completely annuls the effect of the given source for $t = t_o$ and $y > o$); while the dipole image at $+[h + \frac{\rho}{2\pi}(t - t_o)]$, that affects the field in the region $y < o$ (where the given source is situated), is of the same sign as the source (and results in $B_n = B_y = 0$ at the sheet when $t = t_o$).

III. Solution in Terms of Harmonic Series

As before, we write

$$A_z = 2\,P(t)\,\frac{y+h}{x^2+(y+h)^2} + A^I\,(x, y\,;\,t),$$

and recognize that the image contribution A^I to the vector potential will be even in y. Again we require that A^I be a harmonic function ($\nabla^2 A^I = 0$, for $y \neq o$) and that (p.3)

$$\left.\frac{\partial A^I}{\partial t}\right|_{y=o} - \frac{\rho}{2\pi}\left.\frac{\partial A^I}{\partial y}\right|_{y=o+} = -\,2\,P'(t)\,\frac{h}{x^2+h^2}\,.$$

We now employ the harmonic-function representation

$$A^I = \int_{k=o}^{\infty} F(k,\,t)\,e^{-k|y|}\cos kx\,dk$$

and note that[3]

$$\frac{h}{x^2+h^2} = \int_o^{\infty} e^{-kh}\cos kx\,dk.$$

We thus require

$$\int_o^{\infty}\frac{\partial F}{\partial t}\cos kx\,dk + \frac{k\rho}{2\pi}\int_o^{\infty} F\cdot\cos kx\,dk = -\,2\,P'(t)\int_o^{\infty} e^{-kh}\cos kx\,dk;$$

i.e., we require

$$\frac{\partial F}{\partial t} + \frac{k\rho}{2\pi}F = -\,2\,P'(t)\,e^{-kh}.$$

As a solution of this last, first-order differential equation in t, we take[4]

$$F(k,t) \doteq -2\,e^{-kh}\int_{-\infty}^{t} P'(\xi)\, e^{-\frac{k\rho}{2\pi}(t-\xi)}\, d\xi .$$

Then

$$A^{I} = -2\int_{k=0}^{\infty} dk \int_{\xi=-\infty}^{t} d\xi\, P'(\xi)\, e^{-k[h + |y| + \frac{\rho}{2\pi}(t-\xi)]}\cos kx$$

$$= -2\int_{-\infty}^{t} P'(\xi)\, d\xi \int_{k=0}^{\infty} dk\, e^{-k[h + |y| + \frac{\rho}{2\pi}(t-\xi)]}\cos kx$$

$$\doteq -2\int_{-\infty}^{t} P'(\xi)\, \frac{|y| + h + \frac{\rho}{2\pi}(t-\xi)}{x^2 + [|y| + h + \frac{\rho}{2\pi}(t-\xi)]^2}\, d\xi$$

(ref. 3),

and

$$A_z = 2\,P(t)\,\frac{y+h}{x^2 + (y+h)^2} - 2\int_{-\infty}^{t} P'(\xi)\,\frac{|y| + h + \frac{\rho}{2\pi}(t-\xi)}{x^2 + [|y| + h + \frac{\rho}{2\pi}(t-\xi)]^2}\, d\xi,$$

in agreement with the result of the preceding section (p. 4).

IV. Frequency Analysis

Time dependent electrical problems are frequently analyzed in terms of Fourier components (each with a time dependence characterized by $e^{j\omega t}$). It is evident that such an approach may not be the most direct in the present example, but use of the technique may provide a bridge to connect with results obtained by the use of the Fourier time-spectrum method.

Suppose we consider a unit step function for P(t), occuring at t_o.[8] Then

$$P(t) = \frac{1}{2} + \frac{1}{\pi}\int_0^{\infty} \frac{\sin \omega(t - t_o)}{\omega}\, d\omega$$

$$= \frac{1}{2} + \frac{1}{2\pi}\int_{-\infty}^{\infty} \frac{\sin \omega(t - t_o)}{\omega}\, d\omega .$$

For each of the individual a.c. components of P(t) -- e.g., $\frac{1}{2\pi}\,\frac{\sin \omega(t - t_o)}{\omega}\, d\omega$ -- the vector potential will require a supplementary image contribution to account for the presence of the infinite plane conducting sheet. One may seek, then, to refer to the solution of the steady-state problem for an a.c. 2-D double line-current source situated a distance h below an infinite plane conductor (of d.c. surface resistance ρ emu per square). If, as assumed in the previous sections of this note, the sheet is <u>infinitely</u> <u>thin</u>, the sheet will exhibit this same surface resistance ρ emu per square for all <u>finite</u> a.c. frequencies.

For an a.c. source, $P(\omega,t) = \frac{1}{2\pi}\,\frac{\sin \omega(t - t_o)}{\omega}$, the equation for F (bottom of 1st page of Section III),

$$\frac{\partial F}{\partial t} + \frac{k\rho}{2\pi}F = -\,2\,P'(t)\,e^{-kh} ,$$

becomes $$\frac{\partial F}{\partial t} + \frac{k\rho}{2\pi}F = -\,\frac{1}{\pi}\,e^{-kh}\cos \omega(t - t_o)$$

with the steady-state solution

$$F = -\frac{1}{\pi}\;\frac{\omega \sin \omega(t - t_o) + \frac{k\rho}{2\pi} \cos \omega(t - t_o)}{\omega^2 + \left(\frac{k\rho}{2\pi}\right)^2}\; e^{-kh} \quad .$$

Thus, for this Fourier component,

$$A^I(\omega,t) = -\frac{1}{\pi}\int_{k=o}^{\infty} \frac{\omega \sin \omega(t - t_o) + \frac{k\rho}{2\pi} \cos \omega(t - t_o)}{\omega^2 + \left(\frac{k\rho}{2\pi}\right)^2}\; e^{-k(|y| + h)} \cos kx\, dk$$

and, for the entire step-function wave-form,

$$A^I(t) = -\frac{1}{\pi}\int_{k=o}^{\infty} dk \;\; e^{-k(|y| + h)} \cos kx \int_{-\infty}^{\infty} d\omega \;\; \frac{\omega \sin \omega(t - t_o) + \frac{k\rho}{2\pi} \cos \omega(t - t_o)}{\omega^2 + \left(\frac{k\rho}{2\pi}\right)^2} \quad .$$

Performing the integration over ω we obtain [9, 3]

$$A^I(t) = -2\int_{k=o}^{\infty} e^{-k\,[|y| + h + \frac{\rho}{2\pi}(t - t_o)]} \cos kx\, dk$$

$$= -2\,\frac{|y| + h + \frac{\rho}{2\pi}(t - t_o)}{x^2 + [|y| + h + \frac{\rho}{2\pi}(t - t_o)]^2} \;,$$

in agreement with the previous results when interpreted for a unit step function for $P(t)$ that occurs at $t = t_o$.

V. Character of the Solution

If one recalls the solution for A^I when P(t) has the character of a step function (P_o), namely (for a step at t = o):

$$A^I = -2P_o \frac{|y| + h + vt}{x^2 + (|y| + h + vt)^2}, \quad \text{with } v = \frac{\rho}{2\pi},$$

it is evident that A^I does not fall off exponentially with increasing time.

For large t, $A^I \cong -2\frac{P_o}{vt}$.

Also, for the image fields,

$$B_x^I = \frac{\partial A^I}{\partial y} = \pm 2P_o \frac{(|y| + h + vt)^2 - x^2}{[(|y| + h + vt)^2 + x^2]^2} \cong \pm 2\frac{P_o}{(vt)^2}$$

and

$$B_y^I = -\frac{\partial A^I}{\partial x} = -4P_o \frac{x \cdot (|y| + h + vt)}{[(|y| + h + vt)^2 + x^2]^2} \cong -4\frac{P_o x}{(vt)^3} .$$

Finally,

$$\frac{\partial B_x{}^I}{\partial y} = \frac{\partial B_y{}^I}{\partial x} = 4P_o \frac{3x^2 - (|y| + h + vt)^2}{[(|y| + h + vt)^2 + x^2]^3} (|y| + h + vt) \cong -4\frac{P_o}{(vt)^3}$$

while of course

$$\frac{\partial B_x^I}{\partial x} + \frac{\partial B_y^I}{\partial y} = 0,$$ with each individual term

asymptotically $\mp 12 \dfrac{P_o x}{(vt)^4}$, $\pm 12 \dfrac{P_o x}{(vt)^4}$ respectively.

Specifically, at $y = -h$,

$$\frac{A^I(t)}{A^I(t=o)} = \left(1 + \frac{vt}{2h}\right) \frac{\left(\frac{x}{2h}\right)^2 + 1}{\left(\frac{x}{2h}\right)^2 + \left(1 + \frac{vt}{2h}\right)^2}$$

$$\frac{B_x^I(t)}{B_x^I(t=o)} = \frac{\left(1 + \frac{vt}{2h}\right)^2 - \left(\frac{x}{2h}\right)^2}{1 - \left(\frac{x}{2h}\right)^2} \cdot \frac{[1 + \left(\frac{x}{2h}\right)^2]^2}{\left[\left(1 + \frac{vt}{2h}\right)^2 + \left(\frac{x}{2h}\right)^2\right]^2}$$

$$\frac{B_y^I(t)}{B_y^I(t=o)} = \left(1 + \frac{vt}{2h}\right) \frac{\left[\left(\frac{x}{2h}\right)^2 + 1\right]^2}{\left[\left(\frac{x}{2h}\right)^2 + \left(1 + \frac{vt}{2h}\right)^2\right]^2}$$

$$\frac{[\partial B_x/\partial y]_t}{[\partial B_x/\partial y]_{t=o}} = \left(1 + \frac{vt}{2h}\right) \frac{3\left(\frac{x}{2h}\right)^2 - \left(1 + \frac{vt}{2h}\right)^2}{3\left(\frac{x}{2h}\right)^2 - 1} \quad \frac{\left[\left(\frac{x}{2h}\right)^2 + 1\right]^3}{\left[\left(\frac{x}{2h}\right)^2 + \left(1 + \frac{vt}{2h}\right)^2\right]^3} .$$

VI. Numerical Calculations

By way of illustration, numerical values have been computed for the ratios listed on the preceding sheet (end of Section V). Values for these ratios are tabulated vs. $W \equiv x/h$ and $R \equiv vt/h$. The attached program permits these computations to be performed readily by use of the LRL BRF facility.

```
↑EDIT
OK

L

             W = 0
      10     PRINT9, W
             R = 0
      20     U = W/2
             S = R/2
             F = 1 + S
             N1 = 1 + U*U
             D1 = F*F + U*U
             N2 = F*F - U*U
             D2 = 1 - U*U
             N3 = 3*U*U - F*F
             D3 = 3*U*U - 1
             A = F*N1/D1
             BX = (N2/D2)*((N1/D1)**2)
             BY = F*((N1/D1)**2)
             DBXDY = F*(N3/D3)*((N1/D1)**3)
             PRINT9, R, A, BX, BY, DBXDY
             IF (R .GE. 5.9) GO TO 30
             R = R + 0.3
             GO TO 20
      30     IF (W .GE. 2.9) GO TO 40
             W = W + 0.3
             GO TO 10
      40     STOP
OK
```

Numerical results are given in the Appendix.

VII. References and Notes

* Work supported by the U.S. Atomic Energy Commission.

1 The resistance ρ abohms per square is equal to 10^9 times the surface resistance expressed as ohms per square. The velocity $\frac{\rho_{emu}}{2\pi}$ may be expressed in M.K.S. units as $\frac{2\rho}{\mu_o}$. Thus $v_{M/sec} = \frac{2\,\rho_{ohms}}{\mu_o} =$

$$\frac{\rho_{ohms}}{2\pi \times 10^{-7}} = \frac{10^{-9}\,\rho_{emu}}{2\pi \times 10^{-7}} = \frac{1}{100}\,\frac{\rho_{emu}}{2\pi}, \quad \text{or} \quad v_{cm/sec} = \frac{\rho_{emu}}{2\pi} .$$

2 J.C. Maxwell, "Electricity and Magnetism", Sec. 654 ff. See also Sir James Jeans, "Electricity and Magnetism", Sec. 538 ff; W.R. Smythe, "Static and Dynamic Electricity" (Ed. 2), Sec. 11.10.

3 B.O. Peirce, "A Short Table of Integrals", #506, p. 64.

4 If one wishes, one may seek the solution to the differential equation for F, as a function of t, by the use of the Laplace transformation [cf. J.C. Jaeger, "An Introduction to the Laplace Transformation" (Methuen, London; Wiley, New York); the Laplace transform is denoted by a bar, and is defined as $\overline{f} \equiv \int_0^\infty e^{-pt} f(t)\,dt$]. Since[5]

$$\overline{\left[\frac{\partial f}{\partial t}\right]} \equiv \int_0^\infty e^{-pt}\,\frac{\partial f}{\partial t}\,dt = fe^{-pt}\Big|_0^\infty + p\int_0^\infty e^{-pt} f(t)\,dt$$

$$= - f(o) + p\bar{f}$$

$$= p\bar{f} \quad \text{if} \quad f(o) = 0 \quad ,$$

then in application to our first-order differential equation for F:

$$p\,\bar{F} + \frac{k\rho}{2\pi}\,\bar{F} = -\,2\bar{P}'\,e^{-kh} \quad \underline{\text{if}} \quad F \doteq 0 \text{ at } t = 0.$$

In this event

$$\bar{F} = -\,2\,\frac{\overline{P'}}{p + \frac{k\rho}{2\pi}}\,e^{-kh}$$

$$\doteq -\,2\,e^{-kh}\left(\overline{\left[e^{-\frac{k\rho}{2\pi}t}\right]\cdot\overline{P'}}\right) \quad . \quad [6]$$

Hence [7]

$$F \quad -\,2\,e^{-kh}\int_{o}^{t} P'(\zeta)\,e^{-\frac{k\rho}{2\pi}(t-\zeta)}\,d\zeta$$

for cases in which $F = 0$ at $t = o$.

More generally (removing the condition that $F = 0$ at $t = 0$), then,

$$F = -\,2e^{-kh}\int_{-\infty}^{t} P'(\zeta)\,e^{-\frac{k\rho}{2\pi}(t-\zeta)}\,d\zeta, \quad \text{as written in the text}$$

(Sect. III of these notes).

[5] J. C. Jaeger, _op_. _cit_., Theorem III, p. 14.

[6] J. C. Jaeger, _op_. _cit_., Table I, p. 3.

7 By use of the convolution theorem, as stated by Jaeger (op. cit.), Theorem IX, p. 90.

8 B. O. Peirce, op. cit., #484, p. 62

9 I. S. Gradshteyn and I. N. Ryzhik, "Table of Integrals, Series, and Products" (Academic Press, New York, 1965), Sect. 3.723, #3 and #2, p. 406.

APPENDIX

Numerical Results

W= 0.00000

R	A	BX	BY	DBXDY
0.00000	1.00000	1.00000	1.00000	1.00000
0.30000	0.86957	0.75614	0.65752	0.65752
0.60000	0.76923	0.59172	0.45517	0.45517
0.90000	0.68966	0.47562	0.32802	0.32802
1.20000	0.62500	0.39063	0.24414	0.24414
1.50000	0.57143	0.32653	0.18659	0.18659
1.80000	0.52632	0.27701	0.14579	0.14579
2.10000	0.48780	0.23795	0.11607	0.11607
2.40000	0.45455	0.20661	0.09391	0.09391
2.70000	0.42553	0.18108	0.07705	0.07705
3.00000	0.40000	0.16000	0.06400	0.06400
3.30000	0.37736	0.14240	0.05374	0.05374
3.60000	0.35714	0.12755	0.04555	0.04555
3.90000	0.33898	0.11491	0.03895	0.03895
4.20000	0.32258	0.10406	0.03357	0.03357
4.50000	0.30769	0.09467	0.02913	0.02913
4.80000	0.29412	0.08651	0.02544	0.02544
5.10000	0.28169	0.07935	0.02235	0.02235
5.40000	0.27027	0.07305	0.01974	0.01974
5.70000	0.25974	0.06747	0.01752	0.01752
6.00000	0.25000	0.06250	0.01563	0.01563

W= 0.30000

R	A	BX	BY	DBXDY
0.00000	1.00000	1.00000	1.00000	1.00000
0.30000	0.87426	0.76361	0.66463	0.68001
0.60000	0.77620	0.60816	0.46346	0.48143
0.90000	0.69771	0.49267	0.33572	0.35253
1.20000	0.63349	0.40694	0.25082	0.26545
1.50000	0.58002	0.34164	0.19224	0.20465
1.80000	0.53482	0.29080	0.15055	0.16099
2.10000	0.49612	0.25046	0.12007	0.12885
2.40000	0.46262	0.21793	0.09728	0.10470
2.70000	0.43334	0.19132	0.07991	0.08620
3.00000	0.40753	0.16929	0.06643	0.07180
3.30000	0.38462	0.15085	0.05582	0.06043
3.60000	0.36413	0.13526	0.04735	0.05133
3.90000	0.34572	0.12195	0.04052	0.04397
4.20000	0.32907	0.11052	0.03493	0.03794
4.50000	0.31395	0.10062	0.03033	0.03297
4.80000	0.30015	0.09198	0.02650	0.02883
5.10000	0.28751	0.08442	0.02329	0.02535
5.40000	0.27590	0.07774	0.02057	0.02241
5.70000	0.26518	0.07183	0.01827	0.01991
6.00000	0.25527	0.06657	0.01629	0.01776

W= 0.60000

R= 0.00000	A= 1.00000	BX= 1.00000	BY= 1.00000	DBXDY= 1.00000
R= 0.30000	A= 0.88743	BX= 0.80653	BY= 0.68482	DBXDY= 0.76192
R= 0.60000	A= 0.79607	BX= 0.65931	BY= 0.43748	DBXDY= 0.58067
R= 0.90000	A= 0.72087	BX= 0.54660	BY= 0.35388	DBXDY= 0.44725
R= 1.20000	A= 0.65811	BX= 0.45922	BY= 0.27070	DBXDY= 0.34928
R= 1.50000	A= 0.60508	BX= 0.39050	BY= 0.20921	DBXDY= 0.27671
R= 1.80000	A= 0.55973	BX= 0.33570	BY= 0.16489	DBXDY= 0.22225
R= 2.10000	A= 0.52056	BX= 0.29140	BY= 0.13219	DBXDY= 0.18082
R= 2.40000	A= 0.48641	BX= 0.25516	BY= 0.10754	DBXDY= 0.14385
R= 2.70000	A= 0.45639	BX= 0.22516	BY= 0.08864	DBXDY= 0.12386
R= 3.00000	A= 0.42981	BX= 0.20008	BY= 0.07389	DBXDY= 0.10407
R= 3.30000	A= 0.40612	BX= 0.17892	BY= 0.06224	DBXDY= 0.08823
R= 3.60000	A= 0.38487	BX= 0.16090	BY= 0.05290	DBXDY= 0.07540
R= 3.90000	A= 0.36571	BX= 0.14545	BY= 0.04534	DBXDY= 0.06492
R= 4.20000	A= 0.34835	BX= 0.13210	BY= 0.03914	DBXDY= 0.05628
R= 4.50000	A= 0.33255	BX= 0.12049	BY= 0.03403	DBXDY= 0.04909
R= 4.80000	A= 0.31811	BX= 0.11034	BY= 0.02976	DBXDY= 0.04307
R= 5.10000	A= 0.30487	BX= 0.10141	BY= 0.02618	DBXDY= 0.03798
R= 5.40000	A= 0.29267	BX= 0.09351	BY= 0.02315	DBXDY= 0.03366
R= 5.70000	A= 0.28141	BX= 0.08649	BY= 0.02057	DBXDY= 0.02997
R= 6.00000	A= 0.27098	BX= 0.08024	BY= 0.01836	DBXDY= 0.02680

W= 0.90000

R= 0.00000	A= 1.00000	BX= 1.00000	BY= 1.00000	DBXDY= 1.00000
R= 0.30000	A= 0.90680	BX= 0.87321	BY= 0.71504	DBXDY= 1.02709
R= 0.60000	A= 0.82602	BX= 0.75305	BY= 0.52486	DBXDY= 0.91977
R= 0.90000	A= 0.75645	BX= 0.64841	BY= 0.39464	DBXDY= 0.78417
R= 1.20000	A= 0.69647	BX= 0.56013	BY= 0.30317	DBXDY= 0.65648
R= 1.50000	A= 0.64453	BX= 0.48645	BY= 0.23738	DBXDY= 0.54683
R= 1.80000	A= 0.59928	BX= 0.42507	BY= 0.18902	DBXDY= 0.45606
R= 2.10000	A= 0.55962	BX= 0.37377	BY= 0.15277	DBXDY= 0.38197
R= 2.40000	A= 0.52464	BX= 0.33070	BY= 0.12511	DBXDY= 0.32173
R= 2.70000	A= 0.49360	BX= 0.29431	BY= 0.10368	DBXDY= 0.27270
R= 3.00000	A= 0.46590	BX= 0.26337	BY= 0.08683	DBXDY= 0.23262
R= 3.30000	A= 0.44106	BX= 0.23689	BY= 0.07341	DBXDY= 0.19968
R= 3.60000	A= 0.41865	BX= 0.21410	BY= 0.06260	DBXDY= 0.17246
R= 3.90000	A= 0.39836	BX= 0.19435	BY= 0.05379	DBXDY= 0.14981
R= 4.20000	A= 0.37990	BX= 0.17716	BY= 0.04656	DBXDY= 0.13086
R= 4.50000	A= 0.36304	BX= 0.16210	BY= 0.04055	DBXDY= 0.11489
R= 4.80000	A= 0.34759	BX= 0.14884	BY= 0.03553	DBXDY= 0.10137
R= 5.10000	A= 0.33338	BX= 0.13712	BY= 0.03131	DBXDY= 0.08955
R= 5.40000	A= 0.32026	BX= 0.12671	BY= 0.02772	DBXDY= 0.07993
R= 5.70000	A= 0.30813	BX= 0.11742	BY= 0.02466	DBXDY= 0.07148
R= 6.00000	A= 0.29637	BX= 0.10911	BY= 0.02203	DBXDY= 0.06413

W= 1.20000

R= 0.00000	A= 1.00000	BX= 1.00000	BY= 1.00000	DBXDY= 1.00000
R= 0.30000	A= 0.92957	BX= 0.98263	BY= 0.75139	DBXDY= -1.84107
R= 0.60000	A= 0.86244	BX= 0.91462	BY= 0.57215	DBXDY= -2.39427
R= 0.90000	A= 0.80081	BX= 0.83046	BY= 0.44228	DBXDY= -3.12197
R= 1.20000	A= 0.74521	BX= 0.74568	BY= 0.34708	DBXDY= -2.99061
R= 1.50000	A= 0.69540	BX= 0.66677	BY= 0.27633	DBXDY= -2.72112
R= 1.80000	A= 0.65088	BX= 0.59594	BY= 0.22297	DBXDY= -2.41562
R= 2.10000	A= 0.61107	BX= 0.53347	BY= 0.18215	DBXDY= -2.11921
R= 2.40000	A= 0.57538	BX= 0.47882	BY= 0.15049	DBXDY= -1.84931
R= 2.70000	A= 0.54331	BX= 0.43116	BY= 0.12561	DBXDY= -1.61264
R= 3.00000	A= 0.51437	BX= 0.38959	BY= 0.10583	DBXDY= -1.40719
R= 3.30000	A= 0.48818	BX= 0.35329	BY= 0.08993	DBXDY= -1.23064
R= 3.60000	A= 0.46439	BX= 0.32149	BY= 0.07702	DBXDY= -1.07942
R= 3.90000	A= 0.44270	BX= 0.29356	BY= 0.06644	DBXDY= -0.94995
R= 4.20000	A= 0.42287	BX= 0.26894	BY= 0.05768	DBXDY= -0.83898
R= 4.50000	A= 0.40467	BX= 0.24715	BY= 0.05039	DBXDY= -0.74365
R= 4.80000	A= 0.38792	BX= 0.22781	BY= 0.04426	DBXDY= -0.66151
R= 5.10000	A= 0.37246	BX= 0.21057	BY= 0.03908	DBXDY= -0.59052
R= 5.40000	A= 0.35815	BX= 0.19515	BY= 0.03467	DBXDY= -0.52895
R= 5.70000	A= 0.34487	BX= 0.18132	BY= 0.03089	DBXDY= -0.47536
R= 6.00000	A= 0.33252	BX= 0.16888	BY= 0.02764	DBXDY= -0.42855

W= 1.50000

R= 0.00000	A= 1.00000	BX= 1.00000	BY= 1.00000	DBXDY= 1.00000
R= 0.30000	A= 0.95325	BX= 1.19358	BY= 0.79016	DBXDY= 0.34773
R= 0.60000	A= 0.90178	BX= 1.24008	BY= 0.62554	DBXDY= -0.00158
R= 0.90000	A= 0.85014	BX= 1.21001	BY= 0.49844	DBXDY= -0.17641
R= 1.20000	A= 0.80064	BX= 1.14326	BY= 0.40064	DBXDY= -0.25443
R= 1.50000	A= 0.75431	BX= 1.06166	BY= 0.32513	DBXDY= -0.28029
R= 1.80000	A= 0.71150	BX= 0.97682	BY= 0.26644	DBXDY= -0.27901
R= 2.10000	A= 0.67222	BX= 0.89462	BY= 0.22043	DBXDY= -0.26442
R= 2.40000	A= 0.63628	BX= 0.81783	BY= 0.18402	DBXDY= -0.24405
R= 2.70000	A= 0.60343	BX= 0.74752	BY= 0.15495	DBXDY= -0.22194
R= 3.00000	A= 0.57339	BX= 0.68386	BY= 0.13151	DBXDY= -0.20018
R= 3.30000	A= 0.54590	BX= 0.62659	BY= 0.11245	DBXDY= -0.17976
R= 3.60000	A= 0.52068	BX= 0.57521	BY= 0.09682	DBXDY= -0.16113
R= 3.90000	A= 0.49750	BX= 0.52917	BY= 0.08390	DBXDY= -0.14438
R= 4.20000	A= 0.47616	BX= 0.48790	BY= 0.07314	DBXDY= -0.12946
R= 4.50000	A= 0.45646	BX= 0.45088	BY= 0.06411	DBXDY= -0.11624
R= 4.80000	A= 0.43823	BX= 0.41761	BY= 0.05649	DBXDY= -0.10455
R= 5.10000	A= 0.42133	BX= 0.38766	BY= 0.05001	DBXDY= -0.09423
R= 5.40000	A= 0.40563	BX= 0.36063	BY= 0.04447	DBXDY= -0.08511
R= 5.70000	A= 0.39101	BX= 0.33619	BY= 0.03971	DBXDY= -0.07705
R= 6.00000	A= 0.37736	BX= 0.31404	BY= 0.03560	DBXDY= -0.06992

```
W=  1.80000
R=  0.00000   A=  1.00000   BX=  1.00000   BY=  1.00000   DBXDY=  1.00000
R=  0.30000   A=  0.97608   BX=  1.94321   BY=  0.32347   DBXDY=  0.54460
R=  0.60000   A=  0.94125   BX=  2.42776   BY=  0.68143   DBXDY=  0.25530
R=  0.90000   A=  0.90112   BX=  2.62726   BY=  0.56001   DBXDY=  0.07970
R=  1.20000   A=  0.85935   BX=  2.65694   BY=  0.46155   DBXDY= -0.02254
R=  1.50000   A=  0.81795   BX=  2.53991   BY=  0.38231   DBXDY= -0.07904
R=  1.80000   A=  0.77805   BX=  2.47125   BY=  0.31861   DBXDY= -0.10766
R=  2.10000   A=  0.74025   BX=  2.32817   BY=  0.26730   DBXDY= -0.11964
R=  2.40000   A=  0.70478   BX=  2.17677   BY=  0.22578   DBXDY= -0.12190
R=  2.70000   A=  0.67169   BX=  2.02630   BY=  0.19199   DBXDY= -0.11867
R=  3.00000   A=  0.64093   BX=  1.88188   BY=  0.16432   DBXDY= -0.11254
R=  3.30000   A=  0.61238   BX=  1.74610   BY=  0.14151   DBXDY= -0.10503
R=  3.60000   A=  0.58590   BX=  1.62004   BY=  0.12260   DBXDY= -0.09705
R=  3.90000   A=  0.56131   BX=  1.50393   BY=  0.10680   DBXDY= -0.08914
R=  4.20000   A=  0.53843   BX=  1.39750   BY=  0.09354   DBXDY= -0.08158
R=  4.50000   A=  0.51726   BX=  1.30019   BY=  0.08232   DBXDY= -0.07451
R=  4.80000   A=  0.49749   BX=  1.21136   BY=  0.07279   DBXDY= -0.06800
R=  5.10000   A=  0.47907   BX=  1.13029   BY=  0.06465   DBXDY= -0.06206
R=  5.40000   A=  0.46186   BX=  1.05629   BY=  0.05765   DBXDY= -0.05667
R=  5.70000   A=  0.44577   BX=  0.98869   BY=  0.05161   DBXDY= -0.05179
R=  6.00000   A=  0.43070   BX=  0.92689   BY=  0.04637   DBXDY= -0.04738
```

```
W=  2.10000
R=  0.00000   A=  1.00000   BX=  1.00000   BY=  1.00000   DBXDY=  1.00000
R=  0.30000   A=  0.99706   BX= -1.61342   BY=  0.36446   DBXDY=  0.64475
R=  0.60000   A=  0.97378   BX= -3.24915   BY=  0.73693   DBXDY=  0.38893
R=  0.90000   A=  0.95121   BX= -4.19843   BY=  0.62400   DBXDY=  0.21377
R=  1.20000   A=  0.91850   BX= -4.68599   BY=  0.52727   DBXDY=  0.09805
R=  1.50000   A=  0.88340   BX= -4.87275   BY=  0.44594   DBXDY=  0.02390
R=  1.80000   A=  0.84769   BX= -4.86952   BY=  0.37820   DBXDY= -0.02212
R=  2.10000   A=  0.81246   BX= -4.75050   BY=  0.32200   DBXDY= -0.04950
R=  2.40000   A=  0.77838   BX= -4.56448   BY=  0.27540   DBXDY= -0.06471
R=  2.70000   A=  0.74579   BX= -4.34309   BY=  0.23668   DBXDY= -0.07210
R=  3.00000   A=  0.71489   BX= -4.10652   BY=  0.20443   DBXDY= -0.07454
R=  3.30000   A=  0.68574   BX= -3.86744   BY=  0.17745   DBXDY= -0.07393
R=  3.60000   A=  0.65832   BX= -3.63353   BY=  0.15478   DBXDY= -0.07143
R=  3.90000   A=  0.63257   BX= -3.40931   BY=  0.13564   DBXDY= -0.06800
R=  4.20000   A=  0.60842   BX= -3.19719   BY=  0.11941   DBXDY= -0.06401
R=  4.50000   A=  0.58578   BX= -2.99826   BY=  0.10558   DBXDY= -0.05983
R=  4.80000   A=  0.56454   BX= -2.81279   BY=  0.09374   DBXDY= -0.05566
R=  5.10000   A=  0.54461   BX= -2.64051   BY=  0.08355   DBXDY= -0.05163
R=  5.40000   A=  0.52589   BX= -2.48087   BY=  0.07475   DBXDY= -0.04780
R=  5.70000   A=  0.50830   BX= -2.33315   BY=  0.06711   DBXDY= -0.04421
R=  6.00000   A=  0.49174   BX= -2.19656   BY=  0.06045   DBXDY= -0.04085
```

```
W=  2.40000
R=  0.00000    A=  1.00000    BX=  1.00000    BY=  1.00000    DBXDY=  1.00000
R=  0.30000    A=  1.01575    BX=  0.20833    BY=  0.89717    DBXDY=  0.71545
R=  0.60000    A=  1.01342    BX= -0.34529    BY=  0.79001    DBXDY=  0.48786
R=  0.90000    A=  0.99873    BX= -0.71432    BY=  0.68790    DBXDY=  0.31647
R=  1.20000    A=  0.97600    BX= -0.94716    BY=  0.59536    DBXDY=  0.19252
R=  1.50000    A=  0.94836    BX= -1.08294    BY=  0.51394    DBXDY=  0.10549
R=  1.80000    A=  0.91802    BX= -1.15134    BY=  0.44356    DBXDY=  0.04583
R=  2.10000    A=  0.88649    BX= -1.17405    BY=  0.38335    DBXDY=  0.00587
R=  2.40000    A=  0.85478    BX= -1.16651    BY=  0.33211    DBXDY= -0.02021
R=  2.70000    A=  0.82355    BX= -1.13952    BY=  0.28861    DBXDY= -0.03663
R=  3.00000    A=  0.79324    BX= -1.10057    BY=  0.25169    DBXDY= -0.04642
R=  3.30000    A=  0.76403    BX= -1.05477    BY=  0.22031    DBXDY= -0.05171
R=  3.60000    A=  0.73621    BX= -1.00557    BY=  0.19357    DBXDY= -0.05396
R=  3.90000    A=  0.70969    BX= -0.95526    BY=  0.17073    DBXDY= -0.05422
R=  4.20000    A=  0.68452    BX= -0.90537    BY=  0.15115    DBXDY= -0.05318
R=  4.50000    A=  0.66070    BX= -0.85684    BY=  0.13431    DBXDY= -0.05134
R=  4.80000    A=  0.63815    BX= -0.81025    BY=  0.11978    DBXDY= -0.04903
R=  5.10000    A=  0.61684    BX= -0.76595    BY=  0.10718    DBXDY= -0.04646
R=  5.40000    A=  0.59670    BX= -0.72408    BY=  0.09623    DBXDY= -0.04380
R=  5.70000    A=  0.57765    BX= -0.68468    BY=  0.08667    DBXDY= -0.04114
R=  6.00000    A=  0.55963    BX= -0.64773    BY=  0.07830    DBXDY= -0.03854
```

```
W=  2.70000
R=  0.00000    A=  1.00000    BX=  1.00000    BY=  1.00000    DBXDY=  1.00000
R=  0.30000    A=  1.03207    BX=  0.48962    BY=  0.92624    DBXDY=  0.77125
R=  0.60000    A=  1.04463    BX=  0.10402    BY=  0.83942    DBXDY=  0.57034
R=  0.90000    A=  1.04271    BX= -0.17604    BY=  0.74982    DBXDY=  0.40614
R=  1.20000    A=  1.03046    BX= -0.37192    BY=  0.66366    DBXDY=  0.27817
R=  1.50000    A=  1.01113    BX= -0.50330    BY=  0.58422    DBXDY=  0.18172
R=  1.80000    A=  0.98716    BX= -0.58665    BY=  0.51289    DBXDY=  0.11080
R=  2.10000    A=  0.96035    BX= -0.63503    BY=  0.44989    DBXDY=  0.05968
R=  2.40000    A=  0.93201    BX= -0.65842    BY=  0.39484    DBXDY=  0.02349
R=  2.70000    A=  0.90305    BX= -0.66428    BY=  0.34702    DBXDY= -0.00164
R=  3.00000    A=  0.87411    BX= -0.65807    BY=  0.30563    DBXDY= -0.01872
R=  3.30000    A=  0.84563    BX= -0.64378    BY=  0.26985    DBXDY= -0.02997
R=  3.60000    A=  0.81790    BX= -0.62427    BY=  0.23892    DBXDY= -0.03706
R=  3.90000    A=  0.79110    BX= -0.60156    BY=  0.21215    DBXDY= -0.04120
R=  4.20000    A=  0.76534    BX= -0.57710    BY=  0.18895    DBXDY= -0.04326
R=  4.50000    A=  0.74066    BX= -0.55189    BY=  0.16879    DBXDY= -0.04387
R=  4.80000    A=  0.71709    BX= -0.52663    BY=  0.15124    DBXDY= -0.04350
R=  5.10000    A=  0.69462    BX= -0.50179    BY=  0.13591    DBXDY= -0.04247
R=  5.40000    A=  0.67322    BX= -0.47767    BY=  0.12249    DBXDY= -0.04102
R=  5.70000    A=  0.65285    BX= -0.45447    BY=  0.11070    DBXDY= -0.03931
R=  6.00000    A=  0.63347    BX= -0.43231    BY=  0.10032    DBXDY= -0.03746
```

```
W=  3.00000
R=  0.00000   A=  1.00000   BX=  1.00000   BY=  1.00000   DBXDY=  1.00000
R=  0.30000   A=  1.04619   BX=  0.61408   BY=  0.95174   DBXDY=  0.81727
R=  0.60000   A=  1.07234   BX=  0.30483   BY=  0.88454   DBXDY=  0.64208
R=  0.90000   A=  1.08271   BX=  0.06579   BY=  0.80846   DBXDY=  0.43793
R=  1.20000   A=  1.08108   BX= -0.11322   BY=  0.73046   DBXDY=  0.35965
R=  1.50000   A=  1.07059   BX= -0.24327   BY=  0.65495   DBXDY=  0.25695
R=  1.80000   A=  1.05375   BX= -0.33466   BY=  0.58442   DBXDY=  0.17700
R=  2.10000   A=  1.03255   BX= -0.39627   BY=  0.52007   DBXDY=  0.11606
R=  2.40000   A=  1.00846   BX= -0.43538   BY=  0.46227   DBXDY=  0.07039
R=  2.70000   A=  0.98263   BX= -0.45774   BY=  0.41083   DBXDY=  0.03668
R=  3.00000   A=  0.95588   BX= -0.46782   BY=  0.36543   DBXDY=  0.01215
R=  3.30000   A=  0.92882   BX= -0.46904   BY=  0.32555   DBXDY= -0.00541
R=  3.60000   A=  0.90188   BX= -0.46397   BY=  0.29050   DBXDY= -0.01774
R=  3.90000   A=  0.87537   BX= -0.45453   BY=  0.25975   DBXDY= -0.02617
R=  4.20000   A=  0.84949   BX= -0.44215   BY=  0.23279   DBXDY= -0.03173
R=  4.50000   A=  0.82439   BX= -0.42788   BY=  0.20911   DBXDY= -0.03517
R=  4.80000   A=  0.80014   BX= -0.41250   BY=  0.18830   DBXDY= -0.03707
R=  5.10000   A=  0.77681   BX= -0.39655   BY=  0.16998   DBXDY= -0.03786
R=  5.40000   A=  0.75439   BX= -0.38046   BY=  0.15381   DBXDY= -0.03735
R=  5.70000   A=  0.73290   BX= -0.36449   BY=  0.13952   DBXDY= -0.03729
R=  6.00000   A=  0.71233   BX= -0.34885   BY=  0.12685   DBXDY= -0.03634
END XEQ.
```

DECAY OF IMAGE CURRENTS
INDUCED IN A THIN CONDUCTING CIRCULAR CYLINDER
BY A CO-AXIAL LINE-CURRENT PAIR*

L. Jackson Laslett

Lawrence Radiation Laboratory
University of California
Berkeley, California

July 29, 1969

If the wall is absent: The vector potential of a single line current is

$$A_z = -I(t)\ \ln\left[r^2 + s^2 - 2rs\cos\theta\right] - \ln r^2$$

$$= -I(t)\ \ln \frac{r^2 + s^2 - 2rs\cos\theta}{r^2}$$

and for s small (infinitesimal) the potential of a line-current pair, with $\underset{s\to o}{L}\ I(t)\cdot s = P(t)$, becomes

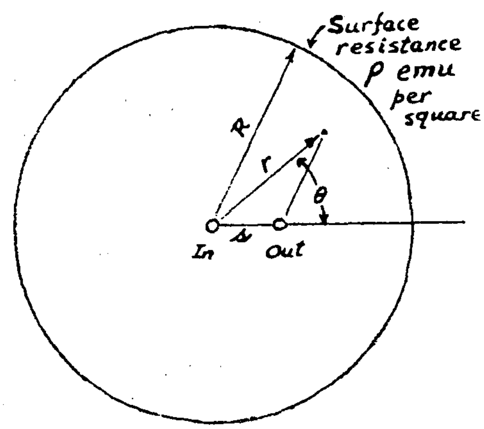

$$A_z = -P(t)\left\{\frac{\partial}{\partial s}\left[\ln\left(\frac{r^2 + s^2 - 2rs\cos\theta}{r^2}\right)\right]\right\}_{s=0}$$

$$= 2\ P(t)\ \frac{r\cos\theta}{r^2 + s^2 - 2rs\cos\theta}\Bigg|_{s=o}$$

$$= 2\ P(t)\ \frac{\cos\theta}{r}\ .$$

We now write, so as to take into account the effect of eddy currents induced in the thin conducting circular cylinder,

$$A_z = 2\ P(t)\ \frac{\cos\theta}{r} + A^I.$$

As is customary, displacement currents will be neglected.

---

* Work supported by the U. S. Atomic Energy Commission. For previous work, see L. Jackson Laslett, "Decay of Image Currents in a Plane Geometry", LRL Report ERAN-37 (July 28, 1969).

Now $B_\theta = -\dfrac{\partial A_z}{\partial r} = 2\,P(t)\,\dfrac{\cos\theta}{r^2} - \dfrac{\partial A^I}{\partial r}$,

while the induced current density in the wall at r = R is

$$J_z^I = -\frac{1}{\rho}\frac{\partial A_z}{\partial t}\bigg|_{r=R}$$

The condition $B_\theta \Big|_{r=R^+} - B_\theta \Big|_{r=R^-} = 4\pi J_z^I$ then becomes

$$\frac{\partial A^I}{\partial r}\bigg|_{r=R^+} - \frac{\partial A^I}{\partial r}\bigg|_{r=R^-} = \frac{4\pi}{\rho}\frac{\partial A_z}{\partial t}\bigg|_{r=R}$$

$$= \frac{4\pi}{\rho}\left[2\,P'(t)\,\frac{\cos\theta}{R} + \frac{\partial A^I}{\partial t}\bigg|_{r=R}\right].$$

We also require continuity of A^I and require that A^I (a Cartesian component of a divergenceless vector $\vec{A}^I$) be harmonic ($\nabla^2 A^I = 0$, for $r \neq R$):

$$\frac{1}{r}\frac{\partial}{\partial r}\left(r\frac{\partial A^I}{\partial r}\right) + \frac{1}{r^2}\frac{\partial^2 A^I}{\partial\theta^2} = 0 .$$

Suppose, then, that A^I is of the form

$$A^I = \begin{cases} F(t)\,\dfrac{r\cos\theta}{R} & \text{for } r \leq R, \\[2ex] F(t)\,\dfrac{R\cos\theta}{r} & \text{for } r \geq R. \end{cases}$$

Then the inhomogeneous differential equation for A^I becomes

$$-\frac{2}{R}F(t)\cos\theta = \frac{4\pi}{\rho}\left[2\,P'(t)\,\frac{\cos\theta}{R} + F'(t)\cos\theta\right],$$

or

$$F' + \frac{\rho}{2\pi R}F = -\frac{2}{R}P'(t).$$

We take the solution of this first-order equation to be

$$F = -\frac{2}{R}\int_{-\infty}^{t} P'(\xi)\, e^{-\frac{\rho}{2\pi R}(t-\xi)}\, d\xi .$$

The vector potential of the induced eddy currents then becomes

$$A^{I} \doteq \begin{cases} -2\,\dfrac{r\cos\theta}{R^2}\displaystyle\int_{-\infty}^{t} P'(\xi)\, e^{-\frac{\rho}{2\pi R}(t-\xi)}\, d\xi & \text{for } r \leqslant R, \\[2ex] -2\,\dfrac{\cos\theta}{r}\displaystyle\int_{-\infty}^{t} P'(\xi)\, e^{-\frac{\rho}{2\pi R}(t-\xi)}\, d\xi & \text{for } r \geqslant R; \end{cases}$$

the total vector potential correspondingly can be written:

$$A_z(r,\theta;t) \doteq 2P(t)\,\frac{\cos\theta}{r} - \frac{2}{R}\left[\int_{-\infty}^{t} P'(\xi)\, e^{-\frac{\rho}{2\pi R}(t-\xi)}\, d\xi\right]\cdot\begin{bmatrix} r/R \\ \text{or} \\ R/r \end{bmatrix}\cos\theta, \quad \text{for} \begin{cases} r \leqslant R \\ r \geqslant R \end{cases}.$$

In the particular case that $P(t)$ is a <u>step function</u>, of magnitude P_o occuring at $t = t_o$ $\left[P' = P_o\,\delta\,(t - t_o)\right]$ and with no changes prior to that time, the above solution for A^I becomes:

$$A^{I} = \begin{cases} -2\,P_o\,\dfrac{r\cos\theta}{R^2}\, e^{-\frac{\rho}{2\pi R}(t-t_o)} & \text{for } r \leqslant R, \\[2ex] -2\,P_o\,\dfrac{\cos\theta}{r}\, e^{-\frac{\rho}{2\pi R}(t-t_o)} & \text{for } r \geqslant R. \end{cases}$$

In this case of a "dipole" line current centered in a thin conducting circular cylinder, we appear to have, in contrast to the case of a plane conducting sheet, an exponential decrease of A^I with time. The characteristic time is $\tau = \frac{R}{v}$, where $v = \frac{\rho}{2\pi}$ (for ρ in emu per square).

Interpretation

Interpretation of the Field Modification resulting from the Eddy Currents generated when P(t) is a Step Function:

1. For $r > R$:

A^I has the form of the vector potential for a 2-D current "dipole" – similar to the actual "dipole source" P_o and similarly situated, but of opposite polarity to the latter – whose strength $P^I(t) = - P_o \, e^{-\frac{\rho}{2\pi R}(t - t_o)}$ decreases exponentially with time from an initial strength $- P_o$ at $t = t_o$. [The external fields ($r > R$) thus build up form a value that is zero at the initial time t_o.]

2. For $r < R$:

The vector potential A^I that characterizes the field produced by the induced eddy currents is of the form that describes a uniform field (as is characteristic of the field produced within a circular cylinder by a current distribution $J_z^I \propto \cos\theta$ on the boundary), and this field has the exponentially-decreasing value

$\vec{H}^I = \frac{2\,P_o}{R^2} \, e^{-\frac{\rho}{2\pi R}(t - t_o)} \, \hat{e}_y$. [Such a uniform "image field" is encountered in magnetostatics (steady-state current problems) when a source approaches the axis and the external images in consequence recede to infinity.]

Appendix: Check of the solution given for $A_z(r, \theta; t)$:

With

$$A_z(r, \theta; t) = 2\,P(t)\,\frac{\cos\theta}{r} - \frac{2}{R}\left[\int_{-\infty}^{t} P'(\xi)\, e^{-\frac{\rho}{2\pi R}(t-\xi)}\,d\xi\right]\cdot\left[\begin{array}{c} r/R \\ \text{or} \\ R/r \end{array}\right]\cdot \cos\theta, \text{ for} \begin{cases} r \leqslant R \\ r \geqslant R, \end{cases}$$

$$J_z^I \doteq -\frac{1}{\rho}\frac{\partial A_z}{\partial t}\bigg|_R = -\frac{2}{R\rho}P'(t)\cos\theta + \frac{2}{R\rho}\left[P'(t) - \frac{\rho}{2\pi R}\int_{-\infty}^{t} P'(\xi)\, e^{-\frac{\rho}{2\pi R}(t-\xi)}\,d\xi\right]\cdot\cos\theta$$

$$\doteq -\frac{1}{\pi R^2}\left[\int_{-\infty}^{t} P'(\xi)\, e^{-\frac{\rho}{2\pi R}(t-\xi)}\,d\xi\right]\cdot\cos\theta.$$

Also, then,

$$B_\theta\bigg|_{R^+} - B_\theta\bigg|_{R^-} = \frac{\partial A_z}{\partial r}\bigg|_{R^-} - \frac{\partial A_z}{\partial r}\bigg|_{R^+} = -\frac{4}{R^2}\left[\int_{-\infty}^{t} P'(\xi)\, e^{-\frac{\rho}{2\pi R}(t-\xi)}\,d\xi\right]\cdot\cos\theta$$

$$\doteq 4\pi J_z^I, \text{ as required.}$$

DECAY OF IMAGE CURRENTS INDUCED IN A THIN CONDUCTING CIRCULAR CYLINDER BY A LINE-CURRENT PAIR THAT IS PARALLEL TO, BUT NOT NECESSARILY COINCIDENT WITH, THE CYLINDER AXIS *

L. Jackson Laslett

Lawrence Radiation Laboratory
University of California
Berkeley, California

31 July 1969

1. Vector Potential With The Wall Absent

We consider a 2-dimensional "current dipole", formed from anti-parallel currents $\pm I(t)$ at $\theta = o$ and $r = h + s$ or h, in the limit $s \to o$ with $P(t) \equiv I(t) \cdot s$. Then the vector potential of this isolated "current dipole" is given by [1]

$$A_z^{(o)} = -P(t) \left[\frac{\partial}{\partial s} \left\{ \ln \left[r^2 + (h+s)^2 - 2r(h+s)\cos\theta \right] \right\} \right]_{s=o}$$

$$= 2\,P(t)\,\frac{r\cos\theta - h}{r^2 + h^2 - 2rh\cos\theta} .$$

By use of the identity [2]

$$-\ln(r^2 + r_o^2 - 2rr_o\cos\theta) = 2\sum_{n=1}^{\infty} \frac{1}{n}\left(\frac{r_o}{r}\right)^n \cos n\theta - \ln r^2 \quad (r_o < r),$$

this $A_z^{(o)}$ can be written in an alternative form as an expansion in terms of familiar plane-polar harmonic functions:

$$A_z^{(o)} = 2\,P(t) \left\{ \frac{\partial}{\partial s} \left[\sum_{n=1}^{\infty} \frac{1}{n} \left(\frac{h+s}{r} \right)^n \cos n\theta \right] \right\}_{s=o}$$

$$= \frac{2}{h}\, P(t) \sum_{n=1}^{\infty} \left(\frac{h}{r} \right)^n \cos n\theta \qquad (h < r).$$

2. Introduction of a Vector Potential to Account for Induced Eddy Currents

We consider now the presence of a thin circular cylinder, with its axis coincident with the polar-coordinate origin. The surface resistance of this cylinder is taken to be ρ emu per square and the radius of the cylinder is denoted by R. The vector potential of the induced eddy currents will be written A^I, so that the total vector potential is (with $\nabla^2 A^I = 0$, for $r \neq R$):

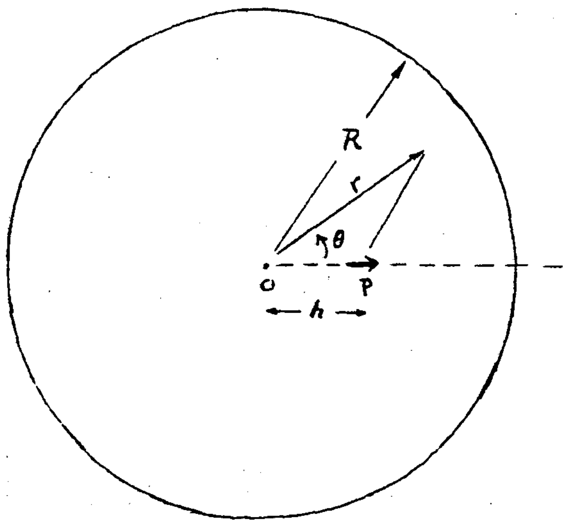

$$A_z = A_z^{(o)} + A^I .$$

With $\vec{E} = -\frac{\partial \vec{A}}{\partial t}$, or $J_z = -\frac{1}{\rho}\frac{\partial A_z}{\partial t}$, and $B_\theta = -\frac{\partial A_z}{\partial r}$, the condition

$$\Delta B_\theta \Big|_{r=R} = 4\pi J_z \quad \text{becomes} \quad \frac{\partial A^I}{\partial r}\Big|_{r=R^+} - \frac{\partial A^I}{\partial r}\Big|_{r=R^-} = \frac{4\pi}{\rho}\frac{\partial A_z}{\partial t}\Big|_{r=R} ;$$

i.e.,

$$\left.\frac{\partial A^I}{\partial r}\right|_{r=R^+} - \left.\frac{\partial A^I}{\partial r}\right|_{r=R^-} = \frac{4\pi}{\rho}\left[2P'(t)\,\frac{R\cos\theta - h}{R^2 + h^2 - 2Rh\cos\theta} + \left.\frac{\partial A^I}{\partial t}\right|_{r=R}\right]$$

or, equivalently,

$$\left.\frac{\partial A^I}{\partial r}\right|_{r=R^+} - \left.\frac{\partial A^I}{\partial r}\right|_{r=R^-} = \frac{4\pi}{\rho}\left[\frac{2}{h}\;P'(t)\sum_{n=1}^{\infty}\left(\frac{h}{R}\right)^n\cos n\theta + \left.\frac{\partial A^I}{\partial t}\right|_{r=R}\right].$$

3. Solution for A^I

To procede directly to obtain a solution for A^I, it is convenient to employ the series expansion for $A^{(o)}$ that led to the last of the equations in Section 2. We then assume A^I to be of the form

$$A^I = \begin{cases} \displaystyle\sum_{n=1}^{\infty} F_n(t)\left(\frac{r}{R}\right)^n \cos n\theta & (r \leqslant R) \\[2ex] \displaystyle\sum_{n=1}^{\infty} F_n(t)\left(\frac{R}{r}\right)^n \cos n\theta & (r \geqslant R), \end{cases}$$

that is manifestly harmonic.

Then we require

$$-\frac{2}{R}\sum_{n=1}^{\infty} nF_n(t)\cos n\theta = \frac{4\pi}{\rho}\left[\frac{2}{h}\;P'(t)\sum_{n=1}^{\infty}\left(\frac{h}{R}\right)^n\cos n\theta + \sum_{n=1}^{\infty} F_n'(t)\cos n\theta\right],$$

so that we obtain the first-order differential equations for the $F_n(t)$:

$$F_n' + n\frac{\rho}{2\pi R}\,F_n = -2\,\frac{h^{n-1}}{R^n}\;P'(t).$$

An appropriate solution for F_n is

$$F_n \doteq - 2 \frac{h^{n-1}}{R^n} \int_{-\infty}^{t} P'(\xi)\, e^{-n \frac{v}{R}(t-\xi)}\, d\xi,$$

where $v \equiv \frac{\rho}{2\pi}$ (dimensions of velocity).

Thus

$$A^I \doteq - \frac{2}{h} \sum_{n=1}^{\infty} \left[\int_{-\infty}^{t} P'(\xi)\, e^{-n \frac{v}{R}(t-\xi)}\, d\xi \right] \cdot \left\{ \begin{matrix} \left(\frac{hr}{R^2}\right)^n \\ \text{or} \\ \left(\frac{h}{r}\right)^n \end{matrix} \right\} \cdot \cos n\theta, \text{ for } \left\{ \begin{matrix} r \leqslant R \\ \\ r \geqslant R. \end{matrix} \right.$$

When $P(t)$ in particular has the form of a single step function, of magnitude P_o and occuring at $t \doteq t_o$ [so that $P'(t) \doteq P_o \cdot \delta(t - t_o)$], this solution becomes

$$A^I = - \frac{2}{h} P_o \sum_{n=1}^{\infty} \left\{ \begin{matrix} \left(\frac{hr}{R^2}\right)^n \\ \text{or} \\ \left(\frac{h}{r}\right)^n \end{matrix} \right\} (\cos n\theta)\ e^{-n \frac{v}{R}(t-t_o)}, \quad \text{for } t > t_o .$$

4. Interpretation of the Step-Function Result

(a) Interpretation of the result for $t = t_o$

At $t = t_o$ the last result in Section 3 may be written

$$A^I(t_o) = - \frac{2}{h} P_o \sum_{n=1}^{\infty} \left\{ \begin{matrix} \left(\frac{hr}{R^2}\right)^n \\ \text{or} \\ \left(\frac{h}{r}\right)^n \end{matrix} \right\} \cdot \cos n\theta \qquad \left\{ \begin{matrix} r \leqslant R \\ \\ r \geqslant R \end{matrix} \right.$$

$$= \begin{cases} -\frac{R^2}{h^2} P_o \left[\frac{\partial}{\partial D} \{ \ln [D^2 + r^2 - 2rD\cos\theta] \} \right]_{D = \frac{R^2}{h}} + \frac{2}{h} P_o & r \leqslant R \\ \text{or} & \\ P_o \left[\frac{\partial}{\partial s} \{ \ln [r^2 + (h+s)^2 - 2r(h+s)\cos\theta] \} \right]_{s = o} & r \geqslant R. \end{cases}$$

Thus, at the instant of creation of the "2-dimensional dipole current" P_o, we have the following image system that will serve to describe the effects of the eddy currents induced in the cylinder:

To account for fields outside the conducting cylinder ($r \geqslant R$), one provides within the cylinder, at the location of the true source ($r = h$), an image that replicates this source but has the opposite sign. The combination then serves, of course, to give zero total field in the region under consideration -- namely in the region outside the cylinder.

To account for magnetic fields inside the cylinder ($r \leqslant R$), one places a 2-dimensional dipole-current image at the familiar image position (outside the cylinder) whose radial coordinate is $D = R^2/h$. This image has the same dipole polarity as the actual source P_o, and a magnitude that is $(R/h)^2 P_o$ [due, one might say, to the "magnification" in imaging a pair of line filaments at h and h + s to radii R^2/h and $R^2/(h + s)$]. The term $\frac{2}{h} P_o$ that appears in $A^I(t_o)$ does not contribute to the magnetic field.

(b) Interpretation of the result for $t \geqslant t_o$

The expression (Section 3) shown for $t > t_o$ (in the case of a step function that occurs at $t = t_o$) is of the form given for $t = t_o$, save that h is replaced by $\tilde{h} = he^{-\frac{v}{R}(t - t_o)}$ and P_o by $\tilde{P}_o = P_o\, e^{-\frac{v}{R}(t - t_o)}$.

These substitutions then suggest the following interpretation:

To describe the field outside the cylinder ($r \geqslant R$), one imagines supplementing the true source by a 2-dimensional current dipole of opposite sign and exponentially decreasing strength, $-P_o e^{-\frac{v}{R}(t-t_o)}$; this image initially is situated at the location ($r = h$) of the true source but moves inward so as to decrease exponentially its distance $\tilde{h}$ from the axis $\left[\tilde{h} = h\, e^{-\frac{v}{R}(t-t_o)}\right]$.

To describe the field inside the cylinder ($r \leqslant R$), we introduce an external current-pair at a distance from the axis that initially is $\frac{R^2}{h}$ and that increases exponentially as $\frac{R^2}{h} e^{\frac{v}{R}(t-t_o)}$; 3 the two dimensional dipole moment of this source is $+P_o\left[\frac{R}{h} e^{\frac{v}{R}(t-t_o)}\right]^2$ (or $P_o R^2/\tilde{h}^2$, with this increase of strength associable with the magnification that would result from imaging a pair of internal line currents situated near $r = \tilde{h}$).

5. Step-Function Solution in Closed Form

Aided by the interpretation of the preceding section (Section 4), one may write the solution for a step-function $P(t)$ in closed form: - Thus for $r \leqslant R$,

$$A^I = -\frac{R^2}{h^2} P_o e^{\frac{v}{R}(t-t_o)} \left[\frac{\partial}{\partial D}\{\ln [D^2 + r^2 - 2rD\cos\theta]\}\right]_{D = \frac{R^2}{h} e^{-\frac{v}{R}(t-t_o)}}$$

$$+ \frac{2}{h} P_o$$

$$= -2\frac{R^2}{h^2} P_o e^{\frac{v}{R}(t-t_o)} \left.\frac{D - r\cos\theta}{D^2 + r^2 - 2rD\cos\theta}\right|_{D = \frac{R^2}{h} e^{-\frac{v}{R}(t-t_o)}} + \frac{2}{h} Po$$

$$= -\frac{2r}{R^2} P_o \frac{\cos\theta - \frac{hr}{R^2} e^{-\frac{v}{R}(t-t_o)}}{1 - 2\frac{hr}{R^2} e^{-\frac{v}{R}(t-t_o)} \cos\theta + \left(\frac{hr}{R^2}\right)^2 e^{-2\frac{v}{R}(t-t_o)}} e^{-\frac{v}{R}(t-t_o)} .$$

Likewise, for $r \geqslant R$,

$$A^I = 2 P_o e^{-\frac{v}{R}(t-t_o)} \left.\frac{\tilde{h} - r\cos\theta}{r^2 + \tilde{h}^2 - 2r\tilde{h}\cos\theta}\right|_{\tilde{h} = he^{-\frac{v}{R}(t-t_o)}}$$

$$= -\frac{2}{h} P_o \frac{\frac{r}{h}\cos\theta - e^{-\frac{v}{R}(t-t_o)}}{\left(\frac{r}{h}\right)^2 - 2\frac{r}{h} e^{-\frac{v}{R}(t-t_o)} \cos\theta + e^{-2\frac{v}{R}(t-t_o)}} e^{-\frac{v}{R}(t-t_o)} .$$

We thus write, for the case in which $P(t)$ is a step function,

$$A^I = -2 P_o \left\{ \begin{array}{l} \dfrac{r}{R^2} \dfrac{\cos\theta - \frac{hr}{R^2} E(t,t_o)}{1 - 2\frac{hr}{R^2} E(t,t_o)\cos\theta + \left[\left(\frac{hr}{R^2}\right) E(t,t_o)\right]^2} \\ \\ \dfrac{1}{r} \dfrac{\cos\theta - \frac{h}{r} E(t,t_o)}{1 - 2\frac{h}{r} E(t,t_o)\cos\theta + \left[\left(\frac{h}{r}\right) E(t,t_o)\right]^2} \end{array} \right\} \cdot E(t,t_o),$$

where $E(t,t_o)$ denotes $e^{-\frac{v}{R}(t - t_o)}$ while the upper and lower forms shown within the curley brackets refer respectively to $r \leqslant R$ or $r \geqslant R$.

The total vector potential is then

$$A_z = 2\,P_o \frac{r \cos\theta - h}{r^2 - 2rh\cos\theta + h^2} + A^I \qquad (t \geqslant t_o),$$

and the induced surface current in this case is

$$J_z = -\frac{1}{\rho}\frac{\partial A_z}{\partial t}$$

$$= -\frac{P_o}{\pi}\,\frac{R^2\cos\theta - 2\,RhE(t,t_o) + [h\cdot E(t,t_o)]^2\cos\theta}{\{R^2 - 2RhE(t,t_o)\cos\theta + [h\cdot E(t,t_o)]^2\}^2}\cdot E(t,t_o) \quad \text{abamp/cm}$$

for $t \geqslant t_o$.

6. General Solution in Closed Form

The results of the preceding section (Section 5) of course can be immediately generalized to describe the results for an arbitrary P(t): 4

$$A = 2\,P(t)\,\frac{r\cos\theta - h}{r^2 - 2rh\cos\theta + h^2}$$

$$-\,2\int_{-\infty}^{t} P'(\xi)\left\{\begin{array}{l} \dfrac{r}{R^2}\;\dfrac{\cos\theta - \frac{hr}{R^2}\,E(t,\xi)}{1 - 2\,\frac{hr}{R^2}\,E(t,\xi)\cos\theta + \left[\left(\frac{hr}{R^2}\right)E(t,\xi)\right]^2} \\[4ex] \dfrac{1}{r}\;\dfrac{\cos\theta - \frac{h}{r}\,E(t,\xi)}{1 - 2\,\frac{h}{r}\,E(t,\xi)\cos\theta + \left[\left(\frac{h}{r}\right)E(t,\xi)\right]^2} \end{array}\right\} E(t,\xi)\,d\xi$$

For $r \leqslant R$ or $r \geqslant R$, respectively;

$$J_z = -\frac{1}{\pi}\int_{-\infty}^{t} P'(\xi)\,\frac{R^2\cos\theta - 2Rh\,E(t,\xi) + [h\cdot E(t,\xi)]^2\cos\theta}{\{R^2 - 2Rh\,E(t,\xi)\cos\theta + [h\,E(t,\xi)]^2\}^2}\cdot E(t,\xi)\,d\xi\ ,$$

with $E(t,\xi) = e^{-\frac{v}{R}(t-\xi)} = e^{-\frac{\rho}{2\pi R}(t-\xi)}$. The components of magnetic field are given by $B_\theta = -\frac{\partial A_z}{\partial r}$, $B_r = \frac{1}{r}\frac{\partial A_z}{\partial\theta}$.

7. Asymptotic Character of the Effects of Eddy Currents That are Induced by a Step-Function P(t)

The solution for A^I, as obtained in Section 3, was (for $r \leqslant R$ or $r \geqslant R$)

$$A^I = -\frac{2}{h}\,P_o\sum_{n=1}^{\infty}\left\{\begin{matrix}\left(\frac{hr}{R^2}\right)^n\\ \text{or}\\ \left(\frac{h}{r}\right)^n\end{matrix}\right\}(\cos n\,\theta)\,e^{-n\frac{v}{R}(t-t_o)}$$

so that

$$A_z = \frac{2}{h}\,P_o\sum_{n=1}^{\infty}\left[\left(\frac{h}{r}\right)^n - \left\{\begin{matrix}\left(\frac{hr}{R^2}\right)^n\\ \text{or}\\ \left(\frac{h}{r}\right)^n\end{matrix}\right\}e^{-n\frac{v}{R}(t-t_o)}\right]\cdot\cos n\,\theta$$

and

$$J_z = -\frac{P_o}{\pi hR}\sum_{n=1}^{\infty} n\left(\frac{h}{R}\right)^n(\cos n\,\theta)\,e^{-n\frac{v}{R}(t-t_o)}$$

Also,

$$B_\theta = 2\,\frac{P_o}{hr}\sum_{n=1}^{\infty} n\left[\left(\frac{h}{r}\right)^n + \left\{\begin{matrix}\left(\frac{hr}{R^2}\right)^n\\ \text{or}\\ -\left(\frac{h}{r}\right)^n\end{matrix}\right\}e^{-n\frac{v}{R}(t-t_o)}\right]\cdot\cos n\,\theta$$

and

$$B_r = -2\,\frac{P_o}{hr}\sum_{n=1}^{\infty} n\left[\left(\frac{h}{r}\right)^n - \left\{\begin{matrix}\left(\frac{hr}{R^2}\right)^n\\ \text{or}\\ \left(\frac{h}{r}\right)^n\end{matrix}\right\}e^{-n\frac{v}{R}(t-t_o)}\right]\cdot\sin n\,\theta\ ,$$

so that the discontinuity of B_θ at $r = R$, namely

$$\Delta B_\theta = -4 \frac{P_o}{hR} \sum_{n=1}^{\infty} n \left(\frac{h}{R}\right)^n (\cos n\theta)\, e^{-n \frac{v}{R}(t - t_o)} ,$$ at all times is

equal to $4\pi J_z$ (as required), and initially ($t = t_o$) the external field vanishes [with $B_r = o$ at $t = t_o$].

When expressed in this form, the results indicate that the various order spatial harmonics decay at increasingly great exponential rates as the harmonic order n under consideration becomes larger $\left[\text{decay proportional to } e^{-n \frac{v}{R}(t - t_o)}, \text{ or to } e^{-\frac{t - t_o}{\tau_n}} \text{ where } \tau_n = \frac{R}{nv} = \frac{1}{n}\, \frac{2\pi R}{\rho}\right]$.

In consequence, the induced eddy currents that remain assume more and more the character of a pure $\cos\theta$ distribution;[5] correspondingly, the external magnetic field becomes more and more that characteristic of a "2-dimensional current dipole", with the numerical factor $1 - e^{-\frac{v}{R}(t - t_o)}$, and the eddy-current modification to the internal field becomes essentially the exponentially decaying uniform field $\frac{2P_o}{R^2}\, e^{-\frac{v}{R}(t - t_o)}\, \hat{e}_y$. These results correspond to those obtained in an earlier report (29 July 1969) for the special case $h = o$.

The asymptotic character of the solution, as just described here (for $t - t_o$ large in comparison to $\frac{R}{v}$), also follows immediately from the closed-form results presented in Section 5. The results of Sections 5 and 6 also become identical, when h is set equal to zero, to results presented in the previous report that considered only the special case of a source situated on the axis of the cylinder.

8. Numerical Computations

(a) Numerical values of the induced current density have been computed at various times, for 10 - degree intervals of the polar-coordinate angle, for cases in which $h = G \cdot R$, with $G = 0$, 0.1, 0.2, 0.3, and 0.4; these values of G are denoted by $G_0, G_1, \cdots G_4$. The corresponding values of current density, for a step-function source (P_o), are given by $J_i \equiv \frac{R^2 J_z}{P_o}$ ($i = o, 1, \cdots 4$), as a function of the angle A (equals θ, in degrees) and of $L = \frac{v(t - t_o)}{R}$.

$$\text{With } E \equiv e^{-L}, \quad J_i = \frac{1}{\pi} \frac{[1 + (G_i \cdot E)^2] \cos\theta - 2 \cdot G_i \cdot E}{[1 + (G_i \cdot E)^2 - 2 \cdot G_i \cdot E \cdot \cos\theta]^2} \; E.$$

Appendix A presents the results of this computation, with each table corresponding to a particular time ($L = 0$, 0.5, ... 3.0), and lists the J_i vs. G_i and A.

(b) Similarly, for the image field and its gradient at the location ($r = h$, $\theta = 0$) of the source, we have

$$B_y{}^I\Big|_{\substack{x=h\\y=o}} = 2\,\frac{P_o E}{R^2\left[1 - \left(\frac{h}{R}\right)^2 E\right]^2} \quad \text{and} \quad \frac{\partial B_y{}^I}{\partial x}\Big|_{\substack{x=h\\y=o}} = \frac{\partial B_x{}^I}{\partial y}\Big|_{\substack{x=h\\y=o}} = 4\,\frac{P_o h E^2}{R^4\left[1 - \left(\frac{h}{R}\right)^2 E\right]^3}$$

Thus, defining $B_i \equiv \frac{R^2 B_y^I}{P_o}$ and $P_i \equiv \frac{R^4 [\partial B_y^I/\partial x]}{hP_o} = \frac{R^4 \left[\partial B_x^I/\partial y\right]}{hP_o}$

at the points $x = h = G_i \cdot R$, $y = o$, we have

$$B_i = 2\,\frac{E}{[1 - G_i^2 E]^2} \quad \text{and} \quad P_i = 4\,\frac{E^2}{[1 - G_i^2 E]^3} .$$

Tables are given in Appendices B and C respectively of the quantities B_i and P_i vs. G_i (0, 0.1, ... 0.4) and L.

9. References and Notes

* Work supported by the U.S. Atomic Energy Commission. For previous work, see L. Jackson Laslett, "Decay of Image Currents in a Plane Geometry" ERAN-37 (28 July 1969) and "Decay of Image currents Induced in a Thin Conducting Circular Cylinder by a Co-Axial Line-Current Pair" ERAN-38 (29 July 1969).

[1] The result $A_z = 2P(t) \dfrac{r \cos \theta - h}{r^2 + h^2 - 2rh \cos \theta}$ will be recognized as that which would be obtained by employing the expression $A_z = 2P(t) \dfrac{\cos \phi}{r_1}$ for a 2-dimensional current dipole on the polar-coordinate axis and then shifting the origin by a distance h.

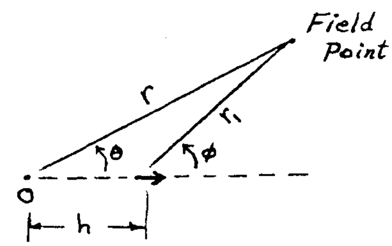

[2] Cf. W.R. Smythe, "Static and Dynamic Electricity" (McGraw-Hill, New York, 1950) Ed. 2, Sect. 4.02, Eqn. (1), p. 65.

[3] It is noted that $\frac{R^2}{h} e^{\frac{v}{R}(t - t_o)} = \frac{R^2}{\tilde{h}}$, so that the external and internal images (used to assist in determination of the magnetic field in the regions $r < R$ and $r > R$, respectively) are images of one another.

[4] It can be confirmed directly that the results presented here in Section 6 do constitute a solution to the problem as it was formulated by the next to last equation of Section 2.

[5] The fact that the current J_z becomes progressively more smoothly distributed is reminiscent of a similar situation for currents induced in an infinite plane

conducting sheet (report of 28 July 1969). The initial eddy-current distribution in the present case is

$$J_z(t_o) = -\frac{P_o}{\pi}\ \frac{(R^2 + h^2)\cos\theta - 2\,Rh}{[R^2 - 2\,Rh\cos\theta + h^2]^2}$$ and only is of a pure cos θ

form if h = o.

INDUCED CURRENT DISTRIBUTION

```
      DIMENSION G(5)
      DIMENSION J(5)
      DO 10 I=1,5
      G(I) = (I - 1)/10
10    CONTINUE
      G0 = G(1)
      G1 = G(2)
      G2 = G(3)
      G3 = G(4)
      G4 = G(5)
      L = 0
20    E = EXP((-L))
      PRINT7, L, G0, G1, G2, G3, G4
30    A = 0
40    C = COS(PI*A/180)
      DO 50 I=1,5
      D = (1 + (G(I)*E)**2 - 2*G(I)*E*C)**2
      J(I) = -((1 + (G(I)*E)**2)*C - 2*G(I)*E)*E/(PI*D)
      IF ((ABS(J(I))) .GT. (5.0E-4)) GO TO 45
      J(I) = 0
45    CONTINUE
50    CONTINUE
      J0 = J(1)
      J1 = J(2)
      J2 = J(3)
      J3 = J(4)
      J4 = J(5)
      PRINT7, A, J0, J1, J2, J3, J4
      IF (A .GT. 175) GO TO 60
      A = A + 10
      GO TO 40
60    IF (L .GT. 2.9) GO TO 70
      L = L + 0.5
      GO TO 20
70    STOP
```

```
L= 0.000   G0= 0.000   G1= 0.100   G2= 0.200   G3= 0.300   G4= 0.400
A= 0.000   J0= -0.318  J1= -0.393  J2= -0.497  J3= -0.650  J4= -0.834
A= 10.00   J0= -0.313  J1= -0.383  J2= -0.476  J3= -0.605  J4= -0.73
A= 20.00   J0= -0.299  J1= -0.353  J2= -0.417  J3= -0.488  J4= -0.554
A= 30.00   J0= -0.276  J1= -0.307  J2= -0.331  J3= -0.337  J4= -0.293
A= 40.00   J0= -0.244  J1= -0.249  J2= -0.235  J3= -0.168  J4= -0.094
A= 50.00   J0= -0.205  J1= -0.184  J2= -0.139  J3= -0.065  J4= 0.041
A= 60.00   J0= -0.159  J1= -0.117  J2= -0.054  J3= 0.026   J4= 0.121
A= 70.00   J0= -0.109  J1= -0.052  J2= 0.017   J3= 0.092   J4= 0.163
A= 80.00   J0= -0.055  J1= 0.006   J2= 0.074   J3= 0.135   J4= 0.183
A= 90.00   J0= 0.000   J1= 0.062   J2= 0.115   J3= 0.161   J4= 0.189
A= 100.0   J0= 0.055   J1= 0.109   J2= 0.150   J3= 0.176   J4= 0.189
A= 110.0   J0= 0.109   J1= 0.149   J2= 0.174   J3= 0.185   J4= 0.185
A= 120.0   J0= 0.159   J1= 0.182   J2= 0.190   J3= 0.189   J4= 0.181
A= 130.0   J0= 0.205   J1= 0.209   J2= 0.202   J3= 0.190   J4= 0.176
A= 140.0   J0= 0.244   J1= 0.229   J2= 0.210   J3= 0.190   J4= 0.171
```

A	J0	J1	J2	J3	J4
150.0	0.276	0.244	0.215	0.190	0.167
160.0	0.299	0.255	0.219	0.189	0.165
170.0	0.313	0.261	0.220	0.187	0.163
180.0	0.318	0.263	0.221	[illegible]	0.162

L= 0.500 G0= 0.000 G1= 0.100 G2= 0.200 G3= 0.300 G4= 0.400

A	J0	J1	J2	J3	J4
0.000	-0.193	-0.219	-0.250	-0.289	-0.337
10.00	-0.190	-0.214	-0.243	-0.277	-0.319
20.00	-0.181	-0.200	-0.222	-0.245	-0.271
30.00	-0.167	-0.179	-0.190	-0.199	-0.204
40.00	-0.148	-0.151	-0.150	-0.145	-0.133
50.00	-0.124	-0.118	-0.107	-0.091	-0.068
60.00	-0.097	-0.083	-0.064	-0.041	-0.013
70.00	-0.066	-0.046	-0.023	0.002	0.030
80.00	-0.034	-0.011	0.014	0.038	0.061
90.00	0.000	0.023	0.045	0.066	0.084
100.0	0.034	0.054	0.072	0.087	0.099
110.0	0.066	0.082	0.094	0.103	0.109
120.0	0.097	0.106	0.112	0.115	0.116
130.0	0.124	0.126	0.126	0.124	0.120
140.0	0.148	0.143	0.137	0.130	0.122
150.0	0.167	0.156	0.144	0.134	0.124
160.0	0.181	0.165	0.150	0.136	0.125
170.0	0.190	0.170	0.153	0.138	0.125
180.0	0.193	0.172	0.154	0.138	0.125

L= 1.000 G0= 0.000 G1= 0.100 G2= 0.200 G3= 0.300 G4= 0.400

A	J0	J1	J2	J3	J4
0.000	-0.117	-0.126	-0.136	-0.148	-0.161
10.00	-0.115	-0.124	-0.133	-0.144	-0.156
20.00	-0.110	-0.117	-0.124	-0.132	-0.140
30.00	-0.101	-0.106	-0.110	-0.114	-0.118
40.00	-0.090	-0.091	-0.092	-0.091	-0.090
50.00	-0.075	-0.073	-0.070	-0.066	-0.061
60.00	-0.059	-0.054	-0.048	-0.041	-0.033
70.00	-0.040	-0.033	-0.025	-0.017	-0.008
80.00	-0.020	-0.012	-0.003	0.006	0.015
90.00	0.000	0.009	0.017	0.025	0.033
100.0	0.020	0.028	0.035	0.042	0.048
110.0	0.040	0.046	0.052	0.056	0.060
120.0	0.059	0.062	0.065	0.068	0.069
130.0	0.075	0.076	0.077	0.077	0.076
140.0	0.090	0.088	0.086	0.084	0.081
150.0	0.101	0.097	0.093	0.089	0.085
160.0	0.110	0.104	0.098	0.092	0.087
170.0	0.115	0.108	0.101	0.094	0.089
180.0	0.117	0.109	0.102	0.095	0.089

L= 1.500 G0= 0.000 G1= 0.100 G2= 0.200 G3= 0.300 G4= 0.400

A	J0	J1	J2	J3	J4
0.000	-0.071	-0.074	-0.078	-0.082	-0.086
10.00	-0.070	-0.073	-0.076	-0.080	-0.083
20.00	-0.067	-0.069	-0.072	-0.075	-0.077
30.00	-0.062	-0.063	-0.065	-0.066	-0.068
40.00	-0.054	-0.055	-0.055	-0.055	-0.056
50.00	-0.046	-0.045	-0.044	-0.043	-0.042
60.00	-0.036	-0.034	-0.032	-0.030	-0.027
70.00	-0.024	-0.022	-0.019	-0.016	-0.013
80.00	-0.012	-0.009	-0.006	-0.003	0.000
90.00	0.000	0.003	0.006	0.009	0.012
100.0	0.012	0.015	0.018	0.021	0.023

A= 110.0	J0= 0.024	J1= 0.027	J2= 0.029	J3= 0.031	J4= 0.033
A= 120.0	J0= 0.036	J1= 0.037	J2= 0.038	J3= 0.039	J4= 0.040
A= 130.0	J0= 0.046	J1= 0.046	J2= 0.046	J3= 0.047	J4= 0.047
A= 140.0	J0= 0.054	J1= 0.054	J2= 0.053	J3= 0.052	J4= 0.052
A= 150.0	J0= 0.062	J1= 0.060	J2= 0.058	J3= 0.057	J4= 0.055
A= 160.0	J0= 0.067	J1= 0.064	J2= 0.062	J3= 0.060	J4= 0.058
A= 170.0	J0= 0.070	J1= 0.067	J2= 0.064	J3= 0.062	J4= 0.059
A= 180.0	J0= 0.071	J1= 0.068	J2= 0.065	J3= 0.062	J4= 0.060

L= 2.000 G0= 0.000 G1= 0.100 G2= 0.200 G3= 0.300 G4= 0.400

A= 0.000	J0= -0.043	J1= -0.044	J2= -0.046	J3= -0.047	J4= -0.048
A= 10.00	J0= -0.042	J1= -0.044	J2= -0.045	J3= -0.046	J4= -0.047
A= 20.00	J0= -0.040	J1= -0.041	J2= -0.042	J3= -0.043	J4= -0.044
A= 30.00	J0= -0.037	J1= -0.038	J2= -0.038	J3= -0.039	J4= -0.040
A= 40.00	J0= -0.033	J1= -0.033	J2= -0.033	J3= -0.033	J4= -0.034
A= 50.00	J0= -0.028	J1= -0.027	J2= -0.027	J3= -0.027	J4= -0.027
A= 60.00	J0= -0.022	J1= -0.021	J2= -0.020	J3= -0.020	J4= -0.019
A= 70.00	J0= -0.015	J1= -0.014	J2= -0.013	J3= -0.012	J4= -0.011
A= 80.00	J0= -0.007	J1= -0.006	J2= -0.005	J3= -0.004	J4= -0.003
A= 90.00	J0= 0.000	J1= 0.001	J2= 0.002	J3= 0.003	J4= 0.005
A= 100.0	J0= 0.007	J1= 0.009	J2= 0.010	J3= 0.011	J4= 0.012
A= 110.0	J0= 0.015	J1= 0.016	J2= 0.016	J3= 0.017	J4= 0.018
A= 120.0	J0= 0.022	J1= 0.022	J2= 0.023	J3= 0.023	J4= 0.024
A= 130.0	J0= 0.028	J1= 0.028	J2= 0.028	J3= 0.028	J4= 0.028
A= 140.0	J0= 0.033	J1= 0.033	J2= 0.033	J3= 0.032	J4= 0.032
A= 150.0	J0= 0.037	J1= 0.037	J2= 0.036	J3= 0.036	J4= 0.035
A= 160.0	J0= 0.040	J1= 0.040	J2= 0.039	J3= 0.038	J4= 0.037
A= 170.0	J0= 0.042	J1= 0.041	J2= 0.040	J3= 0.039	J4= 0.038
A= 180.0	J0= 0.043	J1= 0.042	J2= 0.041	J3= 0.040	J4= 0.039

L= 2.500 G0= 0.000 G1= 0.100 G2= 0.200 G3= 0.300 G4= 0.400

A= 0.000	J0= -0.026	J1= -0.027	J2= -0.027	J3= -0.027	J4= -0.028
A= 10.00	J0= -0.026	J1= -0.026	J2= -0.027	J3= -0.027	J4= -0.027
A= 20.00	J0= -0.025	J1= -0.025	J2= -0.025	J3= -0.026	J4= -0.026
A= 30.00	J0= -0.023	J1= -0.023	J2= -0.023	J3= -0.023	J4= -0.023
A= 40.00	J0= -0.020	J1= -0.020	J2= -0.020	J3= -0.020	J4= -0.020
A= 50.00	J0= -0.017	J1= -0.017	J2= -0.017	J3= -0.017	J4= -0.016
A= 60.00	J0= -0.013	J1= -0.013	J2= -0.013	J3= -0.012	J4= -0.012
A= 70.00	J0= -0.009	J1= -0.009	J2= -0.008	J3= -0.008	J4= -0.008
A= 80.00	J0= -0.005	J1= -0.004	J2= -0.004	J3= -0.003	J4= -0.003
A= 90.00	J0= 0.000	J1= 0.000	J2= 8.57E-04	J3= 0.001	J4= 0.002
A= 100.0	J0= 0.005	J1= 0.005	J2= 0.005	J3= 0.006	J4= 0.006
A= 110.0	J0= 0.009	J1= 0.009	J2= 0.010	J3= 0.010	J4= 0.010
A= 120.0	J0= 0.013	J1= 0.013	J2= 0.013	J3= 0.014	J4= 0.014
A= 130.0	J0= 0.017	J1= 0.017	J2= 0.017	J3= 0.017	J4= 0.017
A= 140.0	J0= 0.020	J1= 0.020	J2= 0.020	J3= 0.020	J4= 0.020
A= 150.0	J0= 0.023	J1= 0.022	J2= 0.022	J3= 0.022	J4= 0.022
A= 160.0	J0= 0.025	J1= 0.024	J2= 0.024	J3= 0.024	J4= 0.023
A= 170.0	J0= 0.026	J1= 0.025	J2= 0.025	J3= 0.025	J4= 0.024
A= 180.0	J0= 0.026	J1= 0.026	J2= 0.025	J3= 0.025	J4= 0.024

L= 3.000 G0= 0.000 G1= 0.100 G2= 0.200 G3= 0.300 G4= 0.400

A= 0.000	J0= -0.016	J1= -0.016	J2= -0.016	J3= -0.016	J4= -0.016
A= 10.00	J0= -0.016	J1= -0.016	J2= -0.016	J3= -0.016	J4= -0.016
A= 20.00	J0= -0.015	J1= -0.015	J2= -0.015	J3= -0.015	J4= -0.015
A= 30.00	J0= -0.014	J1= -0.014	J2= -0.014	J3= -0.014	J4= -0.014
A= 40.00	J0= -0.012	J1= -0.012	J2= -0.012	J3= -0.012	J4= -0.012
A= 50.00	J0= -0.010	J1= -0.010	J2= -0.010	J3= -0.010	J4= -0.010
A= 60.00	J0= -0.008	J1= -0.008	J2= -0.008	J3= -0.008	J4= -0.008

```
A=  70.00   J0= -0.005   J1= -0.005   J2= -0.005   J3= -0.005   J4= -0.005
A=  80.00   J0= -0.003   J1= -0.003   J2= -0.002   J3= -0.002   J4= -0.002
A=  90.00   J0= 0.000    J1= 0.000    J2= 0.000    J3= 0.000    J4= 6.31E-04
A=  100.0   J0= 0.003    J1= 0.003    J2= 0.003    J3= 0.003    J4= 0.003
A=  110.0   J0= 0.005    J1= 0.006    J2= 0.006    J3= 0.006    J4= 0.006
A=  120.0   J0= 0.008    J1= 0.008    J2= 0.008    J3= 0.008    J4= 0.008
A=  130.0   J0= 0.010    J1= 0.010    J2= 0.010    J3= 0.010    J4= 0.010
A=  140.0   J0= 0.012    J1= 0.012    J2= 0.012    J3= 0.012    J4= 0.012
A=  150.0   J0= 0.014    J1= 0.014    J2= 0.014    J3= 0.013    J4= 0.013
A=  160.0   J0= 0.015    J1= 0.015    J2= 0.015    J3= 0.015    J4= 0.014
A=  170.0   J0= 0.016    J1= 0.015    J2= 0.015    J3= 0.015    J4= 0.015
A=  180.0   J0= 0.016    J1= 0.016    J2= 0.016    J3= 0.015    J4= 0.015
```

IMAGE FIELD AT SOURCE LOCATION

```
         DIMENSION G(5)
         DIMENSION B(5)
         DO 10 I=1,5
         G(I) = (I - 1)/10
   10    CONTINUE
         G0 = G(1)
         G1 = G(2)
         G2 = G(3)
         G3 = G(4)
         G4 = G(5)
         A = 0
         PRINT7, A, G0, G1, G2, G3, G4
         L = 0
   20    E = EXP((-L))
         DO 30 I=1,5
         D = (1 - G(I)*G(I)*E)**2
         B(I) = 2*E/D
         IF ((ABS(B(I))) .GT. (5.0E-4)) GO TO 25
         B(I) = 0
   25    CONTINUE
   30    CONTINUE
         B0 = B(1)
         B1 = B(2)
         B2 = B(3)
         B3 = B(4)
         B4 = B(5)
         PRINT7, L, B0, B1, B2, B3, B4
         IF (L .GT. 4.95) GO TO 40
         L = L + 0.1
         GO TO 20
   40    STOP
```

A= 0.000	G0= 0.000	G1= 0.100	G2= 0.200	G3= 0.300	G4= 0.400
L= 0.000	B0= 2.000	B1= 2.041	B2= 2.170	B3= 2.415	B4= 2.834
L= 0.100	B0= 1.810	B1= 1.843	B2= 1.948	B3= 2.145	B4= 2.474
L= 0.200	B0= 1.637	B1= 1.665	B2= 1.750	B3= 1.908	B4= 2.168
L= 0.300	B0= 1.482	B1= 1.504	B2= 1.574	B3= 1.701	B4= 1.907
L= 0.400	B0= 1.341	B1= 1.359	B2= 1.416	B3= 1.518	B4= 1.682
L= 0.500	B0= 1.213	B1= 1.228	B2= 1.274	B3= 1.357	B4= 1.488
L= 0.600	B0= 1.098	B1= 1.110	B2= 1.147	B3= 1.215	B4= 1.319
L= 0.700	B0= 0.993	B1= 1.003	B2= 1.034	B3= 1.088	B4= 1.172
L= 0.800	B0= 0.899	B1= 0.907	B2= 0.932	B3= 0.976	B4= 1.043
L= 0.900	B0= 0.813	B1= 0.820	B2= 0.840	B3= 0.876	B4= 0.930
L= 1.000	B0= 0.736	B1= 0.741	B2= 0.758	B3= 0.787	B4= 0.831
L= 1.100	B0= 0.666	B1= 0.670	B2= 0.684	B3= 0.707	B4= 0.743
L= 1.200	B0= 0.602	B1= 0.606	B2= 0.617	B3= 0.636	B4= 0.665
L= 1.300	B0= 0.545	B1= 0.548	B2= 0.557	B3= 0.573	B4= 0.596
L= 1.400	B0= 0.493	B1= 0.496	B2= 0.503	B3= 0.516	B4= 0.535
L= 1.500	B0= 0.446	B1= 0.448	B2= 0.454	B3= 0.465	B4= 0.480
L= 1.600	B0= 0.404	B1= 0.405	B2= 0.410	B3= 0.419	B4= 0.431
L= 1.700	B0= 0.365	B1= 0.367	B2= 0.371	B3= 0.378	B4= 0.388
L= 1.800	B0= 0.331	B1= 0.332	B2= 0.335	B3= 0.341	B4= 0.349
L= 1.900	B0= 0.299	B1= 0.300	B2= 0.303	B3= 0.307	B4= 0.314
L= 2.000	B0= 0.271	B1= 0.271	B2= 0.274	B3= 0.277	B4= 0.283
L= 2.100	B0= 0.245	B1= 0.246	B2= 0.247	B3= 0.250	B4= 0.255
L= 2.200	B0= 0.222	B1= 0.222	B2= 0.224	B3= 0.226	B4= 0.230
L= 2.300	B0= 0.201	B1= 0.201	B2= 0.202	B3= 0.204	B4= 0.207
L= 2.400	B0= 0.181	B1= 0.182	B2= 0.183	B3= 0.184	B4= 0.187
L= 2.500	B0= 0.164	B1= 0.164	B2= 0.165	B3= 0.167	B4= 0.169
L= 2.600	B0= 0.149	B1= 0.149	B2= 0.149	B3= 0.151	B4= 0.152
L= 2.700	B0= 0.134	B1= 0.135	B2= 0.135	B3= 0.136	B4= 0.137
L= 2.800	B0= 0.122	B1= 0.122	B2= 0.122	B3= 0.123	B4= 0.124
L= 2.900	B0= 0.110	B1= 0.110	B2= 0.111	B3= 0.111	B4= 0.112
L= 3.000	B0= 0.100	B1= 0.100	B2= 0.100	B3= 0.100	B4= 0.101
L= 3.100	B0= 0.090	B1= 0.090	B2= 0.090	B3= 0.091	B4= 0.091
L= 3.200	B0= 0.082	B1= 0.082	B2= 0.082	B3= 0.082	B4= 0.083
L= 3.300	B0= 0.074	B1= 0.074	B2= 0.074	B3= 0.074	B4= 0.075
L= 3.400	B0= 0.067	B1= 0.067	B2= 0.067	B3= 0.067	B4= 0.067
L= 3.500	B0= 0.060	B1= 0.060	B2= 0.061	B3= 0.061	B4= 0.061
L= 3.600	B0= 0.055	B1= 0.055	B2= 0.055	B3= 0.055	B4= 0.055
L= 3.700	B0= 0.049	B1= 0.049	B2= 0.050	B3= 0.050	B4= 0.050
L= 3.800	B0= 0.045	B1= 0.045	B2= 0.045	B3= 0.045	B4= 0.045
L= 3.900	B0= 0.040	B1= 0.041	B2= 0.041	B3= 0.041	B4= 0.041
L= 4.000	B0= 0.037	B1= 0.037	B2= 0.037	B3= 0.037	B4= 0.037
L= 4.100	B0= 0.033	B1= 0.033	B2= 0.033	B3= 0.033	B4= 0.033
L= 4.200	B0= 0.030	B1= 0.030	B2= 0.030	B3= 0.030	B4= 0.030
L= 4.300	B0= 0.027	B1= 0.027	B2= 0.027	B3= 0.027	B4= 0.027
L= 4.400	B0= 0.025	B1= 0.025	B2= 0.025	B3= 0.025	B4= 0.025
L= 4.500	B0= 0.022	B1= 0.022	B2= 0.022	B3= 0.022	B4= 0.022
L= 4.600	B0= 0.020	B1= 0.020	B2= 0.020	B3= 0.020	B4= 0.020
L= 4.700	B0= 0.018	B1= 0.018	B2= 0.018	B3= 0.018	B4= 0.018
L= 4.800	B0= 0.016	B1= 0.016	B2= 0.016	B3= 0.016	B4= 0.017
L= 4.900	B0= 0.015	B1= 0.015	B2= 0.015	B3= 0.015	B4= 0.015
L= 5.000	B0= 0.013	B1= 0.013	B2= 0.013	B3= 0.013	B4= 0.014

END XEQ.

GRADIENT OF IMAGE FIELD, AT SOURCE LOCATION

```
      DIMENSION G(5)
      DIMENSION P(5)
      DO 10 I=1,5
      G(I) = (I - 1)/10
10    CONTINUE
      G0 = G(1)
      G1 = G(2)
      G2 = G(3)
      G3 = G(4)
      G4 = G(5)
      A = 0
      PRINT7, A, G0, G1, G2, G3, G4
      L = 0
20    E = EXP((-L))
      DO 30 I=1,5
      D = (1 - G(I)*G(I)*E)**3
      P(I) = 4*E*E/D
      IF ((ABS(P(I))) .GT. (5.0E-4)) GO TO 25
      P(I) = 0
25    CONTINUE
30    CONTINUE
      P0 = P(1)
      P1 = P(2)
      P2 = P(3)
      P3 = P(4)
      P4 = P(5)
      PRINT7, L, P0, P1, P2, P3, P4
      IF (L .GT. 4.95) GO TO 40
      L = L + 0.1
      GO TO 20
40    STOP
```

```
A= 0.000   G0= 0.000   G1= 0.100   G2= 0.200   G3= 0.300   G4= 0.400
L= 0.000   P0= 4.000   P1= 4.122   P2= 4.521   P3= 5.308   P4= 6.749
L= 0.100   P0= 3.275   P1= 3.365   P2= 3.658   P3= 4.225   P4= 5.236
L= 0.200   P0= 2.681   P1= 2.748   P2= 2.963   P3= 3.373   P4= 4.086
L= 0.300   P0= 2.195   P1= 2.245   P2= 2.403   P3= 2.700   P4= 3.205
L= 0.400   P0= 1.797   P1= 1.834   P2= 1.950   P3= 2.166   P4= 2.526
L= 0.500   P0= 1.472   P1= 1.499   P2= 1.584   P3= 1.741   P4= 1.999
L= 0.600   P0= 1.205   P1= 1.225   P2= 1.288   P3= 1.403   P4= 1.587
L= 0.700   P0= 0.986   P1= 1.001   P2= 1.048   P3= 1.131   P4= 1.264
L= 0.800   P0= 0.808   P1< 0.819   P2= 0.853   P3= 0.914   P4= 1.010
L= 0.900   P0= 0.661   P1= 0.669   P2= 0.695   P3= 0.739   P4= 0.809
L= 1.000   P0= 0.541   P1= 0.547   P2= 0.566   P3= 0.599   P4= 0.649
L= 1.100   P0= 0.443   P1= 0.448   P2= 0.461   P3= 0.486   P4= 0.522
L= 1.200   P0= 0.363   P1= 0.366   P2= 0.376   P3= 0.394   P4= 0.421
L= 1.300   P0= 0.297   P1= 0.300   P2= 0.307   P3= 0.320   P4= 0.340
L= 1.400   P0= 0.243   P1= 0.245   P2= 0.251   P3= 0.260   P4= 0.274
L= 1.500   P0= 0.199   P1= 0.200   P2= 0.205   P3= 0.212   P4= 0.222
L= 1.600   P0= 0.163   P1= 0.164   P2= 0.167   P3= 0.172   P4= 0.180
L= 1.700   P0= 0.133   P1= 0.134   P2= 0.136   P3= 0.140   P4= 0.146
L= 1.800   P0= 0.109   P1= 0.110   P2= 0.111   P3= 0.114   P4= 0.118
L= 1.900   P0= 0.089   P1= 0.090   P2= 0.091   P3= 0.093   P4= 0.096
L= 2.000   P0= 0.073   P1= 0.074   P2= 0.074   P3= 0.076   P4= 0.078
L= 2.100   P0= 0.060   P1= 0.060   P2= 0.061   P3= 0.062   P4= 0.064
L= 2.200   P0= 0.049   P1= 0.049   P2= 0.050   P3= 0.051   P4= 0.052
L= 2.300   P0= 0.040   P1= 0.040   P2= 0.041   P3= 0.041   P4= 0.042
L= 2.400   P0= 0.033   P1= 0.033   P2= 0.033   P3= 0.034   P4= 0.034
L= 2.500   P0= 0.027   P1= 0.027   P2= 0.027   P3= 0.028   P4= 0.028
L= 2.600   P0= 0.022   P1= 0.022   P2= 0.022   P3= 0.023   P4= 0.023
L= 2.700   P0= 0.018   P1= 0.018   P2= 0.018   P3= 0.018   P4= 0.019
L= 2.800   P0= 0.015   P1= 0.015   P2= 0.015   P3= 0.015   P4= 0.015
L= 2.900   P0= 0.012   P1= 0.012   P2= 0.012   P3= 0.012   P4= 0.012
L= 3.000   P0= 0.010   P1= 0.010   P2= 0.010   P3= 0.010   P4= 0.010
L= 3.100   P0= 0.008   P1= 0.008   P2= 0.008   P3= 0.008   P4= 0.008
L= 3.200   P0= 0.007   P1= 0.007   P2= 0.007   P3= 0.007   P4= 0.007
L= 3.300   P0= 0.005   P1= 0.005   P2= 0.005   P3= 0.005   P4= 0.006
L= 3.400   P0= 0.004   P1= 0.004   P2= 0.004   P3= 0.004   P4= 0.005
L= 3.500   P0= 0.004   P1= 0.004   P2= 0.004   P3= 0.004   P4= 0.004
L= 3.600   P0= 0.003   P1= 0.003   P2= 0.003   P3= 0.003   P4= 0.003
L= 3.700   P0= 0.002   P1= 0.002   P2= 0.002   P3= 0.002   P4= 0.002
L= 3.800   P0= 0.002   P1= 0.002   P2= 0.002   P3= 0.002   P4= 0.002
L= 3.900   P0= 0.002   P1= 0.002   P2= 0.002   P3= 0.002   P4= 0.002
L= 4.000   P0= 0.001   P1= 0.001   P2= 0.001   P3= 0.001   P4= 0.001
L= 4.100   P0= 0.001   P1= 0.001   P2= 0.001   P3< 0.001   P4= 0.001
L= 4.200   P0= 8.99E-04   P1= 9.00E-04   P2= 9.01E-04   P3= 9.03E-04
P4= 9.06E-04
L= 4.300   P0= 7.36E-04   P1= 7.37E-04   P2= 7.38E-04   P3= 7.39E-04
P4= 7.41E-04
L= 4.400   P0= 6.03E-04   P1= 6.03E-04   P2= 6.04E-04   P3= 6.05E-04
P4= 6.06E-04
L= 4.500   P0= 0.000   P1= 0.000   P2= 0.000   P3= 0.000   P4= 0.000
L= 4.600   P0= 0.000   P1= 0.000   P2= 0.000   P3= 0.000   P4= 0.000
L= 4.700   P0= 0.000   P1= 0.000   P2= 0.000   P3= 0.000   P4= 0.000
L= 4.800   P0= 0.000   P1= 0.000   P2= 0.000   P3= 0.000   P4= 0.000
L= 4.900   P0= 0.000   P1= 0.000   P2= 0.000   P3= 0.000   P4= 0.000
L= 5.000   P0= 0.000   P1= 0.000   P2= 0.000   P3= 0.000   P4= 0.000
END XEQ.
```

ON HIGH-CURRENT INJECTION*

(Preliminary notes to serve as basis of discussion)

L. Jackson Laslett

Lawrence Radiation Laboratory
University of California
Berkeley, California

October 1, 1969**

* Work supported by the U.S. Atomic Energy Commission.

** Submitted for typing on 22 December 1969.

I. Introduction

The action of self-fields has been mentioned (Kerst, Judd, Lambertson, Hartwig, Faltens) as a possible mechanism for self-inflection. It appears that, even overlooking image effects, there may be several phenomena of this type:

(i) There are radial self forces from bias fields (Laslett; Ivanov et al.) that act in a sense to expand the ring (Kegel).

(ii) The increasing flux through the ring produces a back-EMF that acts to retard the particles, with the result that the orbits gradually would contract in radius from this effect alone.

(iii) The increasing charge on the ring produces an electrostatic potential that acts to retard the particles on injection, and this effect also acts to decrease the radius of the path described in the magnetic field (Faltens).

We attempt to treat these effects, in turn, below. We suppose that at any time $n(t)$ particles have been injected to form a ring, so that we consider the steady injection of $\dot{n}$ highly-relativistic particles (of charge e esu) per second, at an injection momentum p_o. For simplicity, we take the applied magnetic field to be spatially constant ("uniform"), and let R_o denote the trajectory radius for particles of momentum p_o in this field.

We employ r_o to denote the classical particle radius,

$$r_o = \frac{e^2}{m_o c^2} \quad (= 2.82 \times 10^{-13} \text{ cm for electrons}).$$

II. Estimates of $\Delta R/R_o$

(i) The effect of the radial self-forces:

The electric and magnetic "bias fields" lead to an effective radial bias force (Laslett; Ivanov et al.)

$$eF_r)_o = e(E_r + B_z)_o = \frac{m_o c^2 \gamma}{R} \mu P, \tag{1}$$

to employ the notation of Ivanov et al. in which

$$\mu P = \frac{(\text{Particles per unit length}) \times r_o}{\gamma} \left[2 \ln \frac{8R}{\bar{b}}\right]$$

$$= \frac{n r_o}{\pi \gamma R} \ln \frac{8R}{\bar{b}} . \tag{2}$$

Then, for particles of momentum p_o in a magnetic field

$$B_o \text{ (emu)} = \frac{p_o}{(e/c)R_o} ,$$

we have (treating $\beta \cong 1$):

$$\left[\frac{e}{c} B_o - \frac{m_o c\gamma}{R} \mu P\right] R = \frac{e}{c} B_o R_o = m_o \gamma \beta c$$

$$\cong m_o \gamma c$$

$$\frac{e}{c} B_o R - (m_o c\gamma)(\mu P) = \frac{e}{c} B_o R_o \cong m_o \gamma c$$

$$B_o R - \frac{m_o c^2 \gamma}{e} \mu P = B_o R_o \cong \frac{m_o c^2}{e} \gamma$$

$$B_o R - (B_o R_o)\mu P = B_o R_o$$

$$B_o R = B_o R_o (1 + \mu P)$$

or

$$\frac{R}{R_o} = 1 + \mu P \tag{3}$$

[*cf*. Kegel].

This result contrasts the orbit radii of electrons of a *specified kinetic energy* under circumstances of high *vs*. vanishing intensity.

(ii) *The effect of the back electromotance*:

With n particles of charge e esu in the ring, the circulating current in emu is (for $\beta \cong 1$)

$$I = \frac{ne}{2\pi R} \quad \text{emu} \tag{4}$$

and the rate of increase of this current is

$$\dot{I} = \frac{\dot{n}e}{2\pi R} \quad \text{abamp/sec.} \tag{5}$$

The induced electromotance (per turn) is most readily obtained from the self-inductance of the ring, which is given roughly by

$$L \cong 4\pi R \ln \frac{8R}{\bar{b}} \quad \text{emu.} \tag{6}$$

The induced electromotance per turn then is

$$\begin{aligned} E &= - L\dot{I} \\ &= - 2\dot{n}e \ln \frac{8R}{\bar{b}} \quad \text{emu,} \end{aligned} \tag{7}$$

the negative sign indicating that the induced electric field acts to <u>decrease</u> the particle energy when $\dot{n} > o$ (Lenz's Law).

All particles, once they are in the ring, will individually lose momentum at the following rate as a result of the induced electric field associated with the electromotance given by Eqn. (7):

$$\frac{dp}{dt} = \frac{1}{c}\,\frac{dE}{dt} = \frac{Ee}{c^2}\,\frac{\omega}{2\pi} = - \frac{\dot{n}e^2\omega}{\pi c^2} \ln \frac{8R}{\bar{b}} = - \frac{\dot{n}e^2}{\pi cR} \ln \frac{8R}{\bar{b}}\,, \tag{8}$$

or

$$\begin{aligned} \frac{dp/dt}{p_o} &= \frac{\dot{n}e^2}{\pi\gamma m_o Rc^2} \ln \frac{8R}{\bar{b}} \\ &= - \frac{\dot{n}r_o}{\pi\gamma R} \ln \frac{8R}{\bar{b}}\,. \end{aligned} \tag{9}$$

Thus, for an <u>early</u> particle that is injected when the ring has zero intensity,

$$\left.\frac{\Delta p}{p_o}\right)_{\text{early}} = - \frac{nr_o}{\pi\gamma R} \ln \frac{8R}{\bar{b}}\,,$$

while one injected when $n = n_i$ experiences a momentum change given by

$$\left.\frac{\Delta p}{p_o}\right)_i = - \frac{(n - n_i)r_o}{\pi\gamma R} \ln \frac{8R}{\bar{b}}\,. \tag{10}$$

Accordingly, at any given time when the number of particles in the ring is n, the average particle momentum will differ from p_o by an amount

$\Delta p = \langle p \rangle - p_o$ given by

$$\frac{\Delta p}{p_o} = - \frac{\int_o^n (n - n_i)\, dn_i}{\int_o^n dn_i} \;\; \frac{r_o}{\pi \gamma R} \; \ln \frac{8R}{b}$$

$$= - \frac{n r_o}{2\pi\gamma R} \; \ln \frac{8R}{b} \qquad (11)$$

With the ring acting as-a-whole with regard to its curvature in a uniform applied magnetic field, this change of average momentum will imply a corresponding radius change given by

$$\frac{\Delta R}{R_o} = - \; \frac{n r_o}{2\pi\gamma R} \; \ln \frac{8R}{b} \; . \qquad (12)$$

Alternative Derivation: As Faltens has pointed out, the ring contraction derived above for the effect of induced electromotance [effect (ii)] should be readily derivable by consideration of the energy in the magnetic field.

The relevant quantity of interest here is the magnetic energy term that is proportional to the square of the circulating current:

$$W_M = \frac{1}{2} L I^2$$

$$= \frac{n^2 e^2}{2\pi R} \ln \frac{8R}{b} \; . \qquad (13)$$

If this energy is provided by the incoming particles, the departure of the average particle momentum from p_o will be given, for this cause, by

$$\Delta p = \frac{1}{c} \Delta E = - \frac{W_M}{nc} = - \frac{ne^2}{2\pi c R} \ln \frac{8R}{b}$$

and hence

$$\frac{\Delta p}{p_o} = - \; \frac{ne^2}{2\pi\gamma m_o c^2 R} \; \ln \frac{8R}{b}$$

$$= - \frac{nr_o}{2\pi\gamma R} \ln \frac{8R}{b} , \tag{14}$$

a result that is identical to Eqn. (11) on p. 4. Accordingly, we obtain, as before (p. 4),

$$\frac{\Delta R}{R_o} = - \frac{nr_o}{2\pi\gamma R} \ln \frac{8R}{b}$$

$$= - \frac{1}{2} \mu P, \tag{15}$$

or

$$\frac{R}{R_o} = 1 - \frac{1}{2} \mu P. \tag{16}$$

(iii) <u>The effect of the electrostatic potential of the ring:</u>

We may take the electrostatic potential of the ring as essentially

$$V = 2\lambda \ln \frac{8R}{b} = \frac{Q}{\pi R} \ln \frac{8R}{b} = \frac{ne}{\pi R} \ln \frac{8R}{b} \text{ esu.} \tag{17}$$

[This suggests $V/\lambda = 2 \ln \frac{8R}{b} = 2 \ln(320) = 11.54$ at the center of a ring with $\frac{R}{b} = 40$; compare L.J. Laslett, ERAN-7 in the ERA 1968 <u>Proceedings</u> (UCRL-18103).]

A particle injected at a moment when the ring contains n_i particles thus would be expected to experience a loss of momentum, because of the electrostatic field, given by

$$\Delta p = \frac{1}{c} \Delta E = - \frac{n_i e^2}{\pi c R} \ln \frac{8R}{b} \tag{18}$$

or (for $\beta \cong 1$)

$$\frac{\Delta p}{p_o} = - \frac{n_i e^2}{\pi \gamma m_o c^2 R} \ln \frac{8R}{b}$$

$$= - \frac{n_i r_o}{\pi \gamma R} \ln \frac{8R}{b} \tag{19}$$

Accordingly, when the number of particles in the ring has become n, the average particle momentum will differ from p_o by an amount $\Delta p = \langle p \rangle - p_o$ such that

$$\frac{\Delta p}{p_o} = - \frac{\int_o^n n_i dn_i}{\int_o^n dn_i} \frac{r_o}{\pi \gamma R} \ln \frac{8R}{\bar{b}}$$

$$= - \frac{n r_o}{2\pi\gamma R} \ln \frac{8R}{\bar{b}} . \tag{20}$$

As in sub-section (ii), this effect similarly will itself contribute a radius change given by a similar expression

$$\frac{\Delta R}{R_o} = - \frac{n r_o}{2\pi\gamma R} \ln \frac{8R}{\bar{b}} . \tag{21}$$

<u>Alternative Derivation</u>: Analogously to the work on p. 4-5, the ring contraction derived above for the effect of electrostatic fields in reducing the particle kinetic energy can alternatively be derived by following Faltens' suggestion that this effect will follow from consideration of the electrostatic field energy.

We employ the electrostatic field energy term that is proportional to the square of the number of charged particles present:

$$W_E = \frac{1}{2} QV = \frac{n^2 e^2}{2\pi R} \ln \frac{8R}{\bar{b}} . \tag{22}$$

If this energy is provided by the incoming particles, the departure of the average particle momentum from the injector value will be given, for this effect, by

$$\Delta p = \frac{1}{c} \Delta E = - \frac{W_E}{nc} = - \frac{ne^2}{2\pi c R} \ln \frac{8R}{\bar{b}}$$

and hence

$$\frac{\Delta p}{p_o} = - \frac{ne^2}{2\pi\gamma m_o c^2 R} \ln \frac{8R}{\bar{b}}$$

$$= -\frac{nr_o}{2\pi\gamma R} \ln \frac{8R}{b} , \tag{23}$$

a result that agrees with that given as Eqn. (20) on p. 6. Accordingly we obtain, as before (p. 6),

$$\frac{\Delta R}{R_o} = -\frac{nr_o}{2\pi\gamma R} \ln \frac{8R}{b}$$

$$= -\frac{1}{2}\mu P, \tag{24}$$

or

$$\frac{R}{R_o} = 1 - \frac{1}{2}\mu P. \tag{25}$$

III. Summary

Neglecting image-field effects and the influence of trapped ions (that in practice may gradually accumulate in the ring beam, we find the following terms for contributions to $\frac{\Delta R}{R_o}$ in a uniform applied field:

From Radial Self Forces:	$+\mu P$	Sect. II(i), Eqn. (3), p.2;
From Back Electromotance:	$-\frac{1}{2}\mu P$	Sect. II(ii), Eqn. (16), p.5;
From Electrostatic Potential:	$-\frac{1}{2}\mu P$	Sect. II(iii), Eqn. (25), p.7.

The total result of these three effects thus appears to be zero -- at least to the accuracy justified by the foregoing rough calculations.

It undoubtedly will be recognized that, in many situations met in practice, image effects can, however, be of considerable importance. Such effects would, of course, deserve specific study and one can scarcely anticipate that in the end their results will vanish.

IV. Comments (22 December 1969)

The above notes have been circulated to serve as a basis of discussion. There is a continuing interest in these possible effects that may influence the equilibrium-orbit radius at injection, and also in the following allied features: energy change, dispersion of radius, and dispersion of energy. It will be recognized that the model used as a basis for the present treatment is incomplete -- it may be appropriate to attempt careful attention to the following additional aspects (amongst others):

1. Inacuracy of the simple (logarithmic) formulas for the "bias fields".

2. Effect of electric and magnetic images, and the possible decay of the latter (if present).

3. Azimuthal variations

   (a) From the plural-form character of the injection process;

   (b) From localized features of the structure (e.g., the injection snout).

ERAN-44
November 4, 1969

POTENTIAL OF A UNIFORMLY CHARGED BEAM WITH AN ELLIPTICAL SHAPE †

L. Jackson Laslett

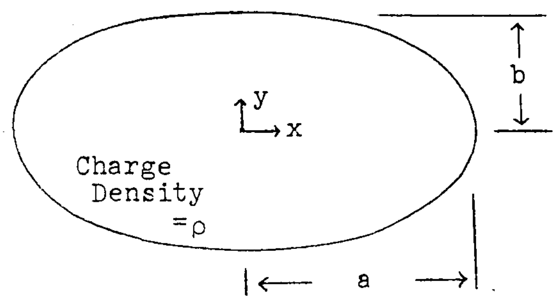

I Write $x = \sqrt{a^2 - b^2}\ \sin u \operatorname{Cosh} v$

$y = \sqrt{a^2 - b^2}\ \cos u \operatorname{Sinh} v.$

Introducing the complex numbers

$\tilde{z} = x + iy,\ \tilde{w} = u + iv,$

this transformation may be written $\tilde{z} = \sqrt{a^2 - b^2}\ \sin \tilde{w}$ and hence is conformal.

(a) It may be noted that, for this transformation,

$$\frac{d\tilde{z}}{d\tilde{w}} = \sqrt{a^2 - b^2}\ \cos \tilde{w} = \sqrt{a^2 - b^2}\ (\cos u \operatorname{Cosh} v - i \sin u \operatorname{Sinh} v),$$

so that

$$\left|\frac{d\tilde{z}}{d\tilde{w}}\right|^2 = (a^2 - b^2)\ (\cos^2 u \operatorname{Cosh}^2 v + \sin^2 u \operatorname{Sinh}^2 v)$$

$$= (a^2 - b^2) \cdot \frac{\cos 2u + \operatorname{Cosh} 2v}{2} .$$

(b) Also, curves of constant v are given by

$$\left(\frac{x}{\sqrt{a^2 - b^2}\ \operatorname{Cosh} v}\right)^2 + \left(\frac{y}{\sqrt{a^2 - b^2}\ \operatorname{Sinh} v}\right)^2 = 1,$$

so that when
$$\left.\begin{aligned} \operatorname{Cosh} v &= \frac{a}{\sqrt{a^2 - b^2}} \\ \operatorname{Sinh} v &= \frac{b}{\sqrt{a^2 - b^2}} \\ v &= \operatorname{Tanh}^{-1} \frac{b}{a} \end{aligned}\right\}$$
we have the ellipse $\left(\frac{x}{a}\right)^2 + \left(\frac{y}{b}\right)^2 = 1.$

† Work supported by the U.S. Atomic Energy Commission.

For this value of v we also have

$$\text{Cosh } 2v = \frac{a^2 + b^2}{a^2 - b^2}$$

$$\text{Sinh } 2v = \frac{2ab}{a^2 - b^2}$$

$$e^{2v} = \frac{a + b}{a - b}$$

$$\epsilon^{-2v} = \frac{a - b}{a + b} .$$

II Write the electrostatic potential as*

$$\Phi = - \frac{2\pi\rho}{a+b} (bx^2 + ay^2)$$

$$= + \frac{\pi\rho}{2} (a-b) \left\{[(a-b)+(a+b) \cos 2u] - [(a+b)+(a-b) \cos 2u]\right\} \text{Cosh } 2v$$

for points <u>inside</u> the elliptical boundary,

$$(v \leq \text{Tanh}^{-1} \frac{b}{a}).$$

The potential as written in the Cartesian form is clearly such that

$\nabla^2_{x,y} \Phi = -4\pi\rho$, as required.

If one wishes to check the $\Phi(u,v)$ in this regard, one may form

$$\nabla^2_{x,y} \Phi = \frac{\nabla^2_{u,v} \Phi}{\left|\frac{d\tilde{z}}{d\tilde{w}}\right|^2}$$

$$= \frac{- 2\pi\rho(a^2 - b^2)(\cos 2u + \text{Cosh } 2v)}{(a^2 - b^2) \cdot \frac{\cos 2u + \text{Cosh } 2v}{2}} = - 4\pi\rho, \text{ as before.}$$

Write the external potential (for the region <u>outside</u> the elliptical boundary of the beam -- <u>i.e.</u>, where the charge density is <u>zero</u>) as of the form

$$\Phi = A + B \cdot v + C \cdot (\cos 2u) e^{-2v}.$$

This form is clearly <u>harmonic</u> ($\nabla^2_{u,v} \Phi = 0$ and hence $\nabla^2_{x,y} \Phi = 0$), its depen-

---

* <u>Cf</u>. L. C. Teng, ANLAD-59 (1963).

dence on u has the same cos 2u form that is employed inside the elliptical boundary, and the e^{-2v} factor is such that the major dependence on distance when $v \cong \ln r$ is large is $\cong B \ln r$. One might, in fact, expect that with this form for the exterior potential one must have $B = -2\lambda = -2\pi ab\rho$.

It remains to adjust the constants so that the potential and the fields are continuous at the beam boundary -- i.e., so that Φ and $\frac{\partial\Phi}{\partial v}$ are continuous at $v = \mathrm{Tanh}^{-1}\frac{b}{a}$.

III To match the boundary conditions, we require, as identities in u,

$$\frac{\pi\rho}{2}(a-b)\left\{[(a-b)+(a+b)\cos 2u] - [(a+b)+(a-b)\cos 2u]\frac{a^2+b^2}{a^2-b^2}\right\}$$

$$\equiv A + B\cdot\mathrm{Tanh}^{-1}\frac{b}{a} + C\cdot(\cos 2u)\frac{a-b}{a+b}$$

and

$$-\pi\rho(a-b)[(a+b)+(a-b)\cos 2u]\frac{2ab}{a^2-b^2}$$

$$\equiv B - 2C(\cos 2u)\frac{a-b}{a+b}$$

i.e.,

$$\left.\begin{aligned} -\pi ab\rho &= A + B\cdot\mathrm{Tanh}^{-1}\frac{b}{a} \\ \pi ab\frac{a-b}{a+b}\rho &= C\frac{a-b}{a+b} \\ -2\pi ab\rho &= B \\ -2\pi ab\frac{a-b}{a+b}\rho &= -2C\frac{a-b}{a+b} \end{aligned}\right\}.$$

These relations are all satisfied by taking

$$A = \pi ab\left[2\,\mathrm{Tanh}^{-1}\frac{b}{a} - 1\right]\rho$$

$$B = -2\pi ab\rho$$

$$C = \pi ab\rho.$$

Thus we may write:

$$\Phi = -\frac{2\pi\rho}{a+b}(bx^2 + ay^2) \quad \underline{\text{inside}}\text{ the beam}$$

and

$$\Phi = -\pi ab\rho\,[1 - 2\cdot \text{Tanh}^{-1}\frac{b}{a} + 2v - e^{-2v}\cos 2u] \quad \underline{\text{outside}}.$$

IV Along the y-axis ($x = 0$), $|y| = \sqrt{a^2 - b^2}\,\text{Sinh}\, v$, so that

$$v = \text{Sinh}^{-1}\left|\frac{y}{\sqrt{a^2 - b^2}}\right| = \ln \frac{\sqrt{y^2 + a^2 - b^2} + |y|}{\sqrt{a^2 - b^2}}$$

and

$$e^{-2v} = \frac{\left(\sqrt{y^2 + a^2 - b^2} - |y|\right)^2}{a^2 - b^2}, \qquad \text{while } \cos 2u = 1.$$

Thus we may write for the potential along this axis

$$\Phi = -2\pi\rho\frac{a}{a+b}y^2, \quad \text{for} \quad |y| \le b\,;$$

and

$$\Phi = -\pi ab\rho\left[1 - 2\cdot\text{Tanh}^{-1}\frac{a}{b} + 2\,\text{Sinh}^{-1}\left|\frac{y}{\sqrt{a^2 - b^2}}\right| - \frac{\left(\sqrt{y^2 + a^2 - b^2} - |y|\right)^2}{a^2 - b^2}\right]$$

$$= -\pi ab\rho\left[1 - \ln\frac{a+b}{a-b} + \ln\frac{\left(\sqrt{y^2 + a^2 - b^2} + |y|\right)^2}{a^2 - b^2} - \frac{\left(\sqrt{y^2 + a^2 - b^2} - |y|\right)^2}{a^2 - b^2}\right]$$

$$= -\pi ab\rho\left[1 - \frac{\left(\sqrt{y^2 + a^2 - b^2} - |y|\right)^2}{a^2 - b^2} + 2\ln\left(\frac{\sqrt{y^2 + a^2 - b^2} + |y|}{a + b}\right)\right]$$

$$= -2\pi ab\rho\left[\frac{|y|\left(\sqrt{y^2 + a^2 - b^2} - |y|\right)}{a^2 - b^2} + \ln\frac{\sqrt{y^2 + a^2 - b^2} + |y|}{a + b}\right],$$

for $|y| \ge b$.

At the boundary points on this axis ($x = 0$, $y = \pm b$),

$$\Phi = -2\pi\rho\frac{ab^2}{a+b} \quad \text{from either formula.}$$

Similarly, $\Phi = 0$ at the origin, and $\Phi \cong -2\pi ab\rho \ln|y| = -2\lambda \ln|y|$ at great distances along this axis.

The interior field is $E_y = 4\pi\rho \frac{a}{a+b} y = 4\lambda \frac{y}{b(a+b)}$ inside, with the value $4\pi\rho \frac{ab}{a+b} = 4\frac{\lambda}{a+b}$ at the edge $(y = b)$;

The exterior field** is $E_y = 4\pi\rho \frac{ab}{a^2-b^2}\left[\sqrt{y^2+a^2-b^2} - y\right]$ for $y > b$,

becoming $4\pi\rho \frac{ab}{a+b}$ at $y = b$ and tending toward $\frac{2\pi\rho ab}{y} = \frac{2\lambda}{y}$ as $y \to \infty$ (or for $b \to a$).

In the special case $b = a$, the expressions for Φ become, after evaluating the limit of the indeterminate form for the exterior potential,

$$\Phi = \begin{cases} -\pi\rho y^2, & |y| \leq a; \\ -\pi\rho a^2\left[1 + 2\ln\left|\frac{y}{a}\right|\right], & |y| \geq a \end{cases} \quad \text{for } b = a.$$

V In application to the Action-Integral programme,

we replace $\pi ab\rho$ by

$$\lambda = \frac{(Nef)\ |e|}{2\pi R} = 1.5288 \times 10^{-10}\ \frac{(Nef)}{2R}$$

and scale Φ by

$$\frac{1}{\beta} = (FP) = \frac{\sqrt{P^2 + (1704.9)^2}}{P}$$

(with P in gauss · cm) to make $A + (-\Phi)_{\text{scaled}}$ an effective "potential".

We thus obtain the working formulas (writing z in place of y)

For $|z| \leq b$:

$$-\Phi_{\text{scaled}} = 1.5288 \times 10^{-10}\ \frac{(FP)(N_e f)}{Rb(a+b)}\ z^2$$

** This expression for the exterior field along the y-axis agrees with the result given as Eqn. (23) in the cited report of Teng (ANLAD-59). The present report has the merit of giving the potential, $\Phi(u,v)$, not only along principal axes but also at an arbitrarily situated point in the neighborhood of the beam.

For $z > b$:

$$-\Phi_{\text{scaled}} = 1.5288 \times 10^{-10} \frac{(FP)(N_e f)}{R}$$

$$\left[\frac{|z|\left(\sqrt{z^2 + a^2 - b^2} - |z|\right)}{a^2 - b^2} + \ln \frac{\sqrt{z^2 + a^2 - b^2} + |z|}{a + b} \right]$$

if $b \neq a$, or

$$-\Phi_{\text{scaled}} = 1.5288 \times 10^{-10} \frac{(FP)(N_e f)}{R} \left[\frac{1}{2} + \ln \left| \frac{z}{a} \right| \right]$$

if $b = a$.

VI For the preparation of numerical tables to illustrate the character of Φ, as a function of z and of the parameters a, b, one may find the following LRL BRF TTY program convenient.

We let $U = \frac{R(-\Phi)}{(Nef)\,|e|}$ $\qquad ZS = \frac{z}{b}$ $\qquad Q = \frac{a}{b}$

We define $S = |ZS|$

Then $U = \frac{1}{\pi} \frac{S^2}{Q + 1}$ $\qquad$ for $|ZS| \leq 1$

$$U = \begin{cases} \frac{1}{\pi} \left[\frac{S\left(\sqrt{S^2 + Q^2 - 1} - S\right)}{Q^2 - 1} + \ln \frac{\sqrt{S^2 + Q^2 - 1} + S}{Q + 1} \right] & \text{for } |ZS| \geq 1 \text{ and } Q \neq 1 \\ \frac{1}{\pi} \left[\frac{1}{2} + \ln S \right] & \text{for } |ZS| \geq 1 \text{ and } Q = 1. \end{cases}$$

LRL BKY BRF TTY Program for Tabulating
Representative Values of $-\Phi$

```
        Q = 1/4
  10    PRINT6, Q
        ZS = -6.0
  20    S = ABS(ZS)
        IF (S .GT. 1) GO TO 30
        U = S*S/(PI*(Q+1))
        GO TO 50
  30    IF (Q .EQ. 1) GO TO 40
        D = SQRT(S*S + Q*Q -1)
        U = (S*(D-S)/(Q*Q-1) + ALOG((D+S)/(Q+1)))/PI
        GO TO 50
  40    U = ((1/2) + ALOG(S))/PI
  50    PRINT12, ZS, U
        IF (ZS .GT. 5.95) GO TO 70
        IF ((ZS .GT. (-2.05)) .AND. (ZS .LT. (1.95))) GO TO 60
        ZS = ZS + 0.1
  60    ZS = ZS + 0.1
        GO TO 20
  70    IF (Q .GT. 4.90) GO TO 80
        Q = Q + 1/4
        GO TO 10
  80    STOP
OK
```

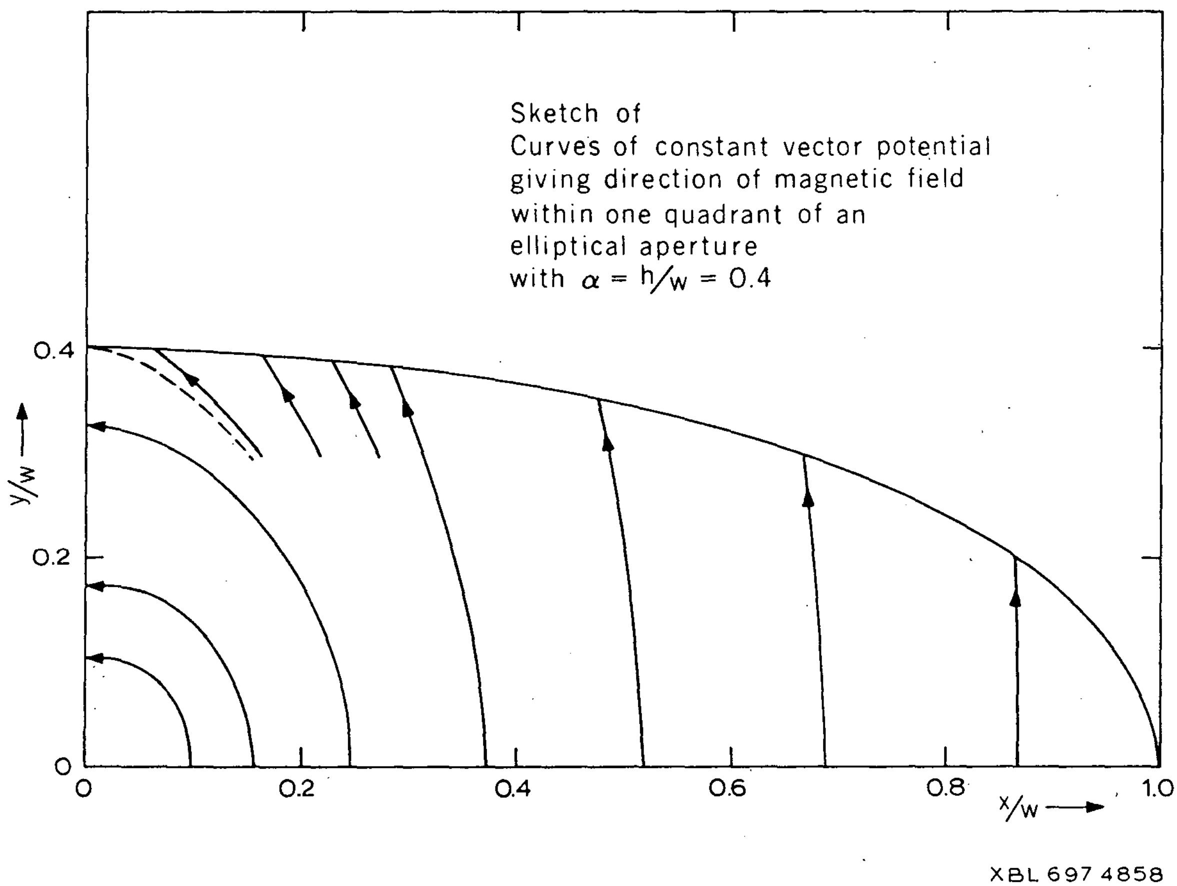
Sketch of
Curves of constant vector potential
giving direction of magnetic field
within one quadrant of an
elliptical aperture
with α = h/w = 0.4
0.4
0.2
0
y/w
0
0.2
0.4
0.6
0.8
1.0
x/w
XBL 697 4858

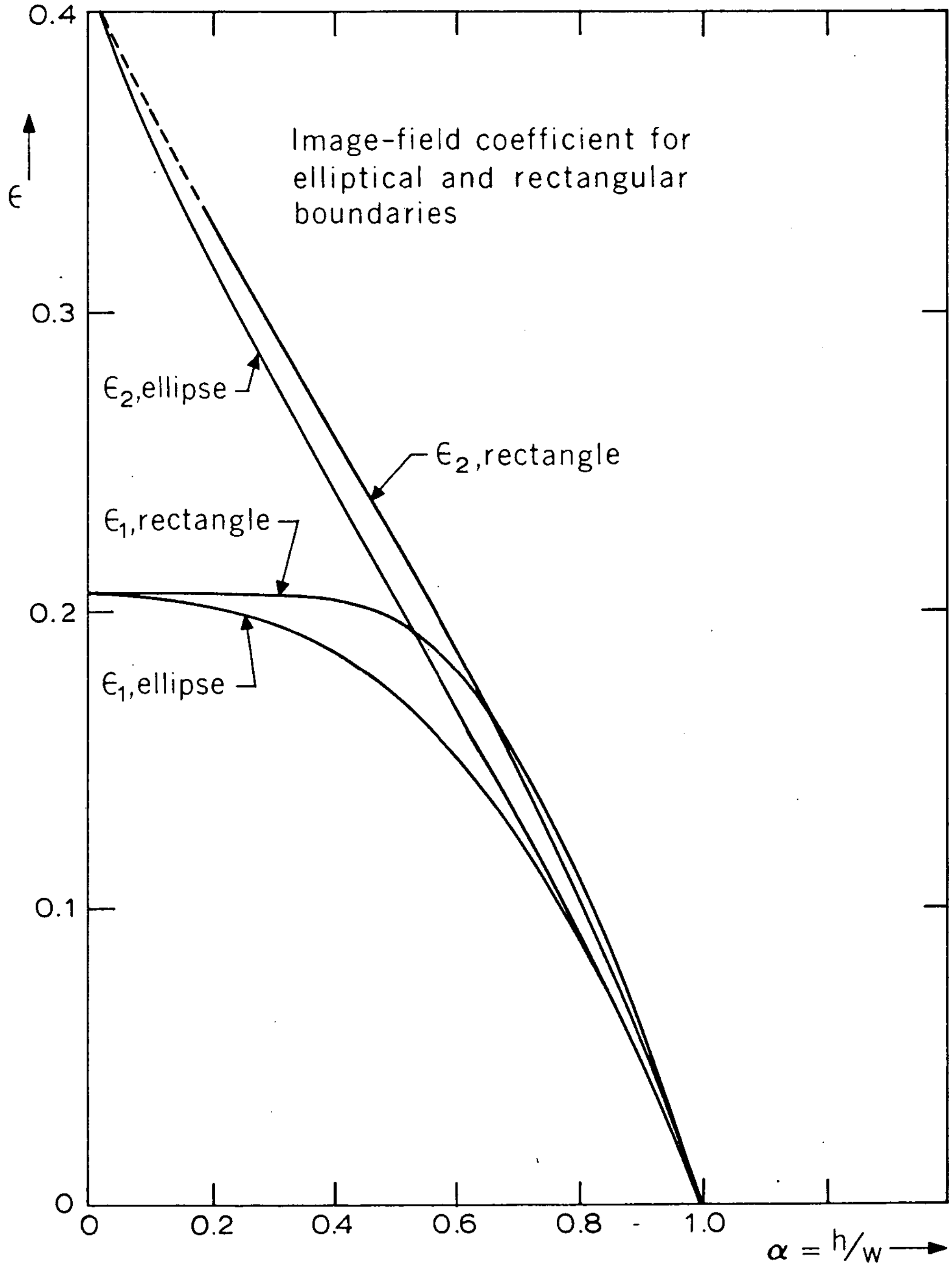
Image-field coefficient for
elliptical and rectangular
boundaries
ϵ
0.4
0.3
0.2
0.1
0
ϵ_2,ellipse
ϵ_2,rectangle
ϵ_1,rectangle
ϵ_1,ellipse
0
0.2
0.4
0.6
0.8
1.0
$\alpha = h/w$

XBL 697-4837

IMAGE FIELD OF A STRAIGHT BEAM OF ELLIPTICAL CROSS-SECTION*

L. Jackson Laslett

13 January 1970

I. Introduction

Image-field coefficients (e.g., ϵ_1)[1] are normally calculated on the supposition that the image field can be taken to be that of a line charge (or line current), and frequently are evaluated for a simple two-dimensional boundary. In this spirit the image field of an electron ring close to a co-axial cylinder may be approximated by "straightening-out" the ring and cylinder into a line source and an infinite plane boundary, respectively, and the image-field coefficient ϵ_1 then assumes the value $\frac{1}{8}$.[2]

The use of a line source appears justified for computing image fields when the boundary surface is somewhat remote in comparison to the transverse dimensions of the beam. Straightening out the source and image surface to a two-dimensional configuration appears suitable in cases for which the transverse dimensions and clearance are each small compared to the major dimensions.

Dr. Perkins has pointed out[3] that the first of these assumptions may not be appropriate for describing some of the experiments performed in the LRL Compressor-III device. In the following report we therefore investigate the image fields of an elliptical beam, taken to be straight and parallel to a conducting plane sheet, within which the charge density is assumed to be constant.

II. Notation

We take the linear charge density to be $-\lambda$ (e.s.u. per cm.) and denote the semi-axes of the beam by "a" (x-direction) and "b" (y-direction) with the center of the beam located at the origin of the coördinate system. An infinite plane conducting sheet is situated at $y = -h$.[4] We wish to compute the image-field contribution to the following quantities:

$$\mathrm{POT} = -\Phi/\lambda$$

$$\mathcal{E}_x = h^2 \frac{E_x}{\lambda} = h^2 \frac{\partial (POT)}{\partial x}$$

and

$$EPS = \epsilon_1 = \frac{h^2}{4\lambda} \frac{E_x}{x} = \frac{h^2}{4} \frac{\partial (POT)}{\partial x}$$

at points along the x axis (in particular for $|x| \leq a$).

III. Derivation

Since each filament of the assumed elliptical beam will give rise to a mirror-image filament of opposite sign, the image field of the entire elliptical beam will be that which would arise from a similar positive beam centered at $y = -2h$. The field of such an image ($+\lambda$ e.s.u. per cm.) is characterized by an exterior potential[5] such that

$$POT = -\frac{\Phi}{\lambda} = 2v - e^{-2v} \cos 2u$$

(if we drop an arbitrary additive constant), where

$$x = F \sin u \operatorname{Cosh} v$$

and

$$y = F \cos u \operatorname{Sinh} v - 2h \quad \text{(for our present choice of origin),}$$

with

$$F = \sqrt{a^2 - b^2} \quad .$$

The x-axis, along which we wish to evaluate the image effects, then is given by the relation

$$F \cos u \operatorname{Sinh} v = 2h.$$

To obtain u in terms of x, we eliminate v to obtain the quadratic equation for $\sin^2 u$:

$$(\sin^2 u)^2 - (1 + M^2 + Z^2)\sin^2 u + Z^2 = 0 \quad \text{(for } y = 0\text{)},$$

where we have written

$$L = 2h, \; M = L/F, \text{ and } Z = x/F.$$

From this equation, sin u and related quantities can be determined.

The curvilinear coördinate v is then given by

$$\operatorname{Sinh} v = M/\cos u$$

and

$$\text{Cosh } v = (\cos^2 u + M^2)^{\frac{1}{2}} / \cos u$$

$$\text{Tanh } v = M/(\cos^2 u + M^2)^{\frac{1}{2}}$$

$$e^{\pm v} = \sqrt{1 + (M/\cos u)^2} \pm M/\cos u$$

$$v = \ell n \left[\sqrt{1 + (M/\cos u)^2} + M/\cos u \right] .$$

From the quantities given above, one can immediately evaluate

$$\text{POT} = -\frac{\Phi}{\lambda} = 2v - e^{-2v} \cos 2u$$
$$= 2v - (e^{-v})^2 (1 - 2 \sin^2 u).$$

To evaluate $\partial(\text{POT})/\partial x$, we note that

$$\frac{\partial(\text{POT})}{\partial x} = 2\left[(1 + e^{-2v} \cos 2u) \frac{dv}{du} + e^{-2v} \sin 2u \right] \frac{du}{dx} .$$

The derivative dv/du [with y held constant (y = 0)] is obtained from

$$\cos u \text{ Sinh } v = \text{constant}.$$
$$\cos u \text{ Cosh } v\, dv - \sin u \text{ Sinh } v\, du = 0$$
$$\frac{dv}{du} = \tan u \text{ Tanh } v.$$

Similarly, from

$$x = F \sin u \text{ Cosh } v$$
$$= F \sqrt{\sin^2 u + M^2 \tan^2 u} \quad ,$$

one obtains the derivative

$$\frac{du}{dx} = \frac{1}{dx/du} = \frac{\sqrt{\sin^2 u + M^2 \tan^2 u}}{F[\sin u \cos u + M^2 \sin u/\cos^3 u]}$$
$$= \frac{x}{F^2} \frac{\cos^3 u/\sin u}{\cos^4 u + M^2} \quad .$$

Accordingly,

$$\text{EPS} = \epsilon_1 = \frac{h^2}{4x} \frac{\partial(\text{POT})}{\partial x}$$

(cont.)

$$= \frac{h^2}{2F^2}\left[(1 + e^{-2v}\cos 2u)\tan u \,\mathrm{Tanh}\, v + e^{-2v}\sin 2u\right]\frac{\cos^3 u/\sin u}{\cos^4 u + M^2}$$

$$= \frac{1}{8}(L/F)^2 \frac{\cos^2 u}{\cos^4 u + M^2}\left[(1 + e^{-2v}\cos 2u)\,\mathrm{Tanh}\, v + 2e^{-2v}\cos^2 u\right]$$

$$= \frac{1}{8}\frac{M^2\cos^2 u}{\cos^4 u + M^2}\left[(1 + e^{-2v}\cos 2u)\,\mathrm{Tanh}\, v + 2e^{-2v}\cos^2 u\right],$$

and

$$\mathcal{E}_x = h^2\frac{E_x}{\lambda} = h^2\frac{\partial(\mathrm{POT})}{\partial x}$$

$$= 4 \cdot x \cdot \mathrm{EPS}.$$

IV. Computational Programme

A short programme has been written, for the LRL BRF system, to evaluate the quantities POT, $\mathcal{E}_x$, and EPS for which expressions have been presented above in Section III.[6] The listing of this programme is given below (next page).[7]

V. Tests

When h is large, we expect that a line image will represent a good approximation and hence that

$$\mathcal{E}_x = h^2\frac{E_x}{\lambda} \cong \frac{2h^2}{x[1+(2h/x)^2]} \approx \begin{cases} \dfrac{2h^2}{x} & \text{for x large} \\ \dfrac{x}{2} & \text{for x small} . \end{cases}$$

Correspondingly,

$$\mathrm{EPS} = \epsilon_1 \approx \begin{cases} \dfrac{1}{2}(h/x)^2 & \text{for x large} \\ \dfrac{1}{8} & \text{for x small} , \end{cases}$$

with the value $\epsilon_1 \sim \frac{1}{8}$ familiar from previous work.[2]

These features are illustrated in the following test runs,[7] wherein one also can check (by numerical differentiation) that

$$\mathcal{E}_x = h^2\frac{\partial(\mathrm{POT})}{\partial x} \quad \text{and} \quad \epsilon_1 = \frac{\mathcal{E}_x}{4x} = \frac{h^2}{4x}\frac{\partial(\mathrm{POT})}{\partial x} .$$

```
T
01/13/70   18.54.11

        10      READ, A, B
                F = SQRT(A*A - B*B)
        20      READ, H
                L = 2*H
                M = L/F
                PRINT8, A, B, F
                PRINT8, H
        30      READ, D, XMAX
                X = D
        40      Z = X/F
                SS = (M*M + Z*Z + 1)/2
                SS = SS - SQRT(SS*SS - Z*Z)
                SU = SQRT(SS)
                U = ASIN(SU)
                CS = 1 - SS
                CU = SQRT(CS)
                C2U = 1 - 2*SS
                SQ = SQRT(1 + (M/CU)*(M/CU))
                EMV = SQ - M/CU
                V = ALOG(SQ + M/CU)
                EM2V = EMV*EMV
                TH = M/SQRT(CS + M*M)
                POT = 2*V - EM2V*C2U
                EPS = (1/8)*M*M*((1 + EM2V*C2U)*TH + 2*EM2V*CS)
                EPS = EPS*CS/(M*M + CS*CS)
                EX = 4*X*EPS
                PRINT11, X, POT, EX, EPS
                IF (X .GE. (XMAX - D/3)) GO TO 20
                X = X + D
                GO TO 40
```


TEST RUNS

a = 5.0

b = 4.0

```
> T
  01/13/70   18.56.59

↑XEQ
 BEGIN XEQ

 ENTER... A, B,
5.0,4.0
 ENTER... H,
200.

  A= 5.0000  B= 4.0000  F= 3.0000
  H= 200.00

 ENTER... D, XMAX,
0.1,1.0

  X= 0.1000000  POT= 11.172013  EX= 0.0499979  EPS= 0.1249947
  X= 0.2000000  POT= 11.172013  EX= 0.0999958  EPS= 0.1249947
  X= 0.3000000  POT= 11.172014  EX= 0.1499936  EPS= 0.1249947
  X= 0.4000000  POT= 11.172014  EX= 0.1999914  EPS= 0.1249946
  X= 0.5000000  POT= 11.172015  EX= 0.2499891  EPS= 0.1249945
  X= 0.6000000  POT= 11.172015  EX= 0.2999867  EPS= 0.1249944
  X= 0.7000000  POT= 11.172016  EX= 0.3499842  EPS= 0.1249943
  X= 0.8000000  POT= 11.172017  EX= 0.3999815  EPS= 0.1249942
  X= 0.9000000  POT= 11.172018  EX= 0.4499787  EPS= 0.1249941
  X= 1.0000000  POT= 11.172019  EX= 0.4999758  EPS= 0.1249939

 ENTER... H,
200.

  A= 5.0000  B= 4.0000  F= 3.0000
  H= 200.00

 ENTER... D, XMAX,
1.0,25.0

  X= 1.0000000  POT= 11.172019  EX= 0.4999758  EPS= 0.1249939
  X= 2.0000000  POT= 11.172038  EX= 0.9999328  EPS= 0.1249916
  X= 3.0000000  POT= 11.172069  EX= 1.4998524  EPS= 0.1249877
  X= 4.0000000  POT= 11.172113  EX= 1.9997157  EPS= 0.1249822
  X= 5.0000000  POT= 11.172169  EX= 2.4995040  EPS= 0.1249752
  X= 6.0000000  POT= 11.172238  EX= 2.9991987  EPS= 0.1249666
 PAUSING
↑GO,5
  X= 7.0000000  POT= 11.172319  EX= 3.4987810  EPS= 0.1249565
  X= 8.0000000  POT= 11.172413  EX= 3.9982321  EPS= 0.1249443
  X= 9.0000000  POT= 11.172519  EX= 4.4975335  EPS= 0.1249315
  X= 10.000000  POT= 11.172638  EX= 4.9966665  EPS= 0.1249167
  X= 11.000000  POT= 11.172769  EX= 5.4956123  EPS= 0.1249003
  X= 12.000000  POT= 11.172912  EX= 5.9943525  EPS= 0.1248823
  X= 13.000000  POT= 11.173069  EX= 6.4928634  EPS= 0.1248629
  X= 14.000000  POT= 11.173237  EX= 6.9911414  EPS= 0.1248418
  X= 15.000000  POT= 11.173418  EX= 7.4891538  EPS= 0.1248192
  X= 16.000000  POT= 11.173612  EX= 7.9868843  EPS= 0.1247951
  X= 17.000000  POT= 11.173817  EX= 8.4843131  EPS= 0.1247694
  X= 18.000000  POT= 11.174036  EX= 8.9814347  EPS= 0.1247421
  X= 19.000000  POT= 11.174267  EX= 9.4782161  EPS= 0.1247134
```

```
X= 20.000000  POT= 11.174510  EX= 9.9746440  EPS= 0.1246330
X= 21.000000  POT= 11.174765  EX= 10.470700  EPS= 0.1246512
X= 22.000000  POT= 11.175033  EX= 10.966366  EPS= 0.1246173
X= 23.000000  POT= 11.175314  EX= 11.461624  EPS= 0.1245829
X= 24.000000  POT= 11.175606  EX= 11.956455  EPS= 0.1245464
X= 25.000000  POT= 11.175911  EX= 12.450841  EPS= 0.1245084

ENTER.... H,
200.

A= 5.0000  B= 4.0000  F= 3.0000
H= 200.00

ENTER... D, XMAX,
25.0,850.

X= 25.000000  POT= 11.175911  EX= 12.450841  EPS= 0.1245084
X= 50.000000  POT= 11.187516  EX= 24.614383  EPS= 0.1230719
X= 75.000000  POT= 11.206564  EX= 36.225006  EPS= 0.1207500
X= 100.00000  POT= 11.232635  EX= 47.057102  EPS= 0.1176428
X= 125.00000  POT= 11.265187  EX= 56.937573  EPS= 0.1138751
X= 150.00000  POT= 11.303585  EX= 65.751393  EPS= 0.1095857
X= 175.00000  POT= 11.347141  EX= 73.440579  EPS= 0.1049151
X= 200.00000  POT= 11.395149  EX= 79.998020  EPS= 0.0999975
X= 225.00000  POT= 11.446910  EX= 85.458080  EPS= 0.0949534
X= 250.00000  POT= 11.501757  EX= 89.885935  EPS= 0.0898859
X= 275.00000  POT= 11.559070  EX= 93.367170  EPS= 0.0848792
X= 300.00000  POT= 11.618289  EX= 95.998652  EPS= 0.0799989
X= 325.00000  POT= 11.678912  EX= 97.881184  EPS= 0.0752932
X= 350.00000  POT= 11.740505  EX= 99.114045  EPS= 0.0707957
X= 375.00000  POT= 11.802689  EX= 99.791257  EPS= 0.0665275
X= 400.00000  POT= 11.865146  EX= 99.999297  EPS= 0.0624996
X= 425.00000  POT= 11.927607  EX= 99.815934  EPS= 0.0587153
X= 450.00000  POT= 11.989849  EX= 99.309873  EPS= 0.0551722
X= 475.00000  POT= 12.051689  EX= 98.540950  EPS= 0.0518637
X= 500.00000  POT= 12.112981  EX= 97.560675  EPS= 0.0487803
X= 525.00000  POT= 12.173605  EX= 96.412966  EPS= 0.0459109
X= 550.00000  POT= 12.233470  EX= 95.134958  EPS= 0.0432432
X= 575.00000  POT= 12.292504  EX= 93.757831  EPS= 0.0407643
X= 600.00000  POT= 12.350652  EX= 92.307600  EPS= 0.0384615
X= 625.00000  POT= 12.407877  EX= 90.805842  EPS= 0.0363223
X= 650.00000  POT= 12.464153  EX= 89.270352  EPS= 0.0343348
X= 675.00000  POT= 12.519461  EX= 87.715724  EPS= 0.0324373
X= 700.00000  POT= 12.573796  EX= 86.153851  EPS= 0.0307692
X= 725.00000  POT= 12.627154  EX= 84.594366  EPS= 0.0291705
X= 750.00000  POT= 12.679541  EX= 83.045012  EPS= 0.0276817
X= 775.00000  POT= 12.730964  EX= 81.511953  EPS= 0.0262942
X= 800.00000  POT= 12.781435  EX= 80.000045  EPS= 0.0250000
X= 825.00000  POT= 12.830969  EX= 78.513061  EPS= 0.0237918
X= 850.00000  POT= 12.879582  EX= 77.053878  EPS= 0.0226629
```

```
ENTER... H,
10.

 A= 5.0000   B= 4.0000   F= 3.0000
 H= 10.000

ENTER... D, XMAX,
0.1,1.0

  X= 0.1000000   POT= 5.1861526   EX= 0.0491706   EPS= 0.1229265
  X= 0.2000000   POT= 5.1862263   EX= 0.0983341   EPS= 0.1229176
  X= 0.3000000   POT= 5.1863492   EX= 0.1474834   EPS= 0.1229028
  X= 0.4000000   POT= 5.1865213   EX= 0.1966114   EPS= 0.1228821
  X= 0.5000000   POT= 5.1867424   EX= 0.2457111   EPS= 0.1228556
  X= 0.6000000   POT= 5.1870127   EX= 0.2947754   EPS= 0.1228231
  X= 0.7000000   POT= 5.1873320   EX= 0.3437973   EPS= 0.1227847
  X= 0.8000000   POT= 5.1877003   EX= 0.3927697   EPS= 0.1227405
  X= 0.9000000   POT= 5.1881175   EX= 0.4416856   EPS= 0.1226904
  X= 1.0000000   POT= 5.1885836   EX= 0.4905381   EPS= 0.1226345

ENTER... H,
10.

 A= 5.0000   B= 4.0000   F= 3.0000
 H= 10.000

ENTER... D, XMAX,
1.0,25.0

  X= 1.0000000   POT= 5.1885836   EX= 0.4905381   EPS= 0.1226345
  X= 2.0000000   POT= 5.1959153   EX= 0.9740645   EPS= 0.1217581
  X= 3.0000000   POT= 5.2080192   EX= 1.4438908   EPS= 0.1203242
  X= 4.0000000   POT= 5.2247271   EX= 1.8939445   EPS= 0.1183715
  X= 5.0000000   POT= 5.2458146   EX= 2.3190065   EPS= 0.1159503
  X= 6.0000000   POT= 5.2710093   EX= 2.7143756   EPS= 0.1131198
  X= 7.0000000   POT= 5.3000044   EX= 3.0784528   EPS= 0.1099447
  X= 8.0000000   POT= 5.3324645   EX= 3.4077432   EPS= 0.1064921
  X= 9.0000000   POT= 5.3680418   EX= 3.7018205   EPS= 0.1028283
  X= 10.000000   POT= 5.4063834   EX= 3.9606661   EPS= 0.0990167
  X= 11.000000   POT= 5.4471403   EX= 4.1850748   EPS= 0.0951153
  X= 12.000000   POT= 5.4899748   EX= 4.3764703   EPS= 0.0911765
  X= 13.000000   POT= 5.5345660   EX= 4.5367494   EPS= 0.0872452
  X= 14.000000   POT= 5.5806135   EX= 4.6631322   EPS= 0.0833595
  X= 15.000000   POT= 5.6278403   EX= 4.7730293   EPS= 0.0795505
  X= 16.000000   POT= 5.6759941   EX= 4.8539316   EPS= 0.0758427
  X= 17.000000   POT= 5.7243472   EX= 4.9133218   EPS= 0.0722547
  X= 18.000000   POT= 5.7741963   EX= 4.9536080   EPS= 0.0688001
  X= 19.000000   POT= 5.8238634   EX= 4.9770760   EPS= 0.0654378
  X= 20.000000   POT= 5.8736894   EX= 4.9853596   EPS= 0.0623232
  X= 21.000000   POT= 5.9235331   EX= 4.9819190   EPS= 0.0593036
  X= 22.000000   POT= 5.9732914   EX= 4.9670494   EPS= 0.0564436
  X= 23.000000   POT= 6.0228479   EX= 4.9428293   EPS= 0.0537264
  X= 24.000000   POT= 6.0721216   EX= 4.9107198   EPS= 0.0511533
  X= 25.000000   POT= 6.1210402   EX= 4.8719333   EPS= 0.0487198
```

```
 ENTER... H,
5.0

  A= 5.0000  B= 4.0000  F= 3.0000
  H= 5.0000

 ENTER... D, XMAX,
0.1,1.0

  X= 0.1000000  POT= 3.8163456  EX= 0.0468557  EPS= 0.1171391
  X= 0.2000000  POT= 3.8166267  EX= 0.0936871  EPS= 0.1171089
  X= 0.3000000  POT= 3.8170950  EX= 0.1404703  EPS= 0.1170586
  X= 0.4000000  POT= 3.8177503  EX= 0.1871811  EPS= 0.1169882
  X= 0.5000000  POT= 3.8185923  EX= 0.2337955  EPS= 0.1168978
  X= 0.6000000  POT= 3.8196205  EX= 0.2802899  EPS= 0.1167874
  X= 0.7000000  POT= 3.8208344  EX= 0.3266405  EPS= 0.1166573
 PAUSING
 GO, 10
  X= 0.8000000  POT= 3.8222334  EX= 0.3728240  EPS= 0.1165075
  X= 0.9000000  POT= 3.8238168  EX= 0.4188172  EPS= 0.1163381
  X= 1.0000000  POT= 3.8255837  EX= 0.4645973  EPS= 0.1161493

 ENTER... H,
5.0

  A= 5.0000  B= 4.0000  F= 3.0000
  H= 5.0000

 ENTER... D, XMAX,
1.0,25.0

  X= 1.0000000  POT= 3.8255837  EX= 0.4645973  EPS= 0.1161493
  X= 2.0000000  POT= 3.8531079  EX= 0.9059309  EPS= 0.1132414
  X= 3.0000000  POT= 3.8974310  EX= 1.3041820  EPS= 0.1086818
  X= 4.0000000  POT= 3.9566799  EX= 1.6454345  EPS= 0.1028423
  X= 5.0000000  POT= 4.0282655  EX= 1.9229337  EPS= 0.0961467
  X= 6.0000000  POT= 4.1096552  EX= 2.1360927  EPS= 0.0890039
  X= 7.0000000  POT= 4.1983544  EX= 2.2894653  EPS= 0.0817666
  X= 8.0000000  POT= 4.2921152  EX= 2.3905833  EPS= 0.0747057
  X= 9.0000000  POT= 4.3890218  EX= 2.4432535  EPS= 0.0680070
  X= 10.000000  POT= 4.4875137  EX= 2.4712605  EPS= 0.0617815
  X= 11.000000  POT= 4.5863673  EX= 2.4675736  EPS= 0.0560813
  X= 12.000000  POT= 4.6846553  EX= 2.4440066  EPS= 0.0509168
  X= 13.000000  POT= 4.7816971  EX= 2.4063903  EPS= 0.0462710
  X= 14.000000  POT= 4.8770102  EX= 2.3532111  EPS= 0.0421109
  X= 15.000000  POT= 4.9702665  EX= 2.3037424  EPS= 0.0383957
  X= 16.000000  POT= 5.0612560  EX= 2.2452343  EPS= 0.0350818
  X= 17.000000  POT= 5.1498569  EX= 2.1845503  EPS= 0.0321262
  X= 18.000000  POT= 5.2360124  EX= 2.1231650  EPS= 0.0294384
  X= 19.000000  POT= 5.3197133  EX= 2.0619336  EPS= 0.0271314
  X= 20.000000  POT= 5.4009837  EX= 2.0017374  EPS= 0.0250217
  X= 21.000000  POT= 5.4798713  EX= 1.9429052  EPS= 0.0231299
  X= 22.000000  POT= 5.5564395  EX= 1.8858147  EPS= 0.0214297
  X= 23.000000  POT= 5.6307623  EX= 1.8306559  EPS= 0.0198984
  X= 24.000000  POT= 5.7029193  EX= 1.7775432  EPS= 0.0185161
  X= 25.000000  POT= 5.7729937  EX= 1.7265247  EPS= 0.0172652
```

```
 ENTER... H,
4.0

  A= 5.0000   B= 4.0000   F= 3.0000
  H= 4.0000

 ENTER... D, XMAX,
0.1,1.0

  X= 0.1000000  POT= 3.3820321  EX= 0.0452714  EPS= 0.1131755
  X= 0.2000000  POT= 3.3825965  EX= 0.0905091  EPS= 0.1131364
  X= 0.3000000  POT= 3.3832133  EX= 0.1356794  EPS= 0.1130662
  X= 0.4000000  POT= 3.3842022  EX= 0.1807439  EPS= 0.1129631
  X= 0.5000000  POT= 3.3854724  EX= 0.2256342  EPS= 0.1128421
  X= 0.6000000  POT= 3.3870230  EX= 0.2704524  EPS= 0.1126885
  X= 0.7000000  POT= 3.3888527  EX= 0.3150208  EPS= 0.1125074
  X= 0.8000000  POT= 3.3909602  EX= 0.3593572  EPS= 0.1122991
  X= 0.9000000  POT= 3.3933441  EX= 0.4034298  EPS= 0.1120638
  X= 1.0000000  POT= 3.3960025  EX= 0.4472076  EPS= 0.1118019

 ENTER... H,
4.0

  A= 5.0000   B= 4.0000   F= 3.0000
  H= 4.0000

 ENTER... D, XMAX,
1.0,25.0

  X= 1.0000000  POT= 3.3960025  EX= 0.4472076  EPS= 0.1118019
  X= 2.0000000  POT= 3.4371705  EX= 0.8624263  EPS= 0.1078033
  X= 3.0000000  POT= 3.5025987  EX= 1.2200735  EPS= 0.1016728
  X= 4.0000000  POT= 3.5881600  EX= 1.5051680  EPS= 0.0940730
  X= 5.0000000  POT= 3.6891520  EX= 1.7141253  EPS= 0.0857063
  X= 6.0000000  POT= 3.8009522  EX= 1.8525347  EPS= 0.0771889
  X= 7.0000000  POT= 3.9194776  EX= 1.9314213  EPS= 0.0689793
  X= 8.0000000  POT= 4.0414087  EX= 1.9636646  EPS= 0.0613645
  X= 9.0000000  POT= 4.1642204  EX= 1.9615053  EPS= 0.0544863
  X= 10.000000  POT= 4.2860973  EX= 1.9352385  EPS= 0.0483322
  X= 11.000000  POT= 4.4053006  EX= 1.8931197  EPS= 0.0430254
  X= 12.000000  POT= 4.5225317  EX= 1.8410289  EPS= 0.0383548
  X= 13.000000  POT= 4.6358134  EX= 1.7833362  EPS= 0.0342949
  X= 14.000000  POT= 4.7453953  EX= 1.7230466  EPS= 0.0307657
  X= 15.000000  POT= 4.8511830  EX= 1.6621962  EPS= 0.0277033
  X= 16.000000  POT= 4.9531364  EX= 1.6021266  EPS= 0.0250332
  X= 17.000000  POT= 5.0514831  EX= 1.5436921  EPS= 0.0227014
  X= 18.000000  POT= 5.1461929  EX= 1.4874090  EPS= 0.0206585
  X= 19.000000  POT= 5.2374601  EX= 1.4335632  EPS= 0.0188627
  X= 20.000000  POT= 5.3254419  EX= 1.3822851  EPS= 0.0172736
  X= 21.000000  POT= 5.4102999  EX= 1.3336019  EPS= 0.0158762
  X= 22.000000  POT= 5.4921954  EX= 1.2874735  EPS= 0.0146304
  X= 23.000000  POT= 5.5712856  EX= 1.2438138  EPS= 0.0135193
  X= 24.000000  POT= 5.6477220  EX= 1.2025299  EPS= 0.0125264
  X= 25.000000  POT= 5.7216457  EX= 1.1634864  EPS= 0.0116349
```

VI. Results

As an example of a physically realistic case, the programme has been applied to a beam for which a = 1.0 (semi-axis in the transverse direction parallel to the conductor, normally the axial or z-direction), b = 0.5 (semi-axis in the transverse direction normal to the conductor, normally the radial or r-direction), and the clearance (h) was given the values

$$h = 2.0,\ 1.5,\ 1.0,\ 0.75, \text{ and } 0.50$$

(the last case corresponding to no clearance for the edge of the beam). In each case of this series, the runs were carried to values of x no greater than "a", because of the interest in "incoherent" image focussing forces felt by some representative particle of the beam.

The values found for $\mathcal{E}_x$ provide a measure of the local image field at the corresponding value of x — the extent to which $\mathcal{E}_x$ is not directly proportional to x (in the range $|x| \leq a$) gives an indication of the non-linearity of this image field. The computed values of EPS ($= \epsilon_1$) are proportional (factor $\frac{1}{4}$) to $\mathcal{E}_x/x$ and would be constant throughout the range of x if the image field were exactly proportional to x.

The computational results are given on the following sheets, and are followed by graphs of $\mathcal{E}_x$ and EPS ($= \epsilon_1$) vs. x.

RESULTS

a = 1.0

b = 0.5

```
↑XEQ
 BEGIN XEQ

 ENTER... A, B,
1.0,0.5

 ENTER... H,
2.00

   A= 1.0000   B= 0.5000   F= 0.8660
   H= 2.0000

 ENTER... D, XMAX,
0.1,1.0

   X= 0.1000000   POT= 4.4587529   EX= 0.0482803   EPS= 0.1207007
   X= 0.2000000   POT= 4.4605613   EX= 0.0963938   EPS= 0.1204923
   X= 0.3000000   POT= 4.4635698   EX= 0.1441757   EPS= 0.1201464
   X= 0.4000000   POT= 4.4677665   EX= 0.1914646   EPS= 0.1196654
   X= 0.5000000   POT= 4.4731376   EX= 0.2381045   EPS= 0.1190522
   X= 0.6000000   POT= 4.4796651   EX= 0.2839463   EPS= 0.1183110
   X= 0.7000000   POT= 4.4873271   EX= 0.3288494   EPS= 0.1174462
   X= 0.8000000   POT= 4.4960986   EX= 0.3726327   EPS= 0.1164634
   X= 0.9000000   POT= 4.5059513   EX= 0.4153259   EPS= 0.1153683
   X= 1.0000000   POT= 4.5168541   EX= 0.4566701   EPS= 0.1141675


 ENTER... H,
1.50

   A= 1.0000   B= 0.5000   F= 0.8660
   H= 1.5000

 ENTER... D, XMAX,
0.1,1.0

   X= 0.1000000   POT= 3.8926604   EX= 0.0470319   EPS= 0.1175796
   X= 0.2000000   POT= 3.8957913   EX= 0.0937920   EPS= 0.1172400
   X= 0.3000000   POT= 3.9009395   EX= 0.1400137   EPS= 0.1166750
   X= 0.4000000   POT= 3.9082252   EX= 0.1854392   EPS= 0.1158995
   X= 0.5000000   POT= 3.9174576   EX= 0.2298251   EPS= 0.1149125
   X= 0.6000000   POT= 3.9286353   EX= 0.2729451   EPS= 0.1137271
 PAUSING
↑GO, 10
   X= 0.7000000   POT= 3.9416976   EX= 0.3145940   EPS= 0.1123550
   X= 0.8000000   POT= 3.9565747   EX= 0.3545901   EPS= 0.1108094
   X= 0.9000000   POT= 3.9731899   EX= 0.3927775   EPS= 0.1091049
   X= 1.0000000   POT= 3.9914596   EX= 0.4290266   EPS= 0.1072566
```

```
ENTER... H,
1.00

  A= 1.0000   B= 0.5000   F= 0.8660
  H= 1.0000

 ENTER... D, XMAX,
0.1,1.0

  X= 0.1000000   POT= 3.1072986   EX= 0.0438319   EPS= 0.1095797
  X= 0.2000000   POT= 3.1138552   EX= 0.0871794   EPS= 0.1089742
  X= 0.3000000   POT= 3.1247027   EX= 0.1295728   EPS= 0.1079774
  X= 0.4000000   POT= 3.1397232   EX= 0.1705710   EPS= 0.1066069
  X= 0.5000000   POT= 3.1587570   EX= 0.2097739   EPS= 0.1048869
  X= 0.6000000   POT= 3.1816065   EX= 0.2468332   EPS= 0.1028472
  X= 0.7000000   POT= 3.2080424   EX= 0.2814604   EPS= 0.1005216
  X= 0.8000000   POT= 3.2378100   EX= 0.3134321   EPS= 0.0979475
  X= 0.9000000   POT= 3.2706351   EX= 0.3425920   EPS= 0.0951645
  X= 1.0000000   POT= 3.3062316   EX= 0.3688507   EPS= 0.0922127

 ENTER... H,
0.75

  A= 1.0000   B= 0.5000   F= 0.8660
  H= 0.7500

 ENTER... D, XMAX,
0.1,1.0

  X= 0.1000000   POT= 2.5656869   EX= 0.0400343   EPS= 0.1002108
  X= 0.2000000   POT= 2.5763331   EX= 0.0795252   EPS= 0.0994065
  X= 0.3000000   POT= 2.5933876   EX= 0.1177033   EPS= 0.0980861
  X= 0.4000000   POT= 2.6180742   EX= 0.1540464   EPS= 0.0962790
  X= 0.5000000   POT= 2.6485209   EX= 0.1880512   EPS= 0.0940256
  X= 0.6000000   POT= 2.6847734   EX= 0.2193011   EPS= 0.0913754
  X= 0.7000000   POT= 2.7263124   EX= 0.2474301   EPS= 0.0883857
  X= 0.8000000   POT= 2.7725719   EX= 0.2723311   EPS= 0.0851191
  X= 0.9000000   POT= 2.8229589   EX= 0.2939075   EPS= 0.0816410
  X= 1.0000000   POT= 2.8768727   EX= 0.3120676   EPS= 0.0780169

 ENTER... H,
0.50

  A= 1.0000   B= 0.5000   F= 0.8660
  H= 0.5000

 ENTER... D, XMAX,
0.1,1.0

  X= 0.1000000   POT= 1.8407919   EX= 0.0324196   EPS= 0.0810489
  X= 0.2000000   POT= 1.8601332   EX= 0.0641040   EPS= 0.0801390
  X= 0.3000000   POT= 1.8918818   EX= 0.0943405   EPS= 0.0786178
  X= 0.4000000   POT= 1.9353234   EX= 0.1224635   EPS= 0.0765397
  X= 0.5000000   POT= 1.9894920   EX= 0.1478355   EPS= 0.0739427
  X= 0.6000000   POT= 2.0532076   EX= 0.1701353   EPS= 0.0708876
  X= 0.7000000   POT= 2.1251278   EX= 0.1888679   EPS= 0.0674528
  X= 0.8000000   POT= 2.2038125   EX= 0.2039415   EPS= 0.0637317
  X= 0.9000000   POT= 2.2877954   EX= 0.2153733   EPS= 0.0598273
  X= 1.0000000   POT= 2.3756563   EX= 0.2233730   EPS= 0.0558445
```

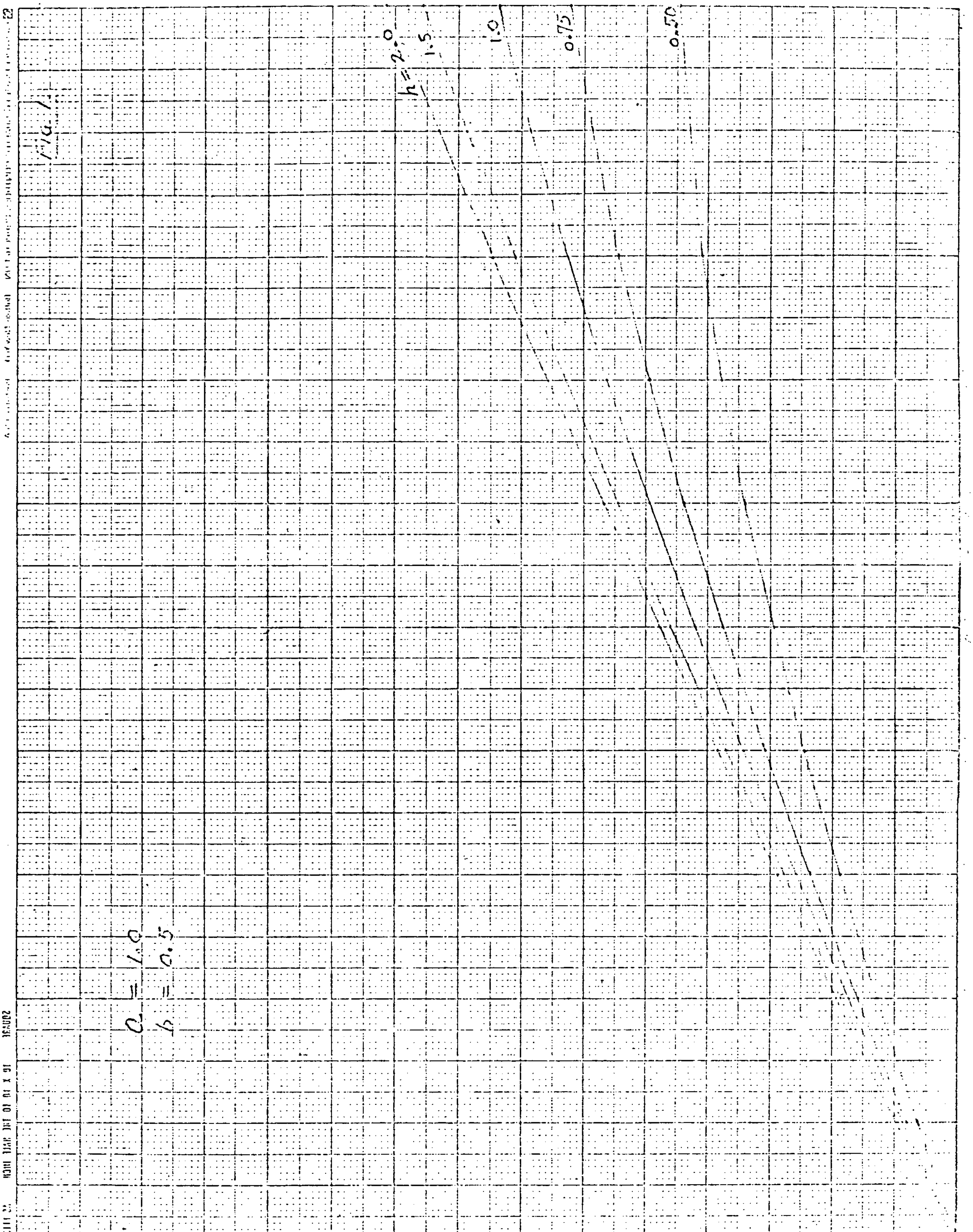
Fig. 1
a = 1.0
b = 0.5
h = 2.0
1.5
1.0
0.75
0.50
0.5
0.4
0.3
0.2
0.1
0

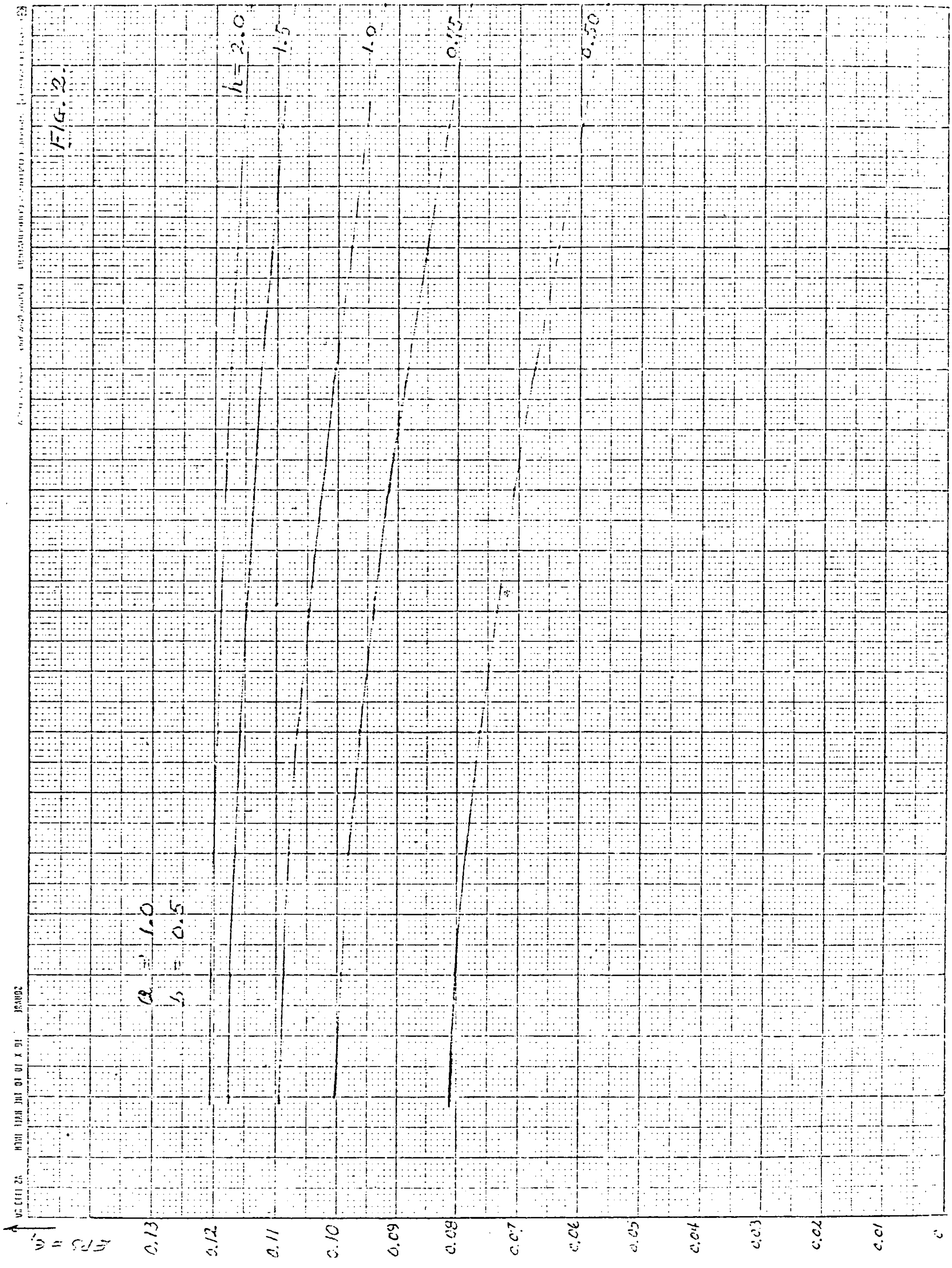
FIG. 2.
h = 2.0
1.5
1.0
0.75
0.50
a = 1.0
b = 0.5
0.13
0.12
0.11
0.10
0.09
0.08
0.07
0.06
0.05
0.04
0.03
0.02
0.01
0

```
1,30P

10    READ, A, B
      F = SQRT(A*A - B*B)
20    READ, H
      L = 2*H
      M = L/F
      PRINT3, A, B, F
      PRINT3, H
30    READ, D, XMAX
      X = D
40    Z = X/F
      SS = (M*M + Z*Z + 1)/2
      SS = SS - SQRT(SS*SS - Z*Z)
      SU = SQRT(SS)
      U = ASIN(SU)
      CS = 1 - SS
      CU = SQRT(CS)
      C2U = 1 - 2*SS
      SQ = SQRT(1 + (M/CU)*(M/CU))
      EMV = SQ - M/CU
      V = ALOG(SQ + M/CU)
      EM2V = EMV*EMV
      TH = M/SQRT(CS + M*M)
      POT = 2*V - EM2V*C2U
      EPS = (1/8)*M*M*((1 + EM2V*C2U)*TH + 2*EM2V*CS)
      EPS = EPS*CS/(M*M + CS*CS)
      EX = 4*X*EPS
      PRINT11, X, POT, EX, EPS
      IF (X .GE. (XMAX - D/8)) GO TO 20
      X = X + D
      GO TO 40
```

```
> T
  01/13/70   19.46.05

> DC.
 OK.
 EQ 72 READY

> T
  01/13/70   19.46.15
 EQ 72 READY
```

VIII. References and Notes

* Work supported by the U.S. Atomic Energy Commission. For previous work, see UCID-10162.

1. BNL-7534, p. 325 ff.

2. ERAN-30

3. Private conversation (13 January 1970).

4. The notation adopted here follows that of reference 5 below. One should note that the transverse dimension parallel to the conductor is x and that the semi-axis of the beam in this direction is denoted by "a" in the present work. We suppose, as is appropriate for the present application, that a $\geq$ b. With respect to notation, the direction here designated by x is frequently termed the z-direction in electron-ring work, and the dimension denoted here by "a" then is commonly written "b".

5. ERAN-44

6. The quantity u is explicitly evaluated in line 14 of the BRF programme, although with the present print statement no direct use is made of this quantity. By adding a suitable print instruction, however, the curvilinear coördinates u and v could be printed.

7. $\mathcal{E}_x$ is typed as EX in the listing and on the output of the BRF programme.

LAWRENCE BER
TECHNICAL INFORMAT ARTMEN
UNIVERSITY OF CA NIA
BERKELEY, CALIFORNIA 94720